

Non-perturbative aspects of (low-dimensional) quantum field theories

Dissertation
zur Erlangung des Doktorgrades
der Naturwissenschaften

vorgelegt beim Fachbereich Physik
der Johann Wolfgang Goethe-Universität
in Frankfurt am Main

von

Adrian Koenigstein

aus Frankfurt am Main

Frankfurt am Main,

2023

(D 30)

vom Fachbereich Physik der

Johann Wolfgang Goethe-Universität als Dissertation angenommen.

Dekan: Prof. Dr. Roger Erb

1. Gutachter: Prof. Dr. Dirk H. Rischke

2. Gutachter: Prof. Dr. Jens Braun

Datum der Disputation: 10. Juli 2023

Preface

This thesis deals with several aspects of non-perturbative calculations in low-dimensional quantum field theories. It is split into two main parts:

The first part focuses on method development and testing. Using exactly integrable QFTs in zero spacetime dimensions as toy models, the need for non-perturbative methods in QFT is demonstrated. In particular, we focus on the functional renormalization group (FRG) as a non-perturbative exact method and present a novel fluid-dynamic reformulation of certain FRG flow equations. This framework and the application of numerical schemes from the field of computational fluid dynamics (CFD) to the FRG is tested and benchmarked against exact results for correlation functions. We also draw several conclusions for the qualitative understanding and interpretation of renormalization group (RG) flows from this fluid-dynamic reformulation and discuss the generalization of our findings to realistic higher-dimensional QFTs.

The topics discussed in the second part are also manifold. In general, the second part of this thesis deals with the Gross-Neveu (GN) model, which is a prototype of a relativistic QFT. Even though being a model in two spacetime dimensions, it shares many features of realistic models and theories for high-energy particle physics, but also emerges as a limiting case from systems in solid state physics. Especially, it is interesting to study the model at non-vanishing temperatures and densities, thus, its thermodynamic properties and phase structure.

First, we use this model to test and apply our findings of the first part of this thesis in a realistic environment. We analyze how the fluid-dynamic aspects of the FRG realize themselves in the RG flow of a full-fledged QFT and how we profit from this numeric framework in actual calculations. Thereby, however, we also aim at answering a long-standing question: Is there still symmetry breaking and condensation at non-zero temperatures in the GN model, if one relaxes the commonly used approximation of an infinite number of fermion species and works with a finite number of fermions? In short: Is matter (in the GN model) in a single spatial dimension at non-zero temperature always gas-like?

In general, we also use the GN model to learn about the correct description of QFTs at non-zero temperatures and densities. This is of utmost relevance for model calculations in low-energy quantum chromodynamics (QCD) or other QFTs in medium and we draw several conclusions for the requirements for stable calculations at non-zero chemical potential.

In any case, both parts come with thorough motivations, introductions, and conclusions and can be studied mostly independently of each other. Either way, the first part can be considered as a standalone work. It is written in a pedagogical manner and may be used as an introduction into the fluid-dynamic framework to the FRG by readers with FRG knowledge, but also as a first introduction for novices in QFT and FRG. The style of the second part is different and basic knowledge about QFT and FRG is required. Nevertheless, especially the second part comes with multiple appendices, which comprise all details of the explicit calculations. This ensures that QFT practitioners, who are not experts on the topic, can in principle follow each step of the calculations. Still, a lot of the numerical calculations are based on the fluid-dynamic framework for FRG, which was put forward in the first part. However, if one is exclusively interested in the physics and results, one does not necessarily need to read the first part in advance.

Disclosure

In my personal view, the way progress is achieved in physics today has changed drastically in the last decades. The era of great geniuses, who can push the boundaries of a field of research almost completely on their own, is basically over. Today, the frontiers of research are mainly moved by projects, where excellent teamwork, high reproducibility, and mutual control of results, as well as interdisciplinary expertise are essential.

By no means I claim that the results presented in this thesis will be a huge advance in the field of high-energy physics. I rather hope and think that at least some aspects of my research will lead to incremental improvements and further knowledge-building.

However, also this thesis is based on the results and publications of several projects that I worked on in close collaboration and fantastic teamwork with colleagues from the research field of high-energy physics during my time as a PhD student.

Without the uncountable discussions, the collaborations, all our cross-checks of results, and also sharing some of the workload, it would have been hardly feasible to obtain significant and correct new results, to have progress in the use of advanced technical methods, and to generate at least some new knowledge.

Though, after several years of joint work, it is oftentimes extremely hard to judge which specific details, ideas, and calculations were contributed by precisely whom. A significant share of ideas and results cannot even be assigned to a single project member, because these ideas in fact formed during discussions and a lot of analytical and numerical calculations were performed together or independently in parallel to ensure their correctness.

Nonetheless, I hereby guarantee that in all of the joint projects a main share of the ideas, the project management, the analytical and numerical calculations, as well as the actual writing of the publications was performed by myself. This thesis, however, is exclusively written by myself.

Therefore – besides all external sources and references, which are cited anyhow – I did my best to indicate whenever ideas or results, which are presented in this thesis, can be originally assigned to other individual members of the projects or other researchers. Otherwise, I will explicitly mention at the beginning of the chapters if these are based on results of the joint projects and publications. Furthermore, I will explicitly mark in figures if they are already published or available as online pre-prints.¹ Apart from this and for the sake of readability, I will abstain from citing all equations and every detail of own published or pre-print works. As a direct consequence of the above, I will also use “we” instead of “I” in almost all active sentences throughout this thesis.

At this point, I also want to explicitly mention that a huge share of the findings of these projects and this thesis is and/or will be also presented in PhD and master theses of my collaborators, who developed and contributed in almost equal shares to the single projects. In particular, these are and will be the theses of M. J. Steil [6], L. Pannullo, J. Stoll [7], M. Winstel, N. Zorbach [8]. The other coauthors of my publications mostly contributed in significantly smaller shares to the projects and publications and/or already graduated, such that there are no corresponding theses.

¹The figures of my own publications were mostly produced by only one of the corresponding authors, while the data were either produced by several authors or crosschecked by several authors. For Refs. [1, 2] the plots were produced by myself, for Ref. [3] M. J. Steil produced the graphics, for Ref. [4] mainly N. Zorbach plotted the data, and for Ref. [5] the graphics are mainly created by L. Pannullo.

Publications

This thesis is predominantly based on the following publications (pre-prints):

- [1] **Numerical fluid dynamics for FRG flow equations: Zero-dimensional QFTs as numerical test cases. I. The $O(N)$ model**,
A. Koenigstein, M. J. Steil, N. Wink, E. Grossi, J. Braun, M. Buballa, D. H. Rischke,
Phys. Rev. D **106** (2022) *6*, 065012 (Sept. 2022),
[arXiv:2108.02504 \[cond-mat.stat-mech\]](#) (Aug. 2021).
- [2] **Numerical fluid dynamics for FRG flow equations: Zero-dimensional QFTs as numerical test cases. II. Entropy production and irreversibility of RG flows**,
A. Koenigstein, M. J. Steil, N. Wink, E. Grossi, J. Braun,
Phys. Rev. D **106** (2022) *6*, 065013 (Sept. 2022),
[arXiv:2108.10085 \[cond-mat.stat-mech\]](#) (Aug. 2021).
- [3] **Numerical fluid dynamics for FRG flow equations: Zero-dimensional QFTs as numerical test cases. III. Shock and rarefaction waves in RG flows reveal limitations of the $N \rightarrow \infty$ limit in $O(N)$ -type models**,
A. Koenigstein, M. J. Steil,
Phys. Rev. D **106** (2022) *6*, 065014 (Sept. 2022),
[arXiv:2108.04037 \[cond-mat.stat-mech\]](#) (Aug. 2021).
- [4] **Bosonic fluctuations in the $(1+1)$ -dimensional Gross-Neveu(-Yukawa) model at varying μ and T and finite N** ,
J. Stoll, N. Zorbach, A. Koenigstein, M. J. Steil, S. Rechenberger,
[arXiv:2108.10616 \[hep-ph\]](#) (Aug. 2021).
- [5] **Detecting inhomogeneous chiral condensation from the bosonic two-point function in the $(1+1)$ -dimensional Gross-Neveu model in the mean-field approximation**,
A. Koenigstein, L. Pannullo, S. Rechenberger, M. J. Steil, M. Winstel,
J. Phys. A **55** (2022) *37*, 375402 (Aug. 2022),
[arXiv:2112.07024 \[hep-ph\]](#) (Dec. 2021).

Other works, whose author I am and which were also produced and published during my time as a PhD student, are,

- [9] **Phenomenology of $J^{PC} = 3^{--}$ tensor mesons**,
S. Jafarzade, A. Koenigstein, and F. Giacosa,
Phys. Rev. D **103** (2021) *9*, 096027 (May 2021),
[arXiv:2101.03195 \[hep-ph\]](#) (Jan. 2021).
- [10] **How the axial anomaly controls flavor mixing among mesons**,
F. Giacosa, A. Koenigstein, and R. D. Pisarski,
Phys. Rev. D **97** (2018) *9*, 091901(R) (May 2018),
[arXiv:1709.07454 \[hep-ph\]](#) (Sept. 2017).

These works are not related to the main topic of this thesis.

Zusammenfassung in deutscher Sprache

Die Vorhersage von makroskopischen (thermodynamischen) Observablen aus mikroskopischen Theorien ist eine der zentralen Aufgaben in der Quantenfeldtheorie (QFT). Hierbei stellt insbesondere die Berechnung von Observablen in stark wechselwirkenden Systemen noch immer eine sehr große Herausforderung dar. Dies gilt insbesondere für Systeme bei nicht-verschwindenden (niedrigen) Temperaturen und großen Nettoteildichten, z.B. bei der Berechnung von Phasendiagrammen. Beispiele für solche Systeme finden sich sowohl im Bereich der (nicht-relativistischen) Festkörperphysik als auch der Hochenergiephysik. In letzterem Bereich ist insbesondere die Beschreibung der starken Kernkraft durch die Quantenchromodynamik (QCD) bei nicht-verschwindenden chemischen Potentialen und Temperaturen von besonderem experimentellem und theoretischem Interesse, da diese die Zustände von Kernmaterie maßgeblich bestimmt.

In jedem Fall versagen im Kontext von stark wechselwirkenden Systemen bewährte störungstheoretische Ansätze. Diese liefern zwar für den Fall sehr kleiner Kopplungen herausragende Resultate, lassen sich jedoch nicht auf Systeme mit multiplen (unendlich vielen) Kopplungen beliebiger Größenordnung anwenden. In diesem Fall ist es notwendig, auf sogenannte nicht-perturbative Methoden zurückzugreifen. Neben der direkten numerischen Berechnung von Erwartungswerten über aufwendige Gitter-Monte-Carlo-Simulationen, welche jedoch häufig bei hohen chemischen Potentialen ihre Vorhersagekraft verlieren, bieten sich funktionale Methoden an. In dieser Arbeit ist die Funktionale Renormierungsgruppe (F(RG)) zur Berechnung von Korrelationsfunktionen von besonderem Interesse. Diese erlaubt das sukzessive Ausintegrieren von Quantenfluktuationen, startend bei der mikroskopischen Theorie im ultravioletten Energiebereich und endend bei einer effektiven makroskopischen Theorie und ihren Observablen im infraroten Energiebereich.

Ursprüngliches Ziel dieser Arbeit war die Anwendung der FRG auf Niederenergiemodelle für QCD zur Beschreibung der Phasenstruktur von Kernmaterie bei moderaten Temperaturen und hohen Dichten, wie sie beispielsweise in kompakten Sternen vorliegen. Während der Arbeit stellte sich jedoch heraus, dass insbesondere zur Beschreibung von nicht-analytischen Strukturen, welche in den RG-Flussgleichungen, z.B. bei hohen chemischen Potentialen oder in der Nähe von Phasenübergängen, auftreten können, Weiterentwicklungen von bislang verwendeten (numerischen) Methoden für diese sehr speziellen, nicht-linearen partiellen Differentialgleichungen (PDGen) notwendig wurden. Im Speziellen kann gezeigt werden, dass sich RG-Flussgleichungen (in bestimmten Modellen und Näherungen) in echte abstrakte fluiddynamische Gleichungen umformen lassen. So können z.B. RG-Flüsse von lokalen bosonischen Potentialen durch Advektions-Diffusions-Gleichungen mit Quellen und Senken beschrieben werden. In direkter Konsequenz kann nicht nur die Dynamik während des RG-Flusses im Feldraum voll fluiddynamisch interpretiert und analysiert werden, sondern auch auf die hochentwickelten Methoden aus der numerischen Strömungsmechanik für die Lösung der PDGen zurückgegriffen werden.

Ein zentrales Ziel dieser Arbeit ist es daher, die fluiddynamische Formulierung von RG-Flussgleichungen weiterzuentwickeln und Methoden aus der numerischen Strömungsmechanik an diese anzupassen, anzuwenden und zu testen. Da jedoch die praktische Anwendung von FRG auf Quantenfeldtheorien fast immer Trunkierungen der (in der Regel unendlichen) Systeme von PDGen beinhaltet und häufig für realistische QFTen keine exakten Vergleichswerte berechnet werden kön-

nen, ist es notwendig, hierfür Systeme zu betrachten, in welchen sowohl exakte Referenzwerte berechenbar sind als auch die FRG-Flussgleichungen exakt (untrunkiert) als PDG betrachtet werden können. Zugleich ist es für realistische Tests notwendig, hinreichend komplizierte Systeme zu verwenden.

Der erste Teil dieser Arbeit befasst sich daher mit skalaren QFTen mit beliebig komplizierten „mikroskopischen“ Wirkungen in einem einzelnen Raumzeitpunkt. Anhand dieser Theorien wird zunächst in der Arbeit die Notwendigkeit von nicht-perturbativen Methoden demonstriert. Anschließend wird die FRG und ihre fluiddynamische Reformulierung präsentiert. Kern der Untersuchung von Teil I ist eine ausgiebige Diskussion der direkten qualitativen Konsequenzen der fluiddynamischen Formulierung, wie z.B. dem Anwachsen von Entropie während der RG-Flüsse sowie der Anpassung einer etablierten Finite-Volumen-Diskretisierung an die spezielle RG-Flussgleichung. Den Abschluss des ersten Teils der Dissertation bilden ausgiebige numerische Benchmark-Tests sowie Diskussionen zur Übertragbarkeit und Anwendbarkeit der entwickelten Methoden auf höherdimensionale realistische Systeme.

Der zweite Teil der Dissertation befasst sich mit ebenjener Anwendung von mitunter in Teil I entwickelten Methoden auf das $(1+1)$ -dimensionale Gross-Neveu (GN)-Modell im Medium. Das GN-Modell stellt eine vollwertige Quantenfeldtheorie dar, welche viele Eigenschaften mit QCD teilt, Anknüpfungspunkte an Modelle der Festkörperphysik bietet und in welcher in verschiedenen Grenzwerten exakte Lösungen bekannt sind. Es eignet sich somit ideal als erster realistischer Anwendungstest. Im Speziellen boten die neu entwickelten Methoden im Rahmen der FRG die Chance, zur Beantwortung der lange ungeklärten Frage beizutragen, ob es im GN-Modell abseits des strikten Limes „unendlich vieler Fermionen“ bei nicht-verschwindenden Temperaturen Kondensationseffekte und Phasenübergänge überhaupt geben kann. In Teil II dieser Arbeit gelang es (innerhalb der verwendeten Näherungen) zu zeigen, dass die lange bestehende Vermutung, dass dies nicht möglich sei, korrekt ist. Des Weiteren wurde die Analyse des GN-Modells zur Weiterentwicklung der sogenannten Stabilitätsanalyse zur Detektion räumlich inhomogener Kondensation verwendet sowie die Effekte verschiedener Trunkierungen und Näherungen auf die Vorhersage von Kondensationseffekten diskutiert.

Acknowledgments

First of all I would like to thank my doctoral supervisors: I am grateful to Prof. Dr. Dirk H. Rischke for the opportunity to perform fundamental research in his working group, his support, and the confidence in my work. I am grateful to Prof. Dr. Jens Braun for his intensive co-supervision, his support, and the opportunity to spend a lot of time in his working group. Of course, I am also grateful for all the discussions with both of my supervisors and their comments on my talks, papers, and the final version of my thesis.

My thanks also go to all members of the working groups of Prof. Dr. Dirk H. Rischke and Prof. Dr. Jens Braun as well as to the members (of the A03 project) of the CRC TR 211. In particular, I want to thank Dr. Florian Divotgey and Dr. Jürgen Eser for uncountable discussions and a great time while sharing an office and also to Dr. Stefan Rechenberger for his support at the start of my PhD.

I also want to thank my collaborators of my PhD projects Dr. Eduardo Grossi, Dr. Nicolas Wink, Laurin Pannullo, Marc Winstel, Niklas Zorbach, Jonas Stoll, and – most importantly – Martin J. Steil very much for the joint work and all the fun during this time. In addition, I thank Dr. Alessandro Sciarra for many discussions and advises on physics and related subjects.

Moreover, I am grateful to my collaborators in some side projects. These are Prof. Dr. Francesco Giacosa, Shahriyar Jafarzade, and Dr. Robert D. Pisarski. I am especially thankful to Prof. Dr. Francesco Giacosa for continuously mentoring me since I entered the field of high-energy particle physics and my research visits at the University of Kielce.

This work was financially supported by the Friedrich-Naumann-Foundation for Freedom via funds of the Federal Ministry of Education and Research. I am grateful for this financial support. Additionally I thank the Friedrich-Naumann-Foundation for Freedom for their non-material supporting program, including, among others: workshops, seminars, and many discussions with other scholars and experts from all fields in science, politics, economy, the cultural sector *etc.*. Within this context I am especially grateful to Prof. Dr. Albrecht Cordes who supported me as a tutor of the scholarship program.

Finally, I thank my friends, my sports team, my family, and Marion C. Seiche for their support and enjoyable distraction from my work.

Contents

Preface	I
Disclosure	III
Zusammenfassung in deutscher Sprache	V
Acknowledgments	VII
Contents	VIII
I The Functional Renormalization Group and (numerical) fluid dynamics from zero-dimensional quantum field theory	1
1. Introduction	3
1.1. Introduction – the everyday challenges of QFT practitioners	3
1.1.1. Solving functional integrals without solving functional integrals	4
1.1.2. Knowing the limitations	4
1.2. Motivation	5
1.2.1. The Functional Renormalization Group and the local potential approximation	5
1.2.2. Innovation and thoroughness – a lesson learned from LPA	6
1.2.3. Complicated and trivial at once – zero-dimensional toy model QFTs	7
1.3. Some applications of zero-dimensional QFT	8
2. A testing ground in zero spacetime dimensions – the $O(N)$ model	11
2.1. The zero-dimensional $O(N)$ model in QFT	11
2.1.1. Expectation values – correlation functions	13
2.1.2. The generating functional	13
2.1.3. The Schwinger functional	14
2.1.4. The effective action	15
2.1.5. Correlation functions for the $O(N)$ model	17
2.2. Symmetry breaking, phase transitions, convexity and all of that	18
2.2.1. Ehrenfest classification	18
2.2.2. Convexity of the generating functionals and the location of the physical point	19
2.2.3. Landau’s classification of phase transitions	20
2.2.4. The CMWHB theorem	20
3. The need for strictly non-perturbative methods	23
3.1. The free theory	23
3.2. Limitations of perturbation theory	24
3.2.1. ϕ^4 -theory	24
3.2.2. Perturbation theory	25

3.3.	The $\frac{1}{N}$ -expansion and its limitations	27
3.3.1.	The $\frac{1}{N}$ -expansion for the zero-dimensional $O(N)$ model	28
3.3.2.	Crosscheck - the free theory	30
3.3.3.	ϕ^4 -theory in the $\frac{1}{N}$ -expansion	31
3.3.4.	An instructive toy model to study the failure of the $\frac{1}{N}$ -expansion and problems of the infinite- N limit	32
3.3.5.	Application of the saddle-point expansion	34
3.3.6.	Summary	36
4.	The Functional Renormalization Group from zero spacetime dimensions	37
4.1.	Solving integrals with flow equations	37
4.1.1.	The scale-dependent partition function	38
4.1.2.	The heat equation – an evolution equation for the scale-dependent generating functional of (connected) correlation functions	39
4.2.	The exact renormalization group equation – the Wetterich equation	42
4.2.1.	A flow equation for $\tilde{\Gamma}(t, \vec{\varphi})$	42
4.2.2.	A proper UV initial condition for the RG flow of the effective average action	43
4.3.	The ERG equation without truncations – a PDE for the local potential of the zero-dimensional $O(N)$ model	45
4.3.1.	The flow equation of the local potential of the $O(N)$ model	45
4.4.	Artificially truncating the ERG equation – the FRG Taylor (vertex) expansion	47
4.4.1.	The formalities of the FRG Taylor expansion	47
4.5.	Symmetry breaking/restoration during the RG flow in zero dimensions	49
4.6.	Summary	50
5.	FRG flow equations and (computational) fluid dynamics	53
5.1.	Flow equations and conservation laws	53
5.1.1.	Turning the LPA flow equation into a conservation law	53
5.1.2.	The LPA flow equation as an advection-diffusion equation	55
5.1.3.	Consequences of the fluid-dynamical interpretation of RG flows	57
5.1.4.	An entropy function in the viscous $N = 1$ limit	60
5.1.5.	The $\frac{1}{N}$ -rescaled flow equations and the $N \rightarrow \infty$ limit	62
5.1.6.	Another entropy function for the inviscid $N \rightarrow \infty$ limit	63
5.1.7.	Method of characteristics in the inviscid $N \rightarrow \infty$ limit	63
5.1.8.	Rankine-Hugoniot condition and shock position in the inviscid $N \rightarrow \infty$ limit	65
5.2.	Numerical implementation	66
5.2.1.	Finite-volume methods	67
5.2.2.	The KT scheme	68
5.2.3.	(Discretized) boundary conditions	72
5.2.4.	Discrete formulation of the entropy function and the TVD property	76
6.	Tests, results, applications, and conclusions	79
6.1.	Introductory remarks	79
6.2.	A testing ground in zero dimensions – some toy models	80
6.2.1.	Test case I: Non-analytic initial condition	81
6.2.2.	Test case II: ϕ^4 potential	83
6.2.3.	Test case III: ϕ^6 potential	84
6.2.4.	Test case IV: the $\sigma = 0$ boundary	84
6.3.	Final remarks on the numerical setup	85
6.4.	Qualitative discussion of RG flows	86
6.5.	Quantitative tests	87
6.5.1.	Spatial resolution	90

6.5.2.	Large- σ boundary condition and size of the computational domain	91
6.5.3.	$\sigma = 0$ boundary condition	93
6.5.4.	Cutoff tests	93
6.6.	Benchmarking the FRG vertex/Taylor expansion	95
6.6.1.	Apparent convergence	97
6.6.2.	Who said “convergence”?	97
6.6.3.	Total collapse instead of convergence	98
6.7.	Entropy production in the viscous $N = 1$ limit	98
6.8.	Large vs. infinite N and shocks in RG flows	101
6.8.1.	Returning to an instructive toy model	102
6.8.2.	RG flows at $N \rightarrow \infty$	102
6.8.3.	Lost in math: How the infinite- N limit leads physics astray	110
6.8.4.	More entropy(!)	112
6.9.	Conclusion and outlook	113
6.9.1.	Conclusion	113
6.9.2.	Generalizations and applications	115
6.9.3.	Applications	116
 II The Gross-Neveu and the Gross-Neveu-Yukawa model		119
7.	Introduction	121
7.1.	The motivation, the scope, and the research questions	121
7.1.1.	The original project – spatially inhomogeneous condensation in QCD at non-zero temperature and non-zero baryon chemical potential	122
7.1.2.	The troubles and redefinition of research objectives	124
7.1.3.	Research questions	127
7.2.	The Gross-Neveu model – an overview and contextualization	128
7.2.1.	Four-fermion models and their applications	129
7.2.2.	Contextualization of the GN model with other QFTs	131
7.3.	Phenomenology of the Gross-Neveu model	133
7.3.1.	The phase diagram of the GN model at infinite N	134
7.4.	To break or not to break – \mathbb{Z}_2 symmetry at finite N	136
7.4.1.	Continuous vs. discrete symmetries	137
7.4.2.	Landau’s argument	137
7.4.3.	Kink configurations in the partition function	138
7.4.4.	Temperature reinterpreted as a spatial box	138
7.4.5.	Explicit calculations at finite N	138
8.	The Gross-Neveu model, the bosonized Gross-Neveu model, and the Gross-Neveu-Yukawa model	141
8.1.	The Gross-Neveu model	141
8.1.1.	The Gross-Neveu action in vacuum	141
8.1.2.	Symmetries of the Gross-Neveu action	144
8.1.3.	The Gross-Neveu action at non-zero temperature and non-zero chemical potential	153
8.2.	The bosonized Gross-Neveu and Gross-Neveu-Yukawa model	156
8.2.1.	Bosonization – Hubbard-Stratonovich transformation	156
8.2.2.	The bosonized Gross-Neveu model and the Gross-Neveu-Yukawa model	159
8.2.3.	Symmetries of the bosonized GN and GNY model	159
9.	The (one-loop) β-function of the four-fermion coupling in the GN model in medium	163
9.1.	Motivation and introduction	164

9.2.	The Gross-Neveu model in the FRG formalism	165
9.2.1.	The ansatz for the effective average action	165
9.2.2.	A necessary evil – the choice of the regulator	166
9.2.3.	The RG flow equation of the four-fermion coupling	167
9.3.	Consistency check and vacuum results	169
9.3.1.	Consistency check	169
9.3.2.	Remarks for two spacetime dimensions	170
9.3.3.	Comment on higher dimensions	171
9.3.4.	Scale dependence of the four-fermion coupling	171
9.4.	The four-fermion coupling at non-zero chemical potential and non-zero temperature	172
9.4.1.	The four-fermion coupling at infinite N	172
9.4.2.	The four-fermion coupling at finite N	177
9.5.	Concluding remarks	183
10.	The Gross-Neveu-Yukawa model via the Functional Renormalization Group	185
10.1.	Motivation and introduction	185
10.2.	The Gross-Neveu-Yukawa model in the FRG formalism	186
10.2.1.	The formal setup – the ansatz for the effective average action and the regulator	186
10.2.2.	The RG flow equations	188
10.2.3.	Discrete chiral symmetry breaking during RG flows and in the IR	191
10.3.	The FRG and (numerical) fluid dynamics	193
10.3.1.	The LPA' truncation as a non-linear heat equation with sink/source terms	193
10.3.2.	The $N \rightarrow \infty$ limit – suppression of diffusion and decoupling in field space	198
11.	The Gross-Neveu(-Yukawa) model at infinite N	201
11.1.	Overview	201
11.2.	Spatially homogeneous condensation	202
11.2.1.	Conventions	202
11.2.2.	Integrating the flow equation of the effective potential	203
11.2.3.	The gap equation and renormalization of the effective potential	204
11.2.4.	The phase diagram	207
11.3.	Stability of the homogeneous solution	215
11.3.1.	The bosonic wave-function renormalization	216
11.3.2.	The bosonic two-point function	219
11.4.	Comment on the computation	227
12.	The Gross-Neveu-Yukawa model at finite N	229
12.1.	Introduction	229
12.2.	“Massaging” the flow equations (again)	230
12.3.	The GNY model in the LPA	232
12.3.1.	The UV initial condition	232
12.3.2.	Numerical tests	235
12.3.3.	Results	236
12.4.	First steps towards the GN(Y) model beyond the LPA approximation	244
12.4.1.	UV initial condition and numerical setup	245
12.4.2.	Results	247
12.5.	Conclusion and outlook	253
12.5.1.	Summary and conclusion	253
12.5.2.	Generalizations and applications	259

III	Appendix	261
A.	Formulary	263
A.1.	Some definitions	263
A.1.1.	Pauli matrices	263
A.1.2.	Dirac delta distribution	263
A.1.3.	Kronecker delta	264
A.1.4.	Volume integrals	264
A.2.	Two-dimensional spacetime	264
A.2.1.	Minkowski metric, Cartesian coordinates, and the Levi-Civita pseudo-tensor	264
A.2.2.	Clifford algebra and gamma matrices in Weyl basis	265
A.2.3.	Euclidean gamma matrices in Weyl basis	265
A.3.	Fourier transformation	266
A.4.	Transcendental functions	266
A.4.1.	Logarithm	266
A.4.2.	Exponential integral	267
A.4.3.	Gamma functions	267
A.4.4.	Zeta and eta functions	268
A.4.5.	Polylogarithms, Fermi-Dirac and Bose-Einstein integrals	269
A.4.6.	IR divergences and the incomplete polylogarithms	272
B.	Matsubara sums and related formula	275
B.1.	Thermal distribution functions and useful identities	276
B.2.	Matsubara sums	277
B.2.1.	Purely bosonic/fermionic Matsubara summation	277
B.2.2.	Mixed bosonic-fermionic Matsubara sums	280
B.2.3.	Matsubara sum of the four-fermion interaction channel with two-fermion exchange	283
C.	RG flow equations in field-space (DeWitt) notation	285
C.1.	Field-space and DeWitt notation	285
C.1.1.	Definitions and general considerations	285
C.1.2.	Functional derivatives in field space	287
C.2.	The FRG in field-space notation	288
C.2.1.	Scale-dependent generating functionals of correlation and vertex functions	288
C.2.2.	RG flow equations for generating functionals	291
C.2.3.	UV initial condition for the ERG equation	293
C.2.4.	Projections and RG flow equations for vertices	294
C.2.5.	Scale-dependent fields	300
D.	RG and loop-integration variables, regulators, and threshold functions	301
D.1.	Relations between the RG time, the RG scale, and the loop momentum	301
D.2.	The flat regulator (Litim regulator)	302
D.2.1.	The bosonic Litim-regulator shape function	302
D.2.2.	The fermionic Litim-regulator shape function	303
D.3.	Propagators and threshold functions	305
D.3.1.	Propagators	305
E.	FRG flow equations of the Gross-Neveu and Gross-Neveu-Yukawa model	307
E.1.	FRG flow equations of the Gross-Neveu model	308
E.1.1.	Fermion two-point vertex – fermion mass & anomalous dimension	311
E.1.2.	Fermion four-point vertex – four-fermion coupling	315

E.2.	FRG flow equations of the Gross-Neveu-Yukawa model	323
E.2.1.	Effective potential	328
E.2.2.	Bosonic two-point function – boson mass & anomalous dimension . .	331
E.2.3.	Infinite- N limit of the two-point function	347
E.2.4.	Fermionic two-point function – fermion mass & anomalous dimension	349
F.	Mean-field Gross-Neveu calculations	359
F.1.	Field-theoretical quantities	359
F.1.1.	The effective potential	359
F.1.2.	The derivative of the effective potential	361
F.1.3.	The bosonic two-point function	362
F.1.4.	The bosonic wave-function renormalization	369
F.2.	Thermodynamic quantities	374
F.2.1.	The pressure	374
F.2.2.	The baryon number density	375
F.2.3.	The internal energy	376
IV	Back matter	379
	Bibliography	381
	List of Figures	422
	List of Tables	424

Part I

The Functional Renormalization Group and (numerical) fluid dynamics from zero-dimensional quantum field theory

Chapter 1

Introduction

Abstract This chapter provides an introduction and brief motivation for why we are dealing with zero-dimensional QFTs to this extent in a Ph.D. thesis. We explain why zero-dimensional models are on the one hand ideal for pedagogical introductions into methods of statistical physics and QFT, but – more importantly – are also perfectly suited for benchmark tests of some of these methods.

Afterwards, we present some works and applications that are (at least partially) built on zero-dimensional models in QFT.

Disclosure The introduction is based in parts on our own publications [1, 2, 3]. References in this chapter are mostly exemplary or have the character of reviews and the citations do not aim to be complete.

1.1. Introduction – the everyday challenges of QFT practitioners

In statistical mechanics and modern QFT we are oftentimes confronted with the problem of computing expectation values or correlation functions for physical observables from a partition of probabilities among the various microscopic states of system [11, 12, 13]. Mathematically this is usually realized in terms of an evaluation of nested sums and complicated high-dimensional integrals over probability distributions.

On the one hand, there are not too many systems where these calculations can be cleverly done by pen and paperwork. On the other hand, also brute-force numerical evaluation is not always feasible or comes along with tremendous demand for computer power and the need for modern Monte-Carlo integration techniques [14, 13]. Usually this is due to the highly involved structure of the microscopic actions, which enter the probability distributions, as well as the high dimensionality of the involved integrals.

In QFT another conceptual aspect that complicates calculations significantly is the general impracticality of Monte-Carlo integration in an infinite volume and in spacetime continuum. However, restricting the theories and computations to some finite-sized spacetime box and discretizing spacetime by the introduction of a spacetime lattice with a minimal length-scale regulates infinities, which stem from otherwise arbitrarily large and small momenta and energies of the particles/fields in Fourier space [15, 14]. This enables numerical Monte-Carlo integration in the first place, but also modifies the quantitative results directly. Another indirect effect, which goes hand in hand with lattice regularizations, is usually the breaking of certain properties of a theory (usually symmetries), which additionally modifies the outcome of the calculations. Hence, it is required to repeatedly perform calculations with lattices of different size, shape, and at different lattice spacing, and to carefully extrapolate to infinite volume and the continuum afterwards, in order to finally obtain reliable predictions for observables, where these artifacts are removed.

On top of these challenges the mathematical description of some QFTs requires to introduce terms into the microscopic actions which render the probability distributions complex and completely impede common statistical integration techniques. This is oftentimes the case for studies of QFT in medium at non-zero chemical potential and is referred to as the “sign problem” [16, 17]. It occurs in various contexts from non-relativistic condensed matter systems to QCD. Among other things these challenges lead to the development of a huge toolbox of (numerical) methods, which eventually either work around the direct computation of the high-dimensional integrals or significantly improve or modify the established lattice Monte-Carlo integration techniques.

1.1.1. Solving functional integrals without solving functional integrals

Historically, one of the first approaches was to treat the computation of correlation functions from path or functional integrals perturbatively [18, 19, 20, 21, 22]. Right from the start this was restricted to theories with a small number of tiny couplings. Hence, perturbative methods are completely inappropriate for systems in their strongly coupled regime with a potentially large or infinite amount of couplings of any scale – which is anyhow repeatedly ignored even in nowadays research. Additionally it is known that even an expansion in small couplings does ultimately not converge [23], even though the inclusion of only the lowest orders can lead to remarkable results as can be seen for example from Quantum Electrodynamics [19, 24, 25]. Also all kinds of resummation techniques, which structure the summation of perturbative contributions and overcome the non-convergence of perturbation series, were developed and surely have valid scopes of application in this context. Otherwise, in the field of modern lattice Monte-Carlo simulations recent developments comprise so-called reweighting techniques to probe topological ground states [26] or calculations at imaginary chemical potential with extrapolation to real chemical potential to tackle the sign problem [27] *etc.*

Anyhow, also many alternative non-perturbative methods emerged to perform computations in strongly interacting systems.¹ These include large- N techniques [28, 29, 30, 31, 32], where the dimensionless expansion parameter is no longer a coupling, but the inverse number of certain degrees of freedom of the system. This is also known as the method of Laplace or saddle-point expansion in statistics [33] and we are dealing with this method several times in this thesis. Then there are functional methods like Dyson-Schwinger equations (DSE) [34], the Bethe-Salpeter equation [25] or the FRG [35], but also effective field theories or other systematic frameworks like chiral perturbation theory [36, 37], QCD sum rules [38], current algebra techniques [39] *etc.* Within the last decades so-called holographic methods, such as the AdS/CFT correspondence [31, 40, 41], gained in importance and are in nowadays part of the standard curriculum.

1.1.2. Knowing the limitations

However, all of these methods come with advantages and disadvantages as well as certain limitations. Thus, it is absolutely essential to have estimates on shortcomings, the range of reliability as well as accuracy of a method, before using it in an unknown and uncontrolled environment. Such ranges of applicability and estimates for the precision are usually worked out from benchmark tests with problems and models whose solutions are known exactly. Thereby it is crucial that these tests encompass, if possible, the hardest plausible scenarios and limiting cases one can think of. In various areas of engineering, natural and computer science, as well as finance this leads to minimal specifications that need to be fulfilled by technical solutions to be later on considered trustworthy for applications in well-defined scopes of application.

Anyhow, in fundamental research, where both, the methods as well as the fields of application, are oftentimes still in an exploratory status, the above approach is not always strictly practicable. In consequence, predictions from such studies should usually be taken with a grain of salt. (This certainly also applies to the work of the author and certain research areas of high-energy particle physics, which is the author’s profession.)

¹Here, the references and methods are mostly from the context of high-energy particle physics.

Howsoever, this does by no means imply that research in such fields is free from steadily trying to improve their methods and from searching for reasonable test cases, which is, however, oftentimes considered as tedious and little productive with respect to (w.r.t.) to new phenomenology. This is because sometimes one has to take a few steps back, reduce the complexity of the problems to well-controlled toy models, and reanalyze the seemingly established techniques from a different perspective.

Exactly this is done in Part I of this thesis and the underlying publications [1, 2, 3]. This thesis is therefore a minor contribution to the general aim of steadily advancing techniques and methods. In particular, we are focusing on the FRG method and in parts also on the infinite- N technique. Within the next lines, we provide a brief motivation of why we believe that this is necessary for certain special aspects and applications of the FRG method.

1.2. Motivation

1.2.1. The Functional Renormalization Group and the local potential approximation

Since its development in the early nineties of the last century [42, 43, 44, 45, 46, 47, 48], the FRG method in terms of the Wetterich equation (also the exact renormalization group (ERG) equation) has proven to be a powerful tool for the calculation of so-called vertex functions in various contexts [35], which are directly related to observables in a QFT and which can also be directly mapped to correlation functions from functional-integral calculations *etc.*. Oversimplified, the formal idea (not to be confused with the physical idea) behind the FRG is to map the problem of solving high-dimensional complicated integrals and sums for the calculation of correlation functions to the problem of solving a set of coupled functional partial integro- and/or ordinary differential equations – the RG flow equations – and extracting the vertex functions from their solution. (A more detailed introduction follows in later chapters.) One could object already at this point that this might not necessarily be an advantage, because solving coupled functional partial differential equations and ordinary differential equations to high precision is by no means a trivial task [49, 50, 51, 52].

Nonetheless, it turns out that in innumerable different contexts the FRG method presents itself as a powerful qualitative and quantitative tool. It already competes with other well-established non-perturbative methods and even provides access to regimes of systems where other methods are currently still doomed to fail, *e.g.*, computations at moderate and high densities or in quantum-gravity calculations. For more details, we refer to Part II and Appendix C of this thesis and for example to Refs. [53, 54, 55, 56, 57, 58, 35].

For this motivational section it suffices to know that among others a specific prominent scope of application of the FRG is the non-perturbative treatment of fluctuations in models for strongly interacting systems from condensed-matter physics and high-energy particle physics, especially in medium. A lot of these calculations within effective models are based, at least to lowest-order approximation, on a truncation of the theoretically infinite number of coupled RG flow equations, which exclusively incorporates local non-derivative couplings of the fields to arbitrary order, see *e.g.*, Refs. [59, 60, 61, 62, 53, 63]. This truncation is called the local potential approximation (LPA). Mathematically it corresponds to a partial differential equation, where a local bosonic potential is evolving in field-space along the RG time from ultra-violet (UV) to infra-red (IR) energy scales. Also much better truncations oftentimes still include this particular flow equation, which is then extended by additional coupled PDEs and ODEs [64, 65, 66, 67, 68, 63, 69, 70, 71, 72, 73]. Structurally, the LPA RG flow equation and its extensions are rather similar for a huge class of these models and problems, such that the following is generic.

1.2.2. Innovation and thoroughness – a lesson learned from LPA

Because the LPA flow equation is a highly non-linear PDE, which is of first order in the temporal derivative and (usually) up to second order in the spatial derivatives of the effective potential, there is little chance to solve it analytically – even though there are a few exactly integrable examples where additional assumptions and limits slightly simplify the PDE [74, 75, 76, 77, 3]. In consequence, a numerical solution is usually required.

Therefore several numerical schemes were developed in the last three decades within the FRG community (in parts specifically for this PDE) and applied to this RG flow equation, see, *e.g.*, Refs. [78, 79, 80, 81, 82, 83, 84, 85, 86, 87, 88, 89, 90] for a few examples. Under some circumstances these methods produce or sometimes seem to produce decent results, which qualitatively and quantitatively agree with expectations.

As it happens, it appears that much more time was spent on qualitative and phenomenological new results than on careful testing all the utilized numerical schemes with exact and challenging reference solutions of standard PDE problems (*e.g.*, the heat equation, Bateman-Burgers equation, shock-tube problems *etc.*) and specific exactly solvable FRG problems. Otherwise it is not explainable what some colleagues and I experienced ourselves: A lot of these numerical schemes turned out to be unstable in certain situations and solutions do not converge against exact reference solutions. Hereby, we are mostly referring to the breakdown of the numerical time stepping due to the generation of ill-conditioned input for the next time step. In addition, we experienced that some of the schemes are not stable against the variation of numerical parameters, like the number of gridpoints or the artificial size of the computational domain or the choice of time-stepper *etc.* Still, in the FRG context there were physical parameter setups for some models where everything was fine and we could not reproduce the instabilities from other situations. Furthermore, we also experienced that there are a lot of publications which are not reproducible, because significant information about the exact numerical setup was simply missing. Certainly, this is not meant as a blanket critique and there are lots of high-quality publications, but the amount of works that fall victim to these problems for this very specific class of FRG calculations is striking.

This puzzling unpredictability of reliability was only resolved when my colleagues Grossi and Wink took the step back and reanalyzed the LPA PDE as a whole, trying to eliminate the bias of the common FRG perspective and existing approaches to this PDE (which I had myself). Indeed they were able to reformulate the LPA flow equation (firstly in the infinite- N limit) in terms of a conservation law for the derivative of the potential [77]. In fact, they (re)discovered, see also Refs. [75, 76, 91], that the PDE is actually a highly non-linear advection equation with all its consequences, such as the possible emergence of discontinuities like shock and rarefaction waves. During these developments it turned out that lifting the infinite- N limit, the LPA flow equation is for most models indeed a non-linear advection-diffusion-sink/source equation and therefore falls into the class of classical fluid-dynamical problems. As it happens, this fact and interpretation of generic RG flow equations had been known in parts already in advance of the modern formulation of the FRG in terms of the Wetterich equation, Refs. [92, 93, 94, 95, 96, 97, 98, 99, 100], but seemed to have been partially forgotten. Currently, work on the extension of this reframing of modern RG flow equations to fluid-dynamical problems is ongoing [101, 4, 102, 103].

After unraveling the true underlying structure of this equation, an explanation for our troublesome experience with some numerical methods is rather obvious. If a certain parameter setup for the PDE allows for the occurrence of non-analytical behavior, which is easily produced in non-linear PDEs [52, 49, 104, 50, 51], all those numerical schemes that are explicitly or implicitly based on smoothness of the solution are doomed and lack convergence, which is unfortunately the case for a lot of them. Otherwise, if the solution was smooth, everything could work out without troubles.

Another direct consequence of these discoveries is that the formulation of RG flow equations as fluid-dynamical problems allows for the direct application or adaption of the methods from the highly developed toolbox of CFD. Therefore, a “from-scratch development” of own and completely

new methods becomes at least questionable, if one is not an absolute expert on non-linear PDEs.

Anyhow, also the application of established methods from the field of CFD to FRG problems needs to be tested. In particular, the special non-linear structure of the PDEs that emerge in the FRG formalism is not always explicitly covered even by modern numerical schemes. This is because most of the schemes are either developed for non-relativistic fluid dynamics – mostly (variants of) the Navier-Stokes problem – or relativistic fluid dynamics in the context of astrophysical problems and nuclear collisions. Especially the involved fluxes are of completely different structure than in the LPA flow equation. Consequently, careful testing is required, when CFD methods are run at their edge of applicability.

To this end E. Grossi and N. Wink first focused on the infinite- N limit of the $O(N)$ model, where the LPA RG flow equation is exact (in terms of a truncation) [74] and integrable in three spacetime dimensions [75, 76, 77]. Besides benchmarking their fluid-dynamical framework, which was based on Discontinuous Galerkin (DG) (finite element) methods, they also studied the relation between phase transitions and shock waves in the effective potential, which would not have been possible to this extent with previously used numerical methods.

1.2.3. Complicated and trivial at once – zero-dimensional toy model QFTs

This is where research covered by Part I of this thesis sets in. Inspired by their findings, my colleague M. J. Steil and I decided to also build up a fluid-dynamical framework for the solution of FRG flows. We went for so-called finite-volume methods in the formulation of A. Kurganov and E. Tadmor [105] – a well-established scheme for conservation laws in fluid dynamics. After also testing this framework with the examples of Ref. [77], we searched for a testing ground with exactly soluble reference solutions beyond the infinite- N limit, but within the FRG framework. Here, inspired by Refs. [106, 107, 108, 109, 110], we came up with the idea to use zero-dimensional QFT to benchmark our setup.

The reason is that structurally the FRG flow equation(s) are identical for zero and non-zero spacetime dimensions. However, in zero dimensions the set of flow equations (PDEs) is finite, because there are no derivative couplings and all (self-)interaction terms can be collected in field- and RG-scale-dependent functions. (Details are presented in later chapters.) For certain models the LPA flow equation is the only existing flow equation and is therefore exact (not a truncation) without any additional assumptions. On the other hand, the complicated functional integrals from calculations in higher-dimensional spacetimes reduce to ordinary integrals in zero spacetime dimensions, such that the computation of reference solutions for correlation or vertex functions to test the FRG turns out to be straightforward. Hence, zero-dimensional QFT presents itself as the ideal testing ground for the newly introduced CFD framework for FRG, because it is complicated within the FRG formalism, but simple(r) from the path-integral perspective – exactly the opposite of what we hope for in non-zero dimensions.

However, in contrast to earlier FRG tests with zero-dimensional $O(N)$ -models, which mostly focused on the FRG Taylor expansion of the effective potential for smooth initial potentials, we mostly² worked with the untruncated PDE for the local potential. Furthermore, in addition to commonly studied smooth initial potentials, we constructed UV initial potentials which comprise non-analytical structures of different kind. These present themselves as hard tests for our (numerical) solution scheme of the flow equation, because they can be related to shock and rarefaction waves in the fluid-dynamical framework.

Another huge advantage of using zero-dimensional QFT for testing and presenting the fluid-dynamical reformulation is that the main structure of the RG flow equations is no longer buried

²Within our work we also present tests for additional artificially introduced truncations of the LPA flow equation, *i.e.*, the infinite- N limit in zero dimensions as well as the FRG Taylor expansion of the LPA flow equation.

under a plethora of additional patterns such as momentum integrals, Matsubara sums, factors from traces in various spaces *etc.*. Hence, it is pedagogically much simpler and the interpretation is easier.

This allowed us to work out further aspects of the FRG, which are rather obvious as soon as one switches perspectives to the fluid-dynamical framework. For example, it is well known that the evolution of dissipative fluid dynamics is irreversible and produces entropy [49, 50], which must therefore also hold true for the FRG flow equations. Hence, irreversibility of the RG seems to be manifest on the level of the PDEs.

All in all, we found that FRG in zero dimensions is the ideal playground to study all kinds of effects, which are present in the ERG, such that we ended up with a three-parts series on this topic, Refs. [1, 2, 3], which M. J. Steil and I worked out with our collaborators and supervisors N. Wink, E. Grossi, J. Braun, M. Buballa, and D. H. Rischke. This is presented and summarized in Part I.

1.3. Some applications of zero-dimensional QFT

The general idea to test and study methods from statistical mechanics and QFT with zero-dimensional toy models is, as already anticipated, not original to the author and collaborators. Indeed, there are a lot of works that used zero-dimensional models for this purpose before, but also tried to describe real-world physical situations or limits with models of this type. In the following, we therefore present a selection of studies which deal with zero-dimensional (toy) models and their application to contextualize our own work.

However, before we start, let us explicitly state what we are referring to when we are talking about zero-dimensional QFT: By zero dimensions, we are always referring to zero spatial and zero temporal dimensions, thus QFT in a single point in space and time. This is to be distinguished from systems with zero spatial dimensions but time/frequency/energy dependence, which are oftentimes also referred to as zero-dimensional QFTs, especially in the context of solid-state theory and/or quantum mechanical systems, *cf.* Refs. [111, 112, 113]. Anyhow, our work deals with quantum fields, which do not have any dependence on space and time at all and can therefore be considered as ultra-localized and maximally interacting.

This is for example realized in Ref. [114]. The authors study grains of superconducting particles. Effectively they consider the zero-volume limit of a static Ginzburg-Landau approximation for the action in the partition function and argue that spatial fluctuations are suppressed in super-small volumes, which allows to ignore derivative contributions in the action. In consequence, their model reduces to an exactly integrable ϕ^4 -theory with $O(2)$ symmetry.

Also inspired by this work, there are some more technically driven publications, which mainly focus on large- N techniques. All of these works are based on $O(N)$ models in zero dimensions with ϕ^4 -interaction and usually positive mass-like term. For example Refs. [115, 107] study the $\frac{1}{N}$ -approximation and find good convergence against an exact solution of the partition function, even for low orders in $\frac{1}{N}$ and rather small N . Similar studies were also performed by Refs. [116, 117, 118, 119, 120, 121, 122]. Some of these works as well as Refs. [123, 124, 125, 126, 127] also use zero-dimensional scalar field theories to pedagogically introduce, discuss, and analyze graph-theoretical aspects and methods in QFT.

In this context, it is for example interesting that the dual-graph representation of the connected Feynman bubble diagrams, which enter the logarithm of the partition function, can be interpreted as randomly branching polymers or chains. In consequence, zero-dimensional $O(N)$ models can be used to study this process of randomly branching one-dimensional objects, *cf.* Refs. [117, 118, 119, 120] (also for illustrations). Hence, these works draw connections to general theories of random surfaces, which play a role for low-dimensional models of topological gravity theories. This is underlined by the fact that the zero-dimensional analogue of the Dyson-Schwinger equations for

ϕ^4 -theory can be mapped to the Virasoro algebra as is shown by these references.

Another interesting application of zero-dimensional ϕ^4 -theory is that it is perfectly suited to learn and benchmark perturbation theory [128, 129, 130, 131, 107, 109, 23, 124, 125] and optimized perturbation theory [132, 125]. With this model it is rather simple to demonstrate that the perturbative series in the coupling constant, even if the coupling constant is small, does not converge w.r.t. conventional convergence criteria. It is only asymptotic to the correct solution, such that the first summands may form a decent approximation very close to vanishing coupling, even though the whole series diverges.

In the recent work [133] a zero-dimensional ϕ^4 -theory with additional complex mass parameter was used to mimic and study the role that is usually played by a chemical potential and thus mimics the sign problem in calculations using stochastic quantization and the complex Langevin method.

However, within this work, we are predominantly interested in testing the FRG method with zero-dimensional QFT. Also this was done partially before. For example, Ref. [106] uses a theory of a single scalar field in zero dimensions to pedagogically introduce the FRG formalism, though explicit calculations are not presented. Also Refs. [109, 108, 134, 125] use it as an introduction to the FRG, but also present tests for the FRG Taylor expansion, where the exact LPA flow equation is artificially expanded in vertex functions, which form a coupled set of ODEs, that is solved numerically. For smooth initial potentials of ϕ^4 -theory with positive mass, all these works find good agreement with exact results. In addition, Refs. [107, 109] also test ϕ^4 potentials with negative mass, but without benchmarking these results against exact solutions. Also an iterative approach to solve the LPA flow equation as well as a mixture of iterative scheme and Taylor expansion are tested and benchmarked for example by Ref. [109] and show good agreement for positive mass.

The above works are all formulated in the 1particle irreducible (PI) effective-action functional formalism for the FRG. Anyhow, it is also possible to work within the 2PI formalism. Also this formalism was analyzed for zero-dimensional $O(N)$ models, with and without FRG framework and also in the context of density-functional theory, see Refs. [110, 135, 136, 137, 125, 138].

Recently, after the completion and publication of the results of our own work in the associated Refs. [1, 2, 3] on solving FRG flow equations in terms of advection-diffusion equations, Ref. [103] used one of our zero-dimensional test cases for demonstrational purposes and comparison for their DG scheme. The same scheme and fluid-dynamical framework was applied in Ref. [102] to various RG flow equations, where RG flows of complex effective actions were studied to ultimately investigate Lee-Yang singularities and PTs. This was also tested for zero-dimensional toy models. Lastly, in the context of FRG publications, we would like to mention Ref. [139], where it is explained for the $O(N)$ model how zero-dimensional QFT emerges as a limiting case in the high-temperature and small-volume limit of higher-dimensional theories after appropriate rescaling of the effective potential.

For reviews concerning zero-dimensional toy models to test and study various (functional) methods in QFT, we refer the interested reader to Refs. [131, 107, 124, 125].

Chapter 2

A testing ground in zero spacetime dimensions – the $O(N)$ model

Abstract In this chapter we introduce the zero-dimensional $O(N)$ model. We present its formulation as a full-fledged QFT. This comprises the calculation formula for and relation between correlation and vertex functions and their systematic derivation from generating functionals for arbitrary $O(N)$ -symmetric classical actions. The chapter closes with a discussion on the absence of spontaneous symmetry breaking and PTs in zero dimensions.

Disclosure None of the material in this chapter is new. Nevertheless, its collection and presentation is original to the author and mostly based on our own Refs. [1, 2, 3]. Similar presentations can be found for example in Refs. [109, 107, 125] and other references from Section 1.3. Thus, the presentation in this chapter is mainly provided as a pedagogical introduction, to introduce our notation, and to have reference formula for later chapters. We therefore mostly refrain from repeatedly citing the “zero-dimensional QFT” literature and instead refer to more generic QFT literature.

2.1. The zero-dimensional $O(N)$ model in QFT

The zero-dimensional $O(N)$ -model is defined as follows. Consider an N -dimensional vector in Euclidean space with real components defined w.r.t. to some complete orthonormal basis,

$$\vec{\phi} = (\phi_1, \phi_2, \dots, \phi_N) \in \mathbb{R}^N, \quad N \in \mathbb{N}. \quad (2.1)$$

This vector describes N identical neutral scalar (quantum) “fields”. In contrast to other field theories, these fields do not exhibit any spacetime dependence. As already said, one might simply assume that the theory is restricted to a single point. A field configuration is therefore given by an N -dimensional vector of real numbers. Since one is dealing with identical scalar fields permutations of the components certainly do not change the state of the system. However, one might also consider continuous rotations in field space, which mix components of the N -dimensional vector. These are mediated by matrix-vector multiplications,

$$\vec{\phi} \mapsto \vec{\phi}' = O \vec{\phi}, \quad (2.2)$$

where the $(N \times N)$ -dimensional matrix O is an element of the $O(N)$ group in its fundamental representation. Componentwise this transformation reads

$$\phi_a \mapsto \phi'_a = O_{ab} \phi_b, \quad a, b \in \{1, 2, \dots, N\}. \quad (2.3)$$

Indeed, these rotations can potentially change the state of the system. This, however, strongly depends on the theory that describes the (self-)interactions of the N scalars.

Such a description is usually formulated (microscopically) in terms of an action or energy functional, whose extremum singles out the most favorable configurations [12]. In zero spacetime dimensions concepts like an action, energy functional, Hamiltonian or Lagrangian basically coincide, because there are no spacetime derivatives and spacetime integrals and we are exclusively dealing with dimensionless quantities. Hence, we will simply refer to this quantity as the action $\mathcal{S}(\vec{\phi})$, which is an ordinary function of $\vec{\phi}$ instead of a functional like in higher dimensions [19, 20]. (By writing $\mathcal{S}(\vec{\phi})$, we mean $\mathcal{S}(\phi_1, \dots, \phi_N)$; this also applies to other function(al)s in this or the following chapters.)

If we think of this field theory in terms of a (quantum) statistical system, one can define a probability-density function (up to a suitable normalization)

$$p(\vec{\phi}) \equiv e^{-\mathcal{S}(\vec{\phi})}, \quad (2.4)$$

which associates a probability to each micro-state of the system according to its (classical) action. Configurations at the minimum of $\mathcal{S}(\vec{\phi})$ are more likely than configurations far away.

Now, similarly to generic systems from statistics and QFT [11, 19, 12, 140] expectation values are calculated according to

$$\langle f(\vec{\phi}) \rangle \equiv \frac{\int_{-\infty}^{\infty} d^N \phi f(\vec{\phi}) p(\vec{\phi})}{\int_{-\infty}^{\infty} d^N \phi p(\vec{\phi})} = \frac{\int_{-\infty}^{\infty} d^N \phi f(\vec{\phi}) e^{-\mathcal{S}(\vec{\phi})}}{\int_{-\infty}^{\infty} d^N \phi e^{-\mathcal{S}(\vec{\phi})}} \quad (2.5)$$

for arbitrary functions/operators $f(\vec{\phi})$, where the denominator ensures appropriate normalization. Here, the functional integral turns into a standard Lebesgue integral [124].

The last ingredient for the construction of $O(N)$ -invariant models is to demand $O(N)$ symmetry of the (microscopic) classical action $\mathcal{S}(\vec{\phi})$. (The integral measures in Eq. (2.5) are $O(N)$ invariant anyhow.) As a direct consequence \mathcal{S} is in fact a function of the $O(N)$ -invariant,

$$\rho \equiv \frac{1}{2} \vec{\phi}^2, \quad (2.6)$$

rather than all components of $\vec{\phi}$ independently.

If one is also studying expectation values which are exclusively functions of $O(N)$ -invariant operators, *viz.* $f(\vec{\phi}) = f(\rho)$, Eq. (2.5) drastically simplifies,

$$\langle f(\rho) \rangle = \frac{\int_0^{\infty} d\rho \rho^{\frac{N}{2}-1} f(\rho) e^{-\mathcal{S}(\rho)}}{\int_0^{\infty} d\rho \rho^{\frac{N}{2}-1} e^{-\mathcal{S}(\rho)}}, \quad (2.7)$$

where we used

$$\int_{-\infty}^{\infty} d^N \phi = \int_{-\infty}^{\infty} d\phi_1 \cdots \int_{-\infty}^{\infty} d\phi_N \stackrel{(A.6)}{=} \Omega_N \int_0^{\infty} d\rho (2\rho)^{\frac{N}{2}-1}. \quad (2.8)$$

Hence, the zero-dimensional QFT of an $O(N)$ -symmetric theory of scalars actually reduces to the calculation of one-dimensional integrals. This makes this system particularly interesting for testing methods and approximation schemes in QFT, because exact reference values for expectations values are easily computed to basically arbitrary precision by standard (numerical) integration, *cf.* Section 1.3 and references therein.

However, note that up to this point we did not further specify $\mathcal{S}(\rho)$. Indeed for the formulation of a valid QFT we can basically think of any continuous function of ρ , which is bounded from below and asymptotically grows at least like $\rho^{\frac{1}{2}}$ to ensure convergence of the integrals. Continuity is required, because in zero spacetime dimensions the action also coincides with the analogue of

the effective bosonic potential, $U(\rho) = \mathcal{S}(\rho)$, which is supposed to be a continuous function of the fields. Otherwise we would completely lose contact to higher-dimensional QFT. Even though this is rarely discussed in QFT, we explicitly do not call for analyticity or smoothness of the action $\mathcal{S}(\rho)$, or the effective potential $U(\rho)$, respectively. In consequence, the commonly discussed ϕ^4 -theory with positive or negative mass, which is certainly inspired from higher-dimensional physics, like the Anderson-Brout-Englert-Guralnik-Hagen-Higgs-Kibble mechanism [141], is only one of many possible setups one can think of. We will find that from the perspective of the FRG and infinite- N methods as well as the study of PTs other initial potentials are much more interesting.

2.1.1. Expectation values – correlation functions

In calculations in QFT one is usually interested in (n -point)¹ correlation functions of fields. Here, these particular expectations values are of course spacetime-independent, because there is no spacetime. Therefore they reduce to correlation functions between components of $\vec{\phi}$. Due to the $O(N)$ symmetry all various correlation functions are proportional to expectation values of (powers of) the $O(N)$ -invariant and it is easy to show, *cf.* also Refs. [107, 125], that

$$\langle \phi_i \phi_j \rangle = \frac{1}{N} \delta_{ij} \langle \vec{\phi}^2 \rangle, \quad (2.9)$$

$$\langle \phi_i \phi_j \phi_k \phi_l \rangle = \frac{1}{N(N+2)} (\delta_{ij} \delta_{kl} + \delta_{ik} \delta_{jl} + \delta_{il} \delta_{jk}) \langle (\vec{\phi}^2)^2 \rangle, \quad (2.10)$$

$$\langle \phi_i \phi_j \phi_k \phi_l \phi_m \phi_n \rangle = \frac{1}{N(N+2)(N+4)} (\delta_{ij} \delta_{kl} \delta_{mn} + \text{all permutations}) \langle (\vec{\phi}^2)^3 \rangle, \quad (2.11)$$

⋮

Correlation functions of an odd number of fields vanish. In consequence by calculating integrals of the form (2.7), *i.e.*,

$$\langle (\vec{\phi}^2)^n \rangle = \frac{2^n \int_0^\infty d\rho \rho^{\frac{N}{2}-1} \rho^n e^{-\mathcal{S}(\rho)}}{\int_0^\infty d\rho \rho^{\frac{N}{2}-1} e^{-\mathcal{S}(\rho)}}, \quad (2.12)$$

one has access to all standard correlation functions between fields. Furthermore, for all $f(\rho)$ from Eq. (2.7) that are expandable in polynomials,² one can use the previous result as well as the expansion coefficients to reconstruct $\langle f(\rho) \rangle$.

2.1.2. The generating functional

Usually the calculation and derivation of correlation functions like Eqs. (2.9) to (2.11) is formalized in statistics and quantum field theory by introducing the moment-generating function(al) [140], the generating function(al) of n -point functions, respectively [20, 142, 19, 124],

$$\mathcal{Z}(\vec{J}) \equiv \mathcal{N} \int_{-\infty}^{\infty} d^N \phi e^{-\mathcal{S}(\vec{\phi}) + \vec{J}^T \cdot \vec{\phi}}. \quad (2.13)$$

Oftentimes it is also called the partition function in the presence of sources or “magnetic” fields \vec{J} . Formally it is a (multidimensional) two-sided Laplace transform of the probability-density function (2.4). Note that definition (2.13) also applies to theories of N real scalars without (full) $O(N)$ symmetry.

¹The term n -point is of course misleading in a “spacetime” which is a single point. Still, we will stick to this notation to keep contact to the higher-dimensional formalism.

²In general, the function $f(\rho)$ does not even need to be analytic. However, in QFT we are mostly confronted with the calculation of expectation values of expandable functions or monomials of fields.

Correlation functions are derived from this object by taking derivatives w.r.t. the source \vec{J} and setting $\vec{J} = 0$. However, one usually also introduces correlation functions in the presence of source fields,

$$\begin{aligned} \langle \phi_{i_n} \cdots \phi_{i_1} \rangle_{\vec{J}} &\equiv \frac{1}{\mathcal{Z}(\vec{J})} \frac{\partial^n \mathcal{Z}(\vec{J})}{\partial J_{i_n} \cdots \partial J_{i_1}} \equiv \\ &\equiv \frac{\mathcal{Z}_{\vec{J}_n \cdots \vec{J}_1}(\vec{J})_{i_n \cdots i_1}}{\mathcal{Z}(\vec{J})} = \\ &= \frac{1}{\mathcal{Z}(\vec{J})} \mathcal{N} \int_{-\infty}^{\infty} d^N \phi \phi_{i_1} \cdots \phi_{i_n} e^{-\mathcal{S}(\vec{\phi}) + \vec{J}^T \cdot \vec{\phi}}. \end{aligned} \quad (2.14)$$

As can be seen from the last line, the normalization factor \mathcal{N} cancels and Eqs. (2.9) to (2.11) are for example recovered via definition (2.5) for $\vec{J} = 0$.

Thus, the entire information about a QFT is either stored in its generating functional (2.13) or all correlation functions – mathematically: the moments.

2.1.3. The Schwinger functional

Another way of deriving correlation functions and storing information about a QFT or a statistical system is the Schwinger function(al). It is simply defined via the logarithm of Eq. (2.13) and therefore directly related to the free energy,

$$\mathcal{W}(\vec{J}) \equiv \ln \mathcal{Z}(\vec{J}). \quad (2.15)$$

It is also called the cumulant-generating function(al) [140], generating function(al) of connected n -point functions [19, 20, 142, 24], or Ursell function in the context of statistical mechanics after Ref. [143].

These cumulants or connected correlation functions (in the presence of sources \vec{J}) are simply defined by derivatives of $\mathcal{W}(\vec{J})$,

$$\langle \phi_{i_n} \cdots \phi_{i_1} \rangle_{\vec{J}}^c \equiv \mathcal{W}_{\vec{J}_n \cdots \vec{J}_1}(\vec{J})_{i_n \cdots i_1}. \quad (2.16)$$

Explicitly one finds that the one-point function – the expectation value of the probability distribution – is the same for both generating functionals,

$$\langle \phi_i \rangle_{\vec{J}}^c = \mathcal{W}_{\vec{J}}(\vec{J})_i = \frac{\mathcal{Z}_{\vec{J}}(\vec{J})_i}{\mathcal{Z}(\vec{J})} = \langle \phi_i \rangle_{\vec{J}}. \quad (2.17)$$

The connected two-point function, which is also called variance, reads

$$\begin{aligned} \langle \phi_{i_2} \phi_{i_1} \rangle_{\vec{J}}^c &= \mathcal{W}_{\vec{J}_2 \vec{J}_1}(\vec{J})_{i_2 i_1} = \\ &= \frac{\mathcal{Z}_{\vec{J}_2 \vec{J}_1}(\vec{J})_{i_2 i_1}}{\mathcal{Z}(\vec{J})} - \frac{\mathcal{Z}_{\vec{J}_2}(\vec{J})_{i_2}}{\mathcal{Z}(\vec{J})} \frac{\mathcal{Z}_{\vec{J}_1}(\vec{J})_{i_1}}{\mathcal{Z}(\vec{J})} = \\ &= \langle \phi_{i_2} \phi_{i_1} \rangle_{\vec{J}} - \langle \phi_{i_2} \rangle_{\vec{J}} \langle \phi_{i_1} \rangle_{\vec{J}}. \end{aligned} \quad (2.18)$$

Analogously, one proceeds with the three-point function,

$$\begin{aligned}
\langle \phi_{i_3} \phi_{i_2} \phi_{i_1} \rangle_{\vec{J}}^c &= \mathcal{W}_{\vec{J}_3 \vec{J}_2 \vec{J}_1}(\vec{J})_{i_3 i_2 i_1} = \\
&= \frac{\mathcal{Z}_{\vec{J}_3 \vec{J}_2 \vec{J}_1}(\vec{J})}{\mathcal{Z}(\vec{J})} - \frac{\mathcal{Z}_{\vec{J}_3}(\vec{J})_{i_3}}{\mathcal{Z}(\vec{J})} \frac{\mathcal{Z}_{\vec{J}_2 \vec{J}_1}(\vec{J})_{i_2 i_1}}{\mathcal{Z}(\vec{J})} - \frac{\mathcal{Z}_{\vec{J}_2}(\vec{J})_{i_2}}{\mathcal{Z}(\vec{J})} \frac{\mathcal{Z}_{\vec{J}_3 \vec{J}_1}(\vec{J})_{i_3 i_1}}{\mathcal{Z}(\vec{J})} - \\
&\quad - \frac{\mathcal{Z}_{\vec{J}_1}(\vec{J})_{i_1}}{\mathcal{Z}(\vec{J})} \frac{\mathcal{Z}_{\vec{J}_3 \vec{J}_2}(\vec{J})_{i_3 i_2}}{\mathcal{Z}(\vec{J})} + 2 \frac{\mathcal{Z}_{\vec{J}_3}(\vec{J})_{i_3}}{\mathcal{Z}(\vec{J})} \frac{\mathcal{Z}_{\vec{J}_2}(\vec{J})_{i_2}}{\mathcal{Z}(\vec{J})} \frac{\mathcal{Z}_{\vec{J}_1}(\vec{J})_{i_1}}{\mathcal{Z}(\vec{J})} = \\
&= \langle \phi_{i_3} \phi_{i_2} \phi_{i_1} \rangle_{\vec{J}} - \langle \phi_{i_3} \rangle_{\vec{J}} \langle \phi_{i_2} \phi_{i_1} \rangle_{\vec{J}} - \langle \phi_{i_2} \rangle_{\vec{J}} \langle \phi_{i_3} \phi_{i_1} \rangle_{\vec{J}} - \langle \phi_{i_1} \rangle_{\vec{J}} \langle \phi_{i_3} \phi_{i_2} \rangle_{\vec{J}} + \\
&\quad + 2 \langle \phi_{i_3} \rangle_{\vec{J}} \langle \phi_{i_2} \rangle_{\vec{J}} \langle \phi_{i_1} \rangle_{\vec{J}}.
\end{aligned} \tag{2.19}$$

Already at this point the advantage of the Schwinger functional in terms of storing information is obvious and proceeding to higher-order correlation functions is straightforward. Redundant information, *e.g.*, contributions of two- and one-point functions to the three-point function, are simply subtracted in the definition of the connected n -point function. The term “connected” hereby refers and derives from the graphical representation of correlation functions, where products of correlation functions appear in terms of unconnected graphs [19, 20, 142].

2.1.4. The effective action

However, when it comes to storing information yet another generating functional is more efficient – the generating functional of 1PI vertex functions. It is directly related to the grand-canonical potential in statistical mechanics [11] and defined in terms of the Legendre transformation of the Schwinger functional (2.15) [144, 145, 146, 18, 19, 24],

$$\Gamma(\vec{\varphi}) \equiv \sup_{\vec{J}} \{ \vec{J} \cdot \vec{\varphi} - \mathcal{W}(\vec{J}) \} = \vec{J}^T(\vec{\varphi}) \cdot \vec{\varphi} - \mathcal{W}(\vec{J}(\vec{\varphi})). \tag{2.20}$$

Usually, we refer to this quantity as the (IR) effective action. Hereby, sup refers to the supremum and the components of the mean-field vector are defined by

$$\varphi_i \equiv \mathcal{W}_{\vec{J}(\vec{\varphi})}(\vec{J}(\vec{\varphi}))_i \equiv \mathcal{W}_{\vec{J}(\vec{\varphi})}(\vec{J})_i \Big|_{\vec{J}=\vec{J}(\vec{\varphi})}. \tag{2.21}$$

The name 1PI again is due to the diagrammatic representation of correlation functions, which exclusively contain contributions of diagrams that cannot be separated by cutting a single internal line [24]. Hence, w.r.t. the connected correlation functions these are even less diagrams, which are sufficient for encoding all information about a QFT. In addition, the (renormalized) vertex functions that are derived from Eq. (2.20) by taking derivatives w.r.t. the components of $\vec{\varphi}$ are directly related to the observables in a QFT in higher-dimensional spacetimes, *e.g.*, scattering amplitudes *etc.*, see, *e.g.*, Ref. [72] for a recent application in the FRG framework to pion scattering. Next, we present certain relations between the 1PI vertex functions,

$$\Gamma^{\vec{\varphi} \dots \vec{\varphi}}(\vec{\varphi})_{i_n \dots i_1} \equiv \frac{\partial^n \Gamma(\vec{\varphi})}{\partial \varphi^{i_n} \dots \partial \varphi^{i_1}}, \tag{2.22}$$

and the previously defined correlation functions. From Eq. (2.20) it is directly found that

$$\Gamma^{\vec{\varphi}}(\vec{\varphi})_i = J_i(\vec{\varphi}). \tag{2.23}$$

As long as this equation is not evaluated at the minimum of $\Gamma(\vec{\varphi})$ the right-hand side (r.h.s.) keeps its dependence on $\vec{\varphi}$.

Furthermore, from Eqs. (2.21) and (2.23) one easily finds,

$$\delta_{ji} = \frac{\delta J_j(\vec{\varphi})}{\delta J_i(\vec{\varphi})} = \frac{\delta J_j(\vec{\varphi})}{\delta \varphi_k} \frac{\delta \varphi_k}{\delta J_i(\vec{\varphi})} = \Gamma^{\vec{\varphi}\vec{\varphi}}(\vec{\varphi})_{jk} \mathcal{W}_{\vec{J}\vec{J}}(\vec{J}(\vec{\varphi}))_{ki}, \quad (2.24)$$

$$\delta_{ij} = \frac{\delta \varphi_j(\vec{J})}{\delta \varphi_i(\vec{J})} = \frac{\delta \varphi_k(\vec{J})}{\delta J_i} \frac{\delta J_j}{\delta \varphi_k(\vec{J})} = \mathcal{W}_{\vec{J}\vec{J}}(\vec{J})_{ik} \Gamma^{\vec{\varphi}\vec{\varphi}}(\vec{\varphi}(\vec{J}))_{kj}, \quad (2.25)$$

which implies that the two-point vertex function and the variance are inverse to each other. We further define

$$G^{\vec{\varphi}\vec{\varphi}}(\vec{\varphi})_{ij} \equiv (\Gamma^{\vec{\varphi}\vec{\varphi}}(\vec{\varphi}(\vec{J})))_{ij}^{-1} \equiv \mathcal{W}_{\vec{J}\vec{J}}(\vec{J})_{ij}, \quad (2.26)$$

which is called the full field-dependent propagator in higher dimensions. In zero dimensions this name is of course absurd in its literal sense but used anyhow.

For more general relations we have to work harder. We need the chain-rule relation between J_i and φ_i derivatives,

$$\frac{\delta}{\delta J_i} = \frac{\delta \varphi_j}{\delta J_i} \frac{\delta}{\delta \varphi_j} = \mathcal{W}_{\vec{J}\vec{J}}(\vec{J}(\vec{\varphi}))_{ij} \frac{\delta}{\delta \varphi_j} = G^{\vec{\varphi}\vec{\varphi}}(\vec{\varphi})_{ij} \frac{\delta}{\delta \varphi_j}, \quad (2.27)$$

Now, by backwards engineering, we obtain an algorithm which relates correlation functions (2.14) with quantities in the framework of the effective action,

$$\begin{aligned} \langle \phi_{i_n} \cdots \phi_{i_1} \rangle_{\vec{J}} &= \frac{\mathcal{Z}_{\vec{J}_n \cdots \vec{J}_1}(\vec{J})_{i_n \cdots i_1}}{\mathcal{Z}(\vec{J})} = \\ &= \left(\frac{\delta}{\delta J_{i_n}} + \varphi_{i_n} \right) \frac{\mathcal{Z}_{\vec{J}_{n-1} \cdots \vec{J}_1}(\vec{J})_{i_{n-1} \cdots i_1}}{\mathcal{Z}(\vec{J})} = \\ &= \left[\prod_{j=1}^{n-1} \left(\frac{\delta}{\delta J_{i_j}} + \varphi_{i_j} \right) \right] \varphi_{i_n} = \\ &= \left[\prod_{j=1}^{n-1} \left(G^{\vec{\varphi}\vec{\varphi}}(\vec{\varphi})_{i_j k} \frac{\delta}{\delta \varphi_k} + \varphi_{i_j} \right) \right] \varphi_{i_n}. \end{aligned} \quad (2.28)$$

Ultimately, this is done by evaluation of the product and the derivatives w.r.t. φ_i in the last line. For an explicit calculation the following identity for the derivative of the propagator (2.26) turns out to be useful,

$$\frac{\delta}{\delta \varphi_k} G^{\vec{\varphi}\vec{\varphi}}(\vec{\varphi})_{ji} = \frac{\delta}{\delta \varphi_k} (\Gamma^{\vec{\varphi}\vec{\varphi}}(\vec{\varphi}))_{ji}^{-1} = -G^{\vec{\varphi}\vec{\varphi}}(\vec{\varphi})_{jn} \Gamma^{\vec{\varphi}\vec{\varphi}}(\vec{\varphi})_{knm} G^{\vec{\varphi}\vec{\varphi}}(\vec{\varphi})_{mi}. \quad (2.29)$$

In the same fashion as for Eq. (2.28), one derives an algorithm that relates connected correlation functions (2.16) to vertex functions (2.22),

$$\langle \varphi_{i_n} \cdots \varphi_{i_1} \rangle_{\vec{J}}^c = \left[\prod_{j=1}^{n-1} \left(G^{\vec{\varphi}\vec{\varphi}}(\vec{\varphi})_{i_j k} \frac{\delta}{\delta \varphi_k} \right) \right] \varphi_{i_n}. \quad (2.30)$$

For more details on this formalism in the context of the FRG, see also Ref. [54].

Explicitly, from Eqs. (2.28) and (2.30) one obtains the following identities for the lowest three

orders,

$$\langle \phi_i \rangle_{\vec{J}}^c = \langle \phi_i \rangle_{\vec{J}} = \varphi_i, \quad (2.31)$$

$$\langle \phi_j \phi_i \rangle_{\vec{J}}^c = G^{\vec{\varphi}\vec{\varphi}}(\vec{\varphi})_{ji}, \quad (2.32)$$

$$\langle \phi_j \phi_i \rangle_{\vec{J}} = G^{\vec{\varphi}\vec{\varphi}}(\vec{\varphi})_{ji} + \varphi_j \varphi_i, \quad (2.33)$$

$$\langle \phi_k \phi_j \phi_i \rangle_{\vec{J}}^c = -G^{\vec{\varphi}\vec{\varphi}}(\vec{\varphi})_{nk} G^{\vec{\varphi}\vec{\varphi}}(\vec{\varphi})_{jm} G^{\vec{\varphi}\vec{\varphi}}(\vec{\varphi})_{il} \Gamma^{\vec{\varphi}\vec{\varphi}\vec{\varphi}}(\vec{\varphi})_{nml}, \quad (2.34)$$

$$\begin{aligned} \langle \phi_k \phi_j \phi_i \rangle_{\vec{J}} = & -G^{\vec{\varphi}\vec{\varphi}}(\vec{\varphi})_{nk} G^{\vec{\varphi}\vec{\varphi}}(\vec{\varphi})_{jm} G^{\vec{\varphi}\vec{\varphi}}(\vec{\varphi})_{il} \Gamma^{\vec{\varphi}\vec{\varphi}\vec{\varphi}}(\vec{\varphi})_{nml} + \\ & + G^{\vec{\varphi}\vec{\varphi}}(\vec{\varphi})_{kj} \varphi_i + G^{\vec{\varphi}\vec{\varphi}}(\vec{\varphi})_{ji} \varphi_k + G^{\vec{\varphi}\vec{\varphi}}(\vec{\varphi})_{ik} \varphi_j + \varphi_k \varphi_j \varphi_i. \end{aligned} \quad (2.35)$$

2.1.5. Correlation functions for the $O(N)$ model

These general relations for zero-dimensional models of N real scalars can be further simplified under the assumption of $O(N)$ symmetry and if they are evaluated for $\vec{J} = 0$, which corresponds to an evaluation at the minimum of $\Gamma(\vec{\varphi})$, which we simply call $\vec{\varphi}_{\min}$ and which is shown in Section 2.2.2 to be trivial in zero dimensions. As already mentioned, correlation functions of an odd number of fields vanish for $\vec{J} = 0$. Using the relations (2.9) to (2.11) we find the following identities, see also, *e.g.*, Refs. [107, 125],

$$\langle \phi_i \phi_i \rangle^c = \langle \phi_i \phi_i \rangle = (\Gamma^{\vec{\varphi}\vec{\varphi}}(\vec{\varphi}_{\min}))_{ii}^{-1}, \quad (2.36)$$

$$\langle \phi_i \phi_i \phi_i \phi_i \rangle^c = \langle \phi_i \phi_i \phi_i \phi_i \rangle - 3 \langle \phi_i \phi_i \rangle^2 = -\langle \phi_i \phi_i \rangle^4 \Gamma^{\vec{\varphi}\vec{\varphi}\vec{\varphi}\vec{\varphi}}(\vec{\varphi}_{\min})_{iiii}, \quad (2.37)$$

$$\begin{aligned} \langle \phi_i \phi_i \phi_i \phi_i \phi_i \phi_i \rangle^c = & \langle \phi_i \phi_i \phi_i \phi_i \phi_i \phi_i \rangle - 15 \langle \phi_i \phi_i \phi_i \phi_i \rangle \langle \phi_i \phi_i \rangle + 30 \langle \phi_i \phi_i \rangle^3 = \\ = & -\langle \phi_i \phi_i \rangle^6 \Gamma^{\vec{\varphi}\vec{\varphi}\vec{\varphi}\vec{\varphi}\vec{\varphi}\vec{\varphi}}(\vec{\varphi}_{\min})_{iiiiii} + 10 \langle \phi_i \phi_i \rangle^{-1} (\langle \phi_i \phi_i \phi_i \phi_i \rangle^c)^2, \end{aligned} \quad (2.38)$$

which can be solved for the vertex functions (evaluated for the same component of $\vec{\varphi}$),

$$\Gamma^{(2)} \equiv \Gamma^{\vec{\varphi}\vec{\varphi}}(\vec{\varphi}_{\min})_{ii} = \frac{N}{\langle \vec{\phi}^2 \rangle}, \quad (2.39)$$

$$\Gamma^{(4)} \equiv \Gamma^{\vec{\varphi}\vec{\varphi}\vec{\varphi}\vec{\varphi}}(\vec{\varphi}_{\min})_{iiii} = 3 \frac{N^2}{\langle \vec{\phi}^2 \rangle^2} \left[1 - \frac{N}{N+2} \frac{\langle (\vec{\phi}^2)^2 \rangle}{\langle \vec{\phi}^2 \rangle^2} \right], \quad (2.40)$$

$$\begin{aligned} \Gamma^{(6)} \equiv \Gamma^{\vec{\varphi}\vec{\varphi}\vec{\varphi}\vec{\varphi}\vec{\varphi}\vec{\varphi}}(\vec{\varphi}_{\min})_{iiiiii} = & 60 \frac{N^3}{\langle \vec{\phi}^2 \rangle^3} \left[1 - \frac{9N}{4(N+2)} \frac{\langle (\vec{\phi}^2)^2 \rangle}{\langle \vec{\phi}^2 \rangle^2} + \frac{3N^2}{2(N+2)^2} \frac{\langle (\vec{\phi}^2)^2 \rangle^2}{\langle \vec{\phi}^2 \rangle^4} - \right. \\ & \left. - \frac{N^2}{4(N+2)(N+4)} \frac{\langle (\vec{\phi}^2)^3 \rangle}{\langle \vec{\phi}^2 \rangle^3} \right]. \end{aligned} \quad (2.41)$$

Deriving relations like these (also for higher-order vertex functions) can be automatized using computer algebra programs like MATHEMATICA [147] as was done for results in later chapters of this thesis.

In the following chapters we are repeatedly making use of these relations between vertex functions and expectation values from the path integral, because the FRG is formulated on the level of the effective action (2.20), while the straightforward calculation of reference values is only possible by direct evaluation of the expectation values from the partition function. Thus, the identities

provide access to exact reference values for the vertex function via the one-dimensional integrals (2.12). For explicit numerical and/or analytical results it still remains to specify the classical action $\mathcal{S}(\vec{\phi})$ as is shown below for various test cases.

2.2. Symmetry breaking, phase transitions, convexity and all of that

Next, we turn to a very special feature of zero-dimensional QFT, namely the absence of (spontaneous) symmetry breaking and PTs and what this has to do with the Coleman-Mermin-Wagner-Hohenberg-Berezinskii (CMWHB) theorem. In this context we also discuss convexity of the generating functionals. Our discussion is a summary of our more detailed Ref. [1, Appendix B], which is in turn partially based on Refs. [109, 13].

2.2.1. Ehrenfest classification

According to Ehrenfest’s classification [148, 11], PTs are defined as discontinuities in the derivatives of thermodynamic potentials, when differentiating is performed w.r.t. an intensive thermodynamic variable. The order n of a PT is given by the lowest n^{th} -order derivative which shows this discontinuity while lower-order derivatives must stay continuous.

However, in zero spacetime dimensions there are no true thermodynamic potentials and state variables. All quantities are dimensionless and concepts like temperature, pressure *etc.* do not exist. Still, as already mentioned before, there are zero-dimensional analogues of thermodynamic potentials, namely the Schwinger functional (2.15), which plays the role of the free energy, and the effective action, which can be associated with the grand canonical potential (2.20). The corresponding “thermodynamic state variables” are the sources \vec{J} and mean fields $\vec{\phi}$. In consequence PTs should show up as discontinuities in derivatives w.r.t. \vec{J} or $\vec{\phi}$, depending on the generating functional.

Having said this, it can be shown that in fact $\mathcal{Z}(\vec{J}) \in C^\infty$ in zero dimensions for $O(N)$ -symmetric actions, thus it is a smooth function of $\vec{J} \in \mathbb{R}^N$. Following Ref. [109] this is demonstrated as follows: (For sake of simplicity we restrict the “physicists proof” to $N = 1$.)

A function is called smooth (or $\in C^\infty$), if for all $n \in \mathbb{N}$ the left- and right-derivatives coincide. For the generating functional (2.13) this is realized if

$$\lim_{\epsilon \rightarrow 0} \left[\frac{\partial^n \mathcal{Z}(J)}{\partial J^n} \Big|_{J+\epsilon} - \frac{\partial^n \mathcal{Z}(J)}{\partial J^n} \Big|_{J-\epsilon} \right] = 0, \quad (2.42)$$

which is easily demonstrated using Def. (2.13) and that $\mathcal{S}(\phi)$ at least grows quadratically and is bounded from below,

$$\begin{aligned} \lim_{\epsilon \rightarrow 0} \left[\frac{\partial^n \mathcal{Z}(J)}{\partial J^n} \Big|_{J+\epsilon} - \frac{\partial^n \mathcal{Z}(J)}{\partial J^n} \Big|_{J-\epsilon} \right] &= \lim_{\epsilon \rightarrow 0} \mathcal{N} \int_{-\infty}^{\infty} d\phi \phi^n e^{-\mathcal{S}(\phi)+J\phi} (e^{\epsilon\phi} - e^{-\epsilon\phi}) = \\ &= \lim_{\epsilon \rightarrow 0} \left[2\epsilon \mathcal{N} \int_{-\infty}^{\infty} d\phi \phi^{n+1} e^{-\mathcal{S}(\phi)+J\phi} + \mathcal{O}(\epsilon^2) \right] = 0. \end{aligned} \quad (2.43)$$

In the second step the exponentials are expanded for small ϵ and it is further used that in zero dimensions the remaining ϕ -integral in the last line is finite.³ The proof can be directly generalized to $N \neq 1$. Note that the convergence of the $\vec{\phi}$ -integration (for arbitrary N) is only guaranteed if $\mathcal{S}(\vec{\phi})$ is an even function of each component of $\vec{\phi}$. For $O(N)$ -symmetric actions this is trivially

³The last aspect is not fulfilled in higher dimensional spacetime as well as the $N \rightarrow \infty$ limit in zero-dimensional spacetime, which is, why PTs in terms of discontinuities *etc.* can exist. Similar violations of theorems affect the convexity of the generating functionals, see below.

fulfilled. Hence, without any terms that explicitly break the $O(N)$ symmetry there are no phase transitions according to Ehrenfest.

Having established that $\mathcal{Z}(\vec{J}) \in C^\infty$, this directly transfers to $\mathcal{W}(\vec{J})$ and $\Gamma(\vec{\varphi})$, because the logarithm of a smooth function is smooth. The same applies to the Legendre transformation of a smooth function.

It is also noteworthy (because it might appear counter-intuitive at first sight) that these arguments applies to any $\mathcal{S}(\vec{\phi})$ which at least grows asymptotically linear in the invariant ρ . This also includes non-differentiable, non-analytic actions, which might have non-trivial degenerate global minima. However, one has to keep in mind that we are integrating over $\vec{\phi}$, respectively ρ , and that smoothness of the generating functional refers to \vec{J} instead. For examples and illustrations, we refer to Ref. [1, Appendix B] and Refs. [149, 13].

2.2.2. Convexity of the generating functionals and the location of the physical point

Before we continue with our discussion on the absence of PTs *etc.*, we have to briefly comment on the convexity of the generating functionals as well as the identification of the physical point where correlation functions and vertex functions are evaluated.

Convexity

A function of several arguments is convex if its Hessian is positive semi-definite. In turn, a matrix M is positive semi-definite if $\vec{x}^T M \vec{x} \geq 0$ for all $\vec{x} \in \mathbb{R}^N$.

Hence, for $\mathcal{Z}(\vec{J})$ we need to study its second derivatives w.r.t. the source-field components J_i . These, however, are directly related to the generic two-point correlation functions in the presence of the sources \vec{J} ,

$$\langle \phi_{i_2} \phi_{i_1} \rangle_{\vec{J}} = \frac{1}{\mathcal{Z}(\vec{J})} \mathcal{N} \int_{-\infty}^{\infty} d^N \phi \phi_{i_1} \phi_{i_2} e^{-\mathcal{S}(\vec{\phi}) + \vec{J}^T \cdot \vec{\phi}}, \quad (2.44)$$

which is clear from definition (2.14). The additional factor $1/\mathcal{Z}(\vec{J})$ is irrelevant for the following, because it is manifestly positive for all \vec{J} . In consequence, we study

$$x_i \langle \phi_i \phi_j \rangle_{\vec{J}} x_j = \frac{1}{\mathcal{Z}(\vec{J})} \mathcal{N} \int_{-\infty}^{\infty} d^N \phi (\vec{x}^T \cdot \vec{\phi})^2 e^{-\mathcal{S}(\vec{\phi}) + \vec{J}^T \cdot \vec{\phi}}. \quad (2.45)$$

The expression is positive semi-definite, which is seen as follows: Consider a substitution of the integration variables in terms of an $O(N)$ rotation (2.2), $O^T \vec{\phi}' = \vec{\phi}$. Next, without loss of generality (w.l.o.g.) choose the rotation matrix such that $\vec{x}^T O^T = (|\vec{x}|, 0, \dots, 0)$. This turns the factor in front of the exponential into $|\vec{x}|^2 \phi_1'^2$, which is positive or zero. The integral measure as well as the action $\mathcal{S}(\vec{\phi})$ are $O(N)$ -invariant and have the same shape in the transformed variables. The source is replaced by $\vec{J}^T O^T$, which ultimately does not alter the fact that the exponential in total is always positive.

We find that the Hessian is positive semi-definite and $\mathcal{Z}(\vec{J})$ is convex.

Analogously we proceed for $\mathcal{W}(\vec{J})$ and show its convexity. Using Eq. (2.18),

$$\begin{aligned} x_i \langle \phi_{i_2} \phi_{i_1} \rangle_{\vec{J}}^c x_j &= \langle (\vec{x}^T \cdot \vec{\phi})^2 \rangle_{\vec{J}} - \langle \vec{x}^T \cdot \vec{\phi} \rangle_{\vec{J}} \langle \vec{x}^T \cdot \vec{\phi} \rangle_{\vec{J}} = \\ &= \langle (\vec{x}^T \cdot \vec{\phi} - \langle \vec{x}^T \cdot \vec{\phi} \rangle_{\vec{J}})^2 \rangle_{\vec{J}} > 0, \end{aligned} \quad (2.46)$$

it is easy to see that the Hessian is always positive semi-definite.

From this we can directly conclude that also $\Gamma(\vec{\varphi})$ is convex, because the Legendre transform of a convex function is convex by definition, *cf.* Refs. [149, 13].

The physical point – the evaluation point for correlation and vertex functions

Taking into account that all three generating functionals are smooth and convex it is obvious that they have their unique minimum at $\vec{J} = 0$ and $\vec{\varphi} = 0$ respectively. The correct evaluation point for correlation functions of $\mathcal{Z}(\vec{J})$ and $\mathcal{W}(\vec{J})$ is of course by construction $\vec{J} = 0$ – their minimum. However, from Eq. (2.23) we also know that the correct evaluation point of the field-dependent vertex functions is the extremum of $\Gamma(\vec{\varphi})$. It follows from the previous considerations that this extremum is a unique minimum in zero dimensions and located at $\vec{\varphi} = 0$.

Again, note that even though the classical $O(N)$ -invariant action $\mathcal{S}(\vec{\phi})$ might have degenerate non-trivial global minima, the physical evaluation point for $\Gamma(\vec{\varphi})$ is always $\vec{\varphi} = 0$ in zero dimensions and the $O(N)$ symmetry of the ground state is always restored. Hence, there is no symmetry breaking in zero spacetime dimensions.

For higher-dimensional QFTs the IR effective action still needs to be convex. However, smoothness and analyticity is no longer required, such that there is an entire “flat region” and the physical minimum can indeed be/stay non-trivial. Symmetry breaking is in general possible.

We refer to Ref. [1, Appendix B] and Refs. [149, 13] for further discussions and illustrations on these topics.

2.2.3. Landau’s classification of phase transitions

According to Landau’s classification, PTs [150] are linked to the spontaneous breaking or restoration of symmetries, while an intensive external thermodynamic state variable is varied. It is signaled by the (dis)appearance of an order parameter, which characterizes the state of the system (its symmetry), *e.g.*, a condensate. On some occasions it is also possible to use an extensive thermodynamic state variable itself as an order parameter. Here, however, it does not make sense to study the variation of its canonically conjugate intensive state variable, since this corresponds to explicit symmetry breaking.

Zero dimensions are again special: The only “intensive state variables” are \vec{J} and their canonically conjugate “extensive” counterparts are $\vec{\varphi}$. However, $\vec{\varphi}$ is directly linked to the condensate. Hence, there is exclusively the option to explicitly break the $O(N)$ symmetry by considering non-vanishing source fields \vec{J} . However, as long as $\vec{J} = 0$, we also have $\vec{\varphi}_{\min} = \langle \vec{\phi} \rangle = 0$ as discussed in Sections 2.2.1 and 2.2.2.

The same applies to the variation of any other parameter in $\mathcal{S}(\vec{\phi})$. It simply has no influence on the location of the physical point, which is always at $\vec{\varphi} = 0$ in the IR, and the condensate $\langle \vec{\phi} \rangle$ always vanishes, as long as the $O(N)$ symmetry is not explicitly broken.

Thus, Ehrenfest and Landau classification lead to identical conclusions on the possible ground state of zero-dimensional $O(N)$ models – namely the trivial state.

2.2.4. The CMWHB theorem

Some readers might interject that this result is already expected from the CMWHB theorem. It states that for systems of spatial dimensions $d \leq 2$ and sufficiently short-range interactions there cannot be spontaneous breaking of continuous symmetries at non-zero temperature [151, 152, 153, 154, 155].

Indeed, zero-dimensional systems fulfill the “dimensional” requirement and interactions are indeed strong and “short-range”, because they are all in a single point. However, there is a priori no notion of temperature.

Still, there is a workaround: It is possible to think of zero-dimensional QFTs in terms of the infinite-temperature limit of a thermal quantum mechanical system or a QFT in a tiny spacetime box. In any case, considering the zero-volume and infinite-temperature limit, only the lowest bosonic Matsubara mode survives and the system is effectively zero-dimensional [109, 139]. In this sense, the CMWHB theorem applies and spontaneous symmetry breaking is forbidden.

Despite everything and strictly speaking, this argument is only valid for systems with $N > 1$ and continuous symmetries, where breaking of this symmetry causes the existence of Nambu-Goldstone modes [156, 157, 144], because the theorem relies on their existence for the symmetry restoration. In fact, we have found, that also for $N = 1$ there is no symmetry breaking either, even though this symmetry is a discrete \mathbb{Z}_2 symmetry. It seems as if the single σ -mode actually suffices to restore the symmetry, totally without the support of Nambu-Goldstone particles. We come back to this fact several times in this thesis and strongly believe that this calls for additional future research.

Chapter 3

The need for strictly non-perturbative methods

Abstract In this chapter we briefly discuss the severe limitations of perturbative methods as well as the large- N expansion. We first provide a short general introduction into the methods. Then their shortcomings are exemplified using two different zero-dimensional $O(N)$ -symmetric toy models. However, for general reference we start this chapter by presenting the trivial model – the free theory.

Note, that our entire discussion does not aim at mathematical rigor and there is a lot more to say about these two and related methods than what is presented in this chapter. Here, we are, however, mainly interested in motivating the use of strictly non-perturbative methods like the FRG in a playful way with seemingly innocent actions and get familiar with aspects of the large- and infinite- N approximation. Experts might want to simply skim over this chapter and continue careful reading in the next chapter.

Disclosure This chapter and especially the part on the saddle-point expansion is mainly based on our own Ref. [3]. Furthermore it contains material from our publications [1, 2]. However, we also comment on well-known results for perturbation theory for the zero-dimensional $O(N)$ model. These results are taken from Refs. [128, 129, 130, 131, 109, 107, 23, 124, 125].

3.1. The free theory

Before we turn to the main subject of this chapter, we briefly present some results for the trivial case – the free theory – as reference. The corresponding action $\mathcal{S}(\vec{\phi})$ of massive non-interacting $O(N)$ -symmetric bosons is given by a potential which exclusively contains the quadratic contribution with positive mass m^2 ,

$$\mathcal{S}(\vec{\phi}) = U_0(\vec{\phi}) = \frac{1}{2} m^2 \vec{\phi}^2 = m^2 \rho = U_0(\rho), \quad (3.1)$$

All corresponding correlation functions (2.9) can therefore be calculated from the moments of a Gaussian-type integral,

$$\begin{aligned} \langle (\vec{\phi}^2)^n \rangle &\stackrel{(2.12)}{=} \frac{2^n \int_0^\infty d\rho \rho^{\frac{N}{2}-1} \rho^n e^{-U_0(\rho)}}{\int_0^\infty d\rho \rho^{\frac{N}{2}-1} e^{-U_0(\rho)}} \stackrel{(3.1)}{=} & t = m^2 \rho, & (3.2) \\ &= \frac{2^n m^{2n} \int_0^\infty dt t^{\frac{N}{2}-1} t^n e^{-t}}{\int_0^\infty dt t^{\frac{N}{2}-1} e^{-t}} \stackrel{(A.37)}{=} \\ &= \frac{2^n m^{2n} \Gamma(\frac{N}{2} + n)}{\Gamma(\frac{N}{2})}. \end{aligned}$$

With Eq. (A.38) we find

$$\langle (\vec{\phi}^2)^0 \rangle = \langle 1 \rangle = 1, \quad \text{and} \quad \forall n > 1 \quad \langle (\vec{\phi}^2)^n \rangle = \frac{2}{m^2} \left(\frac{N}{2} + n - 1 \right) \langle (\vec{\phi}^2)^{n-1} \rangle. \quad (3.3)$$

The corresponding vertex functions are derived by inserting these results into Eqs. (2.39) to (2.41) *etc.*. One finds,

$$\Gamma^{(2)} = m^2, \quad \text{and} \quad \forall n > 2 \quad \Gamma^{(n)} = 0. \quad (3.4)$$

Anyhow, for this special case it is easier to evaluate the Gaussian integral in Eq. (2.13) explicitly for the action (3.1) and determine $\mathcal{W}(\vec{J})$ from Eq. (2.15),

$$\mathcal{W}(\vec{J}) = \ln \mathcal{Z}(\vec{J}) \equiv \ln \left(\mathcal{N} \int_{-\infty}^{\infty} d^N \phi \, e^{-\frac{1}{2} m^2 \vec{\phi}^2 + \vec{J}^T \cdot \vec{\phi}} \right) = \frac{1}{2m^2} \vec{J}^2 + \text{const.} \quad (3.5)$$

As expected for a Gaussian integral it directly follows that exclusively the variance – the connected two-point correlation function (2.18) – is non-zero, while all higher cumulants – connected n -point correlation functions – vanish [140]. Additionally, it turns out that the Legendre transformation to the effective action is trivial and we find

$$\Gamma(\vec{\varphi}) = \frac{1}{2} m^2 \vec{\varphi}^2 + \text{const.}, \quad (3.6)$$

which directly explains Eq. (3.4). This result is also rather intuitive for massive non-interacting particles, because all interaction vertices vanish and exclusively the 1PI two-point function survives.

3.2. Limitations of perturbation theory

Next, we turn to the first real application of the zero-dimensional $O(N)$ model. It serves as the minimal example to study limitations of perturbation theory. To this end, we need a non-trivial $O(N)$ -symmetric action, which contains “interactions” of our bosons in the single spacetime point. As usual in QFT the ϕ^4 -model will do the job.

After presenting the model and exact reference solutions, we first demonstrate the general non-convergence of the perturbation series. Second, we show that considering a low-order expansion may still be useful for an extremely small coupling in the sense of an asymptotic series, while it is totally inappropriate beyond this limit.

Ultimately, we discuss general shortcomings of the idea of the perturbative approach.

3.2.1. ϕ^4 -theory

The zero-dimensional version of the ϕ^4 -theory is defined by the following action/potential

$$\mathcal{S}(\vec{\phi}) = U(\vec{\phi}) = \frac{m^2}{2} \vec{\phi}^2 + \frac{\lambda}{4!} (\vec{\phi}^2)^2, \quad (3.7)$$

with positive mass $m^2 \in \mathbb{R}_{>0}$ and positive quartic coupling $\lambda \in \mathbb{R}_{>0}$. (Later on we also consider the same action with negative mass.) Formulated in terms of the $O(N)$ -invariant (2.6) this reads,

$$U(\rho) = m^2 \rho + \frac{\lambda}{6} \rho^2. \quad (3.8)$$

Exact solution

Interestingly, the zero-dimensional ϕ^4 -theory is one of the rare QFTs that is exactly integrable. Analogously to the free theory the expectation values (2.12) can be calculated in terms of known

functions. This is because the respective integrals are all of the following type,

$$\begin{aligned} \int_0^\infty d\rho \rho^{\frac{N}{2}-1} \rho^n e^{-U(\rho)} &= \int_0^\infty d\rho \rho^{\frac{N}{2}+n-1} e^{-m^2\rho - \frac{\lambda}{6}\rho^2} = \\ &= \left(\frac{6}{\lambda}\right)^{\frac{1}{2}(\frac{N}{2}+n)} \left[\frac{1}{2} \Gamma\left(\frac{1}{2}\left(\frac{N}{2}+n\right)\right) {}_1F_1\left(\frac{1}{2}\left(\frac{N}{2}+n\right); \frac{1}{2}; \frac{6}{\lambda}\left(\frac{m^2}{2}\right)^2\right) - \right. \\ &\quad \left. - \left(\frac{6}{\lambda}\right)^{\frac{1}{2}} \frac{m^2}{2} \Gamma\left(\frac{1}{2}\left(\frac{N}{2}+n+1\right)\right) {}_1F_1\left(\frac{1}{2}\left(\frac{N}{2}+n+1\right), \frac{3}{2}; \frac{6}{\lambda}\left(\frac{m^2}{2}\right)^2\right) \right], \end{aligned} \quad (3.9)$$

such that the correlation functions and vertex functions can all be expressed in terms of functions of this result for the appropriate n . Here ${}_1F_1(a; b; c)$ is the confluent hypergeometric function and $\Gamma(s)$ is the conventional gamma function (A.37).

There are various ways to reshape this result, *e.g.*, in terms of Kummer's and Tricomi's function or modified Bessel functions of the second kind. Anyhow, the result is well-known in literature, see, *e.g.*, Refs. [107, Eq. (3.2)], Ref. [110, Eq. (36)] or other references from Chapter 1.

However, note that for practical applications it is usually much simpler to calculate the (one-dimensional) integrals in the expectation values (2.12) numerically to basically arbitrary precision, which is also done throughout this work.

Anyhow, having exact reference solutions, we can turn to conventional perturbation theory.

3.2.2. Perturbation theory

The following paragraphs are based on Refs. [128, 129, 130, 131, 109, 107, 23, 124, 125] and exclusively serve for introductory and motivational purposes.

Conventional perturbation theory is based on an expansion of the partition function (2.13) and consequently the expectation values (2.12) in the coupling λ under the assumption that $\lambda \lll 1$, thus,

$$\begin{aligned} \langle (\vec{\phi}^2)^n \rangle &= \frac{2^n \int_0^\infty d\rho \rho^{\frac{N}{2}-1} \rho^n e^{-S(\rho)}}{\int_0^\infty d\rho \rho^{\frac{N}{2}-1} e^{-S(\rho)}} = \\ &= \frac{2^n \int_0^\infty d\rho \rho^{\frac{N}{2}-1} \rho^n e^{-\rho - \frac{\lambda}{6}\rho^2}}{\int_0^\infty d\rho \rho^{\frac{N}{2}-1} e^{-\rho - \frac{\lambda}{6}\rho^2}} = \\ &= \frac{2^n \int_0^\infty d\rho \rho^{\frac{N}{2}-1} \rho^n \left[1 - \frac{\lambda}{6}\rho^2 + \frac{\lambda^2}{72}\rho^4 + \mathcal{O}(\lambda^3)\right] e^{-\rho}}{\int_0^\infty d\rho \rho^{\frac{N}{2}-1} \left[1 - \frac{\lambda}{6}\rho^2 + \frac{\lambda^2}{72}\rho^4 + \mathcal{O}(\lambda^3)\right] e^{-\rho}}. \end{aligned} \quad (3.10)$$

For the two-point vertex function, inserting Eq. (3.10) into Eq. (2.39) leads to

$$\Gamma^{(2)} = \frac{N}{\langle \vec{\phi}^2 \rangle} = 1 + (N+2) \frac{\lambda}{6} - 2(N+4)(N+2) \frac{1}{2} \left(\frac{\lambda}{6}\right)^2 + \mathcal{O}(\lambda^3). \quad (3.11)$$

For both results and w.l.o.g. we set $m^2 = 1$, which corresponds to a simple rescaling of the fields and the coupling. For example, for $N = 2$ we find for the expansion to $\mathcal{O}(\lambda^6)$,

$$\Gamma^{(2)} = 1 + \frac{2}{3} \lambda - \frac{2}{3} \lambda^2 + \frac{14}{9} \lambda^3 - \frac{46}{9} \lambda^4 + \frac{562}{27} \lambda^5 - \frac{8054}{81} \lambda^6 + \mathcal{O}(\lambda^7). \quad (3.12)$$

Thus, already from this expression one sees that the modulus of the expansion coefficients is growing rapidly, which should be alarming. Absorbing the factor $\frac{1}{4!}$ from Eq. (3.7) in the coupling does not alter this fact.

This can be analyzed more systematically. To this end and again w.l.o.g. we study the basic integral from the denominator of Eq. (3.10) for $N = 1$ in terms of a perturbation series,

$$\begin{aligned}
& \int_0^\infty d\rho \rho^{\frac{1}{2}-1} e^{-U(\rho)} = \\
& = \int_0^\infty d\rho \rho^{\frac{1}{2}-1} e^{-\rho - \frac{\lambda}{6} \rho^2} = \\
& = \int_0^\infty d\rho \rho^{\frac{1}{2}-1} e^{-\rho} \sum_{m=0}^{\infty} \frac{1}{m!} \left(-\frac{\lambda}{6} \rho^2\right)^m = \\
& = \sum_{m=0}^{\infty} a_m \lambda^m.
\end{aligned} \tag{3.13}$$

In the last step, we exchanged summation and integration and defined the expansion coefficients,

$$\begin{aligned}
a_m & = (-1)^m \frac{1}{6^m} \frac{1}{m!} \int_0^\infty d\rho \rho^{2m+\frac{1}{2}-1} e^{-\rho} \stackrel{\text{(A.37)}}{=} \\
& = (-1)^m \frac{1}{6^m} \frac{1}{m!} \Gamma\left(2m + \frac{1}{2}\right) = \\
& = (-1)^m \frac{1}{6^m} \frac{1}{m!} \frac{(4m)!}{4^{2m}(2m)!} \sqrt{\pi}.
\end{aligned} \tag{3.14}$$

To study the convergence of the series in the last line of Eq. (3.13), we use the ratio test (d'Alembert's criterion) and Eq. (A.43),

$$r = \lim_{m \rightarrow \infty} \left| \frac{a_{m+1} \lambda^{m+1}}{a_m \lambda^m} \right| \propto \lim_{m \rightarrow \infty} m \lambda. \tag{3.15}$$

We find that $r > 1$ for large m , such that the sum does not converge. (This result does not change for other integrals occurring in Eq. (3.10).) In conclusion, the exchange of summation and integration in the last step of Eq. (3.13) was not justified and perturbation theory is in general ill-conditioned. In fact, we can directly argue that the expansion Eq. (3.13) has zero radius of convergence at $\lambda = 0$, because the original integral itself converges for $\lambda > 0$, but diverges for $\lambda < 0$.

The explanation why it is still possible to obtain decent results for very small coupling and finite expansion order is that the series is an asymptotic series at $\lambda = 0$ and it is possible to calculate an optimal finite expansion order with least deviation from the exact result. Hence, for extremely small λ the precision of the perturbation theory is overwhelming and the difference between the Taylor expansion and the partial sum is negligible. However, increasing the coupling leads to large deviations, already for rather small expansion orders, which then grow rapidly.

From a QFT perspective, this is understood as follows. The combinatorial number of graphs which contributes to each order in perturbation theory grows faster (factorial) than the suppression by the powers of the small coupling, λ^m . Thus, suppression of higher-order terms in the perturbation series exclusively works until combinational growth exceeds the suppression by the small coupling. For the $O(N)$ model all this depends on N , the specific order- n correlation function (3.10) and λ .

Here, we do not go any further into detail on this topic. Instead we refer to the textbooks Ref. [23, Sec. 2.1], Ref. [128, Sec. 11], Ref. [129, Sec. 7.5], Ref. [130, Sec. 5.1] or for example Refs. [131, 109, 107, 124, 125]. In this context it is also worth mentioning that there are variants to improve perturbation theory, *e.g.*, using Borel summation or the framework of optimized perturbation theory, which are also discussed within some of the above references.

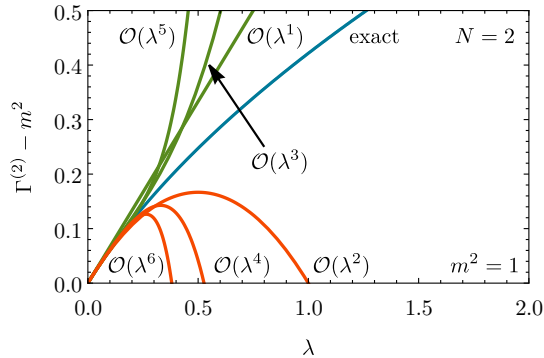


Figure 3.1: The exact result for $\Gamma^{(2)} - m^2$ via Eqs. (2.12), (2.39), and (3.8) and the perturbative result from Eq. (3.12) as functions of λ for $N = 2$. The plot is an adaption from Ref. [107, Fig. 3].

Anyhow, to get an impression of the poor quality of perturbation theory, we plot the exact result for $\Gamma^{(2)}$ and the perturbative result for different expansion orders as a function of λ for fixed $N = 2$ in Fig. 3.1. It is obvious (already without plotting the relative deviations), that perturbation theory is close to the correct result exclusively for $\lambda \ll 1$ and significantly deviates for larger λ . This result does not change drastically for different N , but is even worse for higher-order vertex functions, *cf.* Ref. [107].

However, what about UV actions with large λ , multiple couplings, negative mass term, or cusps? Of course, there are again selected examples where perturbation theory (with certain modifications) could be applied and decent results are obtained. Nevertheless, perturbation theory cannot be seen as a reliable framework beyond these strict limitations. Especially in higher-dimensional systems it is much harder to estimate the point where one leaves the range of applicability, where perturbation theory breaks down. Additionally, calculations are getting much more involved, because UV and IR divergences can emerge in every single expansion order and call for regularization and renormalization.

In conclusion, it is worth turning to alternative techniques, which also avoid direct evaluation of the (functional) integrals and (statistical) integration.

3.3. The $\frac{1}{N}$ -expansion and its limitations

The following subsections are mostly based on our own publication Ref. [3] and in parts closely follow its text. Some introductory examples and figures are taken from Ref. [107] and adopted for our purposes.

We turn to a commonly used “non-perturbative” approach for the calculation of correlation functions in statistical mechanics and QFT. The method is referred to (depending on the context) by many different names, which, strictly speaking, all refer to slightly different, but closely related methods in pure mathematical statistics. In most QFT contexts physicists are not too picky and loosely interchange these names. (Most definitely this is also true for my own work).

The method is known as the $\frac{1}{N}$ -expansion (including the $N \rightarrow \infty$ limit), t’Hooft limit, the Laplace’s method, the saddle-point expansion, the stationary-phase approximation, or method of steepest descent. Oftentimes it is simply referred to as the mean-field approximation, which is probably most unspecific and sometimes even wrong.

Anyhow, the key idea behind the method is the expansion of characteristic quantities of a model or theory, like the correlation and vertex functions, in powers of $\frac{1}{N}$. Here, N is the number of different kinds of (interacting) degrees of freedom in our model or theory. In high-energy physics these can

be particle/field types, spins, molecules, color charges *etc.*. For an expansion in $\frac{1}{N}$ it should therefore be assumed that this number is large, $1 \ll N$. In order to make sense of this expansion, it is required to rescale extensive quantities by appropriate powers of N . This facilitates the comparison between different N and especially the $N \rightarrow \infty$ limit without introducing artificial divergences.

At this point, the question arises why a method that again relies on an expansion in a small parameter, here $\frac{1}{N}$, is considered to be non-perturbative. The explanation is that contrary to conventional perturbation theory, which is based on an expansion in a dimensionless small coupling constant, the $\frac{1}{N}$ -expansion is also applicable to strongly interacting systems with large and multiple coupling constants *etc.*. Indeed, the method enjoyed great successes and oftentimes keeps its predictive power even for systems of unexpectedly small N in their strongly coupled regime, *cf.* for example Refs. [28, 158, 159, 160, 29, 74, 31] in the context of particle physics or see Ref. [30] for a review. This is also demonstrated within this section. Nevertheless, the method also comes with certain problematic features, *e.g.*, non-convex IR potentials or a total failure, if the expansion point is a non-analytic or degenerate global minimum of the potential. Such shortcomings are the key aspect of our critique and motivate the use for strictly non-perturbative methods like the FRG.

Within the next subsections, we introduce the $\frac{1}{N}$ -expansion for our zero-dimensional $O(N)$ model. For this theory the N from the $\frac{1}{N}$ -expansion parameter is of course the dimension N of the group and number of boson fields. We introduce the method for the calculation of arbitrary correlation functions and arbitrary UV potentials. First, we crosscheck the method with the free theory. Afterwards we present established results for the performance of the $\frac{1}{N}$ -expansion for the ϕ^4 -theory, which we already studied within perturbation theory. The limitations of the method are demonstrated using another toy model developed by ourselves in Ref. [3], which is inspired by a higher-dimensional model from Ref. [77] and used to study the large- and infinite- N limit in FRG in the context of shock waves and diffusion in field space.

3.3.1. The $\frac{1}{N}$ -expansion for the zero-dimensional $O(N)$ model

The starting point of our discussion are of course again the general correlation functions (2.12) of zero-dimensional $O(N)$ models,

$$\langle (\vec{\phi}^2)^n \rangle = \frac{2^n \int_0^\infty d\rho \rho^{\frac{N}{2}-1} \rho^n e^{-U(\rho)}}{\int_0^\infty d\rho \rho^{\frac{N}{2}-1} e^{-U(\rho)}}. \quad (3.16)$$

As has just been said, the $\frac{1}{N}$ -expansion requires to rescale extensive quantities with their inverse dependence on N . Therefore, we introduce the rescaled $O(N)$ -invariant and the rescaled potential,

$$\rho \mapsto y = \frac{1}{N} \rho, \quad U(\rho) \mapsto V(y) = \frac{1}{N} U(\rho). \quad (3.17)$$

Expressing the correlation functions by these quantities and slightly rearranging the integrals, we arrive at,

$$\begin{aligned} \langle (\vec{\phi}^2)^n \rangle &= \frac{2^n N^n \int_0^\infty dy y^{\frac{N}{2}-1} y^n e^{-NV(y)}}{\int_0^\infty dy y^{\frac{N}{2}-1} e^{-NV(y)}} = \\ &= \frac{2^n N^n \int_0^\infty dy y^{n-1} e^{-N[V(y) - \frac{1}{2} \ln(y)]}}{\int_0^\infty dy y^{-1} e^{-N[V(y) - \frac{1}{2} \ln(y)]}} = \\ &= \frac{2^n N^n \mathcal{I}^{(N)}[V(y) - \frac{1}{2} \ln(y), y^{n-1}]}{\mathcal{I}^{(N)}[V(y) - \frac{1}{2} \ln(y), y^{-1}]}. \end{aligned} \quad (3.18)$$

In the last line we introduced the integral

$$\mathcal{I}^{(N)}[f, g] \equiv \int_0^\infty dy g(y) e^{-Nf(y)}, \quad (3.19)$$

which is the standard form to apply the saddle point expansion/Laplace's method [33]. (Note, that the cognizant reader can already identify the logarithmic structure in the function $f(y)$, which is also generated in Yukawa-type models in QFT, if fermions are completely integrated out.)

The saddle-point expansion The following general calculations are not original to the author and can be found elsewhere, *e.g.*, in Refs. [33].

The fundamental assumption of the $\frac{1}{N}$ -expansion is that $f(y)$ has a unique global minimum at y_0 . In addition, it is assumed that $f(y)$ and $g(y)$ are analytic in y_0 – expandable to arbitrary order. As long as both functions grow at least like polynomials in y (about y_0), it is possible to derive an asymptotic series of $\mathcal{I}^{(N)}[f, g]$ for large N in powers of $\frac{1}{N}$.

The idea behind is that the integrand of Eq. (3.19) is strongly peaked around the minimum y_0 of $f(y)$ if N is large and can be approximated by a sum of Gaussian integrals. Thus, shifting the integration variable by y_0 ,

$$y = y_0 + \frac{z}{\sqrt{N}}, \quad (3.20)$$

an expansion in $\frac{z}{\sqrt{N}}$ should lead to good approximations already for small expansion orders, as long as N is sufficiently large and vice versa.

Consequently we study this shift in the integral (3.19) and a systematic expansion in $\frac{1}{N}$,

$$\mathcal{I}^{(N)}[f, g] = \quad (3.21)$$

$$= \int_0^\infty dy g(y) e^{-Nf(y)} = \quad (3.22)$$

$$= \frac{1}{\sqrt{N}} \int_{-y_0\sqrt{N}}^\infty dz g(y_0 + \frac{z}{\sqrt{N}}) \exp\left(-Nf(y_0 + \frac{z}{\sqrt{N}})\right) = \quad (3.23)$$

$$= \frac{1}{\sqrt{N}} \int_{-y_0\sqrt{N}}^\infty dz g(y_0 + \frac{z}{\sqrt{N}}) \times \quad (3.24)$$

$$\times \exp\left(-Nf^{(0)} - \frac{1}{2}f^{(2)}z^2 - \frac{1}{6\sqrt{N}}f^{(3)}z^3 - \frac{1}{24N}f^{(4)}z^4 + \mathcal{O}(z^5)\right) \simeq$$

$$\simeq e^{-Nf^{(0)}} \frac{1}{\sqrt{N}} \int_{-\infty}^\infty dz e^{-\frac{1}{2}f^{(2)}z^2} \left(g^{(0)} + \frac{1}{\sqrt{N}}[g^{(1)} - \frac{1}{6}g^{(0)}f^{(3)}z^2]z + \quad (3.25)$$

$$+ \frac{1}{N}[\frac{1}{2}g^{(2)} - \frac{1}{6}g^{(1)}f^{(3)}z^2 + \frac{1}{72}g^{(0)}(f^{(3)})^2z^4 - \frac{1}{24}g^{(0)}f^{(4)}z^2]z^2 + \mathcal{O}(N^{-\frac{3}{2}})\right) =$$

$$= e^{-Nf^{(0)}} \sqrt{\frac{2\pi}{Nf^{(2)}}} \sum_{i=0}^\infty \frac{1}{N^i} \mathcal{C}_i[f, g]. \quad (3.26)$$

In the calculation n -th derivatives of f and g , which are evaluated at y_0 are abbreviated with superscripts (n). The above calculation consists of the following steps

1. An integration-variable substitution via the shift (3.20).
2. An expansion of the exponent in $\frac{z}{\sqrt{N}}$.
3. The extraction of the z -independent zeroth-order term from the integral and separation of the Gaussian factor $\exp(-\frac{1}{2}f^{(2)}z^2)$ in the integrand.
4. An expansion of the remaining exponential contribution and expansion of g in $\frac{z}{\sqrt{N}}$.

5. Extending the integration domain and lower integration bound, using that N is large and that the integrand is peaked.
6. The term-by-term evaluation of Gaussian type integrals and elimination of integrals that are odd in z .
7. Grouping terms in powers of $\frac{1}{N}$.

The result is a power series in $\frac{1}{N}$ with N -independent coefficient $\mathcal{C}_i[f, g]$. The first two coefficients are for example,

$$\mathcal{C}_0[f, g] = g^{(0)}, \quad (3.27)$$

$$\mathcal{C}_1[f, g] = \frac{g^{(2)}}{2f^{(2)}} - \frac{g^{(1)}f^{(3)}}{2(f^{(2)})^2} + \frac{5g^{(0)}(f^{(3)})^2}{24(f^{(2)})^3} - \frac{g^{(0)}f^{(4)}}{8(f^{(2)})^2}. \quad (3.28)$$

Computing higher-order coefficients is simple but tedious and error-prone using pen and paper. It is advisable to use computer algebra systems like MATHEMATICA [147], as was also done in this work and Ref. [3].

Application of the saddle-point expansion to the zero-dimensional $O(N)$ model Taking this expansion for the integrals of type (3.19), it is straightforward to express Eq. (3.18) in a power series in $\frac{1}{N}$. The expansion up to $\mathcal{O}(N^{-2})$ reads,

$$\begin{aligned} \frac{\langle (\vec{\phi}^2)^n \rangle}{N^n} &= \\ &= (2y_0)^n \left(1 + \frac{1}{N} \frac{n[n-1 + (n-3)2y_0^2 V^{(2)}(y_0) - 2y_0^3 V^{(3)}(y_0)]}{[2y_0^2 V^{(2)}(y_0) + 1]^2} + \mathcal{O}\left(\frac{1}{N^2}\right) \right), \end{aligned} \quad (3.29)$$

and is easily extended to higher-order corrections. However, remember that it is exclusively valid for functions $f(y) = V(y) - \frac{1}{2} \ln(y)$ which are analytic around their global minimum y_0 . Using Eq. (3.29) we can again derive expressions for the 1PI vertex functions via Eqs. (2.39) to (2.41) and their generalization.

3.3.2. Crosscheck - the free theory

As a first crosscheck, it is always advisable to return to the free theory, see Section 3.1. (Anyhow, we need these results as being part of our special toy model later on.) For sake of simplicity, we again set $m^2 = 1$ in Eq. (3.1), such that the $\frac{1}{N}$ -rescaled potential reads

$$V_0(y) = y. \quad (3.30)$$

For the corresponding $f(y)$ we find

$$f(y) = V(y) - \frac{1}{2} \ln(y) = y - \frac{1}{2} \ln(y). \quad (3.31)$$

The minimum y_0 of this function is unique and located at

$$0 \stackrel{!}{=} \partial_y f(y) \Big|_{y=y_0} = 1 - \frac{1}{2y_0}. \quad (3.32)$$

Consequently,

$$y_0 = \frac{1}{2}, \quad V(y_0) = \frac{1}{2}, \quad f(y_0) = \frac{1}{2} \left[1 - \ln\left(\frac{1}{2}\right) \right], \quad (3.33)$$

and for the second and third derivatives we have

$$\partial_y^2 V(y)|_{y=y_0} = 0, \quad \partial_y^2 f(y)|_{y=y_0} = 2, \quad (3.34)$$

$$\partial_y^3 V(y)|_{y=y_0} = 0, \quad \partial_y^3 f(y)|_{y=y_0} = -8. \quad (3.35)$$

Obviously, $V(y)$, $f(y)$, and $g(y) = y^{n-1}$ are analytic around $y_0 = \frac{1}{2}$, such that Eq. (3.29) can be used as an approximation. Using the above values in Eq. (3.29) one finds,

$$\frac{1}{N} \langle \vec{\phi}^2 \rangle = 1, \quad \frac{1}{N^2} \langle (\vec{\phi}^2)^2 \rangle = 1 + \frac{2}{N}, \quad \frac{1}{N^3} \langle (\vec{\phi}^2)^3 \rangle = 1 + \frac{6}{N} + \frac{8}{N^2}, \quad \dots \quad (3.36)$$

and from Eqs. (2.39) to (2.41) *etc.*,

$$\Gamma^{(2)} = 1, \quad \text{and} \quad \forall n > 2 \quad \Gamma^{(n)} = 0. \quad (3.37)$$

In fact, these are exact results, as can be seen by direct comparison with Eqs. (3.3) and (3.4). The reason is, that the maximal correction for $\frac{1}{N^n} \langle \vec{\phi}^2 \rangle$ to 1 is always $\mathcal{O}(N^{-(n-1)})$. Expanding to higher order in $\frac{1}{N}$ is therefore useless.

Interestingly, taking the $N \rightarrow \infty$ limit, the result for the vertex functions (3.37) does not change, while the correlation functions (3.36) all reduce to 1. The first result is hardly surprising, because a free theory is a free theory and its IR interaction vertices always have to vanish, independent of the number N of free particles. However, the higher-order correlation functions (3.36) also contain totally unconnected graphs of free propagators, which correspond to many-particle processes, where particles are in fact “passing by” each other and do not interact. These trivial processes depend on the number N of possibly involved non-interacting particles.

3.3.3. ϕ^4 -theory in the $\frac{1}{N}$ -expansion

Next, let us return to the ϕ^4 -theory and see, whether the $\frac{1}{N}$ -expansion yields better performance than perturbation theory, especially for large λ and/or negative mass term m^2 . Hence, w.l.o.g. we consider Eq. (3.8) with $m^2 = \pm 1$,

$$U(\rho) = \pm \rho + \frac{\lambda}{6} \rho^2, \quad \stackrel{(3.17)}{\Rightarrow} \quad V(y) = \pm y + \frac{\lambda'}{6} y^2, \quad \lambda' = N\lambda. \quad (3.38)$$

Checking analyticity of $f(y) = V(y) - \frac{1}{2} \ln(y)$ at its minimum,

$$y_0 = \frac{\mp 3 + \sqrt{9 + 6\lambda'}}{2\lambda'}, \quad (3.39)$$

is trivial, because $y_0 \neq 0$ and all involved functions are analytic for $y > 0$. Hence, we can directly apply the $\frac{1}{N}$ -expansion to both scenarios in Eq. (3.38) at arbitrary λ .

Here, we do not present any further analytic results, even though this would be easily possible. Instead, we evaluate Eqs. (3.29) and (2.39) symbolically using MATHEMATICA [147] and ultimately insert explicit values for n , N , and λ for different expansion orders. These results are compared to exact results for $\Gamma^{(2)}$, which are obtained from brute-force integration of Eqs. (2.12) and (2.39). The idea of benchmarking the $\frac{1}{N}$ -expansion in zero dimensions is not original to ourselves. It was performed in great detail in the excellent Ref. [107] for ϕ^4 -theory with positive mass term. Here, we simply reproduce parts of their Fig. 3, which exemplifies the power of the $\frac{1}{N}$ -expansion already at rather small N by computing $\Gamma^{(2)}$, here for $N = 2$. In Fig. 3.2 we also present an analogous plot for ϕ^4 -theory with negative mass term, which shows similar results concerning the reliability. However, studying higher-order vertex functions, as was also done in Ref. [107], one clearly experiences slower convergence by including higher-order corrections in $\frac{1}{N}$. Furthermore, a more systematic analysis for increasing N at a fixed λ is straightforward and presented in Ref. [107].

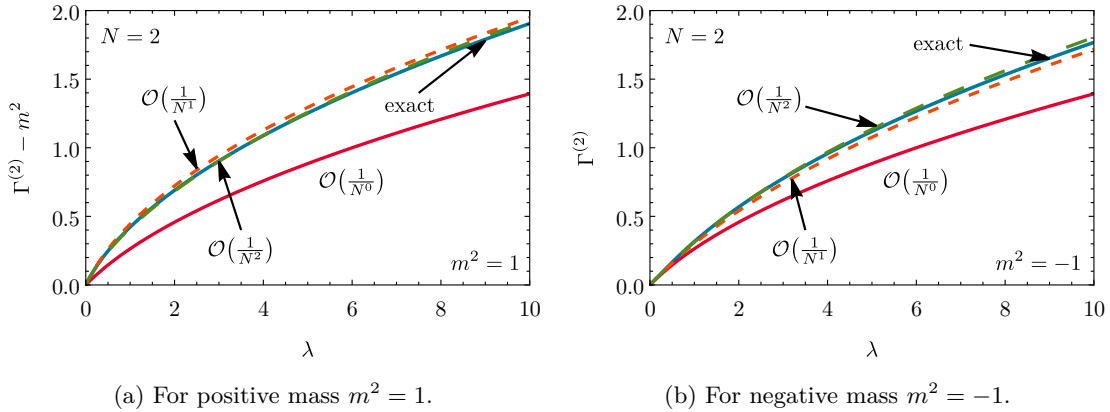


Figure 3.2: The exact result (blue solid line) for $\Gamma^{(2)}$ via Eqs. (2.12), (2.39), and (3.38) and the large- N expansion result from Eqs. (3.29) and (2.39) as functions of λ for $N = 2$. The zeroth order is plotted as a red solid line, the first-order correction as an orange dashed line and the second-order correction as a green dashed line with larger dashing in both panels. The left panel is an adaption of Ref. [107, Fig. 3].

Nonetheless, this work is not about benchmarking the precision of the $\frac{1}{N}$ -expansion with simple toy models, where we totally believe that it yields decent results, also in higher-dimensional generalizations. Rather, we want to demonstrate how the slight modifications in the UV sector of a theory (the UV classical action) can lead the $\frac{1}{N}$ -expansion astray and how the infinite- N limit can totally alter the phenomenology w.r.t. finite N . This is for example of particular relevance in the vicinity of first-order PTs and for condensation/vaporization phenomena, *e.g.*, if an external parameter like the chemical potential is varied. Here, potentials can comprise degenerate global minima and cusps at their physical point. However, in the context of higher-dimensional model calculations it is usually hard to identify these problems, due to a multitude of interfering mathematical challenges and additional approximations.

3.3.4. An instructive toy model to study the failure of the $\frac{1}{N}$ -expansion and problems of the infinite- N limit

To this end we constructed the following seemingly innocent toy model in Ref. [3], which was inspired by Ref. [77]. Its continuous potential is formed by stringing together linear pieces in y , which corresponds to a piecewise quadratic dependence on the scalar field itself. The negative/zero slope of the middle piece depends on some parameter $a \geq 0$. In $\frac{1}{N}$ -rescaled quantities (3.17) it explicitly reads,

$$V(y) = \begin{cases} y & \text{for } 0 \leq y \leq 2, \\ -ay + 2(a+1) & \text{for } 2 < y \leq 8, \\ y - 6(a+1) & \text{for } 8 < y, \end{cases} \quad (3.40)$$

and for its y -derivative we find,

$$v(y) = \partial_y V(y) = \begin{cases} 1 & \text{for } 0 \leq y \leq 2, \\ -a & \text{for } 2 < y \leq 8, \\ 1 & \text{for } 8 < y. \end{cases} \quad (3.41)$$

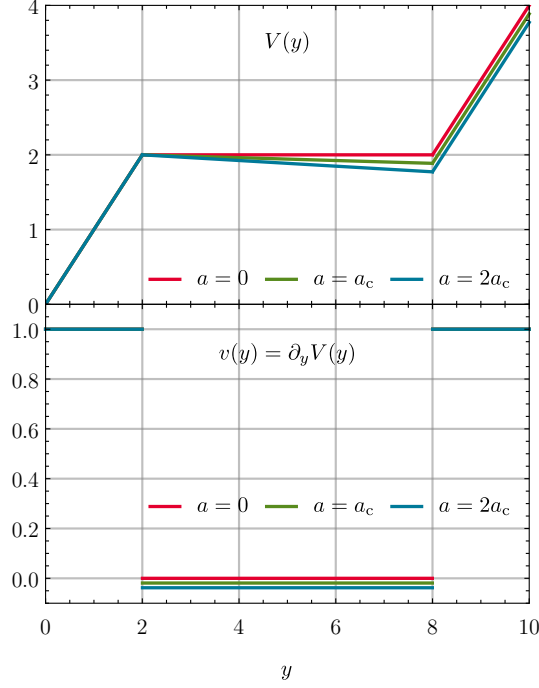


Figure 3.3: The potential $V(y)$ from Eq. (3.40) (upper panel) and its derivative $v(y) = \partial_y V(y)$ from Eq. (3.41) (lower panel) for different values of the parameter a and where a_c is given by Eq. (3.42). From Ref. [3, Fig. 1].

The potential and its y -derivative are illustrated for three different values of a in Fig. 3.3. Here, a_c , which we denote as the critical value for a , is

$$a_c = \frac{1}{4} - \frac{1}{3} \ln(2) \approx 0.018951. \quad (3.42)$$

This terminology and the role of a_c are discussed in the next paragraphs. In addition, another illustration of the potential in the rescaled scalar field

$$x \equiv \frac{1}{\sqrt{N}} \phi, \quad (3.43)$$

is later on provided in Fig. 6.12. It is clearly visible that the UV potential has always a unique global analytic minimum at $y = 0$ for $a \in [0, 2a_c]$. Additionally there is a degenerate flat region for $a = 0$ and a second non-analytic local minimum at $y = 8$ for $0 < a \leq 2a_c$. (Values $a > 2a_c$ are not of relevance for our discussion.)

Exact solution

Before we turn to the actual discussion and the saddle-point expansion, note that this model is exactly integrable. Using the definition of the (incomplete) gamma function (A.36) and (A.37), we find for $a > 0$,

$$\begin{aligned} & \int_0^\infty dy y^{\frac{N}{2}-1} y^n e^{-NV(y)} \stackrel{(3.40)}{=} \\ & = N^{-\left(\frac{N}{2}+n\right)} \left(\Gamma\left(\frac{N}{2}+n\right) - \Gamma\left(\frac{N}{2}+n, 2N\right) + e^{6N(a+1)} \Gamma\left(\frac{N}{2}+n, 8N\right) + \right. \\ & \quad \left. + (-a)^{-\left(\frac{N}{2}+n\right)} e^{-2N(a+1)} \left[\Gamma\left(\frac{N}{2}+n, -2Na\right) - \Gamma\left(\frac{N}{2}+n, -8Na\right) \right] \right), \end{aligned} \quad (3.44)$$

and for $a = 0$,

$$\begin{aligned} & \int_0^\infty dy y^{\frac{N}{2}-1} y^n e^{-NV(y)} \stackrel{(3.40)}{=} \\ & = N^{-(\frac{N}{2}+n)} \left[\Gamma\left(\frac{N}{2} + n\right) - \Gamma\left(\frac{N}{2} + n, 2N\right) + e^{6N} \Gamma\left(\frac{N}{2} + n, 8N\right) + \right. \\ & \quad \left. + e^{-2N} \frac{(4^{\frac{N}{2}+n} - 1)(2N)^{\frac{N}{2}+n}}{\frac{N}{2} + n} \right]. \end{aligned} \quad (3.45)$$

These general integrals can in principle be used to evaluate the arbitrary correlation functions (2.12) by hand and to further obtain the vertex functions (2.39) to (2.41). High-precision numerical evaluation is of course also always possible.

The infinite- N limit of the exact solution

In addition to the exact solution for finite N , we also present the infinite- N limit of this exact solution. For this, we insert Eq. (3.44) or Eq. (3.45), respectively, into the general expression for the correlation function (2.12), which we rescale by $\frac{1}{N^n}$. Afterwards we use Eqs. (A.41) and (A.42) and send $N \rightarrow \infty$. We find for $a = 0$,

$$\lim_{N \rightarrow \infty} \frac{1}{N^n} \langle (\vec{\phi}^2)^n \rangle = 1, \quad (3.46)$$

while for $0 < a \leq 2a_c$,

$$\lim_{N \rightarrow \infty} \frac{1}{N^n} \langle (\vec{\phi}^2)^n \rangle = \begin{cases} 1, & \text{for } a \leq a_c, \\ 16^n, & \text{for } a_c < a \leq 2a_c. \end{cases} \quad (3.47)$$

The corresponding vertex functions in the $N \rightarrow \infty$ limit are

$$\Gamma^{(2)} = \begin{cases} 1, & \text{for } a \leq a_c, \\ \frac{1}{16}, & \text{for } a_c < a \leq 2a_c, \end{cases} \quad \forall n \neq 2 \quad \Gamma^{(n)} = 0. \quad (3.48)$$

For further details we refer to Ref. [3, Appendix A].

3.3.5. Application of the saddle-point expansion

Next, we turn to the saddle-point expansion of the correlation functions for the potential (3.40). To this end, we analyzed and plot the function

$$f(y) = V(y) - \frac{1}{2} \ln(y), \quad (3.49)$$

see Fig. 3.4. We recapitulate that an expansion in $\frac{1}{N}$, thus Eq. (3.29), is exclusively applicable, if $f(y)$ has a unique global minimum y_0 and is analytic around this minimum. Our $f(y)$ has in general two minima $y_{0,1}$ and $y_{0,2}$ with $y_{0,1} < y_{0,2}$. The second minimum is always located at $y_{0,2} = 8$ – the non-analytic cusp of the potential (3.40), while the first minimum agrees with the minimum of $f(y)$ for the free theory, thus $y_{0,1} = \frac{1}{2}$, see Section 3.3.2. The latter is easily understood, because the minimum is always located on the first sector of the potential, where $V(y) = y$, which is identical to the free theory.

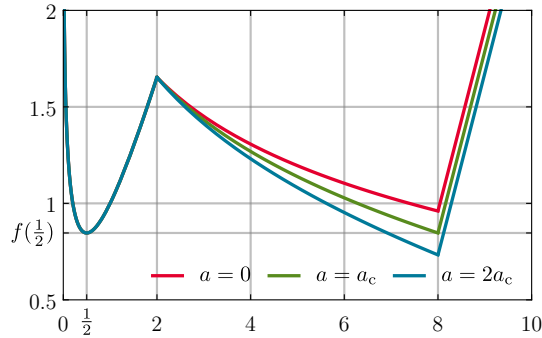


Figure 3.4: The function $f(y) = V(y) - \frac{1}{2} \ln(y)$ for the potential (3.40) for selected values of the parameter a with $a_c = \frac{1}{4} - \frac{1}{3} \ln(2) = 0.018951$. The local minima of $f(y)$ are located at $y_0 = \frac{1}{2}$ and $y_{0,2} = 8$, where y_0 ($y_{0,2}$) is the unique global minimum for $0 \leq a < a_c$ ($a > a_c$). At $a = a_c$ both minima coincide and are global minima of $f(y)$. The non-analyticity of $f(y)$ in $y_{0,2} = 8$ inherited from the piecewise definition of $V(y)$ is clearly visible in the plot. From Ref. [3, Fig. 2].

The number and the position of the minima is independent of the parameter a . However, depending on a , either $y_{0,1}$ or $y_{0,2}$ is the global minimum, while the other one still stays a local minimum. The critical value is $a = a_c$, when both minima of $f(y)$ are degenerate, *i.e.*,

$$f(y_{0,1} = \frac{1}{2}) \stackrel{!}{=} f(y_{0,2} = 8), \quad (3.50)$$

which is exactly the case for a_c previously defined in Eq. (3.42). (This does by no means imply that $V(y_{0,1}) = V(y_{0,2})$.)

We conclude: As long as $a < a_c$ the $\frac{1}{N}$ -expansion of the expectation values (3.29) is perfectly valid, because $f(y)$, $g(y)$, and $V(y)$ are analytic at the expansion point $y_{0,1} = \frac{1}{2}$. Moreover, we simply recover the results of the saddle-point expansion of the free theory from Section 3.3.2, but this time for a highly non-linear interacting theory with non-analytic UV potential. However, in contrast to the free theory, the saddle-point results for the correlation functions (3.36) are an actual approximation to the exact results at finite N , because the latter are calculated from Eqs. (3.45) and (3.44). Now, we could of course start to quantify the quality of this approximation, which is however, not the objective of the discussion. Still, we note that for $N \rightarrow \infty$ the leading order of the $\frac{1}{N}$ -expansion agrees with the $N \rightarrow \infty$ limit of the exact results (3.46) and (3.47). This sounds trivial, but it is not.

On the other hand, if $a \geq a_c$ the situation is totally different. The saddle-point approximation and $\frac{1}{N}$ -expansion is formally¹ no longer applicable, because the expansion point is non-analytic and might not even be unique for $a = a_c$. In this case, we should indeed abstain from using the expansion Eq. (3.29), because an expansion is no longer well-defined. This does of course not alter the fact that the exact result Eq. (3.44) is perfectly valid and also the $N \rightarrow \infty$ limit (3.47) that can be obtained from this result is well-defined.

In summary, we learned:

1. Already tiny variations of parameters in a theory can cause great differences in their phenomenology. This effect is drastically enhanced in the $N \rightarrow \infty$ limit, as can be seen from all correlation functions (3.47), which jump at a_c , while Eq. (3.45) and ratios thereof are continuous functions of a at a_c as long as N is finite. This jump in the correlation functions and vertex functions can be associated with a first-order PT, which is driven by the variation of a , but is totally absent for finite but otherwise arbitrarily large N . In conclusion, the

¹In fact, if one applies the saddle-point expansion at $y_{0,2}$, despite the fact that it is mathematically not allowed, and exclusively uses right-derivatives, one still obtains appropriate results for this toy model. However, this is dangerous and certainly not generalizable.

$N \rightarrow \infty$ limit completely changes the physics of the system. This drastic difference between finite and infinite N and its consequences are again analyzed within the FRG framework for this model.

2. Sometimes it is extremely hard to judge when one is leaving the radius of convergence of an approximation scheme. In the context of smooth UV potentials, which can be written down in closed form, it might be simple to identify the global minimum and judge its quality as an expansion point. Nevertheless, oftentimes the $\frac{1}{N}$ -expansion and the infinite- N limit are applied to UV actions, where this is a highly non-trivial task. For example, consider a boson-fermion system with Yukawa interaction, where the fermions are integrated out. Here, the effective bosonic UV action comprises the logarithm of the fermion determinant and identifying the true ground state of this effective classical action can be challenging. Furthermore, external parameters, like a chemical potential can introduce artificial cusps into these actions, which could even coincide with non-trivial minima of the potential. See Part II for further discussions, details, and examples.

Hence, our simple toy model should be considered as a warning that the $\frac{1}{N}$ -expansion and infinite- N limit can fundamentally spoil the phenomenology. In addition, these methods are not by themselves sensitive to their limitations.

3.3.6. Summary

In this chapter we demonstrated on the basis of two examples, *i.e.*, perturbation theory and the $\frac{1}{N}$ -expansion (including the infinite- N limit), that there is a manifest need for non-perturbative methods, which also avoid the direct evaluation of the integrals in the partition function and expectation values, but which are

1. independent of the number and (relative) strength of couplings.
2. insensitive to the analyticity/smoothness of the involved actions.
3. not based on a specific expansion point.
4. work reliable in all kinds of limits of a theory (*e.g.*, small *vs.* infinite N) and under the variation of external parameters.

In addition, we demonstrated that it needs challenging but exactly solvable test cases to study the quality and predictability of a method under a controlled environment. It is simply not enough to use standard ϕ^4 -theory as a benchmark test, which is anyhow oftentimes the case in the literature.

Chapter 4

The Functional Renormalization Group from zero spacetime dimensions

Abstract In this chapter we provide a pedagogical and perhaps unconventional introduction to the FRG method. Without having to understand the physical concepts of coarse-graining, RG scales, and renormalization *etc.* we derive the ERG equation – the Wetterich equation – in zero-dimensional spacetime. We start off with some simple observations concerning the generating functional for correlation functions and deduce a flow equation for this functional, which smoothly interpolates between a trivial theory and the theories that we are actually interested in. We show how to transform this flow equation into a flow equation for the generating functional for 1PI vertex functions and how to find the correct initial condition for the latter. For the entire discussion we again use the model of N identical real scalars with possible $O(N)$ symmetry. Afterwards we turn to truncations of the flow equation and explain why these are actually not needed in zero spacetime dimensions, which makes zero-dimensional FRG a perfect testing ground. We derive and discuss the exact flow equation for the local potential, but also introduce an artificial truncation scheme, the FRG Taylor expansion. Both are studied numerically in later chapters. Finally, we discuss symmetry breaking/restoration during the RG flow.

Disclosure This chapter is completely based on our own publications [1, 2, 3] and especially follows the discussion of Ref. [1, Chap. II & Appendix B d], which was in turn partially inspired by Refs. [106, 109, 107, 108, 110, 135, 136]. However, the presentation of the material in this thesis slightly differs in its presentation from the corresponding publication [1] and is exclusively written by the author. General introductions to the FRG in higher dimensions can be found for example in Refs. [53, 54, 55, 56, 57, 100, 35].

4.1. Solving integrals with flow equations

Having briefly analyzed two alternative methods to the brute-force calculation of expectation values in the previous chapter, which were not able to produce satisfactory results, we finally turn to the FRG as a possibly more powerful alternative and strictly non-perturbative method.

We start our discussion with a simple observation: As we have already experienced in Section 3.1 there are QFTs where the calculation of all correlation and vertex functions is trivial. These are free non-interacting (massive) theories, which simply correspond to standard Gaussian-type integrals in the functional-integral formalism, and their correlation functions can be identified as

the standard Gaussian moments. This basically generalizes to arbitrary spacetime dimensions and field types.

Let us assume that we add some arbitrary higher-order interacting terms to a free theory, such that the theory is no longer exactly integrable. Furthermore, let us assume that the coefficient of the quadratic term, the positive mass, is huge compared to all other interaction terms in the action. In addition, we know that the probability-distribution function for the microstates is formed by the exponential of the negative action, see Eq. (2.4). This implies that the integrands in the correlation functions (2.5) are completely dominated by the quadratic mass term and almost perfectly approximate Gaussian integrands, because higher-order contributions from interaction terms exclusively enter in the tail of the probability distribution, which hardly contributes to the integrals, due to the strong exponential suppression. Thus, by sending the (positive) mass to extremely large values, basically any theory turns into a quasi-free ultra-massive Gaussian non-interacting integrable theory.

So, what if we introduce an artificial mass term into the partition function of a theory that we are interested in and by hand manipulate its magnitude, such that a complicated interacting theory can be transformed into a trivial quasi-free theory and vice versa? If this transition could be described dynamically by some evolution equation, there was a chance to calculate the correlation and vertex functions of highly complicated theories from a particular evolution starting with trivial Gaussian correlation and vertex functions. Instead of calculating high-dimensional functional integrals, we “only” had to solve the evolution equation(s).

In fact, exactly this is possible and done by the FRG method, which is explained in the following using the zero-dimensional model of N real scalars from Chapter 2.

Of course, the FRG and the RG in general are based on many more physical and mathematical ideas and observations. For a pedagogical introduction to the concepts behind, we refer to Ref. [161] or the FRG-specific Refs. [53, 54, 55, 56, 57, 100, 35]. We come back to these ideas at various occasions throughout the discussions of this thesis, but do not go into detail here.

4.1.1. The scale-dependent partition function

As motivated in the previous paragraph, we use the zero-dimensional model of N real scalars and introduce an artificial mass-like term into the action and the partition function (2.13),

$$\mathcal{Z}(t, \vec{J}) \equiv \mathcal{N} \int_{-\infty}^{\infty} d^N \phi \, e^{-\mathcal{S}(\vec{\phi}) - \Delta\mathcal{S}(t, \vec{\phi}) + \vec{J}^T \cdot \vec{\phi}}. \quad (4.1)$$

This term is sometimes denoted as the regulator insertion and reads

$$\Delta\mathcal{S}(t, \vec{\phi}) \equiv \frac{1}{2} \vec{\phi}^T R(t) \vec{\phi} = \frac{1}{2} \phi_i R_{ij}(t) \phi_j. \quad (4.2)$$

So far we do not assume $O(N)$ symmetry of the theory. Consequently it is advisable to choose a diagonal mass term, which does not introduce additional interactions between the fields, but is still applicable to $O(N)$ -symmetric theories,

$$R(t) \equiv \mathbb{1} r(t), \quad \leftrightarrow \quad R_{ij}(t) = \delta_{ij} r(t). \quad (4.3)$$

The higher-dimensional analogues of R and r are usually called the regulator and the regulator-shape function and are oftentimes energy/momentum-dependent.¹ This directly brings us to their dependence on the so-called RG time t . In higher-dimensional models the RG time t is directly linked to the RG scale k , usually via the UV cutoff Λ , see Appendix D.1. However, in zero spacetime dimensions there is no notion of an energy scale which can serve as a “momentary” reference scale for the energies and momenta occurring in loops, like in higher dimensions, because

¹For details on higher-dimensional regulator(-shape) functions, we refer to Refs. [162, 163, 54, 100, 164, 165, 166, 167].

in zero dimensions there are no loop momenta *etc.*. Anyhow, in zero dimensions we still use the concept of the UV cutoff Λ , which simply refers to a plain number, and is larger than any other “scale” in the model, *e.g.*, couplings, other parameters *etc.*. Here, Λ is simply associated to the maximal artificial “mass” per particle that is introduced by the regulator – the coefficient of the quadratic term in the action. In turn, the RG time is used to smoothly interpolate between a theory with this huge mass Λ (in the UV) and the original theory without the artificial additional mass-like term (in the IR). (The association of small t with the UV and large t with the IR is explained below, when we turn to the 1PI formalism.) In fact, it can be interpreted as the zero-dimensional version of Callan-Symanzik-type regulators, *cf.* Ref. [167]. Therefore, w.l.o.g.² we choose the following regulator-shape function and domain for t ,

$$r(t) = \Lambda e^{-t}, \quad t \in [0, \infty). \quad (4.4)$$

Thus, for $t = 0$ we have $r(t = 0) = \Lambda$ and the theory is approximately Gaussian and all correlation functions are known. Oppositely, for $t \rightarrow \infty$ we recover the original partition function (2.13) and the correlation functions, that we are interested in in the first place.

For practical (and numerical) purposes it usually suffices (is necessary) to stop at some finite t_{IR} , which still has to correspond to an extremely small $r(t_{\text{IR}}) = r_{\text{IR}} \gtrsim 0$, and has to be much smaller than all other “scales” in the model. This is referred to as the IR cutoff time/scale.

The role of the regulator – a visualization

For better understanding of the effect of $r(t)$ on integrals like Eq. (4.1), we plot its integrand for $N = 1$ and $J = 0$ for two different \mathbb{Z}_2 -symmetric actions. In Fig. 4.1a we use the action (3.7) of the ϕ^4 -theory with negative mass term, while Fig. 4.1b shows the dependence on t for a non-analytic but otherwise perfectly valid classical action,

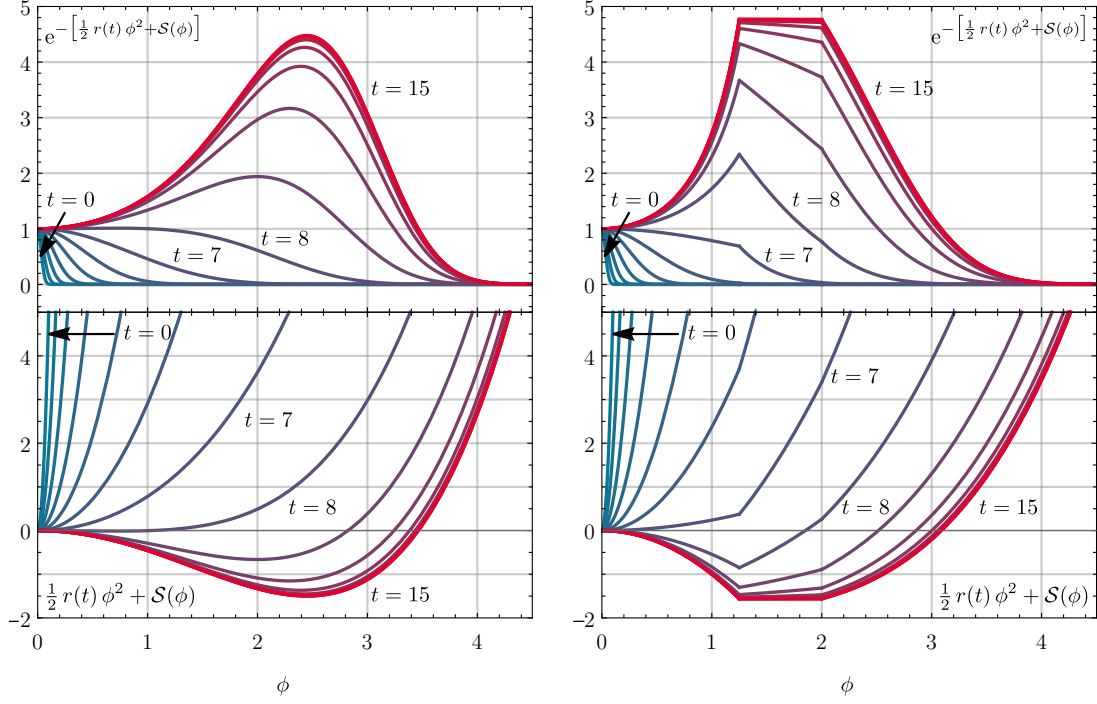
$$\mathcal{S}(\phi) = \begin{cases} -\phi^2, & \text{if } |\phi| \leq \frac{5}{4}, \\ -\left(\frac{5}{4}\right)^2, & \text{if } \frac{5}{4} < |\phi| \leq 2, \\ \frac{1}{48}(\phi^4 - 91), & \text{if } 2 < |\phi|. \end{cases} \quad (4.5)$$

The plots clearly demonstrate how $r(t)$ deforms the actions from ultra-massive free smooth actions, which are quadratic in ϕ , into their actual shape, while the exponential integrand turns from a Gaussian-shape distribution into the more complex original probability distribution. As long as Λ is much larger than the other parameters of the actions, the Gaussian character clearly dominates. However, when $r(t)$ reaches the magnitude of the other parameters in the action, which is of order one, we observe a rapid change until $r(t)$ ultimately becomes irrelevant for large t and the original action/probability distribution is recovered.

4.1.2. The heat equation – an evolution equation for the scale-dependent generating functional of (connected) correlation functions

So far we introduced a term into our original theory, the regulator, which allows to smoothly interpolate between a trivial quasi-free Gaussian theory and the theory that we are originally interested in. Next, we examine how this evolution can be described mathematically.

²The only two requirements for the regulator-shape function, apart from the correct $t = 0$ and $t \rightarrow \infty$ limits, are that $r(t) \in C^1$, such that its first derivative exists for all t , see also Ref. [100]. In addition we demand $\forall t \partial_t r(t) \leq 0$. This guarantees that the regulator can always be interpreted as a mass term and monotonically decreases with t . The need for both aspects becomes clear within the next lines. Furthermore, note that all regulators that fulfill these criteria are reparametrization-invariant in zero dimensions. This does not generalize to higher-dimensional theories.

(a) For the action (3.7) with $m^2 = \lambda = 1$.

(b) For the action (4.5).

Figure 4.1: The integrand (upper panel) and the exponent (classical action plus regulator insertion) of Eq. (4.1) for $N = 1$ at $J = 0$ as a function of the field variable ϕ for various RG times t . The UV cutoff is $\Lambda = 10^3$, which is notably larger than the model parameters, and the IR cutoff $r_{\text{IR}} \simeq 3.06 \cdot 10^{-4}$ is significantly smaller than all model scales and corresponds to $t = 15$. From Ref. [1, Figs. 1 & 2].

A flow equation for $\mathcal{Z}(t, \vec{J})$

As usual, if we study changes of quantities with time – here RG time – we take derivatives w.r.t. t of these quantities. For Eq. (4.1) this leads to

$$\begin{aligned}
 \partial_t \mathcal{Z}(t, \vec{J}) &= - \left[\frac{1}{2} \partial_t r(t) \right] \mathcal{N} \int_{-\infty}^{\infty} d^N \phi \vec{\phi}^2 e^{-S(\vec{\phi}) - \Delta S(t, \vec{\phi}) + \vec{J} \cdot \vec{\phi}} = \\
 &= - \left[\frac{1}{2} \partial_t r(t) \right] \delta_{ij} \frac{\partial^2 \mathcal{Z}(t, \vec{J})}{\partial J_j \partial J_i} = \\
 &= - \left[\frac{1}{2} \partial_t r(t) \right] \Delta_{\vec{J}} \mathcal{Z}(t, \vec{J}),
 \end{aligned} \tag{4.6}$$

where $\Delta_{\vec{J}}$ is the Laplace operator in the space of source-fields \vec{J} . On a formal level, this RG equation constitutes a PDE for the scale-dependent partition function $\mathcal{Z}(t, \vec{J})$ on the infinite domain $\vec{J} \in \mathbb{R}^N$. The RG time plays the role of the evolution parameter – the time – and the source-field space \vec{J} is identified with the spatial domain. The equation is of first order in time and of second order in its spatial derivatives. In fact, we identify Eq. (4.6) as a conventional heat/diffusion equation [168], a fact which is also known in the FRG community [124, 100, 169]. In order to be a well-posed problem with unique (weak) solution and stable convergence according to Hadamard, it is well-known that the diffusion coefficient of the heat equation needs to be

positive semi-definite [168, 49, 50], *i.e.*,

$$D = -\frac{1}{2} \partial_t r(t) \geq 0. \quad (4.7)$$

This is indeed ensured by the monotonicity of the regulator shape function, see also Refs. [100, 164].³

A direct consequence of the RG evolution being described by a diffusion equation, which also generalizes to higher spacetime dimensions, is that the equation itself singles out a unique direction of time from the UV ($t = 0$) to the IR ($t \rightarrow \infty$). The reason is that diffusion is a dissipative manifestly irreversible process and linked to the production of entropy. This introduces a thermodynamic arrow of time and time asymmetry [170] and backwards integration is impeded. It is manifest on the level of the PDE and its numeric solution, as will be discussed in detail in later chapters.

However, to be well-posed, one also needs to specify boundary and initial conditions for the PDE. Formally, boundary conditions are not needed here, because the PDE is defined on all \mathbb{R}^N and an initial condition suffices. It is a pure initial-value/Cauchy problem [104]. Unfortunately, the initial condition is basically identical for any UV action $\mathcal{S}(\vec{\phi})$, because it is by construction an almost perfect Gaussian,

$$\mathcal{Z}(t = 0, \vec{J}) \approx \mathcal{N} \left(\frac{2\pi}{\Lambda} \right)^{\frac{N}{2}} e^{\frac{\vec{J}^2}{2\Lambda}}. \quad (4.8)$$

This implied that RG flows for $\mathcal{Z}(t = 0, \vec{J})$ of totally different classical actions $\mathcal{S}(\vec{\phi})$ are identical, which is nonsense. Thus, one had to include the tiny deviations from the perfect Gaussian shape, which are caused by the different higher-order interaction contributions in $\mathcal{S}(\vec{\phi})$, to obtain different initial conditions. This, however, would require to solve the high-dimensional functional integrals which we wanted to avoid in the first place.

In conclusion, Eq. (4.6) is perfectly valid, but seems to be problematic for practical (numerical) computations, see Ref. [1] for further details. Furthermore, we mentioned several times in Section 2.1 that the generating functional for correlation functions is anyhow not the optimal choice of storing information about a QFT.

Therefore, we turn to the other two generating functionals that were introduced in Section 2.1, *i.e.*, the generating functional of connected correlation functions, Def. (2.15), and the generating functional of 1PI vertex functions, Def. (2.20).

A flow equation for $\mathcal{W}(t, \vec{J})$

It is straightforward to generalize the definition of the generating functional of connected correlation functions to its scale-dependent counterpart. One simply uses Def. (4.1) and defines

$$\mathcal{W}(t, \vec{J}) \equiv \ln \mathcal{Z}(t, \vec{J}), \quad (4.9)$$

which starts off in the UV at $t = 0$ as an almost perfect parabolic function of the source fields \vec{J} , *cf.* Eq. (4.8), and approaches its physical value for $t \rightarrow \infty$.

Using the identities of Section 2.1.3 and the flow equation (4.6), we arrive at an RG flow equation for $\mathcal{W}(t, \vec{J})$,

$$\partial_t \mathcal{W}(t, \vec{J}) = - \left[\frac{1}{2} \partial_t r(t) \right] \left[\Delta_{\vec{J}} \mathcal{W}(t, \vec{J}) + \left(\frac{\partial}{\partial J_i} \mathcal{W}(t, \vec{J}) \right) \left(\frac{\partial}{\partial J_i} \mathcal{W}(t, \vec{J}) \right) \right]. \quad (4.10)$$

In analogy to the flow equation (4.6) we are confronted with a heat equation with manifestly positive diffusion coefficient. However, in addition to the conventional “heat-flux” another term

³Note that zero-dimensional spacetime allows to eliminate $\partial_t r(t)$ from the equation by appropriate reparametrization of the temporal coordinate, which anyhow keeps the structure of the equation unchanged and again emphasizes that all valid regulators are identical up to a reparametrization. In higher-dimensional spacetimes this is no longer the case.

is generated, which is quadratic in the first spatial derivative of the abstract fluid field $\mathcal{W}(t, \vec{J})$. This turns the problem into a non-linear PDE, which in general complicates its solution.

Anyhow, we are again confronted with the same shortcoming as before. The initial condition is to first approximation identical for any possible $\mathcal{S}(\vec{\phi})$. However, incorporating the tiny deviations from $\mathcal{W}(t=0, \vec{J}) \propto \vec{J}^2$ required to solve the functional integral from Eq. (4.1) including interaction terms. However, this was what we wanted to avoid in the first place by turning to perturbation theory, the $\frac{1}{N}$ -expansion, and the FRG method.

Note: Interestingly, the flow equation (4.10) is structurally identical to Polchinski's RG flow equation for the RG flow of effective Lagrangians [171, 100] and similar to the flow equations used in Ref. [102]. In turn, these flow equations do not exhibit the problem of indistinguishable initial conditions, because there the abstract fluid is the effective Lagrangian (Wilson's effective action) itself.

Anyhow, we turn to yet another generating functional and its associated exact RG flow equation and demonstrate that it has well-defined and distinguishable initial conditions for separate theories – the Wetterich equation.

4.2. The exact renormalization group equation – the Wetterich equation

In a first step, we generalize the definition of the generating functional of 1PI vertex functions (2.20) (the effective action) to a scale-dependent version using the Legendre transformation of Eq. (4.9),

$$\Gamma(t, \vec{\varphi}) \equiv \sup_{\vec{J}} \{ \vec{J} \cdot \vec{\varphi} - \mathcal{W}(t, \vec{J}) \} = \vec{J}(t, \vec{\varphi}) \cdot \vec{\varphi} - \mathcal{W}(t, \vec{J}(t, \vec{\varphi})). \quad (4.11)$$

Note that the evaluation on the supremum makes the sources RG-time- and field-dependent. Furthermore, we introduce the so-called effective average action,

$$\bar{\Gamma}(t, \vec{\varphi}) \equiv \Gamma(t, \vec{\varphi}) - \Delta\mathcal{S}(t, \vec{\varphi}), \quad (4.12)$$

where we subtract the regulator insertion (4.2) from Eq. (4.11). Both generating functionals, Eqs. (4.11) and (4.12), have the correct IR limit for $t \rightarrow \infty$ and approach the 1PI IR effective action (2.20). Their UV behavior is, however, different, and discussed below. (Within the next lines it becomes clear why one uses Eq. (4.12) instead of Eq. (4.11) for practical computations.)

4.2.1. A flow equation for $\bar{\Gamma}(t, \vec{\varphi})$

The derivation of the exact RG flow equation for the effective average action (4.12) is straightforward. One starts again by taking the time derivative of the generating functional. The actual calculation is presented in the next lines, with explicit references to the used identities at the end of the lines,

$$\begin{aligned} \partial_t \bar{\Gamma}(t, \vec{\varphi}) &\stackrel{(4.12)}{=} \quad (4.13) \\ &= \partial_t (\Gamma(t, \vec{\varphi}) - \Delta\mathcal{S}(t, \vec{\varphi})) \stackrel{(4.11)}{=} \\ &= \partial_t (\vec{J}(t, \vec{\varphi}) \cdot \vec{\varphi} - \mathcal{W}(t, \vec{J}(t, \vec{\varphi})) - \Delta\mathcal{S}(t, \vec{\varphi})) \stackrel{(4.2)}{=} \\ &= (\partial_t \vec{J}(t, \vec{\varphi})) \cdot \vec{\varphi} - \partial_t \mathcal{W}(t, \vec{J}(t, \vec{\varphi})) - (\partial_t J_i(t, \vec{\varphi})) \left[\frac{\partial}{\partial J_i} \mathcal{W}(t, \vec{J}) \right]_{\vec{J}=\vec{J}(t, \vec{\varphi})} - \left(\frac{1}{2} \partial_t r(t) \right) \vec{\varphi}^2 \stackrel{(2.21)}{=} \end{aligned}$$

$$\begin{aligned}
&= -\partial_t \mathcal{W}(t, \vec{J}(t, \vec{\varphi})) - \left(\frac{1}{2} \partial_t r(t)\right) \vec{\varphi}^2 \stackrel{(4.10), (2.21)}{=} \\
&= \left(\frac{1}{2} \partial_t r(t)\right) \delta_{ij} \frac{\partial^2 \mathcal{W}(t, \vec{J})}{\partial J_j \partial J_i}.
\end{aligned}$$

In a final step, we have to express the scale-dependent connected two-point correlation function to formulate the entire flow equation on the level of the vertex functions. We use Eqs. (2.26) and (4.12) and find,

$$\partial_t \bar{\Gamma}(t, \vec{\varphi}) = \left(\frac{1}{2} \partial_t r(t)\right) \delta_{ij} G^{\vec{\varphi}\vec{\varphi}}(t, \vec{\varphi})_{ji} = \left(\frac{1}{2} \partial_t r(t)\right) \delta_{ij} \left(\bar{\Gamma}^{\vec{\varphi}\vec{\varphi}}(t, \vec{\varphi}) + R(t)\right)_{ji}^{-1}. \quad (4.14)$$

This equation is the zero-dimensional version of the ERG equation or Wetterich equation for a model of N real scalars. In its general form for possibly non-diagonal regulators in arbitrary spacetime dimensions and with arbitrary field content, this equation reads

$$\partial_t \bar{\Gamma}_t[\Phi] = \text{STr} \left[\left(\frac{1}{2} \partial_t R_t\right) G_t[\Phi] \right], \quad (4.15)$$

where Φ contains all degrees of freedom of a system and STr is the “supertrace” that accounts for sign flips due to anti-commutation of fermionic components *etc.*. For further information, we refer to Appendix C.2, where a detailed derivation of the Wetterich equation is presented for arbitrary field content in an arbitrary number of spacetime dimensions, and Refs. [54, 172, 35].

Anyhow, a few comments concerning the form of Eq. (4.14) are in order. In general, the equation is still a diffusion-type equation. It is first order in its temporal derivative and of second order in its spatial derivatives. The spatial domain is now the mean-field space and the spatial coordinates are $\vec{\varphi} \in \mathbb{R}^N$. In contrast to the previous RG flow equations (4.6) and (4.10), we are confronted with an inverse dependence on the second derivative of the abstract fluid field $\bar{\Gamma}(t, \vec{\varphi})$. The equation therefore surely keeps its dissipative character, but diffusion is not necessarily enhanced in regions of high gradients and vice versa. We shed light on the true underlying structure of this equation in the next chapter. For the moment we simply turn to the issue of an appropriate initial condition for this PDE, because the PDE is still a Cauchy problem without boundary conditions, since the domain of the PDE is not compact and not finite.

4.2.2. A proper UV initial condition for the RG flow of the effective average action

To find the initial condition for Eq. (4.14) we have to calculate the $t \rightarrow 0$ limit of the effective average action (4.12). The starting point of this discussion is the identity

$$e^{-\Gamma(t, \vec{\varphi})} = e^{\ln \mathcal{Z}(t, \vec{J}(t, \vec{\varphi})) - \vec{J}^T(t, \vec{\varphi}) \cdot \vec{\varphi}} = \mathcal{N} \int_{-\infty}^{\infty} d^N \phi e^{-S(\vec{\phi}) - \Delta S(t, \vec{\phi}) + \vec{J}^T \cdot (\vec{\phi} - \vec{\varphi})}, \quad (4.16)$$

which simply follows from the Defs. (4.1), (4.9), and (4.11).

Firstly, we shift the integration variables by the mean fields, $\vec{\phi} \mapsto \vec{\phi}' = \vec{\phi} - \vec{\varphi}$, which is the same shift that is frequently deployed in the background-field formalism to study fluctuations about the expectation value of the field [145, 173]. Secondly, we use the t -dependent version of Eq. (2.23) and find,

$$e^{-\bar{\Gamma}(t, \vec{\varphi})} = \mathcal{N} \int_{-\infty}^{\infty} d^N \phi' e^{-S(\vec{\phi}' + \vec{\varphi}) - \Delta S(t, \vec{\phi}') - r(t) \vec{\phi}'^T \cdot \vec{\varphi} + \bar{\Gamma}^{\vec{\varphi}\vec{\varphi}}(t, \vec{\varphi})_i \phi'_i}. \quad (4.17)$$

The two rightmost terms in the exponent can be combined and we have

$$\bar{\Gamma}(t, \vec{\varphi}) = -\ln \int_{-\infty}^{\infty} d^N \phi \left(\frac{r(t)}{2\pi}\right)^{\frac{N}{2}} e^{-S(\vec{\phi} + \vec{\varphi}) - \frac{1}{2} r(t) \vec{\phi}^2 + \bar{\Gamma}^{\vec{\varphi}\vec{\varphi}}(t, \vec{\varphi})_i \cdot \phi_i} - \ln \mathcal{N} \left(\frac{2\pi}{r(t)}\right)^{\frac{N}{2}}. \quad (4.18)$$

Here, we renamed the integration variable and introduced the normalization factor of an N -dimensional Gaussian integral with mass $r(t)$. Now we are ready to analyze the $t \rightarrow 0$ limit of $\bar{\Gamma}(t, \vec{\varphi})$.

In the integral on the r.h.s. the classical action does not depend on t , while the last term in the exponent is of higher order. The middle term of the exponent, however, approaches an N -dimensional Dirac delta distribution

$$\lim_{t \rightarrow 0} \left(\frac{r(t)}{2\pi} \right)^{\frac{N}{2}} e^{-\frac{1}{2} r(t) \vec{\phi}^2} \approx \delta^{(N)}(\vec{\phi}), \quad (4.19)$$

as long as Λ is much larger than all scales in $\mathcal{S}(\vec{\phi})$. Thus, denoting

$$c(t) = -\ln \mathcal{N} \left(\frac{2\pi}{r(t)} \right)^{\frac{N}{2}}, \quad (4.20)$$

the $t \rightarrow 0$ limit of the effective average action is

$$\bar{\Gamma}(t, \vec{\varphi}) \rightarrow -\ln \int_{-\infty}^{\infty} d^N \phi \delta^{(N)}(\vec{\phi}) e^{-\mathcal{S}(\vec{\phi} + \vec{\varphi}) + \bar{\Gamma}^{\vec{\varphi}}(t, \vec{\varphi})_i \phi_i} + c(t) = \mathcal{S}(\vec{\varphi}) + c(t). \quad (4.21)$$

We identify the initial condition for the RG flow equation of the effective average action as the classical action evaluated for the mean fields $\vec{\varphi}$ (up to a scale-dependent constant, which we ignore for a moment). Different models with distinct classical actions $\mathcal{S}(\vec{\varphi})$ therefore correspond to different well-defined initial conditions and generally distinguishable RG flows.

This also explains why $t = 0$ is denoted as the UV and $t \rightarrow \infty$ as the IR: The effective average action simply continuously interpolates between the classical microscopic UV action $\mathcal{S}(\vec{\varphi})$ and the full-quantum IR effective action $\Gamma(\vec{\varphi})$. This transition from micro- to macro-physics is exactly described by the ERG equation (4.14). In higher-dimensional spacetime it goes hand in hand with continuously integrating out momentum shells, which makes the Wetterich equation the direct implementation of Wilson's concept [174, 175, 176, 161] of the RG.

However, it remains to analyze the role of the scale-dependent but field-independent constant (4.20). The problem is that for $t \rightarrow 0$ its absolute value is large, $c(t) \sim \ln r(t)$. Therefore, by including this term, the initial condition for the RG flow would be completely dominated by this large constant and the differences of different $\mathcal{S}(\vec{\varphi})$ would again be hardly visible. Anyhow, an overall field-independent term is always irrelevant for all physical observables, which are either obtained from the IR vertex functions or from relative differences in $\Gamma(\vec{\varphi})$. In both cases the t -dependent constant drops out. In addition, inspecting Eq. (4.14), one finds that the r.h.s. of the PDE exclusively depends on the second derivative of $\bar{\Gamma}(t, \vec{\varphi})$, such that the t -dependent constant does not modify the evolution of $\bar{\Gamma}(t, \vec{\varphi})$ itself. We conclude that the t -dependent term (4.20) can be ignored and dropped from practical calculations.

In summary, the Wetterich equation (4.15) is the evolution equation that we were looking for: It allows to circumvent the brute-force calculation of functional integrals like Eq. (2.12). The price to be paid is that one has to solve in general a highly non-linear multi-dimensional PDE. Instead of calculating the correlation functions, one extracts the vertex functions from the solution of the PDE by taking field-space derivatives at its minimum, *cf.* Section 2.2.2. In zero dimensions, this is of course cumbersome compared to the direct calculation of expectation values, while for higher-dimensional problems, it could be an advantage. Unfortunately, in higher-dimensional spacetimes, the Wetterich equation even turns into a functional partial-integro differential equation, which usually cannot be solved exactly and calls for approximations. The question is therefore how solving this equation is done in practice. This is the topic of the following two sections.

4.3. The ERG equation without truncations – a PDE for the local potential of the zero-dimensional $O(N)$ model

As it stands, even the zero-dimensional Wetterich equation for a model of N real scalars is a tough problem, because it is an N -dimensional PDE, and without further constraints, there is nothing we can do about it.

Fortunately, most problems in QFT are heavily constrained by symmetries of all kind. For the (functional) integrals in the calculation of correlation functions like Eq. (2.7) the $O(N)$ symmetry was used to reduce the dimensionality of the integration from N to 1. A similar approach is usually taken in the FRG formalism: It is known that the IR effective action only comprises terms which are in accordance with the UV symmetries of the system – the symmetries of the partition function [144, 145, 19, 177, 13]. Hence, during the RG flow all kinds of interaction terms and couplings are generated, but all of them have to preserve the symmetries from the UV. (Of course, this is not the case for the vacuum/ground state, which is extracted as the minimum of the IR effective action and can break symmetries, which is spontaneous symmetry breaking during the RG flow.)

Having this in mind, it is advisable to write down the scale-dependent effective average action in terms of scale-dependent function(al)s of invariants of the UV symmetries and to study the RG flow of these function(al)s.

4.3.1. The flow equation of the local potential of the $O(N)$ model

For the zero-dimensional $O(N)$ model this is simple. The only possible $O(N)$ -invariant structure, which is built up from the $O(N)$ invariant of the mean fields $\vec{\varphi}$,

$$\varrho = \frac{1}{2} \vec{\varphi}^2, \quad (4.22)$$

is a scale-dependent effective potential $U(t, \vec{\varphi}) = U(t, \varrho)$. In the UV at $t = 0$ it simply matches the classical potential of Chapter 2. The effective average action is therefore described on all RG scales by

$$\bar{\Gamma}(t, \vec{\varphi}) = U(t, \vec{\varphi}) = U(t, \varrho), \quad (4.23)$$

and starts off in the UV as the classical action/potential $\mathcal{S}(\vec{\varphi}) = \mathcal{S}(\varrho) = U(\varrho)$. Inserting this in the ERG equation (4.14) we obtain an exact flow equation, which is effectively two-dimensional – one temporal coordinate (the RG time t) and a single spatial coordinate (the invariant ϱ).

In order to also reduce the r.h.s. of Eq. (4.14) to a dependence on t and ϱ , we have to invert the matrix-valued two-point function and calculate the propagator. This is done as follows.

We calculate the first two derivatives of Eq. (4.23) w.r.t. the components of $\vec{\varphi}$,

$$\bar{\Gamma}^{\vec{\varphi}}(t, \vec{\varphi})_i \equiv \frac{\partial}{\partial \varphi_i} \bar{\Gamma}(t, \vec{\varphi}) = \varphi_i \partial_\varrho U(t, \varrho), \quad (4.24)$$

$$\bar{\Gamma}^{\vec{\varphi}\vec{\varphi}}(t, \vec{\varphi})_{ji} \equiv \frac{\partial^2}{\partial \varphi_j \partial \varphi_i} \bar{\Gamma}(t, \vec{\varphi}) = \delta_{ji} \partial_\varrho U(t, \varrho) + \varphi_j \varphi_i \partial_\varrho^2 U(t, \varrho). \quad (4.25)$$

These and the Def. (4.3) of the regulator can be used to write down the components of the full field-dependent matrix-valued two-point vertex function,

$$(\bar{\Gamma}^{\vec{\varphi}\vec{\varphi}}(t, \vec{\varphi}) + R(t))_{ji} = \delta_{ji} [r(t) + \partial_\varrho U(t, \varrho)] + \varphi_j \varphi_i \partial_\varrho^2 U(t, \varrho). \quad (4.26)$$

The inverse of this object is generated as follows. We introduce the field-space projectors which project onto the one-dimensional subspace which is parallel (\parallel) to the field-space vector $\vec{\varphi}$, and onto the $(N - 1)$ -dimensional subspace that is perpendicular (\perp) to the same vector respectively,

$$\mathcal{P}_{ji}^{\parallel}(\vec{\varphi}) \equiv \frac{\varphi_j \varphi_i}{\vec{\varphi}^2}, \quad \mathcal{P}_{ji}^{\perp}(\vec{\varphi}) \equiv \delta_{ji} - \frac{\varphi_j \varphi_i}{\vec{\varphi}^2}. \quad (4.27)$$

As is convenient for any reasonable projectors, they are idempotent, orthogonal, and complete. Using these projectors, the two-point function is split into parallel and perpendicular contributions

$$\begin{aligned} (\bar{\Gamma}^{\bar{\varphi}\bar{\varphi}}(t, \bar{\varphi}) + R(t))_{ji} &= \mathcal{P}_{ji}^{\perp}(\bar{\varphi}) [r(t) + \partial_{\varrho}U(t, \varrho)] + \\ &+ \mathcal{P}_{ji}^{\parallel}(\bar{\varphi}) [r(t) + \partial_{\varrho}U(t, \varrho) + 2\varrho \partial_{\varrho}^2U(t, \varrho)], \end{aligned} \quad (4.28)$$

The inversion of this object is now simple, due to the projector properties. One finds

$$\begin{aligned} (\bar{\Gamma}^{\bar{\varphi}\bar{\varphi}}(t, \bar{\varphi}) + R(t))_{ji}^{-1} &= \mathcal{P}_{ji}^{\perp}(\bar{\varphi}) \frac{1}{r(t) + \partial_{\varrho}U(t, \varrho)} + \\ &+ \mathcal{P}_{ji}^{\parallel}(\bar{\varphi}) \frac{1}{r(t) + \partial_{\varrho}U(t, \varrho) + 2\varrho \partial_{\varrho}^2U(t, \varrho)}, \\ &= \mathcal{P}_{ji}^{\perp}(\bar{\varphi}) G^{\pi\pi}(t, \bar{\varphi}) + \mathcal{P}_{ji}^{\parallel}(\bar{\varphi}) G^{\sigma\sigma}(t, \bar{\varphi}). \end{aligned} \quad (4.29)$$

In the last line we defined the full propagators of the so-called radial σ mode and the $N - 1$ pions, which correspond to the Nambu-Goldstone modes of higher-dimensional problems,

$$G^{\sigma\sigma}(t, \bar{\varphi}) = \frac{1}{r(t) + \partial_{\varrho}U(t, \varrho) + 2\varrho \partial_{\varrho}^2U(t, \varrho)}, \quad (4.30)$$

$$G^{\pi\pi}(t, \bar{\varphi}) = \frac{1}{r(t) + \partial_{\varrho}U(t, \varrho)}. \quad (4.31)$$

Next, Eq. (4.29) is inserted into the r.h.s. of the Wetterich equation (4.14) and the summation over field indices (the trace) is evaluated. In total, one obtains the following PDE,

$$\partial_t U(t, \varrho) = (N - 1) \frac{\frac{1}{2} \partial_t r(t)}{r(t) + \partial_{\varrho}U(t, \varrho)} + \frac{\frac{1}{2} \partial_t r(t)}{r(t) + \partial_{\varrho}U(t, \varrho) + 2\varrho \partial_{\varrho}^2U(t, \varrho)}, \quad (4.32)$$

whose spatial domain is parameterized by the invariant $\varrho \in [0, \infty)$.

In contrast to what is usually found in the literature, it turns out, see next chapter, that for certain purposes it is much better to return to the fields instead of the invariant as the domain of PDE. However, instead of using $\bar{\varphi}$ it suffices to pick one field-space direction, *e.g.*, $\bar{\varphi} = (\sigma, 0, \dots, 0)$, such that

$$\varrho = \frac{1}{2} \sigma^2, \quad (4.33)$$

because the Wetterich equation is valid for any field configuration. Using this variable transformation, the PDE is defined for $\sigma \in (-\infty, \infty)$ and reads,

$$\partial_t U(t, \sigma) = (N - 1) \frac{\frac{1}{2} \partial_t r(t)}{r(t) + \frac{1}{\sigma} \partial_{\sigma}U(t, \sigma)} + \frac{\frac{1}{2} \partial_t r(t)}{r(t) + \partial_{\sigma}^2U(t, \sigma)} = \quad (4.34)$$

$$= \text{[Diagram: a dashed red circle with a red cross inside, labeled } \bar{\pi} \text{]} + \text{[Diagram: a solid blue circle with a blue cross inside, labeled } \sigma \text{]}, \quad (4.35)$$

where $U(t, \sigma) = U(t, -\sigma)$, which is a remnant of the $O(N)$ symmetry. In the last line we also introduced the graphical representation of the RG flow equation in terms of Feynman graphs. The

crossed circles represent the regulator term $\frac{1}{2} \partial_t r(t)$, while the full σ and pion propagators are represented by blue jagged and red dashed lines. For further details on this graphical representation, see also Appendices C.2 and E.

Note that in higher spacetime dimensions the derivation of the flow equation of the effective potential in $O(N)$ -type models is very similar and the final result is structurally identical. The difference in higher dimensions are scale-dependent prefactors and that the flow equation for the effective potential is no longer exactly equivalent to the functional integral, but is part of an infinite set of coupled set of PDEs, which is usually truncated, see Appendix C.2.4. Nevertheless, almost all of the upcoming discussion in the next chapters can be generalized or adopted to non-zero spacetime dimensions.

4.4. Artificially truncating the ERG equation – the FRG Taylor (vertex) expansion

As was just said, FRG in higher-dimensional spacetime usually calls for approximations and one is usually confronted with a coupled set of PDEs and ODEs which describe the RG flow of the system.

A commonly used approximation scheme is the so-called vertex expansion [53, 57, 35], where the scale-dependent effective average action is expanded in interaction vertices/field-orders. In non-zero dimensions, these vertices are usually momentum-dependent and high resolution in momentum space is usually the goal, when this approach is used.

Another truncation scheme is the derivative expansion [53, 57, 35], where the effective average action is expanded in powers of momenta, but field dependences are included at all orders. The lowest order contribution of this approximation is the LPA, which is exact in zero dimensions, because there are no momenta. This approximation is believed to work well at small momenta/energies *etc.*

Still, even the LPA flow equation is oftentimes further approximated in terms of a Taylor-expansion of the effective potential in powers of the field, *e.g.*, Refs. [78, 178, 179, 53, 65, 56, 66, 180, 63, 70, 69, 71]. Hereby, the expansion point is usually chosen to be the scale-dependent or the IR minimum of the effective potential. For zero dimensions the IR minimum is trivial as demonstrated in Section 2.2.2. Consequently, in zero dimensions the vertex expansion and the Taylor expansion of the effective potential coincide.

Even though the Taylor expansion of the effective potential is not needed and it is possible to solve Eq. (4.34) (numerically) in full generality, it is instructive to study artificial truncations in zero dimensions. The reason is that in general the effective potential does not need to be analytic during the RG flow and can even develop non-analyticities in the IR in higher dimensions [83, 91, 77, 101, 103]. An expansion in the fields is therefore generally questionable, because the radius of convergence might be strongly limited or not exist at all. Still, this expansion is used frequently without any doubt. Therefore, we believe that it is useful to demonstrate its limited range of applicability via some simple zero-dimensional test cases, similar to what was done in Chapter 3 for perturbation theory and the $\frac{1}{N}$ -expansion. Due to the availability of exact reference values, this may help to get a better intuition on the quality of this truncation scheme and an estimate of its factual range of applicability.

Hopefully, this contributes to the ongoing debate on useful truncation schemes of the Wetterich equation, because so far there is no absolute systematics for the development of correct truncations and their errors. Acting from necessity, truncations are usually simply adopted to the problem at hand by experience rather than quantitative evidence.

4.4.1. The formalities of the FRG Taylor expansion

In this section, we formally introduce the zero-dimensional FRG Taylor expansion as a truncation of the exact flow equations (4.32) and (4.34). This idea is not original to the author and can also

be found in Refs. [107, 108, 109, 110, 125].

The starting point is the equality of the effective average action and the effective potential Eq. (4.23). We expand it in powers of the $O(N)$ invariant $\varrho = \frac{1}{2} \vec{\varphi}^2$, such that the expansion respects the UV symmetry. Explicitly the expansion up to a truncation order m reads,

$$\begin{aligned} \bar{\Gamma}(t, \vec{\varphi}) = U(t, \vec{\varphi}) &= \sum_{n=0}^m \frac{1}{(2n-1)!!} \bar{\Gamma}^{(2n)}(t) \frac{1}{n!} \left(\frac{1}{2} \vec{\varphi}^2\right)^n = \\ &= \bar{\Gamma}^{(0)}(t) + \bar{\Gamma}^{(2)} \left(\frac{1}{2} \vec{\varphi}^2\right) + \frac{1}{3} \bar{\Gamma}^{(4)} \frac{1}{2} \left(\frac{1}{2} \vec{\varphi}^2\right)^2 + \dots, \end{aligned} \quad (4.36)$$

or

$$\bar{\Gamma}(t, \varrho) = U(t, \varrho) = \sum_{n=0}^m \frac{1}{(2n-1)!!} \bar{\Gamma}^{(2n)}(t) \frac{1}{n!} \varrho^n, \quad (4.37)$$

expressed via the invariant itself. Here, $\bar{\Gamma}^{(2n)}(t)$ are the scale-dependent expansion coefficients – the vertices. The additional factors $(2n-1)!!$ and $n!$ are introduced such that the expansion coefficients in the IR exactly match the 1PI $2n$ -point vertex functions with identical field indices (2.39) to (2.41) *etc.*, thus, $\bar{\Gamma}^{(2n)}(t_{\text{IR}}) = \Gamma_{\varphi_i \dots \varphi_i}^{(2n)}$.

This expansion implies that Eqs. (4.32) and (4.34) turn into a coupled set of ODEs for the expansion coefficients. This system is obtained as follows.

We start by inserting the Taylor expansion (4.36) or Eq. (4.37) into Eqs. (4.24) to (4.26) and repeat the projector decomposition of the previous Section 4.3.1. As an intermediate result, we obtain the σ and pion propagators (4.30) and (4.31) in their Taylor-expanded version,

$$\begin{aligned} G^{\pi\pi}(\vec{\varphi}) &= \left[r(t) + \sum_{n=1}^{m+1} \frac{1}{(2n-1)!!} \bar{\Gamma}^{(2n)}(t) \frac{1}{(n-1)!} \left(\frac{1}{2} \vec{\varphi}^2\right)^{n-1} \right]^{-1} = \\ &= \left[r(t) + \sum_{n=1}^{m+1} \frac{1}{(2n-1)!!} \bar{\Gamma}^{(2n)}(t) \frac{1}{(n-1)!} \varrho^{n-1} \right]^{-1} = G^{\pi\pi}(\varrho), \end{aligned} \quad (4.38)$$

$$\begin{aligned} G^{\sigma\sigma}(\vec{\varphi}) &= \left[r(t) + \sum_{n=1}^{m+1} \frac{1}{(2n-3)!!} \bar{\Gamma}^{(2n)}(t) \frac{1}{(n-1)!} \left(\frac{1}{2} \vec{\varphi}^2\right)^{n-1} \right]^{-1} = \\ &= \left[r(t) + \sum_{n=1}^{m+1} \frac{1}{(2n-3)!!} \bar{\Gamma}^{(2n)}(t) \frac{1}{(n-1)!} \varrho^{n-1} \right]^{-1} = G^{\sigma\sigma}(\varrho), \end{aligned} \quad (4.39)$$

Thus, in analogy to the flow equations (4.32) and (4.34), we find

$$\partial_t \bar{\Gamma}_t(\vec{\varphi}) = \left(\frac{1}{2} \partial_t r(t)\right) [(N-1) G^{\pi\pi}(\vec{\varphi}) + G^{\sigma\sigma}(\vec{\varphi})], \quad (4.40)$$

and

$$\partial_t \bar{\Gamma}_t(\varrho) = \left(\frac{1}{2} \partial_t r(t)\right) [(N-1) G^{\pi\pi}(\varrho) + G^{\sigma\sigma}(\varrho)], \quad (4.41)$$

respectively.

In the last step, we also insert Eqs. (4.36) and (4.37) on the left-hand side (l.h.s.) of these equations and expand both sides in $\varrho = \frac{1}{2} \vec{\varphi}^2$ up to the desired expansion order m . Either by comparing coefficients on both sides of the equation or by taking an appropriate number of derivatives w.r.t. the invariant and evaluating at $\varrho = \frac{1}{2} \vec{\varphi}^2 = 0$ afterwards, we obtain the following coupled set of

ODEs [107, 109],

$$\partial_t \bar{\Gamma}^{(0)}(t) = N \frac{\frac{1}{2} \partial_t r(t)}{r(t) + \bar{\Gamma}^{(2)}(t)}, \quad (4.42)$$

$$\partial_t \bar{\Gamma}^{(2)}(t) = -\frac{N+2}{3} \frac{\frac{1}{2} \partial_t r(t)}{[r(t) + \bar{\Gamma}^{(2)}(t)]^2} \bar{\Gamma}^{(4)}(t), \quad (4.43)$$

$$\partial_t \bar{\Gamma}^{(4)}(t) = \frac{2(N+8)}{3} \frac{\frac{1}{2} \partial_t r(t)}{[r(t) + \bar{\Gamma}^{(2)}(t)]^3} [\bar{\Gamma}^{(4)}(t)]^2 - \frac{N+4}{5} \frac{\frac{1}{2} \partial_t r(t)}{[r(t) + \bar{\Gamma}^{(2)}(t)]^2} \bar{\Gamma}^{(6)}(t), \quad (4.44)$$

⋮

and for all $n \geq 2m + 2$

$$\partial_t \bar{\Gamma}^{(n)}(t) = 0. \quad (4.45)$$

As can be seen, the respective flow equation for the coefficient $\bar{\Gamma}^{(2n)}(t)$ always contains $\bar{\Gamma}^{(2n+2)}(t)$ on the r.h.s.. Hence, without truncating this system at an artificial expansion order m , we obtain an infinite tower of coupled ODEs.

This is discussed in detail in Appendix C.2.4. In addition, note, that the UV initial values for the ODE system of vertices are extracted by also expanding the UV potential and mapping its coefficients on the UV coefficients $\bar{\Gamma}^{(2n)}(t_{\text{UV}})$, which already implies analyticity of the initial potential.

Finally, we remark that a computation of high-order Taylor expansions by hand is tedious and error prone. Therefore, we recommend using computer-algebra systems like MATHEMATICA [147] for their derivation as was also done for this thesis and the corresponding publication [1].

4.5. Symmetry breaking/restoration during the RG flow in zero dimensions

In this section we return to the question of symmetry breaking/restoration in zero dimensions as well as smoothness and convexity of the generating functionals. It is a continuation of Section 2.2. The motivation for this discussion is rather simple. In Section 4.2.2 we argued that the correct UV initial condition for the effective average action is the classical action, $\bar{\Gamma}(t=0, \vec{\varphi}) = \mathcal{S}(\vec{\varphi})$. Moreover, we know that the IR limit of the effective average action is the IR effective action $\bar{\Gamma}(t \rightarrow \infty, \vec{\varphi}) = \Gamma(\vec{\varphi})$. For the latter, we demonstrated its smoothness and convexity in Section 2.2. The former classical action, however, neither needs to be convex nor smooth.

This implies that there can be PTs during the RG flow from the UV to the IR on the level of $\bar{\Gamma}(t, \vec{\varphi})$. This transition only allows for a temporary breaking of a symmetry and always leads to a restoration of all symmetries in the IR. Without fermionic degrees of freedom, symmetry breaking has to be imprinted to the dynamics already in the UV initial condition, if it should be present at all at some point during the RG flow, because the bosonic degrees of freedom exclusively work against symmetry breaking.

Of course, this calls for some step-by-step explanation:

Let us start with the RG-scale-dependent versions of the generating functionals of (connected) correlation and vertex functions Eqs. (4.1), (4.9), and (4.11). The plain introduction of the regulator insertion (4.2) simply adds an additional smooth mass term to the classical action and the partition function. In consequence, the proof of smoothness from Section 2.2.1 still applies. The same holds true for the proof of convexity in Section 2.2.2. We conclude that the generating

functionals $\mathcal{Z}(t, \vec{J})$, $\mathcal{W}(t, \vec{J})$, and $\Gamma(t, \vec{\varphi})$ are convex and smooth at all RG times t . The question is how this fits with the discussion of the previous paragraph.

Convexity Concerning convexity, the reasoning is rather simple. In Eq. (4.12) we defined the effective average action as follows

$$\bar{\Gamma}(t, \vec{\varphi}) \equiv \Gamma(t, \vec{\varphi}) - \Delta\mathcal{S}(t, \vec{\varphi}). \quad (4.46)$$

Even though $\Gamma(t, \vec{\varphi})$ is convex for all t , it is obvious from this definition that this is not necessarily the case for $\bar{\Gamma}(t, \vec{\varphi})$ due to the subtraction of the quadratic mass term. This resolves the first puzzle.

Smoothness Nevertheless, the question of smoothness remains. Since $\Gamma(t, \vec{\varphi})$ and $\Delta\mathcal{S}(t, \vec{\varphi})$ are smooth for all t , Eq. (4.46) implies that also $\bar{\Gamma}(t, \vec{\varphi})$ is smooth for all t . But this is in direct opposition to the fact that $\bar{\Gamma}(t, \vec{\varphi})$ is initialized with $\mathcal{S}(\vec{\varphi})$, which can and does contain cusps.

The reason for this discrepancy is hidden in Eq. (4.19). The limit of $\bar{\Gamma}(t \rightarrow 0, \vec{\varphi}) = \mathcal{S}(\vec{\varphi})$ would only be exact for an infinite UV cutoff Λ . This, however, does not make sense, because in this limit, vertices like $\bar{\Gamma}^{(2)}(t=0)$ would diverge, as can be seen from Eq. (3.4) with $m^2 = \Lambda$ and we could hardly calculate at all. Hence, the UV limit is pathologic. The approximation $\bar{\Gamma}(t \rightarrow 0, \vec{\varphi}) = \mathcal{S}(\vec{\varphi})$ is only almost exact for very large Λ and explains the discrepancy in smoothness. For all practical applications this does not have any consequence at all: As long as there is a contribution of the diffusive σ mode in the flow equation, see Eq. (4.34), the flow equation itself will slightly smooth out any cusps already after an infinitesimal RG time step, such that smoothness of $\bar{\Gamma}(t \rightarrow 0, \vec{\varphi})$ is recovered. (We find that this does not need to happen in the $N \rightarrow \infty$ limit of Eq. (4.34).) We can even estimate the error for the observables which stems from the minimal approximation in the initial condition. In fact the error should be of magnitude

$$\text{error} \approx \frac{\text{largest scale in } \mathcal{S}}{\Lambda}, \quad (4.47)$$

because the initial criterion for the choice of Λ was that it should be much larger than all scales and parameters in $\mathcal{S}(\vec{\varphi})$.

Analyticity Still, the above discussion does not say anything about analyticity of the generating functionals at all. A function can easily be smooth, without being analytic and expandable. In consequence, even though smoothness might be restored for $\bar{\Gamma}(t, \vec{\varphi})$ (at finite N) in the RG flow immediately, this does by no means imply that the FRG Taylor expansion of Section 4.4.1 converges and is applicable at all.

In summary, the zero-dimensional $O(N)$ model also allows to study PTs, even though these are not associated with the variations of external thermodynamic parameters. The phase transition that can be studied by our toy model is in fact symmetry restoration of the ground state, if it was initially broken by the ground state of the microscopic UV classical action.

4.6. Summary

In this chapter we presented the FRG method in terms of simple modifications of probability-distribution functions and generating functionals. By introducing an artificial mass-like term in a QFT, which is altered along some evolution parameter t , we derived a partial differential equation which allows to calculate vertex functions without (numerically) calculating functional integrals at all. It is exclusively required to solve this PDE, which sometimes requires approximations.

The peculiar aspect of this chapter is that by using the zero-dimensional $O(N)$ model we were able to reduce the Wetterich equation to its absolute minimal form and essential characteristic properties. We were able to get rid of all additional complications, which usually come with high-dimensional QFTs, such as spacetime symmetry groups, infinities, regularization, renormalization, truncations *etc.*. This sets the stage for reanalyzing the Wetterich equation and working out some novel fluid-dynamical aspects, which also generalize to higher-dimensional applications.

Chapter 5

FRG flow equations and (computational) fluid dynamics

Abstract In this chapter we recast the FRG flow equation for the effective potential of the zero-dimensional $O(N)$ model in the form of a conservation law. We identify advective and diffusive fluxes. This promotes the interpretation of RG flow equation to a fluid-dynamical problem with all its consequences, which are presented in detail. We discuss irreversibility and entropy production as well as shocks and their mathematical formulation in different limits of the flow equation.

Afterwards we deal with the numerical implementation: We first focus on a specific numerical scheme from the field of computational fluid dynamics, the Kurganov-Tadmor (KT) (central) scheme, and then turn to the general formulation of appropriate boundary conditions.

The entire chapter focuses on theoretical considerations, while practical applications and tests of our findings are discussed in the next chapter.

Disclosure This chapter is entirely based on our own work, which is published in Refs. [1, 2, 3]. The compilation of the results is different, but some parts of this chapter closely follow the presentation from the publications. Most of the material is based on work which I performed in equal shares with M. J. Steil and the support of our other coauthors.

Furthermore, this chapter is influenced by the works of our collaborators [77, 101, 102, 103] as well as our related own project Ref. [4], which is presented in Part II of this thesis.

5.1. Flow equations and conservation laws

Already in Section 4.1 we discussed that the RG flow equations for $\mathcal{Z}(t, \vec{J})$ and $\mathcal{W}(t, \vec{J})$ share certain similarities with fluid-dynamical problems, *e.g.*, the heat equation. However, due to difficulties with the initial conditions of these PDEs, we turned to the Wetterich equation for $\bar{\Gamma}(t, \vec{\varphi})$. We finally arrived at a flow equation for the local effective potential $U(t, \sigma) = U(t, \varrho)$ for the zero-dimensional $O(N)$ model, *cf.* Eqs. (4.32) and (4.34). However, a structured analysis of this equation is still outstanding. This is part of this chapter.

5.1.1. Turning the LPA flow equation into a conservation law

For convenience only, we again present the LPA flow equations (4.32) and (4.34) formulated in the $O(N)$ invariant ϱ ,

$$\partial_t U(t, \varrho) = (N-1) \frac{\frac{1}{2} \partial_t r(t)}{r(t) + \partial_\varrho U(t, \varrho)} + \frac{\frac{1}{2} \partial_t r(t)}{r(t) + \partial_\varrho U(t, \varrho) + 2\varrho \partial_\varrho^2 U(t, \varrho)}, \quad \varrho \in [0, \infty), \quad (5.1)$$

and in the background field σ ,

$$\partial_t U(t, \sigma) = (N-1) \frac{\frac{1}{2} \partial_t r(t)}{r(t) + \frac{1}{\sigma} \partial_\sigma U(t, \sigma)} + \frac{\frac{1}{2} \partial_t r(t)}{r(t) + \partial_\sigma^2 U(t, \sigma)}, \quad \sigma \in (-\infty, \infty). \quad (5.2)$$

Both formulations of the flow equation are of first order in the temporal coordinate, comprise a direct dependence on their spatial coordinate, and contain terms with up to second-order derivatives w.r.t. the spatial coordinate. It is notable that the r.h.s. of this flow equation does not depend on U itself, but exclusively on its derivatives. Furthermore, we know that U is not a physically measurable observable. It is only possible to measure derivatives of and relative differences in U . Both facts can be seen as prompts from the equation itself not to study the PDEs as they stand, but to turn to its spatial derivative(s).

Therefore, we calculate the ϱ -derivative of the first version of the PDE,

$$\partial_t u(t, \varrho) = \frac{d}{d\varrho} \left[(N-1) \frac{\frac{1}{2} \partial_t r(t)}{r(t) + u(t, \varrho)} + \frac{\frac{1}{2} \partial_t r(t)}{r(t) + u(t, \varrho) + 2\varrho \partial_\varrho u(t, \varrho)} \right], \quad \varrho \in [0, \infty), \quad (5.3)$$

and the σ -derivative of its second version,

$$\partial_t u(t, \sigma) = \frac{d}{d\sigma} \left[(N-1) \frac{\frac{1}{2} \partial_t r(t)}{r(t) + \frac{1}{\sigma} u(t, \sigma)} + \frac{\frac{1}{2} \partial_t r(t)}{r(t) + \partial_\sigma u(t, \sigma)} \right], \quad \sigma \in (-\infty, \infty). \quad (5.4)$$

Here we introduced

$$u(t, \varrho) = \partial_\varrho U(t, \varrho), \quad (5.5)$$

and,

$$u(t, \sigma) = \partial_\sigma U(t, \sigma), \quad (5.6)$$

respectively. Note that even though both derivatives are labeled with the small letter u , they are different functions due to the chain rule $\frac{\partial}{\partial \sigma} = \frac{\partial \varrho}{\partial \sigma} \frac{\partial}{\partial \varrho}$.

By not executing the derivatives on the r.h.s. of Eqs. (5.1) and (5.2) we can indeed identify the flow equation for the derivative of the potential with a conservation law, where the flux (the square bracket on the r.h.s.) depends on t, ϱ, u , and $\partial_\varrho u$ or t, σ, u , and $\partial_\sigma u$ respectively. (Of course, also other choices of spatial and temporal coordinates are possible and the equation keeps its conservative form.) In general, we identify u as the conserved quantity or the abstract fluid field.

It is important to remark that also the initial condition for the flow equation needs to be adopted and is

$$u(t=0, \varrho) = \partial_\varrho \mathcal{S}(\varrho), \quad \text{or} \quad u(t=0, \sigma) = \partial_\sigma \mathcal{S}(\sigma). \quad (5.7)$$

Moreover, if formulated in σ , the function $u(t, \sigma)$ is \mathbb{Z}_2 -anti-symmetric, $u(t, \sigma) = -u(t, -\sigma)$, while $u(t, \varrho)$ has no additional symmetry and is exclusively defined for $\varrho \geq 0$.

Before we start discussing the single contributions, a few remarks are in order.

1. The conservative form of the flow equation has clear advantages when it comes to an intuitive interpretation of the dynamics. Our entire physical thinking and mathematical description of the world is structured by conservation laws that provide direct access to the behavior of a system. Conservation laws are not only found in all areas of natural science and engineering, but also in finance and economics and have proven to be the most robust laws of Nature.
2. Conservation laws are subject of intensive research and studied numerically in the field of CFD. Extremely powerful tools for their numerical solution were developed within the last century [104, 49, 50, 51, 52]. Hence, formulating RG flow equations in terms of conservation laws provides direct access to this toolbox, which only has to be adopted to the specific problems at hand.

3. The above observation that the LPA flow equation in the FRG formalism should be considered as a fluid-dynamical conservation law is due to Refs. [77, 181]. Some aspects/consequences can already be found in Refs. [76, 75, 91].

Interestingly, it seems as if this reformulation of the RG flow equation in terms of a fluid-dynamical problem is actually in parts a rediscovery. In the “pre-Wetterich” era of flow equations, which was dominated by Polchinski-type equations [171], several works already analyzed the flow equations in this fashion [92, 93, 94, 95, 96, 97, 98, 99, 100].

Moreover, even the notation of RG “flow” equation or RG “time” is not an accident and comparisons of hydrodynamic flow and RG flow can be found in common textbooks [182, 19].

Therefore, it is surprising that these aspects have not been studied further.

5.1.2. The LPA flow equation as an advection-diffusion equation

Next, we dive into a deeper analysis of the single contributions to the flow equation. Therefore, we first split Eqs. (5.3) and (5.4). For the ϱ -formulation we find

$$\partial_t u(t, \varrho) + \frac{d}{d\varrho} F[t, u] = \frac{d}{d\varrho} Q[t, \varrho, u, \partial_\varrho u], \quad (5.8)$$

with fluxes

$$F[t, u] = - (N - 1) \frac{\frac{1}{2} \partial_t r(t)}{r(t) + u(t, \varrho)}, \quad (5.9)$$

$$Q[t, \varrho, u, \partial_\varrho u] = \frac{\frac{1}{2} \partial_t r(t)}{r(t) + u(t, \varrho) + 2\varrho \partial_\varrho u(t, \varrho)}, \quad (5.10)$$

whereas for its formulation in σ , we have

$$\partial_t u(t, \sigma) + \frac{d}{d\sigma} F[t, \sigma, u] = \frac{d}{d\sigma} Q[t, \partial_\sigma u], \quad (5.11)$$

with fluxes

$$F[t, \sigma, u] = - (N - 1) \frac{\frac{1}{2} \partial_t r(t)}{r(t) + \frac{1}{\sigma} u(t, \sigma)}, \quad (5.12)$$

$$Q[t, \partial_\sigma u] = \frac{\frac{1}{2} \partial_t r(t)}{r(t) + \partial_\sigma u(t, \sigma)}. \quad (5.13)$$

Here, we identify F as advection-type fluxes and Q as diffusion-type fluxes, which is explained within the next lines. The full equation is therefore identified as an advection-diffusion problem, which falls into the class of standard fluid-dynamical PDEs.

The pion-loop as a non-linear advection flux

In a first step, let us simply ignore the Q -contributions to the flow equation. Later on, we find that this formally corresponds to the $N \rightarrow \infty$ limit, which is already anticipated from the factor $(N - 1)$ in F . From the derivation of the RG flow equation in Section 4.3, we know that the fluxes F completely stem from the loop contributions of the $N - 1$ pions (the Goldstone modes in higher dimensions).

Now, the question is why we can interpret this contribution as an advection term which transports the fluid u in a directed manner. This is understood by executing the derivatives in Eqs. (5.8) and (5.11) (ignoring Q) [77],

$$\partial_t u(t, \varrho) = -(\partial_u F[t, u]) \partial_\varrho u(t, \varrho), \quad \partial_u F[t, u] = (N - 1) \frac{\frac{1}{2} \partial_t r(t)}{[r(t) + u(t, \varrho)]^2} < 0. \quad (5.14)$$

We clearly see that this equation is an advection equation in its primitive form, where the fluid velocity is given by $\partial_u F$ [104, 49, 50, 51, 52]. Hence, $N \rightarrow \infty$ is the inviscid limit of the flow equation. We find that the fluid velocity depends on the fluid u itself, similar to the famous Bateman-Burgers equation [183, 184], but is also time-dependent. Interestingly, due to the monotonicity of $r(t)$, see Eq. (4.4), the fluid velocity is manifestly negative, which implies that the fluid u is exclusively moved from large ρ towards $\rho = 0$. Hence, there is a unique direction of information propagation.

Similarly, we find for the σ -formulation,

$$\partial_t u(t, \sigma) = -(\partial_u F[t, \sigma, u]) \partial_\sigma u(t, \sigma) - \partial_\sigma F[t, \sigma, u], \quad (5.15)$$

where

$$\partial_u F[t, \sigma, u] = (N - 1) \frac{\frac{1}{2} \partial_t r(t)}{\sigma [r(t) + \frac{1}{\sigma} u(t, \sigma)]^2}. \quad (5.16)$$

Again, we have the structure of an advection equation with dynamical fluid velocity $\partial_u F[t, \sigma, u]$, where $\sigma \in (-\infty, \infty)$. We find that the fluid u simply always moves towards $\sigma = 0$ from positive and negative σ . In addition to the advective term, one also obtains admixtures of a source-like term, because the advection flux in Eq. (5.11) is explicitly σ -dependent. (However, this term is undirected and does not influence the discussion on bulk transport.)

For both formulations the strength of the advection strongly depends on t as well as the ratio of $r(t)$ and $u(t, \rho)$, respectively $\frac{1}{\sigma} u(t, \sigma)$, in the denominators. In general, for large $\rho = \frac{1}{2} \sigma^2$, the advection flux and fluid velocity are strongly suppressed and there is no movement at all, because asymptotically u grows at least linear in $\rho = \frac{1}{2} \sigma^2$. Anyhow, especially for late RG times and small $\rho = \frac{1}{2} \sigma^2$ or regions where $r(t)$ and $u(t, \rho)$, respectively $\frac{1}{\sigma} u(t, \sigma)$ are of opposite sign and almost cancel in the denominators, the flux and velocity can get huge. Among other things, this implies that fast-moving waves of u approach $\rho = \frac{1}{2} \sigma^2 = 0$ and eventually collide with the boundary condition (in ρ) or with waves of opposite sign (in σ). Furthermore, this generically allows for shock- and rarefaction-wave formation, because systems of non-linear advection tend to form non-analytical behavior [104, 49, 50, 51, 52], which was studied in Ref. [77, 101] and recently Ref. [103] in the FRG context.

Also note that the velocity $\partial_u F$ strongly depends on the number of pions and is generally not bounded at all. In consequence, the RG flow falls in the class of non-relativistic classical flow equations and there is no ‘‘causal bound’’ for propagation speed like in relativistic hydrodynamics.

The σ -loop as a non-linear diffusion flux

Next, let us turn to the contribution of the σ -loop and ignore the advective contribution. This is easily done by setting $N = 1$. In complete analogy to the previous discussion, the best way to identify the diffusive nature of the σ -contribution to the RG flow is to execute the spatial derivatives in Eqs. (5.8) and (5.11). This time we start with the σ -version of the flow equation,

$$\partial_t u(t, \sigma) = D[t, \partial_\sigma u] \partial_\sigma^2 u(t, \sigma), \quad (5.17)$$

where

$$D[t, \partial_\sigma u] \equiv \partial_\sigma Q[t, \partial_\sigma u] = -\frac{\frac{1}{2} \partial_t r(t)}{[r(t) + \partial_\sigma u(t, \sigma)]^2} > 0. \quad (5.18)$$

We directly identify the RG flow equation (for $N = 1$) as a heat/diffusion equation with dynamical diffusion coefficient $D[t, \partial_\sigma u]$. Hence, the $N = 1$ scenario is the ‘‘viscous’’ limit. The manifest positivity of the diffusion coefficient ensures stability of the equation and well-posedness of the problem [168, 104, 49, 50, 51, 52]. In general, ordinary diffusion is an undirected process, which tends to eliminate gradients of all kind. There is strong diffusion in the vicinity of jumps, cusps,

and large gradients, while in constant, smooth, and flat regions diffusive processes are slow. Nevertheless, here we are confronted with highly non-linear diffusion. The diffusion coefficient itself is RG-time dependent and inversely depends on the gradient of the fluid. Again, we find that for large $|\sigma|$ and/or early times the diffusion is strongly suppressed. For late times the diffusion gets stronger. However, here it critically depends on the gradient and the second derivative of u . In regions of small gradients and but large curvatures (close to minima of u) diffusion is strong, because the diffusion coefficient as well as $\partial_\sigma^2 u(t, \sigma)$ are large. The effect is even more pronounced in regions where $r(t)$ and $\partial_\sigma u(t, \sigma)$ are of opposite sign, *e.g.*, in the middle part of a mexican-hat-type potential, such that diffusion on the level of the PDE strongly works against symmetry breaking.

In total, we find that both the advective and diffusive contribution tend to be strongest for RG scales close or below model scales and for small $\varrho = \frac{1}{2}\sigma^2$. Especially the diffusive σ -mode is important for a flattening of the potential at small $|\sigma|$, respectively for symmetry restoration. The relative dominance of advection or diffusion for fixed initial condition can be controlled by varying the number of fields N .

So far our discussion of diffusion was based on the σ -formulation of the RG flow equation. The simple reason is that the flux (5.10) cannot be uniquely identified as a diffusion flux due to the additional $u(t, \varrho)$ and ϱ dependences. This is easily seen by executing the ϱ -derivative. Thus, already at this point we conclude that the best choice of spatial variables might strongly depend on the difference between finite and infinite N and the applied numerical schemes, which oftentimes rely on a strict splitting of advective and diffusive fluxes. We come back to the differences of the σ - and ϱ -formulation below.

5.1.3. Consequences of the fluid-dynamical interpretation of RG flows

Identifying the ERG equation as a highly non-linear advection-diffusion equation comes with some direct severe consequences.

Diffusion and irreversibility

As briefly mentioned in Section 4.1, systems that comprise diffusive processes are dissipative, which therefore also applies to the LPA flow equation (except for the $N \rightarrow \infty$ limit). Furthermore, dissipation is always linked to an increase in information that is needed to describe the system, or a loss of information about the initial state (depending on the perspective). This is associated to the growth of an entropy and directly linked to the irreversibility of a process.

In fact, the direct connection between irreversibility, the semi-group property of the RG, and diffusion terms in the LPA flow equation was already discussed for versions of RG flow equations from the “pre-Wetterich” era [97, 98, 99]. For example, Ref. [99] states that the second order field-space derivative of the potential “[...] corresponds to a dissipation in the flow and is responsible for the semi-group property of the RG.” This view is supported by our findings based on the more modern FRG formulation by Wetterich, Morris, Ellwanger *et al.*

Advection and irreversibility

Still, also purely advective systems can show irreversible dynamics and entropy production. This happens, for example, if several characteristic curves, which describe the movement of little portions of the fluid, intersect and a shock wave is formed. Here, the information about the initial state and direction of the movement of the single fluid portions is lost and the dynamics is irreversible and subsequently described by the movement of the shock front. This also comes with an increase of an entropy of the system. For recent discussions in the context of infinite- N FRG flow equations, see Refs. [77, 101, 3].

A “thermodynamic arrow of time” in the RG flow

We conclude that for general N the LPA flow equation describes an irreversible flow of the derivative of the local potential from $t = 0$ (the UV) to $t \rightarrow \infty$ (the IR). Further, this evolution goes hand in hand with the production of entropy and the loss of information about the initial (UV) state of the system. Hence, the RG scale/time can be interpreted as a “thermodynamic arrow of time” in the abstract sense, which is set by the direction of increasing entropy and gradual loss of information about the initial state [170]. These aspects directly generalize to the Wetterich equation for arbitrary systems, because the Wetterich equation is of manifestly diffusive character, as long as truncations and approximations are not applied to the PDE. Truncations may violate this property.

The reinterpretation of the IR

In this context, it is also sensible to rethink the interpretation of the IR solution of RG flow equations. From the fluid-dynamical perspective on the RG flow equation, the IR, where all fluctuations are integrated out and the “PDE dynamics” stops, can be interpreted as a kind of “thermodynamic” equilibrium, which is approached by the diffusive contribution, or a steady flow, from the advective perspective.

In fact, this is conceptually very similar to the equilibration of the air flow around an airfoil, when a plane reaches its travel altitude and should therefore be seen as a manifestly fluid-dynamic process.

This interpretation and its consequences might be of particular interest for RG flow equations of higher-dimensional systems in their rescaled dimensionless form. Here, steady-flow solutions/equilibrium solutions from fluid dynamics are the fixed-point solutions of the RG.

Relation to Kadanoff’s and Wilson’s approach to the RG

From the classical and original non-perturbative RG perspective, which traces back to Wilson’s generalization of Kadanoff’s block-spin transformation [185, 174, 175, 176, 161, 19], the above discussion of the Wetterich formulation of the RG is rather intuitive. Step-by-step block-spin transformations from microscopic to macroscopic scales with appropriate rescaling are a manifestly irreversible process, where the information about the microscopic spin configuration is lost and absorbed in effective macroscopic spins – the coarse-graining process. On top, several distinct microscopic configurations can lead to the same macroscopic physics.

The same applies if formulated in Fourier space on the level of QFTs, to the gradual integration of (Euclidean) momentum shells from the UV to the IR, where all couplings and processes at some energy scale are integrated out and absorbed in effective couplings at lower energy scales until the IR is reached. The possible infinite number of effective measurable IR couplings, vertices, or expectation values comprise all microscopic information from all higher energy scales. Nevertheless, it is impossible to restore the information about the micro-physics once the IR is reached. Backwards integration to higher energy and smaller length scales is only possible theoretically in truncated subsystems.

Relation to the “pre-Wilson” and perturbative RG

It is interesting to ask how these findings relate to the perturbative picture of the RG, which traces back to the early works of Callan, Symanzik, Gell-Mann, Low, t’Hooft, Weinberg, Georgi, Politzer and many more. Here, one does not consider a continuum of infinitely many coupling constants, which is for example collected in an effective potential, but studies the RG flow of a single coupling or selected small number of couplings. (This can also be done with the Wetterich equation using truncations.)

Anyhow, in this case the RG equations reduce to a coupled set of ODEs, and the dissipative and

fluid-dynamical character of the RG is lost. On a formal level,¹ it is possible to integrate this set of ODEs in both directions, to higher and lower RG scales and energies. The most extreme case is certainly the β -function of a single coupling. Hence, also irreversibility and the semi-group property of the RG transformations is spoiled. Working on a finite small set of couplings therefore implies that it would be possible to resolve the microphysics from the macrophysics, which is not possible.

Anyhow, this does not imply that this “pre-Wilson” RG approach is wrong. It is merely the range of applicability that is limited to the weakly interacting perturbative regime of models and theories. As soon as one leaves this regime and encounters strongly interacting physics, one is confronted with a fast rising number of interactions of different scales and one has to turn to a non-perturbative framework, which reflects the previously described effects.

This difference of the perturbative and non-perturbative RG perspectives is already summarized in the recommendable article [161] by Wilson himself.

An entropy function and the connection to the \mathcal{C} -theorem

In the light of the above discussion, the obvious question is, whether it is possible to quantify the dissipative character of RG flow equations by some explicit entropy function.

Basically, this is what is also tried by so-called \mathcal{C} -functions and was first discussed in the context of two-dimensional conformal QFT [95]. In Ref. [95], Zamolodchikov discusses the irreversibility of RG group: “Some of the information on the ultraviolet behavior of the field theory is lost under renormalization transformations with $t > 0$, since in the field theory it is not legitimate to examine correlations at scales smaller than the cutoff. We would therefore expect that a motion of the space Q [a change of the set of all couplings] under the influence of the renormalization group would become an ‘irreversible’ process, similar to the time evolution of dissipative systems.” Therefore, Zamolodchikov proposes and proves that “[t]here exists a function $c(g)$ of the coupling constant g in a 2D renormalizable field theory which decreases monotonically under the influence of a renormalization-group transformation.” The exact properties of such \mathcal{C} -function are [95] (in the notation of Ref. [2]),

1. There exists a positive function

$$\mathcal{C}(\{g_i\}, t) \geq 0. \tag{5.19}$$

of all (possibly infinitely many) dimensionless couplings $\{g_i\}$ of the theory and RG time t , with the additional property

$$\frac{d}{dt} \mathcal{C}(\{g_i\}, t) \leq 0. \tag{5.20}$$

(The choice of sign is convention.)

2. The \mathcal{C} -function takes a fixed value at (critical) fixed points of the theory. These fixed values can be identified with the central charge c (of the Virasoro algebra [187]),

$$\mathcal{C}(\{g_i^*\}, t) = c, \tag{5.21}$$

and the central charge is different for different fixed points.

The terminus “ \mathcal{C} -theorem” is usually restricted to two-dimensional (conformal) QFTs, while generalizations to higher dimensions, *e.g.*, four dimensions, are denoted as \mathcal{A} -theorems, where the central charge is replaced by some anomaly coefficient [188].

Even though there was rather active research on \mathcal{C} - and \mathcal{A} -functions, their construction, and proofs within the last decades, *cf.* Refs. [189, 188, 190, 191, 192, 186, 193, 97, 98, 99, 194, 195, 196, 197,

¹On a practical level, numerical instabilities or the special form of the equations [186] might still prevent the “up-and-down” integration of a system of ODEs.

198, 199, 100], not all questions in this context seem to be settled. Especially the explicit construction of \mathcal{C} -functions for practical models and truncations is still a field of active research.

We shall not further comment in detail on the current status of research in this field as it is beyond the scope of our present studies. Nevertheless, we believe that our work might introduce a new aspect to the discussion, which we were not able to find in the literature so far.

1. In the past, entropy-like functions or \mathcal{C} -functions were oftentimes discussed in the context of a (finite) set of coupling constants. We believe that our zero-dimensional minimal example might hint at another approach, which was also taken by Refs. [97, 98, 99, 100, 190, 164, 198, 199]. The irreversible character of the RG flow is manifestly encoded, if one turns to a global description of the space of couplings, *e.g.*, in terms of a flowing effective potential via some dissipative PDE. Hence, entropy-/ \mathcal{C} -functions might be identified via global descriptions of field/theory space.
2. We believe that our work shows that there should be a direct connection between the \mathcal{C} -theorem and abstract entropy functions of the PDEs that describe the RG flows. This is of particular interest for truncated systems of FRG flow equations or approximations. On the one hand, the approach via entropy functions of the PDEs from the field of CFD might allow to identify \mathcal{C} -functions of truncated systems. On the other hand, this connection could help to identify minimal requirements for truncations, *e.g.*, the presence of irreversibility, dissipation, and an entropy-/ \mathcal{C} -function on the level of the ODEs and PDEs.
3. Furthermore, as discussed below, the existence of an entropy function for a PDE can be used to show stability and convergence of the solution [49, 50]. In addition, discretized versions can in turn be related, used, and studied for finding stable numerical schemes. We further demonstrate that there could be a direct relation between \mathcal{C} -functions, (numerical) entropy functions, and the total variation diminishing (TVD) property below.

In the following, we therefore present the construction of an entropy function from Ref. [2] for our zero-dimensional $O(N)$ model. We comment on possible identification as a \mathcal{C} -function. For generalization to higher dimensions we refer to Ref. [2]. Unfortunately, so far we were only able to construct an entropy function for $N = 1$ and $N = \infty$, while the problem remains unsolved for $N \neq 1$. A possible explanation is sketched in Section 5.1.6 and Refs. [2, 3].

5.1.4. An entropy function in the viscous $N = 1$ limit

Within the next paragraphs, we recapitulate the main steps in the construction of an entropy function for the RG flow equation of the zero-dimensional $O(N)$ model with $N = 1$ from Ref. [2], where also a discussion of subtleties can be found.

As one of the ingredients, we need the spatial derivative of the RG flow equation (5.4),

$$\partial_t[\partial_\sigma u(t, \sigma)] = \frac{d}{d\sigma} \left(\frac{-\frac{1}{2} \partial_t r(t)}{[r(t) + \partial_\sigma u(t, \sigma)]^2} \partial_\sigma^2 u(t, \sigma) \right). \quad (5.22)$$

However, the actual starting point is the definition of the functional

$$S[f(\sigma)] \equiv - \int_{-\infty}^{\infty} d\sigma s(f(\sigma)), \quad (5.23)$$

which we denote as the entropy functional of some real-valued function $f(\sigma)$. The integration domain is the entire field space (the domain of the PDE as well as f). As the integrand, we introduced a continuously (at least) twice differentiable convex function,

$$s : \mathbb{R} \rightarrow \mathbb{R}, \quad y \mapsto s(y), \quad (5.24)$$

with

$$s(y) \in C^2(\mathbb{R}), \quad s''(y) \geq 0, \quad (5.25)$$

which shall not grow faster than y^2 for $|y| \rightarrow \infty$.

In the following we show that by choosing $f(\sigma) = \partial_\sigma u(t, \sigma)$ Eq. (5.23) indeed presents a monotonically increasing function for $t \in [0, \infty)$, *viz.*,

$$\frac{d}{dt} S[\partial_\sigma u] \geq 0, \quad (5.26)$$

and can therefore be interpreted as an entropy-type function (after minor modifications).

We straightforwardly evaluate

$$\begin{aligned} \frac{d}{dt} S[\partial_\sigma u] &= \quad (5.27) \\ &= - \frac{d}{dt} \int_{-\infty}^{\infty} d\sigma s(\partial_\sigma u(t, \sigma)) \stackrel{(5.23)}{=} \\ &= - \int_{-\infty}^{\infty} d\sigma (\partial_t [\partial_\sigma u(t, \sigma)]) s'(\partial_\sigma u(t, \sigma)) \stackrel{(5.22)}{=} \\ &= \int_{-\infty}^{\infty} d\sigma \left[\frac{d}{d\sigma} \left(\frac{\frac{1}{2} \partial_t r(t)}{[r(t) + \partial_\sigma u(t, \sigma)]^2} \partial_\sigma^2 u(t, \sigma) \right) \right] s'(\partial_\sigma u(t, \sigma)) = \\ &= \int_{-\infty}^{\infty} d\sigma \left(\frac{-\frac{1}{2} \partial_t r(t)}{[r(t) + \partial_\sigma u(t, \sigma)]^2} [\partial_\sigma^2 u(t, \sigma)]^2 \right) s''(\partial_\sigma u(t, \sigma)) + \\ &\quad + \left[\frac{\frac{1}{2} \partial_t r(t)}{[r(t) + \partial_\sigma u(t, \sigma)]^2} [\partial_\sigma^2 u(t, \sigma)] s'(\partial_\sigma u(t, \sigma)) \right]_{-\infty}^{\infty}, \end{aligned}$$

where we used integration by parts in the last step.

To understand that the r.h.s. of this equation is indeed greater or equal to zero, it is instructive to analyze the remaining terms separately.

1. By construction, due to its convexity, $s'' \geq 0$. Also $[\partial_\sigma^2 u(t, \sigma)]^2$ is obviously positive. The same holds true for the denominator, even though already $r(t) + \partial_\sigma u(t, \sigma) > 0$ by construction of the FRG. Lastly, because of its monotonicity, $-\partial_t r(t) > 0$. In total, the integrand of the first term is manifestly positive and so is the integral.
2. The second term vanishes, which is seen as follows: First, by construction, $s'(y)$ maximally grows like y for $|y| \rightarrow \infty$. Second, for $|\sigma| \rightarrow \infty$ the potential $U(t, \sigma)$ grows at least quadratically, implying that $\partial_\sigma u(t, \sigma)$ grows at least linearly in σ . We distinguish
 - (a) If $\lim_{|\sigma| \rightarrow \infty} U(t, \sigma) \sim \sigma^2$ the factor $\partial_\sigma^2 u(t, \sigma) = \partial_\sigma^3 U(t, \sigma)$ vanishes, while the other terms do not grow with σ for large $|\sigma|$. This implies that the entire term vanishes, because of the evaluation at $\pm\infty$.
 - (b) If $\lim_{|\sigma| \rightarrow \infty} U(t, \sigma)$ grows faster than σ^2 than the denominator $[r(t) + \partial_\sigma u(t, \sigma)]^2$ always grows faster than the terms in the numerator. Hence, for an evaluation at $\pm\infty$ the term vanishes.

In conclusion, we find that $S[\partial_\sigma u]$ grows monotonically during the RG flow. Further it encodes all information about all possible interactions and dynamics of the field in a global manner and therefore is equivalent to an infinite set of coupling constants/vertices.

Anyhow, there are two remaining issues. A first minor problem is that $S[\partial_\sigma u]$ is by Def. (5.23) negative, which is uncommon for an entropy. Second, $S[\partial_\sigma u]$ is simply divergent, because field-space is infinite and $\partial_\sigma u(t, \sigma)$ is at least constant for $|\sigma| \rightarrow \infty$. This is seen best if we explicitly choose $s(y) = y^2$, which we will keep for all further discussions,

$$S[\partial_\sigma u] = - \int_{-\infty}^{\infty} d\sigma [\partial_\sigma u(t, \sigma)]^2. \quad (5.28)$$

Both doubts are cured by keeping in mind that we are exclusively interested in relative changes or differences of entropy. Therefore, we are allowed to simply subtract the entropy functional of the initial condition. We define the normalized entropy

$$\mathcal{C}[\partial_\sigma u] = \mathcal{S}[\partial_\sigma u(t, \sigma)] - S[\partial_\sigma u(t = 0, \sigma)], \quad (5.29)$$

which is always positive. On top, it is finite, because for large $|\sigma|$ the “fluid” $u(t, \sigma)$ does not evolve at all and the asymptotic contributions of both terms in Eq. (5.29) cancel. This is seen by inspection the PDE (5.4), where the r.h.s. vanishes for large $|\sigma|$.

In total, we were able to construct an explicit entropy function for the PDE and our exact RG problem. This function further fulfills the requirements (5.19) and (5.20) for a \mathcal{C} -function, while Eq. (5.21) does not exist in zero dimensions because there exists no central charge and – as far as we know – no fixed-point solution.²

Below, in Section 5.2.4, we also present a discretized version of this entropy function and provide explicit numerical results for selected UV actions. In addition, we relate this entropy to the TVD property and therefore argue that its existence hints at the existence of stable numerical schemes as well as unique weak solutions.

5.1.5. The $\frac{1}{N}$ -rescaled flow equations and the $N \rightarrow \infty$ limit

For studying the $N \rightarrow \infty$ limit or comparing finite- N and infinite- N calculations, it is advisable to work with the $\frac{1}{N}$ -rescaled version of the RG flow Eqs. (5.3) and (5.4). In analogy to Eq. (3.17) of Section 3.3, we rescale the fields, the $O(N)$ invariant, and the effective potential,

$$\sigma \mapsto x = \frac{1}{\sqrt{N}} \sigma, \quad \rho \mapsto y = \frac{1}{N} \rho, \quad U \mapsto V = \frac{1}{N} U. \quad (5.30)$$

The RG flow equation in the formulation of the rescaled invariant y reads

$$\partial_t v(t, y) = \frac{d}{dy} \left[\frac{N-1}{N} \frac{\frac{1}{2} \partial_t r(t)}{r(t) + v(t, y)} + \frac{1}{N} \frac{\frac{1}{2} \partial_t r(t)}{r(t) + v(t, y) + 2y \partial_y v(t, y)} \right], \quad y \in [0, \infty), \quad (5.31)$$

while the RG flow equation in the formulation of the rescaled field x is

$$\partial_t v(t, x) = \frac{d}{dx} \left[\frac{N-1}{N} \frac{\frac{1}{2} \partial_t r(t)}{r(t) + \frac{1}{x} v(t, x)} + \frac{1}{N} \frac{\frac{1}{2} \partial_t r(t)}{r(t) + \partial_x v(t, x)} \right], \quad x \in (-\infty, \infty). \quad (5.32)$$

Note that the prefactors $\frac{N-1}{N}$ and $\frac{1}{N}$ are the same for LPA flow equations of $O(N)$ models in any dimension, such that the following is general.

Inspecting the structure of the rescaled RG flow equations it is obvious that the PDE gets more and more advection-dominated when N is increased, because the diffusive contribution is suppressed by $\frac{1}{N}$.

²Work on the general absence of zero-dimensional fixed-point solutions for the effective potential in RG flow equations is in progress, but was not finished by completion of this thesis.

In the $N \rightarrow \infty$ limit, the above flow equations simply reduce to their inviscid limit,

$$\lim_{N \rightarrow \infty} \partial_t v(t, y) = \frac{d}{dy} \left[\frac{\frac{1}{2} \partial_t r(t)}{r(t) + v(t, y)} \right], \quad y \in [0, \infty), \quad (5.33)$$

and

$$\lim_{N \rightarrow \infty} \partial_t v(t, x) = \frac{d}{dx} \left[\frac{\frac{1}{2} \partial_t r(t)}{r(t) + \frac{1}{x} v(t, x)} \right], \quad x \in (-\infty, \infty). \quad (5.34)$$

Note that both equations are integrable by applying the method of characteristics as shown in Section 5.1.7, which was already applied to their higher-dimensional counterparts in Refs. [75, 76, 101].

Furthermore, in Section 5.1.8 we use these equations to analytically analyze shock waves in field space.

5.1.6. Another entropy function for the inviscid $N \rightarrow \infty$ limit

In the context of our work on shock and rarefaction waves in the context of the $\frac{1}{N}$ -expansion [3], we noticed that it is possible to also formulate an entropy function for the RG flow equation in the $N \rightarrow \infty$ limit, Eq. (5.33). Thus, similarly to the discussion of Section 5.1.4 we find,

$$\mathcal{C}[v] = \text{TV}[v(t=0, y)] - \text{TV}[v(t, y)], \quad (5.35)$$

where TV denotes the total variation (the arc length of $v(t, y)$)

$$\text{TV}[v(t, y)] \equiv \int_0^\infty dy |\partial_y v(t, y)|. \quad (5.36)$$

Basically, the difference between the entropy functions for $N = 1$ and $N \rightarrow \infty$ is the different integration domain and the change from the square of the derivative to its absolute in the integrand. Anyhow, so far we were not able to formulate a general entropy function for finite $N > 1$. Loosely speaking, the reason is that for finite $N > 1$ the r.h.s. of the PDE always explicitly depends on the position in the spatial domain, see, *e.g.*, Eqs. (5.31) and (5.32). This dependence manifests as a source/sink term after executing spatial derivatives and therefore additionally spoils the arc length of u respectively v .

This is supported by literature from the field of CFD [200, 201, 202, 203, 204].

For further details we refer to our own Ref. [3, Appendix E].

5.1.7. Method of characteristics in the inviscid $N \rightarrow \infty$ limit

A special method for the analytic solution of (quasi-)hyperbolic PDEs is the method of characteristics. Characteristic curves (or oftentimes just characteristics) are parametric curves that form solutions of a PDE. They are defined as those curves where functions of the solution or the solution itself stays constant. The method is applicable to purely advective systems as long as the “fluid” is only transported without “collision” of single fluid cells, hence without or in advance of the formation of shocks.

Within the next paragraphs, we apply this method to the RG flow equations in the $N \rightarrow \infty$ limit, *i.e.*, Eqs. (5.33) and (5.34), which are of quasi-hyperbolic type, and construct their analytic solutions.

In the context of the $N \rightarrow \infty$ FRG flow equation this was first done by Tetradis and Litim [75, 76] and later on by Aoki, Kumamoto, Sato, and Yamada [205, 91]. A comprehensive interpretation of the characteristic curves in the context of CFD was first provided by Grossi and Wink [77] and later on extended in Ref. [101].

General considerations

The construction of the characteristic curves is rather simple, *cf.* Refs. [206, 207, 49]. The general starting point is a quasilinear hyperbolic PDE of type,

$$0 = a(t, y, v) \partial_t v(t, y) + b(t, y, v) \partial_y v(t, y) + c(t, y, v), \quad (5.37)$$

where t is the temporal coordinate, y is the spatial coordinate, and $v = v(t, y)$ is a fluid field. The solution of this equation, if it exists, forms a surface $(t, y, v(t, y)) \in \mathbb{R}^3$. The characteristics are therefore parametric curves $(t(\tau), y(\tau), v(\tau))$ of some parameter τ lying on this surface, where we assume that v stays constant. Thus, via the chain rule,

$$\begin{aligned} 0 &= \frac{d}{d\tau} v(t(\tau), y(\tau), \tau) = \\ &= \frac{\partial t(\tau)}{\partial \tau} \partial_t v(t(\tau), y(\tau), \tau) + \frac{\partial y(\tau)}{\partial \tau} \partial_y v(t(\tau), y(\tau), \tau) + \partial_\tau v(t(\tau), y(\tau), \tau). \end{aligned} \quad (5.38)$$

Comparing this equation to Eq. (5.37) we obtain the so-called Lagrange-Charpit/characteristic equations [206],

$$\frac{\partial t(\tau)}{\partial \tau} = a(t(\tau), y(\tau), v(\tau)), \quad (5.39)$$

$$\frac{\partial y(\tau)}{\partial \tau} = b(t(\tau), y(\tau), v(\tau)), \quad (5.40)$$

$$\frac{\partial v(\tau)}{\partial \tau} = c(t(\tau), y(\tau), v(\tau)), \quad (5.41)$$

which form a set of three coupled ODEs. The initial conditions for these equations are taken from the original PDE problem,

$$t(\tau = 0) = t_0, \quad y(\tau = 0) = y_0, \quad v(\tau = 0) = v_0(t_0, y_0), \quad (5.42)$$

where t_0 is the initial time. Hence, each point y_0 in the domain of the PDE is a starting point of a characteristic curve $(t(\tau), y(\tau), v(\tau))$, which is described by the above three coupled ODEs. Solving the ODE system for each starting point, we have access to the solution of the PDE.

Application to the $N \rightarrow \infty$ flow equations

For the sake of simplicity, we work with the flow equation (5.33)³,

$$\partial_t v(t, y) = \frac{d}{dy} \left[\frac{\frac{1}{2} \partial_t r(t)}{r(t) + v(t, y)} \right] = - \frac{\frac{1}{2} \partial_t r(t)}{[r(t) + v(t, y)]^2} \partial_y v(t, y). \quad (5.43)$$

Here, the y -derivative was already executed to match the shape of Eq. (5.37). Explicitly inserting the regulator (4.4) we identify,

$$\frac{\partial t(\tau)}{\partial \tau} = 1, \quad \frac{\partial y(\tau)}{\partial \tau} = - \frac{\Lambda e^{-t(\tau)}}{2 [\Lambda e^{-t(\tau)} + v(\tau)]^2}, \quad \frac{\partial v(\tau)}{\partial \tau} = 0. \quad (5.44)$$

The corresponding initial conditions of the RG flow equation are,

$$t(\tau = 0) = 0, \quad y(\tau = 0) = y_0 \geq 0, \quad v(\tau = 0) = v(0, y_0). \quad (5.45)$$

Integration of the first and last differential equation from Eq. (5.44) is trivial and we find

$$t(\tau) = \tau, \quad v(\tau) = v(0, y_0), \quad (5.46)$$

³The absence of the explicit dependence on the spatial coordinate slightly simplifies the calculation in comparison to starting with Eq. (5.34), which is also possible.

where we simply identified t and τ by ignoring a possible irrelevant integration constant. Since $v(\tau) = v(0, y_0) = \text{const.}$ the r.h.s. of the remaining differential equation exclusively depends on τ and is directly integrated to,

$$y(t) = y_0 - \int_0^t d\tau \frac{\Lambda e^{-\tau}}{2[\Lambda e^{-\tau} + v(0, y_0)]^2} = y_0 - \frac{1}{2[\Lambda e^{-t} + v(0, y_0)]} + \frac{1}{2[\Lambda + v(0, y_0)]}. \quad (5.47)$$

These are the characteristic curves, where “the fluid” v keeps a constant value.

Applying the transformation $y = \frac{1}{2}x^2$ and using $v(t, y) = \partial_y V(t, y) = \frac{1}{x} \partial_x V(t, x) = \frac{1}{x} v(t, x)$, the solution in the $\frac{1}{N}$ -rescaled field reads,

$$x(t) = \pm \sqrt{2y(t)} = \pm \sqrt{x_0^2 - \frac{1}{\Lambda e^{-t} + \frac{v(0, x_0)}{x_0}} + \frac{1}{\Lambda + \frac{v(0, x_0)}{x_0}}}, \quad v(t) = \frac{v(0, x_0)}{x_0} x(t). \quad (5.48)$$

Note, that here $v(t)$ is no longer constant along the characteristics. Still, the ratio $\frac{1}{x(t)} v(t)$ remains constant.

An useful application of this analytic solution is the simple prediction of the formation of shock or rarefaction waves. A shock wave is formed if characteristic curves intersect and the solution gets multi-valued. Afterwards, the characteristic curves no longer correspond to the correct solution of the PDE.

A rarefaction wave is formed at a point where infinitely many characteristics originate and move apart. Both phenomena have in common that v is non-analytic at the corresponding points and times, see, *e.g.*, Ref. [49] for details.

5.1.8. Rankine-Hugoniot condition and shock position in the inviscid $N \rightarrow \infty$ limit

As already anticipated above, non-linear (quasi-hyperbolic) PDEs of type

$$0 = \partial_t v(t, x) + \frac{d}{dx} F[t, x, v(t, x)] \quad (5.49)$$

tend to form non-analytic structures. One possible scenario is the formation of a shock wave. If analyzed on the level of discretized fluid cells, *e.g.*, in terms of Riemann problems, this happens when the fluid velocities of neighboring cells are directed towards each other or when one fluid cell has higher velocity than its neighboring cell and would outpace the other cell. This causes moving jump discontinuities in the solution. Their propagation can be described using the Rankine-Hugoniot (jump) condition [208, 209], which is recapitulated in the following. For details we refer to Refs. [104, 49, 50, 51] or Ref. [77] in the context of the FRG (even though already Aoki, Kumamoto, Sato, and Yamada discussed shocks in their studies [205, 91], but without the fluid-dynamical context).

Consider some (moving) interval $[x_L(t), x_R(t)]$ in the domain of the PDE, which is supposed to contain a single discontinuity in terms of a shock wave at the position $\xi_s(t)$, *i.e.*, $x_L(t) < \xi_s(t) < x_R(t)$. For this dynamic interval the integrated version of the conservation law (5.49) reads

$$\begin{aligned} \int_{x_L(t)}^{x_R(t)} dx \partial_t v(t, x) &= - \int_{x_L(t)}^{x_R(t)} dx \frac{d}{dx} F[t, x, v(t, x)] = \\ &= - (F[t, x_R(t), v(t, x_R(t))] - F[t, x_L(t), v(t, x_L(t))]). \end{aligned} \quad (5.50)$$

Yet, by definition the integral on the l.h.s. of the equation contains the jump discontinuity. We therefore split this integral about this shock position $\xi_s(t)$ and find,

$$\begin{aligned} \int_{x_L(t)}^{x_R(t)} dx \partial_t v(t, x) &= \int_{x_L(t)}^{\xi_s(t)} dx \partial_t v(t, x) + \int_{\xi_s(t)}^{x_R(t)} dx \partial_t v(t, x) = \\ &= -v(t, \xi_s(t)) \partial_t \xi_s(t) + v(t, x_L(t)) \partial_t x_L(t) + \frac{d}{dt} \int_{x_L(t)}^{\xi_s(t)} dx v(t, x) - \\ &\quad - v(t, x_R(t)) \partial_t x_R(t) + v(t, \xi_s(t)) \partial_t \xi_s(t) + \frac{d}{dt} \int_{\xi_s(t)}^{x_R(t)} dx v(t, x). \end{aligned} \quad (5.51)$$

In the second step, the Leibniz integral rule was applied to extract the t -derivative from the integral. Note that the first and fifth term cancel. This result replaces the l.h.s. of Eq. (5.50). In the next step, we tighten the integration interval in Eqs. (5.50) and (5.51) and study the limits

$$x_R(t) \rightarrow \xi_s^-(t), \quad x_L(t) \rightarrow \xi_s^+(t). \quad (5.52)$$

The remaining integrals in Eq. (5.51) vanish and by introducing the definitions

$$v_L(t) \equiv \lim_{x_L(t) \rightarrow \xi_s^-(t)} v(t, x_L(t)), \quad F_L(t) \equiv \lim_{x_L(t) \rightarrow \xi_s^-(t)} F[t, x_L(t), v(t, x_L(t))], \quad (5.53)$$

$$v_R(t) \equiv \lim_{x_R(t) \rightarrow \xi_s^+(t)} v(t, x_R(t)), \quad F_R(t) \equiv \lim_{x_R(t) \rightarrow \xi_s^+(t)} F[t, x_R(t), v(t, x_R(t))], \quad (5.54)$$

we obtain an equation for the velocity of the shock – the Rankine-Hugoniot (jump) condition,

$$\partial_t \xi_s(t) = \frac{F_R(t) - F_L(t)}{v_R(t) - v_L(t)}. \quad (5.55)$$

This equation can be used to calculate the propagation of a shock wave.

A first application in the FRG context was presented by Ref. [77] for a three-dimensional $O(N)$ model in the $N \rightarrow \infty$ limit. A similar application, which was inspired by Ref. [77], is presented below for the zero-dimensional version of the $\lim_{N \rightarrow \infty} O(N)$ model with the UV potential Eqs. (3.40) and (3.41).

5.2. Numerical implementation

The problem of numerically solving FRG flow equations in various truncations is as old as the Wetterich equation or earlier formulations of RG flow equations, because their analytic solution is rarely possible. This leads to the development of a variety of numerical approaches. Especially for flow equations of effective bosonic local potentials in the LPA and beyond or truncations including field-dependent couplings, there is a lot of literature, which suggests to use some self-developed/adopted discretization schemes. These comprise naive finite-difference discretizations, spline interpolations, or global expansions in terms of polynomials, *e.g.*, Chebyshev polynomials, *etc.*, see Section 1.2.2.

However, in retrospect and from the discussion of the previous Section 5.1 it might be advisable to rely on well-established and tested numerical schemes from experts on numerical mathematics, which can cope with all types of non-analytic structures *etc.*, if one heads for solving non-linear conservation laws.

Therefore, when E. Grossi and N. Wink published their interpretation of the LPA of the $O(N \rightarrow \infty)$ model in terms of an advection equation, they proposed to use modern finite-element methods

from the field of CFD [77]. In fact, they opted for a special sub-type, namely local DG methods, and quantitatively demonstrated their outstanding performance in the context of RG flows. In some follow-up works this framework was extended to coupled sets of PDEs containing a field-dependent Yukawa coupling as well as systems at finite- N , which contain diffusive contributions [101, 102, 103].

For our work we took another, related, and powerful approach from CFD to solve RG flows of effective potentials – finite-volume methods. In the following we briefly sketch the general idea behind the finite-volume methods and present the specific scheme, which we used for our computations, namely a Monotonic Upstream-centered Scheme for Conservation Laws (MUSCL) in the version of Kurganov and Tadmor [105]. This scheme is usually referred to as the KT (central) scheme.

All adequate methods usually have in common that they rely on (quasi-)conservative formulations of PDEs and include methods to avoid artificial oscillations, overshooting *etc.* in the vicinity of non-analyticities.

5.2.1. Finite-volume methods

Consider a one-dimensional PDE of type

$$\partial_t u(t, x) + \frac{d}{dx} F[t, x, u(t, x)] = \frac{d}{dx} Q[t, x, u(t, x), \partial_x u(t, x)] + S[t, x, u(t, x)], \quad (5.56)$$

where F is again an advection flux, Q denotes a diffusion flux, and S is a source-like term, on a finite computational domain $\Omega = \mathcal{V} \times [t_0, t_m]$. Here, $\mathcal{V} \in \mathbb{R}$ is the spatial domain/volume and $[t_0, t_m]$ the temporal domain. Further, we refer to u as the conserved quantity or more general a fluid field.

Of course, generalizations to systems of M conserved quantities $u \rightarrow \{u_1, \dots, u_M\}$ and to $(d + 1)$ dimensional spacetime domains $(t, x) \rightarrow (t, \vec{x}) = (t, x_1, \dots, x_d)$ are possible, but shall not be discussed here.

In addition to the PDE itself and the domain, one needs to specify an initial condition $u(t_0, x)$ and Dirichlet/Neumann boundary conditions, which specifies $(\partial_x)u(t, x)|_{x \in \partial\mathcal{V}}$, such that solving the PDE constitutes a well-posed problem.

The central question is then how $u(t, x)$ is numerically evolved from its initial value at t_0 to its final state at t_m . Here, we motivate the rather popular class of finite-volume (FV) schemes, which serve for this purpose. These schemes are rather popular due to their intuitive interpretation and implementation in terms of balance and conservation laws [49, 50]. However, as already anticipated, there are also alternative high-resolution shock-capturing (HRSC) schemes in CFD, such as finite-difference schemes including flux limiters and numerical viscosity, finite-element methods, and mixtures thereof, see Refs. [104, 49, 51, 52] and references therein.

The central idea between all FV methods is a split of the computational domain Ω into a finite number of spacetime control volumes $\mathcal{V}_j \times [t^i, t^{i+1}]$. In general, the spatial control volumes \mathcal{V}_j do not need to be of the same size and can be of any shape in higher dimensions. The distribution and resolution of spatial cells can even be restructured within each time step by adoptive-mesh-refinement (AMR) techniques. Anyhow, for this work we consider n equally spaced one-dimensional \mathcal{V}_j of size Δx , which shall be centered at positions x_j and are constant during the time evolution. The cell boundaries are located at $x_{j \pm \frac{1}{2}} \equiv x_j \pm \frac{\Delta x}{2}$. For each of these cells, we further define the cell average of the fluid field:

$$\bar{u}(t, x_j) \equiv \frac{1}{\Delta x} \int_{x_{j-\frac{1}{2}}}^{x_{j+\frac{1}{2}}} dx u(t, x). \quad (5.57)$$

Using this definition and integrating Eq. (5.56) over the spacetime control volumes $\mathcal{V}_j \times [t^i, t^{i+1}]$, one obtains

$$\begin{aligned} \bar{u}(t^{i+1}, x_j) &= \\ &= \bar{u}(t^i, x_j) - \int_{t^i}^{t^{i+1}} dt \frac{F[t, x_{j+\frac{1}{2}}, u(t, x_{j+\frac{1}{2}})] - F[t, x_{j-\frac{1}{2}}, u(t, x_{j-\frac{1}{2}})]}{\Delta x} + \dots, \end{aligned} \quad (5.58)$$

due to the Gauss-Ostrogradski (divergence) theorem. The ellipsis denote the integrals over the diffusion flux and source term. Introducing the abbreviation $\bar{u}_j^i \equiv \bar{u}(t^i, x_j)$ for the cell averages the equation compactly reads

$$\bar{u}_j^{i+1} = \bar{u}_j^i - \int_{t^i}^{t^{i+1}} dt \frac{F[t, x_{j+\frac{1}{2}}, u(t, x_{j+\frac{1}{2}})] - F[t, x_{j-\frac{1}{2}}, u(t, x_{j-\frac{1}{2}})]}{\Delta x} + \dots, \quad (5.59)$$

which is a discrete evolution equation for the cell averages \bar{u}_j^i .

The challenge is now to evaluate the integral on the r.h.s. for each cell, which constitutes the solution of a Riemann problem at each cell interface [210, 104, 49, 50, 51, 52]. Thereby, one needs to calculate the fluxes between the cells, which requires a reconstruction of the fluid on the cell interfaces, $u_{j+\frac{1}{2}}(t) \equiv u(t, x_{j+\frac{1}{2}})$, from the cell averages \bar{u}_j^i . This reconstruction is scheme dependent and usually based on some type of polynomial interpolation including the neighboring cell averages. The quality (order) of the reconstruction of course contributes to the overall error of the numerical scheme and usually scales with some power of the cell size Δx .

Still, even after reconstruction of the $u(t^n, x_{j+\frac{1}{2}})$, it remains to solve the Riemann problem, which is the exact evaluation of the time integral in Eq. (5.59). For some fluxes and specific types of PDEs an exact evaluation might be feasible. However, in the FV framework one usually uses approximate Riemann solvers [211, 212, 213] or schemes that do not rely on Riemann solvers at all [105]. Within the next lines, we briefly present a specific FV scheme, the KT (central) scheme [105], which is not based on a Riemann solver and is especially chosen because of its simplicity and flexibility, while still being highly efficient and accurate. For details on alternative schemes and pedagogic introductions to FV and HRSC methods, we refer to Refs. [49, 50, 52, 210].

5.2.2. The KT scheme

Here, we summarize the key aspects of the MUSCL scheme by Kurganov and Tadmor from Ref. [105], which we implemented, as its developers suggest for (systems of) conservation laws like Eq. (5.56), in terms of a black-box solver. For details we refer to the original literature and the more detailed recapitulation in our own publication [1].

The key feature of the KT scheme is that the only additional information (apart from the PDE and its initial and boundary conditions), which is required for the solution, is the spectral radius of the Jacobian of $F[u]$, which reduces to $|\frac{\partial F}{\partial u}|$ for a single fluid field u , and estimates the characteristic fluid velocities. Because these advection velocities dominate the PDE, the core algorithm of the KT scheme exclusively focuses on the correct handling of the advection fluxes. Diffusion and source contributions are treated separately and we ignore them for the moment.

Advection

The KT scheme does not rely on a Riemann solver and the characteristic decomposition of the advection flux. Instead, it is based on a direct evaluation of the flux integrals on the r.h.s. of Eq. (5.59).

An interesting aspect of the KT scheme is that there is an exact limit of $t^{i+1} - t^i = \Delta t \rightarrow 0$ for Eq. (5.59) after evaluation of the flux integrals. In consequence, there is a semi-discrete version of the KT scheme, which is continuous in time but discrete in space. This is of great advantage, because the PDE (5.56) reduces to a coupled set of ODEs, which can be tackled with modern

ready-made ODE solvers. These usually come with several different time-stepping methods and automatic switching between them as well as step-refinement techniques, if this is needed. Usually they can even cope with stiff problems, which is needed for PDEs from FRG in the IR.

In this respect, the KT scheme can be seen as an improvement of its fully discrete predecessor, the Nessyahu-Tadmor scheme [214], which is based on the same piecewise-linear MUSCL reconstruction [215]. Furthermore, w.r.t. the spatial accuracy, which is of second-order, it can be seen as an improved version of the first-order accurate Lax-Friedrichs scheme [216, 217].

Let us now briefly sketch the steps which the KT scheme is made of.

0. The zeroth step, which is usually not mentioned in FV literature and not part of the original KT literature [105], is to calculate the FV cell averages \bar{u}_j^0 for the initial condition $u(t_0, x)$ via Eq. (5.57), before starting the time stepping at all. This step is crucial, especially if there are discontinuities already present in the initial condition. Simply using $u(t_0, x)$ evaluated at the cell centers x_j to approximate \bar{u}_j^0 can lead to significant errors, because for cells which contain discontinuities this procedure leads to a drastic over- or underestimation of the true cell averages. The same happens, if Δx is large compared to tiny structures in $u(t_0, x)$. Here, an average over these structures is by no means identical to an evaluation at the cell center. This averaging in the initial condition, which seems to slightly smear the initial condition and is afterwards handed over to the solver, seems counterintuitive at first sight. Nevertheless, having committed to a FV method this has to be taken serious, because otherwise the reconstruction procedure yields wrong approximate results already in the first time step (see 1.).

Having said this, we turn to the real KT algorithm, which is performed within each time step of the time integration.

1. Because the calculation is performed on the level of the cell averages \bar{u}_j^i , the first step in each time step is to reconstruct the function $u(t^i, x)$ from these cell averages, to have access to the function at all positions x . This is done approximately, which is, why the reconstructed function is called $\tilde{u}(t^i, x)$. Here, we use a piecewise-linear MUSCL reconstruction [215], hence, for $x \in [x_{j-\frac{1}{2}}, x_{j+\frac{1}{2}}]$ (the j^{th} cell),

$$\tilde{u}(t^i, x) = \bar{u}_j^i + (x - x_j) \cdot (\partial_x u)_j^i, \quad (5.60)$$

where the approximate derivatives $(\partial_x u)_j^i$ are given by

$$(\partial_x u)_j^i = \frac{\bar{u}_{j+1}^i - \bar{u}_j^i}{\Delta x} \phi\left(\frac{\bar{u}_j^i - \bar{u}_{j-1}^i}{\bar{u}_{j+1}^i - \bar{u}_j^i}\right). \quad (5.61)$$

The function $\phi(r)$ is a so-called TVD limiter and the entire reconstruction process is referred to as a TVD reconstruction [49, 50, 218]. The idea behind the limiter is to prevent the formation of spurious oscillations around discontinuities, by restricting the possible slopes during the reconstruction process, which would otherwise lead to an over- or underestimation of $u(t^i, x)$ by $\tilde{u}(t^i, x)$.

A list of possible TVD limiters is presented in Refs. [49, 50, 52, 219]. Even though we have tested a lot of these limiters for our FRG applications, we could not identify any significant differences (apart from runtime). Therefore we shall focus on the simplistic minmod limiter [220] in the following:

$$\phi(r) = \max(0, \min(1, r)), \quad (5.62)$$

which is also used in the original Ref. [105].

It is also possible to use higher-order reconstruction schemes (for the KT method) to improve the spatial accuracy. This is not needed for this work and we refer to Refs. [221, 222, 223, 224, 225, 226, 227, 228, 229, 230] for further reading on this topic.

2. As the next step within a time step, the previous reconstruction (5.60) is used to determine $u_{j+\frac{1}{2}}^i$ on the cell boundaries. Thereby one distinguishes between a reconstruction from the left and the right,

$$u_{j+\frac{1}{2}}^{i,-} = \bar{u}_j^i + \frac{\Delta x}{2} (\partial_x u)_j^i, \quad u_{j+\frac{1}{2}}^{i,+} = \bar{u}_{j+1}^i - \frac{\Delta x}{2} (\partial_x u)_{j+1}^i, \quad (5.63)$$

These values are used to estimate the local maximal speed of propagation,

$$a_{j+\frac{1}{2}}^i = \max \left[\rho \left(\frac{\partial F}{\partial u} \left[u_{j+\frac{1}{2}}^{i,+} \right] \right), \rho \left(\frac{\partial F}{\partial u} \left[u_{j+\frac{1}{2}}^{i,-} \right] \right) \right], \quad (5.64)$$

where $\rho(A) \equiv \max\{|\lambda_1|, \dots, |\lambda_\omega|\}$ is the spectral radius of the matrix A , if λ_k are its eigenvalues. For one-dimensional u and F , like for this work, the spectral radius simply reduces to the absolute value.

Note that the estimate for the local velocities via Eq. (5.64) can be further refined, *cf.* Refs. [231, 227]. In addition, if an explicit evaluation of $\frac{\partial F}{\partial u}$ is unfeasible, it is also possible to approximate the local velocities, *cf.* Refs. [105, 232, 233]. Anyhow, for this work it turned out that the estimates (5.64) are adequate.

3. Still, within a time step, using these local velocity estimates (5.64) a spacetime control volume $[x_{j+\frac{1}{2},l}^i, x_{j+\frac{1}{2},r}^i] \times [t^i, t^{i+1}]$ around each cell interface $x_{j+\frac{1}{2}}$ is calculated. It corresponds to the region which can be causally influenced by the discontinuity at the cell boundary,

$$x_{j+\frac{1}{2},l}^i = x_{j+\frac{1}{2}} - \Delta t a_{j+\frac{1}{2}}^i, \quad x_{j+\frac{1}{2},r}^i = x_{j+\frac{1}{2}} + \Delta t a_{j+\frac{1}{2}}^i. \quad (5.65)$$

This grid of staggered cells is used to successively evaluate the integral in Eq. (5.59) using midpoint-rule approximations *etc.*. For details of these lengthy but rather simple steps of the integral evaluation, we refer to the original publication [105], which also contains a detailed sketch of the situation in its Fig. 3.2.

This integration step results in a fully discrete second-order accurate central scheme [105, Eq. (3.9)]. Here, \bar{u}_j^{n+1} is calculated via an algebraic formula from

$$\{\bar{u}_{j-2}^i, \bar{u}_{j-1}^i, \bar{u}_j^i, \bar{u}_{j+1}^i, \bar{u}_{j+2}^i\} \quad (5.66)$$

and the corresponding local velocity estimates $\{a_{j\pm\frac{1}{2}}^i\}$, which are in turn formulae of the sets (5.66).

This algorithm is repeated for every time step (except for step zero).

It is also shown in Ref. [105] that the numerical viscosity of this scheme is, in contrast to the predecessor schemes [214, 216, 217] Δt -independent and $\mathcal{O}(\Delta x^3)$. This Δt -independence allows for a controlled $\Delta t \rightarrow 0$ limit, which results in the following semi-discrete form, which can be used directly with standard ODE integrators:

Including exclusively the advection flux, the semi-discrete evolution equation of the j^{th} cell average reads

$$\partial_t \bar{u}_j(t) = - \frac{H_{j+\frac{1}{2}} - H_{j-\frac{1}{2}}}{\Delta x}. \quad (5.67)$$

The corresponding $H_{j+\frac{1}{2}}$ are

$$H_{j+\frac{1}{2}} \equiv \frac{F[t, x_{j+\frac{1}{2}}, u_{j+\frac{1}{2}}^+] + F[t, x_{j+\frac{1}{2}}, u_{j+\frac{1}{2}}^-]}{2} - \frac{a_{j+\frac{1}{2}}}{2} (u_{j+\frac{1}{2}}^+ - u_{j+\frac{1}{2}}^-), \quad (5.68)$$

using Defs. (5.63) and (5.64). Still, despite its non-trivial structure also the semi-discrete scheme has the overall structure of a five-point stencil and stays second-order accurate in Δx .

Note that without an explicit position dependence of the advection fluxes (and ignoring diffusion and source terms), the scheme is conservative, which implies that detailed balance at the cell interface is maintained and nothing of the fluid field u gets lost (which can even be checked numerically to astonishing precision). Without the position dependence the KT scheme is also proven to be TVD/total variation non-increasing (TVNI) for standard flux limiters.

Diffusion

As soon as non-linear diffusion enters the game, the conservation law exhibits potentially strongly degenerate parabolic contributions, which can lead to non-smooth solutions, even without advection.

In Ref. [105], the advection and diffusion fluxes are strictly split and treated independently. Kurganov and Tadmor suggest to use the following discretized version of the diffusion flux,

$$P_{j+\frac{1}{2}} \equiv \frac{Q[t, x_j, \bar{u}_j, \frac{\bar{u}_{j+1}-\bar{u}_j}{\Delta x}] + Q[t, x_{j+1}, \bar{u}_{j+1}, \frac{\bar{u}_{j+1}-\bar{u}_j}{\Delta x}]}{2}, \quad (5.69)$$

which enters Eq. (5.67) as follows

$$\partial_t \bar{u}_j(t) + \frac{H_{j+\frac{1}{2}} - H_{j-\frac{1}{2}}}{\Delta x} = \frac{P_{j+\frac{1}{2}} - P_{j-\frac{1}{2}}}{\Delta x}. \quad (5.70)$$

This discretization mimics a kind of central difference approximation of the fluxes themselves, was tested in Ref. [105] and also by ourselves with standard diffusion problems, and can be used for problems with and without advection.

An alternative discretization of the diffusion term is presented in Ref. [234, App. B]. For diffusion fluxes of type

$$Q[t, x, u, \partial_x u] = \varphi[t, x, u] \cdot \tilde{Q}[t, x, \partial_x u], \quad (5.71)$$

like for our FRG problem, see Eq. (5.13), the $P_{j+\frac{1}{2}}$ in Eq. (5.70) are

$$P_{j+\frac{1}{2}} = \varphi[t, x_{j+\frac{1}{2}}, \frac{1}{2}(u_{j+\frac{1}{2}}^+ + u_{j+\frac{1}{2}}^-)] \cdot \tilde{Q}[t, x_{j+\frac{1}{2}}, \frac{\bar{u}_{j+1}-\bar{u}_j}{\Delta x}]. \quad (5.72)$$

Both versions of the discretized diffusion fluxes were tested within this work without finding significant differences. All numerical results in this thesis and the corresponding Refs. [1, 2, 3, 4] are calculated via the first version.

We remark that using schemes with higher-order reconstruction these usually also come with higher-order discretization of the diffusion flux, *e.g.*, Ref. [224].

Sinks and sources

The KT scheme also allows for a straightforward inclusion of sink/source terms of type $S[t, x, u]$, if they can be strictly split from advective and diffusive contributions [105].

For u -independent sources of type $S[t, x] = \partial_x s(t, x)$ the spatial integration over FV cells from Eq. (5.56) to Eq. (5.59) can be performed analytically and the sink/source term contributes to Eq. (5.70) as follows

$$\partial_t \bar{u}_j(t) = \dots + \frac{s_{j+\frac{1}{2}} - s_{j-\frac{1}{2}}}{\Delta x}, \quad s_{j+\frac{1}{2}} = s(t, x_{j+\frac{1}{2}}). \quad (5.73)$$

Otherwise, for u -dependent sink/source terms, one may simply use $S[t, x_j, \bar{u}_j(t)]$ as an approximation. For details in the FRG context, we refer to Ref. [4] and Part II of this thesis.

Ultimately, we find the full semi-discrete KT scheme,

$$\partial_t \bar{u}_j(t) + \frac{H_{j+\frac{1}{2}} - H_{j-\frac{1}{2}}}{\Delta x} = \frac{P_{j+\frac{1}{2}} - P_{j-\frac{1}{2}}}{\Delta x} + \text{source}. \quad (5.74)$$

Caveat of applicability to RG flow equations

As already mentioned in Section 1.2.2, care should be taken if numerical methods are run at their edge of applicability. Therefore, we have to remark at this point that also the KT scheme was designed in its original version by Kurganov and Tadmor in Ref. [105] solely for t - and x -independent advection and diffusion fluxes, while FRG problems show t - and x -dependent fluxes. (It is neither stated explicitly by the authors that the scheme works for such systems nor that it is not applicable.)

We do not believe that the t -dependence of the fluxes (5.12) and (5.13) of our FRG problem causes any trouble, because the highly complicated and non-linear dynamics in t is transferred to the ODE time-stepper anyhow. Concerning the explicit x -dependence, things are more involved, because it spoils the fundamental TVD/TVNI and conservative property of the advective part, which is a fundamental feature of the KT scheme. However, to the best of our knowledge, the x -dependence does not alter the correct estimation of the advection velocities via $\frac{\partial F}{\partial u}$, such that the core of the KT algorithm for the evaluation of the flux integrals is working properly.

In any case, using the KT scheme in an uncontrolled environment, like for general FRG applications, calls for detailed testing. This is done in Chapter 6 for our zero-dimensional $O(N)$ toy-models with challenging UV initial conditions. For all our tests, the KT scheme delivered remarkably precise results in terms of extremely small relative deviations from exactly known reference values. Therefore, we strongly believe that the KT scheme is safely applicable for t - and x -dependent advection and diffusion fluxes, but we can not guarantee for this for general FRG setups. Additional research is definitely indispensable.

5.2.3. (Discretized) boundary conditions

Solving a PDE is exclusively a well-posed problem, if, in addition to the PDE itself, its domain, and its initial condition, there are well-defined boundary conditions [104, 49, 50, 51, 52]. Elliptic PDE problems are therefore also called boundary-value problems, because normally there is no initial condition and no time evolution. In the case of (non-linear) PDEs of hyperbolic and parabolic type (like the RG flow equation of the local potential), one usually speaks about a Cauchy or initial(-boundary)-value problem, because the initial (and boundary) condition(s) are needed to propagate the solution to later times.

On the numerical level, it is further necessary that these Dirichlet and/or Neumann boundary conditions are correctly translated to their discretized version. Otherwise it is impossible to obtain correct weak solutions from numerical time stepping. For numerical schemes, like the previously presented FV methods, this is usually done in terms of ghost/dummy cells, which are added artificially outside of the actual physical domain and control the in- and out-fluxes.

Unfortunately, in the FRG literature on flow equations for models and theories, which include a PDE for a local effective potential, there is little discussion on the influence of boundary conditions on the (numerical) solution and their detailed implementation. Some notable exceptions are for example Refs. [84, 85, 235, 196, 82, 83]. Therefore, we also spend some paragraphs in this work to discuss this important issue in great detail and present our reasoning and implementation of boundary conditions for the RG flow equations (5.3) and (5.4).

Identifying the boundary conditions

The domains of the PDEs (5.3) and (5.4) that describe the RG flow of $u(t, \varrho) = \partial_{\varrho} U(t, \varrho)$ in ϱ and $u(t, \sigma) = \partial_{\sigma} U(t, \sigma)$ in σ are $\mathbb{R}_{\geq 0}$ and \mathbb{R} respectively. Therefore, the RG flow of $u(t, \sigma)$ represents a pure initial-value/Cauchy problem without explicit boundary conditions. For $\sigma \rightarrow \pm\infty$ the problem is defined by the asymptotics of the initial condition and the PDE itself and it (theoretically) suffices to know the initial condition to solve the problem. For the version of the PDE in ϱ this is different, because, due to the use of the $O(N)$ symmetry, a domain boundary is introduced at $\varrho = 0$, where boundary conditions for $u(t, \varrho)$ should be imposed. The same happens

if one uses the remaining \mathbb{Z}_2 (anti)-symmetry,

$$U(t, \sigma) = U(t, -\sigma), \quad \Leftrightarrow \quad u(t, \sigma) = -u(t, -\sigma), \quad (5.75)$$

to also reduce the domain of the PDE (5.4) to $\mathbb{R}_{\geq 0}$.⁴ (For the sake of simplicity, we choose $\sigma \geq 0$ and not $\sigma \leq 0$ for the remaining discussion.) Here, the boundary condition is clear by construction, *viz.*, $u(t, \sigma)$ has to be anti-symmetric at $\sigma = 0$. However, for the formulation in ϱ , thus $u(t, \varrho)$, the correct specification of the boundary condition is not clear to us. At first sight, one might be tempted to argue that $u(t, \varrho = 0)$ has to be zero, because by symmetry $\varrho = 0$ has to be a local extremum of the potential. However, if the potential is non-analytic at $\varrho = 0$, which can easily be realized, $u(t, \varrho = 0) = \partial_{\varrho} U(t, \varrho = 0)$ is non-zero and can even diverge. The same is the case for $u(t, \sigma = 0) = \partial_{\sigma} U(t, \sigma = 0)$. Still, in the σ -formulation, there generally exist negative values of σ which allows to cope with possible non-analytic behavior and the anti-symmetry, as is discussed below.

Anyhow, for a numerical solution of the PDE, *e.g.*, with FV methods, it is impossible to work on non-compact domains and a compactification to an effective finite computational domain is required. Basically, there are two options to reduce $\sigma \in [0, \infty)$ and $\varrho \in [0, \infty)$ to a finite domain. Either one compactifies the domain by a mapping function, *e.g.*, $\sigma \mapsto \tilde{\sigma}(\sigma)$, and $u \mapsto \tilde{u}(u)$, which also renders \tilde{u} finite on this domain or, as is also popular in the FRG literature, see for example Refs. [59, 236], one truncates the spatial domain (field space) at some finite σ_{\max} with a suitable boundary condition.

Next, we discuss the $\sigma = 0 = \varrho$ and $\sigma \rightarrow \infty$ ($\varrho \rightarrow \infty$) boundaries in detail.

$\sigma = 0$ boundary condition

We start with an analysis of the boundary condition at $\sigma = 0 = \varrho$. From the PDEs (5.3) and (5.4) it might be appealing to use the ϱ -version of the flow equation, Eq. (5.3), because the advection flux (5.10) does not explicitly depend on ϱ and one avoids the nasty $\frac{1}{\sigma}$ term in the denominator of Eq. (5.12), which makes the flux diverge at $\sigma = 0$. In addition, the $\hat{O}(N)$ symmetry is manifestly encoded already in the domain of the problem if one uses ϱ .

Nevertheless, we believe that a formulation in the background field σ is better suited for numerical calculations, because of the following arguments.

As discussed, highly non-linear advection-diffusion problems tend to form non-analyticities. In FRG, we know that this is indeed the case. For example, in a symmetry-broken phase in the IR bosonic potentials become flat and convex for small field values, but still have non-trivial minima, which can only be realized if the potential is non-analytic around these minima, see, *e.g.* Ref. [13]. The same applies to calculations at non-zero chemical potentials, which introduces moving RG-time-dependent non-differentiable cusps into the potential and possible jumps in its derivative, *cf.* Section 10.3 and Ref. [4]. In consequence, non-analytic behavior can also be present close to or at $\sigma = 0 = \varrho$, such that even though $U(t, \sigma)$ is symmetric and has a local extremum at $\sigma = 0$, this point does not need to be analytic. It follows that $u(t, \sigma)$ (being anti-symmetric) might be discontinuous and jump from $-u$ to u or even have a pole at $\sigma = 0$. Formulated in ϱ , $u(t, \varrho)$ is also not restricted and takes some arbitrary values at $\varrho = 0$ during the RG flow.

It remains the question why this (presently) disfavors the formulation in ϱ ?

⁴If possible, this reduction of the domain is always advisable from a numerical point of view. As long as $u(t, \sigma)$ is perfectly odd about $\sigma = 0$ there is no additional information contained in the second half of the domain. As it happens, spanning the computational domain over positive and negative σ might even introduce tiny numerical errors from the floating-point arithmetic, which are not perfectly symmetric and do not balance, and can lead to artificial symmetry breaking. In addition, using the \mathbb{Z}_2 anti-symmetry can significantly speed up the calculation, because less cells are required to reach the same spatial resolution.

This is seen best on the discrete level. For the FV scheme from the previous section the boundary conditions have to be realized by two ghost cells at each boundary to control the in- and out-fluxes from the physical domain. Other numerical schemes also require additional ghost grid points *etc.*. In any case, it has to be specified where these ghost cells/points are located and how the cell averages of the ghost cells are (re-)constructed/chosen (from the physical cells).

ϱ -formulation In the ϱ -formulation it seems questionable to place the ghost cells outside the physical domain at negative ϱ , because there is no notion of negative ϱ and it is presently unclear to us how the cell averages $\bar{u}_j(t)$ should be chosen there.

So what about positioning the ghost cells inside the physical domain at positive ϱ close to $\varrho = 0$? In this case the ghost cells are well defined, because $\varrho \geq 0$ physically exists. However, the cell averages $\bar{u}_j(t)$ in these cells would have to be reconstructed from the cell averages at larger ϱ via some kind of extrapolation. This, however, does not make sense at all, because the behavior of $u(t, \varrho)$ and the correct extrapolation is not known at small ϱ and finding its dynamics is part of the original problem of solving the PDE. An extrapolation is especially dangerous, because the fluid is in general propagated to smaller ϱ , *cf.* Eq. (5.14), where a lot of dynamics takes place. Further, even the physical point might be located at $\varrho = 0$ and should therefore be part of the solution and not of an extrapolation. If one also takes into account the diffusive contributions, some hand-waving constructions about $\varrho = 0$ sounds even more questionable, because diffusion is undirected and also transports information and possible errors from smaller to larger ϱ , especially, if there was symmetry breaking in the first place. Hence, the artificial boundary condition at $\varrho = 0$ potentially influences all ϱ .

This discussion does by no means imply that there is no solution or workaround for this problem. In fact, we believe that there has to be a valid formulation of a discretized boundary condition in ϱ with ghost cells being located at some fictitious negative ϱ , but we were not able to find it for general setups.

Still, there is an exception to our present objections against choosing ϱ as the spatial coordinate. In the $N \rightarrow \infty$ limit of the $O(N)$ model one finds that information is strictly transported towards $\varrho = 0$, because $\partial F/\partial u$ is always positive. In this scenario ghost cells can be positioned at negative ϱ , because information is never propagated back into the physical domain. Here, we shall not discuss this further, but refer to Refs. [77, 101] and Ref. [3, Appendix E & F] for details.

σ -formulation In this case, there is no problem at all to place ghost cells at negative σ . In addition, from the anti-symmetry of $u(t, \sigma)$ it is obvious that the cell averages of the ghost cells simply need to be chosen as the negative of the first cells in the physical domain.

Still, there is the problem of the factor $\frac{1}{\sigma}$ in the advection flux (5.12), which diverges at $\sigma = 0$. Furthermore, it would be required by the KT scheme to reconstruct the $u(t, \sigma)$ on the cell interface, which is also a problem if $u(t, \sigma)$ is discontinuous at a possible cell interface at $\sigma = 0$.

At least within FV schemes there is a rather simple solution for both issues. If one of the ghost cells or the first physical cell is positioned symmetric about $\sigma = 0$, one never has to evaluate the advection flux at exactly $\sigma = 0$ because the advection flux is always calculated on the cell interfaces, which has a distance of $\pm \frac{\Delta\sigma}{2}$ to the problematic $\sigma = 0$. Hence, the $\frac{1}{\sigma}$ -term no longer causes problems and a reconstruction of $u_{j+\frac{1}{2}}(t)$ is never required at $\sigma = 0$. In addition, we can always fix the cell average $\bar{u}_{j=0}(t)$ to zero, because the average over an odd function always vanishes, even if this function jumps or has a pole at $\sigma = 0$. Hence, we position our FV grid as follows:

The zeroth cell has its center at $\sigma_0 = 0$ and the centers of all physical cells are located at $\sigma_j = \Delta\sigma \cdot j$, $j \in \mathbb{N}$, while their interfaces are at $\sigma_{j+\frac{1}{2}} = \Delta\sigma \cdot (j + \frac{1}{2})$. In turn, the two ghost cells have their cell centers at $\sigma_{-1} = -\Delta\sigma$ and $\sigma_{-2} = -2\Delta\sigma$. The corresponding cell averages of the first three cells are

$$\bar{u}_{-2}(t) = -\bar{u}_2(t), \quad \bar{u}_{-1}(t) = -\bar{u}_1(t), \quad \bar{u}_0(t) = 0, \quad (5.76)$$

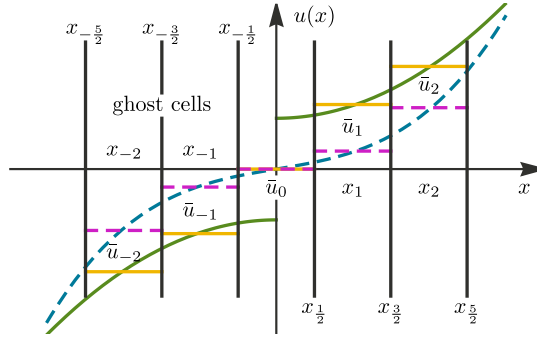


Figure 5.1: Second-order accurate FV implementation of the spatial boundary condition for $u(t, x)$ or $\bar{u}_j(t)$ respectively, at $x = 0$. We use the fact that $u(t, x)$ is an odd function in x by positioning the first computational cell x_0 at $x = 0$, such that the cell average is exactly zero $\bar{u}_0(t) = 0$, which is true for $u(t, x)$ which are analytic (blue-dashed) as well as non-analytic (green-solid) at $x = 0$. The ghost-cell averages can thus be fixed by setting $\bar{u}_{-2}(t) = -\bar{u}_2(t)$ and $\bar{u}_{-1}(t) = -\bar{u}_1(t)$. Corresponding cell averages $\bar{u}_i(t)$ are depicted as horizontal bars (magenta-dashed and yellow-solid). This boundary condition can be generalized to lower- and higher-order accurate FV schemes as well as finite-difference or finite-element schemes, as well as to problems of two or more field-space directions. From Ref. [1, Fig. 3].

for all times t . This forms a valid and stable implementation of the boundary condition, which is valid for any $\Delta\sigma$ and all times t . For illustrative reasons, the situation is again sketched in Fig. 5.1.

Large- σ boundary condition

Next, we turn to the artificial computational boundary condition at large field values. Due to the previous discussion and w.l.o.g. we discuss this for positive $\sigma \in [0, \infty)$.

As already said, formally on the level of the PDE, there is no boundary condition required and the initial condition suffices. This is seen as follows. The effective local potential has to be bounded from below for all RG times and at least grows like σ^2 for large σ . If $U(t, \sigma)$ grows faster than σ^2 the advection and diffusion flux (5.12) and (5.13) both vanish asymptotically, such that $\sigma \rightarrow \infty$ is a zero influx boundary condition and $u(t, \sigma)$ keeps its initial UV asymptotic shape. If the asymptotic behavior of the UV potential is exactly proportional to σ^2 , both fluxes are asymptotically independent of σ , which implies that there is constant in- and outflux in each discretized FV cell. Also here, there is asymptotically no change of $u(t, \sigma)$.

Anyhow, it is impossible to implement this directly for $\sigma \rightarrow \infty$ and there are basically two options to proceed numerically:

1. One could try to map the domain $[0, \infty)$ to the interval $[0, 1)$ by rescaling σ with appropriate rescaling of $u(t, \sigma)$, to keep the values of the fluid field finite. Then, however, one needs to implement the asymptotic boundary conditions at the right boundary of the finite interval, which again brings up questions about the correct positioning of ghost cells and decent extrapolation *etc.*. Further, in order to keep a high resolution of small σ to resolve the physical region and the minimum, the mappings need to be highly non-linear. These distortions come with additional parameters and modify the flow equation, which can lead to additional numerical challenges. After some testing with different map functions, like versions of \tanh , \arctan *etc.*, we discarded this approach and turned to something much simpler – the second option. (This does not imply at all that there are no smart mappings in general.)
2. Another simple and robust option is to split field space into the compact domain $[0, \sigma_{\max}]$ and a non-compact domain $[\sigma_{\max}, \infty)$. Thereby, σ_{\max} has to be chosen larger than the physically

relevant region, but not too large. Approximately three times larger than the physically relevant regions (*e.g.*, defined by a (temporally) non-trivial minimum) turned out to be a good first approach, but this needs to be tested again for every model. Explicit tests are provided later on for zero-dimensional $O(N)$ models and were also performed for the studies of Part II of this thesis in Ref. [4, Appendix F]. Furthermore, we keep a direct identification of the field space with the computational domain. In higher-dimensional calculations a rescaling of field space with the characteristic energy scale (*e.g.*, a condensate, the UV cutoff, a critical temperature) to the appropriate power might be helpful, see again Part II or Ref. [4].

Within the compact domain $[0, \sigma_{\max}]$, one has to ensure a high resolution in terms of FV cells, in order to capture the relevant dynamics. For the non-compact domain at large σ we suggest to expand or approximate $u(t, \sigma)$ in terms of a complete set of functions/polynomials with RG-time-dependent expansion coefficients. As discussed, for large σ , we do not expect a lot of dynamics and deviations from the initial conditions due to decreasing fluxes. Furthermore, for most common UV initial potentials, we do not expect non-analytic structures at large σ , such that a low-order expansion should work out.

Then at the point σ_{\max} the ghost cells for the FV method of the interval $[0, \sigma_{\max}]$ can be fixed via $u(t, \sigma)$ from the asymptotic expansion in the non-compact interval.

The total RG-time evolution and solution consists of an evolution of the cell averages from the first domain and the expansion coefficients of the second domain.

Interestingly, it turned out during our practical tests that the approximation of $u(t, \sigma)$ in $[\sigma_{\max}, \infty)$ is actually not needed, if the interval σ_{\max} is large enough to almost totally suppress the fluxes. This is oftentimes found at surprisingly small σ but strongly depends on the problem at hand. Of course, it also requires a rather large number of FV cells to keep a high resolution via small $\Delta\sigma$.

For this approach it turned out that a simple linear extrapolation of the two last physical cells to the ghost cells, which are located at $\sigma_{\max} + \Delta\sigma$ and $\sigma_{\max} + 2\Delta\sigma$, suffices, as long as $\Delta\sigma$ is small to fix the cell averages in the ghost cells in each time step.⁵ Thus, we simply use for all times t ,

$$\bar{u}_n(t) = 2\bar{u}_{n-1}(t) - \bar{u}_{n-2}(t), \quad \bar{u}_{n+1}(t) = 3\bar{u}_{n-1}(t) - 2\bar{u}_{n-2}(t), \quad (5.77)$$

for the ghost-cell averages, if there are n physical cells centered at $\{\sigma_0, \sigma_1, \dots, \sigma_{n-1}\}$ and the last physical cell is labeled by σ_{n-1} and centered at σ_{\max} . Explicit tests are provided in Section 6.5.2.

Anyhow, if σ_{\max} has to be too large to suppress the influx, it is possible to keep a decent resolution and sensible number of cells, to consider a concatenation of intervals $[0, \sigma_{\max}^{(1)}]$, $[\sigma_{\max}^{(1)}, \sigma_{\max}^{(2)}]$ *etc.*, with different cell size $\Delta\sigma$ in each interval. This ensures high resolution at small σ , while keeping the total computational domain large with a manageable total number of cells and was done with the DG method in the context of the fluid-dynamical approach to FRG [77, 101]. Furthermore, for future improvements one might also think of moving meshes or AMR techniques [237]. Both improvements were not needed for this work.

5.2.4. Discrete formulation of the entropy function and the TVD property

Lastly, before we study explicit tests, we turn to the discretized version of the entropy-/ \mathcal{C} -function for the $O(N = 1)$ model from Section 5.1.4. The task is to formulate Eq. (5.29) with Eq. (5.28) within the FV discretization from Section 5.2.1 and use the discrete boundary conditions from the previous Section 5.2.3.

⁵Higher-order polynomial extrapolation actually perform worse, because these can lead to spurious oscillations, whose error is propagated to smaller σ .

Discrete entropy function

As a first step, we restrict the infinite domains of the σ -integrals to our computational domain $[0, \sigma_{\max}]$. As argued previously, the potential and its derivatives do not change for large field values during the RG flow and as long as σ_{\max} is sufficiently large, we can ignore the contributions from $[\sigma_{\max}, \infty)$ to the two integrals, because they cancel,

$$\mathcal{C}[\partial_\sigma u] = -2 \int_0^{\sigma_{\max}} d\sigma [\partial_\sigma u(t, \sigma)]^2 + 2 \int_0^{\sigma_{\max}} d\sigma [\partial_\sigma u(t=0, \sigma)]^2. \quad (5.78)$$

In the next step, we discretize the spatial derivative using a simple forward finite-difference (FD) stencil.⁶

$$\partial_\sigma u(t, \sigma_i) \simeq \frac{\bar{u}_{i+1}(t) - \bar{u}_i(t)}{\Delta\sigma} + \mathcal{O}(\Delta\sigma). \quad (5.79)$$

Lastly, the integrals are approximated by Riemann sums over the n FV cells and we obtain,

$$\mathcal{C}[\{\bar{u}_i(t)\}] = -\frac{2}{\Delta\sigma} \sum_{i=0}^{n-1} \left(\frac{\bar{u}_{i+1}(t) - \bar{u}_i(t)}{1 + \delta_{i,0} + \delta_{i,n-1}} - \frac{\bar{u}_{i+1}(0) - \bar{u}_i(0)}{1 + \delta_{i,0} + \delta_{i,n-1}} \right). \quad (5.80)$$

The factor $(1 + \delta_{i,0} + \delta_{i,n-1})$ is introduced to compensate for the fact that only the right half of the zeroth cell and the left half of the last volume cell contribute to the integrals of Eq. (5.78). The discrete entropy function Eq. (5.80) can be directly calculated on the discrete solution of the RG flow.

Relation to the TVD property

Let us again emphasize that our entropy function is closely related to the total variation (TV) [218], which is simply defined as the (discretized) arc length of $u(t, \sigma)$ on the computational interval,

$$\text{TV}[u(t, \sigma)] \equiv \int_0^{\sigma_{\max}} d\sigma |\partial_\sigma u(t, \sigma)|, \quad \Leftrightarrow \quad \text{TV}[\{\bar{u}_i(t)\}] \equiv \sum_{i=0}^{n-1} |\bar{u}_{i+1}(t) - \bar{u}_i(t)|. \quad (5.81)$$

Using the absolute value instead of the square in Eq. (5.78) and introducing a normalization as well as a sign-flip solely constitute quantitative differences, while the qualitative interpretation of the TV and entropy function stays the same: For each time step both functions are only non-increasing/decreasing (depending on the sign) and somehow measure the arc length of $u(t, \sigma)$. The property of a solution of a PDE having an arc length that shrinks monotonically is usually called TVD but should actually be denoted as TVNI, *cf.* Ref. [52]. It is fundamentally linked to the existence of (weak) solutions in a huge class of hyperbolic and parabolic conservation laws [238, 200, 104, 49, 50, 218, 51, 239, 52].

From the above construction of the entropy function and its direct relation to the TVNI property, we conclude that the PDE for the RG flow of the effective potential of the zero-dimensional $O(N = 1)$ model is also TVNI. Further, we believe that this points towards a direct relation between the concepts of (numerical) entropy on the level of the PDE and the formal \mathcal{C} -theorem in QFTs. For further discussions we refer to our publication [2].

⁶We are aware of the fact that a FD approximation of the derivative is ill-conditioned at non-analytic points in $u(t, \sigma)$. Hence, the absolute value of $\mathcal{C}[\partial_\sigma u]$ will strongly depend on how the derivative hits possible discontinuities *etc.*, thus on the choice of $\Delta\sigma$ and σ_{\max} . Anyhow, we are not quantitatively interested in this absolute value but its change during the RG flow. Furthermore, for our zero-dimensional toy models the corresponding IR potentials are smooth, such that a FD approximation gets less problematic during the RG flow. Nevertheless, for future works (in higher dimensions) it might be better to use some reconstructed values for the derivatives, like Eq. (5.61).

Chapter 6

Tests, results, applications, and conclusions

Abstract We test the framework of numerical fluid dynamics for FRG flow equations. Introducing challenging test cases, we benchmark the FV-KT scheme against exact reference solutions. This includes tests of numerical parameters belonging to the discretization and FRG parameters such as decent choices of cutoffs. Further, we discuss qualitative aspects of FRG flows from the perspective of fluid dynamics.

Our numeric scheme is also quantitatively compared against an expansion scheme of the flow equation. Here, the FRG Taylor expansion of the effective potential is tested in detail.

Further, we provide quantitative results and a discussion of the entropy function for the RG flow, which was constructed in the previous chapter for the $N = 1$ limit of the $O(N)$ model.

Afterwards, we turn to the inviscid limit, thus $N \rightarrow \infty$. We discuss shocks and rarefaction waves in the FRG flow equation and their relation to PTs. Then, we compare RG flows at infinite N with flows at finite N and demonstrate that even at large N with only little diffusion the dynamics is drastically changed. This is put into context with our previous discussion on the shortcomings of the $N \rightarrow \infty$ limit.

Finally, we summarize the discussion of Part I of this thesis and our novel findings and present possible generalizations and applications.

Disclosure Also this chapter is almost entirely based on our own publications [1, 2, 3] and is a compilation of their mostly novel results. The order of presentation and arrangement of the discussion deviates from the publications, though the content (including figures) is almost the same. Of course, there is some minimal text overlap or similar wording, because the text of these publications was mostly written by M. J. Steil and myself in approximately equal shares and joint work. Again, the discussion is also influenced by works of our collaborators [77, 101, 102, 103] and the related Ref. [4].

6.1. Introductory remarks

In the preceding Chapter 5 we presented a theoretical framework for studying FRG flow equations in terms of fluid-dynamical problems. Furthermore, we discussed several qualitative and quantitative consequences of this interpretation and introduced a numerical scheme to solve the PDE for local bosonic potentials in terms of conservation laws. However, all theory is nothing without explicit testing. This is subject of this chapter.

Similar to Chapter 3 we use that zero-dimensional QFTs are exactly integrable via the path-integral formalism, which provides explicit reference solutions, see Chapter 2. Hence, our novel

fluid-dynamical setup, with numerical methods from CFD for solving the exact¹ RG flow equation of the effective potential, is benchmarked against these solutions. This is done by studying relative deviations of vertex functions obtained from the FRG from their exact counterparts. These errors are analyzed as functions of several parameters which concern the numerical scheme (*e.g.*, the spatial resolution or the size of the computational domain), but also parameters from the FRG formalism (*e.g.*, UV and IR cutoffs). In addition, we also test the correct implementation of boundary conditions *etc.*.

Supplementary, we also use this chapter to benchmark the FRG vertex/Taylor expansion as an artificial truncation of the exact Wetterich equation in zero dimensions. Also here, we discuss relative errors from exact results for vertex functions, *e.g.*, their dependence on the truncation/expansion order.

To be precise, we always use

$$\left| \frac{\Gamma_{\text{test}}^{(2n)}}{\Gamma^{(2n)}} - 1 \right| \quad (6.1)$$

to quantify the relative errors of vertex functions. Here, $\Gamma^{(2n)}$ denotes the exact result from Eqs. (2.12) and (2.39) to (2.41) *etc.* and “test” indicates the respective vertex function that was calculated via FRG flows in some test scenario.

However, all these tests require challenging setups, which push the methods to their limits. Otherwise there is no evidence at all to trust the novel (numerical) approach in an unknown environment, *e.g.*, in higher-dimensional model calculations for theories where no exact solutions are available. Therefore, we first introduce some explicit zero-dimensional toy models with $O(N)$ symmetry in terms of their corresponding classical UV action. These initial potentials are chosen and constructed in a way to cover various severe challenges, which can also be present in one or the other way in RG flow equations of higher-dimensional $O(N)$ -type models.

Afterwards, we turn to the explicit tests and studies of RG flows of these models. We start with a more qualitative discussion of the fluid-dynamical interpretation of the calculated RG flows of the models, but quickly move on to the above described quantitative checks.

In the second part of this chapter, the specific aspect of entropy production and irreversibility of RG flows is presented from a quantitative perspective. We explicitly calculate the (numerical) entropy along the lines of Sections 5.1.4 and 5.2.4 for our toy models in the viscous $N = 1$ limit and discuss the results and their consequences.

As the grand final of this chapter, we return to the $N \rightarrow \infty$ limit and its consequences. This comprises a discussion of shock and rarefaction waves in the derivative of the effective potential in field space and their relation to PTs. Furthermore, we explicitly demonstrate the drastic difference between large and infinite N and discuss the important role of the σ -mode for restoration of convexity and smoothness.

We close this chapter and Part I of this thesis with concluding remarks and comments on possible generalizations.

6.2. A testing ground in zero dimensions – some toy models

In this section, we present some specific UV potentials for our tests. Each test case is provided in terms of its explicit UV initial condition for the RG flow as well as a formula to obtain exact reference solutions for expectation values and vertex functions (if it exists in terms of a closed analytic expression). Furthermore, the presentation of each UV potential is accompanied by some

¹Here, “exact” refers to the fact that there is no truncation needed.

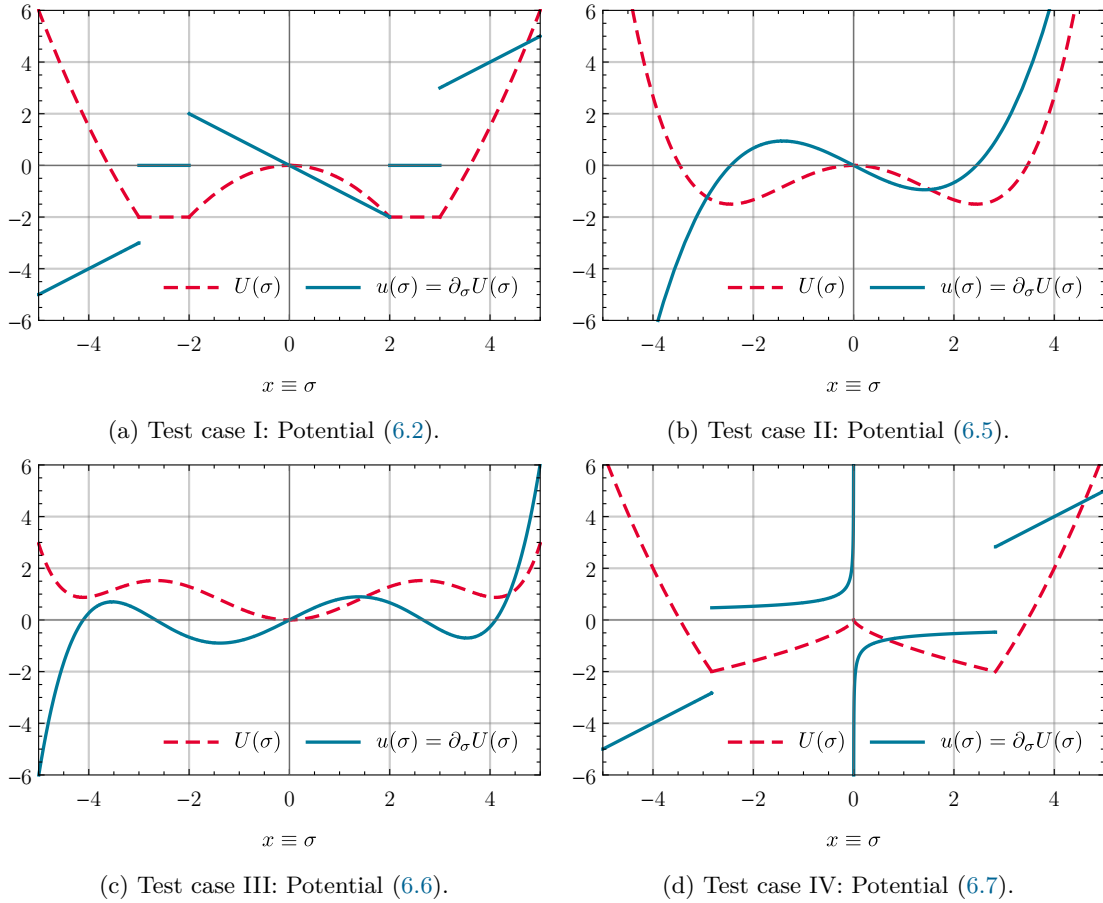


Figure 6.1: The UV potentials $U(\sigma)$ (red-dashed) and their first derivatives $u(\sigma) = \partial_\sigma U(\sigma)$ (blue-solid) evaluated on the constant background-field configuration. From Ref. [1, Figs. 4, 18, 27, 30].

remarks on the reasoning behind the choice/construction w.r.t. possible challenges, because there is no physical phenomenology underlying these potentials in zero dimensions.

All potentials have in common that the parameters and the “physically” interesting dynamical region is of order one. This choice is arbitrary, but it is convenient for a specification of regimes that are larger and smaller scales in the UV and IR. For illustrative reasons Fig. 6.1 provides visualizations of all the UV initial potentials and their derivatives (evaluated on a background-field configuration), while Table 6.1 contains some reference values for the vertex functions which are used in this chapter.

6.2.1. Test case I: Non-analytic initial condition

As our first toy model and test case, we present a non-analytic UV potential, which is defined piecewise,

$$U(\vec{\varphi}) = \begin{cases} -\frac{1}{2} \vec{\varphi}^2, & \text{for } 0 \leq |\vec{\varphi}| \leq 2, \\ -2, & \text{for } 2 < |\vec{\varphi}| \leq 3, \\ +\frac{1}{2} (\vec{\varphi}^2 - 13), & \text{for } 3 < |\vec{\varphi}|. \end{cases} \quad (6.2)$$

Table 6.1: The table lists exact results for various $\Gamma^{(2n)}$ of the $O(N)$ model for selected N for the initial conditions of our test cases (up to numerical integration errors). They are obtained by a high-precision one-dimensional numerical integration of the expectation values $\langle(\vec{\phi}^2)^n\rangle$ using MATHEMATICA's numerical integration routine *NIntegrate* [240] with a *PrecisionGoal* and *AccuracyGoal* of 10. Here, we present the first ten digits only. From Ref. [1, Table I, II, III, IV] & Ref. [2, Table I].

UV potential	N	$\Gamma^{(2)}$	$\Gamma^{(4)}$	$\Gamma^{(6)}$
(6.2)	1	0.1768130358	0.0520549107	0.0865733100
	3	0.3973542395	0.1408641479	0.2249964322
	10	0.8451440328	0.1519326337	-0.0691341063
(6.5) (neg. mass)	1	0.1995098930	0.0622583604	0.1077442107
	4	0.5064440744	0.1824153741	0.2802880035
(6.5) (pos. mass)	1	1.3324252475	0.6078986614	0.7714507237
	4	1.5809246562	0.6118483669	0.5686310448
(6.6)	1	0.1740508127	0.0156179528	0.0134404864
	4	0.2503331837	0.0481313248	0.0432822719
(6.7)	1	0.2046977422	0.0646818943	0.1128487619
	3	0.4216739793	0.1535593029	0.2492523147

Asymptotically, it is quadratic in $|\vec{\varphi}|$. For small $|\vec{\varphi}|$ it is also parabolic, but with negative sign. For an intermediate region, $2 < |\vec{\varphi}| \leq 3$, the potential is flat with an infinite number of degenerate non-trivial minima. The points at $|\vec{\varphi}| = 2$ and $|\vec{\varphi}| = 3$ form non-analytic hyperspheres in field space.

If formulated in the $O(N)$ invariant the potential reads

$$U(\varrho) = \begin{cases} -\varrho, & \text{for } 0 \leq \varrho \leq 2, \\ -2, & \text{for } 2 < \varrho \leq \frac{9}{2}, \\ +\varrho - \frac{13}{2}, & \text{for } \frac{9}{2} < \varrho. \end{cases} \quad (6.3)$$

A plot of the potential and its derivative, evaluated for a constant background-field configuration, is shown in Fig. 6.1a.

Exact solution

The QFT defined by this potential is exactly integrable in terms of transcendental functions. Using

$$\begin{aligned} & \int_0^\infty d\rho \rho^{\frac{N}{2}-1} \rho^n e^{-U(\rho)} \stackrel{(6.3)}{=} \\ & = \left(\frac{N}{2} - n\right)^{-1} \left((-1)^{-\left(\frac{N}{2}-n\right)} \left[\Gamma\left(\frac{N}{2} - n + 1\right) - \left(\frac{N}{2} - n\right) \Gamma\left(\frac{N}{2} - n, -2\right) \right] + \right. \\ & \quad \left. + e^2 \left[\left(\frac{9}{2}\right)^{\frac{N}{2}-n} - 2^{\frac{N}{2}-n} + e^{\frac{9}{2}} \left(\frac{N}{2} - n\right) \Gamma\left(\frac{N}{2} - n, \frac{9}{2}\right) \right] \right), \end{aligned} \quad (6.4)$$

all correlation functions (2.12) and vertex functions, *e.g.*, Eqs. (2.39) to (2.41), can be computed exactly. Nevertheless, for practical purposes a high-precision one-dimensional integration is used to generate floating-point reference results.

Remarks

The potential (6.2) was constructed this way for the following reasons.

1. The UV potential and initial condition for the RG flow start in the symmetry-broken phase. Furthermore, it is non-analytic and non-convex, and comprises an infinite amount of minima. According to Section 2.2 the IR potential has to be smooth, convex, and has exclusively a single trivial minimum. The potential is therefore perfectly suited for studying the restoration of the symmetry during the RG flow as well as the smoothening process.
2. Inspecting the initial condition for the RG flow, namely $u(t = 0, \sigma) = \partial_\sigma U(\sigma)$ in Fig. 6.1a, one further finds that the derivative of the potential contains two discontinuities. These present challenging but soluble tasks for a modern numerical scheme from CFD, like the KT scheme, but cannot be handled by schemes that come without flux/slope limiters or any expansions *etc.*.
3. In order to avoid complications and the possible influx of errors from the boundaries of the computational domain, we choose a quadratic asymptotics, where linear extrapolation of $u(t, \sigma)$ at some large σ_{\max} should definitely be justified as well as smooth quadratic behavior at the artificial $\sigma = 0$ boundary condition. This ensures that IR errors most certainly do not stem from boundary conditions, but exclusively from the numerical scheme and parameters like the cutoffs.

6.2.2. Test case II: ϕ^4 potential

The second toy model is the zero-dimensional version of ϕ^4 -theory, see Section 3.2.1 and Eq. (3.7), with positive and negative mass squared, where, for the sake of simplicity, we set $m^2 = \pm 1$ and $\lambda = 1$,

$$U(\vec{\phi}) = \pm \frac{1}{2} \vec{\phi}^2 + \frac{1}{4!} (\vec{\phi}^2)^2, \quad U(\rho) = \pm \rho + \frac{1}{6} \rho^2. \quad (6.5)$$

A plot of the version with negative mass squared is presented in Fig. 6.1b.

Exact solution

Its exact solutions for correlation and vertex functions was already discussed in Section 3.2.1 and the former can be expressed in terms of the integral (3.9). Again, numerical calculation of reference values yields the same results as using this formula to the desired precision and we are interested in floating-point reference values anyhow.

Remarks

If one is testing methods in QFT, there is of course no way to get around ϕ^4 -theory, because $O(N)$ -type models with such potentials are omnipresent, *e.g.*, in the Anderson-Brout-Englert-Guralnik-Hagen-Higgs-Kibble mechanism [141] in high-energy physics and solid-state theory. Anyhow, since we already used a ϕ^4 -theory with positive and negative mass term in Chapter 3, to demonstrate limitations of perturbation theory and motivate the use of non-perturbative methods, we in fact almost have to show the superiority of FRG for this model.

Apart from these “traditional” reasons, there are of course also practical considerations.

1. In contrast to the previous example, there is a quartic asymptotic behavior of the potential. Consequently, it is especially interesting to examine, whether our linear extrapolation (5.77) at some σ_{\max} still works as an artificial large- σ boundary condition. Other numerical challenges, *e.g.*, at the $\sigma = 0$ boundary condition or the interior of the domain $[0, \sigma_{\max}]$, are not expected, because the potential is already smooth in the UV. Hence, the dominating error in the KT framework should stem from the cell size $\Delta\sigma$, the large- σ boundary condition, and cutoffs.

2. Due to smoothness of the potential a FRG vertex/Taylor expansion seems to be justified (as an artificial truncation) and at least in the UV a truncated Taylor series perfectly describes the potential. Expanding about the IR minimum, which is trivial, we can check, whether the FRG Taylor expansion with constant expansion point from Section 4.4 works for ϕ^4 -theories with positive and negative mass term, respectively. These quantitative results can be further compared to the numerical solution of the exact PDE for the full potential via the KT scheme and the exact reference results. This might shed a different light on the notion of “apparent convergence”, which is oftentimes used in the FRG community to justify vertex expansion schemes as truncations of the Wetterich equation.

Note that, unless stated otherwise, we always use Eq. (6.5) with negative mass term for the upcoming discussion.

6.2.3. Test case III: ϕ^6 potential

As a third test case, we study a potential with $(\vec{\varphi}^2)^3$ asymptotic behavior. The global minimum of the potential is trivial. In addition, the potential comprises a hypersphere of local non-trivial minima,

$$U(\vec{\varphi}) = \frac{1}{2} \vec{\varphi}^2 - \frac{1}{20} (\vec{\varphi}^2)^2 + \frac{1}{6!} (\vec{\varphi}^2)^3, \quad U(\varrho) = \varrho - \frac{1}{5} \varrho^2 + \frac{1}{90} \varrho^3, \quad (6.6)$$

For a visualization of the potential and its derivative, evaluated on a constant background-field configuration, we refer to Fig. 6.1c.

Exact solution

To the best of our knowledge exact solutions for all correlation functions in terms of transcendental functions do not exist. (At least some integral tables, we, and MATHEMATICA [147] could not come up with any.) Therefore, we simply use high-precision numerical integration to generate “exact” reference solutions of desired high accuracy.

Remarks

1. Again, the potential can be used to study the quality of the linear extrapolation at the large- σ boundary condition, similar to what is discussed for the ϕ^4 -theory.
2. Potentials with multiple minima are usually found in RG flows in the vicinity of first-order PTs. Here, the global minimum is already trivial and the system is always in its symmetric phase. Still, the local minima have to vanish during the RG flow to obtain a convex IR potential. The question is, whether this dynamics can also be described in terms of a vertex expansion of the potential, because the expansion point is unique during the entire RG flow. Hence, the potential again allows to directly compare the FRG vertex/Taylor expansion with the full solution of the PDE and the reference solution. As an advantage compared to ϕ^4 -theory with negative mass term, the physical point does not move and always agrees with the expansion point at $\vec{\varphi} = 0$.

6.2.4. Test case IV: the $\sigma = 0$ boundary

The last test scenario is again a potential which is asymptotically proportional to $\vec{\varphi}^2$ and defined piecewise. The small- $|\vec{\varphi}|$ behavior is described by $-(\vec{\varphi}^2)^{\frac{1}{3}}$, which leads to a non-analyticity at $\vec{\varphi} = 0$ and $|\vec{\varphi}| = \sqrt{8}$,

$$U(\vec{\varphi}) = \begin{cases} -(\vec{\varphi}^2)^{\frac{1}{3}}, & \text{for } 0 \leq |\vec{\varphi}| \leq \sqrt{8}, \\ +\frac{1}{2} \vec{\varphi}^2 - 6, & \text{for } \sqrt{8} < |\vec{\varphi}|. \end{cases} \quad (6.7)$$

The latter is a discontinuity on the level of the derivative of the potential, while the cusp at $\vec{\varphi} = 0$ leads to a pole in the derivative.

Rewriting this as a function of the $O(N)$ invariant, we find

$$U(\varrho) = \begin{cases} -(2\varrho)^{\frac{1}{3}}, & \text{for } 0 \leq \varrho \leq 4, \\ +\varrho - 6, & \text{for } 4 < \varrho, \end{cases} \quad (6.8)$$

and a plot of the situation is shown in Fig. 6.1c.

Exact solution

Interestingly, there is an exact expression for the integral

$$\begin{aligned} & \int_0^\infty d\rho \rho^{\frac{N}{2}-1} \rho^n e^{-U(\rho)} \stackrel{(6.8)}{=} \\ & = (-1)^{-3(\frac{N}{2}+n)} 2^{-(\frac{N}{2}+n)} 3 \left[\Gamma\left(3\left(\frac{N}{2}+n\right)\right) - \Gamma\left(3\left(\frac{N}{2}+n\right), -2\right) \right] + e^6 \Gamma\left(\frac{N}{2}+n, 4\right), \end{aligned} \quad (6.9)$$

which can be used to calculate the correlation and vertex functions (2.12) and (2.39) to (2.41), even though simple high-precision one-dimensional numerical integration is also an option.

Remarks

The obvious reason for the construction of this potential is to test the discrete version of the ($\sigma = 0$)-boundary condition (5.76) for the FV scheme. A pole at $\sigma = 0$ is certainly the most extreme case for a discontinuous odd function in σ . The discontinuity at $\sigma = \sqrt{8}$ is an additional challenge, but is already covered by the first toy model (6.2). The linear asymptotic behavior of $u(t, \sigma)$ is again chosen to avoid errors from the large- σ boundary condition.

6.3. Final remarks on the numerical setup

Before we turn to a qualitative analysis of the RG flows for each of the four UV initial potentials, we need to provide some final remarks on the numerical setup, which is used for the remainder of this chapter and is specific to our FRG problems.

As discussed in Section 5.2, we directly identify the background field with the spatial coordinate $x = \sigma$. We use the KT scheme from Section 5.2.2 for the spatial discretization and the boundary conditions (5.76) and (5.77) for the cell averages of the FV method. In total, we use n cells on the domain $[0, \sigma_{\max}]$ and two additional ghost cells at each domain boundary, such that $\Delta\sigma = \Delta x = \frac{\sigma_{\max}}{n-1}$. The cell center of the zeroth cell is at $\sigma = x = 0$ and the cell center of the $(n-1)^{\text{th}}$ cell is at σ_{\max} .

The initial condition for the cell averages is calculated according to

$$\begin{aligned} \bar{u}_j(t=0) & \stackrel{(5.57)}{=} \frac{1}{\Delta\sigma} \int_{\sigma_{j-\frac{1}{2}}}^{\sigma_{j+\frac{1}{2}}} dx u(t=0, \sigma) \\ & = \frac{1}{\Delta\sigma} \int_{\sigma_{j-\frac{1}{2}}}^{\sigma_{j+\frac{1}{2}}} dx \partial_\sigma U(t=0, \sigma) = \\ & = \frac{1}{\Delta\sigma} \left[U(t=0, \sigma_{j+\frac{1}{2}}) - U(t=0, \sigma_{j-\frac{1}{2}}) \right]. \end{aligned} \quad (6.10)$$

The actual time stepping of the semi-discrete KT scheme is performed with the ODE solver `NDSolve` of `MATHEMATICA` [147] with `PrecisionGoal` and `AccuracyGoal` of 10. We used various `MATHEMATICA` versions higher than 12.0 but less than 13.0 on different machines, which all delivered identical results within the precision of this work. For estimates on the performance and required wall time *etc.*, we refer to Ref. [3, Appendices E & F].

After the time stepping, the potential $U(t, \sigma)$ at the cell centers σ_i for arbitrary times t is recovered from the cell averages by standard Riemann integration,

$$U(t, \sigma_i) = \Delta\sigma \sum_{j=0}^i \frac{\bar{u}_j(t)}{1 + \delta_{j0} + \delta_{ji}}, \quad (6.11)$$

where the special denominator compensates for the fact that only half of the first and half of the last cell contribute to the integral. In addition, we ignore the integration constant – a normalization which does not matter for this work.

The vertex functions $\Gamma^{(2n)}$ are extracted from the cell averages using numerical differentiation, thus FD stencils on $u(t, \sigma)$ at the cell centers. Thereby, we approximate $u(t, \sigma)$ at the cell centers σ_j by the cell averages $\bar{u}_j(t)$. If the vertex functions are evaluated at the IR physical point $\sigma = 0$, which is almost always the case in this chapter, the \mathbb{Z}_2 anti-symmetry is used to simplify the FD stencils and to gain one order of accuracy for free, *e.g.*,

$$\Gamma^{(2)} = \partial_\sigma u(t_{\text{IR}}, \sigma)|_{\sigma=0} \simeq \frac{\bar{u}_1(t_{\text{IR}}) - \bar{u}_{-1}(t_{\text{IR}})}{2\Delta\sigma} + \mathcal{O}(\Delta\sigma^2) = \frac{\bar{u}_1(t_{\text{IR}})}{\Delta\sigma} + \mathcal{O}(\Delta\sigma^2). \quad (6.12)$$

The reason why we get one order of accuracy for free is that the last expression is actually identified as the forward FD stencil, which is only first-order accurate,

$$\Gamma^{(2)} = \partial_\sigma u(t_{\text{IR}}, \sigma)|_{\sigma=0} \simeq \frac{\bar{u}_1(t_{\text{IR}}) - \bar{u}_0(t_{\text{IR}})}{\Delta\sigma} + \mathcal{O}(\Delta\sigma) = \frac{\bar{u}_1(t_{\text{IR}})}{\Delta\sigma} + \mathcal{O}(\Delta\sigma). \quad (6.13)$$

Here, it is used that the cell average of the zeroth cell is always zero. For explicit FD formula for higher-order derivatives, which are used in this thesis, we refer to the explicit list in Ref. [1, Appendix A] and the corresponding Refs. [241, 242].

Now, we are readily prepared to start the discussion of our results.

6.4. Qualitative discussion of RG flows

We turn to the qualitative discussion of the RG flows of the four UV initial potentials (6.2) and (6.5) to (6.7).

The explicit parameters that are used in the calculations are listed in the corresponding plots. These are the model parameter N of the $O(N)$ symmetry group, the FRG parameters, namely the UV cutoff Λ , the IR cutoff r_{IR} , which corresponds to some “final” time step t_{IR} , and the numerical parameters, *i.e.*, the size of the computational domain σ_{max} and the number of FV cells n , which results in some $\Delta\sigma$.

For this qualitative discussion, we simply claim that the FRG and numerical parameters are chosen in a way such that errors are negligible. This statement is validated in the next section, where we explicitly test the accurate choice of the parameters by inspecting relative errors.

We further remark that the color-coding in all plots is on purpose, and reddish curves *etc.* correspond to the IR at late RG times, while bluish curves are in the UV at early RG times.

Having said this, let us focus on phenomenological description from the fluid-dynamical perspective first.

W.l.o.g. we first fix $N = 3$ for the two non-analytic UV initial potentials (6.2) and (6.7) and $N = 4$ for the smooth initial potentials Eqs. (6.5) and (6.6). In consequence, we have advective

and diffusive contributions in all RG flows of $u(t, \sigma)$. Inspecting Fig. 6.2, we clearly observe smoothening of $u(t, \sigma)$ for all test cases and a restoration of the symmetry of the ground state. All IR potentials at late t are convex, smooth, and have a single trivial minimum as expected for zero-dimensional models, *cf.* Section 2.2. Remarkably, this also perfectly works out for test case IV, which started with a pole at $\sigma = 0$ in $u(t = 0, \sigma)$, see Fig. 6.2d.

Furthermore, we clearly observe for all test cases that almost all of the (visible) dynamics happens approximately when the regulator $r(t)$ reaches the model scales, which are roughly of order one for all UV potentials. For earlier and later RG times there is almost no dynamics at all, as should be the case. This is actually best seen in the three-dimensional versions of Fig. 6.2a, which are plotted in Fig. 6.3.

As a direct consequence and at first glance, the huge UV cutoffs and tiny IR cutoffs, which lead to an RG flow over several orders of magnitude, seem excessive. However, one should keep in mind that it was explicitly required during the derivation of the (zero-dimensional) Wetterich equation in Chapter 4 that $r(t = 0) = \Lambda \gg 1$ and $t \rightarrow \infty$ with $\lim_{t \rightarrow \infty} r(t) = 0$, while for practical calculations, where $t \rightarrow \infty$ is not possible, $r(t_{\text{IR}}) \ll 1$. In Section 6.5.4 we explicitly demonstrate that rather large/small UV/IR cutoffs are indeed necessary to obtain high-precision vertex functions.

Next, let us turn to the dynamics on the level of $u(t, \sigma)$. Especially, if we inspect the RG flows of the non-analytic initial conditions, Figs. 6.2a and 6.2d, we observe that, as soon as the regulator reaches the model scales, diffusion is present and immediately smears out the discontinuities. We also observe diffusion in regions of negative slope of $u(t, \sigma)$, *e.g.*, in Fig. 6.2b at small $|\sigma|$. However, we also find for all test cases that there is some bulk transport of $u(t, \sigma)$ from large $|\sigma|$ to smaller $|\sigma|$. Especially for Fig. 6.2d it is interesting how bulk motion and diffusion eliminate the pole at $\sigma = 0$.

To get a better intuition for the respective contributions of the diffusive σ -mode and the advective contribution by the $N - 1$ “pions”, we plotted the RG flow of $u(t, \sigma)$ for the initial condition Eq. (6.2) for different N in Fig. 6.4. In the absence of advective contributions, $N = 1$, we find that there is strong non-linear diffusion. The discontinuities are completely smeared out, and it is clearly visible that information is propagated to larger and smaller $|\sigma|$. Increasing N to ten or even 100 renders the problem more and more advection-dominated. For $N = 100$ we almost find complete dominance of the advection and the slight smearing of the edges is barely visible. In addition, comparing $u(t, \sigma)$ for the different N at the same RG times, one observes that the dynamics is much faster and the IR state is reached earlier for larger N . This can be seen as the difference between approaching an equilibrium by diffusion or a state of steady flow by advection. For large N we also observe what we discussed earlier on the level of the fluxes: The advective contribution is uniquely directed towards smaller $|\sigma| = 0$, which can be seen at the discontinuities, which move inwards. Similar behavior for different N can also be found for the other test cases and plots of all test cases in the viscous $N = 1$ limit are presented in Figs. 6.10 and 6.11.

In total, we conclude on the qualitative level that the fluid-dynamical interpretation of $u(t, \sigma)$ is superior for the understanding of the underlying dynamics compared to the inspection of the RG flow of the potentials $U(t, \sigma)$ themselves. In addition, the flows of $u(t, \sigma)$ do not show any signals of numerical instabilities, like wiggles at the discontinuities or artificial over- or undershooting. The FV discretization in terms of the KT scheme seems to perform well – at least by visual inspection.

6.5. Quantitative tests

Next, we turn to quantitative tests of our fluid-dynamical setup to solve the PDE for the effective bosonic potential. These comprise tests of the spatial resolution $\Delta x = \Delta \sigma$, the size of the spatial computational domain $x_{\text{max}} = \sigma_{\text{max}}$, and boundary conditions, as well as tests of UV and IR cutoffs. For all tests we already anticipate optimal parameter setups for the respective other parameters that are presently not under investigation, *e.g.*, for tests of the spatial resolution, we fix the computational domain and cutoffs at some absolutely sufficient values. Note that within

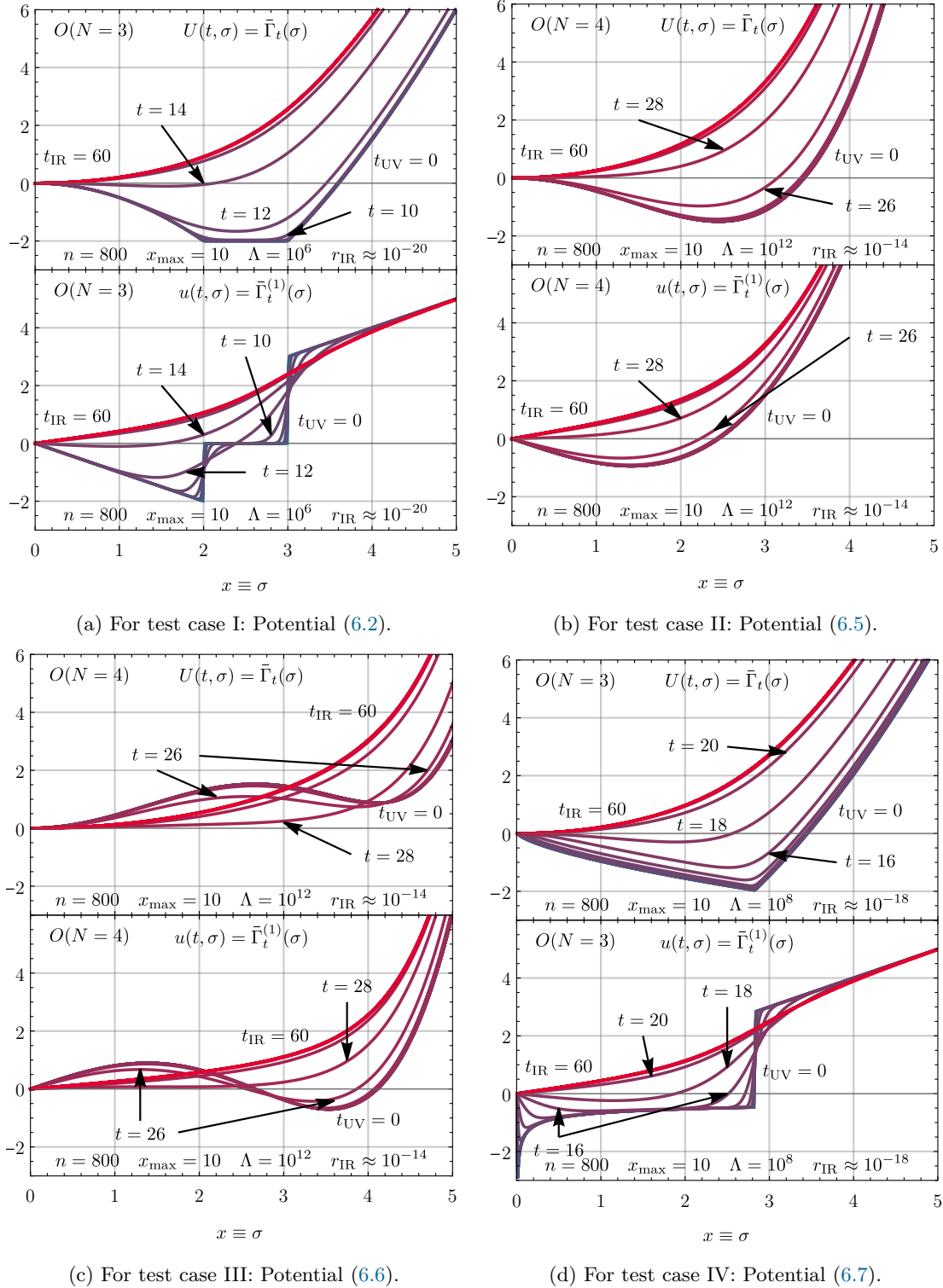


Figure 6.2: The RG flow of the effective potential $U(t, \sigma)$ (upper panel) and its derivative $u(t, \sigma) = \partial_\sigma U(t, \sigma)$ (lower panel) for different UV initial conditions and parameter setups (see panels). From Ref. [1, Figs. 5, 19, 28, 31].

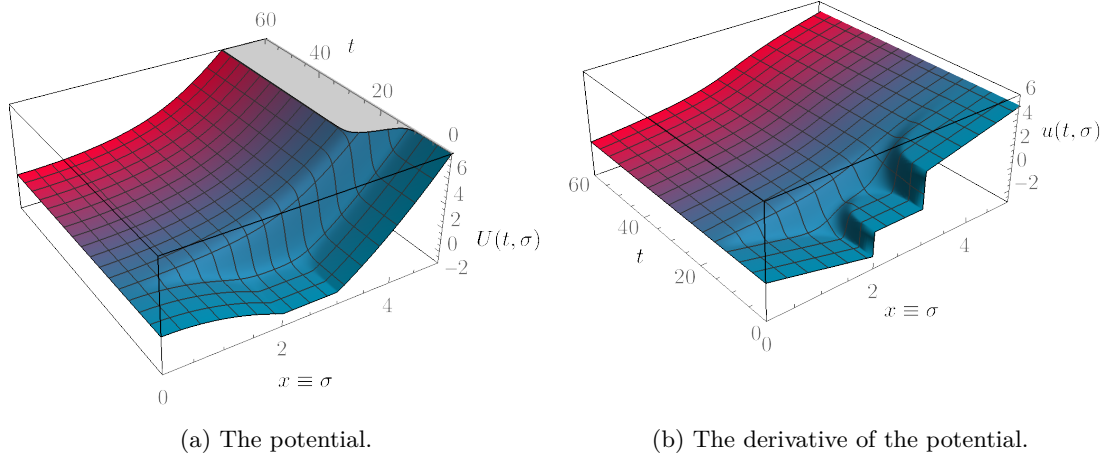


Figure 6.3: Three-dimensional rendering of the RG flow of Fig. 6.2a for the initial condition (6.2) with $N = 3$. From Ref. [1, Figs. 6 & 7].

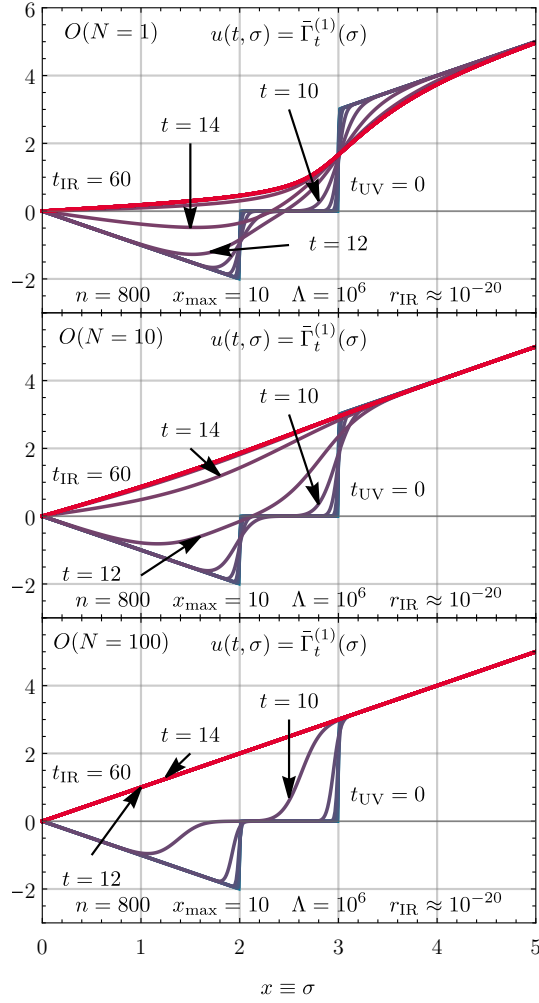


Figure 6.4: The RG flow of the derivative of the effective potential $u(t, \sigma)$ for test case I with different N . From Ref. [1, Fig. 8].

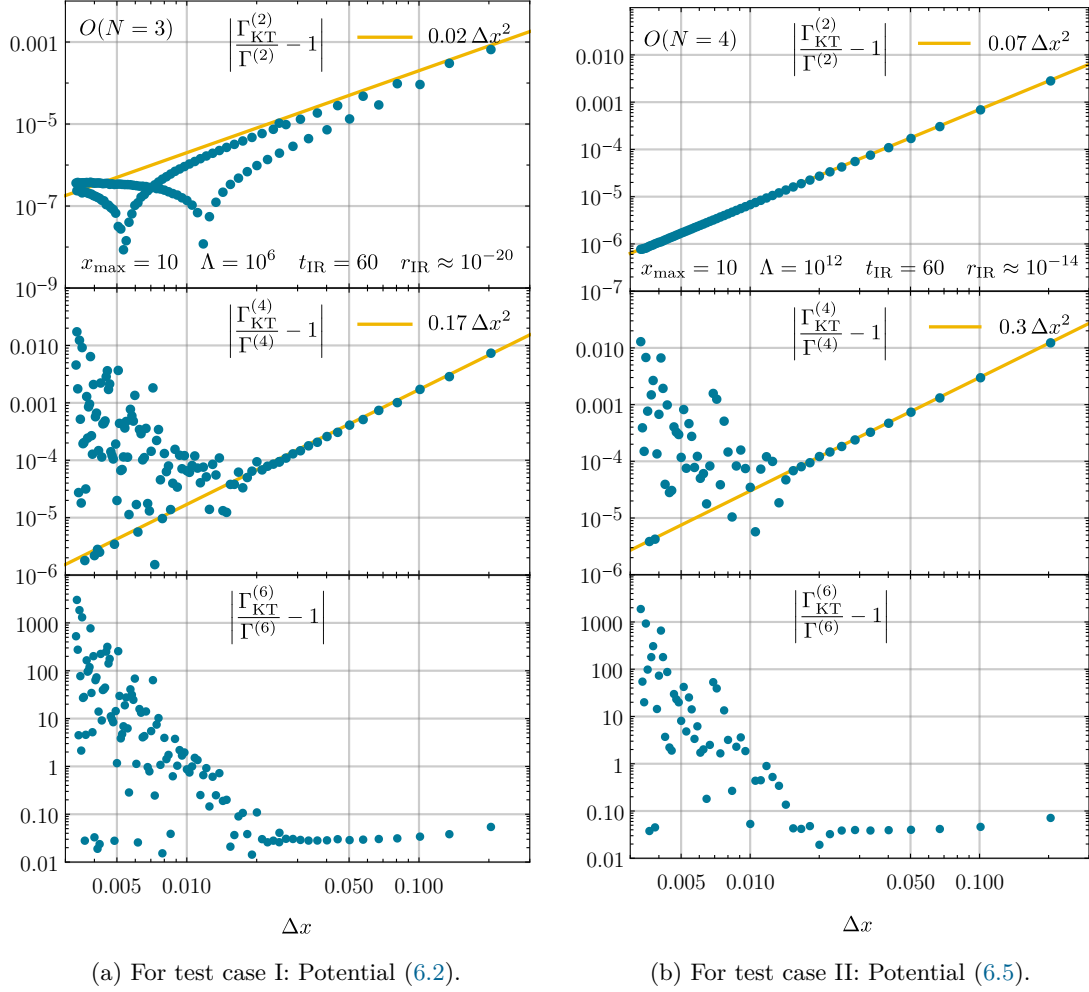


Figure 6.5: The relative error of $\Gamma^{(2m)}$ for $m = 1, 2, 3$ as a function of the cell size $\Delta x = \Delta\sigma$ for two different UV initial potentials and parameter setups (see panels). From Ref. [1, Figs. 9 & 21].

this work, we present selected results for only some of our test scenarios, while all types of tests were performed in detail for each individual UV initial condition.

6.5.1. Spatial resolution

First, we investigate the scaling of the relative errors for the vertex functions, Eq. (6.1), with the spatial resolution of the KT scheme $\Delta x = \Delta\sigma = \frac{\sigma_{\max}}{n-1}$. Here, we simply fix $\sigma_{\max} = 10$, which turns out to be absolutely sufficient (see below) and successively increase the number n of FV cells. For the explicit results, which are presented in Fig. 6.5, we use test cases I and II with UV initial potentials 6.5a and 6.5b. The respective values for N , Λ , and t_{IR} are listed in the plots.

From the KT scheme, we expect that the errors scale approximately with Δx^2 , see Section 5.2.2. Inspecting Fig. 6.5, we identify exactly this error scaling for $\Gamma^{(2)}$ for both initial conditions. Slight deviations from an exact Δx^2 -scaling are expected according to the original publication [105]. In the case of test case I, we additionally observe two dip-like structures in the scaling plots, where the error drastically undershoots its expected value. These stem from the discontinuities in the initial condition, see Fig. 6.1a. Depending on the position of the discontinuities in the respective FV cells, the cell-averaging yields better or worse approximations of the initial condition and can

even lead to results that are by chance much more accurate than the error-scaling suggests.

We also observe almost perfect Δx^2 -scaling of the relative errors of $\Gamma^{(4)}$ – at least for moderately small Δx , while for tiny Δx and for the entire results of $\Gamma^{(6)}$ the scaling breaks down. The question is, what is happening here and especially why we find relative errors at very small Δx which are scattered over all orders of magnitude.

The reason behind is actually rather simple and a fundamental problem of numerical mathematics. In order to calculate $\Gamma^{(2n)}$, we numerically differentiate $u(t_{\text{IR}}, \sigma)$ at $\sigma = 0$. As previously explained, this is done in terms of FD approximations on the level of the IR cell averages $\{\bar{u}_j(t_{\text{IR}})\}$. Typically, these FD stencils also come with an error scaling of some power of Δx , see Eq. (6.12). However, FD formulas are in general ill-conditioned and their error-scaling usually breaks down below a certain Δx , because of rounding errors in the floating-point arithmetic, see, *e.g.*, Ref. [243, Chap. 5.7]. The same happens if FD stencils are evaluated on noisy discrete data, which also causes spurious cancellations. Here, both problems enter at the same time. Even though being extremely precise, the final IR cell averages come with some numerical errors and present discrete “noisy” data. Hence, it is absolutely expected that the error-scaling breaks down at a certain Δx and errors are of all orders of magnitude below. It is well-known that this problem is more severe and occurs already at larger Δx for higher-order derivatives. Also this can be seen in the data, because the performance goes down from $\Gamma^{(2)}$ to $\Gamma^{(4)}$ and is even worse for $\Gamma^{(6)}$. It is clear that the fluctuations in the relative errors for small Δx in $\Gamma^{(4)}$ and $\Gamma^{(6)}$ stem purely from the FD stencils, which are evaluated on top of the solution, and do not originate from the KT scheme and the numerical time stepping, because exclusively a single cell average enters the formula of the numerical derivative for $\Gamma^{(2)}$, see Eq. (6.12), such that spurious cancellations cannot occur. It is therefore absolutely sufficient to use $\Gamma^{(2)}$ to benchmark the KT scheme in the FRG context, while it is of utmost interest which additional problems pop up if one is interested in calculating vertex functions of arbitrary order from the IR potential.

We conclude that we were able to run the KT scheme with its expected performance in an FRG setup and observe the correct error-scaling $\sim \Delta x^2$. We find that the KT scheme is extremely precise, which is directly observed from the super-small relative errors of $\Gamma^{(2)}$, which can easily be pushed below 10^{-5} . Even for $\Gamma^{(4)}$ relatively small deviations from the exact results up to 10^{-4} are safely accessible as long as $\Delta x \gtrsim 0.025$. Similar results are also found for the other two test cases, which are not shown in Fig. 6.5.

For FRG calculations in higher-dimensional systems, which comprise the flow equation of an effective local bosonic potential, this implies, when using the KT scheme with decent resolution, that the dominant errors of IR observables do certainly not stem from the spatial discretization. Instead, the relevant errors are most definitely linked to truncation errors, cutoffs *etc.*. Still, it is required to test this explicitly and check for “independence” of the IR results from the FV cell size. This can be done for example along the lines of Ref. [4, App. F]. Furthermore, we refer to the more detailed discussion in Ref. [1].

6.5.2. Large- σ boundary condition and size of the computational domain

We continue the discussion of the spatial discretization and turn to the artificial restriction of the domain $[0, \infty)$ to the computational domain $[0, \sigma_{\text{max}}]$, which includes the linear extrapolation (5.77) at σ_{max} . Here, we probe with several of our test cases, whether it is possible to increase σ_{max} at constant resolution Δx so much that the relative errors (6.1) become independent of σ_{max} . If this is possible, it also signals that the linear extrapolation works as a boundary condition or that the explicit type of extrapolation is actually irrelevant, because the fluxes basically vanish already.

Some selected results of these tests are presented in Fig. 6.6, where we plot the relative errors for $\Gamma^{(2)}$, $\Gamma^{(4)}$, and $\Gamma^{(6)}$ as functions of σ_{max} . The choices for the other parameters are explicitly listed in the panels and are sufficient according to our other tests. Indeed, we find for all of the

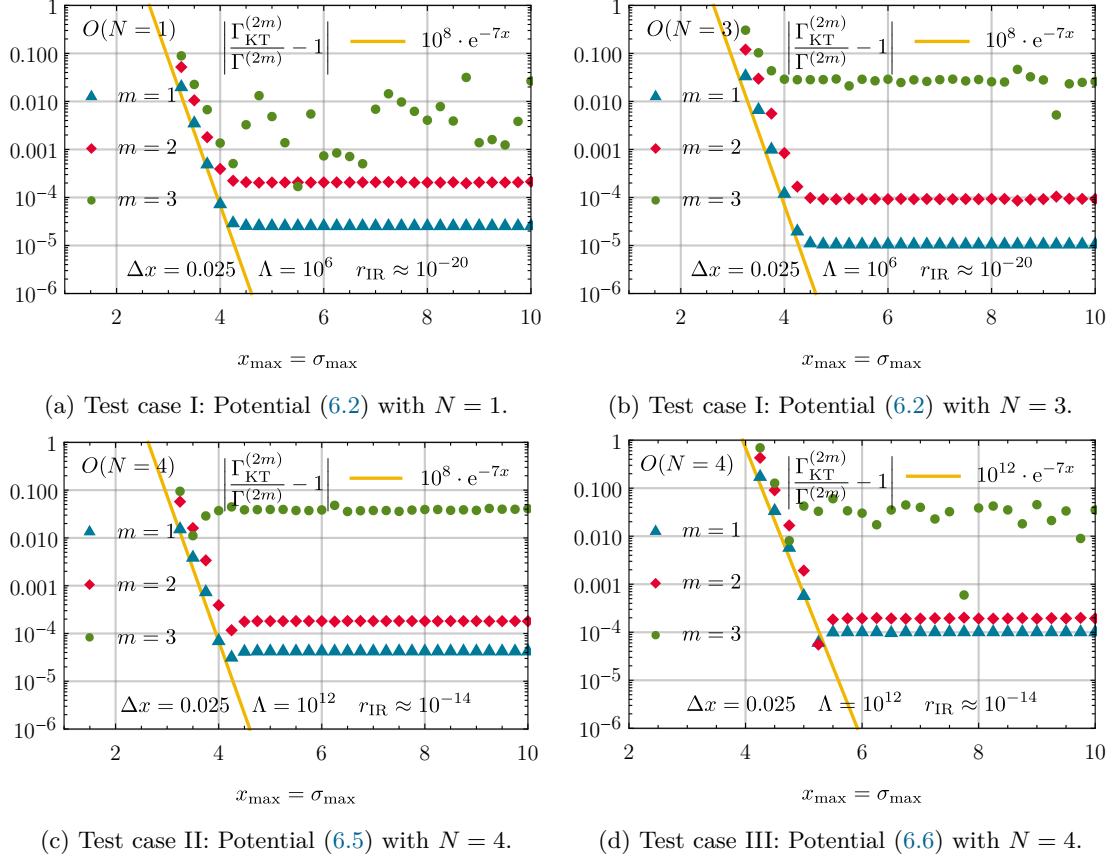


Figure 6.6: The relative error for $\Gamma^{(2m)}$ for $m = 1, 2, 3$ as a function of the size of the computational interval for different UV initial potentials and parameter setups (see panels). From Ref. [1, Figs. 10, 11, 22, 29].

tested examples that it is easily possible to increase σ_{\max} to values where the relative errors of the vertex functions become independent of σ_{\max} and start to be dominated by other sources of errors. For all test cases this decoupling of the relative errors from σ_{\max} happens approximately, when σ_{\max} is considerably larger than the relevant structures in the UV potential, which were all by construction of order one. Here, we are referring to factors 4 or 5 and not several orders of magnitude. However, as soon as σ_{\max} is too small, we observe an exponentially increasing error, which demonstrates the utmost importance of testing the independence of the IR results from this boundary condition, which can also be done in setups without exact reference values, by simply studying the dependence of the IR observables on σ_{\max} . Nevertheless, we could not find any explicit test or comment on tests of this type in common FRG literature. In addition, we have the strong impression that computational domains for similar calculations of RG flows of local bosonic potentials are usually too small and we therefore expect a strong influence of the artificial boundary condition at “large” σ on their results. We thereby hope that our tests may serve as a paradigm for future FRG (model) studies.

Let us close the discussion by mentioning another detail of our own results: By comparing the panels in Fig. 6.6 we find that the linear extrapolation boundary condition also works for the potentials where $u(t, \sigma)$ has a σ^3 or a σ^5 asymptotic behavior. Anyhow, for the test case with σ^5 asymptotic behavior, we clearly observe from Fig. 6.6d that σ_{\max} needs to be significantly larger than for the other test cases. We assume that here the suppression of the fluxes is more important than a decent extrapolation.

6.5.3. $\sigma = 0$ boundary condition

The outstanding precision for the vertex functions, *i.e.*, the extremely low relative errors for $\Gamma^{(2)}$, $\Gamma^{(4)}$, and $\Gamma^{(6)}$, observed in all other tests of this section, clearly demonstrate that the implementation of the boundary condition at $\sigma = 0$ is correct. In particular, the results for test case IV, which comprises the pole at $\sigma = 0$ demonstrate, that our spatial discretization is capable of dealing with challenges of this kind, see, *e.g.*, Figs. 6.2d and 6.7b.

6.5.4. Cutoff tests

In Ref. [1] we present an extensive discussion on identifying the appropriate UV cutoff scales Λ and sufficiently small (artificial) IR cutoffs $r_{\text{IR}}(t_{\text{IR}})$. Here, we summarize some key findings.

The UV cutoff

Recalling the construction of the (zero-dimensional) FRG from Sections 4.1.1 and 4.2.2, there is absolutely no doubt that the UV cutoff Λ needs to be much greater than all relevant scales of the classical UV action such that the effective average action $\bar{\Gamma}(t, \bar{\varphi})$ is correctly initialized with the classical action $\mathcal{S}(\bar{\varphi})$. Still, for conceptual and numerical reasons it has to remain finite.

In higher-dimensional theories, this ensures that really all fluctuations and interactions from high energy scales are incorporated in the effective couplings, which are “measured” at lower energy scales. In zero dimensions, it is of course impossible to speak about energy scales or fluctuations, but the concept of integrating out interaction processes stays conceptually the same and all interactions must be included to obtain correct IR results.

For higher-dimensional theories, it is also easier to state what we mean by “larger than all relevant model scales”: Here, we mean that the UV cutoff Λ has to be larger than all “internal” scales of the model, *e.g.*, dimensionful couplings, initial particle masses, vacuum condensates *etc.*, but also larger than “external” scales, like chemical potentials or temperatures.

In general, starting with a theory with meaningful UV limit, it should be ensured that the IR observables do not depend on the explicit choice of the UV cutoff scale at which the RG flow is initialized. Summarized in a compact equation, this simply reads

$$0 \stackrel{!}{=} \Lambda \frac{d\Gamma[\Phi]}{d\Lambda}. \quad (6.14)$$

(Here, we always assume that there is no artificial IR cutoff and we are able to integrate out all fluctuations.) For example, for some theories, this can be achieved by considering the correct perturbative running of couplings in the UV, *cf.* Part II and Refs. [244, 4], to increase the UV coupling above some external model scales, *e.g.*, a temperature. In general, the task is to send the UV cutoff to larger values or infinity in a sensible way, if this is required, without altering the IR physics. This correct initialization of RG flows at large RG scales, which ultimately ensures Eq. (6.14), is called RG consistency and is discussed in detail in Ref. [244]. However, in lots of practical FRG calculations for effective low-energy models little attention is paid to this issue and UV cutoffs are oftentimes chosen too close to the corresponding model scales (cutoffs are for example of the order of the temperature, the chemical potential or initial curvature masses). For discussions on this and related issues, we also refer to Refs. [245, 246, 247, 248].

However, the question remains how Λ has to be chosen to fulfill Eq. (6.14).

An absolutely lowest limit for Λ is certainly set by the fact the denominators of the propagators have to be manifestly positive by construction of the FRG and should never overshoot their pole, *cf.* Refs. [86, 249]. In our case, this implies

$$\Lambda + \frac{1}{\sigma} u(t=0, \sigma) > 0, \quad \Lambda + \partial_\sigma u(t=0, \sigma) > 0. \quad (6.15)$$

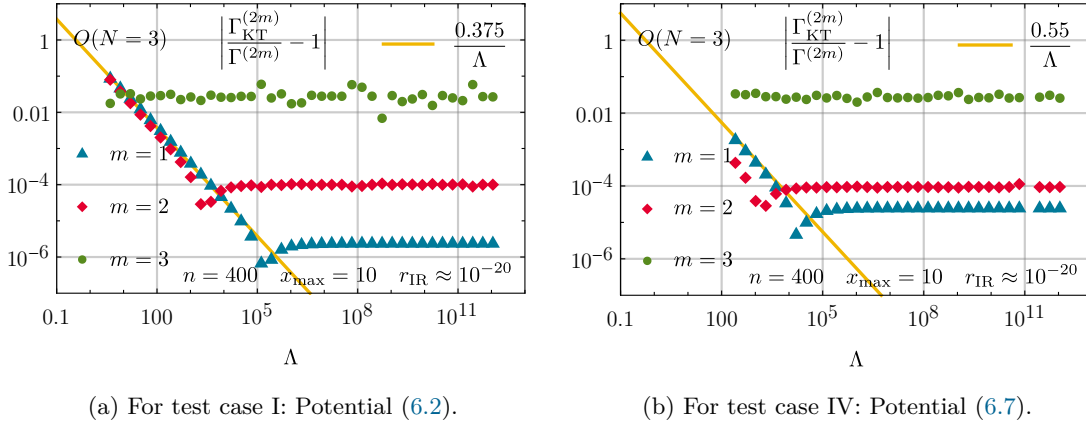


Figure 6.7: The relative error of $\Gamma^{(2m)}$ for $m = 1, 2, 3$ as a function of the UV cutoff Λ for two different UV initial potentials and parameter setups (see panels). From Ref. [1, Figs. 16 & 33].

Usually, this criterion is easy to fulfill, nevertheless it does not suffice to guarantee Eq. (6.14) at all. In any case, if the UV initial condition $u(t = 0, \sigma)$ contains discontinuities or even poles like Eqs. (6.2) and (6.7), its derivative is formally infinite at these points, which also requires infinite Λ . Luckily, on the discretized level, *e.g.*, on the level of cell averages, the derivatives are always finite, but can still be huge, such that very large Λ are already necessary from Eq. (6.15). Interestingly, this implies that the choice of the UV cutoff is also directly linked to the desired resolution in field space.

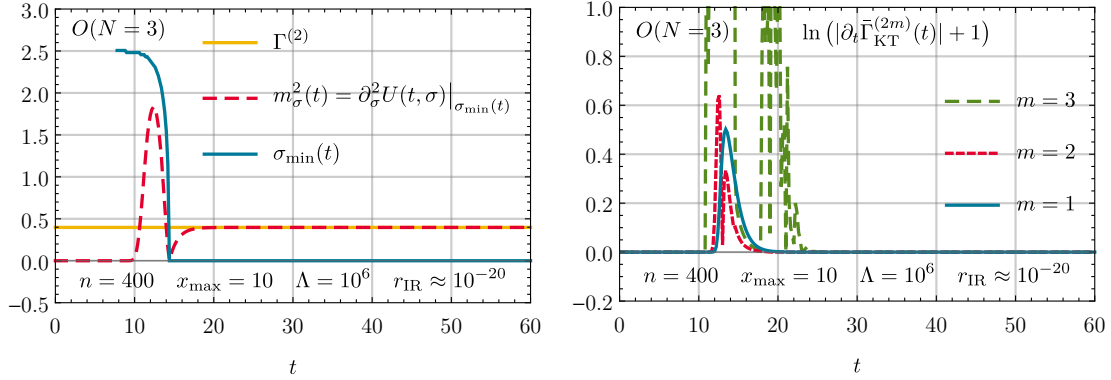
Unfortunately, in some model studies, even the simple condition (6.15) is sometimes ignored or only just fulfilled, see, *e.g.*, Ref. [86].

A much more reliable approach to the correct choice of the UV cutoff is of course to check Eq. (6.14) explicitly, which is easily done for zero-dimensional QFT. Here, one keeps all other (numerical) parameters as well as the artificial IR cutoff fixed and steadily increases Λ until the IR observables do not change with Λ anymore. In this work, we therefore inspect the relative errors of $\Gamma^{(2)}$, $\Gamma^{(4)}$, and $\Gamma^{(6)}$ in the IR as functions of Λ . These are plotted in Fig. 6.7 for the two test cases which contain discontinuities in their UV initial condition. Inspecting these plots, we indeed observe that it is possible to reach RG consistency in the sense that IR errors are dominated by other sources than the cutoff, when Λ is increased to sufficiently large values. In fact, the cutoffs which are necessary to achieve this are surprisingly large, *i.e.*, several orders of magnitude above the typical model scales. This is certainly also caused by the discontinuities and the rather small spatial resolution. In any case, it is clearly visible, especially from Fig. 6.7b, that one has to exercise caution when playing with the UV cutoff, and too small UV cutoffs can lead to huge errors in the IR, which is certainly also of great importance in higher-dimensional setups. Explicit UV-cutoff tests in a higher-dimensional model are presented for example in Ref. [4, Appendix F].

The IR cutoff

To be clear right from the beginning: The IR cutoff is – as already mentioned several times – completely artificial. The effective IR action is uniquely defined as $\Gamma(\vec{\varphi}) = \bar{\Gamma}(t \rightarrow \infty, \vec{\varphi})$ and therefore it does not make sense at all to calculate observables and vertex functions from $\bar{\Gamma}(t, \vec{\varphi})$ at earlier times – or at least to relate them to physical values. Exactly the same holds true for higher-dimensional FRG applications, where the IR effective action is only reached, when the RG scale $k \rightarrow 0$, where ultimately all fluctuations are integrated out.

Exclusively for practical and computational reasons it is of course not possible to exactly end up at $k \rightarrow 0$ or $r(t \rightarrow \infty) \rightarrow 0$ and one has to stop the integration at some non-zero IR scale – the IR cutoff.



(a) RG flows of the minimum and curvature mass.

(b) RG flow of the changing rates $\partial_t \bar{\Gamma}^{(2m)}(t)$ for $m = 1, 2, 3$ at $\sigma = 0$.

Figure 6.8: Indicators of convergence in the IR exemplified for test case I with potential (6.2). From Ref. [1, Figs. 12 & 17].

Admittedly, this fact is oftentimes abused to stop RG flows at rather large cutoff scales. The justifying argument is oftentimes that the RG flow of the effective potential or some other observable is effectively frozen and does not change with the RG time anymore. Another reason to stop the RG flow at rather high cutoff scales is the “numerical stability” of the PDE or related lines of argumentation. The latter reason is of course absurd, because this and related works [1, 2, 3, 4, 77, 101] as well as for example Refs. [235, 84, 85, 249, 83] clearly demonstrate that it is possible to reach extremely low RG scales or carefully extrapolate to $k = 0$, if decent numerical methods are used.

However, also when it is argued that “quantities freeze” in the RG flow, some skepticism is usually in place, if this is not explicitly tested in a given study. Usually different observables and vertex functions freeze out at different RG scales, which can differ by several orders of magnitude. In addition, it is usually better suited to inspect the RG-time derivatives of the observables than to judge freezing by plain visual inspection of their flow itself.

To demonstrate this, we present two plots which are both based on the initial potential (6.2). In Fig. 6.8a, we plot the RG flow of the unique minimum (after a unique minimum has formed from the infinitely many minima) and the RG flow of the curvature mass at the flowing minimum. It is clearly visible that the curvature mass still changes significantly over several orders in the RG scale long after the minimum is already frozen. The change of the vertex functions and their freeze-out at different scales is even better visible in Fig. 6.8b, where we plot the logarithmic changing rates of the vertices at $\sigma = 0$. It is clearly visible from both plots that even though the dynamics of the potential and its derivative seem to be frozen, see Figs. 6.2a and 6.3, this is not the case for the vertex functions and observables.

Additional explicit plots concerning tests of appropriate IR cutoffs $r_{\text{IR}}(t_{\text{IR}})$ can be found in Ref. [1].

In any case, we conclude that it is of great importance to ensure that one really reaches the IR RG scales, where all observables of interest are truly frozen, or to carefully extrapolate, once the scaling regime is reached.

6.6. Benchmarking the FRG vertex/Taylor expansion

Having completed the numerical tests as well as the studies for decent UV cutoff and IR cutoff scales, we shall now compare our novel (numerical) methods from CFD for the solution of the exact PDE of the effective potential to artificial truncations of the Wetterich equation.

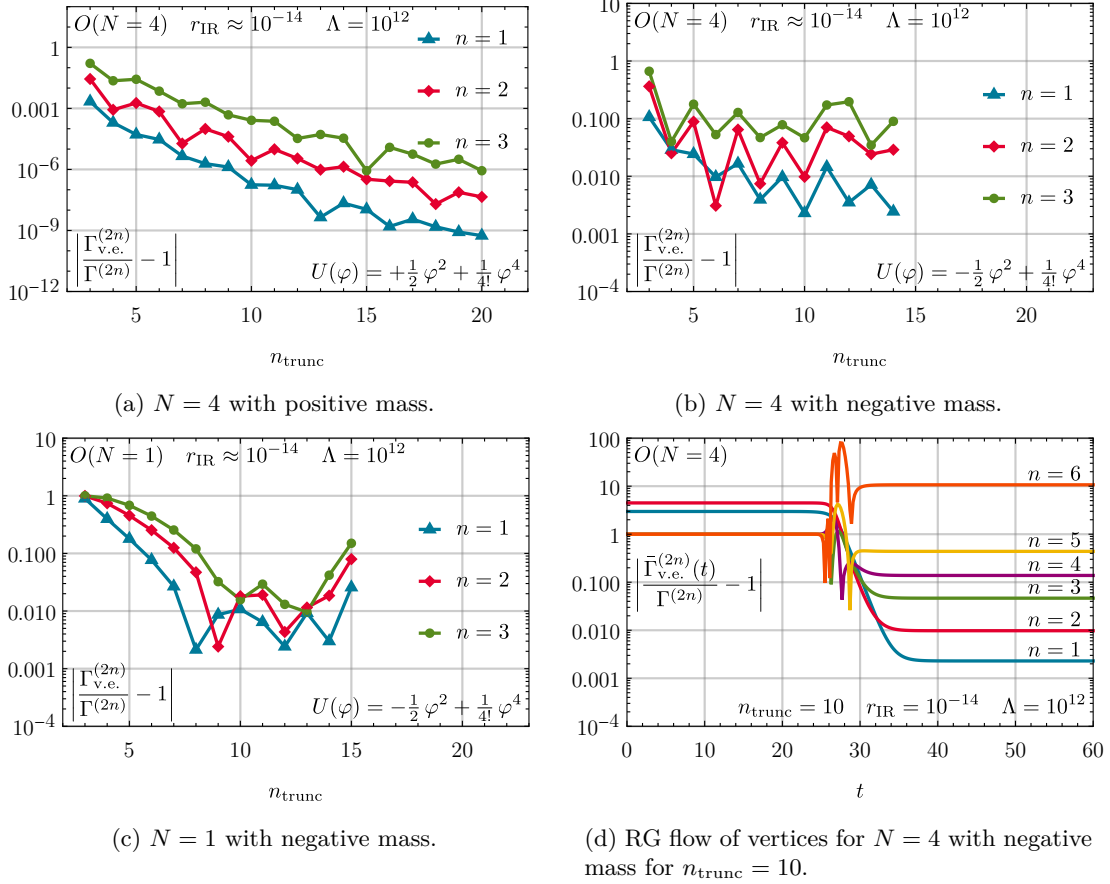


Figure 6.9: Relative errors of the vertices of the FRG vertex/Taylor expansion for test case II with UV potential (6.5) as functions of the truncation order/ RG time. From Ref. [1, Figs. 23, 24, 25, 26].

As outlined and explained in detail in Section 4.4, there exists a version of the FRG vertex expansion which coincides with the Taylor expansion of the effective potential about $\vec{\varphi} = 0$ in zero spacetime dimensions. Taylor expansions of the effective potential are also used in higher-dimensional model calculations, *e.g.*, Refs. [86, 250, 88, 66, 71], such that benchmarking this method seems advisable. Some (maybe too) simple benchmark tests were already performed for example in Refs. [179, 107, 109, 108, 13]. Of course, by definition this scheme can only be applied (if at all) to expandable UV potentials, which are the potentials (6.5) and (6.6) from our test cases.

In the following we therefore numerically solve the ODE system of the scale-dependent vertices, Eqs. (4.43), (4.44), and (4.45), which is generated from the expansions (4.36) and (4.37) and compare the IR results for the vertices to the exact reference values.

This is done for different truncation orders n_{trunc} , where $\bar{\Gamma}^{(2n_{\text{trunc}})}$ is the vertex of highest order, which is included in the truncation. The initial conditions for the ODE systems are obtained by comparing coefficients of the general expansion (4.36) with the UV initial potentials (6.5) and (6.6). As UV and IR cutoffs, we use values which, according to the analysis with the KT scheme in Section 6.5.4, turned out to be absolutely sufficient. These are listed in the result figures. The ODE system is again solved using NDSolve of MATHEMATICA [147] with PrecisionGoal and AccuracyGoal of 10.

Our results are presented subsequently.

6.6.1. Apparent convergence

W.l.o.g. we set $N = 4$ and start our analysis with the presumably most simple scenario, ϕ^4 -theory with positive mass term, thus Eq. (6.5). The corresponding UV initial condition for the ODE system of vertices is

$$\bar{\Gamma}^{(2)}(t=0) = 1, \quad \bar{\Gamma}^{(4)}(t=0) = 1, \quad \forall n > 2 \quad \bar{\Gamma}^{(2n)}(t=0) = 0. \quad (6.16)$$

Solving the ODE system repeatedly for increasing truncation order n_{trunc} , we obtain relative errors for the IR values of $\Gamma^{(2)}$, $\Gamma^{(4)}$, and $\Gamma^{(6)}$, which are plotted in Fig. 6.9a as functions of the truncation order.² The minimal truncation order is $n_{\text{trunc}} = 3$ and we randomly stopped our analysis at truncation order $n_{\text{trunc}} = 20$. One clearly finds that the relative errors are decreasing with increasing truncation order and remarkably precise results are achievable already at low truncation orders. Similar results are also found in Refs. [107, 13, 108, 109]. For this particular example, the FRG vertex/Taylor expansion definitely outperforms the KT scheme for the full solution of the PDE. Moreover, we can estimate the truncation error scaling with n_{trunc} and find that the relative errors of $\Gamma^{(2)}$, $\Gamma^{(4)}$, and $\Gamma^{(6)}$ scale roughly with $n_{\text{trunc}}^{-8.2}$, $n_{\text{trunc}}^{-7.6}$, and $n_{\text{trunc}}^{-7.3}$ respectively. Even though there is no proof, this is a clear sign of “apparent convergence” of the Taylor expansion of the effective potential and the vertex expansion of the Wetterich equation.

6.6.2. Who said “convergence”?

Either way, ϕ^4 -theory with positive mass term cannot be considered as a really challenging test. Neither the global minimum is moving nor is there any significant dynamics. The convex potential simply remains convex and only minimally changes its slope, which is why we do not present any plot. We refer to Ref. [2, Fig. 4] and Ref. [107, Fig. 13] for graphics of the corresponding RG flows.

In consequence, we turn to a slightly more difficult problem, namely ϕ^4 -theory with negative mass term, *i.e.*, the potential (6.5). The initial condition of the ODE system is

$$\bar{\Gamma}^{(2)}(t=0) = -1, \quad \bar{\Gamma}^{(4)}(t=0) = 1, \quad \forall n > 2 \quad \bar{\Gamma}^{(2n)}(t=0) = 0. \quad (6.17)$$

As a fixed expansion point we choose the IR minimum $\bar{\varphi} = 0$. Again solving this system numerically with $N = 4$, we can calculate the relative errors of $\Gamma^{(2)}$, $\Gamma^{(4)}$, and $\Gamma^{(6)}$ in the IR as functions of the truncation order n_{trunc} . This is plotted in Fig. 6.9b. From the plot it is obvious that the “apparent convergence” disappeared and that the relative errors are no longer monotonically decreasing with increasing n_{trunc} .

As a matter of fact, the FRG Taylor/vertex expansion does not work at all for $n_{\text{trunc}} > 14$. During RG flows with $n_{\text{trunc}} \geq 15$ we observe that the ODE system gets unstable at $t \approx 30$, slightly below the typical model scales ($r(t \approx 30) \approx 0.09$). The instability shows up in terms of divergent expansion coefficients. In general the ODE system seems to be ill-conditioned with vertex functions of all orders of magnitude. This can already be seen from Fig. 6.9d, where we plot the running of some expansion coefficients over RG time for $n_{\text{trunc}} = 10$ (which can still be integrated to the IR) and observe that there are drastic variations in the magnitude of the coefficients and higher-order coefficients equilibrate at large relative errors.

The manifest instabilities at large truncation orders cannot be overcome by increasing the precision of the solver and they were present in several independent implementations of the problem. To be sure that this is not artificial, we also studied the same problem for different N , which lead to conceptually identical results, see, *e.g.*, Fig. 6.9c for $N = 1$. Here, the breakdown of the system is observed for $n_{\text{trunc}} > 15$.

Anyhow, even for low-order truncations the relative errors are not systematically decreasing and there is no indication of an “apparent convergence”. Also the observed absolute values for the

²Due to the tiny achievable relative errors, it is necessary to increase the `PrecisionGoal` and `AccuracyGoal` of the time stepper to 12 for this example. Otherwise, the precision of the time stepper instead of the quality of the truncation would set the accessible minimal relative error.

errors, *e.g.*, of $\bar{\Gamma}^{(2)}$ is rather unimpressive compared to the error-scaling of the KT scheme, *cf.* Fig. 6.5b.

The question is why the FRG Taylor/vertex expansion was working so well for ϕ^4 -theory with positive mass term, but does not converge for negative mass term. A possible explanation is that choosing $\vec{\varphi} = 0$ as the expansion point throughout the entire RG flow might be a bad choice, because the global minimum is in the beginning non-trivial and only moves to the expansion point during the RG flow.

In order to exclude that the failure of the FRG Taylor/vertex expansion is linked to the fact that we are not expanding about the moving minimum, we turn to yet another test case.

6.6.3. Total collapse instead of convergence

Hence, we perform the same analysis as before for the UV initial potential (6.6). The corresponding UV initial condition for the ODE system is

$$\bar{\Gamma}^{(2)}(t=0) = 1, \quad \bar{\Gamma}^{(4)}(t=0) = -\frac{6}{5}, \quad \bar{\Gamma}^{(6)}(t=0) = 1, \quad \forall n > 3 \quad \bar{\Gamma}^{(2n)}(t=0) = 0. \quad (6.18)$$

The remarkable result is that the FRG Taylor/vertex expansion does not work at all for this potential and we were not able to find a single choice for N and n_{trunc} where we could integrate to the IR. Using the same UV cutoff as in Fig. 6.2c the RG flow was always breaking down at $t \approx 28$ ($r(t \approx 28) \approx 0.69$) (for $N = 4$), which is, if one inspects Fig. 6.2c, the RG time, where the local minima disappear and the potential turns convex.

The interesting aspect is that for this potential it is not possible to argue that the correct expansion point might have changed during the RG flow, because the global minimum is permanently located at $\vec{\varphi} = 0$.

So, what happened? Again, consulting the result from the KT scheme in Fig. 6.2c, it does not look like there are any cusps appearing during the RG flow and the potential and its derivative seem smooth for all times t . Still, an expansion fails. In consequence, it appears as if the global dynamics of the potential is simply not describable by a local Taylor expansion. A reason behind could be that the potential, even though being differentiable, turns non-analytic (at least for intermediate t), such that an expansion does not converge and an infinite number of expansion coefficients would be required. This can be related to the phenomenon of Wilbraham-Gibbs oscillations [251, 252, 253, 254] in the flat region of the potential at $t \approx 28$, which was already anticipated before in Ref. [85].

Again, we note that this result is not by accident and was carefully checked by our own independent codes. This was also confirmed independently by J. Eser (private communication).

The very harsh conclusion which we draw from these zero-dimensional minimal examples is that a Taylor expansion of local effective bosonic potentials is not trustworthy at all. This is even the case, if the UV potential is smooth and expandable and even for RG flows of potentials that do not show cusps of any type. Furthermore, there is no reason at all, why this should be completely different in higher-dimensional setups. As soon as true non-analytic structures, such as chemical potentials, non-analytic UV initial potentials or non-analyticities of IR potentials (due to non-trivial minima and convexity) enter the game, Taylor expansions of the potential are ill-conditioned anyhow. In total, we think that any kind of expansion that fundamentally relies on analyticity of the potential should be avoided.

6.7. Entropy production in the viscous $N = 1$ limit

At this point, we turn to the quantitative evaluation of the entropy function (5.29) of Section 5.1.4 in terms of its finite-volume discretization by Eq. (5.80) from Section 5.2.4. Basically, we briefly summarize the results of our own Ref. [2], where more details are presented.

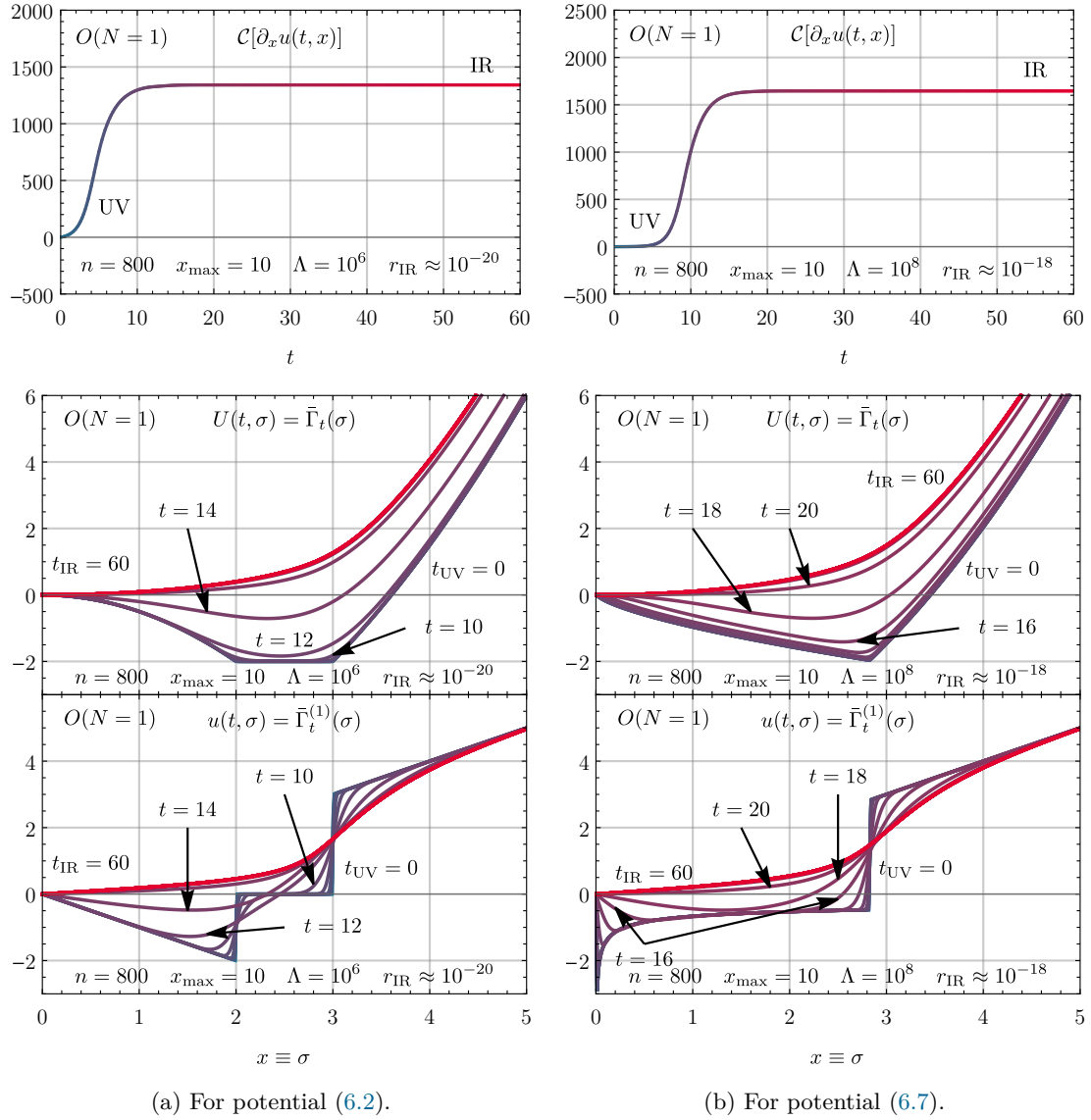


Figure 6.10: The (numerical) entropy function (top panel) and the RG flows of the effective potential (middle panel) $U(t, \sigma)$ and its derivative $u(t, \sigma) = \partial_\sigma U(t, \sigma)$ (bottom panel) for the zero-dimensional $O(N = 1)$ model. From Ref. [2, Figs. 1, 2, 9, 10].

Again, we study all four test cases with the classical UV potentials (6.2) and (6.5) to (6.7). This time, however, we fix $N = 1$ for the entire section, because so far we were not able to generalize the entropy function (5.29) to an arbitrary finite integer N . In Figs. 6.10 and 6.11 we present the corresponding RG flows of the effective potential and its derivatives (lower panels). Remember that these flows correspond to the viscous limit without advection and are exclusively driven by highly non-linear diffusion. In addition, we plot the numerical results for the (numerical) entropy, which was calculated with Eq. (5.80) on the solution. The (numerical) parameters are provided in the figure panels and present solid choices according to our previous analysis of Section 6.5.

Inspecting the numerical results for the entropy function in detail, we observe that the entropy always starts off at zero in the UV. This is of course by construction, because we normalized the entropy of $u(t, \sigma)$ by subtracting its UV initial value. At some later RG time the entropy always rises drastically and ultimately again settles on a plateau in the IR. The time when the entropy

increases most is, as can be seen from the lower panels, exactly when the dynamics in the potential and its derivative set in and when the RG scale approaches model scales. This is also when the arc length of $u(t, \sigma)$ changes most, which underlines a direct connection between the TVD/TVNI property and the numeric entropy. The entropy stops increasing below the model scales. This can be associated with the RG time where the RG flow of $u(t, \sigma)$ approaches an equilibrium state and the diffusion stops, similar to the thermal equilibrium that is approached by the heat equation [168, 49, 170].

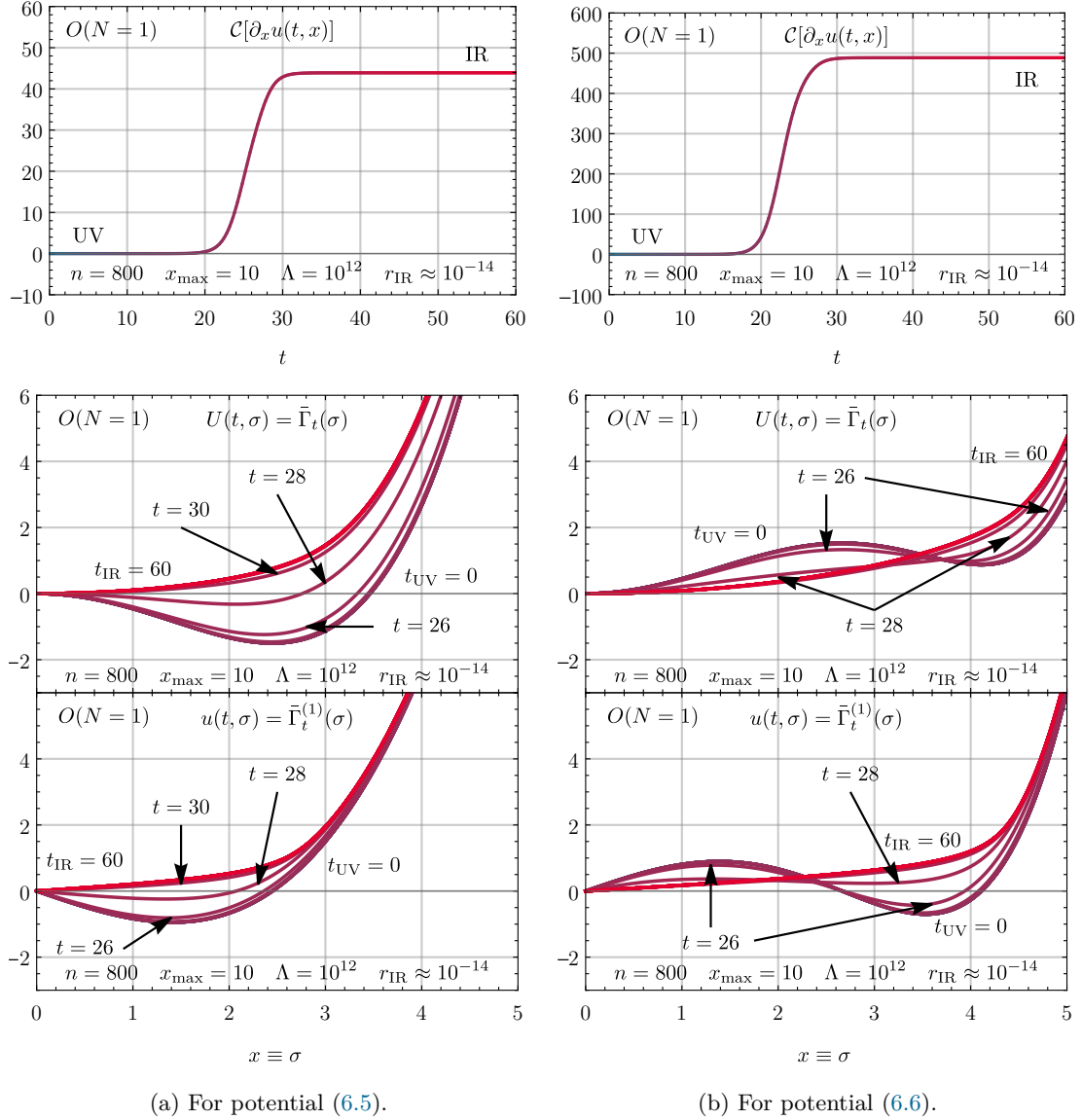


Figure 6.11: The (numerical) entropy function (top panel) and the RG flows of the effective potential (middle panel) $U(t, \sigma)$ and its derivative $u(t, \sigma) = \partial_\sigma U(t, \sigma)$ (bottom panel) for the zero-dimensional $O(N = 1)$ model. From Ref. [2, Figs. 3, 5, 7, 8].

For the non-analytic initial conditions the increase of the entropy sets in earlier, as can be seen from Fig. 6.10. The reason is that the discontinuities are smeared out rather early in the RG flows, because they correspond to huge gradients that enhance diffusion. For the analytic initial potentials, one observes in turn in Fig. 6.11 that the entropy stays (almost) zero for quite some

time, before it starts increasing. Noting that the UV cutoffs of the latter test cases were chosen much larger, the immediate rise of the entropy for the former test cases points towards slightly too small UV cutoff scales. Indeed, if we return to Fig. 6.7 we find that $\Lambda = 10^6$ and $\Lambda = 10^8$ are only just on the plateau, which signals RG consistency and UV cutoff independence.

We conclude that the (numerical) entropy can be used to ensure that the UV cutoff was chosen sufficiently large, but also that the artificial IR cutoff is sufficiently small. Otherwise, the system does not have time to equilibrate and the IR is not reached.

Anyhow, we also associated the increase of the (numerical) entropy with irreversibility of the RG flow and a loss of information about the initial condition and earlier RG times. Also this is understood rather intuitively from Figs. 6.10 and 6.11. First, the entropy increases drastically, when there is strong non-perturbative dynamics by strong diffusion, while it stays constant when almost nothing happens at all. For RG times where the entropy is approximately constant, we can go back and forth in time without noting any significant change of the system. Hence, we are either still in the UV Gaussian regime [177, 255] nor in the IR equilibrium. For both, there is no change of the information which is contained in $u(t, \sigma)$. On the other hand, the information contained in the system changes a lot if $u(t, \sigma)$ changes drastically. In general, we can identify the loss of information about the initial state and the rising entropy with the excessive rise in the number of couplings/vertices that would be necessary to describe the system or the number of vertices that change their value during the flow. For example, only little information was necessary to define the UV initial conditions, while in the IR we find an infinite number of vertex functions that encode scattering processes of all orders in fields. Otherwise, for non-analytic UV initial conditions all vertex functions change drastically during the RG flow.

Next, let us comment on the absolute changes of the numerical entropy for our test cases. We clearly observe that the entropy increases most for the non-analytic initial conditions and littlest for the ϕ^4 -theory. Considering ϕ^4 -theory with positive mass leads to an even smaller increase in the numerical entropy than for all other test cases, see Ref. [2, Fig. 6]. This finding is rather natural, if one thinks of the direct connection between our entropy function and the TV, *i.e.*, the arc length of $u(t, \sigma)$, which of course changes most for the $u(t, \sigma)$ with larger gradients in a purely diffusive setup. However, this difference in absolute numbers may also be interpreted as the amount of information which is required to describe the system during the flow: In the previous Section 6.6, we found that for ϕ^4 -theory with positive mass term a low-order Taylor expansion of the potential suffices to capture the dynamics, while for ϕ^4 -theory with negative mass or ϕ^6 theory convergence of the series gets lost or the expansion does not work at all. Hence, a drastic increase of the entropy function may also signal “how non-perturbative” a system is and how relevant higher-order vertices are for its description. This might be of relevance for higher-dimensional applications of the Taylor expansion of the potential.

In any case, we conclude that our numerical results confirm our analytic construction of the entropy function and its properties. Furthermore, we believe that constructing similar entropy functions for higher-dimensional (truncated) FRG flow equations might help to single out adequate truncations, numerical schemes, but also decent UV and IR cutoffs *etc.*

6.8. Large vs. infinite N and shocks in RG flows

We close this chapter with another demonstration of the great power of the fluid-dynamical framework for the calculation of RG flows of effective potentials. We show its superiority over other (numerical) approaches by studying shock- and rarefaction waves in field space, which cannot be described numerically without modern methods from CFD. We compare our numerical setup with the analytic results from the method of characteristics and the prediction of the shock position from the Rankine-Huguniot condition from Section 5.1.8.

In addition, this setup allows us to show direct connections between shock waves and phase transitions. A lot of these concepts were already worked out for higher-dimensional systems in

Refs. [77, 101], which greatly inspired our own work. Our own work was already presented in Ref. [3].

Finally, we show that even very large N should by no means be confused with the infinite- N limit, and results are not transferable, because the single diffusive σ -mode plays a significant role for the restoration of convexity of effective potentials, such that the $N \rightarrow \infty$ limit can lead to violations of key features of a theory or model.

6.8.1. Returning to an instructive toy model

In order to discuss these topics, we return to our “instructive toy model” from Section 3.3.4. We recall that we work in $\frac{1}{N}$ -rescaled quantities throughout the entire section, which are defined in Eq. (5.30), in order to easily compare finite to infinite N . The same applies to the flow equations, where we use Eqs. (5.31) and (5.32).

Anyhow, in contrast to Section 3.3.4 we work on the level of the rescaled field $x = \frac{1}{\sqrt{N}} \sigma$ and not the rescaled invariant $y = \frac{1}{N} \varrho$. This is because of numerical reasons, *i.e.*, the implementation of the boundary condition at $x = 0$ in the KT scheme, *cf.* Section 5.2.3, and the extremely high resolution which is required at $x = 0$, see below. The corresponding UV initial potential of our model therefore turns from its y -formulation in Eq. (3.40) to

$$V(x) = \begin{cases} \frac{1}{2} x^2 & \text{for } |x| \leq 2, \\ -a \frac{1}{2} x^2 + 2(a+1) & \text{for } 2 < |x| \leq 4, \\ \frac{1}{2} x^2 - 6(a+1) & \text{for } 4 < |x|. \end{cases} \quad (6.19)$$

Its field-space (spatial) derivative reads

$$v(x) = \partial_x V(x) = \begin{cases} x & \text{for } |x| \leq 2, \\ -a x & \text{for } 2 < |x| \leq 4, \\ x & \text{for } 4 < |x|, \end{cases} \quad (6.20)$$

and forms the initial condition of our fluid-dynamical RG flow. Again, we study values $a \in [0, 2a_c]$, where the critical value a_c is given by Eq. (3.42). The role of the critical value a_c in the FRG context is discussed below. Plots of this UV initial condition are presented in Fig. 6.12.

6.8.2. RG flows at $N \rightarrow \infty$

In the next step, we use the initial condition (6.20) to study the RG flow equation (5.32) in the limit $N \rightarrow \infty$, hence, Eq. (5.34), which reads

$$\partial_t v(t, x) = \frac{d}{dx} \left[\frac{\frac{1}{2} \partial_t r(t)}{r(t) + \frac{1}{x} v(t, x)} \right], \quad x \in (-\infty, \infty). \quad (6.21)$$

This is the inviscid limit of the flow equation, which exclusively describes bulk motion of $v(t, x)$. In this limit, we are able, in addition to numerically solving the system with the FV-KT scheme, to analytically integrate the equation via the method of characteristics – at least until characteristic curves intersect. This was discussed and calculated on a theoretical level in detail in Section 5.1.7. In addition, we can analytically capture the position of a shock wave in field space from the Rankine-Hugoniot condition. (The presence of a shock wave is obvious in the y -formulation, where the initial condition presents a Riemann problem, *cf.* Fig. 3.3 and Ref. [77].)

Both analytic approaches can be directly compared to a full numerical solution, which presents another test of the fluid-dynamical approach to FRG. On top of this, the discussion of the analytic solution greatly helps to correctly interpret the dynamics which is observed in the numerical results.

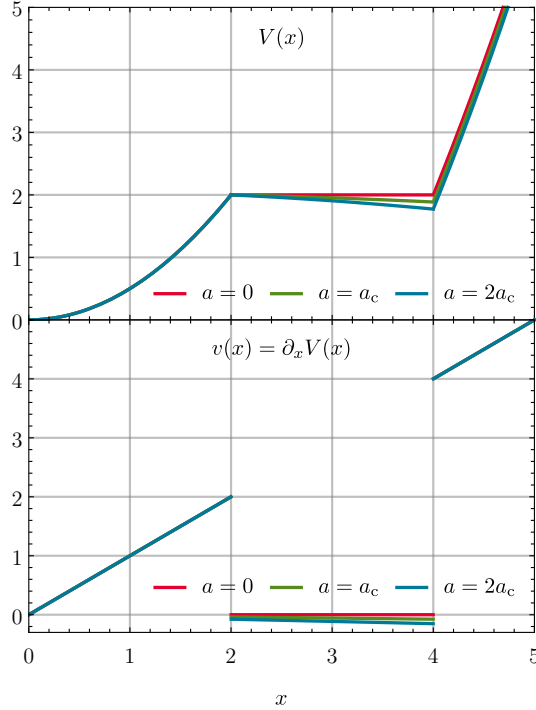


Figure 6.12: The potential $V(x)$ from Eq. (6.19) (upper panel) and its x -derivative $v(x) = \partial_x V(x)$ from Eq. (6.20) (lower panel) for different values of the parameter a and where a_c is given by Eq. (3.42). From Ref. [3, Fig. 3].

Characteristics

For our specific initial condition (6.20) and PDE (6.21) the characteristic curves of the fluid are described by Eq. (5.48). These are parametric curves $(t, x(t))$ in the RG-time-field-space domain $[0, \infty) \times (-\infty, \infty)$, where $\frac{v(t, x(t))}{x(t)}$ stays constant.³ It is possible to reconstruct the full solution $v(t, x)$ of the PDE from these expressions. However, usually this involves an inversion of the expressions, which has to be performed numerically and is not needed for this work. This also partially explains why the method of characteristics breaks down as soon as these curves intersect: An inversion and reconstruction of the full solution is hardly possible if the solution is multi-valued. After an intersection of characteristic curves, a shock is formed and the solution of the PDE exclusively exists in a weak sense. Similarly, infinitely many characteristic curves that originate at a single point and move apart are identified as a rarefaction wave and also form a non-analyticity in the weak solution of the PDE. For details we refer to Refs. [104, 49, 50, 51, 52].

Anyhow, let us turn to the discussion of the results. In Fig. 6.13, we plot the characteristic curves (5.48) for the initial condition (6.20) with $a = 0$ with an UV cutoff $\Lambda = 10^{10}$. (The UV cutoff was chosen after performing numerical benchmark tests for relative errors of $\Gamma^{(2)}$ with the KT scheme and turned out to be absolutely sufficient, see below. Furthermore, we remark that plots for different $a > 0$ look rather similar, which is why we exclusively present a figure for $a = 0$.) We restrict the plot and most of our discussion to positive x , while the situation for negative x is simply mirrored about the t -axis. For the moment, we exclusively focus on the colored lines, which vertically originate at $t = 0$ from the x -axis.

At $t = 0$ the solution $v(t, x(t))$ on the parametric curve takes the values of the initial condition

³The same discussion on the level of y would lead to parametric curves $(t, y(t))$ in the domain $[0, \infty) \times [0, \infty)$, where $v(t, y(t))$ remains constant.

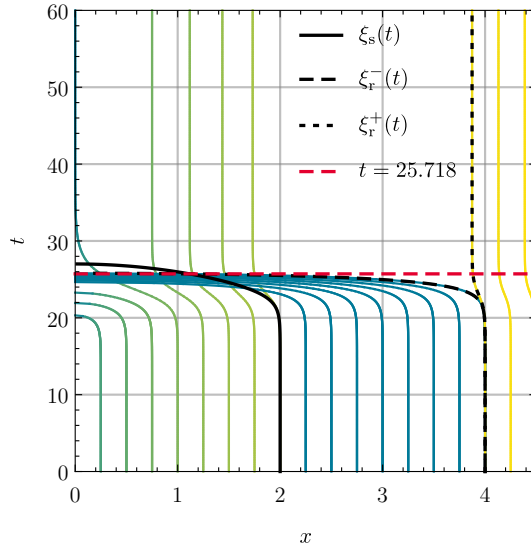


Figure 6.13: Selected characteristic curves $(t, x(t))$, see Eq. (5.48), for $a = 0$ and $\Lambda = 10^{10}$ in blue, green, and yellow, shock position $\xi_s(t)$, see Eq. (6.28), as solid black line, and the tips of the rarefaction fan $\xi_r^\mp(t)$, see Eqs. (6.22) and (6.23) originating at $(t = 0, \xi_r^\mp(0) = 4)$ as dashed black lines. The changing color on the characteristic curves indicates the change of $v(t, x(t))$ along them, see again Eq. (5.48), where blue corresponds to $v(t, x(t)) = 0$ and yellow corresponds to $v(t, x(t)) = 4.5$. The shock wave and the rarefaction fan collide at $(t, x) \approx (25.718, 1.115)$ (the time is marked with the red-dashed line) rendering the expressions $\xi_r^\mp(t)$ and $\xi_s(t)$ as well as the characteristics that intersect with the shock and rarefaction wave invalid for later times. From Ref. [3, Fig. 4].

Eq. (6.21). This is encoded in the colors of the characteristic curves, where blue corresponds to $v(t, x(t)) = 0$ and yellow corresponds to $v(t, x(t)) = 4.5$. Values in between are depicted as mixtures of blue and yellow, thus green. Following the characteristic curves, we find that a lot of them significantly change their color, which implies that $v(t, x(t))$ changes along the curves. However, by definition, the ratio $v(t, x(t))/x(t)$ keeps its value along a characteristic curve.

We remember that the characteristic curves basically describe the motion of little portions of the fluid. Hence, we find that in the beginning the fluid does not move at all. Incidentally, this supports that the UV cutoff was chosen large enough, such that the advection flux is totally suppressed. As soon as the regulator $r(t) = \Lambda e^{-t}$ is approaching the model scales at $t \approx 20$ the dynamics sets in: Overall we see that the characteristic curves are bent towards smaller $|x|$ and $v(t, x(t))$ only decreases (increases) at positive (negative) x . This agrees with the finding that the fluid velocity $\partial_v F[t, x, v]$ is manifestly negative (positive) for positive (negative) x , *cf.* Eq. (5.14). In fact, we find that characteristic curves from negative and positive x hit the t -axis and therefore positive and negative waves of the fluid have to annihilate at $x = 0$.

Either way, this general behavior is superseded by some other dynamics: One finds that fluid elements that start in the region $2 < |x| < 4$ move much faster towards $|x|$ than fluid elements at smaller $|x|$. Their attempt to pass by the slower moving fluid portions leads to their collision. Their characteristics intersect and a shock wave is formed. By construction of the initial condition, this already happens at $t = 0$ at $|x| = 2$. The shock wave propagates and more and more characteristics join the shock and accelerate it towards $x = 0$. The position of the shock wave is marked by the black solid line and its parametric curve is calculated explicitly below.

Anyhow, in advance of this calculation, we turn to another phenomenon which is happening at

about $|x| = 4$. We already discussed that characteristics which start at $|x| < 4$ move fast towards smaller $|x|$. On the other hand, we observe that characteristic curves at $|x| > 4$ only slightly bend towards smaller $|x|$ and then freeze, which is easily understood by inspecting Eq. (5.48) with the initial condition. This results in a rarefaction wave in $v(t, x)$ that originates at $t = 0$ and $|x| = 4$. The rarefaction fan is analytically described by the characteristic curves

$$\xi_r^-(t) = \pm \sqrt{16 - \frac{1}{\Lambda e^{-t} - a} + \frac{1}{\Lambda - a}}, \quad v_r^-(t, \xi_r^-(t)) = -a \xi_r^-(t), \quad (6.22)$$

$$\xi_r^+(t) = \pm \sqrt{16 - \frac{1}{\Lambda e^{-t} + 1} + \frac{1}{\Lambda + 1}}, \quad v_r^+(t, \xi_r^+(t)) = \xi_r^+(t), \quad (6.23)$$

where $\xi_r^\mp(t)$ is the position of a fluid cell that starts at minimally smaller/larger $|x|$ right next to $|x| = 4$ and $v_r^\mp(t, \xi_r^\mp(t))$ is the value of the fluid field on the rarefaction fan. Both curves are plotted in Fig. 6.13 as black dashed lines.

Looking at the black solid and dashed lines for the shock and rarefaction fan in Fig. 6.13 one actually finds that both curves intersect. This happens at $(t, x) \simeq (25.718, 1.115)$, which is marked by the red dashed line. Until this point, where the rarefaction wave catches up with the shock wave, all characteristic curves which did not enter the shock yet are valid solutions and we could in principle integrate backwards in RG time and reconstruct the UV potential. However, after collision of the shock and rarefaction wave, there is some highly non-linear dynamics happening, which cannot be captured by analytic calculations and one has to rely on numerical solutions of the PDE.

This non-linear dynamics causes the manifest irreversibility of the RG flow and should in principle produce entropy of some kind, similar to what was discussed for the purely diffusive systems in Section 6.7. The shock and the rarefaction wave are imprinted already on the initial condition, such that there is no “formation”, which could cause a rise of entropy. We come back to this discussion below in the context of the numerical solution. Before, we insert the analytic detection of the shock position.

A shock wave in field space – application of the Rankine-Hugoniot condition

Here, we use the results of Section 5.1.8 to analytically calculate the position of the shock front in field space. For the sake of simplicity we restrict our discussion to positive x , while the result for negative x is again simply mirrored.

The only thing we need to do at this point is to insert the left and right limits of the initial condition at the shock position $x = 2$ into Eqs. (5.53) and (5.54) and combine these with the Rankine-Hugoniot condition (5.55). The values of $v(t, x(t))$ directly left and right of the shock are

$$v_L(t) = \frac{v_{UV,L}}{x_{UV,L}} x_L(t) = \xi_s^-(t), \quad v_R(t) = \frac{v_{UV,R}}{x_{UV,R}} x_R(t) = -a \xi_s^+(t), \quad (6.24)$$

while the corresponding fluxes are

$$F_L(t) = -\frac{\frac{1}{2} \partial_t r(t)}{r(t) + \frac{v_L(t)}{x_L(t)}} = -\frac{\frac{1}{2} \partial_t r(t)}{r(t) + 1}, \quad F_R(t) = -\frac{\frac{1}{2} \partial_t r(t)}{r(t) + \frac{v_R(t)}{x_R(t)}} = -\frac{\frac{1}{2} \partial_t r(t)}{r(t) - a}. \quad (6.25)$$

Using Eq. (5.55), we obtain a differential equation for the shock position, the Rankine-Hugoniot condition,

$$\partial_t \xi_s(t) = \frac{1}{\xi_s(t)} \frac{1}{a+1} \left[\frac{\frac{1}{2} \partial_t r(t)}{r(t) - a} - \frac{\frac{1}{2} \partial_t r(t)}{r(t) + 1} \right]. \quad (6.26)$$

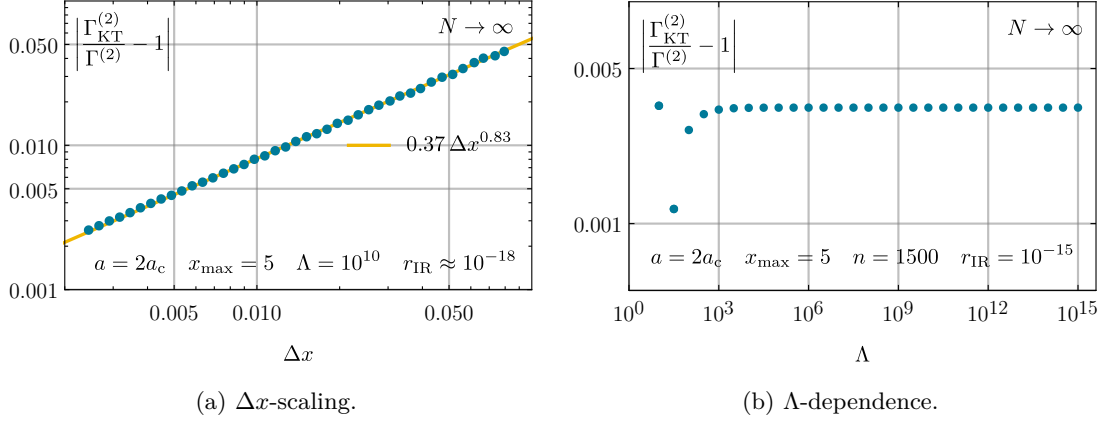


Figure 6.14: Relative errors for $\Gamma^{(2)}$ for the UV initial condition (6.20) for $N \rightarrow \infty$ and $a = 2a_c$. From Ref. [3, Figs. 12 & 13].

Here, we are allowed to set $\xi_s^+(t) = \xi_s^-(t) = \xi_s(t)$. The differential equation is integrable and can be rewritten in terms of the regulator function (due to its monotonicity),

$$\partial_r(\xi_s^2(r)) = \frac{1}{a+1} \left(\frac{1}{r-a} - \frac{1}{r+1} \right). \quad (6.27)$$

Integrating this equation from the UV ($r = \Lambda$) to some arbitrary $r(t) \leq \Lambda$, we find

$$\xi_s(t) = \sqrt{\xi_{s,\text{UV}}^2 + \frac{1}{a+1} \left[\ln \left(\frac{r(t)-a}{\Lambda-a} \right) - \ln \left(\frac{r(t)+1}{\Lambda+1} \right) \right]}. \quad (6.28)$$

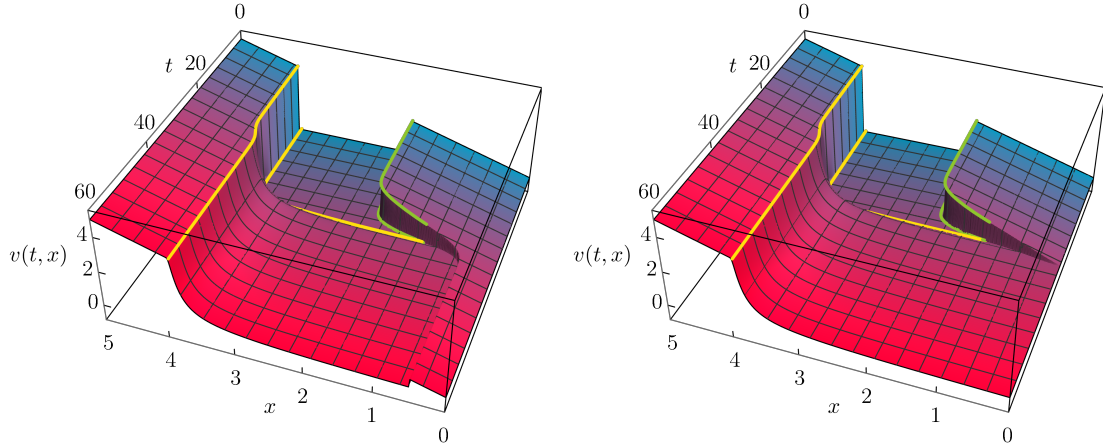
The integration constant $\xi_{s,\text{UV}} = 2$ is the initial shock position. Plotting Eq. (6.28), we obtain the black solid line in Fig. 6.13, which is valid until it intersects with the rarefaction fan.

Numerical results for the RG flow

Next, we turn to the fully numerical results for the purely advective RG flows of Eq. (6.21) with initial condition (6.20).

Numerical setup Explicitly, we present results for three different choices of a , namely $a = 0$, $a = a_c$, and $a = 2a_c$. All calculations are performed with a UV cutoff $\Lambda = 10^{10}$ and IR cutoff $r_{\text{IR}}(t = 60) \approx 10^{-18}$ on a computational domain $x_{\text{max}} = 5$ with $n = 1500$ FV cells, and a resulting cell size $\Delta x \simeq 0.003$. It was explicitly tested that these parameters suffice to achieve relative deviations from the exact $\Gamma^{(2)}$ in the IR which are of order 10^{-14} for $a = 0$ and $a = a_c$ and of order 10^{-3} for $a = 2a_c$ and are therefore of extremely high quality. For a more detailed analysis of the choice of numerical parameters and the performance of the KT scheme as well as its first-order-accurate variant, we refer to our publication [3]. Here, however, we shall focus on the phenomenology which can be resolved by the CFD approach to the flow equation. For reference, we solely present plots for the UV-cutoff independence and the Δx -scaling of the relative errors of $\Gamma^{(2)}$ for the hardest case with $a = 2a_c$ in Fig. 6.14. The reason for the different performance for $a \leq a_c$ as well as the approximate $\Delta x^{0.83}$ instead of Δx^2 scaling becomes clear after the following discussion.

Comparison of numerical and analytical results Our explicit numerical results from the FV-KT scheme for the $N \rightarrow \infty$ RG flows are plotted in Fig. 6.16a. For better visualization, we also present two three-dimensional versions of the upper and the lower panel of Fig. 6.16a in the



(a) Freezing shock waves for $a = 0$: The left tip of the rarefaction fan and the shock are only marked up to $(t, x) \simeq (25.718, 1.115)$, where they meet and the analysis based on the method of characteristics and Rankine-Hugoniot condition breaks down.

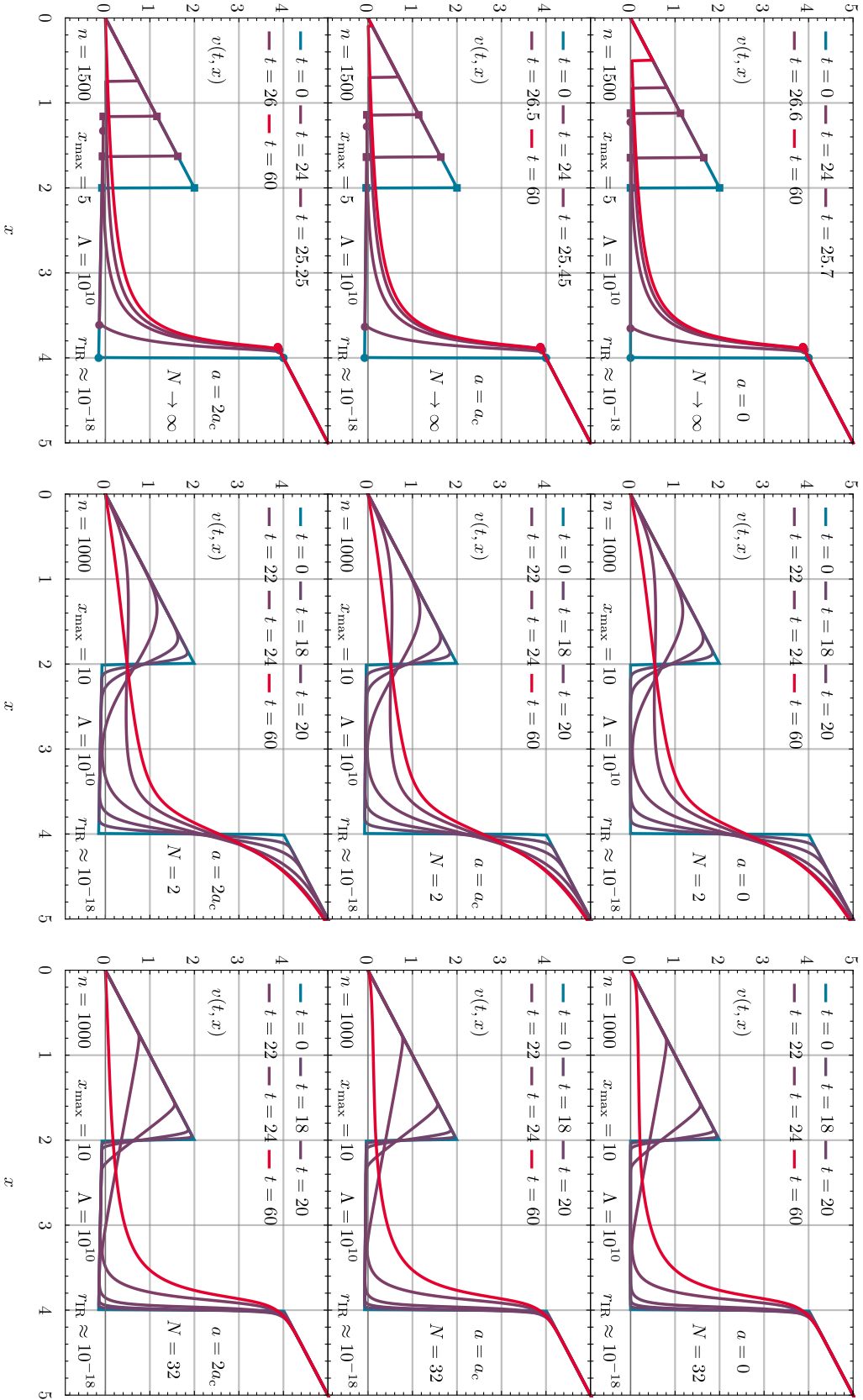
(b) Annihilating shock waves for $a = 2a_c$: The left tip of the rarefaction fan and the shock are only marked up to $(t, x) \simeq (25.718, 1.115)$, where they meet and the analysis based on the method of characteristics and Rankine-Hugoniot condition breaks down.

Figure 6.15: RG flow of $v(t, x)$ as 3D-plot corresponding to the flow displayed in the upper and lower panel of Fig. 6.16a. The left and right tips $(\xi_r^\mp(t), t, v(t, \xi_r^\mp(t)))$ of the rarefaction fan are plotted as yellow lines, while the shock $(\xi_s(t), t, v(t, \xi_s(t)^\pm))$ is marked with green lines. From Ref. [3, Figs. 6 & 7].

separate Fig. 6.15. The other two plots of Fig. 6.16 can be ignored for the moment, because these belong to the discussion of RG flows at finite N in Section 6.8.3. Color coding is analogous to the previous sections: blue curves/regions correspond to the UV and red curves/regions are associated to the IR scales.

Inspecting the plots, we clearly observe the dynamics which is predicted from the method of characteristics: For all choices of a we find exclusively advective transport of $v(t, x)$ from larger to smaller $|x|$. The discontinuity, which starts at $|x| = 2$, propagates as a shock wave to smaller $|x|$. The corresponding analytic reference solution for the shock position $\xi_s(t)$ from Eq. (6.28) is marked in Fig. 6.16a by little square dots as long as the analytic solution is trustworthy, while it is indicated by green lines in Fig. 6.15. The same applies to the other discontinuity at $|x| = 4$, which causes the rarefaction wave. Here, the analytical solution from Eqs. (6.22) and (6.23) of the left and right characteristics $\xi_r^\mp(t)$ of the rarefaction fan are marked with bullets in Fig. 6.16a and yellow lines in Fig. 6.15 as long as the analytical solution is valid. For both, the shock position and the rarefaction fans we find perfect agreement of the numerical and analytical results. This would never be achieved without modern methods from CFD, which are capable of resolving discontinuities with very high precision.

Colliding shocks, criticality, and phase transitions Having briefly discussed the high numerical quality, let us turn to the phenomenology and its peculiar dependence on the choice of a . From Fig. 6.16a, it is clearly visible that for all choices of a the inner rarefaction fan catches up with the shock wave, which was already predicted and discussed from the method of characteristics for $a = 0$. However, we find that depending on the precise value of a , which directly influences the velocity of the rarefaction and shock wave as well as their interaction, the shock wave either freezes at some $|\xi_s(t \rightarrow \infty)| \neq 0$ or it reaches $x = 0$. (This cannot be calculated from the method of characteristics, which is no longer valid after the interaction of the rarefaction and shock wave.) If the shock waves from positive and negative x make it to $x = 0$, they annihilate, which again corresponds to a highly non-linear process. Again, this process has to cause a rise in entropy and



(a) For $N \rightarrow \infty$. From Ref. [3, Fig. 5].

(b) For $N = 2$. From Ref. [3, Fig. 8].

(c) For $N = 32$. From Ref. [3, Fig. 9].

Figure 6.16: The RG flow of $v(t, x)$ for the initial potential (6.20) with $a = 0$, $a = a_c$, and $a = 2a_c$ in the upper, middle, and lower panel respectively.

is definitely irreversible.

Putting numbers on this process, we find that the shock wave freezes for $a = 0$ at $|x| = |\xi_s(t = 60)| \approx 0.496$. This value was extracted from the numerical solution on the level of the cell averages by performing computations at varying Δx but fixed computational domain x_{\max} as well as keeping all other parameters fixed. Fitting 41 data points with n ranging from 64 to 2048 we find

$$|\xi_s(t \rightarrow \infty)| \simeq |\xi_s(t = 60)| = 0.496 + 0.788 \Delta x^{0.869}. \quad (6.29)$$

Using the same fitting procedure, we find for $a = a_c$,

$$|\xi_s(t \rightarrow \infty)| \simeq |\xi_s(t = 60)| = 0.983 \Delta x^{0.413}, \quad (6.30)$$

which clearly shows that the shock exactly ends up at $x = 0$. Nonetheless, exclusively due to the finite Δx -resolution of our FV calculation, we observe in the middle panel of Fig. 6.16a a remnant of a freezing shock at $|x| \approx 0.095$, which is clearly a discretization artifact. For all $a > a_c$, the shock waves from negative and positive x truly collide and annihilate at $x = 0$.

Hence, it turns out that a_c is a critical value for the dynamics and IR physics. A slight variation of the “external” UV parameter a causes huge changes in the IR. On the level of the PDE, this can be seen as a realization of a “butterfly effect”, where a minimal perturbation at some time t causes great effects at later times and totally different locations.

Explicitly, as long as $a < a_c$, there is a small region around $x = 0$ where the fluid $v(t, x)$ remains actually untouched throughout the entire RG flow and keeps its linear slope, while for larger $|x|$ extremely non-linear dynamics happens. The inner region is very similar to the eye of a cyclone, which is not affected by the chaos around. For $a = 0$, this untouched region is exactly between the freezing points of the shocks at $|\xi_s(t \rightarrow \infty)| \simeq 0.496$. Thus, for values $a < a_c$ and for all times t ,

$$\partial_x v(t, x)|_{x=0} = 1, \quad \forall n > 1 \quad \partial_x^n v(t, x)|_{x=0} = 0. \quad (6.31)$$

Yet, in the IR these derivatives are in one-to-one correspondence to the observables, the vertex functions,

$$N^{\frac{n-1}{2}} \Gamma^{(n+1)} = \partial_x^n v(t \rightarrow \infty, x)|_{x=0}, \quad (6.32)$$

which are those of a massive free theory. This is exactly the result which we obtained by exact evaluation of the correlation functions as well as from the zeroth-order contribution of the saddle-point expansion, see Sections 3.3.4 and 3.3.5. We recapitulate that $a < a_c$ corresponds to those values of a where the saddle-point expansion is applicable.

On the other hand, if we turn to the lower panel of Fig. 6.16a, or in general $a > a_c$, there is no longer an “eye of the cyclone” and loosely speaking, the cyclone collapses. The rarefaction waves do not hinder the shocks from annihilating at $x = 0$, and $v(t, x)$ and its derivatives change drastically after this collision at $x = 0$. Extracting the vertex functions numerically one finds (up to numerical errors, see Fig. 6.14a) perfect agreement with the exact results of Eq. (3.48). First of all, this implies that the numeric scheme is trustworthy also under “hard non-linear circumstances”, even though the Δx -scaling is drastically reduced because of the colliding shock waves, which does not come unexpected by Ref. [105].

However, phenomenologically, we find that $\Gamma^{(2)}$ jumped from $\Gamma^{(2)} = 1$ to $\Gamma^{(2)} = \frac{1}{16}$ in the IR due to the collision of two shock waves.

On the level of the QFT this jump in the observable, which is caused by the tuning of an UV and/or external parameter, here a , clearly corresponds to a first-order PT. Hence, there is a direct link between PTs and freezing/annihilating shock waves. This clearly supports the findings of Refs. [77, 101].⁴ (Our work can be seen as a refinement of some of their analysis.)

⁴Looking at the problem from Ehrenfest’s classification of PTs [148, 11] it is almost by definition that (moving) discontinuities in derivatives of (thermodynamic) potentials are in direct correspondence to PTs.

However, this fluid-dynamical FRG calculation also reveals another interesting connection: In our analysis of Section 3.3.5 we found that the saddle-point expansion is doomed to fail for our toy model as soon as a exceeds the critical value a_c . Hence, also using the zeroth order approximation in the $\frac{1}{N}$ -expansion is no longer justified. On the level of the saddle-point expansion, this was signaled by the degeneration of minima or the non-analyticity of minima of the exponent (3.49), see Fig. 3.4, as soon as a exceeds a_c . In the FRG formalism, however, it is realized in terms of irreversible non-linear dynamics of colliding shock waves. We believe that further research is in order to better understand this connection.

“I really don’t care, do u?” Some exhausted readers might ask at this point why we should care about these technical discussions and findings. Real-world physical problems in higher-dimensional QFTs usually seem to be less pathological and the $N \rightarrow \infty$ approximation is used day in-day out without great doubts and seems to deliver great results.

Either way, maybe we should be more careful: Consider some $O(N)$ -type model in a dimensionally reduced setup, where the effect of temperature is mimicked by a coupling constant in the UV action, *e.g.*, Ref. [256], or where temperature is introduced via the Matsubara formalism, *e.g.*, Ref. [257, 22, 13]. Such models are oftentimes analyzed to study PTs, which are triggered by tuning the temperature. They are even discussed as minimal toy models for the chiral PT in the QCD phase diagram, which is oftentimes considered to be of $O(4)$ universality class. As a first approach, these types of calculations are oftentimes performed in the $\frac{1}{N}$ -expansion. Usually, the zeroth-order contribution, which agrees with the $N \rightarrow \infty$ limit in rescaled quantities, is considered to be a good first estimate and simplifies calculations drastically. For example, the FRG flow equations of a d -dimensional $O(N)$ model exactly reduce to the LPA flow equation with exclusive contributions by Goldstone modes [74, 75, 76, 77]. Now, let us assume that we observe some first- or second-order PT by tuning the “temperature” parameter. How can we actually be sure that the order of the PT or the existence of this PT at all is not simply an artifact of the approximation, especially the $N \rightarrow \infty$ limit? Similar situations can also be constructed for other types of theories or models, where exactly the same question arises, and all of them are not too different from our “pathological” zero-dimensional setup: The parameter a could simply be identified with a temperature and a_c with the critical temperature of the first-order PT. Even the non-analytic structures in the UV initial condition can easily be present in higher-dimensional theories, *e.g.*, by introducing a chemical potential.

Anyhow, checking the independence of the phenomenology by comparing different approximations and limits in higher-dimensional setups is usually expensive and cumbersome. Therefore, our minimal and exactly solvable toy model might be better suited to generally discard certain approximations for the investigation of PTs *etc.*. This is discussed in detail in the following paragraphs, where we compare $N \rightarrow \infty$ with finite- N results.

6.8.3. Lost in math: How the infinite- N limit leads physics astray

Before we turn to calculations at finite N , let us again examine the upper panel of Fig. 6.16a and ask how the corresponding potential $V(t, x)$ looks like. In fact, the shape of the potential during the RG flow looks very similar to its initial condition in Fig. 6.12 (upper panel). Only the flat part moves downwards a little bit. (For an illustration of a similar potential, see Ref. [77, Fig. 2b].) In any case, the cusp at $x = 2$ remains and simply moves to smaller $|x|$ and freezes in the IR, because it is the integral of the shock wave in $v(t, x)$. However, this violates fundamental properties of zero-dimensional QFTs, which were discussed in detail in Section 2.2: The potential is neither convex nor smooth in the IR. This can also be seen by calculating the x -derivative of $v(t, x)$, which is clearly negatively divergent at the shock position. Similar non-convex IR potentials are also found in generic models with Yukawa-type interactions in their respective $N \rightarrow \infty$ limit, *e.g.*, the bosonized Gross-Neveu (bGN) model in Part II or quark-/nucleon-meson models. Even though it seems as if the $N \rightarrow \infty$ limit violates a fundamental property of (thermodynamic) IR potentials, this is usually not considered as a fundamental problem in QFT literature and observables, which are calculated from these potentials, are compared to experiment without hesitation.

Thus, let us demonstrate what already happens to the phenomenology of our simple toy model as soon as N is considered to be finite but of arbitrary order.

Numerical setup for RG flows at finite N As soon as we study RG flows at finite N we have to use again the RG-flow equation (5.32), which involves the diffusive contribution of the σ -mode. We still use the KT scheme in the implementation of Section 5.2 as well as the same parameter sets as before. The only difference is that we have to increase the size of the computational domain. Choosing $x_{\max} = 10$ guarantees that the diffusion does not reach the domain boundary and boundary effects are not present in the results. In addition, it is no longer required to have an extremely high resolution, *e.g.*, to resolve a shock wave in great detail, because the diffusion smears out the cusps anyhow. Thus, $n = 1000$ cells are perfectly fine for our purpose and still present a high-resolution setup.

A (non-)trivial tautology: large $N \neq$ infinite N As examples for RG flows with the same initial conditions including diffusion at finite N , we choose $N = 2$ and $N = 32$ and present the results for $a = 0$, $a = a_c$, and $a = 2a_c$ in Figs. 6.16b and 6.16c. From Fig. 6.16b for $N = 2$ the significant effect of the diffusive σ -mode is clearly visible. The shock and rarefaction waves are completely smeared out and a difference of the shapes of $v(t, x)$ for the different values of a is absent by plain visual judgment. The first-order PT at a_c completely disappeared and $\Gamma^{(2)}$ continuously changes with a . This has already been discussed in Section 3.3.5, but was by no means associated with the presence of a diffusive contribution in the RG flow in field space. In addition, we clearly find that $\partial_x v(t \rightarrow \infty, x) > 0$ for all a at all positions x , such that convexity of the IR potential $V(t, x)$ is guaranteed. Also restoration of smoothness in the IR is rather obvious from the plots.

Nevertheless, what happens if N is significantly increased? To gain a first insight, we plot the same RG flows for identical a but $N = 32$ in Fig. 6.16c. Again, we immediately see the drastic effect of the σ -mode: The discontinuity of the shock wave vanishes completely and only a remnant, a moving, significantly smeared cusp, is visible in the flow of $v(t, x)$. At the end of the RG flow we again find smoothness and convexity of the potential and an absence of the first-order phase transition.

We repeated this calculation also for higher values of N but could not identify any qualitative changes of the results. It is simply the minimal diffusion which enters the RG flow equation via the presence of the σ -mode that “totally changes the game”. Hence, common arguments that theories with rather small N can be approximated rather well by the $N \rightarrow \infty$ limit (the zeroth order of a $\frac{1}{N}$ -expansion) are certainly only valid for some observables, but generally wrong. Especially, if one is interested in studying PTs one should be extremely conservative in drawing conclusions from strict approximations like sending $N \rightarrow \infty$.

Another interesting aspect of these results is the following: In a lot of model calculations (ignoring explicit symmetry breaking) symmetries are realized linearly, *e.g.*, the linear sigma model, the quark-meson-(diquark)-model *etc.*. Still, it is oftentimes assumed that the IR regime of RG flows is completely dominated by the massless Goldstone modes and that “massive” radial σ -modes do not contribute to the dynamics below certain energies/momenta. Usually this assumption is transferred from frameworks like chiral perturbation theory, which is ultimately an IR theory of only the lightest modes. However, our calculations clearly demonstrate that this assumption is definitely not correct and that the contribution of the σ -mode even in the deep IR is of utmost importance (independent of the number of Goldstone modes). Interestingly, taking chiral perturbation theory seriously, one should come to exactly the same conclusion: Integrating out the σ -mode reduces the field space to a curved manifold, where the residual symmetry for the Goldstone modes is non-linearly realized. Thus, even though one is left with an IR theory of massless Goldstone modes, the effect of the massive σ -field is always present in the IR vertices via the geometric restrictions of the vacuum manifold.

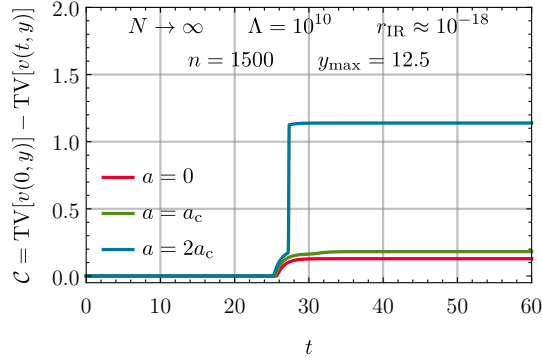


Figure 6.17: The RG flow of the (numerical) entropy/TV (5.35) corresponding to the RG flows of Fig. 6.16a. From Ref. [3, Fig. 11].

6.8.4. More entropy(!)

Before we close the discussion of our results and summarize, let us briefly return to the $N \rightarrow \infty$ results of this section. At several occasions we mentioned that entropy production is not exclusive to diffusion, but is also present in purely advective systems as soon as non-analytic structures like shock or rarefaction waves form or interact. Furthermore, we briefly discussed in Section 5.1.6 that in the y -formulation of the RG flow equation (5.31) it is natural to associate the difference of the arc length/TV of $v(t, y)$ in the UV and some later RG time with a (numerical) entropy of the PDE. The obvious question is, whether Eq. (5.35) really behaves like an entropy function for the RG flows of Fig. 6.16a.

There are various options to check this. For example, one could formulate Eq. (5.35) in x instead of y via a variable transformation and then calculate the integral from the cell averages in the x -formulation.

However, we combined the calculation of the entropy function with additional tests of a first-order reduction of another numerical FV scheme, which, because of the manifestly negative advection velocities $\partial_v F[t, v]$ in the absence of diffusion, can also be implemented for the y -formulation of the flow equation, because it does not require a ghost cell at negative y . For details of these tests, we refer to Ref. [3, Appendix E]. Here, we exclusively present the numerical results for the entropy function (5.35) of the $N \rightarrow \infty$ flows of the initial condition (6.20) for $a = 0$, $a = a_c$, and $a = 2a_c$ in Fig. 6.17.

Exactly as expected from our discussion, we observe for all choices of a that, in the beginning of the RG flow, there is no entropy production at all. The shock and rarefaction wave are not formed during the flow but imprinted in the initial condition, such that there is no loss of information and exclusively bulk motion. As soon as the rarefaction wave catches up with the shock wave, there is non-linear, irreversible, dissipative dynamics. This is clearly visible in Fig. 6.17 from the rising entropy for all choices of a . However, going deeper into the IR, the differences between the three setups are clearly visible. For $a = 0$ the interaction of the rarefaction and shock wave simply causes the freezing of the shock wave, such that also the entropy growth comes to halt. However, when the shocks from negative and positive x collide at $x = 0$ for $a \geq a_c$, we observe another generation of entropy. For $a = a_c$ this rise is minimal but visible, while for $a = 2a_c$ the entropy almost jumps. The latter is rather natural for the collision and complete annihilation of two fast-moving shock waves.

This discussion certainly supports our earlier assertions that there are strong indications for a direct connection of numerical entropy in the PDE, the TVD/TVNI property, and the \mathcal{C} -/ \mathcal{A} -theorem in QFT, which calls for additional research.

6.9. Conclusion and outlook

Let us wrap up the discussion of this Section and Part I of this thesis and present some possible applications, generalizations, and an outlook on prospective projects.

6.9.1. Conclusion

Let us begin with a brief summary of the discussion of Part I.

Summary

We started off in Chapter 1 with a general introduction and motivation for the need of alternative methods to the brute-force calculation of functional integrals and expectation values in statistical physics and QFT. It was discussed that all these methods require explicit benchmark tests in challenging setups, before an application to real-world problems is trustworthy. Furthermore, it was noted that for certain methods, especially some truncation schemes of the FRG, there is significant space for improvement concerning the theoretical formulation of the problem, the numerical setup, and the testing. We mentioned already in the introduction that novel developments concerning the improvement of the numerical approach to some FRG flow equations via concepts from CFD are ongoing. Therefore, we also suggested the framework of zero-dimensional QFTs to continue this work and qualitatively and quantitatively test this novel approach.

In Chapter 2 we provided a detailed introduction into zero-dimensional QFT – in particular the zero-dimensional version of the $O(N)$ model. Hereby, we focused on formal aspects, like the formulation of generating functionals for several types of correlation and vertex functions as well as formulae for their explicit calculation for the generation of exact reference values. This chapter sets the formal playground for Part I. We closed the chapter with a discussion of special aspects of QFT in zero dimensions, *e.g.*, the absence of spontaneous symmetry breaking or the smoothness of generating function(al)s.

In Chapter 3 we demonstrated how zero-dimensional QFT can be used to show that only strictly non-perturbative methods are sufficiently powerful to present true alternatives to the brute-force statistical integration of correlation functions. Furthermore, the chapter was used to become familiar with the application of zero-dimensional QFT for method testing. In particular we presented shortcomings of perturbation theory and limitations of the $\frac{1}{N}$ -expansion.

Afterwards, in Chapter 4, we completely turned to the FRG method and introduced it within our zero-dimensional framework. In a step by step procedure we derived and discussed the corresponding FRG flow equations for the different generating functionals in great detail. We demonstrated, that these form closed PDEs in zero dimensions, but still keep the overall structure of truncated systems of flow equations from higher-dimensional models. This promotes these PDEs to ideal testing grounds for (numerical) solution methods. In addition, we discussed a common approximation scheme – the FRG vertex/Taylor expansion – and its zero-dimensional version, which presents an artificial truncation of the otherwise exact PDE of the effective potential.

Chapter 5 contains a main share of our own findings. Here, we present the extension of the fluid-dynamical approach to certain FRG flow equations that was initiated by Ref. [77]. We showed, how the RG flow equation of the local bosonic potential is turned into an advection-diffusion equation – a conservation law – with all its consequences. The single advective and diffusive contributions to the RG flow are discussed in detail. Furthermore, direct consequences of this reformulation, such as the emergence of non-analyticities, like shock waves, irreversibility, entropy production, *etc.* are addressed. A significant part of this chapter also deals with the consequences for the solution of the corresponding PDE. Different limits of the flow equation are discussed and the analytic method of characteristics as well as the Rankine-Hugoniot condition are introduced.

Additionally, we present (numerical) entropy functions for the RG flow. The second half of the chapter completely focuses on the numerical solution of the PDE, and a particular FV method, the KT central scheme [258], is introduced and adopted to the FRG problem involving appropriate discretization of boundary conditions.

Finally, in Chapter 6 we demonstrated in great detail the power of the fluid-dynamical approach to the FRG flow equation of the effective potential. We qualitatively discussed the individual contributions to the flow and presented quantitative benchmark tests, which showed the superiority of this numerical approach over other commonly used methods. Tests and applications of the fluid-dynamic methods were discussed in different limits of the flow equation. This comprises explicit results for our entropy functions, but also the comparison of analytical and numerical results for shock and rarefaction waves in $N \rightarrow \infty$ RG flows, which showed perfect agreement. Lastly, we returned to the shortcomings of the $\frac{1}{N}$ -expansion and the $N \rightarrow \infty$ limit and their impacts on predictions for PTs from the fluid-dynamical and FRG perspective.

Take-away messages

Even though this work was built entirely on a rather simplistic playground – the zero-dimensional $O(N)$ model – we strongly believe that there are some important outcomes of this work. Here, we shall briefly recapitulate some of these.

First, our work clearly demonstrates that, if used correctly and beyond the minimal example of ϕ^4 -theory with positive mass term, zero-dimensional QFT can serve as a serious testing ground for methods in statistics and QFT. In addition, we hope that those readers who were not confronted with this framework so far might be convinced that it is also of great pedagogical use for the introduction of methods and technical problems in QFT, without having to bother with all kinds of additional challenges which are unrelated to the methods themselves.

Concerning the FRG method, we hope that – despite all the critical remarks – our work is not understood as a criticism of the FRG method itself. Exactly the opposite is the case: We hope that our presentation of the FRG might have convinced some skeptics that the FRG is a truly exact alternative to the brute-force calculation of expectation values and a real circumvention of the path-integral formalism. We clearly demonstrated that it is even quantitatively competitive, as long as the corresponding PDEs are not artificially truncated or truncations are chosen carefully. However, we also learned and clearly showed that the FRG framework is much more than simply deriving the corresponding flow equations and solving them somehow. The correct (re)formulation and analysis – here as a fluid-dynamical conservation law – is of utmost importance to draw the correct conclusions for the interpretation of the dynamics and – most importantly – for choosing the correct numerical approach. We believe that our results should be understood as a clear warning that for applications in higher-dimensional setups, where truncations are unavoidable, great care has to be taken to choose a decent approximation, but on the other hand to also use a powerful and tested numerical scheme to solve this truncated system.

Furthermore, we think that our work contributes to a general better understanding of the concept of renormalization and integrating out interactions. Here, we are especially thinking of the concepts of entropy production and irreversibility and their realization in terms of dissipative dynamics in field space, which we could demonstrate via the fluid-dynamical formulation. These findings and partial rediscoveries could be of relevance for future research on \mathcal{C}/\mathcal{A} -theorems.

Finally, we would like to mention our insights on the difference between large and infinite N and problems of expansions in inverse numbers of degrees of freedom of the system. For sure, a particularly interesting result is the strong effect of the $N \rightarrow \infty$ limit on PTs, which is realized in terms of highly non-linear dynamics in field space in fluid-dynamical RG flows.

6.9.2. Generalizations and applications

Next, let us turn to some possible generalizations and applications.

Generalizations

Despite the fact that a strict distinction between generalization and application is not possible, let us try to start with some direct generalizations.

Multi-dimensional field space First of all, we could expand our technical developments and tests and stay in zero spacetime dimensions.

Here, a possible generalization would be to extend our discussion to problems where the background-field configuration and therefore the spatial domain of the corresponding PDE for the effective potential is no longer one-dimensional. This could be realized by simply not using the $O(N)$ symmetry of our model and keeping the background-field space N -dimensional. Otherwise it is also possible to construct simple models with different symmetry groups and multiple invariants.

The most simple generalization is for sure to use the $O(2)$ model and keep field space two-dimensional, *i.e.*, $\vec{\varphi} = (\varphi_1, \varphi_2)$. In the fluid-dynamical formulation this results in two fluid fields, which correspond to the derivatives of the potential along the two field-space directions,

$$u(t, \varphi_1, \varphi_2) = \partial_{\varphi_1} U(t, \varphi_1, \varphi_2), \quad v(t, \varphi_1, \varphi_2) = \partial_{\varphi_2} U(t, \varphi_1, \varphi_2), \quad (6.33)$$

which evolve in the two-dimensional spatial domain spanned by φ_1 and φ_2 . In total, one obtains a coupled set of two non-linear diffusion equations for u and v , which can for example be solved with a two-dimensional generalization of the KT scheme.

Such a setup can again be used to explicitly benchmark the numerical setup and formulate requirements for trustworthy numerical implementations of general FRG problems, which call for more than one field-space dimension. Work on this generalization is almost completed.

Fermions and field-dependent couplings Another generalization in zero spacetime dimensions is the introduction of fermion-like degrees of freedom. This is realized via the introduction of Grassmann numbers and additional interaction terms with bosonic fields [124]. On the level of the partition function correlation and vertex functions can still be calculated exactly. Here, Grassmann fields are first integrated out and afterwards one is again confronted with ordinary integrals over boson fields, such that exact reference solutions are accessible.

In the FRG formulation the flow equations still form a finite and closed set of coupled PDEs for the effective potential and some field-dependent fermion-boson couplings. This system, however, is highly non-linear and constitutes a numerically challenging problem. We already formulated such systems and also derived appropriate flow equations. Some results are presented in the PhD thesis of M. Steil [6]. However, their explicit formulation in terms of conservation laws without assuming any truncations is missing. The same applies to their full numerical solution.

The reason why such systems are of great interest are:

1. We might learn from these minimal examples how to formulate generic FRG flow equations of fermion-boson systems as advection-diffusion-source/sink equations in conservative form to apply ready-made modern methods from CFD. This could help to further improve the developments started by Ref. [101].
2. Again, we can use these minimal models to test certain truncation schemes. For example, one could study the quality of the results, if Yukawa-type interactions are assumed to be field-independent or expanded in a Taylor series, like we did for the FRG vertex/Taylor expansion of the effective potential in Section 6.6.

Also here, work is in progress [259] and first quantitative results are expected soon.

Periodic field space The framework of this chapter could also be generalized to models which are periodic in field space. This is of great interest for sine-Gordon-type systems or Polyakov-loop models in QCD in higher dimensions [260, 261, 262, 263]. In zero spacetime dimensions, however, testing of the fluid-dynamical framework and numerical methods is much easier and it is surely possible to construct zero-dimensional analogues of higher-dimensional models with non-trivial topology in field space, which are also describable by exact (untruncated) flow equations and exact reference solutions.

Complex actions Especially, if one thinks about the severe problems which are caused by complex-valued probability distributions in higher-dimensional systems, *e.g.*, due to chemical potentials, a direct generalization of our findings is their application to actions which comprise complex couplings, parameters, and/or field space. A first step into this direction was already taken by Ref. [102] but there is definitely room for further testing with zero-dimensional toy models like those of Refs. [133, 264].

2-PI formalism It would be interesting to study whether the fluid-dynamical reformulation of certain flow equations can be generalized to the two- or n -PI formalism for FRG [265]. Here, a great starting point are Refs. [136, 137, 138], which present and test the formalism in zero spacetime dimensions. The obvious question therefore is whether their flow equations are also malleable into advection-diffusion equations.

Other flow equations Already several times within this work we mentioned that there are flow equations from the “pre-Wetterich era”, like Polchinski’s or related equations [171, 94, 96, 97, 98, 99], which – even though not being exact – can also be formulated in terms of conservation laws and were discussed in terms of diffusion equations (at least in the LPA). It would be interesting to derive exactly these PDEs for zero-dimensional models and to study these equations in the same fluid-dynamical setup which was used for the Wetterich equation in this work. Furthermore, their zero-dimensional formulation would probably allow for an easier comparison and mapping between these flow equations. A starting point could be Ref. [266].

6.9.3. Applications

Anyhow, the original goal of this PhD project was not to study zero-dimensional FRG and to push some numerical methods in this setup to their limits. Of course, we were originally and are still interested in simply using the FRG as a non-perturbative tool to study the effects of bosonic fluctuations in low-energy effective models for QCD at non-zero temperature and chemical potential. After clearing up the numerical approach to the corresponding flow equations, we are now in a position to systematically and without great reservations address the PDE of the effective potential in generic fermion-boson systems.

Higher-dimensional $O(N)$ models in the LPA and beyond Of course the first direct application (and in some sense also generalization) is to apply our fluid-dynamical framework to higher-dimensional $O(N)$ models in the LPA. In parts, this was already done by Ref. [77] with the three-dimensional $O(N)$ model in the infinite- N limit. However, it would be interesting to study $O(N)$ models at finite N . Of course, then the LPA constitutes a truncation of the infinite set of PDEs. Nevertheless, it would be interesting to repeat certain $O(N)$ model studies, like Refs. [256, 267, 268, 269, 270, 271, 272], in this truncation with state-of-the-art numerical schemes and compare the results to earlier findings or to extend the truncation by first including a field-independent wave-function renormalization or even higher-derivative couplings. Also trying to formulate a flow equation in conservative form for a field dependent wave-function renormalization would be of great interest.

All these studies could additionally be performed in a finite or infinite physical volume and at zero or non-zero temperature. Hence, the framework could even be used to reanalyze earlier works

on critical exponents or to compare FRG to lattice Monte-Carlo simulations to obtain higher-dimensional benchmark tests.

Fermion-boson systems in LPA Of course another direct application of our findings is to use the fluid-dynamical framework and the numerical methods from CFD to investigate fermion-boson systems with Yukawa interactions. Models of these types are the quark-meson model (QMM) [273, 59, 66, 274, 70, 275, 276], the quark-meson-diquark model (QMDM) [71, 88, 277, 278] or meson-nucleon models [279, 280, 72, 281], and their variants and extensions. Similar models are also found in lower spacetime dimensions, where they are mostly used for applications from solid-state theory, see Part II. In any case, the LPA of all these models at (non-)zero temperature and density has always rather similar structure and can be recast into a system of PDEs for derivatives of the effective local bosonic potential w.r.t. some condensate directions. The contributions from the fluctuating boson fields can be classified as advective or diffusive contributions, while fermions show up as source/sink terms.

In advanced truncations this changes slightly. For example in Ref. [101], the field dependence of a Yukawa coupling was taken into account. This amounts to an additional fluid field (in the fluid-dynamical formulation) which evolves in field space (the spatial domain).

A particular example of an application to a fermion-boson system is presented in Part II of this thesis, where we study the effect of bosonic fluctuations in the GN model at non-zero temperature and (non-)zero chemical potential.

Phase transitions, shocks, condensation phenomena and all that Independently of the particular model under consideration, we are now well equipped to study all kinds of non-analytic structures which can show up in field space in effective bosonic potentials. Furthermore, we now know how to address such structures in other field-dependent quantities [101]. In particular this means that our methods in general enable us to study the deep IR region of RG flows, where potentials need to turn convex, but might show non-analytic points, if the ground state of the system is non-trivial. If, despite the new discretization schemes, one is still not able to robustly integrate to the deep IR, we do have the tools to systematically analyze the underlying reason and eventually trace instabilities back to other issues, such as insufficient truncations.

Moreover, we can systematically address problems which are caused by “external shocks”, such as chemical potentials, which suddenly enter the RG flows in terms of cusps in the derivative of effective bosonic potentials. In general, the CFD schemes are able to handle such structures, such that problems or unphysical behavior of a system, *e.g.*, thermodynamic instabilities, may be systematically traced back to other reasons, such as bad choices of truncations or bad choices of regulator shape functions.

In any case, fluid dynamics simply provides a framework which allows to address previously asked questions concerning the quality and predictability of FRG model calculations more systematically. Finally, it is also possible to include this framework for the effective potential in much more comprehensive FRG setups, which for example start off in the gluonic sector of QCD and dynamically switch over to an effective theory of hadrons.

Part II

The Gross-Neveu and the Gross-Neveu-Yukawa model

Chapter 7

Introduction

Abstract We start by presenting the main motivation and research questions that triggered this work. Phenomenologically these are all related to the dynamics and mechanisms of symmetry breaking and restoration in strongly interacting QFTs at zero and non-zero temperatures and densities. On a mathematical and technical level, the research questions focus on the necessities of an adequate formal and numerical description of these phenomena as well as the strong impact of assumptions and approximation schemes on the results.

Afterwards we give an overview about the GN model, which is used as a playground to address our research issues. Hereby, we first contextualize the model with other QFTs from high-energy particle physics and solid state theory. Thereby, its prominent role as a prototype model for various physical phenomena and its recurrence as the limiting scenario of several theories and models in QFT is emphasized.

Furthermore, we recapitulate the well-known phenomenology of the GN model (in the infinite- N approximation) and summarize the arguments and predictions for its phenomenology beyond this approximation.

Disclosure This introduction partially follows the introductions of Refs. [4, 5]. Both publications – text and results – are produced by my coauthors and myself in almost equal shares. This also holds true for the introductions to these works.

In the introduction to the publications as well as this thesis the aim was to provide a rather comprehensive overview of the milestones and seminal publications in the context of the GN model. Nevertheless, the sheer number of publications (at present almost 2000 listed on INSPIRE HEP) solely directly referring to the original publication by D. J. Gross and A. Neveu somehow limits this aspiration. Especially the discussion of literature that deals with the spectrum and the famous result for the S -matrix, *e.g.*, Refs. [282, 283, 284, 285, 286], as well as generalizations of the GN model fall victim to these restrictions.

Also in the motivational parts and especially in the overview on QCD in medium and the comments on four-fermion theories, we can only provide a small selection of references, which underpins our arguments or serves as an example. The research field is by far too large to provide a comprehensive picture and a choice of references that is completely unbiased by the technical methods of own preference and the own affiliation.

7.1. The motivation, the scope, and the research questions

The motivation for this work is indeed many-faceted and it is worth starting with a few paragraphs on the original goal of my PhD project and research area. This may help understanding why my colleagues and I put so much effort in the better understanding of a model and its phenomenology (the GN model), which seemed to be understood and has – at first sight – little to do with real-world high-energy particle physics, which is our main profession. Besides that it serves as a

brief report on my route through my PhD project and is therefore of slightly different style and intonation than the remaining parts of this thesis.

Readers who are not interested in this “report” are encouraged to skip the next two subsections, and continue reading the listed summary of the main research questions that are covered by Part II this thesis in Section 7.1.3.

7.1.1. The original project – spatially inhomogeneous condensation in QCD at non-zero temperature and non-zero baryon chemical potential

Originally, the objective of my PhD project was to contribute to a better understanding of QCD at moderate non-zero temperature T and non-zero baryon chemical potential μ_b , which is maybe the most challenging region of the QCD phase diagram. This is because lattice Monte-Carlo simulations, which are the number-one tool to directly study QCD at $\mu_b \simeq 0$ and arbitrary T , suffer at $\mu_b \neq 0$ from the QCD sign problem. Simply speaking, complex-valued probability distributions in the partition function impede conventional and advanced statistical simulation techniques, see, *e.g.*, Refs. [287, 288, 289, 16, 290, 291] for details. As we will see, my PhD project indeed contributed to a better understanding of QFTs in medium, but differently than intended in the beginning.

The phase diagram of QCD However, from QCD calculations at very large chemical potential as well as innumerable model studies for QCD it is expected that the low-temperature but non-zero-density region of the QCD phase diagram has a rather rich structure and phenomenology, *cf.* Refs. [292, 293, 294, 295, 296]. It is argued that by increasing the chemical potential, the phase structure will change via several PTs or crossovers, starting off with a gas of hadrons, which consists of equal shares of matter and anti-matter. At $\mu_b \simeq 1$ GeV there is a transition to a nuclear liquid phase, which is dominated by a liquid of mesons, glueballs, and predominantly baryons, which forms ordinary nuclear matter. This feature is rather robust from an experimental and theoretical perspective, see for example Refs. [297, 298, 281] and references therein. Already the question “what comes after the nuclear-liquid phase on the journey towards larger matter-anti-matter asymmetry” is subject of ongoing debate and research. At least most particle physicists agree that the precise phase structure is not known yet and state-of-the-art phenomenological predictions strongly depend on the specific models, their particle content, and the approximations. An aspect which is very well established from a theoretical perspective is the existence of some PT, where chiral symmetry, which is (spatially homogeneously) broken at small chemical potential by the chiral condensate, which in turn gives rise to some fraction of the hadron masses, but most importantly to the mass splitting of hadrons, gets restored for large μ_b .

A scenario in the low- T region which is compatible with a chiral PT is that there is a PT/crossover from the nuclear-liquid phase to a so-called quarkyonic phase, where hadrons, especially pions, are still the dominant degrees of freedom, but densities are so high that nucleons overlap and quarks become “quasi free” and relevant degrees of freedom [299, 300, 301]. It is argued that the chiral PT, where quarks become massless and hadron masses of the same flavor multiplets degenerate, lies somewhere inside the quarkyonic matter region. The confinement-deconfinement PT is generally not expected to follow the chiral PT at large μ_b . Recent studies, *i.e.*, Ref. [302] and references therein, show that – contrary to what was believed for many years – it seems that also at small μ_b and under the assumption of vanishing bare quark masses the chiral PT and the confinement-deconfinement PT do not coincide (not even approximately). It is likely that the confined phase completely engulfs the phase of broken chiral symmetry but also comprises large regions where chiral symmetry is already restored. If and where the confinement-deconfinement PT touches the $T = 0$ axis or if it simply absconds approximately parallel to the μ_b axis at large μ_b is also not settled yet.

For large chemical potential and small temperatures, implying large matter-anti-matter asymmetry, it is also predicted that there is a phase where quark-quark pairing is energetically favored over

quark-anti-quark pairing and the conventional mesons are ousted by all kinds of diquark states. In analogy to superconductivity in condensed-matter systems, so-called color-superconductivity and diquark condensation is studied intensively, see, *e.g.*, Refs. [293, 295, 278, 166, 303, 304].

Spatially inhomogeneous phases Also provoked by calculations from solid-state theory¹ and supported by various (model) studies in rather rough approximation schemes in high-energy physics, it is also speculated about phases of so-called spatially inhomogeneous condensation, where chiral, diquark *etc.* condensation is no longer expected to be homogeneous in space, but comes with some spatially oscillating crystalline-like structures, see Ref. [313] for a review. First works trace back to Ref. [314] in the context of nuclear matter for inhomogeneous pion condensation and Refs. [315, 316, 317] for models of quark matter. From model calculations and calculations in low-dimensional relativistic QFTs it is found that such phases, if they exist, are predominantly located in the region where, when inhomogeneous condensation was excluded in the calculations, the chiral PT is originally located [318]. Hence, they are expected to be variants of the quarkyonic phase at low T and moderate μ_b .

Usually inhomogeneous condensates somehow interpolate between regions in the μ_b - T -plane with spatially homogeneous condensation and the corresponding symmetric phase: Their shape changes with μ_b , *e.g.*, kink-like profiles, which can be seen as domain walls between regions of spatially homogeneous condensation of opposite sign (similar to magnetic domains), change towards rapidly oscillating profiles with rather short wavelength and decreasing amplitudes. The typical crystal momentum is proportional to μ_b , which sets the dominant energy scale at low T , while the amplitude usually decreases towards the symmetric phase. This is only one possible scenario for inhomogeneous condensation. Other options for example comprise so-called chiral spirals, where the direction of condensation in field space rotates, *i.e.*, the Goldstone modes are not the same everywhere in space, or combinations thereof, see Refs. [319, 320].

Also competing or overlapping phases of various (inhomogeneous) phases are possible.

All of these scenarios for the phase structure of QCD at low temperatures are of great relevance for the structure and properties of the matter in our universe and especially the composition of compact stellar objects, like neutron stars. Here, however, also other “external” energy scales, like isospin chemical potential or strong magnetic fields play a crucial role [321, 322], which introduce additional axes in the QCD phase diagram and allow for more complicated (spatially inhomogeneous) phases, which is nevertheless not discussed in this thesis. See Refs. [61, 62, 281, 323] for recent works using functional methods.

My original PhD project Anyhow, as already anticipated, most of the above predictions for the QCD phase diagram for large μ_b strongly rely on model calculations in rather rough approximation schemes, like the mean-field approximation, large- N_f or large- N_c expansions, perturbative arguments or plain four-fermion formulations. Simply speaking, most of the calculations artificially suppress thermal and quantum fluctuations (the back reaction and self interaction) of mesons or diquarks and exclusively incorporate the fluctuations of the fermions (or in the high- μ_b region perturbative corrections from the gluons). The reason for these approximations is mostly without stating this too explicitly in the literature, the manageability of the calculations, which get rather involved already in simple approximations, especially when studying position-dependent condensates. This is absolutely reasonable, however, from a phenomenological perspective, the light mesons are expected to be the dominant driving forces of the dynamics of low-energy QCD and usually work against condensation phenomena. Real-world physics might therefore strongly deviate from these model predictions.

¹The first predictions of such structures in condensed-matter physics go back to P. Fulde, R. A. Ferrel, A. Larkin, and Y. Ovchinnikov in the context of superconducting materials at large magnetic fields [305, 306]. See also Ref. [307] for a review or Refs. [308, 309, 310, 311, 312] as typical applications.

Therefore, the main goal of the PhD project was to study the influence of bosonic fluctuations on possible inhomogeneous chiral condensation in the QCD phase diagram at low T and moderate μ_b by applying non-perturbative functional methods in advanced truncations to effective low-energy models for QCD.

To fall back on well-established effective low-energy models for QCD, like the QMM and its extensions, has several advantages. First, it is widely expected that this circumvents the QCD sign problem and allows for direct calculations at low T and moderate μ_b . Additionally, these models are extensively studied without and with the inclusion of bosonic fluctuations (under the assumption of spatially homogeneous condensation). Furthermore, a lot of these models allow for spatially inhomogeneous condensation if bosonic fluctuations are ignored. Hence, benchmark and limiting results are available as good starting points. Second, the application of non-perturbative functional methods, more specifically the FRG, allows for a rather natural and self-consistent treatment of fermionic and bosonic thermal and quantum fluctuations in infinite volumes and the continuum. It was already applied to all kinds of low-energy models for QCD in the past, but never w.r.t. the search and stability of spatially inhomogeneous condensation².

One of the drawbacks of this approach is of course that the gluon dynamics is completely omitted in the calculations. Another one traces back to the structure of the FRG: In the FRG framework it is extremely challenging to work with so-called ansatz functions for the possible spatial dependence of inhomogeneous condensates, which is oftentimes the starting point of many mean-field calculations. The first point is an unavoidable shortcoming of model calculations and has to be accepted³. The second issue can be bypassed by not studying inhomogeneous condensates directly from ansatz functions for the spatial modulation or a direct prediction of their shape, but by analyzing the stability of the symmetric phase w.r.t. momentum-dependent perturbations. This can be done via a so-called stability analysis of the bosonic two-point functions, which ultimately provides possible PT lines in the μ_b - T -plane to phases of spatially inhomogeneous condensation. Additionally, as a by-product, one obtains estimates for the dominating wave vector of the spatial modulation of the condensate and thereby gets some estimates for the shape. This technique or variants thereof were applied several times before within mean-field approximations and seemed to deliver decent results, see, *e.g.*, Refs. [327, 328, 329, 330, 331, 332, 333, 334] for applications in advance of this project and Ref. [5] for an overview.

In summary, the program was rather clear and settled. However, shortly after the start several pitfalls appeared, which led to the drastic change in the scope and goals of our⁴ research.

7.1.2. The troubles and redefinition of research objectives

In the following, we sketch several issues which popped up while working through this program, as well as the resulting new research questions, which had to be settled before returning to the main program.

Unreliable numerical schemes for FRG flow equations in the existing literature As already mentioned, our approach to the detection of inhomogeneous phases is grounded on a stability analysis of spatially homogeneous condensation, respectively the symmetric phase, by analyzing the momentum structure of the bosonic two-point function. Therefore the basis of this machinery has to be a trouble-free and reliable determination of the “common” phase structure of a model under the assumption of homogeneous chiral condensation. In widely used simple truncations⁵ of the FRG this is done by solving the corresponding RG flow equations for the

²First attempts can be found in parallel works [274, 324].

³One way to include at least some aspects of the gluon dynamics in effective models is to build in the Polyakov-loop potential, which models some aspects of the confinement-deconfinement PT, *cf.* Refs. [325, 326, 318].

⁴By “our” and “we” I am predominantly referring to the close cooperation with M. J. Steil, but also other direct collaborators.

⁵More advanced truncations usually build on this truncation, such that they inherit the issues discussed here.

bosonic potential numerically for each point in the μ_b - T -plane and by extracting the position of its minimum (the condensate) from the solution at the end of the RG flow. Mathematically this flow equation is a highly non-linear (integro-)partial differential equation, which is of first order in the RG time and (in the LPA) up to second order in space.

Because this first part of the project seemed to be fully understood and under control, we completely relied on existing literature and used the common numerical implementations from the community of “FRG practitioners” (which I would also call myself!).

However, when we tried to reproduce existing results we repeatedly failed miserably. The information appears often to be incomplete in the FRG literature.

In a lot of publications crucial information about the exact implementation, *e.g.*, the handling of boundary conditions, the number of spatial discretization points, the termination time of the integrator *etc.* was simply missing and reproducibility was not guaranteed. In other works the numerical solution of the flow equations was simply not stable against slight variations of numerical parameters, like the number of grid points or the order of interpolating polynomials, the choice of coordinates *etc.*

To make a long story short: At a certain point it turned out that a huge amount of the applied numerical schemes (local Taylor expansions, naive finite-difference discretizations, global Chebyshev approximations, global spline interpolations, self-constructed schemes *etc.*) were after all based on the fundamental assumption that the solution of the PDE (the local potential) is smooth in its spatial direction (field space). This, however, is not necessarily the case for the effective bosonic local potential, especially in regions of symmetry breaking or in presence of chemical potentials. In fact the effective potential is non-analytic in the IR or at intermediate RG times for most points in the μ_b - T -plane.

The drastic consequence is that a discretization scheme which calls for analyticity or at least smoothness of the solution is no longer guaranteed to converge against the correct solution of the PDE, if the exact solution does not fulfill these requirements⁶. In retrospect this also explains the lack of convergence while refining the spatial resolution *etc.*

Independent and almost parallel to the observations by M. J. Steil and myself our colleagues E. Grossi and N. Wink experienced basically the same issues. However, slightly earlier than we they came up with a much deeper explanation and solution of these phenomena, which comes in terms of a complete reformulation and reinterpretation of the RG flow equations: It is possible to reshape the flow equation for the potential in terms of a conservation law – an advection-diffusion-source equation, which can be seen as a common fluid -dynamical problem with all its consequences, such as non-analytical behavior, *e.g.*, in terms of shock waves. Such phenomena are well understood in fluid dynamics and adequately handled by modern numerical schemes from the field of CFD. Interestingly, it turns out that parts of these discoveries are actually rediscoveries and can be found for example in literature on RG flow equations from the “pre-Wetterich era”. Here, we refer to Part I and Refs. [77, 101, 1, 2, 3, 4] for all the details on these developments.

Hence, before studying effective models for QCD, we decided to work out the consequences of these findings and transfer the techniques from CFD to FRG problems by using reliable, well-known test cases. Besides the extensive studies in the context of exactly solvable zero-dimensional QFTs in Part I of this thesis, the idea came up to study the GN model in 1 + 1 dimensions in medium for this purpose. In its bosonized version, in terms of the Gross-Neveu-Yukawa (GNY) model, it shares a lot of similarities with common low-energy effective models for QCD, but has several advantages. It is a prototype model for (chiral) symmetry breaking (and possibly also symmetry restoration, if bosonic fluctuations are included). Similarly to effective models, it describes the interaction of fermions and bosons via a Yukawa interaction. However, contrary to the effective models it constitutes a fully fledged QFT in 1 + 1 dimensions with a well-defined weakly coupled UV limit and well-known unique reference results in the infinite- N limit, such that there is no

⁶This does by no means imply that all existing results that are based on such assumptions must be wrong. However, there is also no guarantee at all that they are close to the correct weak solutions of the PDE.

artificial parameter dependence. Further arguments to turn to the GN model first are presented in the next paragraphs and sections.

Counterintuitive results in related lattice Monte-Carlo studies The $(1+1)$ -dimensional GN model takes a special role in the context of related projects on inhomogeneous chiral condensation of our collaborators. It is one of the rarely known fully integrable QFTs in the infinite- N limit. Here, its phase diagram for non-zero μ and non-zero T is completely understood and possesses regions of spatially inhomogeneous condensation. Also variants of the model, with larger symmetry groups, show inhomogeneous condensates in $1+1$ dimensions and these one-dimensional modulations of the condensates even turn out to be the energetically favored solutions in higher-dimensional QFTs.

The GN model and its variants can therefore be seen as the prototype models for spatially inhomogeneous condensation and may therefore serve as testing fields for methods in the context of inhomogeneous condensates. (For details, we also refer to the next (sub)sections.)

However, it is expected for several reasons, which are discussed in detail in Section 7.4, that condensates of any kind are not stable in a single spatial dimension at non-zero temperature, if the large- N limit is relaxed and bosonic fluctuations are taken into account – independently of the specific model. This peculiar feature does of course not generalize to dimensions $d \geq 2$ and/or $T = 0$.

In that sense it was rather surprising when colleagues from associated projects detected signals of possible spatially homogeneous as well as inhomogeneous condensation in lattice Monte-Carlo simulations of the GN model at various finite N [335, 336, 337, 338]. Similar results were also reported in the past by other authors in older studies, see below.

These counterintuitive results triggered our interest for several reasons: In terms of a benchmark model, we anyhow planned to test the FRG machinery in the infinite- N limit and at finite N including the stability analysis of the bosonic two-point function with the GN model due to the aforementioned reasons. However, when searching the literature, we found that most of the arguments against symmetry breaking beyond the infinite- N limit are of qualitative nature and reliable calculations that explicitly show symmetry restoration or breaking for all $T \neq 0$ on a quantitative level in the continuum are not known.

Hence, this opened the opportunity to tackle several interesting questions at the same time: We could test the newly introduced numerical methods for FRG flow equations from CFD within a more realistic QFT and study how symmetry breaking and restoration as well as how effects from the chemical potential and temperature are realized within the fluid-dynamical framework.

Additionally, the GN model makes it possible to study the drastic scale dependence (and separation or interplay) of the various effects (scales of symmetry breaking via fermion interactions; scales at which μ_b and T start to impinge on the dynamics in the RG flow; scales where bosonic quantum fluctuations set in *etc.*). This analysis of the same problem using a continuum and infinite-volume method like FRG and a method that relies on spacetime discretization and finite-size simulation, like lattice Monte Carlo, both including full bosonic quantum fluctuations, also allows to better understand lattice artifacts of the results, but also the effects of truncations in FRG studies. Currently there is even work in progress where the FRG studies of this and related works [7, 8, 6] and the corresponding publication [4] are generalized by artificially introducing a finite-sized box and spacetime grid for the GN model.

Insufficient tests of the stability analysis and how the infinite- N results help to understand advanced FRG truncations Another topic that led to a reshaping of the project relates to the aforementioned stability analysis of homogeneous condensation via the momentum structure of the bosonic two-point function. Although being applied already several times in the past in the context of spatially inhomogeneous condensation, we recognized that a full-featured and pedagogic benchmark study on the reliability of this method seemed to be missing. Existing studies mostly focus on the phenomenology of inhomogeneous phases, sidelining the details and limitations of the applied technique. This pertains especially to the analysis of the momentum

structure of the two-point function and wave-function renormalization in comparison with analytically known solutions for inhomogeneous condensates and an open discussion of the caveats of the entire method.

Hence, we decided that returning to the GN model also in the context of the stability analysis was worth the effort, in order to set a trustworthy basis and guidance for more involved studies. Again, possessing completely understood analytical solutions for all μ_b and T the GN model is the ideal playground for this type of analysis and review.

Interestingly, without previous planning, there was a spin-off product of these infinite- N studies of the GN model, which actually allowed for a much better understanding of advanced truncation schemes of FRG studies of this and other models: Because the RG flow in the GN model is dominated by the fermion-loop contribution in the beginning in the UV, even in calculations that involve bosonic fluctuations at finite N , the RG flow always looks like an infinite- N calculation approximately up to the symmetry-breaking scale. Hence, the full momentum structure of the bosonic two-point function and the bosonic wave-function renormalization from the infinite- N calculations can be used to estimate the requirements that need to be fulfilled by advanced truncations to capture exactly this momentum structure and adequately describe the bosonic back-reaction.

7.1.3. Research questions

In summary this thesis therefore aims to contribute to answering the following research questions, which all concern calculations for QFTs in medium.

Phenomenological questions

1. Is it possible to have PTs in a system in a single spatial dimension? In other words: Is there a different state of aggregation than a disordered gas- or liquid-like state for one-dimensional systems of elementary particles at non-zero temperature? Does this change at zero temperature?
2. The answer to the previous question seems to be partially settled by the CMWHB theorem, which forbids continuous symmetry breaking at non-zero temperature in less than two spatial dimensions. Some qualitative arguments by L. D. Landau and others (see below) seem to also rule out discrete symmetry breaking in $1 + 1$ spacetime dimension at non-zero T . Still, there are conflicting results to the latter arguments in literature. Is there a way to resolve this puzzle also by quantitative calculations?
3. What is the influence of different approximation schemes on quantitative investigations of the previous question(s)?
4. How does the phase diagram of the GN model look like beyond the infinite- N approximation?
5. What are the typical (RG) scales of symmetry breaking (restoration) and the dominance of fermion/bosonic thermal and/or quantum fluctuations?
6. Is the GNY model an appropriate approximation for the GN model? The models differ in its UV initial value for the wave-function renormalization. How large is the influence of the ex-/inclusion of a dynamical wave-function renormalization (and Yukawa coupling) on the phenomenology?

Technical questions

1. What are the necessities and limitations of a stability analysis of the spatially homogeneous ground state?

2. How is dynamical symmetry breaking and restoration (PTs) realized within the fluid-dynamical reformulation of FRG flow equations? What are the roles of the bosons, the fermions, and the chemical potential in the fluid-dynamical framework?
3. What are the numerical necessities for a trustworthy description of symmetry breaking and/or restoration on the level of a dynamic bosonic effective local potential within the FRG framework?
4. How can we systematically improve the truncations of FRG calculations? What can we actually learn from the infinite- N calculations for better truncations?

General questions

1. What can we learn from $(1 + 1)$ -dimensional calculations in strongly interacting systems for non-perturbative descriptions of higher-dimensional QFTs?
2. What are the requirements for an appropriate investigation of the (non-)existence and (in)stability of spatially inhomogeneous condensates under the influence of bosonic quantum fluctuations in relativistic QFTs, especially QCD?
3. What can we learn from simple approximations of QFTs and how can we transfer the relevant knowledge to construct stable, improved truncations, especially in the context of the FRG method?
4. How can we understand recurrently appearing imaginary contributions to the β -functions (RG flow equations) of fermionic vertex functions at non-zero μ and non-zero T and how should we handle them?

7.2. The Gross-Neveu model – an overview and contextualization

The GN model was originally introduced in 1974 by D. J. Gross and A. Neveu [158]. It is constructed as a relativistic QFT, which describes the dynamics of massless Dirac fermions, that are self-interacting via local two-to-two scatterings in one spatial dimension. The model was built as a $(1 + 1)$ -dimensional version of the $(3 + 1)$ -dimensional Nambu-Jona-Lasinio (NJL) model [339, 340], which in turn was constructed in 1960 to describe a relativistic theory of mesons and nucleons via analogies to the Bardeen-Cooper-Schrieffer theory of superconductivity [341]. (We come back to this connection of high-energy physics and non-relativistic condensed-matter physics within the next paragraphs.)

More precisely, D. J. Gross and A. Neveu proposed three versions of their model, featuring either a continuous chiral symmetry (with four-fermion interaction in the scalar and pseudoscalar channel) or a discrete chiral symmetry (exclusively in the scalar channel). In contemporary literature the version with discrete chiral symmetry is usually referred to as the GN model, while the two versions with continuous chiral symmetry are mostly denoted as $SU(N)$ Thirring model [342] and chiral Gross-Neveu (χ GN) model⁷. Furthermore, the designation “GN model” is also used for the single scalar-channel version in an arbitrary number of spacetime dimensions. Today, QFTs like the GN or NJL model can be considered as the most prominent representatives of a huge class of relativistic models of fermions in an arbitrary number of spacetime dimensions, whose dynamics is driven by four-point interactions, thus scattering processes, and which can be seen as generalizations of the most simplistic GN model. Other important and early representatives of this class of QFTs are the Soler model [344] or the Thirring model [345].

⁷For an overview of the different models see also Ref. [343]. Here the $SU(N)$ Thirring model is referred to as NJL₂ model and the χ GN model is referred to as isoNJL₂ model.

7.2.1. Four-fermion models and their applications

Models that are based on four-fermion interactions have a wide field of applications in QFT. Due to our own background, we mainly focus on high-energy physics, more specifically QCD.

High-energy particle physics In the context of relativistic particle physics theories of four-fermion interactions are predominantly used to model the strong nuclear force at a mesoscopic level, thus QCD at moderate and low energy scales in $3 + 1$ spacetime dimensions, see, *e.g.*, Refs. [293, 295, 346, 347, 348, 349, 350, 351, 352, 353, 354, 303, 355] for various approaches.

In a lot of models, the gauge-field dynamics of the gluons is oftentimes considered to be integrated out and absorbed in the four-fermion couplings. The four-fermion couplings are therefore assumed to be effective couplings, which are generated by gluon exchange between quarks in various interaction channels depending on the quantum numbers, kinematics *etc.*, *e.g.*, Refs. [346, 293, 303]. However, these effective four-fermion couplings, which then drive the quark interactions do not form a macroscopic description of QCD yet. At sufficiently low energies QCD is dominated by quark confinement and the degrees of freedom are hadrons. Hence, four-fermion models serve as effective but still microscopic description at intermediate energy scales between the weakly coupled high-energy regime of QCD, where quarks and gluons are the relevant degrees of freedom, and the strongly coupled low-energy regime of QCD, where hadrons as the effective degrees of freedom dominate the dynamics. Therefore, integrating out the dynamics of the quarks from the four-fermion interaction results in a low-energy description of QCD.

This can be done – at least to a certain extent – on the purely fermionic level or via bosonization techniques at low energies in the IR. This transition from high to low energies and the corresponding change in the relevant degrees of freedom is realized as a PT or crossover transition, which is associated to the breaking of symmetries of the microscopic theory and condensation phenomena, if external energy scales like the temperature and the chemical potentials are not too large. In the context of QCD and four-fermion models this affects mostly the $U_L(N_f) \times U_R(N_f)$ flavor symmetry of QCD, which is, apart from anomalies and explicit symmetry breaking by bare quark masses, the symmetry group of the fermionic sector of QCD at high energies. Four-fermion models are ideal tools to describe this process of dynamical symmetry breaking and restoration. One approach is to study the four-fermion couplings themselves, by analyzing their interplay and energy dependence⁸. (Possible divergences of these couplings signal resonant channels, where condensation and associated symmetry breaking is likely.)

Oftentimes one also uses (partial) bosonization techniques, where the four-fermion interactions are replaced by effective bosonic degrees of freedom. Here, the dynamical symmetry breaking and restoration is usually modeled on the level of an effective bosonic local potential, whose shape is determined by fermion and boson self-interactions as well as fermion-boson interactions and which can be directly related to thermodynamic observables.

Modern approaches to a full-fledged description of QCD, especially in the context of functional methods like DSE and FRG, combine these techniques by dynamical hadronization methods in the IR regime. On the other hand, four-fermion models are also directly coupled to full QCD calculations in the UV sector. Here, the starting point is the original QCD action, while the four-fermion interactions are dynamically generated from the quark-gluon dynamics. See Refs. [348, 350, 351, 352, 353, 354, 303] for recent works.

In fact, in any of these approaches, it turns out that the scalar and the pseudoscalar four-fermion interaction channel play an extremely dominant role in the low-energy regime of QCD. The divergence of the scalar four-fermion coupling is associated to the scalar quark-anti-quark condensate, which gives rise to some fraction of the quark masses and massless Goldstone modes⁹ – the pions,

⁸By “energy dependence”, we refer to external energy scales set by the temperature or chemical potential, but also the RG scale, which is used to smoothly integrate out the fluctuations from the UV to the IR into effective renormalized physical couplings.

⁹The pions are massive in Nature [356]. However, their mass originates from the explicit chiral symmetry breaking by the bare quark masses, which stem from the Higgs mechanism in the electroweak sector at much higher energy scales and have nothing to do with QCD.

which are the lightest stable¹⁰ states in QCD [19, 18].

In total, four-fermion models form a perfect tool for investigations of the strong interaction under extreme conditions and provide access to calculations at non-zero temperatures and non-zero quark densities – the QCD phase diagram.

Interestingly, as already mentioned above, four-fermion models, like the NJL model, were originally proposed as effective descriptions of baryons (especially nucleons) and, in their bosonized version, of meson-nucleon interactions. Even today they are still used in this manner, *cf.* Refs. [280, 72, 281, 279]. However, the association of the fermions with quarks seems to dominate modern literature.

A drawback of four-fermion models in $3+1$ dimensions is that they are neither perturbatively nor non-perturbatively renormalizable [158, 357, 346, 358]. Therefore, they lack a well-defined UV (microscopic) limit like asymptotic freedom or safety scenarios. This implies that they need to be considered as effective field theories with a defining scale, the UV cutoff, that is manifestly part of the model. This is cured if an asymptotically free/safe theory like QCD is considered as their UV limit, where the four-fermion couplings are initially not existing and only emerge dynamically. However, as stand-alone models for symmetry-breaking mechanisms they suffer from this fact.

Conceptual aspects of field theories The aspect of non-renormalizability is, however, strongly tied to $3+1$ dimensions and does not generalize to other spacetime dimensions. This was also the reason for D. J. Gross and A. Neveu to turn to $(1+1)$ -dimensional four-fermion models. In $1+1$ dimensions the GN model is perturbatively renormalizable and asymptotically free for any number N of fermions. This was studied for the four-fermion coupling up to fourth order in loop corrections in a purely fermionic or partially bosonized setup [359, 360, 361, 177, 362, 363]. Also (perturbative) corrections at (in)finite N to the effective bosonic potential [364, 365] or critical exponents [366, 367], as well as the relation between boson and fermion mass [368] have been considered. However, inspecting the corresponding β -functions at different loop order, one clearly finds that a perturbative approach to the GN model is more or less useless, if one leaves the UV regime of extremely small coupling, where perturbation theory might be justified, independent of N , *cf.* Ref. [363, Fig. 2 & 3].

At this point it is noteworthy and interesting that the $(2+1)$ -dimensional version of the GN model is perturbatively non-renormalizable. Still, it is shown that it is non-perturbatively renormalizable [369, 370, 371, 357, 372, 373], *e.g.*, via the FRG method, and can be used as a prototype model to study asymptotic safety [374, 375]. Moreover, $(2+1)$ -dimensional four-fermion theories are also interesting from a phenomenological perspective, because they are commonly used to model two-dimensional solid-state systems, *e.g.*, graphene layers, nanotubes, or fullerene (depending on the spatial topology). We briefly comment again on the $2+1$ dimensional GN model in Section 9.3, but otherwise refer to the broad spectrum of literature on this topic.

Returning to the $(1+1)$ -dimensional GN model: Another remarkable feature, which makes this model extremely interesting, is that similar to QCD with massless quarks, it is scale/conformally invariant and asymptotically free in the UV, but undergoes dimensional transmutation during the RG flow towards the IR – the emergence of a dimensionful scale in a theory which has only dimensionless couplings in its UV action [376, 19, 377]. It indeed gets strongly coupled resulting in a mass gap, which breaks dilatation invariance. Again similar to QCD, the mass gap is a manifestly non-perturbative result and was predominantly studied in the large- and infinite- N approximation [158, 378, 177].

Either way, at zero temperature it seems that the mass gap is still a robust feature of the GN model at finite N – as already proposed by D. J. Gross and A. Neveu [158]. This was studied for example at next-to-leading order in the $\frac{1}{N}$ -expansion [368, 379, 380, 381, 382], by the Gaussian

¹⁰Pions are stable w.r.t. the strong interaction. Nevertheless, they can decay via electroweak interactions [356].

approximation with the functional Schrödinger technique [383, 384, 385], an investigation of the exponential fall-off of the two-point function [386], the δ -expansion [387] (which however seems to be inconclusive for small N), working with the 2PI expansion up to second loop order [388], and various lattice simulations, see, *e.g.*, Refs. [389, 390, 391, 392, 393, 394, 395, 396]. An exact result for the vacuum mass gap in terms of the cutoff $\Lambda_{\overline{\text{MS}}}$ (in the modified minimal subtraction scheme) is provided in Ref. [397] for all N , from studying the S -matrix and free energy in comparison with loop corrections of the perturbative β -function,

$$m = \frac{1}{(4e)^{2N-2}} \frac{1}{\Gamma(1 - \frac{1}{2N-2})} \Lambda_{\overline{\text{MS}}} . \quad (7.1)$$

It turns out that the deviations from this exact result for the mass gap from next-to-leading order calculations in the $\frac{1}{N}$ -expansion or loop expansions *etc.* are ranging approximately from 20% to 50% for the smallest $N = 2$, but converge rapidly for larger N . In general bosonic fluctuation exclusively lower the fermion mass gap in comparison to the infinite- N result.

Another interesting conceptual aspect of the GN model is that it can be used to study the equivalence of four-fermion theories with Yukawa-type theories, here, the GNY model. The underlying question affects the kinetic term(s) of the boson fields, because a Hubbard-Stratonovich transformations [398, 399] exclusively transforms four-fermion interactions into Yukawa interactions of the fermion fields with auxiliary bosonic fields, such that a bosonized four-fermion model a priori lacks the bosonic kinetic term in the UV or on the level of the functional integral, see Section 8.2.1. On the other hand, Yukawa models and related non-linear σ -models usually come with kinetic terms for the boson fields by definition. From an RG perspective this amounts to a difference in the initial UV value or asymptotic behavior for the bosonic wave-function renormalization, which is either zero or non-zero. As can be seen from Refs. [400, 401, 378, 177] it is a long-standing discussion, whether these models are equivalent in the IR w.r.t. their phenomenology. Within this work, we will also contribute to this ongoing discussion.

In addition, let us mention that we are not the only ones who are not exclusively interested in the phenomenology of the GN model, but also considered it as a perfect testing ground for mathematical and numerical methods in QFT. For example Ref. [402] used it to study and test the method of Lefschetz thimbles. Due its conformal invariance in the UV sector and its well-known infinite- N limit, the GN model is also of interest for investigations on holographic aspects of QFTs, see, *e.g.*, Refs. [403, 404]. Other examples where the GN model serves as a test field for the study of conceptual aspects of QFTs comprise the influence of spacetime curvature on symmetry breaking/restoration phenomena [405, 406, 407, 408] or the study of entanglement entropy [409]. It was even used to conceptually study the freeze-out in heavy-ion collisions [410] – just to name a few examples.

7.2.2. Contextualization of the GN model with other QFTs

More importantly and as already previously stated, the GN model is also interesting from the perspective of (non-relativistic) condensed-matter physics. It turns out that the GN model (and related four-fermion models in 1+1 dimension) emerge as limiting scenarios from several (discrete) theoretical solid-state systems.

Very recently it was shown [411, 412, 413] that one-dimensional probabilistic cellular automata in their continuum limit are equivalent to relativistic QFTs of fermions. Hereby, the classical bits, respectively cells, are interpreted as Ising spins.

This already hints at a deeper connection to solid-state physics, that was already found years ago: In the $N \rightarrow \infty$ limit it can be shown [414] that the lattice-field theory version of the (1+1)-dimensional Euclidean GN model is equivalent to a (square lattice) two-dimensional Ising model, where the temperature of the Ising model is identified with the four-fermion coupling of the GN model $T = 4g^2$. The latter model was first solved by L. Onsager [415] and one finds an ordered

and a disordered phase, which are separated by a second-order PT. This directly translates to the formation of a condensate in the Euclidean discretized GN model in vacuum, and it is explicitly shown in Ref. [416] that this is due to the Bardeen-Cooper-Schrieffer mechanism [341]. Hence, the infinite- N lattice version of the GN model can be seen as a model for superconductivity, where left-moving fermions are coupled to right-moving anti-fermions and vice versa [416].

A similar relationship also exists for the lattice-field theory version of the $(1 + 1)$ -dimensional Euclidean $SU(N)$ Thirring model and the XY model¹¹ [414]. However, due to the CMWHB theorem [151, 152, 153, 154, 155] there are no Nambu-Goldstone bosons [156, 157, 144] in systems of dimension two or smaller at non-zero temperature, such that there is no symmetry breaking and long-range order in the XY model. Nevertheless, it was shown by V. Berezinskii, J. M. Kosterlitz, and D. J. Thouless [154, 155, 417] that there is still a transition from a disordered high-temperature state to a quasi-long-range ordered low-temperature state mediated by vortex-anti-vortex pairs. This calls into question the (continuum) infinite- N result for the $SU(N)$ Thirring model, where spontaneous symmetry breaking and a Nambu-Goldstone particle is found, as discussed by E. Witten [342].

Note that the Ising and the XY model are both special versions of the N -vector model of spins on a crystalline lattice [418] and prototype condensed-matter (toy) models.

In this context let us also mention that the infinite- N GN model has certain similarities with systems of cold atoms in optical lattices, which are described by so called rotor Jackiw-Rebbi models, as pointed out by Ref. [419]. This does not seem accidental, because there is a direct link to the physics of ultra-cold atoms: The thermodynamic limit of the imbalanced Creutz-Hubbard model [420] can be written as a one-dimensional Wilson-fermion Hamiltonian on the lattice, which in turn is a discretized version of the GN model [421].

Next, we consider the opposite limit: For $N \rightarrow 1$ the GN model is equivalent to the Thirring model [345] model. This accordance is shown using Fierz identities [19, 422, 177, 423]. The Thirring model, however, is the continuum limit of the one-dimensional spin- $\frac{1}{2}$ Heisenberg model [424] – correspondingly the lattice version of the Thirring model describes a chain of antiferromagnetic spins [416, 423]. On the other hand, the Thirring model emerges as the infinite-volume limit of the Luttinger model with strictly local interactions [425] describing the one-dimensional Tomonaga-Luttinger liquid [426, 427], see Ref. [423] for further details. Interestingly, there is another connection of the Thirring model to condensed-matter physics. The continuum limit of the Frenkel-Kontorova model [428] is the sine-Gordon model, which was shown to be equivalent to the massive Thirring model [429, 430]. Note that the equivalence between the bosonic sine-Gordon model and the Thirring model is based on bosonization transformations, which is a feature that is often employed in $(1 + 1)$ -dimensional QFT theories [423, 430].

There are even more direct connections between condensed-matter theory models and the GN model. It can be shown [431] that the continuum limit of the Potts model [432], also known as the Ashkin-Teller model [433] for certain cases, is the GN model. This is again not accidental, because the N -vector model, discussed above, is a generalization of the latter.

One of the principles behind the connection of spin systems and fermionic QFTs in $1 + 1$ dimensions is the mapping of spin operators using the so-called Jordan-Wigner transformation [434], see also Ref. [423]. In turn, bosonization techniques may be used to transform the fermionic QFT into bosonic QFT to study, understand, and even solve these systems, *cf.* Refs. [423, 435, 342, 430, 429].

Furthermore, it turns out that the GN model seems to be a decent description of polymers, more specifically (trans-)polyacetylene, which is a chain of CH groups (CH_x) and understood as follows, *cf.* Refs. [436, 437, 437, 438, 439, 440, 441, 442]. At first, it seems as if there is one free electron per site (C-atom) and therefore a half-filled band. Due to the Peierls instability the electrons form pairs (double bonds), such that polyacetylene is an insulator and not a metal. This is drastically changed and polyacetylene behaves like a metal after doping.

¹¹This model also goes under the name “classical rotor model”, “planar model”, or “ $O(2)$ model”.

The reason is that the formation of the double bonds, the dimerization, is not unique, because taking the view of one CH chain link, the double bond can either go left or right. For a chain of infinite extent this corresponds to two degenerate ground states, because the same pattern continues for the entire chain. On the other hand, the doping leads to CH chain links, which have no or two double bonds, which can be interpreted as domain walls, between regions of the distinct degenerate ground states. These impurities can move and scatter like solitons and lead to conductivity. See Ref. [441] for a review. This is described by the Su-Schrieffer-Heeger model [436] and its continuum limit, the Takayama-Lin-Liu-Maki model [443]. It is shown by Refs. [437, 444, 438] that the latter model and the $N = 2$ GN model are identical, which explains that the GN model is an approximate description of (trans-)polyacetylene. This is also easy to understand, by identifying the degenerate minima of the vacuum potential of the GN with the degenerate ground states of the CH chain and the doping impurities with the soliton solutions of the GN model. The doping concentration is in turn associated with the chemical potential [445, 439].

For more connections between relativistic QFTs and condensed-matter systems we refer to Refs. [446, 423, 442].

Finally, let us mention another interesting connection between (experimental) solid state physics and high-energy particle physics in the context of the GN model. Only recently photonic waveguide arrays were used to study spatially inhomogeneous multi-fermion bound state solutions of the equations of motion of the GN model – the solitons – in the infinite- N limit [447].

7.3. Phenomenology of the Gross-Neveu model

So far we introduced the GN model as a prototype model to study conceptual aspects of QFTs and reported on its generic features as well as its role in connection with other models and theories of relativistic high-energy particle and condensed-matter physics. Next we turn to the presently established phenomenology of the GN model – especially at non-zero chemical potential μ and non-zero temperature T . Most of these theoretical predictions are based on calculations in the lowest order of the $\frac{1}{N}$ -expansion. Beyond this approximation there is little secure knowledge about the phenomenology, besides the vacuum results, which were already mentioned previously.

Before we turn to the in-medium phenomenology, we should nevertheless briefly return to the GN model in vacuum. Already shortly after D. J. Gross and A. Neveu proposed their model R. F. Dashen, B. Hasslacher, and A. Neveu studied the spectrum of bound states in the semi-classical Wentzel-Kramers-Brillouin approximation [282]. They found a rich spectrum of fermion-antifermion and multi-fermion bound states, some of which are so-called time-(in)dependent kink (soliton-like) solutions and can be associated with baryon-like states. This particle spectrum and especially the dynamics of the solitonic solutions was studied extensively with various methods, see, *e.g.*, Refs. [448, 449, 450, 451, 452, 453]. Generically, they seem to be a rather robust feature of all kinds of low-dimensional QFTs. Using semi-classical approximations like the Wentzel-Kramers-Brillouin method or Hartree-Fock method, it is shown that the problem of finding these solutions is oftentimes the same as self-consistently solving a scattering problem of fermions in a potential, which is formed by the fermions itself. These scattering problems, which are formulated in terms of the Schrödinger/Lamé equation, oftentimes fall in the class of super-symmetric quantum-mechanical problems [454, 455]. The corresponding Lamé potentials are ultimately associated to hadrons in the original QFT.

The reason why this is important in the context of the in-medium phenomenology of the GN model and this thesis is as follows. At low temperatures and large chemical potentials baryon-like states become important, meaning that they are energetically favored and certainly influence the vacuum structure. This becomes highly relevant in the context of spatially inhomogeneous condensation in the next paragraphs.

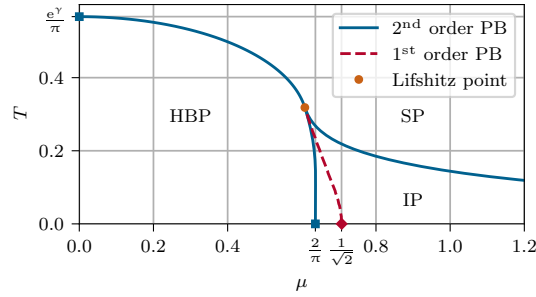


Figure 7.1: The phase diagram of the GN model in the $N \rightarrow \infty$ limit. The dashed red curve corresponds to the first-order phase boundary that is obtained if spatially homogeneous condensation is assumed [456, 457, 458]. The solid blue lines correspond to second-order PTs, if spatially inhomogeneous condensation is taken into account [446, 459, 460, 461]. From Ref. [5, Fig. 1].

7.3.1. The phase diagram of the GN model at infinite N

Finally, we turn to the phase structure of the GN model in medium.

The obvious question that arose already shortly after the initial publications on the vacuum properties of the GN model was how robust the formation of a fermion-anti-fermion condensate is against thermal fluctuations and an imbalance of matter and anti-matter. Another question that is directly related to the previous one concerns the dependence of thermodynamic state variables like the density, the pressure, the energy density, the entropy density, susceptibilities *etc.*, on the temperature and chemical potential. These questions were dealt with and answered in the infinite- N approximation step by step in numerous publications and culminated in a complete picture of the phase diagram of the (massive) GN model presented by O. Schnetz, M. Thies, and K. Urlichs, see Fig. 7.1. In the next paragraphs we summarize the highlights of these developments.

Spatially homogeneous condensation Starting off from the established infinite- N results in vacuum, it was obvious (1) to keep the assumption of spatially homogeneous condensation for the sake of simplicity, (2) to continue working in the infinite- N approximation, and (3) to study the influence of temperature and chemical potential separately.

Using the methods of Ref. [462] it was demonstrated by Refs. [463, 464, 465], that, while cranking up the temperature and keeping $\mu = 0$, the chiral condensate starts to “melt” and one finally reaches a critical temperature T_c where the condensate completely vanishes and the discrete chiral \mathbb{Z}_2 symmetry is restored. This PT was determined to be of second order and the T_c is uniquely related to the vacuum fermion mass by the factor $\frac{e\gamma}{\pi}$.

In parallel Refs. [465, 466] argued that at $T = 0$ the \mathbb{Z}_2 symmetry gets also restored and the condensate is destroyed, if the chemical potential is larger than half the vacuum fermion mass. Qualitatively they were right and one finds a critical chemical potential μ_c where symmetry restoration takes place. Nevertheless, their calculation was implicitly based on the assumption of a second-order PT. This assumption is incorrect for spatially homogeneous condensation and one actually finds a first-order PT at $\mu_c = \frac{1}{\sqrt{2}}$, while $\mu = \frac{1}{2}$ is merely the $T = 0$ endpoint of the so-called spinodal line (all dimensionful quantities are expressed in units of the vacuum fermion mass).

This false determination of the point $(\mu_c, 0)$ was resolved in Ref. [458]. Moreover Ref. [458] revealed the entire phase structure in the μ - T -plane (including the spinodal lines). It turns out that the second-order PT at $\mu = 0$ extends until it reaches a critical (respectively Lifshitz) point at $(\mu_{cp}, T_{cp}) \simeq (0.608, 0.318)$. There the PT between the phases of symmetry breaking and restoration turns into a first-order PT line that approaches $(\mu_c, 0) = (\frac{1}{\sqrt{2}}, 0)$. The spinodal lines engulf the region in the μ - T -plane, where the effective potential exhibits trivial and non-trivial minima. See, *e.g.*, Ref. [458, Fig. 4] for sketches or the discussions in Refs. [4, 5, 467].

At this point it is important to say that the entire infinite- N phase diagram and physics of the GN model is unique, meaning that all dimensionful quantities can be expressed in terms of a single

observable like T_c , μ_c , the vacuum mass of the fermions *etc.*. Hence, it is renormalization-scheme independent!

Interestingly, as discovered by Ref. [446] it seems that the infinite- N phase diagram of the GN model for spatially homogeneous condensation is actually older than the GN model itself. Reference [456] presents the phase diagram for a model where a uniform magnetic field is acting on the spins of the conduction electrons in a superconductor already in 1963. Identifying the strength of the uniform magnetic field with the chemical potential of the GN model, the phase diagrams in units of the respective energy gaps are identical. It is even more remarkable that also the wrong interpretation of the spinodal line with a second-order PT line was resolved already by Ref. [456] 22 years in advance of Ref. [458] and 11 years in advance of the model proposal by D. J. Gross and A. Neveu. Hence, the model was solved before it existed.

Apart from the above mentioned references there are various other works who contributed to a better understanding of the GN phase diagram under the assumption of spatially homogeneous condensation or used the well-established results to test methods in QFT. For example, Ref. [468] presents the dependence of the chiral condensate (the fermion mass) on the temperature using Schwinger's proper-time method and the so-called tadpole formalism. It also provides the temperature dependence of amplitudes of elastic scattering. Another study that reproduces parts of the above results, is Ref. [469], which deals with symmetry breaking and restoration by analyzing the fermion mass along the lines of Refs. [339, 340]. There are also various studies that calculated thermodynamic properties, like entropy densities, baryon-number densities, susceptibilities *etc.*, *e.g.*, Refs. [470, 457].

Spatially inhomogeneous condensation One of the natural follow-up questions is what happens to the infinite- N phase diagram, if the strong restriction of spatially homogeneous condensation is relaxed and spatially varying condensates are taken into account.

Inspired by various model studies at non-zero baryon density but zero temperature, which demonstrated that ground states at large μ might break translational invariance V. Schön and M. Thies studied this phenomenon in the χ GN model [471]. In this work they also raised the question whether similar phenomena take place in the conventional massless GN model. The idea behind this deviation from a spatially homogeneous phase structure stems from the rich bound-state structure, especially baryons, which should strongly influence the phase structure at small temperature and moderate matter-anti-matter asymmetry, as mentioned earlier.

The starting point of the actual investigation seems to be Ref. [472], where the authors demonstrated that a ground state (a gap), that breaks translational invariance and \mathbb{Z}_2 symmetry, is always energetically favored over the translational invariant and \mathbb{Z}_2 -symmetric ground state at $T = 0$. As an ansatz for the spatial dependence of the condensate they chose a concatenation of the single repulsive baryon solutions from the spectrum of the vacuum model of Refs. [451, 282]. It is found that this crystalline-like ground state of equally spaced baryons is even energetically favored over spatial homogeneous condensation for some $\mu < \mu_c$, such that the former first-order PT is covered by a phase with an spatially inhomogeneous ground state. In their concluding remarks the authors already anticipate that at large chemical potentials their crystal of equally spaced and distinct baryons – although being energetically favored over a vanishing condensate – will not be the minimal-energy solution. This was reasonable, because at higher densities spatially distinct baryons are an unrealistic assumption¹². Nevertheless, since already this crucial approximation is energetically favored over a symmetric phase, the authors conclude that the true shape of the condensate at arbitrarily high densities has to have some periodic oscillatory spatial dependence. This spatial dependence of the true ground state was ultimately worked out analytically in Ref. [473] by mapping the Hartee-Fock Dirac equation to a supersymmetric Lamé equation [452, 454, 453].

Slightly earlier M. Thies and K. Urlichs already published a revised version of the infinite- N phase diagram [327] of the GN model, partially relying on numerical minimization, where they

¹²Actually this is the same assumption that lead to the prediction of a quarkyonic phase [299, 301] in QCD.

find exactly this kind of spatially inhomogeneous condensation at large chemical potential but also $T \neq 0$, without presenting the full analytic solution of the ground state for all μ and T .

By generalizing the analytic solution from Ref. [473] from zero to non-zero temperature, the full phase structure and true ground state for the GN model and massive GN model was then ultimately worked out in a series of publications by the former authors and O. Schnetz [446, 459, 460] and the phase structure derived semi-numerically in Ref. [327] was confirmed.

The resulting phase diagram is presented in Fig. 7.1 and ultimately consists of three phases with spatially homogeneous broken \mathbb{Z}_2 symmetry (HBP), spatially inhomogeneous broken \mathbb{Z}_2 symmetry (IP) (additional breaking of continuous translational invariance) and a symmetric phase (SP). All phase boundaries constitute second-order PT lines and the former first-order PT is completely engulfed by the so-called inhomogeneous phase that extends to $\mu \rightarrow \infty$.

The shape of the inhomogeneous phase can be exactly expressed in terms of Jacobi elliptic functions. For increasing μ one finds that the shape of the condensate transforms from a kink-antikink-like structure to a sine-like shape. Furthermore, the amplitude of the oscillations decreases with μ , while their frequency increases. Increasing the temperature also leads to a continuously decreasing amplitude.

Again, the above publications triggered also other authors to use the exact result for the phase diagram with spatially inhomogeneous condensation as a test field for methods for the detection and analysis of inhomogeneous phases in a general context. Some prominent examples are Refs. [332, 333, 474, 475], where lattice field-theory methods were tested with the GN model for the search of inhomogeneous phases and also the influence of the restriction of the spatial dimension to a finite volume was studied. For analytical works, see, *e.g.*, Ref. [476], which invented the so-called “fermion-doubler trick” that is based on a doubling of the fermion degrees of freedom and an expansion of the action about a condensate with cosine-background field dependence, or Ref. [467], that studies the (in)homogeneous phase via a systematic Ginzburg-Landau expansion.

Variations and generalizations Before we continue with our main program, we briefly comment on various generalizations and variants of the above infinite- N calculations. Concerning the phase diagram of the GN model (assuming spatially homogeneous condensation), there is for example Ref. [477] that generalizes the phase diagram to continuous spacetime dimensions $2 \leq d+1 < 4$, or Ref. [478] that uses the GN model at $T = 0$ on a spatial ring S^1 with chemical potential to study multiple phases of a Peierls insulator. A similar study [479] analyzes the GN model for non-zero μ on a torus formed by a periodic spatial dimension and the temperature. Also the generalization to the massive GN model were studied already before M. Thies and collaborators solved it in full generality [480]. Generalizations that considered more possible interaction channels, the possibility of a true superconducting phase in the relativistic QFT framework or more than one condensate can be found in, for example, Refs. [481, 482, 483, 484, 485, 486].

7.4. To break or not to break – \mathbb{Z}_2 symmetry at finite N

Having said all this, the careful reader might object that even if the above results are highly relevant and interesting, the infinite- N limit is extraordinarily special: It completely suppresses all kinds of bosonic fluctuations and thus any direct backreaction of bosonic bound states on the fermions. In addition, and more importantly, all bosonic self-interactions are ignored. This seems to be a crude assumption, because especially in a single spatial dimension it is rather obvious that fluctuations will spread over large distances and easily destabilize long-range order, hence condensation.

Therefore the question is whether \mathbb{Z}_2 -symmetry breaking and condensation of fermion-anti-fermion pairs is still a robust feature of the (1+1)-dimensional GN model at finite N and especially non-zero T .

At first sight, this question seems to be answered and there are indeed a bunch of arguments why we should not expect any kind of condensation phenomena at non-zero temperature under the influence of bosonic thermal and quantum fluctuations. However, on closer inspection things are not as clear as they appear to be or as they are communicated at conference dinners... .

7.4.1. Continuous vs. discrete symmetries

The first argument that is usually played off against symmetry breaking is the CMWHB theorem [153, 151, 152, 154, 155]. This theorem forbids the formation of Nambu-Goldstone bosons [156, 157, 144] in less than two spatial dimensions at non-zero temperature. However, Nambu-Goldstone bosons arise by dynamical symmetry breaking of continuous symmetries, which is not the case for the GN model, which has a discrete \mathbb{Z}_2 symmetry. In conclusion the theorem does exclusively apply to extensions of the GN model, *e.g.*, the χ GN model. This was for example discussed by E. Witten [342], who also argues that the infinite- N limit violates the CMWHB theorem, but discusses the possibility for a phase of Berezinski-Kosterlitz-Thouless type [154, 155, 417] of quasi-long-range order. See also Refs. [487, 488, 489] for recent related works on the χ GN model, which address this issue. Note that generically the theorem is restricted to $T \neq 0$, such that symmetry breaking in vacuum and for $\mu \neq 0$ is always possible.

7.4.2. Landau's argument

Another – maybe the most powerful – argument against any symmetry breaking in all kinds of one-dimensional systems at non-zero temperature was already put forward by L. D. Landau in 1950 and is presented by L. D. Landau and E. M. Lifshitz in Ref. [490, § 163]: Consider a generic bistable system of two possible phases in a single spatial dimension at non-zero temperature. Let us further assume that space is split into M equally sized cells. Each cell either belongs to one or the other phase, such that adjacent cells may form domains of the same phase. In consequence there are also N interfaces (or rather contact points in a single dimension), where neighboring cells belong to different phases. These phase boundaries are oftentimes called domain walls. The Boltzmann entropy of a possible domain configuration therefore is

$$S = \ln \left(\frac{M!}{N!(M-N)!} \right) \simeq M \ln(M) - N \ln(N) - (M - N) \ln(M - N), \quad (7.2)$$

where we used Stirling's approximation. Assume that each interface comes with a constant energy ε , which is reasonable in one dimension, since interface sizes should not depend on the domain size – they are always point-like. The inner energy of the system is thus given by $U = \varepsilon N$ and the free energy by

$$F = U - T S. \quad (7.3)$$

Lets us study how this thermodynamic potential changes with N for fixed M ,

$$\frac{\partial F}{\partial N} = \varepsilon + T \ln \left(\frac{N}{M-N} \right). \quad (7.4)$$

For $N \ll M$ the logarithm is large and negative. Hence, the free energy is lowered, if N is increased. Consequently, the system will automatically produce more and more interfaces and domains of different phases. This process continues until Eq. (7.4) vanishes, *i.e.*,

$$N = \frac{1}{\exp(\frac{\varepsilon}{T}) + 1} M. \quad (7.5)$$

If the domain-wall energy ε is small compared to the temperature, N approaches the same order of magnitude as M . For large systems, this means that “the two phases will tend to intermingle in shorter and shorter sections, and therefore cannot exist as separate phases” [490, § 163]. From the above it is clear that this argument no longer holds true at zero temperature or if the $\frac{\varepsilon}{T}$ is no longer small. The latter is the case in the infinite- N limit of the GN model, *cf.* Ref. [465]

and below. Landau’s argument also fails, if the domain-wall energy is assumed to grow with the domain size. Indeed this is the reason why it does not generalize to $d > 1$, where the size of the cell interfaces depends on the domain size [465]. For further details, we also refer to Ref. [491] that discusses (the absence of) symmetry breaking in small dimensions from various perspectives.

7.4.3. Kink configurations in the partition function

Actually, already in 1975 R. F. Dashen, S. Ma, and R. Rajaraman confirmed Landau’s argument for the GN model on a qualitative level and predicted that $T_c = 0$ for a finite number N of fermions [465]. (The authors exclusively discuss the situation of finite N for $\mu = 0$ and do not comment on $\mu \neq 0$.)

They deduced that field configurations $\sigma(x) \sim \bar{\psi}(x)\psi(x)$ that are spatially oscillating in terms of kinks and anti-kinks, which “interpolate” between the homogeneous vacua of the infinite- N potential, essentially contribute to the partition function – also at low temperatures. Even though each kink comes with a finite energy, which can be interpreted as Landau’s domain-wall energy, these configurations are energetically preferred due to an entropic gain and consequently lead to a net vanishing expectation value for $\langle \bar{\psi}\psi \rangle = 0$, because kinks and anti-kinks average to zero. In addition it was shown that each kink energy is proportional to N , such that large values of N make the occurrence of kinks more and more unlikely (for $\mu = 0$). Ultimately, for $N \rightarrow \infty$, the number of kinks is zero and $\langle \bar{\psi}\psi \rangle \neq 0$ – allowing for spontaneous symmetry breaking. The same applies to the zero-temperature limit, where the entropic gain does no longer exist and the kink energies therefore disfavor oscillating configurations in the partition function¹³.

Hence, Ref. [465] is in agreement with Ref. [490], because Landau’s argument also exclusively applies to finite interface energies and non-zero temperature.

7.4.4. Temperature reinterpreted as a spatial box

Another argument which is put forward against symmetry breaking relates to the special structure of Euclidean $(1+1)$ -dimensional QFTs at non-zero temperature. On a formal level it is impossible to distinguish a $(1+1)$ -dimensional Euclidean QFT in a spatial box at zero temperature from the same QFT in an infinite spatial volume at non-zero temperature, if the temperature is identified with the inverse box size and boundary conditions are matched accordingly. Of course, this kind of duality is restricted to $\mu = 0$. Then again, it is generally assumed that spontaneous symmetry breaking in finite-sized systems is impossible, see, *e.g.*, Ref. [18, 139], which directly translates to the absence of spontaneous symmetry breaking in the GN model at non-zero temperature [458, 457].

Still, certain details of the thermodynamic and/or infinite-volume limit, the inclusion of (infinitesimal) explicit symmetry breaking, as well as studying extremely large volumes might spoil this theoretically strict argument in practical calculations and lead to false signals of spontaneous symmetry breaking. See, *e.g.*, Ref. [492] for details on this topic.

7.4.5. Explicit calculations at finite N

Sometimes decades of qualitative discussions simply call for explicit quantitative investigations. These may either support the theoretical arguments or yield controversial results, which call for further studies and discussions. In the context of the GN model the latter was the case.

Non-perturbative corrections to the infinite- N result Anyhow, let us start by presenting some rather uncontroversial and expected results at finite N . Using a thermodynamic Bethe

¹³Even though the kink configurations are closely related in shape to the inhomogeneous condensates at non-zero μ in the infinite- N limit, they do not refer to vacuum expectation values for the scalar field in this context. For the arguments of Ref. [465] it is crucial to differentiate between expectation values and the actual field configurations that contribute predominantly to the partition function.

ansatz A. Chodos and H. Minakata present the first-order $\frac{1}{N}$ -correction to the critical chemical potential at zero temperature in terms of the vacuum fermion mass [382],

$$\mu_c = \frac{1}{\sqrt{2}} \left(1 - \frac{0.47}{N} \right) + \mathcal{O}(N^2). \quad (7.6)$$

Hence, their calculation predicts, in accordance with the above discussions and references, that condensation still takes place at zero temperature and finite N , though the critical chemical potential μ_c is lowered by the bosonic fluctuations compared to the infinite- N result. For example, for $N = 2$, which is the most extreme case, the first-order correction (7.6) is approximately a 20% effect.

Next, we turn to higher-order $\frac{1}{N}$ -corrections at non-zero temperature. Here, S. K. Gandhi and M. B. Pinto used a non-perturbative δ -expansion up to third order to study corrections to the infinite- N result for T_c at $\mu = 0$ [493]. Their calculation shows that T_c is drastically lowered by including these corrections, which include terms of various orders in $\frac{1}{N}$. Even though they argue that their results point towards $T_c = 0$, the calculations can only be seen as an indication. Similarly, J.-P. Blaizot, R. M. Galain, and N. Wschebor studied the next-to-leading order correction in the $\frac{1}{N}$ -expansion of the effective potential [494]. They reported complementary results at very low temperatures, where their results seem to resemble the infinite- N results, and at very high temperature, where the $\frac{1}{N}$ -correction agrees with perturbative corrections to a free gas. However, for intermediate temperatures the $\frac{1}{N}$ -expansion seems to break down. Still, their results indicate that T_c is lowered by decreasing N [494, Fig. 14].

Other works that also used the δ -expansion, which is also called optimized perturbation theory, find similar results at non-zero μ and non-zero T . In Refs. [495, 496, 440] corrections to the leading-order $\frac{1}{N}$ result are studied, which lead to a lowering of the temperature of the second-order phase transition, including T_c and the critical point. All authors agree that their results point at $T_c = 0$, even though they do not provide a systematic analysis of convergence properties of the δ -expansion or $\frac{1}{N}$ corrections.

Lattice Monte-Carlo studies at finite N On the other hand, there is a significant number of brute-force lattice simulations of the GN model at finite N . Not long ago some of our collaborators and colleagues used lattice Monte-Carlo simulations [335, 336, 337, 338] to search for spatially inhomogeneous condensation in the GN model in medium at finite N . There it turned out that the three phases from Fig. 7.1 still seem to be present, even though the phase of spatially homogeneous condensation appeared to shrink by lowering N . These results are in agreement with older lattice Monte-Carlo simulations at finite N [391, 392, 497, 389], which also found regions with signals of spatially homogeneous condensation in the μ - T -plane.

Since these results in parts contradict the above arguments against symmetry breaking in $1 + 1$ dimensions at $T \neq 0$, the question arises where the discrepancies come from. Indeed, most of these lattice studies do not provide careful continuum extrapolations. Also the infinite-volume limit is usually not performed accurately. Hence, finite-volume and discretization artifacts might spoil the calculations and question their predictive power for the GN model in an infinite volume and continuum. See also Refs. [416, 498, 393, 390, 394, 499, 500] for lattice discretization artifacts in the GN model.

As a matter of fact, we speculated in Ref. [4] that the artificial finite volume of the lattice Monte-Carlo studies might have suppressed infrared fluctuations of the bosons, which are important for symmetry restoration. Ongoing FRG investigations of the GN and GNY model in a finite-sized box in continuum indicate that this is not the case and that the presence of (inhomogeneous) condensates in lattice Monte-Carlo simulations might either be related to the spatial discretization (UV) artifacts or statistical problems.

Chapter 8

The Gross-Neveu model, the bosonized Gross-Neveu model, and the Gross-Neveu-Yukawa model

Abstract In this chapter we discuss the field-theoretical formulation of the GN model in detail. In the first part the action of the original model in $(d + 1)$ -dimensional Minkowski spacetime and its translation into Euclidean spacetime is presented. Furthermore, the symmetries of the model are discussed. Then baryon chemical potential as well as temperature are introduced to enable calculations in medium.

The second part deals with the Hubbard-Stratonovich transformation to a bosonized version of the model – the bGN model. In addition the GNY model is introduced and its relation to the bGN model is discussed. The chapter ends by demonstrating how the symmetries of the purely fermionic theory translate to the bosonized models.

Readers who are familiar with the GN model are encouraged to merely skim over this chapter to familiarize with the notation of this work.

Disclosure None of the concepts discussed in this chapter is really new, though its presentation and compilation is original to the author. Similar material can be found in generic publications on the GN model or related QFTs and we mostly refrain from citing all kinds of standard QFT calculations and techniques. The presentation and compilation in this chapter is partially based on our own publications [4, 5].

8.1. The Gross-Neveu model

The starting point is the presentation of the purely fermionic GN model. We introduce the field-theoretical formulation of the model in terms of an action in Minkowski and Euclidean vacuum and discuss its generalization to non-zero temperature and non-zero chemical potential. Throughout the discussion we mostly keep the number of spatial dimensions general and comment on some peculiar features of the model in different dimensions.

8.1.1. The Gross-Neveu action in vacuum

Let us start with the vacuum formulation of the GN model.

Minkowski spacetime

In a $(d + 1)$ -dimensional Minkowski spacetime, where d is the number of spatial dimensions, the original action of the GN model is given by [158],

$$\mathcal{S}[\bar{\psi}, \psi] = \int_{-\infty}^{\infty} d^{d+1}x \left[\bar{\psi} i \not{\partial} \psi + \frac{1}{2N} g^2 (\bar{\psi} \psi)^2 \right]. \quad (8.1)$$

Hereby g^2 is the four-fermion coupling and N is the number of fermion species (oftentimes denoted as colors or flavors in the GN model literature). The rescaling of the four-fermion coupling by $2N$ is convention and simplifies calculations at various N – including $N \rightarrow \infty$. The fields ψ consist of N copies of spinors that transform under representations of the Lorentz group of the respective spacetime. Hence, one has to exercise caution when d is altered, because with d also the spacetime symmetry groups change their properties and so does the spin group and the spinor representations [501]. In particular this leads to significant differences between even- and odd-dimensional spacetimes, see, *e.g.*, Ref. [502, App. A].

We work in Cartesian coordinates and use the conventions of Appendix A.2 for the metric. (Note that we associate the $(d+1)$ th coordinate with the temporal direction.) Hence, Eq. (8.1) is actually a compact notation for

$$\begin{aligned} \mathcal{S}[\bar{\psi}, \psi] = & \int_{-\infty}^{\infty} d^d x \int_{-\infty}^{\infty} dt \left[\bar{\psi}_{a_1 c_1}(t, \vec{x}) (\mathbf{1})^{c_1}_{c_2} i(\gamma^\mu)^{a_1}_{a_2} \partial_\mu \psi^{a_2 c_2}(t, \vec{x}) - \right. \\ & \left. - \frac{1}{2N} g^2 \left[\bar{\psi}_{a_1 c_1}(t, \vec{x}) (\mathbf{1})^{c_1}_{c_2} (\mathbf{1})^{a_1}_{a_2} \psi^{a_2 c_2}(t, \vec{x}) \right]^2 \right], \end{aligned} \quad (8.2)$$

where t is the time, \vec{x} are the d spatial coordinates, the indices $c_i \in \{1, \dots, N\}$ label the N fermion species, and $a_i \in \{1, \dots, d_\gamma\}$ are the spinor indices, that attach the spinors to the members of the Clifford algebra, the γ -matrices γ^μ . Here, d_γ is the dimension of the representation of the Clifford algebra. (For our two-dimensional calculations, we choose the lowest-dimensional representation, $d_\gamma = 2$, and use the Weyl basis.) The γ -matrices also carry a Lorentz index $\mu \in \{1, \dots, d + 1\}$, that labels the basis vectors of the Minkowski space.

Let us also briefly comment on the physical dimensions of the fermion fields $\bar{\psi}$ and ψ as well as the coupling constant g^2 . In natural units it is straightforward to deduce their canonical energy dimension,

$$[\psi] = \text{energy}^{\frac{(d+1)-1}{2}}, \quad [g^2] = \text{energy}^{-(d+1)+2}. \quad (8.3)$$

We find that the four-fermion coupling has negative energy dimension for $d > 1$, which underpins the previous statements from Section 7.2 on perturbative non-renormalizability of any four-fermion couplings in spacetime dimensions larger than two.

So far we exclusively presented the microscopic action, which describes the fermions at some UV scale. In order to calculate macroscopic observables in terms of vacuum expectation values or rather correlation functions, we define the generating functional for n -point correlation functions (up to an irrelevant normalization factor) as usual in QFT [19, 422, 18, 20, 142],

$$\mathcal{Z}[\bar{\eta}, \eta] \propto \int [d\bar{\psi}, d\psi] \exp \left(i\mathcal{S}_M[\bar{\psi}, \psi] + i \int_{-\infty}^{\infty} d^{d+1}x_M (\bar{\eta} \psi + \bar{\psi} \eta) \right). \quad (8.4)$$

Without the artificially introduced fermionic source terms $\bar{\eta}$ and η the generating functional corresponds to the path or functional integral of the model. Hence, Eq. (8.4) sums (integrates over) all possible microscopic field configurations, which are in turn weighted according to their action. By taking derivatives w.r.t. the sources and by evaluating at vanishing source fields afterwards,

one generates expectation values, respectively correlation functions of fermion fields.

However, the interpretation of the integrand in Eq. (8.4) as an ordinary probability distribution is limited due its complex highly oscillatory nature. Furthermore, the scope of this work is the thermodynamics of the GN model. In any case and without going into detail, one therefore needs to change the spacetime structure from a Minkowski space to a Euclidean spacetime to obtain a conventional probability distribution in the sense of statistical physics. For details, we refer to Refs. [503, 22, 142, 504, 13, 505].

Euclidean spacetime

The change from Minkowski to Euclidean spacetime can be done on a formal level via the following simple “substitutions”, where M indicates Minkowski and E Euclidean quantities,

$$x_M^{d+1} = t_M \quad \mapsto \quad x_E^{d+1} = it_M = ix_M^{d+1}, \quad (8.5)$$

$$\partial_{d+1,M} \quad \mapsto \quad \partial_{d+1,E} = -i\partial_{d+1,M}, \quad (8.6)$$

$$\gamma_M^i \quad \mapsto \quad \gamma_E^i = i\gamma_M^i, \quad i \in \{1, \dots, d\}. \quad (8.7)$$

while all other objects of the QFT are unchanged. These “substitutions” are indeed a special case of a so-called Wick-rotation [506] in the complex plane of the temporal coordinate. On a more fundamental level the actual procedure of linking a “Minkowski path integral” with an “Euclidean partition function” and vice versa is more involved and still subject of todays research in QFT. One might think of this connection in terms of an exchange of integration contours using analytic continuation into the complex plane of the temporal coordinate under the application of Chauchy’s (residue) theorem. Details for fermionic QFTs are provided for example by Ref. [507].

Anyhow, in the following chapters of this work, we are almost exclusively interested in properties of the GN model in medium and we simply do not need any additional knowledge about the connection between the Minkowski and Euclidean spacetime than the above substitutions.

We therefore continue by applying Eqs. (8.5) to (8.7) to Eq. (8.1) and start by analyzing the kinetic term of the fermions in detail,

$$\begin{aligned} \not{\partial}_M &= \gamma_M^\mu \partial_{\mu,M} = \gamma_M^i \partial_{i,M} + \gamma_M^{d+1} \partial_{d+1,M} = \\ &= -\gamma_M^i \partial_M^i + \gamma_M^{d+1} \partial_M^{d+1} = \\ &= i\gamma_E^i \partial_E^i + i\gamma_E^{d+1} \partial_E^{d+1} = i\gamma_E^\mu \partial_{\mu,E} = i\not{\partial}_E. \end{aligned} \quad (8.8)$$

Using this intermediate result, we find that the Minkowski and the Euclidean action can be related as follows,

$$\begin{aligned} \mathcal{S}_M[\bar{\psi}, \psi] &= \int_{-\infty}^{\infty} d^{d+1}x_M \left[\bar{\psi} i\not{\partial}_M \psi + \frac{1}{2N} g^2 (\bar{\psi} \psi)^2 \right] = \\ &= -i \int_{-\infty}^{\infty} d^{d+1}x_E \left[-\bar{\psi} \not{\partial}_E \psi + \frac{1}{2N} g^2 (\bar{\psi} \psi)^2 \right] = i\mathcal{S}_E[\bar{\psi}, \psi], \end{aligned} \quad (8.9)$$

where the Euclidean action is defined by,

$$\mathcal{S}_E[\bar{\psi}, \psi] \equiv \int_{-\infty}^{\infty} d^{d+1}x_E \left[\bar{\psi} \not{\partial}_E \psi - \frac{1}{2N} g^2 (\bar{\psi} \psi)^2 \right]. \quad (8.10)$$

On the level of the path integral (8.4), we find that this transforms the highly oscillatory complex-valued integrand into an (apart from infinities) well-behaved probability distribution. The resulting partition function in the presence of sources is,

$$\begin{aligned} \mathcal{Z}[\bar{\eta}, \eta] &\propto \int [d\bar{\psi}, d\psi] \exp \left(-\mathcal{S}_E[\bar{\psi}, \psi] + \int_{-\infty}^{\infty} d^{d+1}x_E (\bar{\eta}\psi + \bar{\psi}\eta) \right) = \\ &= \int [d\bar{\psi}, d\psi] \exp \left(-\int_{-\infty}^{\infty} d^{d+1}x_E [\bar{\psi} \not{\partial}_E \psi - \frac{1}{2N} g^2 (\bar{\psi}\psi)^2 - \bar{\eta}\psi - \bar{\psi}\eta] \right). \end{aligned} \quad (8.11)$$

After regularization, this expression can be used for a direct computation of correlation functions. In order to recover their counterparts in Minkowski spacetime or for the calculation of spectral functions, one would need to analytically continue the latter, *cf.* Refs. [508, 509, 180, 510, 511, 167] for some recent works in the context of functional methods.

8.1.2. Symmetries of the Gross-Neveu action

Before we continue with the introduction of temperature and a matter-anti-matter asymmetry, we return to the action (8.1) and discuss its properties and symmetries.

We start our presentation with some comments on chirality and the discussion of the discrete symmetries and turn to the continuous symmetries afterwards. In the context of continuous symmetries, Noether's theorem becomes relevant and we repeatedly use the generic expressions for the energy-momentum tensor Θ and the Noether current J for fermionic theories. Componentwise these are [20, 24, 19],

$$\Theta^\mu{}_\nu = (\partial_\nu \bar{\psi}) \frac{\partial \mathcal{L}}{\partial (\partial_\mu \bar{\psi})} + \frac{\partial \mathcal{L}}{\partial (\partial_\mu \psi)} (\partial_\nu \psi) - \delta^\mu_\nu \mathcal{L}, \quad (8.12)$$

$$J^\mu \propto \delta \bar{\psi} \frac{\partial \mathcal{L}}{\partial (\partial_\mu \bar{\psi})} + \frac{\partial \mathcal{L}}{\partial (\partial_\mu \psi)} \delta \psi - \Theta^\mu{}_\nu \delta x^\nu + \mathcal{F}^\mu, \quad (8.13)$$

Here, \mathcal{F}^μ denotes the components of a vector whose divergence vanishes (a surface term).

Within this subsection, we focus on $d = 1$, if not explicitly stated otherwise.

Chirality and chiral symmetry in two dimensions

As stated before, we focus on the lowest-dimensional non-trivial representations of the Clifford algebra, which has $d_\gamma = 2$. These are 2×2 γ -matrices. The associated spinors that transform according to this representations are therefore two-component objects (apart from their flavor/color structure),

$$\psi = \begin{pmatrix} \psi_L \\ \psi_R \end{pmatrix}, \quad \bar{\psi} = \psi^\dagger \gamma^{d+1} = (\psi_L^\dagger, \psi_R^\dagger) \begin{pmatrix} 0 & 1 \\ 1 & 0 \end{pmatrix} = (\psi_R^\dagger, \psi_L^\dagger). \quad (8.14)$$

The entries are denoted with “left-” (L) and “right-handed” (R), which is a slightly misleading denotation and is explained within the next lines. (We keep using the adjoint symbol (\dagger) instead of the complex conjugation symbol ($*$) for the two spinor components, because the implied transposition also targets the flavor/color space.)

In order to project the spinor onto its left- or right-handed components, we can use the so-called chiral projectors,

$$\begin{pmatrix} \psi_L \\ 0 \end{pmatrix} = \gamma_L \psi = \begin{pmatrix} 1 & 0 \\ 0 & 0 \end{pmatrix} \begin{pmatrix} \psi_L \\ \psi_R \end{pmatrix}, \quad \begin{pmatrix} 0 \\ \psi_R \end{pmatrix} = \gamma_R \psi = \begin{pmatrix} 0 & 0 \\ 0 & 1 \end{pmatrix} \begin{pmatrix} \psi_L \\ \psi_R \end{pmatrix}, \quad (8.15)$$

$$(\psi_R^\dagger, 0) = \bar{\psi} \gamma_L = (\psi_R^\dagger, \psi_L^\dagger) \begin{pmatrix} 1 & 0 \\ 0 & 0 \end{pmatrix}, \quad (0, \psi_L^\dagger) = \bar{\psi} \gamma_R = (\psi_R^\dagger, \psi_L^\dagger) \begin{pmatrix} 0 & 0 \\ 0 & 1 \end{pmatrix}. \quad (8.16)$$

The projectors and their properties are defined in Eqs. (A.15) to (A.18). In terms of these left- and right-handed spinors, the GN action (8.1) reads

$$\begin{aligned} \mathcal{S}_M[\bar{\psi}, \psi] &= \\ &= \int_{-\infty}^{\infty} d^2x \left[\bar{\psi} i \not{\partial} \psi + \frac{1}{2N} g^2 (\bar{\psi} \psi)^2 \right] = \\ &= \int_{-\infty}^{\infty} d^2x \left[\psi_R^\dagger i(\partial_x + \partial_t) \psi_R + \psi_L^\dagger i(-\partial_x + \partial_t) \psi_L + \frac{1}{2N} g^2 (\psi_R^\dagger \psi_L + \psi_L^\dagger \psi_R)^2 \right]. \end{aligned} \quad (8.17)$$

Discarding the four-fermion interaction for a moment, we find that the free action completely splits into left- and right-handed components. The equations of motion for these free spinors are

$$0 = (\partial_x + \partial_t) \psi_R, \quad 0 = (-\partial_x + \partial_t) \psi_L, \quad (8.18)$$

which are advection equations for right- and left-moving waves that do not disperse. (The same applies to the equations of motion for the adjoint spinors.) These are the $(1+1)$ -dimensional analogues of the Weyl equation. Since there is no real concept like spin and chirality in $1+1$ dimensions, “left” and “right” simply refer to direction of motion of the particles and correspond to the two irreducible representations of the Lorentz group, see below.

In addition, without the four-fermion interaction, transformations of the left-handed spinors would not affect the right-handed ones and vice versa. Here, we refer to global $U(N)_{L/R}$ transformations, thus complex rotations of the left- or right-handed fermion species among each other. This symmetry is usually denoted as (full) chiral symmetry.

Anyhow, the four-fermion term leads to an interaction of left- and right-movers by local scattering and breaks the global $U(N)_{L/R}$ -symmetry explicitly to its discrete global \mathbb{Z}_2 subgroup. The corresponding transformations read,

$$\psi \mapsto \psi' = \gamma^{\text{ch}} \psi, \quad \bar{\psi} \mapsto \bar{\psi}' = -\bar{\psi} \gamma^{\text{ch}}. \quad (8.19)$$

On the level of the left- and right-handed spinors, this is even more instructive,

$$\psi_L \mapsto \psi'_L = -\psi_L, \quad \psi_R \mapsto \psi'_R = \psi_R. \quad (8.20)$$

The transformation of the hermitian adjoint spinors is analogous. We observe that chiral symmetry is realized in the GN model in terms of a discrete \mathbb{Z}_2 symmetry, which flips the sign of the wave function of the left-handed¹ spinors.

Discrete symmetries

The action (8.1) is invariant under the following discrete symmetry transformations. Here, the transformation law for the adjoint spinor always follows directly from the transformation rule for the spinor itself via $\bar{\psi} = \psi^\dagger \gamma^{d+1} = \psi^\dagger \gamma^2$.

Parity Studying a reflection of the spatial coordinates, while keeping the temporal coordinate untouched,

$$x \mapsto x' = -x, \quad t \mapsto t' = t, \quad (8.21)$$

¹The choice of the minus sign in front of the left-handed spinor is convention and can be moved to the right-handed spinor via a global $U(1)$ transformation, which is another symmetry of the system, see below.

we can derive that the GN action (8.1) is invariant, if the fermion fields transform as follows under these parity transformations²,

$$\psi(t, x) \mapsto \psi'(t, x) = P \psi(t, -x), \quad P = \gamma^{d+1} = \gamma^2. \quad (8.22)$$

This transformation law holds up to a phase factor. On the level of the left- and right-handed spinor components of Eq. (8.14) the parity transformation by γ^2 simply exchanges left- and right-moving spinors.

Time reversal It is also possible to show that the GN action (8.1) is invariant under inversion of the temporal coordinate,

$$x \mapsto x' = x, \quad t \mapsto t' = -t, \quad (8.23)$$

in addition with the transformation,

$$\psi(t, x) \mapsto \psi'(t, x) = T \psi(-t, x), \quad T = \gamma^{d+1} = \gamma^2. \quad (8.24)$$

(Note that in addition to these transformation rules the Dirac operator undergoes complex conjugation.) Again, we could have added a random phase to the transformation law. Note that the time-reversal operator, whose properties are listed in Eq. (A.21), is chosen identical to the parity operator. This is absolutely reasonable in a two-dimensional world, where time reflection leads to a movement in the exactly opposite spatial direction.

Charge conjugation Furthermore, the action (8.1) is invariant under charge-conjugation. The spinor is mapped to its charge conjugated counterpart by,

$$\psi(t, x) \mapsto \psi'(t, x) = C \bar{\psi}^T(t, x), \quad C = \gamma^1, \quad (8.25)$$

where C is the charge conjugation matrix, whose properties are listed in Eq. (A.20). Again, we simply fixed the additional phase factor.

CPT Because the GN action (8.1) is already separately invariant under charge conjugation (8.25), parity transformations (8.22), and time-reversal transformations (8.24), also their concatenation constitutes a symmetry transformation [515, 516, 18] and the GN model fulfills the CPT-theorem. In particular the concatenated transformation reads

$$x \mapsto x' = -x, \quad t \mapsto t' = -t, \quad (8.26)$$

for the coordinates and

$$\psi(t, x) \mapsto \psi'(t, x) = -\gamma^{\text{ch}} \psi^*(-t, -x), \quad (8.27)$$

for the spinor. In addition a complex conjugation of the Dirac operator is required. Interestingly, the matrix which maps the spinor to its transformed version is (the negative of) the chiral gamma matrix and the mapping is the discrete chiral symmetry transformation (8.19).

Continuous symmetries

Next, we turn to the continuous symmetry transformations which leave the GN action (8.1) invariant.

²For an odd number of spacetime dimensions the situation is more involved. In $2+1$ spacetime dimensions, for example, the transformation (8.21) turns out to correspond to a rotation by π and it is appropriate to reflect only one of the spatial coordinates to study parity. For details on parity transformations in four-fermion theories in odd dimensions, see, *e.g.*, Refs. [502, 512, 513, 514]. This is one of the reasons why we limit ourselves to $d = 1$ in this subsection.

Unitary transformations of degree N As already anticipated in the discussion about the chiral symmetry, we note that the GN model is invariant under global unitary transformations of degree N , which act on left- and right-handed fermions simultaneously. This symmetry is realized by unitary transformations that mix the fermion species, where members of the $U(N)$ group act on the spinors in terms of their matrix representation by matrix-vector multiplications. In particular, the spinors are supposed to transform as objects that belong to the fundamental representation,

$$\psi \mapsto \psi' = \mathcal{U} \psi, \quad \bar{\psi} \mapsto \bar{\psi}' = \bar{\psi} \mathcal{U}^\dagger, \quad (8.28)$$

componentwise,

$$\psi^{c_1} \mapsto \psi'^{c_1} = \mathcal{U}^{c_1}_{c_2} \psi^{c_2}, \quad \bar{\psi}_{c_1} \mapsto \bar{\psi}'_{c_1} = \bar{\psi}_{c_2} (\mathcal{U}^\dagger)^{c_2}_{c_1}. \quad (8.29)$$

Here,

$$\mathcal{U} = \exp(-i\vartheta^n T_n) \in U(N), \quad (8.30)$$

are the elements of the group. These are constructed from the N^2 group parameters ϑ^n that parameterize the group manifold, which is spanned by the basis elements of the tangent space T_n , the generators, such that the indices $n \in \{0, 1, \dots, N^2 - 1\}$.

It is convenient to split this group into pure global phase transformations and special unitary transformations $U(N) = U(1) \times SU(N)$, where

$$U = \exp(-i\vartheta^m T_m) \in SU(N), \quad m \in \{1, \dots, N^2 - 1\}, \quad (8.31)$$

and

$$\exp(-i\alpha) \mathbb{1} \equiv \exp(-i\vartheta^0 T_0) \in U(1). \quad (8.32)$$

Here, we set $\alpha = \frac{1}{\sqrt{2N}} \vartheta^0$. Furthermore, we choose

$$T_0 = \frac{1}{\sqrt{2N}} \mathbb{1}, \quad (8.33)$$

where $\mathbb{1}$ is the $N \times N$ unit matrix. The remaining generators T_m of Eq. (8.31) form the $\mathfrak{su}(N)$ algebra

$$[T_{m_1}, T_{m_2}]_- = i f^{m_3}_{m_1 m_2} T_{m_3}, \quad \{T_{m_1}, T_{m_2}\}_+ = \frac{1}{N} \delta_{m_1 m_2} \mathbb{1} + d^{m_3}_{m_1 m_2} T_{m_3}, \quad (8.34)$$

where $f^{m_3}_{m_1 m_2}$ and $d^{m_3}_{m_1 m_2}$ are the (anti-)symmetric structure constants of $\mathfrak{su}(N)$. To be consistent with Def. (8.33) we choose the fundamental representation in terms of matrices that fulfill

$$\text{tr}(T_{n_1} T_{n_2}) = \frac{1}{2} \delta_{n_1 n_2}, \quad n_1, n_2 \in \{0, 1, \dots, N^2 - 1\}. \quad (8.35)$$

These are $N \times N$ traceless Hermitian matrices, that are usually chosen in a fashion that generalizes the Pauli and Gell-Mann matrices for $N > 3$. For more details on the group-theoretical aspects we refer to Refs. [516, 19].

According to Noether's theorem, these symmetries come with conservation laws. The conserved current that is associated to the global $U(1)$ symmetry is

$$\mathcal{J}^\mu = \bar{\psi} \gamma^\mu \psi, \quad (8.36)$$

while the conserved current which comes along with the global $U(N)$ symmetry reads

$$\mathcal{J}_m^\mu = \bar{\psi} \gamma^\mu T_m \psi, \quad m \in \{1, \dots, N^2 - 1\}. \quad (8.37)$$

Depending on the context, both are denoted as vector currents. We come back to these currents when we introduce the GN model in medium. For the moment, we turn to the spacetime symmetries.

Translations The GN action (8.1) is invariant under spacetime translations. Here, the (infinitesimal) transformation of the coordinates are as follows,

$$x^\mu \mapsto x'^\mu = x^\mu + a^\mu, \quad x^\mu \mapsto x'^\mu = x^\mu + \delta a^\mu, \quad (8.38)$$

while the spinor conventionally does not transform when moved from one position to the other

$$\psi(x) \mapsto \psi'(x') = \psi(x). \quad (8.39)$$

However, studying the transformation from the same viewpoint in spacetime, one clearly observes the passive transformation of the shifted field

$$\psi(x) \mapsto \psi'(x) = \psi(x) - i\delta a^\mu P_\mu, \quad P_\mu = -i\mathbb{1}\partial_\mu, \quad (8.40)$$

which involves the generator P_μ of translations, that is identical for all types of fields. From Eq. (8.13) we find that the associated conserved current is the energy-momentum tensor

$$\Theta^\mu{}_\nu = \frac{1}{2} [\bar{\psi} i\gamma^\mu (\partial_\nu \psi) - (\partial_\nu \bar{\psi}) i\gamma^\mu \psi] - \delta^\mu_\nu [\bar{\psi} i\rlap{\not{\partial}} \psi + \frac{1}{2N} g^2 (\bar{\psi} \psi)^2]. \quad (8.41)$$

Using the equations of motion it can be shown that its trace vanishes $\Theta^\mu{}_\mu = 0$.

Lorentz transformations Next, we consider the $(1+1)$ -dimensional Lorentz transformation. We start analogous to the well-known higher-dimensional case by specifying the (infinitesimal) transformation law of the coordinates that leaves the line element invariant,

$$x^\mu \mapsto x'^\mu = \Lambda^\mu{}_\nu x^\nu, \quad x^\mu \mapsto x'^\mu = x^\mu + \delta\omega^\mu{}_\nu x^\nu. \quad (8.42)$$

The boost matrix reads

$$\Lambda = (\Lambda^\mu{}_\nu) = \begin{pmatrix} \cosh(\omega) & \sinh(\omega) \\ \sinh(\omega) & \cosh(\omega) \end{pmatrix}, \quad (8.43)$$

where ω is the rapidity. As expected in $1+1$ dimensions, there is only one boost and one boost parameter ω . The intrinsic transformation law of the fermion fields is

$$\psi(x) \mapsto \psi'(x') = S \psi(x), \quad (8.44)$$

and the GN action (8.1) is invariant under boosts if the standard relation

$$S^{-1} \gamma^\mu S = \Lambda^\mu{}_\nu \gamma^\nu \quad (8.45)$$

holds true. Hence the transformation matrix and the generator read

$$S = \exp\left(-\frac{i}{2} \omega^{\mu\nu} I_{\mu\nu}\right), \quad I^{\mu\nu} = \frac{i}{4} [\gamma^\mu, \gamma^\nu]_- = -\frac{i}{2} \gamma^{\text{ch}} \varepsilon^{\mu\nu}. \quad (8.46)$$

where we used Def. (A.9). The two-dimensional tensor $\omega^{\mu\nu}$ is antisymmetric. Thus, we define $\omega \equiv \omega^{12} = -\omega^{21} = \omega_{21} = -\omega_{12}$ and find

$$S = \exp\left(\frac{1}{2} \omega \gamma^{\text{ch}}\right) = \exp\left(\begin{array}{cc} -\frac{\omega}{2} & 0 \\ 0 & \frac{\omega}{2} \end{array}\right) = \begin{pmatrix} e^{-\frac{\omega}{2}} & 0 \\ 0 & e^{\frac{\omega}{2}} \end{pmatrix} \quad (8.47)$$

for boosts of the fermion fields, *cf.* Ref. [501]. This result is rather intuitive. Left-moving fermion fields get exponentially suppressed, while right-moving fields are scaled by an exponential enhancement factor. If the direction of the boost is inverted, $\omega \rightarrow -\omega$, one finds the opposite result.

The infinitesimal transformation law of the spinor is

$$\psi(x) \mapsto \psi'(x) = \psi(x) - \frac{i}{2} \delta\omega^{\mu\nu} M_{\mu\nu} \psi(x), \quad M_{\mu\nu} = i\mathbb{1}(x_\mu \partial_\nu - x_\nu \partial_\mu) + I_{\mu\nu}, \quad (8.48)$$

where we also included the passive transformation which is identical for any type of field (note the different arguments of ψ' in Eqs. (8.44) and (8.48)). Finally, we present the conserved current, the total spin-angular momentum tensor,

$$M^{\mu\alpha\beta} = \Theta^{\mu\alpha} x^\beta - \Theta^{\mu\beta} x^\alpha, \quad (8.49)$$

where $\Theta^{\mu\nu}$ is given by Eq. (8.41). As already anticipated, the contribution from the spin tensor vanishes. This is because the spin tensor is proportional to $\bar{\psi} \{\gamma^\mu, I^{\alpha\beta}\}_+ \psi$, *cf.* Ref. [517], which is zero in $1+1$ dimensions, due to Eqs. (8.46) and (A.14). In conclusion, there is no notion of spin and handedness in a single spatial dimension.

Lorentz transformations in Euclidean spacetime In contrast to the other continuous spacetime symmetries, which are formulated in principle equivalently in a Euclidean space, the Lorentz transformations are fundamentally related to the metric signature of the spacetime. Therefore, a comment on the consequences for Euclidean spacetime is appropriate.

Taking into account the Wick rotation Eq. (8.5), we can rewrite Eq. (8.42) as follows

$$\begin{aligned} \begin{pmatrix} x'_E \\ -i\tau'_E \end{pmatrix} &= \begin{pmatrix} x'_M \\ t'_M \end{pmatrix} = \begin{pmatrix} \cosh(\omega_M) & \sinh(\omega_M) \\ \sinh(\omega_M) & \cosh(\omega_M) \end{pmatrix} \begin{pmatrix} x_M \\ t_M \end{pmatrix} = \\ &= \begin{pmatrix} \cosh(\omega_M) & \sinh(\omega_M) \\ \sinh(\omega_M) & \cosh(\omega_M) \end{pmatrix} \begin{pmatrix} x_E \\ -i\tau_E \end{pmatrix}, \end{aligned} \quad (8.50)$$

where “M” indicates Minkowski and “E” Euclidean quantities. Moving the factor $-i$ to the transformation matrix and defining the Euclidean coordinates $(x_E^\mu) \equiv (x_E, \tau_E)$, we find

$$\begin{pmatrix} x'_E \\ \tau'_E \end{pmatrix} = \begin{pmatrix} \cosh(\omega_M) & -i \sinh(\omega_M) \\ i \sinh(\omega_M) & \cosh(\omega_M) \end{pmatrix} \begin{pmatrix} x_E \\ \tau_E \end{pmatrix} \quad (8.51)$$

However, we also know that rotations instead of boosts are isometric transformations in the Euclidean spacetime, thus transformations

$$\begin{pmatrix} x'_E \\ \tau'_E \end{pmatrix} = \begin{pmatrix} \cos(\omega_E) & \sin(\omega_E) \\ -\sin(\omega_E) & \cos(\omega_E) \end{pmatrix} \begin{pmatrix} x_E \\ \tau_E \end{pmatrix} \quad (8.52)$$

leave the line element invariant. In consequence, we find (up to a parity transformation) the additional relation $\omega_M = i\omega_E$. Inserting this result into Eq. (8.47), the transformation matrix S for the fermion field turns into

$$S = \exp\left(\frac{i}{2} \omega_E \gamma_E^{\text{ch}}\right) = \begin{pmatrix} e^{-\frac{i\omega_E}{2}} & 0 \\ 0 & e^{\frac{i\omega_E}{2}} \end{pmatrix}, \quad (8.53)$$

because $\gamma_M^{\text{ch}} = \gamma_E^{\text{ch}}$ by construction. In total, these are simultaneous $U(1)$ phase transformations of ψ_L and ψ_R with exactly opposite phase.

It is straightforward to check the invariance of the Euclidean action under these transformations.

Scale transformations We can also consider scale transformations. For the coordinates these are

$$x^\mu \mapsto x'^\mu = e^\lambda x^\mu, \quad x^\mu \mapsto x'^\mu = x^\mu + \delta\lambda x^\mu, \quad (8.54)$$

where $(\delta)\lambda$ is the (infinitesimal) scaling parameter. In order to have the free part of the GN action Eq. (8.1) (without the four-fermion interaction term) invariant under this dilatation³, the spinors need to transform as follows under scale transformations,

$$\psi(x) \mapsto \psi'(x') = e^{\lambda \Delta_\psi} \psi(x), \quad \psi(x) \mapsto \psi'(x') = \psi(x) + \delta\lambda \Delta_\psi \psi(x), \quad (8.55)$$

where the scaling dimension has to be

$$\Delta_\psi = -\frac{(d+1)-1}{2}. \quad (8.56)$$

On the other hand, one finds

$$\Delta_\psi = -\frac{d+1}{4}, \quad (8.57)$$

³Note that a scale transformation affects the volume element of the spacetime integral as well as the derivative in the kinetic term in addition to the fermion fields themselves.

if one additionally claims scale invariance of the four-fermion interaction part of the action (8.1). Both requirements are exclusively fulfilled for $d = 1$ with scaling dimension $\Delta_\psi = -\frac{1}{2}$, implying that the GN model is scale-invariant in 1+1 dimensions. Note that the scaling dimension $\Delta_\psi = -\frac{1}{2}$ agrees with the canonical length (inverse energy) dimension of the field, see Eq. (8.3). Viewing the scale transformation from the original non-scaled position in spacetime, we observe

$$\psi(x) \mapsto \psi'(x) = \psi(x) - i\delta\lambda D\psi(x), \quad D = i\mathbf{1}(\Delta_\psi - x^\mu \partial_\mu), \quad (8.58)$$

where D is the generator of dilatations.

Also the scale transformations come with a conserved current [518], which reduces to

$$J^\mu = \Theta^\mu{}_\nu x^\nu. \quad (8.59)$$

where $\Theta^\mu{}_\nu$ is again the stress-energy-momentum tensor from Eq. (8.41).

Special conformal transformations Lastly, there are special conformal transformations. For the coordinates these read,

$$x^\mu \mapsto x'^\mu = \frac{x^\mu + c^\mu x^2}{1 + 2c \cdot x + c^2 x^2}, \quad x^\mu \mapsto x'^\mu = x^\mu + \delta c^\nu (\delta_\nu^\mu x^2 - 2x^\mu x_\nu), \quad (8.60)$$

which leave the Minkowski line-element invariant up to a position-dependent scaling factor. In fact, special conformal transformations are a succession of an inversion, a translation, and another inversion, *i.e.*,

$$\frac{x'^\mu}{x'^2} = \frac{x^\mu}{x^2} + c^\mu. \quad (8.61)$$

Special conformal transformations can also be interpreted in terms of a transformation into an accelerated reference frame [519]. However, it is convenient to discuss special conformal transformations directly for infinitesimal transformations of the fields,

$$\psi(x) \mapsto \psi'(x') = \psi(x) - i\delta c^\mu 2x^\nu (i\Delta_\psi \eta_{\mu\nu} - S_{\mu\nu}) \psi(x). \quad (8.62)$$

(A formal reason is that finite special conformal transformations not necessarily preserve causality.) This transformation leaves the GN action Eq. (8.1) invariant.

Again, if one fixes the viewpoint and includes the passive transformation, one finds

$$\psi(x) \mapsto \psi'(x) = \psi(x) - i\delta c^\mu K_\mu \psi(x), \quad (8.63)$$

where the full generator reads,

$$K_\mu = i(x^2 \partial_\mu - 2x_\mu x^\nu \partial_\nu) + 2x^\nu (i\Delta_\psi \eta_{\mu\nu} - S_{\mu\nu}). \quad (8.64)$$

The corresponding conserved current is

$$K^{\mu\nu} = 2\Theta^{\mu\rho} x_\rho x^\nu - \Theta^{\mu\nu} x^2, \quad (8.65)$$

because the spin tensor $S_{\mu\nu}$ vanishes.

Global conformal symmetry The just discussed continuous global spacetime symmetry transformations effectively form a larger group, *viz.* the global conformal symmetry group and the

generators (8.40), (8.48), (8.58), and (8.64) fulfill the conformal algebra. All non-vanishing commutators of the algebra read [520, 518]

$$[M_{\alpha\beta}, M_{\gamma\delta}]_- = i(\eta_{\beta\gamma} M_{\alpha\delta} + \eta_{\alpha\delta} M_{\beta\gamma} - \eta_{\alpha\gamma} M_{\beta\delta} - \eta_{\beta\delta} M_{\alpha\gamma}), \quad (8.66)$$

$$[P_\alpha, M_{\gamma\delta}]_- = i(\eta_{\alpha\gamma} P_\delta - \eta_{\alpha\delta} P_\gamma), \quad (8.67)$$

$$[K_\alpha, M_{\gamma\delta}]_- = i(\eta_{\alpha\gamma} K_\delta - \eta_{\alpha\delta} K_\gamma), \quad (8.68)$$

$$[D, P_\beta]_- = iP_\beta, \quad (8.69)$$

$$[K_\alpha, P_\beta]_- = 2i(\eta_{\alpha\beta} D - M_{\alpha\beta}), \quad (8.70)$$

$$[D, K_\alpha]_- = -iK_\alpha \quad (8.71)$$

for spacetimes with Minkowski-type metric signature. This algebra is generic for the generators of conformal transformations in any dimension. Indeed, also QCD with massless quarks shows conformal symmetry in the UV. For the special case of 1+1 dimensions the commutation relations (8.66) to (8.68) and (8.70) further simplify, because there is only a single generator for boosts,

$$M_{\alpha\beta} = \varepsilon_{\alpha\beta} L, \quad L = -\frac{1}{2} \varepsilon^{\alpha\beta} M_{\alpha\beta}. \quad (8.72)$$

For these, we find

$$[L, L]_- = 0, \quad [P_\alpha, L]_- = -i\varepsilon_{\alpha\beta} P^\beta, \quad (8.73)$$

$$[K_\alpha, P_\beta]_- = 2i(\eta_{\alpha\beta} D - \varepsilon_{\alpha\beta} L), \quad [K_\alpha, L]_- = -i\varepsilon_{\alpha\beta} K^\beta. \quad (8.74)$$

In general the structure of the global conformal group is as follows. The basis is formed by the subgroup of Lorentz transformations, which consists of rotations (for $d > 1$) and boosts. In connection with spacetime translations, one obtains the Poincaré subgroup, which form the isometries of $(d+1)$ -dimensional Minkowski spacetimes. As soon as one relaxes the requirement for the preservation of length, one can add pure scale transformations to the Poincaré group and one again finds a closed subgroup of the full conformal group. If also scale and/or special conformal transformations are considered as symmetries of a system, exclusively angles and entities that move on the light-cone with worldlines $ds^2 = 0$ are preserved.

Going from Minkowski to Euclidean signature, small modifications of the above algebra are required, due to the changes in the metric. The generic form is almost similar. However, instead of boosts and rotations, there are exclusively rotations.

Interestingly, one finds that the conformal symmetry group of a $(d+1)$ -dimensional spacetime is isomorphic to the $SO(d+1, 1+1)$ symmetry group of a $((d+1) + (1+1))$ -dimensional spacetime with $d+1$ spatial and two temporal directions and Minkowski-type metric signature. Usually a field theory that exhibits conformal symmetry can therefore be formulated as a higher-dimensional field theory that is exclusively Lorentz invariant.

It might therefore be an interesting exercise to repeat some of the calculations of the GN model in this higher-dimensional framework and thereby link the results of the $(1+1)$ -dimensional GN model to a strongly constrained $(2+2)$ -dimensional QFT, respectively $(3+1)$ -dimensional QFT if one starts from Euclidean two-dimensional spacetime. This might also be of interest for the connection of conformal (quantum) field theories and field theories on anti-de Sitter spaces, *i.e.*, the AdS/CFT correspondence, where conformal QFTs in their infinite- N limit are mapped to field

theories in constantly negatively curved spaces.

At this point we also have to comment on another peculiar feature of two-dimensional conformal QFTs. Conformal field theories in 1+1 dimension usually exhibit a local conformal symmetry with infinite-dimensional Witt algebra in addition to the above discussed global conformal symmetry [520]. This is because the conformal Killing equation reduces to the Cauchy-Riemann equations. Thus, all analytic coordinate transformations are Killing vector fields and there are infinitely many. However, two-dimensional conformal field theory is a giant topic on its own and a huge research field, which cannot be addressed in this thesis even though it might be of some relevance. A certainly oversimplified argument why it might be justified to ignore this field of research and their results is that we are mainly interested in in-medium calculations, where external energy scales like the chemical potential and temperature break any kind of conformal symmetry explicitly, as is discussed below.

O(2N) symmetry In addition to the previously discussed continuous symmetries, it was shown in Ref. [282] that the GN model is actually invariant under $O(2N)$ rotations, such that the previously discussed $U(N)$ symmetry emerges from the $O(2N)$ group in terms of a subgroup. To show the invariance of the GN action (8.1) it is useful to follow Ref. [282] and change the basis of γ -matrices from a Weyl to a Majorana basis. We use the matrices

$$S = \begin{pmatrix} i & 0 \\ 0 & 1 \end{pmatrix}, \quad S^\dagger = \begin{pmatrix} -i & 0 \\ 0 & 1 \end{pmatrix}, \quad (8.75)$$

and

$$\gamma_M^\mu = S \gamma_W^\mu S^\dagger, \quad (8.76)$$

to switch the basis. Here, “W” denotes the Weyl and “M” denotes the Majorana basis. We find

$$\gamma_M^1 = \begin{pmatrix} 0 & i \\ i & 0 \end{pmatrix}, \quad \gamma_M^2 = \begin{pmatrix} 0 & i \\ -i & 0 \end{pmatrix}, \quad \gamma_M^{\text{ch}} = \begin{pmatrix} -1 & 0 \\ 0 & 1 \end{pmatrix}, \quad (8.77)$$

The crucial point in switching the representation of gamma matrices is that γ^2 is now anti-symmetric, thus $(\gamma^2)^T = -\gamma^2$, while $(\gamma^1)^T = \gamma^1$ and γ^{ch} keeps its form.

The spinors transform according to

$$\psi_M = S \psi_W, \quad \bar{\psi}_M = \bar{\psi}_W S^\dagger, \quad (8.78)$$

such that the GN action in the Majorana basis has the same shape as in the Weyl basis, although the spinors are different. (For the following arguments we entirely stay in the Majorana basis and we therefore drop the label “M” again.)

In addition to the basis transformation, let us split the spinors in the Majorana basis into real and imaginary parts,

$$\psi = \psi_{\text{Re}} + i\psi_{\text{Im}}, \quad \psi^\dagger = \psi_{\text{Re}}^T - i\psi_{\text{Im}}^T, \quad (8.79)$$

where ψ_{Re} and ψ_{Im} are real-valued two-component fields in Dirac space and N -component fields in color/flavor space.

Rewriting the GN action (8.1) in the Majorana basis in terms of these fields, we find

$$\begin{aligned} \mathcal{S}[\bar{\psi}, \psi] &= \int_{-\infty}^{\infty} d^2x \left[\bar{\psi} i \not{\partial} \psi + \frac{1}{2N} g^2 (\bar{\psi} \psi)^2 \right] = \\ &= \int_{-\infty}^{\infty} d^2x \left[i\psi_{\text{Re}}^T (\mathbf{1} \partial_t + \gamma^{\text{ch}} \partial_x) \psi_{\text{Re}} + i\psi_{\text{Im}}^T (\mathbf{1} \partial_t + \gamma^{\text{ch}} \partial_x) \psi_{\text{Im}} + \right. \\ &\quad \left. + \frac{1}{2N} g^2 (\psi_{\text{Re}}^T \gamma^2 \psi_{\text{Re}} + \psi_{\text{Im}}^T \gamma^2 \psi_{\text{Im}})^2 \right]. \end{aligned} \quad (8.80)$$

Here, we used integration by parts in the kinetic terms as well as that transposing fermion bilinears results in an additional factor of minus one, because fermions are Grassmann numbers. Note that $\mathbb{1}$ and γ^{ch} are invariant under these transpositions, while γ^2 switches its sign.

Now the $O(2N)$ symmetry is apparent, because we can simply merge ψ_{Re} and ψ_{Im} to a single $O(2N)$ vector and observe the usual $\vec{v}^T \cdot \vec{v}$ structure of $O(N)$ -invariant scalar products of Euclidean vectors \vec{v} . In fact, this $O(2N)$ symmetry plays a crucial role in the classification of the (bound) states in the GN model [282] or mappings to related theories [284].

8.1.3. The Gross-Neveu action at non-zero temperature and non-zero chemical potential

So far we discussed the GN model in the Minkowski and Euclidean vacuum. Anyhow, in this thesis we are interested in the in-medium properties of the model at non-zero density and non-zero temperature. Therefore we introduce a matter-anti-matter asymmetry using a chemical potential and compactify the temporal direction to heat up the system.

Chemical potential

To study how an excess of matter over anti-matter (or vice versa) influences the properties of the GN model, one needs to constrain the energy that is required to add another (anti-)matter particle to the system, which is already full of particles of exactly this species, but allow for particle-number fluctuations. The species of particles can be labeled and counted via their quantum numbers, which are in turn linked to conserved charges and currents. A conserved charge that all N fermions have in common is the baryon number, which is associated to the temporal component of the vector current and derived from the $U(1)$ symmetry of the GN action. This is because global $U(1)$ phase transformations are identical for all N fermions and so is their baryon number. Integrating the temporal component of the associated current over spacetime (and implicitly summing over all N fermion species) therefore gives the total particle number (which agrees with the baryon number up to a proportionality constant).

$$N = \int_{-\infty}^{\infty} d^{d+1}x \bar{\psi} \gamma^{d+1} \psi. \quad (8.81)$$

This number is supposed to fluctuate, while we keep the energy per additional particle in the system fixed – the chemical potential μ .

The chemical potential in the partition function On the level of the partition function this is realized as follows. The chemical potential is introduced in terms of a Lagrange multiplier that associates a probability to configurations with particular particle numbers. The possible fluctuations of the particle number are realized by the functional integral over all field configurations. Hence, analogous to conventional partition functions from classical statistical physics we find [521, 522, 523],

$$\begin{aligned} \mathcal{Z}[\bar{\eta}, \eta] &\propto \\ &\propto \int [d\bar{\psi}, d\psi] \exp \left(- \int_{-\infty}^{\infty} d^{d+1}x \left[\bar{\psi} (\not{\partial} - \mu \gamma^{d+1}) \psi - \frac{1}{2N} g^2 (\bar{\psi} \psi)^2 - \bar{\eta} \psi - \bar{\psi} \eta \right] \right). \end{aligned} \quad (8.82)$$

This modification of the partition function has some consequences for the symmetries of the system. Working with a matter-anti-matter asymmetry, $\mu \neq 0$, it is natural that the classical action is no longer invariant under charge conjugation. Exchanging particles and antiparticles corresponds to a mapping of $\mu \mapsto -\mu$. Anyhow, because the definition of (anti-)matter is arbitrary, (at least the absolute values of) all physical observables should be the identical under replacements of $\mu \mapsto -\mu$ in Eq. (8.82). Therefore, w.l.o.g. one can assume $\mu \geq 0$ for practical calculations.

Other symmetries that are explicitly broken by the chemical potential are (Euclidean) Lorentz invariance, scale invariance, and invariance under conformal transformations. The reason is rather simple and understood immediately in Minkowski spacetime. Having a charged ensemble of particles, the charge is perceived as a current from another boosted frame of reference. Formally, the μ -dependent term in (8.82) is simply not Lorentz covariant. The same applies in Euclidean spacetime. The chemical potential also breaks scale invariance and, thereby, automatically conformal invariance [518], because it introduces an explicit external energy scale to the problem and can be viewed as a coupling constant with non-zero energy dimension on the mathematical level.

The Silver-Blaze property Anyhow, introducing μ also comes with a symmetry and some special properties of correlation functions [524, 525]. This is discussed in great detail in Refs. [348, 166] and references therein in the context of FRG. Here, we simply recapitulate some aspects of the discussion from these two references:

Analogous to electrodynamics, one can study local instead of global $U(1)$ phase transformations. More specifically, the transformation

$$\psi \mapsto \psi' = e^{-i\alpha\tau} \psi, \quad \bar{\psi} \mapsto \bar{\psi}' = e^{i\alpha\tau} \bar{\psi}, \quad \mu \mapsto \mu' = \mu + i\alpha, \quad (8.83)$$

leaves the partition function (8.82) invariant, where τ is the Euclidean temporal coordinate and μ transforms like the temporal component of an electromagnetic potential.

Fourier-transforming the action in the partition function (8.82) using the conventions of Appendix A.3 for $T = 0$ and choosing $\alpha = i\mu$, one finds that μ can be completely eliminated from the partition function if one shifts the Euclidean temporal momentum $p^{d+1} \mapsto p'^{d+1} = p^{d+1} + i\mu$. This is possible if \mathcal{Z} is analytic and done by analytic continuation of p^{d+1} to the complex plane. The same holds true for other generating functionals like the Schwinger functional and the effective action as well as the resulting correlation and vertex functions.

The reason why we still observe the chemical potential (at least for certain values) is that the analytic continuation to complex p^{d+1} is restricted to $|p^{d+1}| \leq m$, where m is the pole mass of the lightest state that carries baryon number.

In consequence and simply speaking, one observes that all correlation functions are supposed to be independent of the chemical potential and identical to their (Euclidean) vacuum counterparts as long as μ is smaller than the mass of the lightest particle that carries baryon number.

Strictly speaking this is exclusively valid for $T = 0$, because a complex shift of the Matsubara frequencies in the summation is ill conditioned. This somewhat weird property is named ‘‘Silver-Blaze’’ after a Sherlock Holmes story [524].

Now, one might ask why this is an important constraint rather than an incidental feature. The reason is that practical calculations and especially regularization schemes are required to respect this property at $T = 0$ and $\mu \neq 0$ to deliver correct results for correlation functions. As discussed in detail in the previously mentioned references it is actually not easy to incorporate this constraint without violating other demands for symmetry *etc.*.

Temperature

Next, we introduce temperature. Instead of providing an excessive discussion of the formalities, we present a motivation why temperature is identified with the inverse of the radius of the compactified temporal direction in Euclidean QFTs.⁴ Similar arguments can also be found elsewhere. For further details and technicalities we refer to the literature on thermal QFT, *e.g.*, Refs. [503, 22, 142, 504, 13, 505].

First of all, temperature is an undirected external source of energy, which affects all particles, independent of their specific properties. Secondly, working in a heat bath in equilibrium implies

⁴This motivation explicitly addresses non-experts and students, like I was when I started working on QFT in medium and was confused about the way temperature entered QFTs. Experts can simply skip the discussion.

that there is no longer a global time evolution of the system but only local fluctuations and microscopic processes. Therefore it is reasonable to introduce temperature via a modification of the spacetime manifold, more specifically the temporal direction, because the spatial properties of the spacetime manifold should be identical at $T = 0$ and $T \neq 0$, but adjustments in the temporal direction still affect all particles. The question is how the temporal direction has to be modified. To this end, we recapitulate some quantum mechanics. Studying the Schrödinger equation in an infinite volume, one finds a continuous spectrum, while its solution in a spatial box (or more generally on a compact manifold) results in a discrete spectrum, which stems from the discrete spatial momenta and the finite domain (boundary conditions). Therefore the allowed momenta are proportional to the inverse box size and there is a minimal momentum.

The same mechanism can formally be used to pump thermal energy into a system. Constraining the Euclidean temporal domain of the quantum fields leads to a minimal energy, which is inversely proportional to the size of the domain. Associating this energy with the temperature, one finds that the minimal energy of the fields is set by their thermal fluctuations, which is reasonable. Therefore we can identify the temperature with the inverse of the temporal box size (up to additional constants). It remains to specify the exact compactification.

If we really introduce a temporal box into a QFT, we need appropriate boundary conditions for the quantum fields and/or their derivatives. However, this leads to artificial “scattering” of the fields with the domain walls. Another option are (anti-)periodic boundary conditions of a compact temporal domain, so that the entire spacetime manifold turns into a $(d + 1)$ -dimensional cylinder of infinite length. Here, the fields are exclusively self-interacting, which is rather natural, if one thinks of a thermodynamic ensemble. The rate of scatterings, hence the amount of thermal fluctuations is of course proportional to the radius of the cylinder, *viz.* proportional to the inverse temperature (small radius = many thermal fluctuations; large radius = little thermal fluctuations).

A final argument which underpins this identification is as follows. Assume we wished to experimentally measure some observable in an ensemble at high temperature. Due to the huge number of thermal fluctuations we only have to wait for a short time until we obtain a reasonable expectation value for the observable from our measurement. On the other hand, for a system at very low temperature, the rate of fluctuations is small, which entails a long measuring time to obtain a reliable average value for the observable. Hence, it is sensible to identify inverse (measurement) time with temperature.

Formally, these arguments result in the simple replacement

$$\int_{-\infty}^{\infty} d^{d+1}x \mapsto \int_{-\infty}^{\infty} d^d x \int_0^{\beta=\frac{1}{T}} d\tau \quad (8.84)$$

for the spacetime integration of the action, where β is the inverse temperature and associated with the radius of the cylinder. Additionally, we enforce periodic boundary conditions for bosons and anti-periodic boundary conditions for fermions. The reason for this choice is simple. Consider a two-point function $\langle \Phi(\tau \neq 0, \vec{x}) \Phi(0, \vec{x}) \rangle$ of two generic fields and study the substitution $\tau \mapsto \tau + \beta$. This moves the first particle exactly once around the cylinder. Thereby it passes the second particle, which results in a minus sign, if the fields are Grassmann-valued. Hence, in order to have generically non-vanishing two-point functions – which is a reasonable assumption – we should establish the above (anti-)periodic boundary conditions for (fermions) bosons.

In total, we find that the GN partition function and action at non-zero T and non-zero μ are generalized to

$$\mathcal{Z}[\bar{\eta}, \eta] \propto \int [d\bar{\psi}, d\psi] e^{-\mathcal{S}[\bar{\psi}, \psi] + \int_{-\infty}^{\infty} d^d x \int_0^{\beta} d\tau (\bar{\eta} \psi + \bar{\psi} \eta)}, \quad (8.85)$$

$$\mathcal{S}[\bar{\psi}, \psi] = \int_{-\infty}^{\infty} d^d x \int_0^{\beta} d\tau [\bar{\psi} (\not{\partial} - \mu \gamma^{d+1}) \psi - \frac{1}{2N} g^2 (\bar{\psi} \psi)^2], \quad (8.86)$$

which is the QFT analogue of the grand canonical ensemble.

Finally some remarks are in order.

1. In Fourier space these adjustments lead to so-called discrete Matsubara frequencies for the temporal Euclidean momenta and corresponding momentum integrals are replaced by Matsubara sums. Details can be found in Refs. [503, 22, 142, 504, 13, 505], while we present our conventions in Appendices A.3 and B.
2. The introduction of temperature (already at $\mu = 0$) naturally breaks symmetries of the vacuum theory. Most obvious is again the explicit breaking of scale and conformal invariance due to the explicit external energy scale. In addition, one loses invariance under (Euclidean) boosts, while invariance under purely spatial rotations is still preserved in $d > 1$, where these exist. Furthermore, invariance under translations along the temporal directions is reduced to translational invariance with periodicity. Also time-reversal symmetry is lost.
3. Having introduced the compactification it has to be checked that for $T \rightarrow 0$, hence $\beta \rightarrow \infty$ the vacuum results as well as its symmetries are recovered. In fact, shifting $\tau \mapsto \tau' + \frac{\beta}{2}$ and sending $\beta \rightarrow \infty$ restores the vacuum theory and a continuum of Euclidean temporal momenta.
4. To be honest, this rather sloppy introduction of temperature, which is easily outperformed by textbooks and publications, is dangerous and actually more care should be taken, if one starts manipulating the spacetime manifold of a QFT. The reason is that fields are directly tied to the representations of the spacetime symmetry groups, such that it is a priori not obvious that objects like gamma matrices on a cylinder are identical to those in a non-compact Euclidean vacuum. The same applies in particular to fermions themselves. However, a mathematically rigorous discussion is beyond the scope of this work and fortunately it turns out that our heuristic arguments seem to be mathematically justified [507]. The underlying reason why we are not confronted with more fundamental problems by switching our spacetime to a cylinder traces back to the fact that a cylinder is still a flat spacetime with a metric identical to a Euclidean space, if certain quantities are rescaled by the cylinder radius, *cf.* Ref. [4, App.]

8.2. The bosonized Gross-Neveu and Gross-Neveu-Yukawa model

In order to study condensation effects in a four-fermion theory one of the standard techniques which was already used by D. Gross and A. Neveu [158] is to partially bosonize the model. For the Gross-Neveu model this means that the purely fermionic GN model is mapped onto the so-called bGN model – a model of the same fermions, which additionally involves an “ultra-massive” scalar constraint field in the UV, that turns dynamical in the IR. Here, we formally derive the relation between the GN model and bGN model. Afterwards we briefly comment on the consequences of the bosonization for the symmetries of the purely fermionic theory.

8.2.1. Bosonization – Hubbard-Stratonovich transformation

For the sake of simplicity we demonstrate the bosonization in the Euclidean vacuum and study the partition function (8.11). We also ignore all types of source terms, which can be reintroduced after bosonization. The generalization to non-zero μ and T is straightforward. Within the next lines we follow our own presentation of Ref. [4, App. B].

Bosonization of the partition function

The bosonization is performed by a so-called Hubbard-Stratonovich transformation [399, 398], where the Gaussian partition function of an auxiliary/constraint field $\xi = \xi(x)$,

$$1 = \# \int [d\xi] e^{-\int_{-\infty}^{\infty} d^{d+1}x \frac{1}{2} \xi^2}, \quad (8.87)$$

is introduced. We choose $\#$ as suitable normalization factor such that the r.h.s. evaluates to one. This identity is inserted into the original partition function (8.11) as follows,

$$\begin{aligned} \mathcal{Z} &\propto \int [d\bar{\psi}, d\psi] \exp\left(-\int_{-\infty}^{\infty} d^{d+1}x [\bar{\psi} \not{\partial} \psi - \frac{1}{2N} g^2 (\bar{\psi} \psi)^2]\right) = \\ &= \int [d\xi, d\bar{\psi}, d\psi] \exp\left(-\int_{-\infty}^{\infty} d^{d+1}x [\bar{\psi} \not{\partial} \psi - \frac{1}{2N} g^2 (\bar{\psi} \psi)^2 + \frac{1}{2} \xi^2]\right), \end{aligned} \quad (8.88)$$

which does not modify the theory. The actual trick is to shift the newly introduced integral over the auxiliary-field configurations by the fermion bilinear $\bar{\psi} \psi$, thus to substitute,

$$\xi = \frac{h}{g} \phi + \frac{g}{\sqrt{N}} \bar{\psi} \psi. \quad (8.89)$$

The resulting partition function and classical action for the bosonized model reads

$$\mathcal{Z} \propto \int [d\phi, d\bar{\psi}, d\psi] e^{-\mathcal{S}[\phi, \bar{\psi}, \psi]}, \quad (8.90)$$

$$\mathcal{S}[\phi, \bar{\psi}, \psi] = \int_{-\infty}^{\infty} d^{d+1}x [\bar{\psi} (\not{\partial} + \frac{1}{\sqrt{N}} h \phi) \psi + \frac{1}{2g^2} h^2 \phi^2], \quad (8.91)$$

where the four-fermion interaction was traded for a Yukawa-type interaction of the fermions with a static massive bosonic field. The factor h , the Yukawa coupling, is introduced because of the following reason. Thinking in terms of an RG flow, the theory will also dynamically generate a kinetic term for the bosons $\sim (\partial_\mu \phi)^2$. To have a dimensionless coefficient in front of this term, namely the bosonic wave-function renormalization, the bosonic field ϕ has to take its canonical energy dimension, *i.e.*,

$$[\phi] = \text{energy}^{\frac{(d+1)-2}{2}}. \quad (8.92)$$

On the other hand, the original constraint field ξ has by definition energy dimension $\frac{d+1}{2}$. This mismatch needs to be compensated by the introduction of the Yukawa coupling, which has dimension

$$[h] = \text{energy}^{\frac{4-(d+1)}{2}}. \quad (8.93)$$

This also ensures that the entire Yukawa-interaction term has the correct energy dimension.

Note that in conventional infinite- N calculations fluctuations of the bosons are suppressed, such that it is oftentimes practical to absorb the Yukawa coupling in the bosonic field. Contrarily, in this thesis we are ultimately interested in a distinct RG-scale evolution of the bosonic wave-function renormalization, the Yukawa coupling, and all local bosonic self-interaction terms, such that it is reasonable to stick to the canonical energy dimensions of the fields.

In total we turned a purely fermionic theory with local fermion-fermion scattering into a theory where fermion-scattering is mediated by the exchange of a massive scalar particle. Due to the absence of propagation of the boson on the level of the classical action (in the UV) the exchange of the scalar particle is basically “ultra-massive”, thus point-like. This visualizes the agreement of both theories.

Correlation functions

Next, let us briefly comment on the implications of the Hubbard-Stratonovich transformation of correlation functions. In the purely fermionic GN model it was only possible to calculate correlation functions of fermion fields. This is different on the level of Eq. (8.90), where the study of purely bosonic or mixed expectation values is possible. However, these new types of correlation functions are not independent from those from which they originate, that exclusively consist of fermion fields, and there are direct relations between them. These relations could be denoted as Ward-Takahashi identities. In fact, there is a one-to-one mapping. For a detailed derivation of several such identities we refer to Ref. [526, Sec. 1.3.1]. Here, we merely sketch the strategy and present the relation between the expectation value of the scalar field and the fermion-anti-fermion correlation function, which is of relevance for this work and also presented in Ref. [526, Sec. 1.3.1].

Consider an infinitesimal shift

$$\phi(x) \mapsto \phi'(x) = \phi(x) + \delta\phi(x) \quad (8.94)$$

of the bosonic field in Eq. (8.90). In the partition function (8.90) are integrating over all bosonic field configurations including all values of the field, so that this shift is supposed to leave the theory invariant. If we ignore terms of order $\mathcal{O}(\delta\phi^2)$, we find

$$\begin{aligned} \mathcal{Z}' &= \mathcal{Z} - \int [d\phi, d\bar{\psi}, d\psi] \left(\int d^{d+1}x h \delta\phi \left(\frac{1}{\sqrt{N}} \bar{\psi} \psi + \frac{1}{g^2} h \phi \right) \right) e^{-\mathcal{S}[\phi, \bar{\psi}, \psi]} = \\ &= \mathcal{Z} - \int d^{d+1}x h \delta\phi \left(\frac{1}{\sqrt{N}} \langle \bar{\psi} \psi \rangle + \frac{1}{g^2} h \langle \phi \rangle \right), \end{aligned} \quad (8.95)$$

The infinitesimal shift is arbitrary and therefore the integrand in the last line has to vanish to have $\mathcal{Z}' = \mathcal{Z}$. It follows, that

$$\frac{1}{\sqrt{N}} \langle \bar{\psi} \psi \rangle = -\frac{1}{g^2} h \langle \phi \rangle. \quad (8.96)$$

This is an identity between the fermion-anti-fermion correlation function and the expectation value of the scalar field.

An equivalent relation is obtained on the level of the (classical) UV fields from the equations of motion of the classical action $\mathcal{S}[\phi, \bar{\psi}, \psi]$ of Eq. (8.91).

We conclude that it is sufficient to study certain bosonic correlation functions to gain information about the full theory.

The generating functional of the bGN model at non-zero μ and T

Lastly, we provide the final expression for the partition function and generating functional at non-zero μ and T , which sets the basis for most of our calculations. (Re)introducing the source fields, the resulting generating functional is,

$$\begin{aligned} \mathcal{Z}[J, \bar{\eta}, \eta] &\propto \int [d\phi, d\bar{\psi}, d\psi] \exp \left(- \int_{-\infty}^{\infty} d^d x \int_0^{\beta} d\tau [\bar{\psi} (\not{\partial} - \mu \gamma^{d+1} + \frac{1}{\sqrt{N}} h \phi) \psi \right. \\ &\quad \left. + \frac{1}{2g^2} h^2 \phi^2 - J \phi - \bar{\eta} \psi - \bar{\psi} \eta] \right), \end{aligned} \quad (8.97)$$

where we introduced the chemical potential and the temperature along the lines of the purely fermionic discussion. The classical action that corresponds to this bGN model in medium with a non-dynamic boson field is

$$\mathcal{S}[\phi, \bar{\psi}, \psi] = \int_{-\infty}^{\infty} d^d x \int_0^{\beta} d\tau [\bar{\psi} (\not{\partial} - \mu \gamma^{d+1} + \frac{1}{\sqrt{N}} h \phi) \psi + \frac{1}{2g^2} h^2 \phi^2]. \quad (8.98)$$

8.2.2. The bosonized Gross-Neveu model and the Gross-Neveu-Yukawa model

So far, two absolutely equivalent formulations of the same theory have been introduced. To distinguish both formulations, we strictly denote the purely fermionic formulation (8.86) as the GN model and the bosonized version (8.98) as the bGN model. Anyhow, during this thesis, we will need yet another model, which is closely related to the latter models, namely the GNY model. The only difference to the bGN model is the by-hand introduction of the standard kinetic term for the bosons already in the classical UV action. As already anticipated before, this term is generated during RG flows in any case, though it is a clear modification of the UV theory. Until today there is an ongoing debate whether the by-hand introduction of the kinetic term of the bosons manifestly alters the IR vertex functions and observables [400, 401, 378, 177]. For the moment, we postpone this discussion to later chapters and only define what we denote as the GNY model, namely the classical action

$$\mathcal{S}[\phi, \bar{\psi}, \psi] = \int_{-\infty}^{\infty} d^d x \int_0^{\beta} d\tau [\bar{\psi} (\not{\partial} - \mu \gamma^{d+1} + \frac{1}{\sqrt{N}} h \phi) \psi - \frac{1}{2} \phi (\square \phi) + \frac{1}{2g^2} h^2 \phi^2], \quad (8.99)$$

where \square is the Euclidean d'Alembert operator – a Laplace operator.

8.2.3. Symmetries of the bosonized GN and GNY model

Before we end the formal introduction of the QFTs which are discussed in this thesis we briefly return to some symmetry considerations. The question that is addressed within the next lines is how the symmetries of the GN model translate to the bGN and GNY model. For this purpose, we again focus on the theories at $\mu = 0$ and $T = 0$ but stick to Euclidean spacetime. In contrast to the GN model we abstain from explicitly presenting conserved currents.

Discrete chiral symmetry

Considering the transformation law for the fermion fields under discrete chiral transformations, Eqs. (8.19) and (8.20), as well as the relation between the expectation value of the boson field and the fermion two-point correlation function (8.96) (or its classical analogue), we find that the boson field transforms as follows,

$$\phi(x) \mapsto \phi'(x) = -\phi(x), \quad (8.100)$$

which leaves the classical actions of the bGN and GNY model invariant and better explains the denotation (discrete chiral) \mathbb{Z}_2 symmetry.

However, Eq. (8.96) also implies that a non-vanishing expectation value of the bosonic field, thus a non-trivial ground state, signals the breaking of discrete chiral symmetry. This is reasonable because the Yukawa interaction term then acts like an effective fermion mass term (with fixed $h \phi$), which leads to an interaction of left- and right-moving fermions that breaks the symmetry,

$$\bar{\psi} \frac{1}{\sqrt{N}} h \phi \psi = \frac{1}{\sqrt{N}} h \phi (\psi_{\text{R}}^{\dagger} \psi_{\text{L}} + \psi_{\text{L}}^{\dagger} \psi_{\text{R}}). \quad (8.101)$$

Discrete chiral symmetry on the level of the classical microscopic UV action is not altered at non-zero μ and non-zero T .

CPT transformations

The fermion bilinear $\bar{\psi} \psi$ and therefore also the scalar field ϕ transform trivially under separate and consecutive C, P, and T transformation. Therefore the bGN and GNY models are C, P, and T invariant. (This is consistent with the fact that the ground state of the vacuum GN model is given by $\bar{\psi} \psi$ condensation, thus a non-trivial expectation value (8.96). Generally, the vacuum state has to be CPT-invariant if CPT symmetry is not explicitly broken in the classical action.) Introducing non-zero μ or T , we are confronted with the same explicit breaking of CPT invariance as for the GN model, see above.

Continuous symmetries

$U(N)$ symmetry From $\phi \sim \bar{\psi}\psi$, which holds classically or on the level of the expectation values, it is directly deduced that the scalar field transforms trivially under global $U(N)$ transformations (8.30) and the bGN and GNY model are still invariant under global $U(N)$ transformations, also at non-zero μ and non-zero T .

Poincaré transformations The denotation “scalar field” already refers to the trivial representation of the Lorentz group. Using $\phi \sim \bar{\psi}\psi$ it follows from the transformation laws of the spinor fields (8.39) and (8.44) that indeed

$$\phi(x) \mapsto \phi'(x') = \phi(x), \quad (8.102)$$

for translations and Lorentz transformations (as well as rotations in Euclidean spacetime). Note that one still experiences the passive transformations of the scalar fields with generators $P_\mu = -i\partial_\mu$ and $M_{\mu\nu} = i(x_\mu\partial_\nu - x_\nu\partial_\mu)$ as for any field, if one does not transform the observation point.

In consequence, the bGN and GNY model are invariant under (Euclidean) Poincaré transformations, while $\mu \neq 0$ and $T \neq 0$ still break this symmetry as discussed before.

Scale and special conformal transformations To figure out how the scalar field is supposed to transform under scale transformation, one might be tempted to use again

$$\frac{1}{\sqrt{N}} \bar{\psi}\psi = -\frac{1}{g^2} h \phi. \quad (8.103)$$

However, h has non-zero energy dimension, such that we should not conclude the scaling dimension from this equation and the transformation law of the fermions (8.55) alone.

Moreover, we should take into account that a kinetic term for the bosons

$$\int d^{d+1}x \frac{1}{2} (\partial_\mu \phi)^2 \quad (8.104)$$

is supposed to have a dimensionless coefficient, which entails

$$\phi(x) \mapsto \phi'(x') = e^{\lambda \Delta_\phi} \phi(x), \quad (8.105)$$

where

$$\Delta_\phi = -\frac{(d+1)-2}{2}, \quad (8.106)$$

which is the canonical length (inverse energy) dimension of the scalar field and the natural scaling dimension for scalar bosons. In $d = 1$ we find $\Delta_\phi = 0$, implying that the scalar field does not scale at all.

In consequence, studying the Yukawa interaction term in the bGN and GNY models, the Yukawa coupling needs to scale like

$$h \mapsto h' = e^{\lambda \frac{(d+1)-4}{2}} h, \quad (8.107)$$

to have a scale-invariant theory. On the level of the classical action the Yukawa coupling does not scale, which means that exclusively in $d = 3$ dimensions this interaction term is scale-invariant and scale invariance is broken in $d = 1$ dimension. Inspecting the classical equation of motion (8.103) of the bGN model or the respective equation for the expectation values (8.96), we find that scale invariance is actually broken in any dimension. One can also argue similarly for the mass term of the bosons $\sim \phi^2$. One finds that also this term breaks scale invariance in $d = 1$ dimension.

The breaking of scale invariance automatically entails breaking of conformal invariance [518] and the Yukawa coupling naturally introduces a mass scale, which is anyhow required for renormalization. This emergence of an energy scale in a scale-invariant theory can already be interpreted as a first sign of dimensional transmutation.

$O(2N)$ **symmetry** Again we can conclude from $\phi \sim \bar{\psi}\psi$ that the scalar fields transform trivially and that the bGN and GNY model are invariant under the $O(2N)$ transformations. This is seen best from the four-fermion interaction in Eq. (8.80), which contains the $O(2N)$ -invariant fermion bilinears $\bar{\psi}\psi$.

Chapter 9

The (one-loop) β -function of the four-fermion coupling in the GN model in medium

Abstract In this chapter we study the (one-loop) β -function of the momentum-independent four-fermion coupling in the purely fermionic GN model. We derive and discuss explicit expressions for the renormalized four-fermion coupling at (non-)zero temperature and (non-)chemical potential within different approximations.

Based on these results we present “phase diagrams” for the purely fermionic GN model, by identifying regions of finite or diverging renormalized IR four-fermion coupling in the μ - T -plane. We determine the dependence of the size and shape of these regions on the number N of fermions as well as the external fermion energies that enter the corresponding loop diagrams via the lowest Matsubara modes.

We work in the FRG framework, which allows for a non-perturbative treatment in any number of spacetime dimensions. Additionally, it keeps the calculations structured and as close as possible to later investigations of the bGN and GNY model. In analogy to common mean-field (MF) studies and to avoid a violation of the Silver-Blaze property, we work with one-dimensional Litim type regulators, which exclusively regulate the spatial loop momenta but lead to other shortcomings, which will be discussed.

Disclosure This chapter shares several similarities with Refs. [527, 346, 528, 347, 348, 350, 351, 355], which also study the “phase structure” of models with four-fermion interactions by analyzing the resonant (diverging) four-fermion interaction channels. It is a technique that is also common in theoretical condensed-matter physics [529, 530]. In fact, our work is much more simplistic than these publications, because we are only analyzing a single scalar channel. Hence, on a conceptual level the approach is not original to this work and is in parts contained in the above references by reducing their work to the one-channel approximation and two spacetime dimensions. In consequence the presentation of this topic was primarily planned as an introduction and motivation for condensation and bosonization.

However, while working out the details of the calculation we found that there are still open questions and subtle issues, which seem to be unresolved in the literature. These are related to the evaluation points of the external fermion lines in the corresponding loop diagrams in Matsubara frequency space – especially at finite N . Depending on the choice of the Matsubara modes at which the β -function is evaluated in medium, the β -function is altered drastically and can even gain complex contributions. This is a well-known phenomenon for generic FRG/loop calculations of fermionic correlation functions, *cf.* Refs. [531, 66, 275]. By reducing the problem of four-fermion flows to the one-channel approximation – the GN model – we incidentally discovered how one might treat these complex contributions correctly. To the best of our knowledge this discussion is new,

complements existing literature, and could influence future investigations that are based on flow equations which include Feynman diagrams with external fermion lines.

9.1. Motivation and introduction

One issue from our list of research questions in Section 7.1.3 is whether there is condensation and symmetry breaking in the GN model at finite N . Another one concerns the influence of different approximation schemes on the answer to this question.

Concerning these two questions the most natural approach is, to start investigating the most simplistic approximation scheme which one can think of. In QFT this is usually the analysis of the (perturbative) one-loop corrections to the microscopic classical action, which of course only provides a rough idea of the true IR physics. For the GN model this implies that it is reasonable to start with the original purely fermionic formulation and calculate the β -function of the four-fermion coupling and the scale evolution of the coupling itself as well as other possible corrections, *e.g.*, to the kinetic term – the wave-function renormalization.

In vacuum, this is a standard QFT textbook exercise [19, 422] and also the derivation of higher-order loop corrections is rather tedious work than conceptually complicated, see also Refs. of Section 7.2.1. However, as we will see below, performing these calculations in medium leads to additional difficulties, already on the level of the first-order correction. These problems are all related to the occurrence of external fermion lines in the corresponding loop diagrams, which can cause complex contributions to the β -function(s) at non-zero μ and non-zero T . Maybe this also explains why a lot of authors in high-energy physics prefer to work in the partially bosonized framework, while those works that are based on a direct calculation of the four-fermion interactions cannot resolve this issue and usually need to construct workarounds. We hope that this chapter might contribute to a better understanding of these technical issues, which is also the reason why we decided to present the calculations in great detail.

The question that was not addressed so far is how we can extract information about the phase structure of the GN model from the β -function and the RG flow of the four-fermion coupling. The argument is as follows: In those regions of the phase diagram where the four-fermion interaction is attractive and strong, we expect (at least temporarily for certain RG scales) the formation of a $\bar{\psi}\psi$ condensate, *i.e.*, a non-trivial expectation value (8.96). This is associated with a diverging four-fermion coupling in the IR, which signals strong attraction of fermions and anti-fermions and the change of the relevant degrees of freedom to bound states of the latter. In regions of the phase diagram where the four-fermion coupling stays finite in the IR condensation is generally not excluded, but more unlikely.

In total, the study of the μ - T -plane via the four-fermion coupling yields a first rough picture of the phase structure, but is inconclusive, because the dynamics of possibly formed $\bar{\psi}\psi$ states *etc.* is not incorporated in the description. In parts, this drawback can be compensated by also resolving the non-trivial momentum structure of the four-fermion coupling and the generation of additional four-fermion channels, which is ignored in this work.

We will start our discussion by setting up the FRG framework for the GN model in medium. This includes a presentation of our minimalist truncation and the choice of regulator as well as the flow equations (the β -functions). We continue by checking consistency of our flow equation with established vacuum results. Afterwards we turn to our in-medium evaluation of the β -function, where we discuss results for infinite and finite N and different strategies for evaluating external fermion lines.

9.2. The Gross-Neveu model in the FRG formalism

We start our discussion by deriving the β -function of the GN model in the FRG formalism. In this section we do not repeat the details of the FRG approach to QFT and the details of the calculations. For this purpose and for readers who are not familiar with the FRG we prepared multiple comprehensive appendices, which contain every single detail of the calculations.¹ Furthermore, we refer to Part I of this thesis or introductory literature and reviews on the FRG, *e.g.*, Refs. [53, 54, 55, 56, 57, 100, 13, 35, 1, 58].

In this section, we shall simply present the ansatz and initial condition for the effective average action that needs to be specified for FRG calculations. It defines an approximation and effectively presents a truncation of the (infinite) tower of coupled ODEs for the running couplings which is derived from the ERG equation, see Appendix C.2.4.

Furthermore, we briefly discuss the regulator that is used throughout this work. The regulator is an essential ingredient for all FRG calculations, but usually comes with some “trouble”, since it modifies the original theory in one or the other way.

We close the section by providing and discussing some aspects of the β -function of the four-fermion coupling, which is obtained from the FRG calculation.

The explicit integration, renormalization, and analysis of the β -function is set aside for the following sections.

9.2.1. The ansatz for the effective average action

The starting point of every FRG calculation is the ansatz for the effective average action. First of all, the ansatz has to be consistent with the microscopic UV action that specifies the model or theory at some UV energy scale k_{UV} . It simply has to have the same shape at k_{UV} as the action that enters the partition function, *cf.* Appendix C.2.3 or Section 4.2.2. In our case, this is the original action of the GN model at non-zero μ and non-zero T , thus Eq. (8.85).

Additionally, an effective action contains all kinds of terms that are in accordance with the (UV) symmetries of the model or theory [54, 57, 18].² As it is not possible to incorporate all of them, one has to decide which of the possible interaction terms are taken into account and on top of that which are considered to be scale-dependent. This decision forms a truncation.

Here, we consider the following ansatz for the effective average action,

$$\bar{\Gamma}_t[\bar{\psi}, \psi] = \int_{-\infty}^{\infty} d^d x \int_0^{\beta} d\tau [\bar{\psi} Z_{\psi}(t) (\not{\partial} - \mu \gamma^{d+1}) \psi - \frac{1}{2N} g^2(t) (\bar{\psi} \psi)^2]. \quad (9.1)$$

It comprises a scale-dependent wave-function renormalization $Z_{\psi}(t)$. Also the four-fermion coupling in the scalar channel $g^2(t)$ is considered to be scale-dependent. Instead of the RG scale k , we used the RG time t to indicate the scale dependence, which is defined in Appendix D.1. At the UV initial scale k_{UV} we choose $Z_{\psi}(t=0) = 1$ and $g^2(t=0) = g_{UV}^2$ to recover the classical action (8.85).

Our ansatz (9.1) is simplistic, but contains already a rather rich phenomenology as is discussed below. However, we should list what is ignored by the ansatz (9.1):

1. The ansatz does not take into account that other four-fermion interaction channels could be dynamically generated during the scale evolution to the IR, which is usually the case – at least at finite N , *cf.* Refs. [348, 350, 351, 355].

¹Appendix C introduces the field-space formalism and DeWitt notation. It includes a derivation of the ERG equation in this formalism for arbitrary QFTs and provides details on the generic calculation of flow equations for vertex functions. In Appendix D we record our conventions for the RG scale and RG time and their interrelation. Furthermore, multiple (integral) identities for the bosonic and fermionic Litim-regulator shape functions are listed and derived. We also introduce shorthand notations for bosonic and fermionic propagators and integral identities for these objects, which are oftentimes called threshold functions in the FRG literature. Ultimately, in Appendix E we provide a detailed derivation of the flow equations of the GN and GNY model.

²Note that these are not only the symmetries of the classical action, but the symmetries of the partition function, which makes a huge difference for gauge theories or theories with anomalies *etc.*

2. Higher-order and momentum-dependent fermion interactions are not taken into account.
3. Higher-order momentum dependences are not considered in the kinetic term. Therefore the ansatz (9.1) can be considered as the lowest order of a derivative expansion.
4. A splitting of the scale-dependent quantities into parts which are parallel and perpendicular to the heat bath is not taken into account by our truncation.

These are crucial restrictions and they all limit the predictability of the model. Still, our ansatz is a reasonable approach and good starting point for a first understanding of the phase structure. During the discussion of this chapter, we return to these assumptions and explain which limitations are related to the latter.

9.2.2. A necessary evil – the choice of the regulator

Handling infinities in QFTs usually calls for some regularization and renormalization scheme. The FRG is overall a framework for the structured regularization of divergences and the renormalization of vertices via a smooth transition between the UV and IR regime to ultimately calculate IR observables.

This regularization is basically done by introducing an RG scale and a possibly momentum-dependent mass-like term in the partition function – the regulator, which has to fulfill certain properties, see Appendix C.2.1 for details. Still, there is some freedom and the particular construction or choice of the regulator is up to the user and should be adopted to the specific problem at hand. Broadly speaking, it is most important that the regulator has a suitable UV behavior that can be matched with the microscopic description and that it indeed acts as an IR regularization. In addition, the regulator is supposed to be local in momentum space and it should not violate any symmetries of the theory. (In the context of this work the symmetries are those discussed in Sections 8.1.2 and 8.2.3.) Again we refer to Appendix C.2.1 and for example Refs. [273, 162, 163, 532, 165, 348, 166, 167, 533] for further details on regulators and abstain from going into great detail here.

In an ideal world where we could solve the ERG equation without a truncation, like for the zero-dimensional models in Part I or the $O(N)$ model in the infinite- N limit, where the LPA truncation is exact [74, 77], the specific choice of the regulator does not influence the results in the IR by construction, as long as the above specifications are fulfilled. This is the case even though the (unphysical) RG flows between the UV and the IR through theory space (the space of all couplings) may look totally different for different regulators. However, the picture drastically changes if one works with truncations of the ERG equation, which is almost always required to do computations at all. Here, different regulators, although they might all fulfill the regulator specifications of Appendix C.2.1, can lead to different results in the IR. This is certainly the case for the FRG calculations in Part II of this work.

On top of that it is sometimes practical or simply not possible to circumvent the breaking of symmetries or a violation for some requirements for the regulator, because there are usually competing demands and properties, see Ref. [167, Fig. 1] for a sketch. For sure it is not by chance that this is oftentimes the case for models and physical situations where also the application of other technical and mathematical methods are getting doubtful or cause great challenges, *e.g.*, in calculations at moderate chemical potentials and low temperatures or in calculations where the preservation of gauge invariance is required.

To make a long story short: Also within this work and the related publication [4] we fall back to a regulator that violates more requirements than presumably necessary. We simply traded a loss of accuracy for practicability of the calculations, which is explained in a moment.

To be precise, we use a regulator that belongs to the class of so-called dimensionally reduced regulators. These types of regulators exclusively work on the spatial momenta, but do not affect the Matsubara frequencies at all. The direct consequence is that the regulator is no longer local in Euclidean momentum space, but takes into account Matsubara modes of all orders at any RG

scale k . Recently, this peculiarity was related to the so-called “back-bending phenomenon” in the quark-meson model [533]. A similar phenomenon is observed in Fig. 12.17 in Section 12.4 at non-zero RG scales k . However, this discussion is beyond the scope of this work and we comment on this elsewhere.

In addition, this class of regulators breaks Poincaré invariance of the theory. At large non-zero T and non-zero μ this might be of minor importance, because Poincaré invariance is strongly broken anyhow. However, close to the vacuum ($T \simeq \mu \simeq 0$) such regulators will surely alter results quantitatively. Hence, one has to exercise caution w.r.t. quantitative predictions, which is why we sometimes wonder about the finetuning of parameters to reproduce experimental data, while predictions are altered anyhow if the truncation is improved or the type of regulator is changed. The reason why we still use this type of regulator is that the Matsubara sums in the loops become completely independent of the regulator and are easily evaluated. In addition, purely spatial regulators straightforwardly ensure that the Silver-Blaze property is not violated in the limit $T \rightarrow 0$, because the temporal momenta are not touched by the regulator at all.

A less important reason in using these type of regulators is the direct comparability of calculations in the FRG formalism in and beyond the infinite- N limit with conventional infinite- N calculations for the GN model, which commonly rely on an exclusive regularization of spatial momenta.

Moreover, we choose the Litim (flat) regulator for the spatial momenta. Also here, the reason is mainly driven by practical considerations. Using Litim regulators it is usually possible to evaluate the remaining loop integration over spatial momenta by pen-and-paper calculation. Together with the complete evaluation of Matsubara sums this results in expressions for RG flow equations that are PDEs instead of partial-integro-differential equations. This turned out to be a big advantage for a first structured analysis of the fluid-dynamical properties of the RG flow equations and the classification of the single contributions along the lines of Part I.

Also note: The role, which is played by flat regulator w.r.t. to optimization of RG trajectories, see Refs. [162, 163, 165], was not of any relevance for our choice and we strongly believe that this aspect is oftentimes used as a superficial reason in some FRG literature to justify the use of the Litim regulator, while the actual reason is similar to ours: manageability and simplification of the equations. This does by no means imply that there is anything wrong about its use. However, one has to keep in mind, that for advanced truncations like derivative expansions $\mathcal{O}(\partial^4)$ or larger, like in Refs. [64, 65, 534, 63, 270, 70, 69, 71, 73], the non-analytic shape of the regulator strongly limits its applicability in practical calculations.

In addition, it seems as if the seemingly simple structure of RG flow equations in the LPA truncation that is caused by this regulator lead to its inflationary use, while it was widely ignored that one is still facing a highly non-linear partial differential equation with all its mathematical and numerical challenges.

We conclude this digression by explicitly recording our choice for the regulator: The regulator (insertion) is given by Eqs. (E.5) to (E.7) in combination with the regulator shape function of Appendix D.2.2.

9.2.3. The RG flow equation of the four-fermion coupling

Using the above ansatz (9.1) for the effective average action as well as the regulator that was discussed in the previous paragraphs, we are ready to derive the explicit flow equations within our truncations, respectively β -functions for $Z_\psi(t)$ and $g^2(t)$.

This lengthy and tedious calculation is actually outsourced to Appendix E.1 and the appendices that are referenced therein. These appendices provide every detail of the derivation and explicitly address FRG novices, which is why we directly continue presenting the results.

The fermion wave-function renormalization The first flow equation that is obtained from Appendix E.1.1 is the (vanishing) scale evolution of the fermion anomalous dimension, respectively

the fermion wave-function renormalization, cf. Def. (C.62),

$$\eta_\psi(t) = \partial_t \ln Z_\psi(t) = 0. \quad (9.2)$$

This simply implies that the fermion wave-function renormalization is constant throughout the scale evolution and keeps its UV initial value from the classical action,

$$\forall t \quad Z_\psi(t) = 1. \quad (9.3)$$

For experts this result is hardly surprising. A wave-function renormalization is defined as the lowest-order Taylor coefficient of the two-point function expanded in momentum space [19]. Hence, its RG flow equation is extracted by deriving the flow equation of the two-point function w.r.t. the external spatial momentum \vec{p} that enters the respective Feynman diagram, and by evaluating the result at vanishing momentum, see Eqs. (E.11) and (E.13) and the corresponding discussion. However, as long as all scale-dependent quantities in the ansatz (9.1) are considered to be momentum-independent, the external momentum does not enter the loop in Eq. (E.11) via the four-fermion vertex, such that the two-point function is independent of the external momentum. In consequence all derivatives w.r.t. the spatial momentum vanish and so does the β -function for $Z_\psi(t)$. This is a generic feature of tadpole-type diagrams and is explained in detail in Appendix E.1.1.

It is also the first effect where we are confronted with shortcomings of our truncation – the momentum independence of $Z_\psi(t)$ and $g^2(t)$. However, it is not expected that this drastically spoils the phenomenology, because fermion wave-function renormalizations are not expected to have a strong RG evolution [66, 63, 70, 535, 71].³

The four-fermion coupling A direct consequence of Eq. (9.3) is that within our truncation the RG flow of the so-called renormalized coupling $g_r^2(t)$ and the bare coupling $g^2(t)$ are identical,

$$g_r^2(t) = Z_\psi^{-2}(t) g^2(t) = g^2(t). \quad (9.4)$$

The renormalized coupling is introduced when the effective average action (9.1) is expressed in terms of renormalized effective IR fermion fields

$$\bar{\psi}_r = Z_\psi^{\frac{1}{2}}(t) \bar{\psi}, \quad \psi_r = Z_\psi^{\frac{1}{2}}(t) \psi, \quad (9.5)$$

and the wave-function renormalization $Z_\psi(t)$ is completely eliminated, see, e.g., Refs. [63, 70, 69, 71, 72].

Using this as well as Eq. (9.3) the RG flow equation for the four-fermion coupling, the flow equation (E.26) which is derived in Appendix E.1.2, “simplifies” to

$$\partial_t g^2(t) = \quad (9.6)$$

$$= -A_d \frac{2}{N} \frac{d_\gamma N - 2}{d_\gamma N - 1} g^4(t) k^{d+2} \times \quad (9.7)$$

$$\times \frac{1}{\beta} \sum_{n=-\infty}^{\infty} \frac{\frac{1}{k^2}(\nu_n + i\mu)[2(\nu_{n+n_{\text{II}}-n_{\text{III}}} + i\mu) - (\nu_n + i\mu)] + 1}{\frac{1}{k^2}(\nu_{n+n_{\text{II}}-n_{\text{III}}} + i\mu)^2 + 1} \frac{1}{[(\nu_n + i\mu)^2 + k^2]^2} +$$

$$+ A_d \frac{2}{N} (d_\gamma N - 1) g^4(t) k^{d+2} \times \quad (9.8)$$

$$\times \frac{1}{\beta} \sum_{n=-\infty}^{\infty} \frac{\frac{1}{k^2}(\nu_n + i\mu)[2(\nu_{n+n_{\text{IV}}-n_{\text{III}}} + i\mu) - (\nu_n + i\mu)] + 1}{\frac{1}{k^2}(\nu_{n+n_{\text{IV}}-n_{\text{III}}} + i\mu)^2 + 1} \frac{1}{[(\nu_n + i\mu)^2 + k^2]^2} -$$

³In addition, we will find that even in the bosonized version of the GN model the fermion wave-function renormalization keeps its UV value (at least for $d = 1$), although the corresponding Feynman diagrams which enter the flow of the fermion two-point function are no longer all of tadpole type, see Eq. (E.89).

$$\begin{aligned}
& - A_d \frac{2}{N} \frac{1}{(d_\gamma N - 1)} g^4(t) k^{d+2} \times \\
& \times \frac{1}{\beta} \sum_{n=-\infty}^{\infty} \frac{-\frac{1}{k^2}(\nu_n + i\mu)[2(\nu_{-n+n_I+n_{III}} + i\mu) + (\nu_n + i\mu)] + 1}{\frac{1}{k^2}(\nu_{-n+n_I+n_{III}} + i\mu)^2 + 1} \frac{1}{[(\nu_n + i\mu)^2 + k^2]^2}.
\end{aligned} \tag{9.9}$$

A few remarks are in order:

1. The prefactor A_d is the typical spacetime-dimension-dependent prefactor in RG flow equations and defined in Eq. (A.7). Table A.1 lists explicit values for various d .
2. d_γ still denotes the dimensionality of the fermion representation and stems from the trace over γ matrices.
3. The flow equation was obtained by a projection on the scalar four-fermion channel, by contracting the open indices of fermion legs ψ_I and $\bar{\psi}_{II}$ as well as ψ_{III} and $\bar{\psi}_{IV}$ in Eq. (E.19). For details we refer to Eq. (E.20) and the corresponding discussion.
4. The flow equation was evaluated at vanishing external spatial momenta, which is reasonable because our ansatz Eq. (9.1) can be seen as the lowest order of a derivative expansion in fermion momenta, which should be valid at $\vec{p} = 0$.
5. The three contributions on the r.h.s. of Eq. (9.6) correspond to the three different types of Feynman diagrams, see Eq. (E.19). The first and last diagram in Eq. (E.19) result in the first term (9.7), while the second and third diagram are summarized in the second summand (9.8). The last summand corresponds to the fourth diagram. The three types of diagrams are the s -, t -, and u -channel of fermion anti-fermion scattering processes. Therefore one could interpret the fermion loop as an exchange of an $\bar{\psi}\psi$ state (a scalar boson) in the s - and t -channel (the first two contributions), while the scattering in the u -channel (the last contribution) can be interpreted as an exchange of a diquark state.
6. The Matsubara-frequency sums are not evaluated yet, because external Matsubara frequencies which enter the diagrams in Eq. (E.19) are not specified. We will use the formulae from Appendix B, after setting n_I to n_{IV} to explicit values. Here, we have to keep in mind that the four-fermion scattering has to conserve energy and momentum. The prefactor $\delta_{n_{II}+n_{IV}, n_I+n_{III}}$ on both sides of Eq. (9.6) was dropped for sake of readability, but has to be respected. It ensures energy conservation and sets the constraint $n_{II} + n_{IV} = n_I + n_{III}$ for the “index” of the Matsubara frequencies.

9.3. Consistency check and vacuum results

Caution: In this section d does not exclusively denote the number of spatial dimensions but is mostly used as the total number of spacetime dimensions!

Before we start with a detailed analysis, integration, and renormalization of the β -function (9.6) in medium, it is crucial to crosscheck that our derivation of the RG flow equations in Appendix E.1 is consistent with the well-known vacuum result(s) for the β -function of the GN model [359, 360, 361, 19, 422, 177, 362, 363].

9.3.1. Consistency check

Naively one might expect that the vacuum phenomenology is directly recovered by studying the $\mu \rightarrow 0$ and $T \rightarrow 0$ limits of Eq. (9.6). As a matter of fact, we cannot expect that this is the case. The reason lies in the choice of our regulator, which solely damps the spatial momenta and breaks Poincaré invariance explicitly. We argued in Section 9.2.2 that this effect might be

mild at sufficiently large temperatures or chemical potentials, where Poincaré invariance is broken anyhow. However, by approaching the zero-temperature limit, it can be expected that we will not recover the “correct” vacuum flow equations, which used covariant regularization throughout their derivation.

Therefore, we crosscheck our results differently:

1. We set $\mu = 0$.
2. We ignore all aspects in Eq. (9.6) that are related to non-zero temperature. Hence, we simply drop the frequency sums including the factor $\frac{1}{\beta}$ and set all Matsubara frequencies ν_n to zero.
3. Afterwards the three different contributions can be combined into one term.

The result reads,

$$\partial_t g^2(t) = 2 A_d \left(d_\gamma - \frac{2}{N} \right) g^4(t) k^{d-2}. \quad (9.10)$$

This equation is the RG flow equation of the d -dimensional GN model in vacuum, where all d momenta are regulated and treated on the same footing. The Litim regulator does not break Euclidean Poincaré invariance anymore, because all d Euclidean momenta are regulated on the same footing.

To study the β -function it is standard to work with dimensionless couplings. Therefore we rescale g^2 by appropriate powers of k according to its canonical energy dimension, see Eq. (8.3) (with $d + 1 \mapsto d$). We define the dimensionless four-fermion coupling as follows,

$$\bar{g}^2(k) \equiv k^{d-2} g^2(k), \quad (9.11)$$

such that the β -function reads

$$\beta(\bar{g}^2) = k \partial_k \bar{g}^2(k) = (d - 2) \bar{g}^2(k) - 2 A_d \left(d_\gamma - \frac{1}{N} \right) \bar{g}^4(k). \quad (9.12)$$

This is a well-known result, see, *e.g.*, Ref. [374, Eq. 14]⁴.

9.3.2. Remarks for two spacetime dimensions

Let us now consider $d = 2$. Here, $\bar{g}^2(k) = g^2(k)$ and the first term on the r.h.s. of Eq. (9.12) drops out. Indeed, Eq. (9.10) is the RG flow equation of the (1 + 1)-dimensional GN model in vacuum in a Euclidean spacetime.

Additionally choosing $d_\gamma = 2$ and using Def. (D.2), we recover its famous β -function, *cf.* Refs. [422, 19, Sec. 12.2]

$$\beta(g^2) = k \partial_k g^2(k) = -\frac{1}{\pi} \left(1 - \frac{1}{N} \right) g^4(k). \quad (9.13)$$

In Fig. 9.1 we drew a sketch of this β -function for $N > 1$.⁵ (For higher-order corrections, see Ref. [363, Figs. 2 & 3].) As we can see from the sketch and Eq. (9.13) the β -function in 1 + 1 spacetime dimensions is manifestly negative. Increasing k therefore leads to a lowering of g^2 and vice versa. The same behavior of the (one-loop) β -function is also observed in various other strongly interacting systems, *e.g.*, in QCD [537, 538, 539, 540, 541]. One refers to this as asymptotic freedom, because the coupling, that mediates the interaction, becomes negligible at extremely large RG scales/energies, respectively small distances. Asymptotic freedom goes hand in hand with a so-called repulsive Gaussian UV fixed point⁶ of the β -function. Among other things this feature

⁴Note that there seems to be a typo in the definition of the rescaled coupling in Ref. [374, Eq. (13)].

⁵For $N = 1$ the β -function vanishes. In this case the GN model is identical to the massless Thirring model, *cf.* Section 7.2.2. This can be shown via Fierz identities [422]. The massless Thirring model is known to have a vanishing β -function for one species of fermions [536, 345], because the Grassmann nature of the fermions leads to a vanishing four-fermion vertex.

⁶A fixed point is a point in the space of dimensionless couplings where the RG flow comes to halt, because all β -functions vanish. These fixed points can be attractive or repulsive, depending on whether a small perturbation of the dimensionless couplings about the fixed points starts growing or dies off. The Gaussian fixed point is the trivial fixed point, where the β -functions vanish due to vanishing couplings.

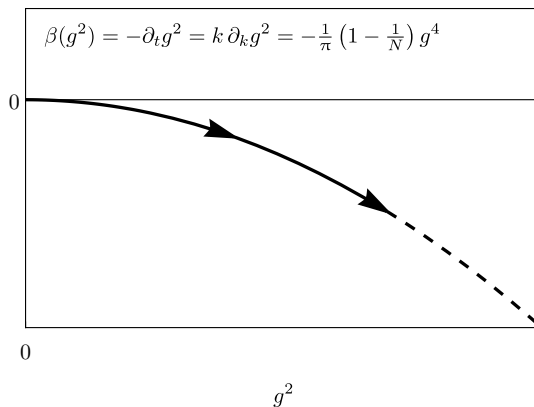


Figure 9.1: Sketch of the (one-loop) β -function (9.13) of the GN model for arbitrary N in vacuum. The dashed line indicates that the β -function is expected to be valid only for sufficiently small g^2 close to the UV. For larger values of g^2 non-perturbative higher-order effects are of relevance and modify the slope.

of the GN model was one reason for its proposal by D. J. Gross and A. Neveu [158]: Having a simple toy model to study asymptotic freedom without the complications of gauge theories, but taking advantage of knowledge about four-fermion theories from solid-state physics.

9.3.3. Comment on higher dimensions

However, note that asymptotic freedom in the GN model is strongly tied to 1 + 1 spacetime dimensions. Switching to a larger number of spacetime dimensions the four-fermion coupling has negative energy dimension, see Eq. (8.3), and the β -function of the dimensionless coupling \bar{g}^2 is no longer manifestly negative, see Eq. (9.12). Here, the negative parabola in Fig. 9.1 is moved to the right and upwards (still intersecting the origin), such there is a region where the β -function is positive, *cf.* Ref. [374, Fig. 1]. This opens the possibility for another non-trivial repulsive UV fixed point, while the trivial Gaussian fixed point turns into an attractive IR fixed point. Having a non-trivial repulsive UV fixed point is a possible realization of a so-called asymptotic-safety scenario, which also constitutes a well-defined microscopic limit of a model or theory⁷. Asymptotic-safety scenarios are manifestly non-perturbative, since the UV fixed point is a (strongly) interacting fixed point. This kind of UV limit was discovered by K. G. Wilson [176], G. Parisi [542], and S. Weinberg [543, 544] and is a promising candidate for a microscopic theory of gravity [545]. In the context of the GN model a first analysis for $d > 2$ is found in Ref. [546], while an extensive and instructive discussion is presented in Ref. [374]. We conclude that we expect a totally different dynamics and phenomenology of the GN model in $d > 2$ than in $d = 2$.

9.3.4. Scale dependence of the four-fermion coupling

Nevertheless, in this thesis we are mainly interested in the GN model in 1+1 spacetime dimensions at non-zero μ and non-zero T . Therefore we return to $d = 2$ in vacuum for the moment and see what we can already anticipate for our later investigations in medium.

By integrating the β -function (9.13) analytically from some UV reference scale k_{UV} towards the

⁷These are necessary conditions for asymptotic safety but they are not sufficient. Higher-order corrections, bosonization *etc.* can rule out asymptotic safety as is the case for the GN model for $d > 3$ [374].

IR we find,

$$-\int_{g^2}^{g_{\text{UV}}^2} d(g^2) \frac{1}{g^4} = \frac{1}{\pi} \left(1 - \frac{1}{N}\right) \int_{k_{\text{IR}}}^{k_{\text{UV}}} dk \frac{1}{k}. \quad (9.14)$$

Here, g_{UV}^2 stands for the initial coupling at k_{UV} and g^2 is the physically “observable” coupling in the IR at k_{IR} . The previous integral equation is solved by

$$\frac{1}{g_{\text{UV}}^2(k_{\text{UV}})} - \frac{1}{g^2(k_{\text{IR}})} = \frac{1}{\pi} \left(1 - \frac{1}{N}\right) \ln \left(\frac{k_{\text{UV}}}{k_{\text{IR}}}\right). \quad (9.15)$$

Note that formally we need to remove the UV and IR cutoff scales by sending $k_{\text{UV}} \rightarrow \infty$ and $k_{\text{IR}} \rightarrow 0$. However, we observe that only one of the two divergences of Eq. (9.15) can be cured by an appropriate renormalization prescription. This can be done by specifying some scale in the IR where the four-fermion coupling is supposed to diverge, and removing the UV cutoff. However, this means that the IR divergence of the four-fermion coupling g^2 is manifest – at least in the vacuum at $\mu = 0$ and $T = 0$. This is absolutely reasonable, since there is no other physical scale which regulates the IR modes and prevents the coupling from diverging in the purely fermionic setup.

In fact, this IR divergence of the attractive four-fermion interaction channel signals a resonance – the formation of a bound state – and condensation phenomena [158, 348, 350, 351], as we will also see below. In consequence, the fermionic degrees of freedom are no longer sufficient for an adequate description of the IR physics, such that the IR divergence of g^2 cannot be resolved at zero μ and zero T in a purely fermionic framework. However, it can be cured in a partially bosonized framework, because the Yukawa coupling effectively introduces a scale, *cf.* Section 8.2.3.

Note that these findings are indeed independent of the (in)finite number N of fermions and condensation is expected anyhow – at least for certain RG scales.

9.4. The four-fermion coupling at non-zero chemical potential and non-zero temperature

Next, we study the flow equation of the four-fermion coupling, Eq. (9.6), at non-zero μ and non-zero T .

In a first step we consider an infinite number N of fermions. This presents as a drastic approximation, but makes our results directly comparable to partially bosonized calculations in the same limit. As a first indicator for the phase structure of the GN model, we search for regions in the μ - T -plane where the four-fermion coupling diverges and signals the formation of a condensate.

In a second step, we work at a finite number N of fermions and repeat the infinite- N investigation in medium.

At finite N , however, the evaluation point of external fermion energies becomes relevant.

9.4.1. The four-fermion coupling at infinite N

Let us start with our discussion in the $N \rightarrow \infty$ limit. From Eq. (9.6) we find that this limit suppresses the contributions (9.7) and (9.9) and we are left with the term (9.8) on the r.h.s.. Hence, the $N \rightarrow \infty$ flow equation reads,

$$\begin{aligned} \partial_t g^2(t) &= \quad (9.16) \\ &= + 2 A_d d_\gamma g^4(t) k^{d+2} \times \\ &\quad \times \frac{1}{\beta} \sum_{n=-\infty}^{\infty} \frac{\frac{1}{k^2} (\nu_n + i\mu) [2(\nu_{n+n_{\text{IV}}-n_{\text{III}}} + i\mu) - (\nu_n + i\mu)] + 1}{\frac{1}{k^2} (\nu_{n+n_{\text{IV}}-n_{\text{III}}} + i\mu)^2 + 1} \frac{1}{[(\nu_n + i\mu)^2 + k^2]^2}. \end{aligned}$$

On a more physical level this could be roughly interpreted as follows: For the derivation of the flow equation, we contracted the external fermion legs ψ_I and $\bar{\psi}_{II}$ as well as ψ_{III} and $\bar{\psi}_{IV}$, see Eqs. (E.19) and (E.20), to project onto the scalar interaction channel. Hence, looking at the diagrammatic expression for the flow equation in Eq. (E.19) these may be viewed as an effective scalar bosonic particle $\phi \propto \bar{\psi}\psi$ that is either propagating bottom-top or top-down. The fermion loops can be considered as processes within this scalar particle on the level of its constituents – the fermions. On this level, the first and the last diagram in Eq. (E.19) (contribution (9.7)) are related to a simultaneous creation and annihilation of a scalar boson, while the fourth diagram (contribution (9.9)) can be seen as the creation and annihilation of a diquark state, which both mediate some force between the fermions. The second and third diagram (contribution (9.8)) are mere propagations of the fermions in the direction of the effective ϕ -particle (vertically). The infinite- N limit, however, suppresses all kinds of bosonic fluctuations, which eliminates the boson exchange processes. This ultimately becomes clear later on, when we work with the bGN and GNY model.

The remaining question is, how to choose n_{III} and n_{IV} in Eq. (9.16). Because we contracted the external fermion legs ψ_{III} and $\bar{\psi}_{IV}$ it seems reasonable to choose $n_{IV} = n_{III}$, which means that their energies are identical. It follows via energy conservation, $n_{II} + n_{IV} = n_I + n_{III}$, that $n_I = n_{II}$. In total the loop is independent of the external energies, see diagram two and three in Eq. (E.19). Although on a formal level we could choose any $n_{III} = n_{IV}$, the derivative expansion of our ansatz (9.1) strongly suggests to consider the smallest possible fermion energies, which are $\nu_n|_{n=0} = 2\pi(n + \frac{1}{2})T|_{n=0} = \pi T$ (at least for $\mu = 0$). We return to this issue below, when we consider finite N .

For the moment, we have

$$\begin{aligned} \partial_t g^2(t) &= 2 A_d d_\gamma g^4(t) k^{d+2} \frac{1}{\beta} \sum_{n=-\infty}^{\infty} \frac{1}{[(\nu_n + i\mu)^2 + k^2]^2} \stackrel{\text{(B.20)}}{=} \\ &= 2 A_d d_\gamma g^4(t) k^{d+2} \frac{1}{4k^3} \left[1 - n_f\left(\frac{k+\mu}{T}\right) - n_f\left(\frac{k-\mu}{T}\right) + \right. \\ &\quad \left. + \frac{k}{T} \left[n_f^2\left(\frac{k+\mu}{T}\right) + n_f^2\left(\frac{k-\mu}{T}\right) - n_f\left(\frac{k+\mu}{T}\right) - n_f\left(\frac{k-\mu}{T}\right) \right] \right], \end{aligned} \quad (9.17)$$

where Eq. (B.20) was used to evaluate the Matsubara sum.

Before integrating and renormalizing this β -function let us discuss which kind of phenomenology is expected at non-zero μ and non-zero T . This helps in choosing an appropriate renormalization point.

Firstly, for almost any system in Nature, one expects that the state of aggregation is gas-like at very high temperatures, because thermal fluctuations destroy any ordering and work against attractive interactions. On the other hand, we discussed in Section 9.3 that the renormalized IR four-fermion coupling diverges in vacuum and that we expect a formation of bound states, respectively condensation, especially in the $N \rightarrow \infty$ limit, where bosonic fluctuations are suppressed and cannot destabilize the condensate. Therefore we conclude that there should be a PT (or cross-over) from a gas-like phase with finite renormalized four-fermion coupling g^2 in the IR to a phase where bound states of fermions and anti-fermions dominate. Presumably this will happen at some non-zero temperature T_\dagger . As an indicator for this PT at T_\dagger , we use the divergence of the four-fermion coupling, which signals a definite breakdown of the purely fermionic theory. (The upwards arrow in T_\dagger stands for the divergence of the coupling.) Note that this is not a sufficient criterion to correctly locate a true PT line, because the description of the entire system by a single coupling is surely inadequate already before this coupling diverges.

Analogously, one can argue that there should also be a PT if the chemical potential μ is increased significantly, because varying the net baryon density introduces an imbalance of matter and anti-

matter, such that a condensate in the scalar four-fermion interaction channel is destabilized. Above some critical μ_\uparrow a suitable matching of fermions and anti-fermions is no longer possible. This can even be anticipated from the second and third Feynman diagram in Eq. (E.19). The chemical potential introduces an asymmetry between the fermion and the anti-fermion in the loop, which can be interpreted as an effective destabilization of the loop and the bosonic ϕ -particle, which we associated to the $\bar{\psi}\psi$ pair.

These considerations also generalize to a simultaneous variation of μ and T .

Consequently, we are actually expecting a region of finite physical IR four-fermion coupling $g^2(k_{\text{IR}})$ for $k_{\text{IR}} \rightarrow 0$ and a transition line in the μ - T -plane, where this coupling diverges. The region that is engulfed by this line at smaller $|\mu|$ and smaller T is not accessible by inspecting the four-fermion coupling alone, because the UV degrees of freedom (the fermions) are no longer sufficient to describe the corresponding state of matter.

Integration Having this in mind, we return to the analysis of the in-medium β -function (9.17). Integrating this equation from some UV scale k_{UV} to an IR scale k_{IR} one finds,

$$\begin{aligned} & \frac{1}{g_{\text{UV}}^2(k_{\text{UV}})} - \frac{1}{g^2(k_{\text{IR}}, \mu, T)} = \\ & = A_d \frac{d_\gamma}{2} \int_{k_{\text{IR}}}^{k_{\text{UV}}} dk k^{d-2} \left[1 - n_f\left(\frac{k+\mu}{T}\right) - n_f\left(\frac{k-\mu}{T}\right) + \right. \\ & \quad \left. + \frac{k}{T} \left[n_f^2\left(\frac{k+\mu}{T}\right) + n_f^2\left(\frac{k-\mu}{T}\right) - n_f\left(\frac{k+\mu}{T}\right) - n_f\left(\frac{k-\mu}{T}\right) \right] \right]. \end{aligned} \quad (9.18)$$

Note that $g_{\text{UV}}^2(k_{\text{UV}})$ is chosen to be independent of μ and T and the UV scale k_{UV} has to be much larger than μ and T to ensure RG consistency [244, 4, 547, 6]. This is anyhow the case after the renormalization, when the cutoff k_{UV} can be safely sent to infinity and is removed from the IR results.

From now on, we also set $d = 1$.

Before turning to the actual renormalization procedure, we consider Eq. (9.18) for vanishing temperature, thus $\beta|\mu| \rightarrow \infty$ and $\beta k \rightarrow \infty$. We use Eq. (B.21) and find

$$\begin{aligned} & \frac{1}{g_{\text{UV}}^2(k_{\text{UV}})} - \frac{1}{g^2(k_{\text{IR}}, \mu, 0)} = \\ & = \frac{d_\gamma}{2\pi} \int_{k_{\text{IR}}}^{k_{\text{UV}}} dk \frac{1}{k} \left(1 - \Theta\left(\frac{|\mu|}{k} - 1\right) - \frac{k}{|\mu|} \left[\delta\left(\frac{k}{|\mu|} + 1\right) + \delta\left(\frac{k}{|\mu|} - 1\right) \right] \right) = \\ & = \frac{d_\gamma}{2\pi} \int_{\frac{k_{\text{IR}}}{|\mu|}}^{\frac{k_{\text{UV}}}{|\mu|}} dt \frac{1}{t} \left(\Theta(t - 1) - t \left[\delta(t + 1) + \delta(t - 1) \right] \right) = \\ & = \frac{d_\gamma}{2\pi} \left[\ln\left(\frac{k_{\text{UV}}}{|\mu|}\right) - 1 \right]. \end{aligned} \quad (9.19)$$

While evaluating the integral, we assumed that $|\mu| > k_{\text{IR}}$, which is justified because ultimately the IR cutoff is sent to zero, $k_{\text{IR}} \rightarrow 0$. Hence, contrarily to the vacuum result (9.15) the chemical potential regulates the integral in the IR and makes it executable. The reason, why we are studying the zero-temperature limit separately will become clear within the next paragraphs.

Returning to Eq. (9.18) we introduce the dimensionless variable $t = \frac{k}{T}$ and use the relation (B.4)

for the Fermi-Dirac distribution function. Integration by parts yields,

$$\begin{aligned}
 & \frac{1}{g_{\text{UV}}^2(k_{\text{UV}})} - \frac{1}{g^2(k_{\text{IR}}, \mu, T)} = \tag{9.20} \\
 &= \frac{d_\gamma}{2\pi} \int_{t_{\text{IR}}}^{t_{\text{UV}}} dt \frac{1}{t} \left([1 - n_f(t + \frac{\mu}{T}) - n_f(t - \frac{\mu}{T})] - \right. \\
 & \quad \left. - t \partial_t [1 - n_f(t + \frac{\mu}{T}) - n_f(t - \frac{\mu}{T})] \right) = \\
 &= -\frac{d_\gamma}{2\pi} \int_{t_{\text{IR}}}^{t_{\text{UV}}} dt t \partial_t \left(\frac{1}{t} [1 - n_f(t + \frac{\mu}{T}) - n_f(t - \frac{\mu}{T})] \right) = \\
 &= -\frac{d_\gamma}{2\pi} \left([1 - n_f(t + \frac{\mu}{T}) - n_f(t - \frac{\mu}{T})]_{t_{\text{IR}}}^{t_{\text{UV}}} - \right. \\
 & \quad \left. - \int_{t_{\text{IR}}}^{t_{\text{UV}}} dt \frac{1}{t} [1 - n_f(t + \frac{\mu}{T}) - n_f(t - \frac{\mu}{T})] \right) = \\
 &= \frac{d_\gamma}{2\pi} \left(n_f(t_{\text{UV}} + \frac{\mu}{T}) + n_f(t_{\text{UV}} - \frac{\mu}{T}) - n_f(t_{\text{IR}} + \frac{\mu}{T}) - n_f(t_{\text{IR}} - \frac{\mu}{T}) + \right. \\
 & \quad \left. + \ln\left(\frac{t_{\text{UV}}}{t_{\text{IR}}}\right) - \lim_{s \rightarrow -1} \int_{t_{\text{IR}}}^{t_{\text{UV}}} dt t^s [n_f(t + \frac{\mu}{T}) + n_f(t - \frac{\mu}{T})] \right).
 \end{aligned}$$

Next, we study this expression in the limits $k_{\text{IR}} \rightarrow 0$ and $k_{\text{UV}} \rightarrow \infty$. For some of the terms the limits can be executed straightforwardly, while other terms require careful treatment. To this end, we express the remaining integral in terms of the (incomplete) Fermi-Dirac integral Eq. (A.85) respectively the (incomplete) polylogarithm Eq. (A.61),

$$\begin{aligned}
 & \lim_{t_{\text{UV}} \rightarrow \infty} \frac{1}{g_{\text{UV}}^2(t_{\text{UV}})} - \frac{1}{g^2(\mu, T)} = \tag{9.21} \\
 &= \frac{d_\gamma}{2\pi} \left(-1 + \lim_{t_{\text{UV}} \rightarrow \infty} \lim_{t_{\text{IR}} \rightarrow 0} \ln\left(\frac{t_{\text{UV}}}{t_{\text{IR}}}\right) + \right. \\
 & \quad \left. + \lim_{t_{\text{IR}} \rightarrow 0} \lim_{s \rightarrow 0} \Gamma(s) [\text{Li}_s(t_{\text{IR}}, -e^{\frac{\mu}{T}}) + \text{Li}_s(t_{\text{IR}}, -e^{-\frac{\mu}{T}})] \right) \stackrel{\text{(A.94)}}{=} \\
 &= \frac{d_\gamma}{2\pi} \left[-1 + \lim_{t_{\text{UV}} \rightarrow \infty} \ln(t_{\text{UV}}) + \gamma + \text{DLi}_0\left(\frac{\mu}{T}\right) \right].
 \end{aligned}$$

In the last step, we used Eq. (A.94) and the discussion of Appendix A.4.6 to resolve the IR divergence.

Similarly, we can formally consider the $k_{\text{UV}} \rightarrow \infty$ and $k_{\text{IR}} \rightarrow 0$ limit of Eq. (9.19) at vanishing temperature,

$$\lim_{t_{\text{UV}} \rightarrow \infty} \frac{1}{g_{\text{UV}}^2(t_{\text{UV}})} - \frac{1}{g^2(\mu, 0)} = \frac{d_\gamma}{2\pi} \left[\lim_{t_{\text{UV}} \rightarrow \infty} \ln\left(\frac{k_{\text{UV}}}{|\mu|}\right) - 1 \right]. \tag{9.22}$$

Renormalization Next, we turn to the actual renormalization procedure. So far, the scale-dependent quantities in our formula for g^2 comprise the chemical potential μ , the temperature T , as well as the UV and IR cutoffs k_{UV} and k_{IR} . However, it is somewhat meaningless to assign values to these quantities, as long as there is no real physical reference scale where we fix the coupling g^2 .

Of course, we could just choose some random $g_{\text{UV}}^2(k_{\text{UV}})$ at the scale k_{UV} – as is oftentimes done in FRG calculations. However, it is more reasonable to choose a physical and observable reference scale for the model and instead remove the UV cutoff from the theory. Such a reasonable physical IR scale, could be a critical temperature and/or chemical potential. Here, this is when the IR four-fermion coupling g^2 diverges, when varying μ and/or T over a critical threshold. Although we could in principle use any point (μ, T) as reference point, it is more convenient to choose either $(\mu_\dagger, 0)$ or $(0, T_\dagger)$ as reference scales.

Renormalization at zero chemical potential As a first choice, we consider $\mu = 0$ and choose T_\dagger as the temperature where four-fermion coupling diverges in the IR. Hence, we set $\frac{1}{g^2(0, T_\dagger)} = 0$ and use Eq. (A.83) to simplify Eq. (9.21). At T_\dagger we have,

$$\lim_{\substack{k_{\text{UV}} \rightarrow \infty \\ T_\dagger}} \frac{1}{g_{\text{UV}}^2(k_{\text{UV}})} = \frac{d_\gamma}{2\pi} \left[-1 + \lim_{k_{\text{UV}} \rightarrow \infty} \ln \left(\frac{k_{\text{UV}}}{T_\dagger} \right) + \gamma - \ln \left(\frac{\pi}{2} \right) \right]. \quad (9.23)$$

This is the renormalization condition, which can be used to remove the UV cutoff k_{UV} and UV coupling from the physical observables. By simply reinserting Eq. (9.23) into Eqs. (9.21) and (9.22), we find

$$\frac{1}{g^2(\mu, T)} = \frac{d_\gamma}{2\pi} \begin{cases} \ln \left(\frac{2T}{\pi T_\dagger} \right) - \text{DLi}_0 \left(\frac{\mu}{T} \right), & \text{if } T \neq 0, \\ \ln \left(\frac{2|\mu|}{\pi T_\dagger} \right) + \gamma, & \text{if } T = 0. \end{cases} \quad (9.24)$$

Hence, we express the four-fermion interaction $g^2(\mu, T)$ exclusively by μ and T and the reference scale T_\dagger . The same is done for example in Ref. [348, Figs. 3 & 5].

Renormalization at zero temperature Another common renormalization prescription is to study the case where $T = 0$ and set the physical scale via some critical μ_\dagger . Here, we define $|\mu_\dagger|$ as the chemical potential where $g^2(\mu_\dagger, 0)$ diverges. Thus we use Eq. (9.22) and find,

$$\lim_{\substack{k_{\text{UV}} \rightarrow \infty \\ |\mu_\dagger|}} \frac{1}{g_{\text{UV}}^2(k_{\text{UV}})} = \frac{d_\gamma}{2\pi} \left[\lim_{k_{\text{UV}} \rightarrow \infty} \ln \left(\frac{k_{\text{UV}}}{|\mu_\dagger|} \right) - 1 \right].$$

This result can be inserted into Eq. (9.21), such that the renormalized inverse four-fermion coupling reads

$$\frac{1}{g^2(\mu, T)} = \frac{d_\gamma}{2\pi} \begin{cases} \ln \left(\frac{T}{|\mu_\dagger|} \right) - \gamma - \text{DLi}_0 \left(\frac{\mu}{T} \right), & \text{if } T \neq 0, \\ \ln \left(\frac{|\mu|}{|\mu_\dagger|} \right), & \text{if } T = 0. \end{cases} \quad (9.25)$$

Again, we observe that the IR value of the coupling solely depends on μ and T and the reference scale μ_\dagger .

Note that we can relate the scales μ_\dagger and T_\dagger from the different renormalization conditions by comparing Eqs. (9.30) and (9.25). We conclude

$$\mu_\dagger = \frac{\pi}{2} e^{-\gamma} T_\dagger. \quad (9.26)$$

Phenomenology at infinite N Now that we have derived formulae for the inverse four-fermion coupling in the IR for arbitrary μ and T , we can start investigating the “phase structure” of the purely fermionic Gross-Neveu model for $N \rightarrow \infty$.

Hence, w.l.o.g. we choose T_\dagger as our reference scale and evaluate Eq. (9.24) numerically in the μ - T -plane. In doing so, we can formally use any numerical value for T_\dagger . All other dimensionful

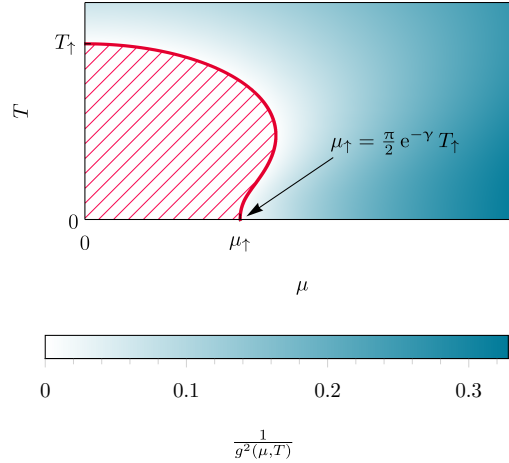


Figure 9.2: Inverse four-fermion coupling as a function of μ and T . The solid red is the line of diverging four-fermion coupling $g^2(\mu, T)$. In the crosshatched region the investigation of the four-fermion interaction breaks down. The blue color map indicates the strength of the four-fermion interaction. The numerical values are calculated with Eq. (9.24). The T - and μ -axis have the same scale.

quantities (here μ and T) are measured w.r.t. T_\dagger .⁸ Our result is plotted in Fig. 9.2. As expected, there is a region in the μ - T -plane at large $|\mu|$ and T where the four-fermion coupling $g^2(\mu, T)$ is always finite. As it happens, it tends to zero for very large $|\mu|$ and/or T . This is another realization of asymptotic freedom – vanishing interactions for asymptotically large energies. In this region the system is in a gas-like state and can be approximately described (perturbatively) by the single four-fermion coupling. Our truncation (9.1) is reasonable there.

On the other hand, for sufficiently low $|\mu|$ and T there is a region where the four-fermion coupling diverges. In this region the approximation breaks down and other degrees of freedom, momentum structure *etc.* might become relevant. This is the region where we expect some condensation phenomena – at least temporarily during the RG flow.

Readers who are familiar with the phenomenology of the infinite- N GN model might find the shape of this region rather familiar. Let us already mention at this point that the $\frac{1}{g^2(\mu, T)} = 0$ line is exactly the spinodal line, see, *e.g.*, Refs. [4, 467], which is discussed later on.

9.4.2. The four-fermion coupling at finite N

Next, we study the four-fermion coupling, respectively its flow equation (9.6), at finite N . In consequence, now all three processes from the Feynman diagrams in Eq. (E.19) contribute. Generally we expect that there is still condensation (a region of diverging four-fermion coupling) within the purely fermionic framework – at least temporarily for some RG scales. However, the region in the μ - T -plane where this might happen is expected to be smaller, since the different types of diagrams in Eq. (E.19) can come with opposite signs in (9.6). Also on a phenomenological level this is expected. Relaxing the $N \rightarrow \infty$ limit allows for fluctuations of bound states, which destabilize condensation, as we will see below.

However, before starting the calculations, we have to return to the intriguing question which are the correct evaluation points for the external fermion lines in Matsubara-frequency space, thus

⁸We used $T_\dagger = \frac{e^\gamma}{\pi}$ for our numerical calculations (in arbitrary energy units), which implies $\mu_\dagger = \frac{1}{2}$. This specific choice becomes clear in Chapter 11, where we study the bosonized theory. The numerical result was obtained using an AMR algorithm – a two-dimensional bisection in the μ - T plane.

how to choose $n_I, n_{II}, n_{III}, n_{IV}$ in Eq. (9.6). In the literature, several approaches are discussed. All rely on the fact that truncations like Eq. (9.1) form some kind of derivative expansion. Unlike bosonic fields, a derivative expansion for fermionic fields comes with two main difficulties, which both concern the temporal direction – the fermion energies. At non-zero temperature a Matsubara zero-mode does not exist for fermions and the smallest fermion energy is πT . In addition, at non-zero chemical potential (even if the temperature is zero) the fermion energies get shifted by $i\mu$. Both facts violate the idea of a derivative expansion about zero spatial momenta and energies. On top of that, a suitable evaluation of the diagrams that enter our flow equation has to respect the Silver-Blaze property. The situation is even made complicated by the specific choice of the fermion regulator, which can in principle spoil a suitable evaluation point. Discussions of this issue are presented for example in Refs. [548, Sec. II B], [348, App. B], [66, Sec. III B & App. B]. Here, we shall simply present two approaches for the evaluation of external fermion lines,

1. Let us first take the concept of the derivative expansion seriously. We naively expand the effective average action about $\nu_n + i\mu = 0$ analogous to what is required in vacuum to fulfill the Silver-Blaze property. At non-zero T this leads to the following evaluation point for the fermion lines,

$$0 = \nu_n + i\mu = 2\pi \left(n + \frac{1}{2}\right) T + i\mu, \quad \Rightarrow \quad n = -\frac{i\mu}{2\pi T} - \frac{1}{2}. \quad (9.27)$$

This seems to be at odds with $n \in \mathbb{Z}$, but is closest to an expansion about the Fermi-surface at $T = 0$. Indeed, without stating it explicitly, this evaluation is oftentimes used in the literature. Thereby, the argument is usually that the temporal Euclidean momentum at $T = 0$ is analytically continued to the complex plane, such that the expansion point is $p_{d+1} + i\mu = 0$. After all formulas are derived for $T = 0$ this relation is simply extended to $\nu_n + i\mu = 0$ and non-zero T .

2. Another option is to choose $n \in \mathbb{Z}$, which is the correct option on a mathematical level and evaluate the flow equation on the lowest lying Matsubara frequency $\nu_0 = \pi T$. This in turn spoils the concept of the derivative expansion, because the flow equations are not evaluated at zero energy. In addition, this version is known to introduce complex contributions to the flow equations of fermionic n -point functions.

We can just test both options in our simple model due to the simplistic truncation.

Evaluation at the Fermi surface We start by evaluating Eq. (9.6) for

$$n_I = n_{II} = n_{III} = n_{IV} = -\frac{i\mu}{2\pi T} - \frac{1}{2}. \quad (9.28)$$

Here, all three contributions sum up to a rather familiar flow equation for the four-fermion coupling,

$$\partial_t g^2(t) = 2 A_d \left(d_\gamma - \frac{2}{N}\right) g^4(t) k^{d-2} \frac{1}{\beta} \sum_{n=-\infty}^{\infty} \frac{1}{[(\nu_n + i\mu)^2 + k^2]^2}. \quad (9.29)$$

Up to a replacement $d_\gamma \mapsto d_\gamma - \frac{2}{N}$ in the prefactor on the r.h.s. it is identical to the infinite- N flow equation (9.17).

The renormalized four-fermion coupling is therefore simply obtained by exchanging the prefactor in Eq. (9.24) and we find,

$$\frac{1}{g^2(\mu, T)} = \frac{1}{2\pi} \left(d_\gamma - \frac{2}{N}\right) \begin{cases} \ln\left(\frac{2T}{\pi T_\dagger}\right) - \text{DLi}_0\left(\frac{\mu}{T}\right), & \text{if } T \neq 0, \\ \ln\left(\frac{2|\mu|}{\pi T_\dagger}\right) + \gamma, & \text{if } T = 0. \end{cases} \quad (9.30)$$

Of course the critical temperature T_\dagger is different for each value of N , because each N effectively stands for a separate model. Nevertheless, the region where the four-fermion coupling diverges will have the same shape for all N and look like the one for $N \rightarrow \infty$ in Fig. 9.2. Additionally, for $N \rightarrow \infty$ Eq. (9.30) reduces to Eq. (9.24).

Evaluation at πT If we evaluate Eq. (9.6) at

$$n_{\text{I}} = n_{\text{II}} = n_{\text{III}} = n_{\text{IV}} = 0, \quad (9.31)$$

hence all fermion legs at energy πT , we obtain,

$$\begin{aligned} \partial_t g^2(t) = & \quad (9.32) \\ = & -A_d \frac{2}{N} \frac{d_\gamma N - 2}{d_\gamma N - 1} g^4(t) k^{d+2} \frac{1}{\beta} \sum_{n=-\infty}^{\infty} \frac{1}{[(\nu_n + i\mu)^2 + k^2]^2} + \\ & + A_d \frac{2}{N} (d_\gamma N - 1) g^4(t) k^{d+2} \frac{1}{\beta} \sum_{n=-\infty}^{\infty} \frac{1}{[(\nu_n + i\mu)^2 + k^2]^2} - \\ & - A_d \frac{2}{N} \frac{1}{d_\gamma N - 1} g^4(t) k^{d+2} \times \\ & \times \frac{1}{\beta} \sum_{n=-\infty}^{\infty} \frac{-(\nu_n + i\mu)[2(\nu_{-n} + i\mu) + (\nu_n + i\mu)] + k^2}{(\nu_{-n} + i\mu)^2 + k^2} \frac{1}{[(\nu_n + i\mu)^2 + k^2]^2}. \end{aligned}$$

Interestingly, the first two contributions (9.7) and (9.8) become proportional to the standard Matsubara sums, which we already encountered before. The third contribution (9.9) is of different shape. This is expected, if we return to the corresponding Feynman diagrams in Eq. (E.19) and consider them as physical processes (scattering or the “vertical” propagation of $\phi \propto \psi \psi$ state): Since the chemical potential introduces an asymmetry between matter and anti-matter, it is clear that the first, second, third, and fifth diagram are affected equally by the chemical potential. These four diagrams involve internal fermion lines that run in opposite directions (from vertex to vertex) and can be viewed as propagation of a (virtual) fermion and a (virtual) anti-fermion in the same direction. However, fermions and anti-fermions are influenced differently by a matter-anti-matter imbalance. This is reflected in the Fermi-Dirac distribution functions, which emerge from the Matsubara sums and come with corresponding arguments $\beta(k \pm \mu)$, *cf.* Eq. (B.20).

Then again there is the fourth diagram, where the internal fermion lines point into the same direction (from one vertex to the other). Here, the chemical potential should not have an influence on this diagram, which we prove below.

Either way, even if $\mu = 0$, we observe that the Matsubara sum in the third term of Eq. (9.32) differs from the others. This is also understandable by returning to the diagrams in Eq. (E.19). If we consider the diagrams as scattering processes at $\mu = 0$, we find that in the case of the fourth diagram, the energy $2\pi T$ has to flow somehow through the fermion loop, while for the other diagrams the external energies πT never enter the loop. Scattering at zero-momentum/energy transfer is – in contrast to the vacuum – not possible for the fourth diagram and the minimal momentum/energy transfer is set by the temperature.

Integration With this we turn to the integration of the β -function Eq. (9.32), which formally reads

$$\begin{aligned} & \frac{1}{g_{\text{UV}}^2(k_{\text{UV}})} - \frac{1}{g_{\text{IR}}^2(k_{\text{IR}}, \mu, T)} = \quad (9.33) \\ = & A_d \frac{2}{N} \frac{1}{d_\gamma N - 1} \times \\ & \times \left[[(d_\gamma N - 1)(d_\gamma N - 2) + 1] \int_{k_{\text{IR}}}^{k_{\text{UV}}} dk k^{d+1} \frac{1}{\beta} \sum_{n=-\infty}^{\infty} \frac{1}{[(\nu_n + i\mu)^2 + k^2]^2} - \right. \end{aligned}$$

$$- \int_{k_{\text{IR}}}^{k_{\text{UV}}} dk k^{d+1} \frac{1}{\beta} \sum_{n=-\infty}^{\infty} \frac{-(\nu_n + i\mu)[2(\nu_{-n} + i\mu) + (\nu_n + i\mu)] + k^2}{(\nu_{-n} + i\mu)^2 + k^2} \frac{1}{[(\nu_n + i\mu)^2 + k^2]^2} \Big].$$

The first Matsubara sum and k -integral is evaluated analogously to Eqs. (9.17), (9.20), and (9.21). The tricky part is the second Matsubara sum and k -integration. The corresponding Matsubara sum was evaluated using MATHEMATICA. Reshaping of the result as well as taking the $\mu \rightarrow 0$ limit is presented in Appendix B.2.3. One finds,

$$\begin{aligned} & \int_0^{\infty} dk k^2 \frac{1}{\beta} \sum_{n=-\infty}^{\infty} \frac{-(\nu_n + i\mu)[2(\nu_{-n} + i\mu) + (\nu_n + i\mu)] + k^2}{(\nu_{-n} + i\mu)^2 + k^2} \frac{1}{[(\nu_n + i\mu)^2 + k^2]^2} = \quad (9.34) \\ &= -\frac{1}{8} \int_0^{\infty} dk k \frac{\partial}{\partial k} \left[\left(\frac{k+\mu}{(k+\mu)^2 + (\pi T)^2} \tanh\left(\frac{k+\mu}{2T}\right) + \frac{k-\mu}{(k-\mu)^2 + (\pi T)^2} \tanh\left(\frac{k-\mu}{2T}\right) \right) \right. \\ & \quad \left. + i\pi T \left(\frac{1}{(k+\mu)^2 + (\pi T)^2} \tanh\left(\frac{k+\mu}{2T}\right) - \frac{1}{(k-\mu)^2 + (\pi T)^2} \tanh\left(\frac{k-\mu}{2T}\right) \right) \right], \end{aligned}$$

This result entails that the β -function (9.32) is manifestly complex for non-zero μ and non-zero T , because the k -integration is not evaluated yet. This was also checked explicitly for random numerical values of μ and T . However, for $\mu = 0$, it is shown in Eq. (B.37) that the imaginary part of the β -function vanishes.

In general, a complex β -function seems to be a puzzling result, because the β -function/RG flow is supposed to describe the change of a coupling while changing the energy scale k . Why should there be a complex contribution? Is the imaginary part physical? Still, similar results are found and discussed for example in Refs. [531, 548, 66, 549, 275] in the context of fermion-two-point functions. Basically, all of these references argue that the imaginary part of the flow equation is unphysical. Their arguments are based on expansions in $\frac{\mu}{T}$ or $\frac{\mu}{k}$ (or their inverse counterparts) and/or exploit the symmetry of the theory under the substitution $\mu \mapsto -\mu$. Usually, this symmetry is not fulfilled by the imaginary contribution. It is mainly argued that the emergence of the imaginary parts traces back to ignoring momentum and frequency dependences of the couplings.

In the following, we present a calculation which may point at a slightly different resolution of the problem, which is not based on any approximation or heuristic argumentation *etc.*.

Assume that the imaginary part of the β -function manifestly exists. However, a β -function is not observable and is in general even regularization-scheme dependent – at least at higher-loop level or for non-perturbative corrections. The physical quantities are the renormalized IR couplings, which can be related to one-PI- n -point-vertex functions and therefore to scattering amplitudes *etc.*, see for example Ref. [72].

Therefore, we should look at the integrated β -function in the limit of vanishing IR cutoff $k_{\text{IR}} \rightarrow 0$ and infinite UV cutoff $k_{\text{UV}} \rightarrow \infty$. Here it can actually be shown that there is no imaginary contribution to the IR four-fermion coupling, thus the k -integral over the imaginary part vanishes exactly. This is shown by studying the imaginary and real part of Eq. (9.34) separately.

Indeed, the imaginary part vanishes

$$\begin{aligned} & \text{Im}(9.34) = \quad (9.35) \\ &= -\frac{\pi}{8} T \int_0^{\infty} dk k \frac{\partial}{\partial k} \left[\frac{1}{(k+\mu)^2 + (\pi T)^2} \tanh\left(\frac{k+\mu}{2T}\right) - \frac{1}{(k-\mu)^2 + (\pi T)^2} \tanh\left(\frac{k-\mu}{2T}\right) \right] = \\ &= -\frac{\pi}{8} T \left[\frac{k}{(k+\mu)^2 + (\pi T)^2} \tanh\left(\frac{k+\mu}{2T}\right) - \frac{k}{(k-\mu)^2 + (\pi T)^2} \tanh\left(\frac{k-\mu}{2T}\right) \right]_0^{\infty} + \\ & \quad + \frac{\pi}{8} T \int_0^{\infty} dk \left[\frac{1}{(k+\mu)^2 + (\pi T)^2} \tanh\left(\frac{k+\mu}{2T}\right) - \frac{1}{(k-\mu)^2 + (\pi T)^2} \tanh\left(\frac{k-\mu}{2T}\right) \right] = \end{aligned}$$

$$\begin{aligned}
 &= \frac{\pi}{8} T \left[\int_{\mu}^{\infty} dk \frac{1}{k^2 + (\pi T)^2} \tanh\left(\frac{k}{2T}\right) - \int_{-\mu}^{\infty} dk \frac{1}{k^2 + (\pi T)^2} \tanh\left(\frac{k}{2T}\right) \right] = \\
 &= -\frac{\pi}{8} T \int_{-\mu}^{\mu} dk \frac{1}{k^2 + (\pi T)^2} \tanh\left(\frac{k}{2T}\right) = \\
 &= 0,
 \end{aligned}$$

while the real part becomes independent of μ as anticipated from the diagrams and our discussion,

$$\begin{aligned}
 \text{Re (9.34)} &= \tag{9.36} \\
 &= -\frac{1}{8} \int_0^{\infty} dk k \frac{\partial}{\partial k} \left[\frac{k+\mu}{(k+\mu)^2 + (\pi T)^2} \tanh\left(\frac{k+\mu}{2T}\right) + \frac{k-\mu}{(k-\mu)^2 + (\pi T)^2} \tanh\left(\frac{k-\mu}{2T}\right) \right] = \\
 &= -\frac{1}{8} \left[\frac{k(k+\mu)}{(k+\mu)^2 + (\pi T)^2} \tanh\left(\frac{k+\mu}{2T}\right) + \frac{k(k-\mu)}{(k-\mu)^2 + (\pi T)^2} \tanh\left(\frac{k-\mu}{2T}\right) \right]_0^{\infty} + \\
 &\quad + \frac{1}{8} \int_0^{\infty} dk \left[\frac{k+\mu}{(k+\mu)^2 + (\pi T)^2} \tanh\left(\frac{k+\mu}{2T}\right) + \frac{k-\mu}{(k-\mu)^2 + (\pi T)^2} \tanh\left(\frac{k-\mu}{2T}\right) \right] = \\
 &= -\frac{1}{4} + \frac{1}{8} \int_0^{\infty} dk \left[\frac{k+\mu}{(k+\mu)^2 + (\pi T)^2} \tanh\left(\frac{k+\mu}{2T}\right) + \frac{k-\mu}{(k-\mu)^2 + (\pi T)^2} \tanh\left(\frac{k-\mu}{2T}\right) \right] = \\
 &= -\frac{1}{4} + \frac{1}{8} \left[\int_{\mu}^{\infty} dk \frac{k}{k^2 + (\pi T)^2} \tanh\left(\frac{k}{2T}\right) + \int_{-\mu}^{\infty} dk \frac{k}{k^2 + (\pi T)^2} \tanh\left(\frac{k}{2T}\right) \right] = \\
 &= -\frac{1}{4} + \frac{1}{8} \int_{-\infty}^{\infty} dk \frac{k}{k^2 + (\pi T)^2} \tanh\left(\frac{k}{2T}\right) \stackrel{\text{(B.2)}}{=} \\
 &= -\frac{1}{4} + \frac{1}{4} \int_0^{\infty} dk \frac{k}{k^2 + (\pi T)^2} [1 - 2 n_f\left(\frac{k}{T}\right)] = \\
 &= -\frac{1}{4} + \lim_{k_{UV} \rightarrow \infty} \frac{1}{8} \ln\left(\frac{k_{UV}^2 + (\pi T)^2}{(\pi T)^2}\right) - \frac{1}{2} \int_0^{\infty} dk \frac{k}{k^2 + (\pi T)^2} n_f\left(\frac{k}{T}\right).
 \end{aligned}$$

In the last step, we reintroduced the UV cutoff, because the integral is UV divergent. This will be cured by renormalization.

Combining the results, we find

$$\begin{aligned}
 &\lim_{k_{UV} \rightarrow \infty} \frac{1}{g_{UV}^2(k_{UV})} - \frac{1}{g^2(\mu, T)} = \tag{9.37} \\
 &= \frac{1}{\pi} \frac{1}{2N} \frac{1}{d_{\gamma} N - 1} \times \\
 &\quad \times \left([(d_{\gamma} N - 1)(d_{\gamma} N - 2) + 1] \left[-1 + \lim_{k_{UV} \rightarrow \infty} \ln\left(\frac{k_{UV}}{T}\right) + \gamma + \text{DLi}_0\left(\frac{\mu}{T}\right) \right] - \right. \\
 &\quad \left. - \left[-1 + \lim_{k_{UV} \rightarrow \infty} \frac{1}{2} \ln\left(\frac{k_{UV}^2 + (\pi T)^2}{(\pi T)^2}\right) - 2 \int_0^{\infty} dk \frac{k}{k^2 + (\pi T)^2} n_f\left(\frac{k}{T}\right) \right] \right),
 \end{aligned}$$

which is real.

At this point, one might ask how this generalizes to calculations with more than one four-fermion interaction channel or fermionic two-point functions in theories with Yukawa interactions. So far, we do not have a definite answer to this question, but work on this topic is already in progress. Currently, we speculate that couplings are generally allowed to gain complex contributions during RG flows. In systems of several couplings, which form coupled ODEs, we therefore expect interference phenomena but ultimately vanishing imaginary parts in the IR.

Renormalization at zero chemical potential Next, we can simply repeat the steps of Section 9.4.2 for the renormalization procedure. We choose $\mu = 0$ and $T = T_\dagger$ as the renormalization point. Again, this is supposed to be the point where the four-fermion coupling diverges first, when the temperature is lowered along the T -axis of the phase diagram. Of course, in principle each N has its own T_\dagger . Still, the renormalization procedure is the same for all N . At T_\dagger the inverse IR four-fermion coupling vanishes, $\frac{1}{g^2(0, T_\dagger)}$, such that

$$\begin{aligned} & \lim_{k_{UV} \rightarrow \infty} \frac{1}{g_{UV}^2(k_{UV})} = \tag{9.38} \\ &= \frac{1}{\pi} \frac{1}{2N} \frac{1}{d_\gamma N - 1} \times \\ & \times \left([(d_\gamma N - 1)(d_\gamma N - 2) + 1] \left[-1 + \lim_{k_{UV} \rightarrow \infty} \ln \left(\frac{k_{UV}}{T_\dagger} \right) + \gamma - \ln \left(\frac{\pi}{2} \right) \right] - \right. \\ & \left. - \left[-1 + \lim_{k_{UV} \rightarrow \infty} \frac{1}{2} \ln \left(\frac{k_{UV}^2 + (\pi T_\dagger)^2}{(\pi T_\dagger)^2} \right) - 2 \int_0^\infty dk \frac{k}{k^2 + (\pi T_\dagger)^2} n_f \left(\frac{k}{T_\dagger} \right) \right] \right), \end{aligned}$$

where we used Eq. (A.83) to simplify the derivative of the polylogarithm. By reinserting this result in Eq. (9.37) we find the final result for the IR four-fermion coupling in the μ - T -plane,

$$\begin{aligned} & \frac{1}{g^2(\mu, T)} = \tag{9.39} \\ &= \frac{1}{\pi} \frac{1}{2N} \frac{1}{d_\gamma N - 1} \times \\ & \times \left([(d_\gamma N - 1)(d_\gamma N - 2) + 1] \left[\ln \left(\frac{2T}{\pi T_\dagger} \right) - \text{DLi}_0 \left(\frac{\mu}{T} \right) \right] - \right. \\ & \left. - \left[\ln \left(\frac{T}{T_\dagger} \right) - 2 \int_0^\infty dk \frac{k}{k^2 + (\pi T_\dagger)^2} n_f \left(\frac{k}{T_\dagger} \right) + 2 \int_0^\infty dk \frac{k}{k^2 + (\pi T)^2} n_f \left(\frac{k}{T} \right) \right] \right). \end{aligned}$$

We were not able to solve the remaining two integrals analytically. Still, these can be straightforwardly evaluated numerically using standard integration routines.

Before studying the area of diverging four-fermion coupling in the μ - T -plane from Eq. (9.39), note that this equation has the correct $N \rightarrow \infty$ limit, where it reduces to Eq. (9.24).

Phenomenology at finite N To study the lines of diverging four-fermion coupling at finite N using Eq. (9.39) we proceed as follows. There is no other dimensionful scale which distinguishes calculations at different N , thus we choose the same T_\dagger for all N of our calculations. For sake of convenience, we use $T_\dagger = \frac{e^\gamma}{\pi}$, which becomes clear below. The actual calculation of the $\frac{1}{g^2(\mu, T)} = 0$ lines is based on bisections in μ -direction up to an accuracy of $\Delta\mu = 0.001$. The bisections are performed at constant temperatures in steps of $\Delta T = 0.001$.

The results of these calculations are shown in Fig. 9.3. We clearly find that by increasing N the curves clearly approach the $N \rightarrow \infty$ result, which was plotted before in Fig. 9.2. For small N there

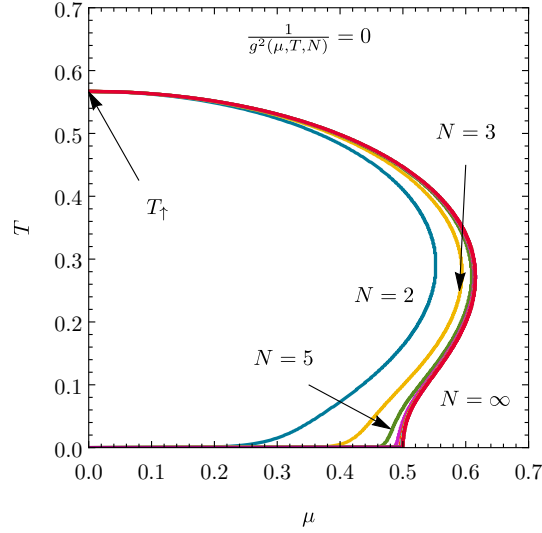


Figure 9.3: Lines of diverging four-fermion coupling for $N \in \{2, 3, 5, 8, 12, 21, 34, 55, 89, \infty\}$ (from left to right). All curves are normalized to the same T_{\dagger} . All curves for finite N end in $\mu = 0$ at $T = 0$, while the curve for $N = \infty$ ends in $\mu = 0.5$ at $T = 0$. The $N = \infty$ curve agrees with Fig. 9.2.

is a significant deviation from the $N \rightarrow \infty$ line, especially for small temperatures. Another crucial difference between all finite N and the infinite- N curve is that for $N \rightarrow \infty$ the curve terminates at non-zero chemical potential for $T \rightarrow 0$, while for any finite N the lines end at $\mu = 0$, $T = 0$. These differences are exclusively driven by the contribution of the fourth diagram in Eq. (E.19), which is independent of μ and gains in importance for small N .

What does this say about our initial question about the presence or absence of symmetry breaking and condensation in the GN model at finite N ? From Fig. 9.3 we deduce that generically the region of diverging four-fermion coupling, which is an indicator of condensation, shrinks while N is reduced. Nevertheless, the difference between $N = 2$ and $N = \infty$ does not seem too large. However, if we take into account that T_{\dagger} itself will change in the real world, if we exclusively change the number N of fermions in the GN model, the effect will be more drastic. In fact the size of the region will shrink in μ - and T -direction, because less fermions leads to less attractive interactions that can work against thermal and bosonic fluctuations. In general, these results are in qualitatively good agreement with earlier investigations of the GN or bGN model at finite N , which we discussed in Section 7.4.5.

9.5. Concluding remarks

In this section we used the FRG approach to calculate the β -function of the purely fermionic GN model in medium. After integration and renormalization we studied the IR four-fermion coupling as a function of μ and T at (in)finite N and its dependence on the external energies – the Matsubara modes that enter the corresponding loop diagrams. We observed that finite- and infinite- N results strongly deviate, especially for low temperatures and that the region with signals of condensation of $\bar{\psi}\psi$ pairs significantly shrinks for small N . Furthermore, we observed a significant dependence of the region where the four-fermion coupling diverges on the choice of the external energies. In this way, however, we were able to show that commonly appearing complex contributions in flow equations of fermionic vertex functions might not be artifacts which need to be ignored, but can possibly be handled systematically by including them in the RG flows.

Concerning the original objective of this work, to study the GN model at finite N , we conclude that the approximation of this section is insufficient and inconclusive. Thus, from here there are basically two routes to proceed:

1. We could start enlarging the basis of four-fermion coupling channels and study Fierz-complete sets of couplings like in Refs. [348, 350, 351]. Here, we could even distinguish contributions, which are parallel and perpendicular to the heat bath. In addition, another improvement would be to resolve the momentum structure of the four-fermion couplings and to include higher-order derivative couplings. If one chooses this route, one should also think about exchanging the dimensionally reduced flat regulator by some covariant smooth regulator, which still guarantees the Silver-Blaze property, but has a better vacuum limit. In this setup, with an enlarged space of couplings, we can repeat our studies at finite and infinite N .
2. Another route is to switch to the partially bosonized description of the GN model, the GNY model. Here, it is much simpler to study condensation phenomena, because $\bar{\psi}\psi$ pairs form bosonic bound states, which are explicitly included in the calculation and interact with the fermions via Yukawa couplings. Also here it is possible to work at finite and infinite N and compare the system with and without bosonic fluctuations.

Even though there is already some work in progress on the first option, we focus on route two throughout the remainder of this thesis.

Chapter 10

The Gross-Neveu-Yukawa model via the Functional Renormalization Group

Abstract In this chapter we summarize the formal setup for FRG calculations for the GNY model. This sets the basis for investigations within different truncation schemes as well as an infinite- N analysis of the bGN model. The discussion is supported by comprehensive appendices involving explicit derivations.

Furthermore, the resulting RG flow equations are analyzed w.r.t. their fluid-dynamical character.

Disclosure The generic structure of the FRG flow equations for boson-fermion systems with Yukawa interaction is well-known for general spatial dimension $d \geq 2$, also in medium. However, we are not aware that the special case $d = 1$ with its peculiar features was discussed in the literature. Furthermore, depending on the respective publication, we find agreement of their and our flow equations w.r.t. the truncation order, the interaction channels, the in-vacuum or in-medium equations, the regulator *etc.*, but never all features at once. Therefore, none of the specific flow equations is really new, but our compilation for $d = 1$ is.

On the other hand, the second part of this chapter is original to the author and his collaborators. Large parts of this chapter are based on Ref. [4] and are also inspired by Refs. [77, 101, 1, 2, 3] and discussions with their authors. This mostly affects the fluid-dynamical interpretation and analysis of the RG flow equations and the resulting numerical setup for their solution.

10.1. Motivation and introduction

In the previous chapter the GN model was analyzed in the μ - T -plane by studying the behavior of the four-fermion coupling. It was found that the position of the line of diverging four-fermion coupling, which was interpreted as a signal of condensation, depends on the number of fermion species N and the fermion energies that enter the loop diagrams via external fermion lines. A dependence on the choice of regulator was not discussed but is certainly present, *cf.* Ref. [348]. Even though the divergence of the four-fermion coupling indicates condensation phenomena, the purely fermionic consideration is inconclusive without studying more than one interaction channel and ignoring their momentum structure.

At this point there are basically two options to proceed. Either one tries to improve the truncation on the fermionic level along the lines of Refs. [348, 350, 351] or one turns to the well-established partially bosonized bGN or GNY model. Of course, the best variant is to combine both approaches, which however presently exceeded the capacities of the people involved in the project, but might be of future interest. We decided for the partially bosonized approach and leave the advanced purely

fermionic approach for future investigations. This is because we are particularly interested in bosonic fluctuations and bosonic self-interactions in the deep IR region, whose description should contain some local effective bosonic potential.

Hence, we turn to the bGN and GNY model in this section, see Section 8.2. Still, this section will not provide any explicit phenomenological and numerical results. Instead, it sets the formal basis for all later calculations in different truncations. Methodical we stick to the FRG formalism. In contrast to the one-loop/FRG analysis of the GN model, the technicalities are more demanding, which is why we spend an entire chapter on their setup.

We therefore start by presenting again the truncation and the regulator. We further comment on the initial conditions for the FRG calculations as well as the concept of dynamical symmetry breaking. The explicit derivation of the RG flow equation is again outsourced to the extensive Appendix E.2.

In the second half of this chapter, we analyze the formal structure of the RG flow equations, especially w.r.t. their fluid-dynamical properties. In particular this affects the RG flow equation of the bosonic local potential, which is decomposed into non-linear diffusive contributions and source-sink terms. We close the chapter with remarks on the role of the chemical potential as a “shock wave” in bosonic field space and briefly recapitulate some aspects of the numerical implementation from Chapter 5.

10.2. The Gross-Neveu-Yukawa model in the FRG formalism

As demonstrated in Section 8.2 it is possible to partially bosonize the GN model via a Hubbard-Stratonovic transformation to obtain the bGN model, which forms an equivalent description of this QFT on the level of the partition function. On the other hand, it is known and discussed in Appendix C.2 or Refs. [550, 54, 57, 100] that during RG flows all possible interaction terms which are compatible with the symmetries of the model are generated on the level of the effective (average) action. Thus, without the artificial truncation of the effective (average) action, we would anyhow end up with an IR theory of interacting fermions and bosons that is most certainly dominated by bosonic self-interactions, irrespective of the starting point being the GN or bGN version.

Hence, the task is to construct a truncation which captures this dynamics best, without going beyond our computational abilities.

10.2.1. The formal setup – the ansatz for the effective average action and the regulator

Having said this, we need a truncation which is on the one hand compatible with the UV theory (either the GN action (8.86) or the bGN action (8.99)) and on the other hand able to describe bosonic and fermionic interactions as well as condensation on all RG scales.

Truncation We choose the following ansatz for the effective average action,

$$\begin{aligned} \bar{\Gamma}_t[\bar{\psi}, \psi, \varphi] &= \\ &= \int_{-\infty}^{\infty} d^d x \int_0^{\beta} d\tau \left[\bar{\psi} \left[Z_{\psi}(t) (\not{\partial} - \mu \gamma^{d+1}) + \frac{1}{\sqrt{N}} h(t, \varphi) \varphi \mathbb{1} \right] \psi - Z_{\varphi}(t) \frac{1}{2} \varphi (\square \varphi) + U(t, \varphi) \right], \end{aligned} \quad (10.1)$$

It comprises a scale-dependent local bosonic potential $U(t, \varphi)$, scale-dependent wave-function renormalizations $Z_{\psi}(t)$ and $Z_{\varphi}(t)$ for the fermions and bosons, and a scale- and field-dependent

Yukawa coupling¹. This truncation can be seen as the first-order contribution of a derivative expansion of the effective average action, where all orders of bosonic self-interactions are considered, but fermion-boson interactions as well as momentum-dependent terms are only included at lowest non-trivial order. The reason why we expect this to be a promising approach to answer the research questions of Section 7.1.3 is the following:

We are especially interested in the low-energy/-momentum limit of the GN model (for external energy scales, μ and T , and deep IR-RG scales), such that a “Taylor-expansion” in powers of derivative couplings seems to be justified.² (As we will see, this assumption seems to be violated already at rather small chemical potential, while large temperatures seem not to be in conflict with the truncation.) If already at small μ and T condensation is not found in the IR, it is unrealistic to find condensation at all.

Since there is only a single spatial dimension, we further expect that once bosonic bound states have formed during the RG flow, the dynamics is dominated by local bosonic scattering. Particles can only go left or right in a single dimension, which implies that also high-order boson self-interaction terms are non-negligible, because particles cannot bypass each other, since there is only one spatial momentum direction. This is where the GN model drastically differs from QCD, where a decent energy and momentum resolution of quark and gluon (self-)interactions is much more important, though higher-order scatterings are simply more unlikely due to the dimensionality and therefore seem to be of minor importance [551, 552, 553, 35]. Oversimplified: the phase space is totally different for different spacetime dimensions. The most extreme example is certainly zero-dimensional QFT, which can be interpreted as an ultra-local QFT in a single point, where self-interaction terms of all orders are of equal relevance, see Part I.

Another advantage of our truncation is that condensation is straightforwardly detected by a non-trivial global minimum of $U(t \rightarrow \infty, \varphi)$, as is discussed in Section 10.2.3.

A splitting of the wave-function renormalizations into components which are orthogonal and perpendicular to the heat bath is not considered in this work, but might be of future interest, see, *e.g.*, Refs. [554, 555].

Truncation continued: matching the UV theory Using the ansatz (10.1) also enables to make contact to the bGN model in terms of the classical microscopic action (8.99) in the UV. Hence, for $t = 0$, which corresponds to $k = \Lambda$ (the UV cutoff scale), the local bosonic effective potential should approach a purely parabolic shape, *i.e.*,

$$U(t = 0, \varphi) = \frac{1}{2g^2} h^2 \varphi^2. \quad (10.2)$$

In addition, the Yukawa coupling is supposed to be field-independent and takes its UV initial value,

$$h(t = 0, \varphi) = h. \quad (10.3)$$

Ultimately, for the bosonic and fermionic wave-function renormalizations we need

$$Z_\psi(t = 0) = 1, \quad Z_\varphi(t = 0) = 0, \quad (10.4)$$

in order to match the bGN action (8.99).³

It remains to choose suitable initial values for h and g^2 that possibly depend on the UV cutoff Λ . In principle this choice should be unique, because the running of the four-fermion coupling with energy is uniquely defined after fixing some reference energy scale, *cf.* the discussion in Sections 9.3 and 9.4. We come back to this issue below, after discussing the RG flow equations as well as the renormalization procedure for the unique infinite- N results.

¹Already at this point we remark that while deriving RG flow equations for a field-dependent Yukawa coupling, we restricted our entire numerical analysis to a field-independent but scale-dependent Yukawa coupling.

²This is for example supported by Ref. [71], which shows that in vacuum it is important to include dynamical wave-function renormalizations, while higher momentum dependences seem to be of secondary importance.

³Note that for numerical calculations it is not possible to choose exactly $Z_\varphi(t = 0) = 0$ as becomes clear from the flow equations. Hence, we choose a negligibly small value for practical considerations, *cf.* Refs. [372, 373, 374].

The regulator Working in the FRG formalism necessitates the choice of a regulator function for the handling of (IR) divergences. For the fermions, we utilize the same regulator as for the four-fermion calculation of Chapter 9. It remains to choose a regulator for the bosons. Here, we also choose a dimensionally reduced Litim regulator, which solely acts on the bosonic spatial momenta, while keeping the Matsubara modes untouched, see Eqs. (E.38) to (E.40). Instead of repeating the reasoning for this choice, we refer to the discussion in Section 9.2.2 and Appendices C.2.1 and D.2 as well as Ref. [4, Sec. III C].

10.2.2. The RG flow equations

Next, we shall present the RG flow equations that result from the ansatz (10.1). A detailed derivation of these equations is presented in Appendix E.2, but is partially also found elsewhere. (The respective references are cited in the appendix.)

However, before we present explicit results, we introduce renormalized and rescaled quantities. The so-called renormalized fields and the renormalized Yukawa coupling are indicated by the letter “r” and defined as follows, see, *e.g.*, Refs. [556, 374, 66],

$$\varphi_r \equiv Z_\varphi^{\frac{1}{2}} \varphi, \quad \psi_r \equiv Z_\psi^{\frac{1}{2}} \psi, \quad \bar{\psi}_r \equiv Z_\psi^{\frac{1}{2}} \bar{\psi}, \quad h_r \equiv Z_\psi^{-1} Z_\varphi^{-\frac{1}{2}} h. \quad (10.5)$$

(Function(al) arguments are dropped for the sake of readability.) In addition, we define the field-dependent fermion mass and its renormalized counterpart,

$$m \equiv \frac{1}{\sqrt{N}} h \varphi, \quad m_r \equiv \frac{1}{\sqrt{N}} h_r \varphi_r = \frac{1}{\sqrt{N}} Z_\psi^{-1} Z_\varphi^{-\frac{1}{2}} h Z_\varphi^{\frac{1}{2}} \varphi = Z_\psi^{-1} m. \quad (10.6)$$

Furthermore, it is convenient to work in so-called $\frac{1}{N}$ -rescaled quantities to allow a connection between finite- N and infinite- N results. A similar approach was taken in Sections 3.3 and 6.8 We therefore substitute

$$\varphi \mapsto \check{\varphi} = \frac{1}{\sqrt{N}} \varphi, \quad U(t, \varphi) \mapsto \check{U}(t, \check{\varphi}) = \frac{1}{N} U(t, \varphi) \quad (10.7)$$

on the level of the bare fields. The substitution is analogous for the renormalized fields. In addition, we introduce the constant background-field configuration

$$\check{\varphi}_{\text{ren}}(\tau, \vec{x}) = \check{\sigma}_r = \text{const.}, \quad (10.8)$$

which is used to reduce the FRG flow equations to a systems of ODEs and PDEs. (The renormalized constant field configuration $\check{\sigma}_r$ still depends on the RG time t .)

Having these definitions at hand, we are ready to present and analyze the RG flow equations of the GNY model in $d = 1$.⁴

Local bosonic potential

The RG flow equation for the local bosonic effective potential is given by Eq. (E.51) and is derived in Appendix E.2.1,

$$\begin{aligned} \partial_t \check{U}(t, \check{\sigma}_r) + \frac{1}{2} \eta_\varphi(t) \check{\sigma}_r \partial_{\check{\sigma}_r} \check{U}(t, \check{\sigma}_r) = & \quad (10.9) \\ = -\frac{1}{\pi} \left[1 - \frac{\eta_\varphi(t)}{3} \right] \frac{1}{N} k^3 \frac{1}{\beta} \sum_{n=-\infty}^{\infty} \frac{1}{\omega_n^2 + k^2 + \partial_{\check{\sigma}_r}^2 \check{U}(t, \check{\sigma}_r)} + \\ & + \frac{1}{\pi} \left[1 - \frac{\eta_\psi(t)}{2} \right] d_\gamma k^3 \frac{1}{\beta} \sum_{n=-\infty}^{\infty} \frac{1}{(\nu_n + i\mu)^2 + k^2 + m_r^2(t, \check{\sigma}_r)}. \end{aligned}$$

⁴Flow equations for $d \neq 1$ are also found in the corresponding appendices.

It comprises a boson and fermion loop contribution and is given on a diagrammatic level by Eq. (E.47). The Matsubara sums can be further evaluated using Eqs. (B.13) and (B.15), which is not done here for the sake of readability. The RG flow equation of the effective potential depends on the scale evolution of the anomalous dimensions, respectively the wave-function renormalizations and the Yukawa coupling, which is absorbed in the fermion mass.

Bosonic anomalous dimension

The corresponding scale evolution of the bosonic anomalous dimension is found from Eq. (E.78),

$$\begin{aligned} \eta_\varphi(t) = & + \frac{1}{\pi} \frac{1}{N} [\partial_{\check{\sigma}_r}^3 \check{U}(t, \check{\sigma}_r)]^2 k^3 \frac{1}{\beta} \sum_{n=-\infty}^{\infty} \frac{1}{[\omega_n^2 + k^2 + \partial_{\check{\sigma}_r}^2 \check{U}(t, \check{\sigma}_r)]^4} + \\ & + 2 \frac{1}{\pi} d_\gamma [\partial_{\check{\sigma}_r} m_r(t, \check{\sigma}_r)]^2 \times \\ & \times \left[-2 m_r^2(t, \check{\sigma}_r) k^3 \frac{1}{\beta} \sum_{n=-\infty}^{\infty} \frac{1}{[(\nu_n + i\mu)^2 + k^2 + m_r^2(t, \check{\sigma}_r)]^4} + \right. \\ & \left. + \frac{1}{4} k \frac{1}{\beta} \sum_{n=-\infty}^{\infty} \frac{1}{[(\nu_n + i\mu)^2 + k^2 + m_r^2(t, \check{\sigma}_r)]^2} \right]. \end{aligned} \quad (10.10)$$

The anomalous dimension is related to the wave-function renormalization by Eq. (C.62) and the derivation of this flow equation is presented in Appendix E.2.2. The diagrammatic equation for the RG flow of the two-point function, Eq. (E.53), does not perfectly match the structure of Eq. (10.10), because additional momentum derivatives and an evaluation at vanishing external momentum is required to arrive at the latter equation. Again Eq. (10.10) still contains Matsubara sums, which can be further evaluated using Eqs. (B.24), (B.20), and (B.25). Further, note that the r.h.s. of this flow equation still depends on the background field $\check{\sigma}_r$, while the l.h.s. is field-independent. This traces back to the fact that we consider a field-independent wave-function renormalization. Hence, the r.h.s. has to be evaluated at a single specific $\check{\sigma}_r$. We come back to the choice of the evaluation point below. We also remark that the RG flow equation of the bosonic anomalous dimension, apart from the standard differences in the prefactors and powers of k *etc.*, strongly depends on the number of spatial dimensions d , as is discussed in Appendix E.2.2.

Fermionic anomalous dimension

Next, we present the scale evolution of the fermionic anomalous dimension, see Eq. (E.114) from Appendix E.2.4, which is in fact trivial in $d = 1$,

$$\eta_\psi(t) = 0. \quad (10.11)$$

This implies that the fermionic wave-function renormalization keeps its initial value, Eq. (10.4). In addition it drastically simplifies the other flow equations. The diagrammatic equation from which this result is derived is Eq. (E.89).

Yukawa coupling – fermion mass

The same (diagrammatic) equation is used to derive Eq. (E.109), thus the RG evolution equation of the field-dependent fermion mass, which is equivalent to the field-dependent flow equation of

the Yukawa coupling, reads

$$\begin{aligned}
& \partial_t m_r(t, \check{\sigma}_r) + \eta_\psi(t) m_r(t, \check{\sigma}_r) + \frac{1}{2} \eta_\varphi(t) \check{\sigma}_r \partial_{\check{\sigma}_r} m_r(t, \check{\sigma}_r) = \tag{10.12} \\
& = -2 \frac{1}{\pi} \left[1 - \frac{\eta_\varphi(t)}{3} \right] \frac{1}{N} [\partial_{\check{\sigma}_r} m_r(t, \check{\sigma}_r)]^2 m_r(t, \check{\sigma}_r) k^3 \times \\
& \quad \times \frac{1}{\beta} \sum_{n=-\infty}^{\infty} \frac{1}{[\omega_n^2 + k^2 + \partial_{\check{\sigma}_r}^2 \check{U}(t, \check{\sigma}_r)]^2} \frac{1}{(\nu_{n+m} + i\mu)^2 + k^2 + m_r^2(t, \check{\sigma}_r)} - \\
& \quad - 2 \frac{1}{\pi} \left[1 - \frac{\eta_\varphi(t)}{3} \right] \frac{1}{N} [\partial_{\check{\sigma}_r} m_r(t, \check{\sigma}_r)]^2 m_r(t, \check{\sigma}_r) k^3 \times \\
& \quad \times \frac{1}{\beta} \sum_{n=-\infty}^{\infty} \frac{1}{\omega_{n-m}^2 + k^2 + \partial_{\check{\sigma}_r}^2 \check{U}(t, \check{\sigma}_r)} \frac{1}{[(\nu_n + i\mu)^2 + k^2 + m_r^2(t, \check{\sigma}_r)]^2} - \\
& \quad - \frac{1}{\pi} \left[1 - \frac{\eta_\varphi(t)}{3} \right] \frac{1}{N} [\partial_{\check{\sigma}_r}^2 m_r(t, \check{\sigma}_r)] k^3 \frac{1}{\beta} \sum_{n=-\infty}^{\infty} \frac{1}{[\omega_n^2 + k^2 + \partial_{\check{\sigma}_r}^2 \check{U}(t, \check{\sigma}_r)]^2}.
\end{aligned}$$

Note that the r.h.s. of this PDE still depends on the “index” m of the external Matsubara mode that enters the loops via the fermion legs.

In complete analogy to the discussion in Section 9.4.2 in the context of the β -function of the four-fermion coupling, we need to choose some m . Again, an evaluation at the Fermi surface with $m = -\frac{i\mu}{2\pi T} - \frac{1}{2}$ renders the Matsubara sums and the entire flow equation real, due to Matsubara sums (B.18), (B.22), and (B.23). However, as already discussed in Section 9.4.2 this evaluation seems to be questionable, because an integer is evaluated at a complex number.

However, choosing $m = 0$ generates complex contributions to the RG flow equations, because the Matsubara sums contain bosonic and fermion frequencies, see Eqs. (B.32) and (B.34). The appearance of complex contributions in this type of flow equations or loop calculations at non-zero μ and T is well-known and discussed at various occasions, *cf.* Refs. [531, 548, 66, 549, 275]. Usually these discussions are valuable but ultimately seem to be inconclusive and mostly lead to some motivational arguments for a certain handling of this issue. In order to study this flow equation numerically it is usually argued in one or the other way that the imaginary part should be ignored and only the real part has to enter the system of ODEs and PDEs. From our discussion in Section 9.4.2 we generally believe that it is not correct to simply ignore the imaginary contribution to the RG flow, because interference effects between various complex contributions may be present at non-zero RG scales k . However, we agree that the IR couplings should be real after RG evolution. Still, imaginary parts may be present during the flow and influence the real parts, *e.g.*, because the fermion mass enters the fermion propagators in all flow equations quadratically.

However, here, in contrast to the Section 9.4.2, we are facing a system of PDEs and ODEs and we were not able to show that the imaginary part adds up to zero after the RG flow, which might be a problem of an inconsistent truncation or incomplete basis. Anyhow, for the moment we leave this highly interesting and relevant topic for future investigations, because it exceeds the scope of this work and we simply take the same approach as everybody else: We drop the imaginary part on the r.h.s. of Eq. (10.12) by hand and hope for the best.

Further remarks on the PDE-ODE system

In total, within this truncation, the above RG flow equations form a system of two PDEs, Eqs. (10.10) and (10.12), and an algebraic equation, Eq. (10.10), where the RG time plays the role of the time – the evolution parameter – and the constant background field (space) can be interpreted as the spatial domain.

Working in bare (unrenormalized) fields, the algebraic equation (10.10) turns into an ODE for the wave-function renormalization and the PDEs are slightly modified. (Actually we will use the

second version for our numerical computations as explained within the next paragraphs.)

It is also possible to further simplify this system by studying even more streamlined truncations and approximations. Within the next Chapters 11 and 12 we are going to analyze the above equations in a bunch of different approximations schemes, which are improved and compared to each other little by little.

However, before diving into these calculations, we need to comment on two leftover topics. The first affects the signals and the detection of discrete chiral \mathbb{Z}_2 symmetry breaking and/or restoration within our truncation, which is discussed within the next paragraphs. The other topic concerns a detailed analysis of the specific type of PDEs and ODEs that we are confronted with as well as the resulting numerical implementation that is needed for their adequate solution. This is discussed in the next Section 10.3.

10.2.3. Discrete chiral symmetry breaking during RG flows and in the IR

In Section 8.2.3 we briefly discussed that the breaking of the discrete chiral \mathbb{Z}_2 symmetry of the GN model is detected on the level of the bosonized partition function via a non-vanishing expectation value for the boson field $\langle\phi\rangle \neq 0$.

In the FRG formalism this translates to a non-trivial ground state of the IR effective action. This means that after solving the RG flow equations, one has to search for the field configuration that minimizes the IR effective action $\Gamma[\Phi]$ to detect the vacuum state of the system [18, 42, 550]. This vacuum field configuration may either break or be symmetric under discrete chiral symmetry transformations (8.19) and (8.100).

On a formal level, *e.g.*, for the specific truncation (10.1), one searches for solutions of the quantum equations of motion for the mean fields $\bar{\psi}$, ψ , and φ ,

$$0 \stackrel{!}{=} \frac{\delta \bar{\Gamma}_{t_{\text{IR}}}[\bar{\psi}, \psi, \varphi]}{\delta \bar{\psi}} = [Z_{\psi}(t_{\text{IR}}) (\not{\partial} - \mu \gamma^{d+1}) + \frac{1}{\sqrt{N}} h(t_{\text{IR}}, \varphi) \varphi \mathbb{1}] \psi, \quad (10.13)$$

$$0 \stackrel{!}{=} \frac{\delta \bar{\Gamma}_{t_{\text{IR}}}[\bar{\psi}, \psi, \varphi]}{\delta \varphi} = \left[\frac{1}{\sqrt{N}} [h(t_{\text{IR}}, \varphi) + \varphi \partial_{\phi} h(t_{\text{IR}}, \varphi)] \bar{\psi} \psi - Z_{\varphi}(t_{\text{IR}}) \square \varphi + \partial_{\varphi} U(t_{\text{IR}}, \varphi) \right], \quad (10.14)$$

(where the equation for $\bar{\psi}$ was not listed separately) and studies these solutions.

Spatially homogeneous symmetry breaking/restoration

Usually one studies these equations for vanishing fermion mean fields, $\bar{\psi}(\tau, \vec{x}) = \psi(\tau, \vec{x}) = 0$, and further assumes that the ground-state field configuration of the bosonic field is constant in spacetime, $\varphi(\tau, \vec{x}) = \text{const.} = \sigma$, thus translationally invariant. In this approximation one arrives at the condition

$$0 \stackrel{!}{=} \partial_{\sigma} U(t_{\text{IR}}, \sigma). \quad (10.15)$$

Furthermore, one needs $0 < \partial_{\sigma}^2 U(t_{\text{IR}}, \sigma)$ at this extremum to ensure that it is a minimum and that the vacuum is stable, *viz.* has a positive IR curvature mass for the bosonic field. Hence, in the FRG framework one detects spatially homogeneous discrete chiral \mathbb{Z}_2 -symmetry breaking by looking for (non-)trivial global minima of the effective local bosonic potential in the IR – the chiral condensate. For a trivial minimum $\sigma_{\text{min}} = 0$ the system is in the symmetric phase, while for $\sigma_{\text{min}} \neq 0$ the system is in the symmetry-broken phase.

Within this thesis and the associated publication [4] we are not only interested in the symmetry of the system in the IR, but also in the dynamics of symmetry breaking and restoration, which can be studied during the RG flow.

From the discussion of the purely fermionic GN model in Chapter 9 and various infinite- N calculations, *cf.* Section 7.3.1, we expect dynamical symmetry breaking at some RG scales during the RG flow by attractive fermion interactions for sufficiently low μ and T . However, based on the arguments from Section 7.4 long-range bosonic fluctuations may also destroy any kind of condensate at non-zero T , such that the \mathbb{Z}_2 symmetry is again restored in the deep IR. This is studied by looking at the RG scale-dependent minimum $\sigma_{\min}(t)$ of $U(t, \sigma)$ during the RG flow.

Condensation and vaporization during a single RG flow is a realization of the so-called precondensation phenomenon, which is discussed in Refs. [557, 558, 559, 560, 561, 278] in the context of FRG applications.

Spatially inhomogeneous condensation

One might wonder whether the restriction to ground states with $\bar{\psi}(\tau, \vec{x}) = \psi(\tau, \vec{x}) = 0$ and $\varphi(\tau, \vec{x}) = \text{const.} = \sigma$ is too restrictive and more involved solutions of the quantum equations of motion (10.13) and (10.14) with even smaller effective action exist. Furthermore, one might ask whether it is always justified in the FRG formalism to assume a constant background-field configuration for the calculation of the IR effective action.

At least in certain approximations there is evidence that so-called spatially inhomogeneous condensates exist, which minimize the effective action, see Sections 7.1.1 and 7.3.1 and Refs. therein, and that these field configurations emerge as self-consistent solutions, where the calculation of the IR effective action already includes them in terms of background fields. Even the possibility of so-called time crystals was discussed in (semi-)classical approximations, *cf.* Refs. [562, 563, 564], where the ground state is formed by an oscillatory condensate. Therefore the answer is certainly that the assumptions are too restrictive.

On the other hand it strongly depends on the specific research question: Sometimes it is sufficient to assume a homogeneous background-field configuration and a homogeneous ground state, *e.g.*, at large T where condensation is absent, and to study perturbations of the homogeneous trivial ground state in terms of a stability analysis. By successively lowering T and μ one detects regions, where this method predicts an instability of the homogeneous solution. This is a perfectly valid approach to detect second-order PTs to regions of spatially homogeneous and inhomogeneous condensation and is discussed and analyzed in detail in Section 11.3.

Another occasion where the assumption of a spatially homogeneous background-field configuration as well as homogeneous ground state might be justified is the following: If there are regions in a phase diagram where inhomogeneous condensation is already excluded in approximations without bosonic fluctuations (infinite- N), *e.g.*, at very low T and μ in the GN model, it is highly unlikely that beyond this approximation any kind of inhomogeneous condensate forms in this region of the phase diagram.

Within this work we are therefore always working with a spatially homogeneous background field and under the assumption of spatially homogeneous condensation. Spatially inhomogeneous condensation is exclusively detected/predicted indirectly via the instability of the homogeneous ground state.⁵

⁵Another formal reason for this approach is that working with position-dependent background-field configurations in the FRG formalism is highly complicated due to the non-trivial momentum structure and off-diagonal contributions in the two-point functions that need to be inverted. Currently there are some advances by deploying properties of very special oscillating background-field configurations such as chiral spirals [6, 547]. Notwithstanding these successes it is unlikely that more complicated field configurations can be used for FRG calculations, because the inversion of the two-point functions is either analytically or numerically far too demanding.

10.3. The FRG and (numerical) fluid dynamics

In the second part of this chapter we turn to the formalities of the system of PDEs and ODEs that is formed by the RG flow equations (10.9) to (10.12) and its numerical implementation. Here we use recently (re)discovered analogies between (computational) fluid dynamics and RG flows, *cf.* Chapter 5 and Refs. [77, 1, 2, 3, 4], which also form the basis of this discussion. The primary observation of these works was that the flow equation for the effective local bosonic potential of a huge class of models and QFTs can be recast into a conservation law – more specifically an advection-diffusion-sink/source equation, where the RG time plays the role of the temporal direction and field space takes the role of the spatial coordinates. Similar considerations are put forward for the flow equation of a field-dependent Yukawa coupling in Ref. [101]. Based on the formulation in terms of conservation laws and coupled ODEs one can adapt advanced methods from the field of CFD as already discussed in Chapters 5 and 6 for the case of the $O(N)$ model.

10.3.1. The LPA' truncation as a non-linear heat equation with sink/source terms

The starting point of our discussion is formed by some additional modifications and simplifications of Eqs. (10.9) to (10.12).

1. Within this work we will not numerically investigate the RG evolution of a field-dependent Yukawa coupling or fermion mass, but restrict ourselves to a field-independent but scale-dependent Yukawa coupling. The simple reason are ongoing technical developments [101] which are not covered by this work. Therefore Eq. (10.12) is evaluated at a specific point in the background-field space, which still needs to be specified.
2. Another modification affects the background-field space itself. Working with renormalized fields and couplings (10.5) has two direct consequences. First, in contrast to RG flow equations for bare fields there are additional terms on the l.h.s. of Eqs. (10.9) and (10.12), which modify the character of the equations and fluid-dynamical analogy. The second consequence is seen from the UV initial condition for the bosonic wave-function renormalization (10.4). When it changes from zero (or a numerically extremely small value) to non-zero values that are numerically several orders of magnitude larger during the RG evolution, the field-space is completely rescaled according to Eq. (10.5). Hence, huge domains in renormalized field space would be required for an adequate description of the bosonic local effective potential, because the physically interesting region is expected to move simply by rescaling of the fields. This is not the case if Eq. (10.9) is solved on the level of bare fields, which also allows for better comparison with conventional infinite- N calculations. The price one has to pay for working in bare fields is that Eq. (10.10) turns into an ODE for $Z_\varphi(t)$, which also appears explicitly in the other flow equations.

Taking into account these two modifications, the actual PDE-ODEs system that is studied in this work is

$$\begin{aligned} \partial_t \check{U}(t, \check{\sigma}) = & -\frac{1}{\pi} \left[1 - \frac{\eta_\varphi(t)}{3} \right] \frac{1}{N} k^3 \frac{1}{\beta} \sum_{n=-\infty}^{\infty} \frac{1}{\omega_n^2 + k^2 + \frac{1}{Z_\varphi(t)} \partial_\sigma^2 \check{U}(t, \check{\sigma})} + \\ & + \frac{1}{\pi} d_\gamma k^3 \frac{1}{\beta} \sum_{n=-\infty}^{\infty} \frac{1}{(\nu_n + i\mu)^2 + k^2 + h^2(t) \check{\sigma}^2}, \end{aligned} \quad (10.16)$$

$$\begin{aligned} \partial_t Z_\varphi(t) = & + \frac{1}{\pi} \frac{1}{N} \frac{1}{Z_\varphi^2(t)} \left[\partial_\sigma^3 \check{U}(t, \check{\sigma}) \right]^2 k^3 \frac{1}{\beta} \sum_{n=-\infty}^{\infty} \frac{1}{[\omega_n^2 + k^2 + \frac{1}{Z_\varphi(t)} \partial_\sigma^2 \check{U}(t, \check{\sigma})]^4} + \\ & + 2 \frac{1}{\pi} d_\gamma h^2(t) \left[-2 h^2(t) \check{\sigma}^2 k^3 \frac{1}{\beta} \sum_{n=-\infty}^{\infty} \frac{1}{[(\nu_n + i\mu)^2 + k^2 + h^2(t) \check{\sigma}^2]^4} + \right. \end{aligned} \quad (10.17)$$

$$\begin{aligned}
& + \frac{1}{4} k \frac{1}{\beta} \sum_{n=-\infty}^{\infty} \frac{1}{[(\nu_n + i\mu)^2 + k^2 + h^2(t) \check{\sigma}^2]^2} \Big]. \\
\partial_t h(t) = & - 2 \frac{1}{\pi} \frac{1}{N} \frac{1}{Z_\varphi(t)} h^3(t) k^3 \operatorname{Re} \left(\left[1 - \frac{\eta_\varphi(t)}{3} \right] \times \right. \\
& \times \frac{1}{\beta} \sum_{n=-\infty}^{\infty} \frac{1}{[\omega_n^2 + k^2 + \frac{1}{Z_\varphi(t)} \partial_{\check{\sigma}}^2 \check{U}(t, \check{\sigma})]^2} \frac{1}{(\nu_n + i\mu)^2 + k^2 + h^2(t) \check{\sigma}^2} + \\
& \left. + \frac{1}{\beta} \sum_{n=-\infty}^{\infty} \frac{1}{\omega_n^2 + k^2 + \frac{1}{Z_\varphi(t)} \partial_{\check{\sigma}}^2 \check{U}(t, \check{\sigma})} \frac{1}{[(\nu_n + i\mu)^2 + k^2 + h^2(t) \check{\sigma}^2]^2} \right). \tag{10.18}
\end{aligned}$$

where we refrained from listing the trivial flow equation for $Z_\psi(t)$. Still, the latter two equations need to be evaluated at a specific $\check{\sigma}$, which turns them into ODEs. Oftentimes this truncation and system of FRG flow equations is denoted as local potential approximation prime (LPA'), which can be seen as the first correction to the famous LPA truncation. However, sometimes LPA and LPA' are also used for truncations that include field-dependent Yukawa couplings, since these still exclusively comprise local-non-derivative interaction terms, see, *e.g.*, Refs. [66, 35, 72, 565, 101, 276] for details.

In total, one simply ends up with a single PDE and two coupled ODEs. Next, one proceeds analogously to what is done in Section 5.1: One takes another derivative of Eq. (10.16) w.r.t. $\check{\sigma}$ and defines

$$\check{u}(t, \check{\sigma}) \equiv \partial_{\check{\sigma}} \check{U}(t, \check{\sigma}). \tag{10.19}$$

The resulting equation has conservative form

$$\partial_t \check{u}(t, \check{\sigma}) = \frac{d}{d\check{\sigma}} Q[t, \partial_{\check{\sigma}} \check{u}(t, \check{\sigma}), Z_\varphi(t), \partial_t Z_\varphi(t), h(t)] + S[t, \check{\sigma}, Z_\varphi(t), h(t)], \tag{10.20}$$

where Q is a diffusion flux and S a source term. (If our QFT also involves Nambu-Goldstone modes, these enter the flow equation in terms of an advection term.) On this level the interpretation of the RG time $t \in [0, \infty)$, *cf.* Eq. (D.1), as a temporal variable and $\check{\sigma} \in (-\infty, \infty)$ as the spatial domain is rather natural, if the ‘‘conserved quantity’’ $\check{u}(t, \check{\sigma})$ is viewed as some abstract fluid field that moves in field space.

The boson loop – diffusion in field space

First, we turn to the bosonic contribution to the flow equation. If we use the formula (B.13) for the Matsubara sum the diffusion flux explicitly reads

$$Q[t, \partial_{\check{\sigma}} \check{u}(t, \check{\sigma}), Z_\varphi(t), \partial_t Z_\varphi(t), h(t)] = -\frac{1}{\pi} \left[1 - \frac{\eta_\varphi(t)}{3} \right] \frac{1}{N} \frac{k^3(t)}{2E_\varphi} \left[1 + 2 n_b \left(\frac{E_\varphi}{T} \right) \right], \tag{10.21}$$

where the bosonic ‘‘energy’’

$$E_\varphi^2 \equiv k^2(t) + \frac{1}{Z_\varphi(t)} \partial_{\check{\sigma}} \check{u}(t, \check{\sigma}), \tag{10.22}$$

is introduced for the sake of readability.

The interpretation of Q in Eq. (10.20) as a diffusion flux becomes apparent by performing the field-space derivative in Eq. (10.20),

$$\begin{aligned}
& \frac{d}{d\check{\sigma}} Q[t, \partial_{\check{\sigma}} \check{u}(t, \check{\sigma}), Z_\varphi(t), \partial_t Z_\varphi(t), h(t)] = \\
& = D[t, \partial_{\check{\sigma}} \check{u}(t, \check{\sigma}), Z_\varphi(t), \partial_t Z_\varphi(t), h(t)] \partial_{\check{\sigma}}^2 u(t, \check{\sigma}). \tag{10.23}
\end{aligned}$$

In the absence of the source term S the RG flow equation for the effective local bosonic potential has turned into a heat equation with a highly non-linear diffusion coefficient D .

Interestingly, there are some direct consequences of this reformulation of the RG flow equation.

As discussed in detail in Section 5.1.3, the reinterpretation of the bosonic contribution to the RG flow in terms of highly non-linear diffusion in field space shows the irreversible character of the RG. Because diffusion is a dissipative process, the bosonic term clearly introduces a “thermodynamic arrow of time” [170] into the RG flow. In total this may be interpreted as a realization of Kadanoff’s irreversible block-spin transformations [185] and the impossibility of integrating backwards in RG time, thus to smaller scales and higher energies, *cf.* Refs. [161, 285, 99]. Furthermore, from this we also expect that it might be possible to identify a quantity, which can be interpreted as an entropy function for the PDE and RG flow, similarly to Section 5.1.4. However, as discussed in this context the presence of sink/source terms violates properties like TVD/TVNI, which is usually needed for the definition of monotonically increasing/decreasing (global) functionals for a PDE.

Another immediate consequence is that the interpretation of the flow equation in terms of a (non-linear) heat equation strongly restricts the particular (numeric) values that can be taken by the factors that enter the diffusion flux, respectively the diffusion coefficient. Actual diffusion equations require manifestly positive diffusion coefficients, here D , to ensure existence of a (weak) solution and stable convergence against this solution while solving the PDE [168].

The fermion loop – source-sink terms in field space

Second, we present the sink-source term, which contributes to the PDE (10.20). In LPA’ truncation without field dependences of the Yukawa coupling and wave-function renormalizations, the fermion loop enters the RG flow of the effective local bosonic potential in terms of a sink-source term in field space, which is (RG-)time and (field-space-)position dependent, *i.e.*,

$$S[t, \check{\sigma}, Z_\varphi(t), h(t)] = \frac{d}{d\check{\sigma}} \left(\frac{1}{\pi} d_\gamma \frac{k^3(t)}{2E_\psi} \left[1 - n_f \left(\frac{E_\psi + \mu}{T} \right) - n_f \left(\frac{E_\psi - \mu}{T} \right) \right] \right), \quad (10.24)$$

where we also defined the fermionic “energy” for the sake of readability,

$$E_\psi^2 \equiv k^2(t) + h^2(t) \check{\sigma}^2, \quad (10.25)$$

and used Eq. (B.15) for the evaluation of the Matsubara sum. Note that this term does not depend on the fluid field $u(t, \check{\sigma})$ itself. As a direct consequence, the fermion contribution to the RG flow is basically independent of the evolution of the effective potential itself – at least in the LPA truncation, where the indirect back-reaction of the potential via the Yukawa coupling and bosonic wave-function renormalization is artificially suppressed.

It is also interesting that the source term (10.24) is on a formal level a classical potential of a conservative (external) force field, which acts on the fluid, *e.g.*, like a Newtonian gravitational potential [105].

If the $\check{\sigma}$ derivative in Eq. (10.24) is evaluated, one finds a positive contribution to the RG flow for $\check{\sigma} < 0$ – a source – and a negative contribution for $\check{\sigma} > 0$ – a sink – for $\mu = 0$. For non-zero μ the situation is more involved and the term no longer strictly positive or negative definite. Especially for small or zero temperatures the chemical potential introduces additional sinks and sources in terms of “moving spikes” into the problem, which are superimposed on the structure with opposite sign. This is discussed within the next paragraphs and interpreted as a kind of shock wave in field space.

(Computational) boundary conditions in field-space

If and only if there are well-defined initial and boundary conditions for a PDE the actual problem of solving the PDE is well-posed. As discussed in detail in Section 5.2.3 the problem at hand presents a pure initial-value problem on \mathbb{R} , because the domain of the RG flow equation for $u(t, \check{\sigma})$ is $\check{\sigma} \in (-\infty, \infty)$. Hence, formally, there are no boundary conditions required and the problem is fully defined via (the derivative of) the UV initial condition (10.2). However, for a numerical

treatment, we explained in detail that it is sensible to deploy the \mathbb{Z}_2 symmetry and introduce an artificial reflective boundary condition for the derivative of the effective potential via its anti-symmetry,

$$u(t, \check{\sigma}) = -u(t, -\check{\sigma}), \quad (10.26)$$

to restrict the problem to $\check{\sigma} \in [0, \infty)$. Furthermore, it is necessary to restrict this infinite domain to a finite computational domain by introducing another artificial boundary condition at some $\check{\sigma}_{\max}$ via some extrapolation.

For details we refer to Section 5.2.3 and Ref. [1, Sec. IV D].

The chemical potential as a “shock wave” in field space

Analyzing the RG flow equation of the derivative of the effective potential in terms of a non-linear diffusion equation with sink-source terms also allows for a better formal understanding of the role of the chemical potential on the level of the PDE. Within the next lines, we argue that the chemical potential presents a kind of external shock wave that enters the problem at a certain (RG-)time and (field-space-)position. This is particularly relevant for very small or zero temperatures, which is why we exemplify the effect for $T = 0$ and $T = 0.01$. Furthermore, we start our discussion by ignoring the diffusive contribution to the RG flow of the effective potential (the boson loop), because μ primarily enters the dynamics via the fermionic sink-source term.⁶

δ -peaks in the fermionic source-sink term We begin by plotting the sink-source term (10.24) for different values of μ , each at several RG scales k , in Fig. 10.1 for $T = 0$ and $T = 0.01$. The RG scales are chosen to be approximately near the model scales, which are set by the dimensionful Yukawa coupling, that was fixed to $h = 1$. In order to make sense of this plot and the underlying dynamics, we focus on the $T = 0$ case⁷, where according to Eq. (B.16) the source term reads,

$$S[t, \check{\sigma}, Z_\varphi(t), h(t)] = \frac{d}{d\check{\sigma}} \left(\frac{1}{\pi} d_\gamma \frac{k^3(t)}{2E_\psi} \Theta \left(\frac{E_\psi}{|\mu|} - 1 \right) \right). \quad (10.27)$$

As expected, one clearly finds that the chemical potential does not enter the dynamics as long as $E_\psi^2 \geq \mu^2$, where the flow is identical to the $\mu = 0$ scenario. However, at $E_\psi^2 \approx \mu^2$ the chemical potential becomes relevant as can be seen by inspecting the Heaviside function in Eq. (10.27). The relevant inequality therefore is

$$E_\psi^2 \stackrel{(10.25)}{=} k^2 + h^2 \check{\sigma}^2 \lesssim \mu^2. \quad (10.28)$$

The first time this inequality is fulfilled is at $k \approx 0.5$ and $k \approx 1.0$ for the middle and lower panel of Fig. 10.1 at $\check{\sigma} \approx 0$. Further lowering k implies that also larger $|\check{\sigma}|$ are affected by μ . The largest value of $\check{\sigma}$ that is ever directly affected by μ is therefore at $h^2 \check{\sigma}^2 \approx \mu^2$, for $t \rightarrow \infty$ and $k(t) \rightarrow 0$ in the deep IR. We conclude that the information about the presence of the chemical potential propagates from $\check{\sigma} = 0$ to large $|\check{\sigma}|$. The associated peaks in the plot are located at $\check{\sigma} \pm \frac{1}{h} \sqrt{\mu^2 - k^2(t)}$ for $\mu^2 > k^2(t)$.

The reason why μ shows up in terms of peaks in the sink-source term is rather obvious from the structure of Eq. (10.27), where the $\check{\sigma}$ -derivative hits the Heaviside Θ -function and thereby produces a δ -peak, which is smeared out for $T \neq 0$.

The informed reader might wonder why this spectacular effect was never discussed this way before. The reason could be the following: As long as bosonic fluctuations are completely suppressed by the $N \rightarrow \infty$ limit, there is

⁶Within this discussion we ignore that the chemical potential also contributes via the flow equations of the Yukawa coupling and bosonic wave-function renormalization, because this is expected to be a sub-leading effect as long as $h(t)$ and $Z_\varphi(t)$ are field-independent.

⁷The approximate signs within this discussion hold for small non-zero temperatures and become exact for $T = 0$.

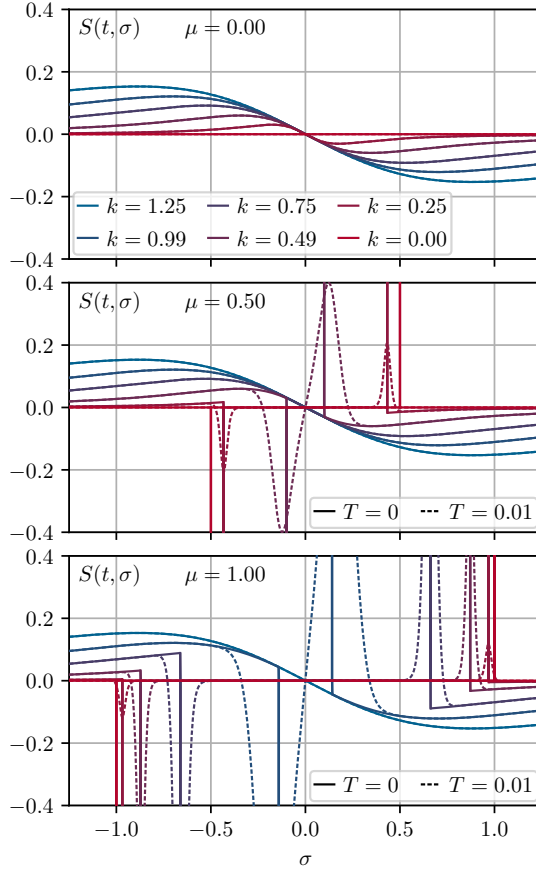


Figure 10.1: Source-sink term of Eq. (10.24) with Yukawa coupling $h = 1$ at zero (solid lines) and small temperature $T = 0.01$ (dashed lines) at various RG scales k (close and below the model scales) between $k = 1.25$ in blue and $k = 0$ in red at $\mu = 0$ (upper panel), $\mu = 0.5$ (middle panel), and $\mu = 1.0$ (lower panel). From Ref. [4, Fig. 1].

1. no reason to work on the level of the derivative of the effective potential.
2. all points in field space decouple and the RG flow can be solved independently for each $\check{\sigma}$, which is rather natural, if the fermion-loop contribution is identified as a local source term in field space.

Together this means that the chemical potential indeed shows up in terms of cusps in the local bosonic potential, due to the Heaviside Θ -functions, though without having any further consequences for mean-field calculations.

The interplay with bosonic fluctuations This is different as soon as bosonic fluctuations are taken into account. Here, as we have just learned, the boson loop introduces a non-linear diffusion and couples points in field space. In the vicinity of jumps or cusps gradients are large, which implies huge diffusive dynamics.⁸ In fact, a cusp in $u(t, \check{\sigma})$ leads to a jump in $\partial_{\check{\sigma}} u(t, \check{\sigma})$, which however has drastic consequences for the stability of the PDE. This is understood easily by inspecting the bosonic energy (10.22). For the sake of simplicity, we assume $Z_{\varphi}(t) = 1$, which

⁸The highly non-linear structure of the diffusion flux (10.21) also leads to a non-linear diffusion, which is indeed driven by the gradients of $u(t, \check{\sigma})$, but strongly depends on the interplay of the single contributions in Eq. (10.21). Therefore it can even enhance cusps and gradients in contrast to an ordinary heat equation.

corresponds to the LPA truncation, *i.e.*,

$$E_\varphi^2 = k^2(t) + \partial_{\check{\sigma}} \check{u}(t, \check{\sigma}). \quad (10.29)$$

As just said, the chemical potential starts entering the dynamics of the RG flow if $\mu^2 \approx k^2$ in terms of δ -distributions in the source term, which lead to jumps/cusps in $u(t, \check{\sigma})$. These lead to jumps in $\partial_{\check{\sigma}} u(t, \check{\sigma})$ with negative sign, as can be seen from the sign of the source terms in Fig. 10.1. In total, this results in a negative bosonic energy (10.29) at $k^2 \approx \mu^2$ for certain points $\check{\sigma}$ in field space. This should not be allowed by construction, because the poles of the Euclidean propagators should never be overshoot during the RG flow. Here, however, the chemical potential enters the dynamics in terms of an external “shock”, which cannot be cushioned smoothly by the PDE, such that the PDE turns ill-conditioned. This is also experienced in numerical computations, see Chapter 12, and as discussed later on, we do not believe that including the dynamics of the scale-dependent Yukawa coupling and wave-function renormalization help much, as long as their field dependences are ignored.

Of course, this effect is only strictly present for the $T \rightarrow 0$ limit of the flow equation, because already very small $T \neq 0$ leads to a smearing of the δ -peaks in the source term and smearing of cusps and jumps in the effective potential and its derivatives. Nevertheless, the smaller T the harder it gets to resolve this dynamics numerically.

The two questions which are immediately arising from this analysis are the following:

1. Why was this effect not discussed before in the context of FRG calculations in the LPA approximation of fermion-boson systems at (non-)zero T and non-zero μ in structurally similar systems like the QMM?
2. Where does this effect come from and is it curable?

A possible explanation why this problem was not described before in numerous FRG model studies at non-zero chemical potential might be that calculations were usually performed on the level of the effective potential itself, where this effect is only visible in terms of (smeared) cusps. Furthermore, on top of this, the effective potential was usually discretized in field space via numerical methods which rely on smoothness or even analyticity, see references in Section 1.2.2. In order to make them work at all in the vicinity of possible non-analytic dynamics, oftentimes an extremely low resolution in terms of a little number of grid points or expansion coefficients was chosen. In consequence, details of the potentials were washed out and buried under low resolution. Furthermore, we have the impression that this also led authors to stop RG flows at rather large IR cutoffs and avoid computations at really low temperatures and non-zero chemical potentials, due to instabilities.

However, even if one chooses a decent discretization scheme, which is in general capable of resolving discontinuities of all kinds, the problem is still present, because it is manifest to the PDE. We are not sure how this problem can be resolved ultimately, but we believe that it will be a combination of improvements of the regulators and truncation. We come back to this discussion in Section 12.4.

Numerical implementation

For all details of the numerical implementation of the PDE for the effective potential we refer the reader to Section 5.2 of this thesis and Refs. [4, Sec. IV E] and [1, Sec. IV B-D], which shall not be repeated here.

10.3.2. The $N \rightarrow \infty$ limit – suppression of diffusion and decoupling in field space

As a last point, before we turn to the explicit calculations in different approximations, let us formally study what happens to the PDE-ODE system (10.16) to (10.18) in the $N \rightarrow \infty$ limit from the field-theoretical and fluid-dynamical perspective.

Due to the $\frac{1}{N}$ -rescaling from Eq. (10.7) we find that all contributions to the RG flow equations which involve internal boson lines are accompanied by prefactors of $\frac{1}{N}$. Hence, taking the $N \rightarrow \infty$ limit is straightforward and we end up with,

$$\partial_t \check{U}(t, \check{\sigma}) = \frac{1}{\pi} d_\gamma k^3 \frac{1}{\beta} \sum_{n=-\infty}^{\infty} \frac{1}{(\nu_n + i\mu)^2 + k^2 + h^2(t) \check{\sigma}^2}, \quad (10.30)$$

$$\begin{aligned} \partial_t Z_\varphi(t) = & 2 \frac{1}{\pi} d_\gamma h^2(t) \left[-2 h^2(t) \check{\sigma}^2 k^3 \frac{1}{\beta} \sum_{n=-\infty}^{\infty} \frac{1}{[(\nu_n + i\mu)^2 + k^2 + h^2(t) \check{\sigma}^2]^4} + \right. \\ & \left. + \frac{1}{4} k \frac{1}{\beta} \sum_{n=-\infty}^{\infty} \frac{1}{[(\nu_n + i\mu)^2 + k^2 + h^2(t) \check{\sigma}^2]^2} \right]. \end{aligned}$$

$$\partial_t h(t) = 0. \quad (10.31)$$

As a first result, we observe that the bare Yukawa coupling is no longer evolving with RG time and keeps its UV initial value. The renormalized Yukawa h_r coupling is still trivially running, if Z_φ changes with RG time, due to Def. (10.5). The same would have happened in a truncation with a field-dependent Yukawa coupling, see Eq. (10.12). As a direct consequence, one can simply use the value of the Yukawa coupling in the UV as a reference scale of dimension energy and express all other dimensionful quantities in terms of the Yukawa coupling. This effectively corresponds to absorbing the Yukawa coupling in the background field and working with a dimensionful background field configuration, as is usually done in MF calculations, *cf.* references in Section 7.3. For the moment, however, we keep the Yukawa coupling explicit but drop its RG-time dependence. Furthermore, we find that the remaining flow equations for the effective potential and the wave-function renormalization decouple. On top of that, the PDE for $\check{U}(t, \check{\sigma})$ reduces to an ODE for each $\check{\sigma}$, because $\check{U}(t, \check{\sigma})$ and its field-space derivatives no longer appear on the r.h.s. of the equation. Hence, the flow equations for the effective potential and the bosonic wave-function renormalization, *i.e.*,

$$\partial_t \check{U}(t, \check{\sigma}) = \frac{1}{\pi} d_\gamma k^3 \frac{1}{\beta} \sum_{n=-\infty}^{\infty} \frac{1}{(\nu_n + i\mu)^2 + k^2 + h^2 \check{\sigma}^2}, \quad (10.32)$$

$$\begin{aligned} \partial_t Z_\varphi(t) = & 2 \frac{1}{\pi} d_\gamma h^2 \left[-2 h^2 \check{\sigma}^2 k^3 \frac{1}{\beta} \sum_{n=-\infty}^{\infty} \frac{1}{[(\nu_n + i\mu)^2 + k^2 + h^2 \check{\sigma}^2]^4} + \right. \\ & \left. + \frac{1}{4} k \frac{1}{\beta} \sum_{n=-\infty}^{\infty} \frac{1}{[(\nu_n + i\mu)^2 + k^2 + h^2 \check{\sigma}^2]^2} \right], \end{aligned} \quad (10.33)$$

can be simply integrated separately, which is done in the next Chapter 11.

From the fluid-dynamical perspective the $N \rightarrow \infty$ limit completely suppresses the diffusion. This is analogous to what was found for the $N \rightarrow \infty$ limit of the zero-dimensional $O(N)$ model in Sections 5.1.5 and 6.8, where $N \rightarrow \infty$ also suppresses the diffusion in the fluid-dynamical picture. In contrast to the $O(N)$ model, where we remain with purely advective contributions from the pion modes, the GNY model does not include pions. Here, we end up with the contribution of the fermion loop, thus exclusively source-sink terms. Now, from this point of view the decoupling in field space is rather natural: The “fluid” is simply too viscous to move, but some fluid is added/removed locally. Already at this point it is obvious that this approximation will spoil fundamental properties of the system, similar to what was found and discussed in Section 6.8.

Chapter 11

The Gross-Neveu(-Yukawa) model at infinite N

Abstract We discuss the phenomenology of the bosonized Gross-Neveu (bGN) model at $N \rightarrow \infty$. We start with the integration and renormalization of the flow equation of the effective bosonic potential. From this, the phase structure under the assumption of spatially homogeneous condensation is calculated. In addition, we present various thermodynamic quantities as functions of μ and T .

In the second half of the chapter we turn to the bosonic momentum structure of the theory which is generated from the fermion fluctuations. The starting point is an analysis of the bosonic wave-function renormalization in the μ - T -plane which indicates the instability of spatially homogeneous condensation in some regions of the phase diagram. Because an analysis of the wave-function renormalization is inconclusive, we turn to the full momentum structure of the bosonic two-point function, to study the stability of the spatially homogeneous ground state. In particular, we compare the predictions from this analysis with the true ground state of the $N \rightarrow \infty$ bGN model, which comprises spatially inhomogeneous condensation, and benchmark the predictive power of the stability analysis.

All results of this section are also discussed w.r.t. their implications on calculations at finite N .

Disclosure Many the results in this chapter are well-known and can be found elsewhere. Explicit references are provided in the text.

The new part of this work is mainly the second part, which comprises detailed tests of the well-known concept of a stability analysis based on the bosonic two-point function. In particular, the explicit results for the bosonic two-point function and wave-function renormalization were not presented to this extent before.

Most of the explicit calculations, results, and plots in this chapter are based on our own publications [4, 5]. Ref. [5] in turn is based on preliminary results and notes by S. Rechenberger [566, 567].

11.1. Overview

In this chapter we turn to explicit solutions of the RG flow equations of the GNY model. Even though we are in general interested in the phenomenology and thermodynamics of the GN model at finite N we entirely focus on the $N \rightarrow \infty$ approximation throughout this chapter. The reason for this is manifold.

First, we show that we recover well-known results for the GN model in the infinite- N limit also from the FRG formalism. We take this opportunity to visualize several (thermodynamic) quantities which were in parts also calculated before, but – to the best of our knowledge – not presented

together. Later on, some of these results also serve as limiting tests for our numerical setup, which is used for calculations at finite N . In addition, we use the $N \rightarrow \infty$ calculations to construct the correct UV initial values for the four-fermion coupling and subsequently the UV potential, see Eq. (10.2), which is required to achieve RG consistency and compare calculations at infinite and finite N by starting with a unique UV theory. Despite better knowledge, we generally assume spatially homogeneous condensation and use constant background field configurations for calculations at any μ and T . The reason underlying this approximation is outlined in Section 10.2.3. Notwithstanding this restriction, we can still get deeper insight into regions of the phase diagram, where this assumption is known to be wrong. To this end, we use the second part of this chapter to focus on the momentum structure of the theory.

Specifically, we first analyze the bosonic wave-function renormalization as an indicator for the instability of spatially homogeneous ground states. With the help of this we scan the μ - T plane and identify regions of negative wave-function renormalization.

We discuss why this analysis is inconclusive and turn to the full momentum structure of the bosonic two-point function. Via a so-called stability analysis of the spatially homogeneous ground state we show that we can recover the established second-order PT between a \mathbb{Z}_2 -symmetric phase at high temperature and a phase of spatially inhomogeneous condensation at small/moderate T and large μ , which is the true ground state at $N \rightarrow \infty$ there. This can be seen as a proof of concept study, which validates the general applicability of this method for the detection of crystalline ground states by simply investigating the stability of a symmetric phase. Furthermore, we compare the details of the momentum structure of the two-point function to the dominating wave vector of the respective true ground state in the inhomogeneous phase.

Thirdly, we draw direct conclusions from the momentum structure of the two-point function at $N \rightarrow \infty$ for the construction of decent truncations of FRG calculations at finite N . Later on this helps in understanding the results of the subsequent chapter and points towards further improvements of FRG truncations in upcoming works.

11.2. Spatially homogeneous condensation

We start by focusing on the solution of the flow equation for the effective bosonic potential at $N \rightarrow \infty$ and ignore the flow equation for the bosonic wave-function renormalization and the momentum structure of the theory for the moment. After adjusting our notation for the sake of readability, we integrate the ODE for the effective potential and present the renormalization procedure. As a byproduct we obtain the UV-cutoff dependence of the UV potential, which we later on need for the RG flows at finite N . After the derivation of a formula for the renormalized IR potential at any μ and T , we extract all kind of information about the phase diagram and thermodynamic observables from this result.

11.2.1. Conventions

For the sake of readability the conventions of this chapter are adjusted as follows:

1. We exclusively work with $\frac{1}{N}$ -rescaled quantities, see Eq. (10.7). Therefore, we can suppress explicit indication of N and replace $\check{\sigma} \rightarrow \sigma$ and $\check{U}(t, \check{\sigma}) \rightarrow U(t, \sigma)$.
2. The only energies which appear in this chapter are the fermionic energies (10.25). Hence, we simply use $E_\psi \mapsto E = \sqrt{k^2 + h^2 \sigma^2}$.
3. Within this chapter we exclusively use the RG scale k instead of the RG time t as argument of RG-time-/scale-dependent quantities. Both are related by Eq. (D.1).

Using these conventions Eqs. (10.32) and (10.33) turn into

$$\partial_k U(k, \sigma) = -\frac{d_\gamma}{\pi} k^2 \frac{1}{\beta} \sum_{n=-\infty}^{\infty} \frac{1}{(\nu_n + i\mu)^2 + E^2}, \quad (11.1)$$

$$\partial_k Z_\varphi(k) = \frac{d_\gamma}{2\pi} h^2 \left[\frac{1}{\beta} \sum_{n=-\infty}^{\infty} \frac{8 h^2 \sigma^2 k^2}{[(\nu_n + i\mu)^2 + E^2]^4} - \frac{1}{\beta} \sum_{n=-\infty}^{\infty} \frac{1}{[(\nu_n + i\mu)^2 + E^2]^2} \right]. \quad (11.2)$$

11.2.2. Integrating the flow equation of the effective potential

We start by analyzing the flow equation (11.1). Before we actually perform the k -integration, we perform the Matsubara sum,

$$\begin{aligned} \partial_k U(k, \sigma) &= -\frac{d_\gamma}{\pi} k^2 \frac{1}{\beta} \sum_{n=-\infty}^{\infty} \frac{1}{(\nu_n + i\mu)^2 + E^2} \stackrel{\text{(B.15)}}{=} \\ &= -\frac{d_\gamma}{\pi} k^2 \frac{1}{2E} \left[1 - n_f\left(\frac{E+\mu}{T}\right) - n_f\left(\frac{E-\mu}{T}\right) \right]. \end{aligned} \quad (11.3)$$

The result in terms of Fermi-Dirac distributions (B.2) or tanh-functions is characteristic for the FRG formalism using dimensionally reduced spatial Litim regulators. Similar results can be found for example in Refs. [245, 66, 568, 569] (for higher dimensional systems).

Next, we perform the RG-scale integration by hand due to the separation and decoupling in field space, which was discussed in Section 10.3.2. Integrating from some large UV (cutoff) scale $k = \Lambda$ to the IR, thus $k = 0$, we formally find

$$U(k=0, \sigma) = U(\Lambda, \sigma) + \frac{d_\gamma}{\pi} \int_0^\Lambda dk \frac{k^2}{2E} \left[1 - n_f\left(\frac{E+\mu}{T}\right) - n_f\left(\frac{E-\mu}{T}\right) \right], \quad (11.4)$$

where $U(k=0, \sigma)$ is the physical IR potential and $U(\Lambda, \sigma)$ is the UV potential, which is defined according to Eq. (10.2),

$$U(\Lambda, \sigma) = \frac{1}{2g^2} h^2 \sigma^2. \quad (11.5)$$

Note that this result looks slightly different than what is usually obtained in “standard” MF calculations, *e.g.*, by studying the $N \rightarrow \infty$ limit in the path-integral formalism, see references in Section 7.3. Both results are simply related by an integration by parts and a surface term,

$$\begin{aligned} U(k=0, \sigma) &= U(\Lambda, \sigma) + \left[\frac{d_\gamma}{2\pi} k \left[E + T \ln \left(1 + e^{-\frac{E+\mu}{T}} \right) + T \ln \left(1 + e^{-\frac{E-\mu}{T}} \right) \right] \right]_0^\Lambda \\ &\quad + \frac{d_\gamma}{\pi} \int_0^\Lambda dk \left[E + T \ln \left(1 + e^{-\frac{E+\mu}{T}} \right) + T \ln \left(1 + e^{-\frac{E-\mu}{T}} \right) \right]. \end{aligned} \quad (11.6)$$

The additional surface term is field-dependent and therefore enters the solution of the vacuum gap equation (see below), which makes the FRG formalism different from conventional MF calculations, *e.g.*, in sharp-cutoff regularization. The reason behind is that flat Litim-type regulators and sharp-cutoff regulators result in slightly different RG flow equations [244, 352, 166]. In order to recover the standard result for the gap equation with sharp-cutoff regularization, we would have to use the FRG analogue of this regularization scheme.

However, in a renormalizable QFT the IR is unique after renormalization and independent of the actual regularization procedure (as long as fundamental properties of the theory are not violated by the regulator). Hence, our next question simply is how we have to choose $\frac{1}{g^2}$ as a function of Λ such that $U(k=0, \sigma)$ is unique and does not depend on the actual choice of Λ – as long as Λ

is significantly greater than all other dimensionful quantities like h , μ , and T . If Λ independence, thus RG consistency, is achieved, we can simply send $\Lambda \rightarrow \infty$ and remove the artificial cutoff from the system – at least in the $N \rightarrow \infty$ calculations, where “pen and paper integration” is possible. Inspecting the first μ - and T -independent contribution to the integral, which is UV divergent, this implies that $\frac{1}{g^2}$ has to diverge in exactly the same way.

11.2.3. The gap equation and renormalization of the effective potential

Before we start our discussion, let us introduce another change in conventions and replace

$$U(k=0, \sigma) \rightarrow U(\sigma, \mu, T). \quad (11.7)$$

In this chapter the IR is always exactly at $k=0$ and we do not have to artificially stop a numerical integration at some IR cutoff k_{IR} . In consequence, it is not required to indicate $k=0$ all the time. However, it will simplify the discussion to explicitly indicate if we are working at vanishing or arbitrary temperature and/or chemical potential.

Let us turn to the actual renormalization procedure. We choose to perform the renormalization in vacuum at $\mu = T = 0$, where Eq. (11.4) reduces to

$$\begin{aligned} U(\sigma, 0, 0) &= \frac{1}{2g^2} h^2 \sigma^2 + \frac{d_\gamma}{2\pi} \int_0^\Lambda dk \frac{k^2}{\sqrt{k^2 + h^2 \sigma^2}} = \\ &= \frac{1}{2g^2} h^2 \sigma^2 + \frac{d_\gamma}{4\pi} \left[\Lambda^2 \sqrt{1 + \frac{h^2 \sigma^2}{\Lambda^2}} - h^2 \sigma^2 \operatorname{artanh} \left(\left[1 + \frac{h^2 \sigma^2}{\Lambda^2} \right]^{-\frac{1}{2}} \right) \right]. \end{aligned} \quad (11.8)$$

The medium contributions (the Fermi-Dirac distributions) are UV-finite anyhow. From our earlier discussion in Chapter 9 we expect that there is condensation, *i.e.*, non-trivial minima in the effective potential, at small μ and T and especially in vacuum. Fixing these minima at the dimensionless values $\sigma = \pm\sigma_0$ and expressing all dimensionful quantities in units of the UV Yukawa coupling h , we can construct the appropriate Λ dependence and therefore divergence structure of $\frac{1}{g^2}$.

The vacuum gap equation

Considering the extremum condition

$$0 = \partial_\sigma U(\sigma, 0, 0) \Big|_{\sigma=\sigma_0} \stackrel{(11.8)}{=} \quad (11.9)$$

$$= h^2 \sigma_0 \left(\frac{1}{g^2} + \frac{d_\gamma}{2\pi} \left[\left(1 + \frac{h^2 \sigma_0^2}{\Lambda^2} \right)^{-\frac{1}{2}} - \operatorname{artanh} \left(\left[1 + \frac{h^2 \sigma_0^2}{\Lambda^2} \right]^{-\frac{1}{2}} \right) \right] \right)$$

under the assumption that there are two non-trivial minima $\pm\sigma_0 \neq 0$, we can discard the $\sigma_0 = 0$ solution as a maximum and find for $\Lambda \gg h\sigma_0$,

$$\frac{1}{g^2} = \frac{d_\gamma}{2\pi} \left[- \left(1 + \frac{h^2 \sigma_0^2}{\Lambda^2} \right)^{-\frac{1}{2}} + \operatorname{artanh} \left(\left[1 + \frac{h^2 \sigma_0^2}{\Lambda^2} \right]^{-\frac{1}{2}} \right) \right] = \quad (11.10)$$

$$= \frac{d_\gamma}{2\pi} \left[-1 + \frac{1}{2} \ln \left(\frac{4\Lambda^2}{h^2 \sigma_0^2} \right) \right] + \mathcal{O} \left(\frac{h^2 \sigma_0^2}{\Lambda^2} \right). \quad (11.11)$$

The explicit crosscheck that $\pm\sigma_0$ are indeed minima is presented below, when we plot the effective potential and present the curvature mass (the second field-space derivative of the potential at the minimum).

In any case, some comments are in order:

1. The asymptotic behavior of Eq. (11.11) for large Λ exactly matches the logarithmic divergence of the inverse four-fermion coupling in the purely fermionic framework, see Eq. (9.15). However, here, $h\sigma_0$ serves as the effective IR cutoff and reference scale, which was not available in the vacuum calculation without bosonic degrees of freedom and had to be mimicked by an IR cutoff k_{IR} in Section 9.3.4. The additional “−1” term in Eq. (11.11) stems from the different regularization prescriptions. In any case, the result again indicates the asymptotic freedom of the GN model in its bosonized version [158, 19, 422, 177],

$$\lim_{\frac{\Lambda}{h\sigma_0} \rightarrow \infty} g^2 = 0. \quad (11.12)$$

2. Formally, we can solve Eq. (11.11) for the minima, *i.e.*,

$$\sigma_0 = \pm \frac{2\Lambda}{h} e^{-\left(\frac{2\pi}{d_\gamma g^2} + 1\right)}. \quad (11.13)$$

Thus, the formation of the two non-trivial minima and \mathbb{Z}_2 -symmetry breaking is directly linked to the asymptotically free behavior and can be seen as a realization of dimensional transmutation [158, 466, 464, 463, 465], where a dimensionful IR theory emerges from a scale-invariant UV theory.

3. Inserting the result (11.10) into Eq. (11.5) by eliminating the four-fermion coupling, we obtain the explicit Λ dependence of the UV potential in units of the vacuum fermion mass $h\sigma_0$,

$$U(\Lambda, \sigma) = \frac{d_\gamma}{4\pi} h^2 \sigma^2 \left[- \left(1 + \frac{h^2 \sigma_0^2}{\Lambda^2} \right)^{-\frac{1}{2}} + \text{artanh} \left(\left[1 + \frac{h^2 \sigma_0^2}{\Lambda^2} \right]^{-\frac{1}{2}} \right) \right]. \quad (11.14)$$

On the level of the bosonic effective potential asymptotic freedom is realized in terms of a decoupling of bosonic modes from the system. For $\frac{\Lambda}{h\sigma_0} \rightarrow \infty$ the effective potential solely comprises the bosonic mass term, which logarithmically diverges, such that the bosons get ultra-massive and vanish as dynamical degrees of freedom. Hence, we are left with a theory of (asymptotically) free fermions.

In the next chapter, we discuss that Eq. (11.14) can also be used as the UV initial condition for FRG flows at finite N .

The renormalized effective potential and its derivatives

Now we are prepared for the renormalization procedure. Inserting the UV potential Eq. (11.14) into the vacuum IR potential (11.8), one finds

$$U(\sigma, 0, 0) = \frac{d_\gamma}{4\pi} \left(\Lambda^2 \sqrt{1 + \frac{h^2 \sigma^2}{\Lambda^2}} + h^2 \sigma^2 \left[- \left(1 + \frac{h^2 \sigma_0^2}{\Lambda^2} \right)^{-\frac{1}{2}} + \text{artanh} \left(\left[1 + \frac{h^2 \sigma_0^2}{\Lambda^2} \right]^{-\frac{1}{2}} \right) - \text{artanh} \left(\left[1 + \frac{h^2 \sigma^2}{\Lambda^2} \right]^{-\frac{1}{2}} \right) \right] \right). \quad (11.15)$$

It is straightforward to crosscheck that $0 = \partial_\sigma U(\sigma, 0, 0)|_{\sigma=\pm\sigma_0}$. Furthermore, even for finite Λ we find

$$\partial_\sigma^2 U(\sigma, 0, 0)|_{\sigma=\pm\sigma_0} = \frac{d_\gamma}{2\pi} \frac{\Lambda^3}{(\Lambda^2 + h^2 \sigma_0^2)^{\frac{3}{2}}} h^2. \quad (11.16)$$

This confirms that the curvature mass is manifestly positive, such that $\pm\sigma_0$ are indeed minima. Ultimately removing the UV cutoff from the theory by sending $\frac{\Lambda}{h\sigma_0} \rightarrow \infty$ results in the famous renormalized vacuum IR potential [158, 466, 464, 463, 465]

$$U(\sigma, 0, 0) = \frac{d_\gamma}{8\pi} h^2 \sigma^2 \left[\ln \left(\frac{h^2 \sigma^2}{h^2 \sigma_0^2} \right) - 1 \right] - \frac{d_\gamma}{4\pi} \Lambda^2 + \mathcal{O} \left(\frac{h^2 \sigma^2}{\Lambda^2} \right), \quad (11.17)$$

with curvature mass

$$m_\sigma^2 = \frac{d_\gamma}{2\pi} h^2 \quad (11.18)$$

at its minima. The infinite constant $\propto \Lambda^2$ is unobservable and can be ignored in the following. Similar to the calculation in vacuum, we can derive the renormalized potential for any μ and T ,

$$U(\sigma, \mu, T) = \quad (11.19)$$

$$= U(\sigma, 0, 0) - \frac{d_\gamma}{\pi} \int_0^\infty dk \frac{k^2}{2E} [n_f(\frac{E+\mu}{T}) + n_f(\frac{E-\mu}{T})] \stackrel{(11.17)}{=} \quad (11.20)$$

$$= \frac{d_\gamma}{4\pi} \left(\frac{1}{2} h^2 \sigma^2 \left[\ln \left(\frac{h^2 \sigma^2}{h^2 \sigma_0^2} \right) - 1 \right] - \int_{-\infty}^\infty dk \frac{k^2}{E} [n_f(\frac{E+\mu}{T}) + n_f(\frac{E-\mu}{T})] \right).$$

Using integration by parts for the thermal contribution we recover the standard form of the renormalized effective potential of the GN model in the $N \rightarrow \infty$ limit [466, 465, 458, 457, 327, 460],

$$U(\sigma, \mu, T) = \quad (11.21)$$

$$= \frac{d_\gamma}{4\pi} \left[\frac{1}{2} (h\sigma)^2 \left[\ln \left(\frac{(h\sigma)^2}{(h\sigma_0)^2} \right) - 1 \right] - \int_{-\infty}^\infty dp \left[T \ln \left(1 + e^{-\frac{E+\mu}{T}} \right) + T \ln \left(1 + e^{-\frac{E-\mu}{T}} \right) \right] \right].$$

For later use, we also present the first and the second field-space derivative of this results,

$$\partial_\sigma U(\sigma, \mu, T) = \quad (11.22)$$

$$\begin{aligned} &= \frac{d_\gamma}{4\pi} h^2 \sigma \left[\ln \left(\frac{(h\sigma)^2}{(h\sigma_0)^2} \right) + \int_{-\infty}^\infty dp \frac{1}{E} [n_f(\frac{E+\mu}{T}) + n_f(\frac{E-\mu}{T})] \right] \stackrel{(B.2)}{=} \\ &= \frac{d_\gamma}{4\pi} h^2 \sigma \left[\ln \left(\frac{(h\sigma)^2}{(h\sigma_0)^2} \right) + \int_{-\infty}^\infty dp \frac{1}{E} \left[1 - \frac{1}{2} \tanh \left(\frac{E+\mu}{2T} \right) - \frac{1}{2} \tanh \left(\frac{E-\mu}{2T} \right) \right] \right], \end{aligned}$$

and

$$\partial_\sigma^2 U(\sigma, \mu, T) = \quad (11.23)$$

$$\begin{aligned} &= \frac{d_\gamma}{4\pi} h^2 \left[\ln \left(\frac{(h\sigma)^2}{(h\sigma_0)^2} \right) + 2 + \int_{-\infty}^\infty dp \frac{1}{E} [n_f(\frac{E+\mu}{T}) + n_f(\frac{E-\mu}{T})] - \right. \\ &\quad \left. - (h\sigma)^2 \int_{-\infty}^\infty dp \frac{1}{E^3} \left(n_f(\frac{E+\mu}{T}) + n_f(\frac{E-\mu}{T}) - \right. \right. \\ &\quad \left. \left. - \frac{E}{T} [n_f^2(\frac{E+\mu}{T}) + n_f^2(\frac{E-\mu}{T}) - n_f(\frac{E+\mu}{T}) - n_f(\frac{E-\mu}{T})] \right) \right] \stackrel{(B.4);(B.2)}{=} \\ &= \frac{d_\gamma}{4\pi} h^2 \left[\ln \left(\frac{(h\sigma)^2}{(h\sigma_0)^2} \right) + 2 + \int_{-\infty}^\infty dp \frac{1}{E} \left[1 - \frac{1}{2} \tanh \left(\frac{E+\mu}{2T} \right) - \frac{1}{2} \tanh \left(\frac{E-\mu}{2T} \right) \right] - \right. \\ &\quad \left. - (h\sigma)^2 \int_{-\infty}^\infty dp \frac{1}{E^3} \left(1 - \frac{1}{2} \tanh \left(\frac{E+\mu}{2T} \right) - \frac{1}{2} \tanh \left(\frac{E-\mu}{2T} \right) + \frac{\frac{E}{2T}}{2 \cosh^2(\frac{E+\mu}{2T})} + \frac{\frac{E}{2T}}{2 \cosh^2(\frac{E-\mu}{2T})} \right) \right]. \end{aligned}$$

Table 11.1: Equation numbers of the explicit expressions for the effective potential and its derivative in Appendices F.1.1 and F.1.2.

(a) For $U(\sigma, \mu, T)$.				(b) For $\partial_\sigma U(\sigma, \mu, T)$.				
T	μ	σ	Eq.	T	μ	σ	Eq.	
$\neq 0$	$\neq 0$	$\neq 0$	(11.21)	$\neq 0$	$\neq 0$	$\neq 0$	(11.22)	
		$= 0$	(F.8)			$= 0$	(F.16)	
	$= 0$	$\neq 0$	(F.9)		$= 0$	$\neq 0$	$\neq 0$	(F.17)
		$= 0$	(F.10)				$= 0$	(F.18)
$= 0$	$\neq 0$	$\neq 0$	(F.11)	$= 0$	$\neq 0$	$\neq 0$	(F.19)	
		$= 0$	(F.12)			$= 0$	(F.20)	
	$= 0$	$\neq 0$	(F.13)		$= 0$	$\neq 0$	$\neq 0$	(F.21)
		$= 0$	(F.14)				$= 0$	(F.22)

Of course, we could try to use these formulae to directly study the minimum structure of Eq. (11.21) depending on μ and T numerically. However, for some positions in field space, *i.e.*, $\sigma = 0$, and/or when μ and/or T vanish, the remaining momentum integral of the thermal contribution can either be simplified drastically or additional IR divergences need to be handled carefully. Doing this by hand in advance via a distinction of cases is advisable to avoid numerical instabilities or spurious cancellations. To this end, we prepared Appendices F.1.1 and F.1.2, where we present explicit calculations. The resulting formulae for Eqs. (11.21) and (11.22) for specific choices of μ , T , and σ are referenced in Table 11.1. For the second field-space derivative we do not provide an extra appendix, because explicit formulae for specific choices of μ , T , and σ can be extracted from the zero-momentum limit of the bosonic two-point function, which is studied below in Section 11.3.2 with corresponding Appendix F.1.3. The corresponding formulae are referenced in the last column of Table 11.3b.

11.2.4. The phase diagram

Next, we turn to the explicit calculation of the phase diagram and some thermodynamic quantities – still under the assumption of homogeneous condensation by ignoring the momentum structure.

General phase structure

The first result which comprises the general phase structure as well as some additional important points and curves is presented in Fig. 11.1, which is identical to Refs. [458, Fig. 4] and [461, Fig. 1], but based on our own data. Within the next paragraphs, we briefly summarize on a technical level how the information for the plot was generated from the previously derived formulae. For a more qualitative discussion, we refer to Section 7.3 or the corresponding references in this section.

The condensate The general location of the first- and second-order PT line is calculated by numerically searching for the global minima of Eq. (11.21) by numerically evaluating the formulae listed in Table 11.1a.¹ This can for example be done via a bisection in field space for each μ and T . Non-trivial global minima at $\pm\sigma_{\min}(\mu, T) \neq 0$ correspond to the phase at small $|\mu|$ and T where the \mathbb{Z}_2 symmetry is broken by the ground state, while a trivial global minimum $\sigma_{\min}(\mu, T) = 0$ belongs to the symmetric phase at large $|\mu|$ and T . The position of the global minimum of the potential, which is identical to the vacuum expectation value – the condensate, is plotted as a function of μ and T in terms of a heat map in Fig. 11.2a. The jump of the minimum at the first-order PT and the steady melting at the second-order PT are clearly visible. For a similar

¹The CP and the endpoint of the first-order PT can be calculated analytically. The latter can be determined from the formulae referenced in Table 11.1 to be $(\mu = 1/\sqrt{2}, T = 0)$.

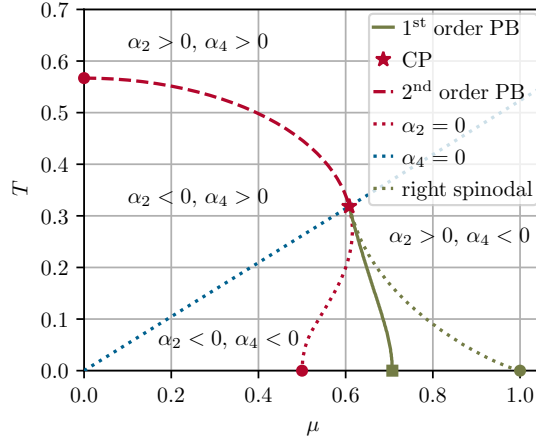


Figure 11.1: The phase diagram of the GN model in the infinite- N limit. The red and blue lines correspond to $\alpha_2 = 0$ and $\alpha_4 = 0$. The red and green dotted lines are the spinodal lines. The green solid line is the first-order PT and goes over to the red dashed line, which marks the second-order PT. The critical point (CP) is marked by the red star. From Ref. [4, Fig. 2].

plot see for example Ref. [526, Fig. 1.1]. The exact location of the PT lines was determined using an AMR algorithm in the μ - T -plane, which is explained below in Section 11.4.

In addition, it is possible to determine the position of the second-order PT line in terms of a closed expression, which is discussed in the subsequent paragraph.

Ginzburg-Landau analysis, spinodal lines, and the curvature mass Before we turn to the other curves in Fig. 11.1, it is instructive to visualize the effective bosonic potential and its derivative explicitly for various positions in the μ - T -plane via the formulae from Table 11.1a. Therefore, we prepared Fig. 11.3. (For similar plots, see Refs. [526, Fig. 1.1] and [457, Figs. 25 & 26].) In Fig. 11.3a for $T = 0$ the non-analytic structure which is induced by the chemical potential is clearly visible in the derivative of the potential, *cf.* our discussion in Section 10.3.1, especially Fig. 10.1. On the other hand, in Fig. 11.3b one finds how increasing the temperature completely smears the cusp that is introduced by the chemical potential. In any case, pumping too much energy into the system by increasing μ or T restores the symmetry by moving the minimum to $\sigma_{\min}(\mu, T) = 0$. Furthermore, we can directly deduce from the plots that there are regions in the μ - T plane where $U(\sigma, \mu, T)$ has exclusively two degenerate global minima, and regions where there exists exclusively a single global trivial minimum. However, there are also values of μ and T around the first-order PT where the potential has three local minima (two degenerate global and one local in the \mathbb{Z}_2 -symmetry-broken region; one global and two degenerate local minima in the \mathbb{Z}_2 -symmetric region). This region is bounded by the so-called spinodal lines (red and green dotted lines in Fig. 11.1). The (green-dotted) spinodal line at larger $|\mu|$ which connects the CP and the point $(\mu = 1.0, T = 0.0)$ can only be extracted numerically, except for its endpoints.²

Still, the (red-dotted) spinodal line, which turns into the (red-dashed) second-order PT line at the CP (the $(\alpha_2 = 0)$ -line), can be calculated in terms of a closed expression. The same applies to the blue-dotted line (the $(\alpha_4 = 0)$ -line), which intersect the $(\alpha_2 = 0)$ -line exactly at the CP. Both can be generated from a Ginzburg-Landau-type expansion of the effective potential Eq. (11.21) about $\sigma = 0$,

$$U(\sigma, \mu, T) = \sum_{n=0}^{\infty} \alpha_{2n}(\mu, T) (\hbar\sigma)^{2n}. \quad (11.24)$$

²The endpoint $(\mu, T) = (1, 0)$ can be read off from Eq. (F.19), see also Fig. 11.3a.

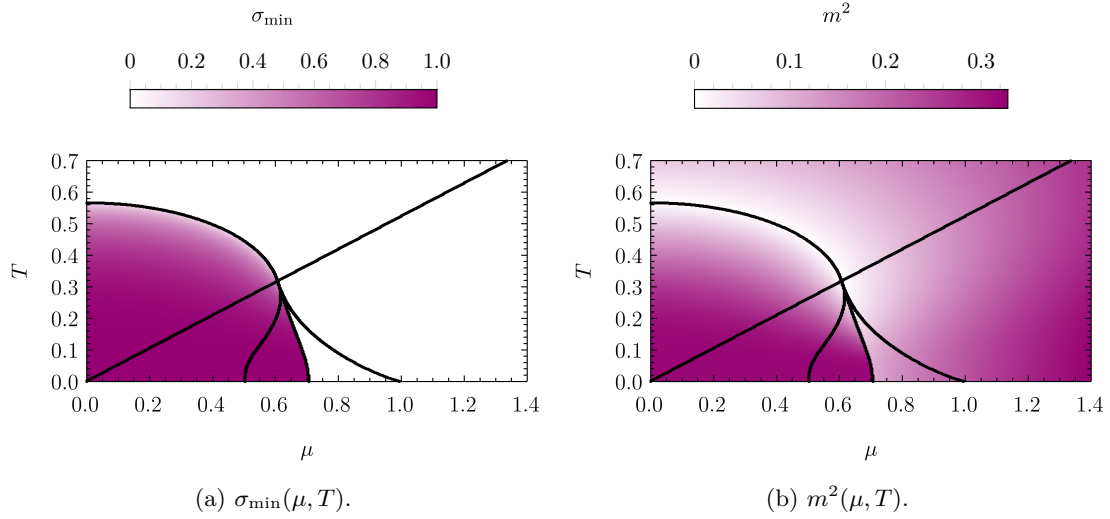


Figure 11.2: The global minimum $\sigma_{\min}(\mu, T)$ of the effective potential and the curvature mass $m^2(\mu, T)$ at this minimum as a function of μ and T .

The coefficients of this expansion are well-known [467, 570, 446]. The zeroth-order coefficient is

$$\alpha_0(\mu, T) = -\frac{\pi}{6} T^2 - \frac{1}{2\pi} \mu^2. \quad (11.25)$$

Below it is identified with the (negative) Stefan-Boltzmann pressure of a massless free gas of fermions in two spacetime dimensions, *cf.* Ref. [377]. The second-order coefficient reads

$$\alpha_2(\mu, T) = \frac{d_\gamma}{4\pi} \begin{cases} \frac{1}{2} \ln \left(\frac{4\mu^2}{h^2 \sigma_0^2} \right), & \text{for } T = 0, \mu > 0, \\ \frac{1}{2} \ln \left(\frac{\pi^2 T^2}{h^2 \sigma_0^2} \right) - \gamma, & \text{for } T > 0, \mu = 0, \\ \frac{1}{2} \ln \left(\frac{4T^2}{h^2 \sigma_0^2} \right) - \gamma - \text{DLi}_0 \left(\frac{\mu}{T} \right), & \text{for } T > 0, \mu > 0, \end{cases} \quad (11.26)$$

where we have used Defs. (A.81). The coefficient is (two times) the curvature mass at $\sigma = 0$, or the bosonic two-point function at vanishing field and vanishing momentum, respectively, see Eqs. (F.37), (F.41), and (F.57). Coefficients for $n > 2$ are given by

$$\alpha_{2n}(\mu, T) = \begin{cases} -\frac{1}{\pi} \frac{(2n-3)!!}{2^{n+1} n! (n-1)!} \mu^{2-2n}, & \text{for } T = 0, \mu > 0, \\ \frac{(-1)^n}{\pi^{2n-1}} \frac{4^{1-2n} (4^n - 2)(2n-2)!}{n! (n-1)!} \zeta(2n-1) T^{2-2n}, & \text{for } T > 0, \mu = 0, \\ -\frac{1}{\pi} \frac{2^{1-2n}}{n! (n-1)!} \text{DLi}_{2-2n} \left(\frac{\mu}{T} \right) T^{2-2n}, & \text{for } T > 0, \mu > 0. \end{cases} \quad (11.27)$$

where ζ is the Riemann zeta function (A.48).

Using this Ginzburg-Landau expansion, we can identify a second-order PT with those lines, where $\alpha_2 = 0$, while $\alpha_4 > 0$. This criterion directly allows to extract the critical temperature $T_c = \frac{e^\gamma}{\pi}$ at $\mu = 0$. Furthermore, as soon as α_4 vanishes on the ($\alpha_2 = 0$)-line, we know that $\alpha_2 = 0$ no longer marks the PT and turns into a spinodal line with $\alpha_2 = 0$ and $\alpha_4 < 0$. This point is identified as the CP $(\mu_{\text{cp}}, T_{\text{cp}}) \simeq (0.608, 0.318)$.

As expected and by construction, a Ginzburg-Landau expansion is incapable of predicting the first-order PT. Also recalling our earlier discussions from Section 3.3, it has to break down as soon

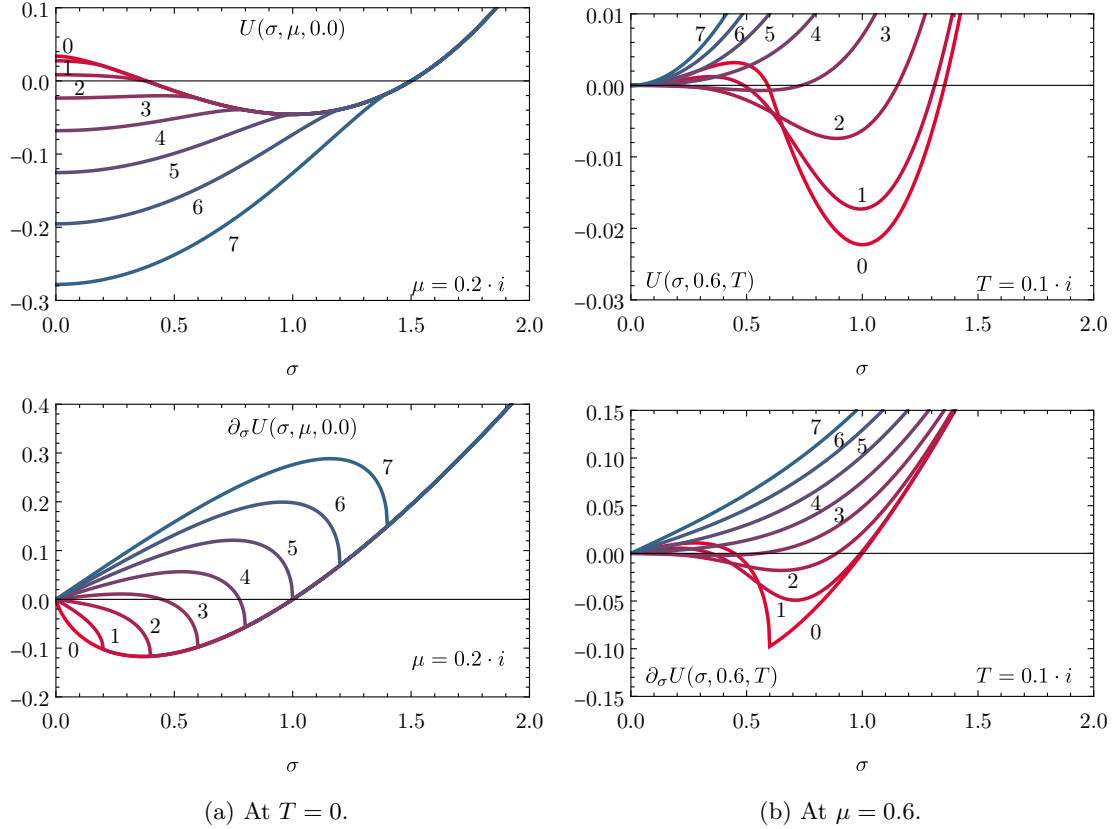


Figure 11.3: The effective potential $U(\sigma, \mu, T)$ and its field-space derivative $\partial_\sigma U(\sigma, \mu, T)$ as functions of σ at varying μ and T . Normalization: left panel: $U(1.5, \mu, 0.0) = 0$; right panel: $U(0.0, 0.6, T) = 0$. (The curves for $i = 3$ of the left panel and the curves for $i = 0$ of the right panel are identical.)

as the relevant information about the phase structure is located at field values σ in the effective potential which are outside the radius of convergence of the expansion. This radius is clearly set by the non-analyticity of the chemical potential.

Nevertheless, Ginzburg-Landau-type studies are a useful tool to approach the effective potential and phase structure [571, 446, 572, 570, 313, 467]. Here, one is not necessarily restricted to constant background-field configurations, but can also assume spatial oscillations of a condensate [313, 573].

In any case, the tricky part is usually the handling of IR divergences. Normally, the IR divergences from the vacuum contribution and the medium contributions cancel in an intriguing way, *cf.* Appendix F. For the calculation of the coefficients Eq. (11.27) we simply used the results of Refs. [574, 575, 523], which comprehensively present the evaluation of high-temperature/Ginzburg-Landau expansions for generic thermodynamic potentials of mean-field models for relativistic Bose and Fermi gases in some background fields and various spacetime dimensions. Before we close the discussion and turn to the thermodynamic observables, some remarks are in order:

1. Interestingly, the ($\alpha_2 = 0$)-spinodal is identical to the line of diverging four-fermion coupling g from the $N \rightarrow \infty$ calculation in the purely fermionic framework of Section 9.4.1, see Fig. 9.2. In retrospect, this is expected, because $\frac{\hbar^2}{g^2}$ is associated to the bosonic mass term (in the symmetric phase) via the Hubbard-Stratonovic transformation, *cf.* Section 8.2.1. Also their RG flow has to be identical at vanishing external momenta and in the $N \rightarrow \infty$ limit, where field space decouples.

Table 11.2: Explicit expressions for some thermodynamic quantities.

(a) For $p(\sigma, \mu, T)$.				(b) For $n(\sigma, \mu, T)$.				(c) For $\mathcal{E}(\sigma, \mu, T)$.						
T	μ	σ	Eq.	T	μ	σ	Eq.	T	μ	σ	Eq.			
$\neq 0$	$\neq 0$	$\neq 0$	(11.32)	$\neq 0$	$\neq 0$	$\neq 0$	(11.35)	$\neq 0$	$\neq 0$	$\neq 0$	(11.40)			
		$= 0$	(F.75)			$= 0$	(F.83)			$= 0$	(F.91)			
	$= 0$	$\neq 0$	(F.76)		$= 0$	$\neq 0$	(F.84)		$= 0$	$\neq 0$	(F.92)	$= 0$	$\neq 0$	(F.93)
		$= 0$	(F.77)			$= 0$	(F.85)			$= 0$	(F.93)			
$= 0$	$\neq 0$	$\neq 0$	(F.78)	$= 0$	$\neq 0$	$\neq 0$	(F.86)	$= 0$	$\neq 0$	$\neq 0$	(F.94)			
		$= 0$	(F.79)			$= 0$	(F.87)			$= 0$	(F.95)			
	$= 0$	$\neq 0$	(F.80)		$= 0$	$\neq 0$	(F.88)		$= 0$	$\neq 0$	(F.96)	$= 0$	$\neq 0$	(F.96)
		$= 0$	(F.81)			$= 0$	(F.89)			$= 0$	(F.97)			

However, extracting the curvature mass always at the global minimum via the second derivative of the effective potential, we obtain a non-vanishing curvature mass at the $\alpha_2 = 0$ spinodal line in the \mathbb{Z}_2 symmetry broken phase. A heat map of the curvature mass in the μ - T -plane is presented in Fig. 11.2b.

2. Finally, we comment again on the shape of the IR potentials and their derivatives, *cf.* Fig. 11.3. As remarked earlier in this work, IR potentials should be convex, see also Refs. [576, 577, 13]. If they have non-trivial minima, then the inner region has to be flat, ending in non-analytical minima. However, as we can see for example from Fig. 11.3, this is not the case for our $N \rightarrow \infty$ results. The reason behind is rather simple: The artificial suppression of bosonic fluctuations manifests as a suppression of diffusion in field space in the RG flow of the derivative of the effective potential. Therefore, we can again conclude that the $N \rightarrow \infty$ approximation violates fundamental properties of a theory and results will drastically change if this restriction is lifted. However, this is the topic of the next Chapter 12 and for the moment we simply ignore this problem.

Thermodynamics

Concerning the phase diagram of a model or theory, one is usually not primarily interested in the location of spinodal lines or the values of certain expansion coefficients of an effective potential. From an experimental and phenomenological standpoint the determination of thermodynamic observables is normally the underlying reason which motivated the calculations in the first place. Therefore, although it is not of utmost importance for the remainder of this work, we consider it instructive to present and plot some standard thermodynamic observables for the GN model at $N \rightarrow \infty$. Plots are presented in Fig. 11.4. These are straightforwardly extracted from the effective potential (11.21) as follows.

The grand canonical potential In thermal QFT the grand canonical potential is defined by [142],

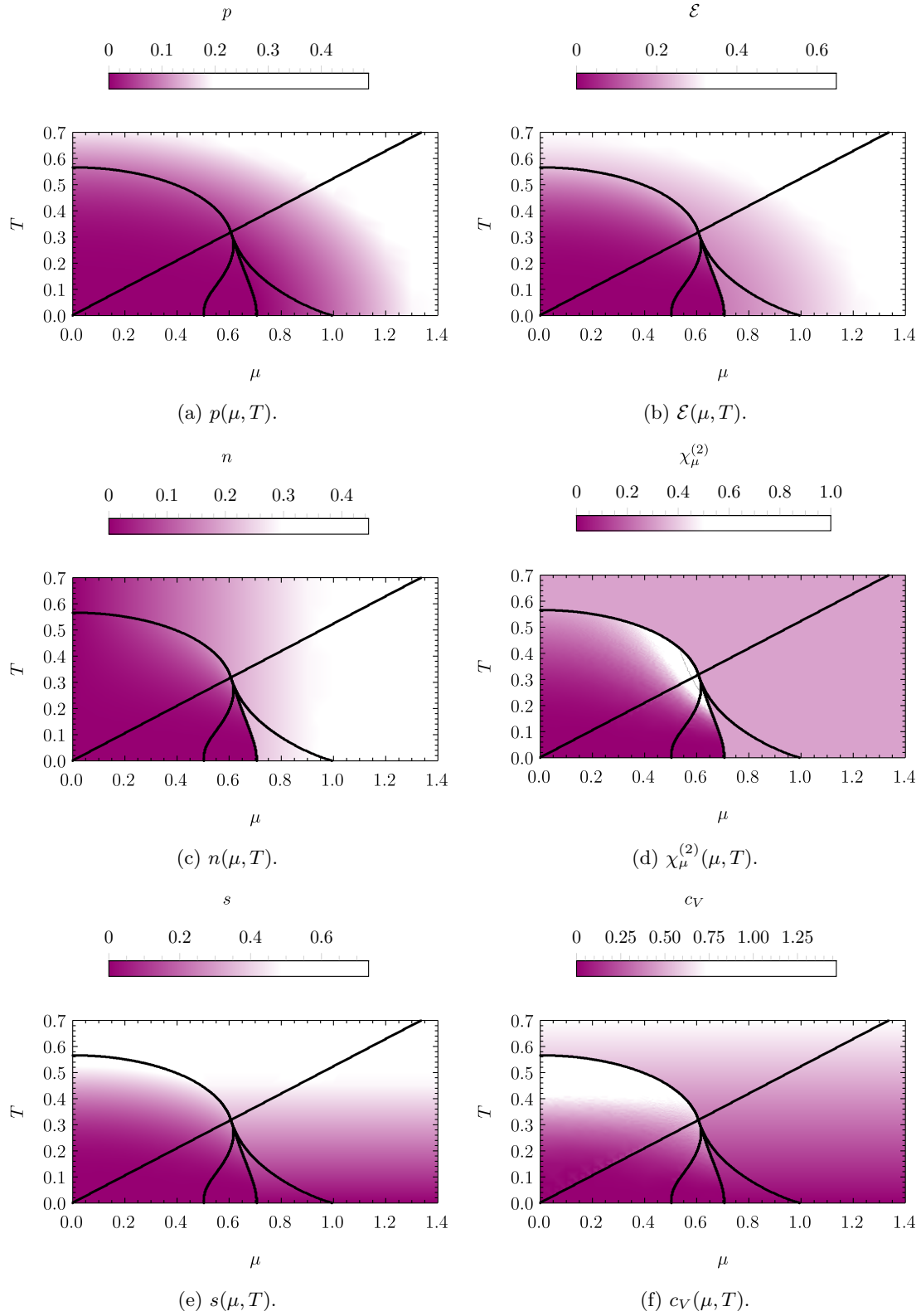
$$\frac{1}{V} \Omega(\mu, T, V) \equiv \frac{1}{V} \left[\Gamma[\bar{\psi}, \psi, \varphi, \mu, T] \Big|_{\text{minimum}} - \Gamma[\bar{\psi}, \psi, \varphi, 0, 0] \Big|_{\text{minimum}} \right]. \quad (11.28)$$

Here, “minimum” implies that the IR effective actions have to be evaluated at their extremal field configurations. These correspond to the classical solutions of the quantum equations of motion, see Section 10.2.3.³ Within our truncation and under the assumption of constant field configurations $\bar{\psi} = \psi = 0$ and $\varphi = \sigma$ Eq. (11.28) simplifies to

$$\frac{1}{V} \Omega(\mu, T, V) = U(\sigma_{\min}(\mu, T), \mu, T) - U(\sigma_0, 0, 0), \quad (11.29)$$

which can be directly calculated from Eq. (11.21).

³Note that Eq. (11.28) is normalized to the vacuum.

Figure 11.4: Thermodynamic observables as functions of μ and T for the infinite- N GN model.

Pressure

The grand canonical potential is directly related to the pressure of the system, *i.e.*,

$$p(\mu, T) = -\frac{1}{V} \Omega(\mu, T, V) = -U(\sigma_{\min}(\mu, T), \mu, T) + U(\sigma_0, 0, 0), \quad (11.30)$$

where the vacuum contribution is given by Eq. (F.13),

$$U(\sigma_0, 0, 0) = -\frac{d_\gamma}{8\pi} (h\sigma_0)^2. \quad (11.31)$$

For the sake of simplicity and explicit calculations of the pressure in the μ - T -plane, we use Eq. (11.21) and define

$$\begin{aligned} p(\sigma, \mu, T) &\equiv -U(\sigma, \mu, T) + U(\sigma_0, 0, 0) = \\ &= \frac{d_\gamma}{4\pi} \left[-\frac{1}{2} (h\sigma)^2 \left[\ln \left(\frac{(h\sigma)^2}{(h\sigma_0)^2} \right) - 1 \right] - \frac{1}{2} (h\sigma_0)^2 + \right. \\ &\quad \left. + \int_{-\infty}^{\infty} dp \left[T \ln \left(1 + e^{-\frac{E+\mu}{T}} \right) + T \ln \left(1 + e^{-\frac{E-\mu}{T}} \right) \right] \right], \end{aligned} \quad (11.32)$$

for any field values σ . In Appendix F.2.1, this formula is further evaluated for different combinations of σ , μ , and T being zero or non-zero. The corresponding formulae are referenced in Table 11.2a and have to be evaluated for the corresponding minimum $\sigma_{\min}(\mu, T)$.

An explicit plot of $p(\mu, T)$ is presented in Fig. 11.4a. At $T = 0$, we find $p(\mu, 0) = 0$ in the symmetry-broken phase. On the other hand, for large μ and T in the symmetric phase the pressure approaches the Stefan-Boltzmann limit of an Fermi gas with multiplicity d_γ [457, 377], see Eq. (F.75).

Particle number density

Next, we turn to the particle number (density). The particle number is defined by

$$N(\mu, T, V) = -\frac{d}{d\mu} \Omega(\mu, T, V). \quad (11.33)$$

However, we are interested in the corresponding density, which is independent of the specific spatial volume of the system,

$$\begin{aligned} n(\mu, T) &= -\frac{1}{V} \frac{d}{d\mu} \Omega(\mu, T, V) \stackrel{(11.29)}{=} \\ &= -\left(\frac{\partial}{\partial \mu} \sigma_{\min}(\mu, T) \right) \left(\frac{\partial}{\partial \sigma} U(\sigma, \mu, T) \right) \Big|_{\sigma=\sigma_{\min}(\mu, T)} - \underbrace{\frac{\partial}{\partial \mu} U(\sigma, \mu, T)}_{\equiv n(\sigma, \mu, T)} \Big|_{\sigma=\sigma_{\min}(\mu, T)}. \end{aligned} \quad (11.34)$$

Here, we use that the derivative of the effective potential vanishes at its minimum. In addition, we define

$$\begin{aligned} n(\sigma, \mu, T) &\equiv -\frac{\partial}{\partial \mu} U(\sigma, \mu, T) = \\ &= -\frac{d_\gamma}{4\pi} \int_{-\infty}^{\infty} dp \left[n_f \left(\frac{E+\mu}{T} \right) - n_f \left(\frac{E-\mu}{T} \right) \right] = \\ &= -\frac{d_\gamma}{4\pi} \int_{-\infty}^{\infty} dp \left[-\frac{1}{2} \tanh \left(\frac{E+\mu}{2T} \right) + \frac{1}{2} \tanh \left(\frac{E-\mu}{2T} \right) \right], \end{aligned} \quad (11.35)$$

which is further evaluated in Appendix F.2.2. Explicit formulae, which have to be evaluated at $\sigma_{\min}(\mu, T)$, are referenced in Table 11.2b. The same result was already presented in Ref. [457, Eq. (264)]. In Fig. 11.4c, we show a plot of $n(\mu, T)$. First, we find that the net particle number is zero on average as long as $\mu = 0$. For increasing μ , the system is more and more unbalanced between matter and anti-matter. Secondly, we find that – as expected from Ehrenfest’s classification of PTs [148, 11] – that $n(\mu, T)$ jumps at the first-order PT, while it stays continuous at the second-order PT.

Entropy density and internal energy

Taking a derivative of the grand canonical potential w.r.t. the temperature, we find the entropy of the system,

$$S(\mu, T, V) = -\frac{\partial}{\partial T} \Omega(\mu, T, V). \quad (11.36)$$

Again, in an infinite spatial volume, it is advisable to study the entropy density,

$$\begin{aligned} s(\mu, T) &= -\frac{1}{V} \frac{d}{dT} \Omega(\mu, T, V) \stackrel{(11.29)}{=} \\ &= -\left(\frac{\partial}{\partial T} \sigma_{\min}(\mu, T)\right) \underbrace{\left(\frac{\partial}{\partial \sigma} U(\sigma, \mu, T)\right)}_{\equiv s(\sigma, \mu, T)} \Big|_{\sigma=\sigma_{\min}(\mu, T)} - \underbrace{\frac{\partial}{\partial T} U(\sigma, \mu, T)}_{\equiv s(\sigma, \mu, T)} \Big|_{\sigma=\sigma_{\min}(\mu, T)}. \end{aligned} \quad (11.37)$$

Analogous to the preceding discussion, the first contribution drops out and we define

$$\begin{aligned} s(\sigma, \mu, T) &\equiv -\frac{\partial}{\partial T} U(\sigma, \mu, T) \stackrel{(11.21)}{=} \\ &= \frac{d_\gamma}{4\pi} \left[\int_{-\infty}^{\infty} dp \left[\ln \left(1 + e^{-\frac{E+\mu}{T}} \right) + \ln \left(1 + e^{-\frac{E-\mu}{T}} \right) \right] + \right. \\ &\quad \left. + \frac{1}{T} \int_{-\infty}^{\infty} dp E \left[n_f \left(\frac{E+\mu}{T} \right) + n_f \left(\frac{E-\mu}{T} \right) \right] + \frac{\mu}{T} \int_{-\infty}^{\infty} dp \left[n_f \left(\frac{E+\mu}{T} \right) - n_f \left(\frac{E-\mu}{T} \right) \right] \right]. \end{aligned} \quad (11.38)$$

The same result can be found in Ref. [457, Eq. (265)]. Before we study the entropy density in detail, we use Euler’s relation for the internal energy (density)⁴

$$\mathcal{E}(\sigma, \mu, T) = T s(\mu, T) - p(\sigma, \mu, T) + \mu n(\sigma, \mu, T). \quad (11.39)$$

With Eqs. (11.35), (11.32), and (11.40) we identify

$$\begin{aligned} \mathcal{E}(\sigma, \mu, T) &= \frac{d_\gamma}{4\pi} \left[\frac{1}{2} (h\sigma)^2 \left[\ln \left(\frac{(h\sigma)^2}{(h\sigma_0)^2} \right) - 1 \right] + \frac{1}{2} (h\sigma_0)^2 + \right. \\ &\quad \left. + \int_{-\infty}^{\infty} dp E \left[n_f \left(\frac{E+\mu}{T} \right) + n_f \left(\frac{E-\mu}{T} \right) \right] \right] \end{aligned} \quad (11.40)$$

as the internal energy density, see also Ref. [457, Eq. (266)]. This formula can be further simplified for certain situations, see Appendix F.2.3. The formulae are referenced in Table 11.2c.

We plot the internal energy in Fig. 11.4b, which of course rises drastically with T^2 and μ^2 in the symmetric gas-like phase.

With Eq. (11.39) we do not need to evaluate Eq. (11.38) explicitly and we can simply use our earlier results for $p(\mu, T)$, $n(\mu, T)$, and $\mathcal{E}(\mu, T)$ to plot the entropy density. The plot is shown in Fig. 11.4e. The small jump of the entropy density at the first-order PT is barely visible.

⁴Of course, this formula exclusively corresponds to the true internal energy if it is evaluated at the physical minimum $\sigma_{\min}(\mu, T)$.

Baryon number susceptibility and heat capacity

In order to correctly identify a second-order PT and distinguish the PT from a crossover, one has to study higher derivatives of the grand canonical potential. Here, these are the baryon-number susceptibility,

$$\chi_{\mu}^{(2)}(\mu, T) = -\frac{1}{V} \frac{d}{d\mu} n(\mu, T) = -\frac{1}{V} \frac{d^2}{d\mu^2} \Omega(\mu, T, V) = -\frac{d^2}{d\mu^2} U(\sigma_{\min}(\mu, T), \mu, T), \quad (11.41)$$

and the heat capacity (at constant volume),

$$c_V = T \frac{d}{dT} s(\mu, T) = -\frac{1}{V} T \frac{d^2}{dT^2} \Omega(\mu, T, V) = -T \frac{d^2}{dT^2} U(\sigma_{\min}(\mu, T), \mu, T). \quad (11.42)$$

Both quantities are evaluated by numerical differentiation of the data for $n(\mu, T)$ and $s(\mu, T)$. Otherwise, one would have to study all contributions which emerge from the chain rules on the r.h.s. of Eqs. (11.41) and (11.42).

Plots of these so-called response functions are presented in Figs. 11.4d and 11.4f, where the jumps at the second-order PT are clearly visible. (The light gray line in Fig. 11.4d indicates the limit of the scale of the heat map.)

In summary, we find that the results for the thermodynamic observables are reasonable and that the system is stable from a thermodynamic perspective.

11.3. Stability of the homogeneous solution

Up to this point, we exclusively investigated the flow equation and the IR result for the effective bosonic potential and derived quantities. In the course of this, we completely ignored the fact that already in lowest non-trivial order of the derivative expansion in the FRG formalism there is another flow equation, which survives the $N \rightarrow \infty$ limit – the flow equation for the bosonic wave-function renormalization (11.2). Thus, the first task of this section is to integrate this equation to the IR to get a more comprehensive picture of the bGN model. Subsequently, we have to evaluate the integral equation for the IR wave-function renormalization in the μ - T -plane.

As we shall see, there are some regions in the phase diagram where the wave-function renormalization becomes negative. This, however, implies that the kinetic term for the bosons, which is quadratic in the momenta, has a negative coefficient in the IR, see Eq. (10.1). Thus, without the generation of higher-order derivative couplings with positive coefficients, the system becomes unstable, although we do not expect an instability from the discussion of the thermodynamic observables. The system could go over from a spatially homogeneous ground state to another one with smaller action by generating gradients (oscillations) in the σ background field. Without higher-order derivative couplings with positive coefficients that disfavor (too) large gradients, this implies that the system generates arbitrarily many and arbitrarily large gradients in the ground-state field configuration and simultaneously approaches states of smaller and smaller action, which is unphysical.

Hence, the second half of this section is dedicated to the full momentum structure of the bosonic two-point function. The bosonic two-point function effectively comprises interaction terms that are of all orders in (spatial) derivatives and of second order in the bosonic fields.⁵ The initial values of these terms are set to zero at the initial scale. They are generated in the RG flow, as we shall demonstrate with the Wetterich equation in Appendix E.2. Because there is no backreaction of these terms to the flow equation, due to the suppression of bosonic fluctuations at $N \rightarrow \infty$, we can simply integrate the RG flow for the bosonic two-point function separately from the flow equation of the effective potential.

⁵Actually, one does not even need to think in terms of an expansion in derivatives/momenta. The two-point function is simply a function of p , which does not even need to be expandable.

As a result, if we think of the IR effective action in terms of a vertex expansion in perturbations $\delta\sigma(x)$ about a spatially constant background-field configuration σ , the bosonic two-point function is simply the quadratic coefficient. From the perspective of a Taylor expansion in powers of perturbations $\delta\sigma(x)$ a negative quadratic coefficient signals an instability of the expansion point (here the spatially homogeneous ground state). Consequently, we can use the bosonic two-point function and in particular its momentum structure to investigate the stability of a spatially homogeneous ground state and predict the presence of spatially oscillating ground states.

One might object at this point that this study seems redundant, cumbersome, and ultimately inaccurate, because the full phase structure of the GN model at $N \rightarrow \infty$, including spatially inhomogeneous ground states is well known for many years. Of course, this is absolutely correct for the GN model and some related theories [473, 327, 578, 579, 461, 580, 564, 581, 582, 583, 584, 585, 586, 343, 587, 588, 446, 459, 460, 589, 590]. Still, for more complicated models and theories in higher-dimensional spacetime there is little knowledge about the true ground state and its exact prediction is usually extremely challenging. Oftentimes, one has to rely on a so-called stability analysis if one is interested in possibly crystalline like ground states. In the past, several studies were based on this or related approaches, *cf.* Refs. [327, 330, 328, 329, 570, 572, 331, 332, 333, 274, 591, 592, 573, 585, 593, 594, 595, 596, 597]. However, to the best of our knowledge a detailed and pedagogical proof of concept study, which benchmarks this method against an exact solution, was missing in literature. The only works which pursue similar goals are Refs. [476, 327, 570], such that our work might be seen as a complement to these publications.

Therefore we considered a detailed analysis of the two-point function and a comparison with the exact results for the GN model as a useful task and performed this analysis in Ref. [5] based on notes and preliminary results by Refs. [566, 567]. Here, we present the main results of this joint research.

In addition, we use the $N \rightarrow \infty$ results of this section to draw direct conclusions for calculations at finite N . This is also discussed throughout this section.

11.3.1. The bosonic wave-function renormalization

We begin with an analysis of the flow equation of the bosonic wave-function renormalization (11.2), *i.e.*,

$$\partial_k Z_\varphi(k) = \frac{d_\gamma}{2\pi} h^2 \frac{1}{\beta} \sum_{n=-\infty}^{\infty} \left[\frac{8 h^2 \sigma^2 k^2}{[(\nu_n + i\mu)^2 + k^2 + h^2 \sigma^2]^4} - \frac{1}{[(\nu_n + i\mu)^2 + k^2 + h^2 \sigma^2]^2} \right]. \quad (11.43)$$

First, we note again that we have not settled the question of the correct evaluation point of the r.h.s. in field space yet.

On the one hand, from the perspective of an expansion of the effective average action in powers of derivatives and fields, the choice $\sigma = 0$ seems to be the correct evaluation point.

On the other hand, at $N \rightarrow \infty$, we can easily promote the field-independent wave-function renormalization $Z_\varphi(k)$ to a field-dependent wave-function renormalization $Z_\varphi(k, \varphi)$ already on the level of Eq. (10.1). Because all bosonic fluctuations are suppressed, there is no feedback of $Z_\varphi(k, \varphi)$ to the flow equation of the effective potential and we do not have to bother about any complications with the bosonic regulator insertion. We simply obtain the above flow equation. In the second case, a field-dependent wave-function renormalization of course needs to be evaluated in the IR on the field configuration which minimizes the action. Under our assumption of a spatially constant configuration this is $\sigma_{\min}(\mu, T)$, the minimum of the effective potential, see Section 10.2.3. For $N \rightarrow \infty$ we believe that the second option is therefore better suited, but also present results for the first option.

Table 11.3: References to the explicit expressions of the bosonic wave-function renormalization and two-point function derived in Appendices F.1.4 and F.1.3.

(a) Equations for $Z(\sigma, \mu, T)$				(b) Equations for $\Gamma^{(2)}(\sigma, \mu, T, q)$					
T	μ	σ	Eq.	T	μ	σ	$q \neq 0$	$q = 0$	
$\neq 0$	$\neq 0$	$\neq 0$	(F.64)	$\neq 0$	$\neq 0$	$\neq 0$	(F.32)	(F.33)	
		$= 0$	(F.65)			$= 0$	(F.36)	(F.37)	
	$= 0$	$\neq 0$	(F.66)		$= 0$	$\neq 0$	$\neq 0$	(F.38)	(F.39)
		$= 0$	(F.67)			$= 0$	(F.40)	(F.41)	
$= 0$	$\neq 0$	$\neq 0$	(F.68)	$= 0$	$\neq 0$	$\neq 0$	(F.49)	(F.50)	
		$= 0$	(F.73)			$= 0$	(F.56)	(F.57)	
	$= 0$	$\neq 0$	(F.74)		$= 0$	$\neq 0$	$\neq 0$	(F.58)	(F.59)
		$= 0$	“ $+\infty$ ”			$= 0$	(F.60)	“ $-\infty$ ”	

Integrating the flow equation of the wave-function renormalization

In either case, we can simply integrate the flow equation from the UV to the IR. We use that according to Eq. (10.4) the UV wave-function renormalization vanishes. Furthermore, we introduce $Z_\varphi(\sigma, \mu, T) = Z_\varphi(k=0)$ as the new notation for its possibly field-dependent IR value. We obtain

$$\begin{aligned}
Z_\varphi(\sigma, \mu, T) &= \tag{11.44} \\
&= \frac{d_\gamma}{2\pi} h^2 \frac{1}{\beta} \sum_{n=-\infty}^{\infty} \int_0^\infty dk \left[\frac{1}{[(\nu_n + i\mu)^2 + k^2 + h^2\sigma^2]^2} - \frac{8h^2\sigma^2 k^2}{[(\nu_n + i\mu)^2 + k^2 + h^2\sigma^2]^4} \right] = \\
&= \frac{d_\gamma}{2\pi} h^2 \frac{1}{\beta} \sum_{n=-\infty}^{\infty} \int_0^\infty dk \left[\frac{1}{[(\nu_n + i\mu)^2 + k^2 + h^2\sigma^2]^2} - \frac{\frac{4}{3}h^2\sigma^2}{[(\nu_n + i\mu)^2 + k^2 + h^2\sigma^2]^3} \right], \tag{11.45}
\end{aligned}$$

where we used integration by parts for the last term. The corresponding surface term vanishes. In the following, we use the version (11.45), which is the standard result that is also obtained in conventional mean-field calculations in sharp-cutoff regularization [4]. A corresponding derivation from the infinite- N limit of the bosonic two-point function is presented in Eq. (F.61).⁶ Within the next steps, we proceed as in the previous Section 11.2. We first evaluate the Matsubara sum in Eq. (11.45). Then, using a distinction of cases for vanishing and non-vanishing σ , μ , and/or T we evaluate the remaining momentum integral as far as possible and cure possible IR divergences. Details can be found in Appendix F.1.4. Here, in the main text, we simply discuss the results, which are based on the formulae listed in Table 11.3a.

The “Frankfurt” phase diagram⁷

By evaluating $Z_\varphi(\sigma, \mu, T)$ in the μ - T -plane for the respective minimum $\sigma_{\min}(\mu, T)$ of the effective potential via the formulae which are listed in Table 11.3a, we can plot $Z_\varphi(\sigma_{\min}(\mu, T), \mu, T)$ in the phase diagram of the GN model. The corresponding heat map is presented in Fig. 11.5, where we ignore the shaded region at low T and large $|\mu|$ for the moment. For the sake of better visualization, we also present two plots with cuts through Fig. 11.5 along lines of constant μ or constant T in Fig. 11.6. We observe the following: Overall, the values of the bosonic wave-function renormalization range approximately between -0.15 and $+0.15$. In absolute values, the wave-function renormalization is smallest in the symmetric phase in regions where μ and T are

⁶This demonstrates that the $N \rightarrow \infty$ limit and the extraction of the wave-function renormalization from the bosonic two-point function are interchangeable, since we extracted the wave-function renormalization from the two-point function before taking the limit.

⁷If you are not Robert D. Pisarski, please, do not use this name for Fig. 11.5.

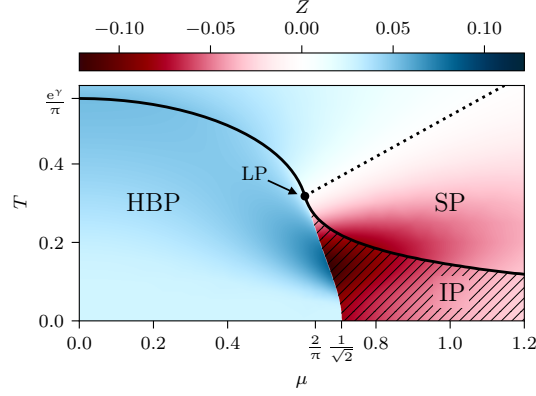


Figure 11.5: The bosonic wave-function renormalization $Z_\varphi(\sigma_{\min}(\mu, T), \mu, T)$, the line of vanishing bosonic wave-function renormalization (black dashed), and the line of vanishing bosonic two-point function $\Gamma^{(2)}(\sigma_{\min}(\mu, T), \mu, T, Q) = 0$ (black solid). The black hatched region indicates $\Gamma^{(2)}(\sigma_{\min}(\mu, T), \mu, T, Q) < 0$ with Q according to Eq. (11.52). From Ref. [5, Fig. 9].

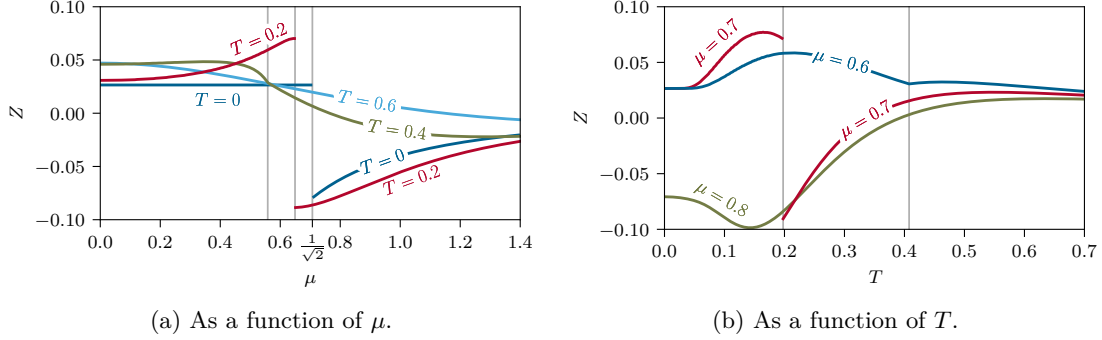


Figure 11.6: The bosonic wave-function renormalization $Z_\varphi(\sigma_{\min}(\mu, T), \mu, T)$ as a function of μ or T . From Ref. [5, Figs. 12 & 13].

both large. This is expected, because there the formation of bosonic bound states is unlikely and we are basically confronted with a relativistic fermion gas. In the phase of spatially homogeneous symmetry breaking, especially at small $|\mu|$ and T , we find positive but relatively small values for Z_φ . There, condensation takes place and, if it was not suppressed by the $N \rightarrow \infty$ limit, the bosons would start fluctuating, because the coefficient of the kinetic term is no longer zero, as it was in the UV.

However, if one considers small constant temperatures, below the temperature of the critical point, and steadily increases $|\mu|$, one first observes a rising bosonic wave-function renormalization until one reaches the first-order PT. At the PT Z_φ jumps to a negative value. In fact, there is a region of infinite size at large $|\mu|$ at temperatures below the dotted diagonal line in Fig. 11.5, where Z_φ is found to be negative.⁸

First, the rising wave-function renormalization close to the first-order PT in the symmetry-broken regime actually tells us that, away from the $N \rightarrow \infty$ limit, the bosons would start to fluctuate more than at smaller $|\mu|$. This is not totally unexpected in the vicinity of a PT. Secondly, in the \mathbb{Z}_2 -symmetric phase close to the first-order PT we have relatively large negative values of Z_φ , which signals a possible instability of the spatially homogeneous ground state.

Of course, only inspecting the wave-function renormalization is inconclusive if one really wants

⁸In fact, it can be shown by comparing the explicit expressions from Table 11.3a with Eq. (11.27) that the black dotted line, where $Z_\varphi = 0$, exactly agrees with the $(\alpha_4 = 0)$ -line in Fig. 11.1 from the Ginzburg-Landau analysis Eq. (11.24).

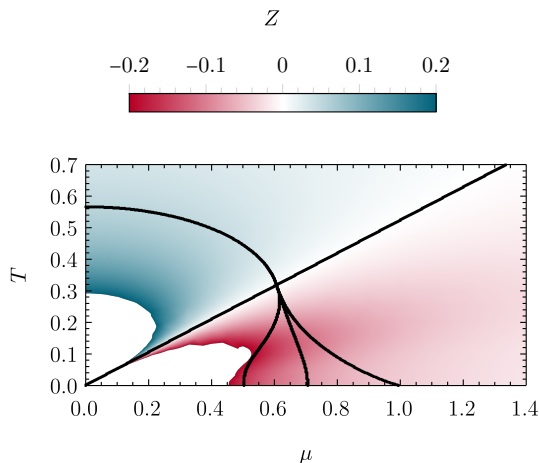


Figure 11.7: The bosonic wave-function renormalization $Z_\varphi(0, \mu, T)$ as a function of μ or T . (The white regions at small $|\mu|$ and T simply indicate that the values for Z_φ are too large/small to be in the range of the color scale. Due to the divergence and pole of Z_φ at $\mu = T = 0$ choosing another plot range would not help much.)

to judge whether spatially oscillating ground states are energetically favorable. These aspects are discussed for example in Refs. [330, 561, 274, 573, 535, 598, 599, 600]. A rather simple argument why negative Z_φ alone is insufficient to predict an instability of a homogeneous ground state is as follows: If we are studying points in the μ - T -plane at large μ and T which are located close but below the dotted black line in Fig. 11.5, we always find negative Z_φ . However, for large μ and T the system simply goes over into a free fermion gas without condensation and there is no reason to expect a non-trivial condensate with some spatial modulation. Here, higher-order derivative terms certainly become important and prevent the instability.

Before we enter the discussion of these terms by analyzing the full momentum structure of the two-point function, let us also present the bosonic wave-function renormalization (11.45) when it is always evaluated at $\sigma = 0$. A plot is shown in Fig. 11.7. In the \mathbb{Z}_2 -symmetric region, where $\sigma_{\min}(\mu, T) = 0$, Figs. 11.5 and 11.7 are of course identical (despite slightly different color coding). However, in the region of homogeneous \mathbb{Z}_2 -symmetry breaking things are drastically different. We find that the diagonal line, where $Z_\varphi(0, \mu, T) = 0$, separates the phase diagram into two regions of negative and positive $Z_\varphi(0, \mu, T)$. In addition, the absolute value of $Z_\varphi(0, \mu, T)$ rises drastically in both regions close to $\mu = T = 0$ and indeed results in a pole, see formulae from Table 11.3a. Recalling that the exact result for the phase diagram of the GN model, see Fig. 7.1, still contains a region of spatially homogeneous condensation at small $|\mu|$ and T , this clearly tells us that $\sigma = 0$ is in fact the wrong evaluation point for the wave-function renormalization – at least in the infinite- N calculations. Otherwise, one would expect crystalline-like ground states for all μ at low T . However, for calculations at finite N things are more complicated and an evaluation at $\sigma = 0$ seems to be appropriate, as anticipated above and discussed below in detail. Here, the results from Fig. 11.7 will be of great relevance.

11.3.2. The bosonic two-point function

Finally, we turn to the analysis of the full momentum structure of the bosonic two-point function. We start with explicit expressions and a few remarks on the derivation from the FRG in comparison to the conventional mean-field derivation. Afterwards, we discuss the explicit functional forms of the two-point function at various μ and T and criteria for the (in)stability of spatially homogeneous condensates. We use these results to present the parts of the phase diagram which can be obtained

from this stability analysis alone and compare this against the exact result. As an amendment, we additionally compare the dominant wave vector of the true ground state to the estimate that is obtained by the minimum of the two-point function. Throughout this discussion we also comment on limitations of the method and consequences for possible calculations at finite N .

The bosonic two-point function from “standard mean-field” and the FRG formalism

The explicit unrenormalized expression for the bosonic two-point function at $N \rightarrow \infty$ is

$$\begin{aligned} \Gamma^{(2)}(\sigma, \mu, T, q) &= \\ &= h^2 \left[\frac{1}{g^2} - d_\gamma \int_{-\infty}^{\infty} \frac{dp}{(2\pi)} \frac{1}{\beta} \sum_{n=-\infty}^{\infty} \left[\frac{1}{(\nu_n + i\mu)^2 + E^2} + \frac{pq - 2(h\sigma)^2}{(\nu_n + i\mu)^2 + E_q^2} \frac{1}{(\nu_n + i\mu)^2 + E^2} \right] \right], \end{aligned} \quad (11.46)$$

where $E_q = \sqrt{(p+q)^2 + h^2\sigma^2}$. Evaluated at $\sigma = 0$, it is the Fourier transform of the quadratic coefficient of the expansion of the IR effective action in small perturbations about the symmetric and spatially homogeneous ground state, *i.e.*,

$$\Gamma[\delta\sigma] = \sum_{n=0}^{\infty} \beta \int_{-\infty}^{\infty} dx \Gamma^{(2n)}(0, \mu, T, x) \delta\sigma^{2n}(x). \quad (11.47)$$

Therefore, it can be used to study the stability of the ($\sigma = 0$)-ground state. An instability is detected if Eq. (11.46) turns negative for some momentum.

In conventional mean-field/ $N \rightarrow \infty$ calculations Eq. (11.46) is derived by expanding the exponent of the path integral

$$\mathcal{Z} \propto \int [d\phi] e^{-N \mathcal{S}_{\text{eff}}[\phi]}, \quad (11.48)$$

i.e.,

$$\mathcal{S}_{\text{eff}}[\phi] = \int_{-\infty}^{\infty} dx \int_0^\beta d\tau \frac{h^2}{2g^2} \phi^2(\tau, x) - \ln \text{Det} (\not{\partial} - \mu \gamma^2 + h\phi(\tau, x)). \quad (11.49)$$

This effective classical action is obtained by integrating out the fermions in Eqs. (8.97) and (8.98) and by rescaling of the boson fields with $\frac{1}{N}$. One uses $\Gamma[\varphi] = \mathcal{S}_{\text{eff}}[\varphi]$, which holds for $N \rightarrow \infty$ after renormalization. The explicit derivation of Eq. (11.46), setting $\phi(\tau, x) = \varphi(\tau, x) = \sigma + \delta\sigma(x)$ in Eq. (11.49) and expanding in perturbations $\delta\sigma(x)$, is presented pedagogically in great detail in Ref. [5], but can also be found elsewhere for similar models [330, 592, 573, 593].

In the FRG formalism, the calculation is slightly different. One has to derive and study the RG flow equation for the bosonic two-point function from the Wetterich equation, see also Refs. [274, 324] (in the context of a stability analysis). Within our truncation (10.1) the general derivation is presented in great detail in Appendix E.2.2 for arbitrary spacetime dimensions and including the possibility for bosonic fluctuations. In terms of Feynman diagrams the corresponding general flow equation is given by Eq. (E.53). For this section, where we are exclusively interested in the $N \rightarrow \infty$ version of this flow equation in $d = 1$, we can drastically simplify the resulting general flow equation (E.73). The correct reduction of this equation to Eq. (11.46), which is unfortunately a little cumbersome, can be found in Appendix E.2.3.

In any case, there are ofcourse various options to arrive at Eq. (11.46), which are studied in the following.

Renormalization and explicit formulae

First, we note that the expression (11.46) for the bosonic two-point function contains a UV divergence in the first term under the integral. This divergence ofcourse cancels against the UV divergence of the inverse four-fermion coupling, see also Ref. [5]. To see this, we can replace $\frac{1}{g^2}$ by its UV-cutoff dependence, hence Eq. (11.11). However, we have to exercise caution, because of the surface term (the “-1” contribution in Eq. (11.11)). As it turns out and is discussed at the end of Appendix E.2.3, we have to ignore this term when we replace $\frac{1}{g^2}$, because via several transformations during the derivation of Eq. (11.46) from the FRG, we got rid of the corresponding contribution in $\Gamma^{(2)}(\sigma, \mu, T, q)$, which has to be respected in the regularization of $\frac{1}{g^2}$. In simple terms, this is required since otherwise we would work with inconsistent regularization schemes. In any case, we obtain

$$\begin{aligned} \Gamma^{(2)}(\sigma, \mu, T, q) = & \tag{11.50} \\ = \frac{d_\gamma}{2\pi} h^2 & \left[\frac{1}{2} \ln \left(\frac{(2\Lambda)^2}{(h\sigma_0)^2} \right) + \mathcal{O} \left(\frac{(h\sigma_0)^2}{\Lambda^2} \right) - \int_{-\infty}^{\infty} dp \frac{1}{2E} \left[1 - n_f \left(\frac{E+\mu}{T} \right) - n_f \left(\frac{E-\mu}{T} \right) \right] - \right. \\ & - \int_{-\infty}^{\infty} dp \left[pq - 2(h\sigma)^2 \right] \left(\frac{1}{2E_q} \frac{1}{E^2 - E_q^2} \left[1 - n_f \left(\frac{E_q+\mu}{T} \right) - n_f \left(\frac{E_q-\mu}{T} \right) \right] + \right. \\ & \left. \left. + \frac{1}{2E} \frac{1}{E^2 - E^2} \left[1 - n_f \left(\frac{E+\mu}{T} \right) - n_f \left(\frac{E-\mu}{T} \right) \right] \right) \right] \end{aligned}$$

for $q \neq 0$ and

$$\begin{aligned} \Gamma^{(2)}(\sigma, \mu, T, 0) = & \tag{11.51} \\ = \frac{d_\gamma}{2\pi} h^2 & \left[\frac{1}{2} \ln \left(\frac{(2\Lambda)^2}{(h\sigma_0)^2} \right) + \mathcal{O} \left(\frac{(h\sigma_0)^2}{\Lambda^2} \right) - \int_{-\infty}^{\infty} dp \frac{1}{2E} \left[1 - n_f \left(\frac{E+\mu}{T} \right) - n_f \left(\frac{E-\mu}{T} \right) \right] + \right. \\ & + 2(h\sigma)^2 \int_{-\infty}^{\infty} dp \frac{1}{4E^3} \left(1 - n_f \left(\frac{E+\mu}{T} \right) - n_f \left(\frac{E-\mu}{T} \right) + \right. \\ & \left. \left. + \frac{E}{T} \left[n_f^2 \left(\frac{E+\mu}{T} \right) + n_f^2 \left(\frac{E-\mu}{T} \right) - n_f \left(\frac{E+\mu}{T} \right) - n_f \left(\frac{E-\mu}{T} \right) \right] \right) \right] \end{aligned}$$

for $q = 0$ after evaluation of the Matsubara sum in Eq. (11.46). The reason why we distinguish between zero and non-zero external momentum q is that taking the $q \rightarrow 0$ limit after the evaluation of the Matsubara sum is more challenging than simply setting $q = 0$ in Eq. (11.46) and using Eqs. (B.15), (B.20), and (11.50) afterwards. Furthermore, Eqs. (11.50) and (11.51) can be further evaluated and renormalized for different combinations of σ , μ , and T being zero or non-zero. For some cases, also depending on (non-)zero external momentum q , one is confronted with additional IR divergences, which have to be handled carefully. Since this is non-trivial but rather dull work, we prepared an extensive Appendix F.1.3 with all necessary details of the calculations, such that all results are understandable and reproducible without huge efforts. In order to have easy access to the explicit equations, we provide Table 11.3b, which points to the respective equations.

Momentum structure of the bosonic two-point function

The basic idea behind the stability analysis is to search for regions in the phase diagram where $\Gamma^{(2)}$ turns negative for some momentum. Therefore, the first step of our discussion is to present $\Gamma^{(2)}$ at different positions (μ, T) to get a clear picture of possible scenarios. To this end, $\Gamma^{(2)}(\sigma, \mu, T, q)$

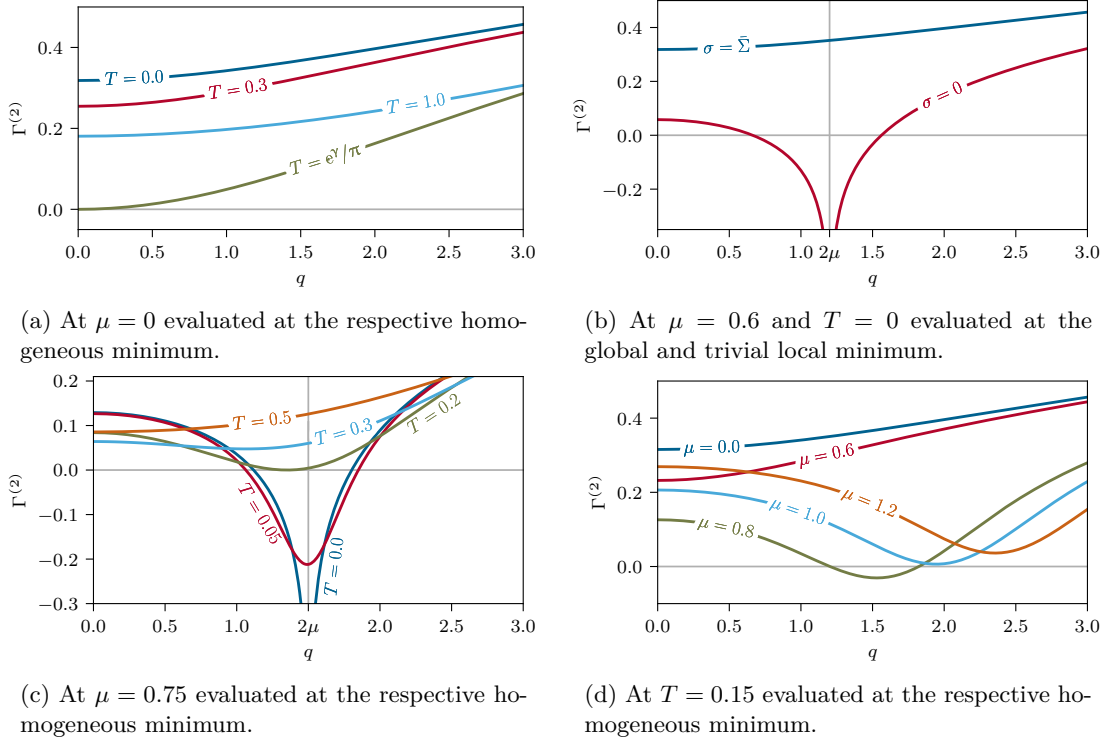


Figure 11.8: The bosonic two-point function Eq. (11.46) as a function of the external momentum q using the renormalized expressions listed in Table 11.3b. From Ref. [5, Figs. 3, 4, 5, 6].

is evaluated on the homogeneous global minimum $\sigma_{\min}(\mu, T)$ of the effective potential. The corresponding plots are depicted in Fig. 11.8.

Zero chemical potential and varying temperature We start our discussion at $\mu = 0$ and Fig. 11.8a. Overall we observe that

1. the bosonic two-point function is always positive for any q and T .
2. the bosonic two-point function is monotonically increasing with q for all T .

These results indicate that the spatially homogeneous minimum is stable against spatially oscillating perturbations. Here, we have to keep in mind that, according to Eq. (11.47), the stability analysis is formally only applicable in the \mathbb{Z}_2 -symmetric phase for an expansion about $\sigma_{\min}(\mu, T) = 0$. The only point where we observe a single root of the two-point function is for $T = \frac{e^{\gamma}}{\pi}$, where find $\Gamma^{(2)} = 0$ at $q = 0$. This, however, is absolutely expected, because for $q = 0$ there is no inhomogeneous perturbation and $\Gamma^{(2)}$ is identical to the curvature mass, which has to vanish at the second-order PT, see Fig. 11.2b. In general, the results at $\mu = 0$ clearly show that inhomogeneous condensation and complicated dispersion relations are not expected at zero net baryon densities.

Before we continue, note that the momentum profiles of the two-point functions at $\mu = 0$ can all be approximated roughly by parabolas with different stretch factors.⁹ This implies that the standard kinetic term, which is quadratic in the bosonic momentum, seems to be sufficient to get a rather accurate description of the bosonic dispersion relation as long as the bosonic wave-function renormalization is included and sets the stretch factor for different temperatures. Since bosonic

⁹This argument still holds true if the bosonic two-point functions are evaluated at $\sigma = 0$ at any temperature and $\mu = 0$.

fluctuations are not expected to produce any types of non-trivial structures in the q -profiles of $\Gamma^{(2)}$, we can already conclude for calculations at finite N that the lowest non-trivial order of a derivative expansion of the effective action, thus truncation (10.1), should lead to an adequate description of the system at zero μ . This result is for example consistent with the findings of Refs. [63, 70, 69, 72, 71] in similar model studies where higher-order derivative couplings are identified to be of sub-leading importance.

Non-zero chemical potential and varying temperature Next, let us turn to non-zero chemical potentials. For our discussion we simply choose $\mu = 0.75$, where the homogeneous condensate always vanishes, compare Fig. 11.1, such that we do not have to bother about the correct expansion point, which is always $\sigma_{\min}(\mu, T) = 0$, where the stability analysis is in general valid. A plot of the two-point function at fixed $\mu = 0.75$ for various T is presented in Fig. 11.8c. For rather high temperatures, *e.g.*, $T = 0.5$, we still observe that $\Gamma^{(2)}$ monotonically grows with q and that the temperature sets the dominating energy scale. However, by lowering T , *e.g.*, $T = 0.3$, we observe an influence of the chemical potential in the shape of the two-point function, which manifests itself in terms of a non-trivial minimum. In general, we denote the minimum of $\Gamma^{(2)}$ for non-trivial q with

$$Q \equiv \operatorname{argmin}_q \Gamma^{(2)}(\sigma_{\min}(\mu, T), \mu, T, q). \quad (11.52)$$

Still, at $T = 0.3$ the two-point function is manifestly positive, such that there is no true instability of the spatially homogeneous condensate. This scenario holds, when we are in the region of the μ - T -plane where the bosonic wave-function renormalization turns negative, see Fig. 11.5, but higher-order momentum contributions still ensure the stability of the homogeneous condensate.

In general, regions in phase diagrams with two-point functions and dispersion relations with such a non-trivial momentum profile have recently been called “moat regimes” [599, 598, 600, 601, 565]. They are discussed as a possibly important general feature of theories at moderate and large densities including QCD. In any case, moat regimes also comprise the situation where $\Gamma^{(2)}$ has a root or even turns negative for some q . In Fig. 11.8c, we find that there is a single root for $T \approx 0.2$, while the two-point function has a manifestly negative region in q for lower temperatures. If there is exactly a single root at $q = Q$, this in fact marks the PT where the \mathbb{Z}_2 -symmetric phase is no longer stable and an inhomogeneous perturbation associated with a finite wave vector Q lowers the energy of the ground state. Hence, at the PT the root at $q = Q$ does not only predict an instability and an inhomogeneous ground state, but also the wave-length of its modulation. If there is an entire region in q where $\Gamma^{(2)}$ is negative, it is not possible to exactly predict the shape of an inhomogeneous condensate. However, as we discuss below, the minimum Q is still a rather good estimate for the dominating wave vector of the true ground state.

Let us also comment on the situation at $T = 0$, where $\Gamma^{(2)}$ turns non-analytic and has a singularity at $q = 2\mu$. To this end, let us imagine how $1/\Gamma^{(2)}$ – the propagator – looks like as a function of the momentum q . Exactly at the position of the two roots of $\Gamma^{(2)}$ the propagator shows poles, which signal a resonance, thus the formation of an anti-fermion-fermion bound state $\sigma \sim \langle \bar{\psi} \psi \rangle$ with non-zero momentum. This is the inhomogeneous condensate, which is also found at small temperatures. The preferred momenta of these states are from the momentum range where $\Gamma^{(2)}$ is negative and the dominating wavelength is associated with the minimum Q . Having a direct relation between $Q \sim 2\mu$ at small and zero temperature is rather common for inhomogeneous condensates, because fermions and anti-fermions pair at the Fermi surface. For details on these mechanisms, we refer to Refs. [319, 320, 313].

Lastly, let us have a quick look on the relevance of the evaluation point of the two-point function in field space. If we for example take $\mu = 0.6$ instead of $\mu = 0.75$ at $T = 0$, we are already safely in the phase of spatially homogeneous symmetry breaking. Thus, the minimum and evaluation point of the two-point function is $\sigma_{\min}(\mu, T) = \sigma_0$. The corresponding two-point function is plotted in Fig. 11.8b and indeed does not signal an instability. However, if we would switch the expansion and evaluation point to $\sigma = 0$, which is actually required by the construction Eq. (11.47), we recover the instability and singularity structure at $q = 2\mu$. This again signals that we should take

Eq. (11.47) seriously and exclusively use the stability analysis in the symmetric phase. We come back to this issue below.

Constant non-zero temperature and varying chemical potential Let us also briefly discuss how the momentum profile of the bosonic two-point function can change with μ if we for example fix $T = 0.15$. The corresponding plot of the $\Gamma^{(2)}$ profiles is Fig. 11.8d. First, at $\mu = 0$ the situation is unspectacular. The two-point function monotonically rises with q , is always positive, and only shows a trivial minimum at $q = 0$. For $\mu = 0.6$, where we are in the homogeneously broken phase between the left spinodal and the first-order PT, things still seem fine. From the stability analysis, we do not expect any instability, because we still find a manifestly positive two-point function without a non-trivial minimum in q . Still, we should not necessarily trust the stability analysis in the homogeneously broken phase.

Only for values of μ which belong already to the \mathbb{Z}_2 -symmetric phase, *e.g.*, $\mu = 0.8$, we observe a true trustworthy instability, which predicts the formation of an inhomogeneous condensate. However, if we further increase μ , here $\mu = 1.0$ and $\mu = 1.2$, $\Gamma^{(2)}$ rises again and turns manifestly positive, even though it still has a “moat”-type structure with $Q \neq 0$. Hence, the inhomogeneous regime seems to approach the μ -axis for large $|\mu|$.

The phase diagram from the stability analysis

Now that we have presented possible scenarios and the ways to detect them, let us present the phase diagram of the $N \rightarrow \infty$ GN, which can be obtained exclusively from the stability analysis. This is plotted in Fig. 11.5.

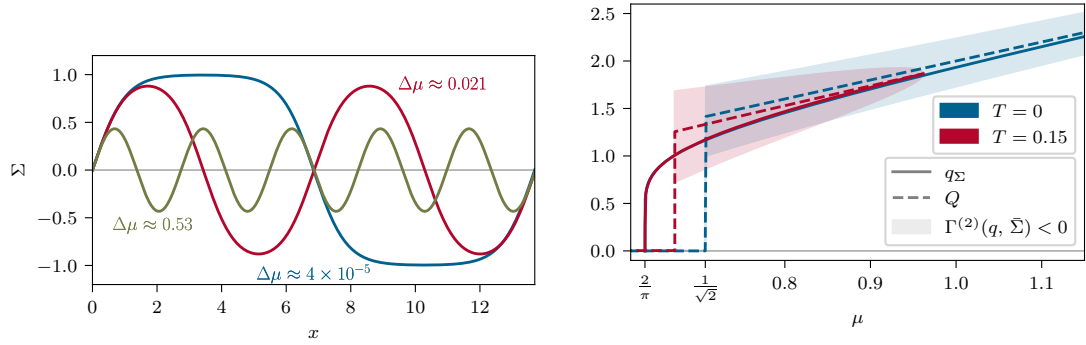
Taking the expansion about $\sigma = 0$ in Eq. (11.47) seriously, we solely work in the \mathbb{Z}_2 -symmetric phase. Starting at high T , we lower the temperature step by step until we detect a single root in the momentum profile of $\Gamma^{(2)}(0, \mu, T, q)$. If this root is at $q = 0$, we simply recover the standard second-order PT between phases, where spatially homogeneous \mathbb{Z}_2 symmetry is broken or restored. If the root is at $q = Q \neq 0$, we detect a PT between the \mathbb{Z}_2 -symmetric phase and a phase, where \mathbb{Z}_2 symmetry and continuous translational invariance are broken. In total, the PT from the \mathbb{Z}_2 -symmetric phase to phases of condensation is the black solid line in Fig. 11.5, which exactly agrees (up to the precision of our AMR method) with the exact results for the PT from Refs. [458, 327, 579, 446, 459, 460]. In conclusion, we can at least identify the entire black shaded region in Fig. 11.5 with a phase of spatially inhomogeneous condensation and further try to estimate the dominant frequency of the spatial modulation.

However, this analysis does not provide any reliable information about the stability of the phase of spatially homogeneous symmetry breaking. Indeed, comparing Fig. 11.5 with the exact result in Fig. 7.1, one identifies a region at small T between $|\mu| = \frac{2}{\pi}$ and $|\mu| = \frac{1}{\sqrt{2}}$, which is located in the former spinodal region with spatially homogeneous symmetry breaking, *cf.* Fig. 11.1. There, the true ground state is indeed inhomogeneous and consists of rather pronounced kink-like oscillations. Hence, in the vicinity of the former first-order PT an expansion in perturbations $\delta\sigma(x)$ about $\sigma = 0$ is no longer justified.

Similar problems of detecting the true PT between the phases of spatially inhomogeneous and homogeneous symmetry breaking were also presented in Ref. [476] or studies of related models [311, 561, 318].

The dominant wave vector

Let us briefly return to the discussion of the wave vector(s) of the inhomogeneous condensate and the position Q of the minimum of the two-point function. We already discussed that in the case where Q is the single root of $\Gamma^{(2)}(0, \mu, T, q)$, we are exactly on the PT line to the inhomogeneous phase and Q defines the only wave vector of the inhomogeneous perturbation. Here, we would like to further compare Q with the dominating wave vector q_Σ of the correct inhomogeneous condensate, which truly minimizes the effective action away from the phase boundary. In general,



(a) Modulation of the spatially inhomogeneous condensate at $T = 0$ for various μ with $\Delta\mu = \mu - \mu_c$, where $\mu_c = \frac{2}{\pi}$. The curves are calculated using exact expressions from Refs. [327, 446, 459]. The plot is inspired by Ref. [327, Fig. 2].

(b) The minimum of the bosonic two-point function Q , Eq. (11.52), and the dominating wave vector q_Σ of the true solution, Eq. (11.53), as functions of μ at constant $T = 0$ and $T = 0.15$. Colored regions mark the momenta q with $\Gamma^{(2)}(\sigma_{\min}(\mu, T), \mu, T, q) < 0$.

Figure 11.9: The spatial modulation of the exact solution for the inhomogeneous condensate, its dominating wave vector, and an estimate for the latter. From Ref. [5, Figs. 2 & 10].

the dominating wave vector is defined by

$$q_\Sigma \equiv \operatorname{argmax}_q \tilde{\Sigma}(\mu, T, q), \quad (11.53)$$

where $\tilde{\Sigma}$ is the Fourier transform of the inhomogeneous spatially oscillating condensate $\Sigma(\mu, T, x)$. For example, at $T = 0$, where we are at maximal distance from the PT, the spatial modulation of the true inhomogeneous ground state is plotted in Fig. 11.9a for several μ that are close to $\mu_c = \frac{2}{\pi}$ of the PT between the phases of spatially homogeneous and inhomogeneous symmetry breaking. Now, we can extract the dominant wave vector from a Fourier transformation of these solutions (which can be expressed in terms of Jacobi elliptic functions, see Refs. [446, 459, 460, 473, 327, 579]) and apply Eq. (11.53). On the other hand, we can extract Q from the two-point function. Both results can be compared to each other, *e.g.*, in Fig. 11.9b. In this figure, we also presented the same comparison at $T = 0.15$.¹⁰ For $T = 0$ one clearly finds from Fig. 11.9b that a sensible comparison is only possible at $|\mu| \geq \frac{1}{\sqrt{2}}$, in the region where the stability analysis is applicable. Close to the first-order PT of the homogeneous phase diagram, we observe significant deviations between Q and q_Σ . This is expected, because perturbations are no longer small and their modulation has a spectrum of many wave vectors. However, for large μ one finds that Q approaches q_Σ , since the amplitude of the inhomogeneous phase decreases and the modulation assumes the shape of a sine function with a single frequency.

For $T = 0.15$ we observe the same deviation of Q and q_Σ close to the former first-order PT. The difference between Q and q_Σ , however, vanishes as soon as μ approaches the PT line to the \mathbb{Z}_2 -symmetric phase, *cf.* Fig. 7.1.

This comparison of Q and q_Σ can of course be extended to the entire μ - T -plane, which is shown in Fig. 11.10. In this figure, we plot Q and q_Σ separately as functions of μ and T as well as their difference. Black regions correspond to vanishing Q and q_Σ , while colored regions indicate non-zero Q and q_Σ . Of course, we find a difference between Q and q_Σ for large μ and T (dark blue region in the middle panel), where inhomogeneous condensates do not exist, while the dispersion relation/bosonic two-point function still shows a “moat”-like structure. On the other hand, there is a significant difference at small T for $|\mu| < \frac{1}{\sqrt{2}}$ (red region in the middle panel), where the

¹⁰Similar plots of the wave vector of some inhomogeneous ground state as a function of baryon density (chemical potential) are also presented for other models by Refs. [314, Fig. 2], [315, Fig. 2], and [317, Figs. 6 & 7].

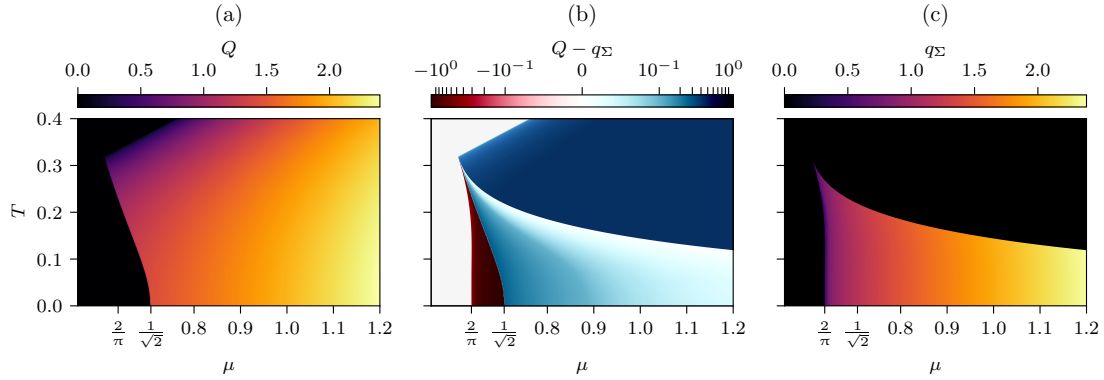


Figure 11.10: The minimum of the bosonic two-point function Q , Eq. (11.52), (a), the dominating wave vector of the exact solution q_Σ , Eq. (11.53), (c), and the difference (b) in the μ - T -plane. (Note that the middle panel has a linear color map for $|Q - q_\Sigma| < 0.1$ and a logarithmic color map for larger absolute values.) From Ref. [5, Figs. 11].

stability analysis fails and predicts no $Q \neq 0$ at all. However, in the formerly \mathbb{Z}_2 -symmetric phase at μ which are away from the first-order PT, the difference between Q and q_Σ is remarkably small. This means that an approximation of the inhomogeneous condensate in terms of conventional sine or cosine functions is feasible.

Consequences for finite- N FRG flows

Lastly, we comment on the consequences of our findings for calculations at finite N . Since the fermionic fluctuations are expected to dominate the dynamics during the RG flow up to a possible symmetry-breaking scale, see, *e.g.*, Ref. [72], the shape of the bosonic two-point function at these scales is not expected to be too different at finite N from what was discussed in this section. However, this implies that at non-zero μ and especially at small T we are confronted with q -profiles which cannot be approximated by simple parabolas. Hence, we cannot assume that the LPA' truncation (10.1), which only contains a quadratic momentum term for the bosons, is sufficient to capture the true dynamics of the system. Moreover, for a scale-dependent $Z_\varphi(t)$ we expect that it even turns negative at finite N , like it does at infinite- N . However, without any other higher-order momentum dependences, this renders the RG flow of a truncated system manifestly unstable.

On the other hand, if we just artificially fix $Z_\varphi(t) = \text{const.} > 0$, there is no chance for the coefficient to turn negative during the RG flow and we expect a stable flow towards the IR. Of course, fixing $Z_\varphi(t) = \text{const.}$, *e.g.*, in the LPA truncation, is a harsh restriction and can only be a crude approximation of the dynamics at small μ . Still, it is expected to be a stable approximation at large μ , while the improved LPA' truncation will clearly show its limitations.

In conclusion, we believe that an adequate description of the GN model at finite N requires, besides an excellent resolution in field space via an effective potential, an excellent resolution of the spatial momentum structure of the bosonic two-point function which enters the propagators. Both is in particular relevant for a precise description of the system at large μ and small T . Exactly the same is expected for higher-dimensional systems, *e.g.*, the QMM or the QMDM *etc.*

Nevertheless, we believe that we can answer the question of the presence/absence of condensation at finite N already with our rather crude truncation schemes in LPA and LPA'. The reason is: If spatially homogeneous condensation is not found at small T and small/vanishing μ , it is not expected to be present at all, because of thermodynamic consistency. At small T and vanishing μ , however, an approximation of the bosonic two-point function via a parabola seems to be justified, *cf.* Fig. 11.8a.

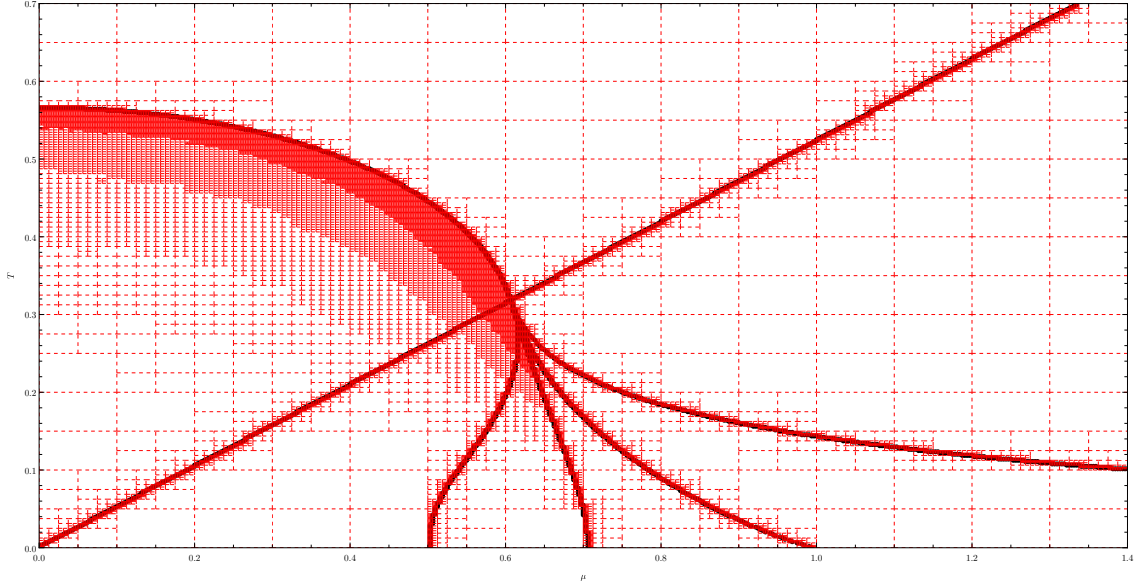


Figure 11.11: Visualization of the AMR algorithm for the $N \rightarrow \infty$ calculations.

11.4. Comment on the computation

As a last point of this chapter, we comment on the generation of the plots for the phase diagrams which are presented in this chapter. All the $N \rightarrow \infty$ data of this chapter were obtained via a simultaneous bisection in μ - and T -direction with multiple bisection criteria. In detail, we used a rectangular AMR algorithm that works as follows: We choose a coarse rectangular initial mesh of points in the μ - T -plane. This generates small rectangular plaquettes, here of initial size $\Delta\mu = 0.1$ and $\Delta T = 0.05$, see Fig. 11.11. At each corner point, all quantities of interest, such as the minimum $\sigma_{\min}(\mu, T)$, the minimum of the two-point function $Q(\mu, T)$, the pressure $p(\mu, T)$ etc., are calculated and stored.

Next, we proceed with an AMR step. To this end, several quantities are compared with each other at the four corners of each plaquette and it is decided whether the plaquette should be subdivided into four plaquettes of equal size. Our parallel refinement criteria are as follows: A refinement for a plaquette takes place, if one of the following conditions evaluates “true”.

1. The standard deviation of $\sigma_{\min}(\mu, T)$ at the four corners is greater than 0.01.
2. The standard deviation of $p(\mu, T)$ at the four corners is greater than 0.01.
3. The number of local minima of the potential at the four corners is unequal.
4. The sign of $Z_{\varphi}(\sigma = 0, \mu, T)$ at the four corners is not identical.
5. The sign of $Z_{\varphi}(\sigma_{\min}(\mu, T), \mu, T)$ at the four corners is not identical.
6. The sign of $\Gamma^{(2)}(\sigma_{\min}(\mu, T), \mu, T, Q)$ at the four corners is not identical.

After deciding which plaquettes require refinement, the corresponding new points on the edges and in the plaquette centers are generated and all necessary quantities are evaluated on these points. Afterwards, the same procedure as before is performed on the refined mesh. This algorithm is repeated until the desired precision in μ - and T -direction is obtained. In this chapter, we used five refinement steps, which results in a resolution

$$\Delta\mu = 0.1 \cdot 2^{-5} = 0.003125, \quad \Delta T = 0.05 \cdot 2^{-5} = 0.0015625. \quad (11.54)$$

However, calculations at higher precision are straightforward. The resulting final mesh of our work is presented in Fig. 11.11.

The challenging aspect of this algorithm is the handling and storage of the generated data and the correct linking of plaquettes, edges, and points such that no point in the μ - T -plane has to be evaluated twice. I am grateful to M. J. Steil, who supported me in setting up a basic version of his AMR algorithm in MATHEMATICA.

Chapter 12

The Gross-Neveu-Yukawa model at finite N

Abstract We present results for FRG calculations in the Gross-Neveu-Yukawa (GNY) model at finite N in different approximations. We start by discussing the correct initial condition for the RG flows and check RG consistency, thus, UV-cutoff independence. In addition, we present some tests for the numerical parameters. Our main discussion of the results starts with RG flows in the LPA approximation. We discuss qualitative aspects of the RG flow, such as the mechanisms for symmetry breaking and restoration. Here, we contrast the finite- N with infinite- N results. This also comprises a discussion of RG flows at low temperature and the dynamics that is introduced by the chemical potential. Afterwards, we turn to a more quantitative analysis and inspect the scaling of the symmetry-restoration scale in the IR as a function of N or T . Ultimately, we present the full phase diagram and the absence of symmetry breaking for all $T > 0$, but also briefly comment on the $T \rightarrow 0$ limit.

The second part focuses on RG flows at finite N in the LPA' truncation without and with the inclusion of a dynamical Yukawa coupling. The preliminary results for these calculations qualitatively confirm the LPA results – absence of symmetry breaking at $T > 0$ – and provide deeper insight into the challenges which are introduced by the chemical potential into FRG calculations.

Disclosure All results of this chapter for calculations in the LPA are presented already in our publication [4], which emerged from a joint work in approximately equal shares and are also part of Refs. [7, 8, 6]. The preliminary results beyond the LPA truncation have been performed exclusively by the author of this thesis and are not yet published.

12.1. Introduction

In the previous chapter, we demonstrated that even for $N \rightarrow \infty$ the bGN model features a non-zero and non-trivial momentum structure for the bosonic field. This indicates that, if they were not artificially suppressed, the bosons (once they have formed) would start fluctuating during the RG flow. Most probably they would even totally dominate the dynamics of the theory in the deep IR. Furthermore, as outlined in detail in Chapter 7 and in particular Section 7.4, there are many reasons to assume that \mathbb{Z}_2 -symmetry breaking of any kind, which was observed for $N \rightarrow \infty$, is absent for finite N , because bosonic fluctuations tend to restore this symmetry completely in a low number of spacetime dimensions.

In this last chapter of this thesis, we therefore turn to explicit FRG calculations for the GNY model at finite N . Most of our results are already presented in great detail in our publication [4], where we performed FRG calculations in the LPA in the novel fluid-dynamical framework. Thus,

in the first Section 12.3 of this chapter we are summarizing these results. Overall, we find that the LPA truncation of the GNY model strongly suggests a general absence of spatially homogeneous \mathbb{Z}_2 -symmetry breaking in the IR. Without spatially homogeneous symmetry breaking at very small $|\mu|$ and T , inhomogeneous condensation at larger $|\mu|$ is extremely unlikely. We therefore believe that there is in fact no symmetry breaking at all in the IR. Still, we observe the general phenomenon of precondensation [557, 558, 559, 560, 561, 278], where the attractive fermion interactions manage to break the symmetry during the RG flow and form bosonic bound states, while the symmetry is again restored in the IR by the bosonic fluctuations.

However, as anticipated already in Section 11.3, using the LPA is certainly a crude approximation, because the bGN model does not comprise a kinetic term for the bosons in the UV, which means that the wave-function renormalization should be initialized at zero. Yet, the LPA uses a constant non-zero wave-function renormalization, which is fixed uniquely in the UV. Therefore, one might argue that the bGN and GNY model are not the same in our FRG framework. Although we believe, as argued below, that the dynamical generation of the wave-function renormalization by the fermion fluctuations is a subleading effect w.r.t. the general question of breaking or restoration of the \mathbb{Z}_2 symmetry, we also extended our study to a dynamical $Z_\varphi(t)$. This allows fix the correct UV initial condition of the theory. Furthermore, we also present calculations with a dynamical Yukawa coupling. These improvements of the LPA truncation are discussed in Section 12.4 of this chapter.

However, we already know at this point that even these calculations are not fully comprehensive, because a single dynamical wave-function renormalization cannot capture the non-trivial momentum structure of the bosonic two-point function, which is generated by the fermion fluctuations and the chemical potential, *cf.* Section 11.3. Still, we believe that for small/zero μ , the above truncation is sufficient and we can argue again that an absence of symmetry breaking at small T and small/vanishing μ makes \mathbb{Z}_2 -symmetry breaking in the remainder of the phase diagram highly unlikely.

12.2. “Massaging” the flow equations (again)

To be explicit, in this chapter we are studying Eqs. (10.16) to (10.18) in three different approximations. For convenience, we recapitulate the equations at this point,

$$\partial_t U(t, \sigma) = -\frac{1}{\pi} \left[1 - \frac{\eta_\varphi(t)}{3} \right] \frac{1}{N} k^3 \frac{1}{\beta} \sum_{n=-\infty}^{\infty} \frac{1}{\omega_n^2 + k^2 + \frac{1}{Z_\varphi(t)} \partial_\sigma^2 U(t, \sigma)} + \quad (12.1)$$

$$+ \frac{1}{\pi} d_\gamma k^3 \frac{1}{\beta} \sum_{n=-\infty}^{\infty} \frac{1}{(\nu_n + i\mu)^2 + k^2 + h^2(t) \sigma^2},$$

$$\partial_t Z_\varphi(t) = + \frac{1}{\pi} \frac{1}{N} \frac{1}{Z_\varphi^2(t)} [\partial_\sigma^3 U(t, \sigma)]^2 k^3 \frac{1}{\beta} \sum_{n=-\infty}^{\infty} \frac{1}{[\omega_n^2 + k^2 + \frac{1}{Z_\varphi(t)} \partial_\sigma^2 U(t, \sigma)]^4} + \quad (12.2)$$

$$+ 2 \frac{1}{\pi} d_\gamma h^2(t) \left[-2 h^2(t) \sigma^2 k^3 \frac{1}{\beta} \sum_{n=-\infty}^{\infty} \frac{1}{[(\nu_n + i\mu)^2 + k^2 + h^2(t) \sigma^2]^4} + \right.$$

$$\left. + \frac{1}{4} k \frac{1}{\beta} \sum_{n=-\infty}^{\infty} \frac{1}{[(\nu_n + i\mu)^2 + k^2 + h^2(t) \sigma^2]^2} \right],$$

$$\partial_t h(t) = -2 \frac{1}{\pi} \frac{1}{N} \frac{1}{Z_\varphi(t)} h^3(t) k^3 \operatorname{Re} \left(\left[1 - \frac{\eta_\varphi(t)}{3} \right] \times \quad (12.3)$$

$$\times \frac{1}{\beta} \sum_{n=-\infty}^{\infty} \frac{1}{[\omega_n^2 + k^2 + \frac{1}{Z_\varphi(t)} \partial_\sigma^2 U(t, \sigma)]^2} \frac{1}{(\nu_n + i\mu)^2 + k^2 + h^2(t) \sigma^2} +$$

$$+ \frac{1}{\beta} \sum_{n=-\infty}^{\infty} \frac{1}{\omega_n^2 + k^2 + \frac{1}{Z_\varphi(t)} \partial_\sigma^2 U(t, \sigma)} \frac{1}{[(\nu_n + i\mu)^2 + k^2 + h^2(t) \sigma^2]^2} \Bigg).$$

We again did not indicate the $\frac{1}{N}$ -rescaling of the boson field and the potential from Eq. (10.7), because we are working in rescaled quantities for the remainder of this chapter.

Of course, for their explicit implementation, we perform the Matsubara sums by hand and use Eqs. (B.13) and (B.15) for the flow equation of the effective potential, Eqs. (B.24), (B.25), and (B.20) for the wave-function renormalization, and Eqs. (B.32) and (B.34) for the Yukawa coupling.

Furthermore, as discussed in detail in Section 10.3, we do not study the flow equation of the effective potential $U(t, \sigma)$ as it stands, but use the flow equation of its σ -derivative $u(t, \sigma) = \partial_\sigma U(t, \sigma)$ in terms of a diffusion-source-sink PDE. Here, we shall not repeat the details.

Lastly, before we can enter the discussion, we have to choose again an evaluation point in field space for the flow equations of $Z_\varphi(t)$ and $h(t)$. We choose $\sigma = 0$ for the following reasons:

1. From the perspective of an expansion of the bosonic kinetic term in powers of momenta and fields, the only reasonable expansion point of the truncation Eq. (10.1) is $\varphi(\tau, x) = 0$. Hence, it seems inconsistent to evaluate the expansion coefficient $Z_\varphi(t)$ at a different position in field space, if this part of the effective average action is constructed from an expansion about vanishing boson field. The same applies to the Yukawa coupling.
2. Another reason to evaluate the flow equations at $\sigma = 0$ is that $\sigma = 0$ represents the constant IR field configuration with least action, because, as we shall see, the system always ends up in the symmetric phase (for $T > 0$). From this perspective, using $\sigma = 0$ as the evaluation point for the flow equations of the Yukawa coupling and wave-function renormalization seems to be a self-consistent approach [71, 66].
3. Evaluating the flow equation for $Z_\varphi(t)$ at $\sigma \neq 0$ seems to violate crucial steps in the derivation of this flow equation, where it was explicitly assumed that it is field-independent. Including a field-dependence of $Z_\varphi(t)$ after derivation of the flow equations was not a problem for $N \rightarrow \infty$, because it did not feed back into the other flow equations, due to the absence of inner boson lines. Now, it would certainly lead to an inconsistency.

Of course, we are aware of the problems which go hand in hand with choosing $\sigma = 0$ as the expansion and evaluation point, such as possibly negative $Z_\varphi(t)$. In addition, we are also aware of possible alternative approaches, such as using a dynamical evaluation point during the RG flow, *i.e.*, the scale-dependent minimum $\sigma_{\min}(t)$ of the effective potential, see, *e.g.*, Refs. [79, 86, 179]. Testing these different approaches against each other is, however, not subject of this work and our results beyond the LPA should be considered as preliminary.

In summary, setting $\sigma = 0$ in the flow equations of $Z_\varphi(t)$ and $h(t)$, we obtain

$$\begin{aligned} \partial_t u(t, \sigma) = & \frac{d}{d\sigma} \left[-\frac{1}{\pi} \left[1 - \frac{\eta_\varphi(t)}{3} \right] \frac{1}{N} k^3 \frac{1}{\beta} \sum_{n=-\infty}^{\infty} \frac{1}{\omega_n^2 + k^2 + \frac{1}{Z_\varphi(t)} \partial_\sigma u(t, \sigma)} + \right. \\ & \left. + \frac{1}{\pi} d_\gamma k^3 \frac{1}{\beta} \sum_{n=-\infty}^{\infty} \frac{1}{(\nu_n + i\mu)^2 + k^2 + h^2(t) \sigma^2} \right], \end{aligned} \quad (12.4)$$

$$\begin{aligned} \partial_t Z_\varphi(t) = & + \frac{1}{\pi} \frac{1}{N} \frac{1}{Z_\varphi^2(t)} [\partial_\sigma^2 u(t, 0)]^2 k^3 \frac{1}{\beta} \sum_{n=-\infty}^{\infty} \frac{1}{[\omega_n^2 + k^2 + \frac{1}{Z_\varphi(t)} \partial_\sigma u(t, 0)]^4} + \\ & + 2 \frac{1}{\pi} d_\gamma h^2(t) \frac{1}{4} k \frac{1}{\beta} \sum_{n=-\infty}^{\infty} \frac{1}{[(\nu_n + i\mu)^2 + k^2]^2}, \end{aligned} \quad (12.5)$$

$$\partial_t h(t) = -2 \frac{1}{\pi} \frac{1}{N} \frac{1}{Z_\varphi(t)} h^3(t) k^3 \operatorname{Re} \left(\left[1 - \frac{\eta_\varphi(t)}{3} \right] \times \right. \quad (12.6)$$

$$\begin{aligned} & \times \frac{1}{\beta} \sum_{n=-\infty}^{\infty} \frac{1}{\left[\omega_n^2 + k^2 + \frac{1}{Z_\varphi(t)} \partial_\sigma u(t, 0)\right]^2} \frac{1}{(\nu_n + i\mu)^2 + k^2} + \\ & + \frac{1}{\beta} \sum_{n=-\infty}^{\infty} \frac{1}{\omega_n^2 + k^2 + \frac{1}{Z_\varphi(t)} \partial_\sigma u(t, 0)} \frac{1}{\left[(\nu_n + i\mu)^2 + k^2\right]^2} \Big). \end{aligned}$$

12.3. The GNY model in the LPA

In this section, we focus on the LPA for the GNY model. At the beginning, we explain how we initialize the RG flow equation (12.4) of the derivative of the potential in the UV. We present checks for RG consistency [244] (UV-cutoff independence of the IR) and a crosscheck of the fluid-dynamical framework with the $N \rightarrow \infty$ results. Furthermore, we discuss the independence of the purely numerical parameters. Afterwards, we turn to the actual discussion of RG flows for (the derivative of) the effective potential. We start with a qualitative discussion and a comparison with RG flows at $N \rightarrow \infty$, *e.g.*, to understand the dynamics which is introduced in the effective potential. We continue by presenting quantitative results at different finite N , *e.g.*, of the symmetry restoration scale in the IR. We end the general-results part with a presentation of the RG-scale dependence of the phase diagram. Lastly, before we switch to the LPA' truncation in Section 12.4 we briefly comment on the situation at $T = 0$.

12.3.1. The UV initial condition

A non-trivial question during the development of the project was how one has to initialize the RG flow of $u(t, \sigma)$ in the UV in a meaningful way. The problem is as follows: At infinite N , the phenomenology in the GN model is uniquely determined as soon as one fixes a single dimensionful quantity to a physical value, see Chapter 11. For example, one could use the critical temperature at $\mu = 0$ to set the scale or fix $h\sigma_0$ to some value. In particular, we set $h\sigma_0 = 1$ and $\sigma_0 = 1$, which implies that all dimensionful quantities in the model are expressed in units of the (UV) Yukawa coupling.¹ This also results in a unique UV potential (in our regularization), *i.e.*, Eq. (11.14), where also the cutoff Λ and $U(\Lambda, \sigma)$ itself can simply be measured in units of h ,

$$U(\Lambda, \sigma) = \frac{d_\gamma}{4\pi} h^2 \sigma^2 \left[- \left(1 + \frac{h^2 \sigma_0^2}{\Lambda^2} \right)^{-\frac{1}{2}} + \operatorname{artanh} \left(\left[1 + \frac{h^2 \sigma_0^2}{\Lambda^2} \right]^{-\frac{1}{2}} \right) \right]. \quad (12.7)$$

However, if we turn to finite N , we are actually confronted with a different theory with possibly different IR physics for each N . Therefore, it seems unconventional to use some unique IR quantity for all N to fix the scale. (This would be similar to comparing calculations for QCD with two, three, and infinite colors(!) by fixing the same proton mass.) Working at constant IR physics simply does not make sense, if we want to compare different N (including infinite N).

However, in the UV, the GN model in its bosonized and $\frac{1}{N}$ -rescaled version should be unique for any N . It is simply an (asymptotically) free relativistic gas of fermions, where bosons decouple by becoming ultra-massive. In addition, due to the $\frac{1}{N}$ -rescaling, it should not play a role whether we are working with $N = 2$ or $N = \infty$ fermion species in the UV. The formal initial condition for $U(t, \sigma)$ should be the same. Therefore, it absolutely makes sense to use the ($N \rightarrow \infty$)-renormalization procedure from Section 11.2.3 to generate the UV-cutoff dependence of the UV potential, Eq. (12.7), to

1. recover the correct ($N \rightarrow \infty$)-IR physics.
2. have a unique UV theory for all N .

Indeed, the explicit choice of N exclusively enters the PDE system Eqs. (12.4) to (12.6) in terms of $\frac{1}{N}$ -factors in front of bosonic propagators, such that “theories” with different N only start to

¹We keep h and σ_0 explicit in all formulae, but set $h\sigma_0 = 1$ and $\sigma_0 = 1$ in all practical calculations and plots.

differ once the bosonic fluctuations set in. This is in the IR, which implies that we can compare IR physics for different N .

Absence of diffusion in the UV

Let us further refine this line of argumentation from the fluid-dynamical perspective on the flow equation Eq. (12.4). In general and independent of the dependence of $\frac{1}{g^2}$ on Λ , the UV potential is quadratic in the fields, see Eq. (10.2). This corresponds to a linear initial condition for $u(t, \sigma)$ at $t = 0$ ($k = \Lambda$). However, the bosonic contribution to the flow equation is of the diffusive type, see Eqs. (10.20) and (10.23). Thus, as long as $\partial_\sigma^2 u(t, \sigma) \simeq 0$ there is no diffusion, which is certainly the case in the UV. Moreover, $\partial_\sigma u(t, \sigma)$ enters the bosonic propagators and therefore also the diffusion coefficient Eq. (10.23) in the denominator. In the UV, $\partial_\sigma u(t = 0, \sigma) = \frac{h^2}{g^2}$, which is supposed to be large (or even diverge for $\Lambda \rightarrow \infty$), which additionally suppresses diffusion. In consequence, already from the quadratic shape of the UV potential and the diffusive character of the flow equation, we can conclude that bosonic fluctuations cannot enter the dynamics until the fermions significantly reshape the potential. This happens approximately at the symmetry-breaking scale. It directly follows that the RG flows at any N will be rather similar up to this scale and closely follow the RG flow for $N \rightarrow \infty$. This already confirms without explicit calculation that switching from $N \rightarrow \infty$ to finite N mainly affects the IR physics. Condensation is even expected at intermediate RG scales in regions of the phase diagram where it is also found for $N \rightarrow \infty$.

Fixing the Yukawa coupling and the wave-function renormalization in the LPA

Implicitly, we have already stated that we fix the non-dynamical Yukawa coupling for all RG times at its UV initial value, which we also use to set the scales of the model. However, for computations in LPA we have to additionally fix the value of $Z_\varphi(t)$ for all RG times. A reasonable approach is certainly to use the infinite- N results from Fig. 11.7 at $\mu = 0$ and small T as an orientation, because this is the region of the phase diagram where we believe that a parabolic momentum profile of $\Gamma^{(2)}$ is most reasonable. However, for $T \rightarrow 0$, Z_φ diverges, while it falls off rapidly for growing temperatures. As a compromise, we simply fix $Z_\varphi = 1$ by hand for all scales. In the UV, this is certainly too large, but also in the IR it is only a rough approximation for most points in the μ - T -plane. However, as just explained, an overestimation of the kinetic term for the bosons is of subordinate importance, because the bosonic fluctuations are suppressed in any case by the shape of the potential up to a possible symmetry-breaking scale. At this scale the bosonic wave-function renormalization is generated for any N and almost takes its $N \rightarrow \infty$ value due to the fermionic fluctuations. In the IR we believe that an under-/overestimation of Z_φ mainly shifts the dynamics slightly to smaller/larger RG scales.

(Numerical) consistency check with the infinite- N solution

Although we have fixed the UV potential and initial condition for all N by Eq. (12.7) and continue to measure all dimensionful quantities in units of the UV Yukawa coupling h , we still have to clarify how large we have to choose Λ . In contrast to the $N \rightarrow \infty$ calculations, it is not possible to send $\Lambda \rightarrow \infty$ in numerical calculations of RG flows. Instead, we have to initialize the RG flows at some very large but finite Λ to ensure RG consistency and independence of the IR observables from Λ . We do not repeat the underlying reasoning at this point, but refer to Section 6.5 and Ref. [244].

Fixing Λ via $N \rightarrow \infty$ calculations A first, rather simple procedure for choosing Λ is to already work in our fluid-dynamical setup for the numerics, but to suppress bosonic fluctuations again by sending $N \rightarrow \infty$. Hence, we initialize the RG flow repeatedly at different values for Λ , flow to the deep IR (here $k_{\text{IR}} = 10^{-4}$ in units of h)² by only including fermion fluctuations, and extract

²We discuss below that this value for the artificial IR cutoff is sufficiently low. Still, we could even integrate to smaller k_{IR} without observing a difference in our results.

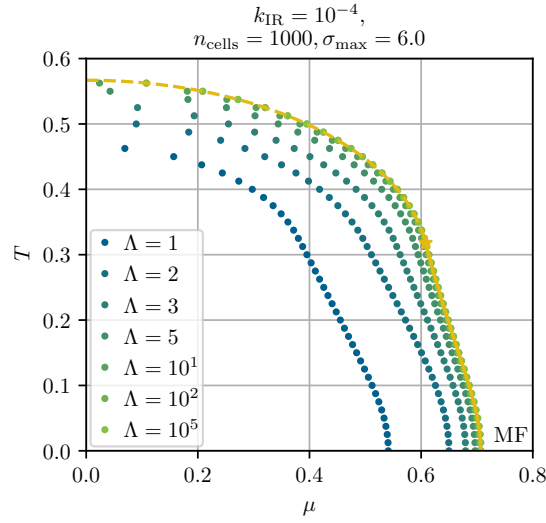


Figure 12.1: PT lines (equally colored dots) for different UV cutoff Λ at $N \rightarrow \infty$. The curves are obtained by integrating the $N \rightarrow \infty$ limit of the RG flow equation (12.4). The exact PT line, *cf.* Fig. 11.1, is plotted in yellow. From Ref. [4, Fig. 3].

the corresponding phase diagram. For large Λ , the phase diagram should go over to the well-known $N \rightarrow \infty$ phase diagram of the renormalized GN model, were the cutoff is entirely removed from the IR potential, see Fig. 11.1. The simple question is how large Λ has to be chosen such that differences between this finite Λ and $\Lambda \rightarrow \infty$ are no longer visible. The corresponding test is presented in Fig. 12.1, where we study the phase boundary for the ($N \rightarrow \infty$)-phase diagram for different UV cutoffs. It is clearly visible that surprisingly large Λ are required to ensure RG consistency already without bosonic fluctuations. We consider $\Lambda = 10^5$ to be a reasonable choice.

UV-cutoff independence with bosonic fluctuations Still, only using the infinite- N calculations to ensure RG consistency seems insufficient and we should at least perform some explicit checks for finite- N calculations. Such type of tests are presented in our own Ref. [4, Appendix F] and we summarize the key idea of these tests in the following. (The concept closely follows the tests from Section 6.5.)

As a non-trivial observable to test UV-cutoff independence, we choose the IR curvature mass. According to Ref. [244], independence of the UV cutoff implies at any μ and T ,

$$\Lambda \frac{d}{d\Lambda} m_\sigma^2 = 0, \quad (12.8)$$

where

$$m_\sigma^2 = \partial_\sigma u(t \rightarrow \infty, \sigma) \Big|_{\sigma = \sigma_{\min}(\mu, T)}. \quad (12.9)$$

(Of course, numerically $t \rightarrow \infty$ is replaced by the artificial cutoff k_{IR} .) The question is how Eq. (12.8) can be tested explicitly. To this end, we solve RG flows with initial condition (12.7) repeatedly for different cutoffs Λ and extract Eq. (12.9). We expect that for sufficiently large Λ the IR values for m_σ^2 do not change anymore. Hence, we plot m_σ^2 as a function of Λ in Fig. 12.2 (upper panels) for two different sample points in the μ - T -plane. Since it is hard to judge by visual inspection only whether m_σ^2 is indeed no longer changing when Λ is further increased, we also plot

$$\frac{\Delta m_\sigma^2}{m_\sigma^2}(\Lambda_i) \equiv \left| \frac{m_\sigma^2(\Lambda_i) - m_\sigma^2(\Lambda = 10^6)}{m_\sigma^2(\Lambda = 10^6)} \right|, \quad (12.10)$$

which is the relative deviation of the IR curvature mass for some Λ_i from the curvature mass at the largest Λ . These are the lower panels of Fig. 12.2.

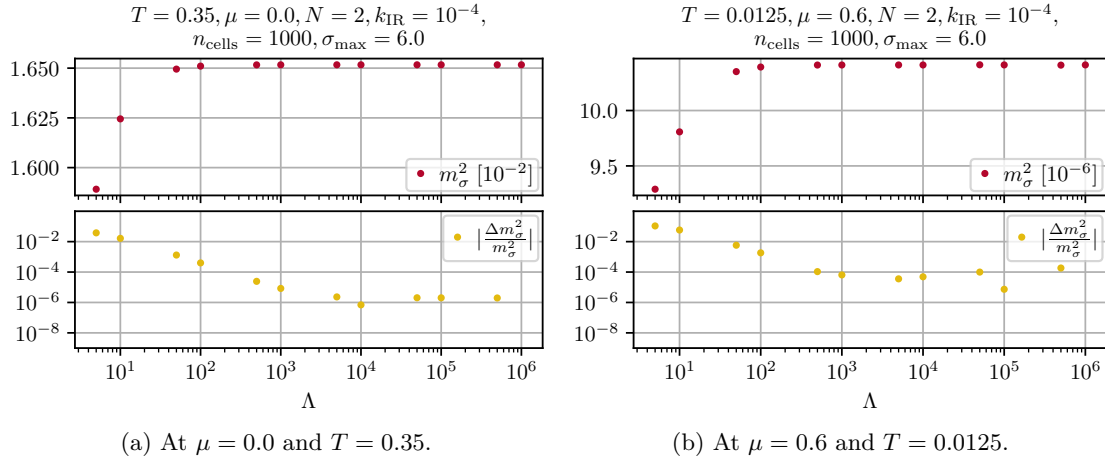


Figure 12.2: IR curvature mass m_σ^2 (upper panels) and Eq. (12.10) (lower panels) as functions of the UV cutoff Λ . From Ref. [4, Figs. 32 & 34].

In total, we observe that both, Eqs. (12.9) and (12.10), saturate on plateaus for large Λ . This is basically a realization of Eq. (12.8) and confirms that $\Lambda = 10^5$ is a suitable choice for the UV initial scale. Similar tests can be performed with other observables. The above tests were also performed at other (μ, T) points, see Ref. [4], and for different N .

Meaningful choices of the numerical parameters σ_{max} and n_{cells} that were used for the tests is briefly discussed in the next paragraphs.

12.3.2. Numerical tests

As discussed in detail in Section 6.5, it is also required to control that the IR results of RG flows are independent of the numerical parameters. Here, these are mainly two parameters, namely σ_{max} , the size of the computational domain, and n_{cells} , the number of FV cells which are used for spatial discretization, *cf.* Sections 5.2, 6.5, and 10.3.1. Of course, in contrast to Section 6.5, we do not have any exact reference solutions to control the independence. In analogy to the previous discussion and as suggested before, we therefore use the largest σ_{max} and the finest grid spacing with smallest $\Delta\sigma$ as corresponding references. Again, the curvature mass (12.9) serves as our observable and we conclude independence of the numerical parameters if we observe plateau-like behavior for σ_{max} -tests and convergence for $\Delta\sigma$ -tests. To this end, we introduce the additional observables

$$\frac{\Delta m_\sigma^2}{m_\sigma^2}(\sigma_{\text{max},i}) \equiv \left| \frac{m_\sigma^2(\sigma_{\text{max},i}) - m_\sigma^2(\sigma_{\text{max}} = 12)}{m_\sigma^2(\sigma_{\text{max}} = 12)} \right| \quad (12.11)$$

and

$$\frac{\Delta m_\sigma^2}{m_\sigma^2}(\Delta\sigma_i) \equiv \left| \frac{m_\sigma^2(\Delta\sigma_i) - m_\sigma^2(\Delta\sigma_{\text{min}})}{m_\sigma^2(\Delta\sigma_{\text{min}})} \right|, \quad (12.12)$$

where the best resolution of our tests is given by

$$\Delta\sigma_{\text{min}} = \frac{\sigma_{\text{max}}}{n_{\text{max}} - 1} = \frac{6}{3000 - 1}. \quad (12.13)$$

The explicit tests are presented in Figs. 12.3 and 12.4 and we conclude that $\sigma_{\text{max}} = 6$ and $\Delta\sigma = 0.006$ are appropriate choices. Tests at two additional points in the μ - T -plane are explicitly presented in Ref. [4] and further tests were performed by the authors of Ref. [4], also for different N .

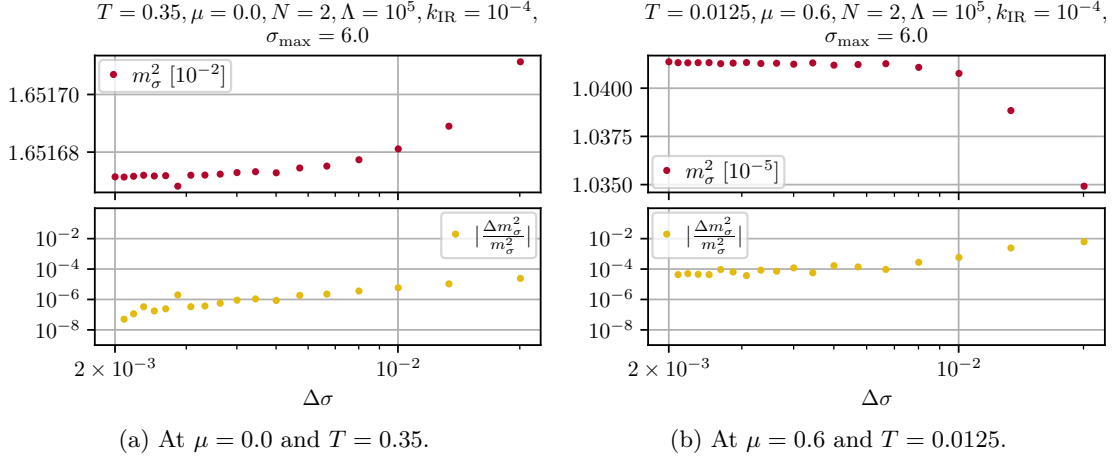


Figure 12.3: IR curvature mass m_σ^2 (upper panels) and Eq. (12.12) (lower panels) as functions of the size of the FV cells $\Delta\sigma$. From Ref. [4, Figs. 28 & 30].

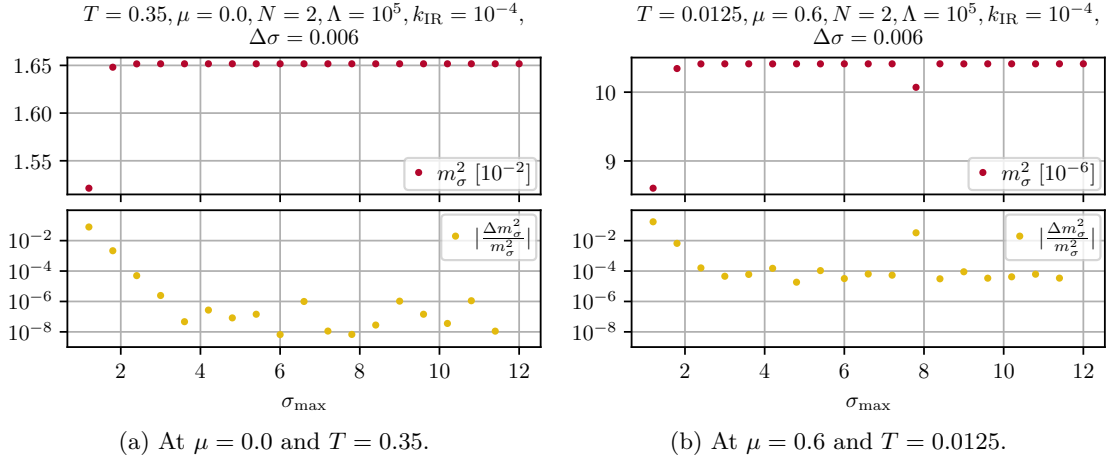


Figure 12.4: IR curvature mass m_σ^2 (upper panels) and Eq. (12.11) (lower panels) as functions of the size of the computational domain σ_{max} . Ref. [4, Fig. 24 & 26].

12.3.3. Results

Having settled the questions of UV initial conditions, a decent choice for the UV cutoff scale, and appropriate choices of the numerical parameters, we can start presenting the results which are obtained within this setup. We begin with a more qualitative discussion of RG flows at selected points in the μ - T -plane and afterwards turn to more quantitative predictions.

Symmetry breaking and restoration in RG flows

In order to understand the overall dynamics of RG flows at finite N and their difference to RG flows at $N \rightarrow \infty$, we simply pick w.l.o.g. the point $\mu = T = 0.1$ and compare calculations at the two extreme choices for N , namely $N = 2$ and $N = \infty$. The corresponding plots are presented in Fig. 12.5.

We start the discussion with Fig. 12.5a, where the RG flow of the derivative of the effective potential was calculated in the absence of bosonic fluctuations. The flow of the potential itself is obtained by integration of $u(t, \sigma)$ in field space. Of course, we could have simply used Eq. (11.21) to plot the IR potential (red curve), which, however, is not the point of this discussion. By integrating

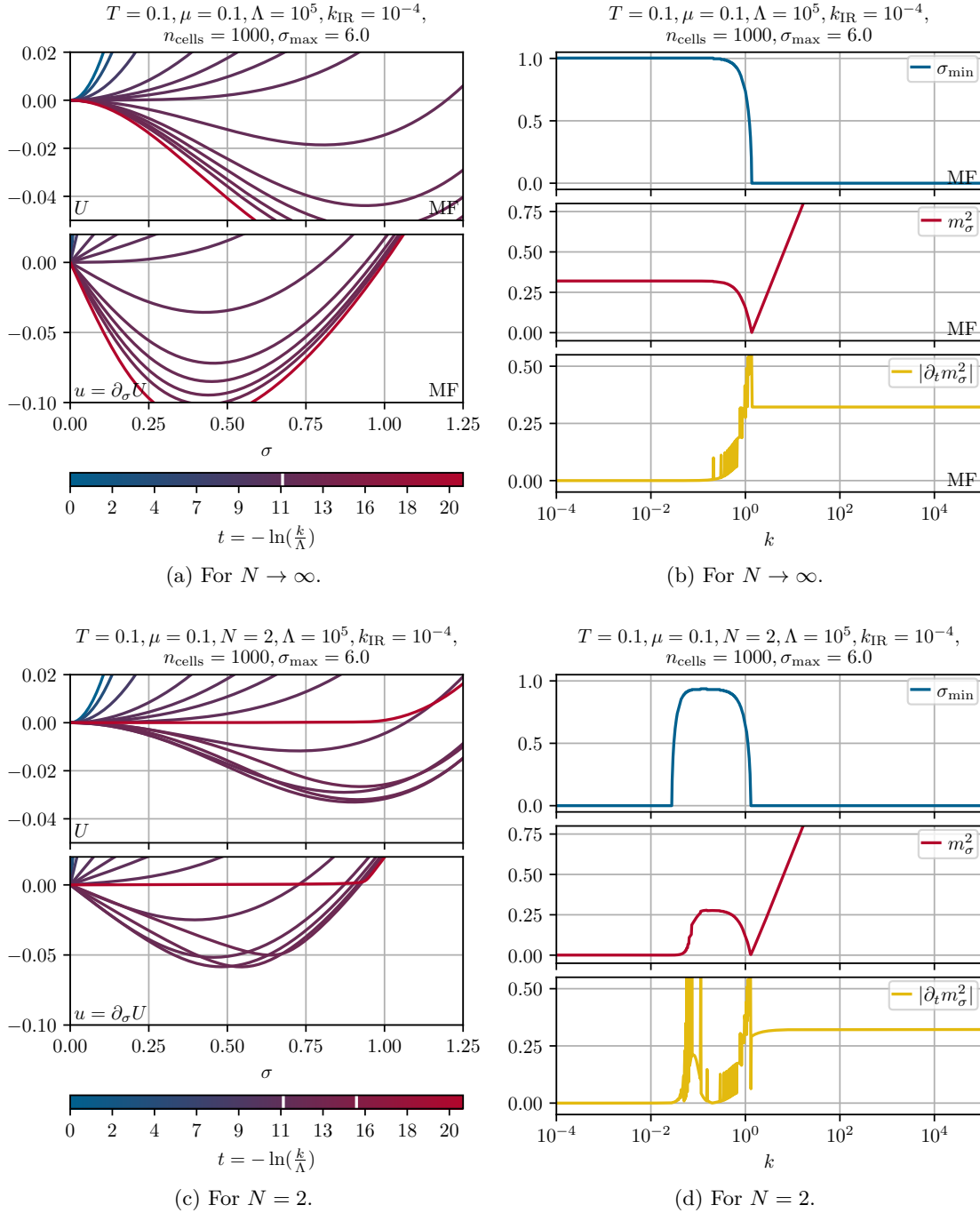


Figure 12.5: RG flow of the effective potential $U(t, \sigma)$, its σ derivative $u(t, \sigma) = \partial_\sigma U(t, \sigma)$, the global minimum σ_{min} , the squared curvature mass m_σ^2 , and the relative change of the squared curvature mass $|\partial_t m_\sigma^2|$ at $\mu = T = 0.1$. (The white vertical bars in the horizontal scaling bar mark the symmetry breaking/restoration RG times.) From Ref. [4, Figs. 4 & 5 & ancillary files on arXiv].

out the fermions step by step one clearly observes how the parabolic UV potential changes its shape as soon as the RG scale reaches model scales (which are set by h) and \mathbb{Z}_2 symmetry of the vacuum gets dynamically broken because a non-trivial minimum forms. This is also observed from Fig. 12.5b, where the corresponding RG flow of the minimum is plotted. Furthermore, we present as an additional observables the curvature mass and its changing rate, which are important to judge whether one has really reached the IR and can stop the RG flow at some finite artificial IR cutoff k_{IR} .

Now, let us compare the $N \rightarrow \infty$ flow with the RG flow for the identical setup, but with $N = 2$. Thus, bosonic fluctuations are no longer suppressed. Even more, $N = 2$ is the smallest possible N and therefore is identified with a maximum of bosonic fluctuations. Interestingly, but as expected from our earlier discussion, we find that the RG flows for $N \rightarrow \infty$ and $N = 2$ lie almost perfectly on top of each other in the UV and only start deviating from each other right after symmetry breaking. (The corresponding plots for the RG flows of the effective potential and its derivative are presented in Fig. 12.5c, while the flow of the minimum, the curvature mass, and its changing rate are shown in Fig. 12.5d.) The agreement of the UV dynamics for all N also confirms our assumption that the explicit choice of Z_φ is of little relevance in the UV and bosonic fluctuations are simply suppressed by the shape of the effective potential and the absence of diffusion in the PDE of $u(t, \sigma)$.

This brings us directly to the dynamics which is going on for $N = 2$ at scales below $k \approx h$. Once a non-trivial minimum has formed and the potential has developed a ‘‘Mexican hat’’-like shape, we find that bosonic fluctuations set in rapidly and start destabilizing the condensate. This is clearly seen on the level of $u(t, \sigma)$ in the lower panel of Fig. 12.5c by comparing it with the lower panel of Fig. 12.5a. Strong diffusion in the small- $|\sigma|$ region, where the slope of $u(t, \sigma)$ is negative and the diffusion coefficient largest, *cf.* Section 10.3, leads to an equilibration of the ‘‘fluid field’’ $u(t, \sigma)$ and a reduction of gradients at small $|\sigma|$. On the level of $U(t, \sigma)$, this corresponds to a flattening of the potential. The non-analytic kink-like structure close to the intermediate minimum (w.r.t. t) is due to the highly non-linear character of the diffusion, which is realized by a highly non-linear diffusion coefficient. Ultimately, the potential $U(t, \sigma)$ itself turns convex, as it should, and the \mathbb{Z}_2 symmetry of the vacuum is restored. This is better seen in the upper panel of Fig. 12.5d and is a realization of precondensation, because $\mu = T = 0.1$ is clearly located in the region of the phase diagram where the bosonic fluctuations and not the thermal fluctuations of the fermions destroy the condensate in the IR.

Overall, the observed dynamics also vividly demonstrates the shortcomings of the $N \rightarrow \infty$ approximation. As soon as we turn to finite N the convexity of the IR potential is recovered, which was artificially violated by the $N \rightarrow \infty$ limit.

Let us finally turn to the changing rates of the curvature masses in the lower panels of Figs. 12.5b and 12.5d. These can be used as a powerful indicator for the freezing of the dynamics in the IR. As soon as this quantity completely falls off to zero, we can reasonably assume that we reached the IR and that we can stop the numerical integration at some small artificial k_{IR} . As is clearly seen from the same plots (upper and middle panel) the minimum and the curvature mass itself are no good observables for reaching the IR.

RG flows at low temperature and the role of the chemical potential

Next, we address the role of the chemical potential during the RG flow by inspecting explicit results and therefore continue the discussion of Section 10.3.1. In this discussion, we identified the dynamics which is introduced by μ into the fluid-dynamical PDE for $u(t, \sigma)$, as a sudden ‘‘external shock’’. It enters field space at $\sigma = 0$ when $k \approx |\mu|$ and moves out to larger $|\sigma|$ for smaller k , see also Fig. 10.1.

In order to visualize this effect, we again choose small and vanishing T , *i.e.*, $T = 0$ and $T = 0.00625$ and fix $\mu = 0.6$. Again, we start by inspecting the step-wise integration of the fermion loop at $N \rightarrow \infty$. The corresponding RG flows of the (derivative) of the effective potential for $T = 0$ and $T = 0.00625$ are plotted in Figs. 12.6a and 12.6b. In Fig. 12.6a for $T = 0$ we clearly observe what was discussed earlier in Section 10.3.1: The chemical potential introduces a discontinuity

into $u(t, \sigma)$, which moves to larger $|\sigma|$ and ultimately freezes for $k = 0$ at $|\sigma| = |\mu|$. On the level of $U(t, \sigma)$, this corresponds to a moving (barely visible) kink. (Note that the IR potential and its derivative agree with Figs. 11.3a and 11.3b.) However, as soon as the temperature is non-vanishing, the Fermi-Dirac distributions lead to a smearing of the discontinuity and the kink, see Fig. 12.6b. Still, remnants of the structures which stem from the chemical potential are clearly visible.

In Section 10.3.1, we discussed that at finite N this sudden externally induced discontinuity may lead to an overshooting of the poles of the Euclidean bosonic propagators for $T = 0$ and therefore presents a severe formal and numerical problem. This behavior was indeed observed as soon as bosonic fluctuations at finite N were included in the RG flows and the numerical integration simply broke. Hence, we are conceptually not able to present RG flows at $T = 0$ for non-vanishing μ . In consequence, in order to study the interplay between the diffusion from the bosonic σ -mode and the non-analyticity, we work at very small non-vanishing temperature, where integration is possible. In Figs. 12.6c and 12.6d, we present explicit RG flows of (the derivative of) the effective potential with $N = 2$ and $N = 16$ at $\mu = 0.6$ and $T = 0.00625$. Again, it is interesting to observe the identical dynamics for all finite and infinite N up to the symmetry-breaking scale and the huge deviations of the finite- N dynamics from the purely fermionic flow in the IR. In any case, we observe how the diffusive σ -mode restores the \mathbb{Z}_2 symmetry in the deep IR and drives the potential convex, which is both violated for the $N \rightarrow \infty$ calculation. However, we can still observe clear imprints of the chemical potential in the shape of $u(t, \sigma)$ in Figs. 12.6c and 12.6d despite the (non-linear) diffusion. An expansion of such a potential or its derivatives in polynomials is certainly not recommendable at RG scales below the symmetry-breaking scale. The same applies when trying to solve the corresponding PDE with discretization schemes which cannot cope with non-analyticities. We therefore believe that insufficient numerical schemes are one of the reasons why there was little success in integrating to the small IR scales with high resolution in field space in a stable and controlled way in various models.

Let us also briefly comment on the differences between the $N = 2$ and $N = 16$ RG flows in Figs. 12.6c and 12.6d. It is clearly visible that for a larger number of fermion species the diffusion sets in at later RG times and symmetry restoration takes place at much smaller RG scales. This is expected, because N exclusively enters the PDE in terms of a $\frac{1}{N}$ -prefactor in front of the bosonic contribution, thus as a $\frac{1}{N}$ factor in the diffusion coefficient, see Eq. (12.4). This simply makes the fluid more viscous such that equilibration takes longer.

Lastly, we note again that the LPA is of course a bad quantitative description of the true dynamics at large μ and small T , because the imprints of the chemical potential in the momentum structure of the bosonic two-point function, which were discussed in Section 11.3, are ignored, see Fig. 11.8. Still, the flows in LPA are stable, even in regions where we expect Z_φ to turn negative, because we simply do not allow for this to influence the dynamics of the potential. This means that, funnily, improving the truncation does not lead to more stability of the RG flows.

Varying N

So far we mainly considered $N = 2$ when we discussed RG flows at finite N or tested the numerical setup. However, the question is whether we are observing the same dynamics, namely symmetry restoration by the bosons for any N or is there maybe a critical N where the \mathbb{Z}_2 symmetry is still broken for some points in the phase diagram in the IR. To answer this question, we first focus again on a single point in the μ - T -plane, namely $\mu = T = 0.1$ and studying the RG flow of the condensate for various N to get an impression of the general behavior. This is plotted in Fig. 12.7a. It is clearly visible that there is condensation for all N . For sufficiently large N we find that $\sigma_{\min}(t)$ even approaches the $N \rightarrow \infty$ vacuum IR values $\sigma_{\min}(\mu = 0.1, T = 0.1) \simeq \sigma_0 = 1$ for RG scales, which are close to the model scales or slightly below. Nevertheless, for any of the randomly chosen N we observe symmetry restoration at some scale k_{res} , which we call the (\mathbb{Z}_2 -symmetry) restoration scale. As expected, there is also a clear hierarchy and k_{res} is decreasing with increasing N . Interestingly, k_{res} is at least one order of magnitude below typical model scales. For larger N , it appears reasonable that it is necessary to integrate several orders of magnitude

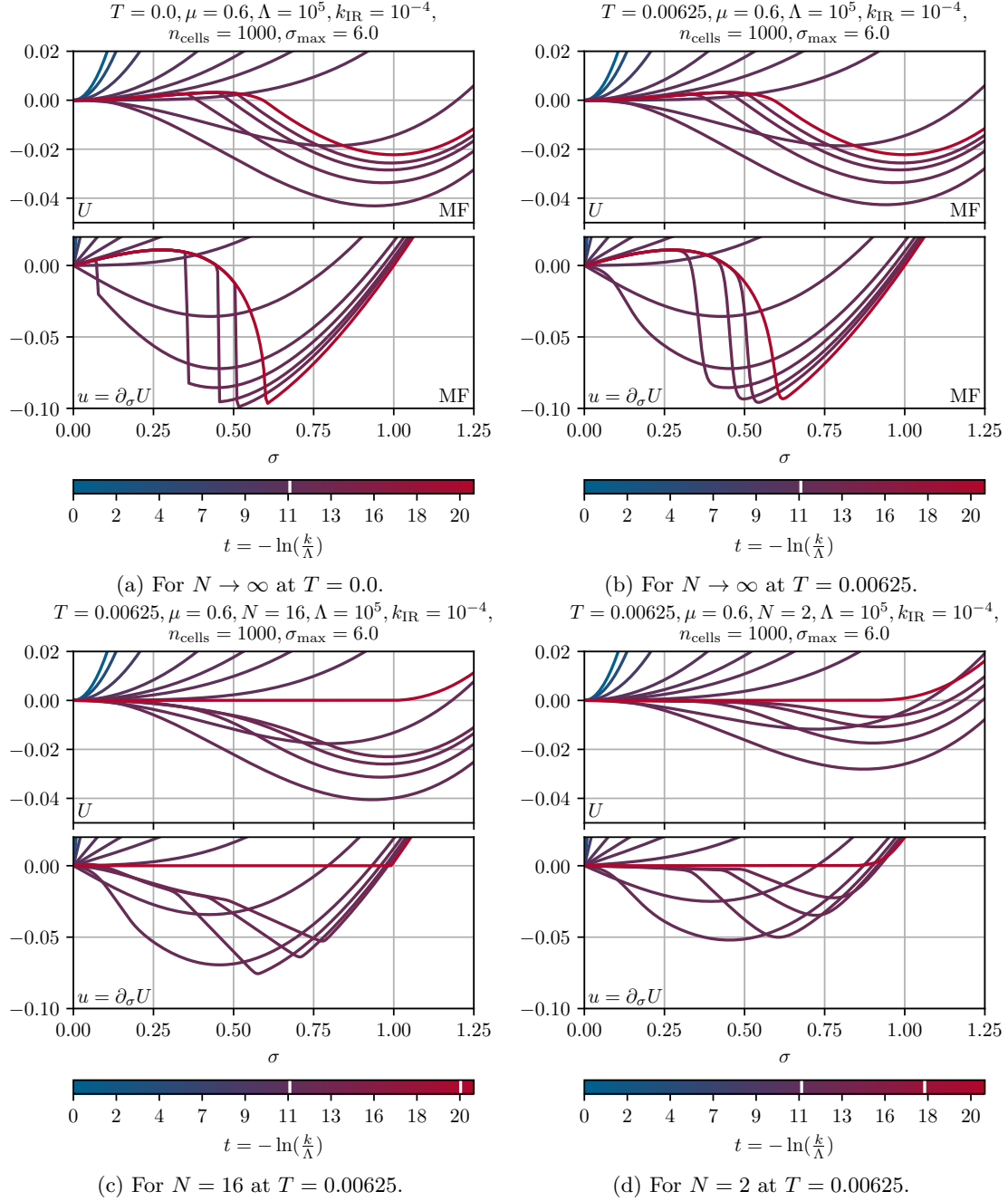


Figure 12.6: RG flows of the effective potential $U(t, \sigma)$ and its σ derivative $u(t, \sigma)$ at small/vanishing temperature and $\mu = 0.6$. (The white vertical bars in the horizontal bar scale mark the symmetry breaking/restoration RG times.) From Ref. [1, Figs. 6, 7, 8, 9].

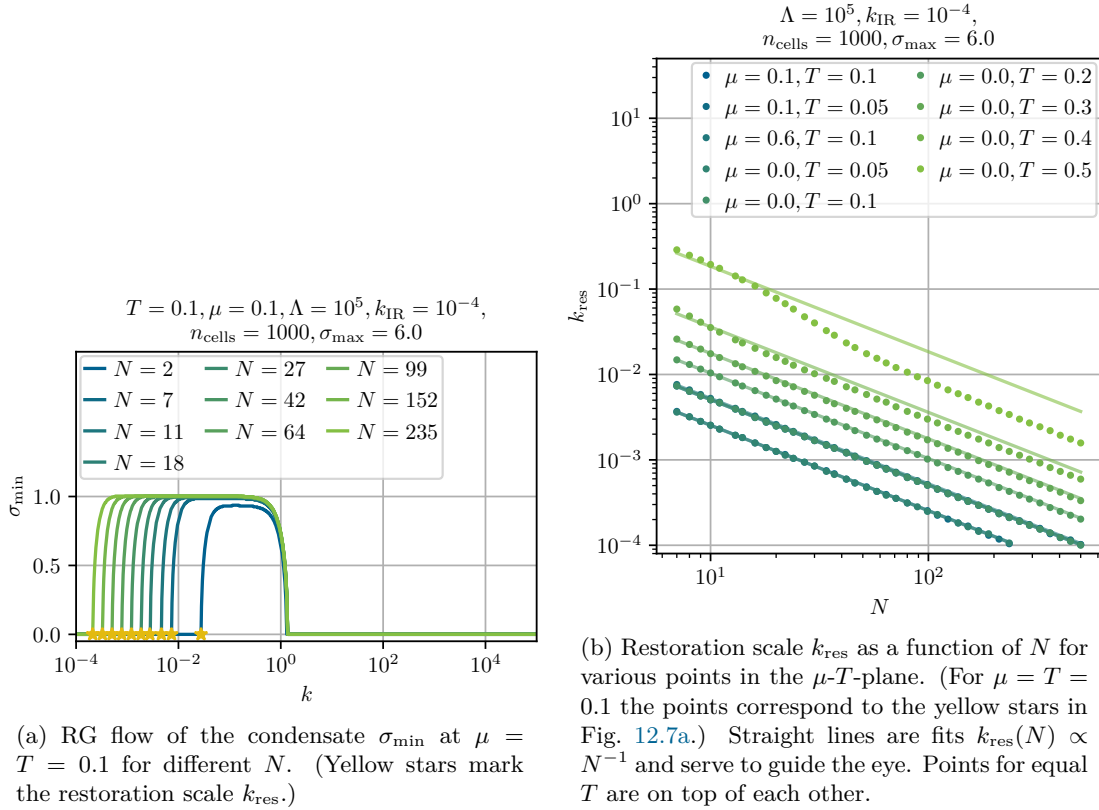


Figure 12.7: Dependence of the \mathbb{Z}_2 -symmetry restoration scale k_{res} on N . From Ref. [4, Figs. 10 & 11].

below model scales. This promotes the solution of the GNY to a true multi-scale problem (from $\Lambda = 10^5$ to $k_{\text{IR}} \approx 10^{-4}$). Recalling that there were multiple approaches to the GN model via lattice Monte-Carlo studies, see references in Section 7.4.5, it seems at least questionable whether these works were able to resolve this range of energies, which seems to be required to capture the entire dynamics.

Anyhow, let us study the dependence of k_{res} on N more systematically for varying μ and T based on Fig. 12.7b. From the plot, we can deduce that $k_{\text{res}}(N) \propto \frac{1}{N}$ for small and moderate temperatures, independent of the choice of μ . Naturally, we exclusively considered values of μ where we expect at least condensation within a finite range of RG scales. As an orientation, we used the infinite- N phase diagram in Fig. 11.1, where the chemical potential alone already restores the symmetry for $|\mu| > \frac{1}{\sqrt{2}}$. We also find deviations from $k_{\text{res}}(N) \propto \frac{1}{N}$ for small $|\mu|$ and temperatures close to the second-order PT line from Fig. 11.1. This is also expected, because in this region already thermal fluctuations of the fermions start to melt the condensate.

Overall, we conclude from this discussion that we do not observe qualitative differences between calculations at different finite N . The only difference is that k_{res} is pushed towards the IR for increasing N . Still, our observed relation $k_{\text{res}}(N) \propto \frac{1}{N}$ predicts the possibility for symmetry breaking in the IR for $N \rightarrow \infty$ and is therefore again consistent with MF calculations.

Varying T

Next, let us more systematically analyze the situation at different temperatures – especially at small temperatures. W.l.o.g. we again fix $N = 2$. We pick different values for $\mu \in [0.0, 0.75]$ and study k_{res} as a function of the temperature. The results are shown in Fig. 12.8. Of course, for $\mu \geq \frac{1}{\sqrt{2}}$, k_{res} at small T becomes independent of T , because the symmetry is already restored by

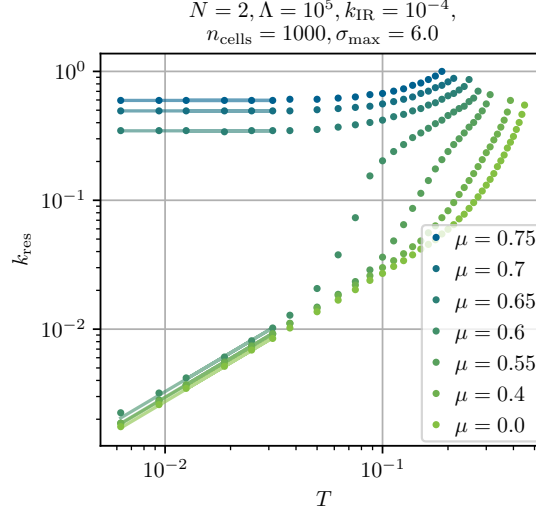


Figure 12.8: T -dependence of the restoration scale k_{res} for $N = 2$. For $T \lesssim 0.03$ we plot $k_{\text{res}}(T) \propto T^0$ for $\mu > 0.6$ and $k_{\text{res}}(T) \propto T$ for $\mu < 0.6$ for optical guidance. From Ref[4, Fig. 13].

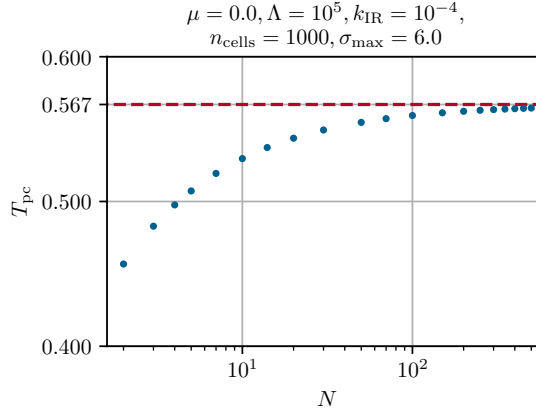


Figure 12.9: The precondensation temperature T_{pc} as a function of N at $\mu = 0$. (The red dashed line marks the $N \rightarrow \infty$ second-order PT line at $T_c = \frac{e^\gamma}{\pi}$, see Fig. 11.1.) From Ref. [4, Fig. 14].

the density fluctuations of fermions (the particle-anti-particle asymmetry) without the help of the bosons. However, for small μ and small T we clearly observe that $k_{\text{res}}(T) \propto T$. This indicates that \mathbb{Z}_2 symmetry is always restored at some IR scale as long as $T > 0$. For $T = 0$, symmetry breaking is in general possible. Both findings are in general agreement with the discussion in Section 7.4.

Precondensation

We have mentioned the phenomenon of precondensation already several times. In simple terms it states, see Refs. [557, 558, 559, 560, 561, 278], that there might be the formation of a condensate at intermediate RG times, because of the attractive fermion interactions, which is nevertheless vaporized by thermal or quantum fluctuations of any kind at deeper IR scales.

As can already be anticipated from the above discussion, we observe this phenomenon in a large region of the phase diagram, which almost matches the region of homogeneous symmetry breaking for $N \rightarrow \infty$. Here, we simply quantify at $\mu = 0$ the actual extent of this region as a function of N . We define the precondensation temperature T_{pc} as the maximal temperature where at least some condensation was observed at any time during the RG flow. For $N \rightarrow \infty$ the temperature T_{pc} should approach $T_c = \frac{e^\gamma}{\pi}$. Exactly this is seen in Fig. 12.9. It is also worth mentioning that

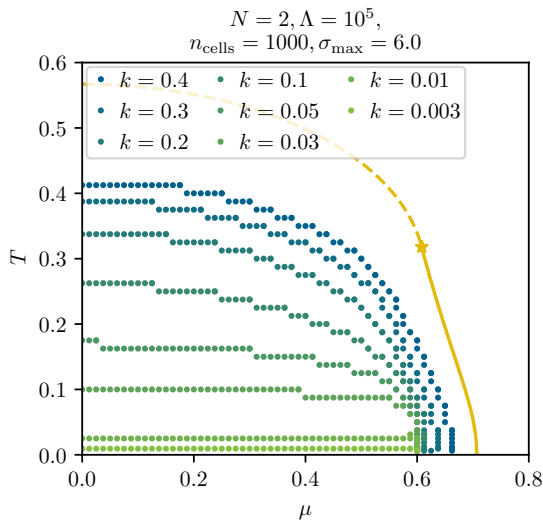


Figure 12.10: PT lines (equally colored dots) depending on the RG scale k for $N = 2$. For RG scales slightly larger or smaller than the values in the plot, there is exclusively a \mathbb{Z}_2 -symmetric phase for $T > 0$. Points are at (μ_i, T_j) with $\mu_i = 0.0125 \cdot i$, $i \in \{0, \dots, 65\}$ and $T_j = 0.0125 \cdot j$, $j \in \{1, \dots, 48\}$. For better resolution at small T , we included calculations at points with $T_j = 0.00625 \cdot j$, $j \in \{1, \dots, 4\}$ and the same μ_i as before. The yellow curve marks the $(N \rightarrow \infty)$ -PT line in the IR, see Fig. 11.1. From Ref. [4, Fig. 19].

there is always a $T_{\text{pc}} \neq 0$ for any N and that T_{pc} is always rather close to T_c even for small N . (Note the axis scaling.)

The phase diagram and absence of symmetry breaking in the IR

Having discussed various details of our findings separately, it is now time to have a look at the bigger picture. We therefore present the entire phase diagram (the PT line between phases where \mathbb{Z}_2 symmetry is spatially homogeneously broken/restored) as a function of the RG scale. For the sake of simplicity, we choose $N = 2$. Results for larger N are qualitatively similar. The output of this calculation is plotted in Fig. 12.10 at a discrete grid of points (μ, T) with $T > 0$. One observes that, as soon as the RG scale is approximately at model scales $k \approx h$, there is a region of non-vanishing condensate. For $N = 2$ this region is not identical to the $N \rightarrow \infty$ phase of broken \mathbb{Z}_2 symmetry, but approaches its shape. Especially for small temperature the difference of the PT for $N = 2$ at $k = 0.4$ and the infinite- N first-order PT is small. However, as soon as one integrates to smaller RG scales and includes more and more bosonic fluctuations the phase of broken \mathbb{Z}_2 symmetry shrinks and ultimately vanishes for $k \lesssim 0.003$.

Especially from the absence of symmetry breaking at small/vanishing μ and non-zero but small T we conclude that condensation is in general not possible in $d = 1$ at $T > 0$.

Towards the vacuum and zero temperature

For $T = 0$ and arbitrary μ the situation is of course not settled and it is unclear whether we can reliably conclude from Fig. 12.8 that there is still condensation.

If we, however, ignore the chemical potential for the moment and turn to the thermodynamic vacuum at $\mu = T = 0$, we can again use our flow equations in LPA and perform stable calculations. Hence, working with the well-defined $T \rightarrow 0$ and $\mu \rightarrow 0$ limit of Eq. (12.4) using Eqs. (B.14) and (B.16), *i.e.*,

$$\partial_t u(t, \sigma) = \frac{d}{d\sigma} \left[-\frac{1}{N} \frac{1}{2\pi} \frac{k^3}{\sqrt{k^2 + \partial_\sigma u(t, \sigma)}} + d_\gamma \frac{1}{2\pi} \frac{k^3}{\sqrt{k^2 + h^2(t) \sigma^2}} \right], \quad (12.14)$$

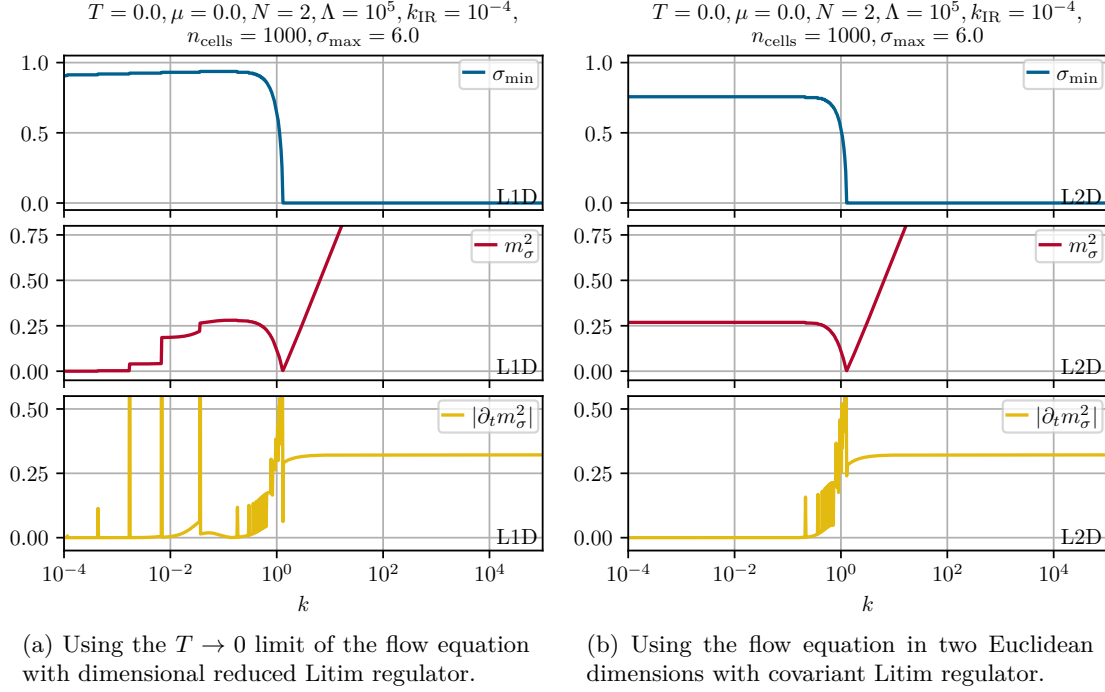


Figure 12.11: RG flow of the minimum σ_{\min} , the squared curvature mass m_σ^2 , and the relative change of the squared curvature mass $|\partial_t m_\sigma^2|$ at $\mu = T = 0$. From Ref. [4, Figs. 18 & 22].

we calculate the RG flows which are plotted in Fig. 12.11a. We observe condensation at any IR scales, which indicates that there is symmetry breaking at $T = 0$ in $d = 1$. The same is found for larger N . Arguing with the Silver-Blaze property, *cf.* Section 8.1.3, the same should hold true at least for small $\mu \neq 0$ (as long as μ is smaller than the pole mass of the fermion).

Nonetheless, we should be careful. As discussed earlier in this work, see Section 9.2.2, taking the $T \rightarrow 0$ and $\mu \rightarrow 0$ limit of Eq. (12.4) does not lead to the true Euclidean vacuum LPA flow equations, which respect Euclidean Poincaré invariance, because we are still working with one-dimensional Litim regulators.

Therefore, it is instructive to also study the RG flow from the vacuum flow equation with a covariant two-dimensional Litim regulator with identical UV initial condition (to work on lines of constant UV physics). This PDE reads

$$\partial_t u(t, \sigma) = \frac{d}{d\sigma} \left[-\frac{1}{N} \frac{1}{8\pi} \frac{k^4}{k^2 + \partial_\sigma u(t, \sigma)} + d_\gamma \frac{1}{8\pi} \frac{k^4}{k^2 + h^2(t) \sigma^2} \right] \quad (12.15)$$

and is solved with the same numerical techniques as before. The result is plotted in Fig. 12.11b and yields qualitatively similar results. There is symmetry breaking in the IR at zero temperature and, due to the Silver-Blaze property, we also expect symmetry breaking for small non-zero μ .

12.4. First steps towards the GN(Y) model beyond the LPA approximation

In this section we turn to calculations beyond LPA. However, we have to note that the analysis in this section is not as systematic as the previous one in LPA and all results are preliminary. Furthermore, the results are not cross-checked by my collaborators yet and they are also not published. The material is completely new. However, we have already made non-trivial checks: Firstly, the flow equations are cross-checked with existing literature (with flow equations of Yukawa-type

models in d -dimensional systems, see Appendix E.2). Secondly, the results are in general agreement with the expectations that were gained from our previous calculations and discussions.

The starting point of this section is again a brief comment on the UV initial conditions for the RG flow equations in LPA', Eqs. (12.4) and (12.5), without and with the flow equation of a running Yukawa coupling, Eq. (12.6). (In the following we use the notation “LPA'+ h ” for the truncation which incorporates the flow of the Yukawa coupling.) Furthermore, we have to explicitly state our choice of numerical parameters, which is done directly afterwards.

Then, we turn to the explicit results. To get a first impression of the outcome of the RG flows in the “improved” truncations, we compare RG flows at infinite N with $N = 2$ RG flows in the LPA, the LPA', and the LPA'+ h at small temperature and zero chemical potential.

Afterwards, we focus on the LPA' and the LPA'+ h truncation. As examples we present results for $N = 2$ and $N = 16$. We show that it is not possible to flow to the deep IR for every point in the μ - T -plane and that the breakdown of the RG flow is closely linked to the dynamics of the bosonic wave-function renormalization, which in turn strongly depends on N , μ , and the truncation. Therefore, we present plots of the bosonic wave-function renormalization and the Yukawa coupling and discuss insufficiencies of the truncations. Finally, we come to one of the main questions of Part II of this thesis: Do we find symmetry breaking at finite N in the IR? Despite the collapse of the RG flows in certain setups and the problems of the truncations, we think that our results still answer this question with “no”. This is elaborated in detail.

12.4.1. UV initial condition and numerical setup

Let us first briefly explain the formal setup.

UV initial condition

Concerning the UV initial condition for the RG flows, we use the following parameters:

The Yukawa coupling We still initialize the Yukawa coupling with $h(t = 0) = 1$, which means that all quantities are still measured in appropriate units of the UV Yukawa coupling. As we shall see from our calculations, it seems appropriate to consider a UV-cutoff independence of the Yukawa coupling in the UV and to initialize $h(t = 0) = 1$, independently from the explicit choice of Λ (as long as Λ is huge compared to $h(t = 0)$). The reason is that the Yukawa coupling does not evolve at very large RG scales and settles on a plateau. There, its value should be the same in all truncations and for finite and infinite N .

The UV cutoff This directly brings us to the UV cutoff Λ . Again, we use $\Lambda = 10^5$. There is no reason to assume that the inclusion of a dynamical bosonic wave-function renormalization or the Yukawa coupling requires a larger UV cutoff than for the LPA calculations in Section 12.3. Of course, explicit checks would be appropriate and are planned for the future. However, inspecting the explicit RG flows of this section, one finds not only a constant Yukawa coupling, but also vanishing bosonic anomalous dimension in the UV for several orders of magnitude in k , which supports the assumption that $\Lambda = 10^5$ is sufficiently large.

The UV potential For the UV potential at $\Lambda = 10^5$ we use Eq. (12.7) as for the RG flows in the LPA. The reasoning behind is the same as before and we refer to Section 12.3.1 for details.

The wave-function renormalization Moreover, the bosonic wave-function renormalization should, according to Eq. (10.4), be zero in the UV for $\Lambda \rightarrow \infty$. This is numerically not possible, which is directly seen from Eqs. (12.4) to (12.6), because of the $1/Z_\varphi(t)$ factors. Still, we are not starting our RG flow at $\Lambda \rightarrow \infty$, but with a finite $\Lambda = 10^5$ such that it is appropriate to assume a small non-vanishing $Z_\varphi(t = 0) \neq 0$. Indeed, it is actually possible to estimate this

value. Inspecting the flow equation for the wave-function renormalization (12.5), we find that the bosonic contribution is proportional to $[\partial_\sigma^2 u(t, 0)]^2$. However, this vanishes exactly in the UV above the cutoff Λ , because the initial condition for the effective potential, Eq. (12.7), is quadratic in σ . Therefore, we can simply use the purely fermionic contribution in Eq. (12.5) to analytically integrate from $\Lambda = \infty$, where the wave-function renormalization has to vanish, to $\Lambda = 10^5$, where it takes a very small value. (We assume that the Yukawa coupling is constant for these RG scales.) This is of course done in vacuum and the corresponding integrated flow equation reads

$$Z_\varphi(k = 10^5) - \cancel{Z_\varphi(k = \infty)} = \frac{d_\gamma}{2\pi} h^2 \int_{10^5}^{\infty} dk \frac{1}{4k^3} \approx 10^{-12}. \quad (12.16)$$

Unfortunately, this value is so small that we experienced that $\eta_\varphi = \partial_t \ln(Z_\varphi)$ is numerically not vanishing at very large Λ , which we trace back to spurious cancellations in the floating-point arithmetic.

We therefore decided to choose a larger (but still very small) value, namely $Z_\varphi(\Lambda = 10^5) = 10^{-5}$, as initial value for the bosonic wave-function renormalization, where we do not see these numerical artifacts. Of course, the question is whether we are now trading a numerical problem for a systematic error. To ensure that this choice does not completely spoil the results, we simply used $Z_\varphi(\Lambda = 10^5) = 10^{-5}$ and returned to the $N \rightarrow \infty$ flow equation. We integrated from $k = \Lambda = 10^5$ to $k = 0$ and compared the numerical result with this slightly wrong UV starting point against the exact results from Table 11.3a of Section 11.3. The differences are indeed marginal. We therefore consider $Z_\varphi(\Lambda = 10^5) = 10^{-5}$ to be a reliable UV initial condition. Of course, this issue should be studied more systematically in future works.

Numerical setup

Next, we comment on the numerical setup.

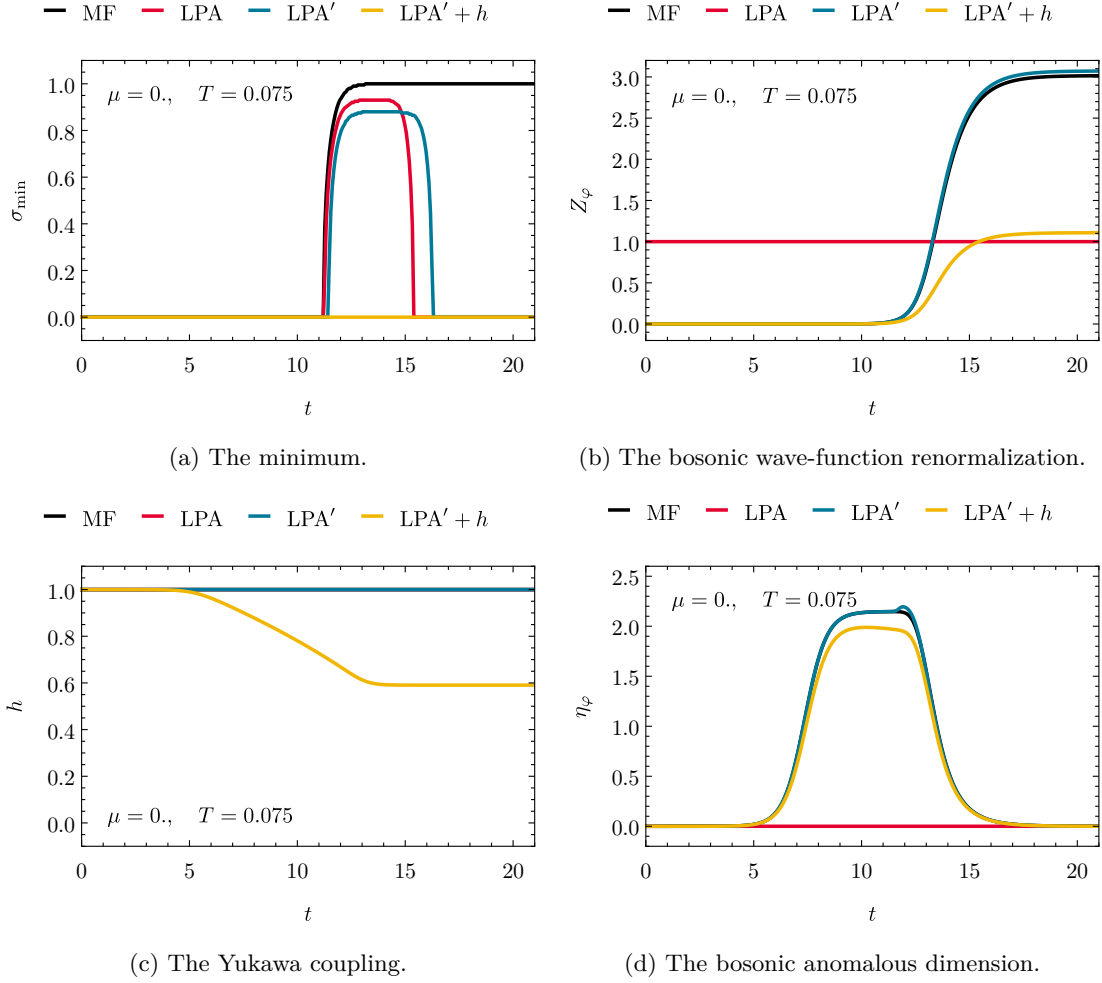
Numerical parameters for the FV-KT scheme Of course, one option would be to completely repeat the tests for an appropriate choice of $\Delta\sigma$ and σ_{\max} , which are the parameters needed for the FV discretization of Eq. (12.4). However, we think that this is not necessary for the following reason: The inclusion of the bosonic wave-function renormalization and of a dynamical Yukawa coupling does not enlarge the dynamical region in field space, which is given by the bare σ field. Hence, we simply use the values which we already considered trustworthy for calculations in the LPA. In particular, we use $\sigma_{\max} = 5$ and $n_{\text{cells}} = 1001$ and thereby fix

$$\Delta\sigma = \frac{\sigma_{\max}}{n_{\text{cells}} - 1} = 0.005. \quad (12.17)$$

As a quick check, we randomly altered these values by hand, *e.g.*, by enlarging σ_{\max} or n_{cells} , but we could not identify a notable change of the IR results. Only for too small choices of σ_{\max} and n_{cells} , which also produced significant deviations in the tests in Section 12.3.2, we observed discrepancies in the respective IR observables.

In addition, we still use the same artificial IR cutoff $k_{\text{IR}} = 10^{-4}$ as for the RG flows in LPA. Especially by inspecting the RG-time evolution of the bosonic anomalous dimension $\eta_\varphi(t) = \partial_t \ln(Z_\varphi(t))$, which is very sensitive to small changes of $Z_\varphi(t)$, as well as the Yukawa coupling $h(t)$, we are confident that this IR cutoff is sufficiently small to ensure that all observables are already “frozen” and all fluctuations are included in their values, *cf.* Figs. 12.12c and 12.12d.

Parameters for plots in the μ - T -plane As becomes clear within the next paragraphs, we have to mention somewhere how we obtained Figs. 12.13 to 12.15 and 12.17. This is here: The underlying data were generated by RG flows on a grid of points in the μ - T -plane with $\mu = 0.025 \cdot i$, $i \in \{0, 1, \dots, 48\}$ and $T = 0.05 \cdot j$, $j \in \{1, \dots, 14\}$. To obtain a better resolution at small T , we added points at the same values of μ with $T = 0.025 + 0.5 \cdot k$, $k \in \{1, \dots, 6\}$ as well as $T = 0.01$ and $T = 0.02$. This underlying grid and the different resolution at different T is visible in the figures.

Figure 12.12: RG flows of several quantities in different truncations for $N = 2$.

12.4.2. Results

Having briefly discussed the formal setup, we proceed with the presentation of the results of our calculations.

A comparison of different truncations at zero chemical potential

In order to gain a first insight into RG flows beyond the LPA, we fix $\mu = 0$ and $T = 0.075$ and compare RG flows in different truncations at constant $N = 2$. We first choose $\mu = 0$ to avoid complications due to the chemical potential and consider a small temperature, $T = 0.075$, to incorporate possible effects of condensation. The plots of the corresponding RG flows are presented in Fig. 12.12.

Here, the black curves correspond to the MF ($N \rightarrow \infty$) results from Chapter 11, while the red curves are the LPA results from Section 12.3. Of course, there is condensation with $\sigma_{\min}(k_{\text{IR}}) \simeq 1$ at $N \rightarrow \infty$ and also a non-trivial evolution of $Z_\varphi(t)$ towards the IR value, which is perfectly expected from Fig. 11.7 and agrees in the IR with the value from Eq. (F.67).

For the LPA, we find the formation of a condensate at almost identical RG time $t \approx 11$. Still, the condensate evaporates again in the IR at $t \approx 15.5$. The wave-function renormalization and Yukawa coupling do not evolve by definition.

As soon as we turn to the LPA' truncation (blue curves), where we still fix $h(t) = 1$, we find from Figs. 12.12b and 12.12d that the wave-function renormalization almost perfectly evolves along the $N \rightarrow \infty$ RG trajectory. There is only a small influence of the bosonic contribution to the RG flow of $Z_\varphi(t)$ at $t \approx 12$, shortly after the time of symmetry breaking, which is again at $t \approx 11$. This is best seen in Fig. 12.12d. Again, we find symmetry restoration in the IR.

Interestingly, if we further improve the truncation by including a running Yukawa coupling (yellow curves), we do no longer find precondensation, thus, the intermediate breaking of the \mathbb{Z}_2 symmetry by a non-trivial minimum of the potential, see Fig. 12.12a. The system stays in its symmetric state. (Below, we discuss that this is not always the case in LPA'+ h , but depends on N .) The drastic impact of a dynamical Yukawa coupling, which drops from $h(t=0) = 1$ to $h(t \rightarrow \infty) \approx 0.6$, is also seen in the flow of the wave-function renormalization, Fig. 12.12b, which strongly differs from the LPA' result.

In any case, we note that we do not find symmetry breaking in the IR for finite $N = 2$ at small T and zero μ , which makes condensation at non-zero μ and larger T highly unlikely from a thermodynamic perspective. How this changes for larger finite values of N is discussed below.

Before we expand the discussion to the entire μ - T -plane, let us also mention that Figs. 12.12c and 12.12d clearly demonstrate that our choices for Λ and k_{IR} seem to be appropriate. We observe plateaus in the UV and in the IR, which imply that

1. there is no non-trivial scaling of the Yukawa coupling in the UV.
2. $Z_\varphi(t=0) = 10^{-5}$ is sufficiently small and does not change until $\eta_\varphi(t)$ rises at $t \approx 5$.
3. we have integrated sufficiently deep into the IR by choosing $k_{\text{IR}} = 10^{-4}$, which is clearly seen from the “freezing” of the Yukawa coupling in LPA'+ h and $\eta_\varphi(t \rightarrow \infty) \simeq 0$.

Remark on the bosonic wave-function renormalization

One might have noticed already from the discussion of the UV initial condition as well as Figs. 12.12b and 12.12d that there is something intriguing about the bosonic loop contribution to the flow equation of $Z_\varphi(t)$, thus, Eq. (12.5). We already stated that the bosonic loop does not contribute to the RG flow in the UV, because the prefactor $[\partial_\sigma^2 u(t, 0)]^2$ vanishes for the quadratic initial condition. Either way, the vanishing of this coefficient does not seem to be restricted to the UV. Being the third σ -derivative of a function which is even in σ , namely $U(t, \sigma)$, it has to be odd about $\sigma = 0$ and should therefore be zero at $\sigma = 0$. Effectively, there is an exception: If $\partial_\sigma^3 U(t, \sigma)$ is discontinuous/non-analytic at $\sigma = 0$, *e.g.*, if it has a discontinuity, it may take non-zero values in terms of left and right limits, $\sigma \rightarrow 0^\pm$, similar to Fig. 5.1. Because it enters the flow equation quadratically anyhow, it is only the absolute value that matters.³

This certainly explains why the RG flow of the bosonic wave-function renormalization is basically independent of the bosonic loop contribution for almost all RG times and solely influenced by the flow of the Yukawa coupling. If also the Yukawa coupling is fixed to a constant, like in LPA', the flow of $Z_\varphi(t)$ therefore has to follow its $N \rightarrow \infty$ path, if the potential is smooth.

Returning to Figs. 12.12b and 12.12d, we find that the bosonic loop only sets in for some RG-time steps shortly after the formation of a non-trivial minimum in the RG flow in LPA'. We conclude that for these RG times the potential is no longer smooth – at least at $\sigma = 0$, while this gets smeared again by the diffusion for later RG times. In total, for this μ - T -point, the difference to MF is still small.

However, there may be more drastic consequences of this term and the dynamics of $Z_\varphi(t)$ in general, which can have significant impact on the RG flows. The reader should keep the following in mind while studying our results:

³Numerically, we simply use a forward FD stencil as a first approximation, which could be refined in future works.

1. If $[\partial_\sigma^2 u(t, 0)]^2$ gets huge or even diverges, which can easily be the case if $\partial_\sigma^3 U(t, \sigma)$ has a pole at $\sigma = 0$, cf. Eq. (11.23) and Section 6.2.4, there is even the possibility that the flow of $Z_\varphi(t)$ diverges and the numerical time-stepper breaks down, because it detects a stiff system. Here, only the extension of the truncation may help.
2. In Section 11.3, we learned that the wave-function renormalization takes negative values for huge domains of the μ - T -plane at $N \rightarrow \infty$, if it is evaluated at $\sigma = 0$, see Fig. 11.7. At least for LPA', where the Yukawa coupling cannot compensate any of this dynamics and the flow of $Z_\varphi(t)$ mostly follows the MF flow, it may therefore easily happen that we observe negative values of $Z_\varphi(t)$ during finite- N RG flows. It is highly unlikely that this is prevented by the bosonic loop contribution due to non-zero $[\partial_\sigma^2 u(t, 0)]^2$ for arbitrary μ and T . Especially large temperatures smoothen the potential drastically. Hence, non-analytic behavior at $\sigma = 0$ is not expected and the bosonic loop stays inactive.

From this we even expect the formation of negative $Z_\varphi(t)$ for huge regions of the phase diagram, especially for large $|\mu|$ and $T > 0$. Since there are no higher-order momentum-dependent terms which render the bosonic two-point function bounded from below, this leads to a breakdown of the RG flow. It is best seen within our truncation from the bosonic propagators in Eqs. (12.4) to (12.6), where a sign flip in $Z_\varphi(t)$ leads to an overshooting of the pole of the propagator. In the fluid-dynamical version of the RG flow equation for $u(t, \sigma)$ this corresponds to the generation of a negative diffusion coefficient. Anyway, within this work, we will simply observe a collapse of the RG flow for these points and the truncation effectively predicts its own insufficiency below a certain k -scale.

Lastly, we have to note that this behavior would change as soon as the flow equation for $Z_\varphi(t)$ was evaluated at non-zero σ or we considered a field-dependent bosonic wave-function renormalization. Both options cause other problems and we are not returning to this discussion here.

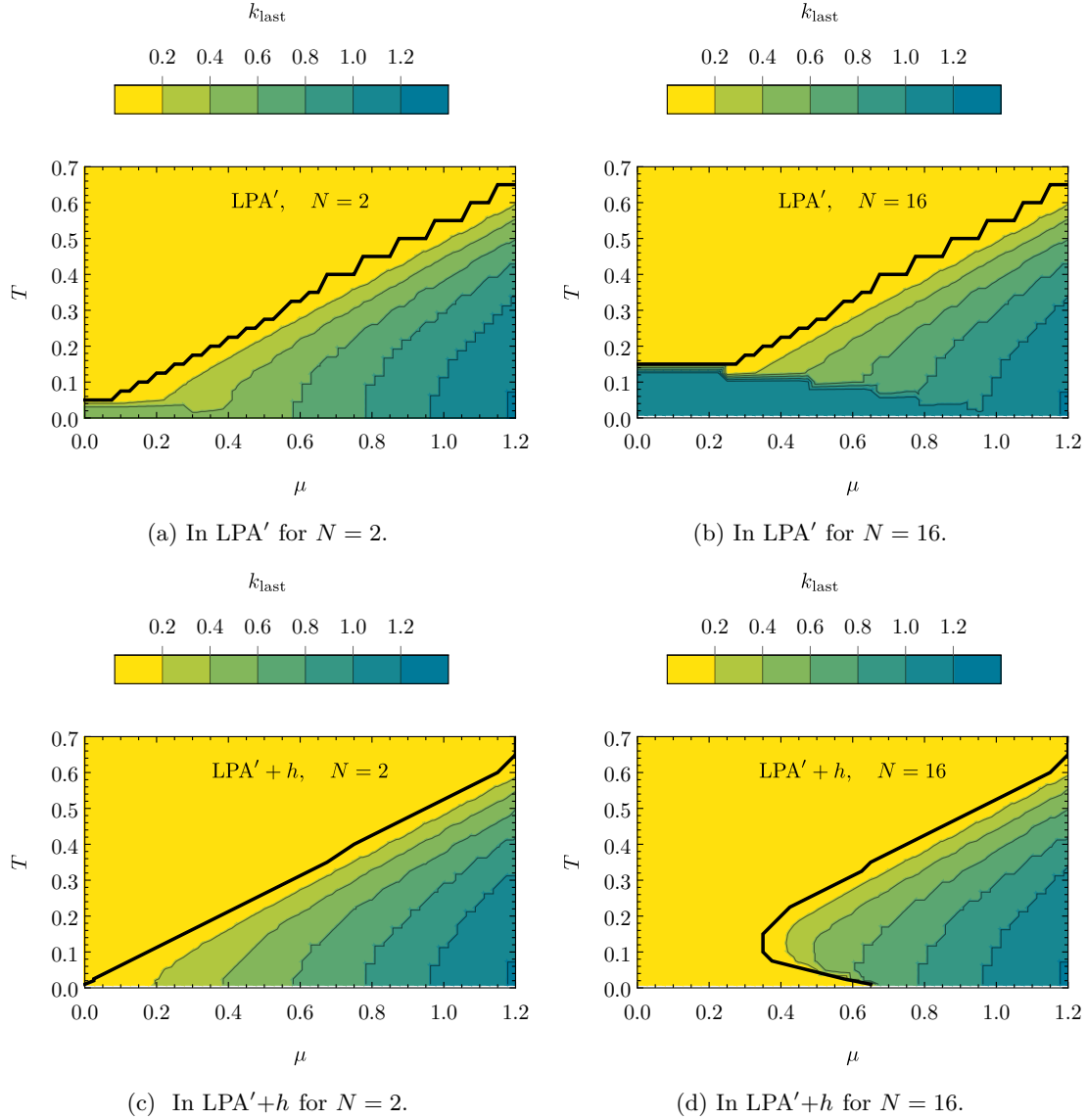
Breakdown of RG flows

Keeping this information in mind, we can turn to RG flows at other points in the μ - T -plane for finite N in LPA' without or with running Yukawa coupling. For the following discussion we use $N = 2$ and $N = 16$, but we also tested other values of N , which did not lead to qualitatively different results. Of course, more systematic tests are planned.

We start by presenting Fig. 12.13, where we introduce and plot the RG scale k_{last} . It is defined as the scale k , before the RG flow breaks down in our approximation, because either the wave-function renormalization turns negative or the time stepper cannot proceed integrating, because of a singularity in the flow equations. The latter is caused, as explained before, by a positive diverging $Z_\varphi(t)$ due to the bosonic loop contribution to its flow. What all four panels of Fig. 12.13 have in common is that integration up to the model scales, which are set by $h(t = 0)$, μ , and T is always possible. Furthermore, in all panels we observe that for small $|\mu|$ and sufficiently large T one can integrate arbitrarily far to the IR, here $k_{\text{last}} \simeq 10^{-4}$ (yellow). This region is separated from all points where the RG flow collapsed at larger k (green and blue) by the solid black line. For large $|\mu|$ and T the black solid line follows approximately the diagonal line from Fig. 11.7, which separates regions of negative and positive Z_φ at infinite N . This approximate separation along this line is expected from our previous discussions.

In addition, all panels have a region at large $|\mu|$ and very small T (blue) where the integration breaks down when $k \approx |\mu|$, while for increasing T integration to (slightly) smaller k is possible. This is in general agreement with the fact that the chemical potential causes an external shock in the system at $k \approx \mu$, which can only be handled by better truncations that can resolve the momentum structure of the bosons.

The main difference in the results from the four setups is seen at small $|\mu|$ and T . Here, it seems that the inclusion of a dynamical Yukawa coupling stabilizes the RG flow in the IR and prevents the bosonic wave-function renormalization from diverging. Furthermore, we find by comparing

Figure 12.13: Last valid RG time step k_{last} as a function of μ and T .

the LPA'+ h results for $N = 2$ and $N = 16$ that a larger finite number of fermions also seems to stabilize the flow and the integration to the IR is even possible at very small T and $|\mu| \neq 0$, where the wave-function renormalization would turn negative for $N \rightarrow \infty$.

It is therefore instructive to look at the explicit values of the wave-function renormalization and Yukawa coupling at the last valid RG step k_{last} , where the flow breaks down or reaches the IR cutoff k_{IR} , hence $Z_\varphi(k_{\text{last}})$ and $h(k_{\text{last}})$. These are shown in Figs. 12.14 and 12.15 for the same truncations and values of N as in Fig. 12.13. Obviously, Fig. 12.14 does not contain plots for the LPA', where $h(t) = 1$ for all RG scales.

From Figs. 12.15a and 12.15b one can deduce that the number of fermion species seems to have little influence on the wave-function renormalization in the region where one can integrate to the IR. The explicit values for $Z_\varphi(k_{\text{last}} = k_{\text{IR}})$ are almost identical there. There are deviations only for small T and small $|\mu|$. Here, loosely speaking, it seems as if more diffusion in field space, hence smaller N , helps to prevent the formation of non-analytic behavior in the potential at $\sigma = 0$.

Meanwhile, if we make the Yukawa coupling RG scale-dependent, things change significantly.

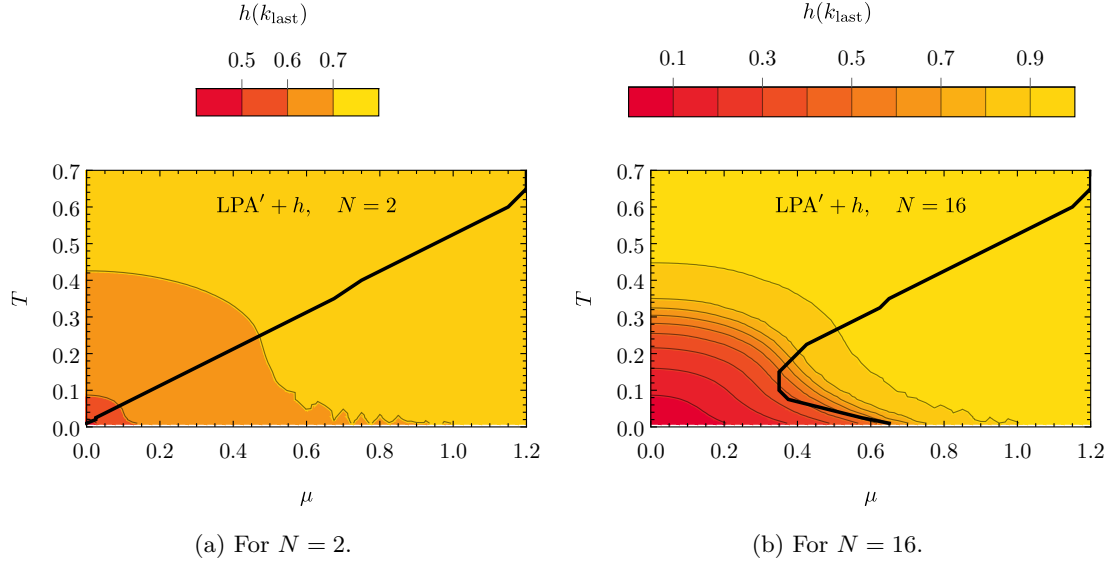


Figure 12.14: Yukawa coupling in the LPA'+h in the μ - T -plane for the last valid RG time step k_{last} .

From Figs. 12.15c and 12.15d we find that $Z_\varphi(k_{\text{last}} = k_{\text{IR}})$ strongly differs for $N = 2$ and $N = 16$ above the diagonal line. This has to be caused by the Yukawa coupling and indeed, we also observe significant differences for the values $h(k_{\text{last}} = k_{\text{IR}})$ itself, see Fig. 12.14. For $N = 16$ the Yukawa coupling falls off to much smaller values already at larger temperatures and is almost zero for a rather large region around $\mu = T = 0$. At this point, we do not have a conclusive explanation for this phenomenon, which is caused by the highly non-linear dynamics of the PDE-ODE system. In any case, we observe that already the variation of the $\frac{1}{N}$ -factors in the flow equations (12.4) to (12.6) can have strong impact on the dynamics.

Before we turn to the main question of symmetry breaking and restoration for these four setups, let us again analyze the RG flow for a single point in the μ - T -plane: In Section 12.3.3 and Ref. [4] we spent quite some time to discuss the dynamics which is caused by the chemical potential at very small temperatures in the RG flows. In Fig. 12.6, we observe remnants of the external shock that stems from μ even in RG flows of $u(t, \sigma)$ at finite N . Therefore, it is interesting to study whether these remnants are still visible in LPA'+h. In Fig. 12.16 we plot the full RG flow of $\eta_\varphi(t)$, $Z_\varphi(t)$, $h(t)$, and $\sigma_{\text{min}}(t)$ at $\mu = 0.4$ and $T = 0.01$ as well as the RG flow of $u(t, \sigma)$. For illustrative reasons, we restricted the plot of $u(t, \sigma)$ to selected values of k in the interesting region about $k \approx 1$.

First, we observe in both panels that there are some intermediate RG times where the \mathbb{Z}_2 symmetry is dynamically broken before the system ultimately turns into its symmetric phase. However, in comparison with the LPA flow at small T from Fig. 12.6c, we find that the absolute value of the condensate is much smaller in LPA'+h. Furthermore, the remnants of the chemical potential are no longer visible. It seems as if the running Yukawa coupling enables stronger diffusion, which effectively smears the non-analytic structures that are caused by μ . An argument which supports that this is not due to the running wave-function renormalization is found by returning to Fig. 12.15b. There, the point $\mu = 0.4$ and $T = 0.01$ corresponds to the regime of collapsing RG flows. Moreover, if we analyze Fig. 12.16a, we find from the dynamics of $\eta_\varphi(t)$ that $Z_\varphi(t)$ changes drastically when the \mathbb{Z}_2 symmetry gets restored and $\sigma_{\text{min}}(t)$ vanishes at $t \approx 12.5$. $Z_\varphi(t)$ almost drops to zero and the system barely prevents $Z_\varphi(t)$ from turning negative. Already at $\mu \approx 0.6$ the drastic decrease and a sign flip of $Z_\varphi(t)$ can no longer be prevented and RG flows are no longer stable, see Fig. 12.15d.

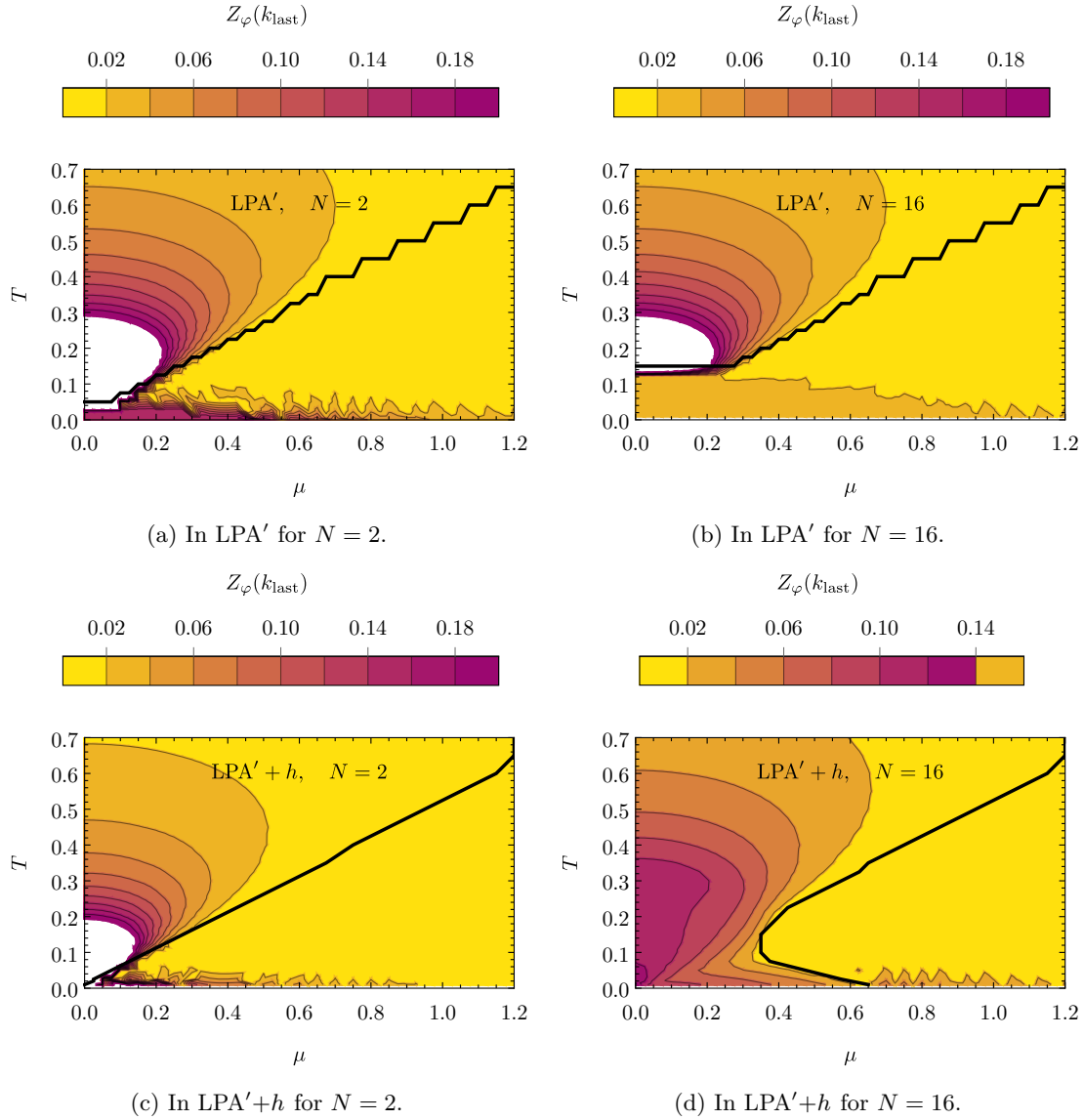


Figure 12.15: Bosonic wave-function renormalization in the LPA'(+ h) in the μ - T -plane for the last valid RG time step k_{last} .

Symmetry restoration

This brings us back to our central question of Part II of this thesis: “To break or not to break \mathbb{Z}_2 symmetry at finite N ?”

Similar to Fig. 12.10 from our calculations in LPA, we therefore consider figures which show the region of condensation in the μ - T -plane as a function of the RG scale k . In particular, we plot the PT line between regions where $\sigma_{\min}(k)$ is either zero or non-zero at a given k . Of course, these lines can only be shown for values of k where a condensate has formed already and where k is not below k_{last} from Fig. 12.13.

Therefore, as a very first result, there is no such figure for the $N = 2$ calculation in LPA'+ h , because we never observe a non-trivial minimum at any non-zero T and any μ , and we refrain from plotting an empty phase diagram.

However, for the other three cases of the above discussion, we find \mathbb{Z}_2 -symmetry breaking at

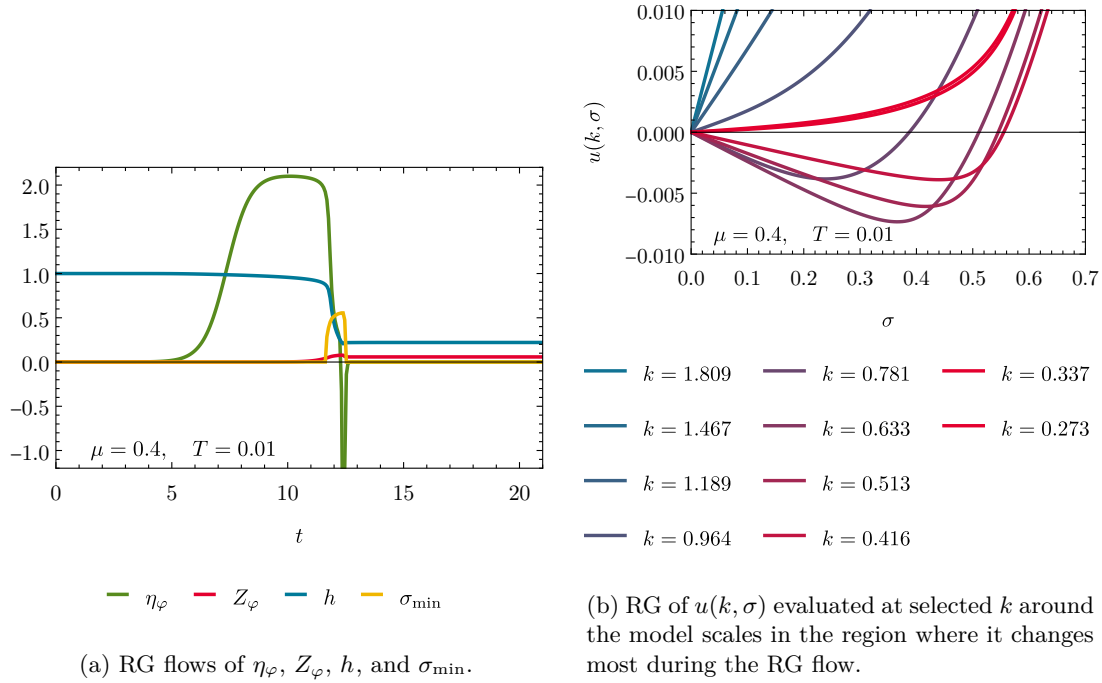


Figure 12.16: RG flow in LPA'+ h at $\mu = 0.4$ and $T = 0.01$ for $N = 16$.

some intermediate k -scales. The corresponding plots are shown in Fig. 12.17. As is visible from Figs. 12.17a and 12.17b, which are both in the LPA' truncation, the maximal region of condensation is larger for larger values of N , which was already seen in LPA, *cf.* Fig. 12.9. For all three scenarios, we clearly observe that the region of condensation drastically shrinks with decreasing k . From Fig. 12.17c, we can even clearly deduce that ultimately there is never condensation in the IR, because the condensate vanishes at each μ - T -point before k_{last} or k_{IR} is reached. Also Figs. 12.17a and 12.17b indicate that we should not expect condensation in the IR. Nevertheless, for small $|\mu|$ and small T the flow breaks down at some k_{last} , before the symmetry is restored. Hence, the LPA' is inconclusive, while the advanced LPA'+ h clearly shows an absence of \mathbb{Z}_2 -symmetry breaking for all $T > 0$ at finite N . We finally add that a systematic scaling analysis with N like in Fig. 12.7b is still missing, but planned for the future.

12.5. Conclusion and outlook

Here, we shall summarize the findings of this chapter and Part II of this thesis. Furthermore, we draw conclusions for promising follow-up projects and similar calculations in higher-dimensional models.

12.5.1. Summary and conclusion

Let us begin with a brief summary of the results in Part II of this thesis.

Summary

We started in Chapter 7 a more general discussion of the search for spatially inhomogeneous chiral condensation in the phase diagram of QCD at non-zero temperature and non-zero baryon chemical potential. It was explained that there are indications from various model studies, especially in MF, that spatially oscillating condensates are expected to form under certain thermodynamic conditions

12. The Gross-Neveu-Yukawa model at finite N

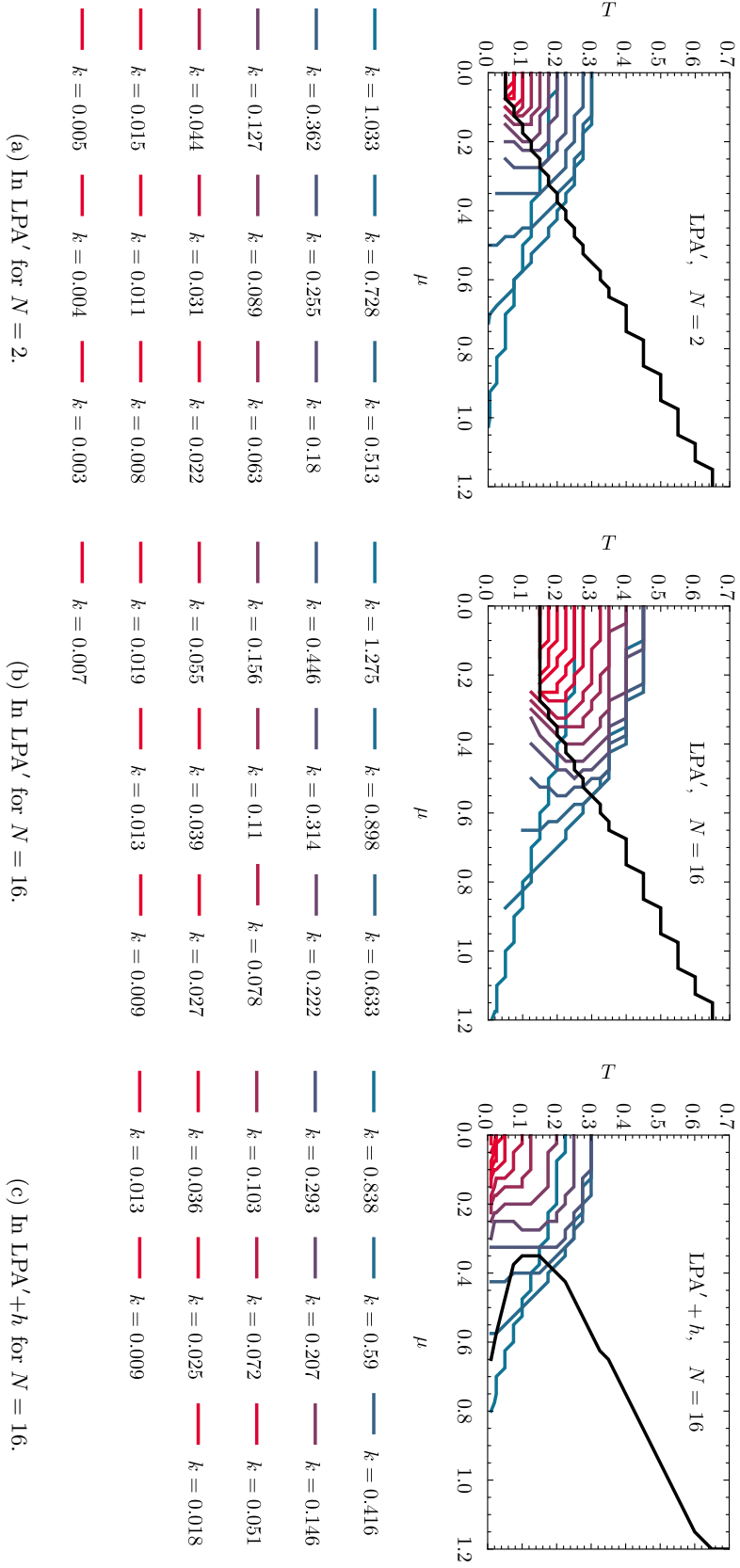


Figure 12.17: RG-scale dependence of the PT line between phases where \mathbb{Z}_2 is broken/restored for the minimum of the effective potential.

at non-zero densities. However, a detailed investigation of the stability of these condensates under the influence of bosonic fluctuations was missing (even in effective models for QCD) and planned as the original topic of my PhD.

Anyhow, we explained in Chapter 7 why we had to strongly reshape the project for several reasons and finally decided to first turn to the (numerical) method development of Part I of this thesis and afterwards to study some aspects of (inhomogeneous) condensation as well as symmetry restoration with a much simpler model – the GN model. Furthermore, in Section 7.1.3, we presented an updated list of research questions, which we planned to answer with our reshaped project, before the return to the problem of inhomogeneous condensation in $3 + 1$ dimensions under the influence of bosonic fluctuations seems feasible.

We proceeded in Chapter 7 with an extensive overview of the GN model and contextualized the model with other QFTs from high-energy particle physics and low-dimensional condensed-matter physics. The presently known phenomenology of the GN model, especially for $N \rightarrow \infty$, was discussed and possible scenarios and preliminary results for the phenomenology at finite N including bosonic fluctuations were outlined.

In Chapter 8, the GN model as well as its bosonized versions were formally introduced as QFTs in Minkowski and Euclidean spacetime. Discrete and continuous symmetries of the model were discussed. Furthermore, the formal description of the model at non-zero temperature and chemical potential was outlined and the consequences for the symmetries of the model were analyzed.

In Chapter 9 we started the actual investigations. We studied the GN model in its purely fermionic formulation and tried to analyze its phase structure. As a framework for our calculations we used the FRG formalism. Based on the possible divergence of the four-fermion coupling, we worked out regions in the μ - T -plane where \mathbb{Z}_2 -symmetry breaking is at least expected at some RG scales at finite and/or infinite N . Nevertheless, it was found that a purely fermionic study is inconclusive without better momentum resolution or the inclusion of the possible formation of bosonic condensates, which motivated us to turn to the partially bosonized versions of the GN model in the subsequent chapter. However, already the four-fermion coupling analysis showed significant differences between the regions of diverging four-fermion coupling at finite and infinite N . Furthermore, the calculations at finite N revealed possible solution strategies for the long-standing problem of the correct evaluation of external fermion legs of Feynman diagrams at non-zero μ and non-zero T , which usually produce complex contributions to the β -functions.

Chapter 10 served as an introduction to our FRG setup to study the partially bosonized version of the GN model – the bGN and GNY model. The truncation, the UV initial condition, and the flow equations for the corresponding RG flows were discussed. Furthermore, we commented on symmetry breaking and restoration during RG flows and the indirect detection of spatially inhomogeneous condensation. In the second half of this chapter, we discussed the FRG flow equations in their fluid-dynamical reformulation and recapitulated the appropriate numerical solution strategy for the PDE-ODE system. A special focus was put on the flow equation for the effective local bosonic potential, its bosonic-diffusive and fermionic-source-sink contributions as well as the role of the chemical potential as an external shock in the system. We ended the chapter by taking the $N \rightarrow \infty$ limit of the RG flows equations, which marked the starting point for Chapter 11.

In Chapter 11, well-known results for the phase structure of the GN model at $N \rightarrow \infty$ were (re)derived from the RG flow equations. First, ignoring the bosonic momentum structure, we focused on the RG flow equation for the effective potential. The renormalization prescription from the FRG formalism (using a dimensionally reduced Litim regulator) was compared against standard MF sharp-cutoff regularization. During the renormalization process we constructed the UV-cutoff dependence of the UV potential, which belongs to our FRG flow equation and which was later on also taken as the initial condition for finite- N calculations. After renormalization, the IR potential at $N \rightarrow \infty$ was used to reproduce the well-known result for the GN phase diagram under the assumption of spatially homogeneous condensation. In addition, we presented various

thermodynamic observables as functions of μ and T and cross-checked our setup with the existing literature.

In the second half of this chapter, we turned to the bosonic momentum structure and analyzed the bosonic two-point function and the bosonic wave-function renormalization in the μ - T -plane. This was part of tests of the so-called stability analysis of the spatially homogeneous ground state, which can be used to detect regions in the phase diagram where spatially inhomogeneous condensation is favored over the homogeneous condensation. As a proof of concept study, we benchmarked this stability analysis with analytically known solutions for crystalline-like ground states and could perfectly recover the correct second-order PT. Furthermore, by examining the infinite- N results for the bosonic momentum structure, we anticipated challenges of certain truncations in finite- N FRG calculations in the GNY model and already speculated about possible solution strategies.

The present chapter, Chapter 12, was dedicated to the actual central research question of presence/absence of condensation phenomena in the GN model at finite N and the decent description of condensation/vaporization in QFTs at non-zero μ and non-zero T . The chapter was split into two main parts.

The first part dealt with results from the LPA for the GNY model. The UV initial condition and an appropriate UV cutoff were chosen to ensure RG consistency. Subsequently, numerical tests for the parameters of the FV discretization of the flow equation of the effective potential were performed. In the section with the actual results, we started with qualitative discussions of explicit RG flows and analyzed symmetry breaking and restoration during the flows. Especially for small T and non-zero μ , we compared RG flows at infinite N with RG flows at finite N and elaborated on the role of the chemical potential. Here, we also commented on consequences for higher-dimensional model calculations in the LPA. Finally, we quantified in detail that the \mathbb{Z}_2 -symmetry is always restored at non-zero T due to bosonic quantum fluctuations in the deep IR, while there is still condensation for some intermediate RG scales in some regions of the phase diagram – so-called precondensation.

Mainly because of the inconsistent choice of the wave-function renormalization in the UV in the LPA, which was initialized at a too large non-zero value and kept constant during the RG flow, we turned to improved truncations in the second half of the chapter. Explicitly, we included a field-independent but dynamical wave-function renormalization. On top of that, also calculations that comprise a dynamical and field-independent Yukawa coupling were performed. Here, the UV initial condition matches exactly the GN model. Again, we started our discussion of the respective results with a qualitative analysis of explicit RG flows in these truncations and afterwards turned to the entire phase structure. The overall result is qualitative identical to the findings in the LPA: \mathbb{Z}_2 symmetry breaking is only found for some N at intermediate RG scales, while at physical IR scales the GN model is in a gas-like state for all $T > 0$.

As anticipated from our discussion of the bosonic momentum structure at $N \rightarrow \infty$, however, we experienced large stability problems of the RG flows beyond the LPA in the deep IR for some regions of the phase diagram. In particular, at small T and moderate and large $|\mu|$ the bosonic wave-function renormalization either diverged or turned negative, which both lead to a collapse of the RG flows. Both effects could be identified as insufficiencies of the truncation scheme and most likely a bad approximation of the two-point function in momentum space. Despite these issues, we consider our finite- N calculations as trustworthy for all μ - T -points where the RG flow did not collapse.

Answers to the research questions raised in Section 7.1.3

Concerning our main research questions of Section 7.1.3 we draw the following conclusions for the respective questions.

Answers to the phenomenological questions

1. Of course, we cannot draw a general conclusion for all systems in a single spatial dimension

from our calculations. Nevertheless, we believe that the calculations for the GN model demonstrated that it is highly unlikely that realistic systems beyond crude approximations exhibit solid, crystalline, or more generally phases with long-range order at non-zero T . As soon as attractive fermion interactions start to form bosonic bound states, their fluctuations seem to ultimately vaporize any type of condensate.

2. A possible explanation why remnants or signals of condensation are still detected in some calculations at finite N and non-zero T , *e.g.*, in lattice Monte Carlo (MC) simulations, might be traced back to an intriguing issue: From the FRG calculations for the GN problem (in all truncations), it seems as if the integration of the GN model is a challenging multi-scale problem. It required to calculate RG flows over more than six orders of magnitude from the UV to the IR to ensure RG consistency as well as the “freezing” of observables in the IR and the detection of symmetry restoration in the IR. It might simply be the case that it is impossible to resolve this range of energy scales in a lattice MC simulation on a finite grid, such that central aspects of the system are destroyed by the lattice regularization.
3. We found that there is always a strong quantitative dependence of the IR results on the truncation scheme. Ignoring the bosonic fluctuations completely by exclusively working in the purely fermionic framework or by suppressing fluctuations with the $N \rightarrow \infty$ limit leads to inconclusive or even wrong qualitative results with different phenomenology. However, as soon as bosonic fluctuations are included, we find that at least the qualitative absence of symmetry breaking in the IR is very robust against the improvement of the truncation.
4. For non-zero T the GN model at finite N is always in a gas-like state without long-range order. At vanishing temperature there is still the option for condensation and \mathbb{Z}_2 -symmetry breaking as well as a quantum phase transition at some critical μ , see also Ref. [382].
5. We found that the UV Yukawa coupling can be used to set the scale of the model. The accessible values of T and $|\mu|$ are basically smaller than one in units of this reference scale. As long as the RG scale is above the reference scale set by the Yukawa coupling, the RG flow is completely dominated by attractive interactions from the fermion fluctuations in all truncations. Only after symmetry breaking at these model scales, the bosonic fluctuations become relevant and start dominating the RG flow of the effective potential. Still, it is required to integrate several orders of magnitude below the reference scale to include all bosonic fluctuations and restore the symmetry. An exception is the bosonic wave-function renormalization, which is mainly driven by the fermion fluctuations even at small k as long as the effective potential is smooth.
6. The qualitative difference between the GNY and GN or bGN model is small w.r.t. the question of symmetry breaking and restoration. However, the quantitative difference is significant. The improvement of the truncation drastically changes the shape of the IR potential and IR physics differs quantitatively.

Answers to the technical questions

1. Using the bosonic two-point function for a stability analysis of the spatially homogeneous ground state is a perfect tool to detect a second-order PT between a symmetric phase and a crystalline-like phase. However, starting from a phase with spatially homogeneous condensation completely spoils the method. For details, we refer to Ref. [5].
2. In the fluid-dynamical description of the RG flow equation of the effective potential, we have to work on the level of its field-space derivative. Hence, symmetry breaking is realized in terms of a non-trivial zero crossing. This is caused by a source-sink-like term in the PDE, which stems from the fermion loop. However, in contrast to calculations at $N \rightarrow \infty$, where non-trivial global/local minima violate the convexity of the effective potential, the bosonic fluctuations ensure convexity in the IR by highly non-linear diffusion in the PDE, which leads

to a flat region in the potential. In the case of symmetry restoration the convex potential simply turns strictly convex. For the truncations which are considered in the work, the chemical potential always enters the PDE in terms of an external shock at late times.

3. The formal necessities for a trustworthy numerical description in field space were discussed in Part I.
4. Especially from the analysis of the bosonic two-point function at $N \rightarrow \infty$ for non-zero μ as well as the calculations in LPA' and LPA'+ h , we draw the conclusion that calculations at large chemical potentials and low temperatures do not only call for stable discretization schemes in field space, but also for a good resolution in momentum space. Here, the inclusion of the standard kinetic term for the bosons with scale-dependent wave-function renormalization turned out as insufficient. We believe that already the inclusion of a quartic term in the bosonic two-point function could stabilize the flows significantly and yields a decent approximation.

Answers to the General questions

1. The technical description of low-dimensional strongly interacting systems and their higher-dimensional counterparts is very similar for most functional methods. Hence, if we for example observe conceptual problems in flow equations in the LPA with dimensionally reduced Litim regulators at zero temperature and high chemical potentials in $1+1$ dimensions, we should not expect that these issues miraculously disappear by simply increasing the dimensions. The same is the case for the stability analysis. Nevertheless, explicit and detailed benchmark tests for a simple low-dimensional model were not done so far. In general, we think that it is oftentimes advisable to use low-dimensional systems to test and benchmark novel techniques, but also to get a first impression of the possible dynamics and challenges that may occur. We therefore consider our $(1+1)$ -dimensional calculations as a great benefit for future calculations in higher-dimensional QFTs.
2. From the projects which are summarized in this thesis, we conclude that the first requirement for studying the influence of bosonic fluctuations on spatially inhomogeneous condensation is an absolutely reliable and stable approach to spatially homogeneous condensation. Within FRG model studies this certainly requires a robust discretization of field space. However, especially at large $|\mu|$ also a profound resolution of momentum space seems to be important. As soon as a reliable and stable flow towards the deep IR is guaranteed for all regions of interest in the μ - T -plane, a stability analysis via the bosonic two-point function can be performed on top of the spatially homogeneous solution – exclusively in the formerly symmetric phase.
3. As we have seen in Chapter 9 from the one-loop β -function, already a rather simple approximation can lead to good estimates of the dynamics and the regions of interest in a phase diagram. The same was the case for the $N \rightarrow \infty$ results for the bosonic two-point function and wave-function renormalization from Section 11.3, which helped in understanding the upcoming challenges of truncations beyond the LPA at finite N . Also the rather simple LPA truncation sufficed to qualitatively capture the dynamics of symmetry restoration. We conclude that the successive improvement of approximations as well as the repeated reinsurance of the consistency of these approximations in certain limits is essential for understanding the relevant requirements of an adequate mathematical description of a system.
4. The appearance of imaginary contributions in β -functions (RG flow equations) of fermionic vertex functions at non-zero μ and non-zero T seems to be a robust feature in relativistic QFTs. Also in this work, we were not able to develop a conclusive solution for this issue. In particular, for the RG flow equation of the Yukawa coupling, we simply followed other works [548, 66, 549, 275] and ignored the imaginary contribution with reference to the symmetry of the theory under the exchange $\mu \leftrightarrow -\mu$. However, in the much simpler flow equation of the

four-fermion coupling in Chapter 9, we found that, even though the imaginary contribution is in general non-zero, it vanishes in the IR after integration over all RG scales. This may also happen for systems of more than one coupling: During the RG flow the couplings could possibly gain nonphysical complex contributions and interference effects might show up, while in the IR only the real parts of the couplings survive.

12.5.2. Generalizations and applications

We end this thesis with brief comments on possible generalizations and applications of the work that was presented in Part II. Here, we just focus on a small selection of direct generalizations and possible follow-up projects.

Enlarging the basis of four-fermion couplings A straightforward and highly interesting generalization of Chapter 9 would be the extension of the basis of four-Fermion couplings. Working along the lines of Refs. [348, 350, 351], one could set up a Fierz-complete basis of four-Fermion couplings, but still initialize the RG flow exclusively with a non-vanishing scalar channel on the GN trajectory. Couplings of other channels would start at zero, but could be dynamically generated. In this way one could identify the important and unimportant channels in all regions of the phase diagram. In contrast to the studies in $3+1$ dimensions, there is a valid UV limit on the purely fermionic level and the system of couplings is renormalizable. Furthermore, the complete basis of couplings is much smaller in $1+1$ dimensions. This might help in better understanding mechanisms like fermion-fermion pairing at high densities. In addition, this setup could be used to systematically return to the question of suitable regulators, which was already addressed by Refs. [348, 350, 351]. An interesting problem which could also be addressed in such a framework is the search for the correct evaluation of external fermion lines and the handling of complex contributions in the RG flows.

Improving truncations in the FRG approach to the GNY model In the spirit of this chapter, one could also continue to improve the truncation for the GNY model in the partially bosonized framework. A first option could be to study the field dependence of the Yukawa coupling in the GNY model in the fluid-dynamical framework similarly to Ref. [101]. This could help to better understand the necessities for the general handling of field-dependent couplings in the FRG. Another option is to improve the resolution in momentum space by the inclusion of higher-order derivative terms, like in Refs. [65, 271, 272, 63, 69, 70, 71], or by even feeding back the full momentum structure of the two-point function. It would be interesting to see whether this fixes the problem of collapsing RG flows due to negative wave-function renormalizations at large chemical potentials. A solution of this problem is also of utmost importance for FRG calculations in higher-dimensional systems of dense matter.

Of course, there are also completely different ways of further improving the truncation, *e.g.*, by combining the four-fermion approach with the partial bosonization.

Regulator dependence As mentioned several times in this thesis, results from truncated FRG calculations are in general regulator-dependent [165, 602, 533, 167]. Naturally, one tries to minimize this dependence, but it is oftentimes extremely hard to quantify this effect. In addition, exchanging the regulator is not necessarily a simple task. Usually, as it is also the case for this work, the choice of the regulator is therefore based on an educated guess. However, because of its simplicity the GNY model at finite and infinite N could be the perfect playground to test different regulators and their impact on the IR physics. Because the GN model shares a lot of features with higher-dimensional models, results from these regulator tests could most certainly be transferred to these systems, which is especially important for calculations at non-zero μ .

GN model in a finite box and/or a spatial lattice In the introduction we discussed that there are several lattice-MC studies for the bGN action. In fact, there is an option to directly

compare these lattice-MC simulations with truncated FRG calculations. In order to reduce the differences between both approaches, a simple option is to study the GN model with the FRG in a finite (periodic) spatial (one-dimensional) box. This spatial domain could be further discretized with a finite number of lattice sites. Thus, without taking the infinite-volume or the continuum limit the lattice MC and the FRG should produce identical results up to the FRG truncation error. Calculations of this type could also be used to search for the reasons why some of the lattice-MC studies identified clear signals of (inhomogeneous) condensation at finite N . Work in this direction is already in progress [603].

Application of the stability analysis to other models The stability analysis of the spatially homogeneous ground state in the infinite- N GN model was initially presented as a pure benchmark test in Ref. [5]. We have stated several times that it was already applied to higher-dimensional models, which are not integrable and lack analytical solutions. Now, after discussing its strengths and weaknesses we clearly advertise and promote its use in arbitrary models with arbitrary methods and arbitrary truncations. We strongly believe that it is an extremely robust tool, as long as the expansion point is in the symmetric phase. Hence, a profound knowledge about regions without any type of condensation is absolutely vital.

Higher-dimensional applications It is obvious that we are also at a point where we can safely use all the insights from the studies of this thesis to return to FRG computations in higher-dimensional QFTs – especially low-energy effective models for QCD at small and moderate $|\mu|$ and T . A particular project could be to start answering the initial research question of this PhD thesis.

Part III

Appendix

Appendix A

Formulary

Abstract We present definitions, formulae, mathematical identities *etc.*, which are used throughout this thesis. This comprises some general definitions, some quantities which are directly linked to two-dimensional spacetime, some relations for Fourier transformations, and a formulary for some transcendental functions.

Disclosure This appendix only presents supplemental material, which is supposed to simplify working with the main text and the other appendices, and there is no original content. It is simply supposed to make the permanent lookup of formulae *etc.* in integral tables like Ref. [242] redundant. In any case, we cite the corresponding reference works.

Only the compilation of the material is original to the author.

A.1. Some definitions

In the following, we present some general and rather unrelated definitions.

A.1.1. Pauli matrices

The Pauli matrices are

$$\sigma_0 \equiv \begin{pmatrix} 1 & 0 \\ 0 & 1 \end{pmatrix}, \quad \sigma_1 \equiv \begin{pmatrix} 0 & 1 \\ 1 & 0 \end{pmatrix}, \quad \sigma_2 \equiv \begin{pmatrix} 0 & -i \\ i & 0 \end{pmatrix}, \quad \sigma_3 \equiv \begin{pmatrix} 1 & 0 \\ 0 & -1 \end{pmatrix}. \quad (\text{A.1})$$

A.1.2. Dirac delta distribution

A representation of the Dirac delta distribution, which is used in this work, is

$$\lim_{a \rightarrow \infty} \frac{a}{2 \cosh^2(ax)} = \delta(x), \quad \int_{-\infty}^{\infty} dx \frac{a}{2 \cosh^2(ax)} = 1. \quad (\text{A.2})$$

We also need the following identity for the Dirac delta distribution,

$$\delta(f(x)) = \sum_i \frac{1}{|f'(x_i)|} \delta(x - x_i), \quad (\text{A.3})$$

where x_i are the roots of $f(x)$.

Table A.1: Volumes of $(d - 1)$ -dimensional spheres and FRG loop prefactors.

d	S^{d-1}	Ω_d	A_d
1	S^0	2	$\frac{1}{\pi}$
2	S^1	2π	$\frac{1}{4\pi}$
3	S^2	4π	$\frac{1}{6\pi^2}$
4	S^3	$2\pi^2$	$\frac{1}{32\pi^2}$

A.1.3. Kronecker delta

The Kronecker delta symbol is defined by

$$\delta^{ab} \equiv \delta_{ab} \equiv \delta_a^b \equiv \begin{cases} 1, & \text{if } a = b, \\ 0, & \text{if } a \neq b. \end{cases} \quad (\text{A.4})$$

where $a, b \in \mathcal{I}$ and \mathcal{I} is a set of indices which are usually chosen as a subset of the natural numbers (including zero), $\mathcal{I} \subseteq \mathbb{N}_0$.

A.1.4. Volume integrals

For various calculations in this work, it is required to evaluate d -dimensional volume integrals. If there is spherical symmetry of the integrand, we usually use

$$\int_{-\infty}^{\infty} \frac{d^d p}{(2\pi)^d} f(|\vec{p}|) = \frac{\Omega_d}{(2\pi)^d} \int_0^{\infty} dp p^{d-1} f(p) = A_d d \int_0^{\infty} dp p^{d-1} f(p), \quad (\text{A.5})$$

where we define the volume of the $(d - 1)$ -dimensional sphere S^{d-1} by

$$\Omega_d \equiv \frac{2\pi^{\frac{d}{2}}}{\Gamma(\frac{d}{2})}. \quad (\text{A.6})$$

For convenience, we also define

$$A_d \equiv \frac{\Omega_d}{d(2\pi)^d} \quad (\text{A.7})$$

for FRG calculations. Explicit values for Eqs. (A.6) and (A.7) for some d are listed in Table A.1.

A.2. Two-dimensional spacetime

Here, we present quantities which are required to describe QFTs in two-dimensional spacetime.

A.2.1. Minkowski metric, Cartesian coordinates, and the Levi-Civita pseudo-tensor

The two-dimensional Minkowski spacetime is defined by the line element and metric,

$$ds^2 \equiv \eta_{\mu\nu} dx^\mu dx^\nu \equiv -d(x^1)^2 + d(x^2)^2 \equiv -dx^2 + dt^2, \quad (\eta_{\mu\nu}) = (\eta^{\mu\nu}) = \begin{pmatrix} -1 & 0 \\ 0 & 1 \end{pmatrix}, \quad (\text{A.8})$$

where we use $x^d = x^1 = x \in (-\infty, \infty)$ for the spatial coordinate and $x^{d+1} = x^2 = t \in (-\infty, \infty)$ for the temporal coordinate.

The two-dimensional Levi-Civita pseudo-tensor is

$$\varepsilon^{\mu\nu} \equiv \begin{cases} +1, & \text{for } \mu = 1, \nu = 2, \\ -1, & \text{for } \mu = 2, \nu = 1, \\ 0, & \text{otherwise.} \end{cases} \quad (\text{A.9})$$

A.2.2. Clifford algebra and gamma matrices in Weyl basis

The two dimensional Clifford algebra is

$$\{\gamma^\mu, \gamma^\nu\}_+ = 2\eta^{\mu\nu} \mathbf{1}, \quad \mu, \nu \in \{1, 2\}, \quad (\text{A.10})$$

where $\eta^{\mu\nu}$ are the components of the metric (A.8). We choose a Weyl basis for the two gamma matrices, thus,

$$\gamma^d = \gamma^1 = i\sigma_2 = \begin{pmatrix} 0 & 1 \\ -1 & 0 \end{pmatrix}, \quad \gamma^{d+1} = \gamma^2 = \sigma_1 = \begin{pmatrix} 0 & 1 \\ 1 & 0 \end{pmatrix}. \quad (\text{A.11})$$

This basis has the advantage that the temporal gamma matrix fulfills

$$(\gamma^{d+1})^\dagger = (\gamma^{d+1})^* = (\gamma^{d+1})^T = \gamma^{d+1}. \quad (\text{A.12})$$

The chiral gamma matrix, which is the two-dimensional equivalent of γ^5 from four-dimensional spacetime, is

$$\gamma^{\text{ch}} = \frac{1}{2} \varepsilon_{\mu\nu} \gamma^\mu \gamma^\nu = -\gamma^1 \gamma^{d+1} = -\gamma^1 \gamma^2 = -\sigma_3 = \begin{pmatrix} -1 & 0 \\ 0 & 1 \end{pmatrix}. \quad (\text{A.13})$$

It fulfills the anti-commutation relation

$$\{\gamma^\mu, \gamma^{\text{ch}}\}_+ = 0. \quad (\text{A.14})$$

The matrices $\mathbf{1}$, γ^1 , γ^2 , and γ^{ch} form a complete basis of the two-dimensional Dirac space and can be used for the construction of bilinear covariants [19, 24].

The chiral gamma matrix is used to define left- and right-handed chiral projectors,

$$\gamma_{\text{L}} = \frac{1}{2}(\mathbf{1} - \gamma^{\text{ch}}) = \begin{pmatrix} 1 & 0 \\ 0 & 0 \end{pmatrix}, \quad \gamma_{\text{R}} = \frac{1}{2}(\mathbf{1} + \gamma^{\text{ch}}) = \begin{pmatrix} 0 & 0 \\ 0 & 1 \end{pmatrix}. \quad (\text{A.15})$$

As projectors, they have the following properties,

$$\gamma_{\text{L}} \gamma_{\text{R}} = \gamma_{\text{R}} \gamma_{\text{L}} = 0, \quad (\text{orthogonality}), \quad (\text{A.16})$$

$$\gamma_{\text{L}} + \gamma_{\text{R}} = \mathbf{1}, \quad (\text{completeness}), \quad (\text{A.17})$$

$$\gamma_{\text{L}} \gamma_{\text{L}} = \gamma_{\text{L}}, \quad \gamma_{\text{R}} \gamma_{\text{R}} = \gamma_{\text{R}}, \quad (\text{idempotency}). \quad (\text{A.18})$$

Furthermore, there is the useful relation

$$\gamma_{\text{L}} \gamma^\mu = \gamma^\mu \gamma_{\text{R}}. \quad (\text{A.19})$$

Lastly, we present the explicit expressions for the charge-conjugation (C) and time-reversal (T) operators in our basis,

$$C \gamma^\mu C^{-1} = -(\gamma^\mu)^T, \quad C = \gamma^1 = i\sigma_2, \quad C = C^* = -C^{-1} = -C^\dagger = -C^T, \quad (\text{A.20})$$

$$T \gamma^\mu T^{-1} = (\gamma^\mu)^T, \quad T = \gamma^2 = \sigma_1, \quad T = T^* = T^{-1} = T^\dagger = T^T. \quad (\text{A.21})$$

A.2.3. Euclidean gamma matrices in Weyl basis

According to Eq. (8.7), the corresponding gamma matrices in two-dimensional Euclidean spacetime in the Weyl basis are

$$\gamma^1 = -\sigma_2 = \begin{pmatrix} 0 & i \\ -i & 0 \end{pmatrix}, \quad \gamma^2 = \sigma_1 = \begin{pmatrix} 0 & 1 \\ 1 & 0 \end{pmatrix}, \quad \gamma^{\text{ch}} = i\gamma^1 \gamma^2 = -\sigma_3 = \begin{pmatrix} -1 & 0 \\ 0 & 1 \end{pmatrix}. \quad (\text{A.22})$$

A.3. Fourier transformation

In this thesis we use the following conventions for Fourier transformations in $(d + 1)$ -dimensional Euclidean spacetime with a single compactified dimension, hence, cylindrical geometry.

For all bosonic fields this reads

$$\varphi(\tau, \vec{x}) = T \sum_{n=-\infty}^{\infty} \int_{-\infty}^{\infty} \frac{d^d p}{(2\pi)^d} \tilde{\varphi}(\omega_n, \vec{p}) e^{+i(\omega_n \tau + \vec{p} \cdot \vec{x})}, \quad (\text{A.23})$$

$$\tilde{\varphi}(\omega_n, \vec{p}) = \int_0^{\frac{1}{T}} d\tau \int_{-\infty}^{\infty} d^d x \varphi(\tau, \vec{x}) e^{-i(\omega_n \tau + \vec{p} \cdot \vec{x})}, \quad (\text{A.24})$$

where we define the bosonic Matsubara frequencies,

$$\omega_n^b \equiv \omega_n = 2\pi T n, \quad n \in \mathbb{Z}, \quad (\text{A.25})$$

to ensure periodic boundary conditions in the compact τ -direction. The Fourier transformations for fermionic fields are

$$\psi(\tau, \vec{x}) = T \sum_{n=-\infty}^{\infty} \int_{-\infty}^{\infty} \frac{d^d p}{(2\pi)^d} \tilde{\psi}(\nu_n, \vec{p}) e^{+i(\nu_n \tau + \vec{p} \cdot \vec{x})}, \quad (\text{A.26})$$

$$\tilde{\psi}(\nu_n, \vec{p}) = \int_0^{\frac{1}{T}} d\tau \int_{-\infty}^{\infty} d^d x \psi(\tau, \vec{x}) e^{-i(\nu_n \tau + \vec{p} \cdot \vec{x})}, \quad (\text{A.27})$$

$$\bar{\psi}(\tau, \vec{x}) = T \sum_{n=-\infty}^{\infty} \int_{-\infty}^{\infty} \frac{d^d p}{(2\pi)^d} \tilde{\bar{\psi}}(\nu_n, \vec{p}) e^{-i(\nu_n \tau + \vec{p} \cdot \vec{x})}, \quad (\text{A.28})$$

$$\tilde{\bar{\psi}}(\nu_n, \vec{p}) = \int_0^{\frac{1}{T}} d\tau \int_{-\infty}^{\infty} d^d x \bar{\psi}(\tau, \vec{x}) e^{+i(\nu_n \tau + \vec{p} \cdot \vec{x})}, \quad (\text{A.29})$$

where

$$\omega_n^f \equiv \nu_n = 2\pi T \left(n + \frac{1}{2}\right), \quad n \in \mathbb{Z}, \quad (\text{A.30})$$

are the fermionic Matsubara frequencies, which ensure anti-symmetric boundary conditions in the temporal direction. In addition to the above definitions, there are two identities which are of relevance for our work,

$$\beta \delta_{n_1, n_2} (2\pi)^d \delta^{(d)}(\vec{p}_1 - \vec{p}_2) = \int_0^\beta d\tau \int_{-\infty}^{\infty} d^d x e^{\pm i[(\omega_{n_1} - \omega_{n_2}) \tau + (\vec{p}_1 - \vec{p}_2) \cdot \vec{x}]}, \quad (\text{A.31})$$

$$\delta(\tau_1 - \tau_2) \delta^{(d)}(\vec{x}_1 - \vec{x}_2) = \frac{1}{\beta} \sum_{n=-\infty}^{\infty} \int_{-\infty}^{\infty} \frac{d^d p}{(2\pi)^d} e^{\pm i[\omega_n (\tau_1 - \tau_2) + \vec{p} \cdot (\vec{x}_1 - \vec{x}_2)]}. \quad (\text{A.32})$$

The same holds true when both bosonic Matsubara frequencies are replaced by fermionic frequencies, $\omega_n \rightarrow \nu_n$, because the additional πT terms cancel.

A.4. Transcendental functions

Here, we list some transcendental functions as well as corresponding formulae, special values, limiting cases *etc.*.

A.4.1. Logarithm

The series representation of the logarithm is

$$\ln(1 + x) = \sum_{n=1}^{\infty} (-1)^{n+1} \frac{1}{n} x^n. \quad (\text{A.33})$$

A.4.2. Exponential integral

The exponential integral function is defined as follows [242, Eq. 5.1.1],

$$E_1(x) = \int_x^\infty dt t^{-1} e^{-t}, \quad |\arg(x)| < \pi. \quad (\text{A.34})$$

Its series expansion reads [242, Eq. 5.1.11],

$$E_1(x) = -\gamma - \ln(x) - \sum_{n=1}^{\infty} \frac{1}{n(n!)} (-x)^n. \quad |\arg(x)| < \pi, \quad (\text{A.35})$$

where γ is the Euler-Mascheroni constant.

A.4.3. Gamma functions

(Incomplete) gamma function

The integral representation of the (lower incomplete) gamma function is [242, Eq. 6.1.1 & 6.5.3],

$$\Gamma(s, x) = \int_x^\infty dt t^{s-1} e^{-t}, \quad \operatorname{Re}(s) > 0, \quad (\text{A.36})$$

$$\Gamma(s) = \Gamma(s, 0) = \int_0^\infty dt t^{s-1} e^{-t}, \quad \operatorname{Re}(s) > 0. \quad (\text{A.37})$$

The gamma function fulfills the recurrence relation [242, Eq. 6.1.15]

$$\Gamma(s+1) = s\Gamma(s). \quad (\text{A.38})$$

From Eqs. (A.34) to (A.36) follows that

$$\Gamma(0, x) = E_1(x) = -\gamma - \ln(x) - \sum_{n=1}^{\infty} \frac{1}{n(n!)} (-x)^n, \quad |\arg(x)| < \pi. \quad (\text{A.39})$$

For positive integers n [604, Eq. 8.4.15], [242, Eq. 6.5.19],

$$\Gamma(-n, x) = \frac{1}{n!} (-1)^n \left[\Gamma(0, x) - e^{-x} \sum_{k=0}^{n-1} \frac{1}{x^{k+1}} (-1)^k k! \right], \quad n \in \mathbb{N}. \quad (\text{A.40})$$

An asymptotic expansion of Eq. (A.36) reads [242, Eq. 6.5.32]

$$\lim_{x \rightarrow \infty} \Gamma(s, x) = e^{-x} x^{s-1} \left[1 + \frac{s-1}{x} + \frac{(s-1)(s-2)}{x^2} + \dots \right], \quad |\arg(x)| < \frac{3}{2} \pi, \quad (\text{A.41})$$

while the asymptotic expansion for Eq. (A.37) is [242, Eq. 6.1.37]

$$\lim_{x \rightarrow \infty} \Gamma(x) = e^{-x} x^x \sqrt{\frac{2\pi}{x}} \left(1 + \frac{1}{12x} + \frac{1}{288x^2} + \dots \right), \quad |\arg(x)| < \pi. \quad (\text{A.42})$$

For positive integers n [242, Eq. 6.1.12],

$$\Gamma\left(n + \frac{1}{2}\right) = \sqrt{\pi} \frac{(2n)!}{4^n n!}, \quad n \in \mathbb{N}. \quad (\text{A.43})$$

Polygamma functions

The digamma function is defined as the first derivative of the logarithm of the gamma function Eq. (A.37) [242, Eq. 6.3.1],

$$\psi(s) = \frac{d}{ds} \ln \Gamma(s) = \frac{\Gamma'(s)}{\Gamma(s)}. \quad (\text{A.44})$$

For positive integers one finds [242, Eq. 6.3.2],

$$\psi(n) = -\gamma + \sum_{k=1}^{n-1} \frac{1}{k}, \quad n \in \mathbb{N}, \quad (\text{A.45})$$

where γ is again the Euler-Mascheroni constant. The polygamma functions are defined as higher derivatives of the gamma function (A.37) or digamma function (A.44) respectively [242, Eq. 6.4.1],

$$\psi^{(n)}(s) = \frac{d^n}{ds^n} \psi(s) = \frac{d^{n+1}}{ds^{n+1}} \ln \Gamma(s) = \quad n \in \mathbb{N}, \operatorname{Re}(s) > 0, \quad (\text{A.46})$$

$$= (-1)^{n+1} \int_0^\infty dt \frac{t^n e^{-st}}{1 - e^{-t}}, \quad (\text{A.47})$$

where $\Gamma(s)$ is again given by Eq. (A.37).

A.4.4. Zeta and eta functions

Riemann zeta function

The integral and series representation of the Riemann zeta function is [242, Eqs. 23.2.1 & 23.2.7],

$$\zeta(s) = \frac{1}{\Gamma(s)} \int_0^\infty dt \frac{t^{s-1}}{e^t - 1} = \sum_{n=1}^{\infty} \frac{1}{n^s}, \quad \operatorname{Re}(s) > 1, \quad (\text{A.48})$$

where $\Gamma(s)$ is the gamma function (A.36).

Some special values of the Riemann zeta function and its derivative are,

$$\zeta(0) = -\frac{1}{2}, \quad [\text{242, Eq. 23.2.11}] \quad (\text{A.49})$$

$$\zeta'(0) = -\frac{1}{2} \ln(2\pi), \quad [\text{242, Eq. 23.2.13}] \quad (\text{A.50})$$

$$\zeta(-2n) = 0, \quad n \in \mathbb{N}, \quad [\text{242, Eq. 23.2.14}] \quad (\text{A.51})$$

$$\zeta'(-2n) = (-1)^n \frac{(2n)!}{2(2\pi)^{2n}} \zeta(2n+1), \quad n \in \mathbb{N}, \quad (\text{A.52})$$

$$\zeta'(-2) = -\frac{1}{4\pi^2} \zeta(3). \quad (\text{A.53})$$

the last expression for $\zeta(3)$ is listed as [OEIS: A240966](#).

Hurwitz zeta function

The integral and series representations of the Hurwitz zeta function are [604, Eq. 25.11.1 & 25.11.25],

$$\zeta(s, z) = \frac{1}{\Gamma(s)} \int_0^\infty dt \frac{t^{s-1} e^{-zt}}{1 - e^{-t}} = \quad \text{Re}(s) > 0, \text{Re}(z) > 0, \quad (\text{A.54})$$

$$= \sum_{n=0}^{\infty} \frac{1}{(n+z)^s}, \quad \text{Re}(s) > 1, z \neq -m, m \in \mathbb{N}_0, \quad (\text{A.55})$$

where $\Gamma(s)$ is given by Eq. (A.37). The relation to the Riemann zeta function (A.48) is [604, Eq. 25.11.2],

$$\zeta(s, 1) = \zeta(s), \quad s \neq 1. \quad (\text{A.56})$$

For positive integer n , we can use the integral representation of the polygamma functions (A.47) to obtain,

$$\psi^{(n)}(s) = (-1)^{n+1} n! \zeta(1+n, s), \quad n \in \mathbb{N}. \quad (\text{A.57})$$

Dirichlet eta function

The integral and series representations of the Dirichlet eta function are defined by [242, Eq. 23.2.19]

$$\eta(s) = \frac{1}{\Gamma(s)} \int_0^\infty dt \frac{t^{s-1}}{e^t + 1} = \sum_{n=1}^{\infty} \frac{1}{n^s} (-1)^{n-1} = \quad \text{Re}(s) > 0 \quad (\text{A.58})$$

$$= (1 - 2^{1-s}) \zeta(s), \quad (\text{A.59})$$

where $\Gamma(s)$ is the gamma function (A.36) and $\zeta(s)$ is the Riemann zeta function (A.48). From the series representation of the Dirichlet eta function (A.58) it directly follows that

$$\sum_{n=1}^{\infty} \ln(n) \frac{1}{n^s} (-1)^n = \eta'(s) = 2^{1-s} \ln(2) \zeta(s) + (1 - 2^{1-s}) \zeta'(s). \quad (\text{A.60})$$

while the second equality follows directly from Eq. (A.59).

A.4.5. Polylogarithms, Fermi-Dirac and Bose-Einstein integrals**(Incomplete) polylogarithm**

The integral and series representations of the (incomplete) polylogarithm are [604, Eq. 25.12.10 & 25.12.11]

$$\text{Li}_s(x, z) = \frac{1}{\Gamma(s)} \int_x^\infty dt \frac{t^{s-1}}{e^t/z - 1} = \frac{1}{\Gamma(s)} \sum_{k=1}^{\infty} \frac{z^k}{k^s} \Gamma(s, kx), \quad (\text{A.61})$$

$$\text{Li}_s(z) = \text{Li}_s(0, z) = \frac{1}{\Gamma(s)} \int_0^\infty dt \frac{t^{s-1}}{e^t/z - 1} = \sum_{k=1}^{\infty} \frac{z^k}{k^s}, \quad (\text{A.62})$$

where $\Gamma(s)$ is the gamma function (A.37) and $\Gamma(s, x)$ is the lower incomplete gamma function (A.36).

From the series representation (A.62), one finds

$$z \frac{\partial}{\partial z} \text{Li}_s(z) = \text{Li}_{s-1}(z), \quad z \frac{\partial}{\partial z} \text{Li}_s(-z) = \text{Li}_{s-1}(-z). \quad (\text{A.63})$$

Substituting $z = e^{\pm x}$,

$$\pm \frac{\partial}{\partial x} \text{Li}_s(e^{\pm x}) = \text{Li}_{s-1}(e^{\pm x}), \quad \pm \frac{\partial}{\partial x} \text{Li}_s(-e^{\pm x}) = \text{Li}_{s-1}(-e^{\pm x}). \quad (\text{A.64})$$

Inverting the differentiation formula (A.63), one obtains

$$\text{Li}_{s+1}(z) = \int_0^z dt t^{-1} \text{Li}_s(t). \quad (\text{A.65})$$

For $z = 1$ the polylogarithm (A.62) reduces to the Riemann zeta function (A.48),

$$\zeta(s) = \text{Li}_s(1). \quad (\text{A.66})$$

For integers $s < 2$, one can use the integral representation (A.62) to derive

$$\text{Li}_1(z) = \int_0^\infty dt \frac{1}{e^t/z - 1} = \int_0^\infty dt \frac{z e^{-t}}{1 - z e^{-t}} = \ln(1 - z e^{-t}) \Big|_0^\infty = -\ln(1 - z). \quad (\text{A.67})$$

From the definition (A.62) and the repeated application of Eq. (A.63) we find

$$\text{Li}_0(z) = \sum_{k=0}^{\infty} z^k = \frac{z}{1-z}, \quad (\text{A.68})$$

$$\text{Li}_{-1}(z) = \sum_{k=0}^{\infty} k z^k = \frac{z}{(1-z)^2}, \quad (\text{A.69})$$

$$\text{Li}_{-2}(z) = \sum_{k=0}^{\infty} k^2 z^k = \frac{z(1+z)}{(1-z)^3}, \quad (\text{A.70})$$

$$\vdots \quad (\text{A.71})$$

Some special relations that directly follow from Eqs. (A.68) to (A.70) are,

$$\text{Li}_0(z) + \text{Li}_0\left(\frac{1}{z}\right) = \frac{z}{1-z} + \frac{\frac{1}{z}}{1-\frac{1}{z}} = -1, \quad (\text{A.72})$$

$$\text{Li}_{-1}(z) + \text{Li}_{-1}\left(\frac{1}{z}\right) = \frac{z}{(1-z)^2} + \frac{\frac{1}{z}}{(1-\frac{1}{z})^2} = 2 \frac{z}{(1-z)^2} = 2 \text{Li}_{-1}(z) = 2 \text{Li}_{-1}\left(\frac{1}{z}\right), \quad (\text{A.73})$$

$$\text{Li}_{-2}(z) + \text{Li}_{-2}\left(\frac{1}{z}\right) = \frac{z(1+z)}{(1-z)^3} + \frac{\frac{1}{z}(1+\frac{1}{z})}{(1-\frac{1}{z})^3} = 0. \quad (\text{A.74})$$

For integers $s \geq 2$ repeated application of Eq. (A.65) defines the polylogarithms. This is also the origin of its naming, because it is a repeated integration of the natural logarithm (A.67). A special case is the dilogarithm for $s = 2$,

$$\text{Li}_2(z) = \int_0^z dt t^{-1} \text{Li}_1(t) = - \int_0^z dt t^{-1} \ln(1-t) = \sum_{k=1}^{\infty} \frac{z^k}{k^2}, \quad (\text{A.75})$$

which is also called Spence's function.

Special identities which are used in Eqs. (F.6) and (F.10) for the dilogarithm are [605],

$$\text{Li}_2(z) + \text{Li}_2\left(\frac{1}{z}\right) = -\frac{\pi^2}{6} - \frac{1}{2} \ln^2(-z), \quad (\text{A.76})$$

$$\text{Li}_2(-1) = -\frac{\pi^2}{12}. \quad (\text{A.77})$$

The next formula is valid for all $s \notin \mathbb{N}_0$ [606]

$$\operatorname{Li}_s(z) = \frac{\Gamma(1-s)}{(2\pi i)^{1-s}} \left[(-1)^{1-s} \zeta\left(1-s, \frac{1}{2} + \frac{\ln(-z)}{2\pi i}\right) + \zeta\left(1-s, \frac{1}{2} - \frac{\ln(-z)}{2\pi i}\right) \right]. \quad (\text{A.78})$$

The derivative of the polylogarithm w.r.t. its index is calculated from its series representation (A.62),

$$\frac{\partial}{\partial s} \operatorname{Li}_s(z) = - \sum_{k=1}^{\infty} \ln(k) \frac{z^k}{k^s}. \quad (\text{A.79})$$

Evaluating Eq. (A.62) for $z = -1$ one finds with Eq. (A.58),

$$\operatorname{Li}_s(-1) = -\eta(s). \quad (\text{A.80})$$

We define

$$\operatorname{DLi}_n(y) \equiv \left[\frac{\partial}{\partial s} \operatorname{Li}_s(-e^y) + \frac{\partial}{\partial s} \operatorname{Li}_s(-e^{-y}) \right]_{s=n}. \quad (\text{A.81})$$

Equation (A.80) can be used to evaluate Eq. (A.81) at $y = 0$,

$$\begin{aligned} \operatorname{DLi}_n(0) &\equiv 2 \left[\frac{\partial}{\partial s} \operatorname{Li}_s(-1) \right]_{s=n} = & (\text{A.82}) \\ &= -2 \eta'(s) \Big|_{s=n} = & (\text{A.60}) \\ &= -2 \left[2^{1-s} \ln(2) \zeta(s) + (1 - 2^{1-s}) \zeta'(s) \right]_{s=n}. \end{aligned}$$

Two special cases are

$$\operatorname{DLi}_0(0) = -\ln\left(\frac{\pi}{2}\right), \quad (\text{A.49}) \text{ and } (\text{A.50}), \quad (\text{A.83})$$

$$\operatorname{DLi}_{-2}(0) = -\frac{7}{2\pi^2} \zeta(3), \quad (\text{A.51}) \text{ and } (\text{A.53}). \quad (\text{A.84})$$

Fermi-Dirac and Bose-Einstein integrals

The (incomplete) Fermi-Dirac integral is defined as follows [604, Eqs. 25.12.14 & 25.12.16],

$$\begin{aligned} F_s(a, x) &= -\operatorname{Li}_{s+1}(a, -e^x) = \frac{1}{\Gamma(s+1)} \int_a^{\infty} dt \frac{t^s}{e^{t-x} + 1} = & (\text{A.85}) \\ &= \frac{1}{\Gamma(s+1)} \int_a^{\infty} dt t^s n_f(t-x), \end{aligned}$$

$$\begin{aligned} F_s(x) &= -\operatorname{Li}_{s+1}(-e^x) = \frac{1}{\Gamma(s+1)} \int_0^{\infty} dt \frac{t^s}{e^{t-x} + 1} = & (\text{A.86}) \\ &= \frac{1}{\Gamma(s+1)} \int_0^{\infty} dt t^s n_f(t-x), \end{aligned}$$

where $n_f(x)$ is the Fermi-Dirac distribution function.

The Bose-Einstein integral is defined as follows [604, Eqs. 25.12.15 & 25.12.16]

$$G_s(a, x) = \text{Li}_{s+1}(a, e^x) = \frac{1}{\Gamma(s+1)} \int_a^\infty dt \frac{t^s}{e^{t-x} - 1} = \quad (\text{A.87})$$

$$= \frac{1}{\Gamma(s+1)} \int_a^\infty dt t^s n_b(t-x),$$

$$G_s(x) = \text{Li}_{s+1}(e^x) = \frac{1}{\Gamma(s+1)} \int_0^\infty dt \frac{t^s}{e^{t-x} - 1} = \quad (\text{A.88})$$

$$= \frac{1}{\Gamma(s+1)} \int_0^\infty dt t^s n_b(t-x),$$

where $n_b(x)$ is the Bose-Einstein distribution function.

Using Eq. (A.64) for Eqs. (A.86) and (A.88) one derives,

$$\partial_x F_s(x) = -\partial_x \text{Li}_{s+1}(-e^x) = -\text{Li}_s(-e^x) = F_{s-1}(x), \quad (\text{A.89})$$

$$\partial_x G_s(x) = \partial_x \text{Li}_{s+1}(e^x) = \text{Li}_s(e^x) = G_{s-1}(x). \quad (\text{A.90})$$

The closed form for the zeroth order Fermi-Dirac integral (A.86) can be calculated using Eq. (A.67),

$$F_0(x) = -\text{Li}_1(-e^x) = \ln(1 + e^x). \quad (\text{A.91})$$

The combination of the two first-order Fermi-Dirac integrals (A.86) can be evaluated using Eq. (A.76),

$$F_1(x) + F_1(-x) = -[\text{Li}_2(-e^x) + \text{Li}_2(-e^{-x})] = \frac{\pi^2}{6} + \frac{1}{2} x^2, \quad F_1(0) = \frac{\pi^2}{12}. \quad (\text{A.92})$$

A.4.6. IR divergences and the incomplete polylogarithms

We evaluate

$$\begin{aligned} & \lim_{\varepsilon \rightarrow 0} \lim_{s \rightarrow 0} \Gamma(s) \text{Li}_s(\varepsilon, -z) = \quad (\text{A.93}) \\ &= \lim_{\varepsilon \rightarrow 0} \lim_{s \rightarrow 0} \sum_{k=1}^{\infty} \frac{1}{k^s} (-z)^k \Gamma(s, k\varepsilon) = \\ &= \lim_{\varepsilon \rightarrow 0} \lim_{s \rightarrow 0} \sum_{k=1}^{\infty} \frac{1}{k^s} (-z)^k \left[-\gamma - \ln(k\varepsilon) - \sum_{n=1}^{\infty} \frac{1}{n(n!)} (-k\varepsilon)^n \right] = \\ &= \lim_{\varepsilon \rightarrow 0} \lim_{s \rightarrow 0} \left[\frac{\partial}{\partial s} \text{Li}_s(-z) + [-\gamma - \ln(\varepsilon)] \text{Li}_s(-z) - \sum_{k=1}^{\infty} \frac{1}{k^s} (-z)^k \sum_{n=1}^{\infty} \frac{1}{n(n!)} (-k\varepsilon)^n \right] = \\ &= \frac{\partial}{\partial s} \text{Li}_s(-z) \Big|_{s=0} - \left[\gamma + \lim_{\varepsilon \rightarrow 0} \ln(\varepsilon) \right] \text{Li}_0(-z). \end{aligned}$$

In the first step, the incomplete polylogarithm is written in terms of its series representation (A.61). Next, one uses the asymptotic expansion (A.39) for the incomplete gamma function (A.36), which is valid in the limit $s \rightarrow 0$. By separating the terms of the sum one identifies the derivative of the polylogarithm w.r.t. its index (A.79), as well as the polylogarithm itself in its series representation (A.62). In the last step, we dropped the nested sums, because each term in the sum vanishes separately for $\varepsilon \rightarrow 0$. The remnant of the IR divergence, $\lim_{\varepsilon \rightarrow 0} \ln(\varepsilon)$, cancels the IR divergence of the vacuum contribution.

Using the identity (A.72) for the zeroth-order polylogarithm as well as definition (A.81), we derive from Eq. (A.93),

$$\lim_{\varepsilon \rightarrow 0} \lim_{s \rightarrow 0} \Gamma(s) [\text{Li}_s(\varepsilon, -z) + \text{Li}_s(\varepsilon, -\frac{1}{z})] = \text{DLi}_0(\ln(z)) + \gamma + \lim_{\varepsilon \rightarrow 0} \ln(\varepsilon). \quad (\text{A.94})$$

Similarly to the previous result(s), we derive an expression for $\lim_{\varepsilon \rightarrow 0} \lim_{s \rightarrow -2} \Gamma(s) \text{Li}_s(\varepsilon, -z)$. During the calculation, we need the identity (A.40) for $n = 2$ and $x = k\varepsilon$,

$$\begin{aligned} \Gamma(-2, k\varepsilon) &= \frac{1}{2} \left[\Gamma(0, k\varepsilon) - e^{-k\varepsilon} \sum_{m=0}^1 \frac{1}{(k\varepsilon)^{m+1}} (-1)^m m! \right] = \\ &= \frac{1}{2} \Gamma(0, k\varepsilon) - \frac{1}{2} e^{-k\varepsilon} \left[\frac{1}{k\varepsilon} - \frac{1}{(k\varepsilon)^2} \right] = \\ &= \frac{1}{2} \Gamma(0, k\varepsilon) + \frac{1}{2} \frac{1}{(k\varepsilon)^2} - \frac{1}{k\varepsilon} + \frac{3}{4} + \mathcal{O}(\varepsilon), \end{aligned} \quad (\text{A.95})$$

as well as the polylogarithms (A.68) to (A.70). Additionally, one again needs the asymptotic expansion of the incomplete gamma function (A.39) and the definition of the polylogarithm (A.62) and its derivative (A.79). It follows that

$$\begin{aligned} \lim_{\varepsilon \rightarrow 0} \lim_{s \rightarrow -2} \Gamma(s) \text{Li}_s(\varepsilon, -z) &= \\ &= \lim_{\varepsilon \rightarrow 0} \lim_{s \rightarrow -2} \sum_{k=1}^{\infty} \frac{1}{k^s} (-z)^k \Gamma(s, k\varepsilon) = \\ &= \lim_{\varepsilon \rightarrow 0} \lim_{s \rightarrow 0} \sum_{k=1}^{\infty} \frac{1}{k^{s-2}} (-z)^k \left[\frac{1}{2} \Gamma(s, k\varepsilon) + \frac{1}{2} \frac{1}{(k\varepsilon)^2} - \frac{1}{k\varepsilon} + \frac{3}{4} + \mathcal{O}(\varepsilon) \right] = \\ &= \lim_{\varepsilon \rightarrow 0} \left[\lim_{s \rightarrow 0} \frac{1}{2} \sum_{k=1}^{\infty} \frac{1}{k^{s-2}} (-z)^k \Gamma(s, k\varepsilon) + \frac{1}{2\varepsilon^2} \text{Li}_0(-z) - \frac{1}{\varepsilon} \text{Li}_{-1}(-z) + \frac{3}{4} \text{Li}_{-2}(-z) \right] = \\ &= \lim_{\varepsilon \rightarrow 0} \left[\lim_{s \rightarrow 0} \frac{1}{2} \sum_{k=1}^{\infty} \frac{1}{k^{s-2}} (-z)^k \left(-\gamma - \ln(k\varepsilon) - \sum_{n=1}^{\infty} \frac{1}{n(n!)} (-k\varepsilon)^n \right) + \right. \\ &\quad \left. + \frac{1}{2\varepsilon^2} \text{Li}_0(-z) - \frac{1}{\varepsilon} \text{Li}_{-1}(-z) + \frac{3}{4} \text{Li}_{-2}(-z) \right] = \\ &= \frac{1}{2} \frac{\partial}{\partial s} \text{Li}_s(-z) \Big|_{s=-2} - \frac{1}{2} \left[\gamma - \frac{3}{2} + \lim_{\varepsilon \rightarrow 0} \ln(\varepsilon) \right] \text{Li}_{-2}(-z) + \lim_{\varepsilon \rightarrow 0} \frac{1}{2\varepsilon^2} \text{Li}_0(-z) - \lim_{\varepsilon \rightarrow 0} \frac{1}{\varepsilon} \text{Li}_{-1}(-z). \end{aligned} \quad (\text{A.96})$$

Again, we were able to split the IR divergences into terms $\sim \ln(\varepsilon)$, $\sim \frac{1}{\varepsilon}$, and $\sim \frac{1}{\varepsilon^2}$. Analogously to Eq. (A.94) one obtains

$$\begin{aligned} \lim_{\varepsilon \rightarrow 0} \lim_{s \rightarrow -2} \Gamma(s) [\text{Li}_s(\varepsilon, -z) + \text{Li}_s(\varepsilon, -\frac{1}{z})] &= \\ &= \frac{1}{2} \text{DLi}_{-2}(\ln(z)) - \frac{1}{2} \lim_{\varepsilon \rightarrow 0} \frac{1}{\varepsilon^2} + 2 \frac{z}{(1+z)^2} \lim_{\varepsilon \rightarrow 0} \frac{1}{\varepsilon}, \end{aligned} \quad (\text{A.97})$$

where we used Eqs. (A.72) to (A.74) and definition (A.81).

Appendix B

Matsubara sums and related formula

Abstract As a huge share of this thesis deals with QFT at non-zero temperature, it is repeatedly required to evaluate so-called Matsubara sums, which are named after T. Matsubara, due to his original work on new techniques in “quantum statistical mechanics” [607].¹ Usually these sums appear at non-zero temperature instead of the integration over the zeroth component of the loop four-momentum during the evaluation of quantum corrections to the UV action. However, since they are a direct consequence of the compactification of the temporal direction, which leads to a discrete (energy) spectrum, similar sums also pop up instead of spatial-momentum integrations if one studies QFTs in a finite spatial volume, see *e.g.*, Refs. [177, 250, 611, 612, 613, 614]. After evaluation the corresponding results of the frequency summations are normally expressed in terms of bosonic and fermionic distribution/occupation functions and their derivatives, respectively the corresponding hyperbolic functions.

In this appendix we provide closed expressions for all Matsubara sums that occur throughout this thesis. We start by introducing our notation for the thermal distribution functions and provide some simple but useful identities for reasons of comprehensibility. Afterwards the results for the Matsubara sums as well as zero-temperature limits of some of the sums are presented.

Disclosure The evaluation of Matsubara sums is a standard problem in statistical mechanics (thermodynamics) and especially thermal QFT. The required mathematical techniques of contour integration in the complex plane are part of the curriculum of any advanced lectures on these subjects and are not recapitulated here. Instead we refer to the following lecture notes and textbooks for details, *i.e.*, Refs. [615, 177, 22, 504, 505, 142] as well as references therein.

All but one result of this appendix are (re)derived by hand by the author, but can in parts also be found elsewhere, because the structure of most of the sums is not exceptional to this work. All results are crosschecked using MATHEMATICA. For these reasons, we only cite selected references where similar results are derived or used.

Still, I would like to mention that some notes by S. Rechenberger [566] were rather useful at the beginning of my doctoral studies to cross-check some of the explicit calculations.

¹Actually similar sums were already derived, evaluated, and studied for example in earlier works on superconductivity by J. Bardeen [608], H. Fröhlich [609], and C. G. Kuper [610], as T. Matsubara states in his own work.

B.1. Thermal distribution functions and useful identities

The Bose-Einstein distribution function [616], n_b , and the Fermi-Dirac distribution function [617, 618], n_f , are defined as follows

$$n_b(x) \equiv \frac{1}{e^x - 1} = \frac{1}{2} \left[-1 + \coth\left(\frac{x}{2}\right) \right], \quad (\text{B.1})$$

$$n_f(x) \equiv \frac{1}{e^x + 1} = \frac{1}{2} \left[1 - \tanh\left(\frac{x}{2}\right) \right]. \quad (\text{B.2})$$

The derivatives of these distribution functions w.r.t. their argument are

$$\frac{\partial}{\partial x} n_b(x) = -n_b^2(x) - n_b(x) = -\frac{1}{4 \sinh^2\left(\frac{x}{2}\right)}, \quad (\text{B.3})$$

$$\frac{\partial}{\partial x} n_f(x) = +n_f^2(x) - n_f(x) = -\frac{1}{4 \cosh^2\left(\frac{x}{2}\right)}. \quad (\text{B.4})$$

Furthermore, we find

$$\frac{\partial^2}{\partial x^2} n_b(x) = 2n_b^3(x) + 3n_b^2(x) + n_b(x) = \frac{\cosh\left(\frac{x}{2}\right)}{4 \sinh^3\left(\frac{x}{2}\right)}, \quad (\text{B.5})$$

$$\frac{\partial^2}{\partial x^2} n_f(x) = 2n_f^3(x) - 3n_f^2(x) + n_f(x) = \frac{\sinh\left(\frac{x}{2}\right)}{4 \cosh^3\left(\frac{x}{2}\right)}, \quad (\text{B.6})$$

for the second derivatives and

$$\frac{\partial^3}{\partial x^3} n_b(x) = -6n_b^4(x) - 12n_b^3(x) - 7n_b^2(x) - n_b^1(x) = -\frac{1+2 \cosh^2\left(\frac{x}{2}\right)}{8 \sinh^4\left(\frac{x}{2}\right)}, \quad (\text{B.7})$$

$$\frac{\partial^3}{\partial x^3} n_f(x) = +6n_f^4(x) - 12n_f^3(x) + 7n_f^2(x) - n_f^1(x) = \frac{1-2 \sinh^2\left(\frac{x}{2}\right)}{8 \cosh^4\left(\frac{x}{2}\right)}, \quad (\text{B.8})$$

for the third derivatives of the distribution functions.

In the limit of vanishing temperature, $T = \frac{1}{\beta} \rightarrow 0$, the Bose-Einstein distribution (B.1) simply vanishes

$$\lim_{\beta E \rightarrow \infty} n_b\left(\frac{E}{T}\right) = 0, \quad (\text{B.9})$$

while for the Fermi-Dirac distribution (B.2) the zero-temperature limit depends on the difference of the energy E and the Fermi level – the chemical potential μ ,

$$\lim_{\beta|\mu|, \beta E \rightarrow \infty} \left[n_f\left(\frac{E+\mu}{T}\right) + n_f\left(\frac{E-\mu}{T}\right) \right] = \Theta\left(\frac{|\mu|}{E} - 1\right), \quad (\text{B.10})$$

$$\lim_{\beta|\mu|, \beta E \rightarrow \infty} \left[n_f\left(\frac{E+\mu}{T}\right) - n_f\left(\frac{E-\mu}{T}\right) \right] = -\text{sgn}(\mu) \Theta\left(\frac{|\mu|}{E} - 1\right). \quad (\text{B.11})$$

According to the previous formulae, this implies that also all derivatives of the Bose-Einstein distribution vanish for vanishing temperature, which is not the case for the Fermi-Dirac distribution. Here, the first derivative spikes and becomes singular for $T \rightarrow 0$. Hence, for Eq. (B.4) the zero-temperature limit is given by

$$\begin{aligned} \lim_{\beta|\mu|, \beta E \rightarrow \infty} \frac{E}{T} \left[n_f^2\left(\frac{E\pm\mu}{T}\right) - n_f\left(\frac{E\pm\mu}{T}\right) \right] &\stackrel{(\text{B.4})}{=} \lim_{\beta|\mu| \rightarrow \infty} -\frac{E}{|\mu|} \frac{\frac{|\mu|}{2T}}{2 \cosh^2\left(\frac{|\mu|}{2T} \left(\frac{E}{|\mu|} \pm \text{sgn}(\mu)\right)\right)} \stackrel{(\text{A.2})}{=} \\ &= -\frac{E}{|\mu|} \delta\left(\frac{E}{|\mu|} \pm \text{sgn}(\mu)\right). \end{aligned} \quad (\text{B.12})$$

Although even higher-order derivatives of the Fermi-Dirac distribution appear in the calculations of this thesis, we will not consider their zero-temperature limit, which is explained in the main text.

B.2. Matsubara sums

B.2.1. Purely bosonic/fermionic Matsubara summation

First, we consider Matsubara sums over powers or products of propagators that exclusively contain bosonic Matsubara frequencies (A.25) or purely fermionic Matsubara frequencies (A.30).

Sums containing a single energy

The most prominent Matsubara sum, which is found in almost any calculation involving bosons at non-zero temperature, is the sum over a single bosonic propagator,

$$\frac{1}{\beta} \sum_{n=-\infty}^{+\infty} \frac{1}{\omega_n^2 + E^2} = \frac{1}{2E} [1 + 2n_b(\frac{E}{T})] \stackrel{(B.1)}{=} \frac{1}{2E} \coth\left(\frac{E}{2T}\right). \quad (B.13)$$

Its zero-temperature limit reads

$$\lim_{\beta E \rightarrow \infty} (B.13) = \frac{1}{2E}. \quad (B.14)$$

The corresponding fermionic counterpart is

$$\begin{aligned} \frac{1}{\beta} \sum_{n=-\infty}^{+\infty} \frac{1}{(\nu_n + i\mu)^2 + E^2} &= \frac{1}{2E} [1 - n_f(\frac{E+\mu}{T}) - n_f(\frac{E-\mu}{T})] \stackrel{(B.2)}{=} \\ &= \frac{1}{2E} \left[\frac{1}{2} \tanh\left(\frac{E+\mu}{2T}\right) + \frac{1}{2} \tanh\left(\frac{E-\mu}{2T}\right) \right]. \end{aligned} \quad (B.15)$$

At vanishing temperature it reduces to

$$\lim_{\beta|\mu|, \beta E \rightarrow \infty} (B.15) = \frac{1}{2E} \Theta\left(\frac{E}{|\mu|} - 1\right). \quad (B.16)$$

Both results can be derived by contour integration and are standard textbook results as explained in the disclosure.

In order to arrive at explicit expressions for the Matsubara sums over higher powers of the propagators, we take the derivative of Eqs. (B.13) and (B.15) w.r.t. the energy E . More explicitly, we apply

$$-\frac{1}{2E} \frac{\partial}{\partial E} \quad (B.17)$$

to both sides of the equations. The same result is obtained via contour integration. For the purely bosonic sum, we find

$$\begin{aligned} \frac{1}{\beta} \sum_{n=-\infty}^{+\infty} \frac{1}{[\omega_n^2 + E^2]^2} &= \frac{1}{4E^3} [1 + 2n_b(\frac{E}{T}) + 2\frac{E}{T} [n_b^2(\frac{E}{T}) + n_b(\frac{E}{T})]] = \\ &= \frac{1}{4E^3} \left[\coth\left(\frac{E}{2T}\right) + \frac{E}{T} \frac{1}{2 \sinh^2\left(\frac{E}{2T}\right)} \right]. \end{aligned} \quad (B.18)$$

The zero-temperature limit is

$$\lim_{\beta E \rightarrow \infty} (B.18) = \frac{1}{4E^3}. \quad (B.19)$$

Similarly one finds the fermionic Matsubara sum over two fermionic propagators,

$$\begin{aligned} & \frac{1}{\beta} \sum_{n=-\infty}^{+\infty} \frac{1}{[(\nu_n + i\mu)^2 + E^2]^2} = \tag{B.20} \\ &= \frac{1}{4E^3} \left[1 - n_f\left(\frac{E+\mu}{T}\right) - n_f\left(\frac{E-\mu}{T}\right) + \frac{E}{T} \left[n_f^2\left(\frac{E+\mu}{T}\right) + n_f^2\left(\frac{E-\mu}{T}\right) - n_f\left(\frac{E+\mu}{T}\right) - n_f\left(\frac{E-\mu}{T}\right) \right] \right] = \\ &= \frac{1}{4E^3} \left(\frac{1}{2} \tanh\left(\frac{E+\mu}{2T}\right) + \frac{1}{2} \tanh\left(\frac{E-\mu}{2T}\right) - \frac{E}{T} \left[\frac{1}{4 \cosh^2\left(\frac{E+\mu}{2T}\right)} + \frac{1}{4 \cosh^2\left(\frac{E-\mu}{2T}\right)} \right] \right). \end{aligned}$$

Using Eqs. (B.10) and (B.12) the zero-temperature limit is easily derived,

$$\lim_{\beta|\mu|, \beta E \rightarrow \infty} (\text{B.20}) = \frac{1}{4E^3} \left[\Theta\left(\frac{E}{|\mu|} - 1\right) - \frac{E}{|\mu|} \left[\delta\left(\frac{E}{|\mu|} + 1\right) + \delta\left(\frac{E}{|\mu|} - 1\right) \right] \right]. \tag{B.21}$$

Analogously, by acting with $-\frac{1}{4E} \frac{\partial}{\partial E}$ on the previous results, we derive

$$\begin{aligned} & \frac{1}{\beta} \sum_{n=-\infty}^{+\infty} \frac{1}{[\omega_n^2 + E^2]^3} = \tag{B.22} \\ &= \frac{3}{16E^5} \left[1 + 2n_b\left(\frac{E}{T}\right) + 2\frac{E}{T} \left[n_b^2\left(\frac{E}{T}\right) + n_b\left(\frac{E}{T}\right) \right] + 2\left(\frac{E}{T}\right)^2 \left[\frac{2}{3} n_b^3\left(\frac{E}{T}\right) + n_b^2\left(\frac{E}{T}\right) + \frac{1}{3} n_b\left(\frac{E}{T}\right) \right] \right] = \\ &= \frac{3}{16E^5} \left[\coth\left(\frac{E}{2T}\right) + \frac{E}{T} \frac{1}{2 \sinh^2\left(\frac{E}{2T}\right)} + \left(\frac{E}{T}\right)^2 \frac{\cosh\left(\frac{E}{2T}\right)}{6 \sinh^3\left(\frac{E}{2T}\right)} \right] \end{aligned}$$

for the bosonic sum and

$$\begin{aligned} & \frac{1}{\beta} \sum_{n=-\infty}^{+\infty} \frac{1}{[(\nu_n + i\mu)^2 + E^2]^3} = \tag{B.23} \\ &= \frac{3}{16E^5} \left[1 - n_f\left(\frac{E+\mu}{T}\right) - n_f\left(\frac{E-\mu}{T}\right) + \frac{E}{T} \left[n_f^2\left(\frac{E+\mu}{T}\right) + n_f^2\left(\frac{E-\mu}{T}\right) - n_f\left(\frac{E+\mu}{T}\right) - n_f\left(\frac{E-\mu}{T}\right) \right] - \right. \\ & \quad \left. - \left(\frac{E}{T}\right)^2 \left[\frac{2}{3} n_f^3\left(\frac{E+\mu}{T}\right) + \frac{2}{3} n_f^3\left(\frac{E-\mu}{T}\right) - n_f^2\left(\frac{E+\mu}{T}\right) - n_f^2\left(\frac{E-\mu}{T}\right) + \frac{1}{3} n_f\left(\frac{E+\mu}{T}\right) + \frac{1}{3} n_f\left(\frac{E-\mu}{T}\right) \right] \right] = \\ &= \frac{3}{16E^5} \left[\frac{1}{2} \tanh\left(\frac{E+\mu}{2T}\right) + \frac{1}{2} \tanh\left(\frac{E-\mu}{2T}\right) - \frac{E}{T} \left[\frac{1}{4 \cosh^2\left(\frac{E+\mu}{2T}\right)} + \frac{1}{4 \cosh^2\left(\frac{E-\mu}{2T}\right)} \right] - \right. \\ & \quad \left. - \left(\frac{E}{T}\right)^2 \left[\frac{\sinh\left(\frac{E+\mu}{2T}\right)}{12 \cosh^3\left(\frac{E+\mu}{2T}\right)} + \frac{\sinh\left(\frac{E-\mu}{2T}\right)}{12 \cosh^3\left(\frac{E-\mu}{2T}\right)} \right] \right] \end{aligned}$$

for the fermionic sum of third powers of the propagators.

For sums over the fourth power of propagators, we apply $-\frac{1}{6E} \frac{\partial}{\partial E}$ to the previous equations and find

$$\begin{aligned} & \frac{1}{\beta} \sum_{n=-\infty}^{+\infty} \frac{1}{[\omega_n^2 + E^2]^4} = \tag{B.24} \\ &= \frac{5}{32E^7} \left[1 + 2n_b\left(\frac{E}{T}\right) + 2\frac{E}{T} \left[n_b^2\left(\frac{E}{T}\right) + n_b\left(\frac{E}{T}\right) \right] + 2\left(\frac{E}{T}\right)^2 \left[\frac{4}{5} n_b^3\left(\frac{E}{T}\right) + \frac{6}{5} n_b^2\left(\frac{E}{T}\right) + \frac{2}{5} n_b\left(\frac{E}{T}\right) \right] + \right. \\ & \quad \left. + 2\left(\frac{E}{T}\right)^3 \left[\frac{2}{5} n_b^4\left(\frac{E}{T}\right) + \frac{4}{5} n_b^3\left(\frac{E}{T}\right) + \frac{7}{15} n_b^2\left(\frac{E}{T}\right) + \frac{1}{15} n_b\left(\frac{E}{T}\right) \right] \right] = \end{aligned}$$

$$= \frac{5}{32E^7} \left[\coth\left(\frac{E}{2T}\right) + \frac{E}{T} \frac{1}{2 \sinh^2\left(\frac{E}{2T}\right)} + \left(\frac{E}{T}\right)^2 \frac{\cosh\left(\frac{E}{2T}\right)}{5 \sinh^3\left(\frac{E}{2T}\right)} + \left(\frac{E}{T}\right)^3 \frac{1+2 \cosh^2\left(\frac{E}{2T}\right)}{60 \sinh^4\left(\frac{E}{2T}\right)} \right],$$

and

$$\begin{aligned} & \frac{1}{\beta} \sum_{n=-\infty}^{+\infty} \frac{1}{[(\nu_n + i\mu)^2 + E^2]^4} = \tag{B.25} \\ &= \frac{5}{32E^7} \left[1 - n_f\left(\frac{E+\mu}{T}\right) - n_f\left(\frac{E-\mu}{T}\right) + \frac{E}{T} \left[n_f^2\left(\frac{E+\mu}{T}\right) + n_f^2\left(\frac{E-\mu}{T}\right) - n_f\left(\frac{E+\mu}{T}\right) - n_f\left(\frac{E-\mu}{T}\right) \right] - \right. \\ & \quad - \left(\frac{E}{T}\right)^2 \left(\frac{4}{5} \left[n_f^3\left(\frac{E+\mu}{T}\right) + n_f^3\left(\frac{E-\mu}{T}\right) \right] - \frac{6}{5} \left[n_f^2\left(\frac{E+\mu}{T}\right) + n_f^2\left(\frac{E-\mu}{T}\right) \right] + \right. \\ & \quad \left. + \frac{2}{5} \left[n_f\left(\frac{E+\mu}{T}\right) + n_f\left(\frac{E-\mu}{T}\right) \right] \right) + \\ & \quad + \left(\frac{E}{T}\right)^3 \left(\frac{2}{5} \left[n_f^4\left(\frac{E+\mu}{T}\right) + n_f^4\left(\frac{E-\mu}{T}\right) \right] - \frac{4}{5} \left[n_f^3\left(\frac{E+\mu}{T}\right) + n_f^3\left(\frac{E-\mu}{T}\right) \right] + \right. \\ & \quad \left. + \frac{7}{15} \left[n_f^2\left(\frac{E+\mu}{T}\right) + n_f^2\left(\frac{E-\mu}{T}\right) \right] - \frac{1}{15} \left[n_f\left(\frac{E+\mu}{T}\right) + n_f\left(\frac{E-\mu}{T}\right) \right] \right) \left. \right] = \\ &= \frac{5}{32E^7} \left[\frac{1}{2} \tanh\left(\frac{E+\mu}{2T}\right) + \frac{1}{2} \tanh\left(\frac{E-\mu}{2T}\right) - \frac{E}{T} \left[\frac{1}{4 \cosh^2\left(\frac{E+\mu}{2T}\right)} + \frac{1}{4 \cosh^2\left(\frac{E-\mu}{2T}\right)} \right] - \right. \\ & \quad \left. - \left(\frac{E}{T}\right)^2 \left[\frac{\sinh\left(\frac{E+\mu}{2T}\right)}{10 \cosh^3\left(\frac{E+\mu}{2T}\right)} + \frac{\sinh\left(\frac{E-\mu}{2T}\right)}{10 \cosh^3\left(\frac{E-\mu}{2T}\right)} \right] + \left(\frac{E}{T}\right)^3 \left[\frac{1-2 \sinh^2\left(\frac{E+\mu}{2T}\right)}{120 \cosh^4\left(\frac{E+\mu}{2T}\right)} + \frac{1-2 \sinh^2\left(\frac{E-\mu}{2T}\right)}{120 \cosh^4\left(\frac{E-\mu}{2T}\right)} \right] \right]. \end{aligned}$$

On the other hand, for example, for the calculation of mean-field effective potentials, the Matsubara sum of the logarithm of the denominator of the propagators is required. One finds,

$$\frac{1}{\beta} \sum_{n=-\infty}^{+\infty} \ln(\beta^2(\omega_n^2 + E^2)) = \tag{B.26}$$

$$= E + \frac{2}{\beta} \ln(1 - e^{-\beta E}) + \text{const.},$$

$$\frac{1}{\beta} \sum_{n=-\infty}^{+\infty} \ln(\beta^2[(\nu_n + i\mu)^2 + E^2]) = \tag{B.27}$$

$$= E + \frac{1}{\beta} \ln(1 + e^{-\beta(E+\mu)}) + \frac{1}{\beta} \ln(1 + e^{-\beta(E-\mu)}) + \text{const.}$$

Both formula can be verified by taking derivatives w.r.t. E of these expressions, which turns them into Eqs. (B.13) and (B.15), *cf.* Ref. [462].

The reason why we provide these sums in terms of distribution functions and hyperbolic functions is that each representation has advantages when it comes to certain applications, *e.g.*, the calculation of limits, the extraction of symmetries, or their numerical evaluation.

Sums containing two energies

For the analysis of the fermionic quantum corrections to the bosonic two-point function, see Section 11.3.2, we need the following Matsubara sum,

$$\begin{aligned}
& \frac{1}{\beta} \sum_{n=-\infty}^{+\infty} \frac{1}{(\nu_n + i\mu)^2 + E_1^2} \frac{1}{(\nu_n + i\mu)^2 + E_2^2} = \tag{B.28} \\
&= \frac{1}{2E_1} \frac{1}{E_2^2 - E_1^2} \left[1 - n_f\left(\frac{E_1 + \mu}{T}\right) - n_f\left(\frac{E_1 - \mu}{T}\right) \right] + \frac{1}{2E_2} \frac{1}{E_1^2 - E_2^2} \left[1 - n_f\left(\frac{E_2 + \mu}{T}\right) - n_f\left(\frac{E_2 - \mu}{T}\right) \right] = \\
&= \frac{1}{2E_1} \frac{1}{E_2^2 - E_1^2} \left[\frac{1}{2} \tanh\left(\frac{E_1 + \mu}{2T}\right) + \frac{1}{2} \tanh\left(\frac{E_1 - \mu}{2T}\right) \right] + \\
&\quad + \frac{1}{2E_2} \frac{1}{E_1^2 - E_2^2} \left[\frac{1}{2} \tanh\left(\frac{E_2 + \mu}{2T}\right) + \frac{1}{2} \tanh\left(\frac{E_2 - \mu}{2T}\right) \right],
\end{aligned}$$

which depends on two different energies E_1 and E_2 , because one of these energies usually contains the external momentum that enters the respective loop diagram.

The zero-temperature limit of this sum is given by

$$\lim_{\beta|\mu|, \beta E \rightarrow \infty} \text{(B.28)} = \frac{1}{2E_1} \frac{1}{E_2^2 - E_1^2} \Theta\left(\frac{E_1}{|\mu|} - 1\right) + \frac{1}{2E_2} \frac{1}{E_1^2 - E_2^2} \Theta\left(\frac{E_2}{|\mu|} - 1\right). \tag{B.29}$$

If the two energies become degenerate, the sum reduces to Eqs. (B.20) and (B.21).

B.2.2. Mixed bosonic-fermionic Matsubara sums

As soon as one is confronted with the computation of loop diagrams that involve internal bosonic and fermionic propagators, see Eq. (E.89), one has to calculate Matsubara sums over bosonic and fermionic Matsubara frequencies. This is not exclusive to FRG calculations, but rather generic in thermal QFT, *e.g.*, Refs. [531, 22]. The most basic sum of this type is

$$\begin{aligned}
& \frac{1}{\beta} \sum_{n=-\infty}^{\infty} \frac{1}{(\nu_n + i\mu)^2 + E_f^2} \frac{1}{\omega_n^2 + E_b^2} = \tag{B.30} \\
&= \left(\frac{1}{E_f^2 - (E_b + \mu - i\pi T)^2} + \frac{1}{E_f^2 - (E_b - \mu + i\pi T)^2} \right) \frac{1}{2E_b} \left[\frac{1}{2} + n_b\left(\frac{E_b}{T}\right) \right] + \\
&\quad + \frac{1}{E_b^2 - (E_f + \mu - i\pi T)^2} \frac{1}{2E_f} \left[\frac{1}{2} - n_f\left(\frac{E_f + \mu}{T}\right) \right] + \frac{1}{E_b^2 - (E_f - \mu + i\pi T)^2} \frac{1}{2E_f} \left[\frac{1}{2} - n_f\left(\frac{E_f - \mu}{T}\right) \right] = \\
&= \left[\left(\frac{E_f^2 - (E_b + \mu)^2 + (\pi T)^2}{E_f^4 - 2E_f^2[(E_b + \mu)^2 - (\pi T)^2] + [(E_b + \mu)^2 + (\pi T)^2]^2} + \frac{E_f^2 - (E_b - \mu)^2 + (\pi T)^2}{E_f^4 - 2E_f^2[(E_b - \mu)^2 - (\pi T)^2] + [(E_b - \mu)^2 + (\pi T)^2]^2} \right) \times \right. \\
&\quad \times \frac{1}{2E_b} \left[\frac{1}{2} + n_b\left(\frac{E_b}{T}\right) \right] + \\
&\quad + \frac{E_b^2 - (E_f + \mu)^2 + (\pi T)^2}{E_b^4 - 2E_b^2[(E_f + \mu)^2 - (\pi T)^2] + [(E_f + \mu)^2 + (\pi T)^2]^2} \frac{1}{2E_f} \left[\frac{1}{2} - n_f\left(\frac{E_f + \mu}{T}\right) \right] + \\
&\quad \left. + \frac{E_b^2 - (E_f - \mu)^2 + (\pi T)^2}{E_b^4 - 2E_b^2[(E_f - \mu)^2 - (\pi T)^2] + [(E_f - \mu)^2 + (\pi T)^2]^2} \frac{1}{2E_f} \left[\frac{1}{2} - n_f\left(\frac{E_f - \mu}{T}\right) \right] \right] + \\
&\quad + i \left[\left(\frac{-2\pi T(E_b + \mu)}{E_f^4 - 2E_f^2[(E_b + \mu)^2 - (\pi T)^2] + [(E_b + \mu)^2 + (\pi T)^2]^2} + \frac{2\pi T(E_b - \mu)}{E_f^4 - 2E_f^2[(E_b - \mu)^2 - (\pi T)^2] + [(E_b - \mu)^2 + (\pi T)^2]^2} \right) \times \right.
\end{aligned}$$

$$\begin{aligned}
& \times \frac{1}{2E_b} \left[\frac{1}{2} + n_b \left(\frac{E_b}{T} \right) \right] \\
& + \frac{-2\pi T(E_f + \mu)}{E_b^4 - 2E_b^2[(E_f + \mu)^2 - (\pi T)^2] + [(E_f + \mu)^2 + (\pi T)^2]^2} \frac{1}{2E_f} \left[\frac{1}{2} - n_f \left(\frac{E_f + \mu}{T} \right) \right] + \\
& + \frac{2\pi T(E_f - \mu)}{E_b^4 - 2E_b^2[(E_f - \mu)^2 - (\pi T)^2] + [(E_f - \mu)^2 + (\pi T)^2]^2} \frac{1}{2E_f} \left[\frac{1}{2} - n_f \left(\frac{E_f - \mu}{T} \right) \right] \Big].
\end{aligned}$$

Here, E_b is the energy of the boson and E_f the fermionic energy. The result in the second and third line is identical to what was derived by Ref. [66, Eq. (B.3)] and Ref. [101, Eq. (H.5)] for their FRG calculations.²

In the second step, the result is split into its real and imaginary part. One can read off that the real part is symmetric in μ , while the imaginary part is anti-symmetric in μ and therefore presumably nonphysical, see Eq. (10.12) and the corresponding discussion.

In the limit of vanishing temperature, we find

$$\begin{aligned}
& \lim_{\beta|\mu|, \beta E \rightarrow \infty} \text{(B.30)} = \tag{B.31} \\
& = \left[\frac{1}{E_f^2 - (E_b + \mu)^2} + \frac{1}{E_f^2 - (E_b - \mu)^2} \right] \frac{1}{4E_b} + \\
& + \frac{1}{E_b^2 - (E_f + \mu)^2} \frac{1}{2E_f} \left[\frac{1}{2} - \Theta \left(-\frac{\mu}{E_f} - 1 \right) \right] + \frac{1}{E_b^2 - (E_f - \mu)^2} \frac{1}{2E_f} \left[\frac{1}{2} - \Theta \left(\frac{\mu}{E_f} - 1 \right) \right],
\end{aligned}$$

which is always real.

Due to the regulator insertion, FRG diagrams always exhibit one additional propagator compared to their perturbative counterparts, see for example Eq. (E.89). Hence, for so-called fermion self-energy-like diagrams, we need to apply $-\frac{1}{2E_b} \frac{\partial}{\partial E_b}$ and $-\frac{1}{2E_f} \frac{\partial}{\partial E_f}$ to Eq. (B.30) to find the corresponding sums. The first one reads

$$\begin{aligned}
& \frac{1}{\beta} \sum_{-\infty}^{\infty} \frac{1}{(\nu_n + i\mu)^2 + E_f^2} \frac{1}{[\omega_n^2 + E_b^2]} = \tag{B.32} \\
& = \left(\frac{1}{E_f^2 - (E_b + \mu - i\pi T)^2} + \frac{1}{E_f^2 - (E_b - \mu + i\pi T)^2} \right) \frac{1}{4E_b^3} \left[\frac{1}{2} + n_b \left(\frac{E_b}{T} \right) + \frac{E_b}{T} \left[n_b^2 \left(\frac{E_b}{T} \right) + n_b \left(\frac{E_b}{T} \right) \right] \right] - \\
& - \left(\frac{E_b + \mu - i\pi T}{[E_f^2 - (E_b + \mu - i\pi T)^2]^2} + \frac{E_b - \mu + i\pi T}{[E_f^2 - (E_b - \mu + i\pi T)^2]^2} \right) \frac{1}{2E_b^2} \left[\frac{1}{2} + n_b \left(\frac{E_b}{T} \right) \right] + \\
& + \frac{1}{[E_b^2 - (E_f + \mu - i\pi T)^2]^2} \frac{1}{2E_f} \left[\frac{1}{2} - n_f \left(\frac{E_f + \mu}{T} \right) \right] + \frac{1}{[E_b^2 - (E_f - \mu + i\pi T)^2]^2} \frac{1}{2E_f} \left[\frac{1}{2} - n_f \left(\frac{E_f - \mu}{T} \right) \right].
\end{aligned}$$

Its physical and real part is symmetric under the exchange of $\mu \leftrightarrow -\mu$ and reads,

$$\begin{aligned}
& \text{Re} \frac{1}{\beta} \sum_{-\infty}^{\infty} \frac{1}{(\nu_n + i\mu)^2 + E_f^2} \frac{1}{[\omega_n^2 + E_b^2]} = \tag{B.33} \\
& = \frac{E_f^2 - (E_b + \mu)^2 + (\pi T)^2}{E_f^4 - 2E_f^2[(E_b + \mu)^2 - (\pi T)^2] + [(E_b + \mu)^2 + (\pi T)^2]^2} \frac{1}{4E_b^3} \left[\frac{1}{2} + n_b \left(\frac{E_b}{T} \right) + \frac{E_b}{T} \left[n_b^2 \left(\frac{E_b}{T} \right) + n_b \left(\frac{E_b}{T} \right) \right] \right] + \\
& + 2(E_b + \mu) \left(\frac{1}{E_f^4 - 2E_f^2[(E_b + \mu)^2 - (\pi T)^2] + [(E_b + \mu)^2 + (\pi T)^2]^2} + \right.
\end{aligned}$$

²However, there seem to be some typos in the corresponding formulae in Ref. [101], because some brackets are missing.

$$\begin{aligned}
& + \frac{2(-E_f^2 + [(E_b + \mu)^2 + (\pi T)^2]) [E_f^2 - (E_b + \mu)^2 + (\pi T)^2]}{(E_f^4 - 2E_f^2[(E_b + \mu)^2 - (\pi T)^2] + [(E_b + \mu)^2 + (\pi T)^2]^2)} \frac{1}{4E_b^2} \left[\frac{1}{2} + n_b\left(\frac{E_b}{T}\right) \right] \\
& - \left(\frac{1}{E_b^4 - 2E_b^2[(E_f + \mu)^2 - (\pi T)^2] + [(E_f + \mu)^2 + (\pi T)^2]^2} - \right. \\
& \left. - \frac{2(E_b^2 - [(E_f + \mu)^2 - (\pi T)^2]) [E_b^2 - (E_f + \mu)^2 + (\pi T)^2]}{(E_b^4 - 2E_b^2[(E_f + \mu)^2 - (\pi T)^2] + [(E_f + \mu)^2 + (\pi T)^2]^2)} \right) \frac{1}{2E_f^2} \left[\frac{1}{2} - n_f\left(\frac{E_f + \mu}{T}\right) \right] + \\
& + (\mu \leftrightarrow -\mu).
\end{aligned}$$

Similarly,

$$\begin{aligned}
& \frac{1}{\beta} \sum_{-\infty}^{\infty} \frac{1}{[(\nu_n + i\mu)^2 + E_f^2]^2} \frac{1}{\omega_n^2 + E_b^2} = \tag{B.34} \\
& = \left(\frac{1}{[E_f^2 - (E_b + \mu - i\pi T)^2]^2} + \frac{1}{[E_f^2 - (E_b - \mu + i\pi T)^2]^2} \right) \frac{1}{2E_b} \left[\frac{1}{2} + n_b\left(\frac{E_b}{T}\right) \right] + \\
& + \frac{1}{E_b^2 - (E_f + \mu - i\pi T)^2} \frac{1}{4E_f^3} \left[\frac{1}{2} - n_f\left(\frac{E_f + \mu}{T}\right) + \frac{E_f}{T} \left[n_f^2\left(\frac{E_f + \mu}{T}\right) - n_f\left(\frac{E_f + \mu}{T}\right) \right] \right] + \\
& + \frac{1}{E_b^2 - (E_f - \mu + i\pi T)^2} \frac{1}{4E_f^3} \left[\frac{1}{2} - n_f\left(\frac{E_f - \mu}{T}\right) + \frac{E_f}{T} \left[n_f^2\left(\frac{E_f - \mu}{T}\right) - n_f\left(\frac{E_f - \mu}{T}\right) \right] \right] \\
& - \frac{E_f + \mu - i\pi T}{[E_b^2 - (E_f + \mu - i\pi T)^2]^2} \frac{1}{2E_f^2} \left[\frac{1}{2} - n_f\left(\frac{E_f + \mu}{T}\right) \right] - \frac{E_f - \mu + i\pi T}{[E_b^2 - (E_f - \mu + i\pi T)^2]^2} \frac{1}{2E_f^2} \left[\frac{1}{2} - n_f\left(\frac{E_f - \mu}{T}\right) \right],
\end{aligned}$$

which has the following real part,

$$\begin{aligned}
& \text{Re} \frac{1}{\beta} \sum_{-\infty}^{\infty} \frac{1}{[(\nu_n + i\mu)^2 + E_f^2]^2} \frac{1}{\omega_n^2 + E_b^2} = \tag{B.35} \\
& = - \left(\frac{1}{E_f^4 - 2E_f^2[(E_b + \mu)^2 - (\pi T)^2] + [(E_b + \mu)^2 + (\pi T)^2]^2} - \right. \\
& \left. - \frac{2(E_f^2 - [(E_b + \mu)^2 - (\pi T)^2]) [E_f^2 - (E_b + \mu)^2 + (\pi T)^2]}{(E_f^4 - 2E_f^2[(E_b + \mu)^2 - (\pi T)^2] + [(E_b + \mu)^2 + (\pi T)^2]^2)} \right) \frac{1}{2E_b} \left[\frac{1}{2} + n_b\left(\frac{E_b}{T}\right) \right] + \\
& + \frac{E_b^2 - (E_f + \mu)^2 + (\pi T)^2}{E_b^4 - 2E_b^2[(E_f + \mu)^2 - (\pi T)^2] + [(E_f + \mu)^2 + (\pi T)^2]^2} \frac{1}{4E_f^3} \left[\frac{1}{2} - n_f\left(\frac{E_f + \mu}{T}\right) + \right. \\
& \left. + \frac{E_f}{T} \left[n_f^2\left(\frac{E_f + \mu}{T}\right) - n_f\left(\frac{E_f + \mu}{T}\right) \right] \right] + \\
& + 2(E_f + \mu) \left(\frac{1}{E_b^4 - 2E_b^2[(E_f + \mu)^2 - (\pi T)^2] + [(E_f + \mu)^2 + (\pi T)^2]^2} + \right. \\
& \left. + \frac{2(-E_b^2 + [(E_f + \mu)^2 + (\pi T)^2]) [E_b^2 - (E_f + \mu)^2 + (\pi T)^2]}{(E_b^4 - 2E_b^2[(E_f + \mu)^2 - (\pi T)^2] + [(E_f + \mu)^2 + (\pi T)^2]^2)} \right) \frac{1}{4E_f^2} \left[\frac{1}{2} - n_f\left(\frac{E_f + \mu}{T}\right) \right] + \\
& + (\mu \leftrightarrow -\mu).
\end{aligned}$$

B.2.3. Matsubara sum of the four-fermion interaction channel with two-fermion exchange

When calculating the β -function of the four-fermion coupling in the Gross-Neveu model at non-zero T and non-zero μ in Appendix E.1.2, one of the three types of diagrams that contributes is a fermion loop, which can be interpreted as the exchange of two virtual quarks or two virtual anti-quarks instead of a quark-anti-quark pair, see Eqs. (E.19) and (E.25). The corresponding Matsubara sum therefore differs from the other two contributions and evaluates to

$$\begin{aligned}
& \frac{1}{\beta} \sum_{n=-\infty}^{\infty} \frac{-(\nu_n + i\mu)[2(\nu_{-n} + i\mu) + (\nu_n + i\mu)] + E_f^2}{(\nu_{-n} + i\mu)^2 + E_f^2} \frac{1}{[(\nu_n + i\mu)^2 + E_f^2]^2} = \quad (\text{B.36}) \\
& = \frac{1}{4E_f} \left[\frac{1}{2(E_f + \mu - i\pi T)^2} \tanh\left(\frac{E_f + \mu}{2T}\right) + \frac{1}{2(E_f - \mu + i\pi T)^2} \tanh\left(\frac{E_f - \mu}{2T}\right) - \right. \\
& \quad \left. - \frac{1}{(E_f + \mu - i\pi T)^2} \frac{E_f + \mu - i\pi T}{T} \frac{1}{4 \cosh^2\left(\frac{E_f + \mu}{2T}\right)} - \frac{1}{(E_f - \mu + i\pi T)^2} \frac{E_f - \mu + i\pi T}{T} \frac{1}{4 \cosh^2\left(\frac{E_f - \mu}{2T}\right)} \right] = \\
& = -\frac{1}{8E_f} \frac{\partial}{\partial E_f} \left[\frac{1}{E_f + \mu - i\pi T} \tanh\left(\frac{E_f + \mu}{2T}\right) + \frac{1}{E_f - \mu + i\pi T} \tanh\left(\frac{E_f - \mu}{2T}\right) \right] = \\
& = -\frac{1}{8E_f} \frac{\partial}{\partial E_f} \left[\frac{E_f + \mu + i\pi T}{(E_f + \mu)^2 + (\pi T)^2} \tanh\left(\frac{E_f + \mu}{2T}\right) + \frac{E_f - \mu - i\pi T}{(E_f - \mu)^2 + (\pi T)^2} \tanh\left(\frac{E_f - \mu}{2T}\right) \right] = \\
& = -\frac{1}{8E_f} \frac{\partial}{\partial E_f} \left[\left(\frac{E_f + \mu}{(E_f + \mu)^2 + (\pi T)^2} \tanh\left(\frac{E_f + \mu}{2T}\right) + \frac{E_f - \mu}{(E_f - \mu)^2 + (\pi T)^2} \tanh\left(\frac{E_f - \mu}{2T}\right) \right) + \right. \\
& \quad \left. + i\pi T \left(\frac{1}{(E_f + \mu)^2 + (\pi T)^2} \tanh\left(\frac{E_f + \mu}{2T}\right) - \frac{1}{(E_f - \mu)^2 + (\pi T)^2} \tanh\left(\frac{E_f - \mu}{2T}\right) \right) \right].
\end{aligned}$$

For the sake of convenience the result is split into real and imaginary parts and expressed in terms of a derivative w.r.t. the fermion energy E_f .

We find that at $\mu = 0$ the imaginary part vanishes,

$$\begin{aligned}
\lim_{\beta\mu, \frac{\mu}{E_f} \rightarrow 0} (\text{B.36}) & = \frac{1}{4E_f} \left[\frac{E_f^2 - (\pi T)^2}{[E_f^2 + (\pi T)^2]^2} \tanh\left(\frac{E_f}{2T}\right) - \frac{1}{E_f^2 + (\pi T)^2} \frac{E_f}{T} \frac{1}{2 \cosh^2\left(\frac{E_f}{2T}\right)} \right] = \quad (\text{B.37}) \\
& = -\frac{1}{4E_f} \frac{\partial}{\partial E_f} \left[\frac{E_f}{E_f^2 + (\pi T)^2} \tanh\left(\frac{E_f}{2T}\right) \right],
\end{aligned}$$

which is discussed in the main text.

Appendix C

RG flow equations in field-space (DeWitt) notation

Abstract The actual and ultimate goal of this appendix is to answer a simple fun question: What is the common feature of FRG and horse-race betting?

Therefore, we introduce the so-called field-space notation and derive the ERG equation for generic systems from statistical physics and QFT with arbitrary field content. The field-space notation and formalism is wildly applied in the derivation of FRG flow equations and DSE to formalize the calculations and keep all steps manageable and trackable. Originally, it was introduced by B. S. DeWitt [145, 619] for all kinds of calculations in QFTs. It can be used in pen and paper calculations, but is also implemented in the DOFUN software package for MATHEMATICA [147] for the algorithmic derivation of functional flow equations [620, 621, 622], see, *e.g.*, Refs. [553, 353, 623, 624, 625, 626, 71, 627, 354, 628, 629, 630, 631] for recent applications or Ref. [632] for a novel implementation of the formalism in terms of another MATHEMATICA [147] package named QMES-DERIVATION for functional flow equations.

We start our presentation by setting up general definitions of objects in the abstract field space and discuss some of their properties as well as calculation rules, *e.g.*, commutation of field components, raising/lowering of field-space indices, or taking functional derivatives. Afterwards, we use the formalism for an elegant derivation of the ERG equation. Furthermore, we discuss projection prescriptions to derive RG flow equations from the ERG equation in field-space notation.

Disclosure This appendix partially follows Ref. [172, Sec. 3.2 and App. A], Ref. [54, especially the Apps.] as well as private notes of M. J. Steil [633]. I am also grateful to F. Divotgey, J. Eser, J. Stoll, and N. Zorbach for discussions on this topic and for sharing some of their material. However, my biggest thanks go to M. J. Steil for sharing his notes and debating the formalism.

C.1. Field-space and DeWitt notation

Here, we introduce the basic notions of the field-space formalism, respectively DeWitt notation. The starting point are some basic definitions. Afterwards we proceed with a bunch of simple calculation rules.

C.1.1. Definitions and general considerations

We start by defining the field-space vector in terms of its contravariant components,

$$(\Phi^a) \equiv (\varphi, \bar{\psi}, -\psi). \tag{C.1}$$

Hereby, φ is a multi-component bosonic field and $\bar{\psi}$ and ψ are multi-component fermionic fields over some spacetime manifold \mathcal{M} . Thus, each \mathbf{a} stands for $\mathbf{a} = a_1 a_2 \cdots a_n$, $n \in \mathbb{N}$, whereas the a_i are by themselves multi-indices of fields in Lorentz, Dirac, color, flavor *etc.* spaces, but also represent continuous arguments of the fields, like momentum dependences or spacetime coordinates, *e.g.*,

$$\varphi^{a_1} = \varphi^{b_1 b_2 \cdots b_i}(\mathbf{x}), \quad (\text{C.2})$$

where \mathbf{x} denotes the coordinates of the spacetime manifold in some basis and the b_i , $i \in \mathbb{N}$, denote the components of the fields in some basis of the corresponding spaces (Lorentz, Dirac, *etc.*). The abstract fields φ , ψ , and $\bar{\psi}$ can even involve fields that are composite objects.

To construct scalar objects in field- and all other spaces, we define a field-space scalar product by introducing the field-space metric

$$\mathbf{g}(\Phi, \Phi) \equiv \Phi^{\mathbf{a}} \Phi^{\mathbf{b}} \mathbf{g}_{\mathbf{ab}} \stackrel{!}{=} \varphi^2 - 2 \bar{\psi} \psi = \varphi^2 - \bar{\psi} \psi + \psi \bar{\psi}. \quad (\text{C.3})$$

In the last step, one uses that the fermionic fields ψ and $\bar{\psi}$ are Grassmann numbers and anti-commute (componentwise). Here, we introduce the DeWitt notation [145, 619] for the remaining contractions over generalized indices,

$$\bar{\psi} \psi \equiv \bar{\psi}_{a_1} \psi^{a_1} = \int_{\mathcal{M}} d^D \mathbf{x} \sqrt{\det(g)} \bar{\psi}_{b_1 b_2 \cdots}(\mathbf{x}) \psi^{b_1 b_2 \cdots}(\mathbf{x}), \quad (\text{C.4})$$

where \mathcal{M} is the D -dimensional spacetime manifold with metric g . (The definition for the bosonic fields φ or a momentum-space representation are analogous.)

For the components of the field-space vectors Φ and Φ' this implies

$$\Phi'^{\mathbf{a}} \Phi^{\mathbf{b}} = (-1)^{\mathbf{ab}} \Phi^{\mathbf{b}} \Phi'^{\mathbf{a}}, \quad (\text{C.5})$$

where we introduced

$$(-1)^{\mathbf{ab}} \equiv \begin{cases} -1, & \text{if } \mathbf{a} \text{ and } \mathbf{b} \text{ are indices of fermionic fields,} \\ +1, & \text{otherwise.} \end{cases} \quad (\text{C.6})$$

Hence, from Eqs. (C.3) and (C.5) it follows (using simple relabeling) that

$$\Phi^{\mathbf{a}} \Phi^{\mathbf{b}} \mathbf{g}_{\mathbf{ab}} = (-1)^{\mathbf{ab}} \Phi^{\mathbf{b}} \Phi^{\mathbf{a}} \mathbf{g}_{\mathbf{ab}} \stackrel{!}{=} \Phi^{\mathbf{b}} \Phi^{\mathbf{a}} \mathbf{g}_{\mathbf{ba}}, \quad \Rightarrow \quad \mathbf{g}_{\mathbf{ab}} = (-1)^{\mathbf{ab}} \mathbf{g}_{\mathbf{ba}}. \quad (\text{C.7})$$

Consequently, the field-space metric needs to be anti-symmetric in its fermionic components. The anti-symmetry of the metric tensor is a crucial difference to ordinary (pseudo-)Riemannian metric tensors, which are symmetric bilinear forms.

A possible choice for the field-space metric that is consistent with Eq. (C.3) is¹

$$(\mathbf{g}_{\mathbf{ab}}) \equiv \begin{pmatrix} 1 & 0 & 0 \\ 0 & 0 & 1 \\ 0 & -1 & 0 \end{pmatrix}. \quad (\text{C.8})$$

For raising and lowering the field space indices, we use the *Northwest–Southeast* (NW–SE) convention [54]. For example, for the components of the field-space vectors, this reads

$$\Phi^{\mathbf{a}} = \mathbf{g}^{\mathbf{ab}} \Phi_{\mathbf{b}} = \Phi_{\mathbf{b}} \mathbf{g}^{\mathbf{ab}}, \quad \Phi_{\mathbf{a}} = \Phi^{\mathbf{b}} \mathbf{g}_{\mathbf{ba}} = \mathbf{g}_{\mathbf{ba}} \Phi^{\mathbf{b}}. \quad (\text{C.9})$$

Here, *North* (*South*) refers to the contravariant (covariant) position of the field-space indices of the field-space metric. On the other hand, *East* (*West*) refers to the right (left) position of the open field-space index of the field-space metric, which is not contracted in Eq. (C.9).

¹Here, it should be noted that Ref. [54] uses a different sign convention.

From definition (C.1) and definition (C.9) we find

$$(\Phi_{\mathbf{a}}) \equiv (\Phi^{\mathbf{b}} \mathbf{g}_{\mathbf{b}\mathbf{a}}) = (\varphi, \psi, \bar{\psi}). \quad (\text{C.10})$$

Consequently, the inverse metric tensor needs to be

$$(\mathbf{g}^{\mathbf{ab}}) = \begin{pmatrix} 1 & 0 & 0 \\ 0 & 0 & 1 \\ 0 & -1 & 0 \end{pmatrix}. \quad (\text{C.11})$$

Otherwise, we could not recover Eq. (C.1) via $\Phi^{\mathbf{a}} = \mathbf{g}^{\mathbf{ab}} \Phi_{\mathbf{b}}$ from Eq. (C.10).

Also the inverse field-space metric tensor is anti-symmetric in its fermionic indices and we summarize,

$$\mathbf{g}^{\mathbf{ab}} = (-1)^{\mathbf{ab}} \mathbf{g}^{\mathbf{ba}}, \quad \mathbf{g}_{\mathbf{ab}} = (-1)^{\mathbf{ab}} \mathbf{g}_{\mathbf{ba}}. \quad (\text{C.12})$$

Lowering the second index of the components of the inverse metric tensor (C.11) (respectively raising the first index of the components of the metric tensor (C.8)), we obtain,

$$\mathbf{g}^{\mathbf{a}}_{\mathbf{b}} = \mathbf{g}^{\mathbf{ac}} \mathbf{g}_{\mathbf{cb}} = (-1)^{\mathbf{ab}} \delta_{\mathbf{b}}^{\mathbf{a}} = \mathbf{g}_{\mathbf{bc}} \mathbf{g}^{\mathbf{ca}}. \quad (\text{C.13})$$

The last two equal signs can be directly read off from Eqs. (C.8) and (C.11). Here, $\delta_{\mathbf{b}}^{\mathbf{a}}$ is the generalization of the Kronecker delta symbol (A.4).

On the other hand, by lowering the first index of the components of the inverse metric tensor, we find

$$\mathbf{g}_{\mathbf{a}}^{\mathbf{b}} = \mathbf{g}^{\mathbf{cb}} \mathbf{g}_{\mathbf{ca}} = \delta_{\mathbf{a}}^{\mathbf{b}} = \mathbf{g}_{\mathbf{ac}} \mathbf{g}^{\mathbf{bc}}. \quad (\text{C.14})$$

Again, the last two equal signs can be directly derived from Eqs. (C.8) and (C.11).

For the contraction of two arbitrary field space vectors Φ and Φ' one derives

$$\Phi^{\mathbf{a}} \Phi'_{\mathbf{a}} = \Phi^{\mathbf{a}} \Phi'^{\mathbf{b}} \mathbf{g}_{\mathbf{ba}} \stackrel{(\text{C.12})}{=} \Phi^{\mathbf{a}} \Phi'^{\mathbf{b}} (-1)^{\mathbf{ab}} \mathbf{g}_{\mathbf{ab}} \stackrel{(\text{C.5})}{=} \Phi'^{\mathbf{b}} \Phi^{\mathbf{a}} \mathbf{g}_{\mathbf{ab}} = \Phi'^{\mathbf{a}} \Phi_{\mathbf{a}}, \quad (\text{C.15})$$

which can also be checked explicitly with Eqs. (C.1) and (C.10).

C.1.2. Functional derivatives in field space

Having introduced some basic notation, we turn to the generalization of the “ordinary” functional derivative to the functional derivative in field space to handle fields that carry bosonic and fermionic components, at once. As usual the field-space derivative works componentwise, *i.e.*,

$$\frac{\delta \Phi_{\mathbf{a}}}{\delta \Phi_{\mathbf{b}}} \equiv \delta_{\mathbf{a}}^{\mathbf{b}}. \quad (\text{C.16})$$

It has to be linear and additive (sum rule) and needs to obey some Leibniz/product rule – as all meaningful derivatives do. Therefore, consider two functionals $\mathcal{F}[\Phi]$ and $\mathcal{G}[\Phi]$.

In order to simplify the notation, we introduce the field-space derivative as a left-derivative and use the following short-hand notation,

$$\mathcal{F}^{\mathbf{a}_n \mathbf{a}_{n-1} \dots \mathbf{a}_2 \mathbf{a}_1}[\Phi] \equiv \frac{\delta}{\delta \Phi_{\mathbf{a}_n}} \mathcal{F}^{\mathbf{a}_{n-1} \dots \mathbf{a}_2 \mathbf{a}_1}[\Phi] \equiv \frac{\delta}{\delta \Phi_{\mathbf{a}_n}} \frac{\delta}{\delta \Phi_{\mathbf{a}_{n-1}}} \dots \frac{\delta}{\delta \Phi_{\mathbf{a}_2}} \frac{\delta}{\delta \Phi_{\mathbf{a}_1}} \mathcal{F}[\Phi]. \quad (\text{C.17})$$

Interchanging the order of any two derivatives results in an additional minus sign for fermionic components,

$$\mathcal{F}^{\mathbf{a}_n \dots \mathbf{a}_j \mathbf{a}_i \dots \mathbf{a}_1}[\Phi] = (-1)^{\mathbf{a}_i \mathbf{a}_j} \mathcal{F}^{\mathbf{a}_n \dots \mathbf{a}_i \mathbf{a}_j \dots \mathbf{a}_1}[\Phi], \quad (\text{C.18})$$

which generalizes Eq. (C.5) to derivatives and correctly describes the derivative w.r.t. Grassmann numbers, *cf.* Refs. [19, 24].

The generalization of the ordinary sum rule is trivial,

$$\frac{\delta}{\delta\Phi_{\mathbf{a}_n}} (f \mathcal{F}^{\mathbf{a}_{n-1}\cdots\mathbf{a}_1}[\Phi] + g \mathcal{G}^{\mathbf{a}_{n-1}\cdots\mathbf{a}_1}[\Phi]) \equiv f \mathcal{F}^{\mathbf{a}_n\cdots\mathbf{a}_1}[\Phi] + g \mathcal{G}^{\mathbf{a}_n\cdots\mathbf{a}_1}[\Phi], \quad (\text{C.19})$$

where f and g are some arbitrary functions that do not depend on Φ .

The generalization of the Leibniz product rule is slightly more involved, because care needs to be taken concerning the fermionic components. One defines

$$\begin{aligned} \frac{\delta}{\delta\Phi_{\mathbf{a}}} (\mathcal{F}^{\mathbf{b}_n\cdots\mathbf{b}_1}[\Phi] \mathcal{G}^{\mathbf{c}_m\cdots\mathbf{c}_1}[\Phi]) &\equiv \\ &\equiv \mathcal{F}^{\mathbf{a}\mathbf{b}_n\cdots\mathbf{b}_1}[\Phi] \mathcal{G}^{\mathbf{c}_m\cdots\mathbf{c}_1}[\Phi] + (-1)^{\mathbf{a}\mathbf{b}_n} \dots (-1)^{\mathbf{a}\mathbf{b}_1} \mathcal{F}^{\mathbf{b}_n\cdots\mathbf{b}_1}[\Phi] \mathcal{G}^{\mathbf{a}\mathbf{c}_m\cdots\mathbf{c}_1}[\Phi]. \end{aligned} \quad (\text{C.20})$$

Finally, we introduce the chain rule,

$$\frac{\delta}{\delta\Phi_{\mathbf{a}}} \mathcal{F}[\mathcal{G}[\Phi]] = \mathcal{G}^{\mathbf{a}\mathbf{b}_m\cdots\mathbf{b}_1}[\Phi] \frac{\delta\mathcal{F}[\mathcal{G}[\Phi]]}{\delta\mathcal{G}^{\mathbf{b}_m\cdots\mathbf{b}_1}[\Phi]}. \quad (\text{C.21})$$

C.2. The FRG in field-space notation

Next, we turn to the derivation of the ERG equation in field-space notation. Starting from the partition function for arbitrary field theories or statistical models, we work our way to the evolution equation for the corresponding (scale-dependent) effective (average) action – the Wetterich or ERG equation. The discussion is completed by providing formulae for the RG evolution of some n -point vertex functions, which are derived from the ERG equation.

This section is not meant to be a self-consistent discussion or review of the FRG method and includes little motivation of the single steps. For these purposes we refer in parts to Part I of this thesis or Refs. [53, 550, 54, 55, 56, 100, 57, 35, 58]. However, this section can be seen as a quick guide that shall enable the reader to reproduce all results of Parts I and II of this work without extensive literature search and without omitting details of the formalism.

C.2.1. Scale-dependent generating functionals of correlation and vertex functions

The generating functional of n -point correlation functions

The generating functional for arbitrary n -point functions (expectation values) in the field-space formalism is defined as follows

$$\mathcal{Z}[\mathbf{J}] \equiv \mathcal{N} \int [d\tilde{\Phi}] \exp(-\mathcal{S}[\tilde{\Phi}] + \mathbf{J}^{\mathbf{a}} \tilde{\Phi}_{\mathbf{a}}). \quad (\text{C.22})$$

Here, the “tilde” indicates that $\tilde{\Phi}$ is the full fluctuating quantum field and the integration variable. The integral ranges over all (gauge-)inequivalent field configurations. \mathbf{J} is introduced as a source of these fields. The abstract source-field vector is assembled from bosonic and fermionic source fields,

$$(\mathbf{J}^{\mathbf{a}}) = (J, \bar{\eta}, -\eta), \quad (\text{C.23})$$

where J is the source of φ , $\bar{\eta}$ is the source of ψ , and η is the source of $\bar{\psi}$. The factor \mathcal{N} is an unobservable normalization, which drops out of any expectation value.

The partition function is simply defined as the generating functional in the absence of sources, thus $\mathcal{Z}[\mathbf{J} = 0]$.

RG-scale dependence and the regulator

In analogy to what is presented for the zero-dimensional toy model in Section 4.1.1, we introduce an additional artificial mass-like term²

$$\Delta\mathcal{S}_k[\Phi] = \frac{1}{2} R_k^{\text{ab}} \Phi_{\text{b}} \Phi_{\text{a}}, \quad (\text{C.24})$$

to the generating functional (C.22),

$$\mathcal{Z}_k[\mathbf{J}] = \mathcal{N} \int [\text{d}\tilde{\Phi}] \exp(-\mathcal{S}[\tilde{\Phi}] - \Delta\mathcal{S}_k[\tilde{\Phi}] + \mathbf{J}^{\text{a}} \tilde{\Phi}_{\text{a}}), \quad (\text{C.25})$$

which is now promoted to the scale-dependent generating functional. Equation (C.24) is called the regulator insertion and depends on the RG scale k , while R_k^{ab} itself is denoted as the regulator. By construction the regulator can only be anti-symmetric in its fermionic indices

$$R_k^{\text{ab}} = (-1)^{\text{ab}} R_k^{\text{ba}} \quad (\text{C.26})$$

and oftentimes we simply have

$$R_k^{\text{ab}} \propto \mathbf{g}^{\text{ab}}. \quad (\text{C.27})$$

Usually the regulator depends on the momenta of the fields, while the momentum integration is absorbed in the summation over field-space indices in Eq. (C.24), *cf.* Eq. (C.4). The RG scale k is of dimension energy and the regulator takes the appropriate mass dimension of the fields.

This approach of modifying the path integral by varying a dimensionful scale k is indeed the basis of the formalization of K. G. Wilson's idea of gradually integrating out momentum shells [174, 175, 19]: Here, the regulator ensures that fluctuations of modes with (Euclidean) momenta $p^2 \lesssim k^2$ are artificially suppressed, while modes of higher momenta $p^2 \gg k^2$ are by construction not affected at all. For $k \rightarrow 0$ the regulator and the regulator insertion (C.24) are supposed to vanish. Thus, the generating functional (C.25) effectively contains all information about the physics above the scale k .

In order to implement K. G. Wilson's idea without completely spoiling the original theory, the regulator therefore needs to fulfill the following requirements.

1. For $\frac{p^2}{k^2} \rightarrow 0$ at non-zero k^2 it needs to stay finite to play the role of an effective particle mass and IR regularization.
2. For $k \rightarrow 0$ it needs to vanish to recover the original QFT.
3. For $k \rightarrow \infty$ it has to diverge suitably such that the effective average action approaches the classical UV action (as will become clear below).
4. The regulator must not break any symmetries of the functional integral.
5. The regulator has to act locally in momentum space for all RG scales k .

Of course there is room for further refinement, amendments, and discussion of these criteria, see also Section 9.2.2. Nonetheless, the peculiarities of different regulators are not the main topic of this work and the interested reader is referred for example to Refs. [162, 54, 634, 165, 166, 602, 533, 167] and especially the excellent Ref. [348, App. B] for further information.

We already remark at this point that it is hardly possible to fulfill all requirements completely. Of course, this statement is to some extent trivial, since the regulator is introduced as a modification of the original theory in the first place to handle divergences and therefore has to alter the theory in one or the other way. Going from large to vanishing k we nevertheless expect at first sight that different regulators, after following different paths through theory space (modifying the path

²Note that the order of indices is different from Ref. [54].

integral in different ways at the same k), all end up at the same point – namely the original theory.

Hence, so far, for $\mathbf{J} = 0$ the scale-dependent generating functional (C.25) effectively interpolates between Gaussian-like partition functions at huge k , where the mass-like term completely dominates, and the partition function of the actual system under consideration at $k \rightarrow 0$.

We also find that the expectation value of some operator \mathcal{O} in the presence of source terms is generalized to

$$\langle \mathcal{O}_{\mathbf{b}_n \dots \mathbf{b}_1}[\tilde{\Phi}] \rangle_{k, \mathbf{J}} = \frac{1}{\mathcal{Z}_k[\mathbf{J}]} \mathcal{N} \int [d\tilde{\Phi}] \mathcal{O}_{\mathbf{b}_n \dots \mathbf{b}_1}[\tilde{\Phi}] \exp(-\mathcal{S}[\tilde{\Phi}] - \Delta \mathcal{S}_k[\tilde{\Phi}_t] + \mathbf{J}^{\mathbf{a}} \tilde{\Phi}_{\mathbf{a}}) \quad (\text{C.28})$$

and also becomes scale-dependent. For $k \rightarrow 0$ also these expectation values approach their correct physical values.

Before we continue and actually turn to the formal implementation of K. G. Wilson's RG, let us provide the field-space derivative of the regulator insertion already at this point of our calculations for later use,

$$\begin{aligned} \Delta \mathcal{S}_k^{\mathbf{ba}}[\Phi] &\stackrel{(\text{C.17})}{=} \frac{\delta}{\delta \Phi_{\mathbf{b}}} \frac{\delta}{\delta \Phi_{\mathbf{a}}} \Delta \mathcal{S}_k[\Phi] = \frac{\delta}{\delta \Phi_{\mathbf{b}}} \frac{\delta}{\delta \Phi_{\mathbf{a}}} \left(\frac{1}{2} R_k^{\mathbf{cd}} \Phi_{\mathbf{d}} \Phi_{\mathbf{c}} \right) \stackrel{(\text{C.20})}{=} \\ &= \frac{\delta}{\delta \Phi_{\mathbf{b}}} \frac{1}{2} [R_k^{\mathbf{ca}} \Phi_{\mathbf{c}} + (-1)^{\mathbf{ad}} R_k^{\mathbf{ad}} \Phi_{\mathbf{d}}] \stackrel{(\text{C.26})}{=} \\ &= \frac{\delta}{\delta \Phi_{\mathbf{b}}} (R_k^{\mathbf{ca}} \Phi_{\mathbf{c}}) = \\ &= R_k^{\mathbf{ba}}. \end{aligned} \quad (\text{C.29})$$

Secondly, we switch from the RG scale k to the RG time t as an evolution parameter. The relation between both is discussed in the first paragraphs of Appendix D.1 and shall not be repeated here.

Scale-dependent Schwinger functional and scale-dependent effective action

Next, as discussed for the zero-dimensional toy model in Section 4.1, it is convenient to switch from the generating functional for n -point correlation functions to the generating functional of their connected counterparts, which is oftentimes denoted as the (scale-dependent) Schwinger functional. Also its scale-dependent version is defined in terms of the logarithm of Eq. (C.25),

$$\mathcal{W}_t[\mathbf{J}] \equiv \ln \mathcal{Z}_t[\mathbf{J}]. \quad (\text{C.30})$$

Again, for later use, we explicitly provide two special expectation values via derivatives w.r.t. the source field. These are the one-point function,

$$\mathcal{W}_{t, \mathbf{a}_1}[\mathbf{J}] \stackrel{(\text{C.17})}{=} \frac{\delta \mathcal{W}_t[\mathbf{J}]}{\delta \mathbf{J}^{\mathbf{a}_1}} = \frac{1}{\mathcal{Z}_t[\mathbf{J}]} \frac{\delta \mathcal{Z}_t[\mathbf{J}]}{\delta \mathbf{J}^{\mathbf{a}_1}} = \frac{\mathcal{Z}_{t, \mathbf{a}_1}[\mathbf{J}]}{\mathcal{Z}_t[\mathbf{J}]} \equiv \langle \tilde{\Phi}_{t, \mathbf{a}_1} \rangle_{\mathbf{J}}, \quad (\text{C.31})$$

and the connected two-point function,

$$\begin{aligned} \mathcal{W}_{t, \mathbf{a}_2 \mathbf{a}_1}[\mathbf{J}] &= \frac{\delta^2 \mathcal{W}_t[\mathbf{J}]}{\delta \mathbf{J}^{\mathbf{a}_2} \delta \mathbf{J}^{\mathbf{a}_1}} = \frac{1}{\mathcal{Z}_t[\mathbf{J}]} \frac{\delta^2 \mathcal{Z}_t[\mathbf{J}]}{\delta \mathbf{J}^{\mathbf{a}_2} \delta \mathbf{J}^{\mathbf{a}_1}} - \frac{1}{(\mathcal{Z}_t[\mathbf{J}])^2} \frac{\delta \mathcal{Z}_t[\mathbf{J}]}{\delta \mathbf{J}^{\mathbf{a}_2}} \frac{\delta \mathcal{Z}_t[\mathbf{J}]}{\delta \mathbf{J}^{\mathbf{a}_1}} = \\ &= \frac{\mathcal{Z}_{t, \mathbf{a}_2 \mathbf{a}_1}[\mathbf{J}]}{\mathcal{Z}_t[\mathbf{J}]} - \frac{\mathcal{Z}_{t, \mathbf{a}_2}[\mathbf{J}]}{\mathcal{Z}_t[\mathbf{J}]} \frac{\mathcal{Z}_{t, \mathbf{a}_1}[\mathbf{J}]}{\mathcal{Z}_t[\mathbf{J}]} \equiv \\ &\equiv \langle \tilde{\Phi}_{t, \mathbf{a}_2} \tilde{\Phi}_{t, \mathbf{a}_1} \rangle_{\mathbf{J}} - \langle \tilde{\Phi}_{t, \mathbf{a}_2} \rangle_{\mathbf{J}} \langle \tilde{\Phi}_{t, \mathbf{a}_1} \rangle_{\mathbf{J}} \equiv \langle \tilde{\Phi}_{t, \mathbf{a}_2} \tilde{\Phi}_{t, \mathbf{a}_1} \rangle_{\mathbf{J}}^{\mathbf{c}}, \end{aligned} \quad (\text{C.32})$$

both in the presence of the source field \mathbf{J} .

However, ultimately we work with the so-called effective action of one-PI vertex functions, respectively its scale-dependent counterpart. It is defined in terms of the Legendre transform of the Schwinger functional,

$$\Gamma_t[\Phi] = \sup_{\mathbf{J}_t} \{ \mathbf{J}^a \Phi_a - \mathcal{W}_t[\mathbf{J}] \} = \hat{\mathbf{J}}_t^a[\Phi] \Phi_a - \mathcal{W}_t[\hat{\mathbf{J}}_t[\Phi]]. \quad (\text{C.33})$$

Here, Φ is called the effective field or mean field and the “hat” symbol indicates an evaluation on the supremum. The name “mean-field” derives from the following equation

$$\langle \tilde{\Phi}_{t,a} \rangle_{\hat{\mathbf{J}}_t} = \mathcal{W}_{t,a}[\hat{\mathbf{J}}_t[\Phi]] = \left. \frac{\delta \mathcal{W}_t[\mathbf{J}]}{\delta \mathbf{J}^a} \right|_{\mathbf{J}=\hat{\mathbf{J}}_t[\Phi]} \equiv \Phi_a, \quad (\text{C.34})$$

which relates Φ to the expectation values of the fluctuating field $\tilde{\Phi}$. On the other hand, we can relate the one-point vertex to the source fields of the composite operators via,

$$\begin{aligned} \Gamma_t^a[\Phi] &\stackrel{(\text{C.17})}{=} \frac{\delta \Gamma_t[\Phi]}{\delta \Phi_a} \stackrel{(\text{C.20})}{=} \frac{\delta \hat{\mathbf{J}}_t^b[\Phi]}{\delta \Phi_a} \Phi_b + (-1)^{ab} \hat{\mathbf{J}}_t^b[\Phi] \frac{\delta \Phi_b}{\delta \Phi_a} - \left. \frac{\delta \hat{\mathbf{J}}_t^b[\Phi]}{\delta \Phi_a} \frac{\delta \mathcal{W}_t[\mathbf{J}]}{\delta \mathbf{J}^b} \right|_{\mathbf{J}=\hat{\mathbf{J}}_t[\Phi]} \stackrel{(\text{C.34})}{=} \\ &= (-1)^{ab} \delta_b^a \hat{\mathbf{J}}_t^b[\Phi] \stackrel{(\text{C.13})}{=} \\ &= \mathbf{g}_b^a \hat{\mathbf{J}}_t^b[\Phi]. \end{aligned} \quad (\text{C.35})$$

Now, we have all ingredients at hand for the derivation of the ERG equation.

C.2.2. RG flow equations for generating functionals

So far we solely defined generating functionals for our theory which are effectively truncated at some sliding IR scale k . In order to describe an evolution from the UV, where $k = \Lambda$, to the IR, thus $k \rightarrow 0$, respectively from $t = 0$ to $t \rightarrow \infty$, we need an evolution equation.³

The flow equation for the generating functional of connected n -point correlation functions Such flow equations for $\mathcal{Z}_t[\mathbf{J}]$ and $\mathcal{W}_t[\mathbf{J}]$ are straightforwardly derived by taking a derivative w.r.t. the RG time t ,

$$\begin{aligned} \frac{d}{dt} \mathcal{W}_t[\mathbf{J}] &\stackrel{(\text{C.30})}{=} \frac{d}{dt} \ln \mathcal{Z}_t[\mathbf{J}] = \frac{1}{\mathcal{Z}_t[\mathbf{J}]} \frac{d}{dt} \mathcal{Z}_t[\mathbf{J}] \stackrel{(\text{C.25})}{=} \\ &= \frac{1}{\mathcal{Z}_t[\mathbf{J}]} \mathcal{N} \int [d\tilde{\Phi}] \frac{d}{dt} \exp\left(-\mathcal{S}[\tilde{\Phi}] - \frac{1}{2} R_t^{ab} \tilde{\Phi}_b \tilde{\Phi}_a + \mathbf{J}^a \tilde{\Phi}_a\right) \stackrel{(\text{C.28}),(\text{C.29})}{=} \\ &= -\left(\frac{1}{2} \partial_t R_t^{ab}\right) \langle \tilde{\Phi}_{t,b} \tilde{\Phi}_{t,a} \rangle_{\mathbf{J}} \stackrel{(\text{C.32})}{=} \\ &= -\left(\frac{1}{2} \partial_t R_t^{ab}\right) \mathcal{W}_{t,ba}[\mathbf{J}] - \left(\frac{1}{2} \partial_t R_t^{ab}\right) \langle \tilde{\Phi}_{t,b} \rangle_{\mathbf{J}} \langle \tilde{\Phi}_{t,a} \rangle_{\mathbf{J}} \stackrel{(\text{C.31})}{=} \\ &= -\left(\frac{1}{2} \partial_t R_t^{ab}\right) (\mathcal{W}_{t,ba}[\mathbf{J}] + \mathcal{W}_{t,b}[\mathbf{J}] \mathcal{W}_{t,a}[\mathbf{J}]), \end{aligned} \quad (\text{C.36})$$

where we used the relations referenced on top of the equal signs.

³Depending on the model at hand, it is possible to send the UV-cutoff Λ to infinity and remove it from the system.

The scale-dependent effective average action Instead of deriving a similar flow equation for the scale-dependent effective action (C.33) itself, we introduce the scale-dependent effective average action,

$$\bar{\Gamma}_t[\Phi] \equiv \Gamma_t[\Phi] - \Delta\mathcal{S}_t[\Phi]. \quad (\text{C.37})$$

In the IR for $k \rightarrow 0$ ($t \rightarrow \infty$) the regulator insertion vanishes and both coincide. In any case, we see below that it is the effective average action that approaches the classical UV action for $k \rightarrow \Lambda$, and not $\Gamma_t[\Phi]$ itself.

For the derivation of the flow equation of Eq. (C.37), we need some additional relations. The first one is a relation for the one-point vertex function,

$$\bar{\Gamma}_t^{\mathbf{a}}[\Phi] + \Delta\mathcal{S}_t^{\mathbf{a}}[\Phi] \equiv (\bar{\Gamma}_t[\Phi] + \Delta\mathcal{S}_t[\Phi])^{\mathbf{a}} = \Gamma_t^{\mathbf{a}}[\Phi] \stackrel{(\text{C.35})}{=} \mathbf{g}_{\mathbf{b}}^{\mathbf{a}} \hat{\mathbf{J}}_t^{\mathbf{b}}[\Phi]. \quad (\text{C.38})$$

Furthermore, using Eq. (C.32) we find

$$\frac{\delta\Phi_{\mathbf{a}}}{\delta\hat{\mathbf{J}}_t^{\mathbf{b}}[\Phi]} = \left. \frac{\delta^2\mathcal{W}_t[\mathbf{J}]}{\delta\mathbf{J}^{\mathbf{b}}\delta\mathbf{J}^{\mathbf{a}}} \right|_{\mathbf{J}=\hat{\mathbf{J}}_t[\Phi]} = \mathcal{W}_{t,\mathbf{ba}}[\hat{\mathbf{J}}_t[\Phi]]. \quad (\text{C.39})$$

From these two results, we can derive a general identity between the connected two-point correlation function in the presence of source fields and the field-dependent two-point vertex function expressed in terms of the scale-dependent effective average action,

$$\begin{aligned} \mathbf{g}_{\mathbf{b}}^{\mathbf{a}} &= \frac{\delta}{\delta\hat{\mathbf{J}}_t^{\mathbf{b}}[\Phi]} (\bar{\Gamma}_t[\Phi] + \Delta\mathcal{S}_t[\Phi])^{\mathbf{a}} = \\ &= \frac{\delta\Phi_{\mathbf{c}}}{\delta\hat{\mathbf{J}}_t^{\mathbf{b}}[\Phi]} \frac{\delta}{\delta\Phi_{\mathbf{c}}} (\bar{\Gamma}_t[\Phi] + \Delta\mathcal{S}_t[\Phi])^{\mathbf{a}} \stackrel{(\text{C.39})}{=} \\ &= \mathcal{W}_{t,\mathbf{bc}}[\hat{\mathbf{J}}_t[\Phi]] (\bar{\Gamma}_t[\Phi] + \Delta\mathcal{S}_t[\Phi])^{\mathbf{ca}}. \end{aligned} \quad (\text{C.40})$$

It follows that these two objects are inverse to each other. Thus,

$$\delta_{\mathbf{b}}^{\mathbf{a}} \stackrel{!}{=} (\bar{\Gamma}_t[\Phi] + \Delta\mathcal{S}_t[\Phi])^{\mathbf{ac}} (\bar{\Gamma}_t[\Phi] + \Delta\mathcal{S}_t[\Phi])_{\mathbf{cb}}^{-1} \quad (\text{C.41})$$

defines the full propagator in terms of the inverse two-point vertex function, respectively the connected two-point correlation function,

$$G_{t,\mathbf{ab}}[\Phi] \equiv \mathbf{g}_{\mathbf{a}}^{\mathbf{c}} (\bar{\Gamma}_t[\Phi] + \Delta\mathcal{S}_t[\Phi])_{\mathbf{cb}}^{-1} = \mathcal{W}_{t,\mathbf{ab}}[\hat{\mathbf{J}}_t[\Phi]]. \quad (\text{C.42})$$

The ERG equation – a flow equation for the scale-dependent effective average action

Now, we have all ingredients at hand to derive a flow equation for the scale-dependent effective average action Eq. (C.37) by taking a derivative w.r.t. RG time t . We further use Eqs. (C.33) and (C.36) and find,

$$\begin{aligned} \frac{d}{dt} \bar{\Gamma}_t[\Phi] &\stackrel{(\text{C.33})}{=} \\ &= (\partial_t \hat{\mathbf{J}}_t^{\mathbf{a}}[\Phi]) \Phi_{\mathbf{a}} - (\partial_t \hat{\mathbf{J}}_t^{\mathbf{a}}[\Phi]) \mathcal{W}_{t,\mathbf{a}}[\hat{\mathbf{J}}_t[\Phi]] - \partial_t \mathcal{W}_t[\hat{\mathbf{J}}_t[\Phi]] - \left(\frac{1}{2} \partial_t R_t^{\mathbf{ab}}\right) \Phi_{\mathbf{b}} \Phi_{\mathbf{a}} = \\ &= -\partial_t \mathcal{W}_t[\hat{\mathbf{J}}_t[\Phi]] - \left(\frac{1}{2} \partial_t R_t^{\mathbf{ab}}\right) \Phi_{\mathbf{b}} \Phi_{\mathbf{a}} \stackrel{(\text{C.36})}{=} \\ &= \left(\frac{1}{2} \partial_t R_t^{\mathbf{ab}}\right) (\mathcal{W}_{t,\mathbf{ba}}[\hat{\mathbf{J}}_t[\Phi]] + \mathcal{W}_{t,\mathbf{b}}[\hat{\mathbf{J}}_t[\Phi]] \mathcal{W}_{t,\mathbf{a}}[\hat{\mathbf{J}}_t[\Phi]]) - \left(\frac{1}{2} \partial_t R_t^{\mathbf{ab}}\right) \Phi_{\mathbf{b}} \Phi_{\mathbf{a}} \stackrel{(\text{C.34})}{=} \end{aligned} \quad (\text{C.43})$$

$$\begin{aligned}
&= \left(\frac{1}{2} \partial_t R_t^{\text{ab}}\right) \mathcal{W}_{t,\text{ba}}[\hat{\mathbf{J}}_t[\Phi]] \stackrel{\text{(C.42)}}{=} \\
&= \left(\frac{1}{2} \partial_t R_t^{\text{ab}}\right) \mathbf{g}_{\mathbf{b}}^{\mathbf{c}} (\bar{\Gamma}_t^{(2)}[\Phi] + R_t)_{\mathbf{ca}}^{-1} \stackrel{\text{(C.42)}}{=} \\
&= \left(\frac{1}{2} \partial_t R_t^{\text{ab}}\right) G_{t,\text{ba}}[\Phi] = \\
&= \text{Tr} \left[\left(\frac{1}{2} \partial_t R_t\right) G_t[\Phi] \right],
\end{aligned}$$

where we again referenced the relations used for each single step at the end of the equation. Hence, in full generality the ERG equation reads

$$\frac{d}{dt} \bar{\Gamma}_t[\Phi] = \text{Tr} \left[\left(\frac{1}{2} \partial_t R_t\right) G_t[\Phi] \right]. \quad (\text{C.44})$$

C.2.3. UV initial condition for the ERG equation

Next, we have to turn to the initial condition of the functional partial-integro differential Eq. (C.44). For this purpose, we return to Defs. (C.25), (C.30), and (C.37) and combine them to study the UV limit, hence $k \rightarrow \Lambda \rightarrow \infty$.

The starting point is the relation,

$$e^{-\bar{\Gamma}_k[\Phi]} = \mathcal{N} \int [d\tilde{\Phi}] \exp(-\mathcal{S}[\tilde{\Phi}] - \Delta \mathcal{S}_k[\tilde{\Phi}] + \hat{\mathbf{J}}_t^{\mathbf{a}}[\Phi] \tilde{\Phi}_{\mathbf{a}} + \Delta \mathcal{S}_k[\Phi] - \hat{\mathbf{J}}_t^{\mathbf{a}}[\Phi] \Phi_{\mathbf{a}}). \quad (\text{C.45})$$

Shifting the integration variable, the fluctuating quantum field $\tilde{\Phi}$, about the mean-field Φ , similar to the background-field formalism [145, 173], we find

$$\begin{aligned}
e^{-\bar{\Gamma}_k[\Phi]} &= \\
&= \mathcal{N} \int [d\tilde{\Phi}] \exp(-\mathcal{S}[\Phi + \tilde{\Phi}] - \Delta \mathcal{S}_k[\Phi + \tilde{\Phi}] + \hat{\mathbf{J}}_k^{\mathbf{a}}[\Phi] \tilde{\Phi}_{\mathbf{a}} + \Delta \mathcal{S}_k[\Phi]) \stackrel{\text{(C.24)}}{=} \\
&= \mathcal{N} \int [d\tilde{\Phi}] \exp(-\mathcal{S}[\Phi + \tilde{\Phi}] - \Delta \mathcal{S}_k[\tilde{\Phi}] + \hat{\mathbf{J}}_k^{\mathbf{a}}[\Phi] \tilde{\Phi}_{\mathbf{a}} - R_k^{\text{ab}} \Phi_{\mathbf{b}} \tilde{\Phi}_{\mathbf{a}}) \stackrel{\text{(C.35)}}{=} \\
&= \mathcal{N} \int [d\tilde{\Phi}] \exp(-\mathcal{S}[\Phi + \tilde{\Phi}] - \Delta \mathcal{S}_k[\tilde{\Phi}] + \Gamma_k^{\mathbf{a}}[\Phi] \tilde{\Phi}_{\mathbf{a}} - \Delta \mathcal{S}_t^{\mathbf{a}}[\Phi] \tilde{\Phi}_{\mathbf{a}}) \stackrel{\text{(C.38)}}{=} \\
&= \mathcal{N} \int [d\tilde{\Phi}] \exp(-\mathcal{S}[\Phi + \tilde{\Phi}] - \Delta \mathcal{S}_k[\tilde{\Phi}] + \bar{\Gamma}_k^{\mathbf{a}}[\Phi] \tilde{\Phi}_{\mathbf{a}}).
\end{aligned} \quad (\text{C.46})$$

Next, we use that the regulator has to diverge for $k \rightarrow \Lambda \rightarrow \infty$, such that we can approximate

$$\lim_{k \rightarrow \Lambda \rightarrow \infty} e^{-\Delta \mathcal{S}_k[\tilde{\Phi}]} \sim \delta[\tilde{\Phi}]. \quad (\text{C.47})$$

This functional δ -distribution leads to a collapse of the integral in the previous expression. We find, as desired, that the scale-dependent effective average action approaches the classical microscopic action for $k \rightarrow \infty$.

$$\bar{\Gamma}_{k \rightarrow \infty}[\Phi] = \mathcal{S}[\Phi] + \text{const.} \quad (\text{C.48})$$

The ‘‘constant’’ term is field-independent, but may diverge for $k \rightarrow \infty$. However, a constant (divergent) shift can be ignored, as discussed in Section 4.2.2 and Ref. [1].

C.2.4. Projections and RG flow equations for vertices

There is only a limited number of QFTs or approximations where the ERG equation (C.44) can be solved (numerically) in full generality. Usually for all kinds of practical applications one uses approximations of this equation. To this end, one formulates an ansatz function for the scale-dependent effective average action that is compatible with the UV initial condition (C.48), but also allows for the evolution of additional/all other couplings *etc.*. In a lot of cases it is therefore required to project Eq. (C.44) onto differential equations for these single couplings/vertices. This is done by taking functional derivatives of Eq. (C.44) w.r.t. the fields Φ and one ends up with an infinite tower of coupled functional differential equations for the field- and scale-dependent one-PI n -point vertex functions. To render this system manageable, one chooses some arbitrary background-field configuration to get rid of the functional structure of the coupled differential equations and one artificially truncates the system. The specifications of an appropriate truncation is up to the user and there is a lot of ongoing debate on sensible truncations. At this point, we do not go into detail, but refer for example to the discussions in Refs. [635, 53, 35]. Here, we exclusively show, how to formalize the derivation of these RG flow equations from the ERG and thus keeping track of all signs for arbitrary QFTs.

Derivatives of the propagator Because it is required to compute field-space derivatives of Eq. (C.44), it is wise to first consider the derivative of the full propagator. We use

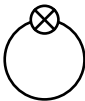
$$\begin{aligned}
 0 &= \frac{\delta}{\delta \Phi_c} \mathbf{g}^a_b = & (C.49) \\
 &= \frac{\delta}{\delta \Phi_c} \left[G_{t,ba_1}[\Phi] (\bar{\Gamma}_t[\Phi] + \Delta \mathcal{S}_t[\Phi])^{a_1 a} \right] \stackrel{(C.20)}{=} \\
 &= \left(\frac{\delta}{\delta \Phi_c} G_{t,ba_1}[\Phi] \right) (\bar{\Gamma}_t[\Phi] + \Delta \mathcal{S}_t[\Phi])^{a_1 a} + (-1)^{cb} (-1)^{ca_1} G_{t,ba_1}[\Phi] \bar{\Gamma}_t^{ca_1 a},
 \end{aligned}$$

and obtain,

$$\begin{aligned}
 \frac{\delta}{\delta \Phi_c} G_{t,ba}[\Phi] &= - (-1)^{cb} (-1)^{ca_1} G_{t,ba_1}[\Phi] \bar{\Gamma}_t^{ca_1 a_2} \mathbf{g}^{a_3}_{a_2} G_{t,a_3 a}[\Phi] = & (C.50) \\
 &= - (-1)^{cb} G_{t,ba_1}[\Phi] \bar{\Gamma}_t^{a_1 ca_2} \mathbf{g}^{a_3}_{a_2} G_{t,a_3 a}[\Phi].
 \end{aligned}$$

RG flow equations for scale-dependent one-PI n -point vertex functions The starting point for the derivation of flow equations for the scale-dependent one-PI n -point vertex functions is the ERG equation,

$$\begin{aligned}
 \partial_t \bar{\Gamma}_t[\Phi] &= \left(\frac{1}{2} \partial_t R_t^{a_1 a_2} \right) G_{t,a_2 a_1}[\Phi] = & (C.51) \\
 &= \text{Tr} \left[\left(\frac{1}{2} \partial_t R_t \right) G_t[\Phi] \right] =
 \end{aligned}$$

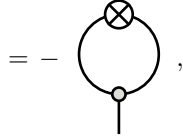
$$= \text{Tr} \left[\text{Diagram} \right].$$


Here, we also introduced the common diagrammatic notation in terms of “FRG-customized” Feynman rules: The derivative of the regulator (including the factor $\frac{1}{2}$) is pictured as a crossed circle.

The full propagator is represented by a black solid line and vertices are depicted as small circles with gray filling and the so-called “amputated” short external legs (see below). The trace is illustrated by the ordered concatenation of the single objects to a closed loop.

Now, let us apply a derivative w.r.t. Φ to the previous equation. Using Eq. (C.50) we find the evolution equation for the one-point vertex function

$$\begin{aligned} \partial_t \bar{\Gamma}_t^{(1)\mathbf{a}}[\Phi] &= -(-1)^{\mathbf{aa}_2} \left(\frac{1}{2} \partial_t R_t^{\mathbf{a}_1 \mathbf{a}_2}\right) G_{t, \mathbf{a}_2 \mathbf{a}_3}[\Phi] \bar{\Gamma}_t^{(3)\mathbf{a}_3 \mathbf{a}_4}[\Phi] \mathbf{g}_{\mathbf{a}_4}^{\mathbf{a}_5} G_{t, \mathbf{a}_5 \mathbf{a}_1}[\Phi] = \\ &= -\text{STr} \left[\left(\frac{1}{2} \partial_t R_t\right) G_t[\Phi] \bar{\Gamma}_t^{(3)\mathbf{a}} G_t[\Phi] \right] = \end{aligned} \quad (\text{C.52})$$



which in turn depends on the three-point vertex function. On a diagrammatic level taking the derivative of Eq. (C.51) w.r.t. Φ simply corresponds to attaching a vertex to the loop.

Taking another derivative w.r.t. Φ , we obtain

$$\begin{aligned} \partial_t \bar{\Gamma}_t^{(2)\mathbf{ba}}[\Phi] &= \\ &= (-1)^{\mathbf{ba}_2} (-1)^{\mathbf{aa}_2} \left(\frac{1}{2} \partial_t R_t^{\mathbf{a}_1 \mathbf{a}_2}\right) G_{t, \mathbf{a}_2 \mathbf{a}_3}[\Phi] \bar{\Gamma}_t^{(3)\mathbf{a}_3 \mathbf{ba}_4}[\Phi] \mathbf{g}_{\mathbf{a}_4}^{\mathbf{a}_5} G_{t, \mathbf{a}_5 \mathbf{a}_6}[\Phi] \bar{\Gamma}_t^{(3)\mathbf{a}_6 \mathbf{aa}_7}[\Phi] \mathbf{g}_{\mathbf{a}_7}^{\mathbf{a}_8} \times \\ &\quad \times G_{t, \mathbf{a}_8 \mathbf{a}_1}[\Phi] - \\ &\quad - (-1)^{\mathbf{ba}_2} (-1)^{\mathbf{aa}_2} \left(\frac{1}{2} \partial_t R_t^{\mathbf{a}_1 \mathbf{a}_2}\right) G_{t, \mathbf{a}_2 \mathbf{a}_3}[\Phi] \bar{\Gamma}_t^{(4)\mathbf{a}_3 \mathbf{baa}_4}[\Phi] \mathbf{g}_{\mathbf{a}_4}^{\mathbf{a}_5} G_{t, \mathbf{a}_5 \mathbf{a}_1}[\Phi] + \\ &\quad + (-1)^{\mathbf{ba}_5} (-1)^{\mathbf{ba}_4} (-1)^{\mathbf{ba}} (-1)^{\mathbf{ba}_2} (-1)^{\mathbf{aa}_2} \left(\frac{1}{2} \partial_t R_t^{\mathbf{a}_1 \mathbf{a}_2}\right) G_{t, \mathbf{a}_2 \mathbf{a}_3}[\Phi] \bar{\Gamma}_t^{(3)\mathbf{a}_3 \mathbf{aa}_4}[\Phi] \mathbf{g}_{\mathbf{a}_4}^{\mathbf{a}_5} \times \\ &\quad \times G_{t, \mathbf{a}_5 \mathbf{a}_6}[\Phi] \bar{\Gamma}_t^{(3)\mathbf{a}_6 \mathbf{ba}_7}[\Phi] \mathbf{g}_{\mathbf{a}_7}^{\mathbf{a}_8} G_{t, \mathbf{a}_8 \mathbf{a}_1}[\Phi] = \\ &= \text{STr} \left[\left(\frac{1}{2} \partial_t R_t\right) G_t[\Phi] \bar{\Gamma}_t^{(3)\mathbf{b}} G_t[\Phi] \bar{\Gamma}_t^{(3)\mathbf{a}} G_t[\Phi] \right] - \\ &\quad - \text{STr} \left[\left(\frac{1}{2} \partial_t R_t\right) G_t[\Phi] \bar{\Gamma}_t^{(4)\mathbf{ba}} G_t[\Phi] \right] + \\ &\quad + \text{STr} \left[\left(\frac{1}{2} \partial_t R_t\right) G_t[\Phi] \bar{\Gamma}_t^{(3)\mathbf{a}} G_t[\Phi] \bar{\Gamma}_t^{(3)\mathbf{b}} G_t[\Phi] \right] = \\ &= \left(\text{Diagram 1} + 1 \text{ permutation} \right) - \text{Diagram 2} . \end{aligned} \quad (\text{C.54})$$

In the second line we used that $\bar{\Gamma}_t^{\mathbf{ba}_3 \mathbf{aa}_4} = (-1)^{\mathbf{ba}_3} \bar{\Gamma}_t^{\mathbf{a}_3 \mathbf{baa}_4}$ such that a factor $(-1)^{\mathbf{ba}_3}$, which stems from the Leibniz rule, cancels. The diagrammatic result is rather intuitive: Either we attach another vertex at the left or right of the first vertex to the loop (first two diagrams) or we increase the order of the existing vertex (third diagram).

Now, we can go on and find,

$$\begin{aligned}
& \partial_t \bar{\Gamma}_t^{(3) \text{cba}}[\Phi] = \tag{C.55} \\
& = -(-1)^{\text{ca}_2} (-1)^{\text{ba}_2} (-1)^{\text{aa}_2} \left(\frac{1}{2} \partial_t R_t^{\text{a}_1 \text{a}_2}\right) G_{t, \text{a}_2 \text{a}_3}[\Phi] \bar{\Gamma}_t^{(3) \text{a}_3 \text{ca}_4}[\Phi] \mathbf{g}_{\text{a}_4}^{\text{a}_5} G_{t, \text{a}_5 \text{a}_6}[\Phi] \times \\
& \quad \times \bar{\Gamma}_t^{(3) \text{a}_6 \text{ba}_7}[\Phi] \mathbf{g}_{\text{a}_7}^{\text{a}_8} G_{t, \text{a}_8 \text{a}_9}[\Phi] \bar{\Gamma}_t^{(3) \text{a}_9 \text{aa}_{10}}[\Phi] \mathbf{g}_{\text{a}_{10}}^{\text{a}_{11}} G_{t, \text{a}_{11} \text{a}_1}[\Phi] + \\
& + (-1)^{\text{ca}_2} (-1)^{\text{ba}_2} (-1)^{\text{aa}_2} \left(\frac{1}{2} \partial_t R_t^{\text{a}_1 \text{a}_2}\right) G_{t, \text{a}_2 \text{a}_3}[\Phi] \bar{\Gamma}_t^{(4) \text{a}_3 \text{cba}_4}[\Phi] \mathbf{g}_{\text{a}_4}^{\text{a}_5} \times \\
& \quad \times G_{t, \text{a}_5 \text{a}_6}[\Phi] \bar{\Gamma}_t^{(3) \text{a}_6 \text{aa}_7}[\Phi] \mathbf{g}_{\text{a}_7}^{\text{a}_8} G_{t, \text{a}_8 \text{a}_1}[\Phi] - \\
& - (-1)^{\text{ca}_5} (-1)^{\text{ca}_4} (-1)^{\text{cb}} (-1)^{\text{ca}_2} (-1)^{\text{ba}_2} (-1)^{\text{aa}_2} \left(\frac{1}{2} \partial_t R_t^{\text{a}_1 \text{a}_2}\right) G_{t, \text{a}_2 \text{a}_3}[\Phi] \times \\
& \quad \times \bar{\Gamma}_t^{(3) \text{a}_3 \text{ba}_4}[\Phi] \mathbf{g}_{\text{a}_4}^{\text{a}_5} G_{t, \text{a}_5 \text{a}_6}[\Phi] \bar{\Gamma}_t^{(3) \text{a}_6 \text{ca}_7}[\Phi] \mathbf{g}_{\text{a}_7}^{\text{a}_8} G_{t, \text{a}_8 \text{a}_9}[\Phi] \times \\
& \quad \times \bar{\Gamma}_t^{(3) \text{a}_9 \text{aa}_{10}}[\Phi] \mathbf{g}_{\text{a}_{10}}^{\text{a}_{11}} G_{t, \text{a}_{11} \text{a}_1}[\Phi] + \\
& + (-1)^{\text{ca}_5} (-1)^{\text{ca}_4} (-1)^{\text{cb}} (-1)^{\text{ca}_2} (-1)^{\text{ba}_2} (-1)^{\text{aa}_2} \left(\frac{1}{2} \partial_t R_t^{\text{a}_1 \text{a}_2}\right) G_{t, \text{a}_2 \text{a}_3}[\Phi] \times \\
& \quad \times \bar{\Gamma}_t^{(3) \text{a}_3 \text{ba}_4}[\Phi] \mathbf{g}_{\text{a}_4}^{\text{a}_5} G_{t, \text{a}_5 \text{a}_6}[\Phi] \bar{\Gamma}_t^{(4) \text{a}_6 \text{caa}_7}[\Phi] \mathbf{g}_{\text{a}_7}^{\text{a}_8} G_{t, \text{a}_8 \text{a}_1}[\Phi] - \\
& - (-1)^{\text{ca}_8} (-1)^{\text{ca}_7} (-1)^{\text{ca}} (-1)^{\text{ca}_5} (-1)^{\text{ca}_4} (-1)^{\text{cb}} (-1)^{\text{ca}_2} (-1)^{\text{ba}_2} (-1)^{\text{aa}_2} \left(\frac{1}{2} \partial_t R_t^{\text{a}_1 \text{a}_2}\right) \times \\
& \quad \times G_{t, \text{a}_2 \text{a}_3}[\Phi] \bar{\Gamma}_t^{(3) \text{a}_3 \text{ba}_4}[\Phi] \mathbf{g}_{\text{a}_4}^{\text{a}_5} G_{t, \text{a}_5 \text{a}_6}[\Phi] \bar{\Gamma}_t^{(3) \text{a}_6 \text{aa}_7}[\Phi] \mathbf{g}_{\text{a}_7}^{\text{a}_8} G_{t, \text{a}_8 \text{a}_9}[\Phi] \times \\
& \quad \times \bar{\Gamma}_t^{(3) \text{a}_9 \text{ca}_{10}}[\Phi] \mathbf{g}_{\text{a}_{10}}^{\text{a}_{11}} G_{t, \text{a}_{11} \text{a}_1}[\Phi] + \\
& + (-1)^{\text{ca}_2} (-1)^{\text{ba}_2} (-1)^{\text{aa}_2} \left(\frac{1}{2} \partial_t R_t^{\text{a}_1 \text{a}_2}\right) G_{t, \text{a}_2 \text{a}_3}[\Phi] \bar{\Gamma}_t^{(3) \text{a}_3 \text{ca}_4}[\Phi] \mathbf{g}_{\text{a}_4}^{\text{a}_5} \times \\
& \quad \times G_{t, \text{a}_5 \text{a}_6}[\Phi] \bar{\Gamma}_t^{(4) \text{a}_6 \text{baa}_7}[\Phi] \mathbf{g}_{\text{a}_7}^{\text{a}_8} G_{t, \text{a}_8 \text{a}_1}[\Phi] - \\
& - (-1)^{\text{ca}_2} (-1)^{\text{ba}_2} (-1)^{\text{aa}_2} \left(\frac{1}{2} \partial_t R_t^{\text{a}_1 \text{a}_2}\right) G_{t, \text{a}_2 \text{a}_3}[\Phi] \bar{\Gamma}_t^{(5) \text{a}_3 \text{cbaa}_4}[\Phi] \mathbf{g}_{\text{a}_4}^{\text{a}_5} G_{t, \text{a}_5 \text{a}_1}[\Phi] + \\
& + (-1)^{\text{ca}_5} (-1)^{\text{ca}_4} (-1)^{\text{ca}} (-1)^{\text{cb}} (-1)^{\text{ca}_2} (-1)^{\text{ba}_2} (-1)^{\text{aa}_2} \left(\frac{1}{2} \partial_t R_t^{\text{a}_1 \text{a}_2}\right) G_{t, \text{a}_2 \text{a}_3}[\Phi] \times \\
& \quad \times \bar{\Gamma}_t^{(4) \text{a}_3 \text{baa}_4}[\Phi] \mathbf{g}_{\text{a}_4}^{\text{a}_5} G_{t, \text{a}_5 \text{a}_6}[\Phi] \bar{\Gamma}_t^{(3) \text{a}_6 \text{ca}_7}[\Phi] \mathbf{g}_{\text{a}_7}^{\text{a}_8} G_{t, \text{a}_8 \text{a}_1}[\Phi] - \\
& - (-1)^{\text{ca}_2} (-1)^{\text{ba}_5} (-1)^{\text{ba}_4} (-1)^{\text{ba}} (-1)^{\text{ba}_2} (-1)^{\text{aa}_2} \left(\frac{1}{2} \partial_t R_t^{\text{a}_1 \text{a}_2}\right) G_{t, \text{a}_2 \text{a}_3}[\Phi] \times \\
& \quad \times \bar{\Gamma}_t^{(3) \text{a}_3 \text{ca}_4}[\Phi] \mathbf{g}_{\text{a}_4}^{\text{a}_5} G_{t, \text{a}_5 \text{a}_6}[\Phi] \bar{\Gamma}_t^{(3) \text{a}_6 \text{aa}_7}[\Phi] \mathbf{g}_{\text{a}_7}^{\text{a}_8} G_{t, \text{a}_8 \text{a}_9}[\Phi] \times \\
& \quad \times \bar{\Gamma}_t^{(3) \text{a}_9 \text{ba}_{10}}[\Phi] \mathbf{g}_{\text{a}_{10}}^{\text{a}_{11}} G_{t, \text{a}_{11} \text{a}_1}[\Phi] + \\
& + (-1)^{\text{ca}_2} (-1)^{\text{ba}_5} (-1)^{\text{ba}_4} (-1)^{\text{ba}} (-1)^{\text{ba}_2} (-1)^{\text{aa}_2} \left(\frac{1}{2} \partial_t R_t^{\text{a}_1 \text{a}_2}\right) G_{t, \text{a}_2 \text{a}_3}[\Phi] \times
\end{aligned}$$

$$\begin{aligned}
&= - \left(\begin{array}{c} \text{Diagram 1} \\ + 5 \text{ permutations} \end{array} \right) + \left(\begin{array}{c} \text{Diagram 2} \\ + 5 \text{ permutations} \end{array} \right) - \\
&\quad - \begin{array}{c} \text{Diagram 3} \end{array} ,
\end{aligned}$$

for the generic flow equation of the three-point vertex, and

$$\partial_t \bar{\Gamma}_t^{(4) \text{ dcba}}[\Phi] = \tag{C.56}$$

$$\begin{aligned}
&= \dots + \\
&\quad + (-1)^{\mathbf{da}_5} (-1)^{\mathbf{da}_4} (-1)^{\mathbf{db}} (-1)^{\mathbf{dc}} (-1)^{\mathbf{da}_2} (-1)^{\mathbf{ca}_2} (-1)^{\mathbf{ba}_2} (-1)^{\mathbf{aa}_2} \times \\
&\quad \times \left(\frac{1}{2} \partial_t R_t^{\mathbf{a}_1 \mathbf{a}_2} \right) G_{t, \mathbf{a}_2 \mathbf{a}_3}[\Phi] \bar{\Gamma}_t^{(4) \mathbf{a}_3 \mathbf{cba}_4}[\Phi] \mathbf{g}_{\mathbf{a}_4}^{\mathbf{a}_5} G_{t, \mathbf{a}_5 \mathbf{a}_6}[\Phi] \bar{\Gamma}_t^{(4) \mathbf{a}_6 \mathbf{daa}_7}[\Phi] \mathbf{g}_{\mathbf{a}_7}^{\mathbf{a}_8} G_{t, \mathbf{a}_8 \mathbf{a}_1}[\Phi] + \\
&\quad + (-1)^{\mathbf{da}_2} (-1)^{\mathbf{ca}_5} (-1)^{\mathbf{ca}_4} (-1)^{\mathbf{cb}} (-1)^{\mathbf{ca}_2} (-1)^{\mathbf{ba}_2} (-1)^{\mathbf{aa}_2} \times \\
&\quad \times \left(\frac{1}{2} \partial_t R_t^{\mathbf{a}_1 \mathbf{a}_2} \right) G_{t, \mathbf{a}_2 \mathbf{a}_3}[\Phi] \bar{\Gamma}_t^{(4) \mathbf{a}_3 \mathbf{dba}_4}[\Phi] \mathbf{g}_{\mathbf{a}_4}^{\mathbf{a}_5} G_{t, \mathbf{a}_5 \mathbf{a}_6}[\Phi] \bar{\Gamma}_t^{(4) \mathbf{a}_6 \mathbf{caa}_7}[\Phi] \mathbf{g}_{\mathbf{a}_7}^{\mathbf{a}_8} G_{t, \mathbf{a}_8 \mathbf{a}_1}[\Phi] + \\
&\quad + (-1)^{\mathbf{da}_2} (-1)^{\mathbf{ca}_2} (-1)^{\mathbf{ba}_2} (-1)^{\mathbf{aa}_2} \times \\
&\quad \times \left(\frac{1}{2} \partial_t R_t^{\mathbf{a}_1 \mathbf{a}_2} \right) G_{t, \mathbf{a}_2 \mathbf{a}_3}[\Phi] \bar{\Gamma}_t^{(4) \mathbf{a}_3 \mathbf{dca}_4}[\Phi] \mathbf{g}_{\mathbf{a}_4}^{\mathbf{a}_5} G_{t, \mathbf{a}_5 \mathbf{a}_6}[\Phi] \bar{\Gamma}_t^{(4) \mathbf{a}_6 \mathbf{baa}_7}[\Phi] \mathbf{g}_{\mathbf{a}_7}^{\mathbf{a}_8} G_{t, \mathbf{a}_8 \mathbf{a}_1}[\Phi] + \\
&\quad + (-1)^{\mathbf{da}_5} (-1)^{\mathbf{da}_4} (-1)^{\mathbf{da}} (-1)^{\mathbf{db}} (-1)^{\mathbf{da}_2} (-1)^{\mathbf{ca}_5} (-1)^{\mathbf{ca}_4} (-1)^{\mathbf{ca}} (-1)^{\mathbf{cb}} (-1)^{\mathbf{ca}_2} \times \\
&\quad \quad \times (-1)^{\mathbf{ba}_2} (-1)^{\mathbf{aa}_2} \times \\
&\quad \times \left(\frac{1}{2} \partial_t R_t^{\mathbf{a}_1 \mathbf{a}_2} \right) G_{t, \mathbf{a}_2 \mathbf{a}_3}[\Phi] \bar{\Gamma}_t^{(4) \mathbf{a}_3 \mathbf{baa}_4}[\Phi] \mathbf{g}_{\mathbf{a}_4}^{\mathbf{a}_5} G_{t, \mathbf{a}_5 \mathbf{a}_6}[\Phi] \bar{\Gamma}_t^{(4) \mathbf{a}_6 \mathbf{dca}_7}[\Phi] \mathbf{g}_{\mathbf{a}_7}^{\mathbf{a}_8} G_{t, \mathbf{a}_8 \mathbf{a}_1}[\Phi] + \\
&\quad + (-1)^{\mathbf{da}_5} (-1)^{\mathbf{da}_4} (-1)^{\mathbf{da}} (-1)^{\mathbf{dc}} (-1)^{\mathbf{da}} (-1)^{\mathbf{ca}_2} (-1)^{\mathbf{ba}_5} (-1)^{\mathbf{ba}_4} (-1)^{\mathbf{ba}} (-1)^{\mathbf{ba}_2} \times \\
&\quad \quad \times (-1)^{\mathbf{aa}_2} \times \\
&\quad \times \left(\frac{1}{2} \partial_t R_t^{\mathbf{a}_1 \mathbf{a}_2} \right) G_{t, \mathbf{a}_2 \mathbf{a}_3}[\Phi] \bar{\Gamma}_t^{(4) \mathbf{a}_3 \mathbf{caa}_4}[\Phi] \mathbf{g}_{\mathbf{a}_4}^{\mathbf{a}_5} G_{t, \mathbf{a}_5 \mathbf{a}_6}[\Phi] \bar{\Gamma}_t^{(4) \mathbf{a}_6 \mathbf{dba}_7}[\Phi] \mathbf{g}_{\mathbf{a}_7}^{\mathbf{a}_8} G_{t, \mathbf{a}_8 \mathbf{a}_1}[\Phi] + \\
&\quad + (-1)^{\mathbf{da}_2} (-1)^{\mathbf{ca}_5} (-1)^{\mathbf{ca}_4} (-1)^{\mathbf{ca}} (-1)^{\mathbf{ca}_2} (-1)^{\mathbf{ba}_5} (-1)^{\mathbf{ba}_4} (-1)^{\mathbf{ba}} (-1)^{\mathbf{ba}_2} (-1)^{\mathbf{aa}_2} \times \\
&\quad \times \left(\frac{1}{2} \partial_t R_t^{\mathbf{a}_1 \mathbf{a}_2} \right) G_{t, \mathbf{a}_2 \mathbf{a}_3}[\Phi] \bar{\Gamma}_t^{(4) \mathbf{a}_3 \mathbf{daa}_4}[\Phi] \mathbf{g}_{\mathbf{a}_4}^{\mathbf{a}_5} G_{t, \mathbf{a}_5 \mathbf{a}_6}[\Phi] \bar{\Gamma}_t^{(4) \mathbf{a}_6 \mathbf{cba}_7}[\Phi] \mathbf{g}_{\mathbf{a}_7}^{\mathbf{a}_8} G_{t, \mathbf{a}_8 \mathbf{a}_1}[\Phi] + \\
&\quad + \dots =
\end{aligned}$$

$$\begin{aligned}
&= \dots + \\
&\quad + \text{STr} \left[\left(\frac{1}{2} \partial_t R_t \right) G_t[\Phi] \bar{\Gamma}_t^{(4) \text{cb}} G_t[\Phi] \bar{\Gamma}_t^{(4) \text{da}} G_t[\Phi] \right] + \\
&\quad + \text{STr} \left[\left(\frac{1}{2} \partial_t R_t \right) G_t[\Phi] \bar{\Gamma}_t^{(4) \text{db}} G_t[\Phi] \bar{\Gamma}_t^{(4) \text{ca}} G_t[\Phi] \right] + \\
&\quad + \text{STr} \left[\left(\frac{1}{2} \partial_t R_t \right) G_t[\Phi] \bar{\Gamma}_t^{(4) \text{dc}} G_t[\Phi] \bar{\Gamma}_t^{(4) \text{ba}} G_t[\Phi] \right] + \\
&\quad + \text{STr} \left[\left(\frac{1}{2} \partial_t R_t \right) G_t[\Phi] \bar{\Gamma}_t^{(4) \text{ba}} G_t[\Phi] \bar{\Gamma}_t^{(4) \text{dc}} G_t[\Phi] \right] + \\
&\quad + \text{STr} \left[\left(\frac{1}{2} \partial_t R_t \right) G_t[\Phi] \bar{\Gamma}_t^{(4) \text{ca}} G_t[\Phi] \bar{\Gamma}_t^{(4) \text{db}} G_t[\Phi] \right] + \\
&\quad + \text{STr} \left[\left(\frac{1}{2} \partial_t R_t \right) G_t[\Phi] \bar{\Gamma}_t^{(4) \text{da}} G_t[\Phi] \bar{\Gamma}_t^{(4) \text{cb}} G_t[\Phi] \right] + \\
&\quad + \dots = \\
&= \left(\begin{array}{c} \text{Diagram 1} \\ + 23 \text{ permutations} \end{array} \right) - \left(\begin{array}{c} \text{Diagram 2} \\ + 35 \text{ permutations} \end{array} \right) + \\
&\quad + \left(\begin{array}{c} \text{Diagram 3} \\ + 7 \text{ permutations} \end{array} \right) + \left(\begin{array}{c} \text{Diagram 4} \\ + 5 \text{ permutations} \end{array} \right) - \\
&\quad - \begin{array}{c} \text{Diagram 5} \end{array}
\end{aligned}$$

for the flow equation of the four-point vertex.

In general we could proceed with this process and derive flow equations for vertices of arbitrary order. However, for generic QFTs the system never terminates, because each n -point vertex depends on the $(n+2)$ -point vertex.

Already at the fourth order, Eq. (C.56), we are confronted with 75 possible terms and diagrams for arbitrary field theories on the r.h.s. of the equation. Of course, in practical applications the actual number is lower due to symmetries of the system and the resulting specific structure of the existing interaction terms. For example, for the QFTs and the corresponding truncations that are studied in this work, we solely need the six contributions that are explicitly provided in terms of formulae in Eq. (C.56).

Nevertheless, the interested reader might ask what happened, if we started to improve of our truncation step by step. How does the number of diagrams and therefore coupled differential equations grow, if one includes higher and higher n -point vertex functions?

FRG and horse-race betting To answer this question, let us return to the initial conundrum that was raised in the abstract of this appendix:

What is the common feature of FRG and horse-race betting?

Looking at the “diagrammatics” of the above equation, the commonality is as follows: The combinatorics, which is needed to obtain all possible diagrams that appear on the r.h.s. of the flow equation of the n^{th} vertex for a generic QFT is identical to the combinatorics of the different possible outcomes of a horse race with n participants. Here, the path along the loop of a diagram (from regulator to regulator) stands for the time when the horses pass the finish line and each horse can be associated with a three-point vertex. If there are ties and m horses finish at exactly the same time, they are depicted as $(m + 2)$ -point vertices instead of single three-point vertices.

Actually, this is a rather old combinatorial problem. Its solution is given by the so-called Bell numbers, which are also denoted as Fubini numbers. The corresponding sequence is given [636] and grows faster than the factorials. Its first terms are

$$1, 1, 3, 13, 75, 541, 4683, 47293, 545835, \dots \quad (\text{C.57})$$

Already this questions the practical possibility of successively increasing the truncation order in any kind of vertex expansion of the ERG equation above fourth- or fifth-order vertices for “real-world” problems, *e.g.*, QCD.

C.2.5. Scale-dependent fields

We close this chapter by showing the modifications that appear in the flow equations, if the ERG equation is evaluated for scale-dependent fields,

$$\Phi \mapsto \Phi_t = \Phi_t[\Phi]. \quad (\text{C.58})$$

Hence, from Eq. (C.44) follows that

$$\frac{d}{dt} \bar{\Gamma}_t[\Phi_t[\Phi]] = \partial_t \bar{\Gamma}_t[\Phi_t] + (\partial_t \Phi_{t,\mathbf{a}}) \left. \frac{\delta \bar{\Gamma}_t[\Phi]}{\delta \Phi_{\mathbf{a}}} \right|_{\Phi=\Phi_t} = \text{STr} \left[\left(\frac{1}{2} \partial_t R_t \right) G_t[\Phi_t[\Phi]] \right]. \quad (\text{C.59})$$

This modification of the flow equation can be used to formulate the flow equations in terms of renormalized fields instead of bare fields [54]. Introducing a field-independent wave-function renormalization via

$$\Phi_t[\Phi] = Z_t^{\frac{1}{2}} \Phi, \quad (\text{C.60})$$

the above equation reduces to

$$\partial_t \bar{\Gamma}_t[\Phi_t] = -\frac{1}{2} \eta_t \Phi_{t,\mathbf{a}} \left. \frac{\delta \bar{\Gamma}_t[\Phi]}{\delta \Phi_{\mathbf{a}}} \right|_{\Phi=\Phi_t} + \text{STr} \left[\left(\frac{1}{2} \partial_t R_t \right) G_t[\Phi_t] \right], \quad (\text{C.61})$$

where we defined the anomalous dimension as follows,

$$\eta_t \equiv \partial_t \ln(Z_t). \quad (\text{C.62})$$

Appendix D

RG and loop-integration variables, regulators, and threshold functions

Abstract This appendix provides some definitions and useful identities which repeatedly occur during the derivation of the FRG flow equations in Appendix E and their discussion in Part II. This comprises relations between the RG time and the RG scale and variable transformations of the loop momentum integration. Additionally, we present explicit formulae and identities for the regulators that are used in this thesis. We also introduce shorthand notations for the propagators and their derivatives. Additionally, we discuss recurring integral identities.

Disclosure None of the material that is presented in this appendix is new on a conceptual level and similar formulae and formularies are part of a lot of FRG publications. Certainly, the compilation and presentation of the material of this appendix is original to the author.

D.1. Relations between the RG time, the RG scale, and the loop momentum

In Part II of this thesis, where we work with QFTs in non-zero dimensions, the sliding RG scale k is of dimension energy. It is related to the RG time t , which serves as a dimensionless evolution parameter in our fluid-dynamical formulation of the RG flow equations, by

$$k(t) = \Lambda e^{-t}, \quad t = -\ln\left(\frac{k}{\Lambda}\right), \quad t \in [0, \infty), \quad (\text{D.1})$$

where Λ is the UV cutoff. The RG time is chosen manifestly positive throughout this work in contrast to most of the modern FRG literature that is based on the ERG equation (C.51). However, for a straightforward interpretation of the RG flow equations in terms of a fluid-dynamical problem, a positive RG time t seems to be more convenient [77, 4, 1, 2, 3]. Interestingly, this was already observed and used in the “pre-Wetterich era” of evolution equations, *cf.* Refs. [94, 96, 97, 193, 98, 99].

A change in RG time and RG scale are related by the chain rule for the derivatives,

$$\partial_t = \frac{\partial k}{\partial t} \frac{\partial}{\partial k} = -k \partial_k. \quad (\text{D.2})$$

During the evaluation of loop integrals in FRG calculations, it is common to introduce another dimensionless variable, see, *e.g.*, Refs. [162, 163, 165],

$$y = \frac{p^2}{k^2}. \quad (\text{D.3})$$

This quantity encodes the ratio of the momentary RG scale k to the absolute value of the loop momentum $p = |\vec{p}|$ during the integration from the UV to the IR. Derivatives w.r.t. the RG scale can be transformed into derivatives w.r.t. the ratio y as follows,

$$k \partial_k = k \frac{\partial y}{\partial k} \frac{\partial}{\partial y} = -2y \partial_y. \quad (\text{D.4})$$

From Eq. (D.2) we additionally find

$$2y \partial_y = \partial_t. \quad (\text{D.5})$$

In Appendix E, where we derive the RG flow equations of the GN and GNY model, we have to execute the (spatial) loop-momentum integrals many times for various diagrams. To this end it is useful to switch the integration variable from p to y . The integration measure transforms as follows

$$dy = 2dp \frac{p}{k^2}, \quad (\text{D.6})$$

and we find that

$$\int_0^\infty dp p^{d+1} f(p) = k^{d+2} \frac{1}{2} \int_0^\infty dy y^{\frac{d}{2}} f(y) \quad (\text{D.7})$$

holds for all integrands, which are functions of the absolute of the momentum \vec{p} only.

D.2. The flat regulator (Litim regulator)

For all FRG calculations in non-zero dimensions of this work, we employ so-called (spatial) flat regulators [634, 165]. Recognizing his seminal paper [163], this type of regulator is also named after D. Litim – the Litim regulator – and we adopt this denotation. It was developed in Ref. [163] to optimize RG flows and is therefore oftentimes also denoted as the (LPA) optimized regulator. Broadly speaking, optimization here refers to the minimization of the artificial errors which are introduced into the IR results of the RG by the regulator in any truncated version of the ERG equation. For details we refer to Refs. [162, 65, 637].

The Litim regulator is in general defined via the corresponding regulator shape functions, which are functions of the ratio (D.3). In this work, we use different versions of the Litim regulator (shape function) for bosons and fermions.

D.2.1. The bosonic Litim-regulator shape function

The bosonic version of the Litim-regulator shape function is defined in Ref. [163, Eq. (2.19)]. The regulator shape function and its derivatives w.r.t. the argument y explicitly read,

$$r_b(y) \equiv \left(\frac{1}{y} - 1\right) \Theta(1 - y), \quad (\text{D.8})$$

$$\dot{r}_b(y) = -\frac{1}{y^2} \Theta(1 - y) - \left(\frac{1}{y} - 1\right) \delta(1 - y), \quad (\text{D.9})$$

$$\ddot{r}_b(y) = \frac{2}{y^3} \Theta(1 - y) + \frac{2}{y^2} \delta(1 - y) - \left(\frac{1}{y} - 1\right) \partial_y \delta(1 - y). \quad (\text{D.10})$$

Two useful identities which are exploited several times during our calculations in Appendix E.2 are,

$$1 + r_b(y) + y \dot{r}_b(y) = 1 - \Theta(1 - y) - (1 - y) \delta(1 - y), \quad (\text{D.11})$$

$$2 \dot{r}_b(y) + y \ddot{r}_b(y) = 2 \delta(1 - y) - (1 - y) \partial_y \delta(1 - y) = \delta(1 - y). \quad (\text{D.12})$$

These combinations automatically appear in the derivatives (D.27) and (D.28) of the bosonic propagator (D.26), see below.

Note that both identities as well as the derivatives of the regulator shape function (D.8) are only valid if they are part of integrands of integrals like Eq. (D.7), because they are distributions. To show the validity of the second equality, we use integration by parts

$$\begin{aligned}
& \int_0^\infty dy f(y) (1-y) \partial_y \delta(1-y) = \\
& = [f(y) (1-y) \delta(1-y)]_0^\infty - \int_0^\infty dy \delta(1-y) \partial_y [f(y) (1-y)] = \\
& = \int_0^\infty dy f(y) \delta(1-y),
\end{aligned} \tag{D.13}$$

where $f(y)$ is some arbitrary test function.

In addition and in combination with the above identities, we are confronted over and over again with integrals of the type [163, Eq. (5.8)],

$$\begin{aligned}
& \frac{d}{2} \int_0^\infty dy y^{\frac{d}{2}} [y \dot{r}_b(y) + \frac{1}{2} \eta_\varphi(t) r_b(y)] f(y) = \\
& = \frac{d}{2} \int_0^\infty dy y^{\frac{d}{2}} \left[-\frac{1}{y} \Theta(1-y) - (1-y) \delta(1-y) + \frac{1}{2} \eta_\varphi(t) \left(\frac{1}{y} - 1\right) \Theta(1-y) \right] f(y) = \\
& = \frac{d}{2} \int_0^1 dy \left[-y^{\frac{d}{2}-1} + \frac{1}{2} \eta_\varphi(t) (y^{\frac{d}{2}-1} - y^{\frac{d}{2}}) \right] f(y).
\end{aligned} \tag{D.14}$$

Here, we inserted the explicit expressions (D.8) and (D.9).

For the special case where $f(y)$ does not depend on y for $y \in [0, 1]$, the integral universally evaluates to

$$= - \left[1 - \frac{\eta_\varphi(t)}{d+2} \right] f. \tag{D.15}$$

D.2.2. The fermionic Litim-regulator shape function

Analogously to Eq. (D.8) one defines a fermionic Litim-regulator shape function [163, Eq. (2.21)]. It is reasonable, see, *e.g.*, the discussions in Ref. [163] and Ref. [273, App. D], to choose the prefactor of the Heaviside step function slightly differently from the prefactor in the bosonic regulator function (D.8) in order to obtain a regulator function which is linear in the fermion momentum, see also Eq. (E.5). A rather natural and common choice for the fermionic regulator shape function in terms of the bosonic regulator shape function, which ensures this linearity, is, *cf.* Refs. [60, 63, 638, 61, 62, 72].

$$1 + r_f(y) \equiv \sqrt{1 + r_b(y)}, \quad \Rightarrow \quad 2[2y \partial_y r_f(y)][1 + r_f(y)] = 2y \partial_y r_b(y). \tag{D.16}$$

The relation has the additional feature for generic regulator shape functions that the IR regularization of fermions and bosons takes place at approximately similar scales k in systems where anti-fermion-fermion pairs can form bosonic particles via Yukawa interactions and vice versa. This can be seen from the relation for the derivatives of the regulators in Eq. (D.16), which relates loop integrals with fermionic regulator insertions, which are of type (D.24), to loop integrals with bosonic regulator insertions, which are of type (D.14) – at least for vanishing anomalous dimensions η_t .

Equations (D.8) and (D.16) imply,

$$r_f(y) \equiv (y^{-\frac{1}{2}} - 1) \Theta(1 - y), \quad (\text{D.17})$$

$$\dot{r}_f(y) = -\frac{1}{2} y^{-\frac{3}{2}} \Theta(1 - y) - (y^{-\frac{1}{2}} - 1) \delta(1 - y), \quad (\text{D.18})$$

$$\ddot{r}_f(y) = \frac{3}{4} y^{-\frac{5}{2}} \Theta(1 - y) + y^{-\frac{3}{2}} \delta(1 - y) - (y^{-\frac{1}{2}} - 1) \partial_y \delta(1 - y). \quad (\text{D.19})$$

There are also some useful identities for the fermionic regulator shape function,

$$1 + r_f(y) + 2y \dot{r}_f(y) = 1 - \Theta(1 - y) - 2(y^{\frac{1}{2}} - y) \delta(1 - y), \quad (\text{D.20})$$

$$3\dot{r}_f(y) + 2y \ddot{r}_f(y) = (-y^{-\frac{1}{2}} + 3) \delta(1 - y) - 2(y^{\frac{1}{2}} - y) \partial_y \delta(1 - y) = \delta(1 - y) \quad (\text{D.21})$$

$$\begin{aligned} \dot{r}_f(y) + y \ddot{r}_f(y) &= \frac{1}{4} y^{-\frac{3}{2}} \Theta(1 - y) + \delta(1 - y) - (y^{\frac{1}{2}} - y) \partial_y \delta(1 - y) = \\ &= \frac{1}{4} y^{-\frac{3}{2}} \Theta(1 - y) + \frac{1}{2} y^{-\frac{1}{2}} \delta(1 - y), \end{aligned} \quad (\text{D.22})$$

where the last two formulae are again derived using integration by parts and some test function $f(y)$,

$$\begin{aligned} &\int_0^\infty dy f(y) (y^{\frac{1}{2}} - y) \partial_y \delta(1 - y) = \\ &= [f(y) (y^{\frac{1}{2}} - y) \delta(1 - y)]_0^\infty - \int_0^\infty dy \delta(1 - y) \partial_y [f(y) (y^{\frac{1}{2}} - y)] = \\ &= - \int_0^\infty dy f(y) (\frac{1}{2} y^{-\frac{1}{2}} - 1) \delta(1 - y). \end{aligned} \quad (\text{D.23})$$

These identities arise within the expressions for the derivatives (D.33) and (D.34) of the denominator of the fermionic propagator (D.32), see below.

Furthermore, we are confronted with integrals of the type [163, Eq. (5.10)],

$$\begin{aligned} &d \int_0^\infty dy y^{\frac{d}{2}} [y \dot{r}_f(y) + \frac{1}{2} \eta_\psi(t) r_f(y)] [1 + r_f(y)] f(y) = \\ &= d \int_0^\infty dy y^{\frac{d}{2}} [-\frac{1}{2} y^{-\frac{1}{2}} \Theta(1 - y) - (y^{-\frac{1}{2}} - 1) \delta(1 - y) + \frac{1}{2} \eta_\psi(t) (y^{-\frac{1}{2}} - 1) \Theta(1 - y)] \times \\ &\quad \times [1 + (y^{-\frac{1}{2}} - 1) \Theta(1 - y)] f(y) = \\ &= d \int_0^1 dy [-\frac{1}{2} y^{\frac{d}{2}-1} + \frac{1}{2} \eta_\psi(t) (y^{\frac{d}{2}-1} - y^{\frac{d-1}{2}})] f(y). \end{aligned} \quad (\text{D.24})$$

The simplifications are done using Eqs. (D.17) and (D.18). Again, if $f(y)$ does not depend on y for $y \in [0, 1]$, the above integral further simplifies to

$$= - \left[1 - \frac{\eta_\psi(t)}{d+1} \right] f. \quad (\text{D.25})$$

D.3. Propagators and threshold functions

Already in the first publications which applied the FRG method to QFTs, so-called *threshold functions* were introduced in order to compactify and systematize the notation of flow equations. In this work, we do not follow this strategy, because most of the threshold functions and notation was established for calculations in vacuum and/or spacetime dimensions greater than two, while our work focuses on in-medium calculations in 1+1 dimensions. Hence, although most of the commonly used threshold functions are provided at first glance for any desired spacetime dimension, some threshold functions are actually not valid for small number of dimensions, due to prefactors like $\frac{1}{d-2}$, cf. Refs. [373, 374]. This distinction of cases for different dimensions is discussed in the context of the flow equation for the Yukawa coupling in Appendix E.2.4, but is oftentimes ignored in the literature.

In consequence, we decided to introduce merely two “threshold functions” – namely shorthand notations for the denominators of the bosonic and fermionic propagators. For the sake of simplicity, we also refer to these quantities as *propagators* throughout this work, even though the true full propagators have additional tensor structures in their numerators, see Eqs. (E.9), (E.43), and (E.44).

In the following paragraphs, we introduce our notation and present some integral identities for the propagators, if one explicitly uses Litim regulators.

D.3.1. Propagators

Bosonic propagator

The (denominator of the) bosonic propagator and its first two derivatives are,

$$\mathfrak{B}_n(y) \equiv \frac{1}{\frac{1}{k^2} \omega_n^2 + y [1 + r_b(y)] + \frac{1}{k^2} \partial_{\sigma_\tau}^2 U(t, \sigma_\tau)}, \quad (\text{D.26})$$

$$\dot{\mathfrak{B}}_n(y) = - [1 + r_b(y) + y \dot{r}_b(y)] \mathfrak{B}_n^2(y), \quad (\text{D.27})$$

$$\ddot{\mathfrak{B}}_n(y) = 2 [1 + r_b(y) + y \dot{r}_b(y)]^2 \mathfrak{B}_n^3(y) - [2 \dot{r}_b(y) + y \ddot{r}_b(y)] \mathfrak{B}_n^2(y). \quad (\text{D.28})$$

Here, y is again the ratio (D.3) of p^2 and k^2 . Note that these formulae are valid for any purely spatial regulator.

However, if one specifically chooses the Litim-regulator shape function (D.8) and studies these expressions as being part of integrands of some y -integrals, which are restricted to $y \in [0, 1]$ by the Heaviside step function from the regulator insertion, like Eqs. (D.14) and (D.24), one can prove the following useful formulae. Explicitly inserting Eqs. (D.8), (D.11), and (D.12) into Eqs. (D.26) to (D.28) one finds,

$$\int_0^\infty dy \Theta(1-y) f(y) \mathfrak{B}_n(y) = \int_0^1 dy f(y) \mathfrak{B}_n(1), \quad (\text{D.29})$$

$$\int_0^\infty dy \Theta(1-y) f(y) \dot{\mathfrak{B}}_n(y) = 0, \quad (\text{D.30})$$

$$\int_0^\infty dy \Theta(1-y) f(y) \ddot{\mathfrak{B}}_n(y) = -\frac{1}{2} f(1) \mathfrak{B}_n^2(1). \quad (\text{D.31})$$

The factor $\frac{1}{2}$ in the last equation stems from the Dirac δ -distribution, being evaluated at the integral boundary.

Fermionic propagators

The (denominator of the) fermionic propagator and its first two derivatives are,

$$\mathfrak{F}_n(y) \equiv \frac{1}{\frac{1}{k^2} (\nu_n + i\mu)^2 + y [1 + r_f(y)]^2 + \frac{1}{k^2} m_r^2(t, \sigma_r)} , \quad (\text{D.32})$$

$$\dot{\mathfrak{F}}_n(y) = - [1 + r_f(y)] [1 + r_f(y) + 2y \dot{r}_f(y)] \mathfrak{F}_n^2(y) , \quad (\text{D.33})$$

$$\ddot{\mathfrak{F}}_n(y) = 2 [1 + r_f(y)]^2 [1 + r_f(y) + 2y \dot{r}_f(y)]^2 \mathfrak{F}_n^3(y) - \quad (\text{D.34})$$

$$- (\dot{r}_f(y) [1 + r_f(y) + 2y \dot{r}_f(y)] + [1 + r_f(y)] [3 \dot{r}_f(y) + 2y \ddot{r}_f(y)]) \mathfrak{F}_n^2(y) ,$$

where we are still using definition Eq. (D.3) for y . Again, these formulae are valid for any kind of purely spatial regulator.

For the special case where $m_r^2(t, \sigma_r) = 0$, which is always the case for the purely fermionic GN model in Appendix E.1 and which is also the case for field-independent flow equations in the GNY model in Appendix E.2, where the flow equations are evaluated at the trivial point $\sigma_r = 0$ in field space, we define,

$$\mathfrak{f}_n(y) \equiv \mathfrak{F}_n(y) \Big|_{m_r^2(t, \sigma_r)=0} . \quad (\text{D.35})$$

All formulae of this appendix which hold for $\mathfrak{F}_n(y)$ do also apply to $\mathfrak{f}_n(y)$.

Choosing the fermionic Litim-regulator shape function (D.17), we can prove certain integral identities. Inserting Eqs. (D.17), (D.20), and (D.21) in Eqs. (D.32) to (D.34) one finds,

$$\int_0^\infty dy \Theta(1-y) f(y) \mathfrak{F}_n(y) = \int_0^1 dy f(y) \mathfrak{F}_n(1) , \quad (\text{D.36})$$

$$\int_0^\infty dy \Theta(1-y) f(y) \dot{\mathfrak{F}}_n(y) = 0 , \quad (\text{D.37})$$

$$\int_0^\infty dy \Theta(1-y) f(y) \ddot{\mathfrak{F}}_n(y) = -\frac{1}{2} f(1) \mathfrak{F}_n^2(1) . \quad (\text{D.38})$$

The factor $\frac{1}{2}$ in the last line stems from the delta distribution being evaluated at the integral boundary. These types of integrals occur if the fermionic propagator and/or its derivatives are part of the integrand of integrals like Eqs. (D.14) and (D.24).

Appendix E

FRG flow equations of the Gross-Neveu and Gross-Neveu-Yukawa model

Abstract This appendix is dedicated to the explicit derivation of the FRG flow equations which are studied and solved in Part II of this thesis. The appendix is split into two parts. The first part exclusively deals with the purely fermionic GN model at non-zero μ and non-zero T . It comprises the calculation of the flow equations of the four-fermion coupling and the trivial flow equation of the fermionic wave-function renormalization in our choice of the truncation. The second part covers the in-medium flow equations of the partially bosonized GN model, the GNY model, in a truncation which involves a scale-dependent local potential, field-independent but scale-dependent wave-function renormalizations for the boson and the fermions, and a field- and scale-dependent Yukawa coupling. Furthermore, we provide an expression for the scale-dependent bosonic two-point function. All derivations are for d spatial dimensions using a purely spatial Litim regulator. Both parts are presented as detailed and self-consistent step-by-step manuals.

Disclosure On a conceptual level, none of the derivations within this appendix are new. FRG flow equations for similar but also much more complicated four-fermion theories or Yukawa-type theories were studied before in numerous contexts, see, *e.g.*, Refs. [527, 346, 528, 347, 348, 350, 351] and Refs. [372, 373, 639, 556, 374, 346, 66, 101], such that the generic form of the flow equations is in principle known in an arbitrary number of spacetime dimensions (in vacuum and in medium) and their shape and derivation is at least in parts discussed elsewhere. Hence, this appendix documents primarily the reproducibility of some of these results and hopefully makes this thesis as self-consistent and pedagogical as possible, because the details of the respective derivations are sometimes very hard to find.

However, to the best of our knowledge the flow equation of the purely fermionic GN model in medium (the β -function of the four-fermion coupling), was never analyzed and evaluated like it is presented in this appendix. Here we refer to a careful analysis and tracing of the external fermionic Matsubara frequencies that have to enter the corresponding diagrams at non-zero temperature in the presence of a chemical potential. Furthermore, although flow equations for the GNY model were already presented for an arbitrary number of dimensions, we are confident, that a careful step-by-step discussion and evaluation of these equations, using a spatial Litim regulator in a small number of dimensions and in medium, is missing in the literature.

E.1. FRG flow equations of the Gross-Neveu model

In this appendix the explicit derivation of the RG flow equation(s) for the GN model in its original and purely fermionic formulation is presented. The starting point of the derivation is the ansatz (9.1) for the effective average action.

For the sake of clarity we write out all dependences of the fermionic fields on the compactified Euclidean spacetime as well as all their color and spinor indices.

$$\begin{aligned} \bar{\Gamma}_t[\bar{\psi}, \psi] &= \\ &= \int_{-\infty}^{\infty} d^d x \int_0^{\beta} d\tau \left[\bar{\psi}_{a_1 c_1}(\tau, \vec{x}) Z_{\psi}(t) (\mathbb{1})_{c_2}^{c_1} (\not{\partial} - \mu \gamma^{d+1})_{a_1 a_2} \psi^{a_2 c_2}(\tau, \vec{x}) - \right. \\ &\quad \left. - \frac{1}{2N} g^2(t) [\bar{\psi}_{a_1 c_1}(\tau, \vec{x}) (\mathbb{1})_{c_2}^{c_1} (\mathbb{1})_{a_2}^{a_1} \psi^{a_2 c_2}(\tau, \vec{x})]^2 \right]. \end{aligned} \quad (\text{E.1})$$

In the first step, the effective average action is transferred to momentum space by inserting the Fourier transformations of the fields, Eqs. (A.26) and (A.28), and applying the identity (A.31),

$$\begin{aligned} \bar{\Gamma}_t[\tilde{\psi}, \tilde{\psi}] &= \\ &= \frac{1}{\beta^2} \sum_{n_1, n_2=-\infty}^{\infty} \int_{-\infty}^{\infty} \frac{d^d p_1}{(2\pi)^d} \frac{d^d p_2}{(2\pi)^d} \tilde{\psi}_{a_1 c_1}(\nu_{n_1}, \vec{p}_1) \beta \delta_{n_1, n_2} (2\pi)^d \delta^{(d)}(\vec{p}_1 - \vec{p}_2) \times \\ &\quad \times Z_{\psi}(t) (\mathbb{1})_{c_2}^{c_1} [i(\nu_{n_2} + i\mu) \gamma^{d+1} + i\vec{p}_2 \cdot \vec{\gamma}]_{a_1 a_2} \tilde{\psi}^{a_2 c_2}(\nu_{n_2}, \vec{p}_2) - \\ &\quad - \frac{1}{\beta^4} \sum_{n_1, \dots, n_4=-\infty}^{\infty} \int_{-\infty}^{\infty} \frac{d^d p_1}{(2\pi)^d} \dots \frac{d^d p_4}{(2\pi)^d} \beta \delta_{n_1+n_3, n_2+n_4} (2\pi)^d \delta^{(d)}(\vec{p}_1 - \vec{p}_2 + \vec{p}_3 - \vec{p}_4) \times \\ &\quad \times \frac{1}{2N} g^2(t) (\mathbb{1})_{a_2}^{a_1} (\mathbb{1})_{a_4}^{a_3} (\mathbb{1})_{c_2}^{c_1} (\mathbb{1})_{c_4}^{c_3} \times \\ &\quad \times \tilde{\psi}_{a_1 c_1}(\nu_{n_1}, \vec{p}_1) \tilde{\psi}^{a_2 c_2}(\nu_{n_2}, \vec{p}_2) \tilde{\psi}_{a_3 c_3}(\nu_{n_3}, \vec{p}_3) \tilde{\psi}^{a_4 c_4}(\nu_{n_4}, \vec{p}_4). \end{aligned} \quad (\text{E.2})$$

Within our our truncation we need explicit expressions for the two- and four-point function for the computation of the RG flow equations. Higher-order n -point functions are omitted from the ansatz (E.1). The odd n -point functions, *i.e.*, the one- and three-point function, vanish if they are evaluated on a constant zero background-field configuration for the fermion fields. Therefore, it remains to derive the two- and four-point function by successively taking derivatives of Eq. (E.2) w.r.t. the Fourier-transformed fermion fields $\tilde{\psi}$ and $\tilde{\psi}$. Here, caution is advised, because the anticommutativity of the fermion fields has to be respected. After taking the required number of derivatives, the result is customarily evaluated $\tilde{\psi} = \psi = 0$.

For the (field-independent) two-point function, one finds

$$\begin{aligned} \bar{\Gamma}_t^{\tilde{\psi}_2 \psi_1}(\nu_{n_2}, \vec{p}_2; \nu_{n_1}, \vec{p}_1)_{a_1 c_1}^{a_2 c_2} &\equiv \\ &\equiv \frac{\beta^2 (2\pi)^{2d} \delta^2 \bar{\Gamma}_t[\tilde{\psi}, \tilde{\psi}]}{\delta \tilde{\psi}_{a_2 c_2}(\nu_{n_2}, \vec{p}_2) \delta \tilde{\psi}^{a_1 c_1}(\nu_{n_1}, \vec{p}_1)} \Big|_{\tilde{\psi}=\psi=0} = \\ &= -\beta \delta_{n_2, n_1} (2\pi)^d \delta^{(d)}(\vec{p}_2 - \vec{p}_1) Z_{\psi}(t) (\mathbb{1})_{c_1}^{c_2} [i(\nu_{n_2} + i\mu) \gamma^{d+1} + i\vec{p}_2 \cdot \vec{\gamma}]_{a_2 a_1} = \end{aligned} \quad (\text{E.3})$$

$$= \begin{array}{c} \bar{\psi}_2 \quad \psi_1 \\ \leftarrow \text{---} \bigcirc \text{---} \rightarrow \end{array},$$

where we adapted the field-space notation of Appendix C.1.2 by strictly indicating all momentum and frequency dependences as well as all open color and spinor indices. In the last line we introduced the graphical representation of the two-point function/vertex for its later use in Feynman diagrams.

Analogously, the four-point function reads as follows,

$$\begin{aligned} & \bar{\Gamma}_t^{\bar{\psi}_4 \psi_3 \bar{\psi}_2 \psi_1}(\nu_{n_4}, \vec{p}_4; \nu_{n_3}, \vec{p}_3; \nu_{n_2}, \vec{p}_2; \nu_{n_1}, \vec{p}_1)^{a_4 a_3 c_4 c_2 c_1} \equiv \tag{E.4} \\ & \equiv \frac{\beta^4 (2\pi)^{4d} \delta^4 \bar{\Gamma}_t[\tilde{\psi}, \tilde{\psi}]}{\delta \tilde{\psi}_{a_4 c_4}(\nu_{n_4}, \vec{p}_4) \delta \tilde{\psi}^{a_3 c_3}(\nu_{n_3}, \vec{p}_3) \delta \tilde{\psi}_{a_2 c_2}(\nu_{n_2}, \vec{p}_2) \delta \tilde{\psi}^{a_1 c_1}(\nu_{n_1}, \vec{p}_1)} \Big|_{\tilde{\psi}=\psi=0} = \\ & = -2 \beta \delta_{n_2+n_4, n_1+n_3} (2\pi)^d \delta^{(d)}(\vec{p}_2 - \vec{p}_1 + \vec{p}_4 - \vec{p}_3) \frac{1}{2N} g^2(t) \times \\ & \times [(\mathbf{1})^{a_2}_{a_1} (\mathbf{1})^{a_4}_{a_3} (\mathbf{1})^{c_2}_{c_1} (\mathbf{1})^{c_4}_{c_3} - (\mathbf{1})^{a_4}_{a_1} (\mathbf{1})^{a_2}_{a_3} (\mathbf{1})^{c_4}_{c_1} (\mathbf{1})^{c_2}_{c_3}] = \\ & = \begin{array}{c} \bar{\psi}_4 \quad \psi_3 \\ \swarrow \quad \searrow \\ \bigcirc \\ \nearrow \quad \nwarrow \\ \psi_1 \quad \bar{\psi}_2 \end{array}. \end{aligned}$$

It is worth mentioning that the tensor structure in the second to last line encodes the two possible “routes” of color-charge flow through the local four-point interaction. Either the color charge that enters at the fermion leg 1 leaves the process at leg 2 or at leg 4, while the color charge that enters the interaction via leg 3 always takes the opposite route to the one from leg 1. This is graphically illustrated by the arrows of the corresponding Feynman graph in the last line, which indicate the direction of color-charge flow.

As discussed in Section 9.2.2 and Appendix C.2.1, the application of the ERG equation (C.51) further requires to specify a regulator function. A construction of fermionic regulator functions is described in Ref. [273, App. D] (in vacuum). Generally, the regulator should be in accordance with all symmetries of the model and additionally fulfill the regulator properties. Within this work, we choose a purely spatial regulator that is diagonal in momentum, frequency, and color space, but mimics the structure of the fermionic spatial kinetic term in Dirac space,

$$\begin{aligned} & R_t^{\bar{\psi}_2 \psi_1}(\nu_{n_2}, \vec{p}_2; \nu_{n_1}, \vec{p}_1)^{a_2 c_2 c_1} = \tag{E.5} \\ & = -\beta \delta_{n_2, n_1} (2\pi)^d \delta^{(d)}(\vec{p}_2 - \vec{p}_1) (\mathbf{1})^{c_2}_{c_1} i\vec{p}_1 \cdot (\vec{\gamma})^{a_2}_{a_1} Z_\psi(t) r_f(t, |\vec{p}_2|). \end{aligned}$$

The corresponding regulator term in the path integral, see Eq. (C.24), is

$$\begin{aligned} & \Delta \mathcal{S}[\tilde{\psi}, \tilde{\psi}] = \tag{E.6} \\ & = \frac{1}{\beta^2} \sum_{n_1, n_2=-\infty}^{\infty} \int_{-\infty}^{\infty} \frac{d^d p_1}{(2\pi)^d} \frac{d^d p_2}{(2\pi)^d} \tilde{\psi}_{a_1 c_1}(\nu_{n_1}, \vec{p}_1) R_t^{\bar{\psi}_2 \psi_1}(\nu_{n_2}, \vec{p}_2; \nu_{n_1}, \vec{p}_1)^{a_2 c_2 c_1} \tilde{\psi}^{a_2 c_2}(\nu_{n_2}, \vec{p}_2). \end{aligned}$$

Despite not being proportional to an actual fermion mass term, the regulator still acts as mass-like damping of spatial IR modes, as can be seen in the fermion propagator below, Eq. (E.9). Furthermore, it satisfies the Silver-Blaze-Property [166] and respects the discrete chiral symmetry – although it breaks (Euclidean) Poincaré invariance. For drawbacks of regulator shape functions that break (Euclidean) spacetime symmetries, we refer to our main discussion in Section 9.2.2 and references therein.

However, for the moment we just focus on the formal derivation of the RG flow equation. Our Feynman graph representation of the regulator insertion in the FRG formalism reads

$$\frac{1}{2} \partial_t R_t^{\bar{\psi}_2 \psi_1}(\nu_{n_2}, \vec{p}_2; \nu_{n_1}, \vec{p}_1)_{a_1 c_2 c_1}^{a_2} = \begin{array}{c} \bar{\psi}_2 \\ \leftarrow \otimes \rightarrow \\ \psi_1 \end{array} . \quad (\text{E.7})$$

By combining the two-point function (E.4) and the regulator function (E.5) the full two-point function (for vanishing fermion background fields) looks as follows,

$$\begin{aligned} & (\bar{\Gamma}_t^{\bar{\psi}_2 \psi_1} + R_t^{\bar{\psi}_2 \psi_1})(\nu_{n_2}, \vec{p}_2; \nu_{n_1}, \vec{p}_1)_{c_1 a_2 a_1}^{c_2} \equiv \\ & \equiv -\beta \delta_{n_2, n_1} (2\pi)^d \delta^{(d)}(\vec{p}_2 - \vec{p}_1) Z_\psi(t) (\mathbb{1})_{c_1}^{c_2} [i(\nu_{n_2} + i\mu) \gamma^{d+1} + i\vec{p}_2 \cdot \vec{\gamma} [1 + r_f(t, |\vec{p}_2|)]]^{a_2 a_1} . \end{aligned} \quad (\text{E.8})$$

The corresponding full propagator (at vanishing fermion background fields) reads

$$\begin{aligned} & (\bar{\Gamma}_t^{\bar{\psi}_2 \psi_1} + R_t^{\bar{\psi}_2 \psi_1})^{-1}(\nu_{n_2}, \vec{p}_2; \nu_{n_1}, \vec{p}_1)_{c_1 a_2 a_1}^{c_2} \equiv \\ & \equiv \beta \delta_{n_2, n_1} (2\pi)^d \delta^{(d)}(\vec{p}_2 - \vec{p}_1) \frac{[i(\nu_{n_2} + i\mu) \gamma^{d+1} + i\vec{p}_2 \cdot \vec{\gamma} [1 + r_f(t, |\vec{p}_2|)]]^{a_2 a_1} (\mathbb{1})_{c_1}^{c_2}}{Z_\psi(t) [(\nu_{n_2} + i\mu)^2 + \vec{p}_2^2 [1 + r_f(t, |\vec{p}_2|)]^2]} = \\ & = \begin{array}{c} \bar{\psi}_2 \\ \leftarrow \\ \psi_1 \end{array} . \end{aligned} \quad (\text{E.9})$$

In the last line, we introduced our Feynman-graph representation of the propagator.

Remember that during the derivation of the ERG equation (C.51) the generic full two-point function is inverted before the ERG equation is evaluated on a specific field configuration. Hence, it incorporates an arbitrary field dependence. Otherwise, it would not be possible to take additional field-space derivatives in order to derive flow equations of higher-order n -point functions, as presented in Appendix C.2.4. However, to obtain the components of the propagators that enter the flow equations, after the entire flow equation is evaluated on a specific background field configuration, one may simply invert the full two-point function (evaluated on a background field configuration), which simplifies the inversion drastically.

Now that all ingredients are at hand, we can start the actual calculation of the flow equations for the single couplings, *i.e.*, the four-fermion coupling $g(t)$ and the wave-function renormalization $Z_\psi(t)$, respectively the corresponding fermion anomalous dimension $\eta_\psi(t)$. In addition, we demonstrate that within the purely fermionic GN model (with vanishing UV fermion masses) a fermionic mass-like term is never generated during the RG flow, which implies that discrete chiral \mathbb{Z}_2 symmetry is never broken, *cf.*, Refs. [158, after Eq. (2.2)], [464, after Eq. (1)].

We begin the derivation of the flow equations by extracting the famous latter result and the (vanishing) flow equation for the fermionic wave-function renormalization $Z_\psi(t)$ from the generic flow equation of the fermionic two-point vertex. Afterwards we turn to the flow equation of the four-fermion coupling.

E.1.1. Fermion two-point vertex – fermion mass & anomalous dimension

Our starting point for the analysis of the (vanishing) RG flow of the fermionic wave-function renormalization $Z_\psi(t)$ and the non-production of fermion mass-like terms is the generic flow equation of the fermionic two-point function.

The two-point vertex

This flow equation is derived by taking a derivative of the ERG equation (C.51) w.r.t. the Fourier-transformed fermion field $\tilde{\psi}$ and another derivative w.r.t. $\tilde{\psi}$. At this point afresh computation is not required and we can simply make use of the general result of Appendix C.2.4 in field-space notation, specifically Eq. (C.53). Evaluating this equation for our specific theory and truncation, the GN model with the previously derived n -point function(s) and propagator, the universal Eq. (C.53) becomes,

$$\begin{aligned}
\partial_t \bar{\Gamma}_t^{(2)} \bar{\psi}_{\text{II}} \psi_{\text{I}} &= \tag{E.10} \\
&= - \text{STr} \left[\left(\frac{1}{2} \partial_t R_t \right) G_t \bar{\Gamma}_t^{(4)} \bar{\psi}_{\text{II}} \psi_{\text{I}} G_t \right] = \\
&= - (-1)^{\bar{\psi}_{\text{II}} \psi_{\text{I}}} (-1)^{\psi_{\text{I}} \psi_{\text{I}}} \left(\frac{1}{2} \partial_t R_t^{\bar{\psi}_{\text{I}} \psi_{\text{I}}} \right) G_{t, \bar{\psi}_2 \psi_3} \bar{\Gamma}_t^{(4)} \bar{\psi}_3 \bar{\psi}_{\text{II}} \psi_{\text{I}} \psi_4 \mathbf{g}_{\bar{\psi}_4}^{\psi_5} G_{t, \bar{\psi}_5 \psi_1} - \\
&\quad - (-1)^{\bar{\psi}_{\text{II}} \psi_{\text{I}}} (-1)^{\psi_{\text{I}} \psi_{\text{I}}} \left(\frac{1}{2} \partial_t R_t^{\psi_{\text{I}} \bar{\psi}_2} \right) G_{t, \psi_2 \bar{\psi}_3} \bar{\Gamma}_t^{(4)} \psi_3 \bar{\psi}_{\text{II}} \psi_{\text{I}} \bar{\psi}_4 \mathbf{g}_{\psi_4}^{\bar{\psi}_5} G_{t, \psi_5 \bar{\psi}_1} = \\
&= - 2 \left(\frac{1}{2} \partial_t R_t^{\bar{\psi}_{\text{I}} \psi_{\text{I}}} \right) G_{t, \bar{\psi}_2 \psi_3} \bar{\Gamma}_t^{(4)} \bar{\psi}_3 \bar{\psi}_{\text{II}} \psi_{\text{I}} \psi_4 \mathbf{g}_{\bar{\psi}_4}^{\psi_5} G_{t, \bar{\psi}_5 \psi_1} = \\
&= - 2 \left(\frac{1}{2} \partial_t R_t^{\bar{\psi}_{\text{I}} \psi_{\text{I}}} \right) (\bar{\Gamma}_t^{(2)} + R_t)^{-1} \bar{\Gamma}_t^{(4)} \bar{\psi}_3 \psi_{\text{I}} \bar{\psi}_{\text{II}} \psi_4 (\bar{\Gamma}_t^{(2)} + R_t)^{-1}_{\bar{\psi}_4 \psi_1}.
\end{aligned}$$

Here, a final evaluation on vanishing fermionic background fields is already implied, such that contributions that involve three-point functions in Eq. (C.53) vanish. In addition, we combined the remaining two contributions by employing that the trace of a transposed operator/matrix is the same as the trace of the object itself. This results in the multiplicity factor “2” of the corresponding diagram. In addition, the $(-1)^{\mathbf{ab}}$ factors, which ensure the correct fermion statistics, are evaluated according to definition (C.6). The same applies to the field-space metric $\mathbf{g}_{\mathbf{b}}^{\mathbf{a}}$, where we use Eq. (C.13), and the propagators $G_{t, \mathbf{ab}}$, where Eq. (C.42) is applied to simplify the equation. Graphically, in terms of Feynman diagrams, the equation looks like

$$\partial_t \left(\bar{\psi}_{\text{II}} \leftarrow \text{---} \circ \leftarrow \psi_{\text{I}} \right) = - 2 \text{---} \bar{\psi}_{\text{II}} \leftarrow \text{---} \circ \leftarrow \psi_{\text{I}} \text{---} \tag{E.11}$$

In the Feynman-graph representation it becomes clear that the multiplicity factor stands for one diagram with an anticlockwise and one diagram with a clockwise propagation of color charge in the loop, which are physically indistinguishable and result in identical contributions to the RG flow.

In order to further evaluate and fill the abstract field-space equations (E.10) and (E.11) with life, one needs to insert the previously derived expressions for the regulator (E.5), the propagator (E.9),

and the four-point function (E.4),

$$\begin{aligned}
& \partial_t \bar{\Gamma}_t^{\bar{\psi}\psi}(\nu_{n_{\text{II}}}, \vec{p}_{\text{II}}; \nu_{n_{\text{I}}}, \vec{p}_{\text{I}})_{a_1 c_1}^{a_{\text{II}} c_{\text{II}}} = \tag{E.12} \\
& = -2 \frac{1}{\beta^4} \sum_{n_1, \dots, n_4 = -\infty}^{\infty} \int_{-\infty}^{\infty} \frac{d^d p_1}{(2\pi)^d} \cdots \frac{d^d p_4}{(2\pi)^d} \times \\
& \quad \times (-1) \beta \delta_{n_1, n_2} (2\pi)^d \delta^{(d)}(\vec{p}_1 - \vec{p}_2) (\mathbb{1})_{c_2}^{c_1} i\vec{p}_1 \cdot (\vec{\gamma})_{a_2}^{a_1} \partial_t [Z_\psi(t) \frac{1}{2} r_f(t, |\vec{p}_1|)] \times \\
& \quad \times \beta \delta_{n_2, n_3} (2\pi)^d \delta^{(d)}(\vec{p}_2 - \vec{p}_3) \frac{[i(\nu_{n_2} + i\mu) \gamma^{d+1} + i\vec{p}_2 \cdot \vec{\gamma} [1 + r_f(t, |\vec{p}_2|)]]^{a_2} (\mathbb{1})_{c_3}^{c_2}}{Z_\psi(t) [(\nu_{n_2} + i\mu)^2 + \vec{p}_2^2 [1 + r_f(t, |\vec{p}_2|)]^2]} \times \\
& \quad \times (-1) 2 \beta \delta_{n_{\text{II}}+n_3, n_4+n_{\text{I}}} (2\pi)^d \delta^{(d)}(\vec{p}_{\text{II}} - \vec{p}_4 + \vec{p}_3 - \vec{p}_{\text{I}}) \frac{1}{2N} g^2(t) \times \\
& \quad \times [(\mathbb{1})_{a_4}^{a_{\text{II}}} (\mathbb{1})_{a_3}^{a_1} (\mathbb{1})_{c_4}^{c_{\text{II}}} (\mathbb{1})_{c_1}^{c_3} - (\mathbb{1})_{a_4}^{a_3} (\mathbb{1})_{a_{\text{I}}}^{a_{\text{II}}} (\mathbb{1})_{c_4}^{c_3} (\mathbb{1})_{c_1}^{c_{\text{I}}}] \times \\
& \quad \times \beta \delta_{n_4, n_1} (2\pi)^d \delta^{(d)}(\vec{p}_4 - \vec{p}_1) \frac{[i(\nu_{n_4} + i\mu) \gamma^{d+1} + i\vec{p}_4 \cdot \vec{\gamma} [1 + r_f(t, |\vec{p}_4|)]]^{a_4} (\mathbb{1})_{c_4}^{c_1}}{Z_\psi(t) [(\nu_{n_4} + i\mu)^2 + \vec{p}_4^2 [1 + r_f(t, |\vec{p}_4|)]^2]}.
\end{aligned}$$

However, to finally obtain an explicit flow equation for $Z_\psi(t)$ or rather $\eta_\psi(t)$ one has to project this flow equation for the two-point function onto a flow equation for $Z_\psi(t)$. The same applies to the flow of the fermion mass.

Projections

Fermionic wave-function renormalization and anomalous dimension From Eqs. (E.2) and (E.3) and the Def. (C.62) of the anomalous dimension it is straightforward to derive (within our truncation),

$$\begin{aligned}
& \beta \delta_{n_{\text{II}}, n_{\text{I}}} (2\pi)^d \delta^{(d)}(\vec{p}_{\text{II}} - \vec{p}_{\text{I}}) \vec{p}_{\text{II}}^2 \eta_\psi(t) = \tag{E.13} \\
& = \frac{1}{N} (\mathbb{1})_{c_{\text{II}}}^{c_{\text{I}}} \frac{1}{d_\gamma} (i\vec{p}_{\text{II}} \cdot \vec{\gamma})_{a_{\text{II}}}^{a_{\text{I}}} Z_\psi^{-1}(t) \frac{\beta^2 (2\pi)^{2d} \delta^2(\partial_t \bar{\Gamma}_t[\bar{\psi}, \psi, \varphi])}{\delta \bar{\psi}_{a_{\text{II}} c_{\text{II}}}(\nu_{n_{\text{II}}}, \vec{p}_{\text{II}}) \delta \bar{\psi}_{a_{\text{I}} c_{\text{I}}}(\nu_{n_{\text{I}}}, \vec{p}_{\text{I}})} \Big|_{\bar{\psi}=\psi=0}.
\end{aligned}$$

However, had we included RG scale dependent couplings via terms that are of higher order in momenta in our initial truncation in Eq. (E.1), such as $\bar{\psi} \square \not{\partial} \psi$ etc., these would show up on the l.h.s. of Eq. (E.13). Hence, in order to avoid admixtures to $\eta_\psi(t)$ which actually belong to those terms, we solely consider the coefficient on the r.h.s. of Eq. (E.13) that is proportional the square of the external spatial momentum, \vec{p}_{II}^2 . In practice, this is realized (especially within automatized derivations of flow equations via computer algebra programs [620, 621, 640, 622, 632]) by

1. Inserting Eq. (E.12) into the r.h.s. of Eq. (E.13).
2. Evaluating all possible traces in internal spaces (here contractions of the Dirac and the color indices) as well as all possible traces in momentum/frequency space (evaluating the Matsubara sums and the momentum integrals).
3. Dropping $\beta \delta_{n_{\text{II}}, n_{\text{I}}} (2\pi)^d \delta^{(d)}(\vec{p}_{\text{II}} - \vec{p}_{\text{I}})$ on both sides of Eq. (E.13).
4. Taking two derivatives w.r.t. the external momentum \vec{p}_{II} and evaluating the result at vanishing external momentum $\vec{p}_{\text{II}} = 0$. This corresponds to a Taylor expansion and comparison

of coefficients on both sides of Eq. (E.13).¹

Fermion mass In order to project the two-point function onto the fermion mass, which might perhaps be generated during the RG flow, we need to extract all terms from the two-point function that are diagonal in color and Dirac space at vanishing external momenta. A suitable projection reads

$$\begin{aligned} & \beta \delta_{n_{\text{II}}, n_{\text{I}}} (2\pi)^d \delta^{(d)}(0) Z_\psi^{-1}(t) \partial_t m(t) = \\ & = \beta \delta_{n_{\text{II}}, n_{\text{I}}} (2\pi)^d \delta^{(d)}(0) [\partial_t m_{\text{r}}(t) + \eta_\psi(t) m_{\text{r}}(t, \sigma_{\text{r}})] = \\ & = -\frac{1}{N} (\mathbb{1})^{c_{\text{I}}} c_{\text{II}} \frac{1}{d_\gamma} (\mathbb{1})^{a_{\text{I}}} a_{\text{II}} Z_\psi^{-1}(t) \frac{\beta^2 (2\pi)^{2d} \delta^2(\partial_t \bar{\Gamma}_t[\bar{\psi}, \psi, \varphi])}{\delta \bar{\psi}_{a_{\text{II}} c_{\text{II}}}(\nu_{n_{\text{II}}}, \vec{p}_{\text{II}}) \delta \bar{\psi}^{a_{\text{I}} c_{\text{I}}}(\nu_{n_{\text{I}}}, \vec{p}_{\text{I}})} \Big|_{\bar{\psi}=\psi=0, \vec{p}_{\text{II}}=\vec{p}_{\text{I}}=0}. \end{aligned} \quad (\text{E.14})$$

Again, after inserting Eq. (E.12) into the r.h.s. of Eq. (E.14) and the evaluation of all kind of traces, one may drop the factors $\beta \delta_{n_{\text{II}}, n_{\text{I}}} (2\pi)^d \delta^{(d)}(0)$, which occur on both sides of the equation. Since we are evaluating for vanishing fermion background fields and vanishing external momenta $\vec{p}_{\text{II}} = 0$ there are no admixtures.

Another possibly generated color-space-diagonal mass-like term for the fermions that breaks (discrete) chiral symmetry, Eqs. (8.19) and (8.20), is proportional to γ^{ch} instead of $\mathbb{1}$ in Dirac space. In order to investigate whether this term is generated if the initial UV action is chirally symmetric (has vanishing bare fermion mass), we can simply replace $\mathbb{1}$ by γ^{ch} in the projection prescription in Eq. (E.14).

Fermion mass

Let us first turn to the question whether there is a generation of fermion mass-like terms in RG flows of the purely fermionic GN model. Evaluating Eq. (E.14) with Eq. (E.12) one finds already by examining the traces in Dirac space,

$$-\frac{1}{N} (\mathbb{1})^{c_{\text{I}}} c_{\text{II}} \frac{1}{d_\gamma} (\mathbb{1})^{a_{\text{I}}} a_{\text{II}} Z_\psi^{-1}(t) (\text{E.12}) \Big|_{\vec{p}_{\text{II}}=\vec{p}_{\text{I}}=0} = 0, \quad (\text{E.15})$$

and

$$\frac{1}{N} (\mathbb{1})^{c_{\text{I}}} c_{\text{II}} \frac{1}{d_\gamma} (i\gamma^{\text{ch}})^{a_{\text{I}}} a_{\text{II}} Z_\psi^{-1}(t) (\text{E.12}) \Big|_{\vec{p}_{\text{II}}=\vec{p}_{\text{I}}=0} = 0. \quad (\text{E.16})$$

Hence, within the purely fermionic formulation of the GN model we will never observe (discrete) chiral symmetry breaking if the UV action is perfectly symmetric under discrete chiral transformations (8.19) and (8.20) and lacks any kind of mass-like term. The situation might differ as soon as discrete chiral symmetry is already explicitly broken by an initial mass term in the UV action, which might then grow and set the physical scale of the system.

¹Note that this Taylor expansion might not always be justified, *e.g.*, the two-point function could be non-analytic at $\vec{p}_{\text{II}} = 0$.

Anomalous dimension

Next, we consider the r.h.s. of the projection Eq. (E.13) for the t -evolution of the fermionic anomalous dimension. We find

$$\begin{aligned}
& \frac{1}{N} (\mathbb{1})^{c_I} c_{II} \frac{1}{d_\gamma} (i\vec{p}_{II} \cdot \vec{\gamma})^{a_I} a_{II} Z_\psi^{-1}(t) \Big|_{\vec{\psi}=\psi=0} \stackrel{(D.35)}{=} \quad (E.17) \\
& = \beta \delta_{n_{II}, n_I} (2\pi)^d \delta^{(d)}(\vec{p}_{II} - \vec{p}_I) \frac{1}{N} g_r^2(t) k^{-2} \times \\
& \quad \times \frac{1}{\beta} \sum_{n=-\infty}^{\infty} \int_{-\infty}^{\infty} \frac{d^d p}{(2\pi)^d} 2\vec{p}^2 \left[\frac{1}{2} \partial_t r_f(t, |\vec{p}|) + \frac{1}{2} \eta_\psi(t) r_f(t, |\vec{p}|) \right] \times \\
& \quad \times \left(f_n^{-1} \left(\frac{\vec{p}^2}{k^2} \right) - 2 \frac{\vec{p}^2}{k^2} [1 + r_f(t, |\vec{p}|)]^2 \right) f_n^2 \left(\frac{\vec{p}^2}{k^2} \right) \stackrel{(A.5)}{=} \\
& = \beta \delta_{n_{II}, n_I} (2\pi)^d \delta^{(d)}(\vec{p}_{II} - \vec{p}_I) \frac{1}{N} g_r^2(t) k^{-2} \times \\
& \quad \times \frac{1}{\beta} \sum_{n=-\infty}^{\infty} A_d d \int_0^\infty dp p^{d+1} 2 \left[\frac{1}{2} \partial_t r_f(t, p) + \frac{1}{2} \eta_\psi(t) r_f(t, p) \right] \times \\
& \quad \times \left(f_n^{-1} \left(\frac{p^2}{k^2} \right) - 2 \frac{p^2}{k^2} [1 + r_f(t, p)]^2 \right) f_n^2 \left(\frac{p^2}{k^2} \right) \stackrel{(D.7)}{=} \\
& = \beta \delta_{n_{II}, n_I} (2\pi)^d \delta^{(d)}(\vec{p}_{II} - \vec{p}_I) \frac{1}{N} g_r^2(t) k^d \times \\
& \quad \times \frac{1}{\beta} \sum_{n=-\infty}^{\infty} A_d d \int_0^\infty dy y^{\frac{d}{2}} \left[y \dot{r}_f(y) + \frac{1}{2} \eta_\psi(t) r_f(y) \right] \left(f_n^{-1}(y) - 2y [1 + r_f(y)]^2 \right) f_n^2(y) \stackrel{(D.24)}{=} \\
& = \beta \delta_{n_{II}, n_I} (2\pi)^d \delta^{(d)}(\vec{p}_{II} - \vec{p}_I) \frac{1}{N} g_r^2(t) k^d \times \\
& \quad \times \frac{1}{\beta} \sum_{n=-\infty}^{\infty} A_d d \int_0^1 dy \left[-\frac{1}{2} y^{\frac{d-1}{2}} + \frac{1}{2} \eta_\psi(t) (y^{\frac{d-1}{2}} - y^{\frac{d}{2}}) \right] [f_n^{-1}(1) - 2] f_n^2(1) = \\
& = -\beta \delta_{n_{II}, n_I} (2\pi)^d \delta^{(d)}(\vec{p}_{II} - \vec{p}_I) A_d \frac{d}{d+1} \left[1 - \frac{\eta_\psi(t)}{d+2} \right] \frac{1}{N} g_r^2(t) k^d \frac{1}{\beta} \sum_{n=-\infty}^{\infty} [f_n^1(1) - 2 f_n^2(1)]
\end{aligned}$$

During the evaluation we made use of various short-hand notations, variable transformations, and identities, which recurrently appear during the evaluation of the traces in RG flow equations. The respective formulae are referenced at the equal signs.

Inspecting our final result, we actually observe that the r.h.s. of Eq. (E.13) is (apart from the delta-distribution) independent of \vec{p}_{II} , such that $\eta_\psi(t) = 0$ and $Z_\psi(t)$ stays constant and keeps its initial UV value.

This result is rather generic for certain types of models and truncations and is easily understood by studying the Feynman graph in Eq. (E.11). The Feynman diagram is actually of “tadpole”-type, which means that the external momentum \vec{p}_{II} does not enter the loop, but exits the self-interaction process directly via the other open leg of the four-fermion vertex. In consequence, the loop momentum integration is not affected by the external momentum and the entire fermion-self-energy correction to the two-point function is momentum-independent. Therefore it does not alter the kinetic part of the two-point function and the corresponding coefficient, the wave-function renormalization $Z_\psi(t)$, is untouched. Nevertheless, one has to keep in mind that this result does not necessarily survive, if advanced truncations are considered. However, within truncations of purely

fermionic models that solely involve the “standard” kinetic term and some local four-fermion interactions, it generalizes to any dimension and model [348, 350, 351]. Furthermore, it is noteworthy that the same result (vanishing quantum corrections) is obtained for an advanced truncation, where the wave-function renormalization is split into two wave-function renormalizations, orthogonal and perpendicular to the heat bath (the temporal direction). We refer to Refs. [348, 350, 351] for further details.

E.1.2. Fermion four-point vertex – four-fermion coupling

Next, we turn to the RG flow equation of the generic four-fermion vertex and extract the flow equation of the four-fermion coupling in the scalar channel.

The four-point vertex

Also for the derivation of the RG flow equation of the four-point vertex the starting point is the ERG equation (C.51), where one takes two derivatives w.r.t. the Fourier-transformed fermion field $\tilde{\psi}$ and another two times w.r.t. $\tilde{\bar{\psi}}$. We do not perform these derivatives again, but utilize the universal field-space result of Appendix C.2.4, namely Eq. (C.56). If this generic equation is evaluated for the GN model in our truncation (9.1), we can again ignore contributions on the r.h.s. with n -point functions of odd order, as well as higher-order n -point functions, which are not included in our truncation. The only contributions that are *a priori* non-vanishing and that are compatible with the four-point vertex (E.4), the regulator (E.5), and the full propagator (E.9) read,

$$\begin{aligned}
& \partial_t \bar{\Gamma}_t^{(4)} \bar{\psi}_{\text{IV}} \psi_{\text{III}} \bar{\psi}_{\text{II}} \psi_{\text{I}} = \tag{E.18} \\
& = + \text{STr} \left[\left(\frac{1}{2} \partial_t R_t \right) G_t \bar{\Gamma}_t^{(4)} \psi_{\text{III}} \bar{\psi}_{\text{II}} G_t \bar{\Gamma}_t^{(4)} \bar{\psi}_{\text{IV}} \psi_{\text{I}} G_t \right] + \\
& + \text{STr} \left[\left(\frac{1}{2} \partial_t R_t \right) G_t \bar{\Gamma}_t^{(4)} \bar{\psi}_{\text{IV}} \bar{\psi}_{\text{II}} G_t \bar{\Gamma}_t^{(4)} \psi_{\text{III}} \psi_{\text{I}} G_t \right] + \\
& + \text{STr} \left[\left(\frac{1}{2} \partial_t R_t \right) G_t \bar{\Gamma}_t^{(4)} \bar{\psi}_{\text{IV}} \psi_{\text{III}} G_t \bar{\Gamma}_t^{(4)} \bar{\psi}_{\text{II}} \psi_{\text{I}} G_t \right] + \\
& + \text{STr} \left[\left(\frac{1}{2} \partial_t R_t \right) G_t \bar{\Gamma}_t^{(4)} \bar{\psi}_{\text{II}} \psi_{\text{I}} G_t \bar{\Gamma}_t^{(4)} \bar{\psi}_{\text{IV}} \psi_{\text{III}} G_t \right] + \\
& + \text{STr} \left[\left(\frac{1}{2} \partial_t R_t \right) G_t \bar{\Gamma}_t^{(4)} \psi_{\text{III}} \psi_{\text{I}} G_t \bar{\Gamma}_t^{(4)} \bar{\psi}_{\text{IV}} \bar{\psi}_{\text{II}} G_t \right] + \\
& + \text{STr} \left[\left(\frac{1}{2} \partial_t R_t \right) G_t \bar{\Gamma}_t^{(4)} \bar{\psi}_{\text{IV}} \psi_{\text{I}} G_t \bar{\Gamma}_t^{(4)} \psi_{\text{III}} \bar{\psi}_{\text{II}} G_t \right] = \\
& = + (-1)^{\bar{\psi}_{\text{IV}} \psi_5} (-1)^{\bar{\psi}_{\text{IV}} \psi_4} (-1)^{\bar{\psi}_{\text{IV}} \bar{\psi}_{\text{II}}} (-1)^{\bar{\psi}_{\text{IV}} \psi_{\text{III}}} (-1)^{\bar{\psi}_{\text{IV}} \psi_2} (-1)^{\psi_{\text{III}} \psi_2} (-1)^{\bar{\psi}_{\text{II}} \psi_2} (-1)^{\psi_1 \psi_2} \times \\
& \quad \times \left(\frac{1}{2} \partial_t R_t^{\bar{\psi}_1 \psi_2} \right) G_{t, \bar{\psi}_2 \psi_3} \bar{\Gamma}_t^{(4)} \bar{\psi}_3 \psi_{\text{III}} \bar{\psi}_{\text{II}} \bar{\psi}_4 \mathbf{g}_{\bar{\psi}_4}^{\psi_5} G_{t, \bar{\psi}_5 \psi_6} \bar{\Gamma}_t^{(4)} \bar{\psi}_6 \bar{\psi}_{\text{IV}} \psi_1 \bar{\psi}_7 \mathbf{g}_{\bar{\psi}_7}^{\psi_8} G_{t, \bar{\psi}_8 \psi_1} + \\
& + (-1)^{\bar{\psi}_{\text{IV}} \psi_5} (-1)^{\bar{\psi}_{\text{IV}} \psi_4} (-1)^{\bar{\psi}_{\text{IV}} \bar{\psi}_{\text{II}}} (-1)^{\bar{\psi}_{\text{IV}} \psi_{\text{III}}} (-1)^{\bar{\psi}_{\text{IV}} \psi_2} (-1)^{\psi_{\text{III}} \psi_2} (-1)^{\bar{\psi}_{\text{II}} \psi_2} (-1)^{\psi_1 \psi_2} \times \\
& \quad \times \left(\frac{1}{2} \partial_t R_t^{\psi_1 \bar{\psi}_2} \right) G_{t, \psi_2 \bar{\psi}_3} \bar{\Gamma}_t^{(4)} \psi_3 \psi_{\text{III}} \bar{\psi}_{\text{II}} \bar{\psi}_4 \mathbf{g}_{\psi_4}^{\bar{\psi}_5} G_{t, \psi_5 \bar{\psi}_6} \bar{\Gamma}_t^{(4)} \bar{\psi}_6 \bar{\psi}_{\text{IV}} \psi_1 \bar{\psi}_7 \mathbf{g}_{\psi_7}^{\bar{\psi}_8} G_{t, \psi_8 \bar{\psi}_1} + \\
& + (-1)^{\bar{\psi}_{\text{IV}} \psi_2} (-1)^{\psi_{\text{III}} \psi_5} (-1)^{\psi_{\text{III}} \psi_4} (-1)^{\psi_{\text{III}} \bar{\psi}_{\text{II}}} (-1)^{\psi_{\text{III}} \psi_2} (-1)^{\bar{\psi}_{\text{II}} \psi_2} (-1)^{\psi_1 \psi_2} \times \\
& \quad \times \left(\frac{1}{2} \partial_t R_t^{\psi_1 \bar{\psi}_2} \right) G_{t, \psi_2 \bar{\psi}_3} \bar{\Gamma}_t^{(4)} \psi_3 \bar{\psi}_{\text{IV}} \bar{\psi}_{\text{II}} \bar{\psi}_4 \mathbf{g}_{\bar{\psi}_4}^{\psi_5} G_{t, \bar{\psi}_5 \psi_6} \bar{\Gamma}_t^{(4)} \bar{\psi}_6 \psi_{\text{III}} \psi_1 \bar{\psi}_7 \mathbf{g}_{\bar{\psi}_7}^{\psi_8} G_{t, \psi_8 \bar{\psi}_1} +
\end{aligned}$$

$$\begin{aligned}
& -2 \left(\frac{1}{2} \partial_t R_t^{\bar{\psi}_1 \psi_2} \right) G_{t, \bar{\psi}_2 \psi_3} \bar{\Gamma}_t^{(4) \bar{\psi}_3 \psi_I \bar{\psi}_{IV} \psi_4} \mathbf{g}_{\bar{\psi}_4}^{\psi_5} G_{t, \bar{\psi}_5 \psi_6} \bar{\Gamma}_t^{(4) \bar{\psi}_6 \psi_{III} \bar{\psi}_{II} \psi_7} \mathbf{g}_{\bar{\psi}_7}^{\psi_8} G_{t, \bar{\psi}_8 \psi_1} = \\
= & +2 \left(\frac{1}{2} \partial_t R_t^{\bar{\psi}_1 \psi_2} \right) (\bar{\Gamma}_t^{(2)} + R_t)^{-1}_{\bar{\psi}_2 \psi_3} \bar{\Gamma}_t^{(4) \bar{\psi}_3 \psi_{III} \bar{\psi}_{II} \psi_4} (\bar{\Gamma}_t^{(2)} + R_t)^{-1}_{\bar{\psi}_4 \psi_5} \times \tag{Atr1} \\
& \times \bar{\Gamma}_t^{(4) \bar{\psi}_5 \psi_I \bar{\psi}_{IV} \psi_6} (\bar{\Gamma}_t^{(2)} + R_t)^{-1}_{\bar{\psi}_6 \psi_1} - \\
& -2 \left(\frac{1}{2} \partial_t R_t^{\bar{\psi}_1 \psi_2} \right) (\bar{\Gamma}_t^{(2)} + R_t)^{-1}_{\bar{\psi}_2 \psi_3} \bar{\Gamma}_t^{(4) \bar{\psi}_3 \psi_{III} \bar{\psi}_{IV} \psi_4} (\bar{\Gamma}_t^{(2)} + R_t)^{-1}_{\bar{\psi}_4 \psi_5} \times \tag{Atr2} \\
& \times \bar{\Gamma}_t^{(4) \bar{\psi}_5 \psi_I \bar{\psi}_{II} \psi_6} (\bar{\Gamma}_t^{(2)} + R_t)^{-1}_{\bar{\psi}_6 \psi_1} - \\
& -2 \left(\frac{1}{2} \partial_t R_t^{\bar{\psi}_1 \psi_2} \right) (\bar{\Gamma}_t^{(2)} + R_t)^{-1}_{\bar{\psi}_2 \psi_3} \bar{\Gamma}_t^{(4) \bar{\psi}_3 \psi_I \bar{\psi}_{IV} \psi_4} (\bar{\Gamma}_t^{(2)} + R_t)^{-1}_{\bar{\psi}_4 \psi_5} \times \tag{Atr3} \\
& \times \bar{\Gamma}_t^{(4) \bar{\psi}_5 \psi_{III} \bar{\psi}_{IV} \psi_6} (\bar{\Gamma}_t^{(2)} + R_t)^{-1}_{\bar{\psi}_6 \psi_1} + \\
& +2 \left(\frac{1}{2} \partial_t R_t^{\bar{\psi}_1 \psi_2} \right) (\bar{\Gamma}_t^{(2)} + R_t)^{-1}_{\bar{\psi}_2 \psi_3} \bar{\Gamma}_t^{(4) \bar{\psi}_3 \psi_{III} \bar{\psi}_4 \psi_I} (\bar{\Gamma}_t^{(2)} + R_t)^{-1}_{\bar{\psi}_4 \psi_5} \times \tag{Atr4} \\
& \times \bar{\Gamma}_t^{(4) \bar{\psi}_{IV} \psi_5 \bar{\psi}_{II} \psi_6} (\bar{\Gamma}_t^{(2)} + R_t)^{-1}_{\bar{\psi}_6 \psi_1} + \\
& +2 \left(\frac{1}{2} \partial_t R_t^{\bar{\psi}_1 \psi_2} \right) (\bar{\Gamma}_t^{(2)} + R_t)^{-1}_{\bar{\psi}_2 \psi_3} \bar{\Gamma}_t^{(4) \bar{\psi}_3 \psi_I \bar{\psi}_{IV} \psi_4} (\bar{\Gamma}_t^{(2)} + R_t)^{-1}_{\bar{\psi}_4 \psi_5} \times \tag{Atr5} \\
& \times \bar{\Gamma}_t^{(4) \bar{\psi}_5 \psi_{III} \bar{\psi}_{II} \psi_6} (\bar{\Gamma}_t^{(2)} + R_t)^{-1}_{\bar{\psi}_6 \psi_1}
\end{aligned}$$

The entire equation was evaluated on a constant background-field configuration with vanishing fermion fields. Additionally, some of the contributions are combined by employing that the trace of an object and its transpose are the same. The $(-1)^{\text{ab}}$ factors are evaluated via Eq. (C.6). In addition Eq. (C.13) and Eq. (C.42) are used for further simplifications.

It is more instructive to depict this equation in terms of its graphic Feynman-diagram representation, which is given by

$$\begin{aligned}
& \partial_t \left(\begin{array}{c} \bar{\psi}_{IV} \quad \psi_{III} \\ \swarrow \quad \nearrow \\ \circ \\ \searrow \quad \swarrow \\ \psi_I \quad \bar{\psi}_{II} \end{array} \right) = \tag{E.19} \\
= & +2 \begin{array}{c} \bar{\psi}_{IV} \quad \psi_{III} \\ \swarrow \quad \nearrow \\ \circ \quad \otimes \quad \circ \\ \searrow \quad \swarrow \\ \psi_I \quad \bar{\psi}_{II} \end{array} - 2 \begin{array}{c} \bar{\psi}_{IV} \quad \psi_{III} \\ \swarrow \quad \nearrow \\ \circ \quad \circ \\ \searrow \quad \swarrow \\ \psi_I \quad \bar{\psi}_{II} \end{array} - 2 \begin{array}{c} \bar{\psi}_{IV} \quad \psi_{III} \\ \swarrow \quad \nearrow \\ \circ \quad \circ \\ \searrow \quad \swarrow \\ \psi_I \quad \bar{\psi}_{II} \end{array} + \\
& +2 \begin{array}{c} \bar{\psi}_{IV} \quad \psi_{III} \\ \swarrow \quad \nearrow \\ \circ \quad \circ \\ \searrow \quad \swarrow \\ \psi_I \quad \bar{\psi}_{II} \end{array} + 2 \begin{array}{c} \bar{\psi}_{IV} \quad \psi_{III} \\ \swarrow \quad \nearrow \\ \circ \quad \otimes \quad \circ \\ \searrow \quad \swarrow \\ \psi_I \quad \bar{\psi}_{II} \end{array} .
\end{aligned}$$

Here the diagrams on the r.h.s. are listed according to the order of the corresponding formulae (Atr1) to (Atr5).

Projection

The RG flow equation for the four-fermion vertex (E.18) and (E.19) is still rather generic and we would obtain the same diagrams for theories with additional local four-fermion interactions, *e.g.*, the χ GN model or NJL type models, *cf.* Refs. [527, 347, 346, 348, 350, 351]. In addition, the diagrams in Eq. (E.19) correspond to different physical processes, depending on the contraction of the external fermion lines. Therefore it is not surprising that the various local four-fermion couplings in advanced models mix and their corresponding RG flow equations form a set of coupled ODEs.

Hence, we would find contributions of the scalar four-fermion coupling $g(t)$ to basically any other relevant four-fermion interaction channel. This implies that in general also other four-fermion couplings, *e.g.*, pseudo-scalar interactions, are generated during the RG flow (at least at finite N), even though they are initially zero. The same holds true the other way round. For details, we refer to Refs. [346, 348, 350, 351]

Within this work, we ignore this effect and restrict our analysis to the scalar interaction channel at finite and infinite N , which is of course a crude approximation.

There are two possible equivalent projections on the scalar four-fermion interaction channel. Either one contracts external fermion lines I+II and III+IV with identity matrices in color and Dirac space or one chooses the combination I+IV and III+II. In any case, the idea behind is that the contracted external fermion legs have the same quantum numbers as a scalar bosonic particle and the initial interaction currents in the four-fermion interaction of our effective average action Eq. (E.1). The entire flow equation is evaluated at zero spatial momentum exchange $\vec{p}_I = \vec{p}_{II} = \vec{p}_{III} = \vec{p}_{IV} = 0$. Evaluating at another momentum configurations would actually spoil our truncation, which corresponds to the lowest order in a derivative expansion about the Fermi surface. Our truncation simply ignores a possible spatial momentum structure of the four-fermion interaction.

However, for the external Matsubara frequencies the situation is slightly different. Fermions do not have a zero mode and the smallest fermion energy is given by the smallest discrete Matsubara frequency (A.30), namely $\nu_0 = \pi T$. Therefore, we cannot simply evaluate our equations at $\nu_0 = 0$. Hence, for the time being, we do not further specify the frequency configuration and keep the “indices” of the Matsubara frequencies n_I, \dots, n_{IV} unspecified.

The actual projection prescription is therefore given by

$$\begin{aligned}
& \beta \delta_{n_{II}+n_{IV}, n_I+n_{III}} (2\pi)^d \delta^{(d)}(0) Z_\psi^{-2}(t) \partial_t g^2(t) = \tag{E.20} \\
& = \beta \delta_{n_{II}+n_{IV}, n_I+n_{III}} (2\pi)^d \delta^{(d)}(0) [\partial_t g_r^2(t) + 2 \eta_\psi(t) g_r^2(t)] = \\
& = - \frac{1}{d_\gamma} \frac{1}{d_\gamma N - 1} Z_\psi^{-2}(t) [(\mathbb{1})^{a_I} (\mathbb{1})^{a_{III}} (\mathbb{1})^{c_I} (\mathbb{1})^{c_{III}} (\mathbb{1})^{c_{IV}}] \times \\
& \quad \times \frac{\beta^4 (2\pi)^{4d} \delta^4(\partial_t \bar{\Gamma}_t[\bar{\psi}, \psi, \varphi])}{\delta \tilde{\psi}_{a_{IV} c_{IV}}(\nu_{n_{IV}}, \vec{p}_{IV}) \delta \tilde{\psi}^{a_{III} c_{III}}(\nu_{n_{III}}, \vec{p}_{III}) \delta \tilde{\psi}_{a_{II} c_{II}}(\nu_{n_{II}}, \vec{p}_{II}) \delta \tilde{\psi}^{a_I c_I}(\nu_{n_I}, \vec{p}_I)} \Big|_{\vec{\psi}=\psi=0, \vec{p}_{IV}=\dots=\vec{p}_I=0},
\end{aligned}$$

where we introduced the renormalized four-fermion coupling $g_r(t)$, which is rescaled by appropriate powers of $Z_\psi(t)$.

Next, we successively discuss the traces (Atr1) to (Atr5) and explicitly insert our formulae for the regulator (E.5), the four-fermion vertex (E.4), and the full propagator (E.9). Afterwards, these expressions are inserted into the r.h.s. of Eq. (E.20) and evaluated for each type of diagram separately. For the evaluation of the traces over spinor indices we used the FORMTRACER software [640].

Traces (Atr1) and (Atr5)

Before we apply our specific projection and evaluate traces, we insert Eqs. (E.5), (E.4), and (E.9) into Eq. (Atr1),

$$\begin{aligned}
(\text{Atr1}) &= 2 \begin{array}{c} \begin{array}{c} \psi \\ \psi_{\text{IV}} \\ \psi_{\text{I}} \end{array} \begin{array}{c} \psi \\ \psi_{\text{III}} \\ \psi_{\text{II}} \end{array} \\ \begin{array}{c} \psi \\ \psi_{\text{II}} \\ \psi_{\text{I}} \end{array} \end{array} = \tag{E.21} \\
&= + 2 \frac{1}{\beta^6} \sum_{n_1, \dots, n_6 = -\infty}^{\infty} \int_{-\infty}^{\infty} \frac{d^d p_1}{(2\pi)^d} \cdots \frac{d^d p_6}{(2\pi)^d} \times \\
&\quad \times (-1) \beta \delta_{n_1, n_2} (2\pi)^d \delta^{(d)}(\vec{p}_1 - \vec{p}_2) (\mathbb{1})^{c_1 c_2} i\vec{p}_1 \cdot (\vec{\gamma})^{a_1 a_2} \partial_t [Z_\psi(t) \frac{1}{2} r_f(t, |\vec{p}_1|)] \times \\
&\quad \times \beta \delta_{n_2, n_3} (2\pi)^d \delta^{(d)}(\vec{p}_2 - \vec{p}_3) \frac{[i(\nu_{n_2} + i\mu) \gamma^{d+1} + i\vec{p}_2 \cdot \vec{\gamma} [1 + r_f(t, |\vec{p}_2|)]]^{a_2} (\mathbb{1})^{c_2 c_3}}{Z_\psi(t) [(\nu_{n_2} + i\mu)^2 + \vec{p}_2^2 [1 + r_f(t, |\vec{p}_2|)]]^2} \times \\
&\quad \times (-1) 2 \beta \delta_{n_{\text{II}} + n_3, n_4 + n_{\text{III}}} (2\pi)^d \delta^{(d)}(\vec{p}_{\text{II}} - \vec{p}_4 + \vec{p}_3 - \vec{p}_{\text{III}}) \frac{1}{2N} g^2(t) \times \\
&\quad \times [(\mathbb{1})^{a_{\text{II}}} (\mathbb{1})^{a_4} (\mathbb{1})^{c_{\text{III}}} (\mathbb{1})^{c_4} (\mathbb{1})^{c_{\text{III}}} - (\mathbb{1})^{a_3} (\mathbb{1})^{a_{\text{II}}} (\mathbb{1})^{c_3} (\mathbb{1})^{c_{\text{III}}}] \times \\
&\quad \times \beta \delta_{n_4, n_5} (2\pi)^d \delta^{(d)}(\vec{p}_4 - \vec{p}_5) \frac{[i(\nu_{n_4} + i\mu) \gamma^{d+1} + i\vec{p}_4 \cdot \vec{\gamma} [1 + r_f(t, |\vec{p}_4|)]]^{a_4} (\mathbb{1})^{c_4 c_5}}{Z_\psi(t) [(\nu_{n_4} + i\mu)^2 + \vec{p}_4^2 [1 + r_f(t, |\vec{p}_4|)]]^2} \times \\
&\quad \times (-1) 2 \beta \delta_{n_{\text{IV}} + n_5, n_6 + n_{\text{I}}} (2\pi)^d \delta^{(d)}(\vec{p}_{\text{IV}} - \vec{p}_6 + \vec{p}_5 - \vec{p}_{\text{I}}) \frac{1}{2N} g^2(t) \times \\
&\quad \times [(\mathbb{1})^{a_{\text{IV}}} (\mathbb{1})^{a_5} (\mathbb{1})^{c_{\text{I}}} (\mathbb{1})^{c_5} (\mathbb{1})^{c_{\text{I}}} - (\mathbb{1})^{a_5} (\mathbb{1})^{a_{\text{IV}}} (\mathbb{1})^{c_5} (\mathbb{1})^{c_{\text{I}}}] \times \\
&\quad \times \beta \delta_{n_6, n_1} (2\pi)^d \delta^{(d)}(\vec{p}_6 - \vec{p}_1) \frac{[i(\nu_{n_6} + i\mu) \gamma^{d+1} + i\vec{p}_6 \cdot \vec{\gamma} [1 + r_f(t, |\vec{p}_6|)]]^{a_6} (\mathbb{1})^{c_6 c_1}}{Z_\psi(t) [(\nu_{n_6} + i\mu)^2 + \vec{p}_6^2 [1 + r_f(t, |\vec{p}_6|)]]^2}.
\end{aligned}$$

Applying our projection (E.20) to this diagram, we obtain

$$\begin{aligned}
&- \frac{1}{d_\gamma} \frac{1}{d_\gamma N - 1} Z_\psi^{-2}(t) [(\mathbb{1})^{a_{\text{I}}} (\mathbb{1})^{a_{\text{III}}} (\mathbb{1})^{c_{\text{I}}} (\mathbb{1})^{c_{\text{III}}} (\mathbb{1})^{c_{\text{IV}}}] (\text{Atr1}) \Big|_{\vec{p}_{\text{IV}} = \dots = \vec{p}_{\text{I}} = 0} \stackrel{(\text{D.35})}{=} \tag{E.22} \\
&= + \beta \delta_{n_{\text{II}} + n_{\text{IV}}, n_{\text{I}} + n_{\text{III}}} (2\pi)^d \delta^{(d)}(0) \frac{1}{N} \frac{d_\gamma N - 2}{d_\gamma N - 1} g_r^4(t) k^{-4} \times \\
&\quad \times \frac{1}{\beta} \sum_{n = -\infty}^{\infty} \int_{-\infty}^{\infty} \frac{d^d p}{(2\pi)^d} 2 \vec{p}^2 \left[\frac{1}{2} \partial_t r_f(t, |\vec{p}|) + \frac{1}{2} \eta_\psi(t) r_f(t, |\vec{p}|) \right] [1 + r_f(t, |\vec{p}|)] \times \\
&\quad \times \frac{(\nu_n + i\mu) [2(\nu_{n+n_{\text{II}}-n_{\text{III}}} + i\mu) - (\nu_n + i\mu)] + \vec{p}^2 [1 + r_f(t, |\vec{p}|)]}{(\nu_{n+n_{\text{II}}-n_{\text{III}}} + i\mu)^2 + \vec{p}^2 [1 + r_f(t, |\vec{p}|)]^2} \hat{f}_n^2 \left(\frac{\vec{p}^2}{k^2} \right) \stackrel{(\text{A.5})}{=} \\
&= + \beta \delta_{n_{\text{II}} + n_{\text{IV}}, n_{\text{I}} + n_{\text{III}}} (2\pi)^d \delta^{(d)}(0) \frac{1}{N} \frac{d_\gamma N - 2}{d_\gamma N - 1} g_r^4(t) k^{-4} \times
\end{aligned}$$

$$\begin{aligned}
& \times \frac{1}{\beta} \sum_{n=-\infty}^{\infty} A_d d \int_0^{\infty} dp p^{d+1} 2 \left[\frac{1}{2} \partial_t r_f(t, p) + \frac{1}{2} \eta_\psi(t) r_f(t, p) \right] [1 + r_f(t, p)] \times \\
& \times \frac{(\nu_n + i\mu) [2(\nu_{n+n_{\text{II}}-n_{\text{III}}} + i\mu) - (\nu_n + i\mu)] + p^2 [1 + r_f(t, p)]}{(\nu_{n+n_{\text{II}}-n_{\text{III}}} + i\mu)^2 + p^2 [1 + r_f(t, p)]^2} \hat{f}_n^2\left(\frac{p^2}{k^2}\right) \stackrel{\text{(D.7)}}{=} \\
& = + \beta \delta_{n_{\text{II}}+n_{\text{IV}}, n_{\text{I}}+n_{\text{III}}} (2\pi)^d \delta^{(d)}(0) \frac{1}{N} \frac{d_\gamma N-2}{d_\gamma N-1} g_r^4(t) k^{d-2} \times \\
& \times \frac{1}{\beta} \sum_{n=-\infty}^{\infty} A_d d \int_0^{\infty} dy y^{\frac{d}{2}} [y \hat{r}_f(y) + \frac{1}{2} \eta_\psi(t) r_f(y)] [1 + r_f(y)] \times \\
& \times \frac{\frac{1}{k^2} (\nu_n + i\mu) (\nu_{n+2(n_{\text{II}}-n_{\text{III}})} + i\mu) + y^2 [1 + r_f(y)]}{\frac{1}{k^2} (\nu_{n+n_{\text{II}}-n_{\text{III}}} + i\mu)^2 + y^2 [1 + r_f(y)]^2} \hat{f}_n^2(y) \stackrel{\text{(D.25)}}{=} \\
& = - \beta \delta_{n_{\text{II}}+n_{\text{IV}}, n_{\text{I}}+n_{\text{III}}} (2\pi)^d \delta^{(d)}(0) A_d \left[1 - \frac{\eta_\psi(t)}{d+1} \right] \frac{1}{N} \frac{d_\gamma N-2}{d_\gamma N-1} g_r^4(t) k^{d-2} \times \\
& \times \frac{1}{\beta} \sum_{n=-\infty}^{\infty} \frac{\frac{1}{k^2} (\nu_n + i\mu) [2(\nu_{n+n_{\text{II}}-n_{\text{III}}} + i\mu) - (\nu_n + i\mu)] + 1}{\frac{1}{k^2} (\nu_{n+n_{\text{II}}-n_{\text{III}}} + i\mu)^2 + 1} \hat{f}_n^2(1) ,
\end{aligned}$$

During the evaluation the formulae which are referenced at the equal signs are used.

Inspecting the final result and the projection, one observes that trace (Atr5) leads to an identical contribution to the RG flow equation, because traces (Atr1) and (Atr5) are related by a simultaneous exchange of $n_{\text{II}} \leftrightarrow n_{\text{IV}}$ and $n_{\text{I}} \leftrightarrow n_{\text{III}}$, which can be directly seen in Eq. (E.19). As we are projecting onto the scalar channel by a contraction of the legs I+II and III+IV, the simultaneous exchange of the external legs has no effect and we obtain the same result.

Traces (Atr2) and (Atr3)

Next, we turn to trace (Atr2) and again insert Eqs. (E.5), (E.4), and (E.9),

$$\begin{aligned}
& \text{(Atr2)} = -2 \begin{array}{c} \bar{\psi}_{\text{IV}} \quad \psi_{\text{III}} \\ \swarrow \quad \searrow \\ \circ \\ \uparrow \quad \downarrow \\ \psi \quad \psi \\ \otimes \\ \psi \quad \psi \\ \swarrow \quad \searrow \\ \psi_{\text{I}} \quad \bar{\psi}_{\text{II}} \end{array} = \tag{E.23} \\
& = -2 \frac{1}{\beta^6} \sum_{n_1, \dots, n_6 = -\infty}^{\infty} \int_{-\infty}^{\infty} \frac{d^d p_1}{(2\pi)^d} \dots \frac{d^d p_6}{(2\pi)^d} \times \\
& \times (-1) \beta \delta_{n_1, n_2} (2\pi)^d \delta^{(d)}(\vec{p}_1 - \vec{p}_2) (\mathbb{1})^{c_1}{}_{c_2} i\vec{p}_1 \cdot (\vec{\gamma})^{a_1}{}_{a_2} \partial_t [Z_\psi(t) \frac{1}{2} r_f(t, |\vec{p}_1|)] \times \\
& \times \beta \delta_{n_2, n_3} (2\pi)^d \delta^{(d)}(\vec{p}_2 - \vec{p}_3) \frac{[i(\nu_{n_2} + i\mu) \gamma^{d+1} + i\vec{p}_2 \cdot \vec{\gamma} [1 + r_f(t, |\vec{p}_2|)]]^{a_2}{}_{a_3} (\mathbb{1})^{c_2}{}_{c_3}}{Z_\psi(t) [(\nu_{n_2} + i\mu)^2 + \vec{p}_2^2 [1 + r_f(t, |\vec{p}_2|)]^2]} \times \\
& \times (-1) 2 \beta \delta_{n_{\text{IV}}+n_3, n_4+n_{\text{III}}} (2\pi)^d \delta^{(d)}(\vec{p}_{\text{IV}} - \vec{p}_4 + \vec{p}_3 - \vec{p}_{\text{III}}) \frac{1}{2N} g^2(t) \times \\
& \times [(\mathbb{1})^{a_{\text{IV}}}{}_{a_4} (\mathbb{1})^{a_3}{}_{a_{\text{III}}} (\mathbb{1})^{c_{\text{IV}}}{}_{c_4} (\mathbb{1})^{c_3}{}_{c_{\text{III}}} - (\mathbb{1})^{a_3}{}_{a_4} (\mathbb{1})^{a_{\text{IV}}}{}_{a_{\text{III}}} (\mathbb{1})^{c_3}{}_{c_4} (\mathbb{1})^{c_{\text{IV}}}{}_{c_{\text{III}}}] \times \\
& \times \beta \delta_{n_4, n_5} (2\pi)^d \delta^{(d)}(\vec{p}_4 - \vec{p}_5) \frac{[i(\nu_{n_4} + i\mu) \gamma^{d+1} + i\vec{p}_4 \cdot \vec{\gamma} [1 + r_f(t, |\vec{p}_4|)]]^{a_4}{}_{a_5} (\mathbb{1})^{c_4}{}_{c_5}}{Z_\psi(t) [(\nu_{n_4} + i\mu)^2 + \vec{p}_4^2 [1 + r_f(t, |\vec{p}_4|)]^2]} \times
\end{aligned}$$

$$\begin{aligned}
& \times (-1) 2 \beta \delta_{n_{\text{II}}+n_5, n_6+n_1} (2\pi)^d \delta^{(d)}(\vec{p}_{\text{II}} - \vec{p}_6 + \vec{p}_5 - \vec{p}_1) \frac{1}{2N} g^2(t) \times \\
& \times [(\mathbb{1})^{a_{\text{II}}} (\mathbb{1})^{a_5} (\mathbb{1})^{c_{\text{II}}} (\mathbb{1})^{c_5} (\mathbb{1})^{c_1} - (\mathbb{1})^{a_5} (\mathbb{1})^{a_{\text{II}}} (\mathbb{1})^{c_5} (\mathbb{1})^{c_{\text{II}}} (\mathbb{1})^{c_1}] \times \\
& \times \beta \delta_{n_6, n_1} (2\pi)^d \delta^{(d)}(\vec{p}_6 - \vec{p}_1) \frac{[\text{i}(\nu_{n_6} + \text{i}\mu) \gamma^{d+1} + \text{i}\vec{p}_6 \cdot \vec{\gamma} [1 + r_{\text{f}}(t, |\vec{p}_6|)]]^{a_6} (\mathbb{1})^{c_6} (\mathbb{1})^{c_1}}{Z_\psi(t) [(\nu_{n_6} + \text{i}\mu)^2 + \vec{p}_6^2 [1 + r_{\text{f}}(t, |\vec{p}_6|)]^2]} .
\end{aligned}$$

Using projection Eq. (E.20), the contribution of trace (Atr2) to the RG flow evaluates to,

$$\begin{aligned}
& - \frac{1}{d_\gamma} \frac{1}{d_\gamma N - 1} Z_\psi^{-2}(t) [(\mathbb{1})^{a_{\text{II}}} (\mathbb{1})^{a_{\text{III}}} (\mathbb{1})^{c_{\text{I}}} (\mathbb{1})^{c_{\text{II}}} (\mathbb{1})^{c_{\text{IV}}}] (\text{Atr2}) \Big|_{\vec{p}_{\text{IV}}=\dots=\vec{p}_{\text{I}}=0} \stackrel{(\text{D.35})}{=} \quad (\text{E.24}) \\
& = - \beta \delta_{n_{\text{II}}+n_{\text{IV}}, n_{\text{I}}+n_{\text{III}}} (2\pi)^d \delta^{(d)}(0) \frac{1}{N} (d_\gamma N - 1) g_{\text{r}}^4(t) k^{-4} \times \\
& \times \frac{1}{\beta} \sum_{n=-\infty}^{\infty} \int_{-\infty}^{\infty} \frac{d^d p}{(2\pi)^d} 2 \vec{p}^2 \left[\frac{1}{2} \partial_t r_{\text{f}}(t, |\vec{p}|) + \frac{1}{2} \eta_\psi(t) r_{\text{f}}(t, |\vec{p}|) \right] [1 + r_{\text{f}}(t, |\vec{p}|)] \times \\
& \times \frac{(\nu_n + \text{i}\mu) [2(\nu_{n+n_{\text{IV}}-n_{\text{III}}} + \text{i}\mu) - (\nu_n + \text{i}\mu)] + \vec{p}^2 [1 + r_{\text{f}}(t, |\vec{p}|)]}{(\nu_{n+n_{\text{IV}}-n_{\text{III}}} + \text{i}\mu)^2 + \vec{p}^2 [1 + r_{\text{f}}(t, |\vec{p}|)]^2} \mathfrak{f}_n^2\left(\frac{\vec{p}^2}{k^2}\right) \stackrel{(\text{A.5})}{=} \\
& = - \beta \delta_{n_{\text{II}}+n_{\text{IV}}, n_{\text{I}}+n_{\text{III}}} (2\pi)^d \delta^{(d)}(0) \frac{1}{N} (d_\gamma N - 1) g_{\text{r}}^4(t) k^{-4} \times \\
& \times \frac{1}{\beta} \sum_{n=-\infty}^{\infty} A_d d \int_0^\infty dp p^{d+1} 2 \left[\frac{1}{2} \partial_t r_{\text{f}}(t, p) + \frac{1}{2} \eta_\psi(t) r_{\text{f}}(t, p) \right] [1 + r_{\text{f}}(t, p)] \times \\
& \times \frac{(\nu_n + \text{i}\mu) [2(\nu_{n+n_{\text{IV}}-n_{\text{III}}} + \text{i}\mu) - (\nu_n + \text{i}\mu)] + p^2 [1 + r_{\text{f}}(t, p)]}{(\nu_{n+n_{\text{IV}}-n_{\text{III}}} + \text{i}\mu)^2 + p^2 [1 + r_{\text{f}}(t, p)]^2} \mathfrak{f}_n^2\left(\frac{p^2}{k^2}\right) \stackrel{(\text{D.7})}{=} \\
& = - \beta \delta_{n_{\text{II}}+n_{\text{IV}}, n_{\text{I}}+n_{\text{III}}} (2\pi)^d \delta^{(d)}(0) \frac{1}{N} (d_\gamma N - 1) g_{\text{r}}^4(t) k^{d-2} \times \\
& \times \frac{1}{\beta} \sum_{n=-\infty}^{\infty} A_d d \int_0^\infty dy y^{\frac{d}{2}} \left[y \dot{r}_{\text{f}}(y) + \frac{1}{2} \eta_\psi(t) r_{\text{f}}(y) \right] [1 + r_{\text{f}}(y)] \times \\
& \times \frac{\frac{1}{k^2} (\nu_n + \text{i}\mu) (\nu_{n+2(n_{\text{IV}}-n_{\text{III}})} + \text{i}\mu) + y^2 [1 + r_{\text{f}}(y)]}{\frac{1}{k^2} (\nu_{n+n_{\text{IV}}-n_{\text{III}}} + \text{i}\mu)^2 + y^2 [1 + r_{\text{f}}(y)]^2} \mathfrak{f}_n^2(y) \stackrel{(\text{D.25})}{=} \\
& = + \beta \delta_{n_{\text{II}}+n_{\text{IV}}, n_{\text{I}}+n_{\text{III}}} (2\pi)^d \delta^{(d)}(0) A_d \left[1 - \frac{\eta_\psi(t)}{d+1} \right] \frac{1}{N} (d_\gamma N - 1) g_{\text{r}}^4(t) k^{d-2} \times \\
& \times \frac{1}{\beta} \sum_{n=-\infty}^{\infty} \frac{\frac{1}{k^2} (\nu_n + \text{i}\mu) [2(\nu_{n+n_{\text{IV}}-n_{\text{III}}} + \text{i}\mu) - (\nu_n + \text{i}\mu)] + 1}{\frac{1}{k^2} (\nu_{n+n_{\text{IV}}-n_{\text{III}}} + \text{i}\mu)^2 + 1} \mathfrak{f}_n^2(1) .
\end{aligned}$$

Similarly to the traces (Atr1) and (Atr5), one finds that the trace (Atr2) and (Atr3) equally contribute to the RG flow.

Trace (Atr4)

It remains to evaluate trace (Atr4). We proceed analogously to the previous traces. However, note that the internal fermion lines in the loop of trace (Atr4) point into the same direction, which leads to a different ordering of the indices than before and an additional minus sign in front of

one of the propagators in the following expression.

$$\begin{aligned}
(\text{Atr4}) &= +2 \begin{array}{c} \bar{\psi}_{\text{IV}} \quad \psi_{\text{III}} \\ \curvearrowright \quad \curvearrowleft \\ \psi \\ \psi_{\text{I}} \quad \psi_{\text{II}} \\ \psi \quad \psi \end{array} = \tag{E.25} \\
&= +2 \frac{1}{\beta^6} \sum_{n_1, \dots, n_6 = -\infty}^{\infty} \int_{-\infty}^{\infty} \frac{d^d p_1}{(2\pi)^d} \cdots \frac{d^d p_6}{(2\pi)^d} \times \\
&\quad \times (-1) \beta \delta_{n_1, n_2} (2\pi)^d \delta^{(d)}(\vec{p}_1 - \vec{p}_2) (\mathbf{1})_{c_2}^{c_1} i\vec{p}_1 \cdot (\vec{\gamma})^{a_1} a_2 \partial_t [Z_\psi(t) \frac{1}{2} r_f(t, |\vec{p}_1|)] \times \\
&\quad \times \beta \delta_{n_2, n_3} (2\pi)^d \delta^{(d)}(\vec{p}_2 - \vec{p}_3) \frac{[i(\nu_{n_2} + i\mu) \gamma^{d+1} + i\vec{p}_2 \cdot \vec{\gamma} [1 + r_f(t, |\vec{p}_2|)]]^{a_2} (\mathbf{1})_{c_3}^{c_2}}{Z_\psi(t) [(\nu_{n_2} + i\mu)^2 + \vec{p}_2^2 [1 + r_f(t, |\vec{p}_2|)]^2]} \times \\
&\quad \times (-1) 2 \beta \delta_{n_4 + n_3, n_1 + n_{\text{III}}} (2\pi)^d \delta^{(d)}(\vec{p}_4 - \vec{p}_1 + \vec{p}_3 - \vec{p}_{\text{III}}) \frac{1}{2N} g^2(t) \times \\
&\quad \times [(\mathbf{1})^{a_4} a_1 (\mathbf{1})^{a_3} a_{\text{III}} (\mathbf{1})^{c_4} c_1 (\mathbf{1})^{c_3} c_{\text{III}} - (\mathbf{1})^{a_3} a_1 (\mathbf{1})^{a_4} a_{\text{III}} (\mathbf{1})^{c_3} c_1 (\mathbf{1})^{c_4} c_{\text{III}}] \times \\
&\quad \times (-1) \beta \delta_{n_5, n_4} (2\pi)^d \delta^{(d)}(\vec{p}_5 - \vec{p}_4) \frac{[i(\nu_{n_5} + i\mu) \gamma^{d+1} + i\vec{p}_5 \cdot \vec{\gamma} [1 + r_f(t, |\vec{p}_5|)]]^{a_5} a_4 (\mathbf{1})^{c_5} c_4}{Z_\psi(t) [(\nu_{n_5} + i\mu)^2 + \vec{p}_5^2 [1 + r_f(t, |\vec{p}_5|)]^2]} \times \\
&\quad \times (-1) 2 \beta \delta_{n_{\text{II}} + n_{\text{IV}}, n_6 + n_5} (2\pi)^d \delta^{(d)}(\vec{p}_{\text{II}} - \vec{p}_6 + \vec{p}_{\text{IV}} - \vec{p}_5) \frac{1}{2N} g^2(t) \times \\
&\quad \times [(\mathbf{1})^{a_{\text{II}}} a_6 (\mathbf{1})^{a_{\text{IV}}} a_5 (\mathbf{1})^{c_{\text{II}}} c_6 (\mathbf{1})^{c_{\text{IV}}} c_5 - (\mathbf{1})^{a_{\text{IV}}} a_6 (\mathbf{1})^{a_{\text{II}}} a_5 (\mathbf{1})^{c_{\text{IV}}} c_6 (\mathbf{1})^{c_{\text{II}}} c_5] \times \\
&\quad \times \beta \delta_{n_6, n_1} (2\pi)^d \delta^{(d)}(\vec{p}_6 - \vec{p}_1) \frac{[i(\nu_{n_6} + i\mu) \gamma^{d+1} + i\vec{p}_6 \cdot \vec{\gamma} [1 + r_f(t, |\vec{p}_6|)]]^{a_6} a_1 (\mathbf{1})^{c_6} c_1}{Z_\psi(t) [(\nu_{n_6} + i\mu)^2 + \vec{p}_6^2 [1 + r_f(t, |\vec{p}_6|)]^2]}.
\end{aligned}$$

Applying the projection Eq. (E.20) to this diagram one finds

$$\begin{aligned}
&- \frac{1}{d_\gamma} \frac{1}{d_\gamma N - 1} Z_\psi^{-2}(t) [(\mathbf{1})^{a_{\text{I}}} a_{\text{III}} (\mathbf{1})^{a_{\text{IV}}} a_{\text{IV}} (\mathbf{1})^{c_{\text{I}}} c_{\text{III}} (\mathbf{1})^{c_{\text{IV}}} c_{\text{IV}}] (\text{Atr4}) \Big|_{\vec{p}_{\text{IV}} = \dots = \vec{p}_{\text{I}} = 0} \stackrel{(\text{D.35})}{=} \\
&= + \beta \delta_{n_{\text{II}} + n_{\text{IV}}, n_1 + n_{\text{III}}} (2\pi)^d \delta^{(d)}(0) \frac{2}{N} \frac{1}{d_\gamma N - 1} g_r^4(t) k^{-4} \times \\
&\quad \times \frac{1}{\beta} \sum_{n = -\infty}^{\infty} \int_{-\infty}^{\infty} \frac{d^d p}{(2\pi)^d} 2 \vec{p}^2 \left[\frac{1}{2} \partial_t r_f(t, |\vec{p}|) + \frac{1}{2} \eta_\psi(t) r_f(t, |\vec{p}|) \right] [1 + r_f(t, |\vec{p}|)] \times \\
&\quad \times \frac{-(\nu_n + i\mu) [2(\nu_{-n + n_1 + n_{\text{III}}} + i\mu) + (\nu_n + i\mu)] + \vec{p}^2 [1 + r_f(t, |\vec{p}|)]}{(\nu_{-n + n_1 + n_{\text{III}}} + i\mu)^2 + \vec{p}^2 [1 + r_f(t, |\vec{p}|)]^2} \hat{f}_n^2 \left(\frac{\vec{p}^2}{k^2} \right) \stackrel{(\text{A.5})}{=} \\
&= + \beta \delta_{n_{\text{II}} + n_{\text{IV}}, n_1 + n_{\text{III}}} (2\pi)^d \delta^{(d)}(0) \frac{2}{N} \frac{1}{d_\gamma N - 1} g_r^4(t) k^{-4} \times \\
&\quad \times \frac{1}{\beta} \sum_{n = -\infty}^{\infty} A_d d \int_0^\infty dp p^{d+1} 2 \left[\frac{1}{2} \partial_t r_f(t, p) + \frac{1}{2} \eta_\psi(t) r_f(t, p) \right] [1 + r_f(t, p)] \times
\end{aligned}$$

$$\begin{aligned}
& \times \frac{-(\nu_n + i\mu)[2(\nu_{-n+n_I+n_{III}} + i\mu) + (\nu_n + i\mu)] + p^2 [1 + r_f(t, p)]}{(\nu_{-n+n_I+n_{III}} + i\mu)^2 + p^2 [1 + r_f(t, p)]^2} \hat{f}_n^2\left(\frac{p^2}{k^2}\right) \stackrel{(D.7)}{=} \\
& = + \beta \delta_{n_{II}+n_{IV}, n_I+n_{III}} (2\pi)^d \delta^{(d)}(0) \frac{2}{N} \frac{1}{d_\gamma N - 1} g_r^4(t) k^{d-2} \times \\
& \quad \times \frac{1}{\beta} \sum_{n=-\infty}^{\infty} A_d d \int_0^\infty dy y^{\frac{d}{2}} [y \dot{r}_f(y) + \frac{1}{2} \eta_\psi(t) r_f(y)] [1 + r_f(y)] \times \\
& \quad \times \frac{-\frac{1}{k^2}(\nu_n + i\mu)[2(\nu_{-n+n_I+n_{III}} + i\mu) + (\nu_n + i\mu)] + y^2 [1 + r_f(y)]}{\frac{1}{k^2}(\nu_{-n+n_I+n_{III}} + i\mu)^2 + y^2 [1 + r_f(y)]^2} \hat{f}_n^2(y) \stackrel{(D.25)}{=} \\
& = - \beta \delta_{n_{II}+n_{IV}, n_I+n_{III}} (2\pi)^d \delta^{(d)}(0) A_d \left[1 - \frac{\eta_\psi(t)}{d+1}\right] \frac{2}{N} \frac{1}{(d_\gamma N - 1)} g_r^4(t) k^{d-2} \times \\
& \quad \times \frac{1}{\beta} \sum_{n=-\infty}^{\infty} \frac{-\frac{1}{k^2}(\nu_n + i\mu)[2(\nu_{-n+n_I+n_{III}} + i\mu) + (\nu_n + i\mu)] + 1}{\frac{1}{k^2}(\nu_{-n+n_I+n_{III}} + i\mu)^2 + 1} \hat{f}_n^2(1) .
\end{aligned}$$

Flow equation four-fermion coupling

Combining the three different contributions, we obtain the RG flow equation for the (renormalized) four-fermion coupling,

$$\begin{aligned}
& \delta_{n_{II}+n_{IV}, n_I+n_{III}} [\partial_t g_r^2(t) + 2 \eta_\psi(t) g_r^2(t)] = \tag{E.26} \\
& = - \delta_{n_{II}+n_{IV}, n_I+n_{III}} A_d \left[1 - \frac{\eta_\psi(t)}{d+1}\right] \frac{1}{N} \frac{d_\gamma N - 2}{d_\gamma N - 1} g_r^4(t) k^{d+2} \times \\
& \quad \times \frac{1}{\beta} \sum_{n=-\infty}^{\infty} \frac{\frac{1}{k^2}(\nu_n + i\mu)[2(\nu_{n+n_{II}-n_{III}} + i\mu) - (\nu_n + i\mu)] + 1}{\frac{1}{k^2}(\nu_{n+n_{II}-n_{III}} + i\mu)^2 + 1} \frac{1}{[(\nu_n + i\mu)^2 + k^2]^2} + \\
& \quad + \delta_{n_{II}+n_{IV}, n_I+n_{III}} A_d \left[1 - \frac{\eta_\psi(t)}{d+1}\right] \frac{1}{N} (d_\gamma N - 1) g_r^4(t) k^{d+2} \times \\
& \quad \times \frac{1}{\beta} \sum_{n=-\infty}^{\infty} \frac{\frac{1}{k^2}(\nu_n + i\mu)[2(\nu_{n+n_{IV}-n_{III}} + i\mu) - (\nu_n + i\mu)] + 1}{\frac{1}{k^2}(\nu_{n+n_{IV}-n_{III}} + i\mu)^2 + 1} \frac{1}{[(\nu_n + i\mu)^2 + k^2]^2} - \\
& \quad - \delta_{n_{II}+n_{IV}, n_I+n_{III}} A_d \left[1 - \frac{\eta_\psi(t)}{d+1}\right] \frac{2}{N} \frac{1}{(d_\gamma N - 1)} g_r^4(t) k^{d+2} \times \\
& \quad \times \frac{1}{\beta} \sum_{n=-\infty}^{\infty} \frac{-\frac{1}{k^2}(\nu_n + i\mu)[2(\nu_{-n+n_I+n_{III}} + i\mu) + (\nu_n + i\mu)] + 1}{\frac{1}{k^2}(\nu_{-n+n_I+n_{III}} + i\mu)^2 + 1} \frac{1}{[(\nu_n + i\mu)^2 + k^2]^2} .
\end{aligned}$$

E.2. FRG flow equations of the Gross-Neveu-Yukawa model

This appendix is dedicated to the detailed derivation of the RG flow equations of the GNY model. The starting point is the ansatz for the effective average action from Eq. (10.1). Writing out all spacetime dependences and spinor and color indices explicitly, this ansatz reads,

$$\begin{aligned}
\bar{\Gamma}_t[\bar{\psi}, \psi, \varphi] = & \int_{-\infty}^{\infty} d^d x \int_0^\beta d\tau \left[\bar{\psi}_{a_1 c_1}(\tau, \vec{x}) (\mathbf{1})^{c_1}_{c_2} [Z_\psi(t) (\not{\partial} - \mu \gamma^{d+1}) + \right. \\
& \left. + \frac{1}{\sqrt{N}} h(t, \varphi(\tau, \vec{x})) \varphi(\tau, \vec{x}) \mathbf{1}]^{a_1}_{a_2} \psi^{a_2 c_2}(\tau, \vec{x}) - \right. \\
& \left. + \frac{1}{\sqrt{N}} h(t, \varphi(\tau, \vec{x})) \varphi(\tau, \vec{x}) \mathbf{1} \right] \tag{E.27}
\end{aligned}$$

$$- Z_\varphi(t) \frac{1}{2} \varphi(\tau, \vec{x}) [\square\varphi(\tau, \vec{x}) + U(t, \varphi(\tau, \vec{x}))].$$

In addition to this ansatz, we also recapitulate the relations between renormalized fields and couplings and their bare counterparts from Section 10.2.1. These are

$$\varphi_r = Z_\varphi^{\frac{1}{2}} \varphi, \quad \psi_r = Z_\psi^{\frac{1}{2}} \psi, \quad \bar{\psi}_r = Z_\psi^{\frac{1}{2}} \bar{\psi}, \quad h_r = Z_\psi^{-1} Z_\varphi^{-\frac{1}{2}} h, \quad (\text{E.28})$$

where the various arguments and indices of the fields and couplings are not written out for sake of readability. In addition, we also repeat the formal definition of the (renormalized) fermion mass

$$m = \frac{1}{\sqrt{N}} h \varphi, \quad m_r = Z_\psi^{-1} m = \frac{1}{\sqrt{N}} Z_\psi^{-1} Z_\varphi^{-\frac{1}{2}} h Z_\varphi^{\frac{1}{2}} \varphi = \frac{1}{\sqrt{N}} h_r \varphi_r. \quad (\text{E.29})$$

Similar to the derivation of the flow equation of the original GN model in Appendix E.1, it is advantageous to work in momentum space. However, a complete Fourier transformation of the effective average action is not useful, due to the field dependence of the Yukawa interaction and the effective potential. This becomes apparent within the next steps. Hence, we solely perform a partial Fourier transformation of the kinetic terms in Eq. (E.27) using the definitions (A.23), (A.26), (A.28), and (A.31).

$$\begin{aligned} \bar{\Gamma}_t[\tilde{\psi}, \tilde{\psi}, \tilde{\varphi}] &= \quad (\text{E.30}) \\ &= \frac{1}{\beta^2} \sum_{n_1, n_2=-\infty}^{\infty} \int_{-\infty}^{\infty} \frac{d^d p_1}{(2\pi)^d} \frac{d^d p_2}{(2\pi)^d} \tilde{\psi}_{a_1 c_1}(\nu_{n_1}, \vec{p}_1) \beta \delta_{n_1, n_2} (2\pi)^d \delta^{(d)}(\vec{p}_1 - \vec{p}_2) \times \\ &\quad \times Z_\psi(t) (\mathbb{1})^{c_1}_{c_2} [i(\nu_{n_2} + i\mu) \gamma^{d+1} + i\vec{p}_2 \cdot \vec{\gamma}]^{a_1}_{a_2} \tilde{\psi}^{a_2 c_2}(\nu_{n_2}, \vec{p}_2) - \\ &\quad - \frac{1}{\beta^2} \sum_{n_1, n_2=-\infty}^{\infty} \int_{-\infty}^{\infty} \frac{d^d p_1}{(2\pi)^d} \frac{d^d p_2}{(2\pi)^d} \tilde{\varphi}(\omega_{n_1}, \vec{p}_1) \beta \delta_{n_1, n_2} (2\pi)^d \delta^{(d)}(\vec{p}_1 + \vec{p}_2) \times \\ &\quad \times Z_\varphi(t) \frac{1}{2} [\omega_{n_2}^2 + \vec{p}_2^2] \tilde{\varphi}(\omega_{n_2}, \vec{p}_2) + \\ &\quad + \int_{-\infty}^{\infty} d^d x \int_0^\beta d\tau \bar{\psi}_{a_1 c_1}(\tau, \vec{x}) \frac{1}{\sqrt{N}} (\mathbb{1})^{c_1}_{c_2} (\mathbb{1})^{a_1}_{a_2} h(t, \varphi(\tau, \vec{x})) \varphi(\tau, \vec{x}) \psi^{a_2 c_2}(\tau, \vec{x}) + \\ &\quad + \int_{-\infty}^{\infty} d^d x \int_0^\beta d\tau U(t, \varphi(\tau, \vec{x})). \end{aligned}$$

Within this approximation we need to derive expressions for the bosonic and fermionic two-point vertex, the purely bosonic three- and four-point vertex, as well as three- and four-point vertices that involve fermion-boson interactions. This is done by successively taking derivatives of Eq. (E.30) w.r.t. the Fourier-transformed fields $\tilde{\varphi}$, $\tilde{\psi}$, and $\tilde{\bar{\psi}}$ and evaluating the result on a (constant) background-field configuration. Within this work we choose $\tilde{\bar{\psi}}(\tau, \vec{x}) = 0$, $\tilde{\psi}(\tau, \vec{x}) = 0$, and $\tilde{\varphi}(\tau, \vec{x}) = \sigma = \text{const.}$ as the background-field configuration.

Before we present the results for these n -point functions, we demonstrate what happens, when the derivatives w.r.t. the Fourier-transformed fields hit one of the terms in the last two-lines of

$$\begin{aligned}
&= -\beta \delta_{n_2, n_1} (2\pi)^d \delta^{(d)}(\vec{p}_2 - \vec{p}_1) Z_\psi(t) (\mathbb{1})_{c_1}^{c_2} \times \\
&\quad \times \left[i(\nu_{n_2} + i\mu) \gamma^{d+1} + i\vec{p}_2 \cdot \vec{\gamma} + \frac{1}{\sqrt{N}} \frac{1}{Z_\psi(t)} h(t, \sigma) \sigma \mathbb{1} \right]_{a_1}^{a_2} = \\
&= -\beta \delta_{n_2, n_1} (2\pi)^d \delta^{(d)}(\vec{p}_2 - \vec{p}_1) Z_\psi(t) (\mathbb{1})_{c_1}^{c_2} \left[i(\nu_{n_2} + i\mu) \gamma^{d+1} + i\vec{p}_2 \cdot \vec{\gamma} + m_r(t, \sigma_r) \mathbb{1} \right]_{a_1}^{a_2} = \\
&= \begin{array}{c} \bar{\psi}_2 \\ \leftarrow \bullet \rightarrow \\ \psi_1 \end{array} .
\end{aligned}$$

Here, we used the identical Feynman-graph representation as in Eq. (E.3). However, there is a crucial difference, because in the GNY model the fermions are coupled to the scalar field via the Yukawa interaction $h_r(t, \sigma_r)$, which enters the two-point function/vertex in terms of a scale- and background-field-dependent mass $m_r(t, \sigma_r)$ for the fermions, while the two-point vertex in the GN model lacks a mass term.

Next, we turn to all those higher n -point correlation functions that are relevant within our truncation and which are generically non-vanishing, if they are evaluated on our specific background-field configuration.

Firstly, these are the three- and four-point vertices with mixed external boson and fermion legs. Both emerge from the Yukawa interaction and have to conserve color-charge and momentum in- and outflow. The three-point vertex reads

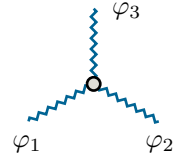
$$\begin{aligned}
&\bar{\Gamma}_t^{\varphi_3 \bar{\psi}_2 \psi_1}[\sigma_r](\omega_{n_3}, \vec{p}_3; \nu_{n_2}, \vec{p}_2; \nu_{n_1}, \vec{p}_1)_{c_1}^{c_2} {}_{a_1}^{a_2} \equiv \dots = \\
&= -\beta \delta_{n_2, n_3+n_1} (2\pi)^d \delta^{(d)}(\vec{p}_3 - \vec{p}_2 + \vec{p}_1) Z_\psi(t) Z_\varphi^{\frac{1}{2}}(t) [\partial_{\sigma_r} m_r(t, \sigma_r)] (\mathbb{1})_{c_1}^{c_2} (\mathbb{1})_{a_1}^{a_2} = \\
&= \begin{array}{c} \varphi_3 \\ \uparrow \\ \bullet \\ \swarrow \quad \searrow \\ \psi_1 \quad \bar{\psi}_2 \end{array} .
\end{aligned} \tag{E.34}$$

The corresponding four-point vertex is given by

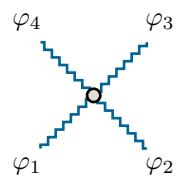
$$\begin{aligned}
&\bar{\Gamma}_t^{\varphi_4 \varphi_3 \bar{\psi}_2 \psi_1}[\sigma_r](\omega_{n_4}, \vec{p}_4; \omega_{n_3}, \vec{p}_3; \nu_{n_2}, \vec{p}_2; \nu_{n_1}, \vec{p}_1)_{c_1}^{c_2} {}_{a_1}^{a_2} \equiv \dots = \\
&= -\beta \delta_{n_2, n_4+n_3+n_1} (2\pi)^d \delta^{(d)}(\vec{p}_4 + \vec{p}_3 - \vec{p}_2 + \vec{p}_1) Z_\psi(t) Z_\varphi(t) [\partial_{\sigma_r}^2 m_r(t, \sigma_r)] (\mathbb{1})_{c_1}^{c_2} (\mathbb{1})_{a_1}^{a_2} = \\
&= \begin{array}{c} \varphi_4 \quad \varphi_3 \\ \swarrow \quad \searrow \\ \bullet \\ \swarrow \quad \searrow \\ \psi_1 \quad \bar{\psi}_2 \end{array}
\end{aligned} \tag{E.35}$$

and only arises, if the Yukawa coupling is assumed to be field-dependent, which is generally the case during the RG flow, *cf.* Refs. [66, 276, 101].

Secondly, there is the purely bosonic three-point vertex

$$\begin{aligned} \bar{\Gamma}_t^{\varphi_3\varphi_2\varphi_1}[\sigma_r](\omega_{n_3}, \vec{p}_3; \omega_{n_2}, \vec{p}_2; \omega_{n_1}, \vec{p}_1) &\equiv \dots = \\ &= \beta \delta_{0, n_3+n_2+n_1} (2\pi)^d \delta^{(d)}(\vec{p}_3 + \vec{p}_2 + \vec{p}_1) Z_{\tilde{\varphi}}^{\frac{3}{2}}(t) \partial_{\sigma_r}^3 U(t, \sigma_r) = \\ &= \text{Diagram} \end{aligned} \quad (\text{E.36})$$


and the purely bosonic four-point vertex

$$\begin{aligned} \bar{\Gamma}_t^{\varphi_4\varphi_3\varphi_2\varphi_1}[\sigma_r](\omega_{n_4}, \vec{p}_4; \omega_{n_3}, \vec{p}_3; \omega_{n_2}, \vec{p}_2; \omega_{n_1}, \vec{p}_1) &\equiv \dots = \\ &= \beta \delta_{0, n_4+n_3+n_2+n_1} (2\pi)^d \delta^{(d)}(\vec{p}_4 + \vec{p}_3 + \vec{p}_2 + \vec{p}_1) Z_{\tilde{\varphi}}^2(t) \partial_{\sigma_r}^4 U(t, \sigma_r) = \\ &= \text{Diagram} \end{aligned} \quad (\text{E.37})$$


In the case of the GNY model, one needs to specify two regulator functions; a regulator for the fermions and a regulator for the bosonic fields. For the fermions we reuse the regulator (E.5). For the bosonic fields the regulator is given by a scale- and momentum-dependent mass term and reads

$$R_t^{\varphi_2\varphi_1}(\omega_{n_2}, \vec{p}_2; \omega_{n_1}, \vec{p}_1) \equiv \beta \delta_{-n_2, n_1} (2\pi)^d \delta^{(d)}(\vec{p}_2 + \vec{p}_1) \vec{p}_2^2 Z_{\varphi}(t) r_b(t, |\vec{p}_2|). \quad (\text{E.38})$$

Also for the bosons only spatial momenta are regulated, while Matsubara frequencies of all orders are taken into account at any RG scale k . For details we refer to Refs. [532] and the discussion in Section 9.2.2. In the scale-dependent partition function and the definition of the effective average action, compare with Eqs. (C.24) and (C.37), the full bosonic regulator term is given by,

$$\begin{aligned} \Delta\mathcal{S}[\tilde{\varphi}] &= \\ &= \frac{1}{\beta^2} \sum_{n_1, n_2=-\infty}^{\infty} \int_{-\infty}^{\infty} \frac{d^d p_1}{(2\pi)^d} \frac{d^d p_2}{(2\pi)^d} \tilde{\varphi}(\omega_{n_1}, \vec{p}_1) \frac{1}{2} R_t^{\varphi_2\varphi_1}(\omega_{n_2}, \vec{p}_2; \omega_{n_1}, \vec{p}_1) \tilde{\varphi}(\omega_{n_2}, \vec{p}_2). \end{aligned} \quad (\text{E.39})$$

On the level of Feynman diagrams for the FRG formalism, the regulator also appears in terms of the regulator insertion, which is graphically represented by a blue-crossed circle,

$$\frac{1}{2} \partial_t R_t^{\varphi_2\varphi_1}(\omega_{n_2}, \vec{p}_2; \omega_{n_1}, \vec{p}_1) = \text{Diagram} \quad (\text{E.40})$$


Finally, one needs to calculate the full fermionic and bosonic propagators. In order to find these quantities, one has to combine the two-point vertices Eqs. (E.32) and (E.33) with the corresponding

regulators (E.38) and (E.5) in advance. This results in the full two-point functions (evaluated on the background-field configurations) for the bosonic fields

$$\begin{aligned} & (\bar{\Gamma}_t^{\varphi_2 \varphi_1}[\sigma_r] + R_t^{\varphi_2 \varphi_1})(\omega_{n_2}, \vec{p}_2; \omega_{n_1}, \vec{p}_1) = \\ & = \beta \delta_{-n_2, n_1} (2\pi)^d \delta^{(d)}(\vec{p}_2 + \vec{p}_1) Z_\varphi(t) [\omega_{n_2}^2 + \vec{p}_2^2 [1 + r_b(t, |\vec{p}_2|)] + \partial_{\sigma_r}^2 U(t, \sigma_r)], \end{aligned} \quad (\text{E.41})$$

and the fermionic fields,

$$\begin{aligned} & (\bar{\Gamma}_t^{\bar{\psi}_2 \psi_1}[\sigma_r] + R_t^{\bar{\psi}_2 \psi_1})(\nu_{n_2}, \vec{p}_2; \nu_{n_1}, \vec{p}_1)^{c_2}_{c_1} a_2 a_1 = \\ & = -\beta \delta_{n_2, n_1} (2\pi)^d \delta^{(d)}(\vec{p}_2 - \vec{p}_1) Z_\psi(t) (\mathbb{1})^{c_2}_{c_1} \times \\ & \quad \times [i(\nu_{n_2} + i\mu) \gamma^{d+1} + i\vec{p}_2 \cdot \vec{\gamma} [1 + r_f(t, |\vec{p}_2|)] + m_r(t, \sigma_r) \mathbb{1}]^{a_2}_{a_1}. \end{aligned} \quad (\text{E.42})$$

By inversion of these two quantities, one arrives at the final expressions for the bosonic propagator

$$\begin{aligned} & (\bar{\Gamma}_t^{\varphi_2 \varphi_1}[\sigma_r] + R_t^{\varphi_2 \varphi_1})^{-1}(\omega_{n_2}, \vec{p}_2; \omega_{n_1}, \vec{p}_1) \equiv \\ & \equiv \beta \delta_{-n_2, n_1} (2\pi)^d \delta^{(d)}(\vec{p}_2 + \vec{p}_1) \frac{1}{Z_\varphi(t) [\omega_{n_2}^2 + \vec{p}_2^2 [1 + r_b(t, |\vec{p}_2|)] + \partial_{\sigma_r}^2 U(t, \sigma_r)]} = \\ & = \text{---} \varphi_2 \text{---} \varphi_1 \text{---}, \end{aligned} \quad (\text{E.43})$$

and the fermionic propagator

$$\begin{aligned} & (\bar{\Gamma}_t^{\bar{\psi}_2 \psi_1}[\sigma_r] + R_t^{\bar{\psi}_2 \psi_1})^{-1}(\nu_{n_2}, \vec{p}_2; \nu_{n_1}, \vec{p}_1)^{c_2}_{c_1} a_2 a_1 \equiv \\ & \equiv \beta \delta_{n_2, n_1} (2\pi)^d \delta^{(d)}(\vec{p}_2 - \vec{p}_1) \frac{[i(\nu_{n_2} + i\mu) \gamma^{d+1} + i\vec{p}_2 \cdot \vec{\gamma} [1 + r_f(t, |\vec{p}_2|)] - m_r(t, \sigma_r)]^{a_2}_{a_1} (\mathbb{1})^{c_2}_{c_1}}{Z_\psi(t) [(\nu_{n_2} + i\mu)^2 + \vec{p}_2^2 [1 + r_f(t, |\vec{p}_2|)]^2 + m_r^2(t, \sigma_r)]} \\ & = \bar{\psi}_2 \text{---} \psi_1 \text{---}. \end{aligned} \quad (\text{E.44})$$

These are all ingredients that are required for the detailed derivation of the flow equations within our truncation.

We proceed as follows: First, in Appendix E.2.1, the RG flow equation for the effective potential is derived. Afterwards, in Appendix E.2.2, we turn to the flow equation of the bosonic two-point function and extract the RG flow equation of the field-dependent bosonic mass term/the second field derivative of the effective potential (as a consistency check) as well as the scale-dependence of the bosonic anomalous dimension. Lastly, we calculate the RG flow equation of the fermionic two-point function in Appendix E.2.4 and extract the RG flow of the Yukawa coupling and fermionic anomalous dimension.

E.2.1. Effective potential

A peculiar feature of a lot of models in the FRG framework is that it is straightforward to derive a flow equation for the entire scale-dependent effective local potential $U(t, \varphi)$, which incorporates all possible local bosonic self-interactions that are in accordance with the symmetry of the system. Here, we shall present this derivation.

Projection onto the effective potential

The flow equation for the scale-dependent effective potential is derived by solely evaluating the ERG equation on the background-field configuration $\bar{\psi}(\tau, \vec{x}) = \psi(\tau, \vec{x}) = 0$, $\varphi(\tau, \vec{x}) = \sigma = \text{const.}$. This projection eliminates all kinetic (momentum-dependent) terms from the ansatz (E.30), as well as all terms that depend on the fermionic fields. The only contribution that is left is the bosonic effective potential evaluated for $\varphi = \sigma$,

$$\begin{aligned} & \beta (2\pi)^d \delta^{(d)}(0) \left[\partial_t U(t, \sigma_r) + \frac{1}{2} \eta_\varphi(t) \sigma_r \partial_{\sigma_r} U(t, \sigma_r) \right] = \\ & = \beta (2\pi)^d \delta^{(d)}(0) \partial_t U(t, \sigma) = \\ & = \partial_t \bar{\Gamma}_t[\bar{\psi}, \psi, \varphi] \Big|_{\bar{\psi}=\psi=0, \varphi=\sigma}. \end{aligned} \quad (\text{E.45})$$

Hence, Eq. (C.51) has the following form for the GNY model,

$$\begin{aligned} & \partial_t \bar{\Gamma}_t[\sigma_r] = \\ & = \text{Tr} \left[\left(\frac{1}{2} \partial_t R_t \right) G_t[\sigma_r] \right] = \\ & = \left(\frac{1}{2} \partial_t R_t^{\varphi_1 \varphi_2} \right) G_{t, \varphi_2 \varphi_1}[\sigma_r] + \left(\frac{1}{2} \partial_t R_t^{\bar{\psi}_1 \psi_2} \right) G_{t, \bar{\psi}_2 \psi_1}[\sigma_r] + \left(\frac{1}{2} \partial_t R_t^{\psi_1 \bar{\psi}_2} \right) G_{t, \psi_2 \bar{\psi}_1}[\sigma_r] = \\ & = \left(\frac{1}{2} \partial_t R_t^{\varphi_1 \varphi_2} \right) G_{t, \varphi_2 \varphi_1}[\sigma_r] + 2 \left(\frac{1}{2} \partial_t R_t^{\bar{\psi}_1 \psi_2} \right) G_{t, \bar{\psi}_2 \psi_1}[\sigma_r] \\ & = + \left(\frac{1}{2} \partial_t R_t^{\varphi_1 \varphi_2} \right) \left(\bar{\Gamma}_t^{(2)}[\sigma_r] + R_t \right)_{\varphi_2 \varphi_1}^{-1} - \\ & \quad - 2 \left(\frac{1}{2} \partial_t R_t^{\bar{\psi}_1 \psi_2} \right) \left(\bar{\Gamma}_t^{(2)}[\sigma_r] + R_t \right)_{\bar{\psi}_2 \psi_1}^{-1}, \end{aligned} \quad (\text{Btr1})$$

where we used that the trace of an operator/matrix and its transposed are identical to combine the two fermionic contributions. The minus sign in front of the fermionic contributions stems from the field-space metric that is contained in the full propagators $G_{t, \mathbf{ab}}$, compare Eqs. (C.13) and (C.42).

On a diagrammatic level, the previous equation reads,

$$\partial_t \left(\circ \right) = \text{loop}_{\varphi} - 2 \text{loop}_{\psi}. \quad (\text{E.47})$$

The two traces/diagrams are evaluated as follows.

Trace (Btr1) – boson loop

In order to evaluate the bosonic loop contribution to the effective potential, Eq. (Btr1), we insert the bosonic regulator (E.38) and (E.40) and the bosonic propagator (E.43) into the trace (Btr1). During the calculation various identities, variable transformations *etc.* are used, which are

indicated at the equal signs at the end of the lines.

$$\begin{aligned}
(\text{Btr1}) &= \text{Diagram} = & (E.48) \\
&= + \frac{1}{\beta^2} \sum_{n_1, n_2 = -\infty}^{\infty} \int_{-\infty}^{\infty} \frac{d^d p_1}{(2\pi)^d} \frac{d^d p_2}{(2\pi)^d} \times \\
&\quad \times \beta \delta_{-n_1, n_2} (2\pi)^d \delta^{(d)}(\vec{p}_1 + \vec{p}_2) \vec{p}_1^2 \partial_t [Z_\varphi(t) \frac{1}{2} r_b(t, |\vec{p}_1|)] \times \\
&\quad \times \beta \delta_{-n_2, n_1} (2\pi)^d \delta^{(d)}(\vec{p}_2 + \vec{p}_1) \frac{1}{Z_\varphi(t) [\omega_{n_2}^2 + \vec{p}_2^2 [1 + r_b(t, |\vec{p}_2|)] + \partial_{\sigma_r}^2 U(t, \sigma_r)]} \stackrel{(D.26)}{=} \\
&= \beta (2\pi)^d \delta^{(d)}(0) k^{-2} \frac{1}{\beta} \sum_{n=-\infty}^{\infty} \int_{-\infty}^{\infty} \frac{d^d p}{(2\pi)^d} \vec{p}^2 [\frac{1}{2} \partial_t r_b(t, |\vec{p}|) + \frac{1}{2} \eta_\varphi(t) r_b(t, |\vec{p}|)] \mathfrak{B}_n \left(\frac{\vec{p}^2}{k^2} \right) \stackrel{(A.5)}{=} \\
&= \beta (2\pi)^d \delta^{(d)}(0) k^{-2} \frac{1}{\beta} \sum_{n=-\infty}^{\infty} A_d d \int_0^\infty dp p^{d+1} [\frac{1}{2} \partial_t r_b(t, p) + \frac{1}{2} \eta_\varphi(t) r_b(t, p)] \mathfrak{B}_n \left(\frac{p^2}{k^2} \right) \stackrel{(D.7)}{=} \\
&= \beta (2\pi)^d \delta^{(d)}(0) k^d \frac{1}{\beta} \sum_{n=-\infty}^{\infty} A_d \frac{d}{2} \int_0^\infty dy y^{\frac{d}{2}} [y \dot{r}_b(y) + \frac{1}{2} \eta_\varphi(t) r_b(y)] \mathfrak{B}_n(y) \stackrel{(D.15)}{=} \\
&= -\beta (2\pi)^d \delta^{(d)}(0) A_d \left[1 - \frac{\eta_\varphi(t)}{d+2} \right] k^{d+2} \frac{1}{\beta} \sum_{n=-\infty}^{\infty} \frac{1}{\omega_n^2 + k^2 + \partial_{\sigma_r}^2 U(t, \sigma_r)}.
\end{aligned}$$

Trace (Btr2) – fermion loop

In complete analogy to the boson loop, the fermion-loop contribution, trace (Btr2), is evaluated using the fermionic regulator (E.5) and (E.7) and the fermionic propagator (E.44).

$$\begin{aligned}
(\text{Btr2}) &= -2 \text{Diagram} = & (E.49) \\
&= -2 \frac{1}{\beta^2} \sum_{n_1, n_2 = -\infty}^{\infty} \int_{-\infty}^{\infty} \frac{d^d p_1}{(2\pi)^d} \frac{d^d p_2}{(2\pi)^d} \times \\
&\quad \times (-1) \beta \delta_{n_1, n_2} (2\pi)^d \delta^{(d)}(\vec{p}_1 - \vec{p}_2) (\mathbf{1})_{c_1}^{c_2} i\vec{p}_1 \cdot (\vec{\gamma})_{a_1}^{a_2} \partial_t [Z_\psi(t) \frac{1}{2} r_f(t, |\vec{p}_1|)] \times \\
&\quad \times \beta \delta_{n_2, n_1} (2\pi)^d \delta^{(d)}(\vec{p}_2 - \vec{p}_1) \times \\
&\quad \times \frac{[i(\nu_{n_2} + i\mu) \gamma^{d+1} + i\vec{p}_2 \cdot \vec{\gamma} [1 + r_f(t, |\vec{p}_2|)] - m_r(t, \sigma_r)]^{a_2} (\mathbf{1})_{a_1}^{c_2} (\mathbf{1})_{c_1}^{a_1}}{Z_\psi(t) [(\nu_{n_2} + i\mu)^2 + \vec{p}_2^2 [1 + r_f(t, |\vec{p}_2|)]^2 + m_r^2(t, \sigma_r)]} \stackrel{(D.32)}{=} \\
&= -\beta (2\pi)^d \delta^{(d)}(0) d_\gamma N k^{-2} \times \\
&\quad \times \frac{1}{\beta} \sum_{n=-\infty}^{\infty} \int_{-\infty}^{\infty} \frac{d^d p}{(2\pi)^d} 2\vec{p}^2 [\frac{1}{2} \partial_t r_f(t, |\vec{p}|) + \frac{1}{2} \eta_\psi(t) r_f(t, |\vec{p}|)] [1 + r_f(t, |\vec{p}|)] \mathfrak{F}_n \left(\frac{\vec{p}^2}{k^2} \right) \stackrel{(A.5)}{=}
\end{aligned}$$

$$\begin{aligned}
&= -\beta (2\pi)^d \delta^{(d)}(0) d_\gamma N k^{-2} \times \\
&\quad \times \frac{1}{\beta} \sum_{n=-\infty}^{\infty} A_d d \int_0^\infty dp p^{d+1} 2 \left[\frac{1}{2} \partial_t r_f(t, p) + \frac{1}{2} \eta_\psi(t) r_f(t, p) \right] [1 + r_f(t, p)] \mathfrak{F}_n \left(\frac{p^2}{k^2} \right) \stackrel{\text{(D.7)}}{=} \\
&= -\beta (2\pi)^d \delta^{(d)}(0) d_\gamma N k^d \times \\
&\quad \times \frac{1}{\beta} \sum_{n=-\infty}^{\infty} A_d d \int_0^\infty dy y^{\frac{d}{2}} \left[y \dot{r}_f(y) + \frac{1}{2} \eta_\psi(t) r_f(y) \right] [1 + r_f(y)] \mathfrak{F}_n(y) \stackrel{\text{(D.25)}}{=} \\
&= \beta (2\pi)^d \delta^{(d)}(0) A_d \left[1 - \frac{\eta_\psi(t)}{d+1} \right] d_\gamma N k^{d+2} \frac{1}{\beta} \sum_{n=-\infty}^{\infty} \frac{1}{(\nu_n + i\mu)^2 + k^2 + m_r^2(t, \sigma_r)}.
\end{aligned}$$

Flow equation of the effective potential

Inserting the results for the traces (E.48) and (E.49) and the projection (E.45) into Eq. (E.46) and dropping the infinite-volume factors $\beta (2\pi)^d \delta^{(d)}(0)$ on both sides of the resulting equation, one obtains the famous RG flow equation for the effective potential,

$$\begin{aligned}
&\partial_t U(t, \sigma_r) + \frac{1}{2} \eta_\varphi(t) \sigma_r \partial_{\sigma_r} U(t, \sigma_r) = \tag{E.50} \\
&= -A_d \left[1 - \frac{\eta_\varphi(t)}{d+2} \right] k^{d+2} \frac{1}{\beta} \sum_{n=-\infty}^{\infty} \frac{1}{\omega_n^2 + k^2 + \partial_{\sigma_r}^2 U(t, \sigma_r)} + \\
&\quad + A_d \left[1 - \frac{\eta_\psi(t)}{d+1} \right] d_\gamma N k^{d+2} \frac{1}{\beta} \sum_{n=-\infty}^{\infty} \frac{1}{(\nu_n + i\mu)^2 + k^2 + m_r^2(t, \sigma_r)}.
\end{aligned}$$

Our result is identical to [373, Eq. (9)], but is basically found in all kinds of FRG publications on models with Yukawa interactions in one or the other variant.

Flow equation effective potential – $\frac{1}{N}$ -rescaled

Rescaling the effective potential and the bosonic fields in Eq. (E.50) with appropriate powers of N , as defined in Eq. (10.7), one obtains the $\frac{1}{N}$ -rescaled RG flow equation,

$$\begin{aligned}
&\partial_t \check{U}(t, \check{\sigma}_r) + \frac{1}{2} \eta_\varphi(t) \check{\sigma}_r \partial_{\check{\sigma}_r} \check{U}(t, \check{\sigma}_r) = \tag{E.51} \\
&= -A_d \left[1 - \frac{\eta_\varphi(t)}{d+2} \right] \frac{1}{N} k^{d+2} \frac{1}{\beta} \sum_{n=-\infty}^{\infty} \frac{1}{\omega_n^2 + k^2 + \partial_{\check{\sigma}_r}^2 \check{U}(t, \check{\sigma}_r)} + \\
&\quad + A_d \left[1 - \frac{\eta_\psi(t)}{d+1} \right] d_\gamma k^{d+2} \frac{1}{\beta} \sum_{n=-\infty}^{\infty} \frac{1}{(\nu_n + i\mu)^2 + k^2 + m_r^2(t, \check{\sigma}_r)}.
\end{aligned}$$

For example, this PDE is identical to Ref. [374, Eq. (39)] (after another rescaling of all dimensionful quantities with appropriate powers of the RG scale k), but is also found elsewhere.

E.2.2. Bosonic two-point function – boson mass & anomalous dimension

Next, we turn to the RG flow equation of the bosonic two-point function. After providing the generic form of this flow equation for our model, we extract the RG flow equation of the field-dependent bosonic mass term and the anomalous dimension.

The bosonic two-point vertex

The starting point for the derivation of the RG flow equation of the bosonic two-point function is the ERG Eq. (C.51), when one takes two derivatives w.r.t. the Fourier-transformed bosonic fields $\tilde{\varphi}$. Again, we make use of the universal field-space result for RG flow equations of arbitrary two-point functions, *i.e.*, Eq. (C.53), and simply evaluate this expression for the GNY model within our truncation (E.27) and our background-field configuration,

$$\begin{aligned}
& \partial_t \bar{\Gamma}_t^{(2) \varphi_{\text{II}} \varphi_{\text{I}}} [\sigma_{\text{r}}] = \tag{E.52} \\
& = \text{STr} \left[\left(\frac{1}{2} \partial_t R_t \right) G_t [\sigma_{\text{r}}] \bar{\Gamma}_t^{(3) \varphi_{\text{II}}} G_t [\sigma_{\text{r}}] \bar{\Gamma}_t^{(3) \varphi_{\text{I}}} G_t [\sigma_{\text{r}}] \right] - \\
& \quad - \text{STr} \left[\left(\frac{1}{2} \partial_t R_t \right) G_t [\sigma_{\text{r}}] \bar{\Gamma}_t^{(4) \varphi_{\text{II}} \varphi_{\text{I}}} G_t [\sigma_{\text{r}}] \right] + \\
& \quad + \text{STr} \left[\left(\frac{1}{2} \partial_t R_t \right) G_t [\sigma_{\text{r}}] \bar{\Gamma}_t^{(3) \varphi_{\text{I}}} G_t [\sigma_{\text{r}}] \bar{\Gamma}_t^{(3) \varphi_{\text{II}}} G_t [\sigma_{\text{r}}] \right] = \\
& = + (-1)^{\varphi_{\text{II}} \varphi_2} (-1)^{\varphi_{\text{I}} \varphi_2} \left(\frac{1}{2} \partial_t R_t^{\varphi_1 \varphi_2} \right) G_{t, \varphi_2 \varphi_3} [\sigma_{\text{r}}] \bar{\Gamma}_t^{(3) \varphi_3 \varphi_{\text{II}} \varphi_4} [\sigma_{\text{r}}] \mathbf{g}_{\varphi_4}^{\varphi_5} G_{t, \varphi_5 \varphi_6} [\sigma_{\text{r}}] \times \\
& \quad \times \bar{\Gamma}_t^{(3) \varphi_6 \varphi_{\text{I}} \varphi_7} [\sigma_{\text{r}}] \mathbf{g}_{\varphi_7}^{\varphi_8} G_{t, \varphi_8 \varphi_1} [\sigma_{\text{r}}] + \\
& \quad + (-1)^{\varphi_{\text{II}} \psi_2} (-1)^{\varphi_{\text{I}} \psi_2} \left(\frac{1}{2} \partial_t R_t^{\bar{\psi}_1 \psi_2} \right) G_{t, \bar{\psi}_2 \psi_3} [\sigma_{\text{r}}] \bar{\Gamma}_t^{(3) \bar{\psi}_3 \varphi_{\text{II}} \psi_4} [\sigma_{\text{r}}] \mathbf{g}_{\bar{\psi}_4}^{\psi_5} G_{t, \bar{\psi}_5 \psi_6} [\sigma_{\text{r}}] \times \\
& \quad \times \bar{\Gamma}_t^{(3) \bar{\psi}_6 \varphi_{\text{I}} \psi_7} [\sigma_{\text{r}}] \mathbf{g}_{\bar{\psi}_7}^{\psi_8} G_{t, \bar{\psi}_8 \psi_1} [\sigma_{\text{r}}] + \\
& \quad + (-1)^{\varphi_{\text{II}} \psi_2} (-1)^{\varphi_{\text{I}} \psi_2} \left(\frac{1}{2} \partial_t R_t^{\psi_1 \bar{\psi}_2} \right) G_{t, \psi_2 \bar{\psi}_3} [\sigma_{\text{r}}] \bar{\Gamma}_t^{(3) \psi_3 \varphi_{\text{II}} \bar{\psi}_4} [\sigma_{\text{r}}] \mathbf{g}_{\psi_4}^{\bar{\psi}_5} G_{t, \psi_5 \bar{\psi}_6} [\sigma_{\text{r}}] \times \\
& \quad \times \bar{\Gamma}_t^{(3) \psi_6 \varphi_{\text{I}} \bar{\psi}_7} [\sigma_{\text{r}}] \mathbf{g}_{\psi_7}^{\bar{\psi}_8} G_{t, \psi_8 \bar{\psi}_1} [\sigma_{\text{r}}] - \\
& \quad - (-1)^{\varphi_{\text{II}} \varphi_2} (-1)^{\varphi_{\text{I}} \varphi_2} \left(\frac{1}{2} \partial_t R_t^{\varphi_1 \varphi_2} \right) G_{t, \varphi_2 \varphi_3} [\sigma_{\text{r}}] \bar{\Gamma}_t^{(4) \varphi_3 \varphi_{\text{II}} \varphi_{\text{I}} \varphi_4} [\sigma_{\text{r}}] \mathbf{g}_{\varphi_4}^{\varphi_5} G_{t, \varphi_5 \varphi_1} [\sigma_{\text{r}}] - \\
& \quad - (-1)^{\varphi_{\text{II}} \psi_2} (-1)^{\varphi_{\text{I}} \psi_2} \left(\frac{1}{2} \partial_t R_t^{\bar{\psi}_1 \psi_2} \right) G_{t, \bar{\psi}_2 \psi_3} [\sigma_{\text{r}}] \bar{\Gamma}_t^{(4) \bar{\psi}_3 \varphi_{\text{II}} \varphi_{\text{I}} \psi_4} [\sigma_{\text{r}}] \mathbf{g}_{\bar{\psi}_4}^{\psi_5} G_{t, \bar{\psi}_5 \psi_1} [\sigma_{\text{r}}] + \\
& \quad - (-1)^{\varphi_{\text{II}} \psi_2} (-1)^{\varphi_{\text{I}} \psi_2} \left(\frac{1}{2} \partial_t R_t^{\psi_1 \bar{\psi}_2} \right) G_{t, \psi_2 \bar{\psi}_3} [\sigma_{\text{r}}] \bar{\Gamma}_t^{(4) \psi_3 \varphi_{\text{II}} \varphi_{\text{I}} \bar{\psi}_4} [\sigma_{\text{r}}] \mathbf{g}_{\psi_4}^{\bar{\psi}_5} G_{t, \psi_5 \bar{\psi}_1} [\sigma_{\text{r}}] + \\
& \quad + (-1)^{\varphi_{\text{II}} \varphi_5} (-1)^{\varphi_{\text{II}} \varphi_4} (-1)^{\varphi_{\text{II}} \varphi_1} (-1)^{\varphi_{\text{II}} \varphi_2} (-1)^{\varphi_{\text{I}} \varphi_2} \left(\frac{1}{2} \partial_t R_t^{\varphi_1 \varphi_2} \right) G_{t, \varphi_2 \varphi_3} [\sigma_{\text{r}}] \times \\
& \quad \times \bar{\Gamma}_t^{(3) \varphi_3 \varphi_{\text{I}} \varphi_4} [\sigma_{\text{r}}] \mathbf{g}_{\varphi_4}^{\varphi_5} G_{t, \varphi_5 \varphi_6} [\sigma_{\text{r}}] \bar{\Gamma}_t^{(3) \varphi_6 \varphi_{\text{II}} \varphi_7} [\sigma_{\text{r}}] \mathbf{g}_{\varphi_7}^{\varphi_8} G_{t, \varphi_8 \varphi_1} [\sigma_{\text{r}}] + \\
& \quad + (-1)^{\varphi_{\text{II}} \psi_5} (-1)^{\varphi_{\text{II}} \psi_4} (-1)^{\varphi_{\text{II}} \varphi_1} (-1)^{\varphi_{\text{II}} \psi_2} (-1)^{\varphi_{\text{I}} \psi_2} \left(\frac{1}{2} \partial_t R_t^{\bar{\psi}_1 \psi_2} \right) G_{t, \bar{\psi}_2 \psi_3} [\sigma_{\text{r}}] \times \\
& \quad \times \bar{\Gamma}_t^{(3) \bar{\psi}_3 \varphi_{\text{I}} \psi_4} [\sigma_{\text{r}}] \mathbf{g}_{\bar{\psi}_4}^{\psi_5} G_{t, \bar{\psi}_5 \psi_6} [\sigma_{\text{r}}] \bar{\Gamma}_t^{(3) \bar{\psi}_6 \varphi_{\text{II}} \psi_7} [\sigma_{\text{r}}] \mathbf{g}_{\bar{\psi}_7}^{\psi_8} G_{t, \bar{\psi}_8 \psi_1} [\sigma_{\text{r}}] + \\
& \quad + (-1)^{\varphi_{\text{II}} \psi_5} (-1)^{\varphi_{\text{II}} \psi_4} (-1)^{\varphi_{\text{II}} \varphi_1} (-1)^{\varphi_{\text{II}} \psi_2} (-1)^{\varphi_{\text{I}} \psi_2} \left(\frac{1}{2} \partial_t R_t^{\psi_1 \bar{\psi}_2} \right) G_{t, \psi_2 \bar{\psi}_3} [\sigma_{\text{r}}] \times \\
& \quad \times \bar{\Gamma}_t^{(3) \psi_3 \varphi_{\text{I}} \bar{\psi}_4} [\sigma_{\text{r}}] \mathbf{g}_{\psi_4}^{\bar{\psi}_5} G_{t, \psi_5 \bar{\psi}_6} [\sigma_{\text{r}}] \bar{\Gamma}_t^{(3) \psi_6 \varphi_{\text{II}} \bar{\psi}_7} [\sigma_{\text{r}}] \mathbf{g}_{\psi_7}^{\bar{\psi}_8} G_{t, \psi_8 \bar{\psi}_1} [\sigma_{\text{r}}] = \\
& = + 2 \left(\frac{1}{2} \partial_t R_t^{\varphi_1 \varphi_2} \right) G_{t, \varphi_2 \varphi_3} [\sigma_{\text{r}}] \bar{\Gamma}_t^{(3) \varphi_3 \varphi_{\text{II}} \varphi_4} [\sigma_{\text{r}}] \mathbf{g}_{\varphi_4}^{\varphi_5} G_{t, \varphi_5 \varphi_6} [\sigma_{\text{r}}] \times
\end{aligned}$$

$$\begin{aligned}
& \times \bar{\Gamma}_t^{(3) \varphi_6 \varphi_1 \varphi_7} [\sigma_r] \mathbf{g}_{\varphi_7}^{\varphi_8} G_{t, \varphi_8 \varphi_1} [\sigma_r] + \\
& + 2 \left(\frac{1}{2} \partial_t R_t^{\bar{\psi}_1 \psi_2} \right) G_{t, \bar{\psi}_2 \psi_3} [\sigma_r] \bar{\Gamma}_t^{(3) \bar{\psi}_3 \varphi_{II} \psi_4} [\sigma_r] \mathbf{g}_{\bar{\psi}_4}^{\psi_5} G_{t, \bar{\psi}_5 \psi_6} [\sigma_r] \times \\
& \quad \times \bar{\Gamma}_t^{(3) \bar{\psi}_6 \varphi_I \psi_7} [\sigma_r] \mathbf{g}_{\bar{\psi}_7}^{\psi_8} G_{t, \bar{\psi}_8 \psi_1} [\sigma_r] + \\
& - \left(\frac{1}{2} \partial_t R_t^{\varphi_1 \varphi_2} \right) G_{t, \varphi_2 \varphi_3} [\sigma_r] \bar{\Gamma}_t^{(4) \varphi_3 \varphi_{II} \varphi_1 \varphi_4} [\sigma_r] \mathbf{g}_{\varphi_4}^{\varphi_5} G_{t, \varphi_5 \varphi_1} [\sigma_r] - \\
& - 2 \left(\frac{1}{2} \partial_t R_t^{\bar{\psi}_1 \psi_2} \right) G_{t, \bar{\psi}_2 \psi_3} [\sigma_r] \bar{\Gamma}_t^{(4) \bar{\psi}_3 \varphi_{II} \varphi_1 \psi_4} [\sigma_r] \mathbf{g}_{\bar{\psi}_4}^{\psi_5} G_{t, \bar{\psi}_5 \psi_1} [\sigma_r] + \\
& + 2 \left(\frac{1}{2} \partial_t R_t^{\bar{\psi}_1 \psi_2} \right) G_{t, \bar{\psi}_2 \psi_3} [\sigma_r] \bar{\Gamma}_t^{(3) \bar{\psi}_3 \varphi_I \psi_4} [\sigma_r] \mathbf{g}_{\bar{\psi}_4}^{\psi_5} G_{t, \bar{\psi}_5 \psi_6} [\sigma_r] \times \\
& \quad \times \bar{\Gamma}_t^{(3) \bar{\psi}_6 \varphi_{II} \psi_7} [\sigma_r] \mathbf{g}_{\bar{\psi}_7}^{\psi_8} G_{t, \bar{\psi}_8 \psi_1} [\sigma_r] = \\
& = + 2 \left(\frac{1}{2} \partial_t R_t^{\varphi_1 \varphi_2} \right) (\bar{\Gamma}_t^{(2)} [\sigma_r] + R_t)_{\varphi_2 \varphi_3}^{-1} \bar{\Gamma}_t^{(3) \varphi_3 \varphi_{II} \varphi_4} [\sigma_r] (\bar{\Gamma}_t^{(2)} [\sigma_r] + R_t)_{\varphi_4 \varphi_5}^{-1} \times \tag{Ctr1} \\
& \quad \times \bar{\Gamma}_t^{(3) \varphi_5 \varphi_I \varphi_6} [\sigma_r] (\bar{\Gamma}_t^{(2)} [\sigma_r] + R_t)_{\varphi_6 \varphi_1}^{-1} + \\
& - 2 \left(\frac{1}{2} \partial_t R_t^{\bar{\psi}_1 \psi_2} \right) (\bar{\Gamma}_t^{(2)} [\sigma_r] + R_t)_{\bar{\psi}_2 \psi_3}^{-1} \bar{\Gamma}_t^{(3) \bar{\psi}_3 \varphi_{II} \psi_4} [\sigma_r] (\bar{\Gamma}_t^{(2)} [\sigma_r] + R_t)_{\bar{\psi}_4 \psi_5}^{-1} \times \tag{Ctr2} \\
& \quad \times \bar{\Gamma}_t^{(3) \bar{\psi}_5 \varphi_I \psi_6} [\sigma_r] (\bar{\Gamma}_t^{(2)} [\sigma_r] + R_t)_{\bar{\psi}_6 \psi_1}^{-1} + \\
& - \left(\frac{1}{2} \partial_t R_t^{\varphi_1 \varphi_2} \right) (\bar{\Gamma}_t^{(2)} [\sigma_r] + R_t)_{\varphi_2 \varphi_3}^{-1} \bar{\Gamma}_t^{(4) \varphi_3 \varphi_{II} \varphi_1 \varphi_4} [\sigma_r] (\bar{\Gamma}_t^{(2)} [\sigma_r] + R_t)_{\varphi_4 \varphi_1}^{-1} - \tag{Ctr3} \\
& + 2 \left(\frac{1}{2} \partial_t R_t^{\bar{\psi}_1 \psi_2} \right) (\bar{\Gamma}_t^{(2)} [\sigma_r] + R_t)_{\bar{\psi}_2 \psi_3}^{-1} \bar{\Gamma}_t^{(4) \bar{\psi}_3 \varphi_{II} \varphi_1 \psi_4} [\sigma_r] (\bar{\Gamma}_t^{(2)} [\sigma_r] + R_t)_{\bar{\psi}_4 \psi_1}^{-1} + \tag{Ctr4} \\
& - 2 \left(\frac{1}{2} \partial_t R_t^{\bar{\psi}_1 \psi_2} \right) (\bar{\Gamma}_t^{(2)} [\sigma_r] + R_t)_{\bar{\psi}_2 \psi_3}^{-1} \bar{\Gamma}_t^{(3) \bar{\psi}_3 \varphi_I \psi_4} [\sigma_r] (\bar{\Gamma}_t^{(2)} [\sigma_r] + R_t)_{\bar{\psi}_4 \psi_5}^{-1} \times \tag{Ctr5} \\
& \quad \times \bar{\Gamma}_t^{(3) \bar{\psi}_5 \varphi_{II} \psi_6} [\sigma_r] (\bar{\Gamma}_t^{(2)} [\sigma_r] + R_t)_{\bar{\psi}_6 \psi_1}^{-1}.
\end{aligned}$$

For the above simplifications, we used Eqs. (C.12) and (C.42) and combined certain contributions by transposing the expressions inside the traces.

In terms of Feynman diagrams Eq. (E.52) can be written as follows,

$$\begin{aligned}
& \partial_t \left(\begin{array}{c} \varphi_{II} \quad \varphi_I \\ \text{---} \circ \text{---} \\ \text{---} \end{array} \right) = \tag{E.53} \\
& = + 2 \begin{array}{c} \varphi \\ \text{---} \circ \text{---} \\ \varphi \\ \text{---} \end{array} - 2 \begin{array}{c} \psi \\ \text{---} \circ \text{---} \\ \psi \\ \text{---} \end{array} - \begin{array}{c} \varphi \\ \text{---} \circ \text{---} \\ \varphi \\ \text{---} \end{array} + \\
& + 2 \begin{array}{c} \psi \\ \text{---} \circ \text{---} \\ \psi \\ \text{---} \end{array} - 2 \begin{array}{c} \psi \\ \text{---} \circ \text{---} \\ \psi \\ \text{---} \end{array},
\end{aligned}$$

where the diagrams on the r.h.s. are ordered according to their appearance in Eqs. (Ctr1) to (Ctr5).

Projections

By inspecting the ansatz for the effective average action (E.30) and the two-point vertex (E.32), one finds that within our truncation

$$\begin{aligned}
& \beta (2\pi)^d \delta^{(d)}(\vec{p}_{\text{II}} + \vec{p}_{\text{I}}) (\eta_\varphi(t) (\omega_{n_{\text{II}}}^2 + \vec{p}_{\text{II}}^2) + Z_\varphi^{-1}(t) \partial_\sigma^2 [\partial_t U(t, \sigma)]) = \\
& = \beta (2\pi)^d \delta^{(d)}(\vec{p}_{\text{II}} + \vec{p}_{\text{I}}) [\eta_\varphi(t) (\omega_{n_{\text{II}}}^2 + \vec{p}_{\text{II}}^2) + \\
& \quad + \partial_t [\partial_{\sigma_r}^2 U(t, \sigma_r)] + \eta_\varphi(t) \partial_{\sigma_r}^2 U(t, \sigma_r) + \frac{1}{2} \eta_\varphi(t) \sigma_r \partial_{\sigma_r}^3 U(t, \sigma_r)] = \\
& = Z_\varphi^{-1}(t) \frac{\beta^2 (2\pi)^{2d} \delta^2(\partial_t \bar{\Gamma}_t[\bar{\psi}, \psi, \varphi])}{\delta \bar{\varphi}(\omega_{n_{\text{II}}}, \vec{p}_{\text{II}}) \delta \bar{\varphi}(\omega_{n_{\text{I}}}, \vec{p}_{\text{I}})} \Big|_{\varphi=\sigma, \bar{\psi}=\psi=0, n_{\text{II}}=n_{\text{I}}}
\end{aligned} \tag{E.54}$$

As already discussed in the context of the fermionic two-point function (E.13) in the GN model, we note that we further need to evaluate this equation at vanishing external momenta $\vec{p}_{\text{I}} = \vec{p}_{\text{II}} = 0$ to obtain the RG flow equation for the field-dependent bosonic mass (the second field-derivative of the effective potential). In order to obtain exclusively the scale evolution of the bosonic anomalous dimension $\eta_\varphi(t)$ and avoid admixtures from higher-order momentum dependent terms of the effective action, which are neglected in our truncation, one needs to extract the coefficient of \vec{p}_{II}^2 on the r.h.s. of Eq. (E.54). This is routinely done by

1. ignoring the factor $\beta (2\pi)^d \delta^{(d)}(\vec{p}_{\text{II}} - \vec{p}_{\text{I}})$, which appears on both sides of the equation,
2. expanding the r.h.s. in a Taylor series of the external momentum \vec{p}_{II} about $\vec{p}_{\text{II}} = 0$,
3. dropping all terms except for the quadratic order.

Within the next steps, all diagrams of Eq. (E.53) are evaluated separately one after the other. To this end we first insert the regulators, propagators, and vertices into the generic traces (Ctr1) to (Ctr5) and afterwards apply Eq. (E.54). Finally, the zeroth- and second-order coefficients of an expansion in the external momentum \vec{p}_{II} are extracted and associated to the flow equations of the field-dependent mass and the anomalous dimension.

Trace (Ctr1) – boson loop

We start our explicit calculations with the analysis of the boson-loop contribution to the RG flow, which is also called the boson self-interaction correction to the two-point function. We insert the explicit expressions (E.38), (E.40), (E.43), and (E.36), into trace (Ctr1) and find,

$$\begin{aligned}
\text{(Ctr1)} & = +2 \text{ } \begin{array}{c} \varphi \\ \text{---} \otimes \text{---} \varphi \\ \text{---} \varphi \end{array} = \\
& = +2 \frac{1}{\beta^6} \sum_{n_1, \dots, n_6 = -\infty}^{\infty} \int_{-\infty}^{\infty} \frac{d^d p_1}{(2\pi)^d} \cdots \frac{d^d p_6}{(2\pi)^d} \times \\
& \quad \times \beta \delta_{-n_1, n_2} (2\pi)^d \delta^{(d)}(\vec{p}_1 + \vec{p}_2) \vec{p}_1^2 \partial_t [Z_\varphi(t) \frac{1}{2} r_b(t, |\vec{p}_1|)] \times
\end{aligned} \tag{E.55}$$

$$\begin{aligned}
& \times \beta \delta_{-n_2, n_3} (2\pi)^d \delta^{(d)}(\vec{p}_2 + \vec{p}_3) \frac{1}{Z_\varphi(t) [\omega_{n_2}^2 + \vec{p}_2^2 [1 + r_b(t, |\vec{p}_2|)] + \partial_{\sigma_r}^2 U(t, \sigma_r)]} \times \\
& \times \beta \delta_{0, n_3 + n_{\text{II}} + n_4} (2\pi)^d \delta^{(d)}(\vec{p}_3 + \vec{p}_{\text{II}} + \vec{p}_4) Z_\varphi^{\frac{3}{2}}(t) \partial_{\sigma_r}^3 U(t, \sigma_r) \times \\
& \times \beta \delta_{-n_4, n_5} (2\pi)^d \delta^{(d)}(\vec{p}_4 + \vec{p}_5) \frac{1}{Z_\varphi(t) [\omega_{n_4}^2 + \vec{p}_4^2 [1 + r_b(t, |\vec{p}_4|)] + \partial_{\sigma_r}^2 U(t, \sigma_r)]} \times \\
& \times \beta \delta_{0, n_5 + n_{\text{I}} + n_6} (2\pi)^d \delta^{(d)}(\vec{p}_5 + \vec{p}_{\text{I}} + \vec{p}_6) Z_\varphi^{\frac{3}{2}}(t) \partial_{\sigma_r}^3 U(t, \sigma_r) \times \\
& \times \beta \delta_{-n_6, n_1} (2\pi)^d \delta^{(d)}(\vec{p}_6 + \vec{p}_1) \frac{1}{Z_\varphi(t) [\omega_{n_6}^2 + \vec{p}_6^2 [1 + r_b(t, |\vec{p}_6|)] + \partial_{\sigma_r}^2 U(t, \sigma_r)]}.
\end{aligned}$$

Inserting this into the r.h.s. of the projection (E.54) one only needs to evaluate traces in momentum space (the integrals and Matsubara sums) as far as possible,

$$\begin{aligned}
& Z_\varphi^{-1}(t) (\text{Ctr1}) \Big|_{n_{\text{II}}=n_{\text{I}}=0} \stackrel{\text{(D.26)}}{=} \tag{E.56} \\
& = \beta (2\pi)^d \delta^{(d)}(\vec{p}_{\text{II}} + \vec{p}_{\text{I}}) 2 [\partial_{\sigma_r}^3 U(t, \sigma_r)]^2 k^{-6} \times \\
& \times \frac{1}{\beta} \sum_{n=-\infty}^{\infty} \int_{-\infty}^{\infty} \frac{d^d p}{(2\pi)^d} \vec{p}^2 \left[\frac{1}{2} \partial_t r_b(t, |\vec{p}|) + \frac{1}{2} \eta_\varphi(t) r_b(t, |\vec{p}|) \right] \mathfrak{B}_n^2 \left(\frac{\vec{p}^2}{k^2} \right) \mathfrak{B}_n \left(\frac{(\vec{p} + \vec{p}_{\text{II}})^2}{k^2} \right).
\end{aligned}$$

Field-dependent bosonic mass Taking only into account the zeroth order of an expansion of Eq. (E.56) in \vec{p}_{II} , which is identical to setting $\vec{p}_{\text{II}} = 0$ and dropping the infinite-volume factor $\beta (2\pi)^d \delta^{(d)}(0)$, one obtains,

$$\begin{aligned}
& 2 [\partial_{\sigma_r}^3 U(t, \sigma_r)]^2 k^{-6} \times \tag{E.57} \\
& \times \frac{1}{\beta} \sum_{n=-\infty}^{\infty} \int_{-\infty}^{\infty} \frac{d^d p}{(2\pi)^d} \vec{p}^2 \left[\frac{1}{2} \partial_t r_b(t, |\vec{p}|) + \frac{1}{2} \eta_\varphi(t) r_b(t, |\vec{p}|) \right] \mathfrak{B}_n^3 \left(\frac{\vec{p}^2}{k^2} \right) \stackrel{\text{(A.5)}}{=} \\
& = 2 [\partial_{\sigma_r}^3 U(t, \sigma_r)]^2 k^{-6} \times \\
& \times \frac{1}{\beta} \sum_{n=-\infty}^{\infty} A_d d \int_0^\infty dp p^{d+1} \left[\frac{1}{2} \partial_t r_b(t, p) + \frac{1}{2} \eta_\varphi(t) r_b(t, p) \right] \mathfrak{B}_n^3 \left(\frac{p^2}{k^2} \right) \stackrel{\text{(D.7)}}{=} \\
& = 2 [\partial_{\sigma_r}^3 U(t, \sigma_r)]^2 k^{d-4} \frac{1}{\beta} \sum_{n=-\infty}^{\infty} A_d \frac{d}{2} \int_0^\infty dy y^{\frac{d}{2}} [y \dot{r}_b(y) + \frac{1}{2} \eta_\varphi(t) r_b(y)] \mathfrak{B}_n^3(y) \stackrel{\text{(D.15)}}{=} \\
& = -2 A_d \left[1 - \frac{\eta_\varphi(t)}{d+2} \right] [\partial_{\sigma_r}^3 U(t, \sigma_r)]^2 k^{d-4} \frac{1}{\beta} \sum_{n=-\infty}^{\infty} \mathfrak{B}_n^3(1).
\end{aligned}$$

Identities, variable substitutions *etc.* are referenced at the end of the lines.

Bosonic anomalous dimension In order to extract the coefficient proportional to \vec{p}_{II}^2 in Eq. (E.56), we simplify the notation by setting $\vec{q} \equiv \vec{p}_{\text{II}}$ and only expand the \vec{q} -dependent con-

tribution about $\vec{q} = 0$,

$$\begin{aligned} \mathfrak{B}_n\left(\frac{(\vec{p}+\vec{q})^2}{k^2}\right) &= \\ &= \mathfrak{B}_n\left(\frac{\vec{p}^2}{k^2}\right) + 2\frac{\vec{q}\cdot\vec{p}}{k^2}\mathfrak{B}_n\left(\frac{\vec{p}^2}{k^2}\right) + \frac{\vec{q}^2}{k^2}\mathfrak{B}_n\left(\frac{\vec{p}^2}{k^2}\right) + 2\frac{(\vec{q}\cdot\vec{p})^2}{k^4}\mathfrak{B}_n\left(\frac{\vec{p}^2}{k^2}\right) + \mathcal{O}\left(\frac{|\vec{q}|^3}{k^3}\right). \end{aligned} \quad (\text{E.58})$$

Inserting this expansion into Eq. (E.56), we can immediately ignore the first two terms, which do not contribute to the \vec{q}^2 coefficient. Additionally, since we are working with Litim-type regulators, we can ignore the $\mathfrak{B}_n(y)$ term, with $y = \frac{\vec{q}^2}{k^2}$, due to the identity (D.30). Finally, under the integral, we replace $(\vec{q}\cdot\vec{p})^2 \mapsto \frac{1}{d}\vec{q}^2\vec{p}^2$, because for terms proportional to $q_i q_j$ with $i \neq j$ the integration is odd and vanishes. Hence, the only contribution at order \vec{q}^2 reads,

$$\begin{aligned} &2\left[\partial_{\sigma_r}^3 U(t, \sigma_r)\right]^2 k^{-6} \frac{1}{\beta} \sum_{n=-\infty}^{\infty} \int_{-\infty}^{\infty} \frac{d^d p}{(2\pi)^d} \vec{p}^2 \left[\frac{1}{2} \partial_t r_b(t, |\vec{p}|) + \frac{1}{2} \eta_\varphi(t) r_b(t, |\vec{p}|)\right] \times \\ &\times \mathfrak{B}_n^2\left(\frac{\vec{p}^2}{k^2}\right) \left[2\frac{(\vec{q}\cdot\vec{p})^2}{k^4} \mathfrak{B}_n\left(\frac{\vec{p}^2}{k^2}\right)\right] \stackrel{(\text{A.5})}{=} \\ &= \vec{q}^2 2\left[\partial_{\sigma_r}^3 U(t, \sigma_r)\right]^2 k^{-8} \frac{1}{\beta} \sum_{n=-\infty}^{\infty} A_d d \int_0^\infty dp p^{d+1} \left[\frac{1}{2} \partial_t r_b(t, p) + \frac{1}{2} \eta_\varphi(t) r_b(t, p)\right] \times \\ &\times \mathfrak{B}_n^2\left(\frac{p^2}{k^2}\right) \left[\frac{2}{d} \frac{p^2}{k^2} \mathfrak{B}_n\left(\frac{p^2}{k^2}\right)\right] \stackrel{(\text{D.7})}{=} \\ &= \vec{q}^2 2\left[\partial_{\sigma_r}^3 U(t, \sigma_r)\right]^2 k^{d-6} \frac{1}{\beta} \sum_{n=-\infty}^{\infty} A_d \frac{d}{2} \int_0^\infty dy y^{\frac{d}{2}} \left[y \dot{r}_b(y) + \frac{1}{2} \eta_\varphi(t) r_b(y)\right] \times \\ &\times \mathfrak{B}_n^2(y) \left[\frac{2}{d} y \mathfrak{B}_n(y)\right] \stackrel{(\text{D.31})}{=} \\ &= \vec{q}^2 A_d \left[\partial_{\sigma_r}^3 U(t, \sigma_r)\right]^2 k^{d-6} \frac{1}{\beta} \sum_{n=-\infty}^{\infty} \mathfrak{B}_n^4(1). \end{aligned} \quad (\text{E.59})$$

Traces (Ctr2) and (Ctr5) – fermion loop

Next, we study the fermion-loop contribution(s) to the bosonic two-point function, *i.e.*, traces (Ctr2) and (Ctr5).

Inserting the explicit expressions for the fermionic regulator Eqs. (E.5) and (E.7), propagator (E.44), and fermion-boson three-point vertex (E.34) into trace (Ctr2), the intermediate result is given by

$$\begin{aligned} (\text{Ctr2}) &= -2 \text{Diagram} = \\ &= -2 \frac{1}{\beta^6} \sum_{n_1, \dots, n_6=-\infty}^{\infty} \int_{-\infty}^{\infty} \frac{d^d p_1}{(2\pi)^d} \cdots \frac{d^d p_6}{(2\pi)^d} \times \\ &\times (-1) \beta \delta_{n_1, n_2} (2\pi)^d \delta^{(d)}(\vec{p}_1 - \vec{p}_2) (\mathbb{1})_{c_1}^{c_1} i\vec{p}_1 \cdot (\vec{\gamma})_{a_1}^{a_1} \partial_t \left[Z_\psi(t) \frac{1}{2} r_f(t, |\vec{p}_1|) \right] \times \\ &\times \beta \delta_{n_2, n_3} (2\pi)^d \delta^{(d)}(\vec{p}_2 - \vec{p}_3) \times \end{aligned} \quad (\text{E.60})$$

$$\begin{aligned}
& \times \frac{[\mathbf{i}(\nu_{n_2} + \mathbf{i}\mu) \gamma^{d+1} + \mathbf{i}\vec{p}_2 \cdot \vec{\gamma} [1 + r_f(t, |\vec{p}_2|)] - m_r(t, \sigma_r)]^{a_2} a_3 (\mathbf{1})^{c_2} c_3}{Z_\psi(t) [(\nu_{n_2} + \mathbf{i}\mu)^2 + \vec{p}_2^2 [1 + r_f(t, |\vec{p}_2|)]^2 + m_r^2(t, \sigma_r)]} \times \\
& \times (-1) \beta \delta_{n_3, n_{\text{II}} + n_4} (2\pi)^d \delta^{(d)}(\vec{p}_{\text{II}} - \vec{p}_3 + \vec{p}_4) Z_\psi(t) Z_\varphi^{\frac{1}{2}}(t) [\partial_{\sigma_r} m_r(t, \sigma_r)] (\mathbf{1})^{c_3} c_4 (\mathbf{1})^{a_3} a_4 \times \\
& \times \beta \delta_{n_4, n_5} (2\pi)^d \delta^{(d)}(\vec{p}_4 - \vec{p}_5) \times \\
& \times \frac{[\mathbf{i}(\nu_{n_4} + \mathbf{i}\mu) \gamma^{d+1} + \mathbf{i}\vec{p}_4 \cdot \vec{\gamma} [1 + r_f(t, |\vec{p}_4|)] - m_r(t, \sigma_r)]^{a_4} a_5 (\mathbf{1})^{c_4} c_5}{Z_\psi(t) [(\nu_{n_4} + \mathbf{i}\mu)^2 + \vec{p}_4^2 [1 + r_f(t, |\vec{p}_4|)]^2 + m_r^2(t, \sigma_r)]} \times \\
& \times (-1) \beta \delta_{n_5, n_{\text{I}} + n_6} (2\pi)^d \delta^{(d)}(\vec{p}_{\text{I}} - \vec{p}_5 + \vec{p}_6) Z_\psi(t) Z_\varphi^{\frac{1}{2}}(t) [\partial_{\sigma_r} m_r(t, \sigma_r)] (\mathbf{1})^{c_5} c_6 (\mathbf{1})^{a_5} a_6 \times \\
& \times \beta \delta_{n_6, n_1} (2\pi)^d \delta^{(d)}(\vec{p}_6 - \vec{p}_1) \times \\
& \times \frac{[\mathbf{i}(\nu_{n_6} + \mathbf{i}\mu) \gamma^{d+1} + \mathbf{i}\vec{p}_6 \cdot \vec{\gamma} [1 + r_f(t, |\vec{p}_6|)] - m_r(t, \sigma_r)]^{a_6} a_1 (\mathbf{1})^{c_6} c_1}{Z_\psi(t) [(\nu_{n_6} + \mathbf{i}\mu)^2 + \vec{p}_6^2 [1 + r_f(t, |\vec{p}_6|)]^2 + m_r^2(t, \sigma_r)]}.
\end{aligned}$$

For the trace (Ctr5) one merely has to exchange I \leftrightarrow II. Consequently, due to momentum conservation, which is encoded in an overall prefactor $\beta \delta_{-n_{\text{II}}, n_{\text{I}}} (2\pi)^d \delta^{(d)}(\vec{p}_{\text{II}} + \vec{p}_{\text{I}})$, both diagrams contribute equally to the RG flow equations of the field-dependent bosonic mass and the anomalous dimension.

Anyhow, applying the projection (E.54) to the latter equation, we find

$$Z_\varphi^{-1}(t) (\text{Ctr2})|_{n_{\text{II}}=n_{\text{I}}=0} \stackrel{(\text{D.32})}{=} \quad (\text{E.61})$$

$$\begin{aligned}
& = + \beta (2\pi)^d \delta^{(d)}(\vec{p}_{\text{II}} + \vec{p}_{\text{I}}) 2 d_\gamma N [\partial_{\sigma_r} m_r(t, \sigma_r)]^2 k^{-6} \times \\
& \times \frac{1}{\beta} \sum_{n=-\infty}^{\infty} \int_{-\infty}^{\infty} \frac{d^d p}{(2\pi)^d} \left[\frac{1}{2} \partial_t r_f(t, |\vec{p}|) + \frac{1}{2} \eta_\psi(t) r_f(t, |\vec{p}|) \right] \mathfrak{F}_n^2\left(\frac{\vec{p}^2}{k^2}\right) \mathfrak{F}_n\left(\frac{(\vec{p} - \vec{p}_{\text{II}})^2}{k^2}\right) \times \\
& \times \left(2 \vec{p}^2 [1 + r_f(t, |\vec{p}|)] \left[k^2 \mathfrak{F}_n^{-1}\left(\frac{\vec{p}^2}{k^2}\right) - 2 m_r^2(t, \sigma_r) - \vec{p}^2 [1 + r_f(t, |\vec{p}|)]^2 \right] + \right. \\
& \left. + (\vec{p}_{\text{II}} \cdot \vec{p} - \vec{p}^2) [1 + r_f(t, |\vec{p} - \vec{p}_{\text{II}}|)] \left[k^2 \mathfrak{F}_n^{-1}\left(\frac{\vec{p}^2}{k^2}\right) - 2 \vec{p}^2 [1 + r_f(t, |\vec{p}|)]^2 \right] \right). \quad (\text{FL1})
\end{aligned}$$

$$+ (\vec{p}_{\text{II}} \cdot \vec{p} - \vec{p}^2) [1 + r_f(t, |\vec{p} - \vec{p}_{\text{II}}|)] \left[k^2 \mathfrak{F}_n^{-1}\left(\frac{\vec{p}^2}{k^2}\right) - 2 \vec{p}^2 [1 + r_f(t, |\vec{p}|)]^2 \right]. \quad (\text{FL2})$$

Here, the traces over fermionic indices were cross-checked with FORMTRACER [640].

Field-dependent bosonic mass The contribution to the flow equation of the second field-derivative of the effective potential is attained by setting $\vec{p}_{\text{II}} = 0$, which drastically simplifies Eq. (E.61),

$$\begin{aligned}
& 2 d_\gamma N [\partial_{\sigma_r} m_r(t, \sigma_r)]^2 k^{-6} \times \quad (\text{E.62}) \\
& \times \frac{1}{\beta} \sum_{n=-\infty}^{\infty} \int_{-\infty}^{\infty} \frac{d^d p}{(2\pi)^d} 2 \vec{p}^2 \left[\frac{1}{2} \partial_t r_f(t, |\vec{p}|) + \frac{1}{2} \eta_\psi(t) r_f(t, |\vec{p}|) \right] [1 + r_f(t, |\vec{p}|)] \times \\
& \times \left[\frac{1}{2} k^2 \mathfrak{F}_n^2\left(\frac{\vec{p}^2}{k^2}\right) - 2 m_r^2(t, \sigma_r) \mathfrak{F}_n^3\left(\frac{\vec{p}^2}{k^2}\right) \right] \stackrel{(\text{A.5})}{=}
\end{aligned}$$

$$\begin{aligned}
&= 2 d_\gamma N [\partial_{\sigma_r} m_r(t, \sigma_r)]^2 k^{-6} \times \\
&\quad \times \frac{1}{\beta} \sum_{n=-\infty}^{\infty} A_d d \int_0^\infty dp p^{d+1} 2 \left[\frac{1}{2} \partial_t r_f(t, p) + \frac{1}{2} \eta_\psi(t) r_f(t, p) \right] [1 + r_f(t, p)] \times \\
&\quad \times \left[\frac{1}{2} k^2 \mathfrak{F}_n^2\left(\frac{p^2}{k^2}\right) - 2 m_r^2(t, \sigma_r) \mathfrak{F}_n^3\left(\frac{p^2}{k^2}\right) \right] \stackrel{(D.7)}{=} \\
&= 2 d_\gamma N [\partial_{\sigma_r} m_r(t, \sigma_r)]^2 k^{d-4} \frac{1}{\beta} \sum_{n=-\infty}^{\infty} A_d d \int_0^\infty dy y^{\frac{d}{2}} \left[y \dot{r}_f(y) + \frac{1}{2} \eta_\psi(t) r_f(y) \right] [1 + r_f(y)] \times \\
&\quad \times \left[\frac{1}{2} k^2 \mathfrak{F}_n^2(y) - 2 m_r^2(t, \sigma_r) \mathfrak{F}_n^3(y) \right] \stackrel{(D.25)}{=} \\
&= -2 A_d \left[1 - \frac{\eta_\psi(t)}{d+1} \right] d_\gamma N [\partial_{\sigma_r} m_r(t, \sigma_r)]^2 k^{d-4} \frac{1}{\beta} \sum_{n=-\infty}^{\infty} \left[\frac{1}{2} k^2 \mathfrak{F}_n^2(y) - 2 m_r^2(t, \sigma_r) \mathfrak{F}_n^3(y) \right].
\end{aligned}$$

Bosonic anomalous dimension The calculation of the coefficient of the \vec{p}_Π^2 -term is more tedious, but in principle straightforward. Again, we define $\vec{q} \equiv \vec{p}_\Pi$ to simplify the notation.

To structure our work, we first consider solely the term in line (FL1) of Eq. (E.61). This term in the round bracket is independent of the external momentum \vec{q} , such that it suffices to expand the factor

$$\mathfrak{F}_n\left(\frac{(\vec{p}-\vec{q})^2}{k^2}\right) = \mathfrak{F}_n\left(\frac{\vec{p}^2}{k^2}\right) - 2 \frac{\vec{q}\cdot\vec{p}}{k^2} \dot{\mathfrak{F}}_n\left(\frac{\vec{p}^2}{k^2}\right) + \frac{\vec{q}^2}{k^2} \ddot{\mathfrak{F}}_n\left(\frac{\vec{p}^2}{k^2}\right) + 2 \frac{(\vec{q}\cdot\vec{p})^2}{k^4} \ddot{\mathfrak{F}}_n\left(\frac{\vec{p}^2}{k^2}\right) + \mathcal{O}\left(\frac{|\vec{q}|^3}{k^3}\right). \quad (E.63)$$

The situation is now analogous to Eq. (E.59), where only the $\ddot{\mathfrak{F}}_n(y)$ -term contributes to the integral at order \vec{q}^2 , because the other terms are not proportional to \vec{q}^2 or the identity (D.37) eliminates the $\dot{\mathfrak{F}}_n(y)$ contribution for the Litim regulator. Hence, we find

$$\begin{aligned}
&(\text{FL1}) = \tag{Ctr2a} \\
&= 2 d_\gamma N [\partial_{\sigma_r} m_r(t, \sigma_r)]^2 k^{-6} \times \\
&\quad \times \frac{1}{\beta} \sum_{n=-\infty}^{\infty} \int_{-\infty}^{\infty} \frac{d^d p}{(2\pi)^d} \left[\frac{1}{2} \partial_t r_f(t, |\vec{p}|) + \frac{1}{2} \eta_\psi(t) r_f(t, |\vec{p}|) \right] \mathfrak{F}_n^2\left(\frac{\vec{p}^2}{k^2}\right) \left[2 \frac{(\vec{q}\cdot\vec{p})^2}{k^4} \ddot{\mathfrak{F}}_n\left(\frac{\vec{p}^2}{k^2}\right) \right] \times \\
&\quad \times \left(2 \vec{p}^2 [1 + r_f(t, |\vec{p}|)] \left[k^2 \mathfrak{F}_n^{-1}\left(\frac{\vec{p}^2}{k^2}\right) - 2 m_r^2(t, \sigma_r) - \vec{p}^2 [1 + r_f(t, |\vec{p}|)]^2 \right] \right) \stackrel{(A.5)}{=} \\
&= \vec{q}^2 2 d_\gamma N [\partial_{\sigma_r} m_r(t, \sigma_r)]^2 k^{-6} \times \\
&\quad \times \frac{1}{\beta} \sum_{n=-\infty}^{\infty} A_d d \int_0^\infty dp p^{d+1} 2 \left[\frac{1}{2} \partial_t r_f(t, p) + \frac{1}{2} \eta_\psi(t) r_f(t, p) \right] [1 + r_f(t, p)] \times \\
&\quad \times \mathfrak{F}_n^2\left(\frac{p^2}{k^2}\right) \left[\frac{2}{d} \frac{p^2}{k^2} \ddot{\mathfrak{F}}_n\left(\frac{p^2}{k^2}\right) \right] \left[\mathfrak{F}_n^{-1}\left(\frac{p^2}{k^2}\right) - 2 \frac{1}{k^2} m_r^2(t, \sigma_r) - \frac{p^2}{k^2} [1 + r_f(t, p)]^2 \right] \stackrel{(D.7)}{=} \\
&= \vec{q}^2 2 d_\gamma N [\partial_{\sigma_r} m_r(t, \sigma_r)]^2 k^{d-4} \times \\
&\quad \times \frac{1}{\beta} \sum_{n=-\infty}^{\infty} A_d d \int_0^\infty dy y^{\frac{d}{2}} \left[y \dot{r}_f(y) + \frac{1}{2} \eta_\psi(t) r_f(y) \right] [1 + r_f(y)] \times
\end{aligned}$$

$$\begin{aligned}
& \times \mathfrak{F}_n^2(y) \left[\frac{2}{d} y \ddot{\mathfrak{F}}_n(y) \right] \left[\mathfrak{F}_n^{-1}(y) - 2 \frac{1}{k^2} m_r^2(t, \sigma_r) - y [1 + r_f(y)]^2 \right] = \\
& = \bar{q}^2 2 A_d d_\gamma N [\partial_{\sigma_r} m_r(t, \sigma_r)]^2 k^{d-4} \frac{1}{\beta} \sum_{n=-\infty}^{\infty} \left[\left(-\frac{1}{2} - \frac{1}{k^2} m_r^2(t, \sigma_r) \right) \mathfrak{F}_n^4(1) + \frac{1}{2} \mathfrak{F}_n^3(1) \right].
\end{aligned}$$

The second term belonging to line (FL2) of Eq. (E.61) is more involved. Again, one has to use the expansion (E.63). This time, however, there are also \bar{q} -dependent terms in line (FL2), which also need to be expanded in \bar{q} . Combining both expansions,

$$\begin{aligned}
& \mathfrak{F}_n \left(\frac{(\bar{p}-\bar{q})^2}{k^2} \right) (\bar{q} \cdot \bar{p} - \bar{p}^2) \left[1 + r_f \left(\frac{(\bar{p}-\bar{q})^2}{k^2} \right) \right] = \tag{E.64} \\
& = \left[\mathfrak{F}_n \left(\frac{\bar{p}^2}{k^2} \right) - 2 \frac{\bar{q} \cdot \bar{p}}{k^2} \dot{\mathfrak{F}}_n \left(\frac{\bar{p}^2}{k^2} \right) + \frac{\bar{q}^2}{k^2} \ddot{\mathfrak{F}}_n \left(\frac{\bar{p}^2}{k^2} \right) + 2 \frac{(\bar{q} \cdot \bar{p})^2}{k^4} \ddot{\mathfrak{F}}_n \left(\frac{\bar{p}^2}{k^2} \right) + \mathcal{O} \left(\frac{|\bar{q}|^3}{k^3} \right) \right] (\bar{q} \cdot \bar{p} - \bar{p}^2) \times \\
& \times \left[1 + r_f \left(\frac{\bar{p}^2}{k^2} \right) - 2 \frac{\bar{q} \cdot \bar{p}}{k^2} \dot{r}_f \left(\frac{\bar{p}^2}{k^2} \right) + \frac{\bar{q}^2}{k^2} \dot{r}_f \left(\frac{\bar{p}^2}{k^2} \right) + 2 \frac{(\bar{q} \cdot \bar{p})^2}{k^4} \ddot{r}_f \left(\frac{\bar{p}^2}{k^2} \right) + \mathcal{O} \left(\frac{|\bar{q}|^3}{k^3} \right) \right],
\end{aligned}$$

one has to extract all terms proportional to \bar{q}^2 . These are

$$\begin{aligned}
& \left[-2 \frac{(\bar{q} \cdot \bar{p})^2}{k^2} \dot{r}_f \left(\frac{\bar{p}^2}{k^2} \right) - \frac{\bar{q}^2 \bar{p}^2}{k^2} \dot{r}_f \left(\frac{\bar{p}^2}{k^2} \right) - 2 \frac{(\bar{q} \cdot \bar{p})^2 \bar{p}^2}{k^4} \ddot{r}_f \left(\frac{\bar{p}^2}{k^2} \right) \right] \mathfrak{F}_n \left(\frac{\bar{p}^2}{k^2} \right) - \tag{E.65} \\
& - 2 \frac{(\bar{q} \cdot \bar{p})^2 \bar{p}^2}{k^4} \left[1 + r_f \left(\frac{\bar{p}^2}{k^2} \right) \right] \ddot{\mathfrak{F}}_n \left(\frac{\bar{p}^2}{k^2} \right),
\end{aligned}$$

where we also dropped all terms proportional to $\dot{\mathfrak{F}}_n(y)$, since these terms vanish anyhow for the Litim regulator due to identity (D.37).

In total, the contribution of from line (FL2) at order \bar{q}^2 is

$$\text{(FL2)} = \tag{Ctr2b}$$

$$\begin{aligned}
& 2 d_\gamma N [\partial_{\sigma_r} m_r(t, \sigma_r)]^2 k^{-6} \times \\
& \times \frac{1}{\beta} \sum_{n=-\infty}^{\infty} \int_{-\infty}^{\infty} \frac{d^d p}{(2\pi)^d} \left[\frac{1}{2} \partial_t r_f(t, |\vec{p}|) + \frac{1}{2} \eta_\psi(t) r_f(t, |\vec{p}|) \right] \mathfrak{F}_n^2 \left(\frac{\bar{p}^2}{k^2} \right) \times \\
& \times \left[k^2 \mathfrak{F}_n^{-1} \left(\frac{\bar{p}^2}{k^2} \right) - 2 \bar{p}^2 \left[1 + r_f \left(\frac{\bar{p}^2}{k^2} \right) \right]^2 \right] \times \\
& \times \left(\left[-2 \frac{(\bar{q} \cdot \bar{p})^2}{k^2} \dot{r}_f \left(\frac{\bar{p}^2}{k^2} \right) - \frac{\bar{q}^2 \bar{p}^2}{k^2} \dot{r}_f \left(\frac{\bar{p}^2}{k^2} \right) - 2 \frac{(\bar{q} \cdot \bar{p})^2 \bar{p}^2}{k^4} \ddot{r}_f \left(\frac{\bar{p}^2}{k^2} \right) \right] \mathfrak{F}_n \left(\frac{\bar{p}^2}{k^2} \right) - \right. \\
& \quad \left. - 2 \frac{(\bar{q} \cdot \bar{p})^2 \bar{p}^2}{k^4} \left[1 + r_f \left(\frac{\bar{p}^2}{k^2} \right) \right] \ddot{\mathfrak{F}}_n \left(\frac{\bar{p}^2}{k^2} \right) \right) \stackrel{\text{(A.5)}}{=} \\
& = \bar{q}^2 2 d_\gamma N [\partial_{\sigma_r} m_r(t, \sigma_r)]^2 k^{-6} \times \\
& \times \frac{1}{\beta} \sum_{n=-\infty}^{\infty} A_d d \int_0^\infty dp p^{d+1} 2 \left[\frac{1}{2} \partial_t r_f(t, p) + \frac{1}{2} \eta_\psi(t) r_f(t, p) \right] \mathfrak{F}_n^2 \left(\frac{p^2}{k^2} \right) \times \\
& \times \left[\frac{1}{2} \mathfrak{F}_n^{-1} \left(\frac{p^2}{k^2} \right) - \frac{p^2}{k^2} \left[1 + r_f \left(\frac{p^2}{k^2} \right) \right]^2 \right] \times
\end{aligned}$$

$$\begin{aligned}
& \times \left(\left[-\frac{2}{d} \dot{r}_f \left(\frac{p^2}{k^2} \right) - \dot{r}_f \left(\frac{p^2}{k^2} \right) - \frac{2}{d} \frac{p^2}{k^2} \ddot{r}_f \left(\frac{p^2}{k^2} \right) \right] \mathfrak{F}_n \left(\frac{p^2}{k^2} \right) - \frac{2}{d} \frac{p^2}{k^2} \left[1 + r_f \left(\frac{p^2}{k^2} \right) \right] \ddot{\mathfrak{F}}_n \left(\frac{p^2}{k^2} \right) \right) \stackrel{\text{(D.7)}}{=} \\
& = \bar{q}^2 2 d_\gamma N \left[\partial_{\sigma_r} m_r(t, \sigma_r) \right]^2 k^{d-4} \times \\
& \times \frac{1}{\beta} \sum_{n=-\infty}^{\infty} A_d d \int_0^\infty dy y^{\frac{d}{2}} \left[y \dot{r}_f(y) + \frac{1}{2} \eta_\psi(t) r_f(y) \right] \mathfrak{F}_n^2(y) \left[\frac{1}{2} \mathfrak{F}_n^{-1}(y) - y [1 + r_f(y)]^2 \right] \times \\
& \times \left(\underbrace{\left[-\dot{r}_f(y) - \frac{2}{d} (\dot{r}_f(y) + y \ddot{r}_f(y)) \right]}_{(2)} \mathfrak{F}_n(y) \underbrace{- \frac{2}{d} y [1 + r_f(y)] \ddot{\mathfrak{F}}_n(y)}_{(1)} \right).
\end{aligned}$$

After some simplifications by certain variable transformations, it remains to evaluate the last y -integral. Also here, it is reasonable to split the evaluation into two separate steps. For both evaluations, several relations and identities for the Litim regulator from Appendix D.2.2 are needed.

The first term is evaluated using Eq. (D.38) plus some results of Appendix D.2.2,

$$(1) = \bar{q}^2 2 A_d d_\gamma N \left[\partial_{\sigma_r} m_r(t, \sigma_r) \right]^2 k^{d-4} \frac{1}{\beta} \sum_{n=-\infty}^{\infty} \left[-\frac{1}{4} \mathfrak{F}_n^3(1) + \frac{1}{2} \mathfrak{F}_n^4(1) \right]. \quad (\text{Ctr2bI})$$

For the second term, we use Eq. (D.36) as well as the results of Appendix D.2.2,

$$\begin{aligned}
(2) & = \bar{q}^2 2 d_\gamma N \left[\partial_{\sigma_r} m_r(t, \sigma_r) \right]^2 k^{d-4} \frac{1}{\beta} \sum_{n=-\infty}^{\infty} A_d d \int_0^\infty dy y^{\frac{d}{2}} \left[y \dot{r}_f(y) + \frac{1}{2} \eta_\psi(t) r_f(y) \right] \times \\
& \times \mathfrak{F}_n^3(y) \left[\frac{1}{2} \mathfrak{F}_n^{-1}(y) - y [1 + r_f(y)]^2 \right] \left[-\dot{r}_f(y) - \frac{2}{d} (\dot{r}_f(y) + y \ddot{r}_f(y)) \right] = \quad (\text{Ctr2bII}) \\
& = \bar{q}^2 2 d_\gamma N \left[\partial_{\sigma_r} m_r(t, \sigma_r) \right]^2 k^{d-4} \frac{1}{\beta} \sum_{n=-\infty}^{\infty} A_d d \int_0^1 dy \left[-\frac{1}{2} y^{\frac{d-1}{2}} + \frac{1}{2} \eta_\psi(t) \left(y^{\frac{d-1}{2}} - y^{\frac{d}{2}} \right) \right] \times \\
& \times \mathfrak{F}_n^3(1) \left[\frac{1}{2} \mathfrak{F}_n^{-1}(1) - 1 \right] \left[\frac{1}{2} y^{-\frac{3}{2}} - \frac{2}{d} \left(\frac{1}{4} y^{-\frac{3}{2}} + \frac{1}{2} y^{-\frac{1}{2}} \delta(1-y) \right) \right] = \\
& = \bar{q}^2 2 d_\gamma N \left[\partial_{\sigma_r} m_r(t, \sigma_r) \right]^2 k^{d-4} \frac{1}{\beta} \sum_{n=-\infty}^{\infty} \left[\frac{1}{2} \mathfrak{F}_n^2(1) - \mathfrak{F}_n^3(1) \right] A_d \times \\
& \times \left[\frac{1}{4} + \left(1 - \frac{1}{d} \right) \frac{d}{2} \int_0^1 dy \left[-\frac{1}{2} y^{\frac{d-4}{2}} + \frac{1}{2} \eta_\psi(t) \left(y^{\frac{d-4}{2}} - y^{\frac{d-3}{2}} \right) \right] \right] \stackrel{d \geq 2}{=} \quad (\text{Ctr2bII-int}) \\
& = \bar{q}^2 2 A_d d_\gamma N \left[\partial_{\sigma_r} m_r(t, \sigma_r) \right]^2 k^{d-4} \frac{1}{\beta} \sum_{n=-\infty}^{\infty} \left[\frac{1}{2} \mathfrak{F}_n^2(1) - \mathfrak{F}_n^3(1) \right] \times \\
& \times \left(\frac{1}{4} - \frac{1}{2} \frac{d-1}{d-2} \left[1 - \frac{\eta_\psi(t)}{d-1} \right] \right) = \\
& = \bar{q}^2 2 A_d d_\gamma N \left[\partial_{\sigma_r} m_r(t, \sigma_r) \right]^2 k^{d-4} \frac{1}{\beta} \sum_{n=-\infty}^{\infty} \left[\frac{1}{2} \mathfrak{F}_n^2(1) - \mathfrak{F}_n^3(1) \right] \left[-\frac{1}{4} - \frac{1+\eta_\psi(t)}{2d-4} \right].
\end{aligned}$$

It remains to combine the two contributions (Ctr2bI) and (Ctr2bII) with our first result in Eq. (Ctr2a).

Here, it is crucial to distinguish between $d > 2$, $d = 2$, and $d = 1$.

For spatial dimensions $d > 2$ there are no ‘‘pitfalls’’ and we find,

$$\begin{aligned}
& (\text{Ctr2a}) + (\text{Ctr2bI}) + (\text{Ctr2bII}) = \tag{E.66} \\
& = \bar{q}^2 2 A_d d_\gamma N [\partial_{\sigma_r} m_r(t, \sigma_r)]^2 k^{d-4} \times \\
& \quad \times \frac{1}{\beta} \sum_{n=-\infty}^{\infty} \left(-\frac{1}{k^2} m_r^2(t, \sigma_r) \mathfrak{F}_n^4(1) + \frac{1}{2} \left[\frac{1+\eta_\psi(t)}{d-2} + 1 \right] \mathfrak{F}_n^3(1) - \frac{1}{2} \left[\frac{1-\eta_\psi(t)}{2d-4} + \frac{1}{4} \right] \mathfrak{F}_n^2(1) \right).
\end{aligned}$$

However, inspecting the calculation and final result of Eq. (Ctr2bII) one observes that the y -integration in line (Ctr2bII-int) is logarithmically IR divergent for $d = 2$. This might point out a non-analyticity of the bosonic two-point function at $\bar{q} = 0$, which leads to a collapse of the expansion in \bar{q} at $\bar{q} = 0$ and an ill-defined flow equation for the wave-function renormalization. However, we are not really interested in $d = 2$ within the scope of this work and postpone a deeper investigation of this puzzling result to future research.

For $d = 1$, it seems as if one runs into the same problems as for $d = 2$. The y -integrals in line (Ctr2bII-int) are IR-divergent. However, the prefactor of these integrals vanishes for $d = 1$, such that they do not contribute to the scale evolution of $\eta_\varphi(t)$ at all. Therefore, the combination of Eqs. (Ctr2a) to (Ctr2bII) for $d = 1$ results in

$$\begin{aligned}
& (\text{Ctr2a}) + (\text{Ctr2bI}) + (\text{Ctr2bII}) = \tag{E.67} \\
& = \bar{q}^2 2 \frac{1}{\pi} d_\gamma N [\partial_{\sigma_r} m_r(t, \sigma_r)]^2 k^{-3} \frac{1}{\beta} \sum_{n=-\infty}^{\infty} \left(-\frac{1}{k^2} m_r^2(t, \sigma_r) \mathfrak{F}_n^4(1) + \frac{1}{8} \mathfrak{F}_n^2(1) \right).
\end{aligned}$$

Trace (Ctr3) – boson tadpole

The evaluation of the next trace is somewhat simpler. It corresponds to the bosonic tadpole diagram, which is attached to the bosonic two-point function via the four-boson interaction vertex. For the evaluation of trace (Ctr3) one needs the bosonic regulator (E.38) and (E.40), the full bosonic propagator (E.43), and the bosonic four-point vertex (E.37),

$$\begin{aligned}
& (\text{Ctr3}) = - \text{Diagram} = \tag{E.68} \\
& = -\frac{1}{\beta^4} \sum_{n_1, \dots, n_4=-\infty}^{\infty} \int_{-\infty}^{\infty} \frac{d^d p_1}{(2\pi)^d} \dots \frac{d^d p_4}{(2\pi)^d} \times \\
& \quad \times \beta \delta_{-n_1, n_2} (2\pi)^d \delta^{(d)}(\vec{p}_1 + \vec{p}_2) \vec{p}_1^2 \partial_t [Z_\varphi(t) \frac{1}{2} r_b(t, |\vec{p}_1|)] \times \\
& \quad \times \beta \delta_{-n_2, n_3} (2\pi)^d \delta^{(d)}(\vec{p}_2 + \vec{p}_3) \frac{1}{Z_\varphi(t) [\omega_{n_2}^2 + \vec{p}_2^2 [1 + r_b(t, |\vec{p}_2|)] + \partial_{\sigma_r}^2 U(t, \sigma_r)]} \times \\
& \quad \times \beta \delta_{0, n_3+n_{11}+n_1+n_4} (2\pi)^d \delta^{(d)}(\vec{p}_3 + \vec{p}_{11} + \vec{p}_1 + \vec{p}_4) Z_\varphi^2(t) \partial_{\sigma_r}^4 U(t, \sigma_r) \times \\
& \quad \times \beta \delta_{-n_4, n_1} (2\pi)^d \delta^{(d)}(\vec{p}_4 + \vec{p}_1) \frac{1}{Z_\varphi(t) [\omega_{n_4}^2 + \vec{p}_4^2 [1 + r_b(t, |\vec{p}_4|)] + \partial_{\sigma_r}^2 U(t, \sigma_r)]}.
\end{aligned}$$

$$\begin{aligned}
& \times \frac{[\mathbf{i}(\nu_{n_2} + \mathbf{i}\mu) \gamma^{d+1} + \mathbf{i}\vec{p}_2 \cdot \vec{\gamma} [1 + r_f(t, |\vec{p}_2|)] - m_r(t, \sigma_r)]^{a_2} a_3 (\mathbf{1})^{c_2} c_3}{Z_\psi(t) [(\nu_{n_2} + \mathbf{i}\mu)^2 + \vec{p}_2^2 [1 + r_f(t, |\vec{p}_2|)]^2 + m_r^2(t, \sigma_r)]} \times \\
& \times (-1) \beta \delta_{n_3, n_{\text{II}} + n_1 + n_4} (2\pi)^d \delta^{(d)}(\vec{p}_{\text{II}} + \vec{p}_1 - \vec{p}_3 + \vec{p}_4) Z_\psi(t) Z_\varphi(t) [\partial_{\sigma_r}^2 m_r(t, \sigma_r)] \times \\
& \times (\mathbf{1})^{c_3} c_4 (\mathbf{1})^{a_3} a_4 \times \\
& \times \beta \delta_{n_4, n_1} (2\pi)^d \delta^{(d)}(\vec{p}_4 - \vec{p}_1) \times \\
& \times \frac{[\mathbf{i}(\nu_{n_4} + \mathbf{i}\mu) \gamma^{d+1} + \mathbf{i}\vec{p}_4 \cdot \vec{\gamma} [1 + r_f(t, |\vec{p}_4|)] - m_r(t, \sigma_r)]^{a_4} a_1 (\mathbf{1})^{c_4} c_1}{Z_\psi(t) [(\nu_{n_4} + \mathbf{i}\mu)^2 + \vec{p}_4^2 [1 + r_f(t, |\vec{p}_4|)]^2 + m_r^2(t, \sigma_r)]}.
\end{aligned}$$

Applying the projection (E.54) to this trace and evaluating the resulting equation as far as possible, one finds

$$\begin{aligned}
& Z_\varphi^{-1}(t) (\text{Ctr4})|_{n_{\text{II}}=n_{\text{I}}=0} \stackrel{\text{(D.32)}}{=} \tag{E.71} \\
& = + \beta (2\pi)^d \delta^{(d)}(\vec{p}_{\text{II}} + \vec{p}_1) 2 d_\gamma N m_r(t, \sigma_r) [\partial_{\sigma_r}^2 m_r(t, \sigma_r)] k^{-4} \times \\
& \quad \times \frac{1}{\beta} \sum_{n=-\infty}^{\infty} \int_{-\infty}^{\infty} \frac{d^d p}{(2\pi)^d} 2 \vec{p}^2 \left[\frac{1}{2} \partial_t r_f(t, |\vec{p}|) + \frac{1}{2} \eta_\psi(t) r_f(t, |\vec{p}|) \right] [1 + r_f(t, |\vec{p}|)] \mathfrak{F}_n^2\left(\frac{\vec{p}^2}{k^2}\right) \stackrel{\text{(A.5)}}{=} \\
& = + \beta (2\pi)^d \delta^{(d)}(\vec{p}_{\text{II}} + \vec{p}_1) 2 d_\gamma N m_r(t, \sigma_r) [\partial_{\sigma_r}^2 m_r(t, \sigma_r)] k^{-4} \times \\
& \quad \times \frac{1}{\beta} \sum_{n=-\infty}^{\infty} A_d d \int_0^\infty dp p^{d+1} 2 \left[\frac{1}{2} \partial_t r_f(t, p) + \frac{1}{2} \eta_\psi(t) r_f(t, p) \right] [1 + r_f(t, p)] \mathfrak{F}_n^2\left(\frac{p^2}{k^2}\right) \stackrel{\text{(D.7)}}{=} \\
& = + \beta (2\pi)^d \delta^{(d)}(\vec{p}_{\text{II}} + \vec{p}_1) 2 d_\gamma N m_r(t, \sigma_r) [\partial_{\sigma_r}^2 m_r(t, \sigma_r)] \times \\
& \quad \times \frac{1}{\beta} \sum_{n=-\infty}^{\infty} A_d k^{d-2} d \int_0^\infty dy y^{\frac{d}{2}} \left[y \dot{r}_f(y) + \frac{1}{2} \eta_\psi(t) r_f(y) \right] [1 + r_f(y)] \mathfrak{F}_n^2(y) \stackrel{\text{(D.25)}}{=} \\
& = - \beta (2\pi)^d \delta^{(d)}(\vec{p}_{\text{II}} + \vec{p}_1) 2 A_d \left[1 - \frac{\eta_\psi(t)}{d+1} \right] d_\gamma N m_r(t, \sigma_r) [\partial_{\sigma_r}^2 m_r(t, \sigma_r)] k^{d-2} \frac{1}{\beta} \sum_{n=-\infty}^{\infty} \mathfrak{F}_n^2(1).
\end{aligned}$$

Here, the situation is identical to the previous tadpole graphs. The external momenta and Matsubara frequencies do not enter the loop. Therefore, there is no \vec{p}_{II} -dependence of the diagram and no contribution to the scale evolution of the anomalous dimension. The diagram entirely contributes to the RG flow of the second derivative of the effective action.

Flow equation of the bosonic two-point function

Combining Eqs. (E.56), (E.61), (E.69), and (E.71) we obtain the RG flow equation for the bosonic two-point function,

$$\begin{aligned}
& Z_\varphi^{-1}(t) \partial_t \bar{\Gamma}_t^{(2)\varphi_{\text{II}}\varphi_{\text{I}}}[\sigma_r](0, \vec{p}_{\text{II}}; 0, \vec{p}_1) = \tag{E.72} \\
& = + \beta (2\pi)^d \delta^{(d)}(\vec{p}_{\text{II}} + \vec{p}_1) \times
\end{aligned}$$

$$\begin{aligned}
& \times \left[+ 2 [\partial_{\sigma_r}^3 U(t, \sigma_r)]^2 k^{-6} \times \right. \\
& \quad \times \frac{1}{\beta} \sum_{n=-\infty}^{\infty} \int_{-\infty}^{\infty} \frac{d^d p}{(2\pi)^d} \bar{p}^2 \left[\frac{1}{2} \partial_t r_b(t, |\vec{p}|) + \frac{1}{2} \eta_\varphi(t) r_b(t, |\vec{p}|) \right] \mathfrak{B}_n^2 \left(\frac{\bar{p}^2}{k^2} \right) \mathfrak{B}_n \left(\frac{(\vec{p} + \vec{p}_{\text{II}})^2}{k^2} \right) + \\
& \quad + 4 d_\gamma N [\partial_{\sigma_r} m_r(t, \sigma_r)]^2 k^{-6} \times \\
& \quad \times \frac{1}{\beta} \sum_{n=-\infty}^{\infty} \int_{-\infty}^{\infty} \frac{d^d p}{(2\pi)^d} \left[\frac{1}{2} \partial_t r_f(t, |\vec{p}|) + \frac{1}{2} \eta_\psi(t) r_f(t, |\vec{p}|) \right] \mathfrak{F}_n^2 \left(\frac{\bar{p}^2}{k^2} \right) \mathfrak{F}_n \left(\frac{(\vec{p} - \vec{p}_{\text{II}})^2}{k^2} \right) \times \\
& \quad \times \left(2 \bar{p}^2 [1 + r_f(t, |\vec{p}|)] \left[k^2 \mathfrak{F}_n^{-1} \left(\frac{\bar{p}^2}{k^2} \right) - 2 m_r^2(t, \sigma_r) - \bar{p}^2 [1 + r_f(t, |\vec{p}|)]^2 \right] + \right. \\
& \quad \left. + (\vec{p}_{\text{II}} \cdot \vec{p} - \bar{p}^2) [1 + r_f(t, |\vec{p} - \vec{p}_{\text{II}}|)] \left[k^2 \mathfrak{F}_n^{-1} \left(\frac{\bar{p}^2}{k^2} \right) - 2 \bar{p}^2 [1 + r_f(t, |\vec{p}|)]^2 \right] \right) + \\
& \quad + A_d \left[1 - \frac{\eta_\varphi(t)}{d+2} \right] [\partial_{\sigma_r}^4 U(t, \sigma_r)] k^{d-2} \frac{1}{\beta} \sum_{n=-\infty}^{\infty} \mathfrak{B}_n^2(1) - \\
& \quad \left. - 2 A_d \left[1 - \frac{\eta_\psi(t)}{d+1} \right] d_\gamma N m_r(t, \sigma_r) [\partial_{\sigma_r}^2 m_r(t, \sigma_r)] k^{d-2} \frac{1}{\beta} \sum_{n=-\infty}^{\infty} \mathfrak{F}_n^2(1) \right].
\end{aligned}$$

Flow equation of the bosonic two-point function – $\frac{1}{N}$ -rescaled

Rewriting Eq. (E.72) in terms of $\frac{1}{N}$ -rescaled quantities, the flow equation turns into

$$\begin{aligned}
& Z_\varphi^{-1}(t) \frac{1}{N} \partial_t \bar{\Gamma}_t^{(2)\bar{\varphi}_{\text{II}}\bar{\varphi}_{\text{I}}}[\sigma_r](0, \vec{p}_{\text{II}}; 0, \vec{p}_{\text{I}}) = \tag{E.73} \\
& = + \beta (2\pi)^d \delta^{(d)}(\vec{p}_{\text{II}} + \vec{p}_{\text{I}}) \times \\
& \quad \times \left[+ 2 \frac{1}{N} [\partial_{\check{\sigma}_r}^3 \check{U}(t, \check{\sigma}_r)]^2 k^{-6} \times \right. \\
& \quad \times \frac{1}{\beta} \sum_{n=-\infty}^{\infty} \int_{-\infty}^{\infty} \frac{d^d p}{(2\pi)^d} \bar{p}^2 \left[\frac{1}{2} \partial_t r_b(t, |\vec{p}|) + \frac{1}{2} \eta_\varphi(t) r_b(t, |\vec{p}|) \right] \mathfrak{B}_n^2 \left(\frac{\bar{p}^2}{k^2} \right) \mathfrak{B}_n \left(\frac{(\vec{p} + \vec{p}_{\text{II}})^2}{k^2} \right) + \\
& \quad + 4 d_\gamma [\partial_{\check{\sigma}_r} m_r(t, \check{\sigma}_r)]^2 k^{-6} \times \\
& \quad \times \frac{1}{\beta} \sum_{n=-\infty}^{\infty} \int_{-\infty}^{\infty} \frac{d^d p}{(2\pi)^d} \left[\frac{1}{2} \partial_t r_f(t, |\vec{p}|) + \frac{1}{2} \eta_\psi(t) r_f(t, |\vec{p}|) \right] \mathfrak{F}_n^2 \left(\frac{\bar{p}^2}{k^2} \right) \mathfrak{F}_n \left(\frac{(\vec{p} - \vec{p}_{\text{II}})^2}{k^2} \right) \times \\
& \quad \times \left(2 \bar{p}^2 [1 + r_f(t, |\vec{p}|)] \left[k^2 \mathfrak{F}_n^{-1} \left(\frac{\bar{p}^2}{k^2} \right) - 2 m_r^2(t, \check{\sigma}_r) - \bar{p}^2 [1 + r_f(t, |\vec{p}|)]^2 \right] + \right. \\
& \quad \left. + (\vec{p}_{\text{II}} \cdot \vec{p} - \bar{p}^2) [1 + r_f(t, |\vec{p} - \vec{p}_{\text{II}}|)] \left[k^2 \mathfrak{F}_n^{-1} \left(\frac{\bar{p}^2}{k^2} \right) - 2 \bar{p}^2 [1 + r_f(t, |\vec{p}|)]^2 \right] \right) + \\
& \quad + A_d \left[1 - \frac{\eta_\varphi(t)}{d+2} \right] \frac{1}{N} [\partial_{\check{\sigma}_r}^4 \check{U}(t, \check{\sigma}_r)] k^{d-2} \frac{1}{\beta} \sum_{n=-\infty}^{\infty} \mathfrak{B}_n^2(1) -
\end{aligned}$$

$$- 2 A_d \left[1 - \frac{\eta_\psi(t)}{d+1} \right] d_\gamma m_r(t, \check{\sigma}_r) \left[\partial_{\check{\sigma}_r}^2 m_r(t, \check{\sigma}_r) \right] k^{d-2} \frac{1}{\beta} \sum_{n=-\infty}^{\infty} \mathfrak{F}_n^2(1) \Big].$$

Flow equation of the bosonic mass

Collecting all contributions to the RG flow of the bosonic two-point function that are independent of the external momentum, namely Eqs. (E.57), (E.62), (E.69), and (E.71), we derive the following result,

$$\begin{aligned} & \partial_t [\partial_{\sigma_r}^2 U(t, \sigma_r)] + \eta_\varphi(t) \partial_{\sigma_r}^2 U(t, \sigma_r) + \frac{1}{2} \eta_\varphi(t) \sigma_r \partial_{\sigma_r}^3 U(t, \sigma_r) = \tag{E.74} \\ & = - 2 A_d \left[1 - \frac{\eta_\psi(t)}{d+2} \right] [\partial_{\sigma_r}^3 U(t, \sigma_r)]^2 k^{d-4} \frac{1}{\beta} \sum_{n=-\infty}^{\infty} \mathfrak{B}_n^3(1) - \\ & \quad - 2 A_d \left[1 - \frac{\eta_\psi(t)}{d+1} \right] d_\gamma N [\partial_{\sigma_r} m_r(t, \sigma_r)]^2 k^{d-4} \frac{1}{\beta} \sum_{n=-\infty}^{\infty} \left[k^2 \mathfrak{F}_n^2(y) - 4 m_r^2(t, \sigma_r) \mathfrak{F}_n^3(y) \right] + \\ & \quad + A_d \left[1 - \frac{\eta_\varphi(t)}{d+2} \right] [\partial_{\sigma_r}^4 U(t, \sigma_r)] k^{d-2} \frac{1}{\beta} \sum_{n=-\infty}^{\infty} \mathfrak{B}_n^2(1) + \\ & \quad - 2 A_d \left[1 - \frac{\eta_\psi(t)}{d+1} \right] d_\gamma N m_r(t, \sigma_r) [\partial_{\sigma_r}^2 m_r(t, \sigma_r)] k^{d-2} \frac{1}{\beta} \sum_{n=-\infty}^{\infty} \mathfrak{F}_n^2(1) = \\ & = - 2 A_d \left[1 - \frac{\eta_\psi(t)}{d+2} \right] [\partial_{\sigma_r}^3 U(t, \sigma_r)]^2 k^{d-4} \frac{1}{\beta} \sum_{n=-\infty}^{\infty} \mathfrak{B}_n^3(1) - \\ & \quad + A_d \left[1 - \frac{\eta_\varphi(t)}{d+2} \right] [\partial_{\sigma_r}^4 U(t, \sigma_r)] k^{d-2} \frac{1}{\beta} \sum_{n=-\infty}^{\infty} \mathfrak{B}_n^2(1) + \\ & \quad + 2 A_d \left[1 - \frac{\eta_\psi(t)}{d+1} \right] d_\gamma N [\partial_{\sigma_r} m_r^2(t, \sigma_r)]^2 k^{d-4} \frac{1}{\beta} \sum_{n=-\infty}^{\infty} \mathfrak{F}_n^3(y) + \\ & \quad - A_d \left[1 - \frac{\eta_\psi(t)}{d+1} \right] d_\gamma N [\partial_{\sigma_r}^2 m_r^2(t, \sigma_r)] k^{d-2} \frac{1}{\beta} \sum_{n=-\infty}^{\infty} \mathfrak{F}_n^2(1). \end{aligned}$$

This flow equation is not of relevance for any practical purposes in this work, but serves as a consistency check of our calculations. Exactly the same equation is obtained if the RG flow equation for the effective potential (E.51) is derived twice w.r.t. the renormalized bosonic background field σ_r .

Flow equation of the bosonic anomalous dimension

Combining all contributions to the bosonic two-point function, that are proportional to \vec{p}_Π^2 , which are Eq. (E.59) and two times Eq. (E.66), one finds the equation that describes the scale evolution of the bosonic anomalous dimension. As already anticipated before, there are distinct expressions for spatial dimensions $d \gtrless 2$.

For $d > 2$ we find,

$$\begin{aligned} \eta_\varphi(t) = & + A_d [\partial_{\sigma_r}^3 U(t, \sigma_r)]^2 k^{d+2} \frac{1}{\beta} \sum_{n=-\infty}^{\infty} \frac{1}{[\omega_n^2 + k^2 + \partial_{\sigma_r}^2 U(t, \sigma_r)]^4} + \tag{E.75} \\ & + 2 A_d d_\gamma N [\partial_{\sigma_r} m_r(t, \sigma_r)]^2 \times \end{aligned}$$

$$\begin{aligned}
& \times \left[-2 \frac{m_r^2(t, \sigma_r)}{k^2} k^{d+4} \frac{1}{\beta} \sum_{n=-\infty}^{\infty} \frac{1}{[(\nu_n + i\mu)^2 + k^2 + m_r^2(t, \sigma_r)]^4} + \right. \\
& + \left[\frac{1-\eta_\psi(t)}{d-2} + 1 \right] k^{d+2} \frac{1}{\beta} \sum_{n=-\infty}^{\infty} \frac{1}{[(\nu_n + i\mu)^2 + k^2 + m_r^2(t, \sigma_r)]^3} - \\
& \left. - \left[\frac{1-\eta_\psi(t)}{2d-4} + \frac{1}{4} \right] k^d \frac{1}{\beta} \sum_{n=-\infty}^{\infty} \frac{1}{[(\nu_n + i\mu)^2 + k^2 + m_r^2(t, \sigma_r)]^2} \right],
\end{aligned}$$

while for $d < 2$, thus $d = 1$,

$$\begin{aligned}
\eta_\varphi(t) = & + \frac{1}{\pi} [\partial_{\sigma_r}^3 U(t, \sigma_r)]^2 k^3 \frac{1}{\beta} \sum_{n=-\infty}^{\infty} \frac{1}{[\omega_n^2 + k^2 + \partial_{\sigma_r}^2 U(t, \sigma_r)]^4} + \\
& + 2 \frac{1}{\pi} d_\gamma N [\partial_{\sigma_r} m_r(t, \sigma_r)]^2 \times \\
& \times \left[-2 m_r^2(t, \sigma_r) k^3 \frac{1}{\beta} \sum_{n=-\infty}^{\infty} \frac{1}{[(\nu_n + i\mu)^2 + k^2 + m_r^2(t, \sigma_r)]^4} + \right. \\
& \left. + \frac{1}{4} k \frac{1}{\beta} \sum_{n=-\infty}^{\infty} \frac{1}{[(\nu_n + i\mu)^2 + k^2 + m_r^2(t, \sigma_r)]^2} \right].
\end{aligned} \tag{E.76}$$

For $d = 2$ we do not provide an expression, because of unresolved IR divergences.

Flow equation of the bosonic anomalous dimension – $\frac{1}{N}$ -rescaled

Similar to Eq. (E.51) for the effective potential, we also provide evolution equations for $\eta_\varphi(t)$ in terms of $\frac{1}{N}$ -rescaled quantities.

For $d > 2$ Eq. (E.75) turns into,

$$\begin{aligned}
\eta_\varphi(t) = & + A_d \frac{1}{N} [\partial_{\check{\sigma}_r}^3 \check{U}(t, \check{\sigma}_r)]^2 k^{d+2} \frac{1}{\beta} \sum_{n=-\infty}^{\infty} \frac{1}{[\omega_n^2 + k^2 + \partial_{\check{\sigma}_r}^2 \check{U}(t, \check{\sigma}_r)]^4} + \\
& + 2 A_d d_\gamma [\partial_{\check{\sigma}_r} m_r(t, \check{\sigma}_r)]^2 \times \\
& \times \left[-2 \frac{m_r^2(t, \check{\sigma}_r)}{k^2} k^{d+4} \frac{1}{\beta} \sum_{n=-\infty}^{\infty} \frac{1}{[(\nu_n + i\mu)^2 + k^2 + m_r^2(t, \check{\sigma}_r)]^4} + \right. \\
& + \left[\frac{1-\eta_\psi(t)}{d-2} + 1 \right] k^{d+2} \frac{1}{\beta} \sum_{n=-\infty}^{\infty} \frac{1}{[(\nu_n + i\mu)^2 + k^2 + m_r^2(t, \check{\sigma}_r)]^3} - \\
& \left. - \left[\frac{1-\eta_\psi(t)}{2d-4} + \frac{1}{4} \right] k^d \frac{1}{\beta} \sum_{n=-\infty}^{\infty} \frac{1}{[(\nu_n + i\mu)^2 + k^2 + m_r^2(t, \check{\sigma}_r)]^2} \right].
\end{aligned} \tag{E.77}$$

This result agrees for example with Refs. [373, Eq. (11)], [374, Eq. (36)], and [346, Eq. (196)] after rearrangement of some of the terms. The result is also consistent with Ref. [556, Eq. (24)].

For $d = 1$ Eq. (E.76) is given by

$$\begin{aligned}
\eta_\varphi(t) = & + \frac{1}{\pi} \frac{1}{N} [\partial_{\check{\sigma}_r}^3 \check{U}(t, \check{\sigma}_r)]^2 k^3 \frac{1}{\beta} \sum_{n=-\infty}^{\infty} \frac{1}{[\omega_n^2 + k^2 + \partial_{\check{\sigma}_r}^2 \check{U}(t, \check{\sigma}_r)]^4} + \\
& + 2 \frac{1}{\pi} d_\gamma [\partial_{\check{\sigma}_r} m_r(t, \check{\sigma}_r)]^2 \times
\end{aligned} \tag{E.78}$$

$$\begin{aligned} & \times \left[-2 m_r^2(t, \check{\sigma}_r) k^3 \frac{1}{\beta} \sum_{n=-\infty}^{\infty} \frac{1}{[(\nu_n + i\mu)^2 + k^2 + m_r^2(t, \check{\sigma}_r)]^4} + \right. \\ & \left. + \frac{1}{4} k \frac{1}{\beta} \sum_{n=-\infty}^{\infty} \frac{1}{[(\nu_n + i\mu)^2 + k^2 + m_r^2(t, \check{\sigma}_r)]^2} \right]. \end{aligned}$$

E.2.3. Infinite- N limit of the two-point function

Within the next paragraphs we shall demonstrate how the $N \rightarrow \infty$ expression for the bosonic two-point function is extracted from the FRG flow equations of the GNY model. The starting point is Eq. (E.73). Inspecting the single contributions on the r.h.s. of Eq. (E.73), we observe that the bosonic loop contributions are accompanied by factors $\frac{1}{N}$ and vanish in the $N \rightarrow \infty$ limit. The same applies to the fermionic anomalous dimension in any spacetime dimension for $N \rightarrow \infty$, see Eq. (E.115). In addition, the fermionic tadpole diagram does not contribute, because we are studying a field-independent Yukawa coupling. The Yukawa coupling itself does also not flow with RG time for $N \rightarrow \infty$, see Eq. (10.31). Hence, Eq. (E.73) reduces to

$$\begin{aligned} & Z_\varphi^{-1}(t) \frac{1}{N} \partial_t \bar{\Gamma}_t^{(2)\bar{\varphi}_{\text{II}}\bar{\varphi}_{\text{I}}}[\check{\sigma}_r](0, \vec{p}_{\text{II}}; 0, \vec{p}_{\text{I}}) = \tag{E.79} \\ & = + \beta (2\pi)^d \delta^{(d)}(\vec{p}_{\text{II}} + \vec{p}_{\text{I}}) \times \\ & \quad \times 4 d_\gamma h_r^2 k^{-6} \frac{1}{\beta} \sum_{n=-\infty}^{\infty} \int_{-\infty}^{\infty} \frac{d^d p}{(2\pi)^d} \left[\frac{1}{2} \partial_t r_f(t, |\vec{p}|) \right] \mathfrak{F}_n^2\left(\frac{\vec{p}^2}{k^2}\right) \mathfrak{F}_n\left(\frac{(\vec{p}-\vec{p}_{\text{II}})^2}{k^2}\right) \times \\ & \quad \times \left(2 \vec{p}^2 [1 + r_f(t, |\vec{p}|)] \left[k^2 \mathfrak{F}_n^{-1}\left(\frac{\vec{p}^2}{k^2}\right) - 2 h_r^2 \check{\sigma}_r^2 - \vec{p}^2 [1 + r_f(t, |\vec{p}|)]^2 \right] + \right. \\ & \quad \left. + (\vec{p}_{\text{II}} \cdot \vec{p} - \vec{p}^2) [1 + r_f(t, |\vec{p} - \vec{p}_{\text{II}}|)] \left[k^2 \mathfrak{F}_n^{-1}\left(\frac{\vec{p}^2}{k^2}\right) - 2 \vec{p}^2 [1 + r_f(t, |\vec{p}|)]^2 \right] \right). \end{aligned}$$

Next, we can eliminate the bosonic wave-function renormalization from the equation by replacing the renormalized fields $\check{\sigma}_r$ and Yukawa coupling h_r by their bare counterparts according to Eq. (10.5). Furthermore, we define the $\frac{1}{N}$ -rescaled two-point function with argument $\vec{q} = \vec{p}_{\text{II}}$,

$$\beta (2\pi)^d \delta^{(d)}(\vec{q} + \vec{p}_{\text{I}}) \partial_t \check{\Gamma}_t^{(2)}(\check{\sigma}, \mu, T, |\vec{q}|) \equiv \frac{1}{N} \partial_t \bar{\Gamma}_t^{(2)\bar{\varphi}_{\text{II}}\bar{\varphi}_{\text{I}}}[\check{\sigma}](0, \vec{q}; 0, \vec{p}_{\text{I}}). \tag{E.80}$$

For the sake of readability, we additionally stop indicating the $\frac{1}{N}$ -rescaling as discussed in Section 11.2.1.

It remains to insert Def. (D.32), *i.e.*,

$$k^2 \mathfrak{F}_n^{-1}\left(\frac{\vec{p}^2}{k^2}\right) = (\nu_n + i\mu)^2 + \vec{p}^2 [1 + r_f(k, |\vec{p}|)]^2 + h^2 \sigma^2. \tag{E.81}$$

From here, it is straightforward but tedious to show that

$$\begin{aligned} & k \partial_k \bar{\Gamma}_k^{(2)}(\sigma, \mu, T, |\vec{q}|) = \tag{E.82} \\ & = -k \partial_k \left[d_\gamma h^2 \frac{1}{\beta} \sum_{n=-\infty}^{\infty} \int_{-\infty}^{\infty} \frac{d^d p}{(2\pi)^d} \frac{1}{(\nu_n + i\mu)^2 + \vec{p}^2 [1 + r_f(k, |\vec{p}|)]^2 + h^2 \sigma^2} \times \right. \\ & \quad \left. \times \frac{(\nu_n + i\mu)^2 - h^2 \sigma^2 + \vec{p} \cdot (\vec{p} - \vec{q}) [1 + r_f(k, |\vec{p}|)] [1 + r_f(k, |\vec{p} - \vec{q}|)]}{(\nu_n + i\mu)^2 + (\vec{p} - \vec{q})^2 [1 + r_f(k, |\vec{p} - \vec{q}|)]^2 + h^2 \sigma^2} \right]. \end{aligned}$$

The easiest way to demonstrate this is to perform the k -derivative on the r.h.s. of Eq. (E.82) to recover all contributions in Eq. (E.79).

We find that Eq. (E.82) can be integrated trivially from the UV cutoff scale $k = \Lambda$ to the IR at $k = 0$. According to the truncation Eq. (10.1) and Eqs. (10.2) and (10.4) the UV initial condition for the two-point function is $\bar{\Gamma}_{k=\Lambda}^{(2)}(\sigma, \mu, T, |\vec{q}|) = \frac{h^2}{g^2}$. For the IR two-point function, we use $\Gamma^{(2)}(\sigma, \mu, T, |\vec{q}|) \equiv \bar{\Gamma}_{k=0}^{(2)}(\sigma, \mu, T, |\vec{q}|)$.

Hence, formally we find

$$\begin{aligned} \Gamma^{(2)}(\sigma, \mu, T, |\vec{q}|) &= \tag{E.83} \\ &= \frac{h^2}{g^2} + \left[d_\gamma h^2 \frac{1}{\beta} \sum_{n=-\infty}^{\infty} \int_{-\infty}^{\infty} \frac{d^d p}{(2\pi)^d} \frac{1}{(\nu_n + i\mu)^2 + \vec{p}^2 [1 + r_f(k, |\vec{p}|)]^2 + h^2 \sigma^2} \times \right. \\ &\quad \left. \times \frac{(\nu_n + i\mu)^2 - h^2 \sigma^2 + \vec{p} \cdot (\vec{p} - \vec{q}) [1 + r_f(k, |\vec{p}|)] [1 + r_f(k, |\vec{p} - \vec{q}|)]}{(\nu_n + i\mu)^2 + (\vec{p} - \vec{q})^2 [1 + r_f(k, |\vec{p} - \vec{q}|)]^2 + h^2 \sigma^2} \right]_0^\Lambda. \end{aligned}$$

Evaluation of the square bracket at $k = 0$ is simple, due to $\lim_{k \rightarrow 0} r_f(k, |\vec{p}|) = 0$. Furthermore, sending $\Lambda \rightarrow \infty$, the expression vanishes and we obtain

$$\begin{aligned} \Gamma^{(2)}(\sigma, \mu, T, |\vec{q}|) &= \tag{E.84} \\ &= h^2 \left[\frac{1}{g^2} - d_\gamma \frac{1}{\beta} \sum_{n=-\infty}^{\infty} \int_{-\infty}^{\infty} \frac{d^d p}{(2\pi)^d} \left[\frac{1}{(\nu_n + i\mu)^2 + \vec{p}^2 + h^2 \sigma^2} \times \right. \right. \\ &\quad \left. \left. \times \frac{(\nu_n + i\mu)^2 - h^2 \sigma^2 + \vec{p} \cdot (\vec{p} - \vec{q})}{(\nu_n + i\mu)^2 + (\vec{p} - \vec{q})^2 + h^2 \sigma^2} \right] \right] = \\ &= h^2 \left[\frac{1}{g^2} - d_\gamma \frac{1}{\beta} \sum_{n=-\infty}^{\infty} \int_{-\infty}^{\infty} \frac{d^d p}{(2\pi)^d} \left[\frac{1}{(\nu_n + i\mu)^2 + \vec{p}^2 + h^2 \sigma^2} + \right. \right. \\ &\quad \left. \left. + \frac{1}{(\nu_n + i\mu)^2 + \vec{p}^2 + h^2 \sigma^2} \frac{\vec{p} \cdot \vec{q} - 2h^2 \sigma^2}{(\nu_n + i\mu)^2 + (\vec{p} + \vec{q})^2 + h^2 \sigma^2} \right] \right]. \end{aligned}$$

This is the unrenormalized standard mean-field result in arbitrary dimensions, *cf.* Refs. [593, 5, 592].

As a consistency check, let us compare this result for $\vec{q} = 0$, $d = 1$, and $\mu = T = 0$, *i.e.*,

$$\Gamma^{(2)}(\sigma, \mu, T, 0) = h^2 \left[\frac{1}{g^2} - \frac{d_\gamma}{2} \int_{-\infty}^{\infty} \frac{dp}{2\pi} \left[\frac{1}{(p^2 + h^2 \sigma^2)^{\frac{1}{2}}} - \frac{h^2 \sigma^2}{(p^2 + h^2 \sigma^2)^{\frac{3}{2}}} \right] \right], \tag{E.85}$$

where we used Eqs. (B.16) and (B.21) for the Matsubara sum, with the second σ -derivative of the flow equation Eq. (11.1) of the effective potential for $\mu = T = 0$, *i.e.*,

$$\partial_k (\partial_\sigma^2 U(k, \sigma)) = h^2 d_\gamma \frac{1}{2\pi} k^2 \left[\frac{1}{(k^2 + h^2 \sigma^2)^{\frac{3}{2}}} - \frac{3h^2 \sigma^2}{(k^2 + h^2 \sigma^2)^{\frac{5}{2}}} \right]. \tag{E.86}$$

Integrated from the UV for $k = \Lambda \rightarrow \infty$ to the IR at $k = 0$ Eq. (E.86) has to be identical to

Eq. (E.85). Using the UV initial potential (10.2), we obtain,

$$\begin{aligned} (\partial_\sigma^2 U(k=0, \sigma)) &= h^2 \left[\frac{1}{g^2} - d_\gamma \int_0^\infty \frac{dk}{2\pi} k^2 \left[\frac{1}{(k^2 + h^2 \sigma^2)^{\frac{3}{2}}} - \frac{3h^2 \sigma^2}{(k^2 + h^2 \sigma^2)^{\frac{5}{2}}} \right] \right] = \\ &= h^2 \left[\frac{1}{g^2} + \frac{d_\gamma}{2\pi} - \frac{d_\gamma}{2} \int_{-\infty}^\infty \frac{dk}{2\pi} \left[\frac{1}{(k^2 + h^2 \sigma^2)^{\frac{1}{2}}} - \frac{h^2 \sigma^2}{(k^2 + h^2 \sigma^2)^{\frac{3}{2}}} \right] \right] \end{aligned} \quad (\text{E.87})$$

Interestingly, this expression differs from Eq. (E.85) by a non-vanishing surface term. This is exactly the same term which appeared in Eq. (11.11) and stems from the choice of the Litim-type regulator and cancels during the renormalization procedure. Hence, for a consistent renormalization of Eq. (E.84), we have to insert the asymptotic behavior of $\frac{1}{g^2}$ from Eq. (11.11) without this surface term.

E.2.4. Fermionic two-point function – fermion mass & anomalous dimension

In the next step, we derive the RG flow equation of the fermionic two-point function and extract the flow equations for the Yukawa coupling, respectively the fermion mass, and the flow equation for the fermionic wave-function renormalization, respectively the anomalous dimension.

The fermionic two-point vertex

To derive the RG flow equation for the fermionic two-point function, we take two derivatives of the ERG Eq. (C.51) w.r.t. the Fourier-transformed fermion fields $\tilde{\psi}$ and $\tilde{\psi}$. Taking these derivatives again is not necessary and we may simply use the generic expression (C.53). Keeping only those contributions on the r.h.s. of the equation that are compatible with our truncation of the GNY model the universal equation turns into,

$$\begin{aligned} \partial_t \bar{\Gamma}_t^{(2)} \bar{\psi}_{\text{II}} \psi_{\text{I}}[\sigma] &= \\ &= \text{STr} \left[\left(\frac{1}{2} \partial_t R_t \right) G_t[\sigma] \bar{\Gamma}_t^{(3)} \bar{\psi}_{\text{II}} G_t[\sigma] \bar{\Gamma}_t^{(3)} \psi_{\text{I}} G_t[\sigma] \right] - \\ &\quad - \text{STr} \left[\left(\frac{1}{2} \partial_t R_t \right) G_t[\sigma] \bar{\Gamma}_t^{(4)} \bar{\psi}_{\text{II}} \psi_{\text{I}} G_t[\sigma] \right] + \\ &\quad + \text{STr} \left[\left(\frac{1}{2} \partial_t R_t \right) G_t[\sigma] \bar{\Gamma}_t^{(3)} \psi_{\text{I}} G_t[\sigma] \bar{\Gamma}_t^{(3)} \bar{\psi}_{\text{II}} G_t[\sigma] \right] = \\ &= + (-1)^{\bar{\psi}_{\text{II}} \varphi_2} (-1)^{\psi_{\text{I}} \varphi_2} \left(\frac{1}{2} \partial_t R_t^{\varphi_1 \varphi_2} \right) G_{t, \varphi_2 \varphi_3}[\sigma] \bar{\Gamma}_t^{(3)} \varphi_3 \bar{\psi}_{\text{II}} \psi_4[\sigma] \mathbf{g}_{\bar{\psi}_4}^{\psi_5} G_{t, \bar{\psi}_5 \psi_6}[\sigma] \times \\ &\quad \times \bar{\Gamma}_t^{(3)} \bar{\psi}_6 \psi_1 \varphi_7[\sigma] \mathbf{g}_{\varphi_7}^{\varphi_8} G_{t, \varphi_8 \varphi_1}[\sigma] + \\ &\quad + (-1)^{\bar{\psi}_{\text{II}} \psi_2} (-1)^{\psi_{\text{I}} \psi_2} \left(\frac{1}{2} \partial_t R_t^{\psi_1 \bar{\psi}_2} \right) G_{t, \psi_2 \bar{\psi}_3}[\sigma] \bar{\Gamma}_t^{(3)} \psi_3 \bar{\psi}_{\text{II}} \varphi_4[\sigma] \mathbf{g}_{\varphi_4}^{\varphi_5} G_{t, \varphi_5 \varphi_6}[\sigma] \times \\ &\quad \times \bar{\Gamma}_t^{(3)} \varphi_6 \psi_1 \bar{\psi}_7[\sigma] \mathbf{g}_{\psi_7}^{\bar{\psi}_8} G_{t, \psi_8 \bar{\psi}_1}[\sigma] - \\ &\quad - (-1)^{\bar{\psi}_{\text{II}} \varphi_2} (-1)^{\psi_{\text{I}} \varphi_2} \left(\frac{1}{2} \partial_t R_t^{\varphi_1 \varphi_2} \right) G_{t, \varphi_2 \varphi_3}[\sigma] \bar{\Gamma}_t^{(4)} \varphi_3 \bar{\psi}_{\text{II}} \psi_1 \varphi_4[\sigma] \mathbf{g}_{\varphi_4}^{\varphi_5} G_{t, \varphi_5 \varphi_1}[\sigma] + \\ &\quad + (-1)^{\bar{\psi}_{\text{II}} \psi_5} (-1)^{\bar{\psi}_{\text{II}} \psi_4} (-1)^{\bar{\psi}_{\text{II}} \psi_1} (-1)^{\bar{\psi}_{\text{II}} \varphi_2} (-1)^{\psi_{\text{I}} \varphi_2} \left(\frac{1}{2} \partial_t R_t^{\varphi_1 \varphi_2} \right) G_{t, \varphi_2 \varphi_3}[\sigma] \times \\ &\quad \times \bar{\Gamma}_t^{(3)} \varphi_3 \psi_1 \bar{\psi}_4[\sigma] \mathbf{g}_{\psi_4}^{\bar{\psi}_5} G_{t, \psi_5 \bar{\psi}_6}[\sigma] \bar{\Gamma}_t^{(3)} \psi_6 \bar{\psi}_{\text{II}} \varphi_7[\sigma] \mathbf{g}_{\varphi_7}^{\varphi_8} G_{t, \varphi_8 \varphi_1}[\sigma] + \end{aligned} \quad (\text{E.88})$$

$$\begin{aligned}
& \times (-1) \beta \delta_{n_{\text{II}}, n_3+n_4} (2\pi)^d \delta^{(d)}(\vec{p}_3 - \vec{p}_{\text{II}} + \vec{p}_4) Z_\psi(t) Z_\varphi^{\frac{1}{2}}(t) [\partial_{\sigma_r} m_r(t, \sigma_r)] (\mathbf{1})^{c_{\text{II}}} c_4 (\mathbf{1})^{a_{\text{II}}} a_4 \times \\
& \times \beta \delta_{n_4, n_5} (2\pi)^d \delta^{(d)}(\vec{p}_4 - \vec{p}_5) \times \\
& \quad \times \frac{[\mathbf{i}(\nu_{n_4} + \mathbf{i}\mu) \gamma^{d+1} + \mathbf{i}\vec{p}_4 \cdot \vec{\gamma} [1 + r_f(t, |\vec{p}_4|)] - m_r(t, \sigma_r)]^{a_4} a_5 (\mathbf{1})^{c_4} c_5}{Z_\psi(t) [(\nu_{n_4} + \mathbf{i}\mu)^2 + \vec{p}_4^2 [1 + r_f(t, |\vec{p}_4|)]^2 + m_r^2(t, \sigma_r)]} \times \\
& \times (-1) \beta \delta_{n_5, n_6+n_{\text{I}}} (2\pi)^d \delta^{(d)}(\vec{p}_5 - \vec{p}_6 + \vec{p}_{\text{I}}) Z_\psi(t) Z_\varphi^{\frac{1}{2}}(t) [\partial_{\sigma_r} m_r(t, \sigma_r)] (\mathbf{1})^{c_5} c_{\text{I}} (\mathbf{1})^{a_5} a_{\text{I}} \times \\
& \times \beta \delta_{-n_6, n_{\text{I}}} (2\pi)^d \delta^{(d)}(\vec{p}_6 + \vec{p}_{\text{I}}) \frac{1}{Z_\varphi(t) [\omega_{n_6}^2 + \vec{p}_6^2 [1 + r_b(t, |\vec{p}_6|)] + \partial_{\sigma_r}^2 U(t, \sigma_r)]}.
\end{aligned}$$

Yukawa coupling The contribution to the RG flow of the fermion mass term is extracted via the projection (E.90) and results in,

$$\begin{aligned}
& -\frac{1}{N} (\mathbf{1})^{c_{\text{I}}} c_{\text{II}} \frac{1}{d_\gamma} (\mathbf{1})^{a_{\text{I}}} a_{\text{II}} Z_\psi^{-1}(t) (\text{Dtr}\mathbf{1})^{a_{\text{II}}} c_{\text{II}} c_{\text{I}} \Big|_{\vec{p}_{\text{II}}=\vec{p}_{\text{I}}=0} \stackrel{(\text{D.26}), (\text{D.32})}{=} \quad (\text{E.93}) \\
& = + \beta \delta_{n_{\text{II}}, n_{\text{I}}} (2\pi)^d \delta^{(d)}(0) 2 [\partial_{\sigma_r} m_r(t, \sigma_r)]^2 m_r(t, \sigma_r) k^{-6} \times \\
& \quad \times \frac{1}{\beta} \sum_{n=-\infty}^{\infty} \int_{-\infty}^{\infty} \frac{d^d p}{(2\pi)^d} \vec{p}^2 \left[\frac{1}{2} \partial_t r_b(t, |\vec{p}|) + \frac{1}{2} \eta_\varphi(t) r_b(t, |\vec{p}|) \right] \mathfrak{B}_n^2 \left(\frac{\vec{p}^2}{k^2} \right) \mathfrak{F}_{n+n_{\text{II}}} \left(\frac{\vec{p}^2}{k^2} \right) \stackrel{(\text{A.5})}{=} \\
& = + \beta \delta_{n_{\text{II}}, n_{\text{I}}} (2\pi)^d \delta^{(d)}(0) 2 [\partial_{\sigma_r} m_r(t, \sigma_r)]^2 m_r(t, \sigma_r) k^{-6} \times \\
& \quad \times \frac{1}{\beta} \sum_{n=-\infty}^{\infty} A_d d \int_0^\infty dp p^{d+1} \left[\frac{1}{2} \partial_t r_b(t, p) + \frac{1}{2} \eta_\varphi(t) r_b(t, p) \right] \mathfrak{B}_n^2 \left(\frac{p^2}{k^2} \right) \mathfrak{F}_{n+n_{\text{II}}} \left(\frac{p^2}{k^2} \right) \stackrel{(\text{D.7})}{=} \\
& = + \beta \delta_{n_{\text{II}}, n_{\text{I}}} (2\pi)^d \delta^{(d)}(0) 2 [\partial_{\sigma_r} m_r(t, \sigma_r)]^2 m_r(t, \sigma_r) \times \\
& \quad \times \frac{1}{\beta} \sum_{n=-\infty}^{\infty} A_d k^{d-4} \frac{d}{2} \int_0^\infty dy y^{\frac{d}{2}} [y \dot{r}_b(y) + \frac{1}{2} \eta_\varphi(t) r_b(y)] \mathfrak{B}_n^2(y) \mathfrak{F}_{n+n_{\text{II}}}(y)
\end{aligned}$$

For the Litim regulator and integration formula Eq. (D.25) this further simplifies and we find

$$-2 A_d \left[1 - \frac{\eta_\varphi(t)}{d+2} \right] [\partial_{\sigma_r} m_r(t, \sigma_r)]^2 m_r(t, \sigma_r) k^{d-4} \frac{1}{\beta} \sum_{n=-\infty}^{\infty} \mathfrak{B}_n^2(1) \mathfrak{F}_{n+n_{\text{II}}}(1). \quad (\text{E.94})$$

Here, we dropped the infinite-volume factor *etc.*. Note that we still need to evaluate this expression for a specific Matsubara index n_{II} .

Anomalous dimension To obtain the contribution of the same diagram to the scale evolution of the anomalous dimension, we use projection Eq. (E.91),

$$\begin{aligned}
& \frac{1}{N} (\mathbf{1})^{c_{\text{I}}} c_{\text{II}} \frac{1}{d_\gamma} (\mathbf{i}\vec{p}_{\text{II}} \cdot \vec{\gamma})^{a_{\text{I}}} a_{\text{II}} Z_\psi^{-1}(t) (\text{Dtr}\mathbf{1})^{a_{\text{II}}} c_{\text{II}} c_{\text{I}} = \quad (\text{E.95}) \\
& = + \beta \delta_{n_{\text{II}}, n_{\text{I}}} (2\pi)^d \delta^{(d)}(\vec{p}_{\text{II}} - \vec{p}_{\text{I}}) 2 [\partial_{\sigma_r} m_r(t, \sigma_r)]^2 k^{-6} \times
\end{aligned}$$

$$\begin{aligned} & \times \frac{1}{\beta} \sum_{n=-\infty}^{\infty} \int_{-\infty}^{\infty} \frac{d^d p}{(2\pi)^d} \vec{p}^2 \left[\frac{1}{2} \partial_t r_b(t, |\vec{p}|) + \frac{1}{2} \eta_\varphi(t) r_b(t, |\vec{p}|) \right] \mathfrak{B}_n^2 \left(\frac{\vec{p}^2}{k^2} \right) \mathfrak{F}_{n-n_{\text{II}}} \left(\frac{(\vec{p}-\vec{p}_{\text{II}})^2}{k^2} \right) \times \\ & \times \vec{p}_{\text{II}} \cdot (\vec{p} - \vec{p}_{\text{II}}) [1 + r_f(t, |\vec{p} - \vec{p}_{\text{II}}|)]. \end{aligned}$$

We simplify the notation by defining $\vec{q} \equiv \vec{p}_{\text{II}}$ and $m = n_{\text{II}}$ as the external spatial momentum and “index” of the Matsubara mode. The coefficient of \vec{q}^2 on the r.h.s. of Eq. (E.95) is obtained by expanding all \vec{q} -dependent terms in a Taylor series about $\vec{q} = 0$,

$$\begin{aligned} & \mathfrak{F}_{n-m} \left(\frac{(\vec{p}-\vec{q})^2}{k^2} \right) (\vec{q} \cdot \vec{p} - \vec{q}^2) \left[1 + r_f \left(\frac{(\vec{p}-\vec{q})^2}{k^2} \right) \right] = \tag{E.96} \\ & = \left[\mathfrak{F}_{n-m} \left(\frac{\vec{p}^2}{k^2} \right) - 2 \frac{\vec{q} \cdot \vec{p}}{k^2} \dot{\mathfrak{F}}_{n-m} \left(\frac{\vec{p}^2}{k^2} \right) + \frac{\vec{q}^2}{k^2} \ddot{\mathfrak{F}}_{n-m} \left(\frac{\vec{p}^2}{k^2} \right) + 2 \frac{(\vec{q} \cdot \vec{p})^2}{k^4} \check{\mathfrak{F}}_{n-m} \left(\frac{\vec{p}^2}{k^2} \right) + \mathcal{O} \left(\frac{|\vec{q}|^3}{k^3} \right) \right] \times \\ & \times (\vec{q} \cdot \vec{p} - \vec{q}^2) \left[1 + r_f \left(\frac{\vec{p}^2}{k^2} \right) - 2 \frac{\vec{q} \cdot \vec{p}}{k^2} \dot{r}_f \left(\frac{\vec{p}^2}{k^2} \right) + \frac{\vec{q}^2}{k^2} \ddot{r}_f \left(\frac{\vec{p}^2}{k^2} \right) + 2 \frac{(\vec{q} \cdot \vec{p})^2}{k^4} \check{r}_f \left(\frac{\vec{p}^2}{k^2} \right) + \mathcal{O} \left(\frac{|\vec{q}|^3}{k^3} \right) \right], \end{aligned}$$

and keeping the only relevant term, which is of order \vec{q}^2 and not proportional to $\dot{\mathfrak{F}}_{n-m}(y)$ (which vanishes under the loop integral for the Litim regulator due to Eq. (D.37)). The relevant contribution from the above expansion is

$$\left(-2 \frac{(\vec{q} \cdot \vec{p})^2}{k^2} \dot{r}_f \left(\frac{\vec{p}^2}{k^2} \right) - \vec{q}^2 \left[1 + r_f \left(\frac{\vec{p}^2}{k^2} \right) \right] \right) \mathfrak{F}_{n-m} \left(\frac{\vec{p}^2}{k^2} \right). \tag{E.97}$$

Hence, at order \vec{q}^2 the loop contribution reads

$$\begin{aligned} & 2 [\partial_{\sigma_r} m_r(t, \sigma_r)]^2 k^{-6} \frac{1}{\beta} \sum_{n=-\infty}^{\infty} \int_{-\infty}^{\infty} \frac{d^d p}{(2\pi)^d} \vec{p}^2 \left[\frac{1}{2} \partial_t r_b(t, |\vec{p}|) + \frac{1}{2} \eta_\varphi(t) r_b(t, |\vec{p}|) \right] \mathfrak{B}_n^2 \left(\frac{\vec{p}^2}{k^2} \right) \times \\ & \times \left(-2 \frac{(\vec{q} \cdot \vec{p})^2}{k^2} \dot{r}_f \left(\frac{\vec{p}^2}{k^2} \right) - \vec{q}^2 \left[1 + r_f \left(\frac{\vec{p}^2}{k^2} \right) \right] \right) \mathfrak{F}_{n-m} \left(\frac{\vec{p}^2}{k^2} \right) \stackrel{\text{(A.5)}}{=} \tag{E.98} \\ & = \vec{q}^2 2 [\partial_{\sigma_r} m_r(t, \sigma_r)]^2 k^{-6} \frac{1}{\beta} \sum_{n=-\infty}^{\infty} A_d d \int_0^\infty dp p^{d+1} \left[\frac{1}{2} \partial_t r_b(t, p) + \frac{1}{2} \eta_\varphi(t) r_b(t, p) \right] \mathfrak{B}_n^2 \left(\frac{p^2}{k^2} \right) \times \\ & \times \left(-\frac{2}{d} \frac{p^2}{k^2} \dot{r}_f \left(\frac{p^2}{k^2} \right) - \left[1 + r_f \left(\frac{p^2}{k^2} \right) \right] \right) \mathfrak{F}_{n-m} \left(\frac{p^2}{k^2} \right) \stackrel{\text{(D.7)}}{=} \\ & = \vec{q}^2 2 [\partial_{\sigma_r} m_r(t, \sigma_r)]^2 k^{d-4} \frac{1}{\beta} \sum_{n=-\infty}^{\infty} A_d \frac{d}{2} \int_0^\infty dy y^{\frac{d}{2}} [y \dot{r}_b(y) + \frac{1}{2} \eta_\varphi(t) r_b(y)] \mathfrak{B}_n^2(y) \mathfrak{F}_{n-m}(y) \times \\ & \times \left(-\frac{2}{d} y \dot{r}_f(y) - \left[1 + r_f(y) \right] \right). \end{aligned}$$

Before we further evaluate the y -integrals, we note that for $d = 1$ the entire expression vanishes, since the integrand (the factor in the last line) is exactly zero when Eqs. (D.17) and (D.18) are used.

Otherwise, for $d > 1$ the y -integration is worked out to

$$\begin{aligned} & -\vec{q}^2 2 [\partial_{\sigma_r} m_r(t, \sigma_r)]^2 k^{d-2} \frac{1}{\beta} \sum_{n=-\infty}^{\infty} A_d \frac{1}{2} (d-1) \int_0^1 dy \left[-y^{\frac{d-3}{2}} + \frac{1}{2} \eta_\varphi(t) \left(y^{\frac{d-3}{2}} - y^{\frac{d-1}{2}} \right) \right] \times \\ & \times \mathfrak{B}_n^2(y) \mathfrak{F}_{n-m}(y) \tag{E.99} \\ & = \vec{q}^2 2 A_d \left[1 - \frac{\eta_\varphi(t)}{d+1} \right] [\partial_{\sigma_r} m_r(t, \sigma_r)]^2 k^{d-2} \frac{1}{\beta} \sum_{n=-\infty}^{\infty} \mathfrak{B}_n^2(y) \mathfrak{F}_{n-m}(y). \end{aligned}$$

Trace (Dtr2) – boson tadpole

The evaluation of the following diagram is again a little bit simpler than the previous diagram, because it is of tadpole type. The trace (Dtr2) corresponding to the bosonic tadpole is first expressed in terms of the explicit regulators, propagators, and vertices. These are provided by Eqs. (E.38), (E.40), (E.35), and (E.43).

$$\begin{aligned}
 \text{(Dtr2)} &= - \text{Diagram} = \tag{E.100} \\
 &= - \frac{1}{\beta^4} \sum_{n_1, \dots, n_4 = -\infty}^{\infty} \int_{-\infty}^{\infty} \frac{d^d p_1}{(2\pi)^d} \cdots \frac{d^d p_4}{(2\pi)^d} \times \\
 &\quad \times \beta \delta_{-n_1, n_2} (2\pi)^d \delta^{(d)}(\vec{p}_1 + \vec{p}_2) \vec{p}_1^2 \partial_t [Z_\varphi(t) \frac{1}{2} r_b(t, |\vec{p}_1|)] \times \\
 &\quad \times \beta \delta_{-n_2, n_3} (2\pi)^d \delta^{(d)}(\vec{p}_2 + \vec{p}_3) \frac{1}{Z_\varphi(t) [\omega_{n_2}^2 + \vec{p}_2^2 [1 + r_b(t, |\vec{p}_2|)] + \partial_{\sigma_r}^2 U(t, \sigma_r)]} \times \\
 &\quad \times (-1) \beta \delta_{n_{\text{II}}, n_3 + n_4 + n_1} (2\pi)^d \delta^{(d)}(\vec{p}_3 + \vec{p}_4 - \vec{p}_{\text{II}} + \vec{p}_1) Z_\psi(t) Z_\varphi(t) [\partial_{\sigma_r}^2 m_r(t, \sigma_r)] (\mathbb{1})^{c_{\text{II}} c_1} (\mathbb{1})^{a_{\text{II}} a_1} \times \\
 &\quad \times \beta \delta_{-n_4, n_1} (2\pi)^d \delta^{(d)}(\vec{p}_4 + \vec{p}_1) \frac{1}{Z_\varphi(t) [\omega_{n_4}^2 + \vec{p}_4^2 [1 + r_b(t, |\vec{p}_4|)] + \partial_{\sigma_r}^2 U(t, \sigma_r)]} .
 \end{aligned}$$

Yukawa coupling Inserting the previous equation into the r.h.s. of Eq. (E.90), which is the projection onto the fermion mass term, we obtain

$$\begin{aligned}
 &- \frac{1}{N} (\mathbb{1})^{c_{\text{II}}} \frac{1}{d_\gamma} (\mathbb{1})^{a_{\text{I}}} Z_\psi^{-1}(t) \text{(Dtr2)}^{a_{\text{II}} c_{\text{II}}} \Big|_{\vec{p}_{\text{II}} = \vec{p}_{\text{I}} = 0} \stackrel{\text{(D.26)}}{=} \tag{E.101} \\
 &= + \beta \delta_{n_{\text{II}}, n_{\text{I}}} (2\pi)^d \delta^{(d)}(0) [\partial_{\sigma_r}^2 m_r(t, \sigma_r)] k^{-4} \times \\
 &\quad \times \frac{1}{\beta} \sum_{n=-\infty}^{\infty} \int_{-\infty}^{\infty} \frac{d^d p}{(2\pi)^d} \vec{p}^2 \left[\frac{1}{2} \partial_t r_b(t, |\vec{p}|) + \frac{1}{2} \eta_\varphi(t) r_b(t, |\vec{p}|) \right] \mathfrak{B}_n^2 \left(\frac{\vec{p}^2}{k^2} \right) \stackrel{\text{(A.5)}}{=} \\
 &= + \beta \delta_{n_{\text{II}}, n_{\text{I}}} (2\pi)^d \delta^{(d)}(0) [\partial_{\sigma_r}^2 m_r(t, \sigma_r)] k^{-4} \times \\
 &\quad \times \frac{1}{\beta} \sum_{n=-\infty}^{\infty} A_d d \int_0^\infty dp p^{d+1} \left[\frac{1}{2} \partial_t r_b(t, p) + \frac{1}{2} \eta_\varphi(t) r_b(t, p) \right] \mathfrak{B}_n^2 \left(\frac{p^2}{k^2} \right) \stackrel{\text{(D.7)}}{=} \\
 &= + \beta \delta_{n_{\text{II}}, n_{\text{I}}} (2\pi)^d \delta^{(d)}(0) [\partial_{\sigma_r}^2 m_r(t, \sigma_r)] k^{d-2} \times \\
 &\quad \times \frac{1}{\beta} \sum_{n=-\infty}^{\infty} A_d \frac{d}{2} \int_0^\infty dy y^{\frac{d}{2}} [y \dot{r}_b(y) + \frac{1}{2} \eta_\varphi(t) r_b(y)] \mathfrak{B}_n^2(y) .
 \end{aligned}$$

Using the Litim regulator and the integration formula Eq. (D.15) the tadpole contribution to the RG flow of the fermion mass boils down to,

$$- A_d \left[1 - \frac{\eta_\varphi(t)}{d+2} \right] [\partial_{\sigma_r}^2 m_r(t, \sigma_r)] k^{d-2} \frac{1}{\beta} \sum_{n=-\infty}^{\infty} \mathfrak{B}_n^2(1) . \tag{E.102}$$

Anomalous dimension The bosonic tadpole diagram does not contribute to the scale evolution of the anomalous dimension for two reasons: Firstly, applying the projection Eq. (E.91) the trace in Dirac space vanishes, because it is a trace over an odd number of gamma matrices,

$$\frac{1}{N} (\mathbf{1})^{c_I}{}_{c_{II}} \frac{1}{d_\gamma} (i\vec{p}_{II} \cdot \vec{\gamma})^{a_I}{}_{a_{II}} Z_\psi^{-1}(t) (\text{Dtr}2)^{a_{II}}{}_{a_I}{}^{c_{II}}{}_{c_I} = 0 \quad (\text{E.103})$$

Secondly, the external spatial momentum does not enter the tadpole loop anyhow, such that this diagram has no non-trivial momentum structure and a vanishing \vec{q}^2 -coefficient.

Trace (Dtr3) – mixed fermion-boson loop (fermionic regulator)

The last trace that needs to be evaluated is of the same type as (Dtr1). However, the regulator insertion is moved from the internal boson lines to the internal fermion lines of the diagram. The regulators, propagators, and vertices of this diagram are replaced by their explicit formulae from Eqs. (E.5), (E.7), (E.34), (E.43), and (E.44),

$$\begin{aligned} (\text{Dtr}3) &= +2 \text{Diagram} = \quad (\text{E.104}) \\ &= +2 \frac{1}{\beta^6} \sum_{n_1, \dots, n_6 = -\infty}^{\infty} \int_{-\infty}^{\infty} \frac{d^d p_1}{(2\pi)^d} \cdots \frac{d^d p_6}{(2\pi)^d} \times \\ &\quad \times (-1) \beta \delta_{n_1, n_2} (2\pi)^d \delta^{(d)}(\vec{p}_1 - \vec{p}_2) (\mathbf{1})^{c_1}{}_{c_2} i\vec{p}_1 \cdot (\vec{\gamma})^{a_1}{}_{a_2} \partial_t [Z_\psi(t) \frac{1}{2} r_f(t, |\vec{p}_1|)] \times \\ &\quad \times \beta \delta_{n_2, n_3} (2\pi)^d \delta^{(d)}(\vec{p}_2 - \vec{p}_3) \times \\ &\quad \times \frac{[i(\nu_{n_2} + i\mu) \gamma^{d+1} + i\vec{p}_2 \cdot \vec{\gamma} [1 + r_f(t, |\vec{p}_2|)] - m_r(t, \sigma_r)]^{a_2}{}_{a_3} (\mathbf{1})^{c_2}{}_{c_3}}{Z_\psi(t) [(\nu_{n_2} + i\mu)^2 + \vec{p}_2^2 [1 + r_f(t, |\vec{p}_2|)]^2 + m_r^2(t, \sigma_r)]} \times \\ &\quad \times (-1) \beta \delta_{n_3, n_4+n_I} (2\pi)^d \delta^{(d)}(\vec{p}_4 - \vec{p}_3 + \vec{p}_I) Z_\psi(t) Z_\varphi^{\frac{1}{2}}(t) [\partial_{\sigma_r} m_r(t, \sigma_r)] (\mathbf{1})^{c_3}{}_{c_I} (\mathbf{1})^{a_3}{}_{a_I} \times \\ &\quad \times \beta \delta_{-n_4, n_5} (2\pi)^d \delta^{(d)}(\vec{p}_4 + \vec{p}_5) \frac{1}{Z_\varphi(t) [\omega_{n_4}^2 + \vec{p}_4^2 [1 + r_b(t, |\vec{p}_4|)] + \partial_{\sigma_r}^2 U(t, \sigma_r)]} \times \\ &\quad \times (-1) \beta \delta_{n_{II}, n_5+n_6} (2\pi)^d \delta^{(d)}(\vec{p}_5 - \vec{p}_{II} + \vec{p}_6) Z_\psi(t) Z_\varphi^{\frac{1}{2}}(t) [\partial_{\sigma_r} m_r(t, \sigma_r)] (\mathbf{1})^{c_{II}}{}_{c_6} (\mathbf{1})^{a_{II}}{}_{a_6} \times \\ &\quad \times \beta \delta_{n_6, n_1} (2\pi)^d \delta^{(d)}(\vec{p}_6 - \vec{p}_1) \times \\ &\quad \times \frac{[i(\nu_{n_6} + i\mu) \gamma^{d+1} + i\vec{p}_6 \cdot \vec{\gamma} [1 + r_f(t, |\vec{p}_6|)] - m_r(t, \sigma_r)]^{a_6}{}_{a_1} (\mathbf{1})^{c_6}{}_{c_1}}{Z_\psi(t) [(\nu_{n_6} + i\mu)^2 + \vec{p}_6^2 [1 + r_f(t, |\vec{p}_6|)]^2 + m_r^2(t, \sigma_r)]}. \end{aligned}$$

Yukawa coupling Projecting the diagram onto its contribution to the RG of the fermion mass via Eq. (E.90) one has to simplify the following expression,

$$\begin{aligned} & - \frac{1}{N} (\mathbf{1})^{c_I}{}_{c_{II}} \frac{1}{d_\gamma} (\mathbf{1})^{a_I}{}_{a_{II}} Z_\psi^{-1}(t) (\text{Dtr}3)^{a_{II}}{}_{a_I}{}^{c_{II}}{}_{c_I} \Big|_{\vec{p}_{II}=\vec{p}_I=0} \stackrel{(\text{D.26}), (\text{D.32})}{=} \quad (\text{E.105}) \\ & = + \beta \delta_{n_{II}, n_I} (2\pi)^d \delta^{(d)}(0) 2 [\partial_{\sigma_r} m_r(t, \sigma_r)]^2 m_r(t, \sigma_r) k^{-6} \times \end{aligned}$$

$$\begin{aligned}
& \times \frac{1}{\beta} \sum_{n=-\infty}^{\infty} \int_{-\infty}^{\infty} \frac{d^d p}{(2\pi)^d} 2 \bar{p}^2 \left[\frac{1}{2} \partial_t r_f(t, |\vec{p}|) + \frac{1}{2} \eta_\psi(t) r_f(t, |\vec{p}|) \right] [1 + r_f(t, |\vec{p}|)] \times \\
& \times \mathfrak{B}_{n-n_{\text{II}}} \left(\frac{\bar{p}^2}{k^2} \right) \mathfrak{F}_n^2 \left(\frac{\bar{p}^2}{k^2} \right) \stackrel{\text{(A.5)}}{=} \\
& = + \beta \delta_{n_{\text{II}}, n_{\text{I}}} (2\pi)^d \delta^{(d)}(0) 2 \left[\partial_{\sigma_r} m_r(t, \sigma_r) \right]^2 m_r(t, \sigma_r) k^{-6} \times \\
& \times \frac{1}{\beta} \sum_{n=-\infty}^{\infty} A_d d \int_0^\infty dp p^{d+1} 2 \left[\frac{1}{2} \partial_t r_f(t, p) + \frac{1}{2} \eta_\psi(t) r_f(t, p) \right] [1 + r_f(t, p)] \times \\
& \times \mathfrak{B}_{n-n_{\text{II}}} \left(\frac{p^2}{k^2} \right) \mathfrak{F}_n^2 \left(\frac{p^2}{k^2} \right) \stackrel{\text{(D.7)}}{=} \\
& = + \beta \delta_{n_{\text{II}}, n_{\text{I}}} (2\pi)^d \delta^{(d)}(0) 2 \left[\partial_{\sigma_r} m_r(t, \sigma_r) \right]^2 m_r(t, \sigma_r) k^{d-4} \times \\
& \times \frac{1}{\beta} \sum_{n=-\infty}^{\infty} A_d d \int_0^\infty dy y^{\frac{d}{2}} \left[y \dot{r}_f(y) + \frac{1}{2} \eta_\psi(t) r_f(y) \right] [1 + r_f(y)] \mathfrak{B}_{n-n_{\text{II}}}(y) \mathfrak{F}_n^2(y) .
\end{aligned}$$

Finally, using again the Litim regulator and the integration formula Eq. (D.25), we find

$$- 2 A_d \left[1 - \frac{\eta_\psi(t)}{d+1} \right] \left[\partial_{\sigma_r} m_r(t, \sigma_r) \right]^2 m_r(t, \sigma_r) k^{d-4} \frac{1}{\beta} \sum_{n=-\infty}^{\infty} \mathfrak{B}_{n-n_{\text{II}}}(1) \mathfrak{F}_n^2(1) . \quad (\text{E.106})$$

Anomalous dimension On the other hand, the projection Eq. (E.91) leads to

$$\begin{aligned}
& \frac{1}{N} (\mathbb{1})_{c_{\text{II}}}^{c_{\text{I}}} \frac{1}{d_\gamma} (i\vec{p}_{\text{II}} \cdot \vec{\gamma})_{a_{\text{II}}}^{a_{\text{I}}} Z_\psi^{-1}(t) (\text{Dtr3})_{a_{\text{I}}}^{a_{\text{II}}} c_{\text{I}} = \quad (\text{E.107}) \\
& = + \beta \delta_{n_{\text{II}}, n_{\text{I}}} (2\pi)^d \delta^{(d)}(\vec{p}_{\text{II}} - \vec{p}_{\text{I}}) 2 \left[\partial_{\sigma_r} m_r(t, \sigma_r) \right]^2 k^{-4} \times \\
& \times \frac{1}{\beta} \sum_{n=-\infty}^{\infty} \int_{-\infty}^{\infty} \frac{d^d p}{(2\pi)^d} 2 \left[\frac{1}{2} \partial_t r_f(t, |\vec{p}|) + \frac{1}{2} \eta_\psi(t) r_f(t, |\vec{p}|) \right] \mathfrak{B}_{n-n_{\text{II}}} \left(\frac{(\vec{p} - \vec{p}_{\text{II}})^2}{k^2} \right) \mathfrak{F}_n^2 \left(\frac{\vec{p}^2}{k^2} \right) \times \\
& \times (\vec{p}_{\text{II}} \cdot \vec{p}) \left[\mathfrak{F}_n^{-1} \left(\frac{\vec{p}^2}{k^2} \right) - 2 \frac{\vec{p}^2}{k^2} [1 + r_f(t, |\vec{p}|)]^2 \right] ,
\end{aligned}$$

Again, we rename $\vec{q} \equiv \vec{p}_{\text{II}}$ and $m \equiv n_{\text{II}}$ and expand the \vec{q} -dependent factors about $\vec{q} = 0$ up to terms of order \vec{q}^2 ,

$$\mathfrak{B}_{n-m} \left(\frac{(\vec{p} - \vec{q})^2}{k^2} \right) (\vec{q} \cdot \vec{p}) = \left[\mathfrak{B}_{n-m} \left(\frac{\vec{p}^2}{k^2} \right) - 2 \frac{\vec{q} \cdot \vec{p}}{k^2} \mathfrak{B}_{n-m} \left(\frac{\vec{p}^2}{k^2} \right) + \mathcal{O} \left(\frac{|\vec{q}|^2}{k^3} \right) \right] (\vec{q} \cdot \vec{p}) .$$

The first term on the r.h.s. of the previous equation is not of order \vec{q}^2 and can be ignored. However, the second term, which is proportional to $\mathfrak{B}_{n-m}(y)$, does also vanish in the loop-integral due to Eq. (D.30). Consequently, there is no contribution of this diagram to the RG flow of the anomalous dimension.

Flow equation of the fermion mass

Finally, we can combine our intermediate results (E.94), (E.102), and (E.106). For the RG flow equation of the fermion-mass (Yukawa coupling) we find in $d \geq 1$,

$$\begin{aligned}
& \partial_t m_r(t, \sigma_r) + \eta_\psi(t) m_r(t, \sigma_r) + \frac{1}{2} \eta_\varphi(t) \sigma_r \partial_{\sigma_r} m_r(t, \sigma_r) = \tag{E.108} \\
& = -2 A_d \left[1 - \frac{\eta_\varphi(t)}{d+2} \right] [\partial_{\sigma_r} m_r(t, \sigma_r)]^2 m_r(t, \sigma_r) k^{d+2} \times \\
& \quad \times \frac{1}{\beta} \sum_{n=-\infty}^{\infty} \frac{1}{[\omega_n^2 + k^2 + \partial_{\sigma_r}^2 U(t, \sigma_r)]^2} \frac{1}{(\nu_{n+m} + i\mu)^2 + k^2 + m_r^2(t, \sigma_r)} - \\
& - 2 A_d \left[1 - \frac{\eta_\psi(t)}{d+1} \right] [\partial_{\sigma_r} m_r(t, \sigma_r)]^2 m_r(t, \sigma_r) k^{d+2} \times \\
& \quad \times \frac{1}{\beta} \sum_{n=-\infty}^{\infty} \frac{1}{\omega_{n-m}^2 + k^2 + \partial_{\sigma_r}^2 U(t, \sigma_r)} \frac{1}{[(\nu_n + i\mu)^2 + k^2 + m_r^2(t, \sigma_r)]^2} - \\
& - A_d \left[1 - \frac{\eta_\varphi(t)}{d+2} \right] [\partial_{\sigma_r}^2 m_r(t, \sigma_r)] k^{d+2} \frac{1}{\beta} \sum_{n=-\infty}^{\infty} \frac{1}{[\omega_n^2 + k^2 + \partial_{\sigma_r}^2 U(t, \sigma_r)]^2}.
\end{aligned}$$

Flow equation of the fermion mass – $\frac{1}{N}$ -rescaled

Rescaling the appropriate variables in Eq. (E.108) with N , the $\frac{1}{N}$ -rescaled flow equation reads,

$$\begin{aligned}
& \partial_t m_r(t, \check{\sigma}_r) + \eta_\psi(t) m_r(t, \check{\sigma}_r) + \frac{1}{2} \eta_\varphi(t) \check{\sigma}_r \partial_{\check{\sigma}_r} m_r(t, \check{\sigma}_r) = \tag{E.109} \\
& = -2 A_d \left[1 - \frac{\eta_\varphi(t)}{d+2} \right] \frac{1}{N} [\partial_{\check{\sigma}_r} m_r(t, \check{\sigma}_r)]^2 m_r(t, \check{\sigma}_r) k^{d+2} \times \\
& \quad \times \frac{1}{\beta} \sum_{n=-\infty}^{\infty} \frac{1}{[\omega_n^2 + k^2 + \partial_{\check{\sigma}_r}^2 \check{U}(t, \check{\sigma}_r)]^2} \frac{1}{(\nu_{n+m} + i\mu)^2 + k^2 + m_r^2(t, \check{\sigma}_r)} - \\
& - 2 A_d \left[1 - \frac{\eta_\psi(t)}{d+1} \right] \frac{1}{N} [\partial_{\check{\sigma}_r} m_r(t, \check{\sigma}_r)]^2 m_r(t, \check{\sigma}_r) k^{d+2} \times \\
& \quad \times \frac{1}{\beta} \sum_{n=-\infty}^{\infty} \frac{1}{\omega_{n-m}^2 + k^2 + \partial_{\check{\sigma}_r}^2 \check{U}(t, \check{\sigma}_r)} \frac{1}{[(\nu_n + i\mu)^2 + k^2 + m_r^2(t, \check{\sigma}_r)]^2} - \\
& - A_d \left[1 - \frac{\eta_\varphi(t)}{d+2} \right] \frac{1}{N} [\partial_{\check{\sigma}_r}^2 m_r(t, \check{\sigma}_r)] k^{d+2} \frac{1}{\beta} \sum_{n=-\infty}^{\infty} \frac{1}{[\omega_n^2 + k^2 + \partial_{\check{\sigma}_r}^2 \check{U}(t, \check{\sigma}_r)]^2}.
\end{aligned}$$

This result agrees for example with Refs. [373, Eq. (13)], [374, Eq. (35)], and [346, Eq. (195)]. It is also consistent with Ref. [556, Eq. (23)]. However, the contribution of the field-dependent Yukawa coupling (the tadpole diagram) was not considered in Refs. [373, 374].

Flow equation of the fermion mass – $N \rightarrow \infty$ limit

Considering the flow equation (E.109) in the limit $N \rightarrow \infty$, we find that the r.h.s. vanishes, because this limit suppresses all contributions of Feynman diagrams with internal boson lines (bosonic propagators) via factors $\frac{1}{N}$,

$$\partial_t m_r(t, \check{\sigma}_r) + \eta_\psi(t) m_r(t, \check{\sigma}_r) + \frac{1}{2} \eta_\varphi(t) \check{\sigma}_r \partial_{\check{\sigma}_r} m_r(t, \check{\sigma}_r) = 0. \tag{E.110}$$

Flow equation of the anomalous dimension fermion

The only non-vanishing contribution to the fermionic anomalous dimension in $d > 1$ is given by Eq. (E.99) such that

$$\begin{aligned} \eta_\psi(t) &= 2 A_d \left[1 - \frac{\eta_\varphi(t)}{d+1} \right] [\partial_{\sigma_r} m_r(t, \sigma_r)]^2 k^{d+2} \times \\ &\times \frac{1}{\beta} \sum_{n=-\infty}^{\infty} \frac{1}{[\omega_n^2 + k^2 + \partial_{\sigma_r}^2 U(t, \sigma_r)]^2} \frac{1}{(\nu_{n-m} + i\mu)^2 + k^2 + m_r^2(t, \sigma_r)}. \end{aligned} \quad (\text{E.111})$$

This result agrees with Ref. [346, Eq. (197)]. It is also consistent with Ref. [556, Eq. (25)]. For the special case $d = 1$ the fermion anomalous dimension vanishes,

$$\eta_\psi(t) = 0. \quad (\text{E.112})$$

Flow equation of the anomalous dimension fermion – $\frac{1}{N}$ -rescaled

In terms of $\frac{1}{N}$ -rescaled quantities the Eq. (E.111) is given by

$$\begin{aligned} \eta_\psi(t) &= 2 A_d \left[1 - \frac{\eta_\varphi(t)}{d+1} \right] \frac{1}{N} [\partial_{\check{\sigma}_r} m_r(t, \check{\sigma}_r)]^2 k^{d+2} \times \\ &\times \frac{1}{\beta} \sum_{n=-\infty}^{\infty} \frac{1}{[\omega_n^2 + k^2 + \partial_{\check{\sigma}_r}^2 \check{U}(t, \check{\sigma}_r)]^2} \frac{1}{(\nu_{n-m} + i\mu)^2 + k^2 + m_r^2(t, \check{\sigma}_r)}, \end{aligned} \quad (\text{E.113})$$

while for $d = 1$ we still find

$$\eta_\psi(t) = 0. \quad (\text{E.114})$$

Flow equation of the anomalous dimension fermion – $N \rightarrow \infty$ limit

In the limit $N \rightarrow \infty$ one finds that the fermionic anomalous dimension does not evolve at all – independent of the number of spatial dimensions d ,

$$\lim_{N \rightarrow \infty} \eta_\psi(t) = 0. \quad (\text{E.115})$$

Appendix F

Mean-field Gross-Neveu calculations

Abstract In this appendix we provide supplemental material to Chapter 11. This comprises renormalization and explicit evaluation of several quantities in the $N \rightarrow \infty$ bGN model for zero or non-zero values of μ , T , σ , (and q). We provide formulae for the effective potential and its field-space derivative, the bosonic wave-function renormalization, and the bosonic two-point function in Appendix F.1. In the second half, in Appendix F.2, we present formulae for some thermodynamic quantities.

Disclosure The explicit calculations and results for the bosonic wave-function renormalization and bosonic two-point function are – to the best of our knowledge – mostly new and complement our own Ref. [5]. Also the evaluation of the other quantities up to this level of details seems to be new. Still, the general expressions can be found elsewhere, see main text.

F.1. Field-theoretical quantities

First, we renormalize and evaluate several field-theoretical quantities of the GN model at $N \rightarrow \infty$.

F.1.1. The effective potential

Consider the renormalized effective potential (11.21),

$$\begin{aligned} U(\sigma, \mu, T) &= \\ &= \frac{d_\gamma}{4\pi} \left[\frac{1}{2} (h\sigma)^2 \left[\ln \left(\frac{(h\sigma)^2}{(h\sigma_0)^2} \right) - 1 \right] - \int_{-\infty}^{\infty} dp \left[T \ln \left(1 + e^{-\frac{E+\mu}{T}} \right) + T \ln \left(1 + e^{-\frac{E-\mu}{T}} \right) \right] \right]. \end{aligned} \quad (\text{F.1})$$

For the sake of simplicity, we define the “thermal contribution” to the effective potential,

$$U^{\text{th}}(\sigma, \mu, T) \equiv - \frac{d_\gamma}{4\pi} \int_{-\infty}^{\infty} dp \left[T \ln \left(1 + e^{-\frac{E+\mu}{T}} \right) + T \ln \left(1 + e^{-\frac{E-\mu}{T}} \right) \right]. \quad (\text{F.2})$$

To obtain an expression for $T = 0$, we first study the limit

$$\lim_{x \rightarrow \infty} \frac{1}{x} \ln (1 + e^{-xb}), \quad (\text{F.3})$$

where $x = \frac{|\mu|}{T}$ and $b = \frac{E}{|\mu|} \pm 1$. For $b \geq 0$ the expression vanishes, which is always true for the positive sign in b . However, for $b < 0$ we can use l'Hôpital's rule, because the limit

$$\lim_{x \rightarrow \infty} -\frac{b}{e^{xb} + 1} = -b, \quad (\text{F.4})$$

exists. Hence, we find for Eq. (F.2),

$$\begin{aligned} U^{\text{th}}(\sigma, \mu, 0) &= \frac{d_\gamma}{4\pi} |\mu| \int_{-\infty}^{\infty} dp \left(\frac{E}{|\mu|} - 1 \right) \Theta \left(\frac{|\mu|}{E} - 1 \right) = \\ &= \frac{d_\gamma}{2\pi} \mu^2 \Theta \left(\frac{\mu^2}{(h\sigma)^2} - 1 \right) \int_0^{\sqrt{1 - \frac{(h\sigma)^2}{\mu^2}}} dt \left[\sqrt{t^2 + \frac{(h\sigma)^2}{\mu^2}} - 1 \right] = \\ &= \begin{cases} \frac{d_\gamma}{4\pi} (h\sigma)^2 \left[\operatorname{arsinh} \left(\sqrt{\frac{\mu^2}{(h\sigma)^2} - 1} \right) - \frac{\mu^2}{(h\sigma)^2} \sqrt{1 - \frac{(h\sigma)^2}{\mu^2}} \right], & \text{if } (h\sigma)^2 < \mu^2, \\ 0, & \text{if } (h\sigma)^2 \geq \mu^2. \end{cases} \end{aligned} \quad (\text{F.5})$$

Here, the Heaviside function in the second line is to be understood symbolically as a distinction of cases. From Eq. (F.5) we directly observe that the vacuum part of the effective potential (F.1) at $T = 0$ is only modified for field values $(h\sigma)^2 < \mu^2$.

On the other hand, setting $\sigma = 0$ in Eq. (F.2), we can use the definition of the dilogarithm (A.75) and the corresponding identity (A.76),

$$\begin{aligned} U^{\text{th}}(0, \mu, T) &= \\ &= -\frac{d_\gamma}{2\pi} T^2 \int_0^\infty du \left(\ln [1 + e^{-(u + \frac{\mu}{T})}] + \ln [1 + e^{-(u - \frac{\mu}{T})}] \right) = \\ &= -\frac{d_\gamma}{2\pi} T^2 \left[\int_0^{-e^{-\frac{\mu}{T}}} dt \frac{1}{t} \ln(1 - t) + \int_0^{-e^{\frac{\mu}{T}}} dt \frac{1}{t} \ln(1 - t) \right] = \\ &= \frac{d_\gamma}{2\pi} T^2 [\operatorname{Li}_2(-e^{-\tilde{\mu}}) + \operatorname{Li}_2(-e^{+\tilde{\mu}})] = \\ &= -\frac{d_\gamma}{2\pi} \left[\frac{\pi^2}{6} T^2 + \frac{1}{2} \mu^2 \right]. \end{aligned} \quad (\text{F.6})$$

From the second to the third line we substituted

$$t = -e^{-u \mp \frac{\mu}{T}}, \quad du = -\frac{dt}{t}. \quad (\text{F.7})$$

Apart from the normalization of the vacuum pressure, the thermal contribution to the effective potential from Eq. (F.6) actually corresponds to the negative of the Boltzmann pressure of a free gas in 1 + 1 dimensions.

Summarizing, we find from Eqs. (F.1) and (F.6) for $\sigma = 0$,

$$U(0, \mu, T) = -\frac{d_\gamma}{2\pi} \left[\frac{\pi^2}{6} T^2 + \frac{1}{2} \mu^2 \right], \quad (\text{F.8})$$

which is especially relevant in the \mathbb{Z}_2 -symmetric phase, where the physical minimum is located at $\sigma = 0$. For $\mu = 0$ and $\sigma \neq 0$ Eq. (F.1) slightly simplifies,

$$U(\sigma, 0, T) = \frac{d_\gamma}{4\pi} \left[\frac{1}{2} (h\sigma)^2 \left[\ln \left(\frac{(h\sigma)^2}{(h\sigma_0)^2} \right) - 1 \right] - 4 \int_0^\infty dp T \ln \left(1 + e^{-\frac{E}{T}} \right) \right]. \quad (\text{F.9})$$

Setting $\sigma = 0$ in this result, we can again use the dilogarithm Eq. (A.75) and relation (A.77) to simplify

$$U(0, 0, T) = \frac{d_\gamma}{2\pi} T^2 2 \operatorname{Li}_2(-1) = -\frac{d_\gamma}{2\pi} \frac{\pi^2}{6} T^2. \quad (\text{F.10})$$

This is consistent with Eq. (F.8).

On the other hand, combining Eqs. (F.1) and (F.5), we find for $T = 0$,

$$\begin{aligned} U(\sigma, \mu, 0) &= \quad (\text{F.11}) \\ &= \frac{d_\gamma}{8\pi} (h\sigma)^2 \left[\ln \left(\frac{(h\sigma)^2}{(h\sigma_0)^2} \right) - 1 \right] + \\ &\quad + \begin{cases} \frac{d_\gamma}{4\pi} (h\sigma)^2 \left[\operatorname{arsinh} \left(\sqrt{\frac{\mu^2}{(h\sigma)^2} - 1} \right) - \frac{\mu^2}{(h\sigma)^2} \sqrt{1 - \frac{(h\sigma)^2}{\mu^2}} \right], & \text{if } (h\sigma)^2 < \mu^2, \\ 0, & \text{if } (h\sigma)^2 \geq \mu^2. \end{cases} \end{aligned}$$

Evaluating the last expression for $\mu \neq 0$ and taking the limit $\sigma \rightarrow 0$ or evaluating Eq. (F.8) for $T = 0$, we find

$$U(0, \mu, 0) = -\frac{d_\gamma}{4\pi} \mu^2. \quad (\text{F.12})$$

In vacuum, for $T = 0$ and $\mu = 0$, we obtain

$$U(\sigma, 0, 0) = \frac{d_\gamma}{8\pi} (h\sigma)^2 \left[\ln \left(\frac{(h\sigma)^2}{(h\sigma_0)^2} \right) - 1 \right], \quad (\text{F.13})$$

$$U(0, 0, 0) = 0. \quad (\text{F.14})$$

All results of this section can in principle be modified by an overall additional constant, which cannot be observed since one can only measure energy differences and not absolute energies.

F.1.2. The derivative of the effective potential

The starting point is Eq. (11.22),

$$\begin{aligned} \partial_\sigma U(\sigma, \mu, T) &= \frac{d_\gamma}{2\pi} h^2 \sigma \left[\frac{1}{2} \ln \left(\frac{(h\sigma)^2}{(h\sigma_0)^2} \right) + \int_0^\infty dp \frac{1}{E} \left[n_f \left(\frac{E+\mu}{T} \right) + n_f \left(\frac{E-\mu}{T} \right) \right] \right] = \quad (\text{F.15}) \\ &= \frac{d_\gamma}{2\pi} h^2 \sigma \left[\frac{1}{2} \ln \left(\frac{(h\sigma)^2}{(h\sigma_0)^2} \right) + \int_0^\infty dp \frac{1}{E} \left[1 - \frac{1}{2} \tanh \left(\frac{E+\mu}{2T} \right) - \frac{1}{2} \tanh \left(\frac{E-\mu}{2T} \right) \right] \right]. \end{aligned}$$

First, we study non-zero temperatures. For $\sigma = 0$ this expression vanishes,

$$\partial_\sigma U(0, \mu, T) = 0, \quad (\text{F.16})$$

because both terms in the square bracket in Eq. (F.15) are merely logarithmically divergent at $\sigma = 0$. This divergence is regulated by the linear prefactor σ .

On the other hand, for $\mu = 0$, only the momentum integral in Eq. (F.15) simplifies slightly,

$$\begin{aligned} \partial_\sigma U(\sigma, 0, T) &= \frac{d_\gamma}{2\pi} h^2 \sigma \left[\frac{1}{2} \ln \left(\frac{(h\sigma)^2}{(h\sigma_0)^2} \right) + 2 \int_0^\infty dp \frac{1}{E} n_f \left(\frac{E}{T} \right) \right] = \quad (\text{F.17}) \\ &= \frac{d_\gamma}{2\pi} h^2 \sigma \left[\frac{1}{2} \ln \left(\frac{(h\sigma)^2}{(h\sigma_0)^2} \right) + \int_0^\infty dp \frac{1}{E} \left[1 - \tanh \left(\frac{E}{2T} \right) \right] \right]. \end{aligned}$$

Again, taking $\sigma = 0$ in this expression, we find

$$\partial_\sigma U(0, 0, T) = 0. \quad (\text{F.18})$$

For $T = 0$ we can use Eq. (B.10) to rewrite Eq. (F.15),

$$\begin{aligned} \partial_\sigma U(\sigma, \mu, 0) &= \frac{d_\gamma}{2\pi} h^2 \sigma \left[\frac{1}{2} \ln \left(\frac{(h\sigma)^2}{(h\sigma_0)^2} \right) + \int_0^\infty dp \frac{1}{E} \Theta \left(\frac{|\mu|}{E} - 1 \right) \right] = \\ &= \frac{d_\gamma}{4\pi} h^2 \sigma \ln \left(\frac{(h\sigma)^2}{(h\sigma_0)^2} \right) + \begin{cases} \frac{d_\gamma}{2\pi} h^2 \sigma \operatorname{arsinh} \left(\sqrt{\frac{\mu^2}{(h\sigma)^2} - 1} \right), & \text{if } (h\sigma)^2 < \mu^2, \\ 0, & \text{if } (h\sigma)^2 \geq \mu^2. \end{cases} \end{aligned} \quad (\text{F.19})$$

This result is consistent with taking a σ -derivative of Eq. (F.11). Setting $T = 0$ in Eq. (F.16) or considering the limit $\sigma \rightarrow 0$ in Eq. (F.19) results in,

$$\partial_\sigma U(0, \mu, 0) = 0. \quad (\text{F.20})$$

Finally, for $\mu = 0$ and $T = 0$ we consistently obtain from the above equations

$$\partial_\sigma U(\sigma, 0, 0) = \frac{d_\gamma}{4\pi} h^2 \sigma \ln \left(\frac{(h\sigma)^2}{(h\sigma_0)^2} \right), \quad (\text{F.21})$$

$$\partial_\sigma U(0, 0, 0) = 0. \quad (\text{F.22})$$

F.1.3. The bosonic two-point function

In this appendix, we evaluate the bosonic two-point function as far as possible in terms of known functions. For this purpose, we distinguish the 16 cases where the variables σ , μ , T , and q take values that are either zero or non-zero.

The starting point of our discussion are the intermediate results (11.50) and (11.51) after evaluation of the Matsubara sum in Eq. (11.46) for (non-)vanishing external momentum,

$$\Gamma^{(2)}(\sigma, \mu, T, q) = \quad (\text{F.23})$$

$$\begin{aligned} &= \frac{d_\gamma}{2\pi} h^2 \left[\frac{1}{2} \ln \left(\frac{(2\Lambda)^2}{(h\sigma_0)^2} \right) + \mathcal{O} \left(\frac{(h\sigma_0)^2}{\Lambda^2} \right) - \int_{-\infty}^\infty dp \frac{1}{2E} [1 - n_f \left(\frac{E+\mu}{T} \right) - n_f \left(\frac{E-\mu}{T} \right)] - \right. \\ &\quad \left. - \int_{-\infty}^\infty dp [pq - 2(h\sigma)^2] \left(\frac{1}{2E_q} \frac{1}{E^2 - E_q^2} [1 - n_f \left(\frac{E_q+\mu}{T} \right) - n_f \left(\frac{E_q-\mu}{T} \right)] + \right. \right. \\ &\quad \left. \left. + \frac{1}{2E} \frac{1}{E^2 - E^2} [1 - n_f \left(\frac{E+\mu}{T} \right) - n_f \left(\frac{E-\mu}{T} \right)] \right) \right], \end{aligned}$$

$$\Gamma^{(2)}(\sigma, \mu, T, 0) = \quad (\text{F.24})$$

$$\begin{aligned} &= \frac{d_\gamma}{2\pi} h^2 \left[\frac{1}{2} \ln \left(\frac{(2\Lambda)^2}{(h\sigma_0)^2} \right) + \mathcal{O} \left(\frac{(h\sigma_0)^2}{\Lambda^2} \right) - \int_{-\infty}^\infty dp \frac{1}{2E} [1 - n_f \left(\frac{E+\mu}{T} \right) - n_f \left(\frac{E-\mu}{T} \right)] + \right. \\ &\quad \left. + 2(h\sigma)^2 \int_{-\infty}^\infty dp \frac{1}{4E^3} (1 - n_f \left(\frac{E+\mu}{T} \right) - n_f \left(\frac{E-\mu}{T} \right)) + \right. \\ &\quad \left. + \frac{E}{T} [n_f^2 \left(\frac{E+\mu}{T} \right) + n_f^2 \left(\frac{E-\mu}{T} \right) - n_f \left(\frac{E+\mu}{T} \right) - n_f \left(\frac{E-\mu}{T} \right)] \right]. \end{aligned}$$

We start our analysis considering non-zero temperatures, $T \neq 0$. First, we analyze the case $\mu \neq 0$ and $\sigma \neq 0$. Having $\sigma \neq 0$ is crucial in the next steps, because the non-zero fermion mass $h\sigma$ in the energies E renders all integrals in Eqs. (F.23) and (F.24) IR-finite.

To treat the UV-divergent contribution, which is identical for both expressions and q -independent, we have to use a sharp UV-cutoff Λ ,

$$\begin{aligned} \int_{-\infty}^{\infty} dp \frac{1}{2E} &\Rightarrow \int_0^{\Lambda} dp \frac{1}{\sqrt{p^2 + (h\sigma)^2}} = \operatorname{arcoth} \left(\sqrt{1 + \frac{(h\sigma)^2}{\Lambda^2}} \right) = \\ &= \frac{1}{2} \ln \left(\frac{(2\Lambda)^2}{(h\sigma)^2} \right) + \mathcal{O} \left(\frac{(h\sigma)^2}{\Lambda^2} \right). \end{aligned} \quad (\text{F.25})$$

With the substitution $p' = -(p + q)$ we rewrite the second integral in Eq. (F.23) as follows

$$\begin{aligned} & - \int_{-\infty}^{\infty} dp [pq - 2(h\sigma)^2] \left(\frac{1}{2E_q} \frac{1}{E^2 - E_q^2} [1 - n_f(\frac{E_q + \mu}{T}) - n_f(\frac{E_q - \mu}{T})] + \right. \\ & \quad \left. + \frac{1}{2E} \frac{1}{E_q^2 - E^2} [1 - n_f(\frac{E + \mu}{T}) - n_f(\frac{E - \mu}{T})] \right) = \\ & = 2 \left[\frac{q^2}{(2h\sigma)^2} + 1 \right] (h\sigma)^2 \int_{-\infty}^{\infty} dp \frac{1}{E} \frac{1}{E_q^2 - E^2} [1 - n_f(\frac{E + \mu}{T}) - n_f(\frac{E - \mu}{T})] = \\ & = 2 \left[\frac{q^2}{(2h\sigma)^2} + 1 \right] (h\sigma)^2 \int_0^{\infty} dp \frac{1}{E} \left(\frac{1}{E_q^2 - E^2} + \frac{1}{E^2 - E_q^2} \right) [1 - n_f(\frac{E + \mu}{T}) - n_f(\frac{E - \mu}{T})]. \end{aligned} \quad (\text{F.26})$$

In the last step, we split the integral at $p = 0$ and substituted $p \rightarrow -p$ in the domain of negative p . To the best of our knowledge, the contribution to the integral involving the Fermi-Dirac distribution functions (B.2) cannot be further evaluated analytically in a reasonable way for $T \neq 0$, $\mu \neq 0$, and $\sigma \neq 0$ and a numerical calculation is needed. Here, some care is required, due to the pole at $p = \frac{|q|}{2}$.

However, the T -independent part can be integrated analytically. In a first step, we introduce the variables $t = \frac{p}{h\sigma}$ and $a = \frac{q}{h\sigma}$.

$$(h\sigma)^2 \int_0^{\infty} dp \frac{1}{E} \left(\frac{1}{E_q^2 - E^2} + \frac{1}{E^2 - E_q^2} \right) = \int_0^{\infty} dt \frac{1}{\sqrt{t^2 + 1}} \left(\frac{1}{(t+a)^2 - t^2} + \frac{1}{(t-a)^2 - t^2} \right) \quad (\text{F.27})$$

For the sake of simplicity, we for the moment assume that $q > 0$ and $h\sigma > 0$, thus also $a > 0$, which will not alter the final result. To handle the pole at $t = \frac{a}{2}$ in the second term, one has to split the integral about the pole into two integration domains $[0, \frac{a}{2} - \varepsilon]$ and $[\frac{a}{2} + \varepsilon, \infty]$ and use the Cauchy principal value [33] for the integral. The solution of the integral over the first term is

$$\begin{aligned} \int_0^{\infty} dt \frac{1}{\sqrt{t^2 + 1}} \frac{1}{(t+a)^2 - t^2} &= \frac{1}{a} \frac{1}{\sqrt{a^2 + 4}} \operatorname{artanh} \left(\frac{at - 2}{\sqrt{a^2 + 4} \sqrt{1 + t^2}} \right) \Big|_0^{\infty} = \\ &= \frac{1}{a} \frac{1}{\sqrt{a^2 + 4}} \left[\operatorname{arcoth} \left(\sqrt{\frac{4}{a^2} + 1} \right) + \operatorname{arcoth} \left(\sqrt{\frac{a^2}{4} + 1} \right) \right]. \end{aligned} \quad (\text{F.28})$$

The Cauchy principal value, for $\varepsilon \rightarrow 0$, of the integral over the second term is

$$\text{p. v.} \int_0^{\infty} dt \frac{1}{\sqrt{t^2 + 1}} \frac{1}{(t-a)^2 - t^2} = \frac{1}{a} \frac{1}{\sqrt{a^2 + 4}} \left[\operatorname{arcoth} \left(\sqrt{\frac{4}{a^2} + 1} \right) - \operatorname{arcoth} \left(\sqrt{\frac{a^2}{4} + 1} \right) \right]. \quad (\text{F.29})$$

Combining these intermediate results, we find

$$\begin{aligned} & 2 \left[\frac{q^2}{(2h\sigma)^2} + 1 \right] (h\sigma)^2 \int_0^\infty dp \frac{1}{E} \left(\frac{1}{E_q^2 - E^2} + \frac{1}{E_{-q}^2 - E^2} \right) = \\ & = \sqrt{\frac{(2h\sigma)^2}{q^2} + 1} \operatorname{arcoth} \left(\sqrt{\frac{(2h\sigma)^2}{q^2} + 1} \right), \end{aligned} \quad (\text{F.30})$$

which is again formulated symmetrically in q and $h\sigma$ and therefore also valid for negative values of q and $h\sigma$.

It remains to evaluate the T -independent integral

$$2 (h\sigma)^2 \int_{-\infty}^\infty dp \frac{1}{4E^3} = \int_0^\infty dt (t^2 + 1)^{-\frac{3}{2}} = 1, \quad (\text{F.31})$$

from Eq. (F.24).

Combing Eqs. (F.23), (F.25), (F.26), and (F.30) and sending the UV cutoff to infinity our first renormalized final result for the bosonic two-point function is

$$\begin{aligned} & \Gamma^{(2)}(\sigma, \mu, T, q) = \\ & = \frac{d_\gamma}{2\pi} h^2 \left[\frac{1}{2} \ln \left(\frac{(h\sigma)^2}{(h\sigma_0)^2} \right) + \sqrt{\frac{(2h\sigma)^2}{q^2} + 1} \operatorname{arcoth} \left(\sqrt{\frac{(2h\sigma)^2}{q^2} + 1} \right) + \right. \\ & \quad \left. + \int_0^\infty dp \frac{1}{E} \left[n_f \left(\frac{E+\mu}{T} \right) + n_f \left(\frac{E-\mu}{T} \right) \right] - \right. \\ & \quad \left. - 2 \left[\frac{q^2}{(2h\sigma)^2} + 1 \right] (h\sigma)^2 \int_0^\infty dp \frac{1}{E} \left(\frac{1}{E_q^2 - E^2} + \frac{1}{E_{-q}^2 - E^2} \right) \left[n_f \left(\frac{E+\mu}{T} \right) + n_f \left(\frac{E-\mu}{T} \right) \right] \right], \end{aligned} \quad (\text{F.32})$$

Note that the remaining integral in the last line still has a pole at $p = \frac{|q|}{2}$.

For vanishing external momentum, it follows from Eqs. (F.24), (F.25), and (F.31),

$$\begin{aligned} & \Gamma^{(2)}(\sigma, \mu, T, 0) = \\ & = \frac{d_\gamma}{2\pi} h^2 \left[\frac{1}{2} \ln \left(\frac{(h\sigma)^2}{(h\sigma_0)^2} \right) + 1 + \int_0^\infty dp \frac{1}{E} \left[n_f \left(\frac{E+\mu}{T} \right) + n_f \left(\frac{E-\mu}{T} \right) \right] - \right. \\ & \quad \left. - (h\sigma)^2 \int_0^\infty dp \frac{1}{E^3} \left(n_f \left(\frac{E+\mu}{T} \right) + n_f \left(\frac{E-\mu}{T} \right) - \right. \right. \\ & \quad \left. \left. - \frac{E}{T} \left[n_f^2 \left(\frac{E+\mu}{T} \right) + n_f^2 \left(\frac{E-\mu}{T} \right) - n_f \left(\frac{E+\mu}{T} \right) - n_f \left(\frac{E-\mu}{T} \right) \right] \right) \right]. \end{aligned} \quad (\text{F.33})$$

Next, we study the cases where σ vanishes. However, we restart with Eqs. (F.23) and (F.24) and do not use our previous results, to better handle the newly introduced IR divergences. This can be seen from the second term in the first line and the integral in the last line of Eq. (F.32), which are separately IR-divergent, but arise from the second integral in Eq. (F.23) that is actually IR-finite for $\sigma \rightarrow 0$. This is seen best by analyzing the limit $p \rightarrow 0$ of the argument of the integral in the

last line of Eq. (F.26) with $\sigma = 0$,

$$\begin{aligned}
& \lim_{p \rightarrow 0} \frac{1}{E} \left(\frac{1}{E_q^2 - E^2} + \frac{1}{E_{-q}^2 - E^2} \right) \left[1 - n_f \left(\frac{E+\mu}{T} \right) - n_f \left(\frac{E-\mu}{T} \right) \right] \Big|_{\sigma=0} = \\
& = \lim_{p \rightarrow 0} \frac{1}{2p} \left(\frac{1}{2pq+q^2} - \frac{1}{2pq-q^2} \right) \left[\tanh \left(\frac{p+\mu}{2T} \right) + \tanh \left(\frac{p-\mu}{2T} \right) \right] = \\
& = \frac{1}{q^2} \frac{1}{T} \frac{1}{\cosh^2 \left(\frac{\mu}{2T} \right)},
\end{aligned} \tag{F.34}$$

which does not diverge as long as $T \neq 0$ and $q \neq 0$. The same is true for the second integral in Eq. (F.24), which vanishes due to the $(h\sigma)^2$ prefactor. This is directly understood by returning to Eq. (11.46), before the Matsubara frequencies are evaluated and where $h\sigma$ can be safely set to zero.

Hence, the q -independent and identical parts of Eqs. (F.23) and (F.24) are the problematic IR- (and UV-)divergent contributions, which are evaluated as follows,

$$\begin{aligned}
& \int_0^\infty dp \frac{1}{p} \left[1 - n_f \left(\frac{p+\mu}{T} \right) - n_f \left(\frac{p-\mu}{T} \right) \right] \Rightarrow \\
& \Rightarrow \int_\varepsilon^{\frac{\Lambda}{T}} dt t^{-1} - \int_\varepsilon^\infty dt t^{-1} \left[n_f \left(\frac{p+\mu}{T} \right) + n_f \left(\frac{p-\mu}{T} \right) \right] = \\
& = \ln \left(\frac{\Lambda}{\varepsilon T} \right) + \lim_{s \rightarrow 0} \Gamma(s) \left[\text{Li}_s \left(\varepsilon, -e^{-\frac{\mu}{T}} \right) + \text{Li}_s \left(\varepsilon, -e^{\frac{\mu}{T}} \right) \right] \\
& = \ln \left(\frac{\Lambda}{\varepsilon T} \right) + \text{DLi}_0 \left(\frac{\mu}{T} \right) - \gamma + \ln(\varepsilon) = \\
& = \ln \left(\frac{\Lambda}{T} \right) + \text{DLi}_0 \left(\frac{\mu}{T} \right) + \gamma.
\end{aligned} \tag{F.35}$$

Here, we first introduced the new variable $t = \frac{p}{T}$, the same UV-cutoff Λ as before (for the UV-divergent contribution), and the dimensionless IR-cutoff ε . Additionally, we used the definition of the incomplete polylogarithm Eq. (A.61). The limit $s \rightarrow 0$ from the third to fourth line can be evaluated according to Eq. (A.94) for small ε . In total the IR divergences perfectly cancel. Inserting this result into Eqs. (F.23) and (F.24) for $\sigma = 0$ also the UV divergence cancels and we obtain the renormalized results

$$\begin{aligned}
\Gamma^{(2)}(0, \mu, T, q) &= \frac{d_\gamma}{2\pi} h^2 \left[\frac{1}{2} \ln \left(\frac{(2T)^2}{(h\sigma_0)^2} \right) - \gamma - \text{DLi}_0 \left(\frac{\mu}{T} \right) + \right. \\
& \quad \left. + \frac{q^2}{2} \int_0^\infty dp \frac{1}{p} \left(\frac{1}{(p+q)^2 - p^2} + \frac{1}{(p-q)^2 - p^2} \right) \left[1 - n_f \left(\frac{p+\mu}{T} \right) - n_f \left(\frac{p-\mu}{T} \right) \right] \right],
\end{aligned} \tag{F.36}$$

$$\Gamma^{(2)}(0, \mu, T, 0) = \frac{d_\gamma}{2\pi} h^2 \left[\frac{1}{2} \ln \left(\frac{(2T)^2}{(h\sigma_0)^2} \right) - \gamma - \text{DLi}_0 \left(\frac{\mu}{T} \right) \right]. \tag{F.37}$$

The remaining integral in Eq. (F.36) again needs numerical evaluation with careful treatment of the pole at $p = \frac{|q|}{2}$, but is, as already mentioned, IR-finite for $T \neq 0$ and $q \neq 0$.

Next, we provide the results for $\mu = 0$, but $T \neq 0$, $\sigma \neq 0$. These can be derived by setting $\mu = 0$

in Eqs. (F.32) and (F.33) and slightly simplifying the integrals,

$$\begin{aligned} \Gamma^{(2)}(\sigma, 0, T, q) &= \tag{F.38} \\ &= \frac{d_\gamma}{2\pi} h^2 \left[\frac{1}{2} \ln \left(\frac{(h\sigma)^2}{(h\sigma_0)^2} \right) + \sqrt{\frac{(2h\sigma)^2}{q^2} + 1} \operatorname{arccoth} \left(\sqrt{\frac{(2h\sigma)^2}{q^2} + 1} \right) + 2 \int_0^\infty dp \frac{1}{E} n_f \left(\frac{E}{T} \right) - \right. \\ &\quad \left. - 4 \left[\frac{q^2}{(2h\sigma)^2} + 1 \right] (h\sigma)^2 \int_0^\infty dp \frac{1}{E} \left(\frac{1}{E_q^2 - E^2} + \frac{1}{E_{-q}^2 - E^2} \right) n_f \left(\frac{E}{T} \right) \right], \end{aligned}$$

$$\begin{aligned} \Gamma^{(2)}(\sigma, 0, T, 0) &= \tag{F.39} \\ &= \frac{d_\gamma}{2\pi} h^2 \left[\frac{1}{2} \ln \left(\frac{(h\sigma)^2}{(h\sigma_0)^2} \right) + 1 + 2 \int_0^\infty dp \frac{1}{E} n_f \left(\frac{E}{T} \right) - \right. \\ &\quad \left. - 2 (h\sigma)^2 \int_0^\infty dp \frac{1}{E^3} \left(n_f \left(\frac{E+\mu}{T} \right) - \frac{E}{T} \left[n_f^2 \left(\frac{E}{T} \right) - n_f \left(\frac{E}{T} \right) \right] \right) \right]. \end{aligned}$$

In order to study the scenario $\mu = 0$ at vanishing σ , we return to Eqs. (F.36) and (F.37) and use Eq. (A.83). We find,

$$\begin{aligned} \Gamma^{(2)}(0, 0, T, q) &= \frac{d_\gamma}{2\pi} h^2 \left[\frac{1}{2} \ln \left(\frac{(\pi T)^2}{(h\sigma_0)^2} \right) - \gamma + \right. \tag{F.40} \\ &\quad \left. + \frac{q^2}{2} \int_0^\infty dp \frac{1}{p} \left(\frac{1}{(p+q)^2 - p^2} + \frac{1}{(p-q)^2 - p^2} \right) [1 - 2 n_f \left(\frac{p}{T} \right)] \right], \end{aligned}$$

$$\Gamma^{(2)}(0, 0, T, 0) = \frac{d_\gamma}{2\pi} h^2 \left[\frac{1}{2} \ln \left(\frac{(\pi T)^2}{(h\sigma_0)^2} \right) - \gamma \right]. \tag{F.41}$$

The integral Eq. (F.40) is still IR-finite, compare Eq. (F.34) at $\mu = 0$, but again needs numerical treatment with focus on the pole at $p = \frac{|q|}{2}$.

To analyze Eqs. (F.23) and (F.24) in the limit of vanishing temperature, we first study the zero-temperature limit of the integral

$$\begin{aligned} &\lim_{\frac{|\mu|}{T} \rightarrow \infty} \int_0^\infty dp \frac{1}{E^3} \frac{E}{T} \left[n_f^2 \left(\frac{E+\mu}{T} \right) + n_f^2 \left(\frac{E-\mu}{T} \right) - n_f \left(\frac{E+\mu}{T} \right) - n_f \left(\frac{E-\mu}{T} \right) \right] = \tag{F.42} \\ &= \lim_{\frac{|\mu|}{T} \rightarrow \infty} -\frac{1}{|\mu|} \int_0^\infty dp \frac{1}{E^2} \left[\frac{\frac{|\mu|}{2T}}{2 \cosh^2 \left(\frac{|\mu|}{2T} \left(\frac{E}{|\mu|} + 1 \right) \right)} + \frac{\frac{|\mu|}{2T}}{2 \cosh^2 \left(\frac{|\mu|}{2T} \left(\frac{E}{|\mu|} - 1 \right) \right)} \right] = \\ &= -\frac{1}{|\mu|} \int_0^\infty dp \frac{1}{E^2} \left[\delta \left(\frac{E}{|\mu|} + 1 \right) + \delta \left(\frac{E}{|\mu|} - 1 \right) \right]. \end{aligned}$$

In the first step, we used relation (B.4). In the second step the representation (A.2) of the Dirac delta distribution was used. This result as well as Eq. (B.10) is inserted into Eqs. (F.32) and (F.33),

$$\begin{aligned} \Gamma^{(2)}(\sigma, \mu, 0, q) &= \tag{F.43} \\ &= \frac{d_\gamma}{2\pi} h^2 \left[\frac{1}{2} \ln \left(\frac{(h\sigma)^2}{(h\sigma_0)^2} \right) + \sqrt{\frac{(2h\sigma)^2}{q^2} + 1} \operatorname{arccoth} \left(\sqrt{\frac{(2h\sigma)^2}{q^2} + 1} \right) + \int_0^\infty dp \frac{1}{E} \Theta \left(\frac{|\mu|}{E} - 1 \right) - \right. \end{aligned}$$

$$\begin{aligned}
& -2 \left[\frac{q^2}{(2h\sigma)^2} + 1 \right] (h\sigma)^2 \int_0^\infty dp \frac{1}{E} \left(\frac{1}{E_q^2 - E^2} + \frac{1}{E_{-q}^2 - E^2} \right) \Theta \left(\frac{|\mu|}{E} - 1 \right), \\
\Gamma^{(2)}(\sigma, \mu, 0, 0) = & \\
= \frac{d_\gamma}{2\pi} h^2 \left[\frac{1}{2} \ln \left(\frac{(h\sigma)^2}{(h\sigma_0)^2} \right) + 1 + \int_0^\infty dp \frac{1}{E} \Theta \left(\frac{|\mu|}{E} - 1 \right) - \right. \\
& \left. - (h\sigma)^2 \left(\int_0^\infty dp \frac{1}{E^3} \Theta \left(\frac{|\mu|}{E} - 1 \right) + \frac{1}{|\mu|} \int_0^\infty dp \frac{1}{E^2} \left[\delta \left(\frac{E}{|\mu|} + 1 \right) + \delta \left(\frac{E}{|\mu|} - 1 \right) \right] \right) \right].
\end{aligned} \tag{F.44}$$

Next, we evaluate the individual contributions. The integral in the first lines of Eqs. (F.43) and (F.44) evaluates to

$$\int_0^\infty dp \frac{1}{E} \Theta \left(\frac{|\mu|}{E} - 1 \right) = \begin{cases} \operatorname{artanh} \left(\sqrt{1 - \frac{(h\sigma)^2}{\mu^2}} \right), & \text{if } (h\sigma)^2 < \mu^2, \\ 0, & \text{if } (h\sigma)^2 \geq \mu^2. \end{cases} \tag{F.45}$$

The integrals in the third line of Eq. (F.44) are solved by

$$(h\sigma)^2 \int_0^\infty dp \frac{1}{E^3} \Theta \left(\frac{|\mu|}{E} - 1 \right) = \begin{cases} \sqrt{1 - \frac{(h\sigma)^2}{\mu^2}}, & \text{if } (h\sigma)^2 < \mu^2, \\ 0, & \text{if } (h\sigma)^2 \geq \mu^2, \end{cases} \tag{F.46}$$

and

$$\frac{(h\sigma)^2}{|\mu|} \int_0^\infty dp \frac{1}{E^2} \left[\delta \left(\frac{E}{|\mu|} + 1 \right) + \delta \left(\frac{E}{|\mu|} - 1 \right) \right] = \begin{cases} \frac{(h\sigma)^2}{\mu^2} \frac{1}{\sqrt{1 - \frac{(h\sigma)^2}{\mu^2}}} & \text{if } (h\sigma)^2 < \mu^2, \\ 0 & \text{if } (h\sigma)^2 \geq \mu^2, \end{cases} \tag{F.47}$$

where we used identity (A.3).

The tricky contribution is the integral in the last line of Eq. (F.43),

$$-2 \left[\frac{q^2}{(2h\sigma)^2} + 1 \right] (h\sigma)^2 \int_0^\infty dp \frac{1}{E} \left(\frac{1}{E_q^2 - E^2} + \frac{1}{E_{-q}^2 - E^2} \right) \Theta \left(\frac{|\mu|}{E} - 1 \right). \tag{F.48}$$

If $(h\sigma)^2 \geq \mu^2$ this integral vanishes, due to the Heaviside function. Otherwise, for $(h\sigma)^2 < \mu^2$, the integral is cut off in the UV at momenta $\sqrt{\mu^2 - h^2\sigma^2}$. The challenge in evaluating the latter case is again the pole $p = \frac{|q|}{2}$ in the second term. If the pole is outside the integration domain, hence $\frac{|q|}{2} > \sqrt{\mu^2 - h^2\sigma^2}$ the integral can be solved directly. If the pole is inside the integration domain, thus $\frac{|q|}{2} < \sqrt{\mu^2 - h^2\sigma^2}$, one has to use again the Cauchy principal value by splitting the integral about the pole, *cf.* Eq. (F.30).

In total, the combined results are

$$\begin{aligned}
\Gamma^{(2)}(\sigma, \mu, 0, q) = & \\
= \frac{d_\gamma}{2\pi} h^2 \left[\frac{1}{2} \ln \left(\frac{(h\sigma)^2}{(h\sigma_0)^2} \right) + \sqrt{1 + \frac{(2h\sigma)^2}{q^2}} \operatorname{arccoth} \left(\sqrt{1 + \frac{(2h\sigma)^2}{q^2}} \right) \right] + &
\end{aligned} \tag{F.49}$$

Combining these results, we find that all IR divergences perfectly cancel, such that the final results read

$$\Gamma^{(2)}(0, \mu, 0, q) = \frac{d_\gamma}{4\pi} h^2 \ln \left(\frac{|(2\mu)^2 - q^2|}{(h\sigma_0)^2} \right), \quad (\text{F.56})$$

$$\Gamma^{(2)}(0, \mu, 0, 0) = \frac{d_\gamma}{4\pi} h^2 \ln \left(\frac{(2\mu)^2}{(h\sigma_0)^2} \right). \quad (\text{F.57})$$

To study the cases where $T = 0$, $\mu = 0$, but $\sigma \neq 0$ we can again use Eqs. (F.49) and (F.50) and just set $\mu = 0$,

$$\Gamma^{(2)}(\sigma, 0, 0, q) = \frac{d_\gamma}{2\pi} h^2 \left[\frac{1}{2} \ln \left(\frac{(h\sigma)^2}{(h\sigma_0)^2} \right) + \sqrt{1 + \frac{(2h\sigma)^2}{q^2}} \operatorname{arccoth} \left(\sqrt{1 + \frac{(2h\sigma)^2}{q^2}} \right) \right], \quad (\text{F.58})$$

$$\Gamma^{(2)}(\sigma, 0, 0, 0) = \frac{d_\gamma}{2\pi} h^2 \left[\frac{1}{2} \ln \left(\frac{(h\sigma)^2}{(h\sigma_0)^2} \right) + 1 \right]. \quad (\text{F.59})$$

Both expressions are consistent for $\sigma \neq 0$ because of Eq. (F.51).

However, keeping $q \neq 0$ and sending $\sigma \rightarrow 0$, we can use Eq. (F.54) to derive the last renormalized result

$$\Gamma^{(2)}(0, 0, 0, q) = \frac{d_\gamma}{4\pi} h^2 \ln \left(\frac{q^2}{(h\sigma_0)^2} \right). \quad (\text{F.60})$$

The same result is found, by setting $\mu = 0$ in Eq. (F.56).

For $T = \mu = q = 0$ and $\sigma \rightarrow 0$ the bosonic two-point function diverges.

F.1.4. The bosonic wave-function renormalization

In this appendix we present detailed calculations for the bosonic wave-function renormalization $Z_\sigma(\sigma, \mu, T)$ in the mean-field approximation. We start with the derivation of Eq. (11.44), which is the generic formula for $Z_\sigma(\sigma, \mu, T)$ before the Matsubara sums are performed. Afterwards, we evaluate this result as far as possible in terms of known functions and regularize and renormalize divergent contributions, if needed. However, some leftover integrals still call for a numerical treatment. Finally, we end up with eight different cases for $Z_\sigma(\sigma, \mu, T)$, where σ , μ , and T take either values that are zero or non-zero.

The starting point for the derivation of Eq. (11.44) is the generic formula for the bosonic two-point function in Eq. (11.46). The bosonic wave-function renormalization is defined as the second-order coefficient of the Taylor series of $\Gamma^{(2)}(\sigma, \mu, T, q)$ in q about $q = 0$, as long as $\Gamma^{(2)}(\sigma, \mu, T, q)$ is expandable about $q = 0$. A straightforward calculation demonstrates the correctness of Eq. (11.44),

$$\begin{aligned} Z_\sigma(\sigma, \mu, T) &\equiv \quad (\text{F.61}) \\ &\equiv \frac{1}{2} \frac{d^2 \Gamma^{(2)}(\sigma, \mu, T, q)}{dq^2} \Big|_{q=0} = \\ &= -\frac{d_\gamma h^2}{2} \int_{-\infty}^{\infty} \frac{dp}{(2\pi)} T \sum_{n=-\infty}^{\infty} \frac{1}{(\nu_n + i\mu)^2 + E^2} \frac{d^2}{dq^2} \left[\frac{pq - 2(h\sigma)^2}{(\nu_n + i\mu)^2 + E_q^2} \right] \Big|_{q=0} = \\ &= -\frac{d_\gamma h^2}{2} \int_{-\infty}^{\infty} \frac{dp}{(2\pi)} T \sum_{n=-\infty}^{\infty} \frac{1}{(\nu_n + i\mu)^2 + E^2} \times \end{aligned}$$

$$\begin{aligned}
& \times \frac{d}{dq} \left[\frac{p}{(\nu_n + i\mu)^2 + E_q^2} - \frac{2(p+q)[pq - 2(h\sigma)^2]}{[(\nu_n + i\mu)^2 + E_q^2]^2} \right] \Big|_{q=0} = \\
& = -\frac{d_\gamma h^2}{2} \int_{-\infty}^{\infty} \frac{dp}{(2\pi)} T \sum_{n=-\infty}^{\infty} \frac{1}{(\nu_n + i\mu)^2 + E^2} \times \\
& \times \left[-\frac{4(p+q)p + 2[pq - 2(h\sigma)^2]}{[(\nu_n + i\mu)^2 + E_q^2]^2} + \frac{8(p+q)^2[pq - 2(h\sigma)^2]}{[(\nu_n + i\mu)^2 + E_q^2]^3} \right] \Big|_{q=0} = \\
& = -\frac{d_\gamma h^2}{2} \int_{-\infty}^{\infty} \frac{dp}{(2\pi)} T \sum_{n=-\infty}^{\infty} \left[-\frac{4p^2}{[(\nu_n + i\mu)^2 + E^2]^3} + \frac{4(h\sigma)^2}{[(\nu_n + i\mu)^2 + E^2]^3} - \right. \\
& \quad \left. - \frac{16p^2(h\sigma)^2}{[(\nu_n + i\mu)^2 + E^2]^4} \right] = \\
& = -\frac{d_\gamma h^2}{2} \int_{-\infty}^{\infty} \frac{dp}{(2\pi)} T \sum_{n=-\infty}^{\infty} \left[p \left(\frac{d}{dp} \frac{1}{[(\nu_n + i\mu)^2 + E^2]^2} \right) + \frac{4(h\sigma)^2}{[(\nu_n + i\mu)^2 + E^2]^3} + \right. \\
& \quad \left. + p \left(\frac{d}{dp} \frac{\frac{8}{3}(h\sigma)^2}{[(\nu_n + i\mu)^2 + E^2]^3} \right) \right] = \\
& = \frac{d_\gamma h^2}{2} \int_{-\infty}^{\infty} \frac{dp}{(2\pi)} T \sum_{n=-\infty}^{\infty} \left(\frac{1}{[(\nu_n + i\mu)^2 + E^2]^2} - \frac{\frac{4}{3}(h\sigma)^2}{[(\nu_n + i\mu)^2 + E^2]^3} \right).
\end{aligned}$$

It remains to perform the Matsubara sums, which can be evaluated by hand. Using the results of the sums (B.20) and (B.23) and identities (B.2), (B.4), and (B.6) one finds

$$\begin{aligned}
& Z_\sigma(\sigma, \mu, T) = \tag{F.62} \\
& = \frac{d_\gamma h^2}{16\pi} \left[\int_{-\infty}^{\infty} dp \frac{1}{E^3} (1 - n_f(\frac{E+\mu}{T}) - n_f(\frac{E-\mu}{T})) + \right. \\
& \quad + \frac{E}{T} [n_f^2(\frac{E+\mu}{T}) + n_f^2(\frac{E-\mu}{T}) - n_f(\frac{E+\mu}{T}) - n_f(\frac{E-\mu}{T})] - \\
& \quad - (h\sigma)^2 \int_{-\infty}^{\infty} dp \frac{1}{E^5} (1 - n_f(\frac{E+\mu}{T}) - n_f(\frac{E-\mu}{T})) + \\
& \quad + \frac{E}{T} [n_f^2(\frac{E+\mu}{T}) + n_f^2(\frac{E-\mu}{T}) - n_f(\frac{E+\mu}{T}) - n_f(\frac{E-\mu}{T})] - \\
& \quad - \frac{1}{3} \frac{E^2}{T^2} [2n_f^3(\frac{E+\mu}{T}) + 2n_f^3(\frac{E-\mu}{T}) - 3n_f^2(\frac{E+\mu}{T}) - 3n_f^2(\frac{E-\mu}{T}) + \\
& \quad \left. + n_f(\frac{E+\mu}{T}) + n_f(\frac{E-\mu}{T})] \right] = \\
& = \frac{d_\gamma h^2}{16\pi} \left[\int_{-\infty}^{\infty} dp \frac{1}{E^3} \left(\frac{1}{2} \tanh\left(\frac{E+\mu}{2T}\right) + \frac{1}{2} \tanh\left(\frac{E-\mu}{2T}\right) - \frac{\frac{E}{2T}}{2 \cosh^2(\frac{E+\mu}{2T})} - \frac{\frac{E}{2T}}{2 \cosh^2(\frac{E-\mu}{2T})} \right) - \right. \\
& \quad - (h\sigma)^2 \int_{-\infty}^{\infty} dp \frac{1}{E^5} \left(\frac{1}{2} \tanh\left(\frac{E+\mu}{2T}\right) + \frac{1}{2} \tanh\left(\frac{E-\mu}{2T}\right) - \frac{\frac{E}{2T}}{2 \cosh^2(\frac{E+\mu}{2T})} - \frac{\frac{E}{2T}}{2 \cosh^2(\frac{E-\mu}{2T})} - \right. \\
& \quad \left. \left. - \frac{1}{3} \frac{(\frac{E}{2T})^2 \sinh(\frac{E+\mu}{2T})}{\cosh^3(\frac{E+\mu}{2T})} - \frac{1}{3} \frac{(\frac{E}{2T})^2 \sinh(\frac{E-\mu}{2T})}{\cosh^3(\frac{E-\mu}{2T})} \right) \right].
\end{aligned}$$

This is our starting point for a detailed analysis of the various cases.

First, we analyze this result for non-zero temperatures, $T \neq 0$, and $\sigma \neq 0$ as well as $\mu \neq 0$. In this setup, all terms that are contributing to $Z_\sigma(\sigma, \mu, T)$ are UV- and IR-finite. However, the only contributions which can be further simplified are the two vacuum contributions,

$$\int_{-\infty}^{\infty} dp \frac{1}{E^3} = \frac{2}{(h\sigma)^2}, \quad \int_{-\infty}^{\infty} dp \frac{1}{E^5} = \frac{4}{3} \frac{1}{(h\sigma)^4}. \quad (\text{F.63})$$

Hence, the first (renormalized) result reads,

$$\begin{aligned} Z_\sigma(\sigma, \mu, T) &= \quad (\text{F.64}) \\ &= \frac{d_\gamma h^2}{8\pi} \left[\frac{1}{3} \frac{1}{(h\sigma)^2} - \int_0^\infty dp \frac{1}{E^3} (n_f(\frac{E+\mu}{T}) + n_f(\frac{E-\mu}{T}) - \right. \\ &\quad \left. - \frac{E}{T} [n_f^2(\frac{E+\mu}{T}) + n_f^2(\frac{E-\mu}{T}) - n_f(\frac{E+\mu}{T}) - n_f(\frac{E-\mu}{T})] \right) + \\ &\quad + (h\sigma)^2 \int_0^\infty dp \frac{1}{E^5} (n_f(\frac{E+\mu}{T}) + n_f(\frac{E-\mu}{T}) - \\ &\quad \left. - \frac{E}{T} [n_f^2(\frac{E+\mu}{T}) + n_f^2(\frac{E-\mu}{T}) - n_f(\frac{E+\mu}{T}) - n_f(\frac{E-\mu}{T})] \right) + \\ &\quad \left. + \frac{1}{3} \frac{E^2}{T^2} [2 n_f^3(\frac{E+\mu}{T}) + 2 n_f^3(\frac{E-\mu}{T}) - 3 n_f^2(\frac{E+\mu}{T}) - 3 n_f^2(\frac{E-\mu}{T}) + \right. \\ &\quad \left. + n_f(\frac{E+\mu}{T}) + n_f(\frac{E-\mu}{T})] \right] = \\ &= \frac{d_\gamma h^2}{8\pi} \left[\frac{1}{3} \frac{1}{(h\sigma)^2} - \int_0^\infty dp \frac{1}{E^3} \left(1 - \frac{1}{2} \tanh\left(\frac{E+\mu}{2T}\right) - \frac{1}{2} \tanh\left(\frac{E-\mu}{2T}\right) + \right. \right. \\ &\quad \left. \left. + \frac{\frac{E}{2T}}{2 \cosh^2(\frac{E+\mu}{2T})} + \frac{\frac{E}{2T}}{2 \cosh^2(\frac{E-\mu}{2T})} \right) + \right. \\ &\quad \left. + (h\sigma)^2 \int_0^\infty dp \frac{1}{E^5} \left(1 - \frac{1}{2} \tanh\left(\frac{E+\mu}{2T}\right) - \frac{1}{2} \tanh\left(\frac{E-\mu}{2T}\right) + \frac{\frac{E}{2T}}{2 \cosh^2(\frac{E+\mu}{2T})} + \frac{\frac{E}{2T}}{2 \cosh^2(\frac{E-\mu}{2T})} + \right. \right. \\ &\quad \left. \left. + \frac{1}{3} \frac{(\frac{E}{2T})^2 \sinh(\frac{E+\mu}{2T})}{\cosh^3(\frac{E+\mu}{2T})} + \frac{1}{3} \frac{(\frac{E}{2T})^2 \sinh(\frac{E-\mu}{2T})}{\cosh^3(\frac{E-\mu}{2T})} \right) \right]. \end{aligned}$$

The same result is obtained when $\frac{1}{2} \frac{d^2}{dq^2}$ is directly applied to the renormalized bosonic two-point function (F.32) and evaluated for $q \rightarrow 0$. This was cross-checked using MATHEMATICA [147].

The more tricky scenario at non-zero temperature is when $\sigma = 0$, because the first integral in Eq. (F.62) is strongly IR-divergent without the fermion mass $(h\sigma)^2$ in the energies E . The second integral does no longer contribute to $Z_\sigma(\sigma, \mu, T)$, due to the $(h\sigma)^2$ prefactor. This is easily understood from the last line of Eq. (F.61), where the Matsubara sums are not yet evaluated. Consequently, within the following steps it is required to introduce a (dimensionless) IR-cutoff ε , which is removed after renormalization. To this end we also substitute $t = \frac{p}{T}$ during the calculation.

$$Z_\sigma(0, \mu, T) = \quad (\text{F.65})$$

$$\begin{aligned}
&= \frac{d_\gamma h^2}{8\pi} \int_0^\infty dp \frac{1}{p^3} (1 - n_f(\frac{p+\mu}{T}) - n_f(\frac{p-\mu}{T}) + \\
&\quad + \frac{p}{T} [n_f^2(\frac{p+\mu}{T}) + n_f^2(\frac{p-\mu}{T}) - n_f(\frac{p+\mu}{T}) - n_f(\frac{p-\mu}{T})]) = \\
&= -\frac{d_\gamma h^2}{8\pi} \frac{1}{T^2} \lim_{\varepsilon \rightarrow 0} \int_\varepsilon^\infty dt \frac{1}{t} \frac{\partial}{\partial t} (\frac{1}{t} [1 - n_f(t + \frac{\mu}{T}) - n_f(t - \frac{\mu}{T})]) = \\
&= -\frac{d_\gamma h^2}{8\pi} \frac{1}{T^2} \lim_{\varepsilon \rightarrow 0} \left[\frac{1}{t^2} [1 - n_f(t + \frac{\mu}{T}) - n_f(t - \frac{\mu}{T})]_\varepsilon^\infty + \int_\varepsilon^\infty dt \frac{1}{t^3} + \right. \\
&\quad \left. + \lim_{s \rightarrow -2} \Gamma(s) [\text{Li}_s(\varepsilon, -\exp(\frac{\mu}{T})) + \text{Li}_s(\varepsilon, -\exp(-\frac{\mu}{T}))] \right] = \\
&= -\frac{d_\gamma h^2}{8\pi} \frac{1}{T^2} \left[-\frac{1}{2 \cosh^2(\frac{\mu}{2T})} \lim_{\varepsilon \rightarrow 0} \frac{1}{\varepsilon} + \frac{1}{2} \lim_{\varepsilon \rightarrow 0} \frac{1}{\varepsilon^2} + \right. \\
&\quad \left. + \frac{1}{2} \text{DLi}_{-2}(\frac{\mu}{T}) - \frac{1}{2} \lim_{\varepsilon \rightarrow 0} \frac{1}{\varepsilon^2} + \frac{1}{2 \cosh^2(\frac{\mu}{T})} \lim_{\varepsilon \rightarrow 0} \frac{1}{\varepsilon} \right] = \\
&= -\frac{d_\gamma h^2}{16\pi} \frac{1}{T^2} \text{DLi}_{-2}(\frac{\mu}{T}).
\end{aligned}$$

In this calculation, we first used integration by parts to formulate the problem in terms of (incomplete) polylogarithms Eq. (A.61). The last step, the limit $s \rightarrow -2$, which corresponds to a careful extraction of the IR divergences, is actually derived in Eq. (A.97). Since all IR-cutoff dependent terms cancel exactly, the cutoff is easily removed from the final result.

Again, we cross-checked our result with directly taking the derivative of Eq. (F.36) w.r.t. q and evaluating at $q = 0$.

A result that trivially follows from Eq. (F.64) for $\sigma \neq 0$, $\mu = 0$, and $T \neq 0$ is

$$\begin{aligned}
Z_\sigma(\sigma, 0, T) &= \tag{F.66} \\
&= \frac{d_\gamma h^2}{8\pi} \left[\frac{1}{3} \frac{1}{(h\sigma)^2} - 2 \int_0^\infty dp \frac{1}{E^3} (n_f(\frac{E}{T}) - \frac{E}{T} [n_f^2(\frac{E}{T}) - n_f(\frac{E}{T})]) + \right. \\
&\quad + 2 (h\sigma)^2 \int_0^\infty dp \frac{1}{E^5} (n_f(\frac{E}{T}) - \frac{E}{T} [n_f^2(\frac{E}{T}) - n_f(\frac{E}{T})]) + \\
&\quad \left. + \frac{1}{3} \frac{E^2}{T^2} [2 n_f^3(\frac{E}{T}) - 3 n_f^2(\frac{E}{T}) + n_f(\frac{E}{T})] \right] = \\
&= \frac{d_\gamma h^2}{8\pi} \left[\frac{1}{3} \frac{1}{(h\sigma)^2} - \int_0^\infty dp \frac{1}{E^3} \left(1 - \tanh\left(\frac{E}{2T}\right) + 2 \frac{\frac{E}{2T}}{2 \cosh^2(\frac{E}{2T})} \right) + \right. \\
&\quad \left. + (h\sigma)^2 \int_0^\infty dp \frac{1}{E^5} \left(1 - \tanh\left(\frac{E}{2T}\right) + 2 \frac{\frac{E}{2T}}{2 \cosh^2(\frac{E}{2T})} + \frac{2}{3} \frac{(\frac{E}{2T})^2 \sinh(\frac{E}{2T})}{\cosh^3(\frac{E}{2T})} \right) \right].
\end{aligned}$$

The last case, where $T \neq 0$, but $\sigma = 0$ and $\mu = 0$ can be derived from Eq. (F.65) making use of Eq. (A.84),

$$Z_\sigma(0, 0, T) = \frac{7d_\gamma h^2}{32\pi^3} \frac{1}{T^2} \zeta(3). \tag{F.67}$$

Next, we turn to the zero-temperature results for the bosonic wave-function renormalization. In this limit, the powers and combinations of the Fermi-Dirac distribution functions turn into

Heaviside functions, Dirac delta distributions and derivatives of the latter, *cf.* Appendix B.1. We find,

$$\begin{aligned}
Z_\sigma(\sigma, \mu, 0) &= \tag{F.68} \\
&= \frac{d_\gamma h^2}{8\pi} \left[\frac{1}{3} \frac{1}{(h\sigma)^2} - \int_0^\infty dp \frac{1}{E^3} \Theta\left(\frac{|\mu|}{E} - 1\right) - \frac{1}{|\mu|} \int_0^\infty dp \frac{1}{E^2} \left[\delta\left(\frac{E}{|\mu|} + 1\right) + \delta\left(\frac{E}{|\mu|} - 1\right) \right] + \right. \\
&\quad + (h\sigma)^2 \left(\int_0^\infty dp \frac{1}{E^5} \Theta\left(\frac{|\mu|}{E} - 1\right) + \frac{1}{|\mu|} \int_0^\infty dp \frac{1}{E^4} \left[\delta\left(\frac{E}{|\mu|} + 1\right) + \delta\left(\frac{E}{|\mu|} - 1\right) \right] - \right. \\
&\quad \left. \left. - \frac{1}{3\mu^2} \int_0^\infty dp \frac{1}{E^3} \left[\delta'\left(\frac{E}{|\mu|} + 1\right) + \delta'\left(\frac{E}{|\mu|} - 1\right) \right] \right) \right] = \\
&= \frac{d_\gamma h^2}{24\pi} \frac{1}{(h\sigma)^2} - \frac{d_\gamma h^2}{24\pi} \frac{1}{(h\sigma)^2} \begin{cases} \frac{1}{\left(1 - \frac{(h\sigma)^2}{\mu^2}\right)^{\frac{3}{2}}}, & \text{if } (h\sigma)^2 < \mu^2, \\ 0, & \text{if } (h\sigma)^2 \geq \mu^2. \end{cases}
\end{aligned}$$

Here, we used Eqs. (F.46) and (F.47) for the integrals in the second line. The first integral in the third line evaluates to

$$\begin{aligned}
(h\sigma)^2 \int_0^\infty dp \frac{1}{E^5} \Theta\left(\frac{|\mu|}{E} - 1\right) &= \tag{F.69} \\
&= \frac{1}{3} \frac{1}{(h\sigma)^2} \begin{cases} 3 \left(1 - \frac{(h\sigma)^2}{\mu^2}\right)^{\frac{1}{2}} - \left(1 - \frac{(h\sigma)^2}{\mu^2}\right)^{\frac{3}{2}}, & \text{if } (h\sigma)^2 < \mu^2, \\ 0, & \text{if } (h\sigma)^2 \geq \mu^2, \end{cases}
\end{aligned}$$

while the second integral in the third line is

$$\frac{(h\sigma)^2}{|\mu|} \int_0^\infty dp \frac{1}{E^4} \left[\delta\left(\frac{E}{|\mu|} + 1\right) + \delta\left(\frac{E}{|\mu|} - 1\right) \right] = \begin{cases} \frac{(h\sigma)^2}{\mu^4} \frac{1}{\left(1 - \frac{(h\sigma)^2}{\mu^2}\right)^{\frac{1}{2}}} & \text{if } (h\sigma)^2 < \mu^2, \\ 0 & \text{if } (h\sigma)^2 \geq \mu^2. \end{cases} \tag{F.70}$$

The last integral involving the derivatives of the Dirac delta distribution yields,

$$\begin{aligned}
-\frac{1}{3|\mu|} \int_0^\infty dp \frac{1}{E^3} \left[\delta'\left(\frac{E}{|\mu|} + 1\right) + \delta'\left(\frac{E}{|\mu|} - 1\right) \right] &= \tag{F.71} \\
&= \begin{cases} -\frac{1}{3} \frac{1}{(h\sigma)^2} \frac{(h\sigma)^4}{\mu^4} \frac{1}{\left(1 - \frac{(h\sigma)^2}{\mu^2}\right)^{\frac{1}{2}}} \left[\frac{1}{\left(1 - \frac{(h\sigma)^2}{\mu^2}\right)} + 2 \right] & \text{if } (h\sigma)^2 < \mu^2, \\ 0 & \text{if } (h\sigma)^2 \geq \mu^2. \end{cases}
\end{aligned}$$

Altogether, we obtain a result that is also found when applying $\frac{1}{2} \frac{d^2}{dq^2}$ to Eq. (F.49) and evaluating the result at $q = 0$. This consistency check was explicitly done with MATHEMATICA [147].

If we want to study Eq. (F.68) for $\sigma = 0$, we need to consider the following asymptotic expansion,

$$\lim_{|\sigma| \rightarrow 0} \frac{1}{(h\sigma)^2} \left[1 - \frac{1}{\left(1 - \frac{(h\sigma)^2}{\mu^2}\right)^{\frac{3}{2}}} \right] = -\frac{3}{2\mu^2} + \mathcal{O}(\sigma^2). \tag{F.72}$$

We conclude,

$$Z_\sigma(0, \mu, 0) = -\frac{d_\gamma h^2}{16\pi} \frac{1}{\mu^2}. \quad (\text{F.73})$$

However, to study $\sigma \neq 0$ in vacuum, we merely have to evaluate Eq. (F.68) at $\mu = 0$, which corresponds to the second case in the distinction of cases,

$$Z_\sigma(\sigma, 0, 0) = \frac{d_\gamma h^2}{24\pi} \frac{1}{(h\sigma)^2}. \quad (\text{F.74})$$

It is also possible to derive the last two results directly from Eqs. (F.56) and (F.58), which was explicitly checked. For $\sigma = 0$, $\mu = 0$, and $T = 0$, the bosonic wave-function renormalization diverges. Anyhow, this case is not physical.

F.2. Thermodynamic quantities

Here, we present calculations for some thermodynamic observables.

F.2.1. The pressure

Here, we provide the explicit expressions listed in Table 11.2a. First, we consider the pressure at non-zero temperature.

Subtracting the vacuum pressure (11.31) from Eq. (F.8) we find for $\sigma = 0$, $\mu \neq 0$ and $T \neq 0$,

$$p(0, \mu, T) = \frac{d_\gamma}{2\pi} \left[\frac{\pi^2}{6} T^2 + \frac{1}{2} \mu^2 - \frac{1}{4} (h\sigma_0)^2 \right], \quad (\text{F.75})$$

which is only physical in the \mathbb{Z}_2 -symmetric phase.

For $\sigma \neq 0$ and $\mu = 0$ we combine Eqs. (11.31) and (F.9) and find

$$p(\sigma, 0, T) = \frac{d_\gamma}{4\pi} \left[-\frac{1}{2} (h\sigma)^2 \left[\ln \left(\frac{(h\sigma)^2}{(h\sigma_0)^2} \right) - 1 \right] - \frac{1}{2} (h\sigma_0)^2 + \right. \\ \left. + 4 \int_0^\infty dp T \ln \left(1 + e^{-\frac{E}{T}} \right) \right]. \quad (\text{F.76})$$

This result can be used in the \mathbb{Z}_2 -symmetry broken phase along the T -axis.

From the above two results or by combining Eqs. (11.31) and (F.10) it directly follows that

$$p(0, 0, T) = \frac{d_\gamma}{2\pi} \left[\frac{\pi^2}{6} T^2 - \frac{1}{4} (h\sigma_0)^2 \right], \quad (\text{F.77})$$

which is physical on the T -axis above the critical temperature $T_c = \frac{e^\gamma}{\pi}$.

Next, we turn to $T = 0$ and find from Eqs. (11.31) and (F.11),

$$p(\sigma, \mu, 0) = \quad (\text{F.78}) \\ = -\frac{d_\gamma}{8\pi} \left[(h\sigma)^2 \left[\ln \left(\frac{(h\sigma)^2}{(h\sigma_0)^2} \right) - 1 \right] + (h\sigma_0)^2 \right] - \\ - \begin{cases} \frac{d_\gamma}{4\pi} (h\sigma)^2 \left[\operatorname{arsinh} \left(\sqrt{\frac{\mu^2}{(h\sigma)^2} - 1} \right) - \frac{\mu^2}{(h\sigma)^2} \sqrt{1 - \frac{(h\sigma)^2}{\mu^2}} \right], & \text{if } (h\sigma)^2 < \mu^2, \\ 0, & \text{if } (h\sigma)^2 \geq \mu^2. \end{cases}$$

Only the second case is physical for $\sigma \neq 0$.

For vanishing σ , the combination of Eqs. (11.31) and (F.12) or the limit $\sigma \rightarrow 0$ of the previous result yields

$$p(0, \mu, 0) = \frac{d_\gamma}{4\pi} \left[\mu^2 - \frac{1}{2} (h\sigma_0)^2 \right], \quad (\text{F.79})$$

which describes the physical situation in the \mathbb{Z}_2 -symmetric phase on the μ -axis. At $\mu = 0$ and $T = 0$, we obtain the physically relevant result from combining Eqs. (11.31) and (F.13),

$$p(\sigma, 0, 0) = -\frac{d_\gamma}{8\pi} \left[(h\sigma)^2 \left[\ln \left(\frac{(h\sigma)^2}{(h\sigma_0)^2} \right) - 1 \right] + (h\sigma_0)^2 \right], \quad (\text{F.80})$$

which vanishes for $\sigma = \sigma_0$ by construction. From Eqs. (11.31) and (F.14) we also find the non-physical expression,

$$p(0, 0, 0) = -\frac{d_\gamma}{8\pi} (h\sigma_0)^2. \quad (\text{F.81})$$

F.2.2. The baryon number density

In Section 11.2.4 we derived the formula for the baryon number density (11.35). Here, we derive the formula for the various limits and cases listed in Table 11.2b. We start with Eq. (11.35),

$$\begin{aligned} n(\sigma, \mu, T) &= -\frac{\partial}{\partial \mu} U(\sigma, \mu, T) = \quad (\text{F.82}) \\ &= -\frac{d_\gamma}{4\pi} \int_{-\infty}^{\infty} dp \left[n_f \left(\frac{E+\mu}{T} \right) - n_f \left(\frac{E-\mu}{T} \right) \right] = \\ &= -\frac{d_\gamma}{4\pi} \int_{-\infty}^{\infty} dp \left[-\frac{1}{2} \tanh \left(\frac{E+\mu}{2T} \right) + \frac{1}{2} \tanh \left(\frac{E-\mu}{2T} \right) \right]. \end{aligned}$$

For $\sigma = 0$ we identify the integral as a Fermi-Dirac integral (A.86) with $s = 0$, thus Eq. (A.91), which can be solved analytically,

$$\begin{aligned} n(0, \mu, T) &= -\frac{d_\gamma}{4\pi} \int_{-\infty}^{\infty} dp \left[n_f \left(\frac{p+\mu}{T} \right) - n_f \left(\frac{p-\mu}{T} \right) \right] = \quad (\text{F.83}) \\ &= -\frac{d_\gamma}{2\pi} T \int_0^{\infty} dt \left[n_f \left(t + \frac{\mu}{T} \right) - n_f \left(t - \frac{\mu}{T} \right) \right] = \\ &= -\frac{d_\gamma}{2\pi} T \Gamma(1) \left[F_0 \left(-\frac{\mu}{T} \right) - F_0 \left(\frac{\mu}{T} \right) \right] = \\ &= -\frac{d_\gamma}{2\pi} T \ln \left(\frac{1+e^{-\frac{\mu}{T}}}{1+e^{\frac{\mu}{T}}} \right) = \\ &= \frac{d_\gamma}{2\pi} \mu. \end{aligned}$$

This expression is the physical result in the \mathbb{Z}_2 -symmetric phase at non-zero μ and non-zero T and consistent with taking the negative of the μ -derivative of Eq. (F.8).

The baryon number density is anti-symmetric in μ and therefore vanishes for $\mu = 0$ along the T -axis of the phase diagram, independent of whether one is in the \mathbb{Z}_2 -symmetric or symmetry broken phase, hence independent of σ ,

$$n(\sigma, 0, T) = 0, \quad (\text{F.84})$$

$$n(0, 0, T) = 0, \quad (\text{F.85})$$

Assuming $\sigma \neq 0$, one finds along the μ -axis for $T = 0$ from Eq. (B.11),

$$n(\sigma, \mu, 0) = \frac{d_\gamma}{2\pi} \operatorname{sgn}(\mu) \int_0^\infty dp \Theta\left(\frac{|\mu|}{E} - 1\right) = \begin{cases} \frac{d_\gamma}{2\pi} \mu \sqrt{1 - \frac{(h\sigma)^2}{\mu^2}} & \text{if } (h\sigma)^2 < \mu^2, \\ 0 & \text{if } (h\sigma)^2 \geq \mu^2. \end{cases} \quad (\text{F.86})$$

This result is consistent with taking the negative μ -derivative of Eq. (F.11). The upper case, where $(h\sigma)^2 < \mu^2$ is of physical relevance in the \mathbb{Z}_2 -symmetric phase for $T = 0$, where σ is evaluated at the trivial minimum, thus $\sigma = 0$. In this scenario, the expression further simplifies and we again obtain Eq. (F.83), which is T -independent,

$$n(0, \mu, 0) = \frac{d_\gamma}{2\pi} \mu, \quad (\text{F.87})$$

In the \mathbb{Z}_2 -symmetry broken phase $(h\sigma)^2$ evaluated at the physical minimum is always larger than μ^2 and the second case of Eq. (F.86) applies where the baryon density vanishes. In vacuum, $\mu = 0$ and $T = 0$,

$$n(\sigma, 0, 0) = 0, \quad (\text{F.88})$$

$$n(0, 0, 0) = 0. \quad (\text{F.89})$$

Even though both expressions are consistent with all previous equations, the physical situation for $\mu = 0$ and $T = 0$ is described by a non-vanishing condensate, thus Eq. (F.88).

F.2.3. The internal energy

The internal energy density is discussed for all limiting cases of Table 11.2c. We start by considering Eq. (11.40),

$$\begin{aligned} \mathcal{E}(\sigma, \mu, T) &= \frac{d_\gamma}{4\pi} \left[\frac{1}{2} (h\sigma)^2 \left[\ln\left(\frac{(h\sigma)^2}{(h\sigma_0)^2}\right) - 1 \right] + \frac{1}{2} (h\sigma_0)^2 + \right. \\ &\quad \left. + \int_{-\infty}^{\infty} dp E \left[n_f\left(\frac{E+\mu}{T}\right) + n_f\left(\frac{E-\mu}{T}\right) \right] \right]. \end{aligned} \quad (\text{F.90})$$

Using the definition of the Fermi-Dirac integral (A.86) and relation (A.92), one arrives at

$$\begin{aligned} \mathcal{E}(0, \mu, T) &= \frac{d_\gamma}{4\pi} \left[\frac{1}{2} (h\sigma_0)^2 + 2 \int_0^\infty dp p \left[n_f\left(\frac{p+\mu}{T}\right) + n_f\left(\frac{p-\mu}{T}\right) \right] \right] = \\ &= \frac{d_\gamma}{2\pi} \left[\frac{1}{4} (h\sigma_0)^2 + T^2 \left[F_1\left(-\frac{\mu}{T}\right) + F_1\left(\frac{\mu}{T}\right) \right] \right] = \\ &= \frac{d_\gamma}{2\pi} \left[\frac{1}{4} (h\sigma_0)^2 + \frac{\pi^2}{6} T^2 + \frac{1}{2} \mu^2 \right]. \end{aligned} \quad (\text{F.91})$$

Keeping $\sigma \neq 0$ but setting $\mu = 0$ in Eq. (F.90) only the momentum integral simplifies,

$$\mathcal{E}(\sigma, 0, T) = \frac{d_\gamma}{4\pi} \left[\frac{1}{2} (h\sigma)^2 \left[\ln\left(\frac{(h\sigma)^2}{(h\sigma_0)^2}\right) - 1 \right] + \frac{1}{2} (h\sigma_0)^2 + 4 \int_0^\infty dp E n_f\left(\frac{E}{T}\right) \right]. \quad (\text{F.92})$$

However, for $\sigma = 0$ the previous expression can be written in terms of Fermi-Dirac integral (A.86) and one can use relation (A.92),

$$\begin{aligned}\mathcal{E}(0, 0, T) &= \frac{d_\gamma}{4\pi} \left[\frac{1}{2} (h\sigma_0)^2 + 4 \int_0^\infty dp p n_f\left(\frac{p}{T}\right) \right] = \\ &= \frac{d_\gamma}{2\pi} \left[\frac{1}{4} (h\sigma_0)^2 + 2 T^2 F_1(0) \right] = \\ &= \frac{d_\gamma}{2\pi} \left[\frac{1}{4} (h\sigma_0)^2 + \frac{\pi^2}{6} T^2 \right],\end{aligned}\tag{F.93}$$

which is consistent with $\mu = 0$ in Eq. (F.91).

Equation (F.90) at vanishing temperature is evaluated as follows,

$$\begin{aligned}\mathcal{E}(\sigma, \mu, 0) &= \frac{d_\gamma}{4\pi} \left[\frac{1}{2} (h\sigma)^2 \left[\ln\left(\frac{(h\sigma)^2}{(h\sigma_0)^2}\right) - 1 \right] + \frac{1}{2} (h\sigma_0)^2 + 2 \int_0^\infty dp E \Theta\left(\frac{|\mu|}{E} - 1\right) \right] \\ &= \frac{d_\gamma}{8\pi} \left[(h\sigma)^2 \left[\ln\left(\frac{(h\sigma)^2}{(h\sigma_0)^2}\right) - 1 \right] + (h\sigma_0)^2 \right] + \\ &\quad + \frac{d_\gamma}{2\pi} \begin{cases} \frac{1}{2} \mu^2 \left[\sqrt{1 - \frac{(h\sigma)^2}{\mu^2}} + \frac{(h\sigma)^2}{\mu^2} \operatorname{arsinh}\left(\sqrt{\frac{\mu^2}{(h\sigma)^2} - 1}\right) \right], & \text{if } (h\sigma)^2 < \mu^2, \\ 0, & \text{if } (h\sigma)^2 \geq \mu^2. \end{cases}\end{aligned}\tag{F.94}$$

Here, only the latter case corresponds to physically meaningful situations.

The correct limit of Eq. (F.94) for $\sigma \rightarrow 0$ and Eq. (F.91) for $T = 0$ is,

$$\mathcal{E}(0, \mu, 0) = \frac{d_\gamma}{2\pi} \left[\frac{1}{4} (h\sigma_0)^2 + \frac{1}{2} \mu^2 \right].\tag{F.95}$$

Consistently from Eqs. (F.92) and (F.94),

$$\mathcal{E}(\sigma, 0, 0) = \frac{d_\gamma}{8\pi} \left[(h\sigma)^2 \left[\ln\left(\frac{(h\sigma)^2}{(h\sigma_0)^2}\right) - 1 \right] + (h\sigma_0)^2 \right].\tag{F.96}$$

Finally and consistent with all above results, we find the non-physical expression

$$\mathcal{E}(0, 0, 0) = \frac{d_\gamma}{8\pi} (h\sigma_0)^2.\tag{F.97}$$

Part IV

Back matter

Bibliography

- [1] Adrian Koenigstein et al. “Numerical fluid dynamics for FRG flow equations: Zero-dimensional QFTs as numerical test cases. I. The $O(N)$ model”. In: *Phys. Rev. D* 106.6 (2022), p. 065012. DOI: [10.1103/PhysRevD.106.065012](https://doi.org/10.1103/PhysRevD.106.065012). arXiv: [2108.02504](https://arxiv.org/abs/2108.02504) [[cond-mat.stat-mech](#)] (cit. on pp. [III](#), [IV](#), [3](#), [5](#), [8](#), [9](#), [11](#), [18–20](#), [23](#), [37](#), [40](#), [41](#), [49](#), [53](#), [68](#), [71](#), [75](#), [79](#), [81](#), [82](#), [86](#), [88–96](#), [125](#), [165](#), [185](#), [193](#), [196](#), [198](#), [240](#), [293](#), [301](#)).
- [2] Adrian Koenigstein et al. “Numerical fluid dynamics for FRG flow equations: Zero-dimensional QFTs as numerical test cases. II. Entropy production and irreversibility of RG flows”. In: *Phys. Rev. D* 106.6 (2022), p. 065013. DOI: [10.1103/PhysRevD.106.065013](https://doi.org/10.1103/PhysRevD.106.065013). arXiv: [2108.10085](https://arxiv.org/abs/2108.10085) [[cond-mat.stat-mech](#)] (cit. on pp. [III](#), [IV](#), [3](#), [5](#), [8](#), [9](#), [11](#), [23](#), [37](#), [53](#), [59](#), [60](#), [71](#), [77](#), [79](#), [82](#), [95](#), [97–101](#), [125](#), [185](#), [193](#), [301](#)).
- [3] Martin J. Steil and Adrian Koenigstein. “Numerical fluid dynamics for FRG flow equations: Zero-dimensional QFTs as numerical test cases. III. Shock and rarefaction waves in RG flows reveal limitations of the $N \rightarrow \infty$ limit in $O(N)$ -type models”. In: *Phys. Rev. D* 106.6 (2022), p. 065014. DOI: [10.1103/PhysRevD.106.065014](https://doi.org/10.1103/PhysRevD.106.065014). arXiv: [2108.04037](https://arxiv.org/abs/2108.04037) [[cond-mat.stat-mech](#)] (cit. on pp. [III](#), [IV](#), [3](#), [5](#), [6](#), [8](#), [9](#), [11](#), [23](#), [27](#), [28](#), [30](#), [32–35](#), [37](#), [53](#), [57](#), [60](#), [63](#), [71](#), [74](#), [79](#), [86](#), [95](#), [102–104](#), [106–108](#), [112](#), [125](#), [185](#), [193](#), [301](#)).
- [4] Jonas Stoll et al. *Bosonic fluctuations in the (1 + 1)-dimensional Gross-Neveu(-Yukawa) model at varying μ and T and finite N* . Aug. 2021. arXiv: [2108.10616](https://arxiv.org/abs/2108.10616) [[hep-ph](#)] (cit. on pp. [III](#), [IV](#), [6](#), [53](#), [71](#), [73](#), [76](#), [79](#), [91](#), [93–95](#), [121](#), [125](#), [126](#), [134](#), [139](#), [141](#), [156](#), [166](#), [174](#), [177](#), [185](#), [188](#), [192](#), [193](#), [197](#), [198](#), [201](#), [208](#), [217](#), [229](#), [234–237](#), [241–244](#), [251](#), [301](#)).
- [5] Adrian Koenigstein et al. “Detecting inhomogeneous chiral condensation from the bosonic two-point function in the (1 + 1)-dimensional Gross-Neveu model in the mean-field approximation*”. In: *J. Phys. A* 55.37 (2022), p. 375402. DOI: [10.1088/1751-8121/ac820a](https://doi.org/10.1088/1751-8121/ac820a). arXiv: [2112.07024](https://arxiv.org/abs/2112.07024) [[hep-ph](#)] (cit. on pp. [III](#), [IV](#), [121](#), [124](#), [134](#), [141](#), [201](#), [216](#), [218](#), [220–222](#), [225](#), [226](#), [257](#), [260](#), [348](#), [359](#)).
- [6] Martin Jakob Steil. “From zero-dimensional theories to inhomogeneous phases with the functional renormalization group”. in preparation. PhD thesis. Technische Universität Darmstadt, 2022 (cit. on pp. [III](#), [115](#), [126](#), [174](#), [192](#), [229](#), [325](#)).
- [7] Jonas Stoll. “Das (1 + 1)-dimensionale Gross-Neveu-(Yukawa)-Modell jenseits des large- N -Limes”. Master thesis. Goethe University Frankfurt, 2021 (cit. on pp. [III](#), [126](#), [229](#)).
- [8] Niklas Zorbach. “Bosonische Fluktuationen im (1 + 1)-dimensionalen Gross-Neveu-Yukawa-Modell mit endlichen N ”. Master thesis. Goethe University Frankfurt, 2021 (cit. on pp. [III](#), [126](#), [229](#)).
- [9] Shahriyar Jafarzade, Adrian Koenigstein, and Francesco Giacosa. “Phenomenology of $J^{PC} = 3^{--}$ tensor mesons”. In: *Phys. Rev. D* 103.9 (May 2021), p. 096027. DOI: [10.1103/PhysRevD.103.096027](https://doi.org/10.1103/PhysRevD.103.096027). arXiv: [2101.03195](https://arxiv.org/abs/2101.03195) [[hep-ph](#)] (cit. on p. [IV](#)).
- [10] Francesco Giacosa, Adrian Koenigstein, and Robert D. Pisarski. “How the axial anomaly controls flavor mixing among mesons”. In: *Phys. Rev. D* 97.9 (May 2018), p. 091901. DOI: [10.1103/PhysRevD.97.091901](https://doi.org/10.1103/PhysRevD.97.091901). arXiv: [1709.07454](https://arxiv.org/abs/1709.07454) [[hep-ph](#)] (cit. on p. [IV](#)).

- [11] Walter Greiner, Ludwig Neise, and Horst Stöcker. *Thermodynamics and Statistical Mechanics*. Springer, New York, 1995. ISBN: 978-0-387-94299-5. DOI: [10.1007/978-1-4612-0827-3](https://doi.org/10.1007/978-1-4612-0827-3) (cit. on pp. [3](#), [12](#), [15](#), [18](#), [109](#), [214](#)).
- [12] Hagen Kleinert. *Path integrals in quantum mechanics, statistics, polymer physics, and financial markets*. 5th ed. World Scientific, May 2004, p. 1624. ISBN: 978-981-4273-55-8. DOI: [10.1142/7305](https://doi.org/10.1142/7305) (cit. on pp. [3](#), [12](#)).
- [13] Andreas Wipf. *Statistical Approach to Quantum Field Theory*. Lect.Notes Phys. 864. Berlin, Germany: Springer-Verlag, 2013. ISBN: 978-3-642-33104-6. DOI: [10.1007/978-3-642-33105-3](https://doi.org/10.1007/978-3-642-33105-3) (cit. on pp. [3](#), [18–20](#), [45](#), [73](#), [96](#), [97](#), [110](#), [143](#), [154](#), [156](#), [165](#), [211](#)).
- [14] Christof Gattringer, Verena Hermann, and Markus Limmer. “Fermion loop simulation of the lattice Gross-Neveu model”. In: *Phys. Rev. D* 76 (July 2007), p. 014503. DOI: [10.1103/PhysRevD.76.014503](https://doi.org/10.1103/PhysRevD.76.014503). arXiv: [0704.2277](https://arxiv.org/abs/0704.2277) [[hep-lat](#)] (cit. on p. [3](#)).
- [15] Kenneth G. Wilson. “Confinement of Quarks”. In: *Phys. Rev. D* 10 (Oct. 1974). Ed. by John C. Taylor, pp. 2445–2459. DOI: [10.1103/PhysRevD.10.2445](https://doi.org/10.1103/PhysRevD.10.2445) (cit. on p. [3](#)).
- [16] Gert Aarts. “Introductory lectures on lattice QCD at nonzero baryon number”. In: *J. Phys. Conf. Ser.* 706.2 (2016), p. 022004. DOI: [10.1088/1742-6596/706/2/022004](https://doi.org/10.1088/1742-6596/706/2/022004). arXiv: [1512.05145](https://arxiv.org/abs/1512.05145) [[hep-lat](#)] (cit. on pp. [4](#), [122](#)).
- [17] Casey E. Berger et al. “Complex Langevin and other approaches to the sign problem in quantum many-body physics”. In: *Phys. Rept.* 892 (Jan. 2021), pp. 1–54. DOI: [10.1016/j.physrep.2020.09.002](https://doi.org/10.1016/j.physrep.2020.09.002). arXiv: [1907.10183](https://arxiv.org/abs/1907.10183) [[cond-mat.quant-gas](#)] (cit. on p. [4](#)).
- [18] Steven Weinberg. *The quantum theory of fields: Modern applications*. Vol. 2. Cambridge, England, UK: Cambridge University Press, Aug. 1996. DOI: [10.1017/CB09781139644174](https://doi.org/10.1017/CB09781139644174) (cit. on pp. [4](#), [15](#), [130](#), [138](#), [142](#), [146](#), [165](#), [191](#)).
- [19] Michael E. Peskin and Daniel V. Schroeder. *An introduction to quantum field theory*. Reading, USA: Addison-Wesley, 1995. ISBN: 978-0-201-50397-5 (cit. on pp. [4](#), [12–15](#), [45](#), [55](#), [58](#), [130](#), [132](#), [142](#), [144](#), [147](#), [164](#), [168–170](#), [205](#), [265](#), [288](#), [289](#)).
- [20] Dirk H. Rischke. *Lecture notes on: Quantenfeldtheorie I + II*. [Online; accessed 2022.03.23]. 2021. URL: https://www.uni-frankfurt.de/65315388/Arbeitsgruppe_Dirk_Rischke (cit. on pp. [4](#), [12–15](#), [142](#), [144](#)).
- [21] Dirk H. Rischke. *Lecture notes on: Statistische Mechanik*. [Online; accessed 2022.03.23]. 2012. URL: https://www.uni-frankfurt.de/65315388/Arbeitsgruppe_Dirk_Rischke (cit. on p. [4](#)).
- [22] Joseph I. Kapusta and Charles Gale. *Finite-temperature field theory: Principles and applications*. Cambridge Monographs on Mathematical Physics. Cambridge University Press, 2011. ISBN: 978-0-521-17322-3, 978-0-521-82082-0, 978-0-511-22280-1. DOI: [10.1017/CB09780511535130](https://doi.org/10.1017/CB09780511535130) (cit. on pp. [4](#), [110](#), [143](#), [154](#), [156](#), [275](#), [280](#)).
- [23] Franco Strocchi. *An introduction to non-perturbative foundations of quantum field theory*. Vol. 158. Oxford University Press, Oxford, May 2013. ISBN: 978-0-19-967157-1. DOI: [10.1093/acprof:oso/9780199671571.001.0001](https://doi.org/10.1093/acprof:oso/9780199671571.001.0001) (cit. on pp. [4](#), [9](#), [23](#), [25](#), [26](#)).
- [24] Walter Greiner and Joachim Reinhardt. *Field quantization*. Springer, Berlin Heidelberg, 1996. ISBN: 978-3-540-78048-9. DOI: [10.1007/978-3-642-61485-9](https://doi.org/10.1007/978-3-642-61485-9) (cit. on pp. [4](#), [14](#), [15](#), [144](#), [265](#), [288](#)).
- [25] Walter Greiner and Reinhardt. *Quantum Electrodynamics*. 4th ed. Berlin, Heidelberg, Germany: Springer, 2009. ISBN: 978-3-540-87560-4. DOI: [10.1007/978-3-540-87561-1](https://doi.org/10.1007/978-3-540-87561-1) (cit. on p. [4](#)).
- [26] Peter Thomas Jahn, Guy D. Moore, and Daniel Robaina. “ $\chi_{\text{top}}(T \gg T_c)$ in pure-gluon QCD through reweighting”. In: *Phys. Rev. D* 98.5 (2018), p. 054512. DOI: [10.1103/PhysRevD.98.054512](https://doi.org/10.1103/PhysRevD.98.054512). arXiv: [1806.01162](https://arxiv.org/abs/1806.01162) [[hep-lat](#)] (cit. on p. [4](#)).

- [27] Philippe de Forcrand and Owe Philipsen. “The QCD phase diagram for small densities from imaginary chemical potential”. In: *Nucl. Phys. B* 642 (2002), pp. 290–306. DOI: [10.1016/S0550-3213\(02\)00626-0](https://doi.org/10.1016/S0550-3213(02)00626-0). arXiv: [hep-lat/0205016](https://arxiv.org/abs/hep-lat/0205016) (cit. on p. 4).
- [28] Gerardus 't Hooft. “A planar diagram theory for strong interactions”. In: *Nucl. Phys. B* 72.3 (Apr. 1974). Ed. by John C. Taylor, pp. 461–473. DOI: [10.1016/0550-3213\(74\)90154-0](https://doi.org/10.1016/0550-3213(74)90154-0) (cit. on pp. 4, 28).
- [29] Edward Witten. “Baryons in the $1/N$ expansion”. In: *Nucl. Phys. B* 160.1 (Nov. 1979), pp. 57–115. DOI: [10.1016/0550-3213\(79\)90232-3](https://doi.org/10.1016/0550-3213(79)90232-3) (cit. on pp. 4, 28).
- [30] Moshe Moshe and Jean Zinn-Justin. “Quantum field theory in the large N limit: A Review”. In: *Phys. Rept.* 385 (2003), pp. 69–228. DOI: [10.1016/S0370-1573\(03\)00263-1](https://doi.org/10.1016/S0370-1573(03)00263-1). arXiv: [hep-th/0306133](https://arxiv.org/abs/hep-th/0306133) (cit. on pp. 4, 28).
- [31] Juan Martin Maldacena. “The large N limit of superconformal field theories and supergravity”. In: *Int. J. Theor. Phys.* 38 (Apr. 1999), pp. 1113–1133. DOI: [10.1023/A:1026654312961](https://doi.org/10.1023/A:1026654312961). arXiv: [hep-th/9711200](https://arxiv.org/abs/hep-th/9711200) (cit. on pp. 4, 28).
- [32] Ofer Aharony et al. “Large N field theories, string theory and gravity”. In: *Phys. Rept.* 323 (Jan. 2000), pp. 183–386. DOI: [10.1016/S0370-1573\(99\)00083-6](https://doi.org/10.1016/S0370-1573(99)00083-6). arXiv: [hep-th/9905111](https://arxiv.org/abs/hep-th/9905111) (cit. on p. 4).
- [33] George B. Arfken and Hans J. Weber. *Mathematical Methods for Physicists*. 6. ed. California: Elsevier Academic Press, 2005 (cit. on pp. 4, 29, 363).
- [34] Christian S. Fischer. “QCD at finite temperature and chemical potential from Dyson–Schwinger equations”. In: *Prog. Part. Nucl. Phys.* 105 (Mar. 2019), pp. 1–60. DOI: [10.1016/j.pnpnp.2019.01.002](https://doi.org/10.1016/j.pnpnp.2019.01.002). arXiv: [1810.12938](https://arxiv.org/abs/1810.12938) [[hep-ph](#)] (cit. on p. 4).
- [35] Nicolas Dupuis et al. “The nonperturbative functional renormalization group and its applications”. In: *Phys. Rept.* 910 (May 2021), pp. 1–114. DOI: [10.1016/j.physrep.2021.01.001](https://doi.org/10.1016/j.physrep.2021.01.001). arXiv: [2006.04853](https://arxiv.org/abs/2006.04853) [[cond-mat.stat-mech](#)] (cit. on pp. 4, 5, 37, 38, 43, 47, 165, 187, 194, 288, 294).
- [36] Stefan Scherer. “Introduction to Chiral Perturbation Theory”. In: *Adv. Nucl. Phys.* 27 (2003). Ed. by John W. Negele and Erich W. Vogt, pp. 277–538. DOI: [10.1007/0-306-47916-8_2](https://doi.org/10.1007/0-306-47916-8_2). arXiv: [hep-ph/0210398](https://arxiv.org/abs/hep-ph/0210398) (cit. on p. 4).
- [37] Evgeny Epelbaum, Hans-Werner Hammer, and Ulf-G. Meissner. “Modern Theory of Nuclear Forces”. In: *Rev. Mod. Phys.* 81 (Dec. 2009), pp. 1773–1825. DOI: [10.1103/RevModPhys.81.1773](https://doi.org/10.1103/RevModPhys.81.1773). arXiv: [0811.1338](https://arxiv.org/abs/0811.1338) [[nucl-th](#)] (cit. on p. 4).
- [38] Mikhail A. Shifman. “Snapshots of hadrons or the story of how the vacuum medium determines the properties of the classical mesons which are produced, live and die in the QCD vacuum”. In: *Prog. Theor. Phys. Suppl.* 131 (1998), pp. 1–71. DOI: [10.1143/PTPS.131.1](https://doi.org/10.1143/PTPS.131.1). arXiv: [hep-ph/9802214](https://arxiv.org/abs/hep-ph/9802214) (cit. on p. 4).
- [39] Sam Treiman, Roman Jackiw, and David J. Gross. *Lectures on Current Algebra and Its Applications*. Princeton University Press, 1972. ISBN: 9781400871506. DOI: [doi:10.1515/9781400871506](https://doi.org/10.1515/9781400871506) (cit. on p. 4).
- [40] Edward Witten. “Anti-de Sitter space and holography”. In: *Adv. Theor. Math. Phys.* 2 (Jan. 1998), pp. 253–291. DOI: [10.4310/ATMP.1998.v2.n2.a2](https://doi.org/10.4310/ATMP.1998.v2.n2.a2). arXiv: [hep-th/9802150](https://arxiv.org/abs/hep-th/9802150) (cit. on p. 4).
- [41] Leonard Susskind. “The world as a hologram”. In: *J. Math. Phys.* 36 (June 1998), pp. 6377–6396. DOI: [10.1063/1.531249](https://doi.org/10.1063/1.531249). arXiv: [hep-th/9409089](https://arxiv.org/abs/hep-th/9409089) (cit. on p. 4).
- [42] Christof Wetterich. “The average action for scalar fields near phase transitions”. In: *Z. Phys. C* 57 (Sept. 1993), pp. 451–470. DOI: [10.1007/BF01474340](https://doi.org/10.1007/BF01474340) (cit. on pp. 5, 191).
- [43] Christof Wetterich. “Exact evolution equation for the effective potential”. In: *Phys. Lett. B* 301 (Feb. 1993), pp. 90–94. DOI: [10.1016/0370-2693\(93\)90726-X](https://doi.org/10.1016/0370-2693(93)90726-X). arXiv: [1710.05815](https://arxiv.org/abs/1710.05815) [[hep-th](#)] (cit. on p. 5).

- [44] Martin Reuter and Christof Wetterich. “Effective average action for gauge theories and exact evolution equations”. In: *Nucl. Phys. B* 417 (Apr. 1994), pp. 181–214. DOI: [10.1016/0550-3213\(94\)90543-6](https://doi.org/10.1016/0550-3213(94)90543-6) (cit. on p. 5).
- [45] Tim R. Morris. “The Exact Renormalization Group and approximate solutions”. In: *Int. J. Mod. Phys. A* 09.14 (June 1994), pp. 2411–2450. DOI: [10.1142/S0217751X94000972](https://doi.org/10.1142/S0217751X94000972). arXiv: [hep-ph/9308265](https://arxiv.org/abs/hep-ph/9308265) (cit. on p. 5).
- [46] Nikolaos Tetradis and Christof Wetterich. “Critical exponents from effective average action”. In: *Nucl. Phys. B* 422 (July 1994), pp. 541–592. DOI: [10.1016/0550-3213\(94\)90446-4](https://doi.org/10.1016/0550-3213(94)90446-4). arXiv: [hep-ph/9308214](https://arxiv.org/abs/hep-ph/9308214) (cit. on p. 5).
- [47] Ulrich Ellwanger. “Flow equations for N point functions and bound states”. In: *Z. Phys. C* 62 (Sept. 1994), pp. 503–510. DOI: [10.1007/BF01555911](https://doi.org/10.1007/BF01555911). arXiv: [hep-ph/9308260](https://arxiv.org/abs/hep-ph/9308260) (cit. on p. 5).
- [48] Ulrich Ellwanger, Manfred Hirsch, and Axel Weber. “Flow equations for the relevant part of the pure Yang-Mills action”. In: *Z. Phys. C* 69 (Dec. 1996), pp. 687–698. DOI: [10.1007/s002880050073](https://doi.org/10.1007/s002880050073). arXiv: [hep-th/9506019](https://arxiv.org/abs/hep-th/9506019) (cit. on p. 5).
- [49] Randall J. LeVeque. *Numerical methods for conservation laws*. 2nd ed. Basel: Birkhäuser, 1992. ISBN: 978-3-7643-2723-1. DOI: [10.1007/978-3-0348-8629-1](https://doi.org/10.1007/978-3-0348-8629-1) (cit. on pp. 5, 6, 8, 41, 54, 56, 60, 64, 65, 67–69, 72, 77, 100, 103).
- [50] Randall J. LeVeque. *Finite-volume methods for hyperbolic problems*. Cambridge Texts in Applied Mathematics. Cambridge University Press, 2002. ISBN: 9780511791253. DOI: [10.1017/CB09780511791253](https://doi.org/10.1017/CB09780511791253) (cit. on pp. 5, 6, 8, 41, 54, 56, 60, 65, 67–69, 72, 77, 103).
- [51] Jan S. Hesthaven and Tim Warburton. *Nodal Discontinuous Galerkin Methods: Algorithms, Analysis, and Applications*. 1st. Springer Publishing Company, Incorporated, 2007. DOI: [10.5555/1557392](https://doi.org/10.5555/1557392) (cit. on pp. 5, 6, 54, 56, 65, 67, 68, 72, 77, 103).
- [52] Luciano Rezzolla and Olindo Zanotti. *Relativistic hydrodynamics*. Oxford, England, UK: Oxford University Press, 2018. ISBN: 9780198807599. DOI: [10.1093/acprof:oso/9780198528906.001.0001](https://doi.org/10.1093/acprof:oso/9780198528906.001.0001) (cit. on pp. 5, 6, 54, 56, 67–69, 72, 77, 103).
- [53] Juergen Berges, Nikolaos Tetradis, and Christof Wetterich. “Nonperturbative renormalization flow in quantum field theory and statistical physics”. In: *Phys. Rept.* 363 (June 2002), pp. 223–386. DOI: [10.1016/S0370-1573\(01\)00098-9](https://doi.org/10.1016/S0370-1573(01)00098-9). arXiv: [hep-ph/0005122](https://arxiv.org/abs/hep-ph/0005122) (cit. on pp. 5, 37, 38, 47, 165, 288, 294).
- [54] Jan M. Pawłowski. “Aspects of the functional renormalisation group”. In: *Annals Phys.* 322 (Dec. 2007), pp. 2831–2915. DOI: [10.1016/j.aop.2007.01.007](https://doi.org/10.1016/j.aop.2007.01.007). arXiv: [hep-th/0512261](https://arxiv.org/abs/hep-th/0512261) (cit. on pp. 5, 16, 37, 38, 43, 165, 186, 285, 286, 288, 289, 300).
- [55] Holger Gies. “Introduction to the Functional RG and applications to gauge theories”. In: *Lect. Notes Phys.* 852 (June 2012), pp. 287–348. DOI: [10.1007/978-3-642-27320-9_6](https://doi.org/10.1007/978-3-642-27320-9_6). arXiv: [hep-ph/0611146](https://arxiv.org/abs/hep-ph/0611146) (cit. on pp. 5, 37, 38, 165, 288).
- [56] Bertrand Delamotte. “An introduction to the nonperturbative Renormalization Group”. In: *Lect. Notes Phys.* 852 (2012), pp. 49–132. DOI: [10.1007/978-3-642-27320-9_2](https://doi.org/10.1007/978-3-642-27320-9_2). arXiv: [cond-mat/0702365](https://arxiv.org/abs/cond-mat/0702365) (cit. on pp. 5, 37, 38, 47, 165, 288).
- [57] Peter Kopietz, Lorenz Bartosch, and Florian Schütz. *Introduction to the Functional Renormalization Group*. Vol. 798. Lecture Notes in Physics. Springer-Verlag Berlin Heidelberg, 2010. ISBN: 978-3-642-05093-0. DOI: [10.1007/978-3-642-05094-7](https://doi.org/10.1007/978-3-642-05094-7) (cit. on pp. 5, 37, 38, 47, 165, 186, 288).
- [58] Jan M. Pawłowski et al. “The functional renormalization group - applications to gauge theories and gravity”. unpublished lecture notes, in preparation (cit. on pp. 5, 165, 288).
- [59] Bernd-Jochen Schaefer and Jochen Wambach. “The phase diagram of the quark meson model”. In: *Nucl. Phys. A* 757 (Aug. 2005), pp. 479–492. DOI: [10.1016/j.nuclphysa.2005.04.012](https://doi.org/10.1016/j.nuclphysa.2005.04.012). arXiv: [nuc1-th/0403039](https://arxiv.org/abs/nuc1-th/0403039) (cit. on pp. 5, 73, 117).

- [60] Mario Mitter and Bernd-Jochen Schaefer. “Fluctuations and the axial anomaly with three quark flavors”. In: *Phys. Rev. D* 89.5 (Mar. 2014), p. 054027. DOI: [10.1103/PhysRevD.89.054027](https://doi.org/10.1103/PhysRevD.89.054027). arXiv: [1308.3176 \[hep-ph\]](https://arxiv.org/abs/1308.3176) (cit. on pp. 5, 303).
- [61] Konstantin Otto, Micaela Oertel, and Bernd-Jochen Schaefer. “Hybrid and quark star matter based on a nonperturbative equation of state”. In: *Phys. Rev. D* 101.10 (May 2020), p. 103021. DOI: [10.1103/PhysRevD.101.103021](https://doi.org/10.1103/PhysRevD.101.103021). arXiv: [1910.11929 \[hep-ph\]](https://arxiv.org/abs/1910.11929) (cit. on pp. 5, 123, 303).
- [62] Konstantin Otto, Micaela Oertel, and Bernd-Jochen Schaefer. “Nonperturbative quark matter equations of state with vector interactions”. In: *Eur. Phys. J. ST* 229.22-23 (Dec. 2020), pp. 3629–3649. DOI: [10.1140/epjst/e2020-000155-y](https://doi.org/10.1140/epjst/e2020-000155-y). arXiv: [2007.07394 \[hep-ph\]](https://arxiv.org/abs/2007.07394) (cit. on pp. 5, 123, 303).
- [63] Jürgen Eser et al. “Low-energy limit of the $O(4)$ quark-meson model from the functional renormalization group approach”. In: *Phys. Rev. D* 98.1 (July 2018), p. 014024. DOI: [10.1103/PhysRevD.98.014024](https://doi.org/10.1103/PhysRevD.98.014024). arXiv: [1804.01787 \[hep-ph\]](https://arxiv.org/abs/1804.01787) (cit. on pp. 5, 47, 167, 168, 223, 259, 303).
- [64] Tim R. Morris. “Derivative expansion of the exact renormalization group”. In: *Phys. Lett. B* 329 (June 1994), pp. 241–248. DOI: [10.1016/0370-2693\(94\)90767-6](https://doi.org/10.1016/0370-2693(94)90767-6). arXiv: [hep-ph/9403340](https://arxiv.org/abs/hep-ph/9403340) (cit. on pp. 5, 167).
- [65] Leonie Canet et al. “Optimization of the derivative expansion in the nonperturbative Renormalization Group”. In: *Phys. Rev. D* 67 (2003), p. 065004. DOI: [10.1103/PhysRevD.67.065004](https://doi.org/10.1103/PhysRevD.67.065004). arXiv: [hep-th/0211055](https://arxiv.org/abs/hep-th/0211055) (cit. on pp. 5, 47, 167, 259, 302).
- [66] Jan M. Pawłowski and Fabian Rennecke. “Higher order quark-mesonic scattering processes and the phase structure of QCD”. In: *Phys. Rev. D* 90.7 (Oct. 2014), p. 076002. DOI: [10.1103/PhysRevD.90.076002](https://doi.org/10.1103/PhysRevD.90.076002). arXiv: [1403.1179 \[hep-ph\]](https://arxiv.org/abs/1403.1179) (cit. on pp. 5, 47, 96, 117, 163, 168, 178, 180, 188, 190, 194, 203, 231, 258, 281, 307, 326).
- [67] Jens Braun et al. “From Quarks and Gluons to Hadrons: Chiral Symmetry Breaking in Dynamical QCD”. In: *Phys. Rev. D* 94.3 (Aug. 2016), p. 034016. DOI: [10.1103/PhysRevD.94.034016](https://doi.org/10.1103/PhysRevD.94.034016). arXiv: [1412.1045 \[hep-ph\]](https://arxiv.org/abs/1412.1045) (cit. on p. 5).
- [68] Fabian Rennecke. “Vacuum structure of vector mesons in QCD”. In: *Phys. Rev. D* 92.7 (Oct. 2015), p. 076012. DOI: [10.1103/PhysRevD.92.076012](https://doi.org/10.1103/PhysRevD.92.076012). arXiv: [1504.03585 \[hep-ph\]](https://arxiv.org/abs/1504.03585) (cit. on p. 5).
- [69] Jürgen Eser, Florian Divotgey, and Mario Mitter. “Low-energy limit of the $O(4)$ quark-meson model”. In: *PoS CD2018* (2019), p. 060. DOI: [10.22323/1.317.0060](https://doi.org/10.22323/1.317.0060). arXiv: [1902.04804 \[hep-ph\]](https://arxiv.org/abs/1902.04804) (cit. on pp. 5, 47, 167, 168, 223, 259).
- [70] Florian Divotgey, Jürgen Eser, and Mario Mitter. “Dynamical generation of low-energy couplings from quark-meson fluctuations”. In: *Phys. Rev. D* 99.5 (Mar. 2019), p. 054023. DOI: [10.1103/PhysRevD.99.054023](https://doi.org/10.1103/PhysRevD.99.054023). arXiv: [1901.02472 \[hep-ph\]](https://arxiv.org/abs/1901.02472) (cit. on pp. 5, 47, 117, 167, 168, 223, 259).
- [71] Niklas Cichutek, Florian Divotgey, and Jürgen Eser. “Fluctuation-induced higher-derivative couplings and infrared dynamics of the quark-meson-diquark model”. In: *Phys. Rev. D* 102.3 (Aug. 2020), p. 034030. DOI: [10.1103/PhysRevD.102.034030](https://doi.org/10.1103/PhysRevD.102.034030). arXiv: [2006.12473 \[hep-ph\]](https://arxiv.org/abs/2006.12473) (cit. on pp. 5, 47, 96, 117, 167, 168, 187, 223, 231, 259, 285).
- [72] Jürgen Eser and Jean-Paul Blaizot. “S-wave pion-pion scattering lengths from nucleon-meson fluctuations”. In: *Phys. Rev. D* 105.7 (Apr. 2022), p. 074031. DOI: [10.1103/PhysRevD.105.074031](https://doi.org/10.1103/PhysRevD.105.074031). arXiv: [2112.14579 \[hep-ph\]](https://arxiv.org/abs/2112.14579) (cit. on pp. 5, 15, 117, 130, 168, 180, 194, 223, 226, 303).
- [73] Gonzalo De Polsi, Guzmán Hernández-Chifflet, and Nicolás Wschebor. “Precision calculation of universal amplitude ratios in $O(N)$ universality classes: Derivative expansion results at order $O(\partial^4)$ ”. In: *Phys. Rev. E* 104.6 (Dec. 2021), p. 064101. DOI: [10.1103/PhysRevE.104.064101](https://doi.org/10.1103/PhysRevE.104.064101). arXiv: [2109.14731 \[cond-mat.stat-mech\]](https://arxiv.org/abs/2109.14731) (cit. on pp. 5, 167).

- [74] Marco D’Attanasio and Tim R. Morris. “Large N and the renormalization group”. In: *Phys. Lett. B* 409 (Sept. 1997), pp. 363–370. DOI: [10.1016/S0370-2693\(97\)00866-6](https://doi.org/10.1016/S0370-2693(97)00866-6). arXiv: [hep-th/9704094](https://arxiv.org/abs/hep-th/9704094) (cit. on pp. 6, 7, 28, 110, 166).
- [75] Nikolaos Tetradis and Daniel F. Litim. “Analytical solutions of exact renormalization group equations”. In: *Nucl. Phys. B* 464 (Apr. 1996), pp. 492–511. DOI: [10.1016/0550-3213\(95\)00642-7](https://doi.org/10.1016/0550-3213(95)00642-7). arXiv: [hep-th/9512073](https://arxiv.org/abs/hep-th/9512073) (cit. on pp. 6, 7, 55, 63, 110).
- [76] D. Litim and N. Tetradis. *Approximate solutions of exact renormalization group equations*. Jan. 1995. arXiv: [hep-th/9501042](https://arxiv.org/abs/hep-th/9501042) (cit. on pp. 6, 7, 55, 63, 110).
- [77] Eduardo Grossi and Nicolas Wink. *Resolving phase transitions with Discontinuous Galerkin methods*. Mar. 2019. arXiv: [1903.09503 \[hep-th\]](https://arxiv.org/abs/1903.09503) (cit. on pp. 6, 7, 28, 32, 47, 53, 55–57, 63, 65–67, 74, 76, 79, 95, 102, 109, 110, 113, 116, 125, 166, 185, 193, 301).
- [78] Jennifer A. Adams et al. “Solving nonperturbative flow equations”. In: *Mod. Phys. Lett. A* 10 (July 1995), pp. 2367–2380. DOI: [10.1142/S0217732395002520](https://doi.org/10.1142/S0217732395002520). arXiv: [hep-th/9507093](https://arxiv.org/abs/hep-th/9507093) (cit. on pp. 6, 47).
- [79] Dirk-Uwe Jungnickel and Christof Wetterich. “Nonperturbative flow equations, low-energy QCD and the chiral phase transition”. In: *NATO Advanced Study Institute on Confinement, Duality and Nonperturbative Aspects of QCD*. Oct. 1997. arXiv: [hep-ph/9710397](https://arxiv.org/abs/hep-ph/9710397) (cit. on pp. 6, 231).
- [80] Jürgen Berges and Christof Wetterich. “Equation of state and coarse grained free energy for matrix models”. In: *Nucl. Phys. B* 487 (Mar. 1997), pp. 675–720. DOI: [10.1016/S0550-3213\(96\)00670-0](https://doi.org/10.1016/S0550-3213(96)00670-0). arXiv: [hep-th/9609019](https://arxiv.org/abs/hep-th/9609019) (cit. on p. 6).
- [81] T. Umekawa, K. Naito, and M. Oka. *Renormalization group approach to the $O(N)$ linear sigma model at finite temperature*. May 1999. arXiv: [hep-ph/9905502](https://arxiv.org/abs/hep-ph/9905502) (cit. on p. 6).
- [82] Julia Borchardt and Benjamin Knorr. “Global solutions of functional fixed point equations via pseudospectral methods”. In: *Phys. Rev. D* 91.10 (May 2015). [Erratum: *Phys.Rev.D* 93, 089904 (2016)], p. 105011. DOI: [10.1103/PhysRevD.91.105011](https://doi.org/10.1103/PhysRevD.91.105011). arXiv: [1502.07511 \[hep-th\]](https://arxiv.org/abs/1502.07511) (cit. on pp. 6, 72).
- [83] Julia Borchardt and Benjamin Knorr. “Solving functional flow equations with pseudo-spectral methods”. In: *Phys. Rev. D* 94 (July 2016), p. 025027. DOI: [10.1103/PhysRevD.94.025027](https://doi.org/10.1103/PhysRevD.94.025027). arXiv: [1603.06726 \[hep-th\]](https://arxiv.org/abs/1603.06726) (cit. on pp. 6, 47, 72, 95).
- [84] Vincent Pangon et al. “Onset of symmetry breaking by the Functional RG method”. In: *Int. J. Mod. Phys. A* 26 (Mar. 2011), pp. 1327–1345. DOI: [10.1142/S0217751X11052839](https://doi.org/10.1142/S0217751X11052839). arXiv: [0907.0144 \[hep-th\]](https://arxiv.org/abs/0907.0144) (cit. on pp. 6, 72, 95).
- [85] Vincent Pangon. “Structure of the broken phase of the sine-Gordon model using Functional Renormalization”. In: *Int. J. Mod. Phys. A* 27 (Feb. 2012), p. 1250014. DOI: [10.1142/S0217751X12500145](https://doi.org/10.1142/S0217751X12500145). arXiv: [1008.0281 \[hep-th\]](https://arxiv.org/abs/1008.0281) (cit. on pp. 6, 72, 95, 98).
- [86] Bernd-Jochen Schaefer, Oliver Bohr, and Jochen Wambach. “Finite temperature gluon condensate with renormalization group flow equations”. In: *Phys. Rev. D* 65 (Apr. 2002), p. 105008. DOI: [10.1103/PhysRevD.65.105008](https://doi.org/10.1103/PhysRevD.65.105008). arXiv: [hep-th/0112087](https://arxiv.org/abs/hep-th/0112087) (cit. on pp. 6, 93, 94, 96, 231).
- [87] Ralf-Arno Tripolt. “The QCD Phase Diagram for Finite Volumes”. Master thesis. University of Graz, 2011. URL: <https://unipub.uni-graz.at/obvugrhs/download/pdf/216945?originalFilename=true> (cit. on p. 6).
- [88] Nils Strodthoff, Bernd-Jochen Schaefer, and Lorenz von Smekal. “Quark-meson-diquark model for two-color QCD”. In: *Phys. Rev. D* 85 (Apr. 2012), p. 074007. DOI: [10.1103/PhysRevD.85.074007](https://doi.org/10.1103/PhysRevD.85.074007). arXiv: [1112.5401 \[hep-ph\]](https://arxiv.org/abs/1112.5401) (cit. on pp. 6, 96, 117).
- [89] G. G. Barnafoldi, A. Jakovac, and P. Posfay. “Harmonic expansion of the effective potential in a functional renormalization group at finite chemical potential”. In: *Phys. Rev. D* 95.2 (2017), p. 025004. DOI: [10.1103/PhysRevD.95.025004](https://doi.org/10.1103/PhysRevD.95.025004). arXiv: [1604.01717 \[hep-th\]](https://arxiv.org/abs/1604.01717) (cit. on p. 6).

- [90] Bin Qin et al. “Nonperturbative renormalization group for the Landau–de Gennes model”. In: *Phys. Rev. B* 98.1 (July 2018), p. 014102. DOI: [10.1103/PhysRevB.98.014102](https://doi.org/10.1103/PhysRevB.98.014102). arXiv: [1803.03683](https://arxiv.org/abs/1803.03683) [[cond-mat.stat-mech](#)] (cit. on p. 6).
- [91] Ken-Ichi Aoki, Shin-Ichiro Kumamoto, and Masatoshi Yamada. “Phase structure of NJL model with weak renormalization group”. In: *Nucl. Phys. B* 931 (2018), pp. 105–131. DOI: [10.1016/j.nuclphysb.2018.04.005](https://doi.org/10.1016/j.nuclphysb.2018.04.005). arXiv: [1705.03273](https://arxiv.org/abs/1705.03273) [[hep-th](#)] (cit. on pp. 6, 47, 55, 63, 65).
- [92] David J. Wallace and Royce K. P. Zia. “Gradient flow and the Renormalization Group”. In: *Phys. Lett. A* 48 (July 1974), p. 325. DOI: [10.1016/0375-9601\(74\)90449-6](https://doi.org/10.1016/0375-9601(74)90449-6) (cit. on pp. 6, 55).
- [93] David J. Wallace and Royce K. P. Zia. “Gradient properties of the Renormalization Group Equations in multicomponent systems”. In: *Annals Phys.* 92 (July 1975), p. 142. DOI: [10.1016/0003-4916\(75\)90267-5](https://doi.org/10.1016/0003-4916(75)90267-5) (cit. on pp. 6, 55).
- [94] Anna Hasenfratz and Peter Hasenfratz. “Renormalization Group study of scalar field theories”. In: *Nucl. Phys. B* 270 (Jan. 1986), pp. 687–701. DOI: [10.1016/0550-3213\(86\)90573-0](https://doi.org/10.1016/0550-3213(86)90573-0) (cit. on pp. 6, 55, 116, 301).
- [95] Alexander B. Zamolodchikov. “Irreversibility of the flux of the Renormalization Group in a 2D field theory”. In: *JETP Lett.* 43 (June 1986), pp. 730–732. URL: http://jetpletters.ru/ps/1413/article_21504.shtml (cit. on pp. 6, 55, 59).
- [96] Giovanni Felder. “Renormalization Group in the local potential approximation”. In: *Comm. Math. Phys.* 111 (Mar. 1987), pp. 101–121. DOI: [10.1007/BF01239018](https://doi.org/10.1007/BF01239018) (cit. on pp. 6, 55, 116, 301).
- [97] Gil Zumbach. “Almost second order phase transitions”. In: *Phys. Rev. Lett.* 71 (Oct. 1993), pp. 2421–2424. DOI: [10.1103/PhysRevLett.71.2421](https://doi.org/10.1103/PhysRevLett.71.2421) (cit. on pp. 6, 55, 57, 59, 60, 116, 301).
- [98] Gil Zumbach. “The Local Potential Approximation of the Renormalization Group and its applications”. In: *Phys. Lett. A* 190 (July 1994), pp. 225–230. DOI: [10.1016/0375-9601\(94\)90746-3](https://doi.org/10.1016/0375-9601(94)90746-3) (cit. on pp. 6, 55, 57, 59, 60, 116, 301).
- [99] Gil Zumbach. “The Renormalization Group in the Local Potential Approximation and its applications to the $O(N)$ model”. In: *Nucl. Phys. B* 413 (Feb. 1994), pp. 754–770. DOI: [10.1016/0550-3213\(94\)90011-6](https://doi.org/10.1016/0550-3213(94)90011-6) (cit. on pp. 6, 55, 57, 59, 60, 116, 195, 301).
- [100] Oliver J. Rosten. “Fundamentals of the Exact Renormalization Group”. In: *Phys. Rept.* 511.4 (Feb. 2012), pp. 177–272. DOI: [10.1016/j.physrep.2011.12.003](https://doi.org/10.1016/j.physrep.2011.12.003). arXiv: [1003.1366](https://arxiv.org/abs/1003.1366) [[hep-th](#)] (cit. on pp. 6, 37–42, 55, 60, 165, 186, 288).
- [101] Eduardo Grossi et al. “Shocks and quark-meson scatterings at large density”. In: *Phys. Rev. D* 104.1 (Feb. 2021), p. 016028. DOI: [10.1103/PhysRevD.104.016028](https://doi.org/10.1103/PhysRevD.104.016028). arXiv: [2102.01602](https://arxiv.org/abs/2102.01602) [[hep-ph](#)] (cit. on pp. 6, 47, 53, 56, 57, 63, 67, 74, 76, 79, 95, 102, 109, 115, 117, 125, 185, 193, 194, 259, 281, 307, 326).
- [102] Friederike Ihssen and Jan M. Pawłowski. *Functional flows for complex effective actions*. July 2022. arXiv: [2207.10057](https://arxiv.org/abs/2207.10057) [[hep-th](#)] (cit. on pp. 6, 9, 42, 53, 67, 79, 116).
- [103] Friederike Ihssen et al. *Local Discontinuous Galerkin for the Functional Renormalisation Group*. July 2022. arXiv: [2207.12266](https://arxiv.org/abs/2207.12266) [[hep-th](#)] (cit. on pp. 6, 9, 47, 53, 56, 67, 79).
- [104] William F. Ames. *Numerical Methods for Partial Differential Equations*. 3. ed., 1. [Dr.] Computer science and scientific computing. Boston [u.a.]: Academic Press, 1992. ISBN: 012056761X (cit. on pp. 6, 41, 54, 56, 65, 67, 68, 72, 77, 103).
- [105] Alexander Kurganov and Eitan Tadmor. “New High-Resolution Central Schemes for Non-linear Conservation Laws and Convection–Diffusion Equations”. In: *Journal of Computational Physics* 160.1 (2000), pp. 241–282. ISSN: 0021-9991. DOI: [10.1006/jcph.2000.6459](https://doi.org/10.1006/jcph.2000.6459) (cit. on pp. 7, 67–72, 90, 109, 195).

- [106] Stefan Flörchinger. “Functional Renormalization and Ultracold Quantum Gases”. In: *Springer Theses* (2010). ISSN: 2190-5061. DOI: [10.1007/978-3-642-14113-3](https://doi.org/10.1007/978-3-642-14113-3). URL: <http://dx.doi.org/10.1007/978-3-642-14113-3> (cit. on pp. 7, 9, 37).
- [107] Jan Keitel and Lorenz Bartosch. “The zero-dimensional $O(N)$ vector model as a benchmark for perturbation theory, the large- N expansion and the Functional Renormalization Group”. In: *J. Phys.* A45 (Feb. 2012), p. 105401. DOI: [10.1088/1751-8113/45/10/105401](https://doi.org/10.1088/1751-8113/45/10/105401). arXiv: [1109.3013](https://arxiv.org/abs/1109.3013) [[cond-mat.stat-mech](https://arxiv.org/abs/1109.3013)] (cit. on pp. 7–9, 11, 13, 17, 23, 25–27, 31, 32, 37, 48, 49, 96, 97).
- [108] Jan M. Pawłowski. *Solving integrals with flow equations*. Slides for the lecture *Non-perturbative aspects of gauge theories* winter term 2012/2013. [Online; accessed 2020.10.29]. 2013. URL: <https://www.thphys.uni-heidelberg.de/~pawłowski/NPgauge12/bonus/idea.pdf> (cit. on pp. 7, 9, 37, 48, 96, 97).
- [109] Sergej Moroz. “Few-body physics with functional renormalization”. PhD thesis. University of Heidelberg, Mar. 2011. DOI: [10.11588/heidok.00011602](https://doi.org/10.11588/heidok.00011602) (cit. on pp. 7, 9, 11, 18, 21, 23, 25, 26, 37, 48, 49, 96, 97).
- [110] Sandra Kemler and Jens Braun. “Towards a Renormalization Group approach to density functional theory – general formalism and case studies”. In: *J. Phys. G* 40 (July 2013), p. 085105. DOI: [10.1088/0954-3899/40/8/085105](https://doi.org/10.1088/0954-3899/40/8/085105). arXiv: [1304.1161](https://arxiv.org/abs/1304.1161) [[nucl-th](https://arxiv.org/abs/1304.1161)] (cit. on pp. 7, 9, 25, 37, 48).
- [111] Ralf Hedden et al. “A functional renormalization group approach to zero-dimensional interacting systems”. In: *Journal of Physics: Condensed Matter* 16.29 (July 2004), pp. 5279–5296. DOI: [10.1088/0953-8984/16/29/019](https://doi.org/10.1088/0953-8984/16/29/019). URL: <https://doi.org/10.1088/0953-8984/16/29/019> (cit. on p. 8).
- [112] Christoph Karrasch et al. “A finite-frequency functional renormalization group approach to the single impurity Anderson model”. In: *Journal of Physics: Condensed Matter* 20.34 (Aug. 2008), p. 345205. DOI: [10.1088/0953-8984/20/34/345205](https://doi.org/10.1088/0953-8984/20/34/345205). URL: <https://doi.org/10.1088/0953-8984/20/34/345205> (cit. on p. 8).
- [113] Jan F. Rentrop, Severin G. Jakobs, and Volker Meden. “Two-particle irreducible Functional Renormalization Group schemes – a comparative study”. In: *Journal of Physics A: Mathematical and Theoretical* 48.14 (Mar. 2015), p. 145002. ISSN: 1751-8121. DOI: [10.1088/1751-8113/48/14/145002](https://doi.org/10.1088/1751-8113/48/14/145002). URL: <http://dx.doi.org/10.1088/1751-8113/48/14/145002> (cit. on p. 8).
- [114] B. Mühlischlegel, D. J. Scalapino, and R. Denton. “Thermodynamic Properties of Small Superconducting Particles”. In: *Phys. Rev. B* 6 (5 Sept. 1972), pp. 1767–1777. DOI: [10.1103/PhysRevB.6.1767](https://doi.org/10.1103/PhysRevB.6.1767) (cit. on p. 8).
- [115] Alan J. Bray. “Statistical mechanics of zero-dimensional Ginzburg-Landau fields: Accuracy of the screening approximation”. In: *J. Stat. Phys.* 11 (July 1974), pp. 29–50. DOI: [10.1007/BF01019476](https://doi.org/10.1007/BF01019476) (cit. on p. 8).
- [116] Shinobu Hikami and Edouard Brezin. “Large order behavior of the $1/N$ expansion in zero and one dimensions”. In: *J. Phys. A* 12 (1979), pp. 759–770. DOI: [10.1088/0305-4470/12/6/006](https://doi.org/10.1088/0305-4470/12/6/006) (cit. on p. 8).
- [117] Paolo Di Vecchia, Mitsuhiro Kato, and Nobuyoshi Ohta. “Double scaling limit in $O(N)$ vector models”. In: *Nucl. Phys. B* 357 (Mar. 1991), pp. 495–520. DOI: [10.1016/0550-3213\(91\)90478-G](https://doi.org/10.1016/0550-3213(91)90478-G) (cit. on p. 8).
- [118] Paolo Di Vecchia, Mitsuhiro Kato, and Nobuyoshi Ohta. “Double scaling limit in $O(N)$ vector models in D -dimensions”. In: *Int. J. Mod. Phys. A* 7 (Mar. 1992), pp. 1391–1414. DOI: [10.1142/S0217751X92000612](https://doi.org/10.1142/S0217751X92000612) (cit. on p. 8).
- [119] Shinsuke Nishigaki and Tamiaki Yoneya. “A nonperturbative theory of randomly branching chains”. In: *Nucl. Phys. B* 348 (Jan. 1991), pp. 787–807. DOI: [10.1016/0550-3213\(91\)90215-J](https://doi.org/10.1016/0550-3213(91)90215-J) (cit. on p. 8).

- [120] Shinsuke Nishigaki and Tamiaki Yoneya. “The double scaling limit of $O(N)$ vector models and the KP hierarchy”. In: *Phys. Lett. B* 268 (Oct. 1991), pp. 35–39. DOI: [10.1016/0370-2693\(91\)90918-G](https://doi.org/10.1016/0370-2693(91)90918-G) (cit. on p. 8).
- [121] Sigurd Schelstraete and Henri Verschelde. “Large N limit of $O(N)$ vector models”. In: *Phys. Lett. B* 332 (1994), pp. 36–43. DOI: [10.1016/0370-2693\(94\)90855-9](https://doi.org/10.1016/0370-2693(94)90855-9). arXiv: [hep-th/9405158](https://arxiv.org/abs/hep-th/9405158) (cit. on p. 8).
- [122] Jean Zinn-Justin. “Vector models in the large N limit: A Few applications”. In: *11th Taiwan Spring School on Particles and Fields*. Mar. 1998. arXiv: [hep-th/9810198](https://arxiv.org/abs/hep-th/9810198) (cit. on p. 8).
- [123] Daniel Bessis, Claude Itzykson, and Jean-Bernard Zuber. “Quantum field theory techniques in graphical enumeration”. In: *Adv. Appl. Math.* 1 (June 1980), pp. 109–157. DOI: [10.1016/0196-8858\(80\)90008-1](https://doi.org/10.1016/0196-8858(80)90008-1) (cit. on p. 8).
- [124] David Skinner. *Lecture notes: Quantum Field Theory II*. [Online; accessed 2021.01.12]. Cambridge, United Kingdom: Department of Applied Mathematics and Theoretical Physics, Centre for Mathematical Sciences, 2018. URL: <http://www.damtp.cam.ac.uk/user/dbs26/AQFT.html> (cit. on pp. 8, 9, 12, 13, 23, 25, 26, 40, 115).
- [125] Kilian Fraboulet. “Path-integral approaches to strongly-coupled quantum many-body systems”. PhD thesis. LPMC - Palaiseau - IJCLab, Orsay, Dec. 2021 (cit. on pp. 8, 9, 11, 13, 17, 23, 25, 26, 48).
- [126] Kilian Fraboulet and Jean-Paul Ebran. *Addressing energy density functionals in the language of path-integrals I: Comparative study of diagrammatic techniques applied to the $(0+0)$ -D $O(N)$ -symmetric φ^4 -theory*. Aug. 2022. arXiv: [2208.13044](https://arxiv.org/abs/2208.13044) [[nucl-th](#)] (cit. on p. 8).
- [127] Kilian Fraboulet and Jean-Paul Ebran. *Addressing energy density functionals in the language of path-integrals II: Comparative study of functional renormalization group techniques applied to the $(0+0)$ -D $O(N)$ -symmetric φ^4 -theory*. Oct. 2022. arXiv: [2210.07748](https://arxiv.org/abs/2210.07748) [[cond-mat.str-el](#)] (cit. on p. 8).
- [128] Lawrence S. Schulman. *Techniques and applications of path integration*. New York: John Wiley & Sons, 1981 (cit. on pp. 9, 23, 25, 26).
- [129] John W. Negele and Henri Orland. *Quantum many-particle systems*. Westview Press, 1988. ISBN: 0-7382-0052-2 (cit. on pp. 9, 23, 25, 26).
- [130] Alexander Altland and Ben D. Simons. *Condensed matter field theory*. Cambridge, England, UK: Cambridge University Press, 2006. ISBN: 978-0-521-76975-4 (cit. on pp. 9, 23, 25, 26).
- [131] Vincent Rivasseau. “Constructive Field Theory in Zero Dimension”. In: *Adv. Math. Phys.* 2010 (Dec. 2009), p. 180159. DOI: [10.1155/2009/180159](https://doi.org/10.1155/2009/180159). arXiv: [0906.3524](https://arxiv.org/abs/0906.3524) [[math-ph](#)] (cit. on pp. 9, 23, 25, 26).
- [132] Dérick S. Rosa, Ricardo L. S. Farias, and Rudnei O. Ramos. “Reliability of the optimized perturbation theory in the 0-dimensional $O(N)$ scalar field model”. In: *Physica A* 464 (Dec. 2016), pp. 11–26. DOI: [10.1016/j.physa.2016.07.067](https://doi.org/10.1016/j.physa.2016.07.067). arXiv: [1604.00537](https://arxiv.org/abs/1604.00537) [[hep-ph](#)] (cit. on p. 9).
- [133] Lukas Kades et al. “Monte Carlo sampling of complex actions in extended state spaces”. In: *Phys. Rev. E* 105.4 (Apr. 2022), p. 045315. DOI: [10.1103/PhysRevE.105.045315](https://doi.org/10.1103/PhysRevE.105.045315). arXiv: [2106.09367](https://arxiv.org/abs/2106.09367) [[hep-lat](#)] (cit. on pp. 9, 116).
- [134] Alberto G. Catalano. “Application of renormalization group techniques to the solution of integrals and Schrödinger eigenvalue equations”. master’s thesis. Politecnico di Torino, 2019. URL: <http://webthesis.biblio.polito.it/id/eprint/18673> (cit. on p. 9).
- [135] Haozhao Liang, Yifei Niu, and Tetsuo Hatsuda. “Functional Renormalization Group and Kohn-Sham scheme in density functional theory”. In: *Phys. Lett. B* 779 (Apr. 2018), pp. 436–440. DOI: [10.1016/j.physletb.2018.02.034](https://doi.org/10.1016/j.physletb.2018.02.034). arXiv: [1710.00650](https://arxiv.org/abs/1710.00650) [[cond-mat.str-el](#)] (cit. on pp. 9, 37).

- [136] Peter Millington and Paul M. Saffin. “Visualising quantum effective action calculations in zero dimensions”. In: *J. Phys. A* 52.40 (Sept. 2019), p. 405401. DOI: [10.1088/1751-8121/ab37e6](https://doi.org/10.1088/1751-8121/ab37e6). arXiv: [1905.09674](https://arxiv.org/abs/1905.09674) [hep-th] (cit. on pp. 9, 37, 116).
- [137] Peter Millington and Paul M. Saffin. “Benchmarking regulator-sourced 2PI and average 1PI flow equations in zero dimensions”. In: *J. Phys. A* 54.46 (Oct. 2021), p. 465401. DOI: [10.1088/1751-8121/ac2d00](https://doi.org/10.1088/1751-8121/ac2d00). arXiv: [2107.12914](https://arxiv.org/abs/2107.12914) [hep-th] (cit. on pp. 9, 116).
- [138] Peter Millington and Paul M. Saffin. “Vertex functions and their flow equations from the 2PI effective action”. In: *J. Phys. A* 55.43 (Nov. 2022), p. 435402. DOI: [10.1088/1751-8121/ac99ae](https://doi.org/10.1088/1751-8121/ac99ae). arXiv: [2206.08865](https://arxiv.org/abs/2206.08865) [hep-th] (cit. on pp. 9, 116).
- [139] Leonard Fister and Jan Martin Pawłowski. “Functional renormalization group in a finite volume”. In: *Phys. Rev. D* 92.7 (Oct. 2015), p. 076009. DOI: [10.1103/PhysRevD.92.076009](https://doi.org/10.1103/PhysRevD.92.076009). arXiv: [1504.05166](https://arxiv.org/abs/1504.05166) [hep-ph] (cit. on pp. 9, 21, 138).
- [140] Peter McCullagh and John Kolassa. “Cumulants”. In: *Scholarpedia* 4.3 (2009). revision #137322, p. 4699. DOI: [10.4249/scholarpedia.4699](https://doi.org/10.4249/scholarpedia.4699) (cit. on pp. 12–14, 24).
- [141] Tom W. B. Kibble. “Englert-Brout-Higgs-Guralnik-Hagen-Kibble mechanism”. In: *Scholarpedia* 4.1 (2009). revision #91222, p. 6441. DOI: [10.4249/scholarpedia.6441](https://doi.org/10.4249/scholarpedia.6441) (cit. on pp. 13, 83).
- [142] Dirk H. Rischke. *Lecture notes on: Statistische Feldtheorie*. [Online; accessed 2022.03.23]. 2022. URL: https://www.uni-frankfurt.de/65315388/Arbeitsgruppe_Dirk_Rischke (cit. on pp. 13–15, 142, 143, 154, 156, 211, 275).
- [143] Harold D. Ursell. “The evaluation of Gibbs’ phase-integral for imperfect gases”. In: *Mathematical Proceedings of the Cambridge Philosophical Society* 23.6 (Apr. 1927), 685–697. DOI: [10.1017/S0305004100011191](https://doi.org/10.1017/S0305004100011191) (cit. on p. 14).
- [144] Jeffrey Goldstone, Abdus Salam, and Steven Weinberg. “Broken symmetries”. In: *Phys. Rev.* 127 (Aug. 1962), pp. 965–970. DOI: [10.1103/PhysRev.127.965](https://doi.org/10.1103/PhysRev.127.965) (cit. on pp. 15, 21, 45, 132, 137).
- [145] Bryce S. DeWitt. *Dynamical theory of groups and fields*. New York, USA: Gordon and Breach, 1965 (cit. on pp. 15, 43, 45, 285, 286, 293).
- [146] Giovanni Jona-Lasinio. “Relativistic field theories with symmetry breaking solutions”. In: *Nuovo Cim.* 34 (Aug. 1964), pp. 1790–1795. DOI: [10.1007/BF02750573](https://doi.org/10.1007/BF02750573) (cit. on p. 15).
- [147] Wolfram Research, Inc. *Mathematica, Version 12.2*. Champaign, IL. 2020. URL: <https://www.wolfram.com/mathematica> (cit. on pp. 17, 30, 31, 49, 84, 86, 96, 285, 371, 373).
- [148] Paul Ehrenfest. “Phasenumwandlungen im ueblichen und erweiterten Sinn, classifiziert nach den entsprechenden Singularitaeten des thermodynamischen Potentiales”. In: *Proc. Royal Acad. Amsterdam* 36.2 (Feb. 1933). Supplement No 75b zu den Mitteilungen aus dem Kamerlingh Onnes-Institute, Leiden, pp. 153–157. URL: <https://www.dwc.knaw.nl/DL/publications/PU00016385.pdf> (cit. on pp. 18, 109, 214).
- [149] Yasushi Fujimoto, Lochlainn O’Raifeartaigh, and Guido Parravicini. “Effective potential for non-convex potentials”. In: *Nucl. Phys. B* 212 (Feb. 1983), pp. 268–300. DOI: [10.1016/0550-3213\(83\)90305-X](https://doi.org/10.1016/0550-3213(83)90305-X) (cit. on pp. 19, 20).
- [150] Lev D. Landau. “On the theory of phase transitions”. In: *Zh. Eksp. Teor. Fiz.* 7 (1937), pp. 19–32. URL: <http://archive.ujp.bitp.kiev.ua/files/journals/53/si/53SI08p.pdf> (cit. on p. 20).
- [151] Nathaniel D. Mermin and Herbert Wagner. “Absence of ferromagnetism or antiferromagnetism in one- or two-dimensional isotropic Heisenberg models”. In: *Phys. Rev. Lett.* 17 (22 Nov. 1966), pp. 1133–1136. DOI: [10.1103/PhysRevLett.17.1133](https://doi.org/10.1103/PhysRevLett.17.1133) (cit. on pp. 20, 132, 137).
- [152] Pierre C. Hohenberg. “Existence of long-range order in one and two dimensions”. In: *Phys. Rev.* 158 (2 June 1967), pp. 383–386. DOI: [10.1103/PhysRev.158.383](https://doi.org/10.1103/PhysRev.158.383) (cit. on pp. 20, 132, 137).

- [153] Sidney Richard Coleman. “There are no Goldstone bosons in two-dimensions”. In: *Commun. Math. Phys.* 31 (Dec. 1973), pp. 259–264. DOI: [10.1007/BF01646487](https://doi.org/10.1007/BF01646487) (cit. on pp. [20](#), [132](#), [137](#)).
- [154] Vadim L. Berezinskii. “Destruction of Long-range Order in One-dimensional and Two-dimensional Systems having a Continuous Symmetry Group I. Classical Systems”. In: *Sov. Phys. JETP* 32 (3 Mar. 1971), p. 493 (cit. on pp. [20](#), [132](#), [137](#)).
- [155] Vadim L. Berezinsky. “Destruction of Long-range Order in One-dimensional and Two-dimensional Systems Possessing a Continuous Symmetry Group. II. Quantum Systems.” In: *Sov. Phys. JETP* 34.3 (Mar. 1972), p. 610 (cit. on pp. [20](#), [132](#), [137](#)).
- [156] Yoichiro Nambu. “Quasiparticles and gauge invariance in the theory of superconductivity”. In: *Phys. Rev.* 117 (Feb. 1960). Ed. by John C. Taylor, pp. 648–663. DOI: [10.1103/PhysRev.117.648](https://doi.org/10.1103/PhysRev.117.648) (cit. on pp. [21](#), [132](#), [137](#)).
- [157] Jeffrey Goldstone. “Field theories with superconductor solutions”. In: *Nuovo Cim.* 19 (Jan. 1961), pp. 154–164. DOI: [10.1007/BF02812722](https://doi.org/10.1007/BF02812722) (cit. on pp. [21](#), [132](#), [137](#)).
- [158] David J. Gross and André Neveu. “Dynamical Symmetry Breaking in Asymptotically Free Field Theories”. In: *Phys. Rev. D* 10 (Nov. 1974), p. 3235. DOI: [10.1103/PhysRevD.10.3235](https://doi.org/10.1103/PhysRevD.10.3235) (cit. on pp. [28](#), [128](#), [130](#), [142](#), [156](#), [171](#), [172](#), [205](#), [310](#)).
- [159] Gabriele Veneziano. “ $U(1)$ Without Instantons”. In: *Nucl. Phys. B* 159 (Nov. 1979), pp. 213–224. DOI: [10.1016/0550-3213\(79\)90332-8](https://doi.org/10.1016/0550-3213(79)90332-8) (cit. on p. [28](#)).
- [160] Edward Witten. “Current Algebra Theorems for the $U(1)$ Goldstone Boson”. In: *Nucl. Phys. B* 156 (Sept. 1979), pp. 269–283. DOI: [10.1016/0550-3213\(79\)90031-2](https://doi.org/10.1016/0550-3213(79)90031-2) (cit. on p. [28](#)).
- [161] Kenneth G. Wilson. “Problems in physics with many scales of length”. In: *Sci. Am.* 241 (Aug. 1979), pp. 158–179. DOI: [10.1038/scientificamerican0879-158](https://doi.org/10.1038/scientificamerican0879-158) (cit. on pp. [38](#), [44](#), [58](#), [59](#), [195](#)).
- [162] Daniel F. Litim. “Optimization of the exact renormalization group”. In: *Phys. Lett. B* 486 (July 2000), pp. 92–99. DOI: [10.1016/S0370-2693\(00\)00748-6](https://doi.org/10.1016/S0370-2693(00)00748-6). arXiv: [hep-th/0005245](https://arxiv.org/abs/hep-th/0005245) (cit. on pp. [38](#), [166](#), [167](#), [289](#), [301](#), [302](#)).
- [163] Daniel F. Litim. “Optimized renormalization group flows”. In: *Phys. Rev. D* 64 (Oct. 2001), p. 105007. DOI: [10.1103/PhysRevD.64.105007](https://doi.org/10.1103/PhysRevD.64.105007). arXiv: [hep-th/0103195](https://arxiv.org/abs/hep-th/0103195) (cit. on pp. [38](#), [166](#), [167](#), [301–304](#)).
- [164] Hugh Osborn and David E. Twigg. “Remarks on Exact RG equations”. In: *Annals Phys.* 327 (Jan. 2012), pp. 29–73. DOI: [10.1016/j.aop.2011.10.011](https://doi.org/10.1016/j.aop.2011.10.011). arXiv: [1108.5340 \[hep-th\]](https://arxiv.org/abs/1108.5340) (cit. on pp. [38](#), [41](#), [60](#)).
- [165] Jan M. Pawłowski et al. “Physics and the choice of regulators in functional renormalisation group flows”. In: *Annals Phys.* 384 (Sept. 2017), pp. 165–197. DOI: [10.1016/j.aop.2017.06.017](https://doi.org/10.1016/j.aop.2017.06.017). arXiv: [1512.03598 \[hep-th\]](https://arxiv.org/abs/1512.03598) (cit. on pp. [38](#), [166](#), [167](#), [259](#), [289](#), [301](#), [302](#)).
- [166] Jens Braun et al. “Renormalization group studies of dense relativistic systems”. In: *Phys. Rev. D* 104.9 (Nov. 2021), p. 096002. DOI: [10.1103/PhysRevD.104.096002](https://doi.org/10.1103/PhysRevD.104.096002). arXiv: [2008.05978 \[hep-ph\]](https://arxiv.org/abs/2008.05978) (cit. on pp. [38](#), [123](#), [154](#), [166](#), [203](#), [289](#), [310](#)).
- [167] Jens Braun et al. *Renormalised spectral flows*. June 2022. arXiv: [2206.10232 \[hep-th\]](https://arxiv.org/abs/2206.10232) (cit. on pp. [38](#), [39](#), [144](#), [166](#), [259](#), [289](#)).
- [168] John R. Cannon. *The one-dimensional heat equation*. Cambridge University Press, 1984. ISBN: 9781139086967. DOI: [10.1017/CB09781139086967](https://doi.org/10.1017/CB09781139086967) (cit. on pp. [40](#), [41](#), [56](#), [100](#), [195](#)).
- [169] Manfred Salmhofer. *Rigorous Renormalization Group*. Talk at the 10th International Conference on Exact Renormalization Group 2020 (ERG2020). [Online; accessed 2021.01.12]. Kyoto, Japan (online conference): Yukawa Institute for Theoretical Physics, Kyoto University, Nov. 2020. URL: https://www2.yukawa.kyoto-u.ac.jp/~erg2020/ERG2020_slides/Salmhofer.pdf (cit. on p. [40](#)).

- [170] Joel L. Lebowitz. “Time’s arrow and Boltzmann’s entropy”. In: *Scholarpedia* 3.4 (2008). revision #137152, [Online; accessed 2021.02.01], p. 3448. DOI: [10.4249/scholarpedia.3448](https://doi.org/10.4249/scholarpedia.3448) (cit. on pp. 41, 58, 100, 195).
- [171] Joseph Polchinski. “Renormalization and Effective Lagrangians”. In: *Nucl. Phys. B* 231 (1984), pp. 269–295. DOI: [10.1016/0550-3213\(84\)90287-6](https://doi.org/10.1016/0550-3213(84)90287-6) (cit. on pp. 42, 55, 116).
- [172] Fabian Rennecke. “The chiral phase transition of QCD”. PhD thesis. University of Heidelberg, July 2015. DOI: [10.11588/heidok.00019205](https://doi.org/10.11588/heidok.00019205) (cit. on pp. 43, 285).
- [173] Laurence F. Abbott. “Introduction to the Background Field Method”. In: *Acta Phys. Polon. B* 13.1–2 (1982), pp. 33–50. URL: <https://www.actaphys.uj.edu.pl/R/13/1/33/pdf> (cit. on pp. 43, 293).
- [174] Kenneth G. Wilson. “Renormalization group and critical phenomena. 1. Renormalization group and the Kadanoff scaling picture”. In: *Phys. Rev. B* 4 (Nov. 1971), pp. 3174–3183. DOI: [10.1103/PhysRevB.4.3174](https://doi.org/10.1103/PhysRevB.4.3174) (cit. on pp. 44, 58, 289).
- [175] Kenneth G. Wilson. “Renormalization group and critical phenomena. 2. Phase space cell analysis of critical behavior”. In: *Phys. Rev. B* 4 (Nov. 1971), pp. 3184–3205. DOI: [10.1103/PhysRevB.4.3184](https://doi.org/10.1103/PhysRevB.4.3184) (cit. on pp. 44, 58, 289).
- [176] Kenneth G. Wilson and John B. Kogut. “The Renormalization group and the epsilon expansion”. In: *Phys. Rept.* 12 (Aug. 1974), pp. 75–199. DOI: [10.1016/0370-1573\(74\)90023-4](https://doi.org/10.1016/0370-1573(74)90023-4) (cit. on pp. 44, 58, 171).
- [177] Jean Zinn-Justin. *Quantum field theory and critical phenomena*. 4th ed. Vol. 113. Int. Ser. Monogr. Phys. A Clarendon Press Publication. Oxford University Press, Apr. 2002, pp. 1–1054. ISBN: 9780198509233. DOI: [10.1093/acprof:oso/9780198509233.001.0001](https://doi.org/10.1093/acprof:oso/9780198509233.001.0001) (cit. on pp. 45, 101, 130–132, 159, 169, 205, 275).
- [178] Bernd-Jochen Schaefer and Hans-Jurgen Pirner. “Renormalization group flow and equation of state of quarks and mesons”. In: *Nucl. Phys. A* 660 (Dec. 1999), pp. 439–474. DOI: [10.1016/S0375-9474\(99\)00409-1](https://doi.org/10.1016/S0375-9474(99)00409-1). arXiv: [nucl-th/9903003](https://arxiv.org/abs/nuc1-th/9903003) (cit. on p. 47).
- [179] Gabor Papp et al. “On the convergence of the expansion of renormalization group flow equation”. In: *Phys. Rev. D* 61 (Mar. 2000), p. 096002. DOI: [10.1103/PhysRevD.61.096002](https://doi.org/10.1103/PhysRevD.61.096002). arXiv: [hep-ph/9909246](https://arxiv.org/abs/hep-ph/9909246) (cit. on pp. 47, 96, 231).
- [180] Jan M. Pawłowski, Nils Strodthoff, and Nicolas Wink. “Finite temperature spectral functions in the $O(N)$ -model”. In: *Phys. Rev. D* 98.7 (Oct. 2018), p. 074008. DOI: [10.1103/PhysRevD.98.074008](https://doi.org/10.1103/PhysRevD.98.074008). arXiv: [1711.07444](https://arxiv.org/abs/1711.07444) [hep-th] (cit. on pp. 47, 144).
- [181] Nicolas Wink. *Resolving phase transitions with Discontinuous Galerkin methods*. Talk at the EMMI Workshop Functional Methods in Strongly Correlated Systems. [Online; accessed 2020.11.24]. Hirschegg, Austria, Apr. 2019. URL: <https://indico.gsi.de/event/8375/contributions/36534/> (cit. on p. 55).
- [182] Sidney R. Coleman. *Aspects of Symmetry: Selected Erice Lectures*. Cambridge, U.K.: Cambridge University Press, 1985. ISBN: 978-0-521-31827-3. DOI: [10.1017/CB09780511565045](https://doi.org/10.1017/CB09780511565045) (cit. on p. 55).
- [183] Harry Bateman. “Some recent researches on the motion of fluids”. In: *Monthly Weather Review* 43 (4 Apr. 1915), pp. 163–170. DOI: [10.1175/1520-0493\(1915\)43<163:SRROTM>2.0.CO;2](https://doi.org/10.1175/1520-0493(1915)43<163:SRROTM>2.0.CO;2) (cit. on p. 56).
- [184] Johannes M. Burgers. “A mathematical model illustrating the theory of turbulence”. In: *Advances in Applied Mechanics* 1 (1948). Ed. by Richard von Mises and Theodore von Kármán, pp. 171–199. ISSN: 0065-2156. DOI: [10.1016/S0065-2156\(08\)70100-5](https://doi.org/10.1016/S0065-2156(08)70100-5). URL: <http://www.sciencedirect.com/science/article/pii/S0065215608701005> (cit. on p. 56).
- [185] Leo P. Kadanoff. “Scaling laws for Ising models near T_c ”. In: *Physics Physique Fizika* 2 (June 1966), pp. 263–272. DOI: [10.1103/PhysicsPhysiqueFizika.2.263](https://doi.org/10.1103/PhysicsPhysiqueFizika.2.263) (cit. on pp. 58, 195).

- [186] Thomas L. Curtright, Xiang Jin, and Cosmas K. Zachos. “RG flows, cycles, and c -theorem folklore”. In: *Phys. Rev. Lett.* 108 (Mar. 2012), p. 131601. DOI: [10.1103/PhysRevLett.108.131601](https://doi.org/10.1103/PhysRevLett.108.131601). arXiv: [1111.2649](https://arxiv.org/abs/1111.2649) [hep-th] (cit. on p. 59).
- [187] Miguel A. Virasoro. “Subsidiary conditions and ghosts in dual resonance models”. In: *Phys. Rev. D* 1 (May 1970), pp. 2933–2936. DOI: [10.1103/PhysRevD.1.2933](https://doi.org/10.1103/PhysRevD.1.2933) (cit. on p. 59).
- [188] John L. Cardy. “Is there a c -theorem in four dimensions?” In: *Phys. Lett. B* 215 (Dec. 1988), pp. 749–752. DOI: [10.1016/0370-2693\(88\)90054-8](https://doi.org/10.1016/0370-2693(88)90054-8) (cit. on p. 59).
- [189] Tom Banks and Emil J. Martinec. “The Renormalization Group and String Field Theory”. In: *Nucl. Phys. B* 294 (1987), pp. 733–746. DOI: [10.1016/0550-3213\(87\)90605-5](https://doi.org/10.1016/0550-3213(87)90605-5) (cit. on p. 59).
- [190] Hugh Osborn. “Derivation of a four dimensional c -theorem for renormalisable quantum field theories”. In: *Phys. Lett. B* 222 (May 1989), pp. 97–102. DOI: [10.1016/0370-2693\(89\)90729-6](https://doi.org/10.1016/0370-2693(89)90729-6) (cit. on pp. 59, 60).
- [191] Ian Jack and Hugh Osborn. “Analogues for the c -theorem for four-dimensional renormalizable field theories”. In: *Nucl. Phys. B* 343 (1990), pp. 647–688. DOI: [10.1016/0550-3213\(90\)90584-Z](https://doi.org/10.1016/0550-3213(90)90584-Z) (cit. on p. 59).
- [192] Zohar Komargodski and Adam Schwimmer. “On Renormalization Group flows in four dimensions”. In: *JHEP* 12 (Dec. 2011), p. 099. DOI: [10.1007/JHEP12\(2011\)099](https://doi.org/10.1007/JHEP12(2011)099). arXiv: [1107.3987](https://arxiv.org/abs/1107.3987) [hep-th] (cit. on p. 59).
- [193] Peter E. Haagensen et al. “Gradient flows from an approximation to the Exact Renormalization Group”. In: *Phys. Lett. B* 323 (Mar. 1994), pp. 330–338. DOI: [10.1016/0370-2693\(94\)91228-9](https://doi.org/10.1016/0370-2693(94)91228-9). arXiv: [hep-th/9310032](https://arxiv.org/abs/hep-th/9310032) (cit. on pp. 59, 301).
- [194] Jacek Generowicz, Chris Harvey-Fros, and Tim R. Morris. “ C function representation of the Local Potential Approximation”. In: *Phys. Lett. B* 407 (Aug. 1997), pp. 27–32. DOI: [10.1016/S0370-2693\(97\)00729-6](https://doi.org/10.1016/S0370-2693(97)00729-6). arXiv: [hep-th/9705088](https://arxiv.org/abs/hep-th/9705088) (cit. on p. 59).
- [195] Stefano Forte and José I. Latorre. “A proof of the irreversibility of Renormalization Group flows in four-dimensions”. In: *Nucl. Phys. B* 535 (Dec. 1998), pp. 709–728. DOI: [10.1016/S0550-3213\(98\)00631-2](https://doi.org/10.1016/S0550-3213(98)00631-2). arXiv: [hep-th/9805015](https://arxiv.org/abs/hep-th/9805015) (cit. on p. 59).
- [196] Alessandro Codello, Giulio D’Odorico, and Carlo Pagani. “A Functional RG equation for the c -function”. In: *JHEP* 07 (July 2014), p. 040. DOI: [10.1007/JHEP07\(2014\)040](https://doi.org/10.1007/JHEP07(2014)040). arXiv: [1312.7097](https://arxiv.org/abs/1312.7097) [hep-th] (cit. on pp. 59, 72).
- [197] Alessandro Codello, Giulio D’Odorico, and Carlo Pagani. “Functional and local Renormalization Groups”. In: *Phys. Rev. D* 91.12 (July 2015), p. 125016. DOI: [10.1103/PhysRevD.91.125016](https://doi.org/10.1103/PhysRevD.91.125016). arXiv: [1502.02439](https://arxiv.org/abs/1502.02439) [hep-th] (cit. on p. 59).
- [198] Daniel Becker and Martin Reuter. “Towards a C -function in $4D$ quantum gravity”. In: *JHEP* 03 (Mar. 2015), p. 065. DOI: [10.1007/JHEP03\(2015\)065](https://doi.org/10.1007/JHEP03(2015)065). arXiv: [1412.0468](https://arxiv.org/abs/1412.0468) [hep-th] (cit. on p. 60).
- [199] Daniel Becker. “Asymptotically safe quantum gravity: Bimetric actions, boundary terms, & a C -function”. PhD thesis. Johannes Gutenberg University Mainz, Feb. 2016. DOI: [10.25358/openscience-2831](https://doi.org/10.25358/openscience-2831) (cit. on p. 60).
- [200] R. M. Redheffer and W. Walter. “The total variation of solutions of parabolic differential equations and a maximum principle in unbounded domains”. In: *Math. Ann.* 209.1 (Mar. 1974), pp. 57–67. DOI: [10.1007/BF01432886](https://doi.org/10.1007/BF01432886) (cit. on pp. 63, 77).
- [201] L.A. Monthé. “A study of splitting scheme for hyperbolic conservation laws with source terms”. In: *Journal of Computational and Applied Mathematics* 137.1 (2001), pp. 1–12. ISSN: 0377-0427. DOI: [10.1016/S0377-0427\(00\)00615-4](https://doi.org/10.1016/S0377-0427(00)00615-4). URL: <https://www.sciencedirect.com/science/article/pii/S0377042700006154> (cit. on p. 63).

- [202] R. Donat Beneito and A. Martínez Gavara. “A ‘TVD-like’ Scheme for Conservation Laws with Source Terms”. In: *Numerical Mathematics and Advanced Applications*. Ed. by Karl Kunisch, Günther Of, and Olaf Steinbach. Berlin, Heidelberg: Springer Berlin Heidelberg, 2008, pp. 265–272. ISBN: 978-3-540-69777-0 (cit. on p. 63).
- [203] Rongsan Chen and De-kang Mao. “Entropy-TVD Scheme for Nonlinear Scalar Conservation Laws”. In: *J. Sci. Comput.* 47.2 (May 2011), pp. 150–169. DOI: [10.1007/s10915-010-9431-9](https://doi.org/10.1007/s10915-010-9431-9) (cit. on p. 63).
- [204] Marianne Bessemoulin-Chatard and Francis Filbet. “A Finite Volume Scheme for Nonlinear Degenerate Parabolic Equations”. In: *SIAM Journal on Scientific Computing* 34.5 (Jan. 2012), B559–B583. ISSN: 1095-7197. DOI: [10.1137/110853807](https://doi.org/10.1137/110853807). URL: <http://dx.doi.org/10.1137/110853807> (cit. on p. 63).
- [205] Ken-Ichi Aoki, Shin-Ichiro Kumamoto, and Daisuke Sato. “Weak solution of the non-perturbative renormalization group equation to describe dynamical chiral symmetry breaking”. In: *PTEP* 2014.4 (2014), 043B05. DOI: [10.1093/ptep/ptu039](https://doi.org/10.1093/ptep/ptu039). arXiv: [1403.0174](https://arxiv.org/abs/1403.0174) [hep-th] (cit. on pp. 63, 65).
- [206] Manuel Delgado. “Classroom Note: The Lagrange–Charpit Method”. In: *SIAM Rev.* (Aug. 2006). DOI: [10.1137/S0036144595293534](https://doi.org/10.1137/S0036144595293534) (cit. on p. 64).
- [207] A.D. Polyanin and V.F. Zaitsev. *Handbook of Nonlinear Partial Differential Equations, Second Edition*. 2. ed. A Chapman & Hall book. Florida, USA: CRC Press, Jan. 2016. DOI: [10.1201/b11412](https://doi.org/10.1201/b11412) (cit. on p. 64).
- [208] William J. M. Rankine. “On the thermodynamic theory of waves of finite longitudinal disturbance”. In: *Phil. Trans. R. Soc.* 160 (15 Jan. 1870), pp. 277–288. DOI: [10.1098/rstl.1870.0015](https://doi.org/10.1098/rstl.1870.0015) (cit. on p. 65).
- [209] Pierre-Henri Hugoniot. “On the propagation of motion in bodies and in perfect gases in Particular – I”. In: *Classic papers in shock compression science*. translation of: Hugoniot, Pierre-Henri, *Journal de l’École Polytechnique*, Vol. 57, pp. 3 – 97 (1887). New York: Springer, 1998, pp. 161–243. ISBN: 978-1-4612-2218-7. DOI: [10.1007/978-1-4612-2218-7_7](https://doi.org/10.1007/978-1-4612-2218-7_7) (cit. on p. 65).
- [210] Sergei K. Godunov. “Eine Differenzenmethode für die Näherungsberechnung unstetiger Lösungen der hydrodynamischen Gleichungen”. In: *Mat. Sb., Nov. Ser.* 47 (1959), pp. 271–306 (cit. on p. 68).
- [211] Philip L. Roe. “Approximate Riemann solvers, parameter vectors, and difference schemes”. In: *Journal of Computational Physics* 135.2 (Aug. 1997), pp. 250–258. DOI: [10.1006/jcph.1997.5705](https://doi.org/10.1006/jcph.1997.5705) (cit. on p. 68).
- [212] Amiram Harten, Peter D. Lax, and Bram van Leer. “On upstream differencing and Godunov-type schemes for hyperbolic conservation laws”. In: *SIAM Review* 25.1 (1983), pp. 35–61. DOI: [10.1137/1025002](https://doi.org/10.1137/1025002) (cit. on p. 68).
- [213] Bernd Einfeldt. “On Godunov-type Methods for Gas Dynamics”. In: *SIAM Journal on Numerical Analysis* 25.2 (1988), pp. 294–318. DOI: [10.1137/0725021](https://doi.org/10.1137/0725021) (cit. on p. 68).
- [214] Haim Nessyahu and Eitan Tadmor. “Non-oscillatory central differencing for hyperbolic conservation laws”. In: *Journal of Computational Physics* 87.2 (1990), pp. 408–463. DOI: [10.1016/0021-9991\(90\)90260-8](https://doi.org/10.1016/0021-9991(90)90260-8) (cit. on pp. 69, 70).
- [215] Bram van Leer. “Towards the ultimate conservative difference scheme. V. A second-order sequel to Godunov’s method”. In: *Journal of Computational Physics* 32.1 (1979), pp. 101–136. DOI: [10.1016/0021-9991\(79\)90145-1](https://doi.org/10.1016/0021-9991(79)90145-1) (cit. on p. 69).
- [216] Peter D. Lax. “Weak solutions of nonlinear hyperbolic equations and their numerical computation”. In: *Communications on Pure and Applied Mathematics* 7.1 (Feb. 1954), pp. 159–193. DOI: [10.1002/cpa.3160070112](https://doi.org/10.1002/cpa.3160070112) (cit. on pp. 69, 70).

- [217] Kurt O. Friedrichs. “Symmetric hyperbolic linear differential equations”. In: *Communications on Pure and Applied Mathematics* 7.2 (May 1954), pp. 345–392. DOI: [10.1002/cpa.3160070206](https://doi.org/10.1002/cpa.3160070206) (cit. on pp. 69, 70).
- [218] Amiram Harten. “High resolution schemes for hyperbolic conservation laws”. In: *Journal of Computational Physics* 49.3 (1983), pp. 357–393. DOI: [https://doi.org/10.1016/0021-9991\(83\)90136-5](https://doi.org/10.1016/0021-9991(83)90136-5) (cit. on pp. 69, 77).
- [219] Wikipedia contributors. *Flux limiter*. [Online; accessed 2020.10.15]. 2020. URL: https://en.wikipedia.org/wiki/Flux_limiter (cit. on p. 69).
- [220] Philip L. Roe. “Characteristic-Based Schemes for the Euler Equations”. In: *Annual Review of Fluid Mechanics* 18.1 (1986), pp. 337–365. DOI: [10.1146/annurev.fl.18.010186.002005](https://doi.org/10.1146/annurev.fl.18.010186.002005) (cit. on p. 69).
- [221] Xu-Dong Liu, Stanley Osher, and Tony Chan. “Weighted Essentially Non-oscillatory Schemes”. In: *Journal of Computational Physics* 115.1 (1994), pp. 200–212. DOI: [10.1006/jcph.1994.1187](https://doi.org/10.1006/jcph.1994.1187) (cit. on p. 69).
- [222] Doron Levy, Gabriella Puppo, and Giovanni Russo. “Central WENO Schemes for hyperbolic systems of conservation laws”. In: *Mathematical Modelling and Numerical Analysis* 33 (May 1999), pp. 547–571. DOI: [10.1051/m2an:1999152](https://doi.org/10.1051/m2an:1999152) (cit. on p. 69).
- [223] Doron Levy, Gabriella Puppo, and Giovanni Russo. “Compact Central WENO Schemes for Multidimensional Conservation Laws”. In: *Siam Journal on Scientific Computing* 22 (Sept. 2000). DOI: [10.1137/S1064827599359461](https://doi.org/10.1137/S1064827599359461). arXiv: [math/9911089](https://arxiv.org/abs/math/9911089) [cs.NA] (cit. on p. 69).
- [224] Alexander Kurganov and Doron Levy. “A Third-Order Semi-Discrete Central Scheme for Conservation Laws and Convection-Diffusion Equations”. In: *SIAM Journal on Scientific Computing* 22 (Mar. 2000). DOI: [10.1137/S1064827599360236](https://doi.org/10.1137/S1064827599360236). arXiv: [math/0002133](https://arxiv.org/abs/math/0002133) [math.NA] (cit. on pp. 69, 71).
- [225] Guang-Shan Jiang and Chi-Wang Shu. “Efficient Implementation of Weighted ENO Schemes”. In: *Journal of Computational Physics* 126.1 (1996), pp. 202–228. DOI: [10.1006/jcph.1996.0130](https://doi.org/10.1006/jcph.1996.0130) (cit. on p. 69).
- [226] Jing Shi, Changqing Hu, and Chi-Wang Shu. “A Technique of Treating Negative Weights in WENO Schemes”. In: *J. Comput. Phys.* 175.1 (Jan. 2002), pp. 108–127. DOI: [10.1006/jcph.2001.6892](https://doi.org/10.1006/jcph.2001.6892) (cit. on p. 69).
- [227] Alexander Kurganov, Guergana Petrova, and Bojan Popov. “Adaptive Semidiscrete Central-Upwind Schemes for Nonconvex Hyperbolic Conservation Laws”. In: *SIAM J. Scientific Computing* 29 (Jan. 2007), pp. 2381–2401. DOI: [10.1137/040614189](https://doi.org/10.1137/040614189) (cit. on pp. 69, 70).
- [228] Ambady Suresh and Hung T. Huynh. “Accurate Monotonicity-Preserving Schemes with Runge–Kutta Time Stepping”. In: *J. Comput. Phys.* 136.1 (1997), pp. 83–99. DOI: <https://doi.org/10.1006/jcph.1997.5745> (cit. on p. 69).
- [229] Thomas Jourdan et al. “An accurate scheme to solve cluster dynamics equations using a Fokker–Planck approach”. In: *Comput. Phys. Commun.* 207 (2016), pp. 170–178. DOI: <https://doi.org/10.1016/j.cpc.2016.06.001> (cit. on p. 69).
- [230] Philipp Mösta et al. “GRHydro: A new open source general-relativistic magnetohydrodynamics code for the Einstein Toolkit”. In: *Class. Quant. Grav.* 31 (2014), p. 015005. DOI: [10.1088/0264-9381/31/1/015005](https://doi.org/10.1088/0264-9381/31/1/015005). arXiv: [1304.5544](https://arxiv.org/abs/1304.5544) [gr-qc] (cit. on p. 69).
- [231] Alexander Kurganov, Sebastian Noelle, and Guergana Petrova. “Semidiscrete Central-Upwind Schemes for Hyperbolic Conservation Laws and Hamilton–Jacobi Equations”. In: *SIAM J. Sci. Comput.* 23.3 (Mar. 2001), pp. 707–740. DOI: [10.1137/S1064827500373413](https://doi.org/10.1137/S1064827500373413) (cit. on p. 70).
- [232] Xu-dong Liu and Eitan Tadmor. “Third Order Nonoscillatory Central Scheme For Hyperbolic Conservation Laws”. In: *Numerische Mathematik* 79 (Nov. 2000). DOI: [10.1007/s002110050345](https://doi.org/10.1007/s002110050345) (cit. on p. 70).

- [233] Guang-shan Jiang and Eitan Tadmor. “Non-oscillatory Central Schemes for Multidimensional Hyperbolic Conservation Laws”. In: *SIAM J. Sci. Comput* 19 (1997), pp. 1892–1917. DOI: [10.1137/S106482759631041X](https://doi.org/10.1137/S106482759631041X) (cit. on p. 70).
- [234] Alina Chertock, Alexander Kurganov, and Philip Rosenau. “On degenerate saturated-diffusion equations with convection”. In: *Nonlinearity* 18 (Mar. 2005), pp. 609–630. DOI: [10.1088/0951-7715/18/2/009](https://doi.org/10.1088/0951-7715/18/2/009) (cit. on p. 71).
- [235] Jean-Michel Caillol. “The non-perturbative renormalization group in the ordered phase”. In: *Nucl. Phys. B* 855 (Sept. 2012), pp. 854–884. DOI: [10.1016/j.nuclphysb.2011.10.026](https://doi.org/10.1016/j.nuclphysb.2011.10.026). arXiv: [1109.4024](https://arxiv.org/abs/1109.4024) [[cond-mat.stat-mech](#)] (cit. on pp. 72, 95).
- [236] Christopher Jung et al. “Self-consistent O(4) model spectral functions from analytically continued functional renormalization group flows”. In: *Phys. Rev. D* 104.9 (Nov. 2021), p. 094011. DOI: [10.1103/PhysRevD.104.094011](https://doi.org/10.1103/PhysRevD.104.094011). arXiv: [2107.10748](https://arxiv.org/abs/2107.10748) [[hep-ph](#)] (cit. on p. 73).
- [237] Huazhong Tang and Tao Tang. “Adaptive Mesh Methods for One- and Two-Dimensional Hyperbolic Conservation Laws”. In: *SIAM Journal on Numerical Analysis* 41 (Apr. 2003), pp. 487–515. DOI: [10.1137/S003614290138437X](https://doi.org/10.1137/S003614290138437X) (cit. on p. 76).
- [238] Peter D. Lax. “1. Hyperbolic Systems of Conservation Laws and the Mathematical Theory of Shock Waves”. In: *Hyperbolic Systems of Conservation Laws and the Mathematical Theory of Shock Waves*. Society for Industrial and Applied Mathematics, 1973, pp. 1–48. DOI: [10.1137/1.9781611970562.ch1](https://doi.org/10.1137/1.9781611970562.ch1) (cit. on p. 77).
- [239] Eleuterio F. Toro. *Riemann Solvers and Numerical Methods for Fluid Dynamics*. 3rd ed. Berlin, Germany: Springer-Verlag, 2009. ISBN: 978-3-540-25202-3. DOI: [10.1007/978-3-540-49834-6](https://doi.org/10.1007/978-3-540-49834-6) (cit. on p. 77).
- [240] Wolfram Research, Inc. *Mathematica, Version 12.1*. Champaign, IL. 2020. URL: <https://www.wolfram.com/mathematica> (cit. on p. 82).
- [241] Bengt Fornberg. “Generation of finite difference formulas on arbitrarily spaced grids”. In: *Math. Comput.* 51.184 (1988), pp. 699–706. ISSN: 0025-5718. DOI: [10.1090/S0025-5718-1988-0935077-0](https://doi.org/10.1090/S0025-5718-1988-0935077-0) (cit. on p. 86).
- [242] Milton Abramowitz and Irene A. Stegun. *Handbook of Mathematical Functions with Formulas, Graphs, and Mathematical Tables*. ninth Dover printing, tenth GPO printing. Mineola, NY, USA: Dover Publications Inc., 1964 (cit. on pp. 86, 263, 267–269).
- [243] William H. Press et al. *Numerical Recipes in C: The art of scientific computing*. 2nd ed. Cambridge, USA: Cambridge University Press, 1992. ISBN: 0-521-43108-5 (cit. on p. 91).
- [244] Jens Braun, Marc Leonhardt, and Jan M. Pawłowski. “Renormalization group consistency and low-energy effective theories”. In: *SciPost Phys.* 6.5 (May 2019), p. 056. DOI: [10.21468/SciPostPhys.6.5.056](https://doi.org/10.21468/SciPostPhys.6.5.056). arXiv: [1806.04432](https://arxiv.org/abs/1806.04432) [[hep-ph](#)] (cit. on pp. 93, 174, 203, 232–234).
- [245] Jens Braun, Kai Schwenzer, and Hans-Jurgen Pirner. “Linking the quark meson model with QCD at high temperature”. In: *Phys. Rev. D* 70 (Oct. 2004), p. 085016. DOI: [10.1103/PhysRevD.70.085016](https://doi.org/10.1103/PhysRevD.70.085016). arXiv: [hep-ph/0312277](https://arxiv.org/abs/hep-ph/0312277) (cit. on pp. 93, 203).
- [246] Tina Katharina Herbst et al. “Thermodynamics of QCD at vanishing density”. In: *Phys. Lett. B* 731 (Apr. 2014), pp. 248–256. DOI: [10.1016/j.physletb.2014.02.045](https://doi.org/10.1016/j.physletb.2014.02.045). arXiv: [1308.3621](https://arxiv.org/abs/1308.3621) [[hep-ph](#)] (cit. on p. 93).
- [247] Lisa M. Haas et al. “Improved Polyakov-loop potential for effective models from functional calculations”. In: *Phys. Rev. D* 87.7 (Apr. 2013), p. 076004. DOI: [10.1103/PhysRevD.87.076004](https://doi.org/10.1103/PhysRevD.87.076004). arXiv: [1302.1993](https://arxiv.org/abs/1302.1993) [[hep-ph](#)] (cit. on p. 93).
- [248] Paul Springer et al. “QCD-inspired determination of NJL model parameters”. In: *EPJ Web Conf.* 137 (2017). Ed. by Y. Foka, N. Brambilla, and V. Kovalenko, p. 03022. DOI: [10.1051/epjconf/201713703022](https://doi.org/10.1051/epjconf/201713703022). arXiv: [1611.06020](https://arxiv.org/abs/1611.06020) [[hep-ph](#)] (cit. on p. 93).

- [249] Marcela Peláez and Nicolás Wschebor. “Ordered phase of the $O(N)$ model within the nonperturbative renormalization group”. In: *Phys. Rev. E* 94.4 (Oct. 2016), p. 042136. DOI: [10.1103/PhysRevE.94.042136](https://doi.org/10.1103/PhysRevE.94.042136). arXiv: [1510.05709](https://arxiv.org/abs/1510.05709) [[cond-mat.stat-mech](https://arxiv.org/abs/1510.05709)] (cit. on pp. 93, 95).
- [250] Jens Braun, Benjamin Klein, and Hans-Juergen Pirner. “Volume dependence of the pion mass in the quark-meson-model”. In: *Phys. Rev. D* 71 (Jan. 2005), p. 014032. DOI: [10.1103/PhysRevD.71.014032](https://doi.org/10.1103/PhysRevD.71.014032). arXiv: [hep-ph/0408116](https://arxiv.org/abs/hep-ph/0408116) (cit. on pp. 96, 275).
- [251] Henry Wilbraham. “On a certain periodic function”. In: *Cambridge and Dublin Mathematical Journal* 3 (1848), pp. 198–201 (cit. on p. 98).
- [252] Josiah W. Gibbs. “Fourier’s series”. In: *Nature* 59 (Dec. 1898), pp. 200–200. DOI: [10.1038/059200b0](https://doi.org/10.1038/059200b0) (cit. on p. 98).
- [253] Josiah W. Gibbs. “Fourier’s series”. In: *Nature* 59 (Apr. 1899), pp. 606–606. DOI: [10.1038/059606a0](https://doi.org/10.1038/059606a0) (cit. on p. 98).
- [254] John P. Boyd. *Chebyshev and Fourier spectral methods*. 2nd ed. 1st ed. in 1969 by Springer-Verlag, Berlin Heidelberg, in the series *Lecture Notes in Engeneering, Vol. 49*. Mineola, New York: Dover Publications, 2001. ISBN: 978-0486411835. URL: <https://depts.washington.edu/ph506/Boyd.pdf> (cit. on p. 98).
- [255] Jean Zinn-Justin. “Critical Phenomena: field theoretical approach”. In: *Scholarpedia* 5.5 (2010). revision #148508, p. 8346. DOI: [10.4249/scholarpedia.8346](https://doi.org/10.4249/scholarpedia.8346) (cit. on p. 101).
- [256] Bernd-Jochen Schaefer, Oliver Bohr, and Jochen Wambach. “Renormalization group flow equations for the scalar $O(N)$ theory”. In: *Int. J. Mod. Phys. A* 16 (Apr. 2001). Ed. by S. Arnone et al., pp. 2119–2124. DOI: [10.1142/S0217751X01004803](https://doi.org/10.1142/S0217751X01004803). arXiv: [hep-ph/0011371](https://arxiv.org/abs/hep-ph/0011371) (cit. on pp. 110, 116).
- [257] Jonathan T. Lenaghan and Dirk H. Rischke. “The $O(N)$ model at finite temperature: Renormalization of the gap equations in Hartree and large- N approximation”. In: *J. Phys. G* 26 (2000), pp. 431–450. DOI: [10.1088/0954-3899/26/4/309](https://doi.org/10.1088/0954-3899/26/4/309). arXiv: [nuc1-th/9901049](https://arxiv.org/abs/nuc1-th/9901049) (cit. on p. 110).
- [258] Alexander Kurganov et al. “Adaptive Moving Mesh Central-Upwind Schemes for Hyperbolic System of PDEs: Applications to Compressible Euler Equations and Granular Hydrodynamics”. In: *Communications on Applied Mathematics and Computation* (Sept. 2020), pp. 1–35. DOI: [10.1007/s42967-020-00082-6](https://doi.org/10.1007/s42967-020-00082-6) (cit. on p. 114).
- [259] Martin J. Steil, Adrian Koenigstein, and Jens Braun. *Numerical fluid dynamics for FRG flow equations: Zero-dimensional QFTs as numerical test cases - Part IV: A fermion-boson model*. in preparation (cit. on p. 115).
- [260] Jens Braun, Holger Gies, and Hans-Juergen Pirner. “RG flow of the Polyakov-loop potential: First status report”. In: *AIP Conf. Proc.* 775.1 (June 2005). Ed. by Jean-Philippe Lansberg, Jean-Rene Cudell, and Joseph Cugnon, pp. 162–172. DOI: [10.1063/1.1961053](https://doi.org/10.1063/1.1961053). arXiv: [hep-ph/0610341](https://arxiv.org/abs/hep-ph/0610341) (cit. on p. 116).
- [261] Romain Daviet and Nicolas Dupuis. “Nonperturbative functional renormalization-group approach to the sine-Gordon model and the Lukyanov-Zamolodchikov conjecture”. In: *Phys. Rev. Lett.* 122.15 (Apr. 2019), p. 155301. DOI: [10.1103/PhysRevLett.122.155301](https://doi.org/10.1103/PhysRevLett.122.155301). arXiv: [1812.01908](https://arxiv.org/abs/1812.01908) [[cond-mat.stat-mech](https://arxiv.org/abs/1812.01908)] (cit. on p. 116).
- [262] Florian Marhauser and Jan M. Pawłowski. *Confinement in Polyakov Gauge*. Dec. 2008. arXiv: [0812.1144](https://arxiv.org/abs/0812.1144) [[hep-ph](https://arxiv.org/abs/0812.1144)] (cit. on p. 116).
- [263] Patrick Jentsch et al. “Physical properties of the massive Schwinger model from the nonperturbative functional renormalization group”. In: *Phys. Rev. D* 105.1 (Jan. 2022), p. 016028. DOI: [10.1103/PhysRevD.105.016028](https://doi.org/10.1103/PhysRevD.105.016028). arXiv: [2106.08310](https://arxiv.org/abs/2106.08310) [[hep-th](https://arxiv.org/abs/2106.08310)] (cit. on p. 116).
- [264] Jan M. Pawłowski and Julian M. Urban. *Flow-based density of states for complex actions*. Mar. 2022. arXiv: [2203.01243](https://arxiv.org/abs/2203.01243) [[hep-lat](https://arxiv.org/abs/2203.01243)] (cit. on p. 116).

- [265] Jean-Paul Blaizot, Jan M. Pawłowski, and Urko Reinosa. “Functional renormalization group and 2PI effective action formalism”. In: *Annals Phys.* 431 (2021), p. 168549. DOI: [10.1016/j.aop.2021.168549](https://doi.org/10.1016/j.aop.2021.168549). arXiv: [2102.13628](https://arxiv.org/abs/2102.13628) [hep-th] (cit. on p. 116).
- [266] Daniel F. Litim and Matthew J. Trott. “Asymptotic safety of scalar field theories”. In: *Phys. Rev. D* 98.12 (2018), p. 125006. DOI: [10.1103/PhysRevD.98.125006](https://doi.org/10.1103/PhysRevD.98.125006). arXiv: [1810.01678](https://arxiv.org/abs/1810.01678) [hep-th] (cit. on p. 116).
- [267] Oliver Bohr, Bernd-Jochen Schaefer, and Jochen Wambach. “Renormalization group flow equations and the phase transition in $O(N)$ models”. In: *Int. J. Mod. Phys. A* 16 (Sept. 2001), pp. 3823–3852. DOI: [10.1142/S0217751X0100502X](https://doi.org/10.1142/S0217751X0100502X). arXiv: [hep-ph/0007098](https://arxiv.org/abs/hep-ph/0007098) (cit. on p. 116).
- [268] Shunsuke Yabunaka and Bertrand Delamotte. “Surprises in $O(N)$ Models: Nonperturbative Fixed Points, Large N Limits, and Multicriticality”. In: *Phys. Rev. Lett.* 119.19 (Nov. 2017), p. 191602. DOI: [10.1103/PhysRevLett.119.191602](https://doi.org/10.1103/PhysRevLett.119.191602). arXiv: [1707.04383](https://arxiv.org/abs/1707.04383) [cond-mat.stat-mech] (cit. on p. 116).
- [269] Shunsuke Yabunaka and Bertrand Delamotte. “Why Might the Standard Large N Analysis Fail in the $O(N)$ Model: The Role of Cusps in the Fixed Point Potentials”. In: *Phys. Rev. Lett.* 121.23 (Dec. 2018), p. 231601. DOI: [10.1103/PhysRevLett.121.231601](https://doi.org/10.1103/PhysRevLett.121.231601). arXiv: [1807.04681](https://arxiv.org/abs/1807.04681) [cond-mat.stat-mech] (cit. on p. 116).
- [270] Ivan Balog et al. “Convergence of nonperturbative approximations to the Renormalization Group”. In: *Phys. Rev. Lett.* 123.24 (Dec. 2019), p. 240604. DOI: [10.1103/PhysRevLett.123.240604](https://doi.org/10.1103/PhysRevLett.123.240604). arXiv: [1907.01829](https://arxiv.org/abs/1907.01829) [cond-mat.stat-mech] (cit. on pp. 116, 167).
- [271] Federico Benitez et al. “Solutions of renormalization group flow equations with full momentum dependence”. In: *Phys. Rev. E* 80 (Sept. 2009), p. 030103. DOI: [10.1103/PhysRevE.80.030103](https://doi.org/10.1103/PhysRevE.80.030103). arXiv: [0901.0128](https://arxiv.org/abs/0901.0128) [cond-mat.stat-mech] (cit. on pp. 116, 259).
- [272] Federico Benitez et al. “Non-perturbative renormalization group preserving full-momentum dependence: implementation and quantitative evaluation”. In: *Phys. Rev. E* 85 (Feb. 2012), p. 026707. DOI: [10.1103/PhysRevE.85.026707](https://doi.org/10.1103/PhysRevE.85.026707). arXiv: [1110.2665](https://arxiv.org/abs/1110.2665) [cond-mat.stat-mech] (cit. on pp. 116, 259).
- [273] Dirk-Uwe Jungnickel and Christof Wetterich. “Effective action for the chiral quark-meson model”. In: *Phys. Rev. D* 53 (May 1996), pp. 5142–5175. DOI: [10.1103/PhysRevD.53.5142](https://doi.org/10.1103/PhysRevD.53.5142). arXiv: [hep-ph/9505267](https://arxiv.org/abs/hep-ph/9505267) (cit. on pp. 117, 166, 303, 309).
- [274] Ralf-Arno Tripolt et al. “Low-temperature behavior of the quark-meson model”. In: *Phys. Rev. D* 97.3 (Feb. 2018), p. 034022. DOI: [10.1103/PhysRevD.97.034022](https://doi.org/10.1103/PhysRevD.97.034022). arXiv: [1709.05991](https://arxiv.org/abs/1709.05991) [hep-ph] (cit. on pp. 117, 124, 216, 219, 220).
- [275] Friederike J. Ihssen. “Low-energy effective models of QCD at finite temperatures and densities”. master’s thesis. University of Heidelberg, 2020 (cit. on pp. 117, 163, 180, 190, 258).
- [276] G. Fejős and A. Patkós. “Field dependence of the Yukawa coupling in the three flavor quark-meson model”. In: *Phys. Rev. D* 103.5 (2021), p. 056015. DOI: [10.1103/PhysRevD.103.056015](https://doi.org/10.1103/PhysRevD.103.056015). arXiv: [2011.08387](https://arxiv.org/abs/2011.08387) [hep-ph] (cit. on pp. 117, 194, 326).
- [277] Nils Strodthoff and Lorenz von Smekal. “Polyakov-Quark-Meson-Diquark Model for two-color QCD”. In: *Phys. Lett. B* 731 (Apr. 2014), pp. 350–357. DOI: [10.1016/j.physletb.2014.03.008](https://doi.org/10.1016/j.physletb.2014.03.008). arXiv: [1306.2897](https://arxiv.org/abs/1306.2897) [hep-ph] (cit. on p. 117).
- [278] Naseemuddin Khan et al. *The Phase Diagram of QC2D from Functional Methods*. Dec. 2015. arXiv: [1512.03673](https://arxiv.org/abs/1512.03673) [hep-ph] (cit. on pp. 117, 123, 192, 230, 242).
- [279] Johannes Weyrich, Nils Strodthoff, and Lorenz von Smekal. “Chiral mirror-baryon-meson model and nuclear matter beyond mean-field approximation”. In: *Phys. Rev. C* 92.1 (July 2015), p. 015214. DOI: [10.1103/PhysRevC.92.015214](https://doi.org/10.1103/PhysRevC.92.015214). arXiv: [1504.02697](https://arxiv.org/abs/1504.02697) [nucl-th] (cit. on pp. 117, 130).

- [280] Ralf-Arno Tripolt et al. “Vector and axial-vector mesons in nuclear matter”. In: *Phys. Rev. D* 104.5 (Sept. 2021), p. 054005. DOI: [10.1103/PhysRevD.104.054005](https://doi.org/10.1103/PhysRevD.104.054005). arXiv: [2105.00861](https://arxiv.org/abs/2105.00861) [[hep-ph](#)] (cit. on pp. [117](#), [130](#)).
- [281] Len Brandes, Norbert Kaiser, and Wolfram Weise. “Fluctuations and phases in baryonic matter”. In: *Eur. Phys. J. A* 57.7 (July 2021), p. 243. DOI: [10.1140/epja/s10050-021-00528-2](https://doi.org/10.1140/epja/s10050-021-00528-2). arXiv: [2103.06096](https://arxiv.org/abs/2103.06096) [[nucl-th](#)] (cit. on pp. [117](#), [122](#), [123](#), [130](#)).
- [282] Roger F. Dashen, Brosl Hasslacher, and Andre Neveu. “Semiclassical Bound States in an Asymptotically Free Theory”. In: *Phys. Rev. D* 12 (Oct. 1975), p. 2443. DOI: [10.1103/PhysRevD.12.2443](https://doi.org/10.1103/PhysRevD.12.2443) (cit. on pp. [121](#), [133](#), [135](#), [152](#), [153](#)).
- [283] Alexander B. Zamolodchikov and Alexei B. Zamolodchikov. “Exact S Matrix of Gross-Neveu Elementary Fermions”. In: *Phys. Lett. B* 72 (Jan. 1978), pp. 481–483. DOI: [10.1016/0370-2693\(78\)90738-4](https://doi.org/10.1016/0370-2693(78)90738-4) (cit. on p. [121](#)).
- [284] Edward Witten. “Some Properties of the $(\bar{\psi}\psi)^2$ Model in Two-Dimensions”. In: *Nucl. Phys. B* 142 (Sept. 1978), pp. 285–300. DOI: [10.1016/0550-3213\(78\)90204-3](https://doi.org/10.1016/0550-3213(78)90204-3) (cit. on pp. [121](#), [153](#)).
- [285] Alexander B. Zamolodchikov and Alexei B. Zamolodchikov. “Factorized s Matrices in Two-Dimensions as the Exact Solutions of Certain Relativistic Quantum Field Models”. In: *Annals Phys.* 120 (Aug. 1979). Ed. by I. M. Khalatnikov and V. P. Mineev, pp. 253–291. DOI: [10.1016/0003-4916\(79\)90391-9](https://doi.org/10.1016/0003-4916(79)90391-9) (cit. on pp. [121](#), [195](#)).
- [286] Bernd A. Berg et al. “Scattering Amplitudes of the Gross-Neveu and Nonlinear σ Models in Higher Orders of the $1/N$ Expansion”. In: *Phys. Lett. B* 76 (June 1978), pp. 502–504. DOI: [10.1016/0370-2693\(78\)90916-4](https://doi.org/10.1016/0370-2693(78)90916-4) (cit. on p. [121](#)).
- [287] Christopher R. Allton et al. “The QCD thermal phase transition in the presence of a small chemical potential”. In: *Phys. Rev. D* 66 (Oct. 2002), p. 074507. DOI: [10.1103/PhysRevD.66.074507](https://doi.org/10.1103/PhysRevD.66.074507). arXiv: [hep-lat/0204010](https://arxiv.org/abs/hep-lat/0204010) (cit. on p. [122](#)).
- [288] Owe Philipsen. “The QCD equation of state from the lattice”. In: *Prog. Part. Nucl. Phys.* 70 (May 2013), pp. 55–107. DOI: [10.1016/j.pnpnp.2012.09.003](https://doi.org/10.1016/j.pnpnp.2012.09.003). arXiv: [1207.5999](https://arxiv.org/abs/1207.5999) [[hep-lat](#)] (cit. on p. [122](#)).
- [289] Heng-Tong Ding, Frithjof Karsch, and Swagato Mukherjee. “Thermodynamics of strong-interaction matter from Lattice QCD”. In: *Int. J. Mod. Phys. E* 24.10 (Sept. 2015), p. 1530007. DOI: [10.1142/S0218301315300076](https://doi.org/10.1142/S0218301315300076). arXiv: [1504.05274](https://arxiv.org/abs/1504.05274) [[hep-lat](#)] (cit. on p. [122](#)).
- [290] Jana N. Guenther et al. “Recent lattice QCD results at non-zero baryon densities”. In: *PoS CPOD2017* (Jan. 2018), p. 032. DOI: [10.22323/1.311.0032](https://doi.org/10.22323/1.311.0032) (cit. on p. [122](#)).
- [291] Felipe Attanasio, Benjamin Jäger, and Felix P. G. Ziegler. “Complex Langevin simulations and the QCD phase diagram: Recent developments”. In: *Eur. Phys. J. A* 56.10 (Oct. 2020), p. 251. DOI: [10.1140/epja/s10050-020-00256-z](https://doi.org/10.1140/epja/s10050-020-00256-z). arXiv: [2006.00476](https://arxiv.org/abs/2006.00476) [[hep-lat](#)] (cit. on p. [122](#)).
- [292] Edward V. Shuryak. “Quantum Chromodynamics and the Theory of Superdense Matter”. In: *Phys. Rept.* 61 (May 1980), pp. 71–158. DOI: [10.1016/0370-1573\(80\)90105-2](https://doi.org/10.1016/0370-1573(80)90105-2) (cit. on p. [122](#)).
- [293] Michael Buballa. “NJL model analysis of quark matter at large density”. In: *Phys. Rept.* 407 (Feb. 2005), pp. 205–376. DOI: [10.1016/j.physrep.2004.11.004](https://doi.org/10.1016/j.physrep.2004.11.004). arXiv: [hep-ph/0402234](https://arxiv.org/abs/hep-ph/0402234) (cit. on pp. [122](#), [123](#), [129](#)).
- [294] Dirk H. Rischke. “The Quark gluon plasma in equilibrium”. In: *Prog. Part. Nucl. Phys.* 52 (Mar. 2004), pp. 197–296. DOI: [10.1016/j.pnpnp.2003.09.002](https://doi.org/10.1016/j.pnpnp.2003.09.002). arXiv: [nuc1-th/0305030](https://arxiv.org/abs/nuc1-th/0305030) (cit. on p. [122](#)).
- [295] Stefan B. Ruester et al. “The Phase diagram of neutral quark matter: Self-consistent treatment of quark masses”. In: *Phys. Rev. D* 72 (Aug. 2005), p. 034004. DOI: [10.1103/PhysRevD.72.034004](https://doi.org/10.1103/PhysRevD.72.034004). arXiv: [hep-ph/0503184](https://arxiv.org/abs/hep-ph/0503184) (cit. on pp. [122](#), [123](#), [129](#)).

- [296] Phillip Lakaschus, Michael Buballa, and Dirk H. Rischke. “Competition of inhomogeneous chiral phases and two-flavor color superconductivity in the NJL model”. In: *Phys. Rev. D* 103.3 (Feb. 2021), p. 034030. DOI: [10.1103/PhysRevD.103.034030](https://doi.org/10.1103/PhysRevD.103.034030). arXiv: [2012.07520](https://arxiv.org/abs/2012.07520) [[hep-ph](#)] (cit. on p. [122](#)).
- [297] Stefan Floerchinger and Christof Wetterich. “Chemical freeze-out in heavy ion collisions at large baryon densities”. In: *Nucl. Phys. A* 890-891 (Oct. 2012), pp. 11–24. DOI: [10.1016/j.nuclphysa.2012.07.009](https://doi.org/10.1016/j.nuclphysa.2012.07.009). arXiv: [1202.1671](https://arxiv.org/abs/1202.1671) [[nucl-th](#)] (cit. on p. [122](#)).
- [298] Matthias Drews and Wolfram Weise. “Functional renormalization group studies of nuclear and neutron matter”. In: *Prog. Part. Nucl. Phys.* 93 (Mar. 2017), pp. 69–107. DOI: [10.1016/j.ppnp.2016.10.002](https://doi.org/10.1016/j.ppnp.2016.10.002). arXiv: [1610.07568](https://arxiv.org/abs/1610.07568) [[nucl-th](#)] (cit. on p. [122](#)).
- [299] Larry McLerran and Robert D. Pisarski. “Phases of cold, dense quarks at large N_c ”. In: *Nucl. Phys. A* 796 (Nov. 2007), pp. 83–100. DOI: [10.1016/j.nuclphysa.2007.08.013](https://doi.org/10.1016/j.nuclphysa.2007.08.013). arXiv: [0706.2191](https://arxiv.org/abs/0706.2191) [[hep-ph](#)] (cit. on pp. [122](#), [135](#)).
- [300] Yoshimasa Hidaka, Larry D. McLerran, and Robert D. Pisarski. “Baryons and the phase diagram for a large number of colors and flavors”. In: *Nucl. Phys. A* 808 (Aug. 2008), pp. 117–123. DOI: [10.1016/j.nuclphysa.2008.05.009](https://doi.org/10.1016/j.nuclphysa.2008.05.009). arXiv: [0803.0279](https://arxiv.org/abs/0803.0279) [[hep-ph](#)] (cit. on p. [122](#)).
- [301] Larry McLerran. “Quarkyonic Matter and the Revised Phase Diagram of QCD”. In: *Nucl. Phys. A* 830 (Nov. 2009). Ed. by Paul Stankus et al., pp. 709C–712C. DOI: [10.1016/j.nuclphysa.2009.10.063](https://doi.org/10.1016/j.nuclphysa.2009.10.063). arXiv: [0907.4489](https://arxiv.org/abs/0907.4489) [[nucl-th](#)] (cit. on pp. [122](#), [135](#)).
- [302] Leonid Ya. Glozman, Owe Philipsen, and Robert D. Pisarski. *Chiral spin symmetry and the QCD phase diagram*. Apr. 2022. arXiv: [2204.05083](https://arxiv.org/abs/2204.05083) [[hep-ph](#)] (cit. on p. [122](#)).
- [303] Jens Braun and Benedikt Schallmo. “From quarks and gluons to color superconductivity at supranuclear densities”. In: *Phys. Rev. D* 105.3 (Feb. 2022), p. 036003. DOI: [10.1103/PhysRevD.105.036003](https://doi.org/10.1103/PhysRevD.105.036003). arXiv: [2106.04198](https://arxiv.org/abs/2106.04198) [[hep-ph](#)] (cit. on pp. [123](#), [129](#)).
- [304] Jens Braun and Benedikt Schallmo. “Zero-temperature thermodynamics of dense asymmetric strong-interaction matter”. In: *Phys. Rev. D* 106.7 (Oct. 2022), p. 076010. DOI: [10.1103/PhysRevD.106.076010](https://doi.org/10.1103/PhysRevD.106.076010). arXiv: [2204.00358](https://arxiv.org/abs/2204.00358) [[nucl-th](#)] (cit. on p. [123](#)).
- [305] Peter Fulde and Richard A. Ferrell. “Superconductivity in a Strong Spin-Exchange Field”. In: *Phys. Rev.* 135 (Aug. 1964), A550–A563. DOI: [10.1103/PhysRev.135.A550](https://doi.org/10.1103/PhysRev.135.A550) (cit. on p. [123](#)).
- [306] Anatoly I. Larkin and Yuri N. Ovchinnikov. “Nonuniform state of superconductors”. In: *Zh. Eksp. Teor. Fiz.* 47 (1964), pp. 1136–1146 (cit. on p. [123](#)).
- [307] George Gruner. “The dynamics of spin-density waves”. In: *Rev. Mod. Phys.* 66 (Jan. 1994), pp. 1–24. DOI: [10.1103/RevModPhys.66.1](https://doi.org/10.1103/RevModPhys.66.1) (cit. on p. [123](#)).
- [308] Aurel Bulgac and Michael McNeil Forbes. “A Unitary Fermi Supersolid: The Larkin-Ovchinnikov Phase”. In: *Phys. Rev. Lett.* 101 (Nov. 2008), p. 215301. DOI: [10.1103/PhysRevLett.101.215301](https://doi.org/10.1103/PhysRevLett.101.215301). arXiv: [0804.3364](https://arxiv.org/abs/0804.3364) [[cond-mat.supr-con](#)] (cit. on p. [123](#)).
- [309] Leo Radzihovsky. “Quantum liquid-crystal order in resonant atomic gases”. In: *Physica C* 481 (Nov. 2012), p. 189. DOI: [10.1016/j.physc.2012.04.014](https://doi.org/10.1016/j.physc.2012.04.014). arXiv: [1112.0773](https://arxiv.org/abs/1112.0773) [[cond-mat.quant-gas](#)] (cit. on p. [123](#)).
- [310] Koos B. Gubbels and Henk T. C. Stoof. “Imbalanced Fermi gases at unitarity”. In: *Phys. Rept.* 525 (Apr. 2013), pp. 255–313. DOI: [10.1016/j.physrep.2012.11.004](https://doi.org/10.1016/j.physrep.2012.11.004). arXiv: [1205.0568](https://arxiv.org/abs/1205.0568) [[cond-mat.quant-gas](#)] (cit. on p. [123](#)).
- [311] Dietrich Roscher, Jens Braun, and Joaquín E. Drut. “Inhomogeneous phases in one-dimensional mass- and spin-imbalanced Fermi gases”. In: *Phys. Rev. A* 89.6 (June 2014), p. 063609. DOI: [10.1103/PhysRevA.89.063609](https://doi.org/10.1103/PhysRevA.89.063609). arXiv: [1311.0179](https://arxiv.org/abs/1311.0179) [[cond-mat.quant-gas](#)] (cit. on pp. [123](#), [224](#)).

- [312] Jildou E. Baarsma and Henk T. C. Stoof. *Inhomogeneous Superfluid Phases in the Unitary Li6-K40 Mixture*. May 2013. arXiv: [1212.5450 \[cond-mat.quant-gas\]](#) (cit. on p. [123](#)).
- [313] Michael Buballa and Stefano Carignano. “Inhomogeneous chiral condensates”. In: *Prog. Part. Nucl. Phys.* 81 (Mar. 2015), pp. 39–96. DOI: [10.1016/j.pnpnp.2014.11.001](#). arXiv: [1406.1367 \[hep-ph\]](#) (cit. on pp. [123](#), [210](#), [223](#)).
- [314] Francois Dautry and Ebbe M. Nyman. “Pion condensation and the σ -model in liquid neutron matter”. In: *Nucl. Phys. A* 319 (May 1979), pp. 323–348. DOI: [10.1016/0375-9474\(79\)90518-9](#) (cit. on pp. [123](#), [225](#)).
- [315] Marek Kutschera, Wojciech Broniowski, and Andrzej Kotlorz. “Quark matter with neutral pion condensate”. In: *Phys. Lett. B* 237 (Mar. 1990), pp. 159–163. DOI: [10.1016/0370-2693\(90\)91421-7](#) (cit. on pp. [123](#), [225](#)).
- [316] Wojciech Broniowski, Andrzej Kotlorz, and Marek Kutschera. “Quarks with a pion condensate. A new phase of matter”. In: *Acta Phys. Polon. B* 22 (1991). Ed. by W. Czyz, pp. 145–166 (cit. on p. [123](#)).
- [317] Marek Kutschera, Wojciech Broniowski, and Andrzej Kotlorz. “Quark matter with pion condensate in an effective chiral model”. In: *Nucl. Phys. A* 516 (Oct. 1990), pp. 566–588. DOI: [10.1016/0375-9474\(90\)90128-9](#) (cit. on pp. [123](#), [225](#)).
- [318] Jens Braun et al. “Crystalline ground states in Polyakov-loop extended Nambu–Jona-Lasinio models”. In: *Phys. Rev. D* 93.1 (Jan. 2016), p. 014032. DOI: [10.1103/PhysRevD.93.014032](#). arXiv: [1510.04012 \[hep-ph\]](#) (cit. on pp. [123](#), [124](#), [224](#)).
- [319] Toru Kojo et al. “Quarkyonic Chiral Spirals”. In: *Nucl. Phys. A* 843 (Oct. 2010), pp. 37–58. DOI: [10.1016/j.nuclphysa.2010.05.053](#). arXiv: [0912.3800 \[hep-ph\]](#) (cit. on pp. [123](#), [223](#)).
- [320] Toru Kojo et al. “Interweaving Chiral Spirals”. In: *Nucl. Phys. A* 875 (Feb. 2012), pp. 94–138. DOI: [10.1016/j.nuclphysa.2011.11.007](#). arXiv: [1107.2124 \[hep-ph\]](#) (cit. on pp. [123](#), [223](#)).
- [321] Bastian B. Brandt, Gergely Endrodi, and Sebastian Schmalzbauer. “QCD phase diagram for nonzero isospin-asymmetry”. In: *Phys. Rev. D* 97.5 (Mar. 2018), p. 054514. DOI: [10.1103/PhysRevD.97.054514](#). arXiv: [1712.08190 \[hep-lat\]](#) (cit. on p. [123](#)).
- [322] Bastian B. Brandt et al. “New class of compact stars: Pion stars”. In: *Phys. Rev. D* 98.9 (Nov. 2018), p. 094510. DOI: [10.1103/PhysRevD.98.094510](#). arXiv: [1802.06685 \[hep-ph\]](#) (cit. on p. [123](#)).
- [323] Jens Braun, Andreas Geißel, and Benedikt Schallmo. *Speed of sound in dense strong-interaction matter*. June 2022. arXiv: [2206.06328 \[nucl-th\]](#) (cit. on p. [123](#)).
- [324] Phillip Lakaschus. “Inhomogeneous chiral condensates in low-energy color-superconductivity models of QCD”. PhD thesis. Goethe University Frankfurt, 2021 (cit. on pp. [124](#), [220](#)).
- [325] Bernd-Jochen Schaefer, Jan M. Pawłowski, and Jochen Wambach. “The Phase Structure of the Polyakov–Quark–Meson Model”. In: *Phys. Rev. D* 76 (Oct. 2007), p. 074023. DOI: [10.1103/PhysRevD.76.074023](#). arXiv: [0704.3234 \[hep-ph\]](#) (cit. on p. [124](#)).
- [326] Tina Katharina Herbst, Jan M. Pawłowski, and Bernd-Jochen Schaefer. “The phase structure of the Polyakov–quark–meson model beyond mean field”. In: *Phys. Lett. B* 696 (Jan. 2011), pp. 58–67. DOI: [10.1016/j.physletb.2010.12.003](#). arXiv: [1008.0081 \[hep-ph\]](#) (cit. on p. [124](#)).
- [327] Michael Thies and Konrad Urlichs. “Revised phase diagram of the Gross-Neveu model”. In: *Phys. Rev. D* 67 (12 June 2003), p. 125015. DOI: [10.1103/PhysRevD.67.125015](#). arXiv: [hep-th/0302092](#) (cit. on pp. [124](#), [135](#), [136](#), [206](#), [216](#), [224](#), [225](#)).

- [328] Christian Boehmer, Michael Thies, and Konrad Urlichs. “Tricritical behavior of the massive chiral Gross-Neveu model”. In: *Phys. Rev. D* 75 (May 2007), p. 105017. DOI: [10.1103/PhysRevD.75.105017](https://doi.org/10.1103/PhysRevD.75.105017). arXiv: [hep-th/0702201](https://arxiv.org/abs/hep-th/0702201) (cit. on pp. 124, 216).
- [329] Christian Boehmer et al. “Phase structure of the massive chiral Gross-Neveu model from Hartree-Fock”. In: *Phys. Rev. D* 78 (Sept. 2008), 065043. DOI: [10.1103/PhysRevD.78.065043](https://doi.org/10.1103/PhysRevD.78.065043). arXiv: [0807.2571 \[hep-th\]](https://arxiv.org/abs/0807.2571) (cit. on pp. 124, 216).
- [330] Eiji Nakano and Takumi Tatsumi. “Chiral symmetry and density wave in quark matter”. In: *Phys. Rev. D* 71 (June 2005), p. 114006. DOI: [10.1103/PhysRevD.71.114006](https://doi.org/10.1103/PhysRevD.71.114006). arXiv: [hep-ph/0411350](https://arxiv.org/abs/hep-ph/0411350) (cit. on pp. 124, 216, 219, 220).
- [331] Hiroaki Abuki, Daisuke Ishibashi, and Katsuhiko Suzuki. “Crystalline chiral condensates off the tricritical point in a generalized Ginzburg-Landau approach”. In: *Phys. Rev. D* 85 (Apr. 2012), p. 074002. DOI: [10.1103/PhysRevD.85.074002](https://doi.org/10.1103/PhysRevD.85.074002). arXiv: [1109.1615 \[hep-ph\]](https://arxiv.org/abs/1109.1615) (cit. on pp. 124, 216).
- [332] Philippe de Forcrand and Urs Wenger. “New baryon matter in the lattice Gross-Neveu model”. In: *PoS LAT2006* (Dec. 2006). Ed. by Tom Blum et al., p. 152. DOI: [10.22323/1.032.0152](https://doi.org/10.22323/1.032.0152). arXiv: [hep-lat/0610117](https://arxiv.org/abs/hep-lat/0610117) (cit. on pp. 124, 136, 216).
- [333] Marc Wagner. “Fermions in the pseudoparticle approach”. In: *Phys. Rev. D* 76 (2007), p. 076002. DOI: [10.1103/PhysRevD.76.076002](https://doi.org/10.1103/PhysRevD.76.076002). arXiv: [0704.3023 \[hep-lat\]](https://arxiv.org/abs/0704.3023) (cit. on pp. 124, 136, 216).
- [334] Hiroaki Abuki. “Ginzburg-Landau phase diagram of QCD near chiral critical point - chiral defect lattice and solitonic pion condensate”. In: *Phys. Lett. B* 728 (Jan. 2014), pp. 427–432. DOI: [10.1016/j.physletb.2013.11.037](https://doi.org/10.1016/j.physletb.2013.11.037). arXiv: [1307.8173 \[hep-ph\]](https://arxiv.org/abs/1307.8173) (cit. on p. 124).
- [335] Laurin Pannullo et al. “Inhomogeneous phases in the 1+1 dimensional Gross-Neveu model at finite number of fermion flavors”. In: *Acta Phys. Polon. Supp.* 13 (2020), p. 127. DOI: [10.5506/APhysPo1BSupp.13.127](https://doi.org/10.5506/APhysPo1BSupp.13.127). arXiv: [1902.11066 \[hep-lat\]](https://arxiv.org/abs/1902.11066) (cit. on pp. 126, 139).
- [336] Laurin Pannullo et al. “Lattice investigation of the phase diagram of the 1+1 dimensional Gross-Neveu model at finite number of fermion flavors”. In: *PoS LATTICE2019* (Aug. 2019), p. 063. DOI: [10.22323/1.363.0063](https://doi.org/10.22323/1.363.0063). arXiv: [1909.11513 \[hep-lat\]](https://arxiv.org/abs/1909.11513) (cit. on pp. 126, 139).
- [337] Julian Lenz et al. “Inhomogeneous phases in the Gross-Neveu model in 1+1 dimensions at finite number of flavors”. In: *Phys. Rev. D* 101.9 (May 2020), p. 094512. DOI: [10.1103/PhysRevD.101.094512](https://doi.org/10.1103/PhysRevD.101.094512). arXiv: [2004.00295 \[hep-lat\]](https://arxiv.org/abs/2004.00295) (cit. on pp. 126, 139).
- [338] Julian J. Lenz et al. “Baryons in the Gross-Neveu model in 1+1 dimensions at finite number of flavors”. In: *Phys. Rev. D* 102.11 (Dec. 2020), p. 114501. DOI: [10.1103/PhysRevD.102.114501](https://doi.org/10.1103/PhysRevD.102.114501). arXiv: [2007.08382 \[hep-lat\]](https://arxiv.org/abs/2007.08382) (cit. on pp. 126, 139).
- [339] Yoichiro Nambu and Giovanni Jona-Lasinio. “Dynamical model of elementary particles based on an analogy with superconductivity. I”. In: *Phys. Rev.* 122 (Apr. 1961). Ed. by Tohru Eguchi, pp. 345–358. DOI: [10.1103/PhysRev.122.345](https://doi.org/10.1103/PhysRev.122.345) (cit. on pp. 128, 135).
- [340] Yoichiro Nambu and Giovanni Jona-Lasinio. “Dynamical model of elementary particles based on an analogy with superconductivity. II”. In: *Phys. Rev.* 124 (Oct. 1961). Ed. by Tohru Eguchi, pp. 246–254. DOI: [10.1103/PhysRev.124.246](https://doi.org/10.1103/PhysRev.124.246) (cit. on pp. 128, 135).
- [341] John Bardeen, Leon N. Cooper, and John R. Schrieffer. “Microscopic theory of superconductivity”. In: *Phys. Rev.* 106 (Apr. 1957), p. 162. DOI: [10.1103/PhysRev.106.162](https://doi.org/10.1103/PhysRev.106.162) (cit. on pp. 128, 132).
- [342] Edward Witten. “Chiral Symmetry, the 1/n Expansion, and the SU(N) Thirring Model”. In: *Nucl. Phys. B* 145 (July 1978), pp. 110–118. DOI: [10.1016/0550-3213\(78\)90416-9](https://doi.org/10.1016/0550-3213(78)90416-9) (cit. on pp. 128, 132, 137).
- [343] Michael Thies. “Duality study of the chiral Heisenberg-Gross-Neveu model in 1+1 dimensions”. In: *Phys. Rev. D* 102.9 (2020), p. 096006. DOI: [10.1103/PhysRevD.102.096006](https://doi.org/10.1103/PhysRevD.102.096006). arXiv: [2008.13119 \[hep-th\]](https://arxiv.org/abs/2008.13119) (cit. on pp. 128, 216).

- [344] Mario Soler. “Classical, stable, nonlinear spinor field with positive rest energy”. In: *Phys. Rev. D* 1 (May 1970), pp. 2766–2769. DOI: [10.1103/PhysRevD.1.2766](https://doi.org/10.1103/PhysRevD.1.2766) (cit. on p. 128).
- [345] Walter E. Thirring. “A soluble relativistic field theory”. In: *Annals Phys.* 3.1 (Jan. 1958), pp. 91–112. DOI: [10.1016/0003-4916\(58\)90015-0](https://doi.org/10.1016/0003-4916(58)90015-0) (cit. on pp. 128, 132, 170).
- [346] Jens Braun. “Fermion Interactions and Universal Behavior in Strongly Interacting Theories”. In: *J. Phys. G* 39 (Jan. 2012), p. 033001. DOI: [10.1088/0954-3899/39/3/033001](https://doi.org/10.1088/0954-3899/39/3/033001). arXiv: [1108.4449](https://arxiv.org/abs/1108.4449) [hep-ph] (cit. on pp. 129, 130, 163, 307, 318, 346, 357, 358).
- [347] Ken-Ichi Aoki and Masatoshi Yamada. “The RG flow of Nambu–Jona-Lasinio model at finite temperature and density”. In: *Int. J. Mod. Phys. A* 30.27 (Sept. 2015), p. 1550180. DOI: [10.1142/S0217751X15501808](https://doi.org/10.1142/S0217751X15501808). arXiv: [1504.00749](https://arxiv.org/abs/1504.00749) [hep-ph] (cit. on pp. 129, 163, 307, 318).
- [348] Jens Braun, Marc Leonhardt, and Martin Pospiech. “Fierz-complete NJL model study: Fixed points and phase structure at finite temperature and density”. In: *Phys. Rev. D* 96.7 (Oct. 2017), p. 076003. DOI: [10.1103/PhysRevD.96.076003](https://doi.org/10.1103/PhysRevD.96.076003). arXiv: [1705.00074](https://arxiv.org/abs/1705.00074) [hep-ph] (cit. on pp. 129, 154, 163, 165, 166, 172, 176, 178, 184, 185, 259, 289, 307, 315, 318).
- [349] Wei-jie Fu and Yu-xin Liu. “Four-fermion interactions and the chiral symmetry breaking in an external magnetic field”. In: *Phys. Rev. D* 96.7 (Oct. 2017), p. 074019. DOI: [10.1103/PhysRevD.96.074019](https://doi.org/10.1103/PhysRevD.96.074019). arXiv: [1705.09841](https://arxiv.org/abs/1705.09841) [hep-ph] (cit. on p. 129).
- [350] Jens Braun, Marc Leonhardt, and Martin Pospiech. “Fierz-complete NJL model study. II. Toward the fixed-point and phase structure of hot and dense two-flavor QCD”. In: *Phys. Rev. D* 97.7 (Apr. 2018), p. 076010. DOI: [10.1103/PhysRevD.97.076010](https://doi.org/10.1103/PhysRevD.97.076010). arXiv: [1801.08338](https://arxiv.org/abs/1801.08338) [hep-ph] (cit. on pp. 129, 163, 165, 172, 184, 185, 259, 307, 315, 318).
- [351] Jens Braun, Marc Leonhardt, and Martin Pospiech. “Fierz-complete NJL model study III: Emergence from quark-gluon dynamics”. In: *Phys. Rev. D* 101.3 (Feb. 2020), p. 036004. DOI: [10.1103/PhysRevD.101.036004](https://doi.org/10.1103/PhysRevD.101.036004). arXiv: [1909.06298](https://arxiv.org/abs/1909.06298) [hep-ph] (cit. on pp. 129, 163, 165, 172, 184, 185, 259, 307, 315, 318).
- [352] Marc Leonhardt. “Phase Structure and Equation of State of Dense Strong-Interaction Matter”. PhD thesis. Technical University of Darmstadt, Oct. 2019 (cit. on pp. 129, 203).
- [353] Martin Pospiech. “From Hot to Cold, from Dense to Dilute – Renormalization Group Studies of Strongly-Interacting Matter”. PhD thesis. Technical University of Darmstadt, Sept. 2019 (cit. on pp. 129, 285).
- [354] Jens Braun et al. *Chiral and effective $U(1)_A$ symmetry restoration in QCD*. Dec. 2020. arXiv: [2012.06231](https://arxiv.org/abs/2012.06231) [hep-ph] (cit. on pp. 129, 285).
- [355] Wei-jie Fu et al. *Four-quark scatterings in QCD I*. Sept. 2022. arXiv: [2209.13120](https://arxiv.org/abs/2209.13120) [hep-ph] (cit. on pp. 129, 163, 165).
- [356] Piotr A. Zyla et al. “Review of Particle Physics”. In: *PTEP* 2020.8 (Aug. 2020). and 2021 update, p. 083C01. DOI: [10.1093/ptep/ptaa104](https://doi.org/10.1093/ptep/ptaa104) (cit. on pp. 129, 130).
- [357] Vladimir E. Rochev and Pavel A. Saponov. “The four fermion interaction in $D = 2$, $D = 3$, $D = 4$: A Nonperturbative treatment”. In: *Int. J. Mod. Phys. A* 13 (Aug. 1998), pp. 3649–3666. DOI: [10.1142/S0217751X98001712](https://doi.org/10.1142/S0217751X98001712). arXiv: [hep-th/9710006](https://arxiv.org/abs/hep-th/9710006) (cit. on p. 130).
- [358] Jens Braun and Tina K. Herbst. *On the Relation of the Deconfinement and the Chiral Phase Transition in Gauge Theories with Fundamental and Adjoint Matter*. May 2012. arXiv: [1205.0779](https://arxiv.org/abs/1205.0779) [hep-ph] (cit. on p. 130).
- [359] Werner Wetzel. “Two Loop Beta Function for the Gross-Neveu Model”. In: *Phys. Lett. B* 153 (1985), pp. 297–299. DOI: [10.1016/0370-2693\(85\)90551-9](https://doi.org/10.1016/0370-2693(85)90551-9) (cit. on pp. 130, 169).
- [360] John A. Gracey. “Three loop calculations in the $O(N)$ Gross-Neveu model”. In: *Nucl. Phys. B* 341 (Sept. 1990), pp. 403–418. DOI: [10.1016/0550-3213\(90\)90186-H](https://doi.org/10.1016/0550-3213(90)90186-H) (cit. on pp. 130, 169).

- [361] John A. Gracey. “Computation of the three loop Beta function of the $O(N)$ Gross-Neveu model in minimal subtraction”. In: *Nucl. Phys. B* 367 (Dec. 1991), pp. 657–674. DOI: [10.1016/0550-3213\(91\)90012-M](https://doi.org/10.1016/0550-3213(91)90012-M) (cit. on pp. 130, 169).
- [362] John A. Gracey, Thomas Luthe, and York Schroder. “Four loop renormalization of the Gross-Neveu model”. In: *Phys. Rev. D* 94.12 (Dec. 2016), p. 125028. DOI: [10.1103/PhysRevD.94.125028](https://doi.org/10.1103/PhysRevD.94.125028). arXiv: [1609.05071](https://arxiv.org/abs/1609.05071) [[hep-th](#)] (cit. on pp. 130, 169).
- [363] Gongjun Choi, Thomas A. Ryttov, and Robert Shrock. “Question of a possible infrared zero in the beta function of the finite- N Gross-Neveu model”. In: *Phys. Rev. D* 95.2 (Jan. 2017), p. 025012. DOI: [10.1103/PhysRevD.95.025012](https://doi.org/10.1103/PhysRevD.95.025012). arXiv: [1612.05580](https://arxiv.org/abs/1612.05580) [[hep-th](#)] (cit. on pp. 130, 169, 170).
- [364] Cristina Luperini and Paolo Rossi. “Three-loop β function(s) and effective potential in the Gross-Neveu model”. In: *Annals Phys.* 212 (Dec. 1991), pp. 371–401. DOI: [10.1016/0003-4916\(91\)90120-W](https://doi.org/10.1016/0003-4916(91)90120-W) (cit. on p. 130).
- [365] Andres G. Quinto, Roberto Vega Monroy, and Alysson F. Ferrari. “Renormalization group improvement of the effective potential in a $(1 + 1)$ dimensional Gross-Neveu model”. In: *Nucl. Phys. B* 984 (Nov. 2022), p. 115959. DOI: [10.1016/j.nuclphysb.2022.115959](https://doi.org/10.1016/j.nuclphysb.2022.115959). arXiv: [2108.04079](https://arxiv.org/abs/2108.04079) [[hep-th](#)] (cit. on p. 130).
- [366] John A. Gracey. “Calculation of exponent η to $O(1/N^{*2})$ in the $O(N)$ Gross-Neveu model”. In: *Int. J. Mod. Phys. A* 6 (Jan. 1991). [Erratum: *Int.J.Mod.Phys.A* 6, 2755 (1991)], pp. 395–408. DOI: [10.1142/S0217751X91000241](https://doi.org/10.1142/S0217751X91000241) (cit. on p. 130).
- [367] John A. Gracey. “Computation of $\beta'(g_c)$ at $O(1/N^2)$ in the $O(N)$ Gross-Neveu model in arbitrary dimensions”. In: *Int. J. Mod. Phys. A* 9 (Feb. 1994), pp. 567–590. DOI: [10.1142/S0217751X94000285](https://doi.org/10.1142/S0217751X94000285). arXiv: [hep-th/9306106](https://arxiv.org/abs/hep-th/9306106) (cit. on p. 130).
- [368] Jonathan F. Schonfeld. “Higher Orders in Inverse n in the Gross-Neveu Model”. In: *Nucl. Phys. B* 95 (Aug. 1975), pp. 148–172. DOI: [10.1016/0550-3213\(75\)90486-1](https://doi.org/10.1016/0550-3213(75)90486-1) (cit. on p. 130).
- [369] Baruch Rosenstein, Brian J. Warr, and Seon H. Park. “The Four Fermi Theory Is Renormalizable in $(2+1)$ -Dimensions”. In: *Phys. Rev. Lett.* 62 (Mar. 1989), pp. 1433–1436. DOI: [10.1103/PhysRevLett.62.1433](https://doi.org/10.1103/PhysRevLett.62.1433) (cit. on p. 130).
- [370] Baruch Rosenstein, Brian J. Warr, and Seon H. Park. “Thermodynamics of $(2+1)$ -dimensional Four Fermi Models”. In: *Phys. Rev. D* 39 (May 1989), p. 3088. DOI: [10.1103/PhysRevD.39.3088](https://doi.org/10.1103/PhysRevD.39.3088) (cit. on p. 130).
- [371] Baruch Rosenstein, Brian J. Warr, and Seon H. Park. “Dynamical symmetry breaking in four Fermi interaction models”. In: *Phys. Rept.* 205 (June 1991), pp. 59–108. DOI: [10.1016/0370-1573\(91\)90129-A](https://doi.org/10.1016/0370-1573(91)90129-A) (cit. on p. 130).
- [372] Luigi Rosa, Patrizia Vitale, and Christof Wetterich. “Critical exponents of the Gross-Neveu model from the effective average action”. In: *Phys. Rev. Lett.* 86 (Feb. 2001), pp. 958–961. DOI: [10.1103/PhysRevLett.86.958](https://doi.org/10.1103/PhysRevLett.86.958). arXiv: [hep-th/0007093](https://arxiv.org/abs/hep-th/0007093) (cit. on pp. 130, 187, 307).
- [373] Felix Hofling, Claus Nowak, and Christof Wetterich. “Phase transition and critical behavior of the $D = 3$ Gross-Neveu model”. In: *Phys. Rev. B* 66 (2002), p. 205111. DOI: [10.1103/PhysRevB.66.205111](https://doi.org/10.1103/PhysRevB.66.205111). arXiv: [cond-mat/0203588](https://arxiv.org/abs/cond-mat/0203588) (cit. on pp. 130, 187, 305, 307, 331, 346, 357).
- [374] Jens Braun, Holger Gies, and Daniel D. Scherer. “Asymptotic safety: a simple example”. In: *Phys. Rev. D* 83 (2011), p. 085012. DOI: [10.1103/PhysRevD.83.085012](https://doi.org/10.1103/PhysRevD.83.085012). arXiv: [1011.1456](https://arxiv.org/abs/1011.1456) [[hep-th](#)] (cit. on pp. 130, 170, 171, 187, 188, 305, 307, 331, 346, 357).
- [375] Benjamin Knorr. “Asymptotic safety in QFT: from quantum gravity to graphene”. PhD thesis. Friedrich-Schiller-Universität Jena, Sept. 2017 (cit. on p. 130).
- [376] John C. Collins, Anthony Duncan, and Satish D. Joglekar. “Trace and Dilatation Anomalies in Gauge Theories”. In: *Phys. Rev. D* 16 (July 1977), pp. 438–449. DOI: [10.1103/PhysRevD.16.438](https://doi.org/10.1103/PhysRevD.16.438) (cit. on p. 130).

- [377] Hagen Kleinert. *Particles and Quantum Fields*. 2nd ed. Singapore: World Scientific Publishing Company, May 2016 (cit. on pp. 130, 209, 213).
- [378] Jean Zinn-Justin. “Four fermion interaction near four-dimensions”. In: *Nucl. Phys. B* 367 (Dec. 1991), pp. 105–122. DOI: [10.1016/0550-3213\(91\)90043-W](https://doi.org/10.1016/0550-3213(91)90043-W) (cit. on pp. 130, 131, 159).
- [379] Chaiho Rim and William I. Weisberger. “Ultraviolet Divergences in $1/N$ Expansions of Asymptotically Free Theories”. In: *Phys. Rev. D* 30 (Oct. 1984), p. 1763. DOI: [10.1103/PhysRevD.30.1763](https://doi.org/10.1103/PhysRevD.30.1763) (cit. on p. 130).
- [380] Anne-Christine Davis et al. “Mass generation and renormalization of supersymmetric σ -models and some other two-dimensional theories”. In: *Nucl. Phys. B* 314 (Feb. 1989), pp. 439–466. DOI: [10.1016/0550-3213\(89\)90161-2](https://doi.org/10.1016/0550-3213(89)90161-2) (cit. on p. 130).
- [381] Peter Forgacs, Ferenc Niedermayer, and Peter Weisz. “The Exact mass gap of the Gross-Neveu model (II). The $1/N$ expansion”. In: *Nucl. Phys. B* 367 (Dec. 1991), pp. 144–157. DOI: [10.1016/0550-3213\(91\)90045-Y](https://doi.org/10.1016/0550-3213(91)90045-Y) (cit. on p. 130).
- [382] Alan Chodos and Hisakazu Minakata. “The Thermodynamic Bethe ansatz and the $1/N$ correction to the density phase transition in the Gross-Neveu model”. In: *Nucl. Phys. B* 490 (Apr. 1997), pp. 687–700. DOI: [10.1016/S0550-3213\(97\)00094-1](https://doi.org/10.1016/S0550-3213(97)00094-1). arXiv: [hep-th/9610150](https://arxiv.org/abs/hep-th/9610150) (cit. on pp. 130, 139, 257).
- [383] Ichiro Yotsuyanagi. “Variational study of the Gross-Neveu model”. In: *Phys. Rev. D* 39 (May 1989), p. 3034. DOI: [10.1103/PhysRevD.39.3034](https://doi.org/10.1103/PhysRevD.39.3034) (cit. on p. 131).
- [384] Sung K. Kim et al. “Gaussian approximation of the Gross-Neveu model in the functional Schrödinger picture”. In: *Phys. Rev. D* 40 (Oct. 1989), p. 2647. DOI: [10.1103/PhysRevD.40.2647](https://doi.org/10.1103/PhysRevD.40.2647) (cit. on p. 131).
- [385] Sung K. Kim et al. “Variational study of the bound states in the functional Schrodinger picture”. In: *Annals Phys.* 214 (Feb. 1992), pp. 142–151. DOI: [10.1016/0003-4916\(92\)90064-S](https://doi.org/10.1016/0003-4916(92)90064-S) (cit. on p. 131).
- [386] Christoph Kopper, Jacques Magnen, and Vincent Rivasseau. “Mass generation in the large N Gross-Neveu model”. In: *Commun. Math. Phys.* 169 (Apr. 1995), pp. 121–180. DOI: [10.1007/BF02101599](https://doi.org/10.1007/BF02101599) (cit. on p. 131).
- [387] Anthony Duncan and Moshe Moshe. “Nonperturbative physics from interpolating actions”. In: *Phys. Lett. B* 215 (Dec. 1988), pp. 352–358. DOI: [10.1016/0370-2693\(88\)91447-5](https://doi.org/10.1016/0370-2693(88)91447-5) (cit. on p. 131).
- [388] David Dudal and Henri Verschelde. “The mass gap and vacuum energy of the Gross-Neveu model via the 2-point-particle-irreducible expansion”. In: *Phys. Rev. D* 67 (Jan. 2003), p. 025011. DOI: [10.1103/PhysRevD.67.025011](https://doi.org/10.1103/PhysRevD.67.025011). arXiv: [hep-th/0210098](https://arxiv.org/abs/hep-th/0210098) (cit. on p. 131).
- [389] Frithjof Karsch. “Lattice QCD at finite density”. In: *Nucl. Phys. A* 461 (Jan. 1987), pp. 305C–316C. DOI: [10.1016/0375-9474\(87\)90490-8](https://doi.org/10.1016/0375-9474(87)90490-8) (cit. on pp. 131, 139).
- [390] Asit Kumar De. *A microcanonical study of the lattice Gross-Neveu model using staggered fermions*. Mar. 1987 (cit. on pp. 131, 139).
- [391] Yuval Cohen, Shmuel Elitzur, and Eliezer Rabinovici. “Monte Carlo Study of Chiral Structure: The Gross-Neveu Model”. In: *Phys. Lett. B* 104 (Sept. 1981), pp. 289–293. DOI: [10.1016/0370-2693\(81\)90128-3](https://doi.org/10.1016/0370-2693(81)90128-3) (cit. on pp. 131, 139).
- [392] Yuval Cohen, Shmuel Elitzur, and Eliezer Rabinovici. “A Monte Carlo study of the Gross-Neveu model”. In: *Nucl. Phys. B* 220 (Mar. 1983), pp. 102–118. DOI: [10.1016/0550-3213\(83\)90136-0](https://doi.org/10.1016/0550-3213(83)90136-0) (cit. on pp. 131, 139).
- [393] Norbert Attig et al. “The lattice Gross-Neveu model and the Langevin algorithm”. In: *International Symposium on Field Theory of the Lattice*. Dec. 1987, p. 0595 (cit. on pp. 131, 139).

- [394] Massimo Campostrini, Giuseppe Curci, and Paolo Rossi. “The Gross-Neveu model and the pseudofermion algorithm”. In: *Nucl. Phys. B* 314 (Feb. 1989), pp. 467–518. DOI: [10.1016/0550-3213\(89\)90162-4](https://doi.org/10.1016/0550-3213(89)90162-4) (cit. on pp. 131, 139).
- [395] L. Belanger et al. “Simulating the Gross-Neveu Model With the Langevin Algorithm: A Comparison of Analytical and Numerical Results”. In: *Nucl. Phys. B* 340 (Aug. 1990), pp. 245–279. DOI: [10.1016/0550-3213\(90\)90163-8](https://doi.org/10.1016/0550-3213(90)90163-8) (cit. on p. 131).
- [396] Robert Lacaze, Andre Morel, and Bengt Petersson. “A Langevin simulation of the Gross-Neveu spectrum”. In: *Nucl. Phys. B Proc. Suppl.* 17 (Sept. 1990). Ed. by N. Cabibbo et al., pp. 736–739. DOI: [10.1016/0920-5632\(90\)90354-W](https://doi.org/10.1016/0920-5632(90)90354-W) (cit. on p. 131).
- [397] Peter Forgacs, Ferenc Niedermayer, and Peter Weisz. “The Exact mass gap of the Gross-Neveu model (I). The Thermodynamic Bethe ansatz”. In: *Nucl. Phys. B* 367 (Dec. 1991), pp. 123–143. DOI: [10.1016/0550-3213\(91\)90044-X](https://doi.org/10.1016/0550-3213(91)90044-X) (cit. on p. 131).
- [398] John Hubbard. “Calculation of partition functions”. In: *Phys. Rev. Lett.* 3 (July 1959), pp. 77–80. DOI: [10.1103/PhysRevLett.3.77](https://doi.org/10.1103/PhysRevLett.3.77) (cit. on pp. 131, 157).
- [399] Ruslan L. Stratonovich. “On a Method of Calculating Quantum Distribution Functions”. In: *Soviet Physics Doklady* 2 (July 1957), p. 416 (cit. on pp. 131, 157).
- [400] Ramamurti Rajaraman. “On the alleged equivalence of certain field theories”. In: *Pramana* 11 (Oct. 1978), p. 491. DOI: [10.1007/BF02848170](https://doi.org/10.1007/BF02848170) (cit. on pp. 131, 159).
- [401] Kyriakos Tamvakis and Gerald S. Guralnik. “Irrelevant operators and equivalent field theories”. In: *Nucl. Phys. B* 146 (Dec. 1978), pp. 224–246. DOI: [10.1016/0550-3213\(78\)90440-6](https://doi.org/10.1016/0550-3213(78)90440-6) (cit. on pp. 131, 159).
- [402] Takuya Kanazawa and Yuya Tanizaki. “Structure of Lefschetz thimbles in simple fermionic systems”. In: *JHEP* 03 (Mar. 2015), p. 044. DOI: [10.1007/JHEP03\(2015\)044](https://doi.org/10.1007/JHEP03(2015)044). arXiv: [1412.2802](https://arxiv.org/abs/1412.2802) [hep-th] (cit. on p. 131).
- [403] Andreas Klotzke and Michael Thies. “Kink dynamics, sinh-Gordon solitons and strings in AdS_3 from the Gross-Neveu model”. In: *J. Phys. A* 43 (July 2010), p. 375401. DOI: [10.1088/1751-8113/43/37/375401](https://doi.org/10.1088/1751-8113/43/37/375401). arXiv: [1006.0324](https://arxiv.org/abs/1006.0324) [hep-th] (cit. on p. 131).
- [404] Simone Giombi. “Higher Spin — CFT Duality”. In: *Theoretical Advanced Study Institute in Elementary Particle Physics: New Frontiers in Fields and Strings*. July 2016. DOI: [10.1142/9789813149441_0003](https://doi.org/10.1142/9789813149441_0003). arXiv: [1607.02967](https://arxiv.org/abs/1607.02967) [hep-th] (cit. on p. 131).
- [405] Emilio Elizalde et al. “Phase structure of renormalizable four fermion models in space-times of constant curvature”. In: *Phys. Rev. D* 53 (Feb. 1996), pp. 1917–1926. DOI: [10.1103/PhysRevD.53.1917](https://doi.org/10.1103/PhysRevD.53.1917). arXiv: [hep-th/9505065](https://arxiv.org/abs/hep-th/9505065) (cit. on p. 131).
- [406] Tomohiro Inagaki, Seiji Mukaigawa, and Teizo Muta. “A soluble model of four-fermion interactions in de Sitter space”. In: *Phys. Rev. D* 52 (Oct. 1995), R4267–R4271. DOI: [10.1103/PhysRevD.52.R4267](https://doi.org/10.1103/PhysRevD.52.R4267). arXiv: [hep-th/9505058](https://arxiv.org/abs/hep-th/9505058) (cit. on p. 131).
- [407] Tomohiro Inagaki. “Curvature induced phase transition in a four fermion theory using the weak curvature expansion”. In: *Int. J. Mod. Phys. A* 11 (Oct. 1996), pp. 4561–4576. DOI: [10.1142/S0217751X9600211X](https://doi.org/10.1142/S0217751X9600211X). arXiv: [hep-th/9512200](https://arxiv.org/abs/hep-th/9512200) (cit. on p. 131).
- [408] Ken-Ichi Ishikawa, Tomohiro Inagaki, and Teizo. Muta. *Dynamical symmetry breaking in Einstein universe*. Dec. 1995. arXiv: [hep-th/9512202](https://arxiv.org/abs/hep-th/9512202) (cit. on p. 131).
- [409] Jordan S. Cotler and Mark T. Mueller. *Entanglement Entropy of the Gross-Neveu Model*. Nov. 2015. arXiv: [1512.00023](https://arxiv.org/abs/1512.00023) [hep-th] (cit. on p. 131).
- [410] N. G. Antoniou, A. I. Karanikas, and Costas G. Papadopoulos. “The Gross-Neveu model near the critical temperature. A mechanism for quark-hadron phase transition in relativistic ion collisions”. In: *Phys. Lett. B* 233 (Dec. 1989), pp. 423–428. DOI: [10.1016/0370-2693\(89\)91334-8](https://doi.org/10.1016/0370-2693(89)91334-8) (cit. on p. 131).

- [411] Christof Wetterich. “Quantum fermions from classical bits”. In: *Phil. Trans. A. Math. Phys. Eng. Sci.* 380.2216 (Dec. 2021), p. 20210066. DOI: [10.1098/rsta.2021.0066](https://doi.org/10.1098/rsta.2021.0066). arXiv: [2106.15517](https://arxiv.org/abs/2106.15517) [[quant-ph](#)] (cit. on p. 131).
- [412] Christof Wetterich. “Fermionic quantum field theories as probabilistic cellular automata”. In: *Phys. Rev. D* 105.7 (Apr. 2022), p. 074502. DOI: [10.1103/PhysRevD.105.074502](https://doi.org/10.1103/PhysRevD.105.074502). arXiv: [2111.06728](https://arxiv.org/abs/2111.06728) [[hep-lat](#)] (cit. on p. 131).
- [413] Christof Wetterich. *Fermion picture for cellular automata*. Mar. 2022. arXiv: [2203.14081](https://arxiv.org/abs/2203.14081) [[nlin.CG](#)] (cit. on p. 131).
- [414] Ian K. Affleck. “Phase Transition in the Lattice Gross-Neveu Model”. In: *Phys. Lett. B* 109 (Feb. 1982), pp. 307–310. DOI: [10.1016/0370-2693\(82\)90441-5](https://doi.org/10.1016/0370-2693(82)90441-5) (cit. on pp. 131, 132).
- [415] Lars Onsager. “Crystal statistics. 1. A Two-dimensional model with an order disorder transition”. In: *Phys. Rev.* 65 (Feb. 1944), pp. 117–149. DOI: [10.1103/PhysRev.65.117](https://doi.org/10.1103/PhysRev.65.117) (cit. on p. 131).
- [416] Anthony Zee. “Dynamical Symmetry Breaking on a Lattice”. In: *Phys. Rev. D* 12 (Nov. 1975), p. 3251. DOI: [10.1103/PhysRevD.12.3251](https://doi.org/10.1103/PhysRevD.12.3251) (cit. on pp. 132, 139).
- [417] John M. Kosterlitz and David J. Thouless. “Ordering, metastability and phase transitions in two-dimensional systems”. In: *J. Phys. C* 6.7 (Apr. 1973), pp. 1181–1203. DOI: [10.1088/0022-3719/6/7/010](https://doi.org/10.1088/0022-3719/6/7/010) (cit. on pp. 132, 137).
- [418] H. Eugene Stanley. “Dependence of critical properties on dimensionality of spins”. In: *Phys. Rev. Lett.* 20 (Mar. 1968), p. 589. DOI: [10.1103/PhysRevLett.20.589](https://doi.org/10.1103/PhysRevLett.20.589) (cit. on p. 132).
- [419] Daniel González-Cuadra et al. “The rotor Jackiw-Rebbi model: a cold-atom approach to chiral symmetry restoration and quark confinement”. In: *PRX Quantum* 1 (Dec. 2020), p. 020321. DOI: [10.1103/PRXQuantum.1.020321](https://doi.org/10.1103/PRXQuantum.1.020321). arXiv: [2008.02045](https://arxiv.org/abs/2008.02045) [[cond-mat.quant-gas](#)] (cit. on p. 132).
- [420] Michael Creutz. “End states, ladder compounds, and domain wall fermions”. In: *Phys. Rev. Lett.* 83 (Sept. 1999), pp. 2636–2639. DOI: [10.1103/PhysRevLett.83.2636](https://doi.org/10.1103/PhysRevLett.83.2636). arXiv: [hep-lat/9902028](https://arxiv.org/abs/hep-lat/9902028) (cit. on p. 132).
- [421] Monika Aidelsburger et al. “Cold atoms meet lattice gauge theory”. In: *Phil. Trans. Roy. Soc. Lond. A* 380 (Dec. 2021), p. 20210064. DOI: [10.1098/rsta.2021.0064](https://doi.org/10.1098/rsta.2021.0064). arXiv: [2106.03063](https://arxiv.org/abs/2106.03063) [[cond-mat.quant-gas](#)] (cit. on p. 132).
- [422] Zhong-Zhi Xianyu. *A Complete Solution to Problems in “An Introduction to Quantum Field Theory” by Peskin and Schroeder*. [Online; accessed 2021.12.07]. 2016. URL: https://zxxianyu.files.wordpress.com/2017/01/peskin_problems.pdf (cit. on pp. 132, 142, 164, 169, 170, 205).
- [423] Eduardo Fradkin. *Field Theories of Condensed Matter Physics*. 2nd ed. Cambridge: Cambridge University Press, 2013. DOI: [10.1017/CB09781139015509](https://doi.org/10.1017/CB09781139015509) (cit. on pp. 132, 133).
- [424] Werner Heisenberg. “Zur Theorie des Ferromagnetismus”. In: *Z. Phys.* 49.9-10 (Sept. 1928), pp. 619–636. DOI: [10.1007/BF01328601](https://doi.org/10.1007/BF01328601) (cit. on p. 132).
- [425] R. Heidenreich, R. Seiler, and D. A. Uhlenbrock. “The Luttinger model”. In: *J. Stat. Phys.* 22.1 (Jan. 1980), pp. 27–57. ISSN: 1572-9613. DOI: [10.1007/BF01007986](https://doi.org/10.1007/BF01007986) (cit. on p. 132).
- [426] Sin-itiro Tomonaga. “Remarks on Bloch’s Method of Sound Waves applied to Many-Fermion Problems”. In: *Progress of Theoretical Physics* 5.4 (July 1950), pp. 544–569. DOI: [10.1143/ptp/5.4.544](https://doi.org/10.1143/ptp/5.4.544) (cit. on p. 132).
- [427] Joaquin M. Luttinger. “An Exactly Soluble Model of a Many Fermion System”. In: *Journal of Mathematical Physics* 4.9 (Sept. 1963), pp. 1154–1162. DOI: [10.1063/1.1704046](https://doi.org/10.1063/1.1704046) (cit. on p. 132).
- [428] Yakov Frenkel and Tatiana Kontorova. “On the theory of plastic deformation and twinning”. In: *Izv. Akad. Nauk, Ser. Fiz.* 1 (1939), pp. 137–149 (cit. on p. 132).

- [429] Sidney R. Coleman. “The Quantum Sine-Gordon Equation as the Massive Thirring Model”. In: *Phys. Rev. D* 11 (Apr. 1975). Ed. by M. Stone, p. 2088. DOI: [10.1103/PhysRevD.11.2088](https://doi.org/10.1103/PhysRevD.11.2088) (cit. on p. 132).
- [430] D. Delepine, R. Gonzalez Felipe, and J. Weyers. “Equivalence of the sine-Gordon and massive Thirring models at finite temperature”. In: *Phys. Lett. B* 419 (Feb. 1998), pp. 296–302. DOI: [10.1016/S0370-2693\(97\)01436-6](https://doi.org/10.1016/S0370-2693(97)01436-6). arXiv: [hep-th/9709039](https://arxiv.org/abs/hep-th/9709039) (cit. on p. 132).
- [431] Ramamurti Shankar. “Ashkin-Teller and Gross-Neveu models: New relations and results”. In: *Phys. Rev. Lett.* 55 (5 July 1985), pp. 453–456. DOI: [10.1103/PhysRevLett.55.453](https://doi.org/10.1103/PhysRevLett.55.453) (cit. on p. 132).
- [432] Renfrey B. Potts. “Some generalized order - disorder transformations”. In: *Proc. Cambridge Phil. Soc.* 48 (1952), pp. 106–109. DOI: [10.1017/S0305004100027419](https://doi.org/10.1017/S0305004100027419) (cit. on p. 132).
- [433] Julius Ashkin and Edward Teller. “Statistics of Two-Dimensional Lattices with Four Components”. In: *Phys. Rev.* 64 (5-6 Sept. 1943), pp. 178–184. DOI: [10.1103/PhysRev.64.178](https://doi.org/10.1103/PhysRev.64.178) (cit. on p. 132).
- [434] Pascual Jordan and Eugene P. Wigner. “Über das Paulische Äquivalenzverbot”. In: *Zeitschrift für Physik* 47.9-10 (Sept. 1928), pp. 631–651. DOI: [10.1007/BF01331938](https://doi.org/10.1007/BF01331938) (cit. on p. 132).
- [435] Michael C. Ogilvie. “The Gross-Neveu model: dynamical symmetry breaking at a Kosterlitz-Thouless phase transition”. In: *J. Phys. A* 14 (Dec. 1981), p. L519. DOI: [10.1088/0305-4470/14/12/008](https://doi.org/10.1088/0305-4470/14/12/008) (cit. on p. 132).
- [436] W. P. Su, John R. Schrieffer, and Alan J. Heeger. “Solitons in polyacetylene”. In: *Phys. Rev. Lett.* 42 (1979), pp. 1698–1701. DOI: [10.1103/PhysRevLett.42.1698](https://doi.org/10.1103/PhysRevLett.42.1698) (cit. on pp. 132, 133).
- [437] David K. Campbell and Alan R. Bishop. “Soliton Excitations in Polyacetylene and Relativistic Field Theory Models”. In: *Nucl. Phys. B* 200 (Feb. 1982), pp. 297–328. DOI: [10.1016/0550-3213\(82\)90089-X](https://doi.org/10.1016/0550-3213(82)90089-X) (cit. on pp. 132, 133).
- [438] Eduardo Fradkin and Jorge E. Hirsch. “Phase diagram of one-dimensional electron-phonon systems. I. The Su-Schrieffer-Heeger model”. In: *Phys. Rev. B* 27 (3 Feb. 1983), pp. 1680–1697. DOI: [10.1103/PhysRevB.27.1680](https://doi.org/10.1103/PhysRevB.27.1680) (cit. on pp. 132, 133).
- [439] Heron Caldas. “Asymmetrically doped polyacetylene”. In: *Nucl. Phys. B* 807 (Feb. 2009), pp. 651–658. DOI: [10.1016/j.nuclphysb.2008.09.002](https://doi.org/10.1016/j.nuclphysb.2008.09.002). arXiv: [0809.0722](https://arxiv.org/abs/0809.0722) [[cond-mat.str-el](https://arxiv.org/abs/0809.0722)] (cit. on pp. 132, 133).
- [440] Heron Caldas et al. “Critical dopant concentration in polyacetylene and phase diagram from a continuous four-Fermi model”. In: *Phys. Rev. B* 77 (May 2008), p. 205109. DOI: [10.1103/PhysRevB.77.205109](https://doi.org/10.1103/PhysRevB.77.205109). arXiv: [0804.2675](https://arxiv.org/abs/0804.2675) [[cond-mat.soft](https://arxiv.org/abs/0804.2675)] (cit. on pp. 132, 139).
- [441] Alan J. Heeger et al. “Solitons in conducting polymers”. In: *Rev. Mod. Phys.* 60 (July 1988), pp. 781–850. DOI: [10.1103/RevModPhys.60.781](https://doi.org/10.1103/RevModPhys.60.781) (cit. on pp. 132, 133).
- [442] Ryosuke Yoshii and Muneto Nitta. “Nambu-Jona Lasinio and Nonlinear Sigma Models in Condensed Matter Systems”. In: *Symmetry* 11.5 (May 2019), p. 636. DOI: [10.3390/sym11050636](https://doi.org/10.3390/sym11050636). arXiv: [1904.01216](https://arxiv.org/abs/1904.01216) [[cond-mat.supr-con](https://arxiv.org/abs/1904.01216)] (cit. on pp. 132, 133).
- [443] Hajime Takayama, Y. R. Lin-Liu, and Kazumi Maki. “Continuum model for solitons in polyacetylene”. In: *Phys. Rev. B* 21 (1980), pp. 2388–2393. DOI: [10.1103/PhysRevB.21.2388](https://doi.org/10.1103/PhysRevB.21.2388) (cit. on p. 133).
- [444] Serguei Brazovskii and Natasha Kirova. “Excitons, polarons, and bipolarons in conducting polymers”. In: *JETP Lett.* 33 (1 1981), p. 6. URL: http://jetpletters.ru/ps/1500/article_22916.pdf (cit. on p. 133).

- [445] Alan Chodos and Hisakazu Minakata. “The Gross-Neveu model as an effective theory for polyacetylene”. In: *Phys. Lett. A* 191 (Aug. 1994), p. 39. DOI: [10.1016/0375-9601\(94\)90557-6](https://doi.org/10.1016/0375-9601(94)90557-6) (cit. on p. 133).
- [446] Oliver Schnetz, Michael Thies, and Konrad Urlichs. “Phase diagram of the Gross-Neveu model: Exact results and condensed matter precursors”. In: *Annals Phys.* 314 (Dec. 2004), pp. 425–447. DOI: [10.1016/j.aop.2004.06.009](https://doi.org/10.1016/j.aop.2004.06.009). arXiv: [hep-th/0402014](https://arxiv.org/abs/hep-th/0402014) (cit. on pp. 133–136, 209, 210, 216, 224, 225).
- [447] Felix Karbstein et al. *Exploring new states of matter with a photonic emulator*. Apr. 2022. arXiv: [2204.06887](https://arxiv.org/abs/2204.06887) [[physics.optics](https://arxiv.org/abs/2204.06887)] (cit. on p. 133).
- [448] Abraham Klein. “Bound States and Solitons in the Gross-Neveu Model”. In: *Phys. Rev. D* 14 (July 1976), p. 558. DOI: [10.1103/PhysRevD.14.558](https://doi.org/10.1103/PhysRevD.14.558) (cit. on p. 133).
- [449] Junko Shigemitsu and Shmuel Elitzur. “Lattice Hamiltonian Results for the Spectrum of a (1+1)-Dimensional Asymptotically Free Field Theory”. In: *Phys. Rev. D* 14 (Oct. 1976), p. 1988. DOI: [10.1103/PhysRevD.14.1988](https://doi.org/10.1103/PhysRevD.14.1988) (cit. on p. 133).
- [450] Friedhelm Kuypers and Pavel Weber. “Bound State Spectrum of the Gross-Neveu Model on the Lattice”. In: *Nucl. Phys. B* 132 (Jan. 1978), pp. 77–87. DOI: [10.1016/0550-3213\(78\)90259-6](https://doi.org/10.1016/0550-3213(78)90259-6) (cit. on p. 133).
- [451] R. Pausch, Michael Thies, and V. L. Dolman. “Solving the Gross-Neveu model with relativistic many body methods”. In: *Z. Phys. A* 338 (Dec. 1991), pp. 441–453. DOI: [10.1007/BF01295773](https://doi.org/10.1007/BF01295773) (cit. on pp. 133, 135).
- [452] Joshua Feinberg. “On kinks in the Gross-Neveu model”. In: *Phys. Rev. D* 51 (Apr. 1995), pp. 4503–4511. DOI: [10.1103/PhysRevD.51.4503](https://doi.org/10.1103/PhysRevD.51.4503). arXiv: [hep-th/9408120](https://arxiv.org/abs/hep-th/9408120) (cit. on pp. 133, 135).
- [453] Joshua Feinberg. “All about the static fermion bags in the Gross-Neveu model”. In: *Annals Phys.* 309 (Jan. 2004), pp. 166–231. DOI: [10.1016/j.aop.2003.08.004](https://doi.org/10.1016/j.aop.2003.08.004). arXiv: [hep-th/0305240](https://arxiv.org/abs/hep-th/0305240) (cit. on pp. 133, 135).
- [454] Gerald V. Dunne and Joshua Feinberg. “Self isospectral periodic potentials and supersymmetric quantum mechanics”. In: *Phys. Rev. D* 57 (Jan. 1998), pp. 1271–1276. DOI: [10.1103/PhysRevD.57.1271](https://doi.org/10.1103/PhysRevD.57.1271). arXiv: [hep-th/9706012](https://arxiv.org/abs/hep-th/9706012) (cit. on pp. 133, 135).
- [455] Fred Cooper, Avinash Khare, and Uday Sukhatme. *Supersymmetry and quantum mechanics*. World Scientific, June 2001. DOI: [10.1142/4687](https://doi.org/10.1142/4687) (cit. on p. 133).
- [456] G. Sarma. “On the influence of a uniform exchange field acting on the spins of the conduction electrons in a superconductor”. In: *Journal of Physics and Chemistry of Solids* 24.8 (Aug. 1963), pp. 1029–1032. ISSN: 0022-3697. DOI: [10.1016/0022-3697\(63\)90007-6](https://doi.org/10.1016/0022-3697(63)90007-6) (cit. on pp. 134, 135).
- [457] Verena Schön and Michael Thies. “2-D model field theories at finite temperature and density”. In: *At The Frontier of Particle Physics: Handbook of QCD, Boris Ioffe Festschrift*. Vol. 3. World Scientific, Aug. 2000. Chap. 33, pp. 1945–2032. DOI: [10.1142/9789812810458_0041](https://doi.org/10.1142/9789812810458_0041). arXiv: [hep-th/0008175](https://arxiv.org/abs/hep-th/0008175) (cit. on pp. 134, 135, 138, 206, 208, 213, 214).
- [458] Ulli Wolff. “The phase diagram of the infinite-N Gross-Neveu model at finite temperature and chemical potential”. In: *Phys. Lett. B* 157 (July 1985), pp. 303–308. DOI: [10.1016/0370-2693\(85\)90671-9](https://doi.org/10.1016/0370-2693(85)90671-9) (cit. on pp. 134, 135, 138, 206, 207, 224).
- [459] Oliver Schnetz, Michael Thies, and Konrad Urlichs. “Full phase diagram of the massive Gross-Neveu model”. In: *Annals Phys.* 321 (Nov. 2006), pp. 2604–2637. DOI: [10.1016/j.aop.2005.12.007](https://doi.org/10.1016/j.aop.2005.12.007). arXiv: [hep-th/0511206](https://arxiv.org/abs/hep-th/0511206) (cit. on pp. 134, 136, 216, 224, 225).
- [460] Oliver Schnetz, Michael Thies, and Konrad Urlichs. *The Phase diagram of the massive Gross-Neveu model, revisited*. July 2005. arXiv: [hep-th/0507120](https://arxiv.org/abs/hep-th/0507120) (cit. on pp. 134, 136, 206, 216, 224, 225).

- [461] Michael Thies. “From relativistic quantum fields to condensed matter and back again: Updating the Gross-Neveu phase diagram”. In: *J. Phys. A* 39 (Sept. 2006), pp. 12707–12734. DOI: [10.1088/0305-4470/39/41/S04](https://doi.org/10.1088/0305-4470/39/41/S04). arXiv: [hep-th/0601049](https://arxiv.org/abs/hep-th/0601049) (cit. on pp. 134, 207, 216).
- [462] Louise A. Dolan and Roman W. Jackiw. “Symmetry behavior at finite temperature”. In: *Phys. Rev. D* 9 (June 1974), pp. 3320–3341. DOI: [10.1103/PhysRevD.9.3320](https://doi.org/10.1103/PhysRevD.9.3320) (cit. on pp. 134, 279).
- [463] Laurence Jacobs. “Critical behavior in a class of $O(N)$ -invariant field theories in two dimensions”. In: *Phys. Rev. D* 10 (Dec. 1974), p. 3956. DOI: [10.1103/PhysRevD.10.3956](https://doi.org/10.1103/PhysRevD.10.3956) (cit. on pp. 134, 205).
- [464] Barry J. Harrington and Asim Yildiz. “Restoration of Dynamically Broken Symmetries at Finite Temperature”. In: *Phys. Rev. D* 11 (Feb. 1975), p. 779. DOI: [10.1103/PhysRevD.11.779](https://doi.org/10.1103/PhysRevD.11.779) (cit. on pp. 134, 205, 310).
- [465] Roger F. Dashen, Shang-keng Ma, and Ramamurti Rajaraman. “Finite temperature behavior of a relativistic field theory with dynamical symmetry breaking”. In: *Phys. Rev. D* 11 (Mar. 1975), p. 1499. DOI: [10.1103/PhysRevD.11.1499](https://doi.org/10.1103/PhysRevD.11.1499) (cit. on pp. 134, 137, 138, 205, 206).
- [466] Barry J. Harrington and Asim Yildiz. “Chiral Symmetry Behavior at Large Densities”. In: *Phys. Rev. D* 11 (Mar. 1975), p. 1705. DOI: [10.1103/PhysRevD.11.1705](https://doi.org/10.1103/PhysRevD.11.1705) (cit. on pp. 134, 205, 206).
- [467] Anees Ahmed. *Ginzburg-Landau Type Approach to the 1+1 Gross Neveu Model - Beyond Lowest Non-Trivial Order*. Feb. 2018. arXiv: [1802.09095](https://arxiv.org/abs/1802.09095) [[hep-th](https://arxiv.org/abs/hep-th)] (cit. on pp. 134, 136, 177, 209, 210).
- [468] Walter Dittrich and Berthold-Georg Englert. “One Loop Thermal Corrections in the Gross-Neveu Model”. In: *Nucl. Phys. B* 179 (Feb. 1981), pp. 85–105. DOI: [10.1016/0550-3213\(81\)90250-9](https://doi.org/10.1016/0550-3213(81)90250-9) (cit. on p. 135).
- [469] Ted F. Treml. “Dynamical mass generation in the Gross-Neveu model at finite temperature and density”. In: *Phys. Rev. D* 39 (2 Jan. 1989), pp. 679–682. DOI: [10.1103/PhysRevD.39.679](https://doi.org/10.1103/PhysRevD.39.679) (cit. on p. 135).
- [470] Michele Modugno. “Thermodynamics of the Gross-Neveu model beyond the mean field approximation”. In: *Riv. Nuovo Cim.* 23N5 (May 2000), pp. 1–67 (cit. on p. 135).
- [471] Verena Schön and Michael Thies. “Emergence of Skyrme crystal in Gross-Neveu and ’t Hooft models at finite density”. In: *Phys. Rev. D* 62 (Sept. 2000), p. 096002. DOI: [10.1103/PhysRevD.62.096002](https://doi.org/10.1103/PhysRevD.62.096002). arXiv: [hep-th/0003195](https://arxiv.org/abs/hep-th/0003195) (cit. on p. 135).
- [472] Andrej Brzoska and Michael Thies. “No first order phase transition in the Gross-Neveu model?” In: *Phys. Rev. D* 65 (May 2002), p. 125001. DOI: [10.1103/PhysRevD.65.125001](https://doi.org/10.1103/PhysRevD.65.125001). arXiv: [hep-th/0112105](https://arxiv.org/abs/hep-th/0112105) (cit. on p. 135).
- [473] Michael Thies. “Analytical solution of the Gross-Neveu model at finite density”. In: *Phys. Rev. D* 69 (Mar. 2004), p. 067703. DOI: [10.1103/PhysRevD.69.067703](https://doi.org/10.1103/PhysRevD.69.067703). arXiv: [hep-th/0308164](https://arxiv.org/abs/hep-th/0308164) (cit. on pp. 135, 136, 216, 225).
- [474] Achim Heinz et al. “Inhomogeneous condensation in effective models for QCD using the finite-mode approach”. In: *Phys. Rev. D* 93.1 (2016), p. 014007. DOI: [10.1103/PhysRevD.93.014007](https://doi.org/10.1103/PhysRevD.93.014007). arXiv: [1508.06057](https://arxiv.org/abs/1508.06057) [[hep-ph](https://arxiv.org/abs/hep-ph)] (cit. on p. 136).
- [475] Rajamani Narayanan. “Phase diagram of the large N Gross-Neveu model in a finite periodic box”. In: *Phys. Rev. D* 101.9 (May 2020), p. 096001. DOI: [10.1103/PhysRevD.101.096001](https://doi.org/10.1103/PhysRevD.101.096001). arXiv: [2001.09200](https://arxiv.org/abs/2001.09200) [[hep-th](https://arxiv.org/abs/hep-th)] (cit. on p. 136).
- [476] Jens Braun et al. “Search for inhomogeneous phases in fermionic models”. In: *Phys. Rev. D* 91.11 (June 2015), p. 116006. DOI: [10.1103/PhysRevD.91.116006](https://doi.org/10.1103/PhysRevD.91.116006). arXiv: [1410.8181](https://arxiv.org/abs/1410.8181) [[hep-ph](https://arxiv.org/abs/hep-ph)] (cit. on pp. 136, 216, 224).

- [477] Tomohiro Inagaki, T. Kouno, and Teizo Muta. “Phase structure of four fermion theories at finite temperature and chemical potential in arbitrary dimensions”. In: *Int. J. Mod. Phys. A* 10 (Sept. 1995), pp. 2241–2268. DOI: [10.1142/S0217751X95001091](https://doi.org/10.1142/S0217751X95001091). arXiv: [hep-ph/9409413](https://arxiv.org/abs/hep-ph/9409413) (cit. on p. 136).
- [478] M. A. Vdovichenko and A. K. Klimenko. “Oscillation phenomena in polyacetylene: $R^{*1} \times S(1)$ Gross-Neveu model with a chemical potential”. In: *JETP Lett.* 68 (Sept. 1998), pp. 460–466. DOI: [10.1134/1.567890](https://doi.org/10.1134/1.567890) (cit. on p. 136).
- [479] Tomohiro Inagaki, Yamato Matsuo, and Hiromu Shimoji. “Precise phase structure in a four-fermion interaction model on a torus”. In: *PTEP* 2022.1 (Dec. 2022), 013B09. DOI: [10.1093/ptep/ptab160](https://doi.org/10.1093/ptep/ptab160). arXiv: [2108.03583](https://arxiv.org/abs/2108.03583) [[hep-ph](https://arxiv.org/abs/hep-ph)] (cit. on p. 136).
- [480] Konstantin G. Klimenko. “Massive Gross-Neveu Model in Leading Order of $1/N$ Expansion: Consideration for Temperature and Chemical Potential”. In: *Theor. Math. Phys.* 75 (May 1988), p. 487. DOI: [10.1007/BF01017488](https://doi.org/10.1007/BF01017488) (cit. on p. 136).
- [481] Izumi Ojima and Reijiro Fukuda. *Another Phase in the Gross-Neveu Model: Two-Dimensional Superconductivity*. Oct. 1976 (cit. on p. 136).
- [482] Alan Chodos, Fred Cooper, and Hisakazu Minakata. *Competing condensates in two-dimensions*. May 1999. arXiv: [hep-ph/9905521](https://arxiv.org/abs/hep-ph/9905521) (cit. on p. 136).
- [483] Alan Chodos et al. “A two-dimensional model with chiral condensates and Cooper pairs having QCD - like phase structure”. In: *Phys. Rev. D* 61 (Jan. 2000), p. 045011. DOI: [10.1103/PhysRevD.61.045011](https://doi.org/10.1103/PhysRevD.61.045011). arXiv: [hep-ph/9909296](https://arxiv.org/abs/hep-ph/9909296) (cit. on p. 136).
- [484] Hiroaki Kohyama. *Phase diagram of chiral and diquark condensates at finite temperature and density in the 2-dimensional Gross Neveu model*. May 2008. arXiv: [0805.0003](https://arxiv.org/abs/0805.0003) [[hep-ph](https://arxiv.org/abs/hep-ph)] (cit. on p. 136).
- [485] Konstantin G. Klimenko. “Phase Structure of Generalized Gross-Neveu Models”. In: *Z. Phys. C* 37 (Sept. 1988), p. 457. DOI: [10.1007/BF01578141](https://doi.org/10.1007/BF01578141) (cit. on p. 136).
- [486] Tamaz G. Khunjua, Konstantin G. Klimenko, and Roman N. Zhokhov. “Charged pion condensation and duality in dense and hot chirally and isospin asymmetric quark matter in the framework of the NJL₂ model”. In: *Phys. Rev. D* 100.3 (Aug. 2019), p. 034009. DOI: [10.1103/PhysRevD.100.034009](https://doi.org/10.1103/PhysRevD.100.034009). arXiv: [1907.04151](https://arxiv.org/abs/1907.04151) [[hep-ph](https://arxiv.org/abs/hep-ph)] (cit. on p. 136).
- [487] Gertian Roose et al. “The chiral Gross-Neveu model on the lattice via a Landau-forbidden phase transition”. In: *JHEP* 06 (June 2022), p. 019. DOI: [10.1007/JHEP06\(2022\)019](https://doi.org/10.1007/JHEP06(2022)019). arXiv: [2111.14652](https://arxiv.org/abs/2111.14652) [[hep-th](https://arxiv.org/abs/hep-th)] (cit. on p. 137).
- [488] Julian J. Lenz, Michael Mandl, and Andreas Wipf. “Inhomogeneities in the two-flavor chiral Gross-Neveu model”. In: *Phys. Rev. D* 105.3 (Feb. 2022), p. 034512. DOI: [10.1103/PhysRevD.105.034512](https://doi.org/10.1103/PhysRevD.105.034512). arXiv: [2109.05525](https://arxiv.org/abs/2109.05525) [[hep-lat](https://arxiv.org/abs/hep-lat)] (cit. on p. 137).
- [489] Riccardo Ciccone, Lorenzo Di Pietro, and Marco Serone. “Inhomogeneous Phase of the Chiral Gross-Neveu Model”. In: *Phys. Rev. Lett.* 129.7 (Aug. 2022), p. 071603. DOI: [10.1103/PhysRevLett.129.071603](https://doi.org/10.1103/PhysRevLett.129.071603). arXiv: [2203.07451](https://arxiv.org/abs/2203.07451) [[hep-th](https://arxiv.org/abs/hep-th)] (cit. on p. 137).
- [490] L. D. Landau and E. M. Lifshitz. *Statistical Physics, Part 1 & 2*. Vol. 5 & 9. Course of Theoretical Physics. Oxford: Butterworth-Heinemann, 1980 (cit. on pp. 137, 138).
- [491] Nikos Theodorakopoulos. “Phase transitions in one dimension: Are they all driven by domain walls?” In: *Physica D: Nonlinear Phenomena* 216.1 (Apr. 2006), 185–190. ISSN: 0167-2789. DOI: [10.1016/j.physd.2005.12.016](https://doi.org/10.1016/j.physd.2005.12.016). URL: <http://dx.doi.org/10.1016/j.physd.2005.12.016> (cit. on p. 138).
- [492] Nicolaas P. Landsman. “Spontaneous symmetry breaking in quantum systems: Emergence or reduction?” In: *Stud. Hist. Philos. Sci.* 44.4 (Nov. 2013), pp. 379–394. DOI: [10.1016/j.shpsb.2013.07.003](https://doi.org/10.1016/j.shpsb.2013.07.003). arXiv: [1305.4473](https://arxiv.org/abs/1305.4473) [[math-ph](https://arxiv.org/abs/math-ph)] (cit. on p. 138).

- [493] Sunil K. Gandhi and Marcus B. Pinto. “Thermodynamics of four fermion models in the δ expansion”. In: *Phys. Rev. D* 49 (Apr. 1994), pp. 4258–4264. DOI: [10.1103/PhysRevD.49.4258](https://doi.org/10.1103/PhysRevD.49.4258) (cit. on p. 139).
- [494] Jean-Paul Blaizot, Ramon Mendez-Galain, and Nicolas Wschebor. “The Gross-Neveu model at finite temperature at next to leading order in the $1/N$ expansion”. In: *Annals Phys.* 307 (Oct. 2003), pp. 209–271. DOI: [10.1016/S0003-4916\(03\)00072-1](https://doi.org/10.1016/S0003-4916(03)00072-1). arXiv: [hep-ph/0212084](https://arxiv.org/abs/hep-ph/0212084) (cit. on p. 139).
- [495] Jean-Loic Kneur, Marcus Benghi Pinto, and Rudnei O. Ramos. “Critical and tricritical points for the massless 2D Gross-Neveu model beyond large N ”. In: *Phys. Rev. D* 74 (Dec. 2006), p. 125020. DOI: [10.1103/PhysRevD.74.125020](https://doi.org/10.1103/PhysRevD.74.125020). arXiv: [hep-th/0610201](https://arxiv.org/abs/hep-th/0610201) (cit. on p. 139).
- [496] Jean-Loic Kneur, Marcus Benghi Pinto, and Rudnei O. Ramos. “The 2d Gross-Neveu model at finite temperature and density with finite N corrections”. In: *Braz. J. Phys.* 37 (Mar. 2007), pp. 258–264. DOI: [10.1590/S0103-97332007000200016](https://doi.org/10.1590/S0103-97332007000200016). arXiv: [0704.2843](https://arxiv.org/abs/0704.2843) [[hep-ph](https://arxiv.org/abs/hep-ph)] (cit. on p. 139).
- [497] Frithjof Karsch, John B. Kogut, and Henry W. Wyld. “The Gross-Neveu Model at finite temperature and density”. In: *Nucl. Phys. B* 280 (June 1987), pp. 289–303. DOI: [10.1016/0550-3213\(87\)90149-0](https://doi.org/10.1016/0550-3213(87)90149-0) (cit. on p. 139).
- [498] Sinya Aoki and Kiyoshi Higashijima. “The recovery of the chiral symmetry in lattice Gross-Neveu model”. In: *Prog. Theor. Phys.* 76 (Aug. 1986), p. 521. DOI: [10.1143/PTP.76.521](https://doi.org/10.1143/PTP.76.521) (cit. on p. 139).
- [499] Vikram Vyas. “Regularizing the Gross-Neveu model on the lattice without fermion doubling”. In: *Phys. Lett. B* 266 (Aug. 1991), pp. 453–457. DOI: [10.1016/0370-2693\(91\)91068-7](https://doi.org/10.1016/0370-2693(91)91068-7) (cit. on p. 139).
- [500] Francesco Knechtli et al. “Universality in the Gross-Neveu model”. In: *Nucl. Phys. B Proc. Suppl.* 140 (Mar. 2005). Ed. by Geoffrey T. Bodwin et al., pp. 785–787. DOI: [10.1016/j.nuclphysbps.2004.11.147](https://doi.org/10.1016/j.nuclphysbps.2004.11.147). arXiv: [hep-lat/0410018](https://arxiv.org/abs/hep-lat/0410018) (cit. on p. 139).
- [501] Andreas Wipf. *Lecture notes on: Introduction to Supersymmetry*. [Online; accessed 2022.07.20]. 2016. URL: <https://www.tpi.uni-jena.de/~wipf/lectures/susy/susyhead.pdf> (cit. on pp. 142, 148).
- [502] Konrad Urlichs. “Baryons and baryonic matter in four-fermion interaction models”. PhD thesis. Friedrich-Alexander-Universität Erlangen Nürnberg, Feb. 2007. URL: https://opus4.kobv.de/opus4-fau/frontdoor/deliver/index/docId/409/file/doktorarbeit_ohnelebenslauf.pdf (cit. on pp. 142, 146).
- [503] Michel Le Bellac. *Quantum and statistical field theory*. [Translation by G. Barton]. Oxford, England, UK: Oxford University Press, 1991. ISBN: 978-0-19-853964-3 (cit. on pp. 143, 154, 156).
- [504] Michel Le Bellac. *Thermal Field Theory*. Cambridge Monographs on Mathematical Physics. Cambridge University Press, Mar. 2011. ISBN: 978-0-511-88506-8, 978-0-521-65477-7. DOI: [10.1017/CB09780511721700](https://doi.org/10.1017/CB09780511721700) (cit. on pp. 143, 154, 156, 275).
- [505] Mikko Laine and Aleksi Vuorinen. *Basics of Thermal Field Theory*. Lect. Notes Phys. 925. Springer, 2016, pp. 1–281. DOI: [10.1007/978-3-319-31933-9](https://doi.org/10.1007/978-3-319-31933-9). arXiv: [1701.01554](https://arxiv.org/abs/1701.01554) [[hep-ph](https://arxiv.org/abs/hep-ph)] (cit. on pp. 143, 154, 156, 275).
- [506] Gian C. Wick. “Properties of Bethe-Salpeter Wave Functions”. In: *Phys. Rev.* 96 (Nov. 1954), pp. 1124–1134. DOI: [10.1103/PhysRev.96.1124](https://doi.org/10.1103/PhysRev.96.1124) (cit. on p. 143).
- [507] Christof Wetterich. “Spinors in euclidean field theory, complex structures and discrete symmetries”. In: *Nucl. Phys. B* 852 (2011), pp. 174–234. DOI: [10.1016/j.nuclphysb.2011.06.013](https://doi.org/10.1016/j.nuclphysb.2011.06.013). arXiv: [1002.3556](https://arxiv.org/abs/1002.3556) [[hep-th](https://arxiv.org/abs/hep-th)] (cit. on pp. 143, 156).

- [508] Stefan Floerchinger. “Analytic Continuation of Functional Renormalization Group Equations”. In: *JHEP* 05 (May 2012), p. 021. DOI: [10.1007/JHEP05\(2012\)021](https://doi.org/10.1007/JHEP05(2012)021). arXiv: [1112.4374](https://arxiv.org/abs/1112.4374) [[hep-th](#)] (cit. on p. 144).
- [509] Kazuhiko Kamikado et al. “Real-time correlation functions in the $O(N)$ model from the functional renormalization group”. In: *Eur. Phys. J. C* 74.3 (Mar. 2014), p. 2806. DOI: [10.1140/epjc/s10052-014-2806-6](https://doi.org/10.1140/epjc/s10052-014-2806-6). arXiv: [1302.6199](https://arxiv.org/abs/1302.6199) [[hep-ph](#)] (cit. on p. 144).
- [510] Jan Horak, Jan M. Pawłowski, and Nicolas Wink. “Spectral functions in the ϕ^4 -theory from the spectral DSE”. In: *Phys. Rev. D* 102 (Dec. 2020), p. 125016. DOI: [10.1103/PhysRevD.102.125016](https://doi.org/10.1103/PhysRevD.102.125016). arXiv: [2006.09778](https://arxiv.org/abs/2006.09778) [[hep-th](#)] (cit. on p. 144).
- [511] Johannes V. Roth et al. “Real-time methods for spectral functions”. In: *Phys. Rev. D* 105.11 (June 2022), p. 116017. DOI: [10.1103/PhysRevD.105.116017](https://doi.org/10.1103/PhysRevD.105.116017). arXiv: [2112.12568](https://arxiv.org/abs/2112.12568) [[hep-ph](#)] (cit. on p. 144).
- [512] Holger Gies et al. “Phase transition and critical behavior of d=3 chiral fermion models with left/right asymmetry”. In: *Phys. Rev. D* 81 (Jan. 2010), p. 025009. DOI: [10.1103/PhysRevD.81.025009](https://doi.org/10.1103/PhysRevD.81.025009). arXiv: [0910.0764](https://arxiv.org/abs/0910.0764) [[hep-th](#)] (cit. on p. 146).
- [513] Holger Gies and Lukas Janssen. “UV fixed-point structure of the three-dimensional Thirring model”. In: *Phys. Rev. D* 82 (Oct. 2010), p. 085018. DOI: [10.1103/PhysRevD.82.085018](https://doi.org/10.1103/PhysRevD.82.085018). arXiv: [1006.3747](https://arxiv.org/abs/1006.3747) [[hep-th](#)] (cit. on p. 146).
- [514] Friedrich Gehring, Holger Gies, and Lukas Janssen. “Fixed-point structure of low-dimensional relativistic fermion field theories: Universality classes and emergent symmetry”. In: *Phys. Rev. D* 92.8 (Oct. 2015), p. 085046. DOI: [10.1103/PhysRevD.92.085046](https://doi.org/10.1103/PhysRevD.92.085046). arXiv: [1506.07570](https://arxiv.org/abs/1506.07570) [[hep-th](#)] (cit. on p. 146).
- [515] Ray F. Streater and Arthur S. Wightman. *PCT, spin and statistics, and all that*. Vol. 52. Princeton Landmarks in Mathematical Physics. Princeton, New Jersey, USA: Princeton University Press, 1989. ISBN: 978-0-691-07062-9 (cit. on p. 146).
- [516] Walter Greiner and Berndt Müller. *Quantenmechanik: Symmetrien*. 5th ed. Haan-Gruiten, Germany: Europa Lehrmittel, 2014. ISBN: 978-3-8085-5639-9 (cit. on pp. 146, 147).
- [517] Enrico Speranza and Nora Weickgenannt. “Spin tensor and pseudo-gauges: from nuclear collisions to gravitational physics”. In: *Eur. Phys. J. A* 57.5 (May 2021), p. 155. DOI: [10.1140/epja/s10050-021-00455-2](https://doi.org/10.1140/epja/s10050-021-00455-2). arXiv: [2007.00138](https://arxiv.org/abs/2007.00138) [[nucl-th](#)] (cit. on p. 148).
- [518] Gerhard Mack and Abdus Salam. “Finite component field representations of the conformal group”. In: *Annals Phys.* 53 (June 1969), pp. 174–202. DOI: [10.1016/0003-4916\(69\)90278-4](https://doi.org/10.1016/0003-4916(69)90278-4) (cit. on pp. 150, 151, 154, 160).
- [519] Edward L. Hill. “On Accelerated Coordinate Systems in Classical and Relativistic Mechanics”. In: *Phys. Rev.* 67 (11-12 June 1945), pp. 358–363. DOI: [10.1103/PhysRev.67.358](https://doi.org/10.1103/PhysRev.67.358) (cit. on p. 150).
- [520] Philippe Di Francesco, Pierre Mathieu, and David Senechal. *Conformal Field Theory*. Graduate Texts in Contemporary Physics. New York, New York, USA: Springer-Verlag, 1997. ISBN: 978-0-387-94785-3, 978-1-4612-7475-9. DOI: [10.1007/978-1-4612-2256-9](https://doi.org/10.1007/978-1-4612-2256-9) (cit. on pp. 151, 152).
- [521] Barry A. Freedman and Larry D. McLerran. “Fermions and Gauge Vector Mesons at Finite Temperature and Density. 1. Formal Techniques”. In: *Phys. Rev. D* 16 (Aug. 1977), p. 1130. DOI: [10.1103/PhysRevD.16.1130](https://doi.org/10.1103/PhysRevD.16.1130) (cit. on p. 153).
- [522] Joseph I. Kapusta. “Bose-Einstein condensation, spontaneous symmetry breaking, and gauge theories”. In: *Phys. Rev. D* 24 (July 1981), pp. 426–439. DOI: [10.1103/PhysRevD.24.426](https://doi.org/10.1103/PhysRevD.24.426) (cit. on p. 153).
- [523] Alfred Actor. “Zeta Function Regularization of High Temperature Expansions in Field Theory”. In: *Nucl. Phys. B* 265 (Apr. 1986), pp. 689–719. DOI: [10.1016/0550-3213\(86\)90336-6](https://doi.org/10.1016/0550-3213(86)90336-6) (cit. on pp. 153, 210).

- [524] Thomas D. Cohen. “Functional integrals for QCD at nonzero chemical potential and zero density”. In: *Phys. Rev. Lett.* 91 (Nov. 2003), p. 222001. DOI: [10.1103/PhysRevLett.91.222001](https://doi.org/10.1103/PhysRevLett.91.222001). arXiv: [hep-ph/0307089](https://arxiv.org/abs/hep-ph/0307089) (cit. on p. 154).
- [525] Gergely Markó, Urko Reinosa, and Zsolt Szép. “Bose-Einstein condensation and Silver Blaze property from the two-loop Φ -derivable approximation”. In: *Phys. Rev. D* 90.12 (Dec. 2014), p. 125021. DOI: [10.1103/PhysRevD.90.125021](https://doi.org/10.1103/PhysRevD.90.125021). arXiv: [1410.6998](https://arxiv.org/abs/1410.6998) [[hep-ph](#)] (cit. on p. 154).
- [526] Laurin Pannullo. “Inhomogeneous Phases in the 1 + 1-Dimensional Gross-Neveu Model at Finite Number of Fermion Flavors”. Updated version from June 30, 2020 with minor corrections. Master thesis. Goethe University Frankfurt, June 2020. URL: https://itp.uni-frankfurt.de/~mwagner/theses/MA_Pannullo.pdf (cit. on pp. 158, 208).
- [527] Ken-Ichi Aoki et al. “Wilson renormalization group equations for the critical dynamics of chiral symmetry”. In: *Prog. Theor. Phys.* 102 (Dec. 1999), pp. 1151–1162. DOI: [10.1143/PTP.102.1151](https://doi.org/10.1143/PTP.102.1151). arXiv: [hep-th/9908042](https://arxiv.org/abs/hep-th/9908042) (cit. on pp. 163, 307, 318).
- [528] Jens Braun et al. “Phase structure of many-flavor QED₃”. In: *Phys. Rev. D* 90.3 (Aug. 2014), p. 036002. DOI: [10.1103/PhysRevD.90.036002](https://doi.org/10.1103/PhysRevD.90.036002). arXiv: [1404.1362](https://arxiv.org/abs/1404.1362) [[hep-ph](#)] (cit. on pp. 163, 307).
- [529] Manfred Salmhofer and Carsten Honerkamp. “Fermionic renormalization group flows: Technique and theory”. In: *Prog. Theor. Phys.* 105 (Jan. 2001), pp. 1–35. DOI: [10.1143/PTP.105.1](https://doi.org/10.1143/PTP.105.1) (cit. on p. 163).
- [530] Walter Metzner et al. “Functional renormalization group approach to correlated fermion systems”. In: *Rev. Mod. Phys.* 84 (Mar. 2012), p. 299. DOI: [10.1103/RevModPhys.84.299](https://doi.org/10.1103/RevModPhys.84.299). arXiv: [1105.5289](https://arxiv.org/abs/1105.5289) [[cond-mat.str-el](#)] (cit. on p. 163).
- [531] G Gatoff and Joseph I. Kapusta. “Fermions at high temperature”. In: *Phys. Rev. D* 41 (Jan. 1990), p. 611. DOI: [10.1103/PhysRevD.41.611](https://doi.org/10.1103/PhysRevD.41.611) (cit. on pp. 163, 180, 190, 280).
- [532] Daniel F. Litim and Jan M. Pawłowski. “Non-perturbative thermal flows and resummations”. In: *JHEP* 11 (Nov. 2006), p. 026. DOI: [10.1088/1126-6708/2006/11/026](https://doi.org/10.1088/1126-6708/2006/11/026). arXiv: [hep-th/0609122](https://arxiv.org/abs/hep-th/0609122) (cit. on pp. 166, 327).
- [533] Konstantin Otto, Christopher Busch, and Bernd-Jochen Schaefer. “Regulator scheme dependence of the chiral phase transition at high densities”. In: *Phys. Rev. D* 106.9 (Nov. 2022), p. 094018. DOI: [10.1103/PhysRevD.106.094018](https://doi.org/10.1103/PhysRevD.106.094018). arXiv: [2206.13067](https://arxiv.org/abs/2206.13067) [[hep-ph](#)] (cit. on pp. 166, 167, 259, 289).
- [534] Leonie Canet et al. “Nonperturbative Renormalization Group approach to the Ising model: A derivative expansion at order ∂^4 ”. In: *Phys. Rev. B* 68 (Aug. 2003), p. 064421. DOI: [10.1103/PhysRevB.68.064421](https://doi.org/10.1103/PhysRevB.68.064421). arXiv: [hep-th/0302227](https://arxiv.org/abs/hep-th/0302227) (cit. on p. 167).
- [535] Wei-jie Fu, Jan M. Pawłowski, and Fabian Rennecke. “QCD phase structure at finite temperature and density”. In: *Phys. Rev. D* 101.5 (Mar. 2020), p. 054032. DOI: [10.1103/PhysRevD.101.054032](https://doi.org/10.1103/PhysRevD.101.054032). arXiv: [1909.02991](https://arxiv.org/abs/1909.02991) [[hep-ph](#)] (cit. on pp. 168, 219).
- [536] Bernhard Klaiber. “The thirring model”. In: *Lect. Theor. Phys. A* 10 (1968), pp. 141–176 (cit. on p. 170).
- [537] David J. Gross and Frank A. Wilczek. “Ultraviolet behavior of non-Abelian gauge theories”. In: *Phys. Rev. Lett.* 30 (June 1973). Ed. by John C. Taylor, pp. 1343–1346. DOI: [10.1103/PhysRevLett.30.1343](https://doi.org/10.1103/PhysRevLett.30.1343) (cit. on p. 170).
- [538] David J. Gross and Frank A. Wilczek. “Asymptotically free gauge theories I”. In: *Phys. Rev. D* 8 (Nov. 1973), pp. 3633–3652. DOI: [10.1103/PhysRevD.8.3633](https://doi.org/10.1103/PhysRevD.8.3633) (cit. on p. 170).
- [539] David J. Gross and Frank A. Wilczek. “Asymptotically free gauge theories II”. In: *Phys. Rev. D* 9 (Feb. 1974), pp. 980–993. DOI: [10.1103/PhysRevD.9.980](https://doi.org/10.1103/PhysRevD.9.980) (cit. on p. 170).

- [540] H. David Politzer. “Reliable perturbative results for strong interactions?” In: *Phys. Rev. Lett.* 30 (June 1973). Ed. by John C. Taylor, pp. 1346–1349. DOI: [10.1103/PhysRevLett.30.1346](https://doi.org/10.1103/PhysRevLett.30.1346) (cit. on p. 170).
- [541] H. David Politzer. “Asymptotic Freedom: An Approach to Strong Interactions”. In: *Phys. Rept.* 14 (Nov. 1974), pp. 129–180. DOI: [10.1016/0370-1573\(74\)90014-3](https://doi.org/10.1016/0370-1573(74)90014-3) (cit. on p. 170).
- [542] Giorgio Parisi. “On Nonrenormalizable Interactions”. In: *Cargese Summer Institute: New Developments in Quantum Field Theory and Statistical Mechanics*. Jan. 1977 (cit. on p. 171).
- [543] Steven Weinberg. “Critical Phenomena for Field Theorists”. In: *14th International School of Subnuclear Physics: Understanding the Fundamental Constituents of Matter*. Aug. 1976. DOI: [10.1007/978-1-4684-0931-4_1](https://doi.org/10.1007/978-1-4684-0931-4_1) (cit. on p. 171).
- [544] Steven Weinberg. *Ultraviolet divergences in quantum theories of gravitation*. 1980 (cit. on p. 171).
- [545] Andreas Nink, Martin Reuter, and Frank Saueressig. “Asymptotic Safety in quantum gravity”. In: *Scholarpedia* 8.7 (2013). revision #135541, p. 31015. DOI: [10.4249/scholarpedia.31015](https://doi.org/10.4249/scholarpedia.31015) (cit. on p. 171).
- [546] Krzysztof Gawedzki and Antti Kupiainen. “Renormalizing the Nonrenormalizable”. In: *Phys. Rev. Lett.* 55 (May 1985), pp. 363–365. DOI: [10.1103/PhysRevLett.55.363](https://doi.org/10.1103/PhysRevLett.55.363) (cit. on p. 171).
- [547] Martin Jakob Steil, Michael Buballa, and Bernd-Jochen Schaefer. *Inhomogeneous chiral condensates in the quark-meson model with the functional renormalization group*. in preparation. 2021 (cit. on pp. 174, 192).
- [548] Jens Braun. “The QCD Phase Boundary from Quark-Gluon Dynamics”. In: *Eur. Phys. J. C* 64 (Sept. 2009), pp. 459–482. DOI: [10.1140/epjc/s10052-009-1136-6](https://doi.org/10.1140/epjc/s10052-009-1136-6). arXiv: [0810.1727](https://arxiv.org/abs/0810.1727) [[hep-ph](https://arxiv.org/abs/hep-ph)] (cit. on pp. 178, 180, 190, 258).
- [549] Wei-jie Fu and Jan M. Pawłowski. “Relevance of matter and glue dynamics for baryon number fluctuations”. In: *Phys. Rev. D* 92.11 (Dec. 2015), p. 116006. DOI: [10.1103/PhysRevD.92.116006](https://doi.org/10.1103/PhysRevD.92.116006). arXiv: [1508.06504](https://arxiv.org/abs/1508.06504) [[hep-ph](https://arxiv.org/abs/hep-ph)] (cit. on pp. 180, 190, 258).
- [550] Christof Wetterich. “Effective average action in statistical physics and quantum field theory”. In: *Int. J. Mod. Phys. A* 16 (Apr. 2001). Ed. by Z. Horvath and L. Palla, pp. 1951–1982. DOI: [10.1142/S0217751X01004591](https://doi.org/10.1142/S0217751X01004591). arXiv: [hep-ph/0101178](https://arxiv.org/abs/hep-ph/0101178) (cit. on pp. 186, 191, 288).
- [551] Anton K. Cyrol et al. “Landau gauge Yang-Mills correlation functions”. In: *Phys. Rev. D* 94.5 (Sept. 2016), p. 054005. DOI: [10.1103/PhysRevD.94.054005](https://doi.org/10.1103/PhysRevD.94.054005). arXiv: [1605.01856](https://arxiv.org/abs/1605.01856) [[hep-ph](https://arxiv.org/abs/hep-ph)] (cit. on p. 187).
- [552] Anton K. Cyrol et al. “Nonperturbative quark, gluon, and meson correlators of unquenched QCD”. In: *Phys. Rev. D* 97.5 (2018), p. 054006. DOI: [10.1103/PhysRevD.97.054006](https://doi.org/10.1103/PhysRevD.97.054006). arXiv: [1706.06326](https://arxiv.org/abs/1706.06326) [[hep-ph](https://arxiv.org/abs/hep-ph)] (cit. on p. 187).
- [553] Markus Q. Huber. “Nonperturbative properties of Yang–Mills theories”. In: *Phys. Rept.* 879 (Oct. 2020), pp. 1–92. DOI: [10.1016/j.physrep.2020.04.004](https://doi.org/10.1016/j.physrep.2020.04.004). arXiv: [1808.05227](https://arxiv.org/abs/1808.05227) [[hep-ph](https://arxiv.org/abs/hep-ph)] (cit. on pp. 187, 285).
- [554] Jens Braun. “Thermodynamics of QCD low-energy models and the derivative expansion of the effective action”. In: *Phys. Rev. D* 81 (Jan. 2010), p. 016008. DOI: [10.1103/PhysRevD.81.016008](https://doi.org/10.1103/PhysRevD.81.016008). arXiv: [0908.1543](https://arxiv.org/abs/0908.1543) [[hep-ph](https://arxiv.org/abs/hep-ph)] (cit. on p. 187).
- [555] Shi Yin, Rui Wen, and Wei-jie Fu. “Mesonic dynamics and the QCD phase transition”. In: *Phys. Rev. D* 100.9 (Nov. 2019), p. 094029. DOI: [10.1103/PhysRevD.100.094029](https://doi.org/10.1103/PhysRevD.100.094029). arXiv: [1907.10262](https://arxiv.org/abs/1907.10262) [[hep-ph](https://arxiv.org/abs/hep-ph)] (cit. on p. 187).

- [556] Holger Gies and Michael M. Scherer. “Asymptotic safety of simple Yukawa systems”. In: *Eur. Phys. J. C* 66 (Feb. 2010), pp. 387–402. DOI: [10.1140/epjc/s10052-010-1256-z](https://doi.org/10.1140/epjc/s10052-010-1256-z). arXiv: [0901.2459](https://arxiv.org/abs/0901.2459) [[hep-th](#)] (cit. on pp. [188](#), [307](#), [346](#), [357](#), [358](#)).
- [557] Igor Boettcher, Jan M. Pawłowski, and Sebastian Diehl. “Ultracold atoms and the Functional Renormalization Group”. In: *Nucl. Phys. B Proc. Suppl.* 228 (July 2012). Ed. by Bernd-Jochen Schaefer, Reinhard Alkofer, and Christian S. Fischer, pp. 63–135. DOI: [10.1016/j.nuclphysbps.2012.06.004](https://doi.org/10.1016/j.nuclphysbps.2012.06.004). arXiv: [1204.4394](https://arxiv.org/abs/1204.4394) [[cond-mat.quant-gas](#)] (cit. on pp. [192](#), [230](#), [242](#)).
- [558] Igor Boettcher et al. “Tan contact and universal high momentum behavior of the fermion propagator in the BCS-BEC crossover”. In: *Phys. Rev. A* 87.2 (Feb. 2013), p. 023606. DOI: [10.1103/PhysRevA.87.023606](https://doi.org/10.1103/PhysRevA.87.023606). arXiv: [1209.5641](https://arxiv.org/abs/1209.5641) [[cond-mat.quant-gas](#)] (cit. on pp. [192](#), [230](#), [242](#)).
- [559] Igor Boettcher, Jan M. Pawłowski, and Christof Wetterich. “Critical temperature and superfluid gap of the Unitary Fermi Gas from Functional Renormalization”. In: *Phys. Rev. A* 89.5 (May 2014), p. 053630. DOI: [10.1103/PhysRevA.89.053630](https://doi.org/10.1103/PhysRevA.89.053630). arXiv: [1312.0505](https://arxiv.org/abs/1312.0505) [[cond-mat.quant-gas](#)] (cit. on pp. [192](#), [230](#), [242](#)).
- [560] Igor Boettcher et al. “Phase structure of spin-imbalanced unitary Fermi gases”. In: *Phys. Rev. A* 91.1 (Jan. 2015), p. 013610. DOI: [10.1103/PhysRevA.91.013610](https://doi.org/10.1103/PhysRevA.91.013610). arXiv: [1409.5070](https://arxiv.org/abs/1409.5070) [[cond-mat.quant-gas](#)] (cit. on pp. [192](#), [230](#), [242](#)).
- [561] Dietrich Roscher, Jens Braun, and Joaquín E. Drut. “Phase structure of mass- and spin-imbalanced unitary Fermi gases”. In: *Phys. Rev. A* 91.5 (May 2015), p. 053611. DOI: [10.1103/PhysRevA.91.053611](https://doi.org/10.1103/PhysRevA.91.053611). arXiv: [1501.05544](https://arxiv.org/abs/1501.05544) [[cond-mat.quant-gas](#)] (cit. on pp. [192](#), [219](#), [224](#), [230](#), [242](#)).
- [562] Frank Wilczek. “Quantum Time Crystals”. In: *Phys. Rev. Lett.* 109 (Oct. 2012), p. 160401. DOI: [10.1103/PhysRevLett.109.160401](https://doi.org/10.1103/PhysRevLett.109.160401). arXiv: [1202.2539](https://arxiv.org/abs/1202.2539) [[quant-ph](#)] (cit. on p. [192](#)).
- [563] Alfred Shapere and Frank Wilczek. “Classical Time Crystals”. In: *Phys. Rev. Lett.* 109 (Oct. 2012), p. 160402. DOI: [10.1103/PhysRevLett.109.160402](https://doi.org/10.1103/PhysRevLett.109.160402). arXiv: [1202.2537](https://arxiv.org/abs/1202.2537) [[cond-mat.other](#)] (cit. on p. [192](#)).
- [564] Michael Thies. *Semiclassical time crystal in the chiral Gross-Neveu model*. Nov. 2014. arXiv: [1411.4236](https://arxiv.org/abs/1411.4236) [[hep-th](#)] (cit. on pp. [192](#), [216](#)).
- [565] Wei-jie Fu. “QCD at finite temperature and density within the fRG approach: an overview”. In: *Commun. Theor. Phys.* 74.9 (Sept. 2022), p. 097304. DOI: [10.1088/1572-9494/ac86be](https://doi.org/10.1088/1572-9494/ac86be). arXiv: [2205.00468](https://arxiv.org/abs/2205.00468) [[hep-ph](#)] (cit. on pp. [194](#), [223](#)).
- [566] Stefan Rechenberger. *private communication*. 2018 (cit. on pp. [201](#), [216](#), [275](#)).
- [567] Stefan Rechenberger. *Inhomogeneous phases at high density: In Search for Instabilities*. Talk at the 1st retreat of the CRC-TR 211 presented by D. H. Rischke, March 12-16, ZiF Bielefeld and corresponding private notes. 2018 (cit. on pp. [201](#), [216](#)).
- [568] Gabor Almasi, Robert Pisarski, and Vladimir Skokov. “Volume dependence of baryon number cumulants and their ratios”. In: *Phys. Rev. D* 95.5 (Mar. 2017), p. 056015. DOI: [10.1103/PhysRevD.95.056015](https://doi.org/10.1103/PhysRevD.95.056015). arXiv: [1612.04416](https://arxiv.org/abs/1612.04416) [[hep-ph](#)] (cit. on p. [203](#)).
- [569] Wei-jie Fu, Jan M. Pawłowski, and Fabian Rennecke. “Strangeness Neutrality and QCD Thermodynamics”. In: *SciPost Phys. Core* 2 (Feb. 2020), p. 002. DOI: [10.21468/SciPostPhysCore.2.1.002](https://doi.org/10.21468/SciPostPhysCore.2.1.002). arXiv: [1808.00410](https://arxiv.org/abs/1808.00410) [[hep-ph](#)] (cit. on p. [203](#)).
- [570] Gokce Basar, Gerald V. Dunne, and Michael Thies. “Inhomogeneous condensates in the thermodynamics of the chiral NJL₂ model”. In: *Phys. Rev. D* 79 (10 May 2009), p. 105012. DOI: [10.1103/PhysRevD.79.105012](https://doi.org/10.1103/PhysRevD.79.105012). arXiv: [0903.1868](https://arxiv.org/abs/0903.1868) [[hep-th](#)] (cit. on pp. [209](#), [210](#), [216](#)).
- [571] Sandra P. Klevansky. “The Nambu-Jona-Lasinio model of quantum chromodynamics”. In: *Rev. Mod. Phys.* 64 (July 1992), pp. 649–708. DOI: [10.1103/RevModPhys.64.649](https://doi.org/10.1103/RevModPhys.64.649) (cit. on p. [210](#)).

- [572] Dominik Nickel. “How many phases meet at the chiral critical point?” In: *Phys. Rev. Lett.* 103 (2009), p. 072301. DOI: [10.1103/PhysRevLett.103.072301](https://doi.org/10.1103/PhysRevLett.103.072301). arXiv: [0902.1778](https://arxiv.org/abs/0902.1778) [[hep-ph](#)] (cit. on pp. [210](#), [216](#)).
- [573] Michael Buballa and Stefano Carignano. “Inhomogeneous chiral phases away from the chiral limit”. In: *Phys. Lett. B* 791 (Apr. 2019), pp. 361–366. DOI: [10.1016/j.physletb.2019.02.045](https://doi.org/10.1016/j.physletb.2019.02.045). arXiv: [1809.10066](https://arxiv.org/abs/1809.10066) [[hep-ph](#)] (cit. on pp. [210](#), [216](#), [219](#), [220](#)).
- [574] Alfred Actor. “Compactification at finite temperature in noncompact electrodynamics”. In: *Annals Phys.* 159 (Feb. 1985), pp. 445–466. DOI: [10.1016/0003-4916\(85\)90119-8](https://doi.org/10.1016/0003-4916(85)90119-8) (cit. on p. [210](#)).
- [575] Alfred Actor. “Chemical potentials in gauge theories”. In: *Phys. Lett. B* 157 (July 1985), pp. 53–56. DOI: [10.1016/0370-2693\(85\)91210-9](https://doi.org/10.1016/0370-2693(85)91210-9) (cit. on p. [210](#)).
- [576] Daniel F. Litim, Jan M. Pawłowski, and Lautaro Vergara. *Convexity of the effective action from functional flows*. Feb. 2006. arXiv: [hep-th/0602140](https://arxiv.org/abs/hep-th/0602140) (cit. on p. [211](#)).
- [577] Julia Borchardt. “From condensed matter to higgs physics : solving functional renormalization group equations globally in field space”. PhD thesis. Friedrich Schiller University Jena, 2017 (cit. on p. [211](#)).
- [578] Michael Thies and Konrad Urlichs. “Baryons in massive Gross-Neveu models”. In: *Phys. Rev. D* 71 (May 2005), p. 105008. DOI: [10.1103/PhysRevD.71.105008](https://doi.org/10.1103/PhysRevD.71.105008). arXiv: [hep-th/0502210](https://arxiv.org/abs/hep-th/0502210) (cit. on p. [216](#)).
- [579] Michael Thies and Konrad Urlichs. “From non-degenerate conducting polymers to dense matter in the massive Gross-Neveu model”. In: *Phys. Rev. D* 72 (Nov. 2005), p. 105008. DOI: [10.1103/PhysRevD.72.105008](https://doi.org/10.1103/PhysRevD.72.105008). arXiv: [hep-th/0505024](https://arxiv.org/abs/hep-th/0505024) (cit. on pp. [216](#), [224](#), [225](#)).
- [580] Michael Thies. “Integrable Gross-Neveu models with fermion-fermion and fermion-antifermion pairing”. In: *Phys. Rev. D* 90.10 (Nov. 2014), p. 105017. DOI: [10.1103/PhysRevD.90.105017](https://doi.org/10.1103/PhysRevD.90.105017). arXiv: [1408.5506](https://arxiv.org/abs/1408.5506) [[hep-th](#)] (cit. on p. [216](#)).
- [581] Michael Thies. “Non-Abelian twisted kinks in chiral Gross-Neveu model with isospin”. In: *Phys. Rev. D* 93.8 (Apr. 2016), p. 085024. DOI: [10.1103/PhysRevD.93.085024](https://doi.org/10.1103/PhysRevD.93.085024). arXiv: [1512.03894](https://arxiv.org/abs/1512.03894) [[hep-th](#)] (cit. on p. [216](#)).
- [582] Michael Thies. *Solving the $U(2)_L \times U(2)_R$ symmetric Nambu–Jona-Lasinio model in 1+1 dimensions*. Mar. 2016. arXiv: [1603.06218](https://arxiv.org/abs/1603.06218) [[hep-th](#)] (cit. on p. [216](#)).
- [583] Michael Thies. “Fermion number of twisted kinks in the NJL₂ model, revisited”. In: *Phys. Rev. D* 97.5 (Mar. 2018), p. 056012. DOI: [10.1103/PhysRevD.97.056012](https://doi.org/10.1103/PhysRevD.97.056012). arXiv: [1710.03420](https://arxiv.org/abs/1710.03420) [[hep-th](#)] (cit. on p. [216](#)).
- [584] Michael Thies. “Chiral spiral in the presence of chiral imbalance”. In: *Phys. Rev. D* 98.9 (Nov. 2018), p. 096019. DOI: [10.1103/PhysRevD.98.096019](https://doi.org/10.1103/PhysRevD.98.096019). arXiv: [1810.03921](https://arxiv.org/abs/1810.03921) [[hep-th](#)] (cit. on p. [216](#)).
- [585] Michael Thies. “Phase structure of the (1 + 1)-dimensional Nambu-Jona-Lasinio model with isospin”. In: *Phys. Rev. D* 101.1 (Jan. 2020), p. 014010. DOI: [10.1103/PhysRevD.101.014010](https://doi.org/10.1103/PhysRevD.101.014010). arXiv: [1911.11439](https://arxiv.org/abs/1911.11439) [[hep-th](#)] (cit. on p. [216](#)).
- [586] Michael Thies. “First-order phase boundaries of the massive (1+1)-dimensional Nambu–Jona-Lasinio model with isospin”. In: *Phys. Rev. D* 101.7 (Apr. 2020), p. 074013. DOI: [10.1103/PhysRevD.101.074013](https://doi.org/10.1103/PhysRevD.101.074013). arXiv: [2002.01190](https://arxiv.org/abs/2002.01190) [[hep-th](#)] (cit. on p. [216](#)).
- [587] Michael Thies. “Twisted kink dynamics in multiflavor chiral Gross–Neveu model”. In: *J. Phys. A* 55.1 (Jan. 2022), p. 015401. DOI: [10.1088/1751-8121/ac3cde](https://doi.org/10.1088/1751-8121/ac3cde). arXiv: [2106.03522](https://arxiv.org/abs/2106.03522) [[hep-th](#)] (cit. on p. [216](#)).
- [588] Michael Thies. “Exact tricritical point from next-to-leading-order stability analysis”. In: *Phys. Rev. D* 105.11 (June 2022), p. 116003. DOI: [10.1103/PhysRevD.105.116003](https://doi.org/10.1103/PhysRevD.105.116003). arXiv: [2203.08503](https://arxiv.org/abs/2203.08503) [[hep-th](#)] (cit. on p. [216](#)).

- [589] Christian Boehmer and Michael Thies. “Large N solution of generalized Gross-Neveu model with two coupling constants”. In: *Phys. Rev. D* 80 (Dec. 2009), p. 125038. DOI: [10.1103/PhysRevD.80.125038](https://doi.org/10.1103/PhysRevD.80.125038). arXiv: [0909.3714](https://arxiv.org/abs/0909.3714) [hep-th] (cit. on p. 216).
- [590] Christian Boehmer and Michael Thies. “Competing mechanisms of chiral symmetry breaking in a generalized Gross-Neveu model”. In: *Phys. Rev. D* 81 (May 2010), p. 105027. DOI: [10.1103/PhysRevD.81.105027](https://doi.org/10.1103/PhysRevD.81.105027). arXiv: [0912.2664](https://arxiv.org/abs/0912.2664) [hep-th] (cit. on p. 216).
- [591] Marc Winstel, Jonas Stoll, and Marc Wagner. “Lattice investigation of an inhomogeneous phase of the 2 + 1-dimensional Gross-Neveu model in the limit of infinitely many flavors”. In: *J. Phys. Conf. Ser.* 1667.1 (2020). Ed. by Marco Destefanis et al., p. 012044. DOI: [10.1088/1742-6596/1667/1/012044](https://doi.org/10.1088/1742-6596/1667/1/012044). arXiv: [1909.00064](https://arxiv.org/abs/1909.00064) [hep-lat] (cit. on p. 216).
- [592] Stefano Carignano and Michael Buballa. “Inhomogeneous chiral condensates in three-flavor quark matter”. In: *Phys. Rev. D* 101.1 (Jan. 2020), p. 014026. DOI: [10.1103/PhysRevD.101.014026](https://doi.org/10.1103/PhysRevD.101.014026). arXiv: [1910.03604](https://arxiv.org/abs/1910.03604) [hep-ph] (cit. on pp. 216, 220, 348).
- [593] Michael Buballa et al. “Regulator dependence of inhomogeneous phases in the (2+1)-dimensional Gross-Neveu model”. In: *Phys. Rev. D* 103.3 (Feb. 2021), p. 034503. DOI: [10.1103/PhysRevD.103.034503](https://doi.org/10.1103/PhysRevD.103.034503). arXiv: [2012.09588](https://arxiv.org/abs/2012.09588) [hep-lat] (cit. on pp. 216, 220, 348).
- [594] Michael Buballa, Stefano Carignano, and Lennart Kurth. “Inhomogeneous phases in the quark-meson model with explicit chiral-symmetry breaking”. In: *Eur. Phys. J. ST* 229.22-23 (Dec. 2020), pp. 3371–3385. DOI: [10.1140/epjst/e2020-000101-x](https://doi.org/10.1140/epjst/e2020-000101-x). arXiv: [2006.02133](https://arxiv.org/abs/2006.02133) [hep-ph] (cit. on p. 216).
- [595] Marc Winstel, Laurin Pannullo, and Marc Wagner. “Phase diagram of the 2+1-dimensional Gross-Neveu model with chiral imbalance”. In: *38th International Symposium on Lattice Field Theory*. Sept. 2021. arXiv: [2109.04277](https://arxiv.org/abs/2109.04277) [hep-lat] (cit. on p. 216).
- [596] Laurin Pannullo, Marc Wagner, and Marc Winstel. “Inhomogeneous Phases in the Chirally Imbalanced 2 + 1-Dimensional Gross-Neveu Model and Their Absence in the Continuum Limit”. In: *Symmetry* 14.2 (2022), p. 265. DOI: [10.3390/sym14020265](https://doi.org/10.3390/sym14020265). arXiv: [2112.11183](https://arxiv.org/abs/2112.11183) [hep-lat] (cit. on p. 216).
- [597] Marc Winstel and Laurin Pannullo. “Stability of homogeneous chiral phases against inhomogeneous perturbations in 2+1 dimensions”. In: *39th International Symposium on Lattice Field Theory*. Nov. 2022. arXiv: [2211.04414](https://arxiv.org/abs/2211.04414) [hep-ph] (cit. on p. 216).
- [598] Robert D. Pisarski et al. “The Lifshitz Regime and its Experimental Signals”. In: *Nucl. Phys. A* 1005 (Jan. 2021). Ed. by Feng Liu et al., p. 121910. DOI: [10.1016/j.nuclphysa.2020.121910](https://doi.org/10.1016/j.nuclphysa.2020.121910). arXiv: [2005.00045](https://arxiv.org/abs/2005.00045) [nucl-th] (cit. on pp. 219, 223).
- [599] Robert D. Pisarski, Alexei M. Tsvelik, and Semeon Valgushev. “How transverse thermal fluctuations disorder a condensate of chiral spirals into a quantum spin liquid”. In: *Phys. Rev. D* 102.1 (July 2020), p. 016015. DOI: [10.1103/PhysRevD.102.016015](https://doi.org/10.1103/PhysRevD.102.016015). arXiv: [2005.10259](https://arxiv.org/abs/2005.10259) [hep-ph] (cit. on pp. 219, 223).
- [600] Robert D. Pisarski and Fabian Rennecke. “Signatures of Moat Regimes in Heavy-Ion Collisions”. In: *Phys. Rev. Lett.* 127.15 (Oct. 2021), p. 152302. DOI: [10.1103/PhysRevLett.127.152302](https://doi.org/10.1103/PhysRevLett.127.152302). arXiv: [2103.06890](https://arxiv.org/abs/2103.06890) [hep-ph] (cit. on pp. 219, 223).
- [601] Fabian Rennecke and Robert D. Pisarski. “Moat Regimes in QCD and their Signatures in Heavy-Ion Collisions”. In: *International Conference on Critical Point and Onset of Deconfinement*. Oct. 2021. arXiv: [2110.02625](https://arxiv.org/abs/2110.02625) [hep-ph] (cit. on p. 223).
- [602] Gonzalo De Polsi and Nicolás Wschebor. “Regulator dependence in the functional renormalization group: A quantitative explanation”. In: *Phys. Rev. E* 106.2 (Aug. 2022), p. 024111. DOI: [10.1103/PhysRevE.106.024111](https://doi.org/10.1103/PhysRevE.106.024111). arXiv: [2204.09170](https://arxiv.org/abs/2204.09170) [cond-mat.stat-mech] (cit. on pp. 259, 289).
- [603] Niklas Zorbach, Laurin Pannullo, and Jens Braun. *A comparison of FRG on a spacetime lattice with lattice simulations via the Gross-Neveu model*. in preparation (cit. on p. 260).

- [604] F. W. J. Olver et al. *NIST Digital Library of Mathematical Function*. Release 1.1.2 of 2021-06-15. [Online; accessed 2020.06.24]. 2021. URL: <http://dlmf.nist.gov/> (cit. on pp. 267, 269, 271, 272).
- [605] Don Zagier. “The Dilogarithm Function”. In: *Les Houches School of Physics: Frontiers in Number Theory, Physics and Geometry*. 2007, pp. 3–65. DOI: [10.1007/978-3-540-30308-4_1](https://doi.org/10.1007/978-3-540-30308-4_1) (cit. on p. 270).
- [606] Alfred Jonquière. “Note sur la série $\sum_{n=1}^{n=\infty} \frac{x^n}{n^s}$ ”. In: *Bulletin de la Société Mathématique de France* 17 (Apr. 1889), pp. 142–152. DOI: [10.24033/bsmf.392](https://doi.org/10.24033/bsmf.392) (cit. on p. 271).
- [607] Takeo Matsubara. “A new approach to quantum statistical mechanics”. In: *Prog. Theor. Phys.* 14 (Oct. 1955), pp. 351–378. DOI: [10.1143/PTP.14.351](https://doi.org/10.1143/PTP.14.351) (cit. on p. 275).
- [608] John Bardeen. “Relation between lattice vibration and London Theories of superconductivity”. In: *Phys. Rev.* 81 (5 Mar. 1951), pp. 829–834. DOI: [10.1103/PhysRev.81.829](https://doi.org/10.1103/PhysRev.81.829) (cit. on p. 275).
- [609] Herbert Frölich. “On the theory of superconductivity: The one-dimensional case”. In: *Proc. R. Soc. Lond. A* 223 (1154 May 1954), pp. 296–305. DOI: [10.1098/rspa.1954.0116](https://doi.org/10.1098/rspa.1954.0116) (cit. on p. 275).
- [610] Charles G. Kuper. “The thermal decomposition of ammonium perchlorate II. The kinetics of the decomposition, the effect of particle size, and discussion of results”. In: *Proc. R. Soc. Lond. A* 227 (1169 Jan. 1955), pp. 214–228. DOI: [10.1098/rspa.1955.0005](https://doi.org/10.1098/rspa.1955.0005) (cit. on p. 275).
- [611] Jens Braun et al. “Volume and quark mass dependence of the chiral phase transition”. In: *Phys. Rev. D* 73 (Apr. 2006), p. 074010. DOI: [10.1103/PhysRevD.73.074010](https://doi.org/10.1103/PhysRevD.73.074010). arXiv: [hep-ph/0512274](https://arxiv.org/abs/hep-ph/0512274) (cit. on p. 275).
- [612] Jens Braun, Benjamin Klein, and Hans-Juergen Pirner. “Influence of quark boundary conditions on the pion mass in finite volume”. In: *Phys. Rev. D* 72 (Aug. 2005), p. 034017. DOI: [10.1103/PhysRevD.72.034017](https://doi.org/10.1103/PhysRevD.72.034017). arXiv: [hep-ph/0504127](https://arxiv.org/abs/hep-ph/0504127) (cit. on p. 275).
- [613] Jens Braun, Bertram Klein, and Bernd-Jochen Schaefer. “On the Phase Structure of QCD in a Finite Volume”. In: *Phys. Lett. B* 713 (July 2012), pp. 216–223. DOI: [10.1016/j.physletb.2012.05.053](https://doi.org/10.1016/j.physletb.2012.05.053). arXiv: [1110.0849](https://arxiv.org/abs/1110.0849) [hep-ph] (cit. on p. 275).
- [614] Jens Braun, Sebastian Diehl, and Michael M. Scherer. “Finite-size and Particle-number Effects in an Ultracold Fermi Gas at Unitarity”. In: *Phys. Rev. A* 84 (Dec. 2011), p. 063616. DOI: [10.1103/PhysRevA.84.063616](https://doi.org/10.1103/PhysRevA.84.063616). arXiv: [1109.1946](https://arxiv.org/abs/1109.1946) [cond-mat.quant-gas] (cit. on p. 275).
- [615] Jean Zinn-Justin. *Quantum field theory at finite temperature: An Introduction*. May 2000. arXiv: [hep-ph/0005272](https://arxiv.org/abs/hep-ph/0005272) (cit. on p. 275).
- [616] Satyendra N. Bose. “Planck’s law and light quantum hypothesis”. In: *Z. Phys.* 26 (Dec. 1924), pp. 178–181. DOI: [10.1007/BF01327326](https://doi.org/10.1007/BF01327326) (cit. on p. 276).
- [617] Enrico Fermi. “Sulla quantizzazione del gas perfetto monoatomico”. In: *Rend. Lincei* 3 (1926), pp. 145–149 (cit. on p. 276).
- [618] Paul A. M. Dirac. “On the theory of quantum mechanics”. In: *Proc. Roy. Soc. Lond. A* 112 (Oct. 1926), pp. 661–677. DOI: [10.1098/rspa.1926.0133](https://doi.org/10.1098/rspa.1926.0133) (cit. on p. 276).
- [619] Bryce S. DeWitt. *The global approach to quantum field theory. Vol. 1, 2*. Vol. 114. Int. Ser. Monogr. Phys. Oxford, England, UK: Oxford University Press, 2003 (cit. on pp. 285, 286).
- [620] Reinhard Alkofer, Markus Q. Huber, and Kai Schwenzer. “Algorithmic derivation of Dyson-Schwinger Equations”. In: *Comput. Phys. Commun.* 180 (June 2009), pp. 965–976. DOI: [10.1016/j.cpc.2008.12.009](https://doi.org/10.1016/j.cpc.2008.12.009). arXiv: [0808.2939](https://arxiv.org/abs/0808.2939) [hep-th] (cit. on pp. 285, 312).

- [621] Markus Q. Huber and Jens Braun. “Algorithmic derivation of functional renormalization group equations and Dyson-Schwinger equations”. In: *Comput. Phys. Commun.* 183 (June 2012), pp. 1290–1320. DOI: [10.1016/j.cpc.2012.01.014](https://doi.org/10.1016/j.cpc.2012.01.014). arXiv: [1102.5307](https://arxiv.org/abs/1102.5307) [[hep-th](#)] (cit. on pp. [285](#), [312](#)).
- [622] Markus Q. Huber, Anton K. Cyrol, and Jan M. Pawłowski. “DoFun 3.0: Functional equations in Mathematica”. In: *Comput. Phys. Commun.* 248 (Mar. 2020), p. 107058. DOI: [10.1016/j.cpc.2019.107058](https://doi.org/10.1016/j.cpc.2019.107058). arXiv: [1908.02760](https://arxiv.org/abs/1908.02760) [[hep-ph](#)] (cit. on pp. [285](#), [312](#)).
- [623] Romain Contant and Markus Q. Huber. “Dense two-color QCD from Dyson-Schwinger equations”. In: *Phys. Rev. D* 101.1 (Jan. 2020), p. 014016. DOI: [10.1103/PhysRevD.101.014016](https://doi.org/10.1103/PhysRevD.101.014016). arXiv: [1909.12796](https://arxiv.org/abs/1909.12796) [[hep-ph](#)] (cit. on p. [285](#)).
- [624] Ouraman Hajizadeh et al. “Exploring the Tan contact term in Yang-Mills theory”. In: *Phys. Rev. D* 103.3 (Feb. 2021), p. 034023. DOI: [10.1103/PhysRevD.103.034023](https://doi.org/10.1103/PhysRevD.103.034023). arXiv: [1909.12727](https://arxiv.org/abs/1909.12727) [[hep-ph](#)] (cit. on p. [285](#)).
- [625] Nicolas Wink. “Towards the spectral properties and phase structure of QCD”. PhD thesis. University of Heidelberg, 2020. DOI: [10.11588/heidok.00028503](https://doi.org/10.11588/heidok.00028503) (cit. on p. [285](#)).
- [626] Markus Q. Huber. “Correlation functions of Landau gauge Yang-Mills theory”. In: *Phys. Rev. D* 101 (June 2020), p. 114009. DOI: [10.1103/PhysRevD.101.114009](https://doi.org/10.1103/PhysRevD.101.114009). arXiv: [2003.13703](https://arxiv.org/abs/2003.13703) [[hep-ph](#)] (cit. on p. [285](#)).
- [627] Gustavo P. de Brito, Astrid Eichhorn, and Marc Schiffer. “Light charged fermions in quantum gravity”. In: *Phys. Lett. B* 815 (Apr. 2021), p. 136128. DOI: [10.1016/j.physletb.2021.136128](https://doi.org/10.1016/j.physletb.2021.136128). arXiv: [2010.00605](https://arxiv.org/abs/2010.00605) [[hep-th](#)] (cit. on p. [285](#)).
- [628] Marc Schiffer. “Probing Quantum Gravity: Theoretical and phenomenological consistency tests of asymptotically safe quantum gravity”. PhD thesis. University of Heidelberg, Oct. 2021. DOI: [10.11588/heidok.00030645](https://doi.org/10.11588/heidok.00030645) (cit. on p. [285](#)).
- [629] Jonas von Milczewski, Félix Rose, and Richard Schmidt. “Functional-renormalization-group approach to strongly coupled Bose-Fermi mixtures in two dimensions”. In: *Phys. Rev. A* 105.1 (Jan. 2022), p. 013317. DOI: [10.1103/PhysRevA.105.013317](https://doi.org/10.1103/PhysRevA.105.013317). arXiv: [2104.14017](https://arxiv.org/abs/2104.14017) [[cond-mat.quant-gas](#)] (cit. on p. [285](#)).
- [630] Gustavo P. de Brito, Astrid Eichhorn, and Rafael Robson Lino dos Santos. “The weak-gravity bound and the need for spin in asymptotically safe matter-gravity models”. In: *JHEP* 11 (Nov. 2021), p. 110. DOI: [10.1007/JHEP11\(2021\)110](https://doi.org/10.1007/JHEP11(2021)110). arXiv: [2107.03839](https://arxiv.org/abs/2107.03839) [[gr-qc](#)] (cit. on p. [285](#)).
- [631] Markus Q. Huber, Christian S. Fischer, and Helios Sanchis-Alepuz. “Higher spin glueballs from functional methods”. In: *Eur. Phys. J. C* 81.12 (Dec. 2021), p. 1083. DOI: [10.1140/epjc/s10052-021-09864-5](https://doi.org/10.1140/epjc/s10052-021-09864-5). arXiv: [2110.09180](https://arxiv.org/abs/2110.09180) [[hep-ph](#)] (cit. on p. [285](#)).
- [632] Jan M. Pawłowski, Coralie S. Schneider, and Nicolas Wink. *QMeS-Derivation: Mathematica package for the symbolic derivation of functional equations*. Feb. 2021. arXiv: [2102.01410](https://arxiv.org/abs/2102.01410) [[hep-ph](#)] (cit. on pp. [285](#), [312](#)).
- [633] Martin J. Steil. *Wetterich equation in FS notation*. Notes. unpublished notes, private communication. Aug. 2019 (cit. on p. [285](#)).
- [634] Istvan Nandori. “Functional renormalization group with a compactly supported smooth regulator function”. In: *JHEP* 04 (Apr. 2013), p. 150. DOI: [10.1007/JHEP04\(2013\)150](https://doi.org/10.1007/JHEP04(2013)150). arXiv: [1208.5021](https://arxiv.org/abs/1208.5021) [[hep-th](#)] (cit. on pp. [289](#), [302](#)).
- [635] Tim R. Morris. “On truncations of the exact renormalization group”. In: *Phys. Lett. B* 334 (Aug. 1994), pp. 355–362. DOI: [10.1016/0370-2693\(94\)90700-5](https://doi.org/10.1016/0370-2693(94)90700-5). arXiv: [hep-th/9405190](https://arxiv.org/abs/hep-th/9405190) (cit. on p. [294](#)).
- [636] John H. Conway. *Sequence A000670: Fubini numbers*. The On-Line Encyclopedia of Integer Sequences. [Online; accessed 2021.03.16]. 2021. URL: <https://oeis.org/A000670> (cit. on p. [300](#)).

- [637] Daniel F. Litim. “Critical exponents from optimized renormalization group flows”. In: *Nucl. Phys. B* 631 (2002), pp. 128–158. DOI: [10.1016/S0550-3213\(02\)00186-4](https://doi.org/10.1016/S0550-3213(02)00186-4). arXiv: [hep-th/0203006](https://arxiv.org/abs/hep-th/0203006) (cit. on p. 302).
- [638] Reinhard Alkofer et al. “Bound state properties from the functional renormalization group”. In: *Phys. Rev. D* 99.5 (Mar. 2019), p. 054029. DOI: [10.1103/PhysRevD.99.054029](https://doi.org/10.1103/PhysRevD.99.054029). arXiv: [1810.07955](https://arxiv.org/abs/1810.07955) [[hep-ph](#)] (cit. on p. 303).
- [639] Joerg Jaeckel and Christof Wetterich. “Flow equations without mean field ambiguity”. In: *Phys. Rev. D* 68 (July 2003), p. 025020. DOI: [10.1103/PhysRevD.68.025020](https://doi.org/10.1103/PhysRevD.68.025020). arXiv: [hep-ph/0207094](https://arxiv.org/abs/hep-ph/0207094) (cit. on p. 307).
- [640] Anton K. Cyrol, Mario Mitter, and Nils Strodthoff. “FormTracer - A Mathematica Tracing Package Using FORM”. In: *Comput. Phys. Commun.* 219 (2017), pp. 346–352. DOI: [10.1016/j.cpc.2017.05.024](https://doi.org/10.1016/j.cpc.2017.05.024). arXiv: [1610.09331](https://arxiv.org/abs/1610.09331) [[hep-ph](#)] (cit. on pp. 312, 318, 337).

List of Figures

3.1	Perturbation theory in zero dimensions	27
3.2	$1/N$ -expansion in zero dimensions	32
3.3	Infinite- N initial potential for RG flows with shocks (invariant)	33
3.4	Exponent of the infinite- N initial potential for RG flows with shocks	35
4.1	Deformation integrand of the path integral with RG time	40
5.1	FV implementation of the boundary condition at $\sigma = 0$	75
6.1	(Derivatives of the) UV initial potentials for tests in zero dimensions	81
6.2	RG flows of test cases in zero dimensions	88
6.3	3D plots of the RG flow of test case I	89
6.4	Comparison of RG flows for $N = 1, 10, 100$ for test case I	89
6.5	Tests for the error scaling with Δx	90
6.6	Tests for the error scaling with x_{\max}	92
6.7	Tests for the error scaling with Λ	94
6.8	IR convergence tests	95
6.9	FRG vertex/Taylor expansion tests	96
6.10	Entropy production in the RG flow – non-analytic UV potentials	99
6.11	Entropy production in the RG flow – analytic UV potentials	100
6.12	Infinite- N initial potential for RG flows with shocks (field)	103
6.13	Characteristic curves	104
6.14	Parameter tests for infinite- N RG flows	106
6.15	3D plots of infinite- N RG flows with shocks and rarefaction waves	107
6.16	Comparison of infinite- and finite- N RG flows	108
6.17	Entropy production in infinite- N RG flows	112
7.1	The full phase diagram of the GN model at $N \rightarrow \infty$	134
9.1	(One-loop) β -function of the GN model	171
9.2	Inverse four-fermion coupling at infinite N	177
9.3	Inverse four-fermion coupling at finite N	183
10.1	Source-sink term of the PDE for the GNY model	197
11.1	Phase diagram of the GN model at $N \rightarrow \infty$	208
11.2	Minimum and curvature mass of the $N \rightarrow \infty$ GN model	209
11.3	(Derivative of the) effective potential in the infinite- N GN model	210
11.4	Thermodynamic observables in the infinite- N GN model	212
11.5	Phase diagram of the infinite- N GN model from the stability analysis	218
11.6	Bosonic wave-function renormalization at $N \rightarrow \infty$	218
11.7	Bosonic wave-function renormalization at $N \rightarrow \infty$ at $\sigma = 0$	219
11.8	Bosonic two-point function at $N \rightarrow \infty$	222
11.9	Spatially inhomogeneous condensate and the dominating wave vector	225
11.10	The dominating wave vector and the minimum of the bosonic two-point function	226

11.11	Visualization of the AMR algorithm	227
12.1	UV cutoff test for the infinite- N GN model with the phase diagram	234
12.2	UV cutoff tests for the infinite- N GN model with the curvature mass	235
12.3	$\Delta\sigma$ tests for the infinite- N GN model with the curvature mass	236
12.4	σ_{\max} tests for the infinite- N GN model with the curvature mass	236
12.5	Comparison of MF and LPA RG flows in the GNY model	237
12.6	MF and LPA RG flows in the GNY model at small/vanishing temperature	240
12.7	Dependence of the symmetry restoration scale on N of the GNY model in LPA	241
12.8	Dependence of the k_{res} on the T of the GNY model in LPA	242
12.9	Precondensation temperature in the GNY model in LPA	242
12.10	RG-scale-dependence of the PT lines of the GNY model in LPA	243
12.11	Vacuum RG flows of the GNY model in LPA	244
12.12	RG flows at $N = 2$ for different truncations	247
12.13	RG breakdown scale in the μ - T -plane in LPA' + h	250
12.14	Yukawa coupling in the μ - T -plane in LPA' + h	251
12.15	Z_ϕ in the μ - T -plane in LPA' + h	252
12.16	RG flow in LPA' + h coupling at small T and non-zero μ	253
12.17	Phase transition lines in the μ - T -plane in LPA' + h	254

List of Tables

6.1	Reference values for vertex functions of the zero-dimensional test models	82
11.1	Explicit expressions for (the derivative of) the effective potential	207
11.2	Explicit expressions for some thermodynamic quantities	211
11.3	Explicit expressions for the wave-function renormalization and two-point function .	217
A.1	Volumes of $(d - 1)$ -dimensional spheres and FRG loop prefactors	264

